NUREG/CR-2229
EPRI NP-1783
GEAP-24962-2
Vol. 2

JUL 30 1982
ASLBP LIBRARY

3WR Large Break Simulation Tests — 3WR Blowdown/Emergency Core Cooling Program

/olume 2
\ppendices I-N

repared by L. S. Lee, G. L. Sozzi, S. A. Allison

uclear Engineering Division
ieneral Electric Company

repared for
.S. Nuclear Regulatory Commission

nd
lectric Power Research Institute

nd
eneral Electric Company

NOTICE

This report was prepared as an account of work sponsored by an agency of the United States Government. Neither the United States Government nor any agency thereof, or any of their employees, makes any warranty, expressed or implied, or assumes any legal liability of responsibility for any third party's use, or the results of such use, of any information, apparatus, product or process disclosed in this report, or represents that its use by such third party would not infringe privately owned rights.

Availability of Reference Materials Cited in NRC Publications

Most documents cited in NRC publications will be available from one of the following sources:

1. The NRC Public Document Room, 1717 H Street, N.W.
   Washington, DC 20555
2. The NRC/GPO Sales Program, U.S. Nuclear Regulatory Commission,
   Washington, DC 20555
3. The National Technical Information Service, Springfield, VA 22161

Although the listing that follows represents the majority of documents cited in NRC publications, it is not intended to be exhaustive.

Referenced documents available for inspection and copying for a fee from the NRC Public Document Room include NRC correspondence and internal NRC memoranda; NRC Office of Inspection and Enforcement bulletins, circulars, information notices, inspection and investigation notices; Licensee Event Reports; vendor reports and correspondence; Commission papers; and applicant and licensee documents and correspondence.

The following documents in the NUREG series are available for purchase from the NRC/GPO Sales Program: formal NRC staff and contractor reports, NRC-sponsored conference proceedings, and NRC booklets and brochures. Also available are Regulatory Guides, NRC regulations in the *Code of Federal Regulations,* and *Nuclear Regulatory Commission Issuances.*

Documents available from the National Technical Information Service include NUREG series reports and technical reports prepared by other federal agencies and reports prepared by the Atomic Energy Commission, forerunner agency to the Nuclear Regulatory Commission.

Documents available from public and special technical libraries include all open literature items, such as books, journal and periodical articles, and transactions. *Federal Register* notices, federal and state legislation, and congressional reports can usually be obtained from these libraries.

Documents such as theses, dissertations, foreign reports and translations, and non-NRC conference proceedings are available for purchase from the organization sponsoring the publication cited.

Single copies of NRC draft reports are available free upon written request to the Division of Technical Information and Document Control, U.S. Nuclear Regulatory Commission, Washington, DC 20555.

Copies of industry codes and standards used in a substantive manner in the NRC regulatory process are maintained at the NRC Library, 7920 Norfolk Avenue, Bethesda, Maryland, and are available there for reference use by the public. Codes and standards are usually copyrighted and may be purchased from the originating organization or, if they are American National Standards, from the American National Standards Institute, 1430 Broadway, New York, NY 10018.

GPO Printed copy price: $13.00

NUREG/CR-2229
EPRI NP-1783
GEAP-24962-2
Vol. 2
R2

BWR Large Break Simulation Tests — BWR Blowdown/Emergency Core Cooling Program

Volume 2
Appendices I-N

Manuscript Completed: March 1981
Date Published: July 1982

Prepared by
L. S. Lee, G. L. Sozzi, S. A. Allison

Nuclear Engineering Division
General Electric Company
San Jose, CA 95125

Prepared for
Division of Accident Evaluation
Office of Nuclear Regulatory Research
U.S. Nuclear Regulatory Commission
Washington, D.C. 20555
NRC FIN No. B3014

and
Electric Power Research Institute
3412 Hillview Avenue
Palo Alto, CA 94303

and
Nuclear Engineering Division
General Electric Company
San Jose, CA 95125

NUREG/CR-2229
EPRI NP-1783
GEAP-24962-2
March 1981
DRF E00-66

BWR LARGE BREAK SIMULATION TESTS
BWR BLOWDOWN/EMERGENCY CORE COOLING PROGRAM

Volume 2

L. S. Lee
G. L. Sozzi
S. A. Allison

Contributors:

J. Ashjaee
D. W. Danielson
W. S. Hwang
D. A. Wilhelmson

Approved: J. C. Black, Sr. Program Manager
BWR/BD/ECC Program

Approved: G. L. Sozzi, Manager
LOCA System Technology

Approved: G. E. Dix, Manager
Safety and Thermal Hydraulics Technology

Approved: J. E. Wood, Manager
Core Methods and Analysis

Prepared for the
U.S. Nuclear Regulatory Commission
and Electric Power Research Institute
Under Contract NRC-04-76-215

Printed in the United States of America
Available from
National Technical Information Service
U.S. Department of Commerce
5285 Port Royal Road
Springfield, VA 22161
Price: Printed Copy $4.00; Microfiche $2.25

NUCLEAR ENGINEERING DIVISION • GENERAL ELECTRIC COMPANY
SAN JOSE, CALIFORNIA 95125

GENERAL ELECTRIC

LEGAL NOTICE

This report was prepared by the General Electric Company as an account of work sponsored by the Nuclear Regulatory Commission, the Electric Power Research Institute, and the General Electric Company. No person acting on behalf of the NRC, the Institute, or members of the Institute, or General Electric Company:

A. Makes any warranty or representation, express or implied, with respect to the accuracy, completeness, or usefulness of the information contained in this report, or that information, apparatus, method or process disclosed in this report may not infringe privately owned rights, or

B. Assumes any liabilities with respect to the use of, or for damages resulting from the use of any information, apparatus, method or process disclosed in this report.

CONTENTS

		Page
	APPENDICES	
I.	SCOPING SERIES RESULTS	I-1
J.	DATA REPORT FOR TEST 6425/RUN 2 (REFERENCE TEST)	J-1
K.	DATA REPORT FOR TEST 6424/RUN 1	K-1
L.	DATA REPORT FOR TEST 6426/RUN 1 AND TEST 6421/RUN 2	L-1
M.	DATA REPORT FOR TEST 6422/RUN 3	M-1
N.	DATA REPORT FOR TEST 6423/RUN 3	N-1

ACKNOWLEDGMENTS

This report was completed as a team effort. In addition to those listed whose contributions were integrated into the report, credits are due the following persons: S. D. Stevens for reducing the data and preparing figures and H. Ngo for assisting in conducting the tests as well as contributing to data reduction. Gratefully acknowledged are technical guidance rendered by Dr. G. E. Dix, B. Matzner, and the Program Management Group: Dr. W. D. Beckner of the Nuclear Regulatory Commission, Dr. S. P. Kalra of the Electric Power Research Institute, and G. W. Burnette of General Electric Company.

Appendix I

SCOPING SERIES RESULTS
(L. S. Lee)

I-1. SUMMARY OF THE SCOPING SERIES

I-1.1 Introduction

The BD/ECC-1A phase of the Blowdown/Emergency Core Cooling (BD/ECC) Program was intended to obtain information on the effect of ECC injection on boiling water reactor (BWR) system responses. The original test plan (I-1) identified a matrix of 20 tests. Six of these tests were selected (I-2) by the Program Management Group (PMG) to scope the outcome of the test series. The scoping series is comprised of five of the six tests.

Four matrix tests plus a repeat of the reference test without ECC injection were completed by September 1978. The bundle power, ECC pump rated flow conditions, and the temperature of the ECC water were parameters in these tests. Table I-1 shows the variation of the parameters throughout the matrix tests.

To summarize the scoping series results, a scenario of the reference test (6406/Run 1) is presented, and the differences between tests with and without ECC injection are described. Highlights of other tests in the scoping series are also briefly summarized. This series of tests was conducted in TLTA-5, which had a nonrepresentative simulation of the core leakage flow path. This flow path was improved in TLTA-5A.

I-1.2 Scenario of the Reference Test

I-1.2.1 Controlled Parameters. Controlled parameters refer to those quantities whose transient responses are designed and controlled to be similar to those predicted for a reactor counterpart. Included and shown in Figure I-1 are bundle power, steamline flow, ECC injection flow characteristics, and drive pump coastdown.

The steamline flow (Figure I-1a) was controlled during the test by the pressure control valve, which opened and closed in response to the vessel pressure. The setpoint for the valve was 1050 psia. The valve closed completely at ∿12 sec for the reference test.

The ECC injections are shown in Figure I-1b. The high pressure core spray (HPCS) was activated at 27* sec, and injection began immediately. The low pressure core spray (LPCS) and low pressure coolant injection (LPCI) were activated at 37* sec, but actual flow began at 78 sec for LPCS and 86 sec for LPCI. Both the timings and the ECCS pump operating characteristics were designed (I-3) to simulate the characteristics of the BWR ECCS.

The bundle power transient is shown in Figure I-1c. The power supplied to the bundle was programmed to simulate the stored heat and fission decay heat [based on American Nuclear Society Standard (ANS) + 20%] of a BWR bundle. However, the capability of the mechanical controller provided accurate simulation for only the first 50 sec. Beyond that time the power supplied to the bundle was held constant. The actual bundle power became proportionally higher with time than the fission decay heat calculated from ANS + 20 percent, reaching ∿1.8 times that value at the end of the test (∿300 sec). A detailed discussion of the bundle power supply is included in Subsection I-2.

Coastdown of the intact loop drive pump began immediately in response to the loss of power (Figure I-1d). The response of pump coastdown is governed by the inertia of the rotating components. The inertia of the test pump has been designed to simulate that of the BWR counterpart.

I-1.2.2 Early Responses. The responses from BD/ECC-1A tests, before HPCS injection at 27 sec, are similar to those of the previous 8x8 blowdown heat transfer (BDHT) tests (with no ECC). The early responses are governed by the liquid level in the downcomer region (Figure 1-2a). This level reaches the jet pump suction plane at 7.6 sec and the recirculation line suction inlet at about 10.5 sec.

The initial drop in the bundle inlet flow (Figure I-2b) is due to the loss of jet pump flow in the broken loop. The inlet flow then decreases following the coastdown of the intact loop drive pump (Figure I-1d). The flow reaches a near zero

*NOTE: The time delays of 27 sec for HPCS and 37 sec for LPCS and LPCI are designed to simulate the startup of the diesel generator and the opening of valves in the BWR.

value when the jet pump suction is uncovered at 7.6 sec. The flow surge associated with lower plenum flashing occurs at 11.8 sec, shortly after recirculation line suction uncovery.

The early pressure and temperature responses are shown in Figures I-2c and I-2d, respectively. The peak power plane temperature steadily decreases until after HPCS is initiated. The system depressurization rate increases after the recirculation line suction uncovery because of an increased volumetric discharge which accompanies the transition from predominantly liquid to vapor blowdown. The system depressurization rate decreases after lower plenum flashing.

I-1.2.3 "Snapshots" Presentation. A series of "snapshots," pictorial depictions of the system at selected instants of the transient, is presented in Figure I-3. These "snapshots" convey a sequential qualitative overview of the thermal-hydraulic responses of the two-loop test apparatus (TLTA). The details of the responses shown in Figures I-4 to I-7 were the bases from which the scenario for the reference test was constructed.

The first "snapshot" (Figure I-3a) depicts the system conditions at the onset of HPCS injection, which occurs at ∿27 sec, shortly after lower plenum flashing (LPF). Substantial mass inventory is seen in the upper plenum, as shown by the high two-phase level in Figure I-4a. This inventory was transferred there as a result of LPF which redistributed fluid from the lower plenum to the core and upper plenum. An apparent continuum of liquid (or two-phase mixture) keeps the bundle in nucleate boiling, as is evident from Figure I-5 which presents the thermal responses throughout the bundle.

As the blowdown proceeds and mass inventory in the lower plenum continues to decrease, the receding two-phase level reaches the jet pump exit plane at ∿34 sec, as shown in Figure I-4a. The lower plenum mixture level remains at the jet pump exit plane until the lower plenum begins to refill later in the transient.

The flashing lower plenum fluid discharges with increasing vapor fraction through the jet pumps. The void fraction in the jet pump increases, reducing the hydrostatic head, which in turn reduces the pressure difference across the jet pump. Accordingly, the pressure drop across the bundle path, which is in parallel with the jet pump path, also decreases. The diversion of vapor out the jet pump path reduces the holdup of liquid caused by counter-current flow limiting (CCFL) within the bundle. The liquid continuum within the bundle then drops below the bottom of

heated length (BHL) at ∿40 sec, as shown in Figure I-4a.

At 40 sec (Figure I-3b), the bundle is filled with a vapor continuum with dispersed liquid. Heater rods begin to dry out, and bulk heatup occurs, as shown by the increasing temperatures in Figure I-5. In contrast, the upper plenum inventory remains essentially unchanged during this period. HPCS flow replenishes the loss of fluid from the upper plenum, while CCFL at the upper tieplate prevents complete draining into the bundle or bypass.

The CCFL conditions at the upper tieplate shift in response to a reduced vapor flow from the bundle. This reduction is due to a decrease in vapor flow from the lower plenum after the uncovery of the jet pump exit plane and the reduction in heat transfer that accompanies the loss of the liquid continuum in the bundle. With the reduction of vapor flow at the upper tieplate, an increased amount of liquid drains into the bundle (Figure I-3c), and a few of the previously dried-out rods are seen to rewet (Figure I-5b). During this period (∿64 sec), rewetting is limited to the upper bundle.

LPCS injection begins at ∿76 sec. The injection rate increases toward the rated flow as the system pressure decreases. The upper plenum inventory is maintained by this LPCS mass influx in conjunction with that of HPCS. The vapor upflow from the lower plenum, in the meantime, diminishes as the rate of system depressurization decreases. The liquid downflow at the upper tieplate increases as the CCFL conditions shift at ∿90 sec (Figure I-3d). Rewetting of previously dried-out thermocouple locations is seen at the bottom as well as at the upper part of the bundle (Figure I-5).

Also at ∿90 sec, LPCI begins to flow into the bypass region in increasing amounts (until rated flow has been reached). The net vapor outflow from this region decreases as the influx of subcooled ECC water condenses some of the steam. At ∿105 sec, the CCFL conditions at the bypass outlet shift to allow the liquid in the upper plenum to drain more rapidly into the bypass region (Figure I-3e). More fluid is now in the bypass region and less in the upper plenum, as shown by the two-phase levels in Figure I-4b. The hydrostatic head in the upper plenum is then decreased, which allows for a higher pressure drop in the core to balance the imposed head of the jet pump. The resultant increased vapor upflow contributes to an increase in bundle heat transfer, which results in a decrease in the bulk heatup rate at ∿105 sec (Figures I-5a and I-5b).

This phase of the refilling process is somewhat different from that in TLTA-5A because of the addition of the leakage path between the bypass and bundle in TLTA-5A.

As the bypass region is being filled, some liquid drains into the guide tubes and, consequently, into the lower plenum. The mixture level in the lower plenum rises (Figure I-4a). This level rises steadily and at a faster rate after the guide tube is completely full. The jet pump exit becomes sealed by the rising mixture level at ∿150 sec (Figure I-3f). As the mixture fills the jet pumps, the hydrostatic head and hence the pressure drop across the jet pumps increase. The pressure drop across the bundle increases correspondingly with increased vapor flow from the lower plenum. The increased vapor flow contributes to a further increase in bulk heat transfer that results in the further decrease in bundle heat-up rate noted in Figures I-5a and I-5b at 150 sec.

The bundle begins to reflood as the lower plenum level continues to rise at a more rapid pace after the bypass region has become full (Figure I-3g). The reflooding of the bundle results in rapid quenching below the mixture level as shown in Figures I-5a and I-5b. The extent of the bundle reflood is limited by the static head corresponding to the jet pump suction plane, as illustrated in Figure I-6. The bundle mixture level reaches its height limit at ∿250 sec. The system is maintained at quasi-steady state for the balance of the test, which ends at ∿300 sec (Figure I-3h).

I-1.3 Comparison of Tests with and without ECC Injection

Comparisons of data from average-power tests with and without ECC are made in this section. Data from Test 6406/R1 (average power, average ECC) are compared with those from Test 6406/R3 and/or Test 6007/R26 (average power, no ECC).

Figure I-7 shows that the system depressurization rate for the test with ECC is lower after ∿65 sec. The flow emanating from the lower plenum for the test with ECC has a higher moisture content as well as a higher discharge rate through the jet pumps. The combined effect is a sequential reduction of volumetric flow through, first, the drive/blowdown line, and then the suction/blowdown line. Slower depressurization results from these lower volumetric flows through the breaks.

The system mass inventory is higher, as expected, for the test with ECC. In the upper plenum (Figure I-8a), the fluid is prevented from completely draining because of CCFL at the upper tieplate. In the test without ECC, the inventory there depletes steadily as it continues to flash throughout the transient. In the test

with ECC, the core spray maintains the inventory until ∿100 sec. At that time, the LPCI has taken effect in the bypass region to reduce the vapor up-flow, allowing the upper plenum fluid to drain into the region. The ECC injection rate is given in Figure I-8d.

The bundle mass inventories for the two tests are virtually the same (Figure I-8b). In both tests, the bundle is filled with a vapor continuum after ∿40 sec. The mass inventory is derived from the bundle pressure drop measurements which show nearly identical responses for the tests with and without ECC (Figure I-9). The transition from liquid to vapor continuum is shown to occur between 34 to 40 sec. In the test with ECC, reflooding causes liquid accumulation in the lower part of the bundle later in the transient (∿200 sec).

The lower plenum mass for the test with ECC is maintained rather constant from 35 to 120 sec (Figure I-8c). The fluid discharged through the jet pump is balanced by the ECC fluid draining from the upper plenum. For the test without ECC, in contrast, the mass inventory in the lower plenum depletes continuously as the fluid flashes off throughout the transient.

The bypass region mass inventories for the two tests are similar prior to LPCI injection (Figure I-8e). Following the LPCI injection (∿90 sec), the bypass region refills only for the test with ECC. The guide tube mass inventories (Figure I-8f) also show a similar early response. A discernible difference between the responses occurs when ECC fluid in the upper plenum begins (∿75 sec) to drain into and accumulate in the guide tube for the test with ECC.

The two-phase levels at different regions in TLTA are shown in Figure I-10. The upper plenum two-phase levels reflect the mass inventories shown in Figure I-8a. In the case with ECC, the mixture level holds up longer because of the core spray fluid. The mixture level in the bundle drops to the bottom of the heated length at ∿40 sec for both tests. The mixture level for the test without ECC remains above the level for the test with ECC until bundle reflood occurs for the test with ECC.

The lower plenum mixture level for both tests falls rather rapidly after lower plenum flashing, reaching the jet pump exit plane at ∿34 sec. The level in the test with ECC lingers at this elevation until it rises later in the transient (∿120 sec). In contrast, the level for the test without ECC falls and holds momentarily at the exit plane before falling below the jet pump exit at ∿65 sec.

In the bypass region, the levels for the two tests are initially similar. For the test with ECC, the level rises later in the transient (∿98 sec) as the ECC fluid drains into the region. Similarly, the level in the guide tube rises later in the transient for the case with ECC.

As a consequence of the differences in hydraulic responses for the two tests, the thermal responses are also different. In the test without ECC, bundle rewetting and heat-up rate reduction are not observed.

The thermal responses for the two tests are compared in Figure I-11. The lower part of the bundle is cooler in the test without ECC for the first ∿100 sec. This is consistent with the observation (Figure I-10a) that, with less static head in the upper plenum, the mixture level in the core is higher for the test without ECC during this period.

Responses from the upper part of the bundle (Figure I-11b) provide evidence of improved heat transfer with ECC. At ∿150 sec, a temperature difference of 375°F is seen between the tests at the location of the peak cladding temperature (90 in. elevation).

I-1.4 Highlights of Significant Differences of Other Tests with ECC Injection

I-1.4.1 Average Power, Low ECC Test (6405/Run 3). Responses from this test are, in general, similar to those from the reference test, as can be seen from Figure I-12. The system pressure of the two tests with ECC starts deviating from that of the test without ECC at ∿65 sec because of the difference in volumetric break flows. The difference at ∿100 sec between the two tests with ECC is due to the same effect (i.e., the difference in liquid content in the break flow). The lower ECC flow results in a lower liquid fraction in the downcomer region and a higher volumetric break flow.

The lower ECC injection also causes a slower system refill as expected. Nevertheless, the responses and phenomena observed are similar. The overall thermal response of the bundle shows that less ECC fluid results in higher cladding temperature at the peak power plane (Figure I-13).

I-1.4.2 Peak Power, Low Flow, and High Temperature ECC Test (6414/Run 3). The parameters for this test were intentionally chosen to provide an upper bound bundle heat-up response. The ECC systems were degraded to have low flows and high temperatures, and the test was conducted with a peak bundle power of 6.49 MW.

Nevertheless, the system response from this test is comparable with that from the average power (5.05 MW), average ECC test. The hydraulic response of the bundle for the peak power test is similar to that of the average power test, as shown by the comparison of pressure drop across the bundle (Figure I-14). Because of the higher bundle power, the temperature response of the rods is different, as can be seen from Figure I-13. The peak power bundle has a higher temperature as expected. A temperature difference of ∿450°F is observed at ∿170 sec when the peak power test was terminated.

I-1.4.3 Low Power, High ECC Test (6401/Run 4). The goal of this low-power (1.62 MW), high-spray flow test was to obtain a data base of system response for a peripheral-power bundle. Significant differences of hydraulic responses are seen in this test as compared with the reference test. The differences are:

(a) more liquid drains into the bundle caused by the combined effect of higher spray flow and lower bundle power,

(b) CCFL at side entry orifice holds up liquid in the bundle throughout the test,

(c) the bundle is kept well cooled (below 600°F) throughout the transient (Figure I-13) because of the liquid holdup, and

(d) subcooling of upper plenum fluid leads to a significant increase of liquid downflow into the bundle.

I-2. BUNDLE POWER DECAY TRANSIENT FOR THE BD/ECC 1A TESTS

The power decay transients that were programmed for BD/ECC 1A tests are shown in Figure I-15. (I-3) In the first 50 seconds, the power supplied to the test bundles was based on values calculated from stored heat and ANS + 20 percent for decay heat. The objectives of the BD/ECC 1A tests are to evaluate the early interaction of the subcooled ECC injection during the blowdown (30-100 sec) and to provide baseline data for comparison of BDHT tests conducted without ECC injection. As such, the power transient used in the BDHT tests was utilized for the early BD/ECC 1A tests. The mechanical power controller was programmed to provide accurate simulation during the blowdown phase (0-50 sec). After 50 sec the power controller held the applied power to the bundle constant (at the 50-sec value). As a result, the test bundle received significantly more power than it would have if the power controller had been allowed to follow the ANS + 20% decay rate throughout the transient.

The difference between the actual bundle power in the tests and the power based on stored heat plus ANS + 20% for fission heat is shown in Figure I-16. For the average power bundle, the power measured beyond 140 sec exceeded the calculated power for the peak power bundle. The significance of this is:

(a) For the average power test, the power applied to the bundle during the post dryout period (period of sustained dryout and heatup) actually exceeded that calculated for a peak power bundle assuming ANS + 20% fission heat and stored heat. Thus, this test was more typical of a peak power test.

(b) For the peak power bundle, the power applied during the sustained dryout period exceeded that calculated from assuming ANS + 20 percent and stored heat by over 16 percent. This test, therefore, represents an overpower bundle.

A new power controller was installed for the tests conducted in TLTA-5A. As was mentioned in Subsection 2.2.4, the new controller was capable of controlling the bundle power over the entire test transient. The power decay transient was based on stored heat plus ANS + 5 percent for fission heat.

I-3. SUMMARY AND DATA REPORT

Initial conditions for the reference test are shown in Table I-2. The bundle power decay and system pressure response are shown in Figures I-17 and I-18, respectively. The ECC systems were activated at nominal times: HPCS at 27 sec, LPCS and LPCI at 37 sec. HPCS begins immediately after activation at 27 sec (Figure I-19); LPCS commences at about 78 sec (Figure I-20) and LPCI begins at about 86 sec (Figure I-21).

The ECC flows lead to accumulation of fluid mass in the system. This mass accumulation is exemplified by the fluid density increase in the lower plenum (Figure I-22). It should be noted that because the refill/reflood phase of the LOCA transient is beyond the scope of Phase 1A, the test apparatus has not been designed to produce representative data during this phase (from about 150 sec on). In particular, the short jet pump in TLTA prevents complete refilling of the lower plenum and bundle (I-4).

The effects of ECC flows on the bundle thermal response are characterized by rewet of dried-out rods and mitigation of heat-up rate. The cladding temperature measurements at different elevations of the bundle are shown in Figures I-23 through I-36. The peak cladding temperature, shown in Figure I-37, stays below 1300°F for the length of this test (power tripped at 296 sec).

The benefit of the ECC flows has been evaluated by comparing results from the two reference tests: Test 6406 Run 1 with ECC and Test 6007 Run 26 without ECC. Comparison of cladding temperatures at and above the peak power location (Figures I-38 and I-39) shows that ECC injection delays the time of sustained heatup that follows dryout. This delaying action is more clearly illustrated in Figure I-40 which shows the approximate dryout front (which closely follows the mixture level) throughout the bundle. Additionally, the decrease of heating rate, also shown in Figures I-38 and I-39, is indicative of enhanced cooling of the bundle. The overall bundle temperature is reduced because of the ECC flows, as can be seen from the lower percentage of thermocouples reaching 1000°F in Figure I-41. The net effect of ECC injection is, therefore, a reduction in peak cladding temperature as a result of improved heat transfer throughout the system.

I-4. REFERENCES

I-1. J. C. Wood and A. F. Morrison, BWR Blowdown/Emergency Core Cooling Program - 64-Rod Bundle Core Spray Interaction (BD/ECC-1A) Test Plan, February 1978 (GEAP-21638A).

I-2. D. L. Galyardt, BWR Blowdown Emergency Core Cooling Fourteenth Quarterly Progress Report, April 1 - June 30, 1979, August 1979 (GEAP-21304-14).

I-3. C. G. Hayes, BWR Blowdown/Emergency Core Cooling Program ECC System Calibration and Performance Verification, July 1978 (NEDG-21956).

I-4. W. J. Letzring, Editor, BWR Blowdown/Emergency Core Cooling Program, Preliminary Facility Description Report for the BD/ECC-1A Test Phase, December 1977 (GEAP-23592).

Table I-1

TEST PARAMETERS FOR BD/ECC 1A SCOPING TEST SERIES

- ECC Flow Variation Tests

Test No.	Power	ECCS Flow	ECC Temperature
6007/26[a]	5.05 MW	No	-
6405/3	5.05 MW	Low	∿120°F
6406/1[b]	5.05 MW	Ave.	∿120°F

[a]Repeated as 6406/3
[b]Reference Test

- Power Variation Tests

Test No.	Power	ECCS Flow	ECC Temperature
6401/4	1.62 MW	High	∿120°F
6414/3	6.49 MW	Low	∿200°F

Table I-2

BD/ECC-1A REFERENCE TEST 6406, RUN 1

Initial Conditions	
Bundle Power	5.04 ± 0.15* MW
Steam Dome Pressure	1056 ± 4 psia
Lower Plenum Pressure	1076 ± 4 psia
Lower Plenum Enthalpy	539 ± 5 Btu/lbm
Initial Water Level	126 ± 6 in. elevation or 50 ± 6 in. above JP suction
Feedwater Enthalpy	45 ± 2 Btu/lbm
Bundle Inlet to Outlet ΔP	15 ± 2 psi
Steam Flow	6.3 ± 0.6 lbm/sec
Feedwater Flow	0.35 ± 0.05 lbm/sec
Drive Pump 1 Flow	8.8 ± 0.8 lbm/sec
Drive Pump 2 Flow	9.6 ± 0.9 lbm/sec
Jet Pump 1 Flow	18.4 ± 2 lbm/sec
Jet Pump 2 Flow	20 ± 2 lbm/sec
Bundle Inlet Flow	35.5 ± 3.5 lbm/sec

*NOTE: All uncertainty bands are judged from the maximum of data fluctuation or the maximum absolute uncertainties of the measurement.

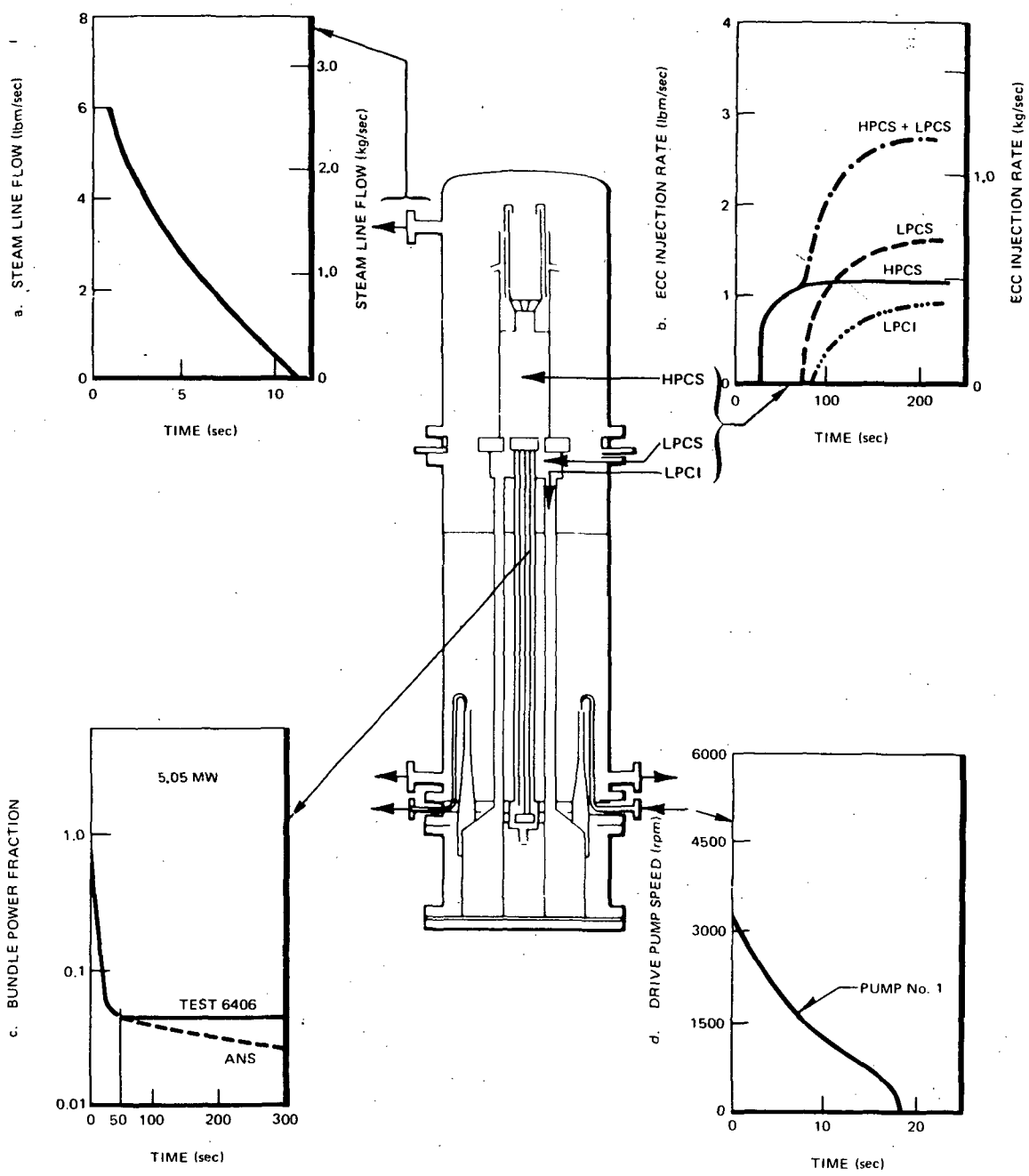

Figure I-1. Controlled Parameter Responses of Reference Test (6406 Run 1, Average Power, Average ECC)

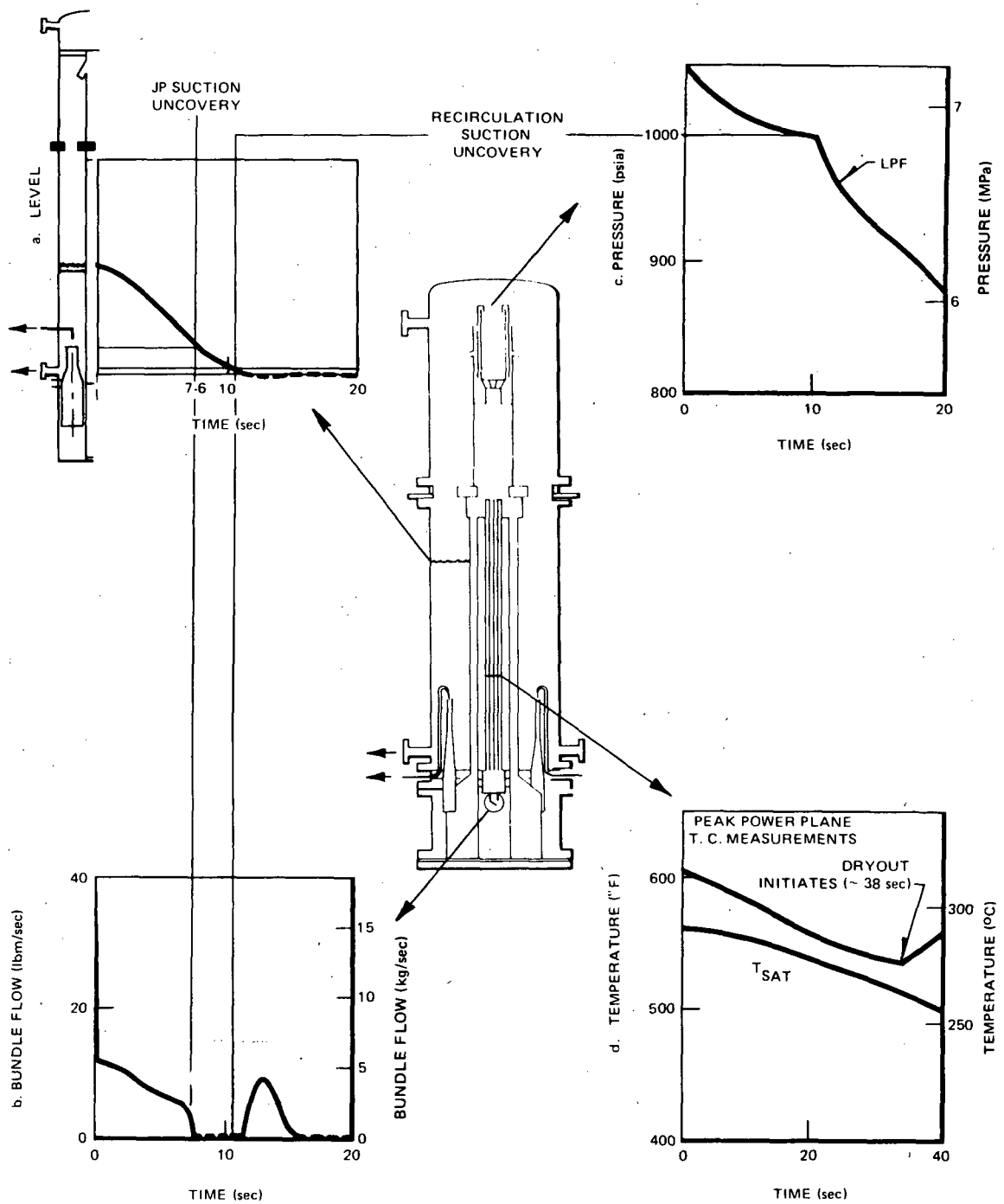

Figure I-2. System Responses in the Early Stage of the BD/ECC Transient for the Reference Test (6406 Run 1, Average Power, Average ECC)

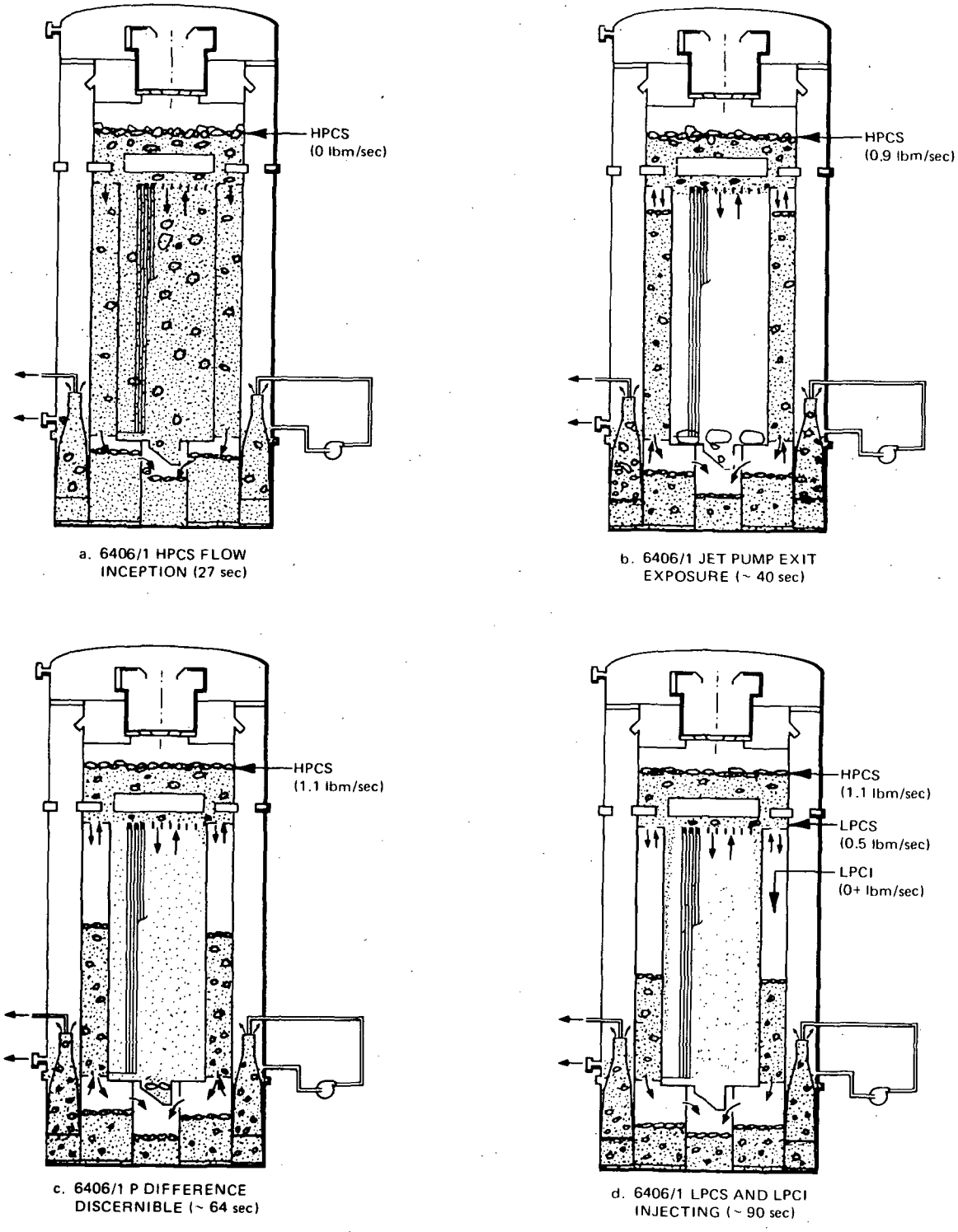

a. 6406/1 HPCS FLOW INCEPTION (27 sec)

b. 6406/1 JET PUMP EXIT EXPOSURE (~ 40 sec)

c. 6406/1 P DIFFERENCE DISCERNIBLE (~ 64 sec)

d. 6406/1 LPCS AND LPCI INJECTING (~ 90 sec)

Figure I-3. "Snapshots" at Selected Instances for the Reference Test (6406 Run 1, Average Power, Average ECC)

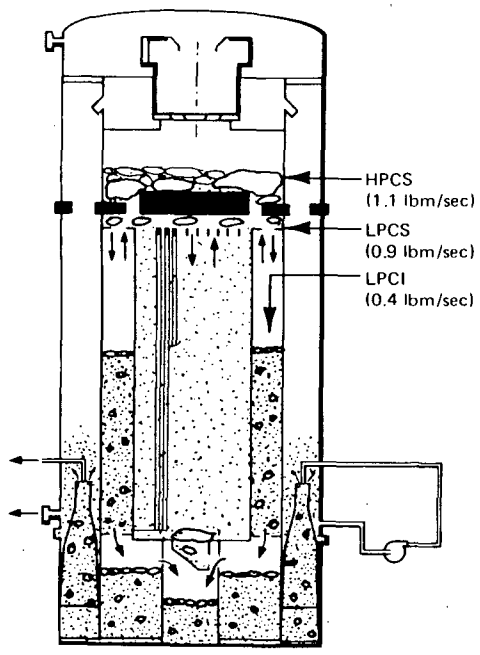

e. 6406/1 CCFL BREAKDOWN AT BYPASS (~ 105 sec)

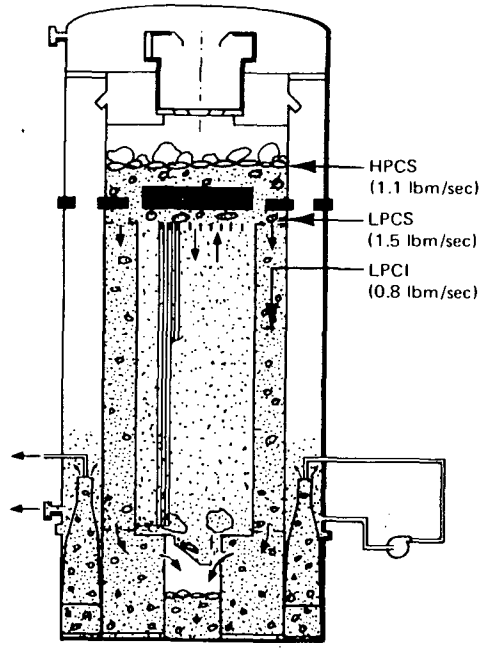

f. 6406/1 JET PUMP REFILLED WITH LIQUID (~ 150 sec)

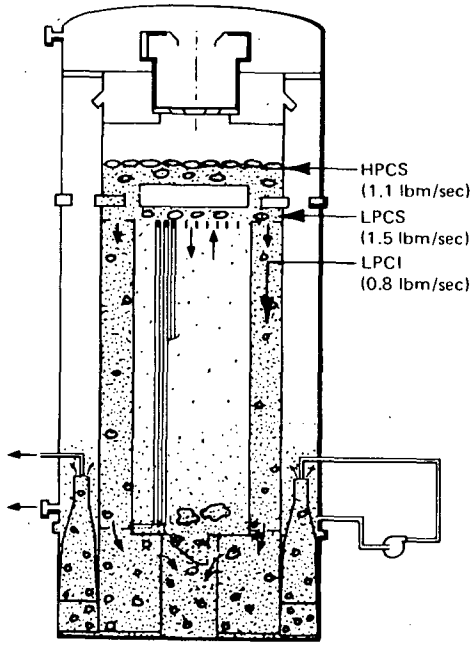

g. 6406/1 SYSTEM FILLING (~ 160 sec)

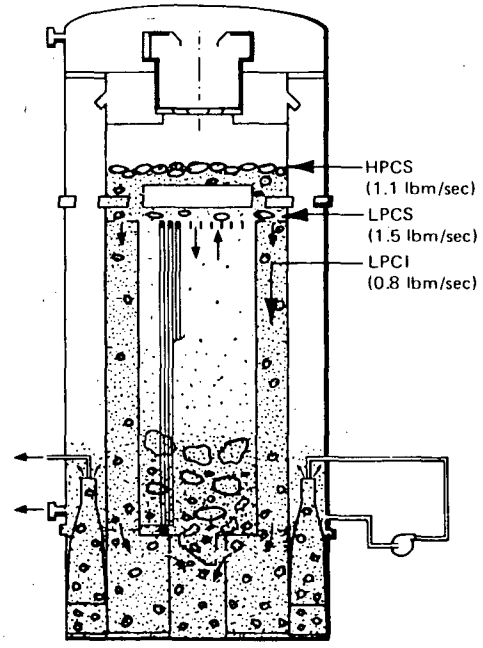

h. 6406/1 TLTA REFILLED (200-300 sec)

Figure I-3. Snapshots at Selected Instances for the Reference Test (6406 Run 1, Average Power, Average ECC) (Continued)

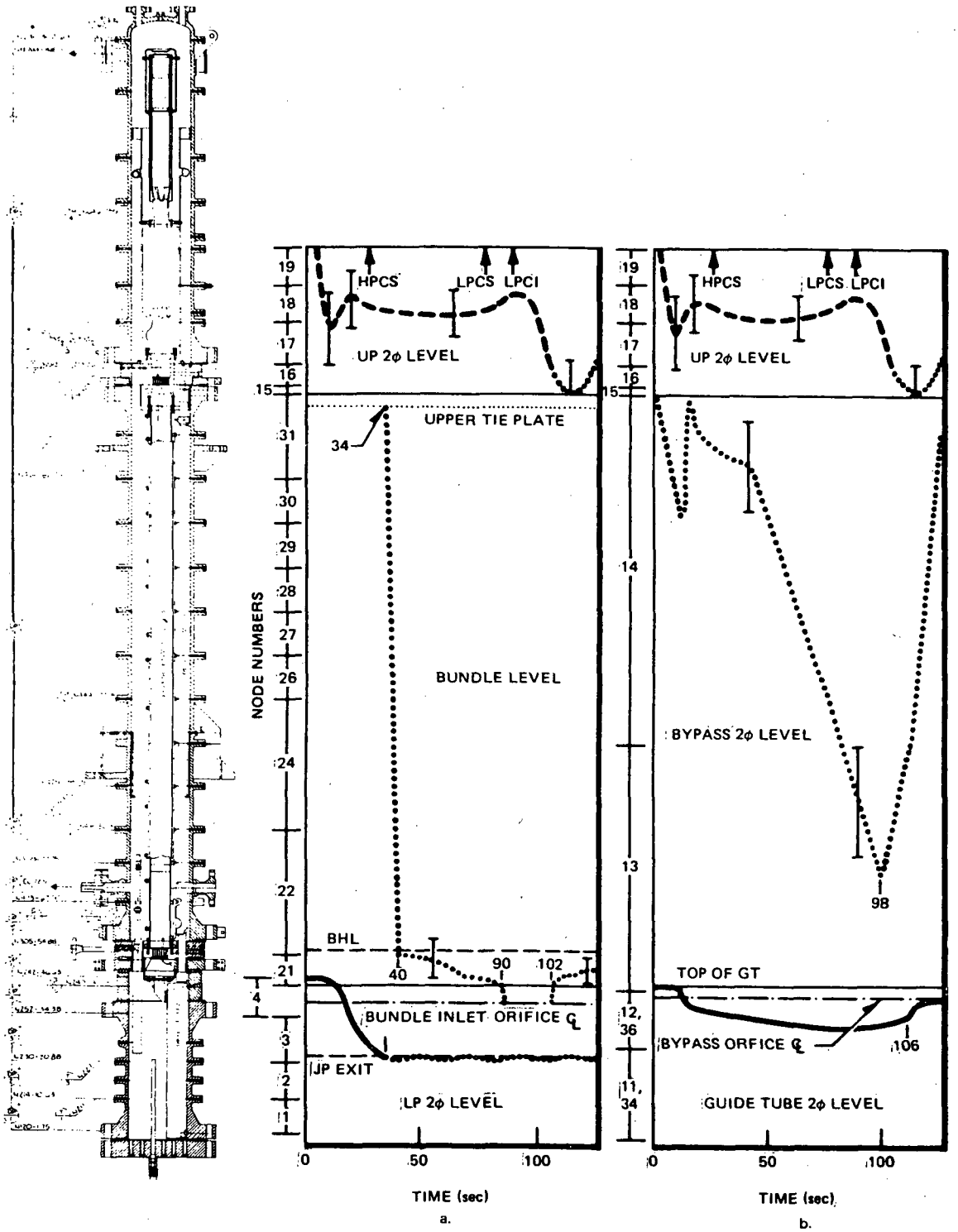

Figure I-4. Two-Phase Mixture Level Responses for the Reference Test (6406 Run 1, Average Power, Average ECC)

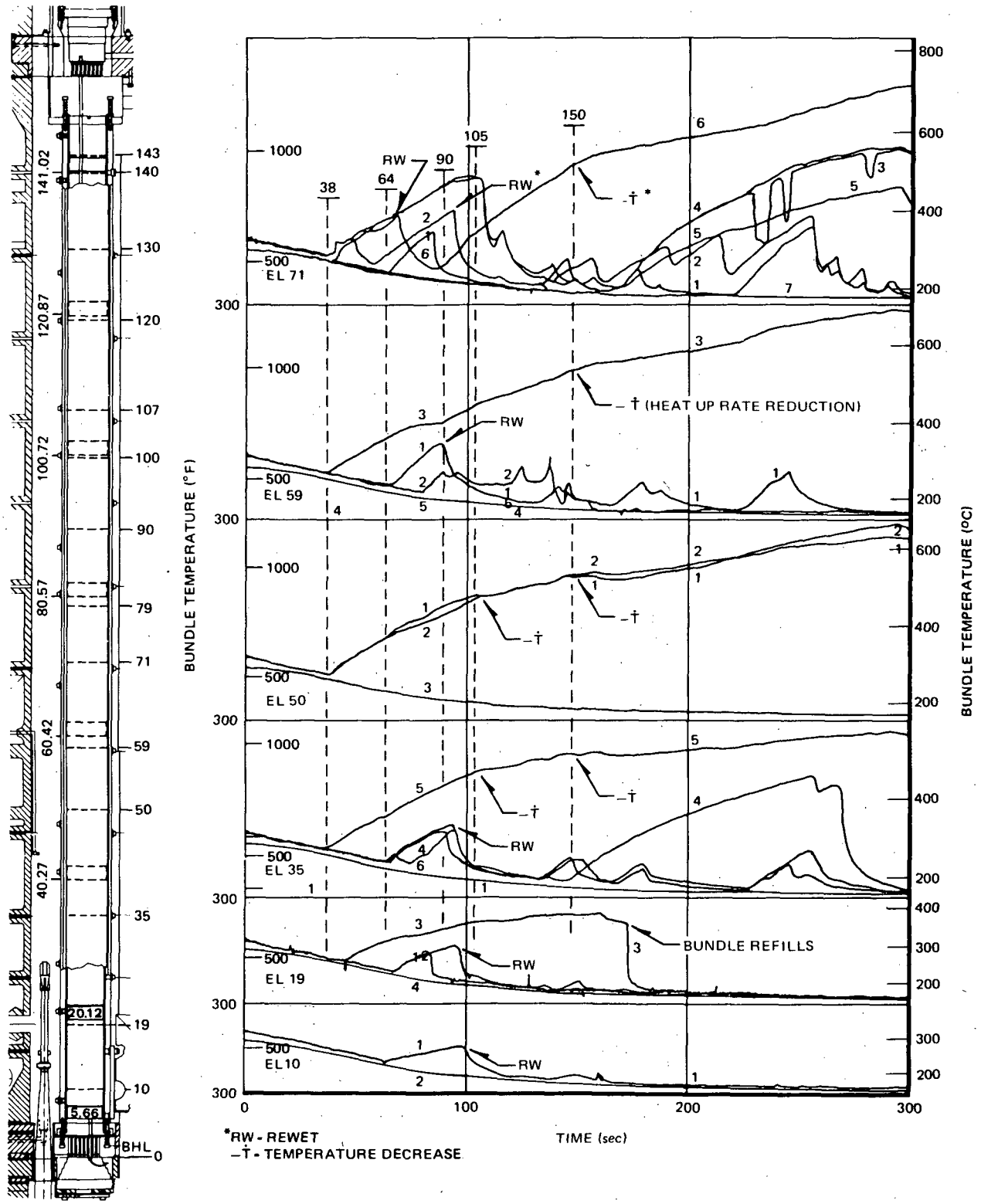

Figure I-5a. Temperature Responses of Lower Half of Bundle for Reference Test (6406 Run 1, Average Power, Average ECC)

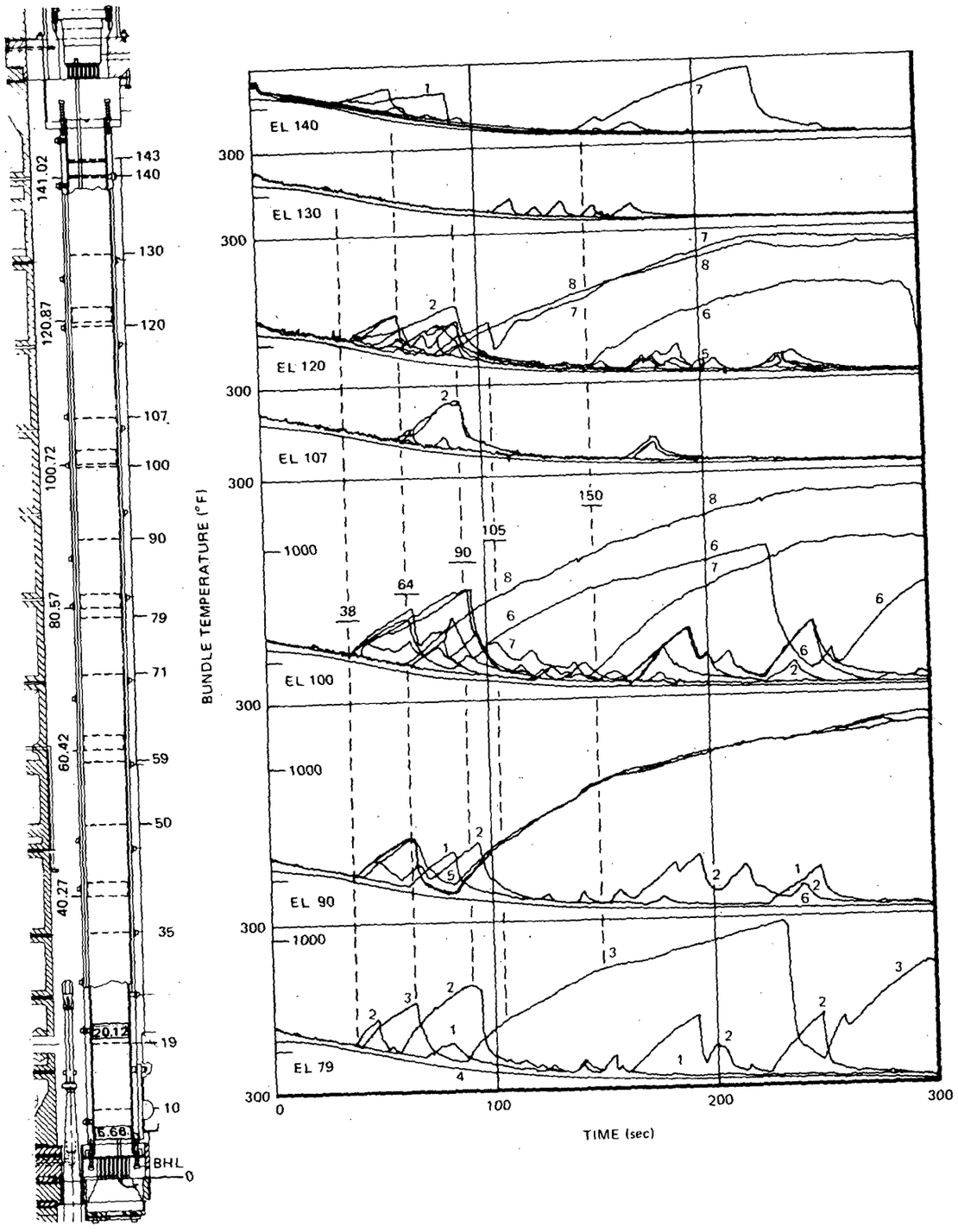

Figure I-5b. Temperature Responses of Upper Half of Bundle for Reference Test (6406 Run 1, Average Power, Average ECC)

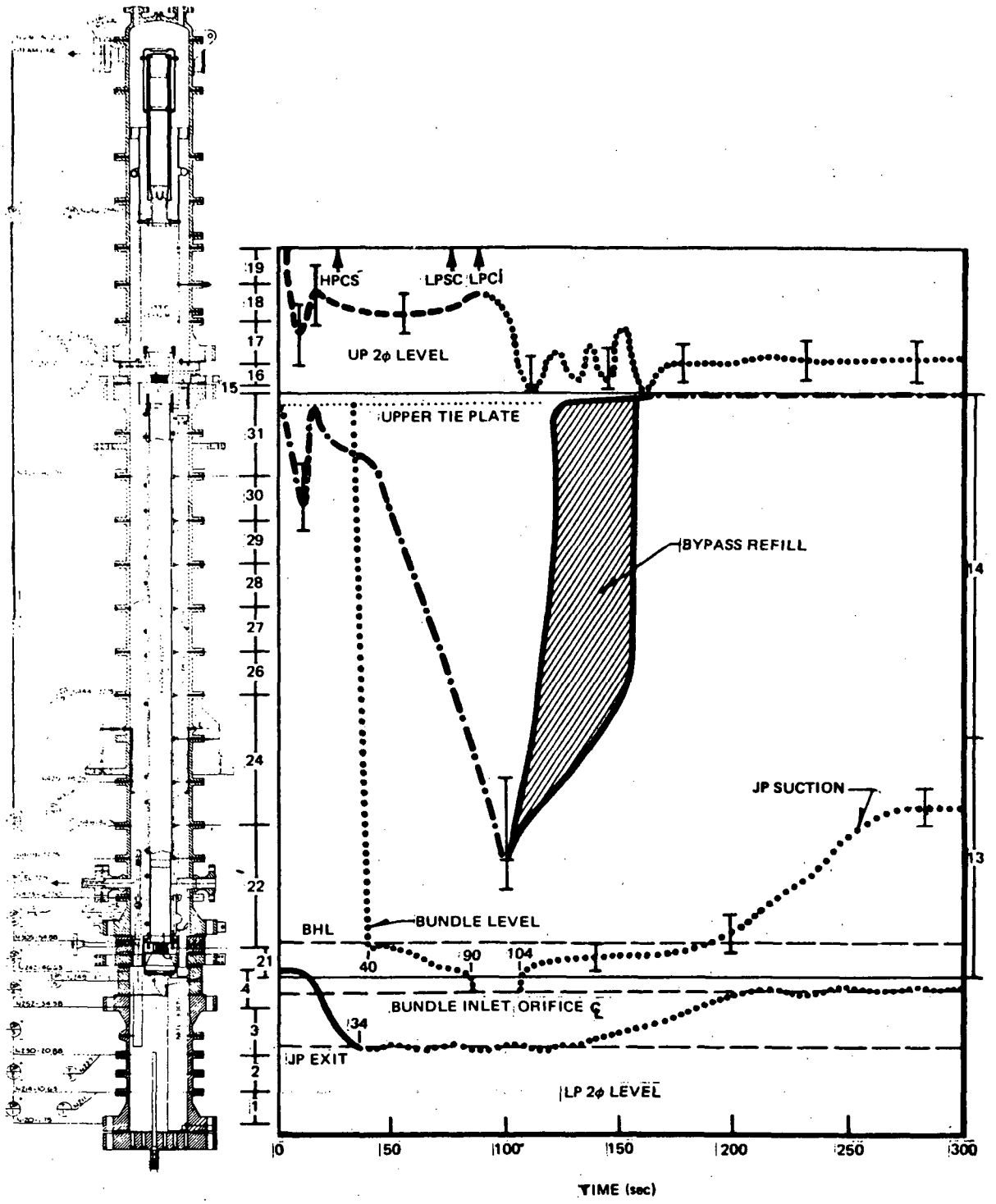

Figure I-6. Two-Phase Mixture Level Responses Illustrating Bundle Refill for Reference Test (6406 Run 1, Average Power, Average ECC)

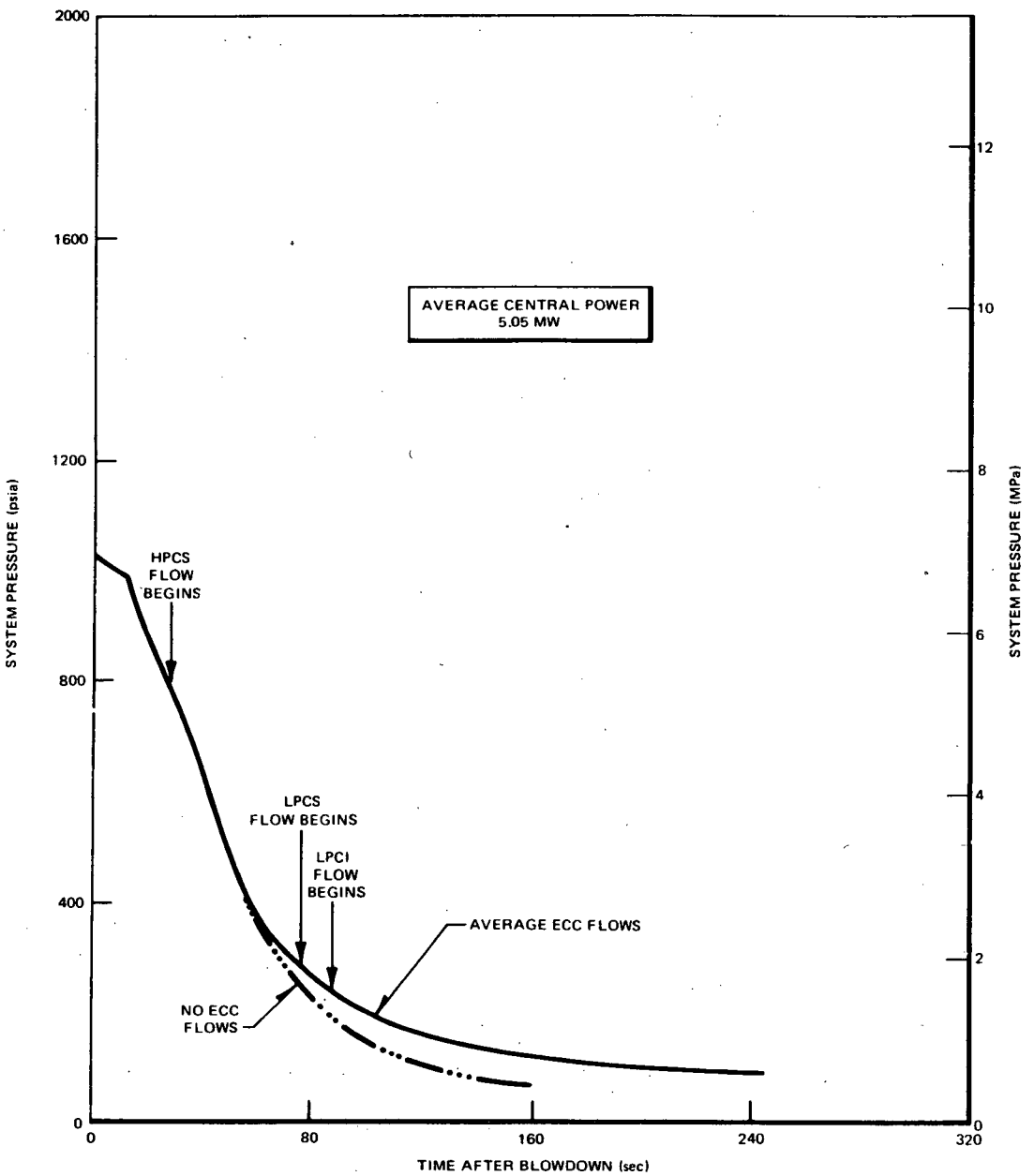

Figure I-7. Comparison of System Pressure Responses between Tests with and without ECC

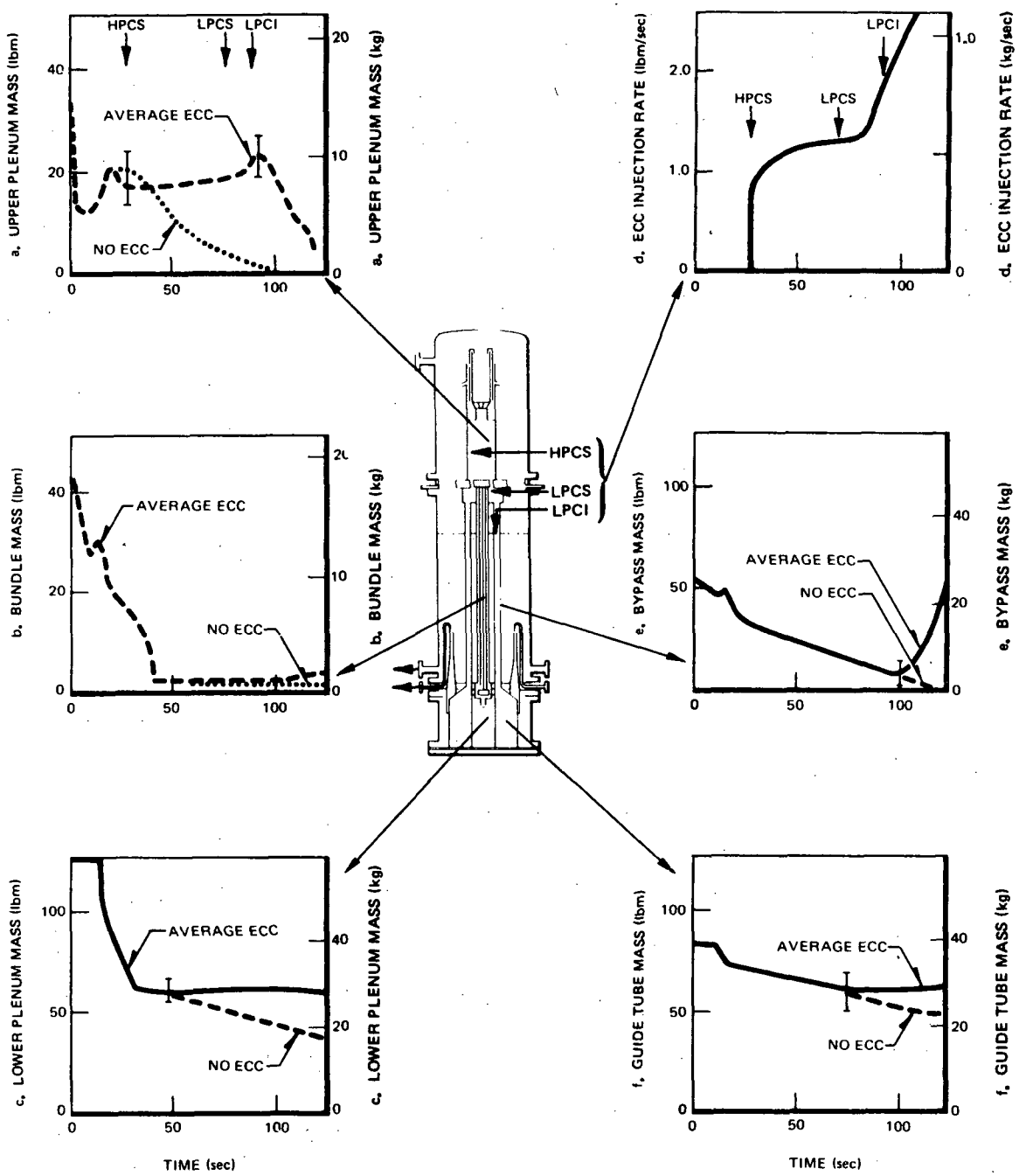

Figure I-8. Comparison of Mass Inventories between Tests with and without ECC

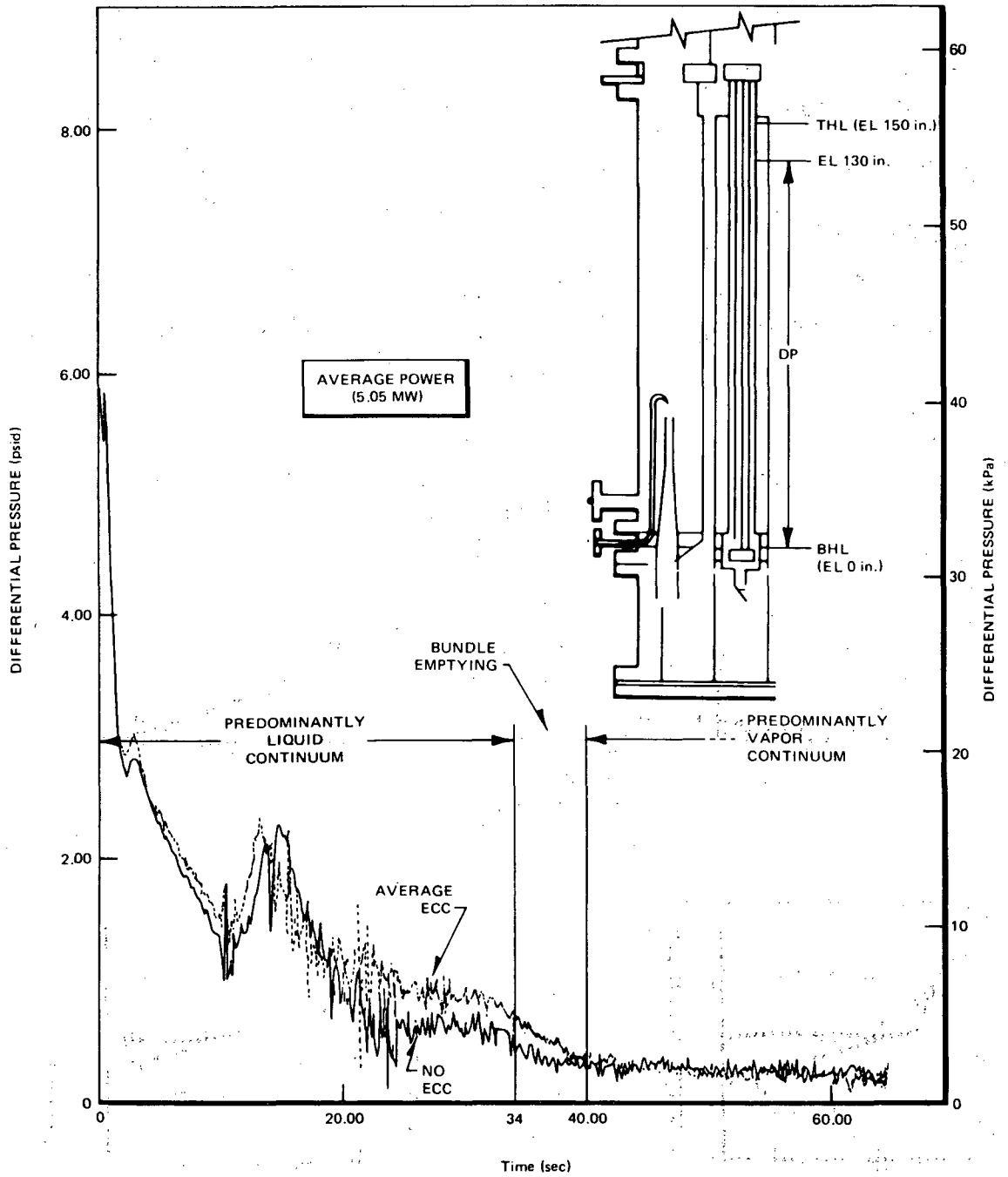

Figure I-9. Comparison of Bundle Differential Pressures between Tests with and without ECC

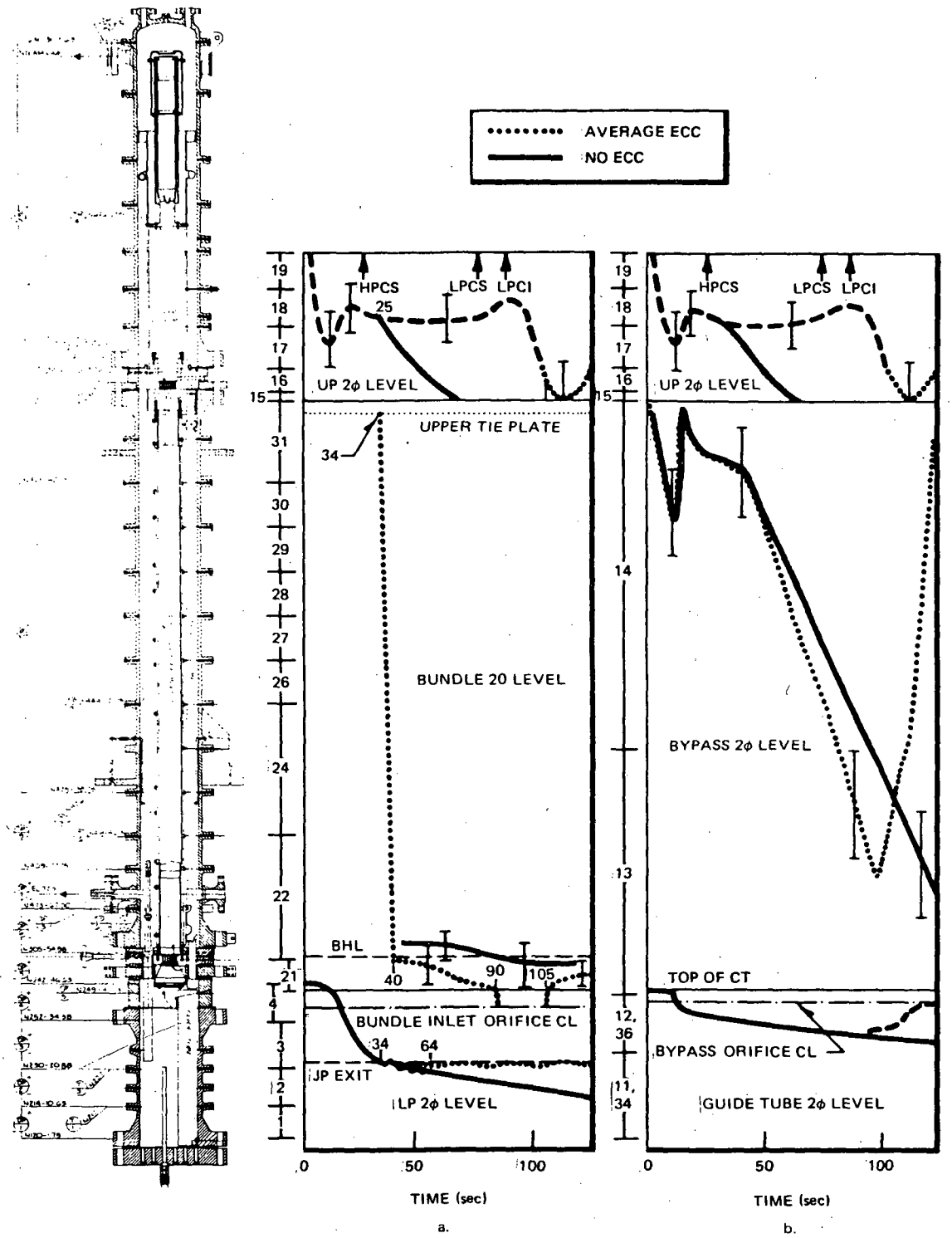

Figure I-10. Comparison of Mixture Level Responses between Tests with and without ECC

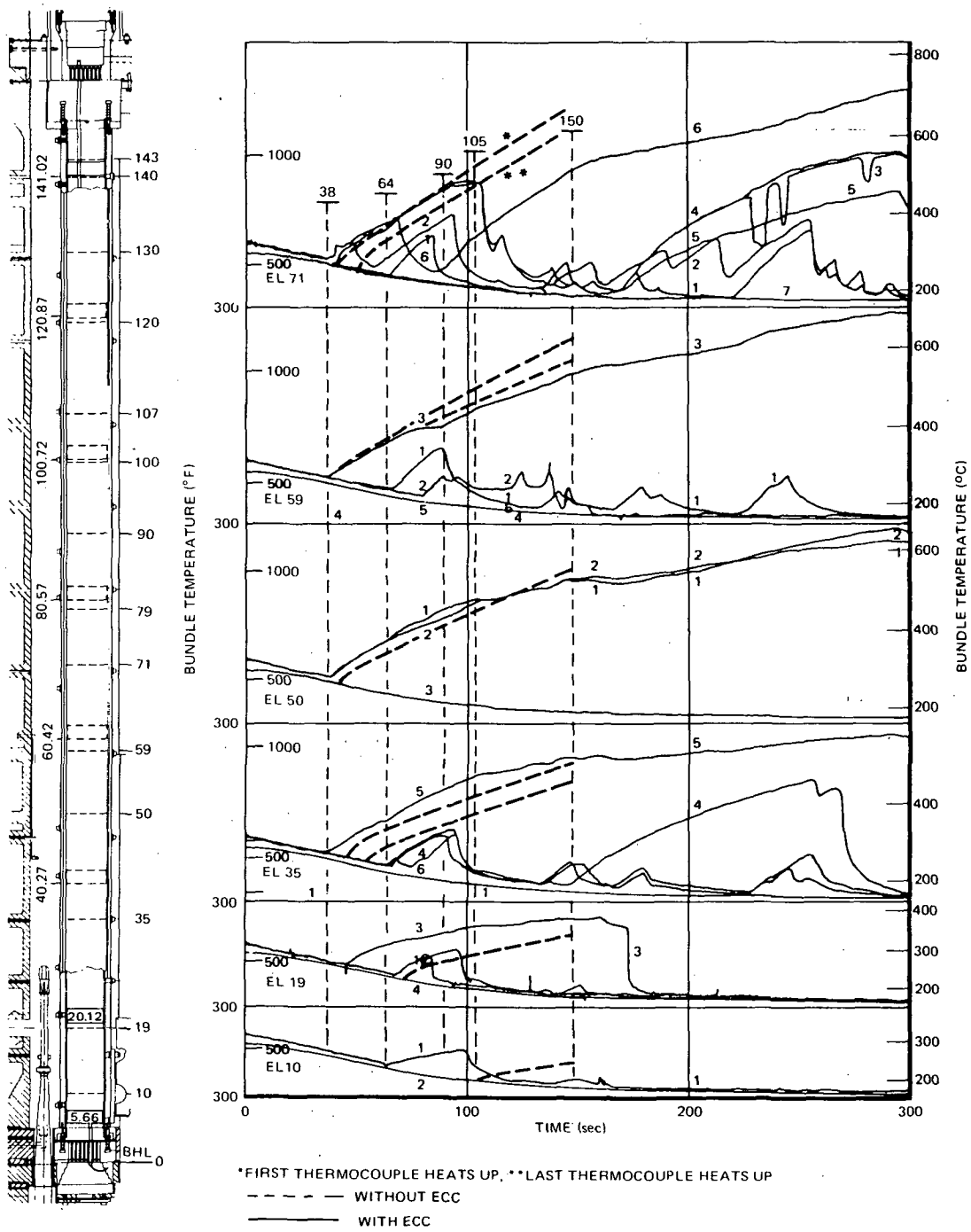

Figure I-11a. Comparison of Temperature Responses in Lower Half of Bundle between Tests with and without ECC

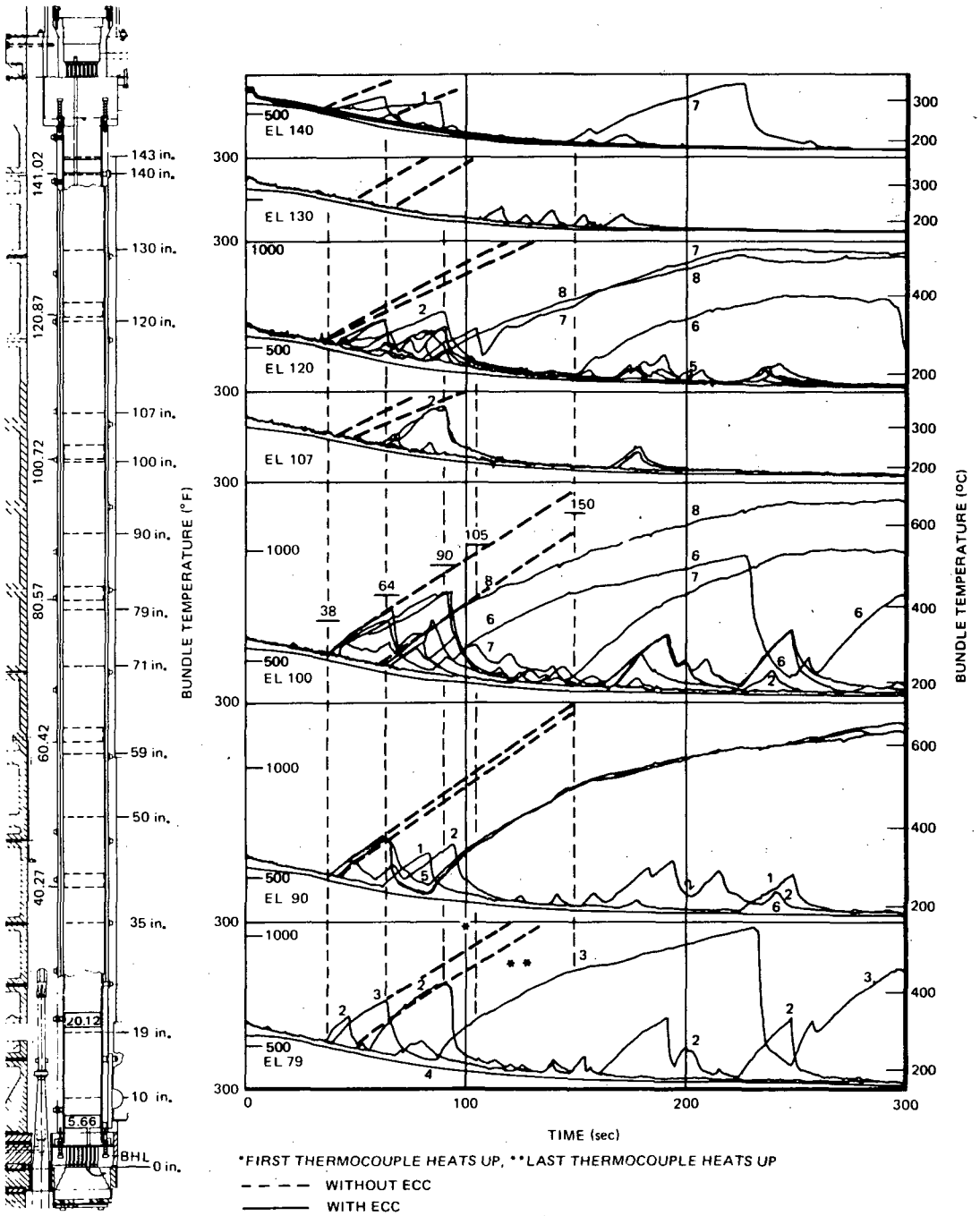

Figure I-11b. Comparison of Temperature Responses in Upper Half of Bundle between Tests with and without ECC

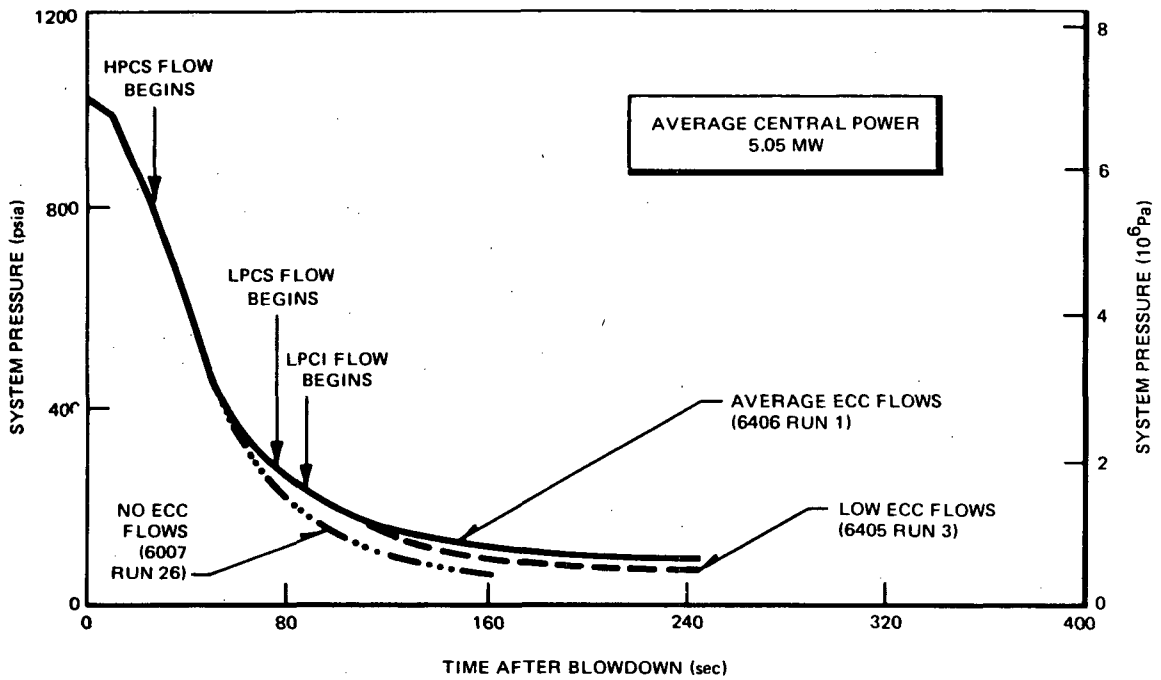

Figure I-12. Comparison of System Pressure Responses of Average Power Tests

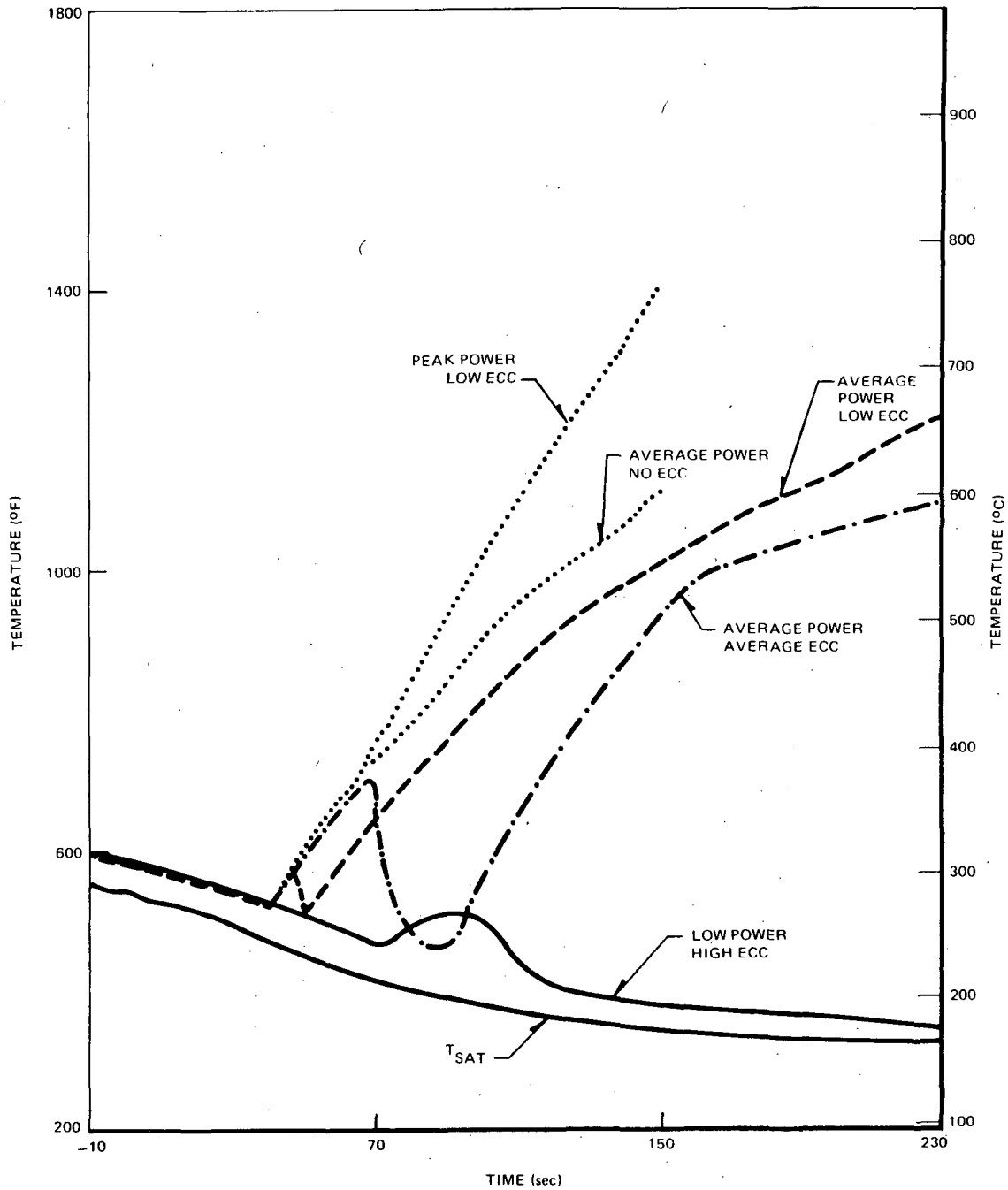

Figure I-13. Comparison of Cladding Temperatures at Peak-Power Elevation (71 in.)

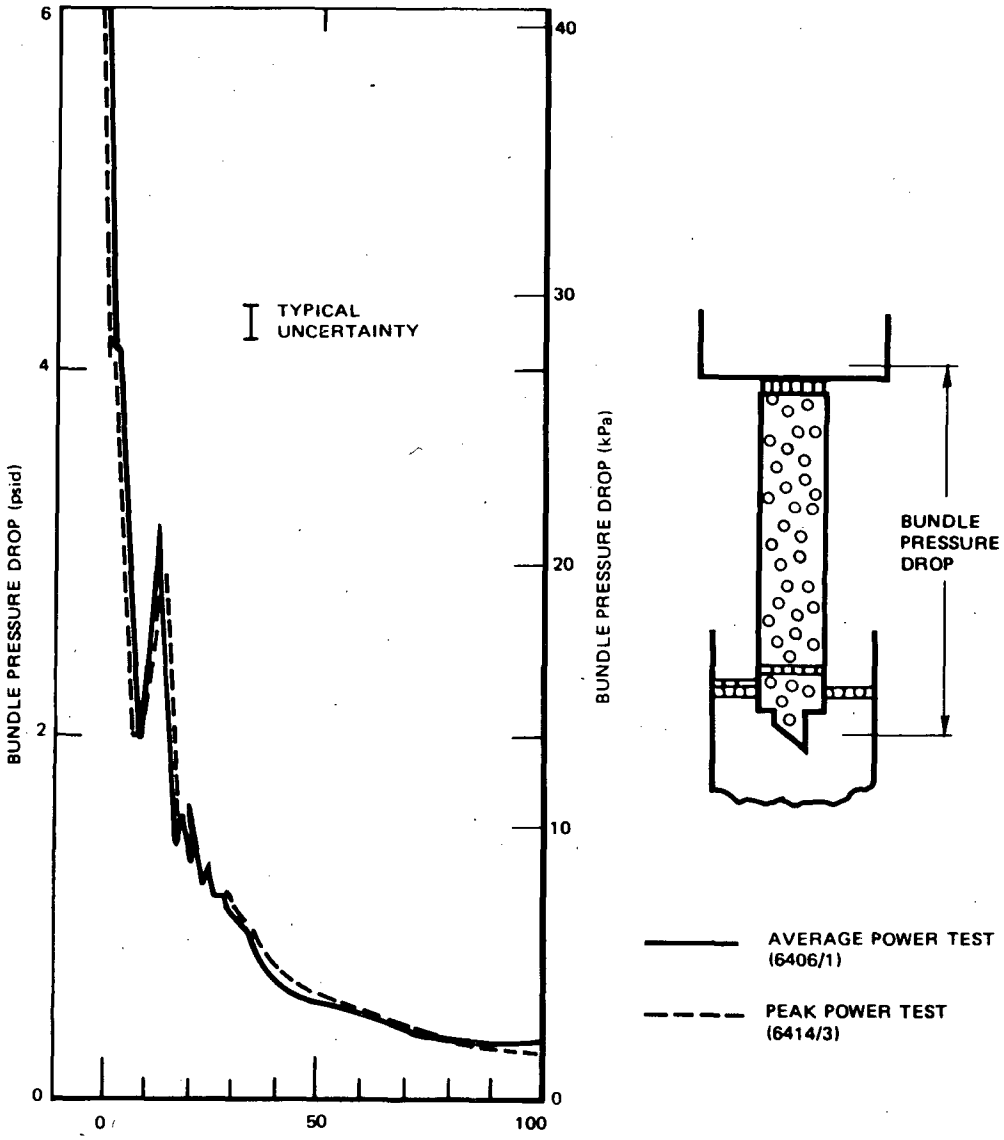

Figure I-14. Comparison of Bundle Inlet to Outlet Differential Pressures

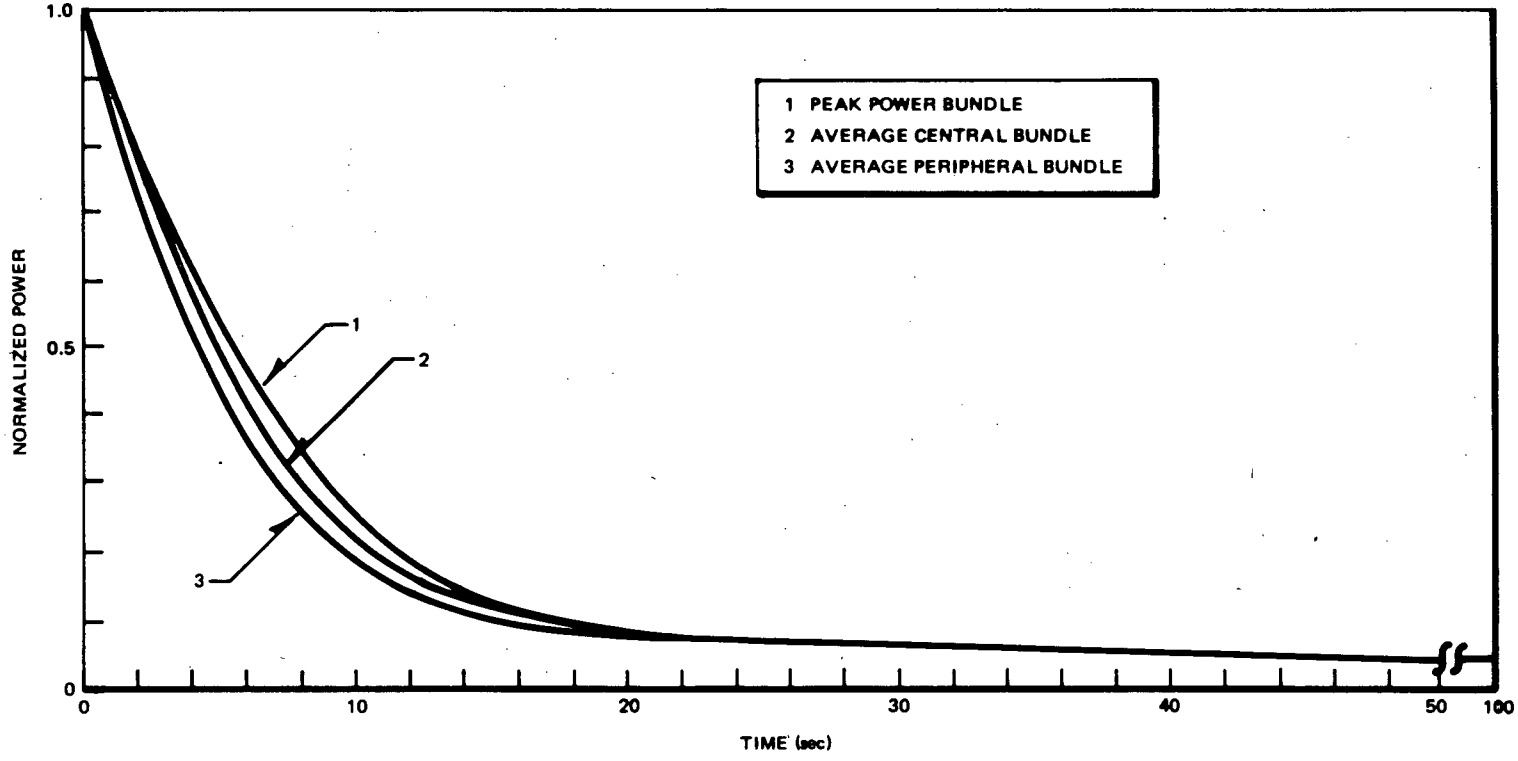

Figure I-15. Power Decay Histories Used in Scoping Test Series

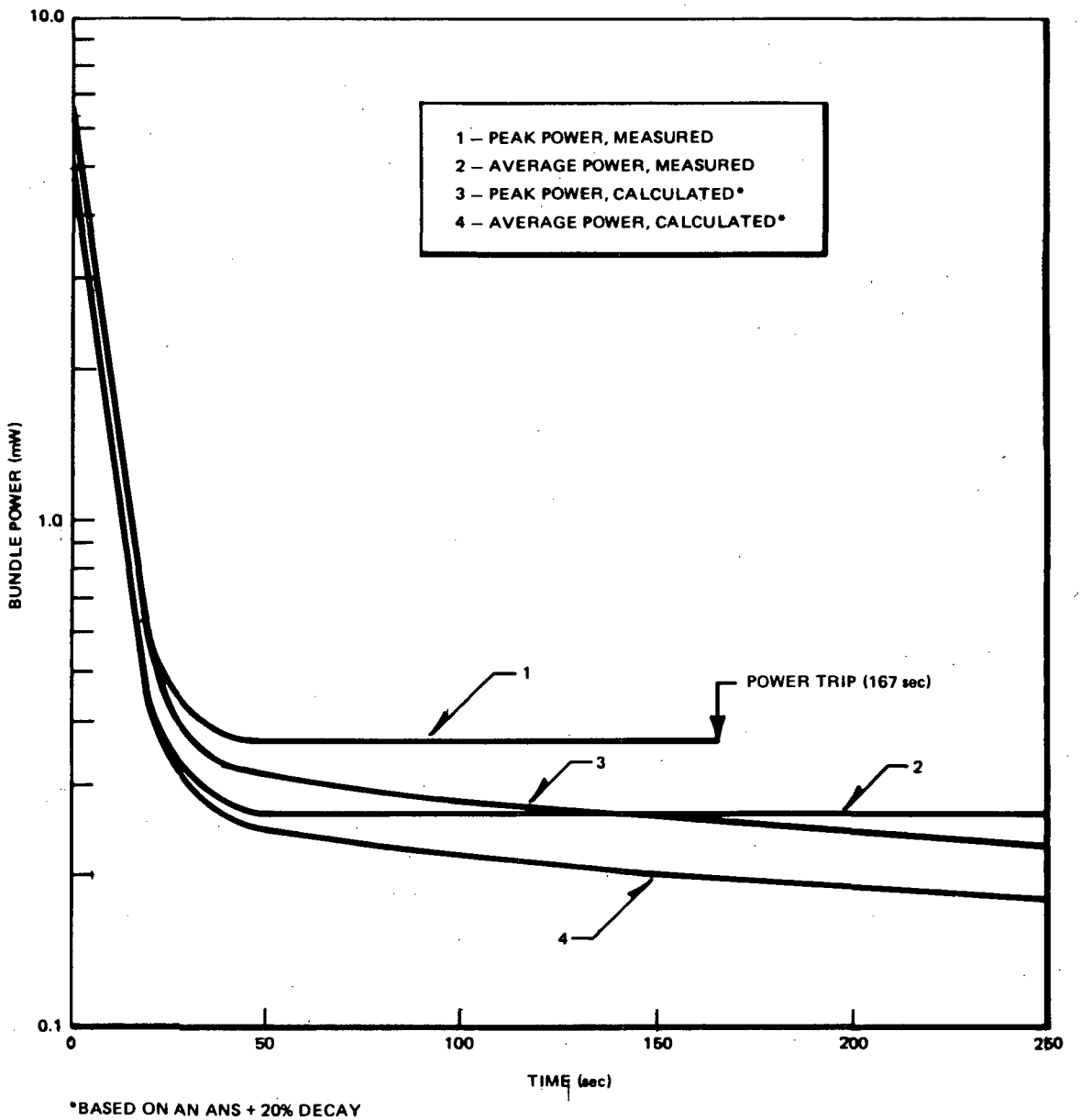

Figure I-16. Comparison of Measured Bundle Power with Calculated Bundle Power

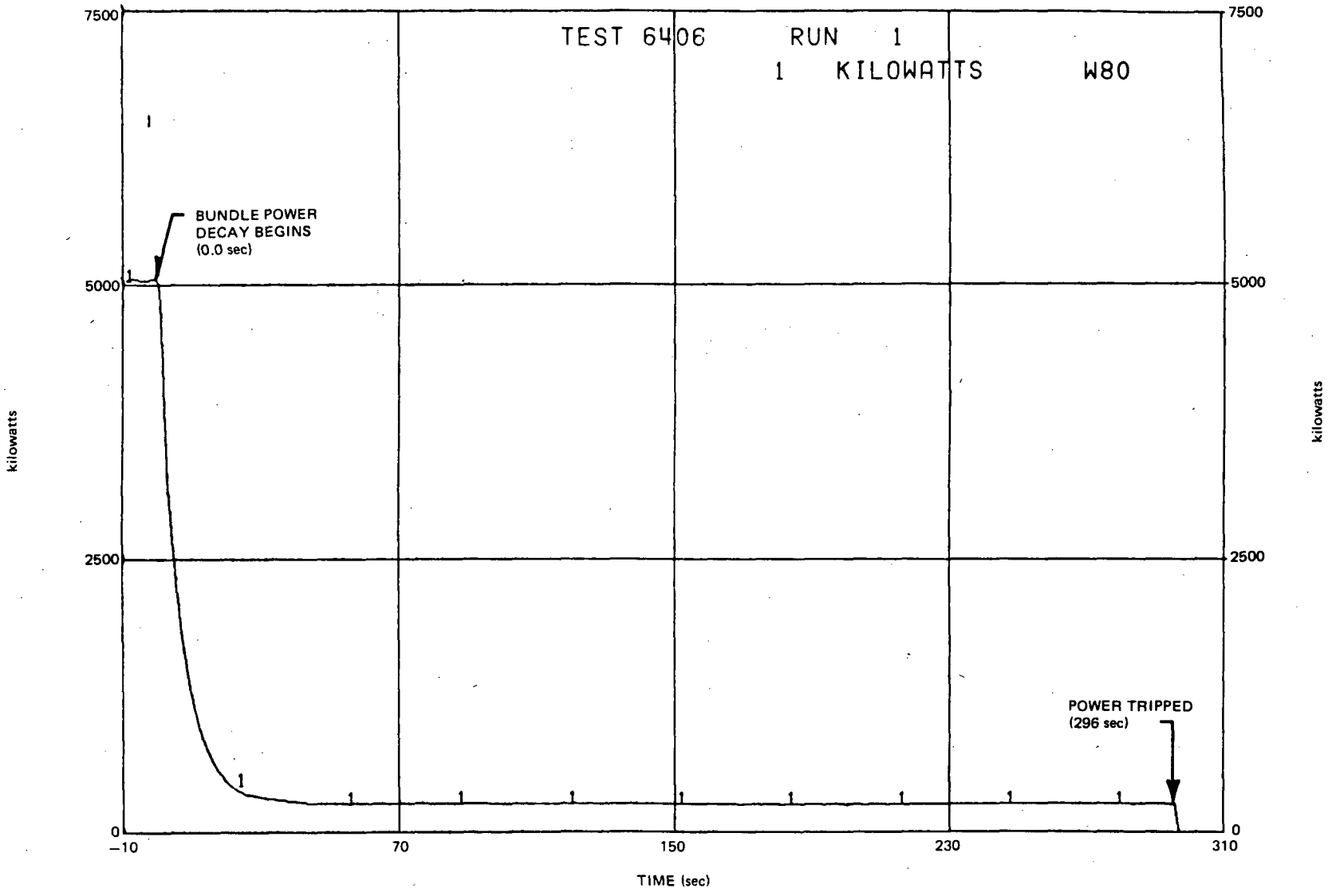

Figure I-17. Bundle Power Decay

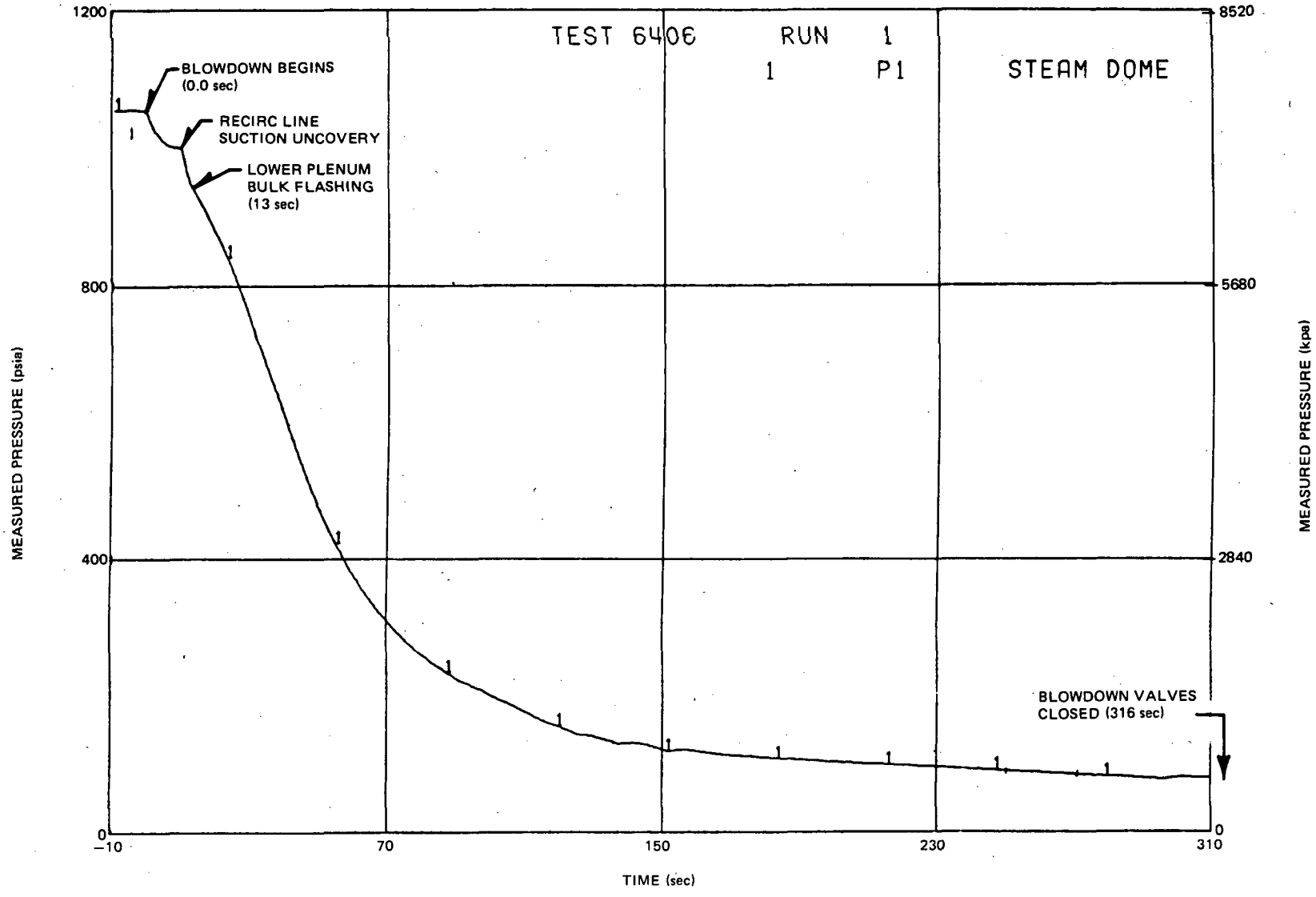

Figure I-18. System Pressure Response

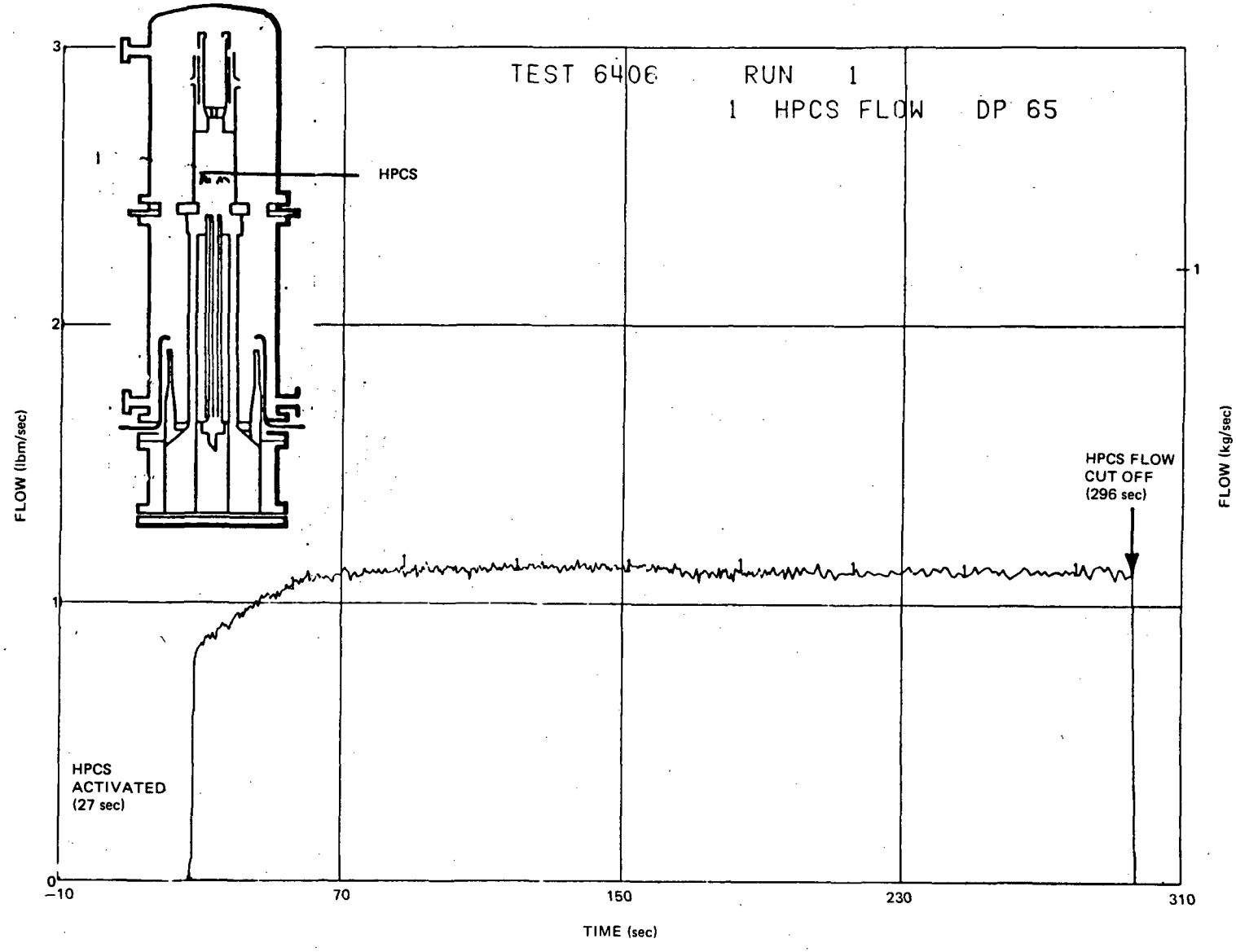

Figure I-19. High Pressure Core Spray Flow

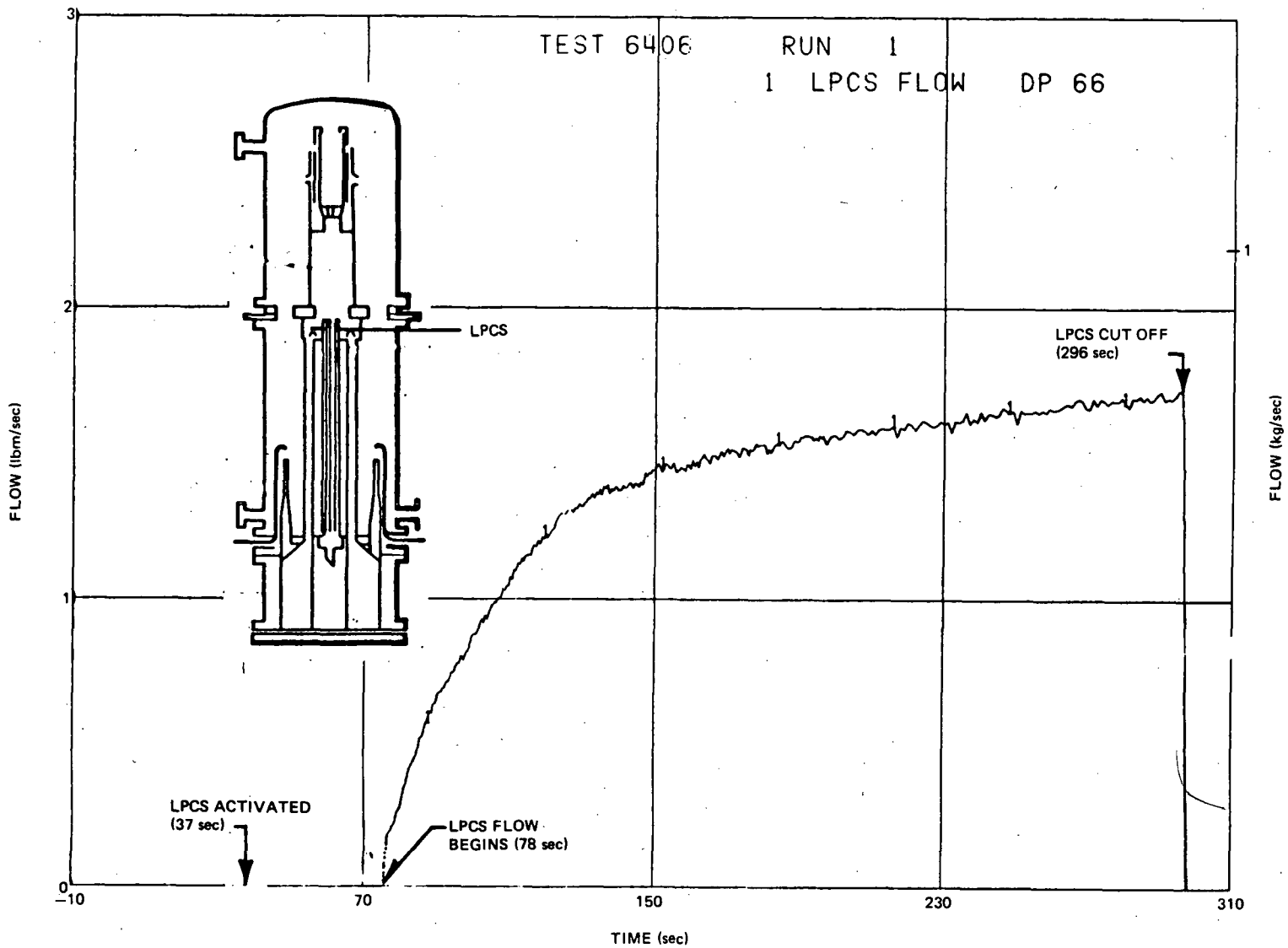

Figure I-20. Low Pressure Core Spray Flow

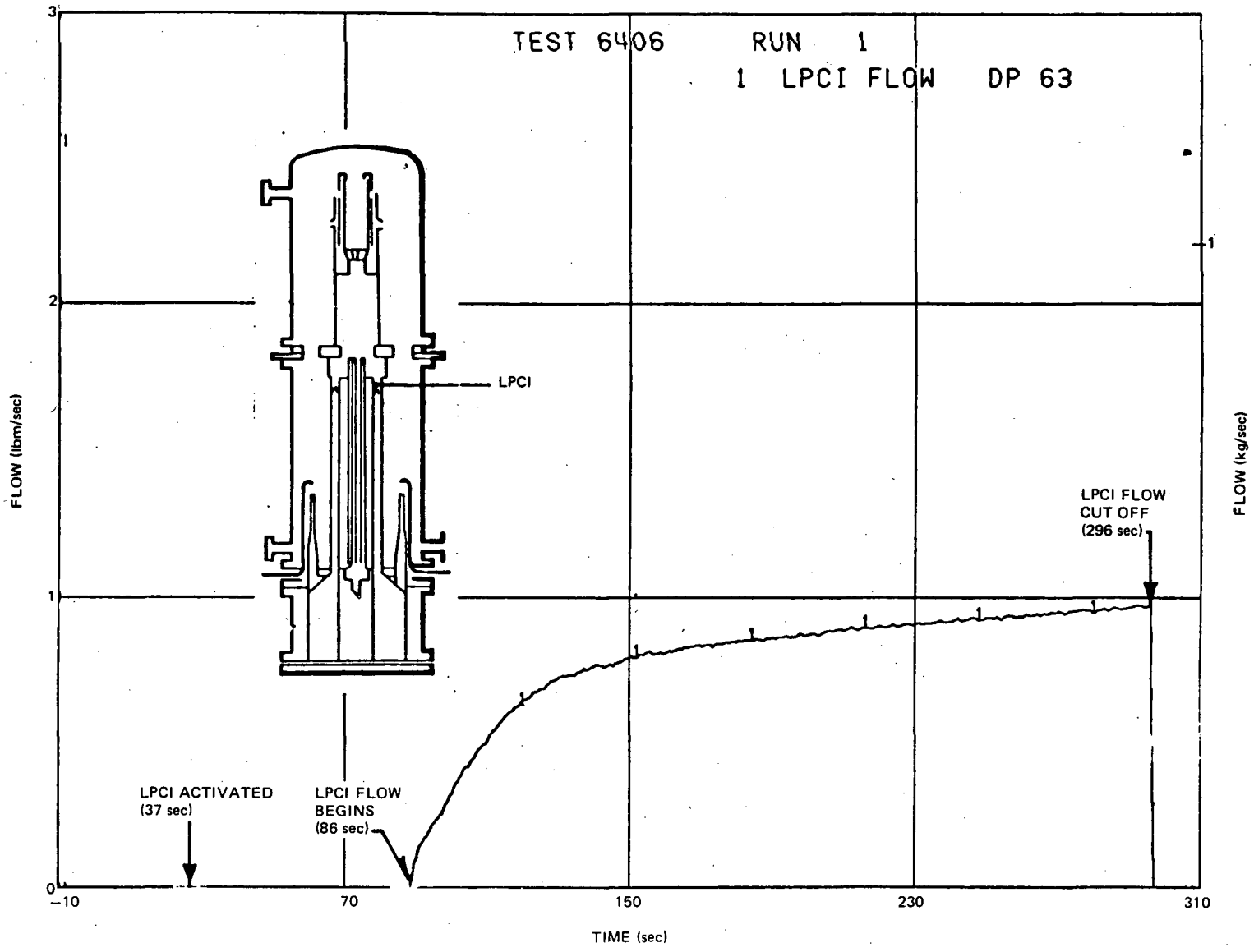

Figure I-21. Low Pressure Core Injection Flow

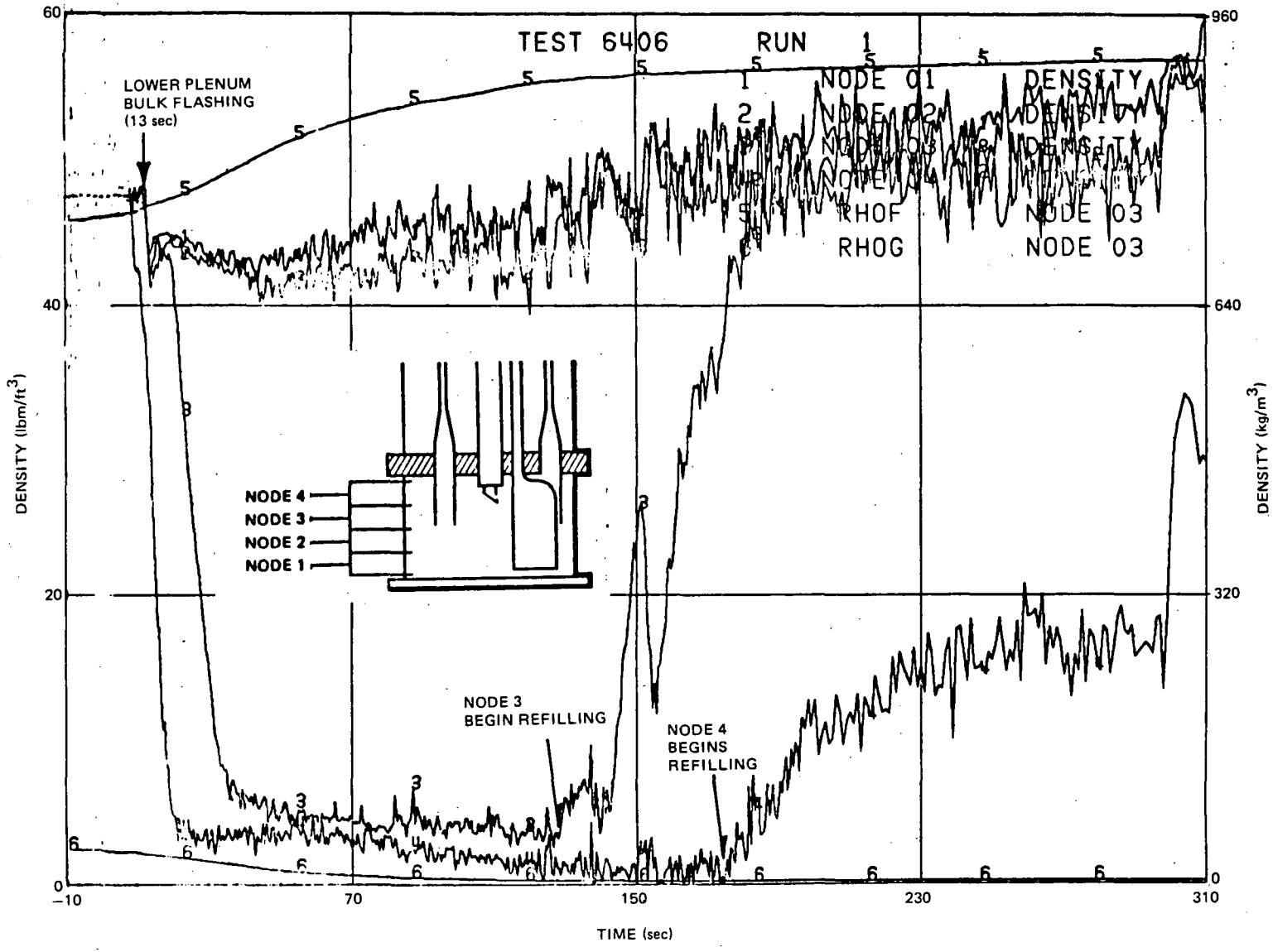

Figure I-22. Lower Plenum Fluid Density

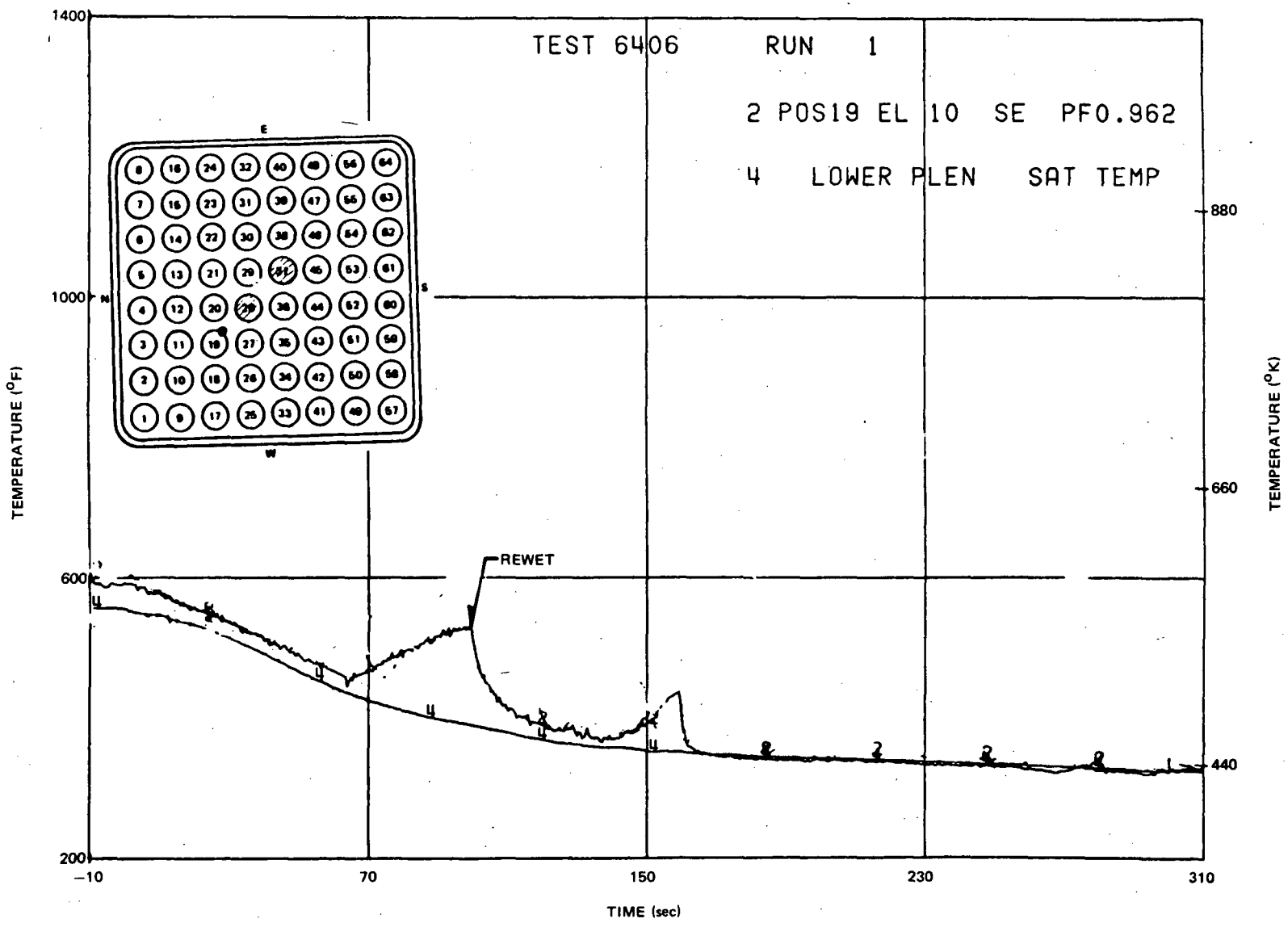

Figure I-23. Bundle Temperature at 10 in. Elevation

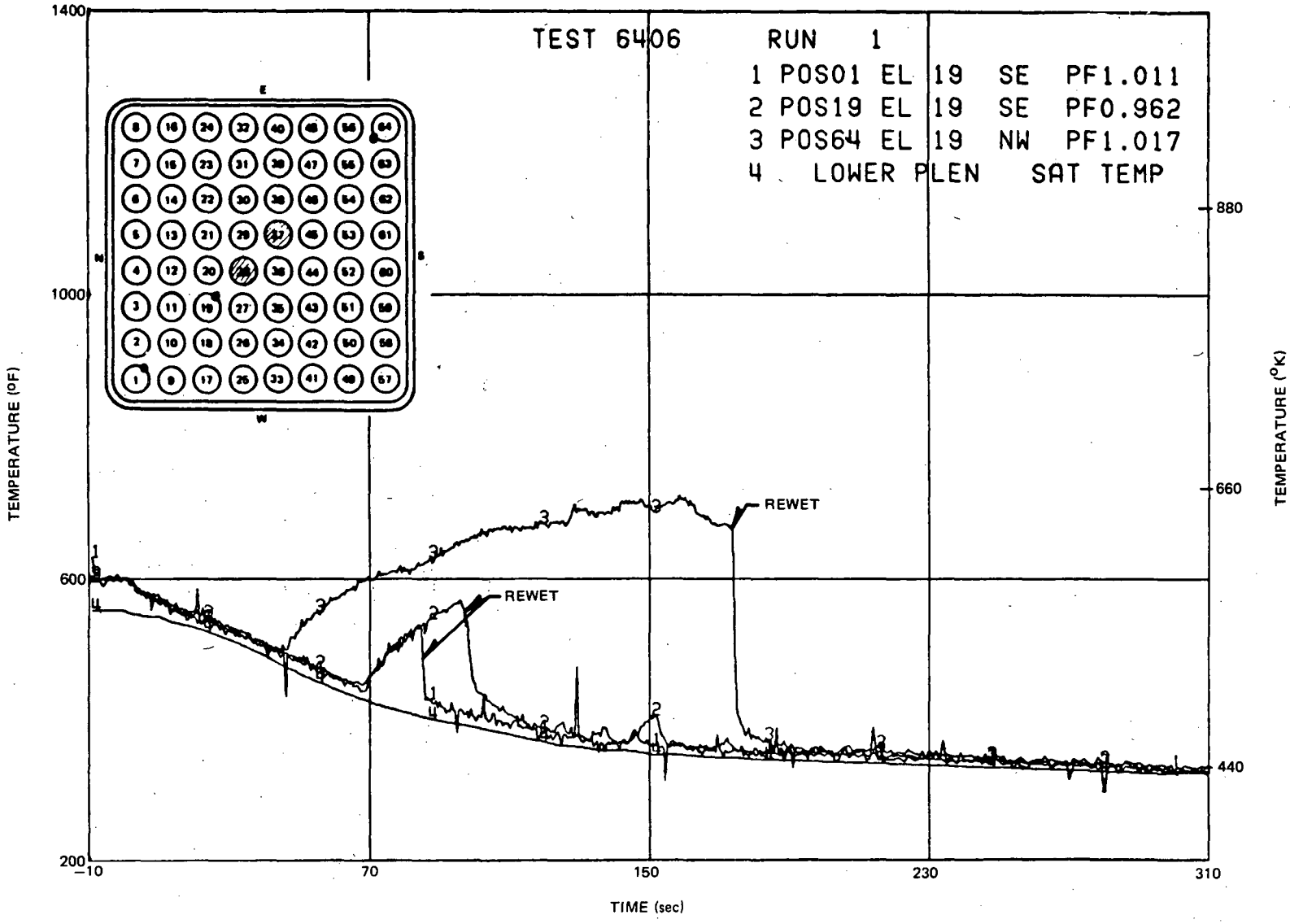

Figure I-24. Bundle Temperature at 19 in. Elevation

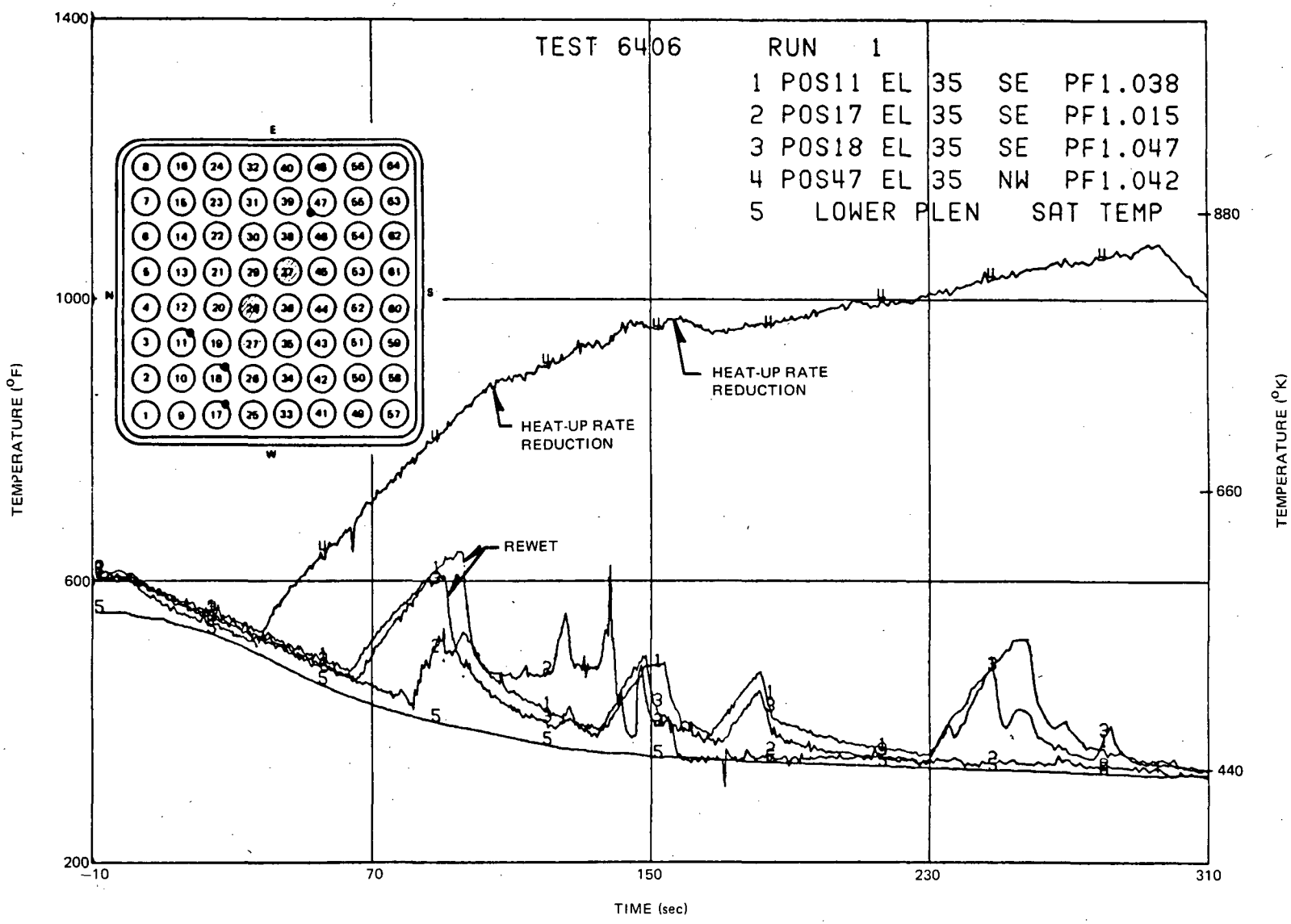

Figure I-25. Bundle Temperature at 35 in. Elevation

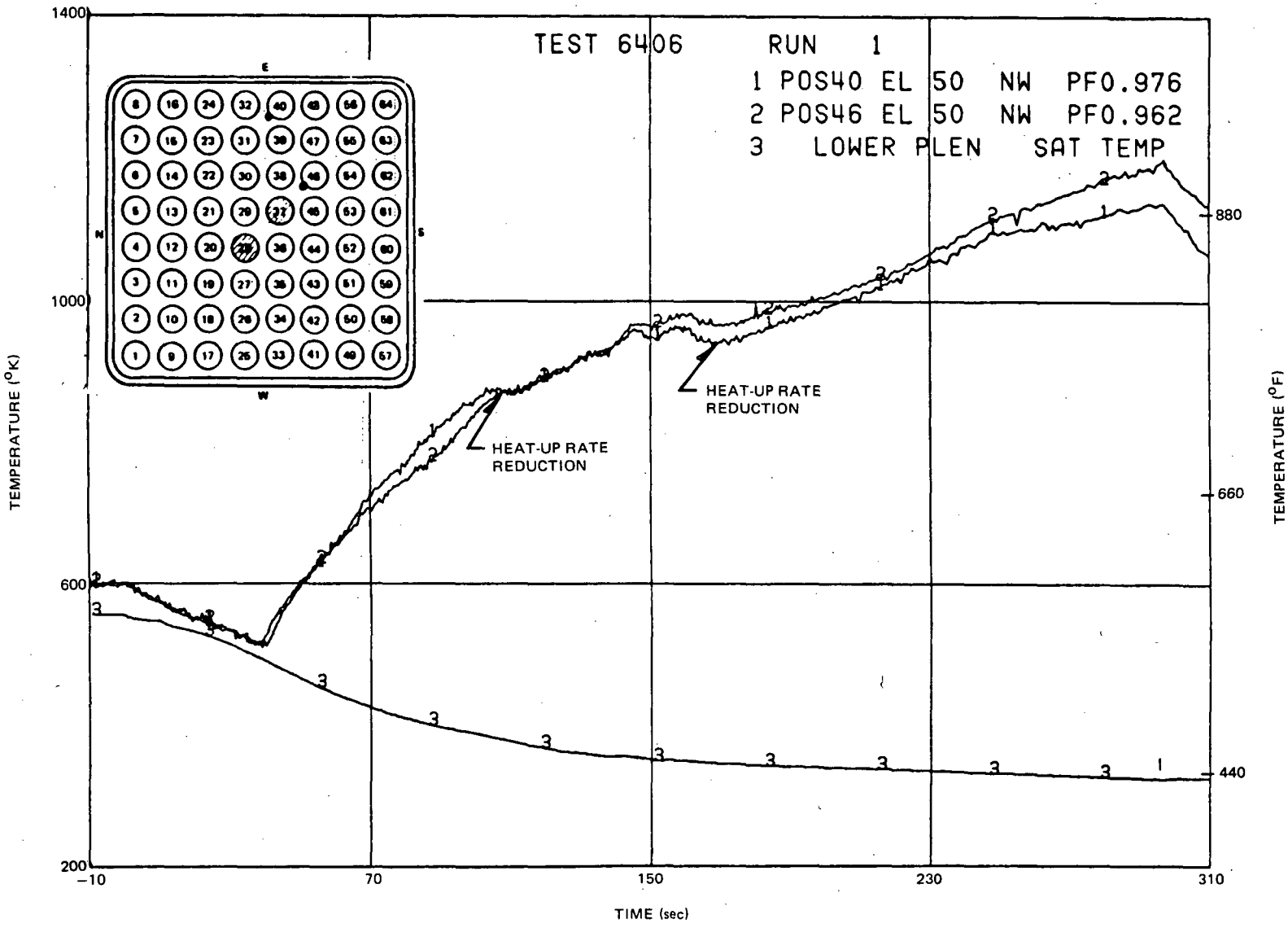

Figure I-26. Bundle Temperature at 50 in. Elevation

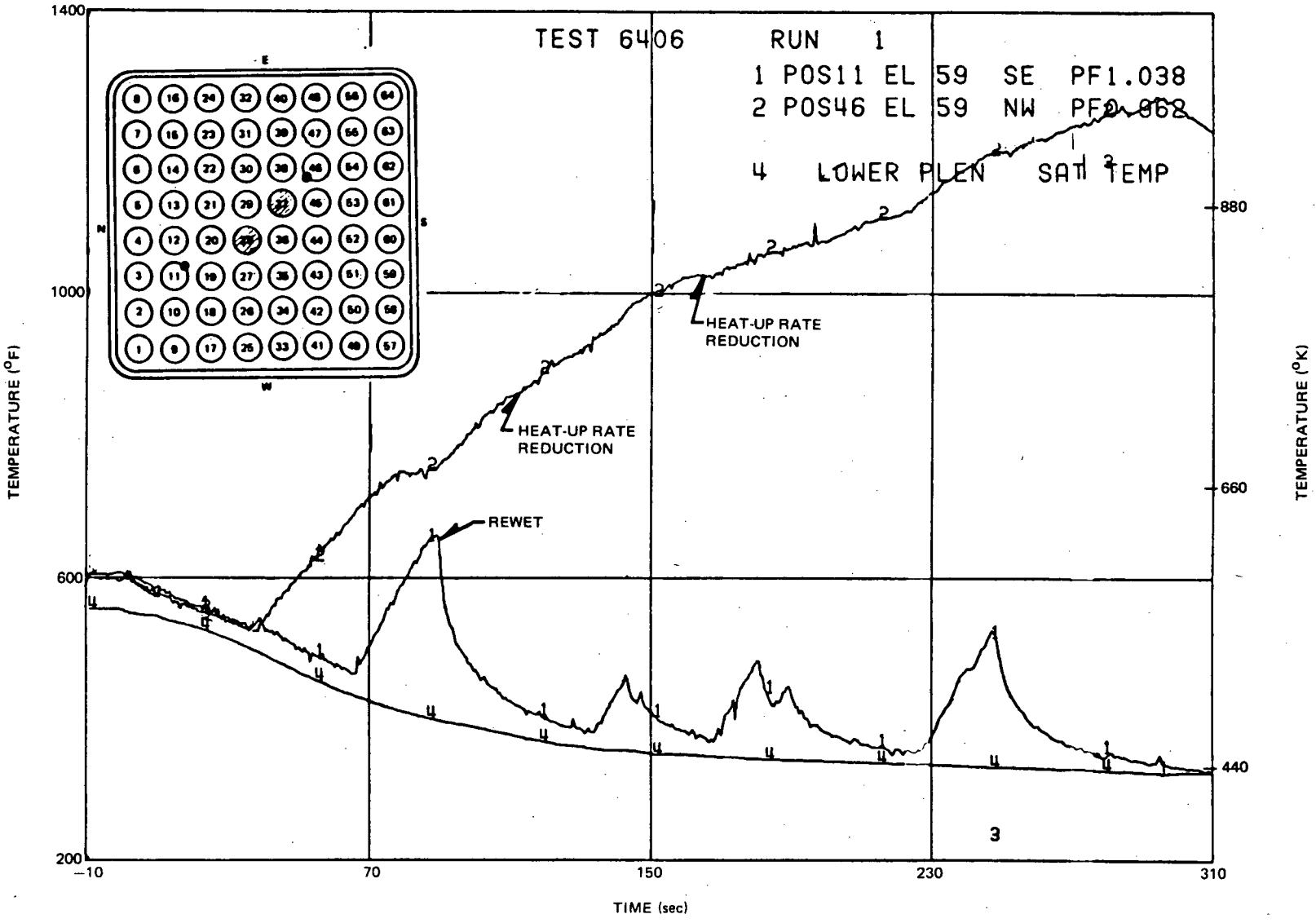

Figure I-27. Bundle Temperature at 59 in. Elevation

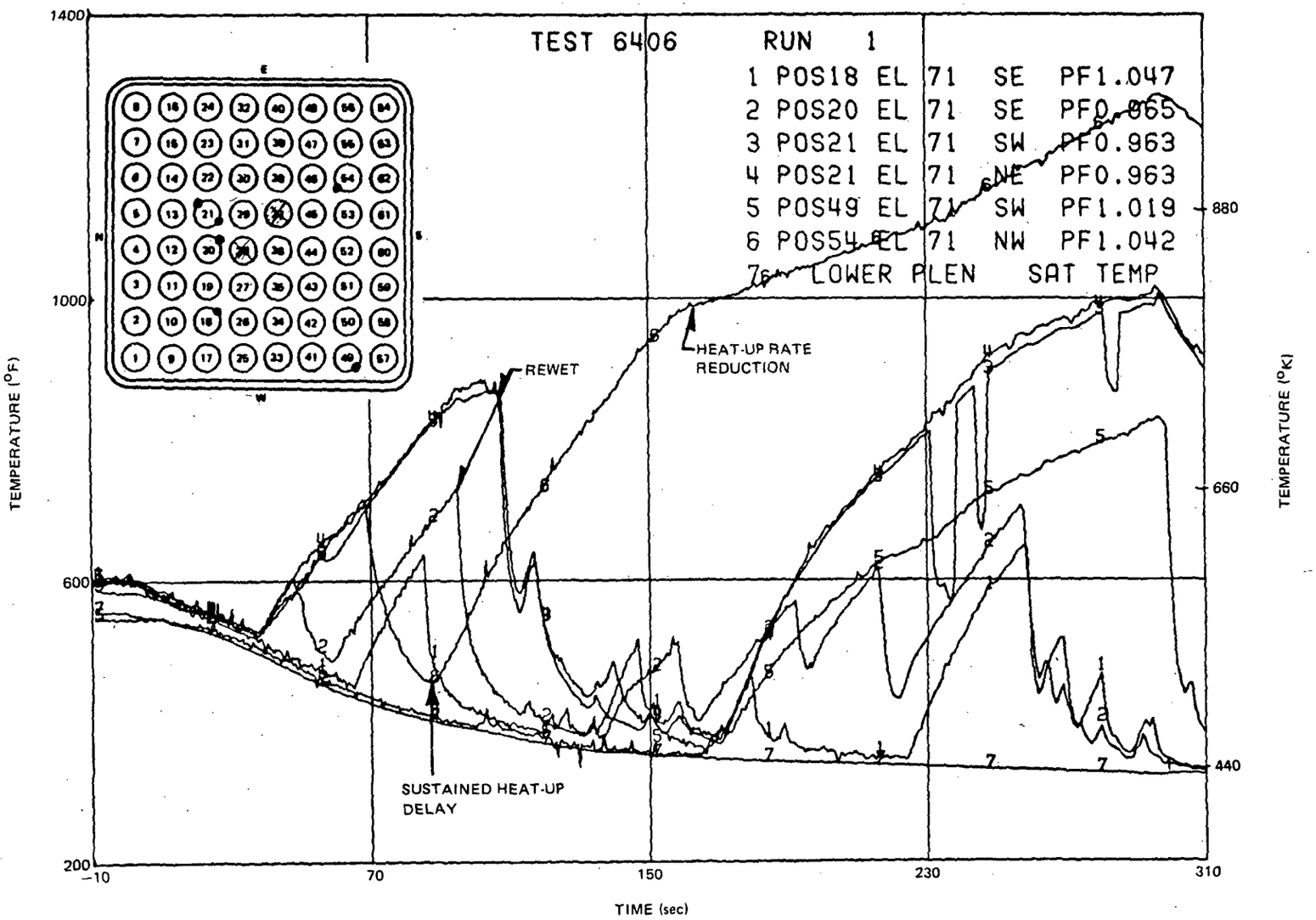

Figure I-28. Bundle Temperature at 71 in. Elevation

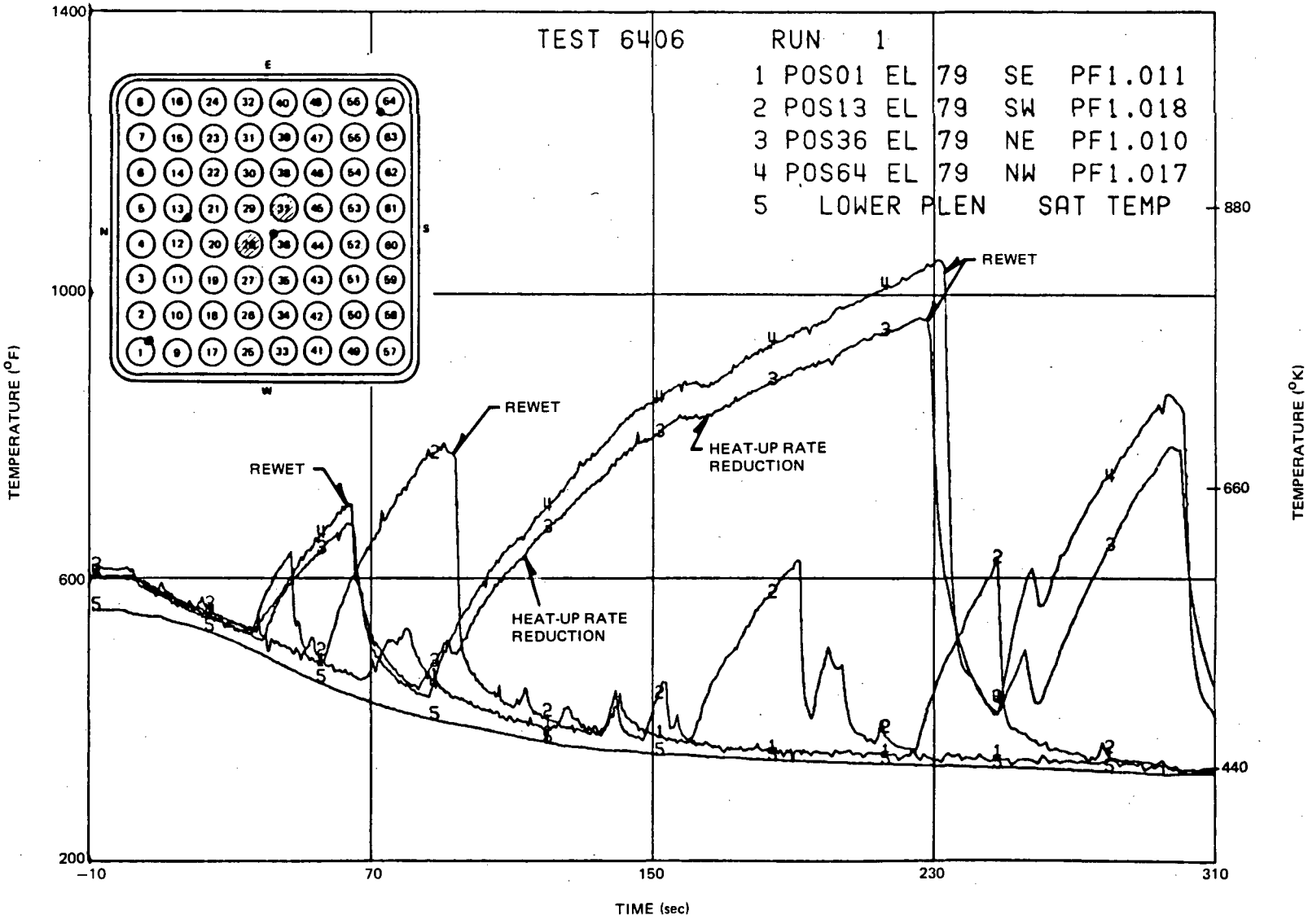

Figure I-29. Bundle Temperature at 79 in. Elevation

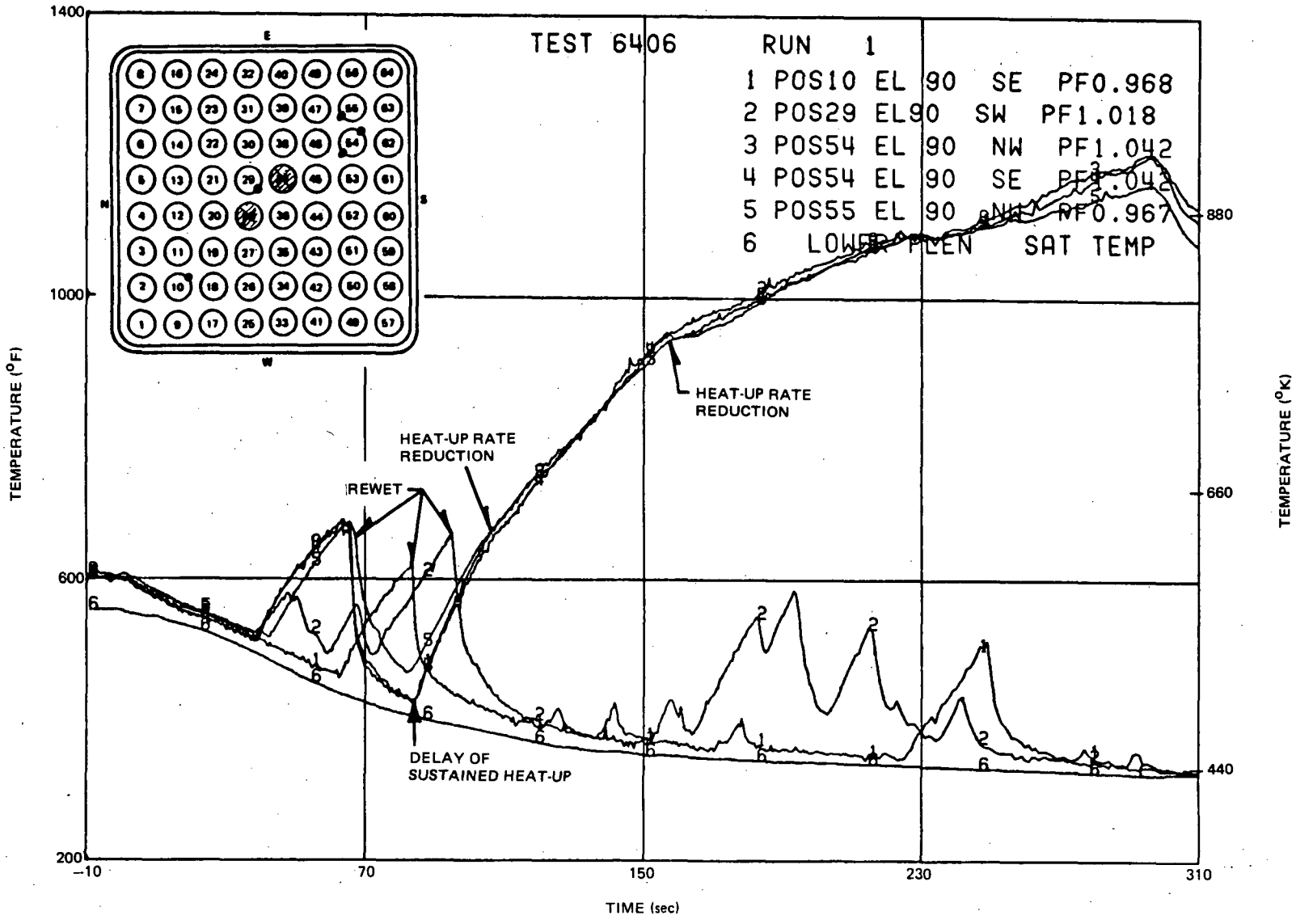

Figure I-30. Bundle Temperature at 90 in. Elevation

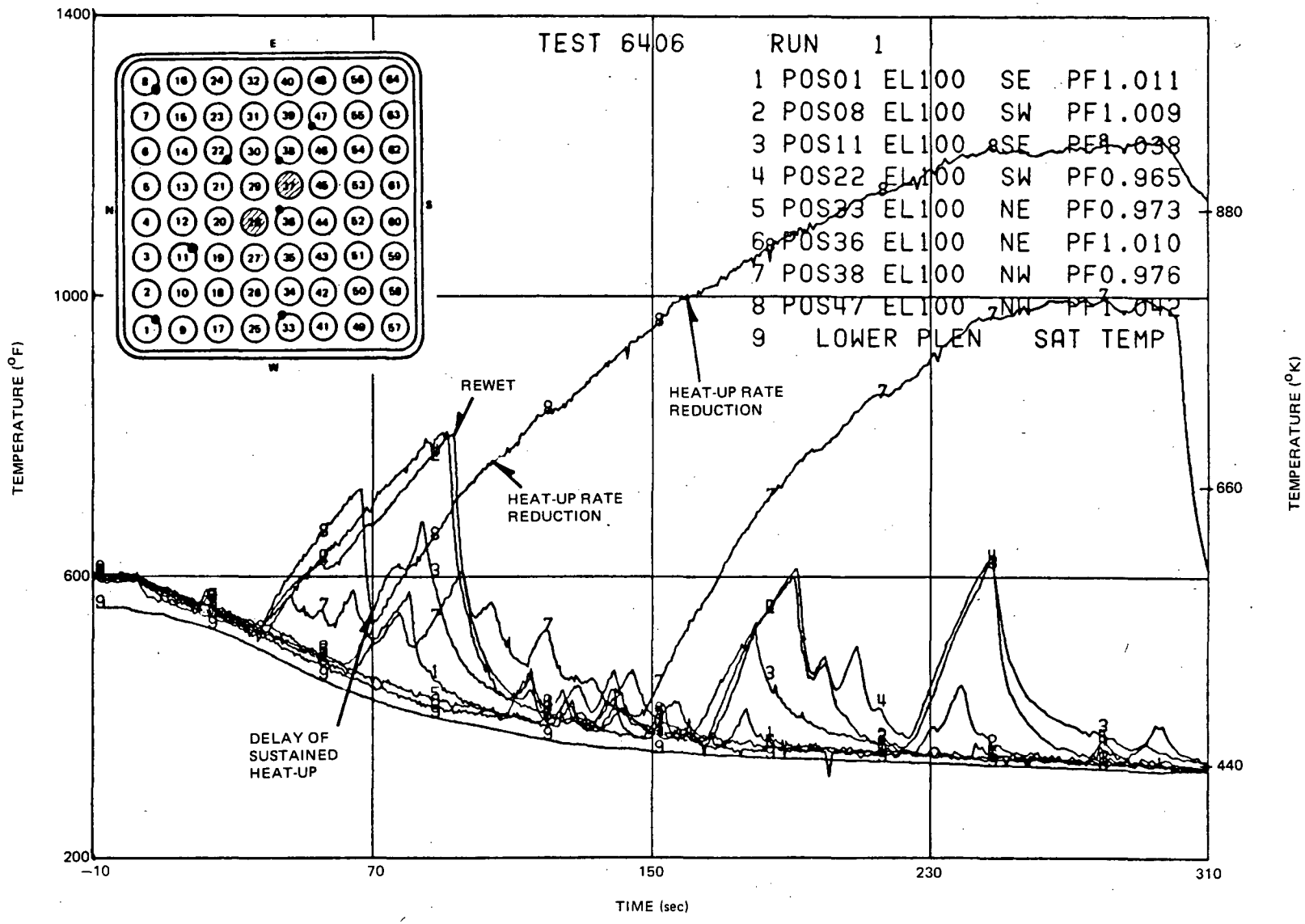

Figure I-31. Bundle Temperature at 100 in. Elevation

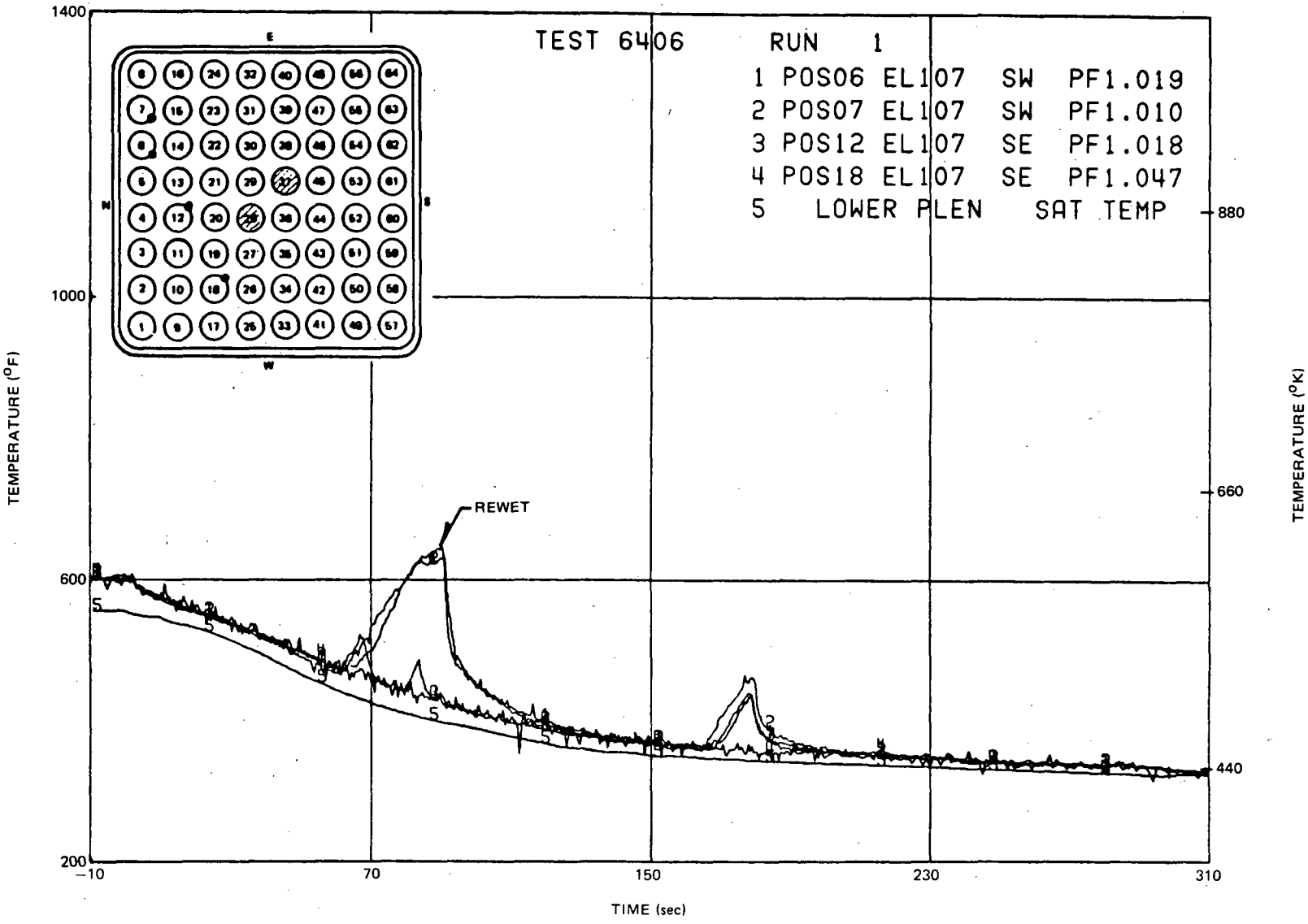

Figure I-32. Bundle Temperature at 107 in. Elevation

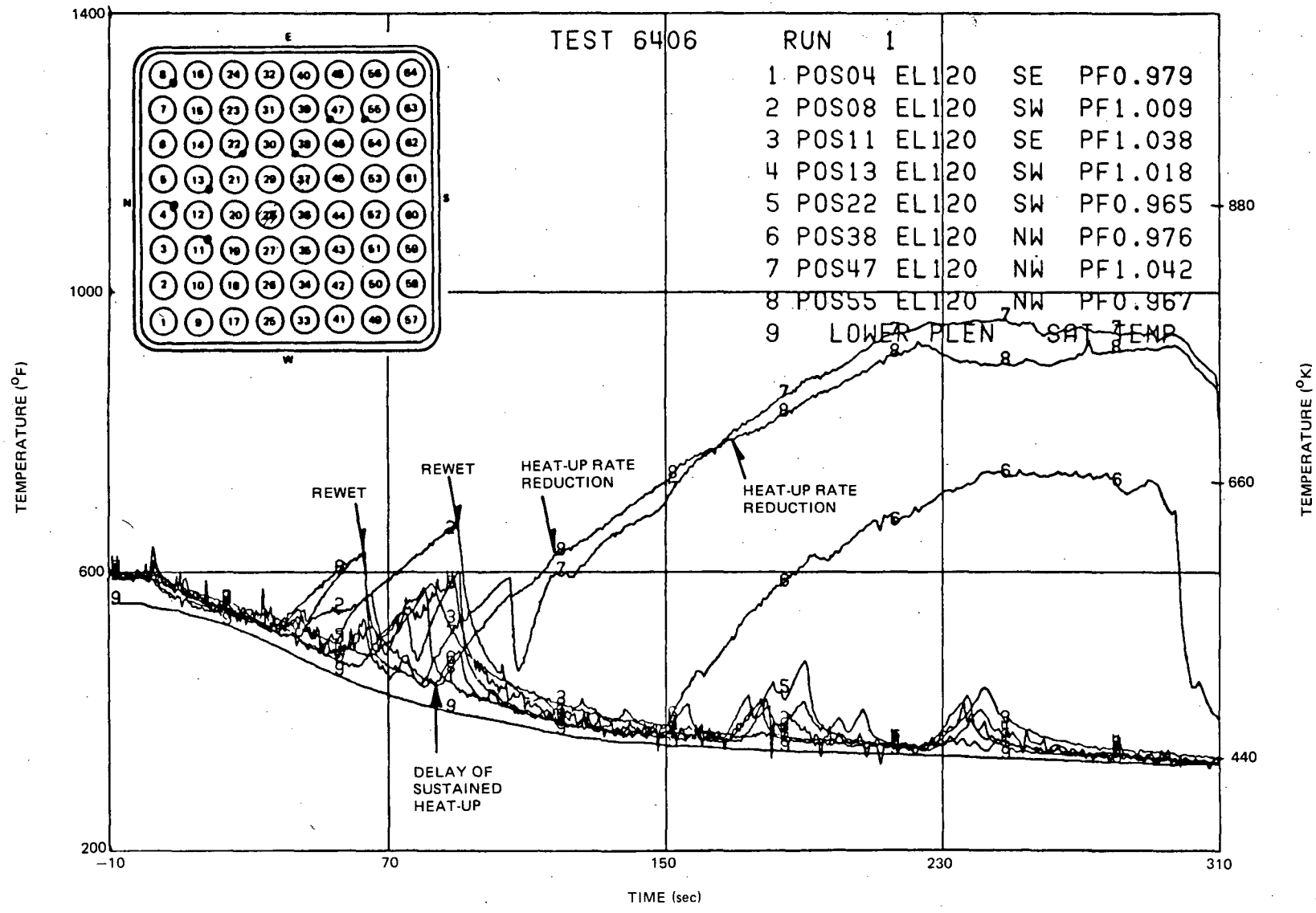

Figure I-33. Bundle Temperature at 120 in. Elevation

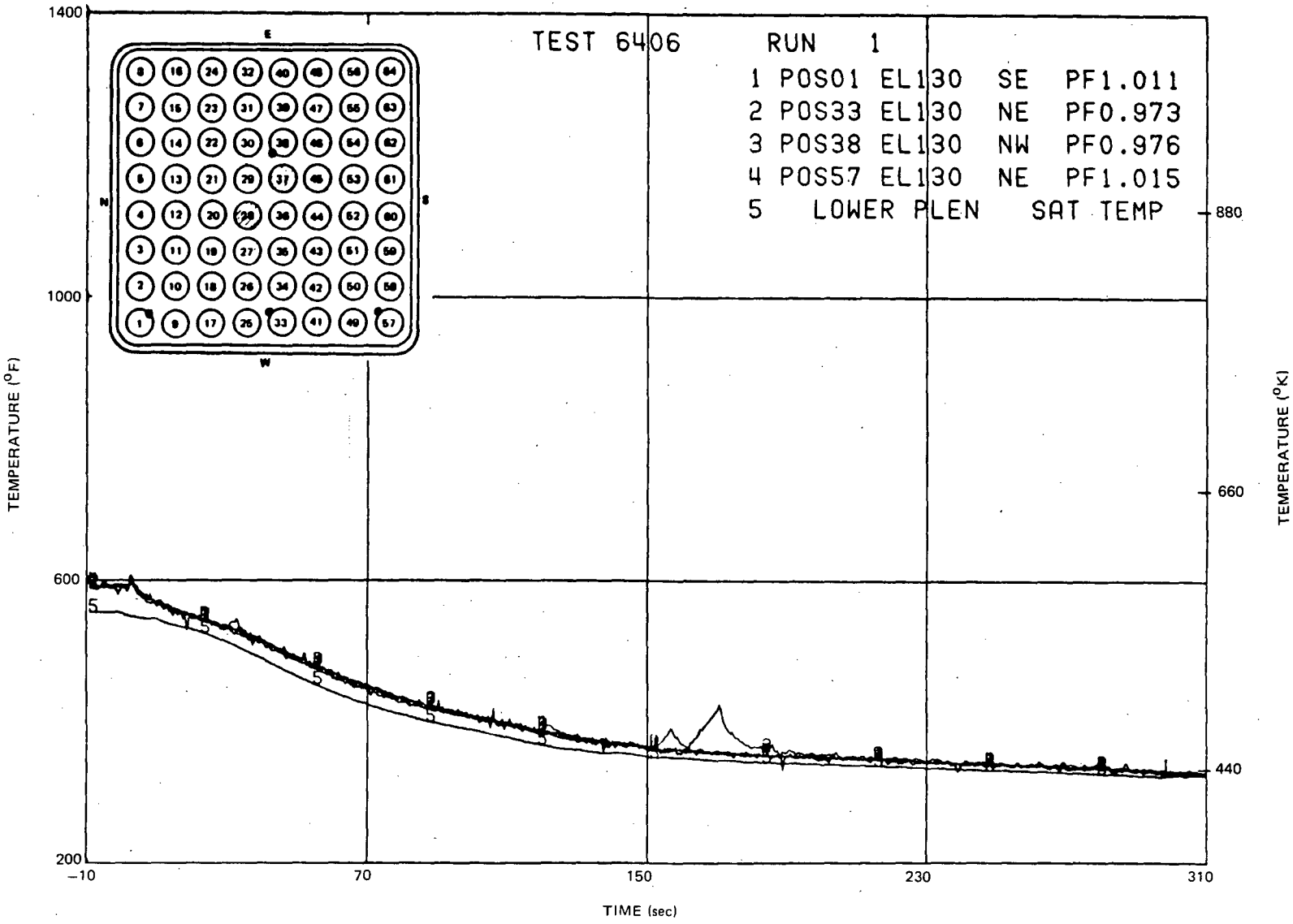

Figure I-34. Bundle Temperature at 130 in. Elevation

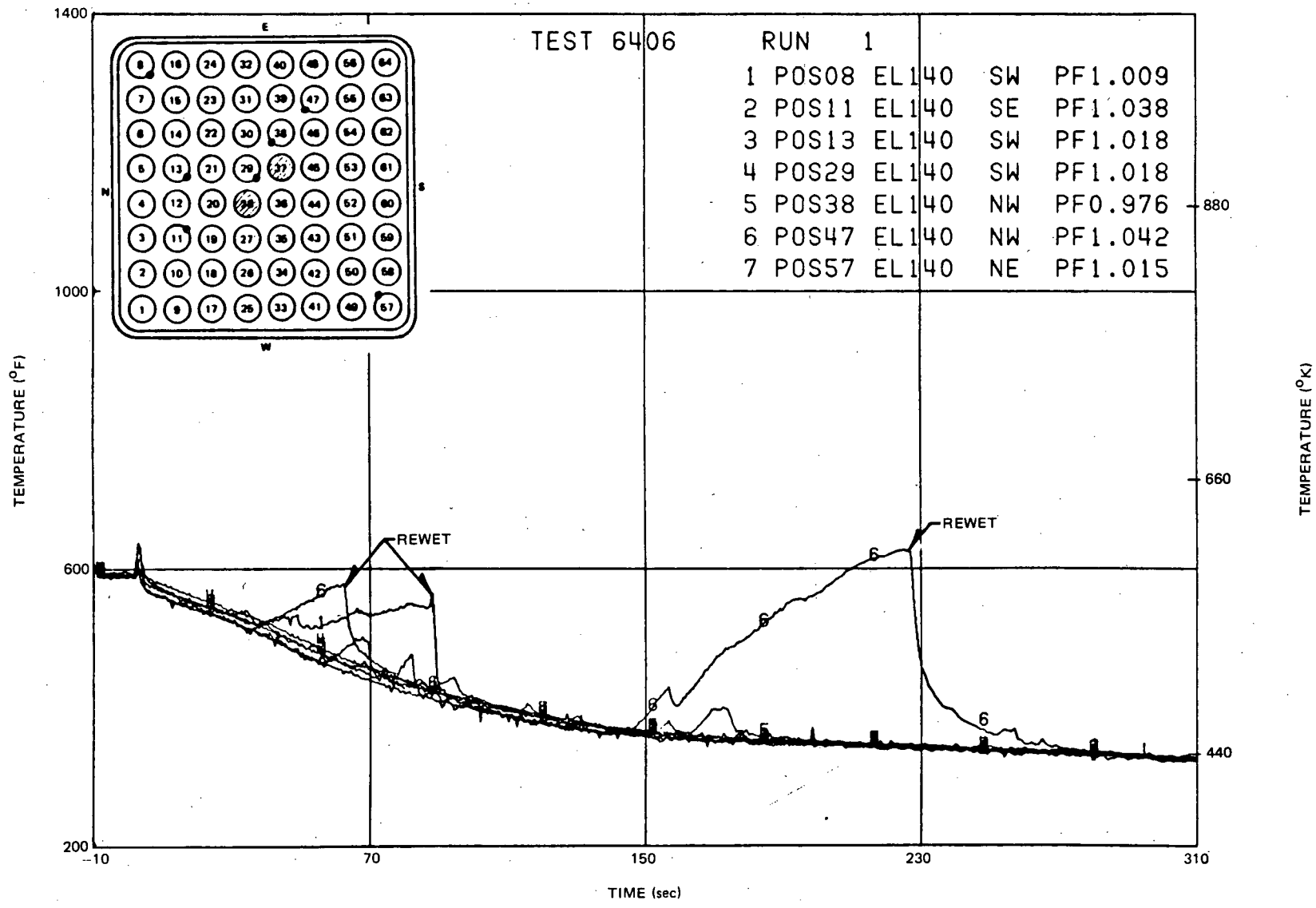

Figure I-35. Bundle Temperature at 140 in. Elevation

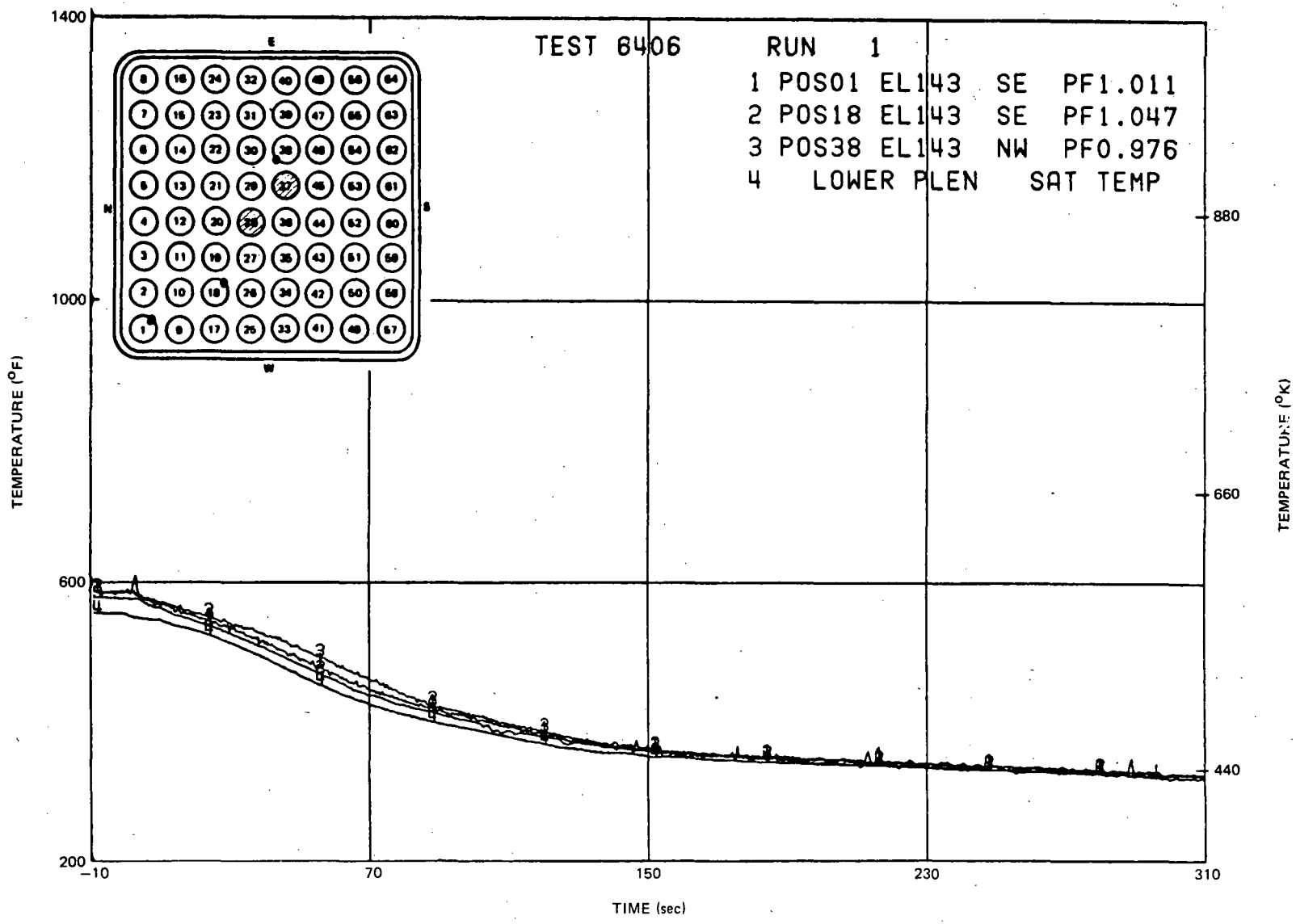

Figure I-36. Bundle Temperature at 143 in. Elevation

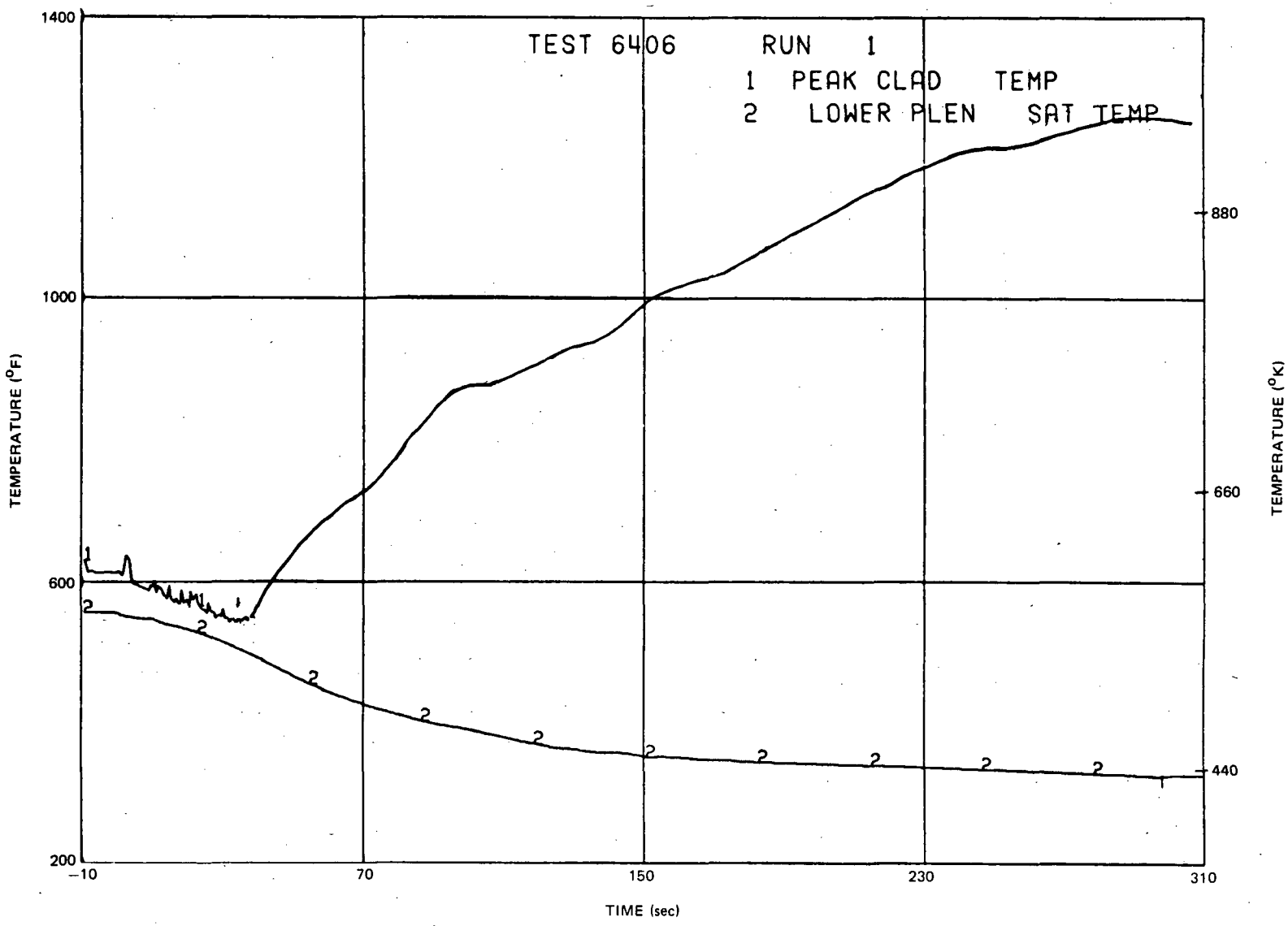

Figure I-37. Peak Cladding Temperature

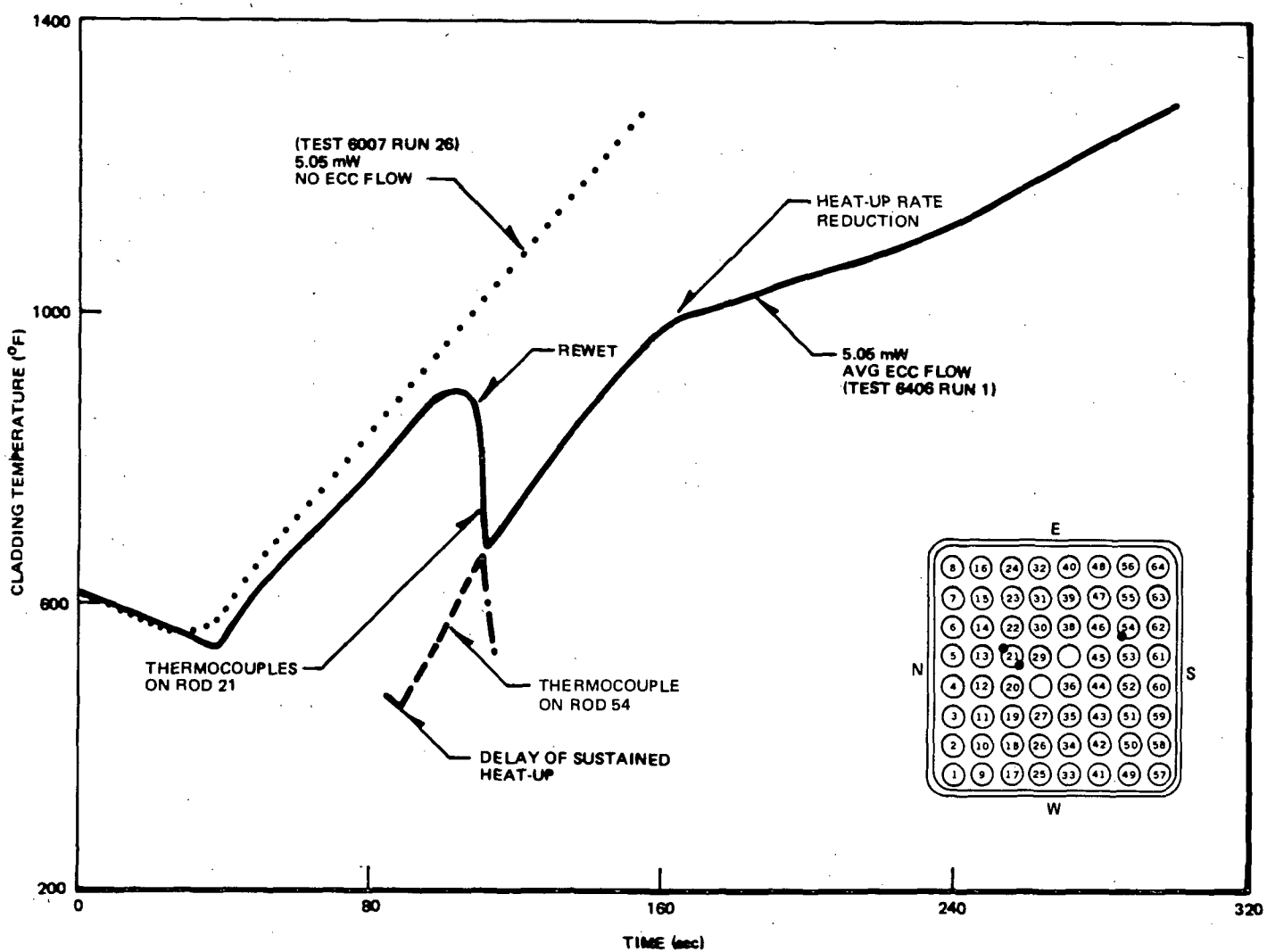

Figure I-38. Comparison of Cladding Temperatures at 71 in. Elevation

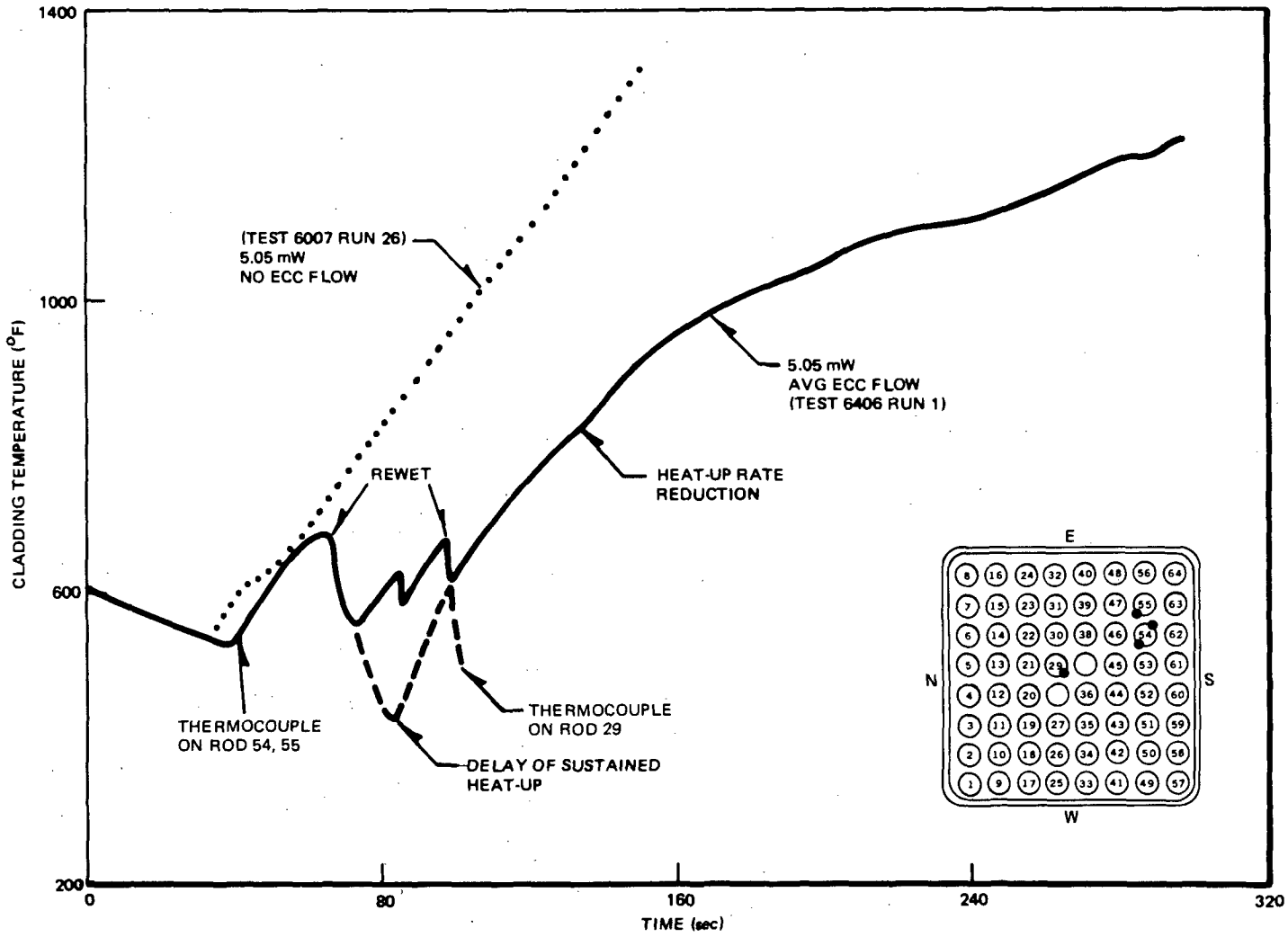

Figure I-39. Comparison of Cladding Temperatures at 90 in. Elevation

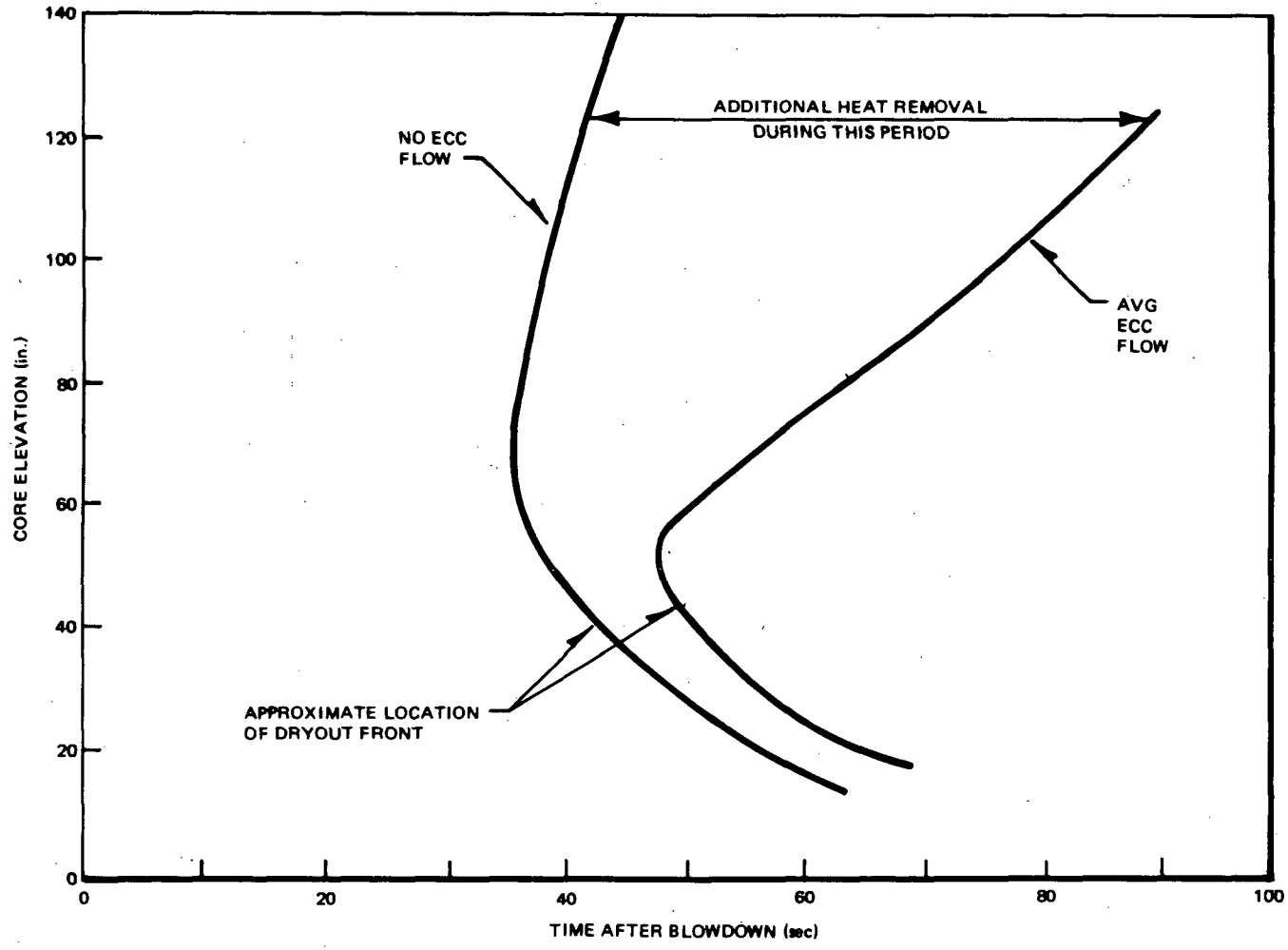

Figure I-40. Effect of ECC Flows on Bundle Dryout Inception

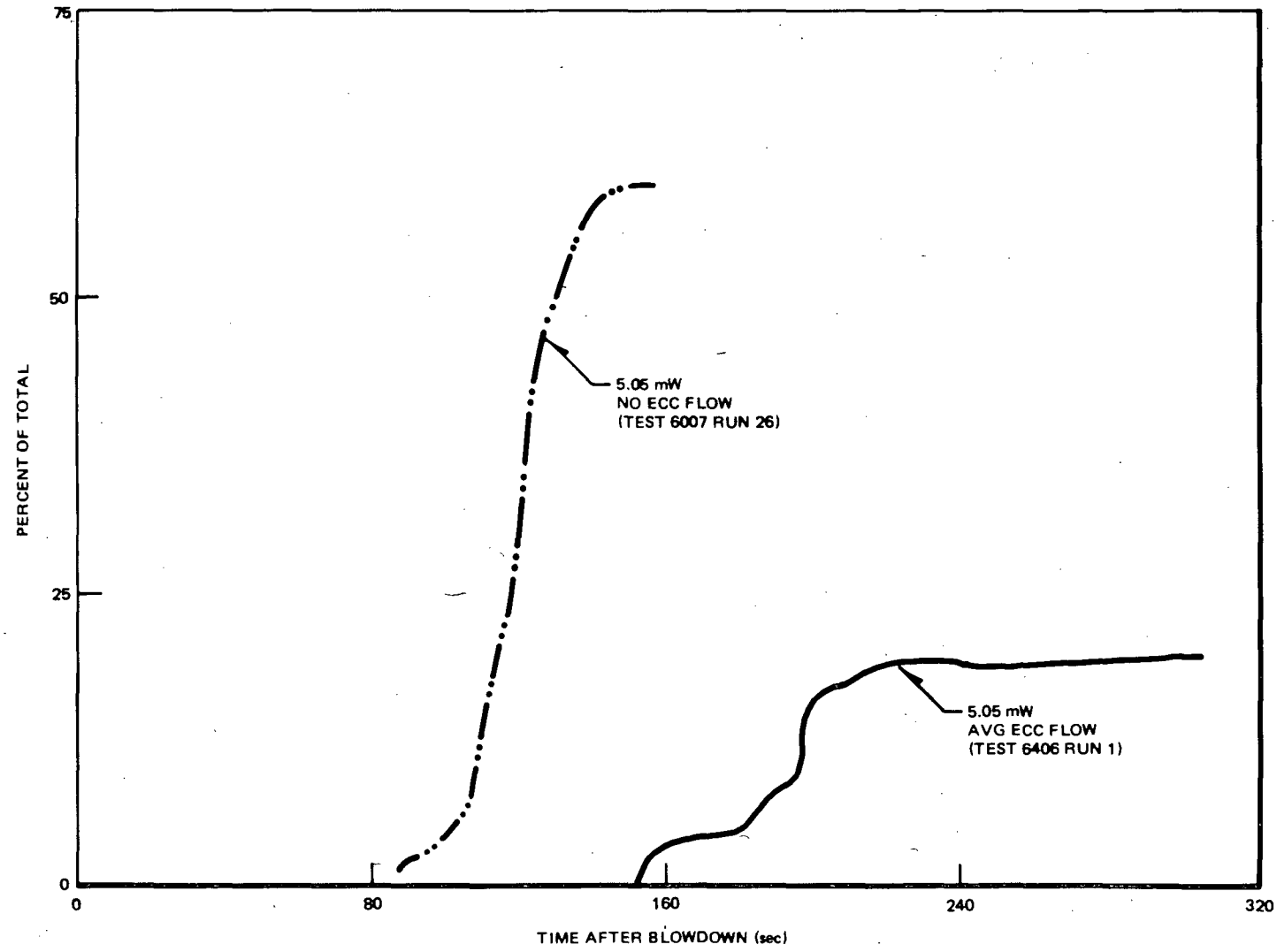

Figure I-41. Comparison of Percentage of Thermocouples Measuring Temperatures Greater than 1000°F in Average Power (5.05 MW) Tests

Appendix J

DATA REPORT FOR TEST 6425/RUN 2 (REFERENCE TEST)

Test 6425/2 was an average power, average ECC flow, nominal ECC temperature test conducted in the TLTA 5A facility. A diagram of the system instrumentation showing measurement nodes is given in Figure J-1. Figure J-2 shows a schematic of the bundle and locations of the pressure transducer taps and thermocouples. The core lattice arrangement and the local peaking factor distribution are shown in Figure J-3.

Tables J-1 and J-2 summarize the initial conditions and sequence of events for Test 6425/2. Primary measurements throughout the transient are given in Figures J-4 to J-38. Quantities such as nodal density, mass, and flow that are derived from the primary measurements are shown in Figures J-39 through J-76. A guide for interpreting bundle temperature plots is shown in Figure J-77, and the bundle temperature measurements are given in Figures J-78 to J-97. Figure J-98 gives the peak cladding temperature.

Table J-1

INITIAL CONDITIONS OF THE BD/ECC 1A REFERENCE TEST (6425 RUN 2)

Initial Conditions	TLTA	
Bundle power	5.05[a] ± 0.03 MW	
Steam dome pressure	1044 ± 5 psia	(7198 Pa)
Lower plenum pressure	1071 ± 5 psia	(7384 Pa)
Lower plenum enthalpy	528 ± 5 Btu/lbm	(1228 kJ/kg)
Initial water level[b]	73 ± 6 in.	(1.85m)
Feedwater enthalpy	41 ± 2 Btu/lbm	(95 kJ/kg)
Bundle inlet to outlet DP	17 ± 2 psi	(117 Pa)
Steam flow	6 ± 1 lbm/sec	(2.7 kg/s)
Feedwater flow	1.4 ± 0.3 lbm/sec	(0.5 kg/s)
Drive Pump 1 flow	9.1 ± 1 lbm/sec	(4.1 kg/s)
Drive Pump 2 flow	8.4 ± 1 lbm/sec	(3.8 kg/s)
Jet Pump 1 flow	22 ± 2 lbm/sec	(10 kg/s)
Jet Pump 2 flow	20 ± 2 lbm/sec	(9 kg/s)
Bundle inlet flow	39 ± 5 lbm/sec	(18 kg/s)

All uncertainty bands are judged from the maximum of data fluctuation and/or absolute uncertainties of the measurements.

[a]NOTE: 5.05 mW is central average bundle power; core average power is 4.60 mW for the reference BWR/6.

[b]NOTE: Relative to jet pump support plate.

Table J-2

SEQUENCE OF EVENTS FOR 6425 RUN 2 (AVG. POWER, AVG. ECC)

Events	Time (sec)
Blowdown valves open	0.0
Bundle power decay initiated	0.5
Blowdown loop jet pump flow reverses	0.5
Feedwater flow stops	0.5
Bypass flow reverses	1.7
Jet pump suction uncovers	6.7
Steamline valve completely closed	9.0
Recirc. suction line begins to uncover	9.4
Lower plenum bulk flashing	11
Guide tube flashing	11.2
Core inlet uncovers (SEO center line)	20
Loop 1 isolated	20
HPCS injection begins	27
Lower plenum mixture level reaches jet pump exit plane	35
LPCS, LPCI activated	37
LPCS flow begins	64
LPCI flow begins	75
Bypass/guide tube region begins to refill	85
CCFL breaks down at bypass outlet	95
Bundle begins to refill	114
Bypass region refilled	125
Bundle reflood with two-phase mixture	130
CCFL breaks down at upper tieplate	125
Bundle quenched	150
End of test	400

NOTES:

1. P - PRESSURE
   DP - DIFFERENTIAL PRESSURE
   T - TEMPERATURE (RTD - RESISTANCE THERM)
   SP - VALVE STEM POSITION
   RO - RESTRICTING ORIFICE
   FE - FLOW ELEMENT
   S - PUMP SPEED
   LP - LEVEL PROBE
   DD - DRAG DISK
   TM - TURBINE METER

2. N305 - 54.88 MEANS NOZZLE NO. 305 IS AT AN ELEVATION OF 54.88 INCHES. IT DOES NOT REFER TO ACTUAL LOCATION OF THE NODAL POINT.

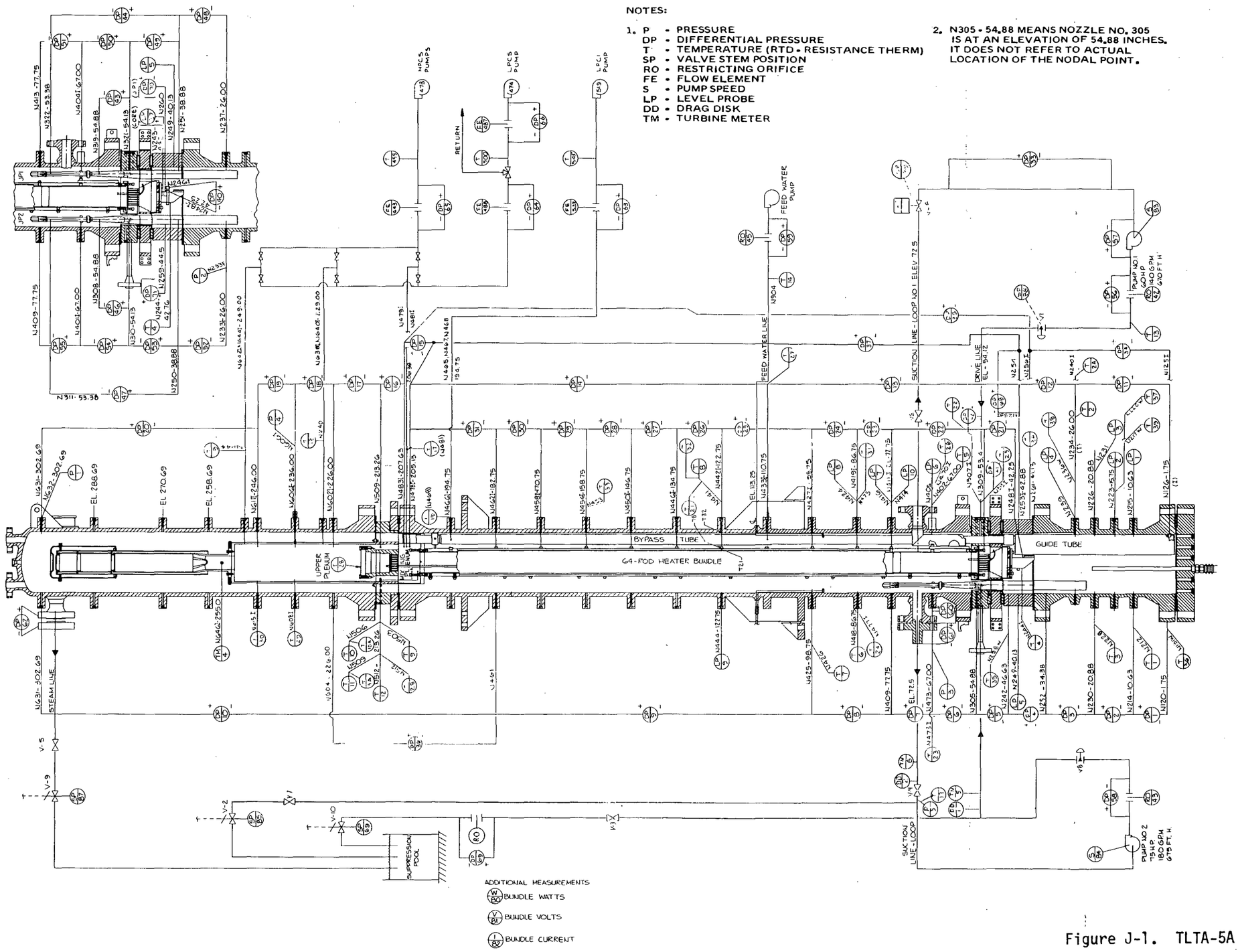

Figure J-1. TLTA-5A Instrumentation

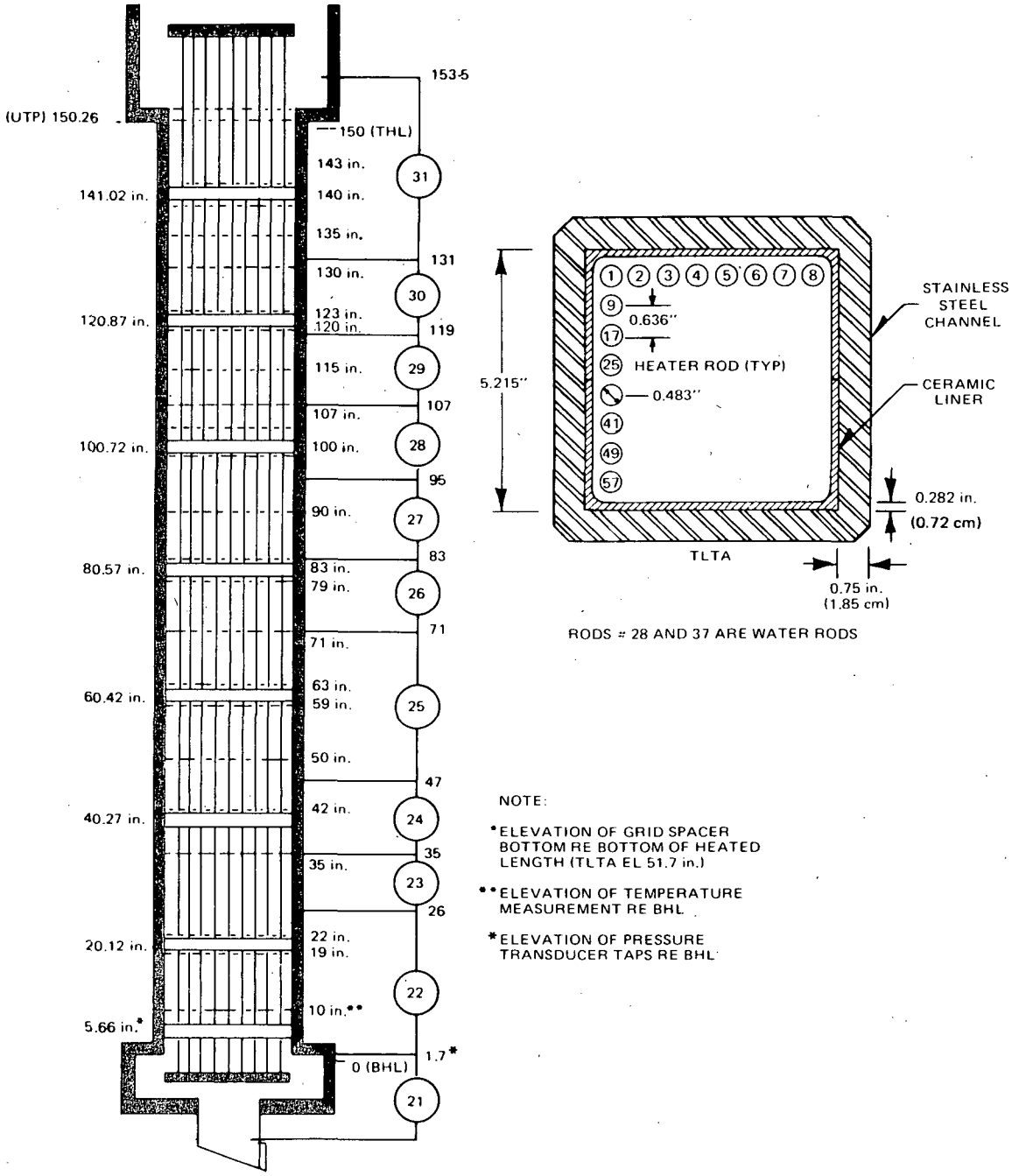

Figure J-2. TLTA-5A Bundle Instrumentation and Dimensions

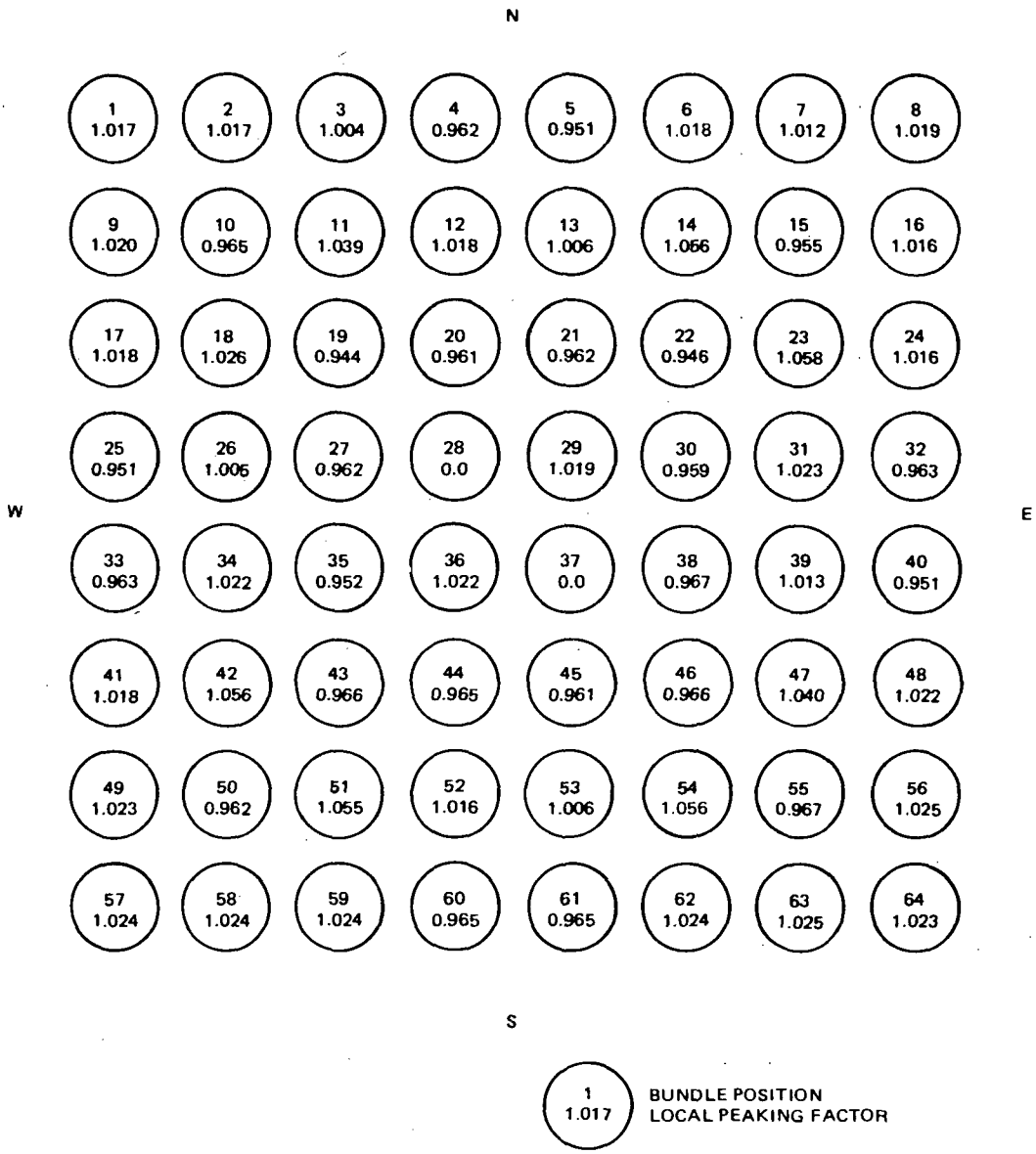

Figure J-3. Local Peaking Factor Distribution

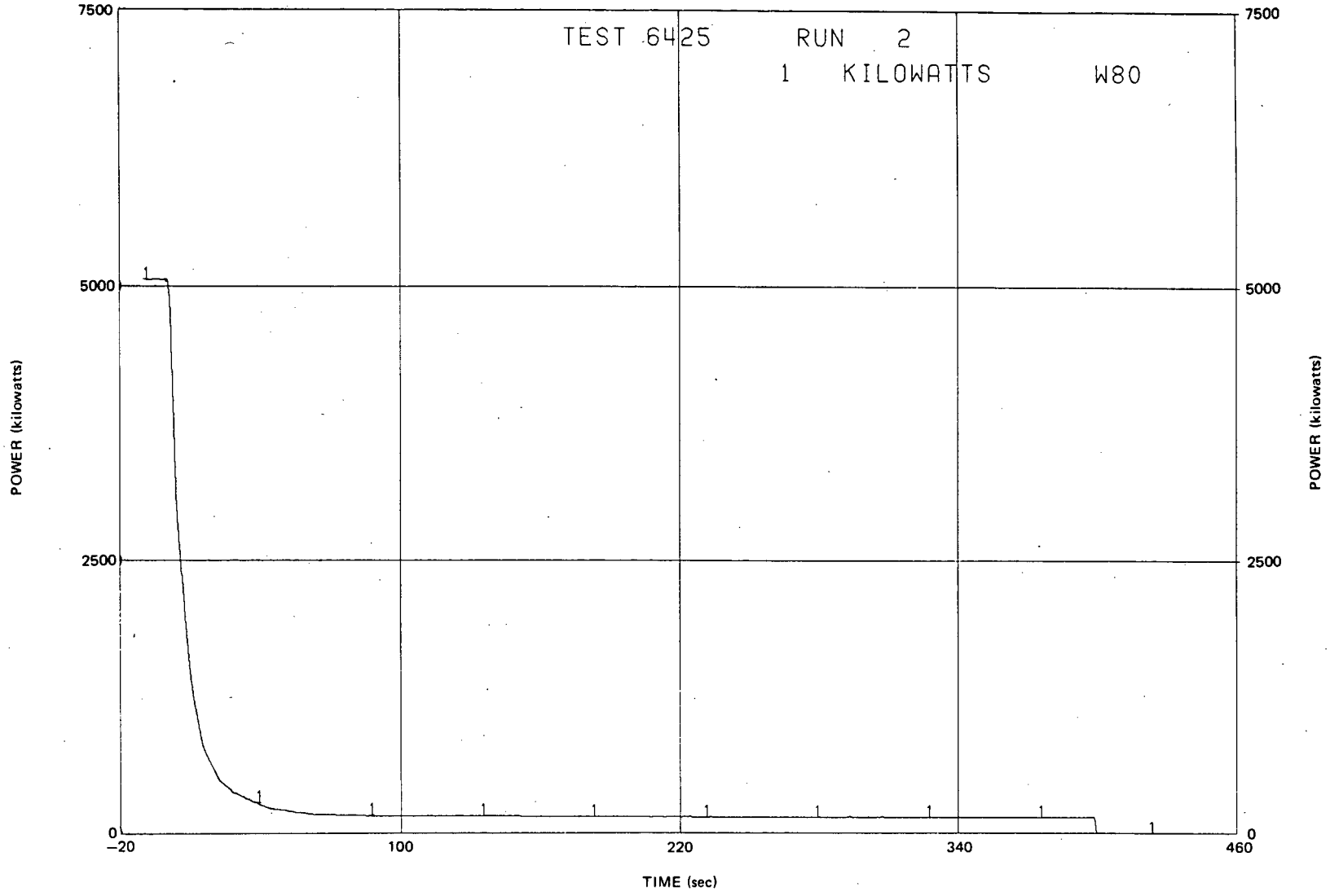

Figure J-4. Bundle Power Decay

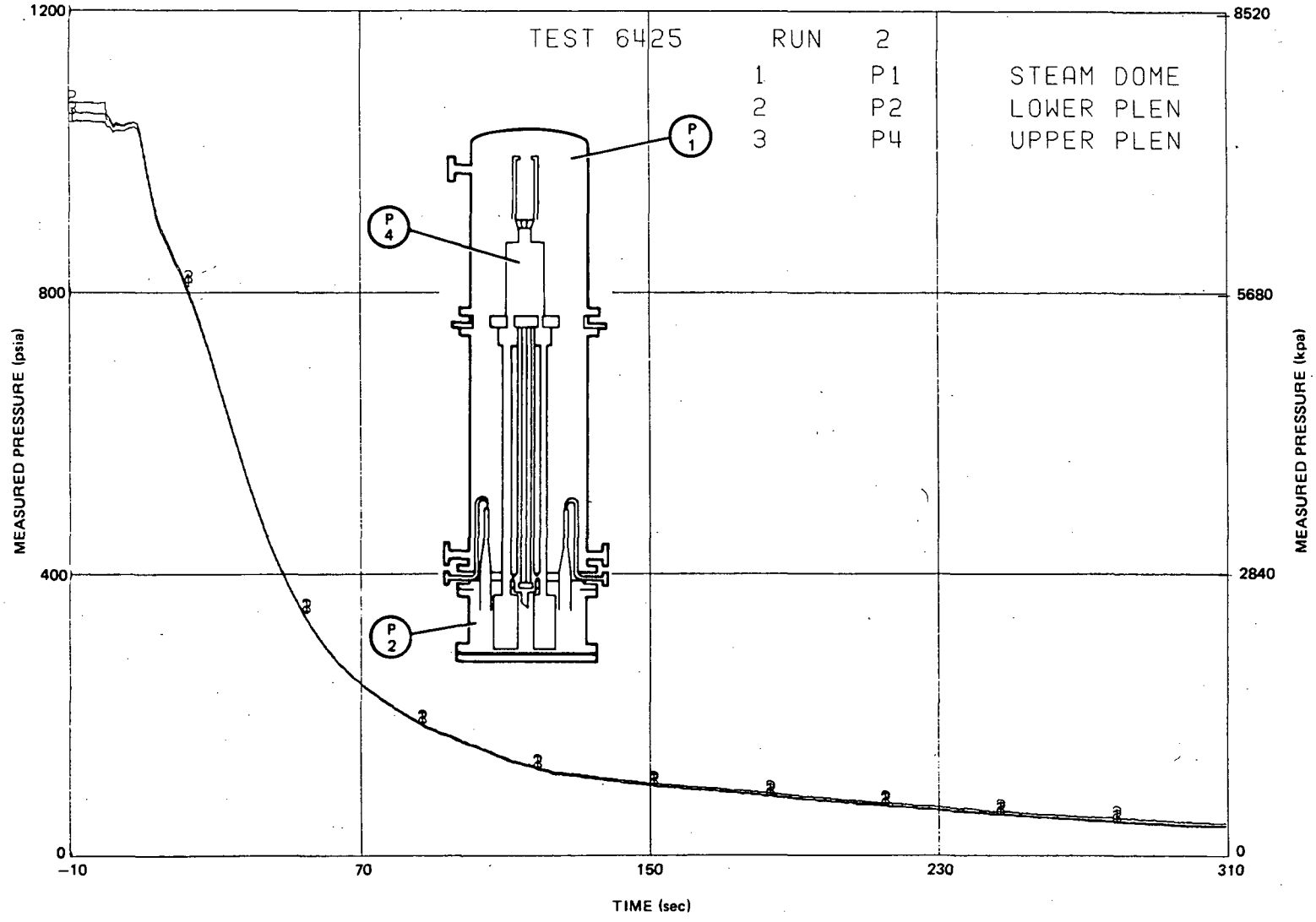

Figure J-5. System Pressures

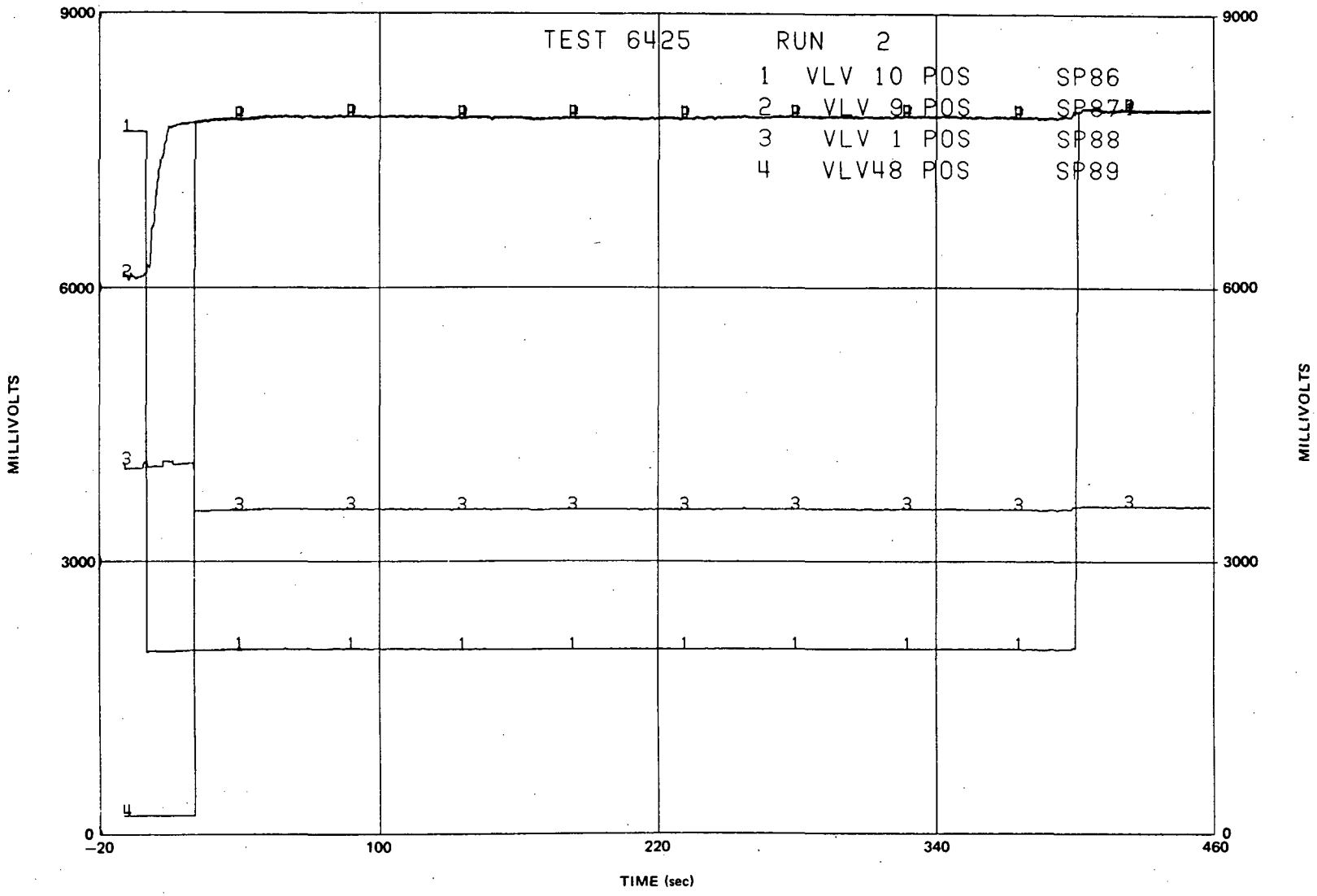

Figure J-6. Valve Positions

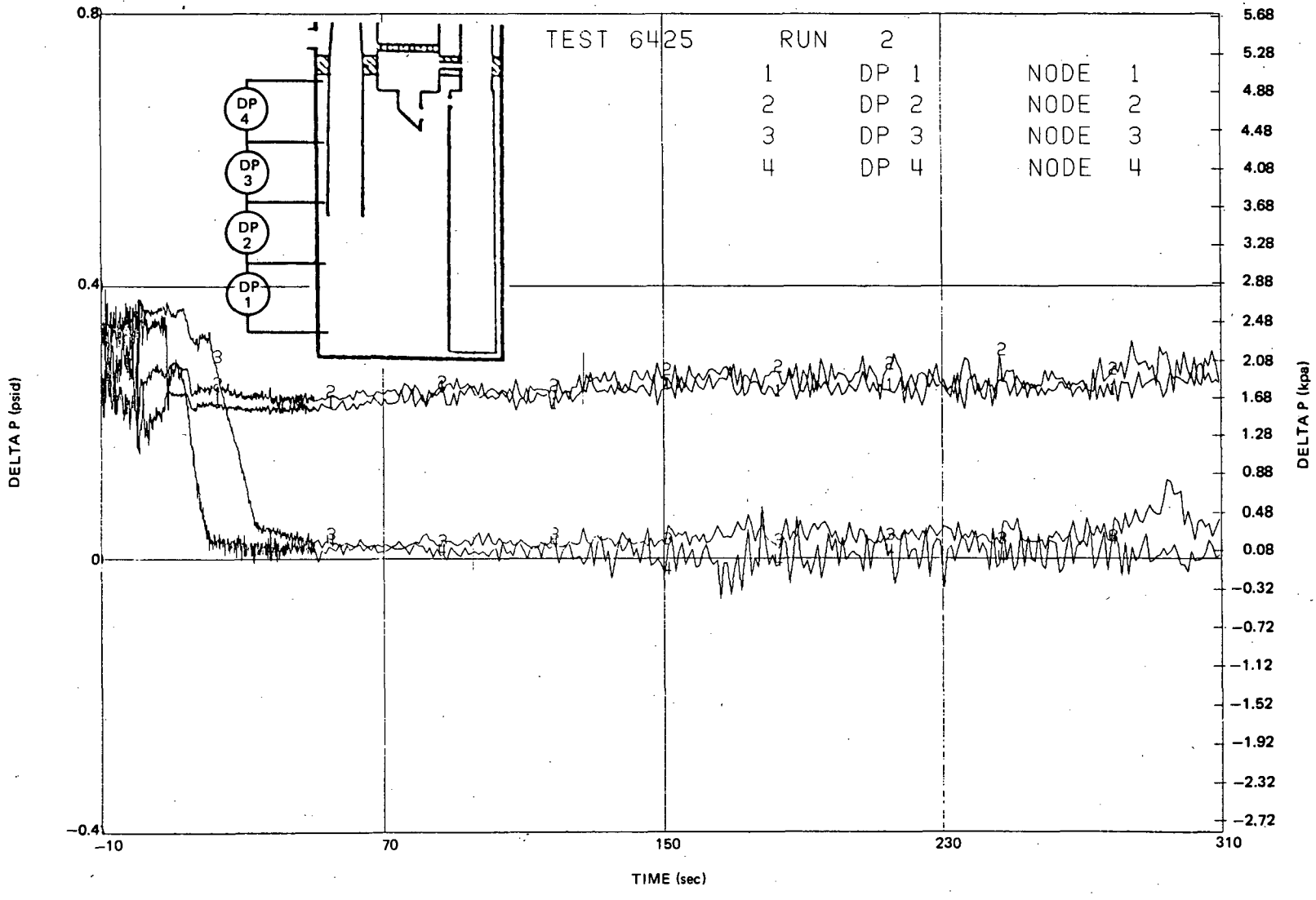

Figure J-7. Lower Plenum Differential Pressures

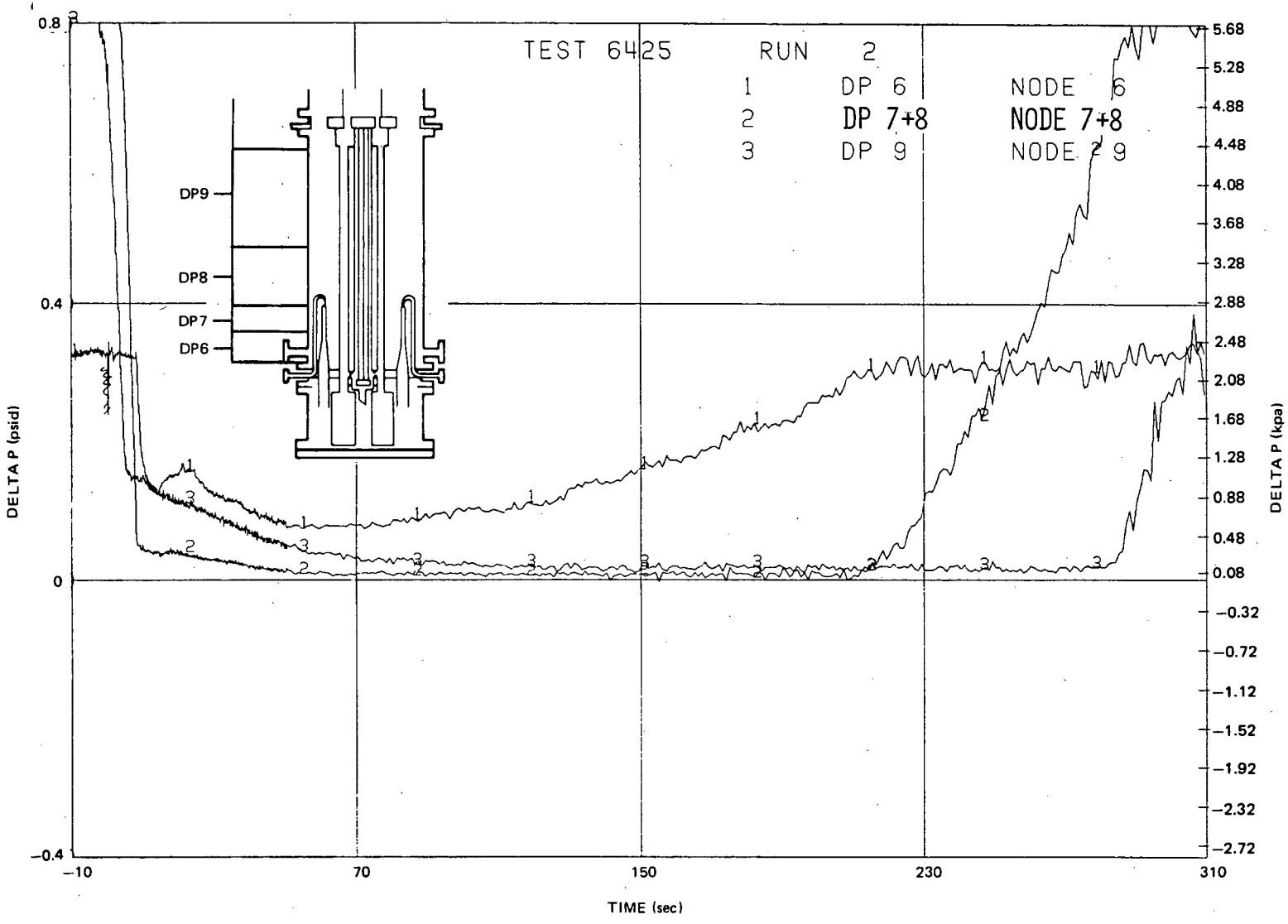

Figure J-8. Annulus Differential Pressures

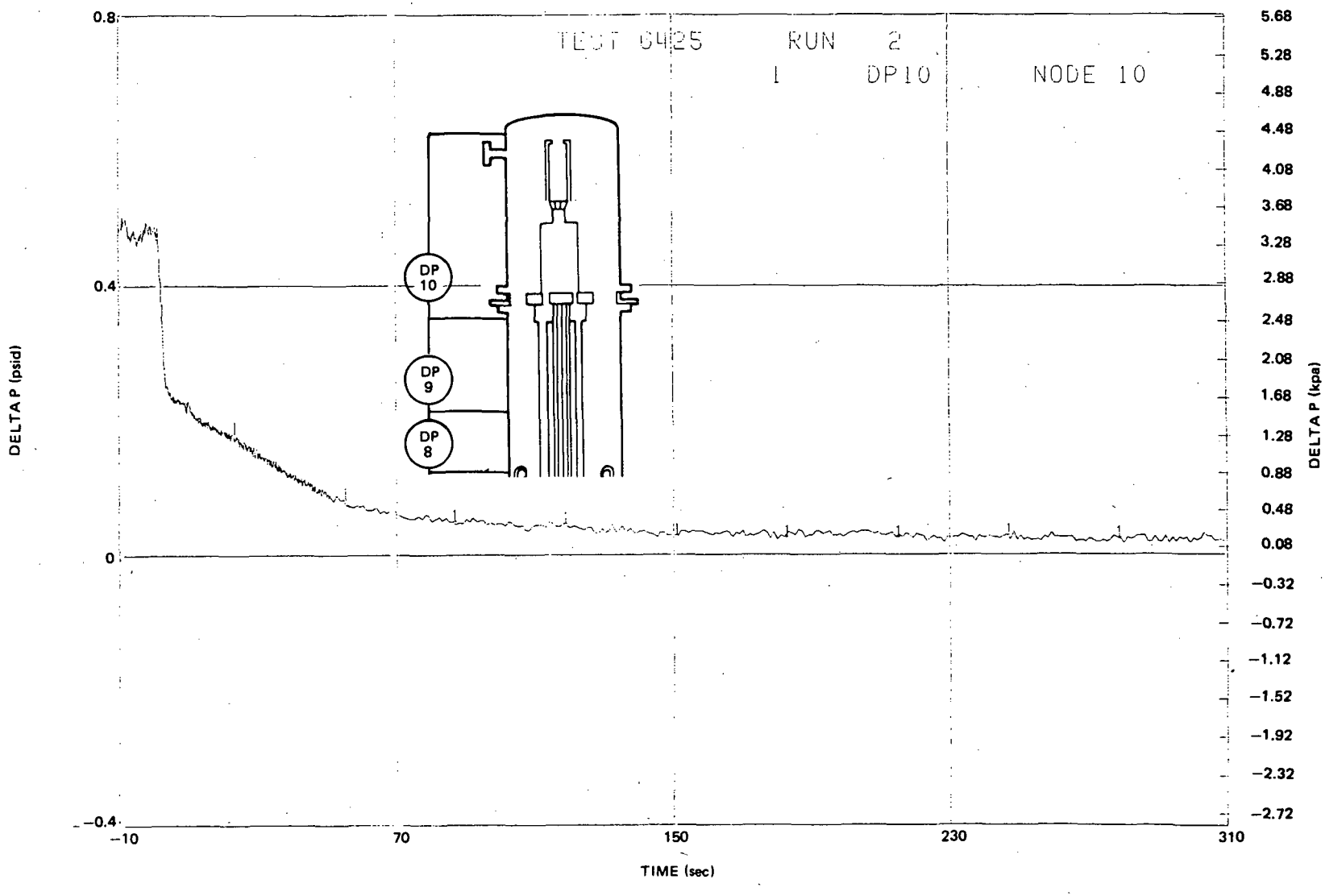

Figure J-9. Upper Annulus Differential Pressure

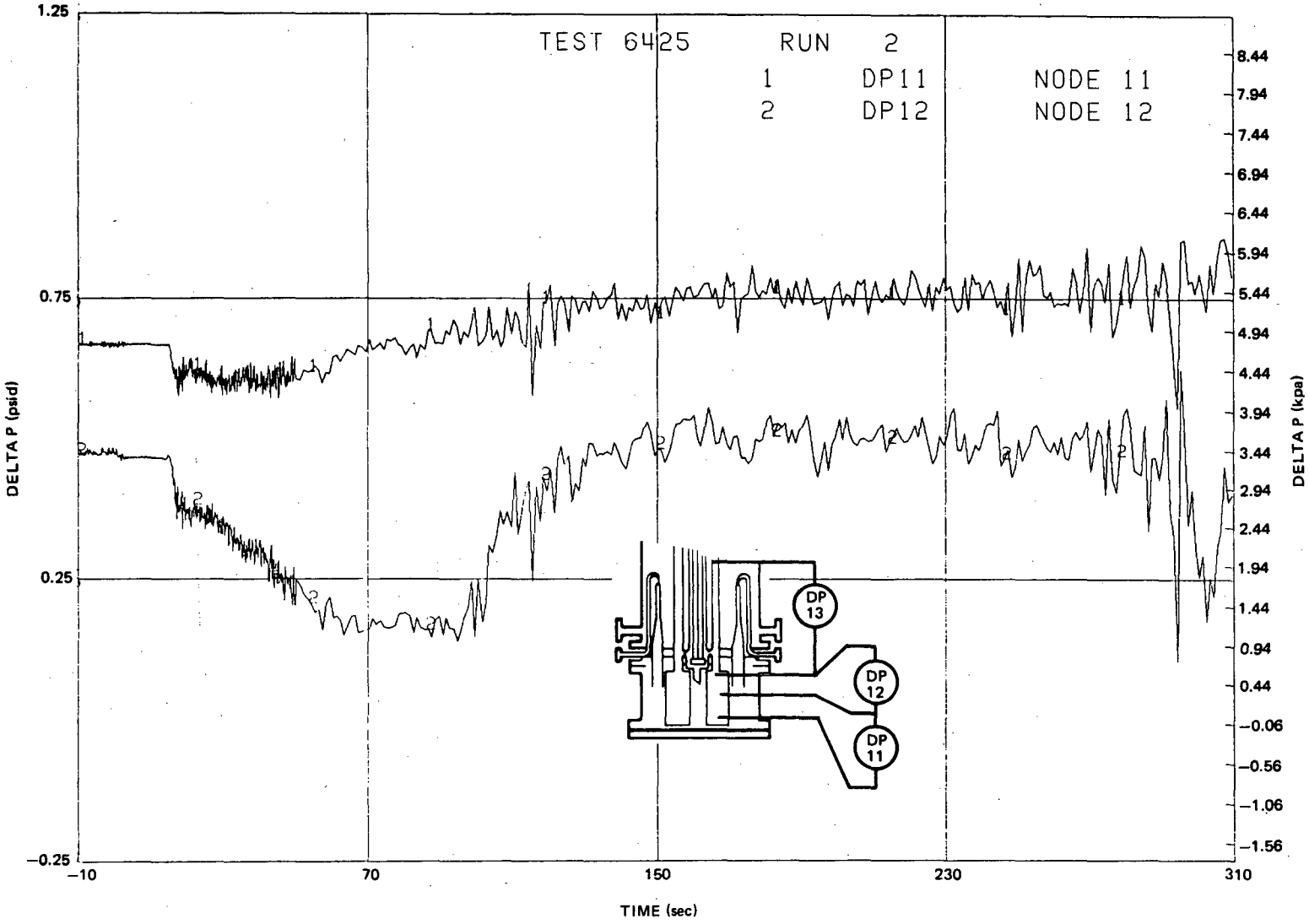

Figure J-10. Guide Tube Differential Pressures

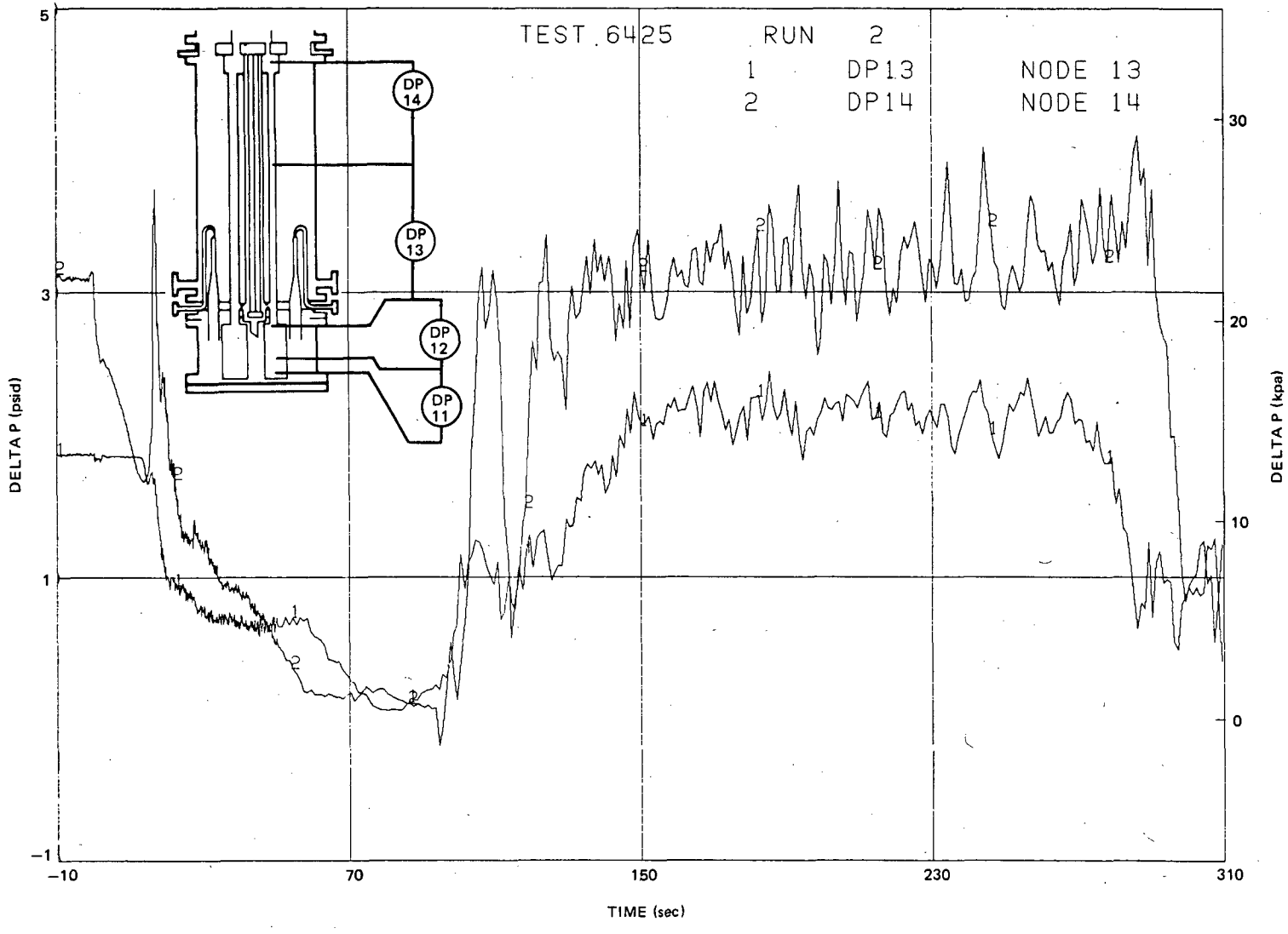

Figure J-11. Bypass Differential Pressures

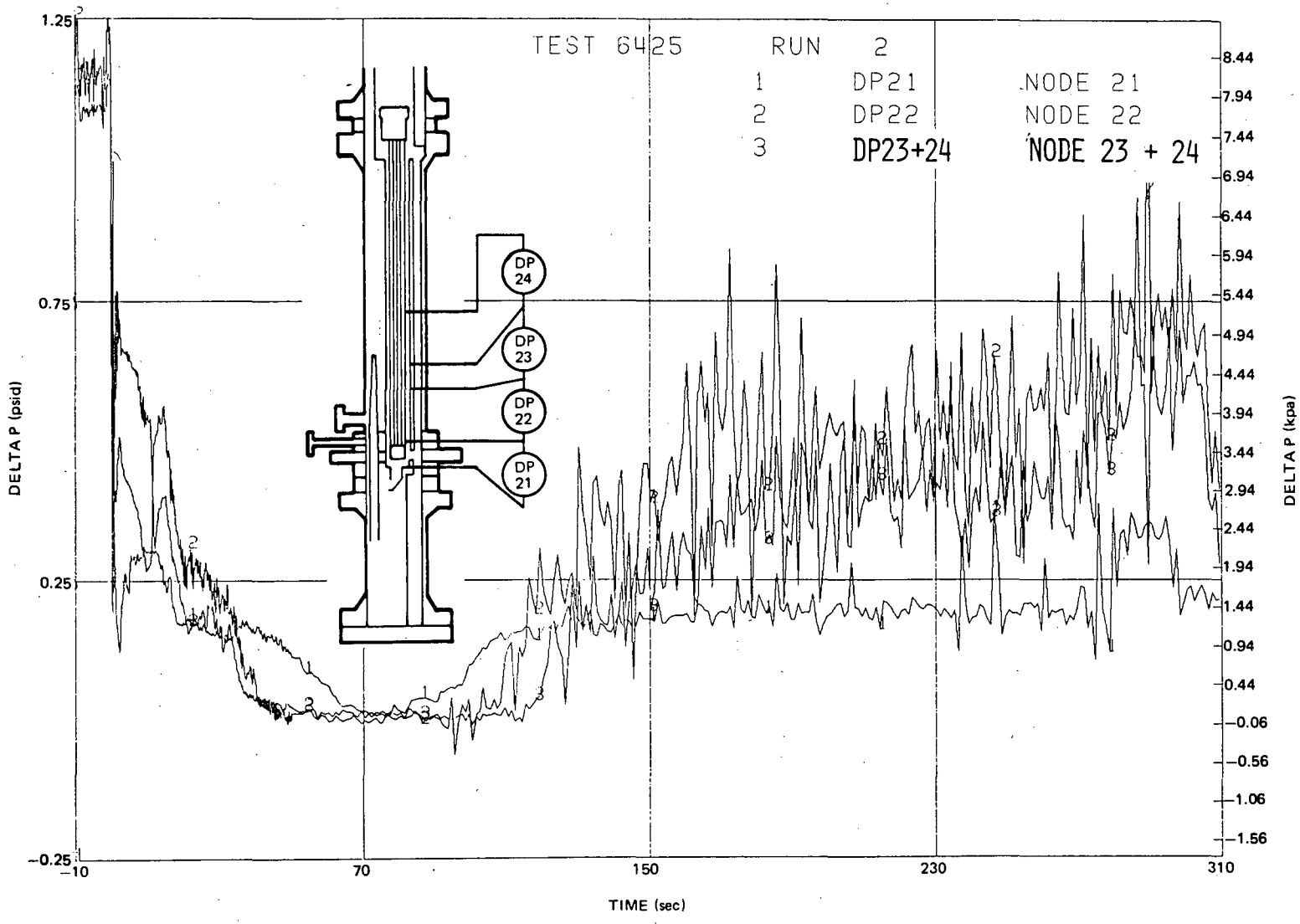

Figure J-12. Lower Bundle Differential Pressures

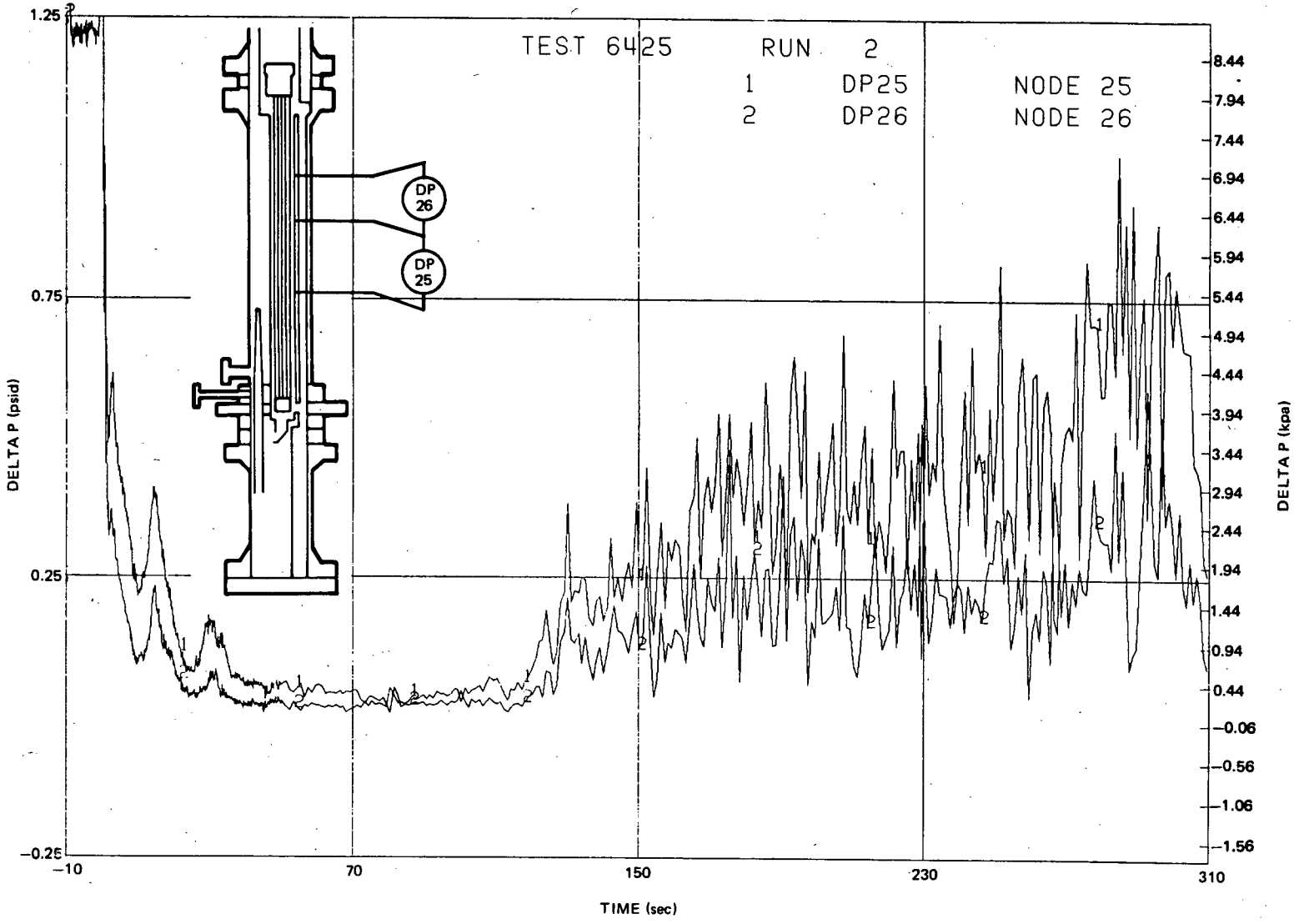

Figure J-13. Middle Bundle Differential Pressures

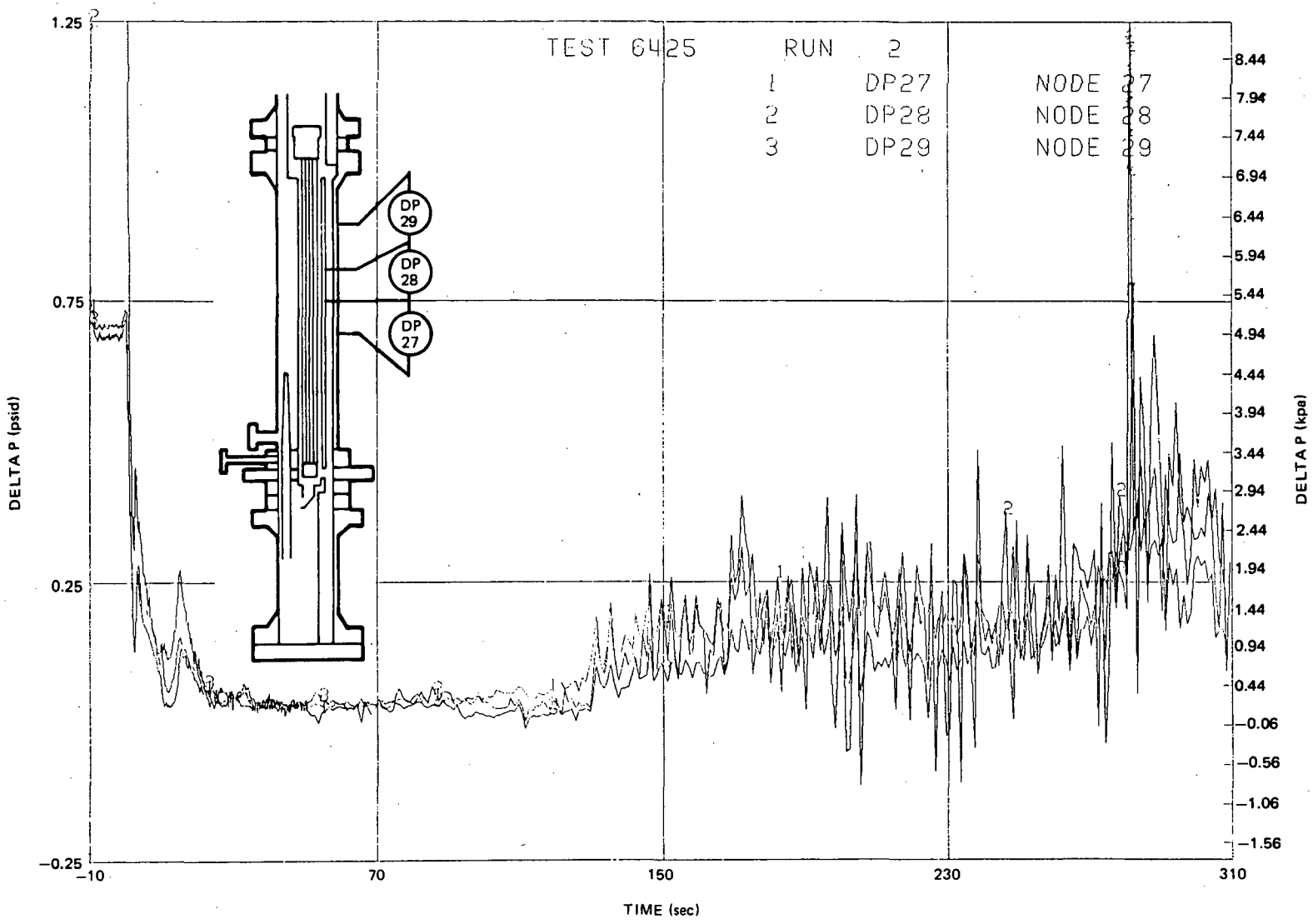

Figure J-14. Upper Bundle Differential Pressures

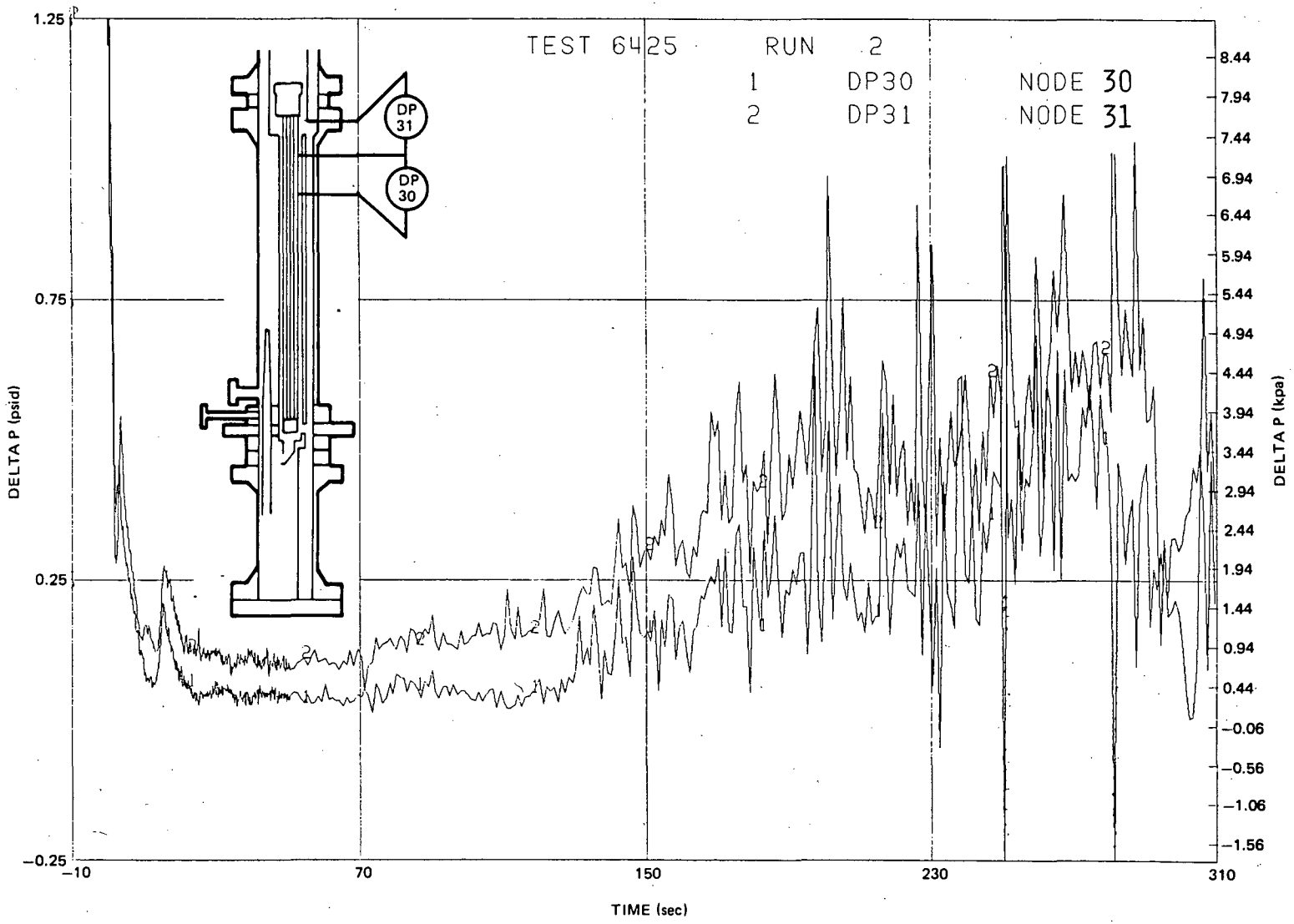

Figure J-15. Top Bundle Differential Pressures

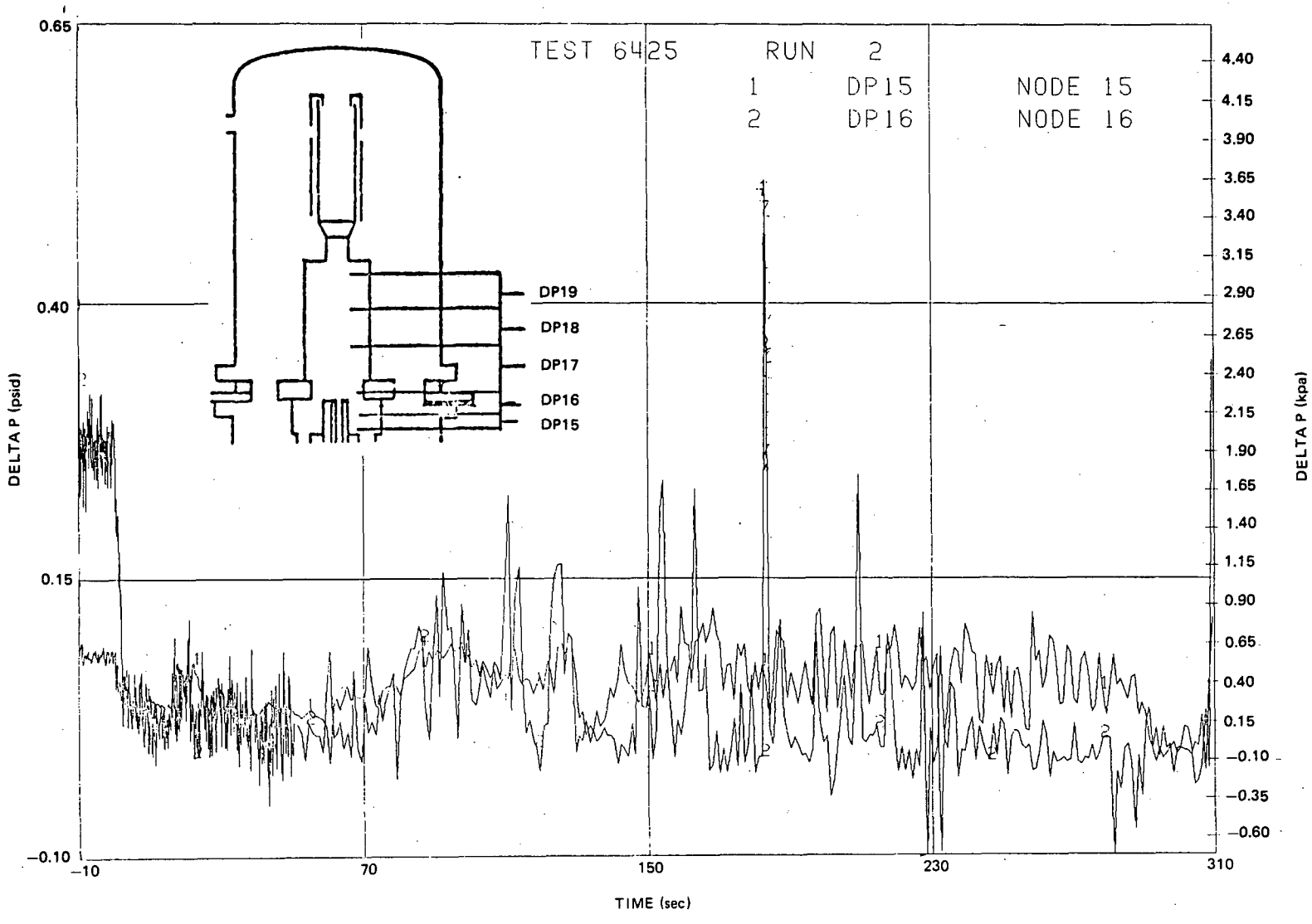

Figure J-16. Mixing Plenum Differential Pressures

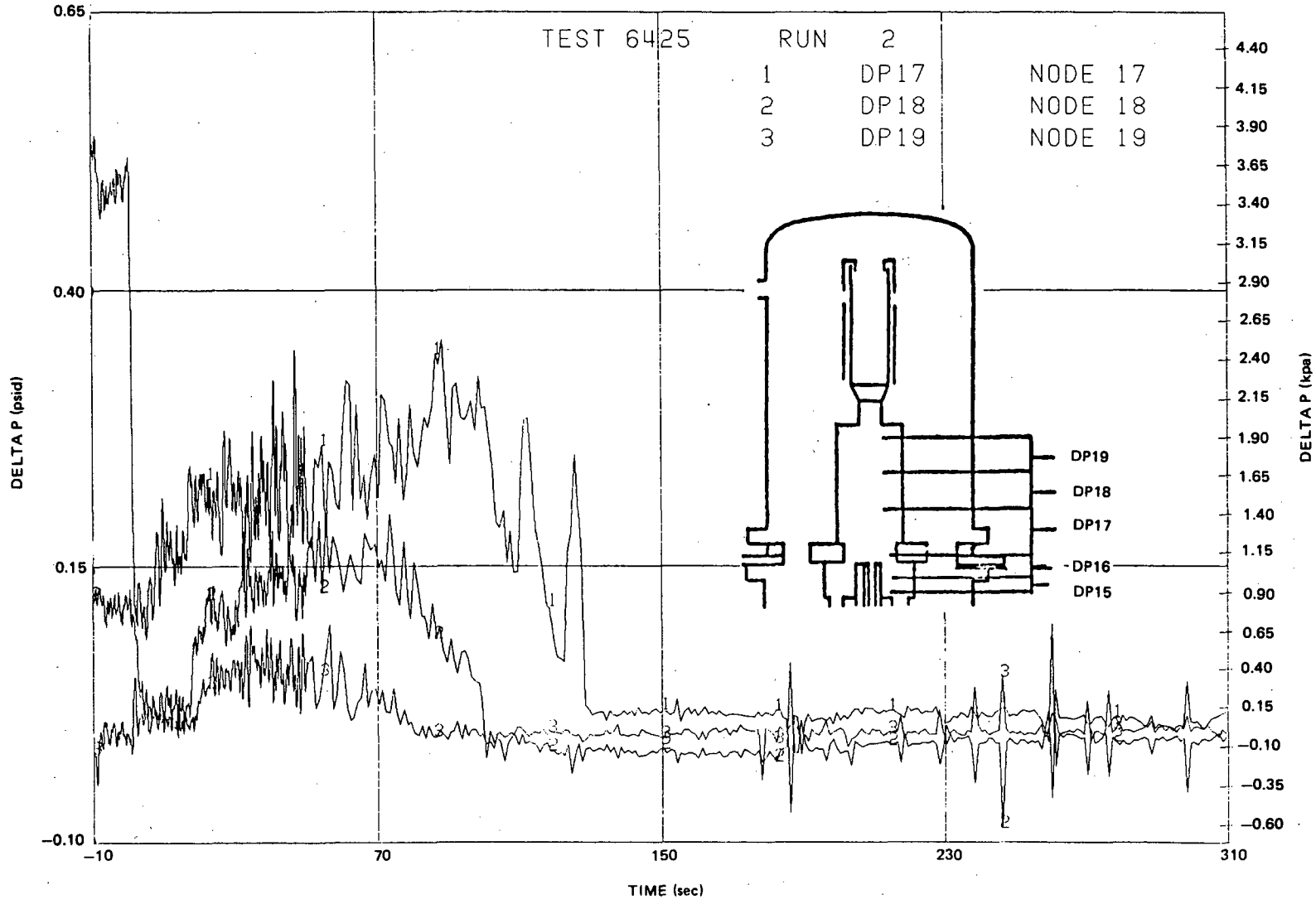

Figure J-17. Upper Plenum Differential Pressures

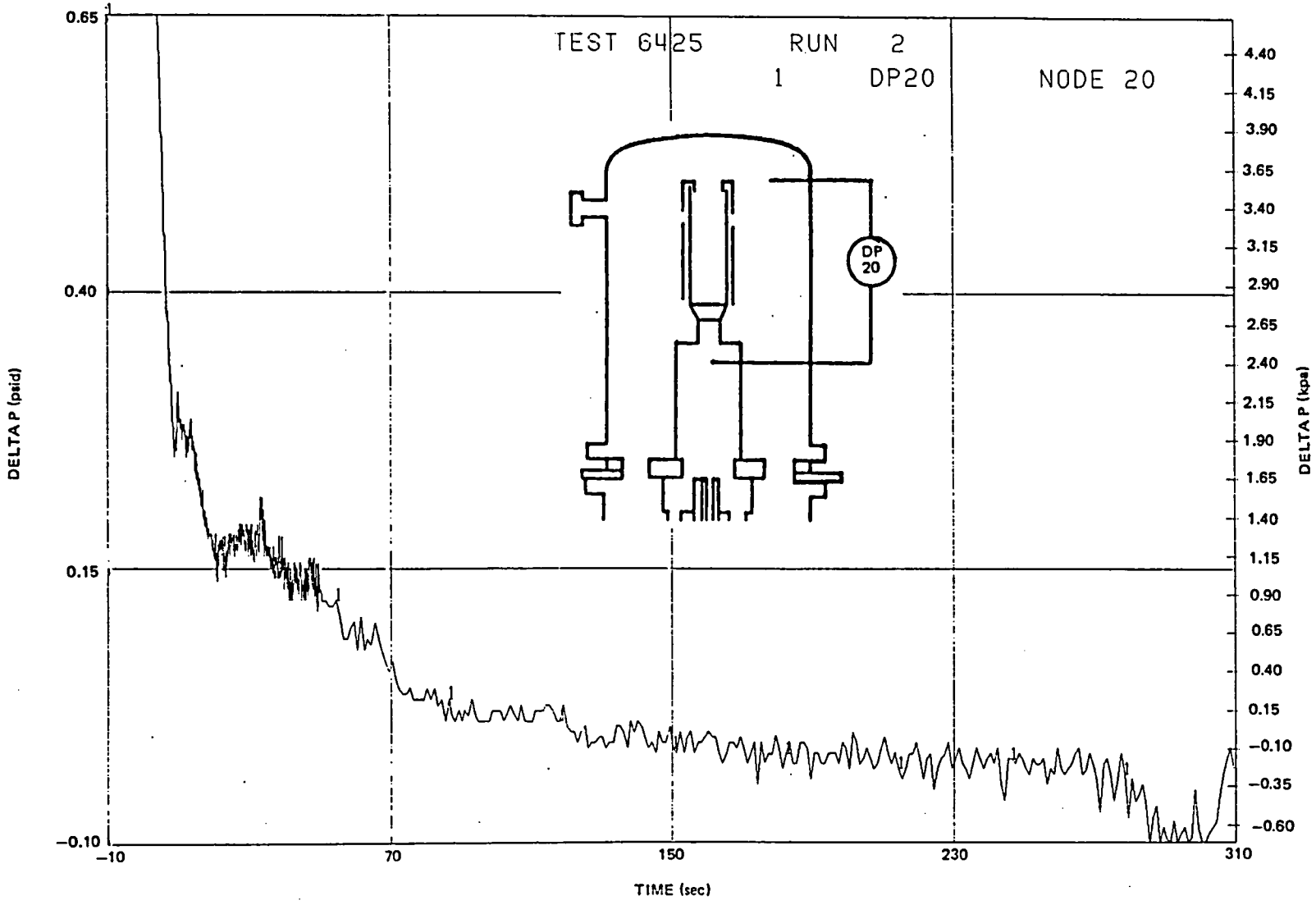

Figure J-18. Steam Separator Differential Pressure

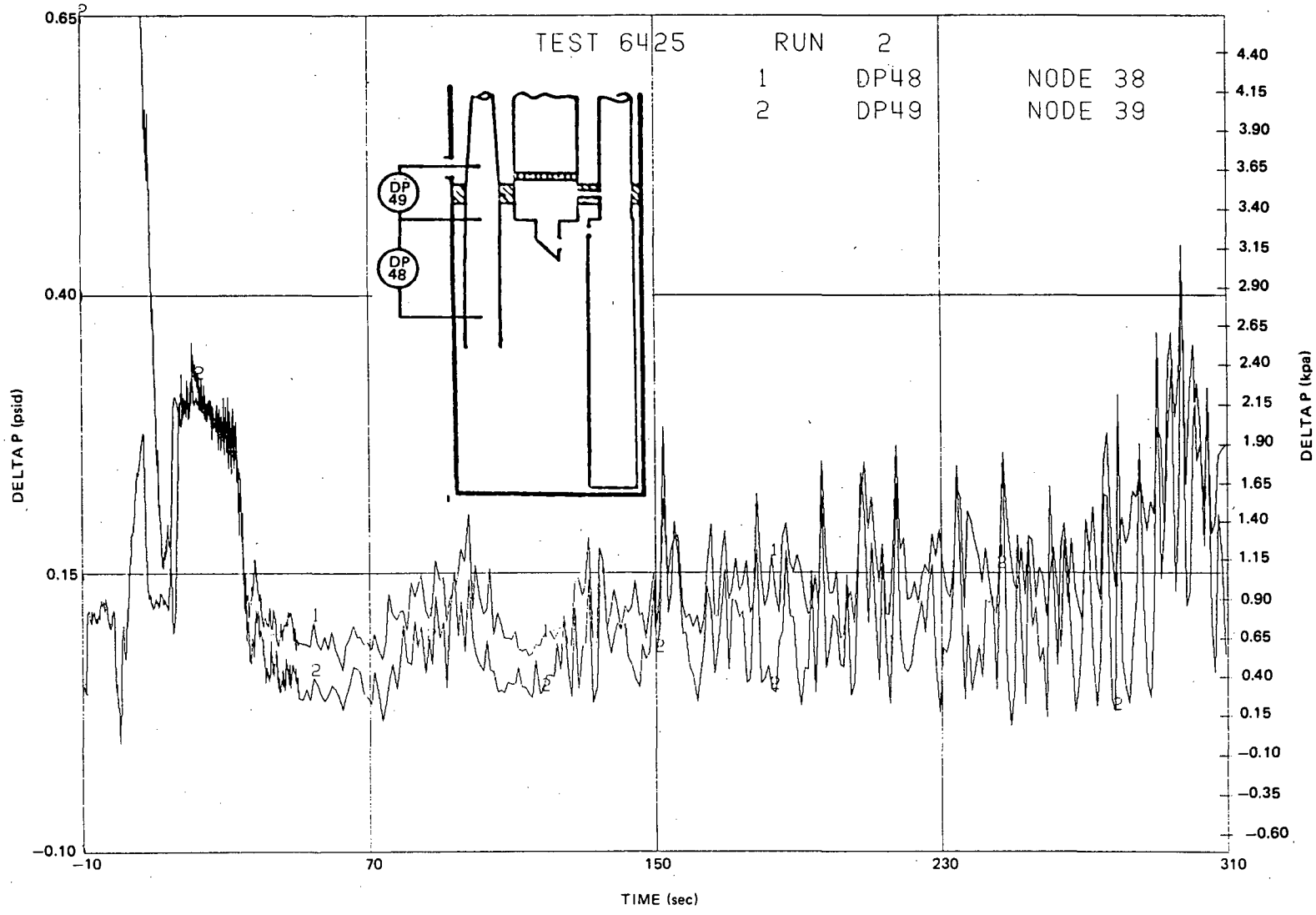

Figure J-19. Intact Loop Jet Pump Differential Pressures

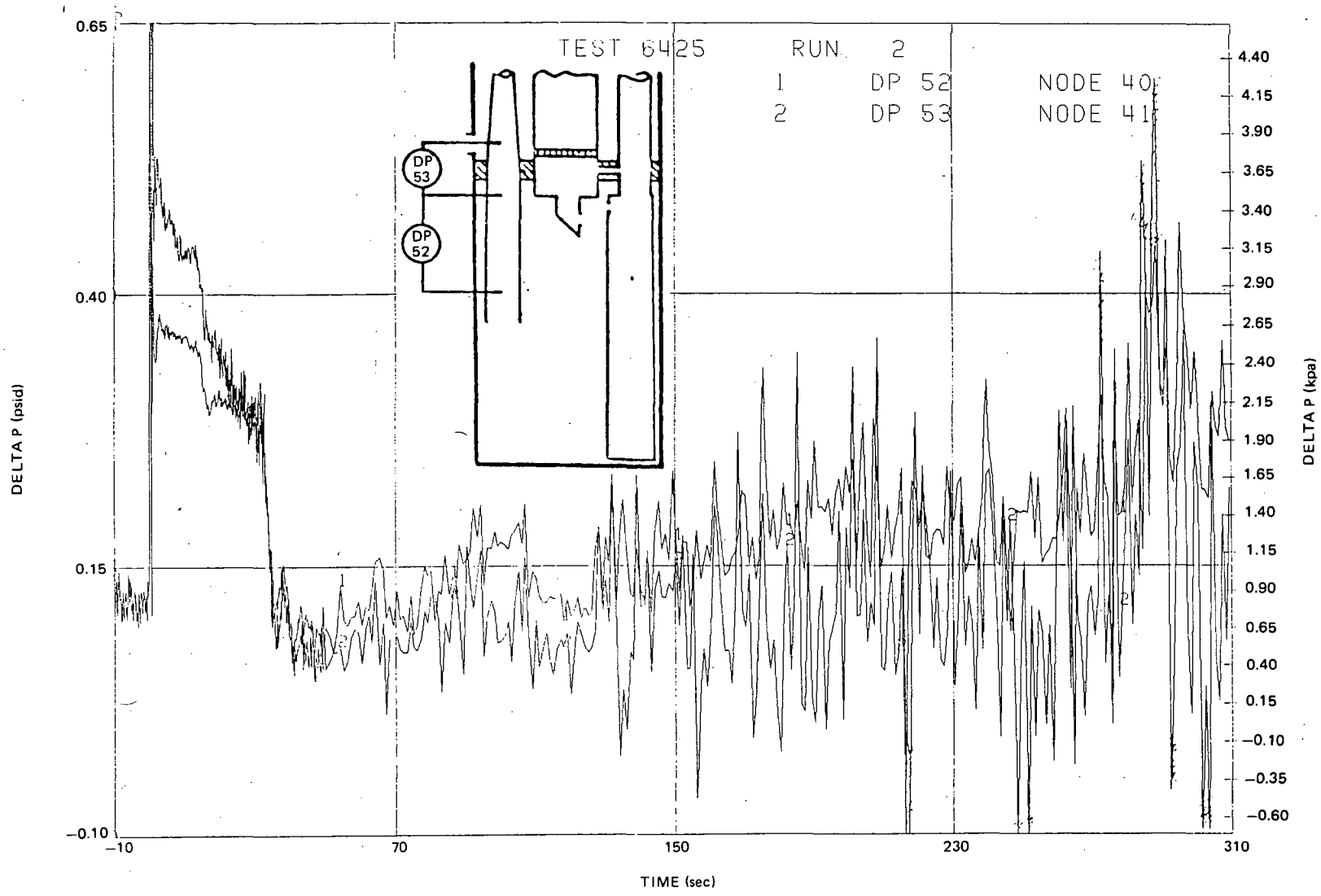

Figure J-20. Broken Loop Jet Pump Differential Pressures

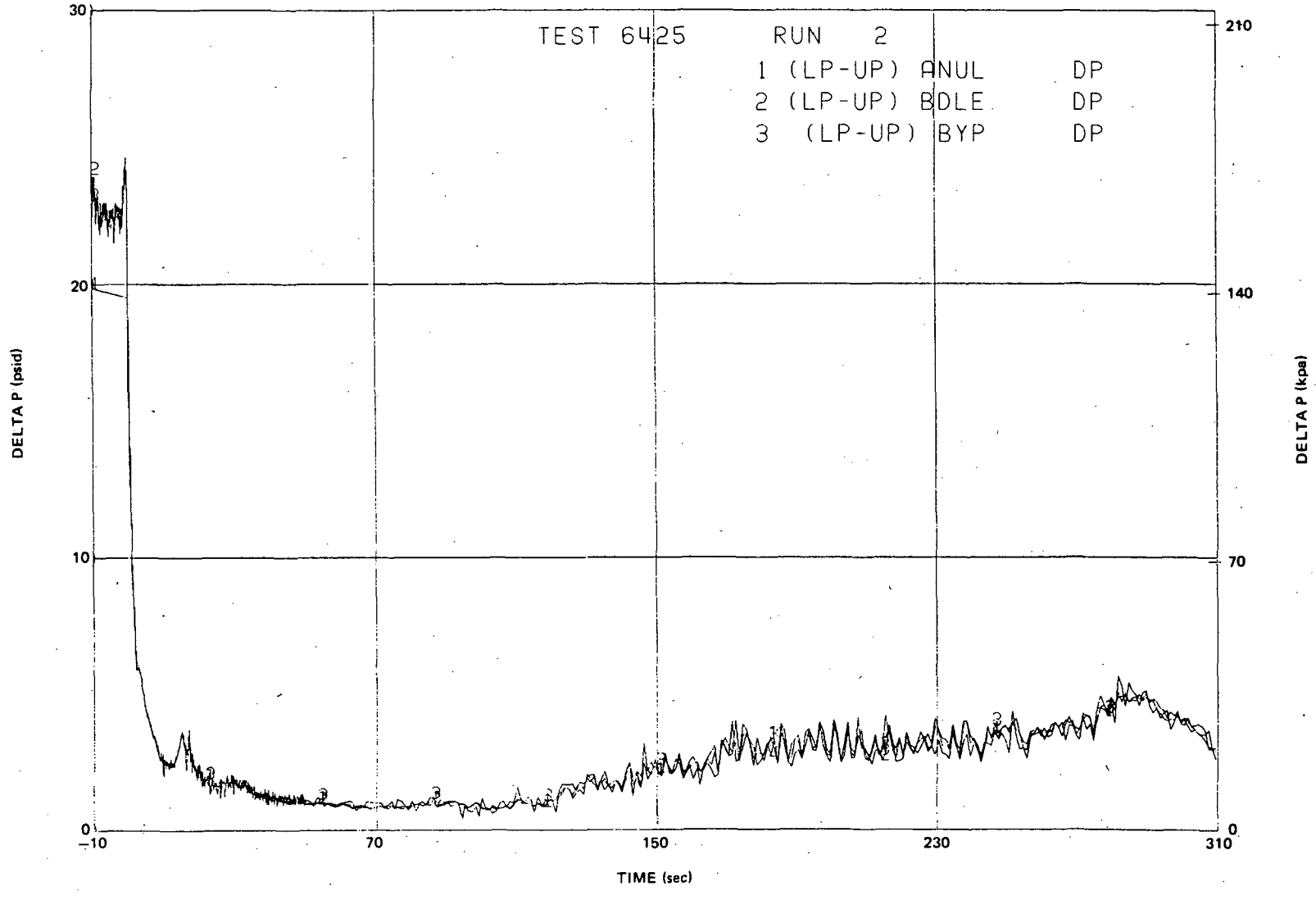

Figure J-21. Lower Plenum to Upper Plenum Differential Pressures for the Annulus, Bundle, and Bypass

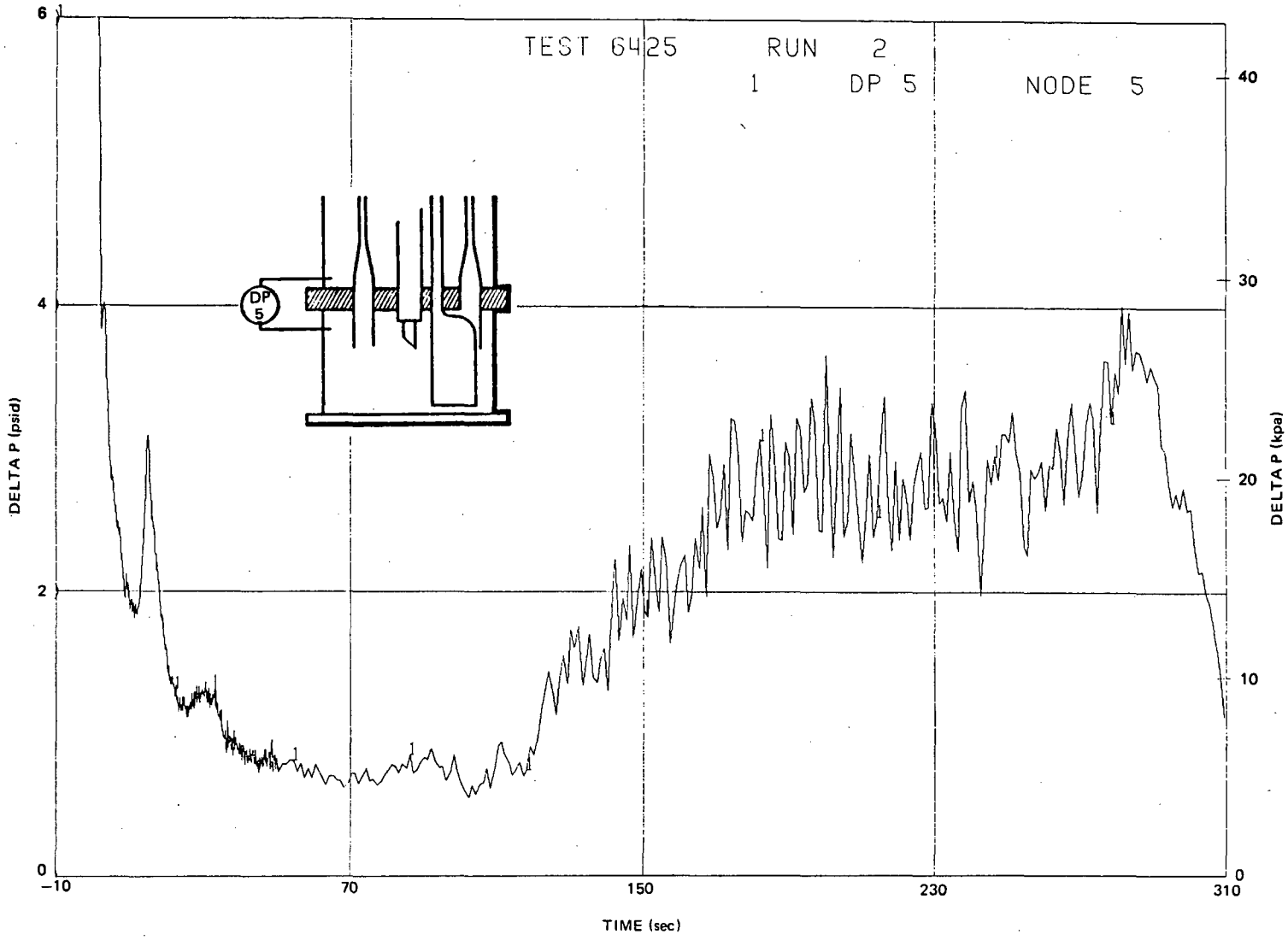

Figure J-22. Lower Plenum to Annulus Differential Pressure

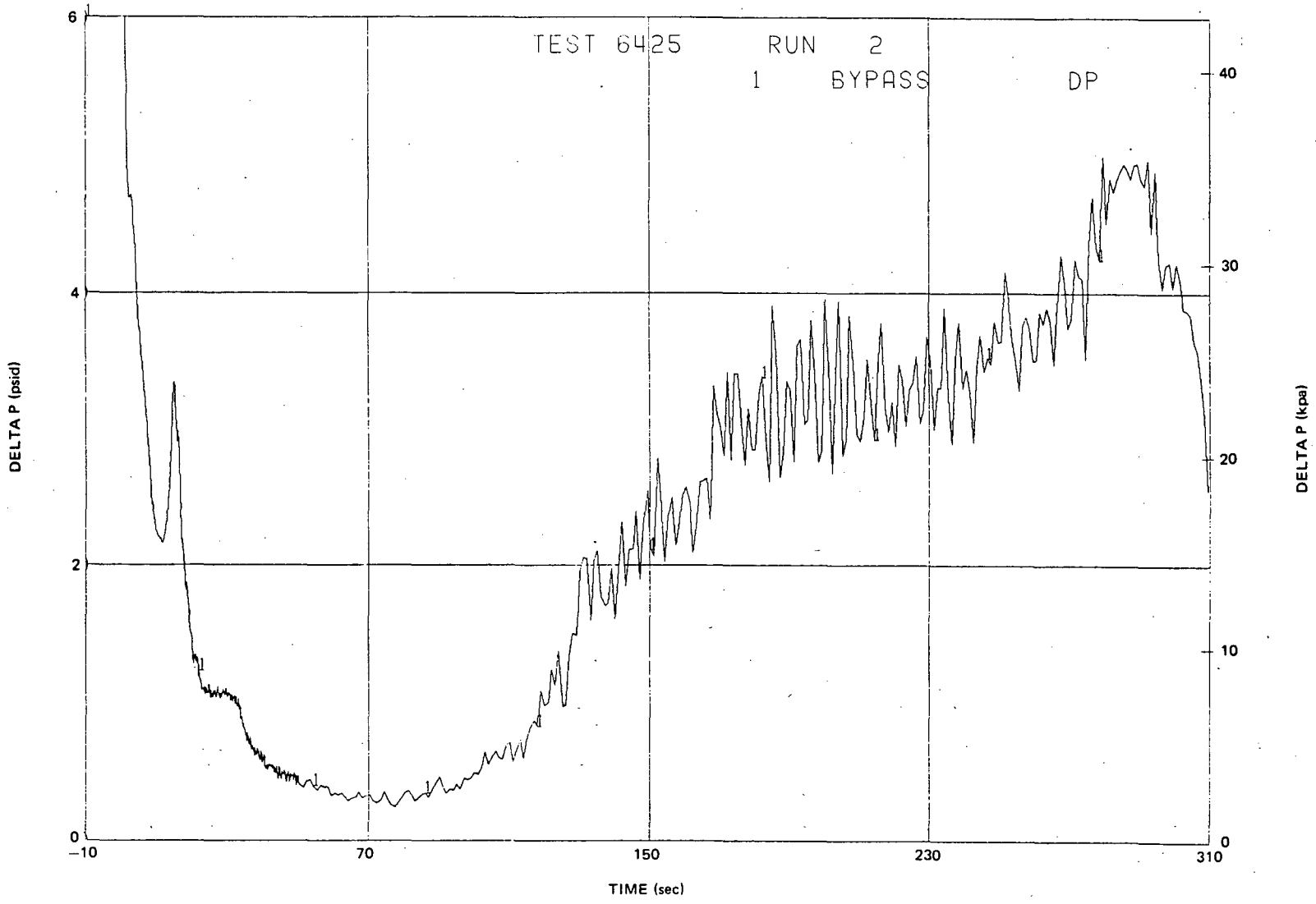

Figure J-23. Bypass Differential Pressure

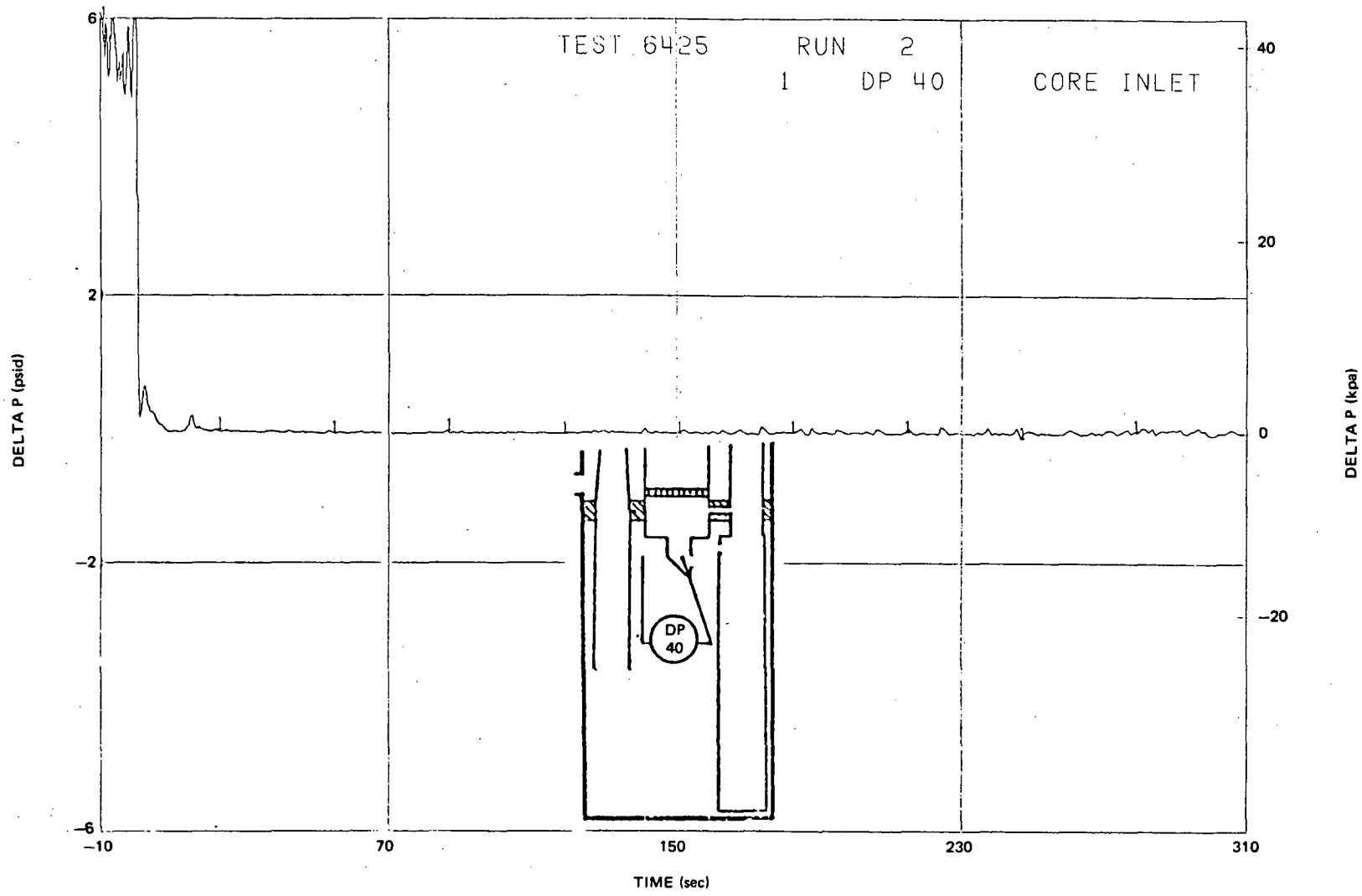

Figure J-24. Bundle Inlet Side Entry Orifice Differential Pressure

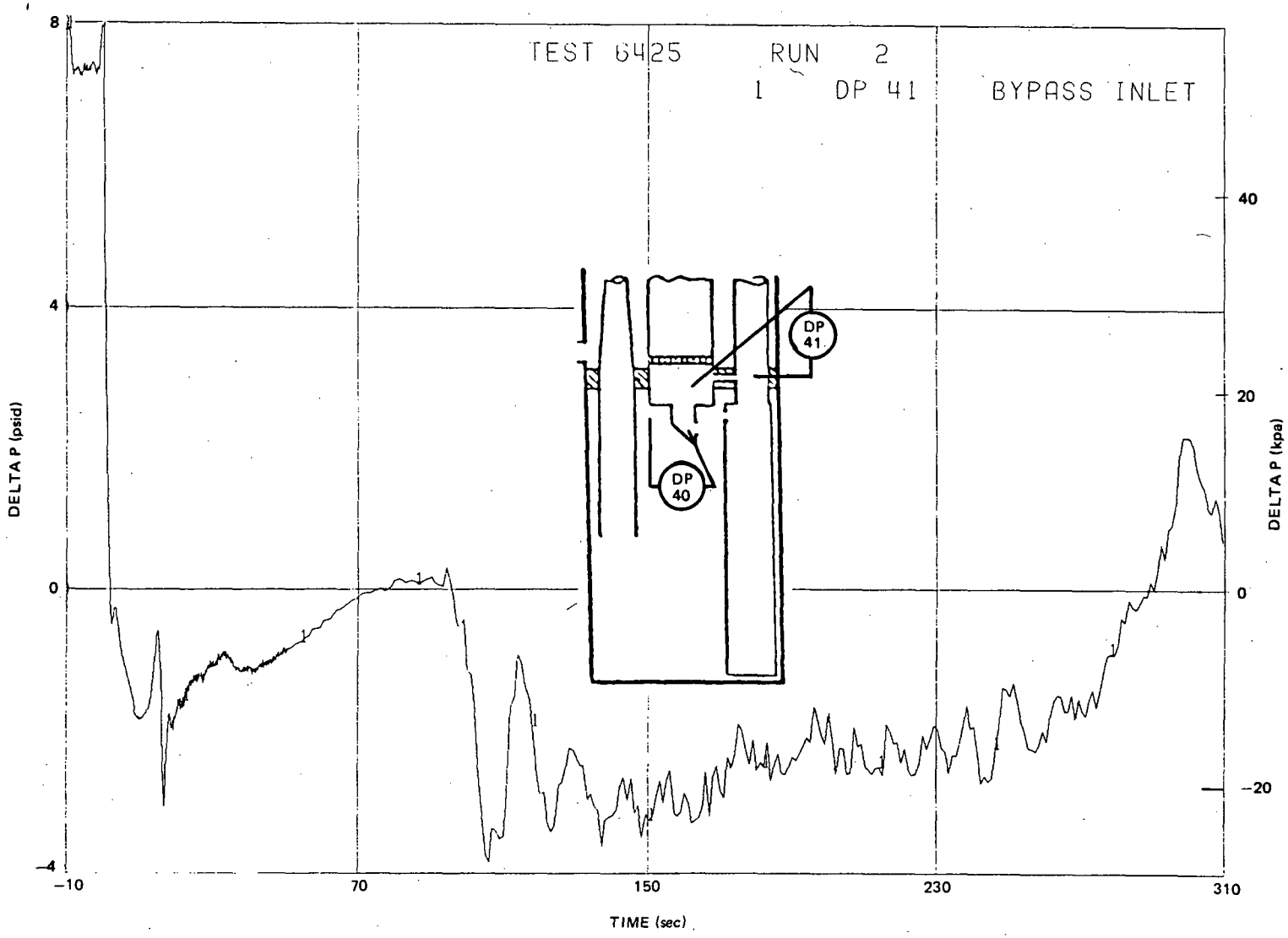

Figure J-25. Bypass Leakage Path Differential Pressure

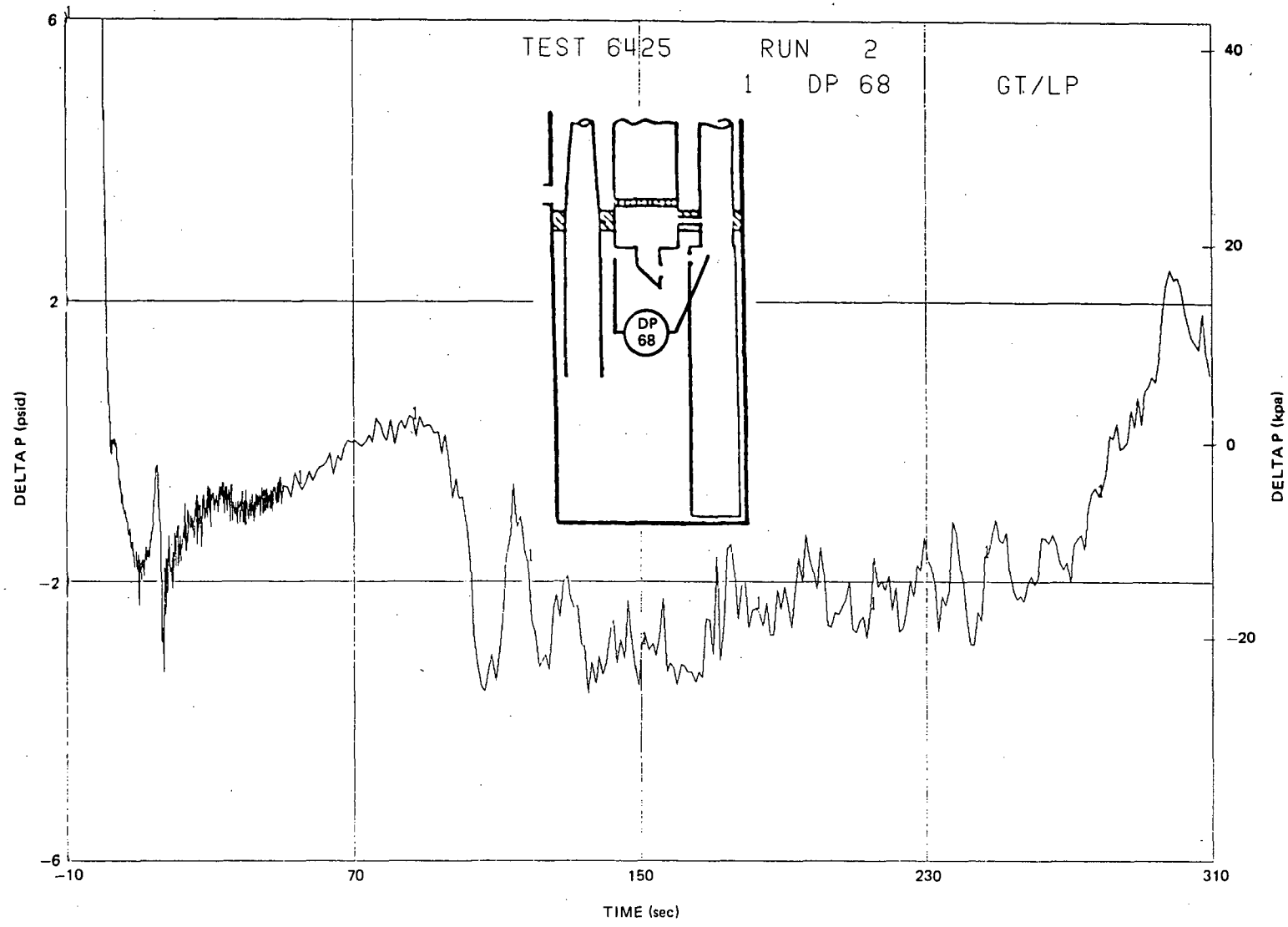

Figure J-26. Lower Plenum to Guide Tube Differential Pressure

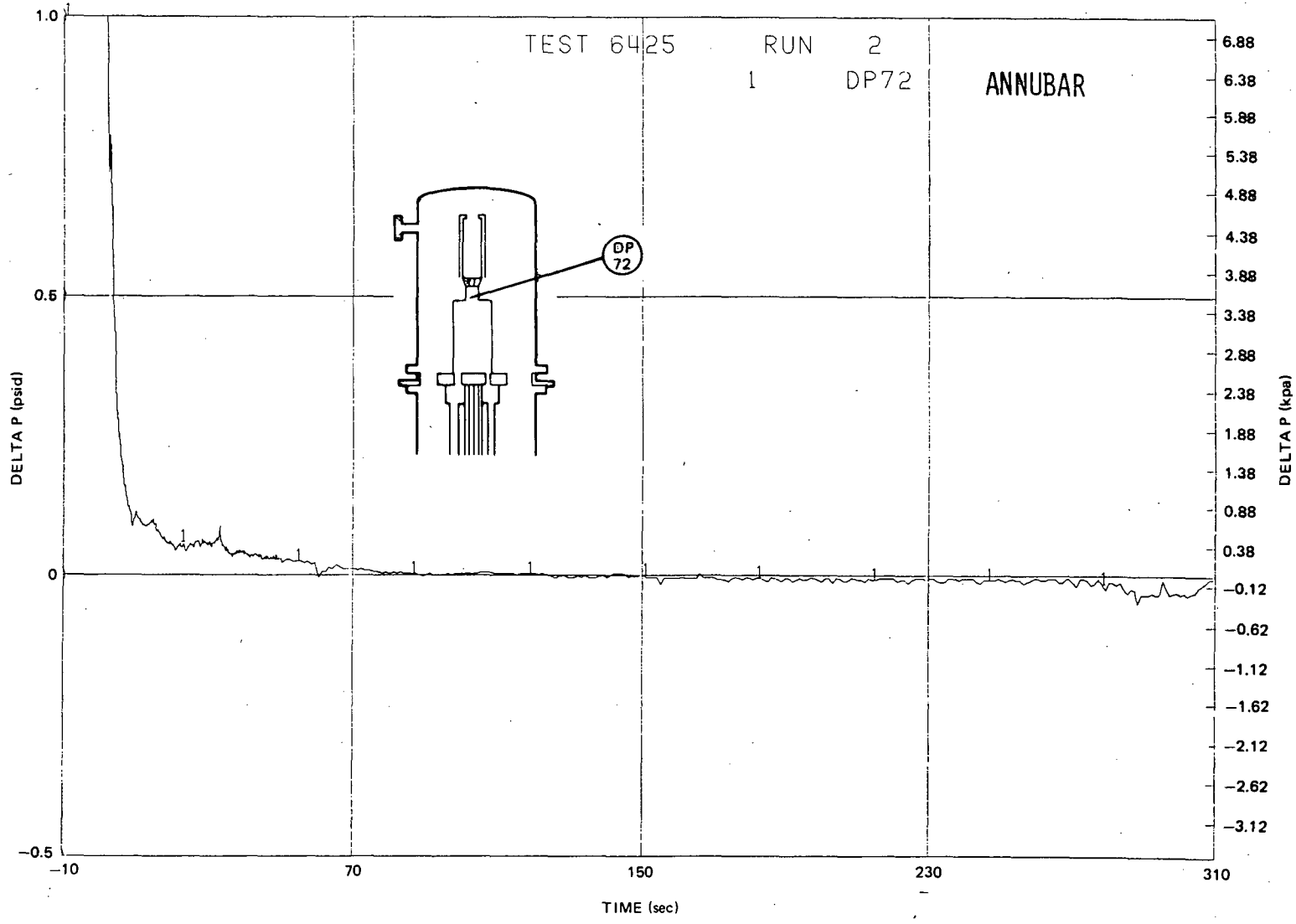

Figure J-27. Upper Plenum Exit Differential Pressure

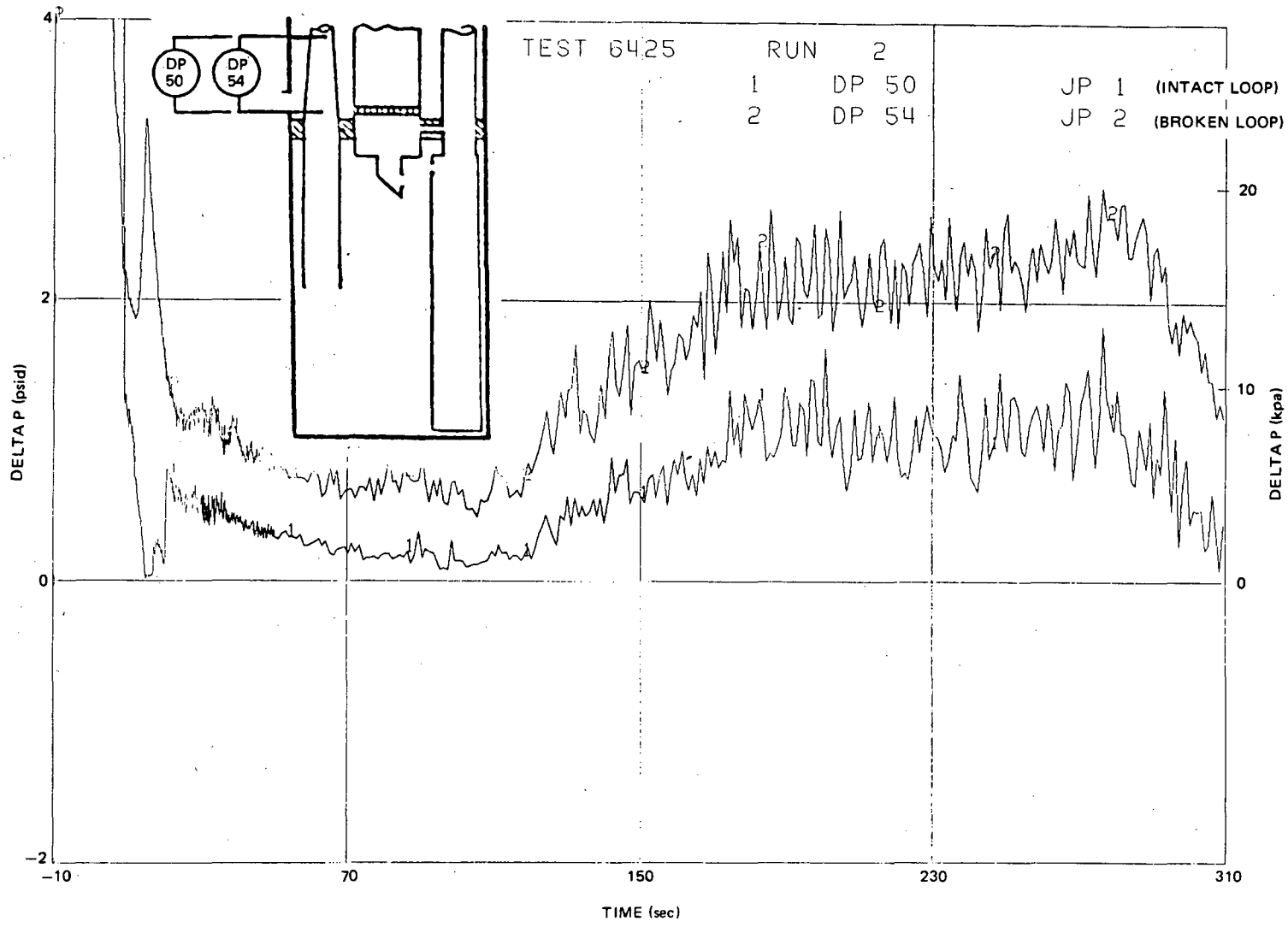

Figure J-28. Intact Loop and Broken Loop Jet Pump Diffuser to Throat Differential Pressures

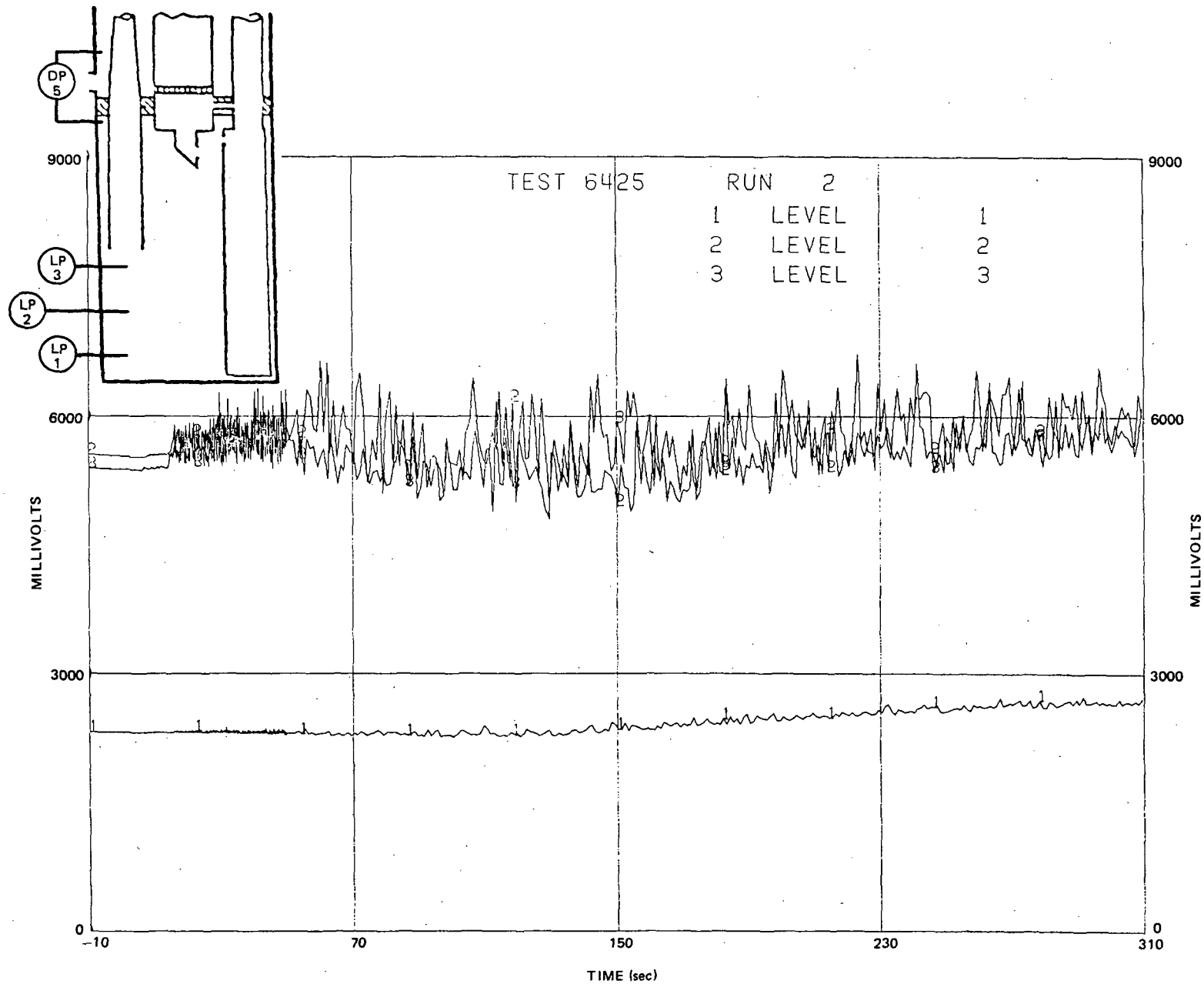

Figure J-29. Bottom Lower Plenum Conductivity Probe Measurements

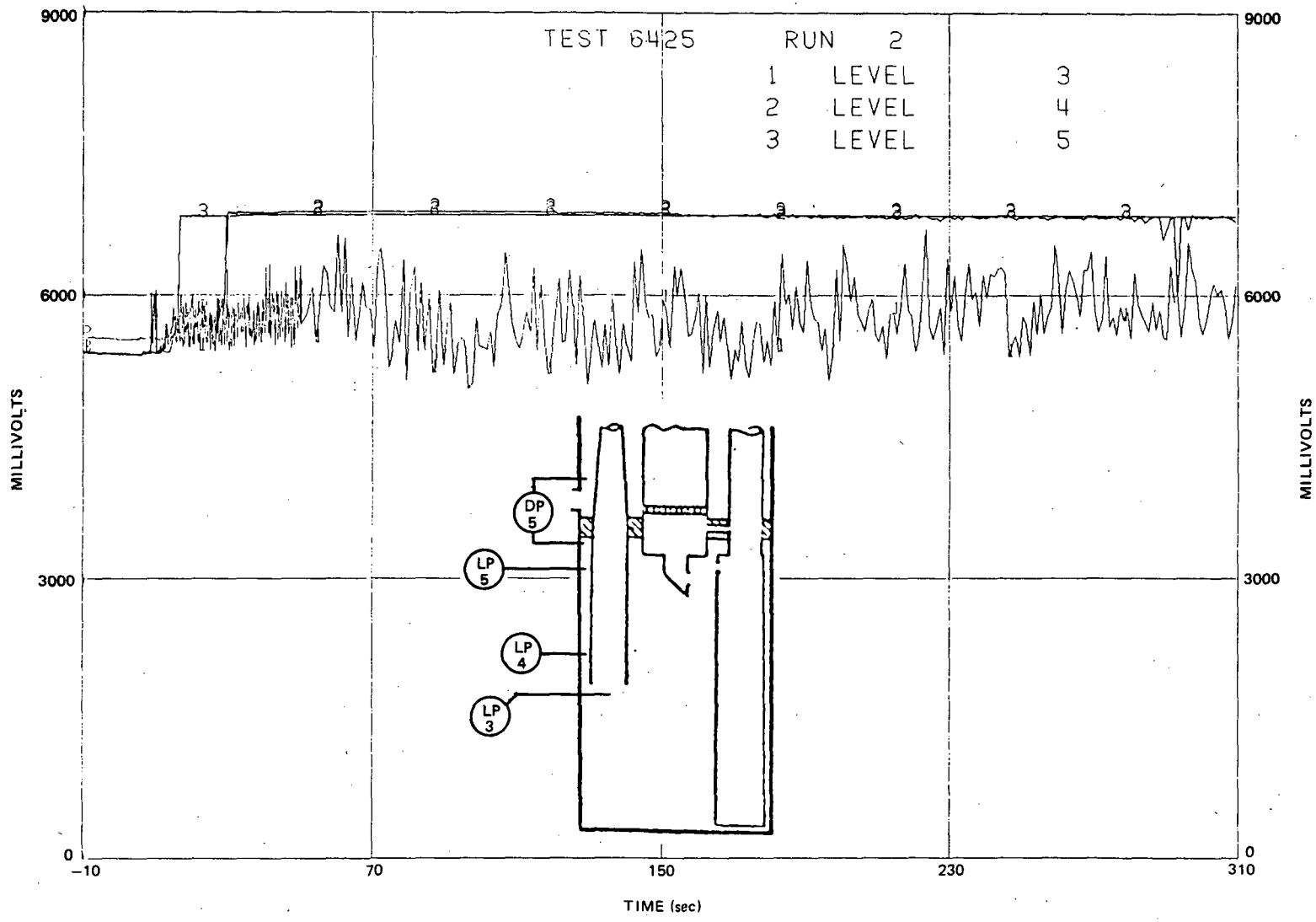

Figure J-30. Upper Lower Plenum Conductivity Probe Measurements

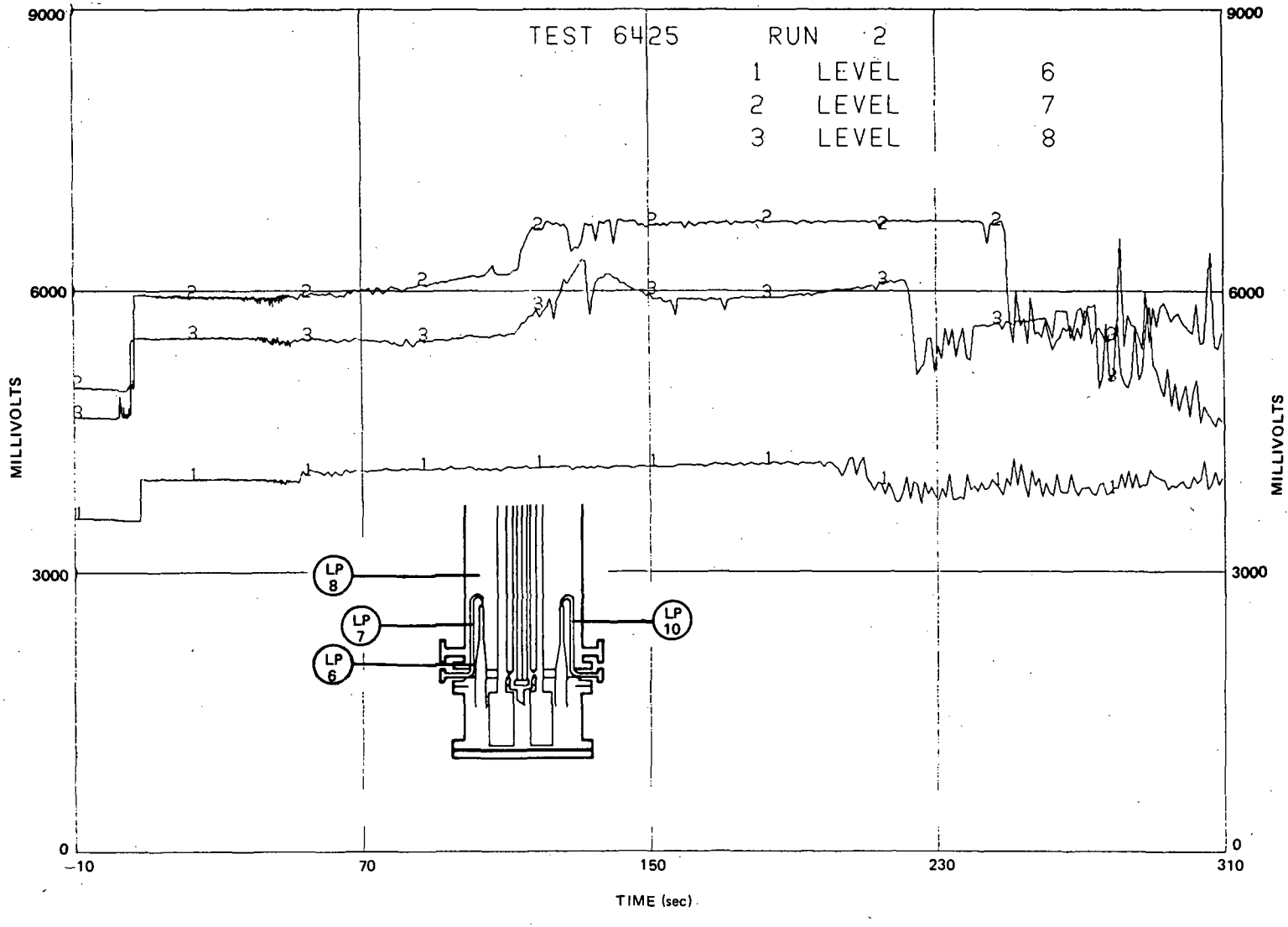

Figure J-31. Lower Annulus Conductivity Probe Measurements

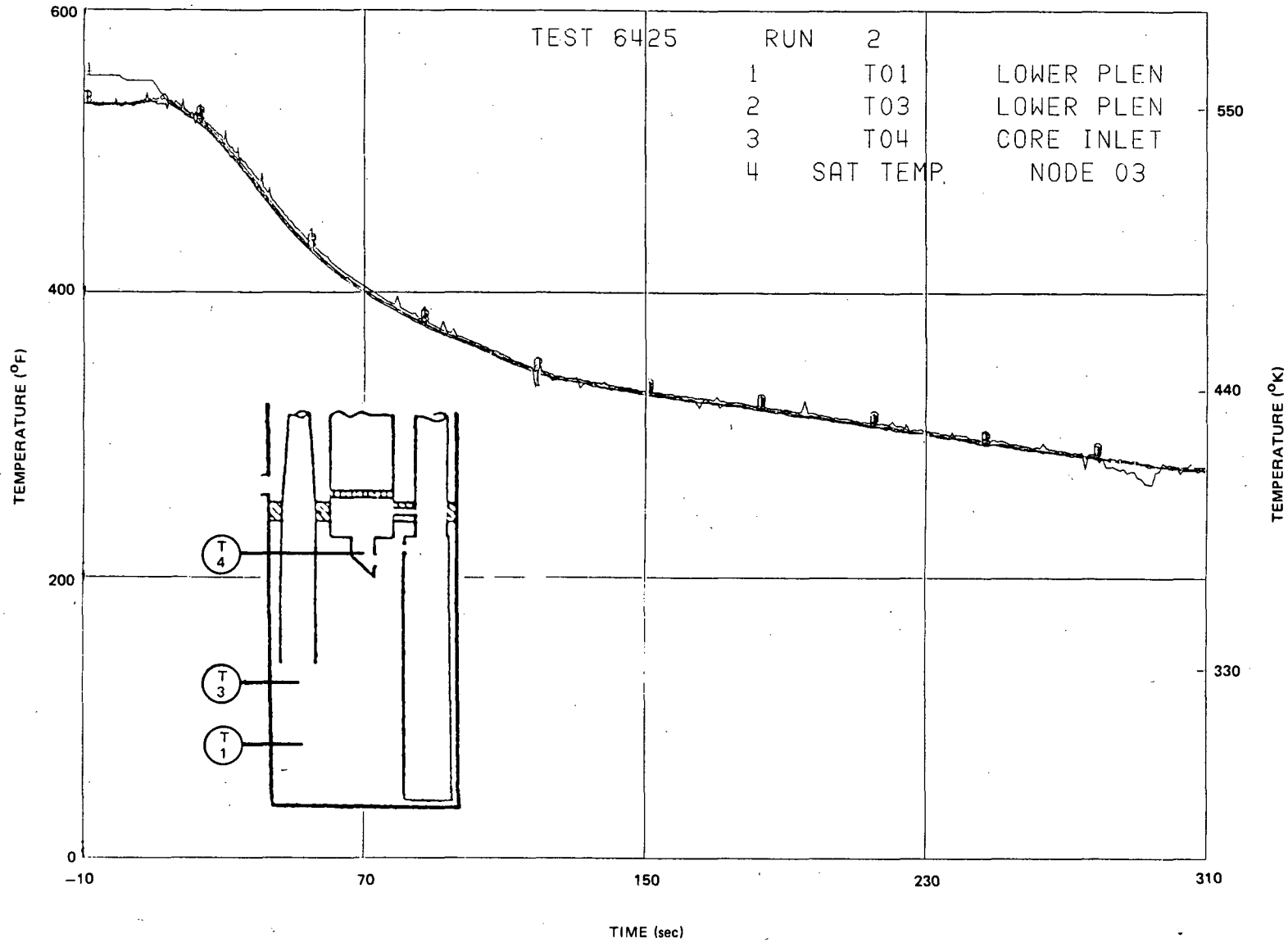

Figure J-32. Lower Plenum Fluid Temperatures

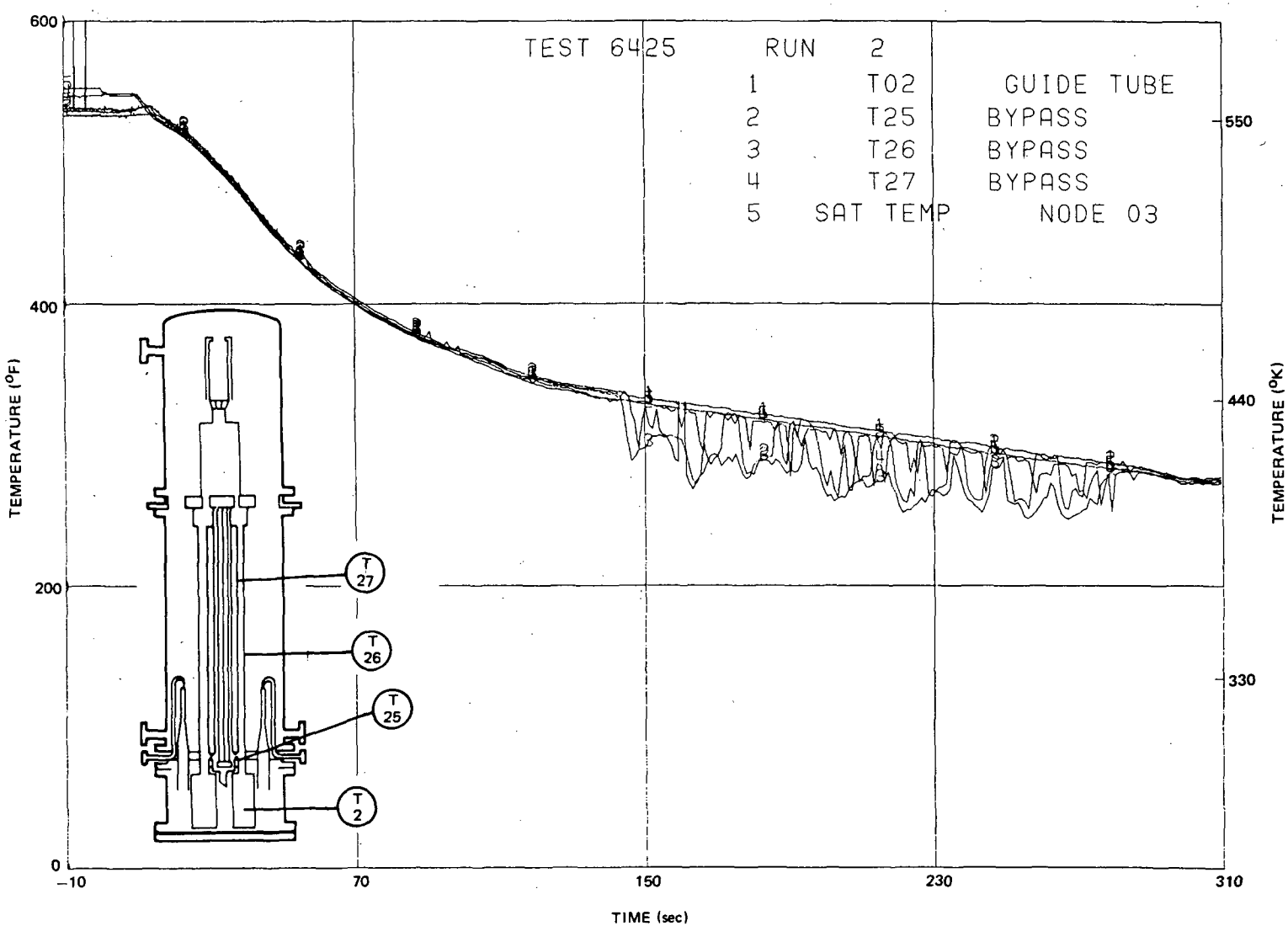

Figure J-33. Guide Tube and Bypass Fluid Temperatures

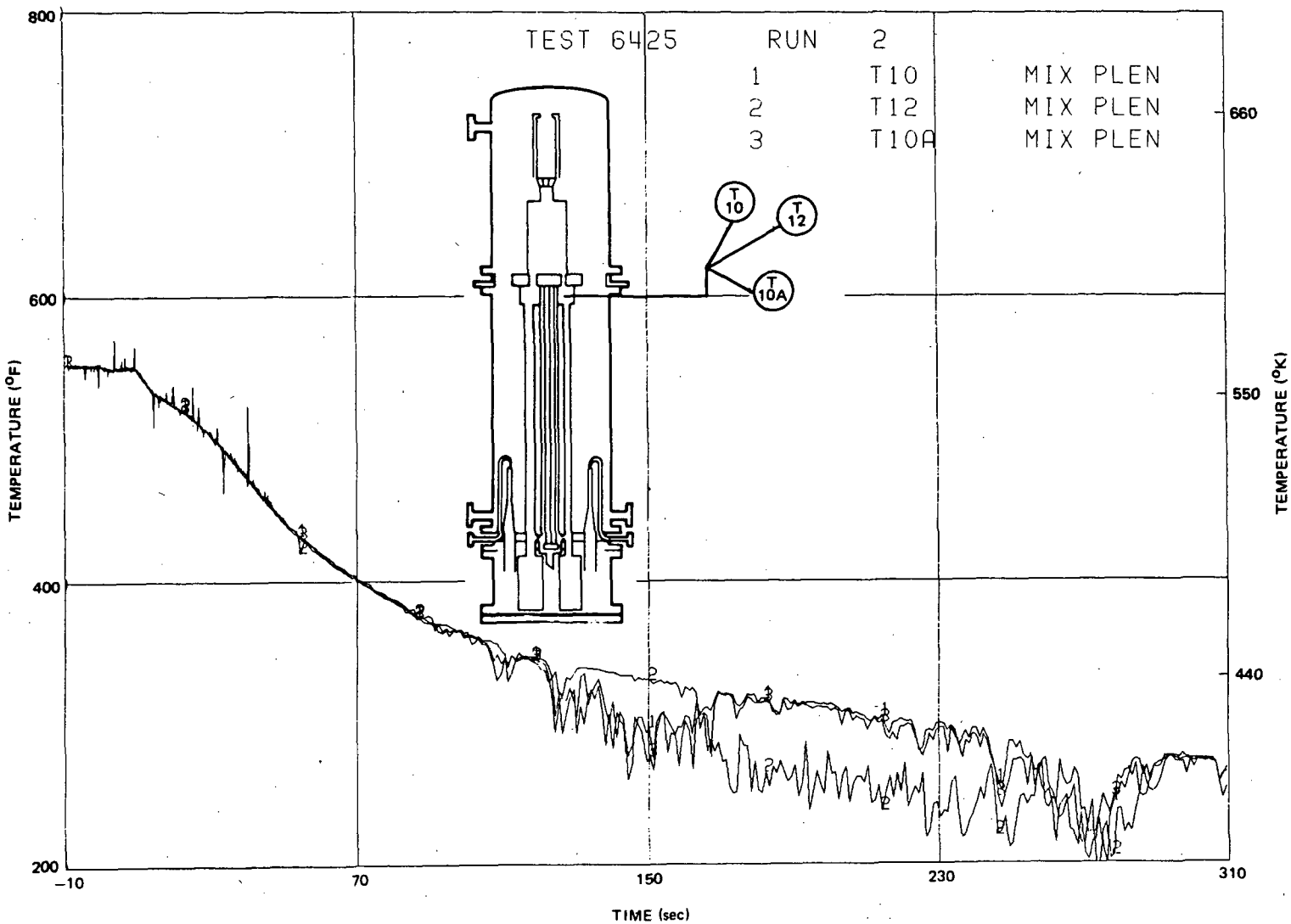

Figure J-34. Mixing Plenum Fluid Temperatures

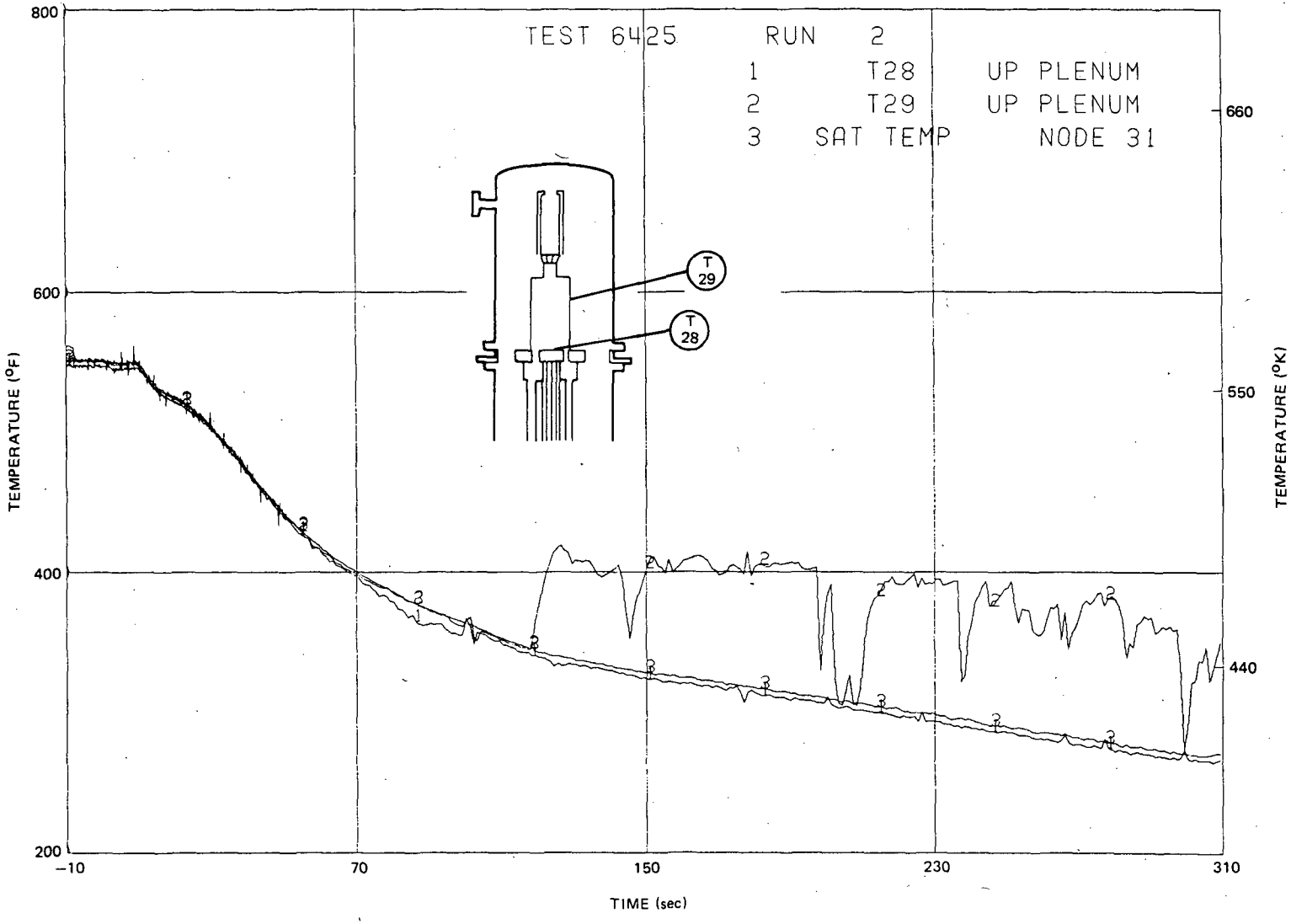

Figure J-35. Upper Plenum Fluid Temperatures

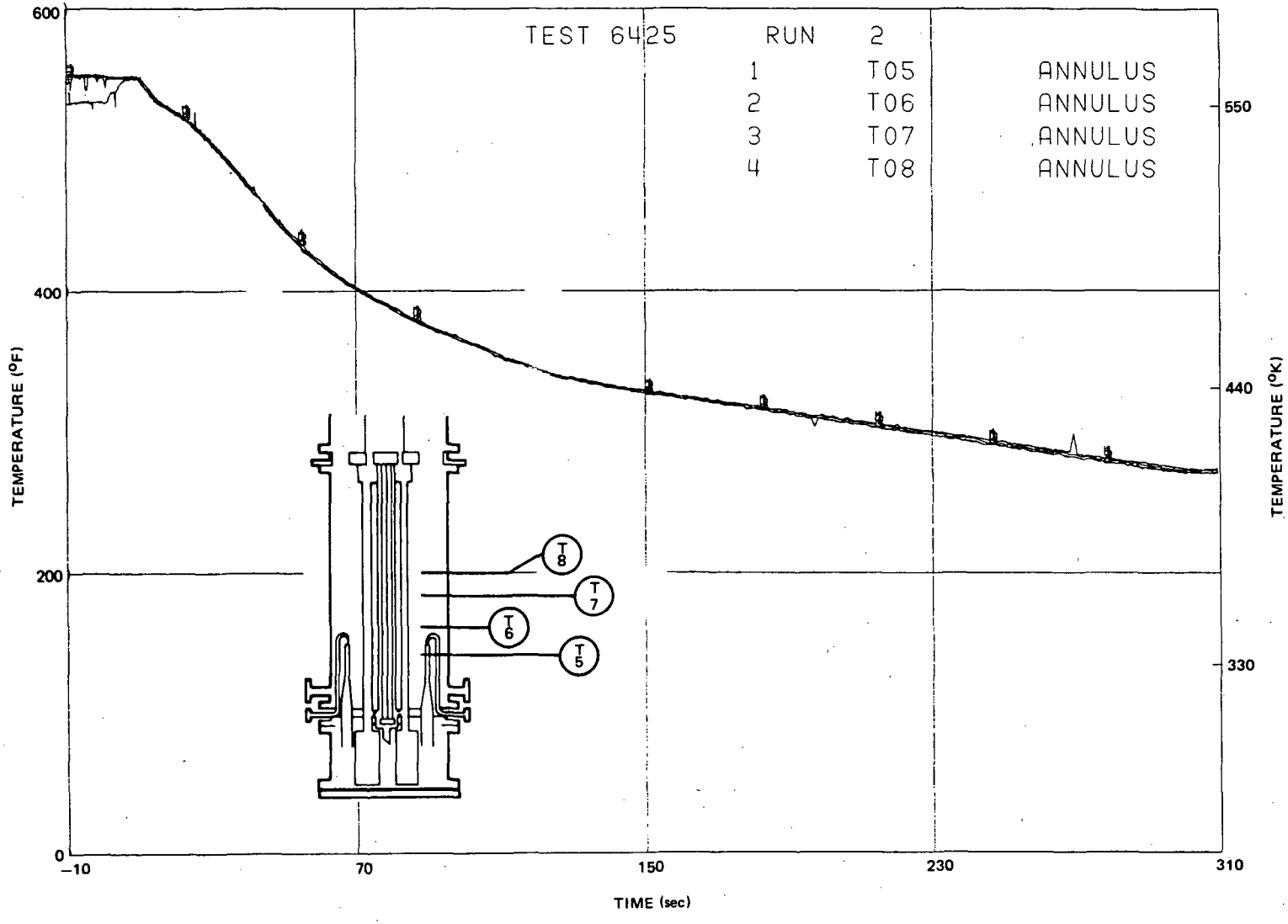

Figure J-36. Annulus Fluid Temperatures

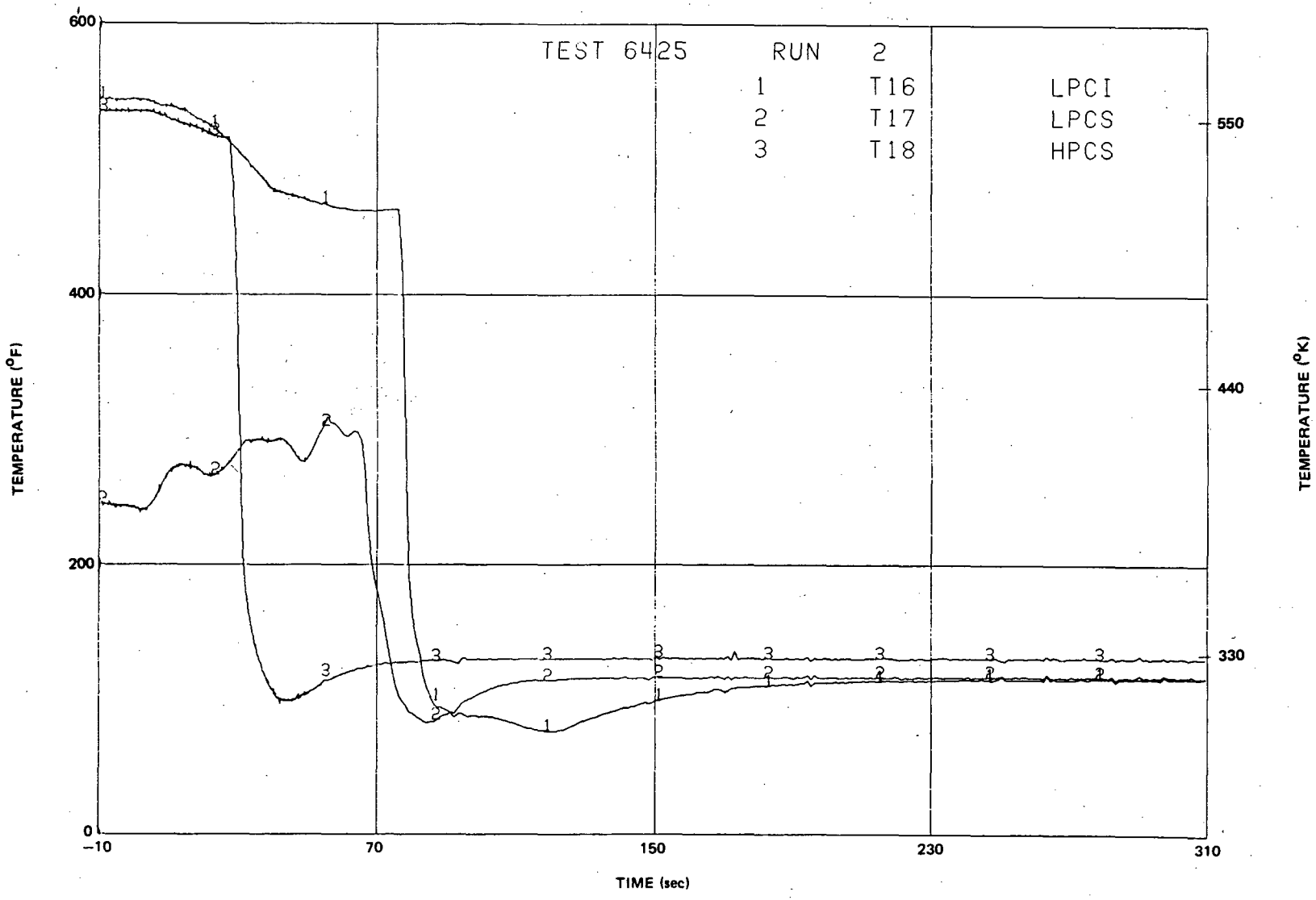

Figure J-37. ECC Fluid Temperatures

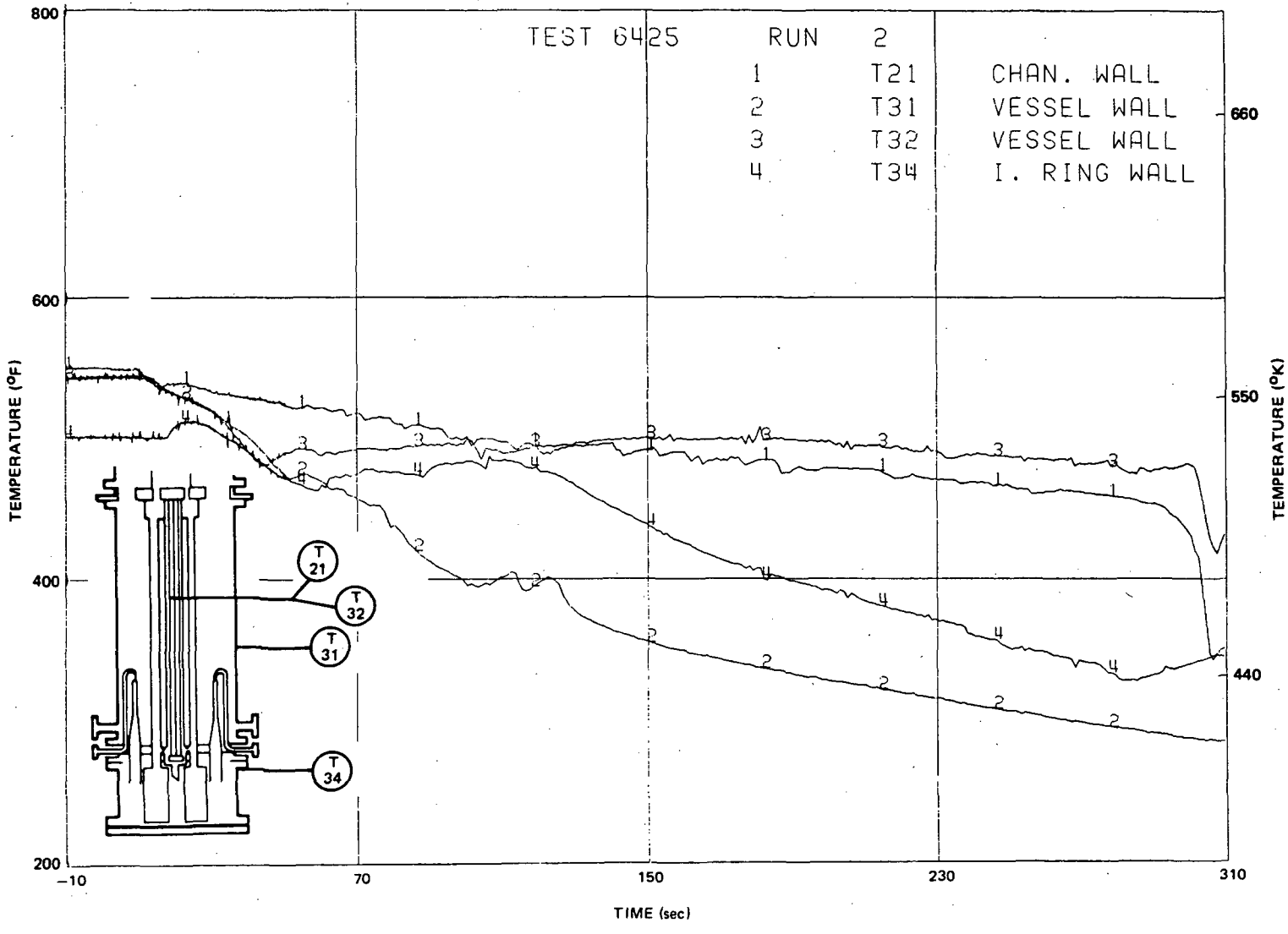

Figure J-38. Wall Temperatures

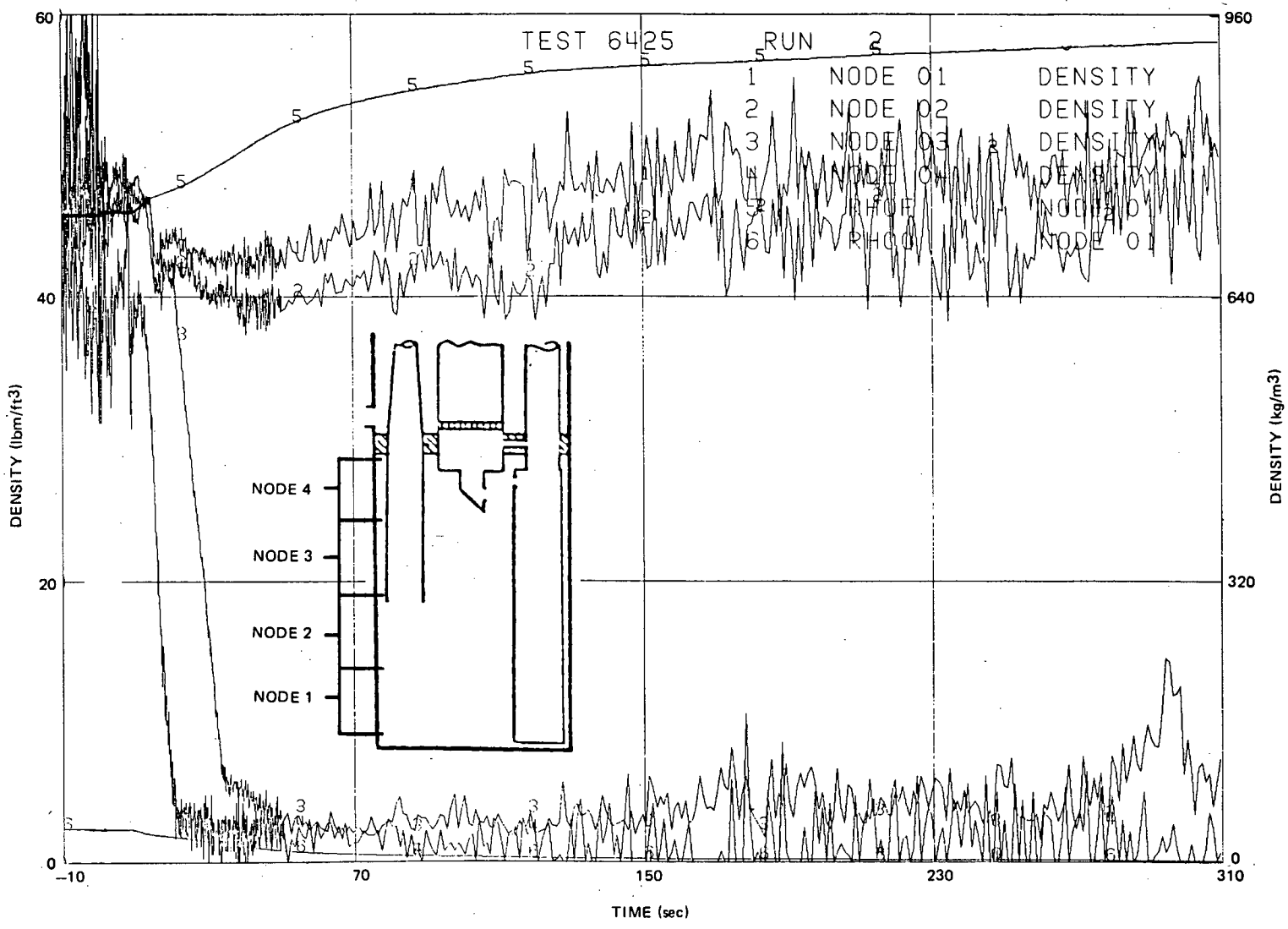

Figure J-39. Lower Plenum Nodal Densities

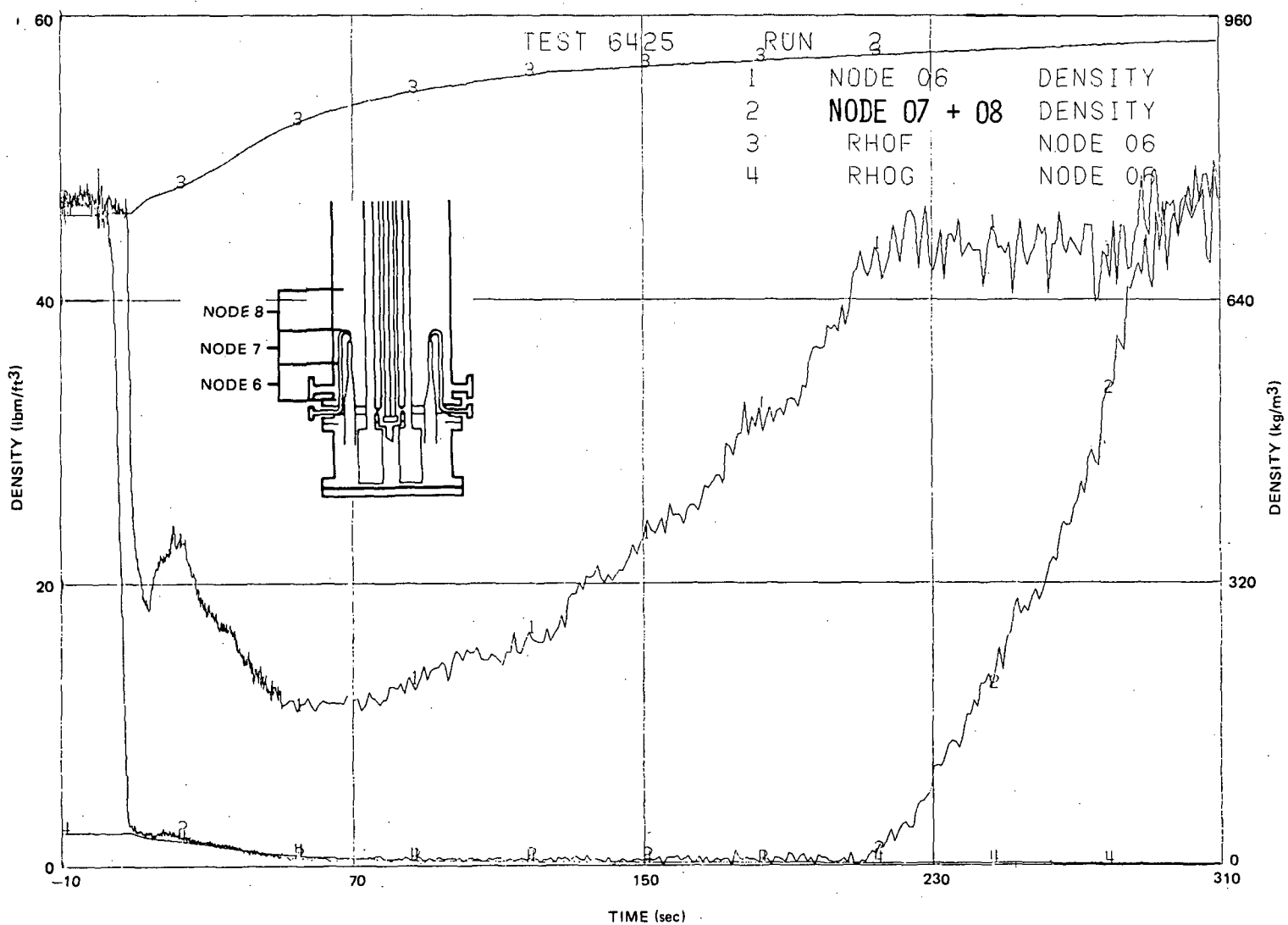

Figure J-40. Annulus Nodal Densities

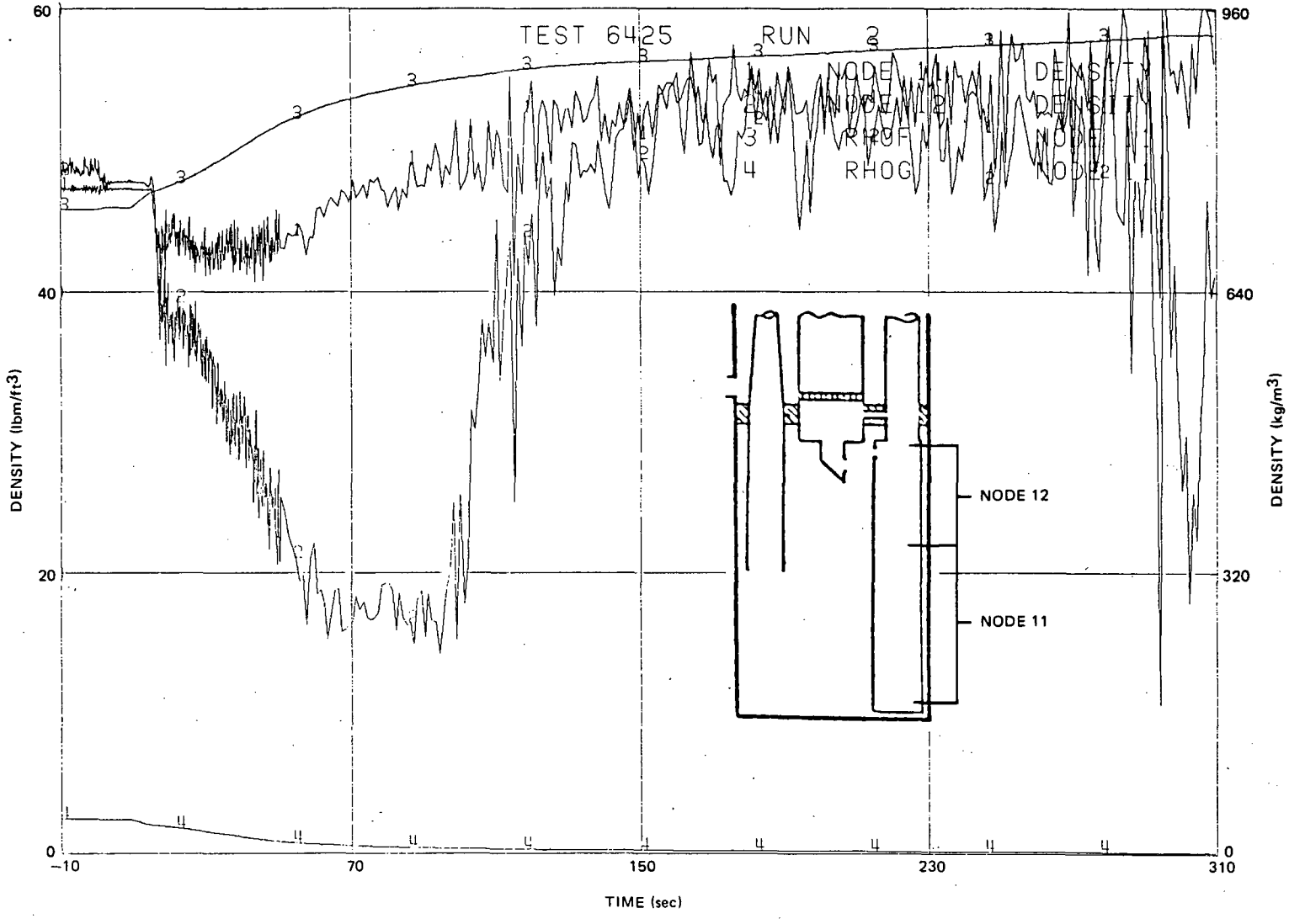

Figure J-41. Guide Tube Nodal Densities

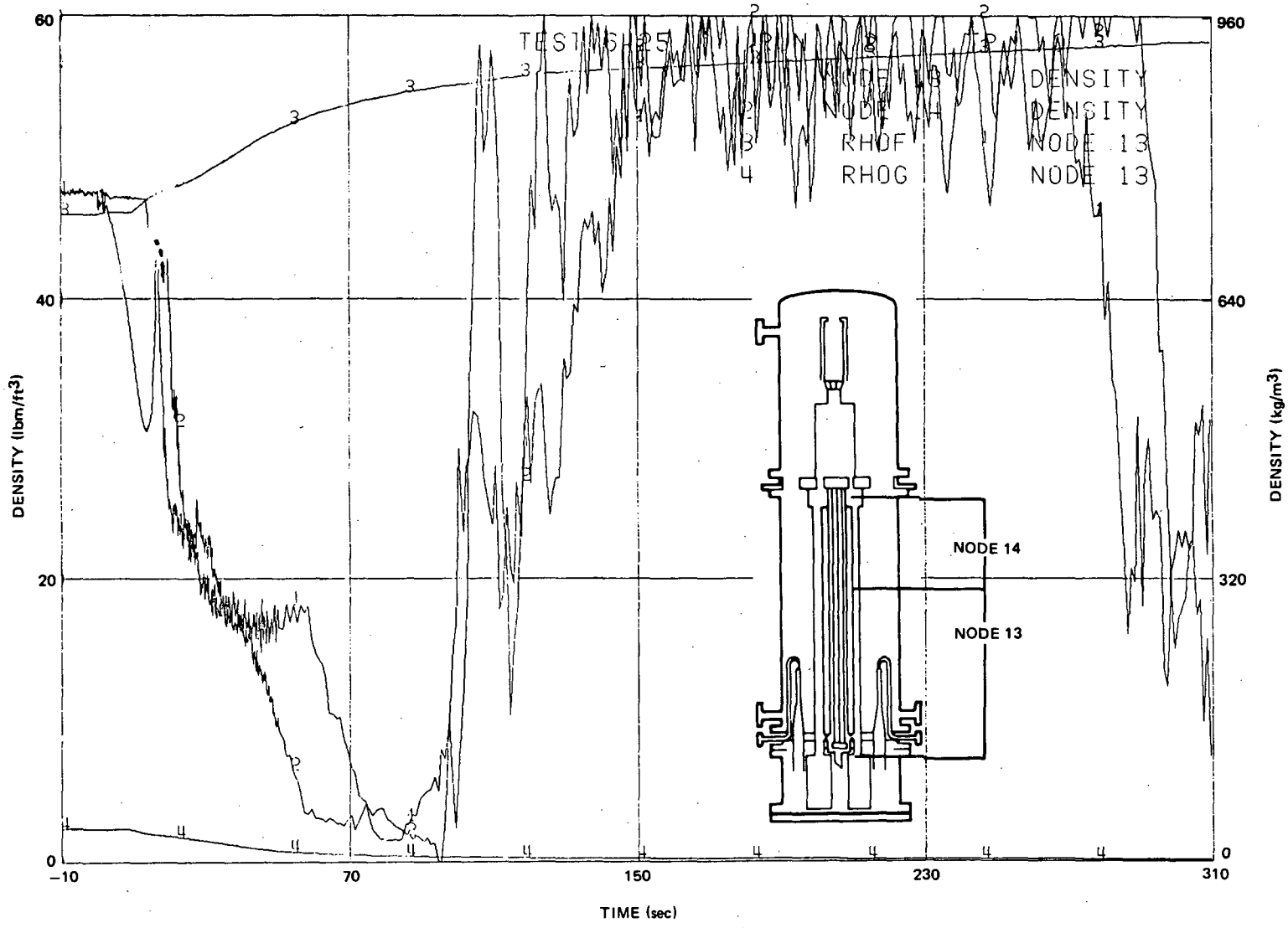

Figure J-42. Bypass Nodal Densities

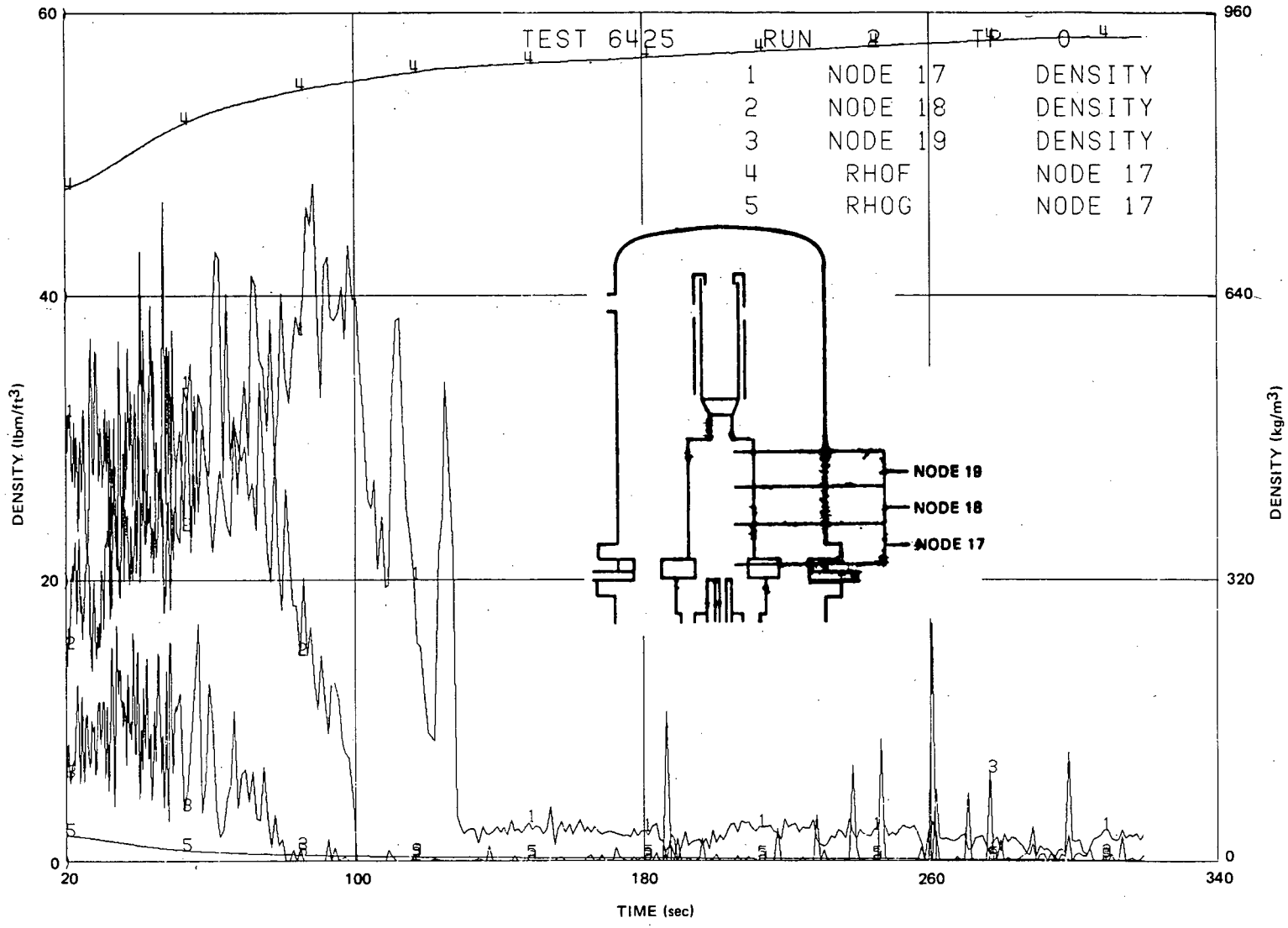

Figure J-43. Upper Plenum Nodal Densities

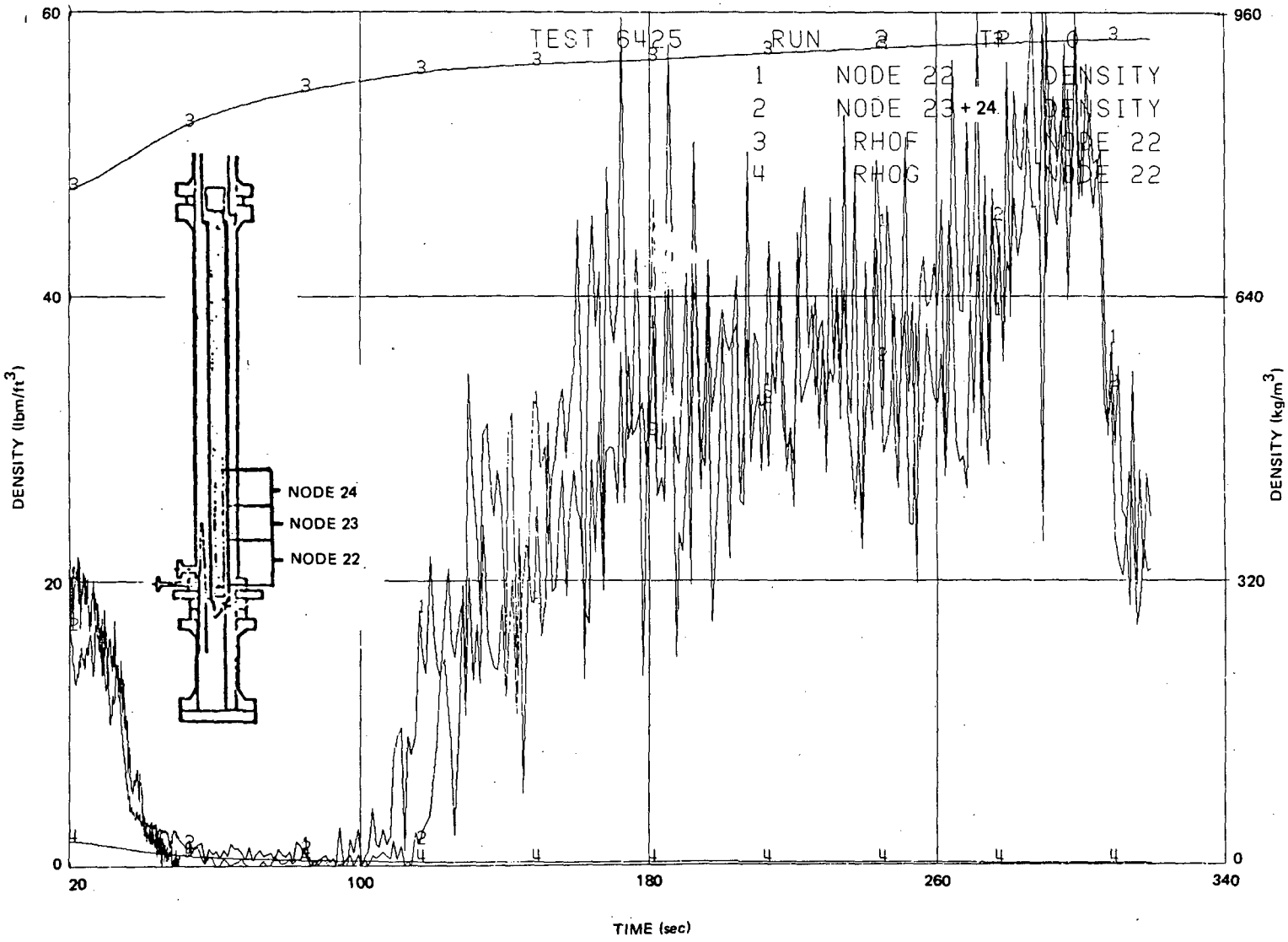

Figure J-44. Lower Bundle Nodal Densities

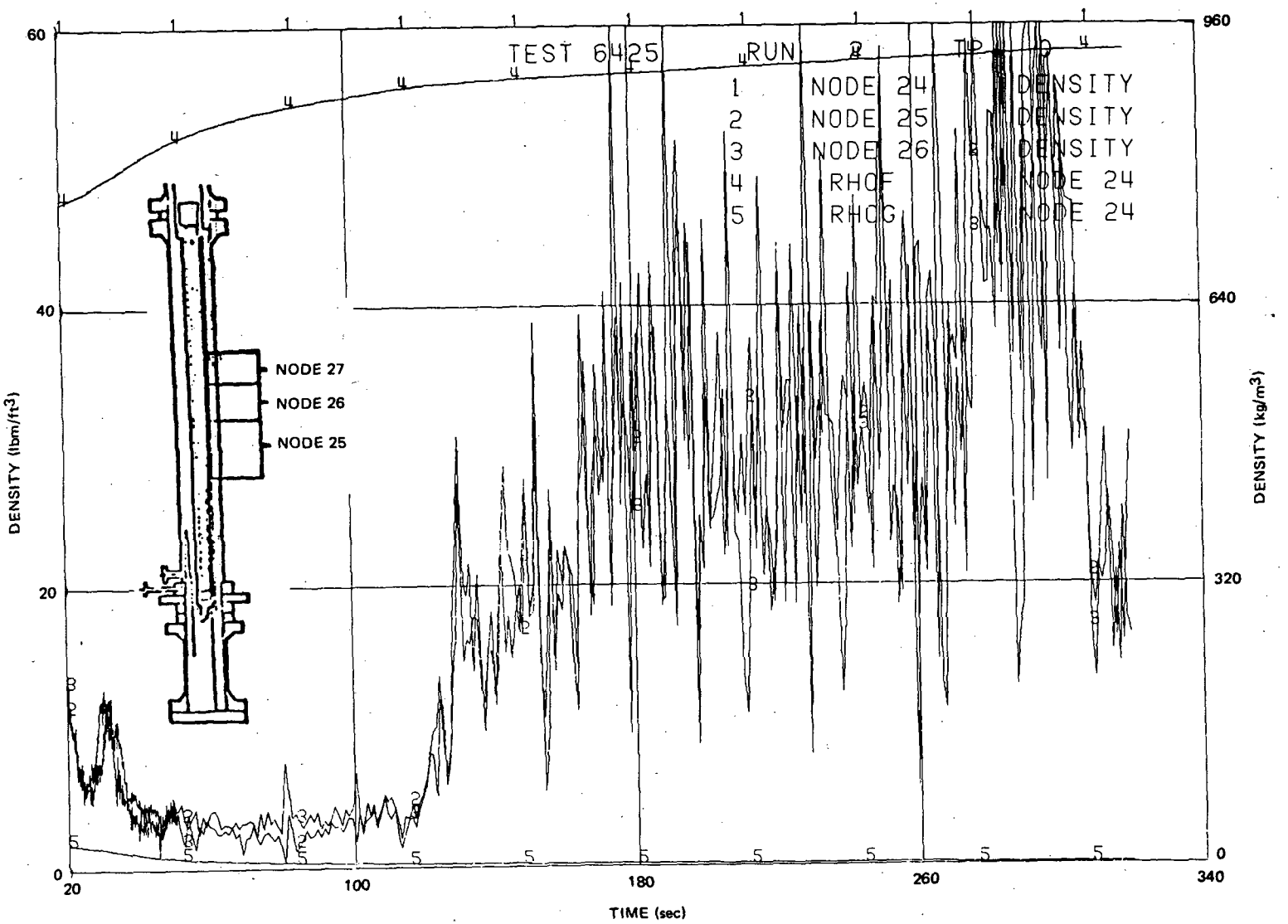

Figure J-45. Middle Bundle Nodal Densities

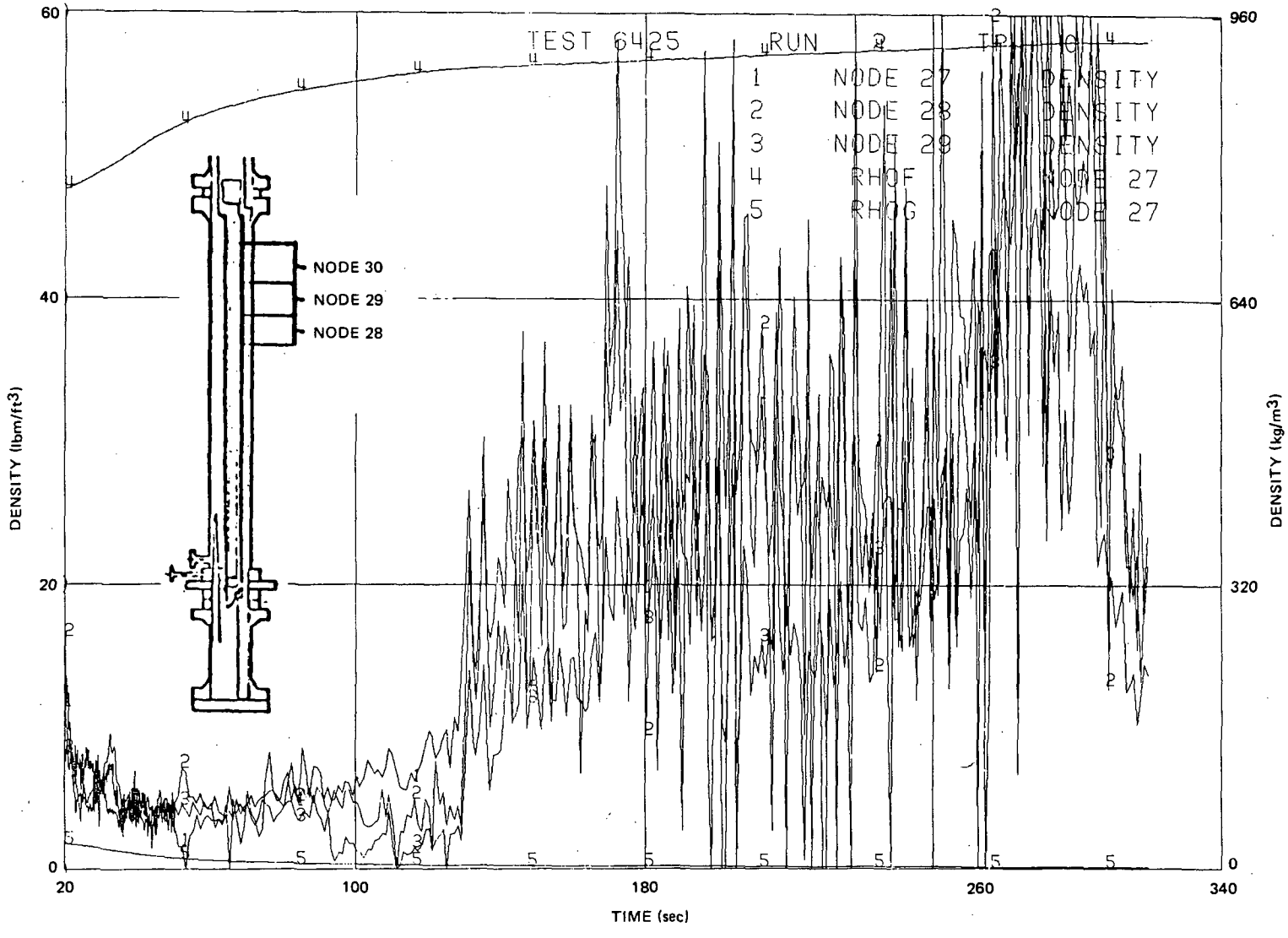

Figure J-46. Upper Bundle Nodal Densities

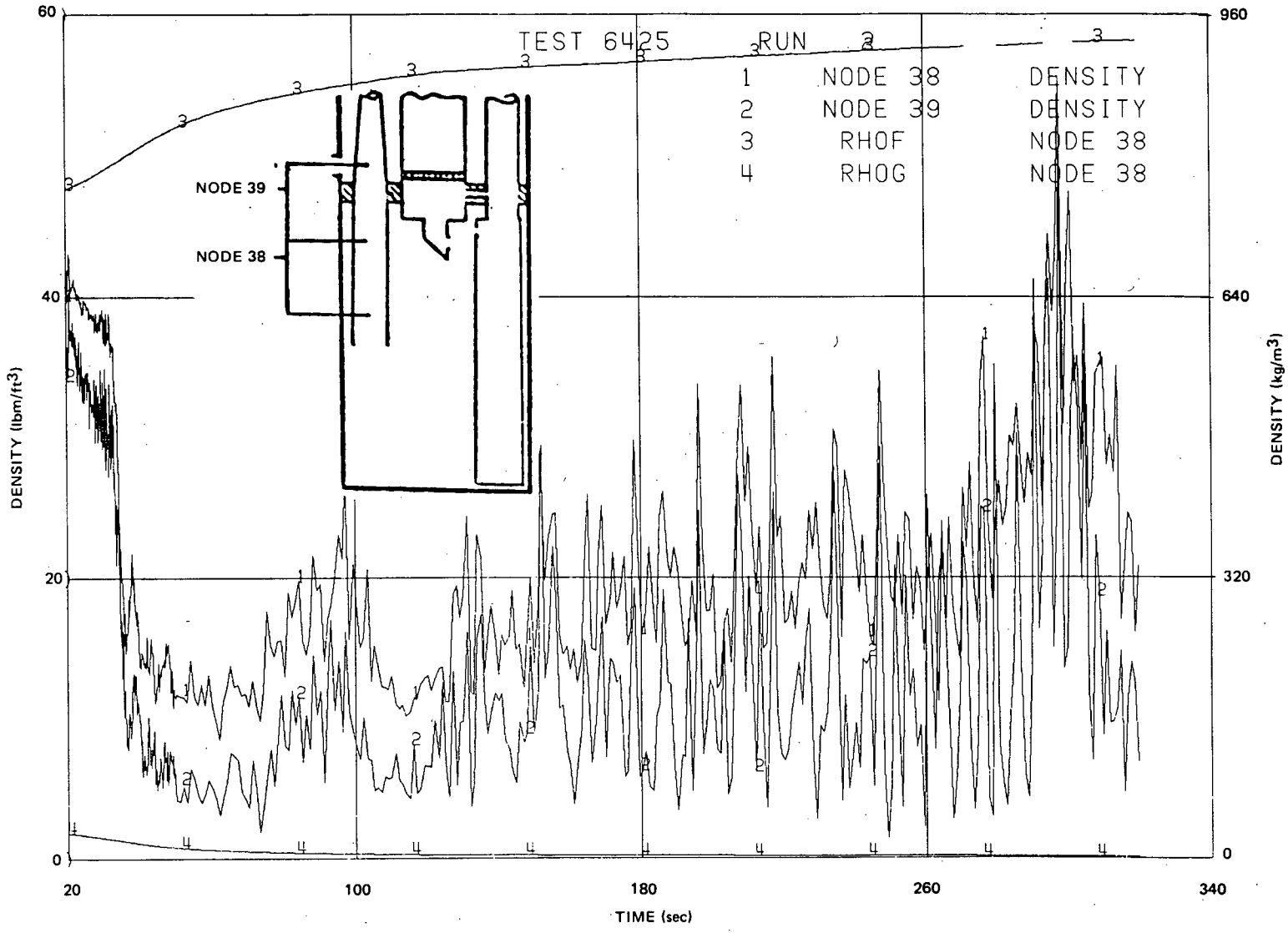

Figure J-47. Intact Loop Jet Pump Nodal Densities

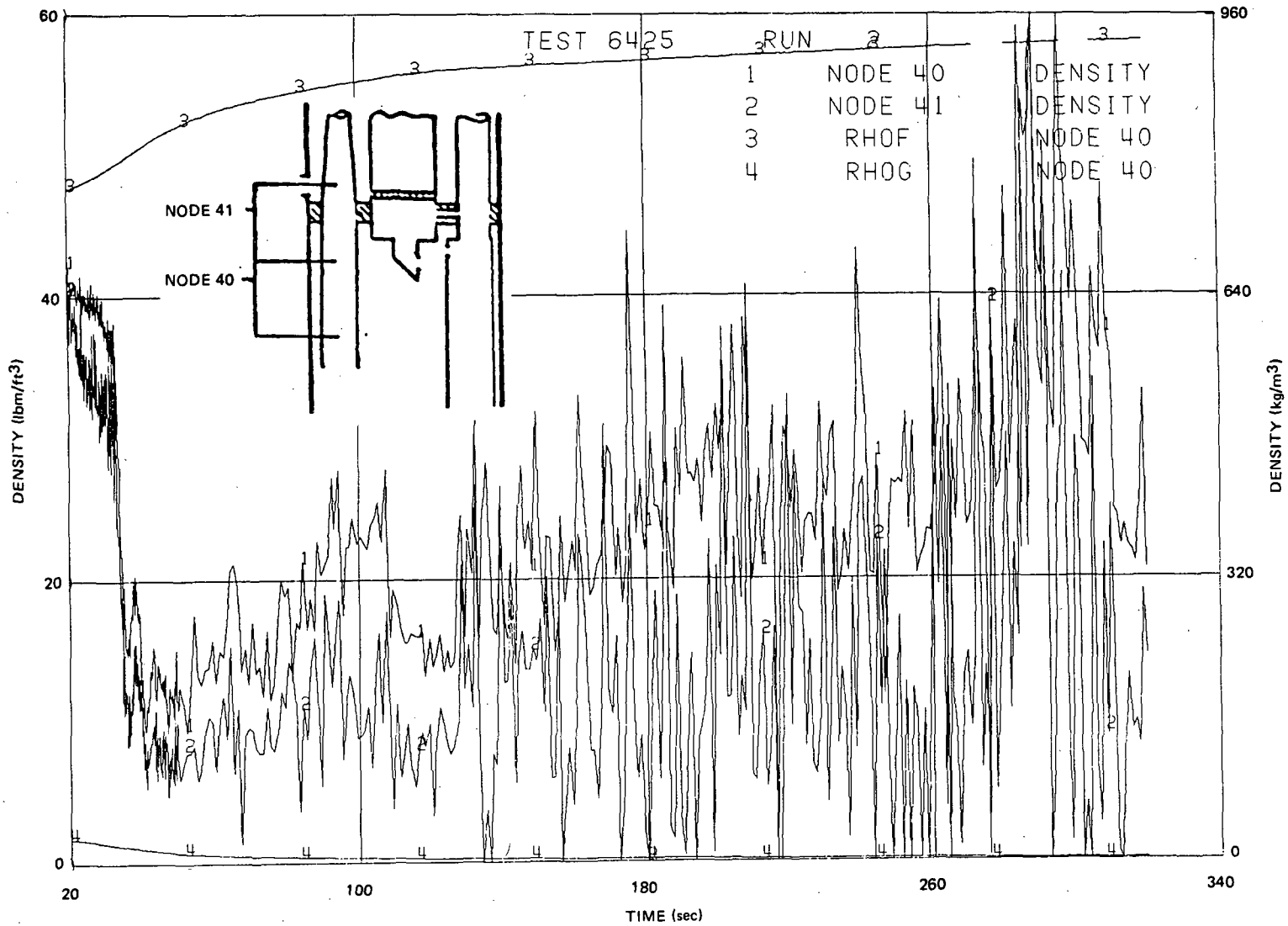

Figure J-48. Broken Loop Jet Pump Nodal Densities

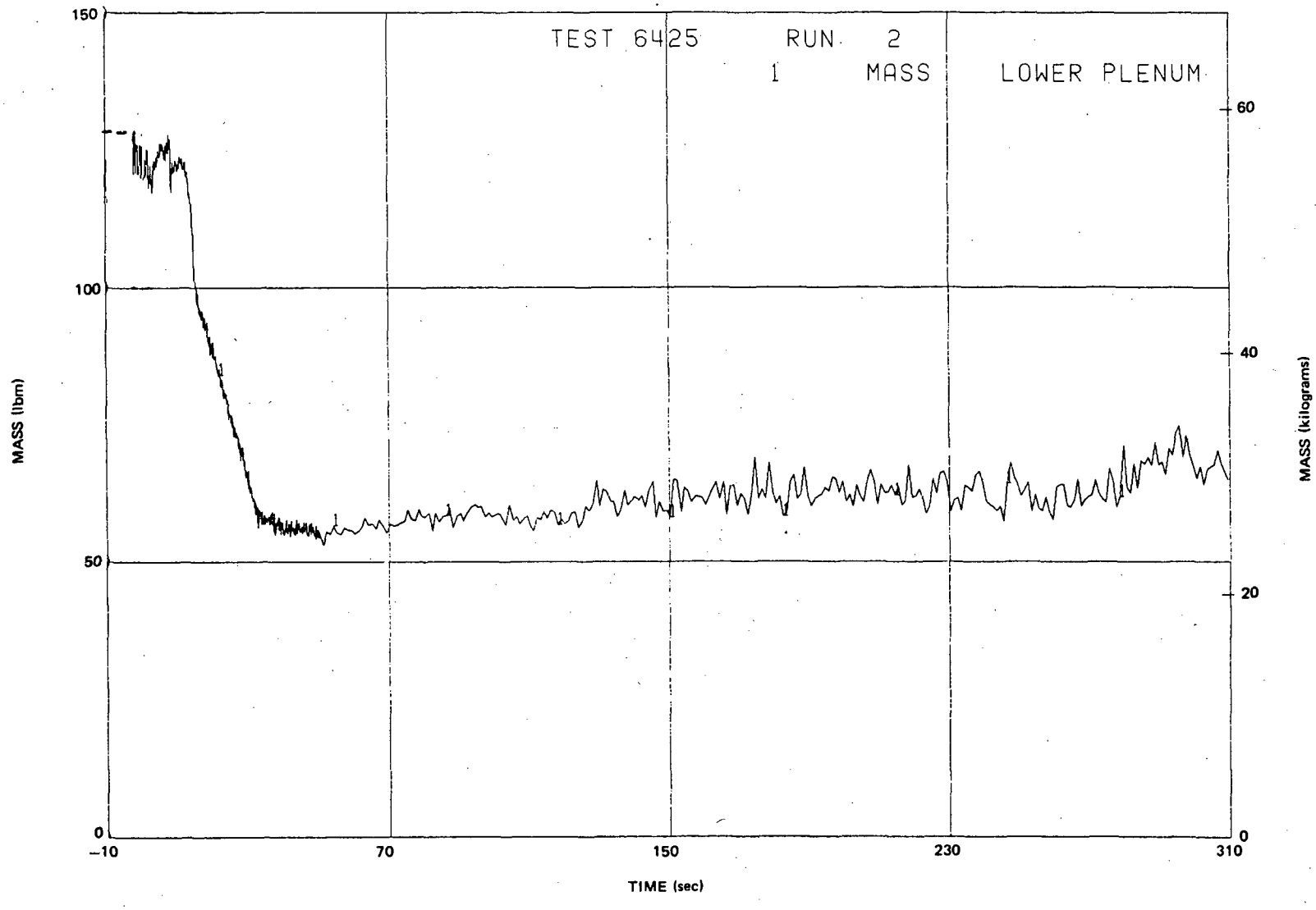

Figure J-49. Lower Plenum Fluid Mass

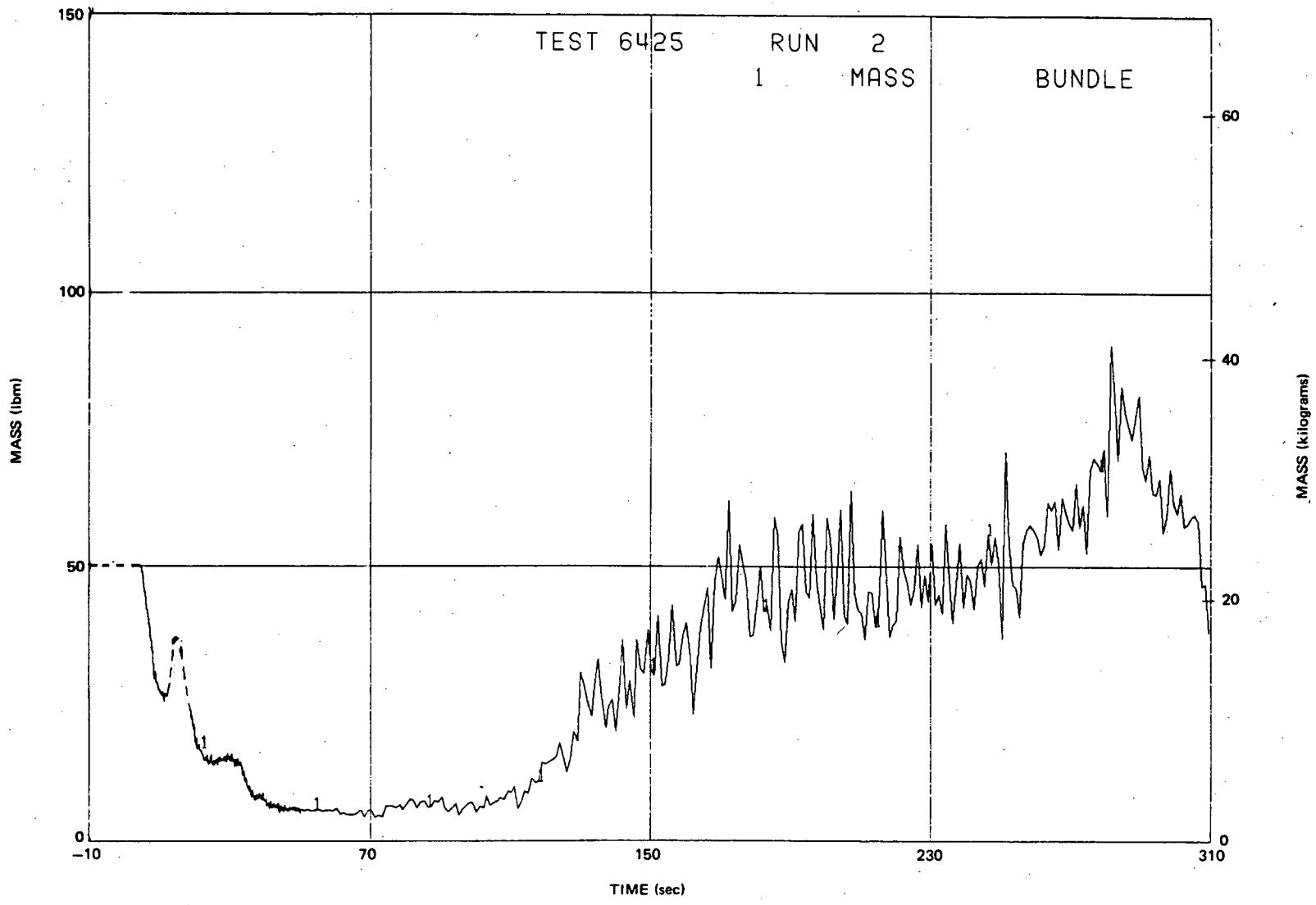

Figure J-50. Bundle Fluid Mass

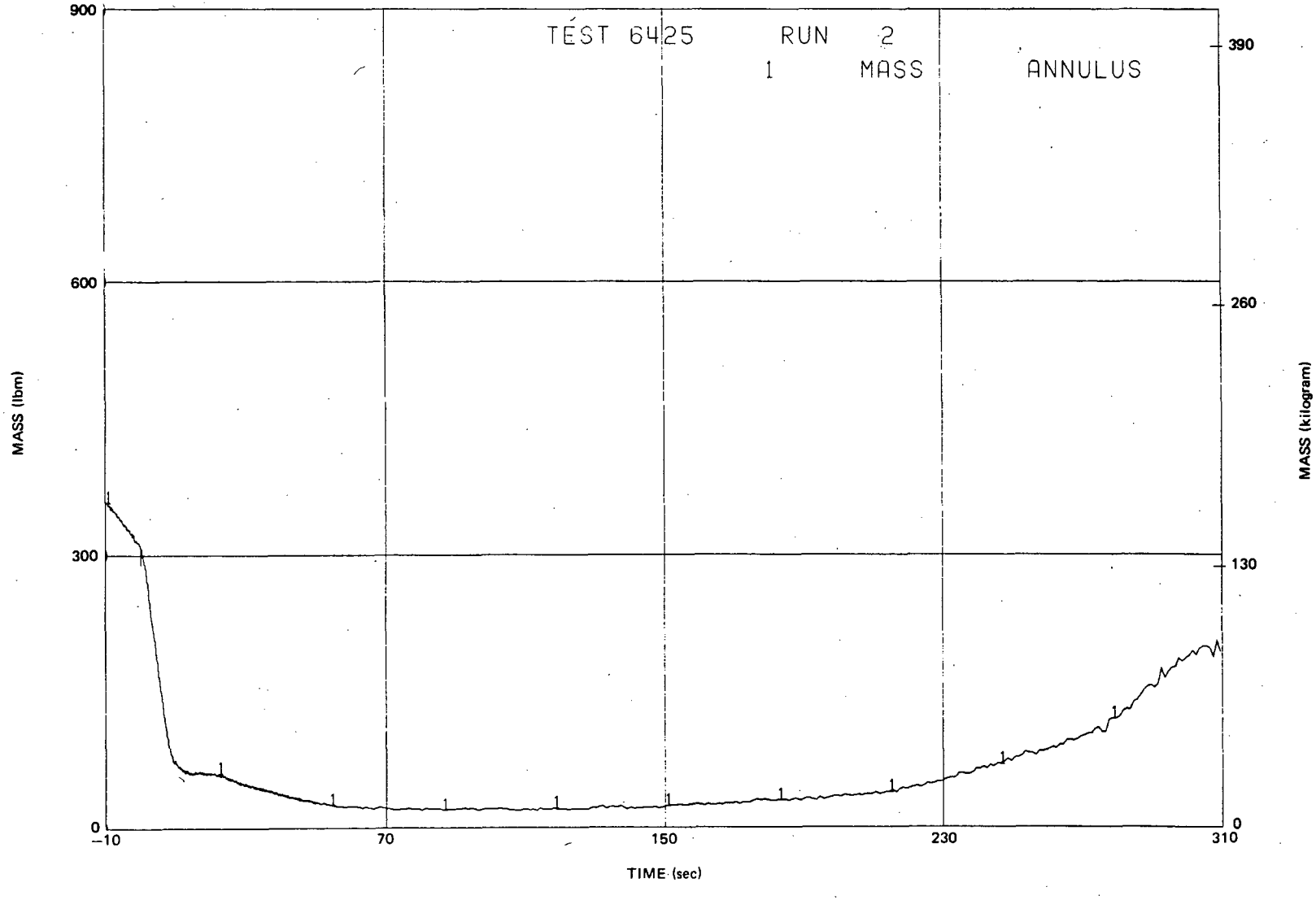

Figure J-51. Annulus Fluid Mass

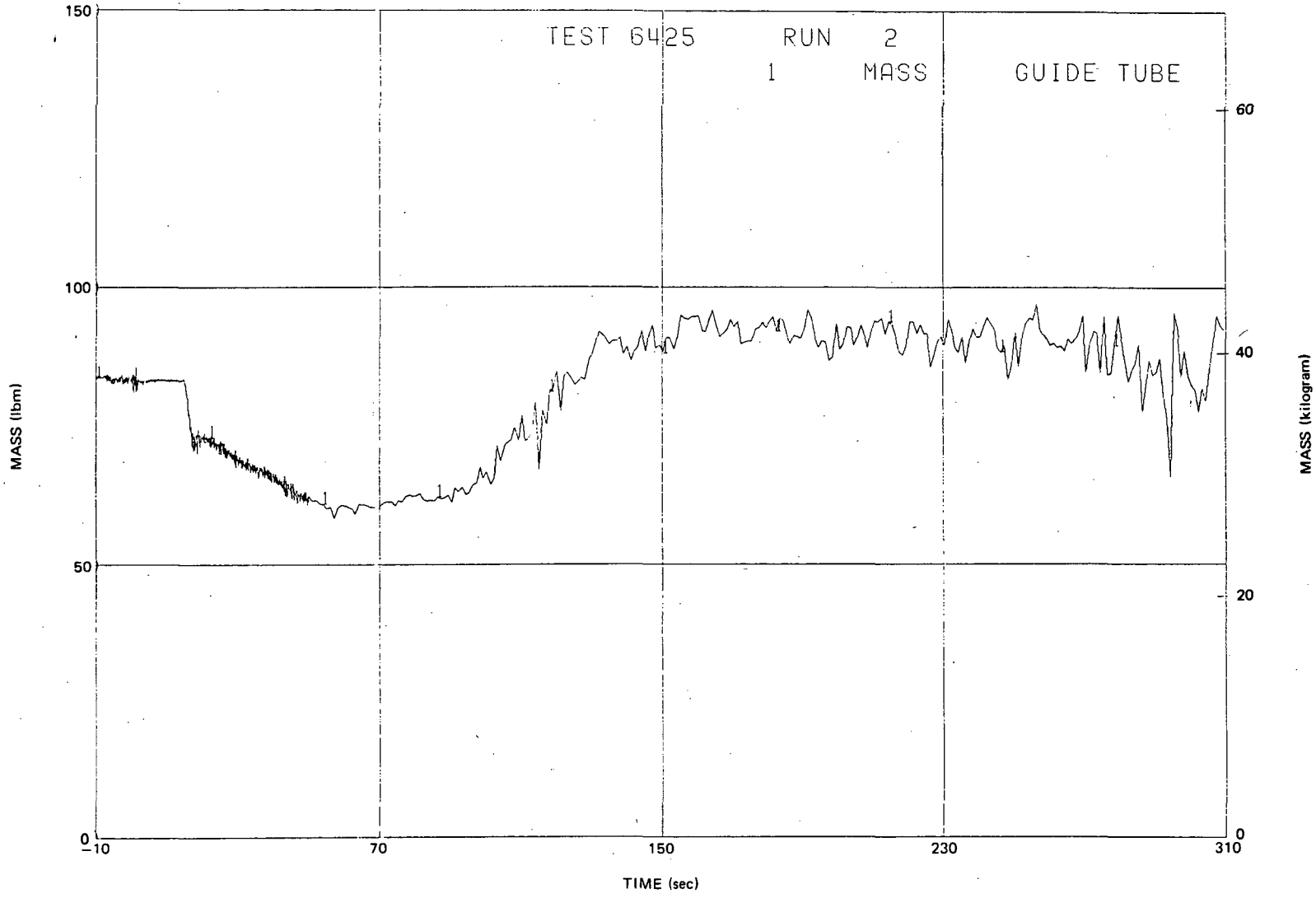

Figure J-52. Guide Tube Fluid Mass

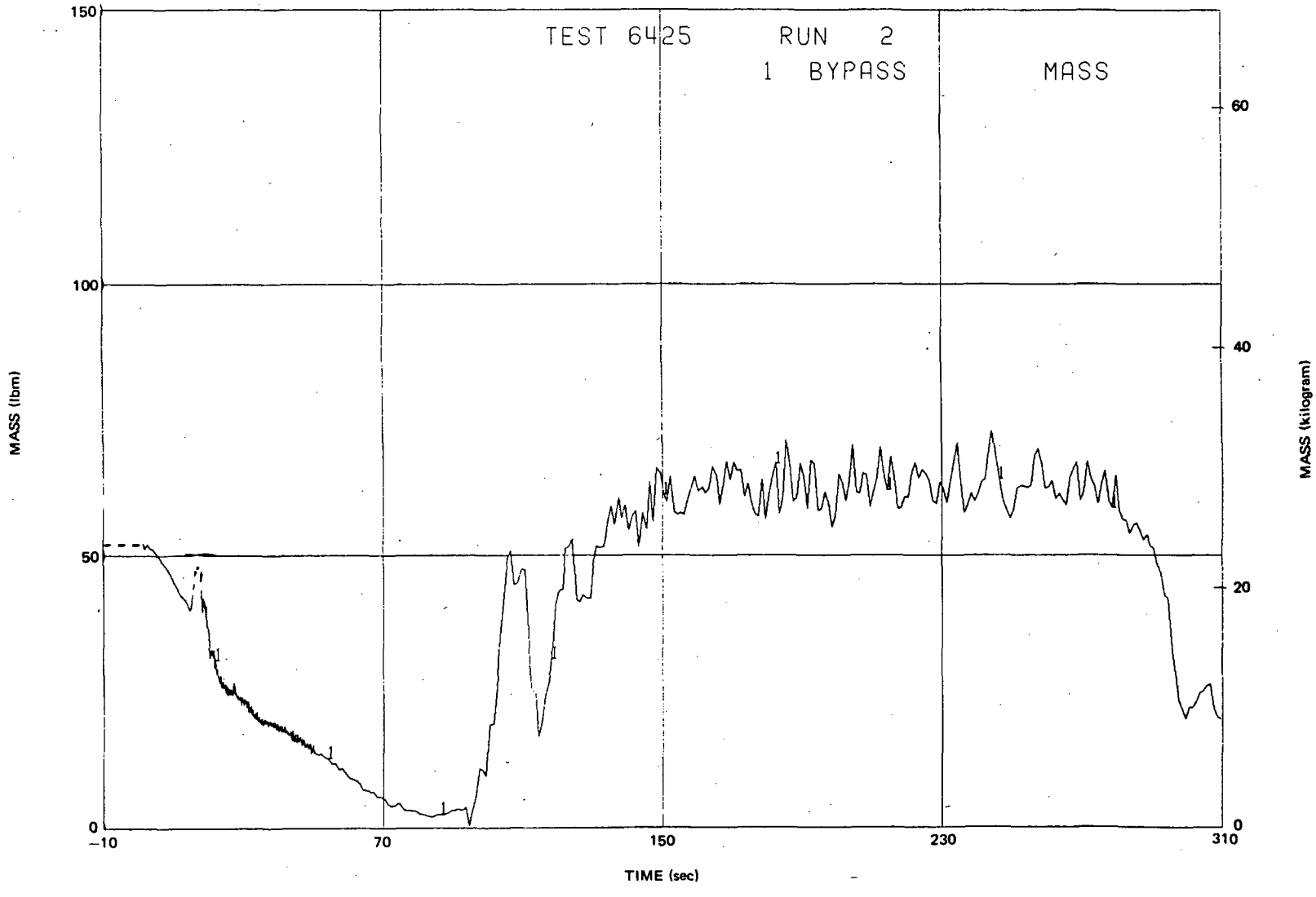

Figure J-53. Bypass Fluid Mass

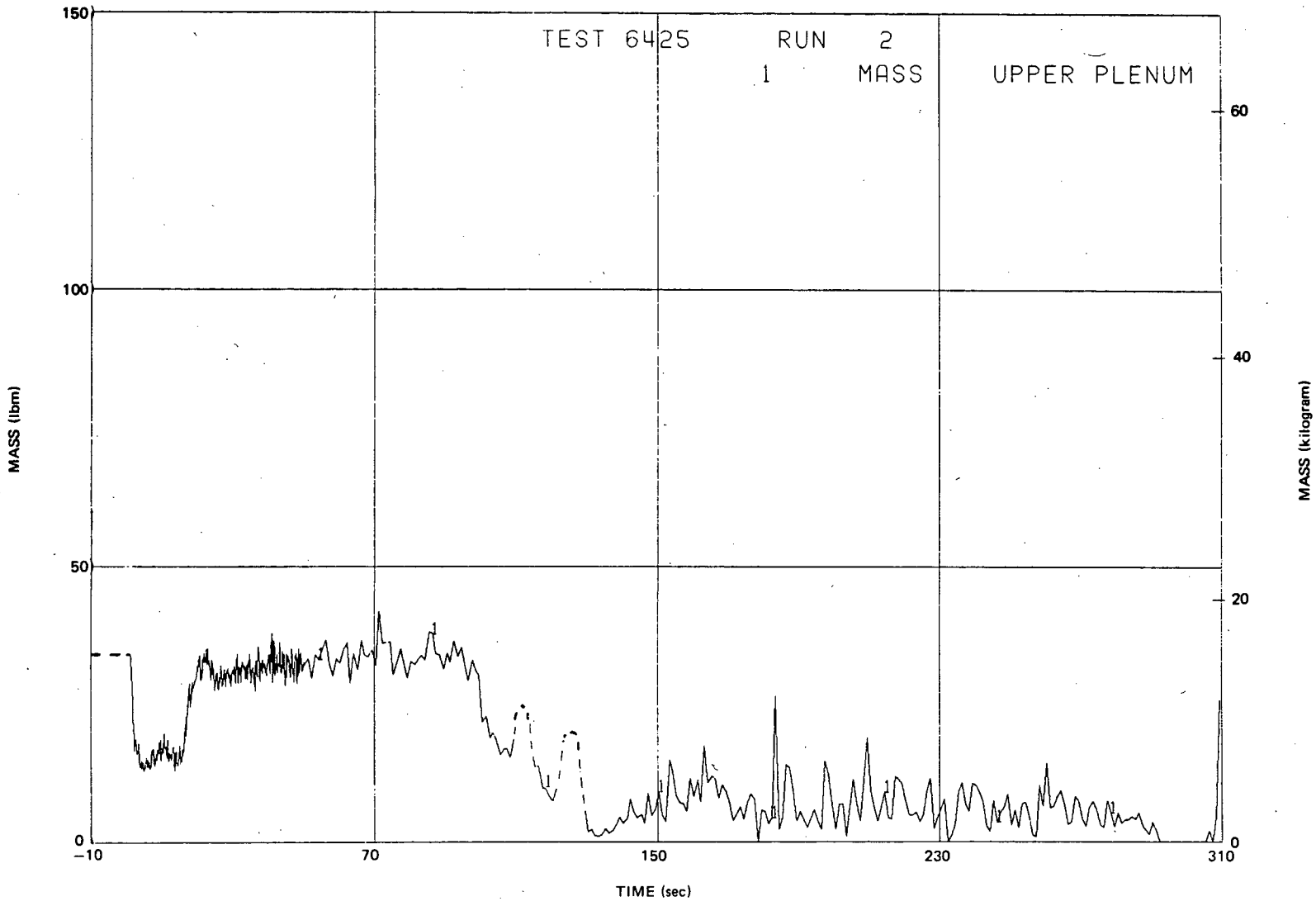

Figure J-54. Upper Plenum Fluid Mass

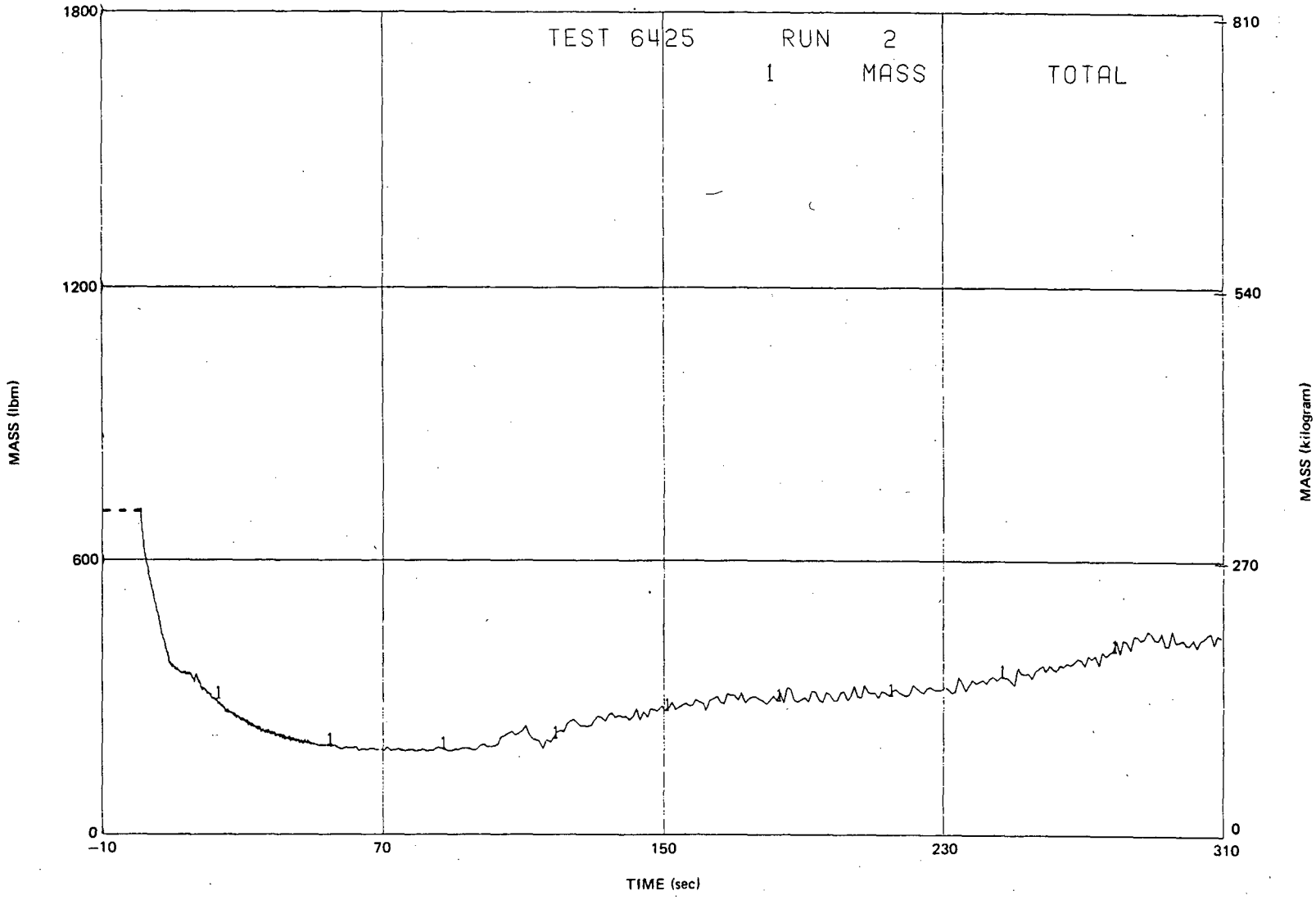

Figure J-55. Total Vessel Fluid Mass

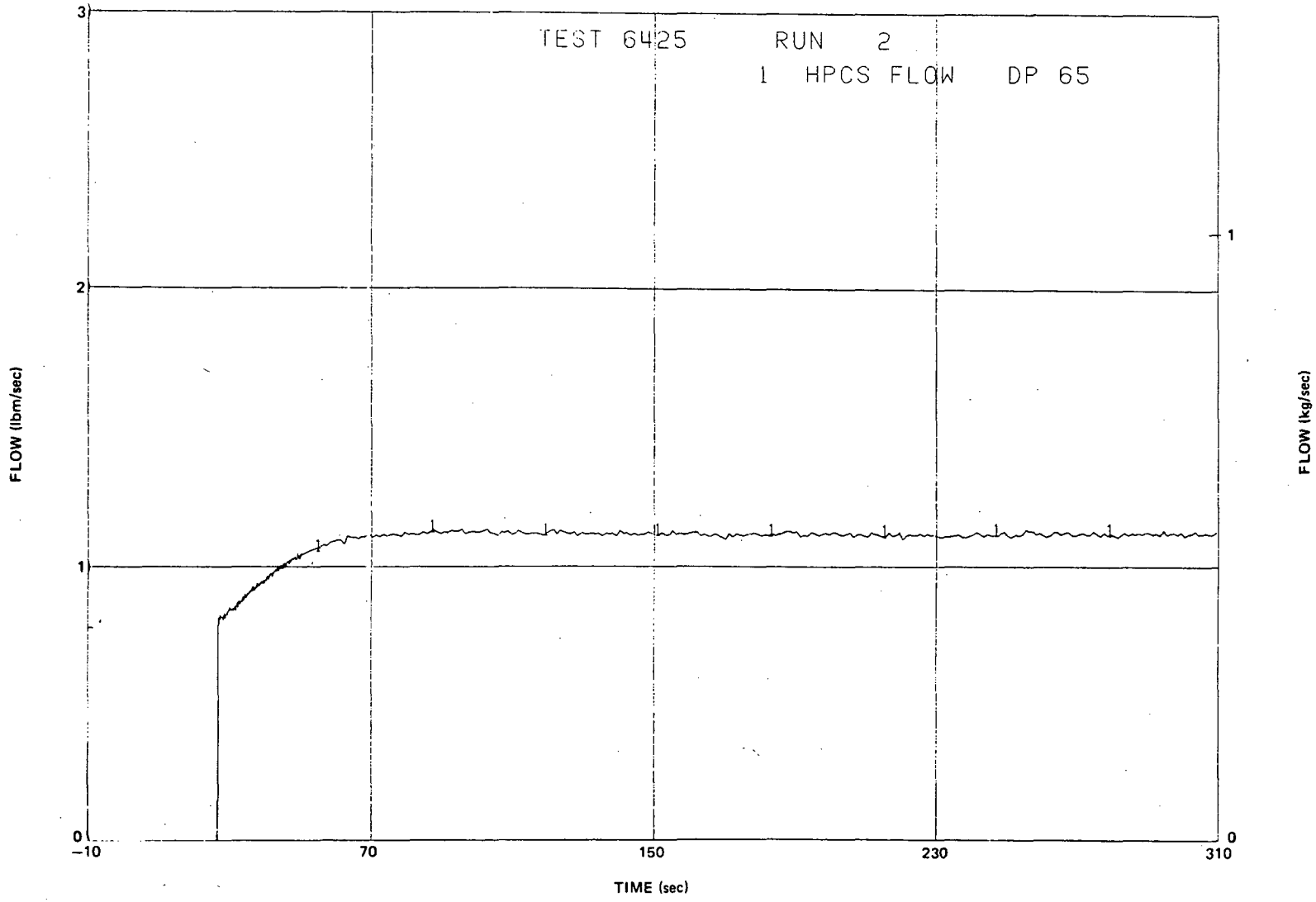

Figure J-56. HPCS Mass Flow Rate

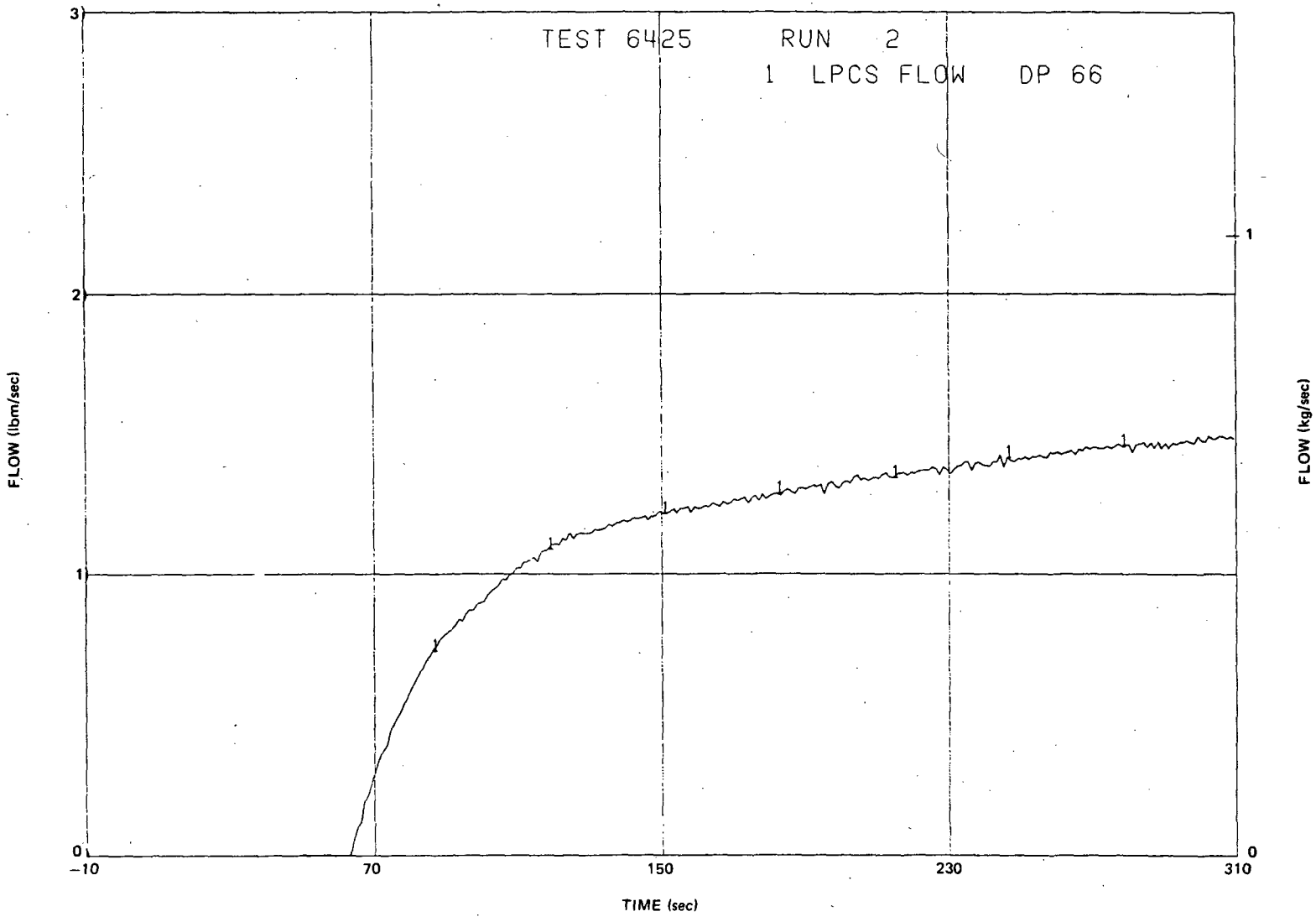

Figure J-57. LPCS Mass Flow Rate

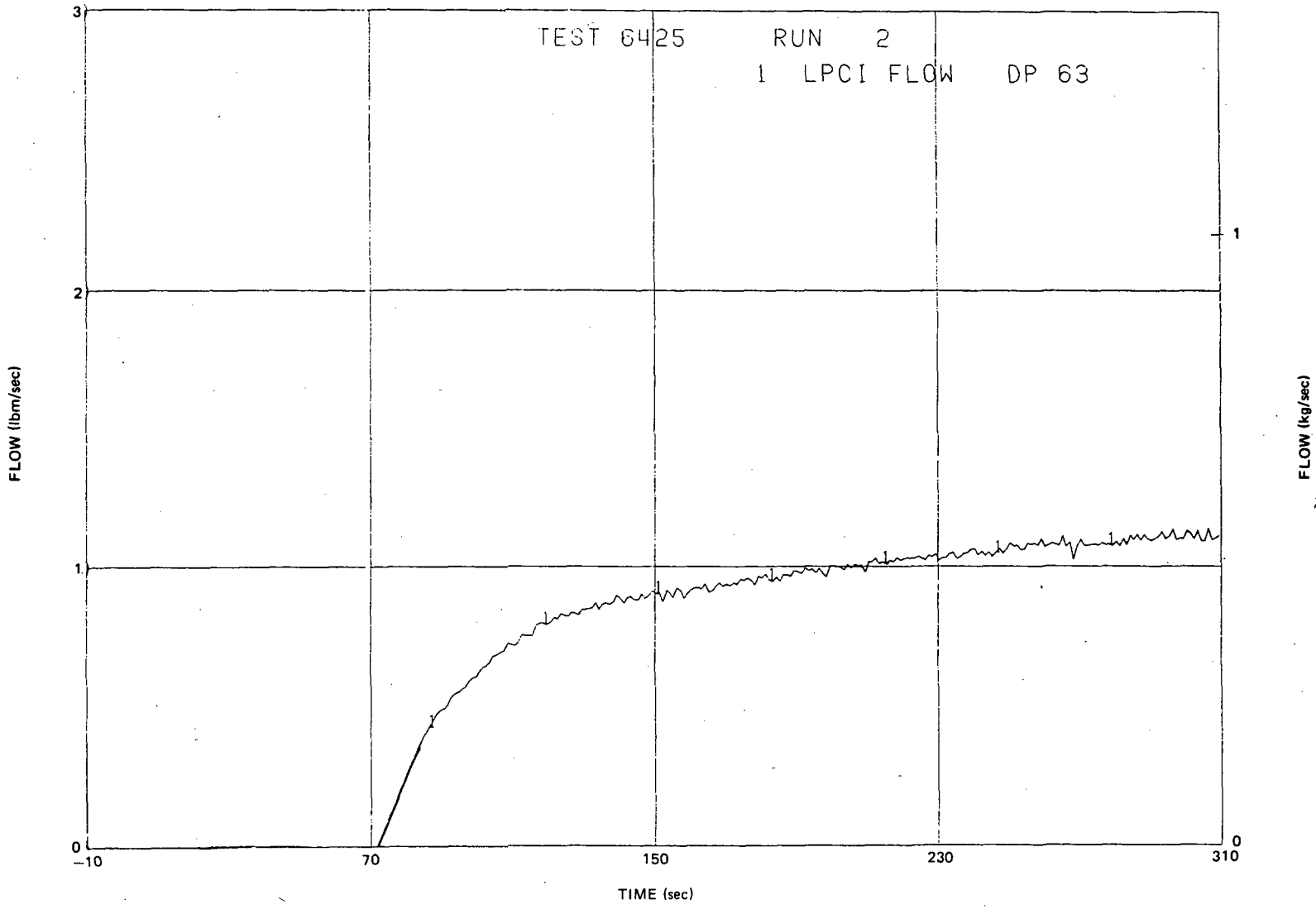

Figure J-58. LPCI Mass Flow Rate

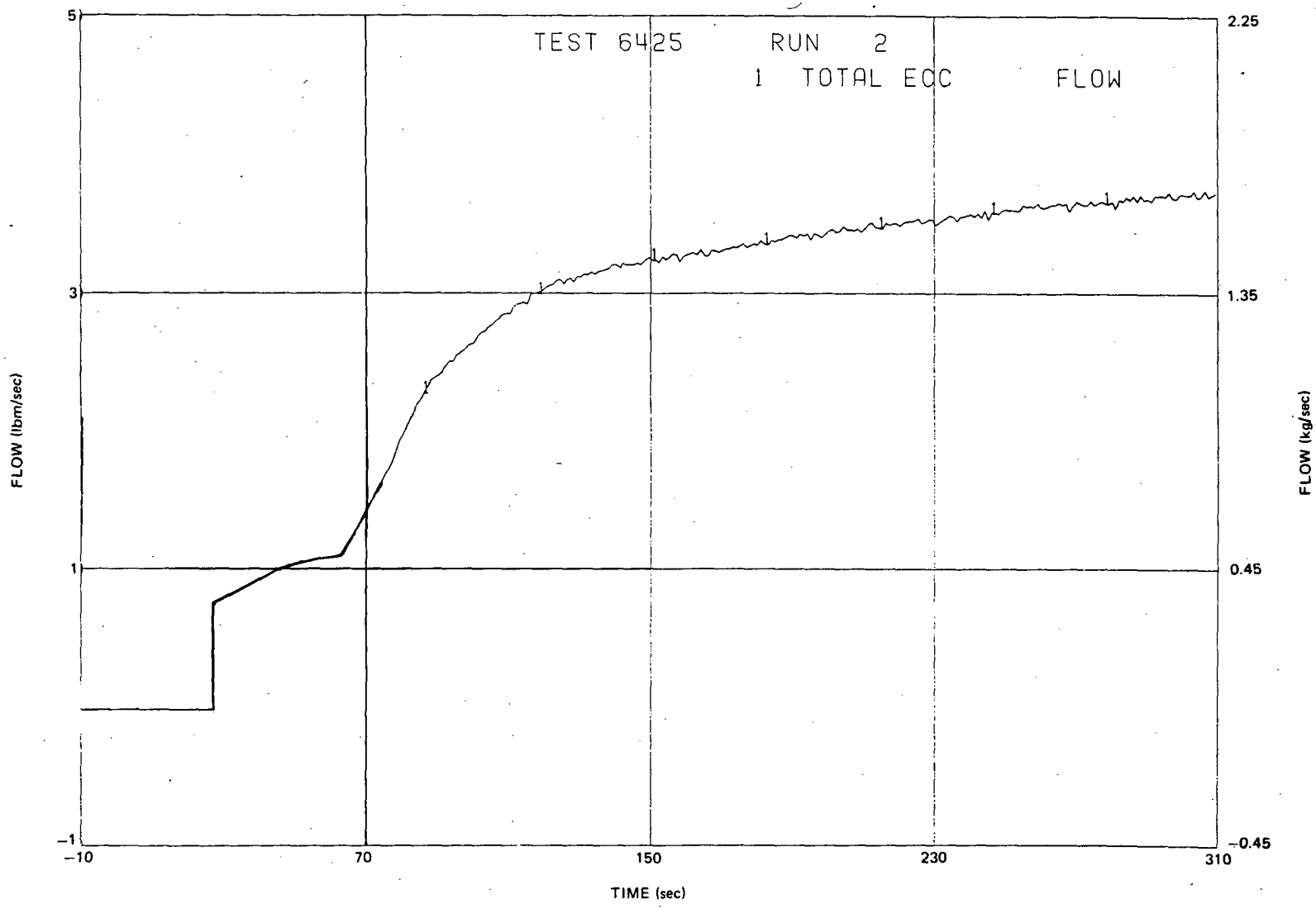

Figure J-59. Total ECC Mass Flow Rate

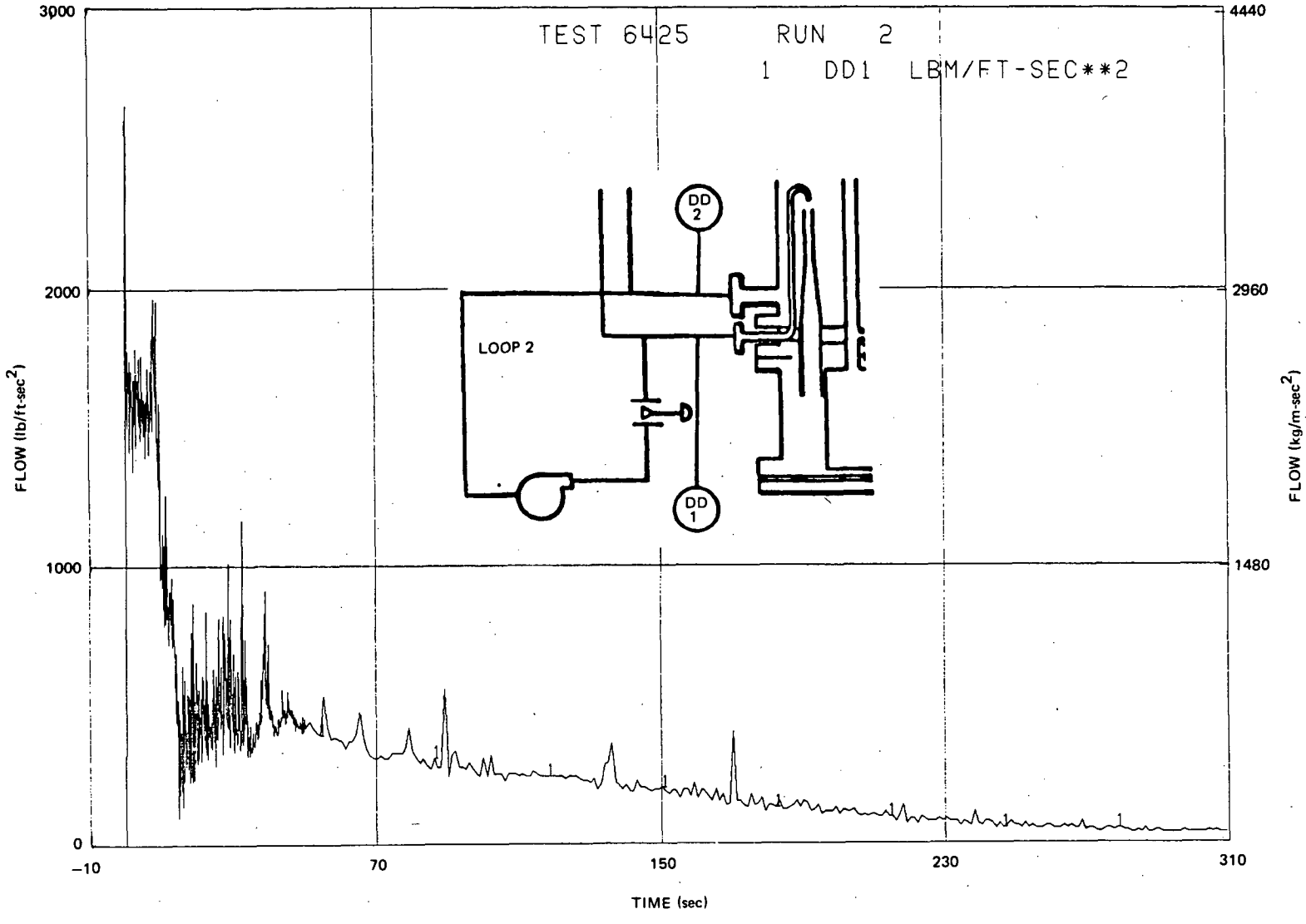

Figure J-60. Drag Disc Measurement on Drive Line Side of Broken Loop

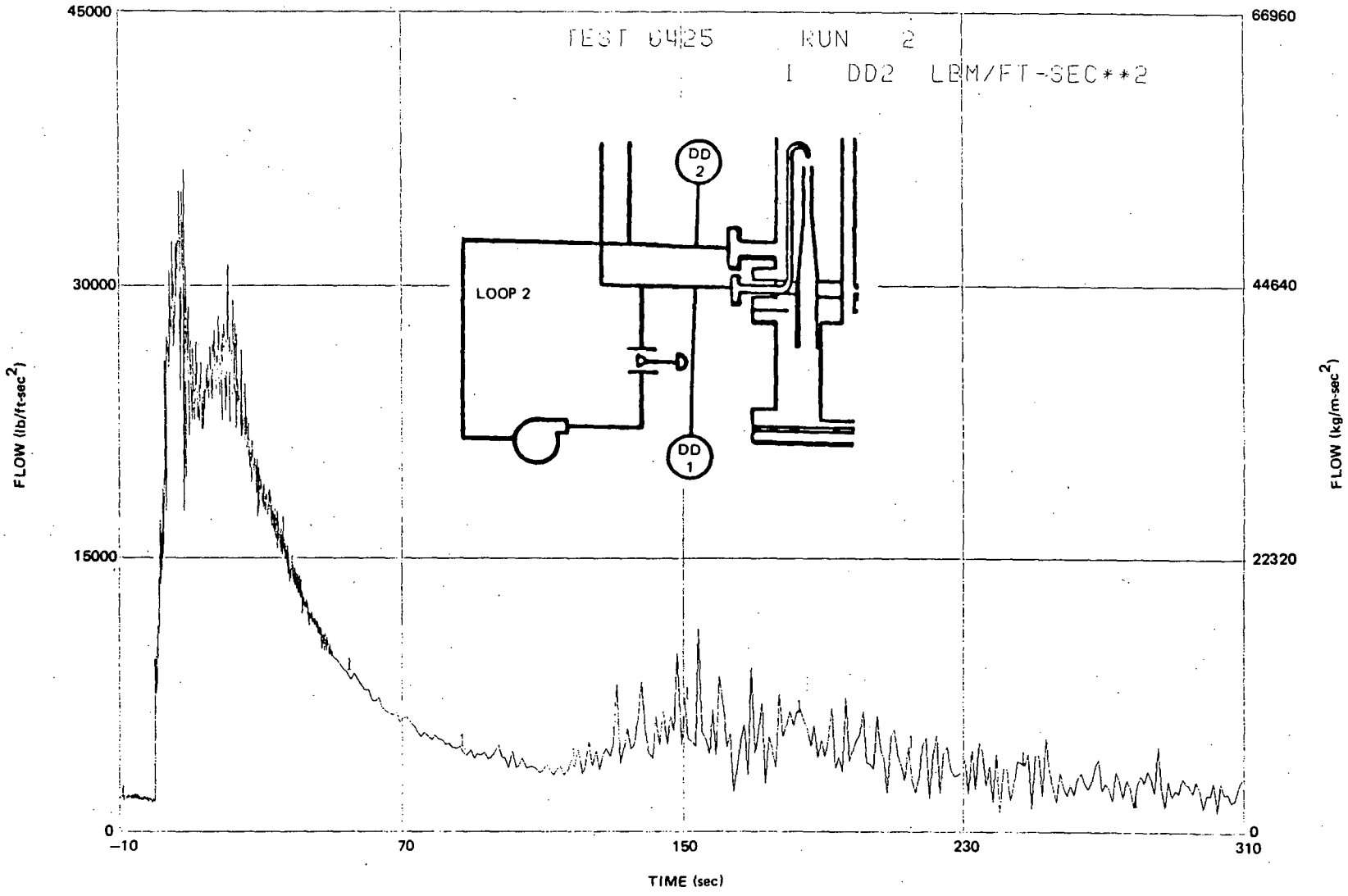

Figure J-61. Drag Disc Measurement on Suction Side of Broken Loop

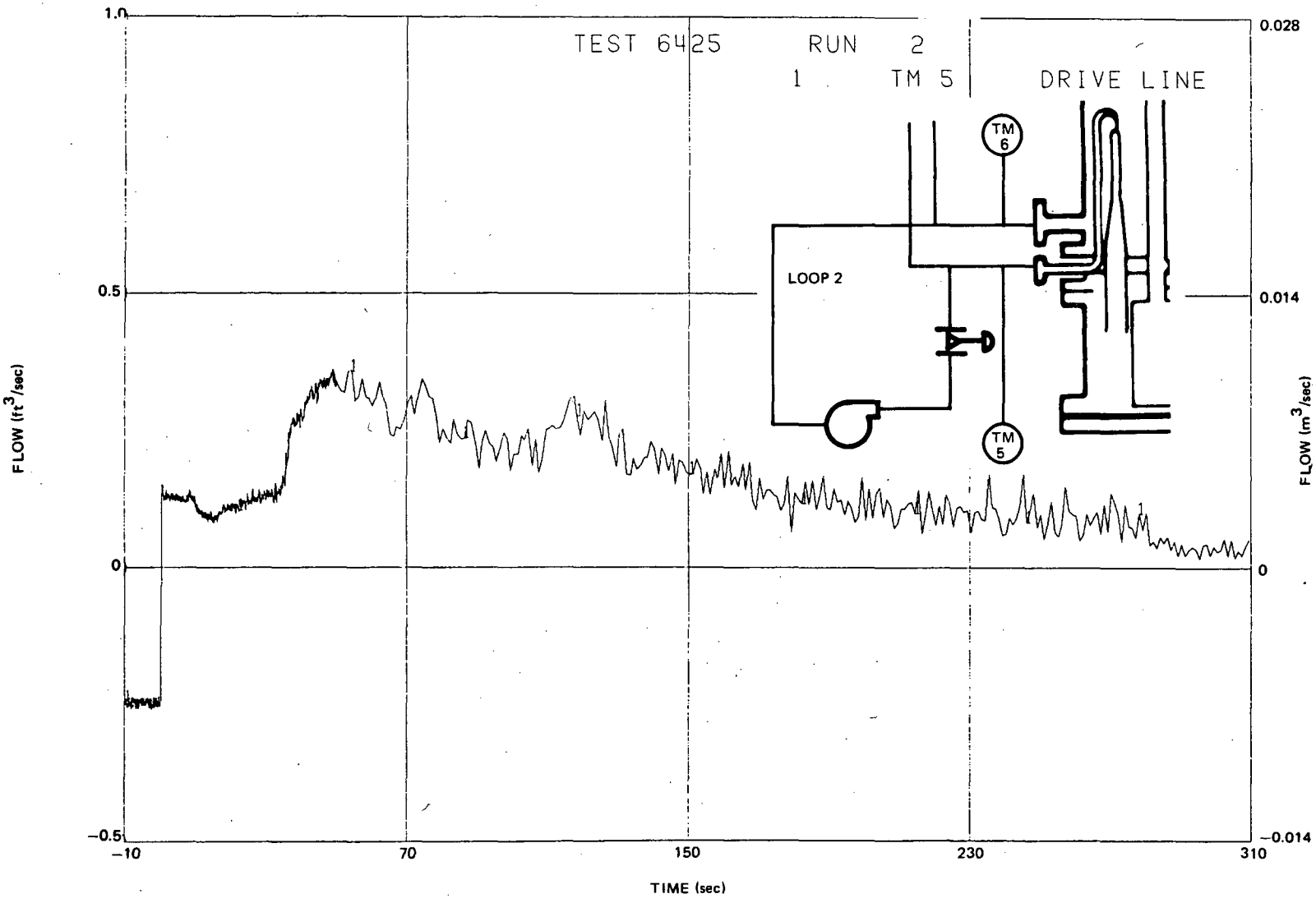

Figure J-62. Turbinemeter Measurement on Drive Line Side of Broken Loop

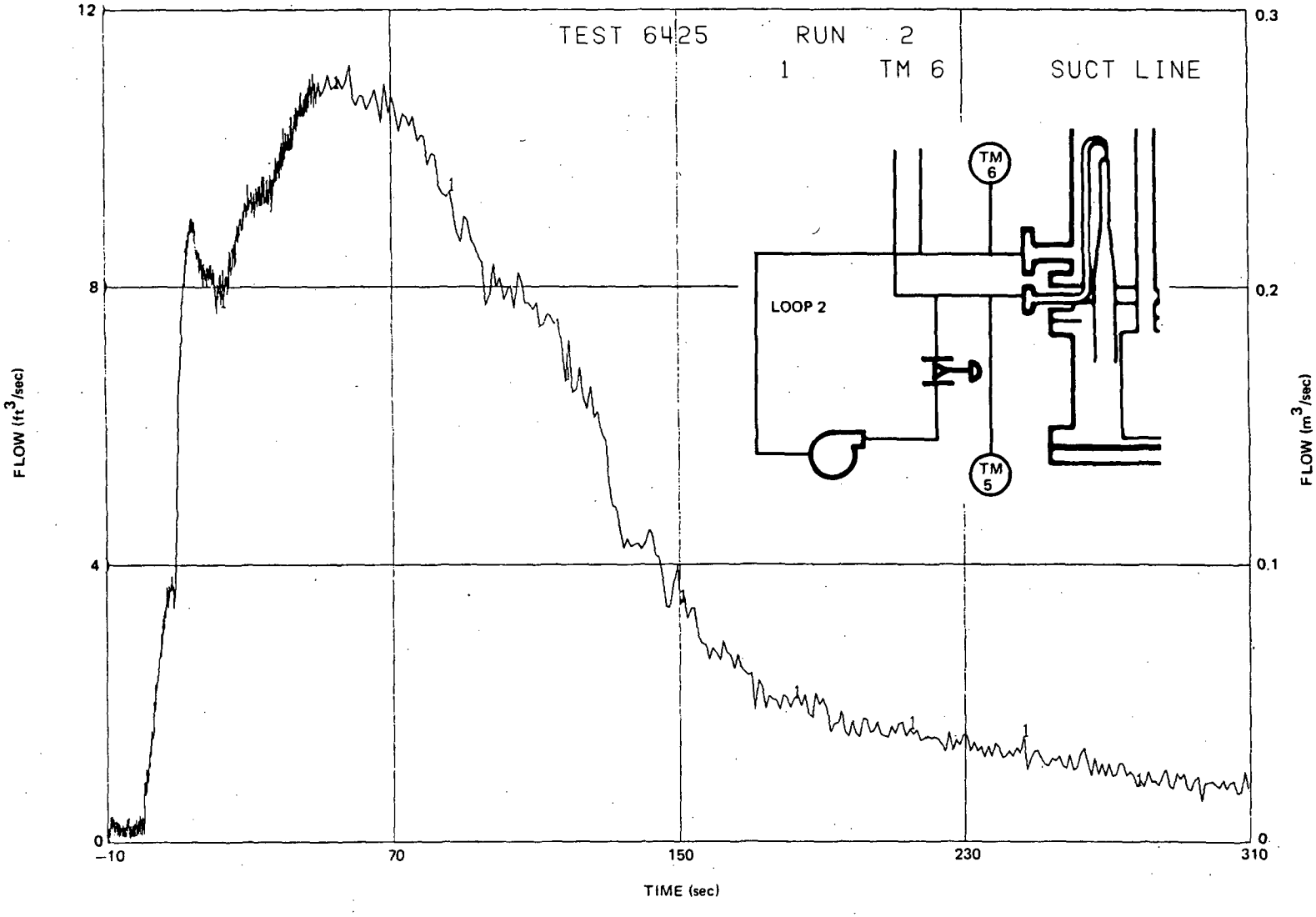

Figure J-63. Turbinemeter Measurement on Suction Line Side of Broken Loop

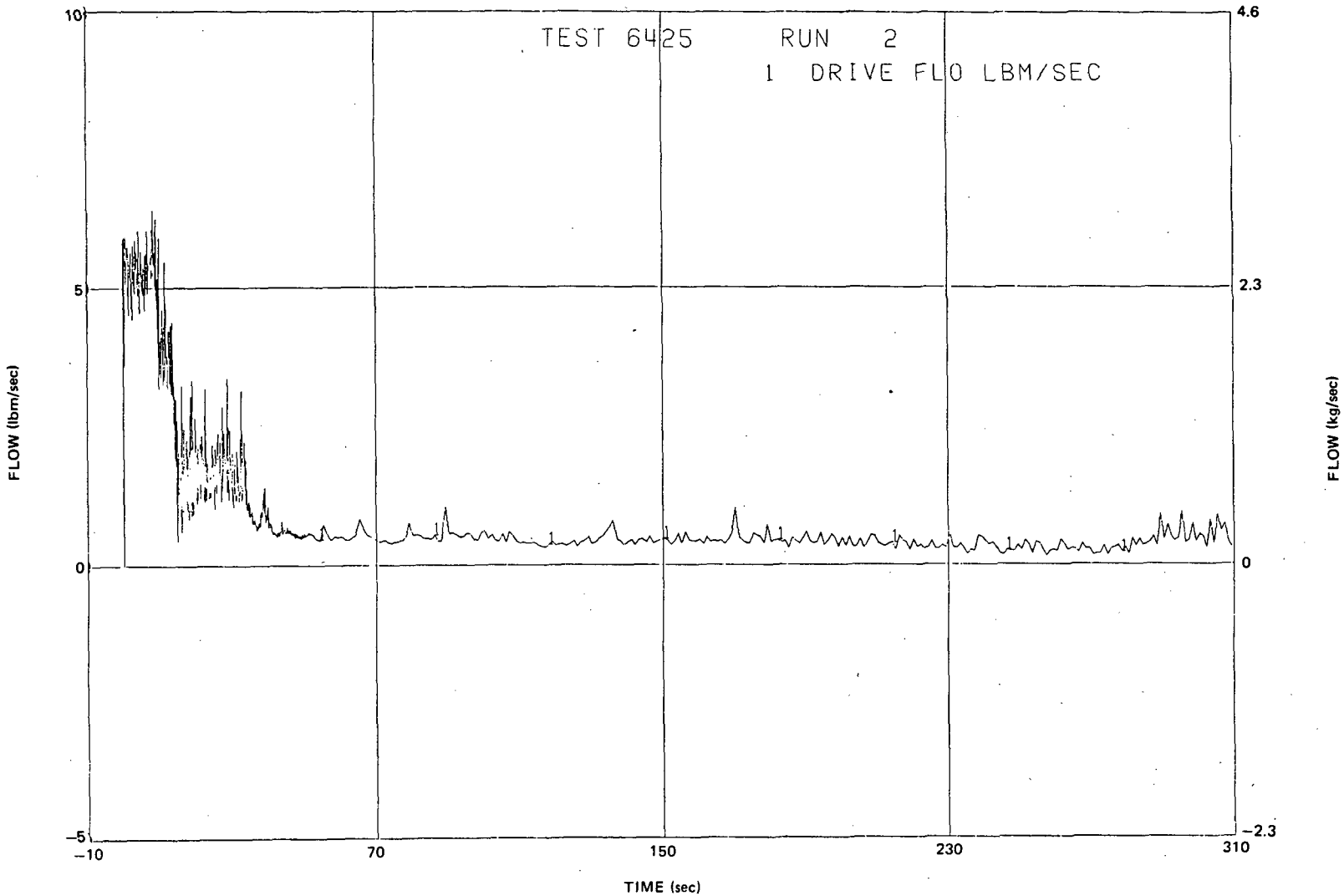

Figure J-64. Drive Line Break Mass Flow Rate

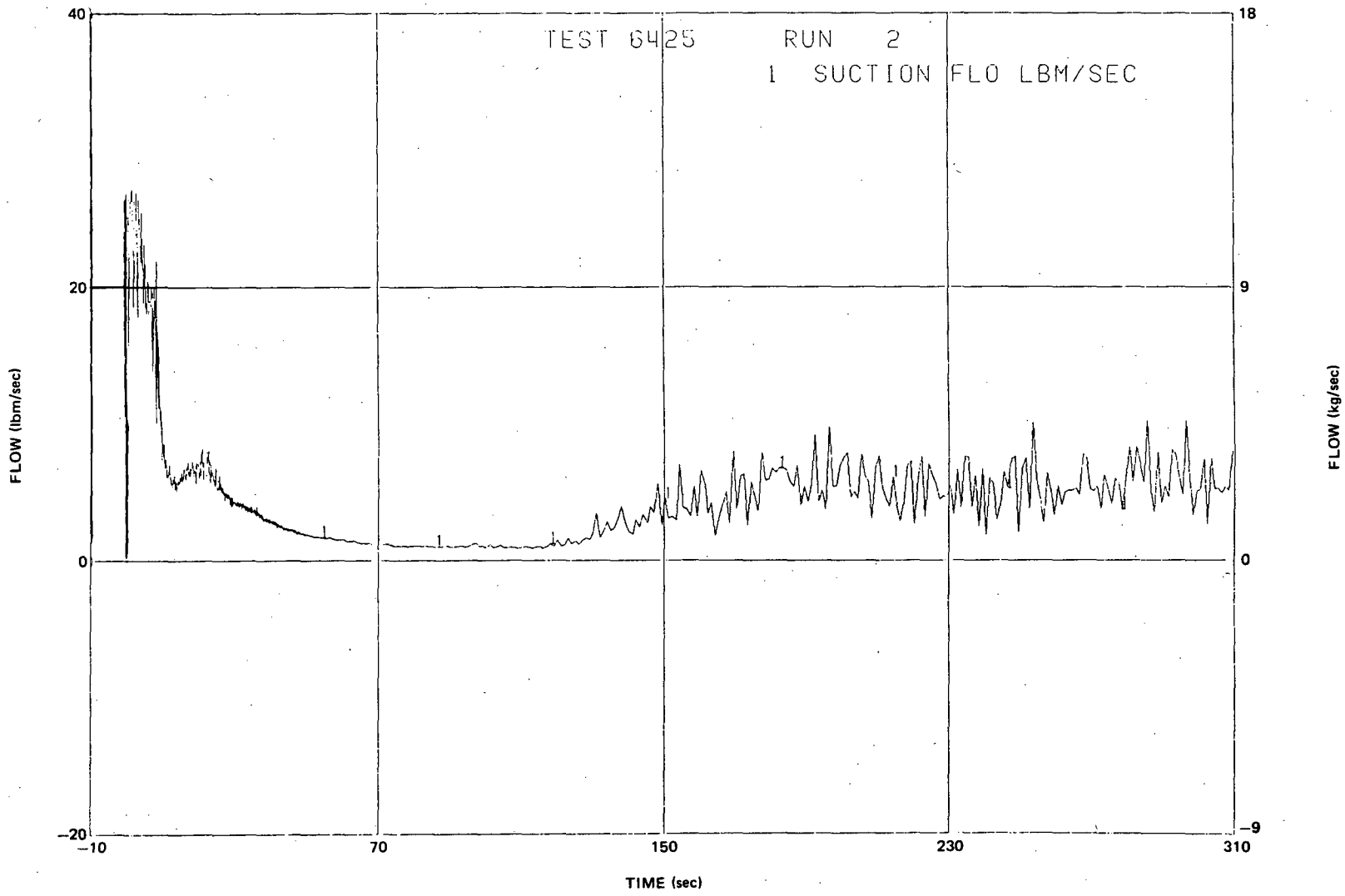

Figure J-65. Suction Line Break Mass Flow Rate

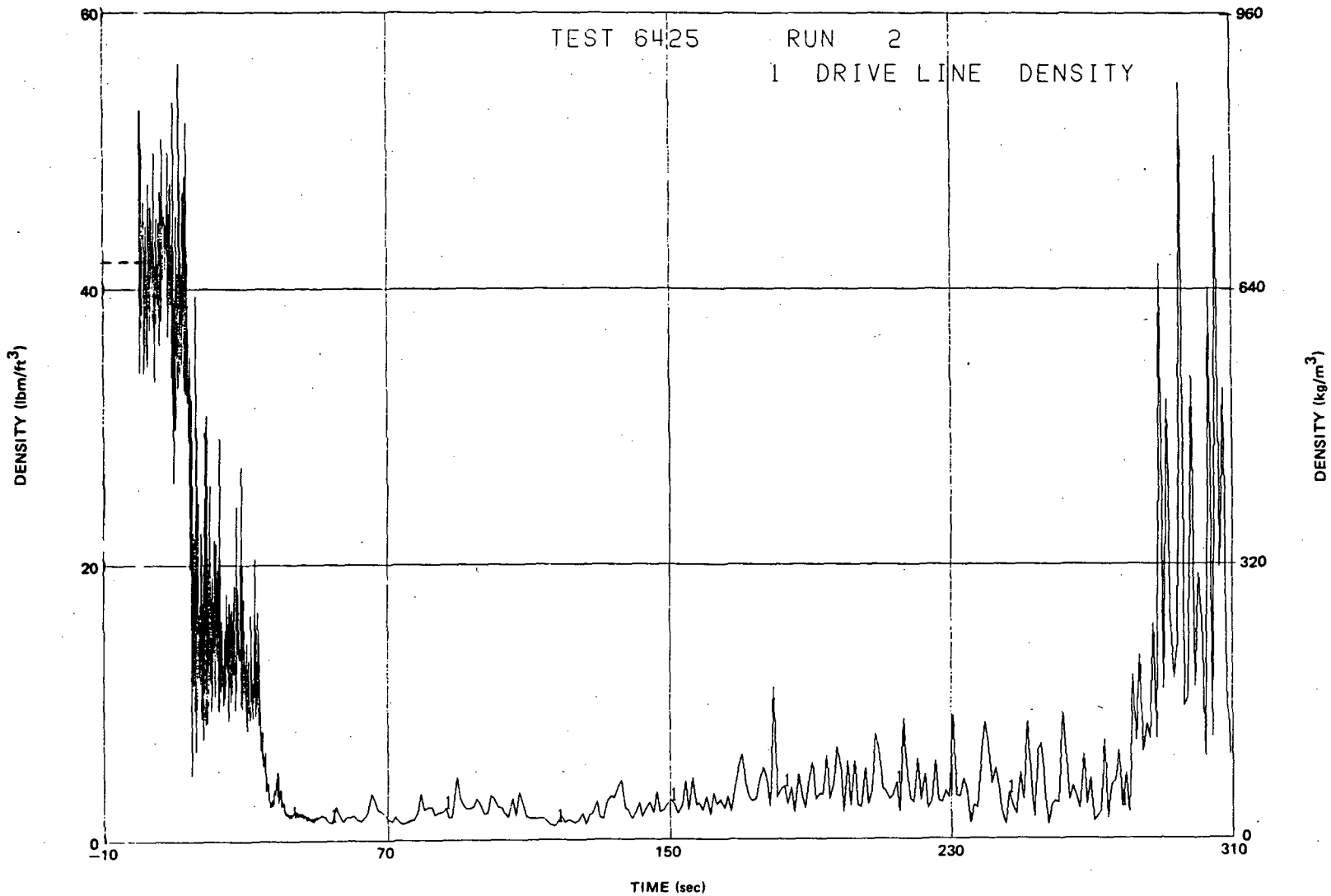

Figure J-66. Drive Line Break Density

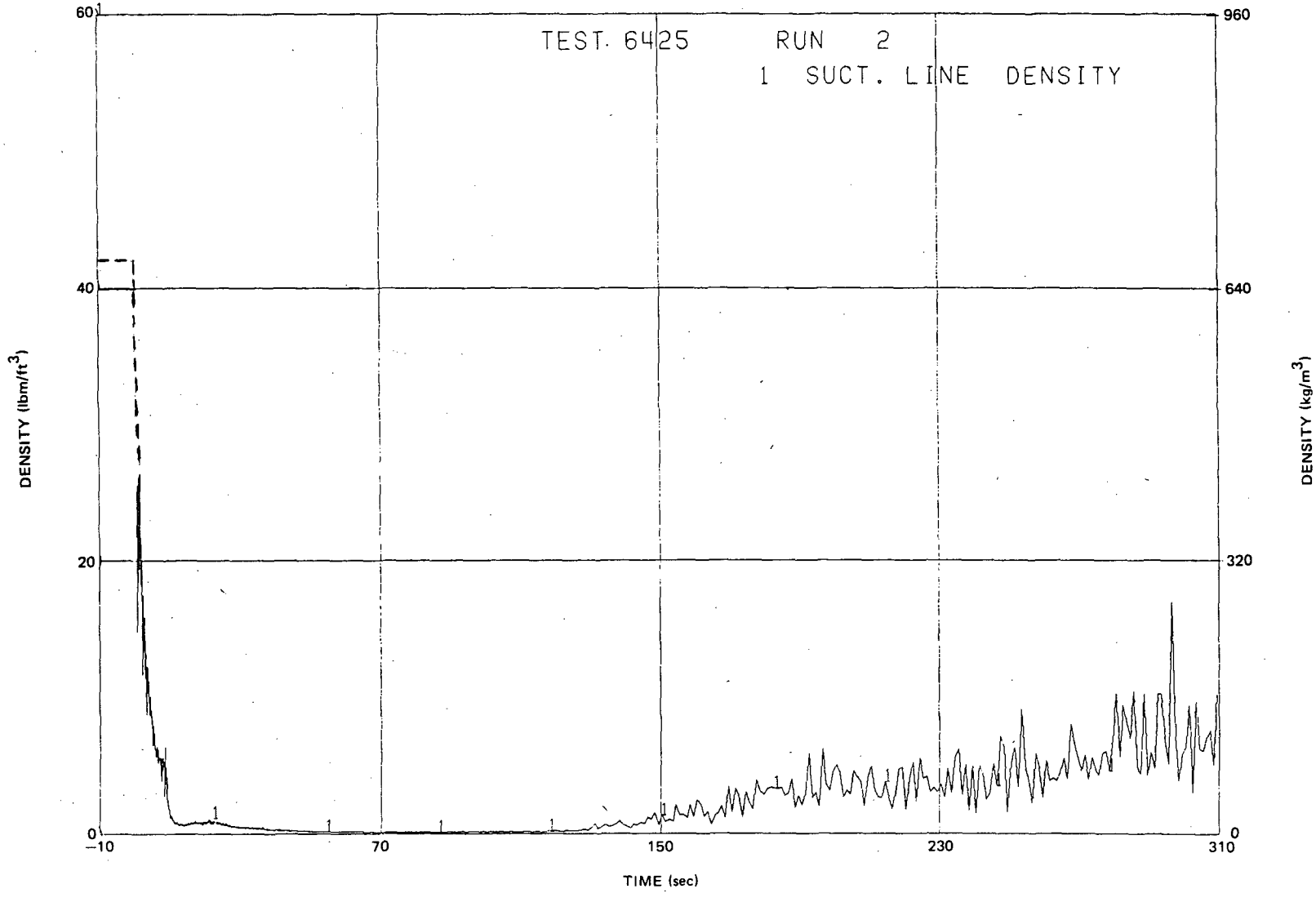

Figure J-67. Suction Line Break Density

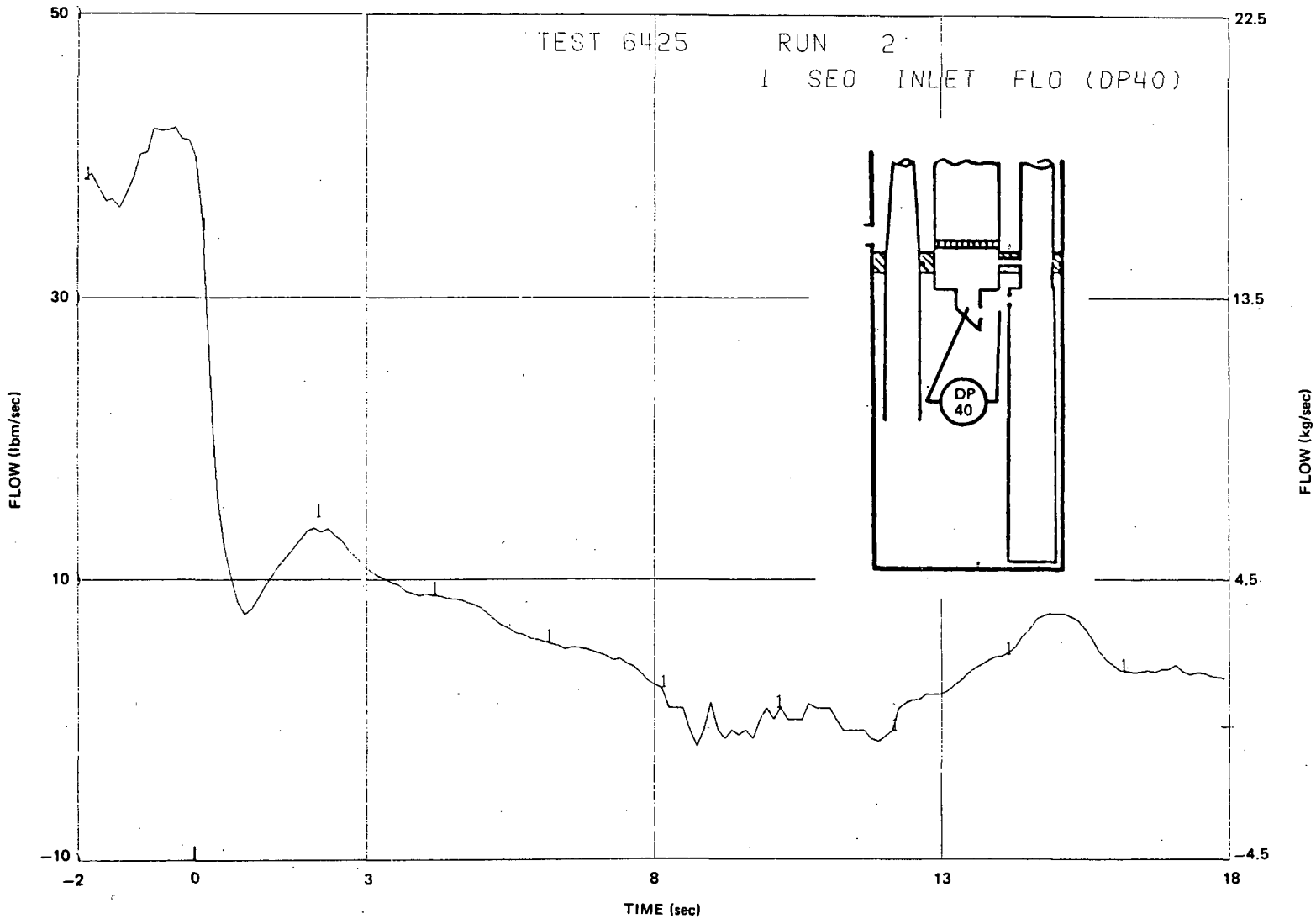

Figure J-68. Bundle Inlet Side Entry Orifice Mass Flow Rate

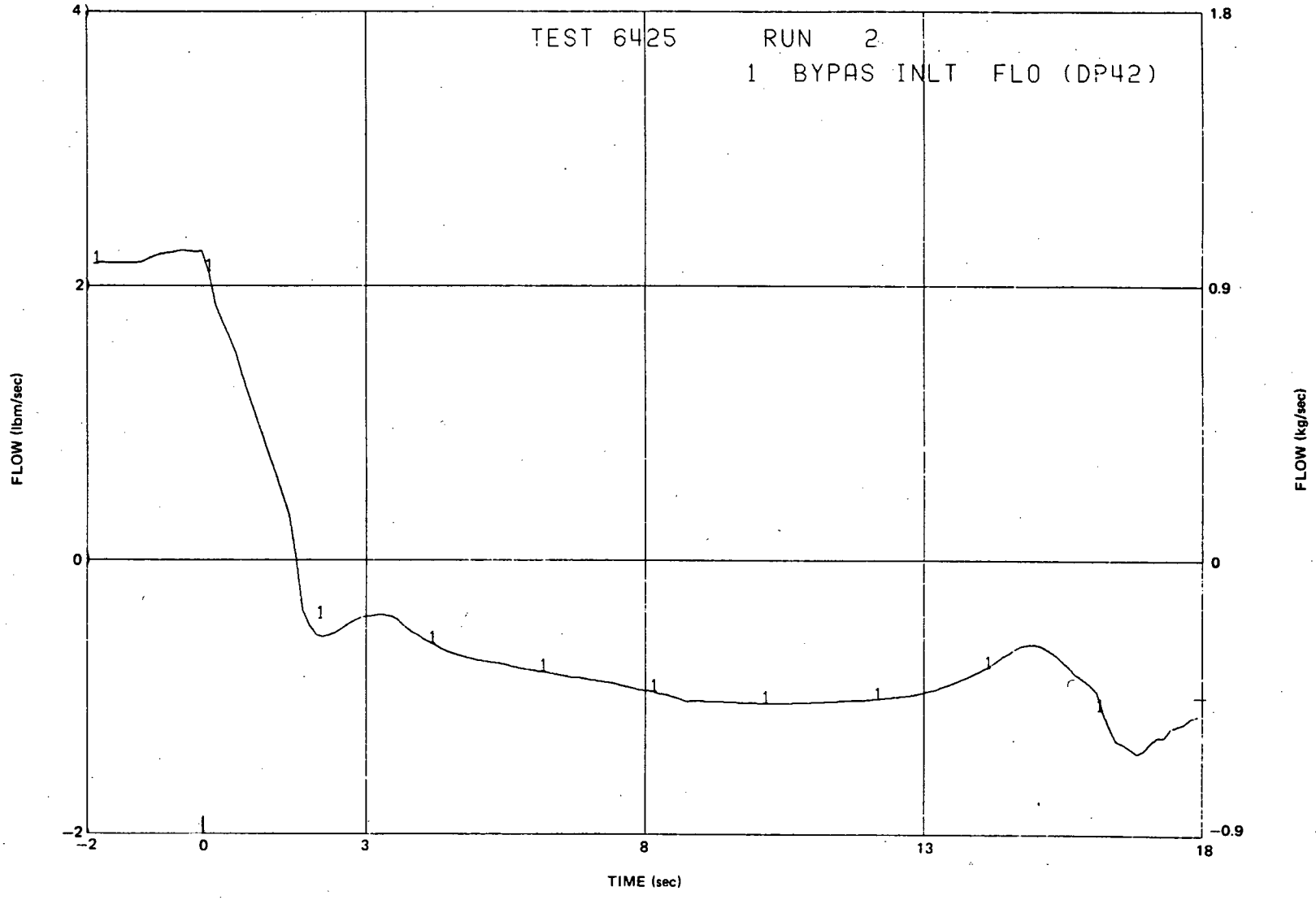

Figure J-69. Bypass Leakage Path Mass Flow Rate

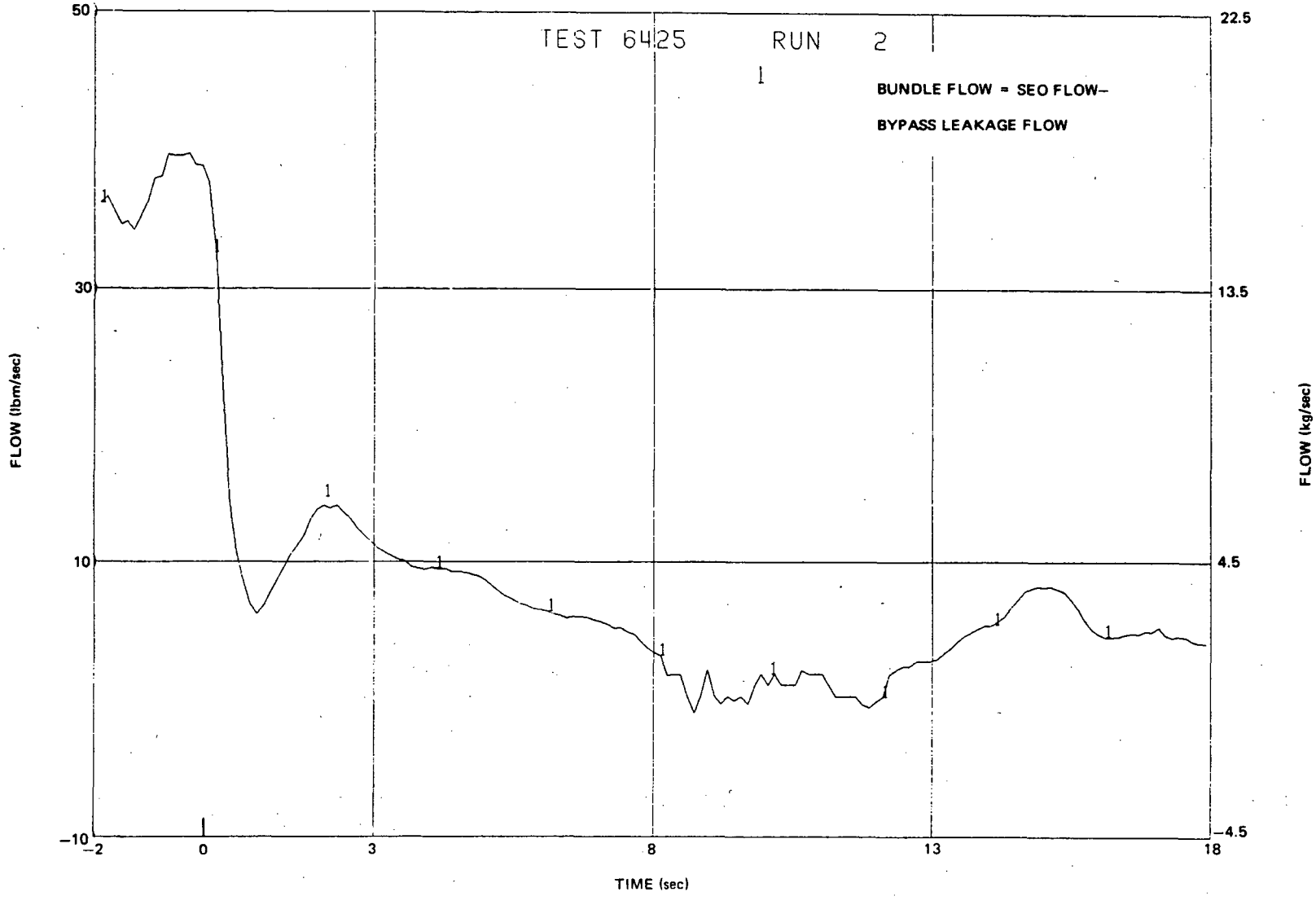

Figure J-70. Bundle Mass Flow Rate

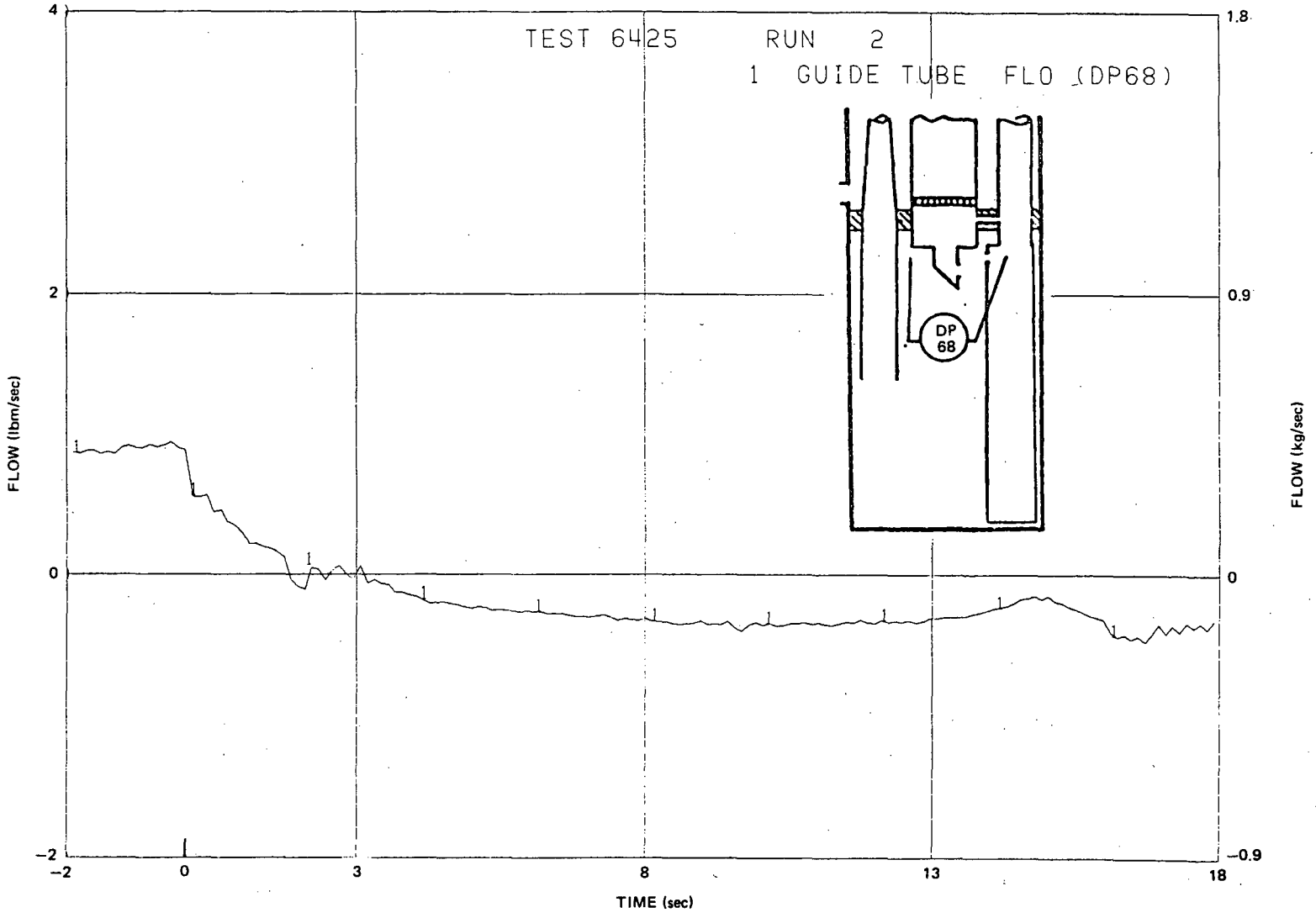

Figure J-71. Lower Plenum to Guide Tube Mass Flow Rate

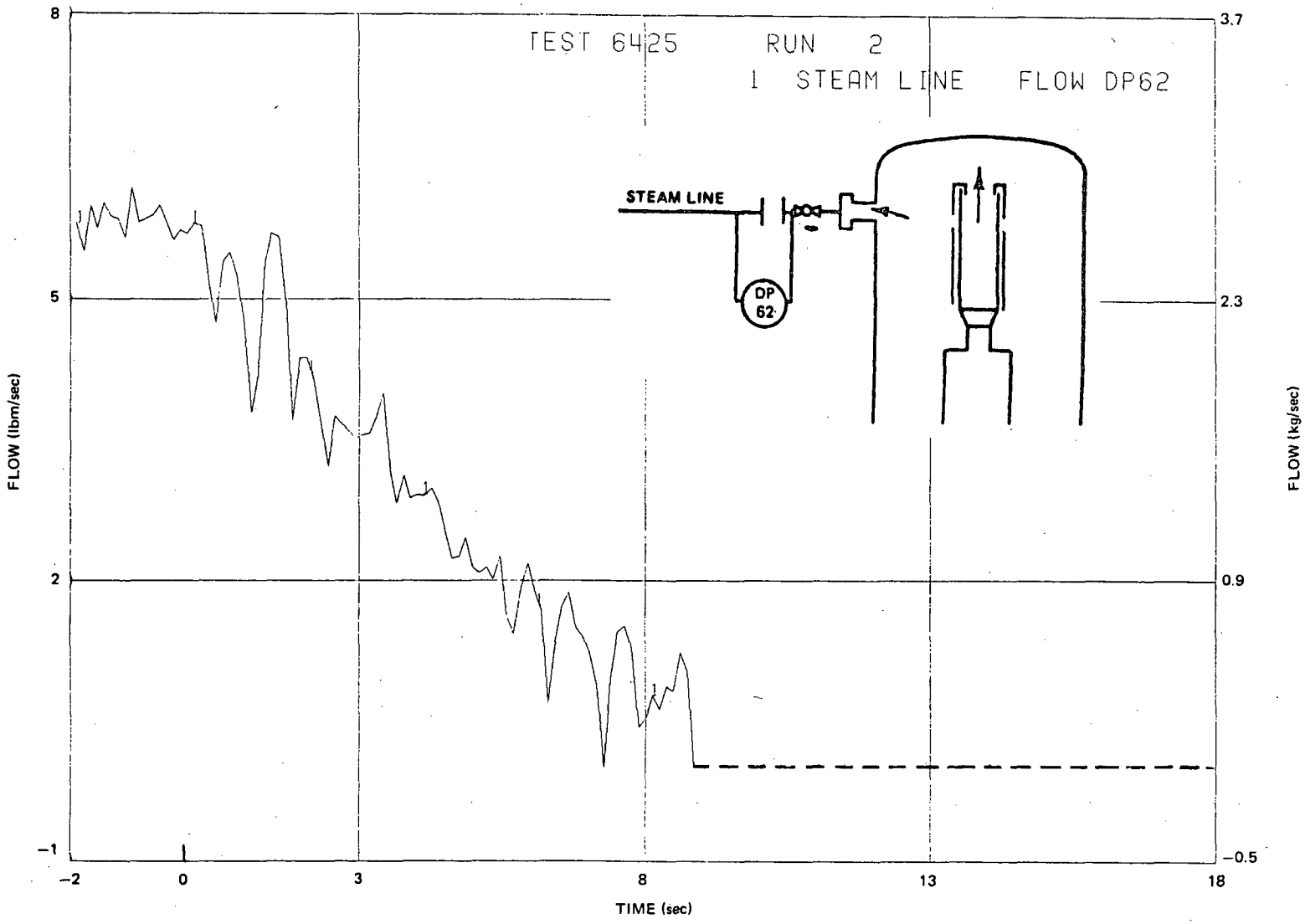

Figure J-72. Steam Line Mass Flow Rate

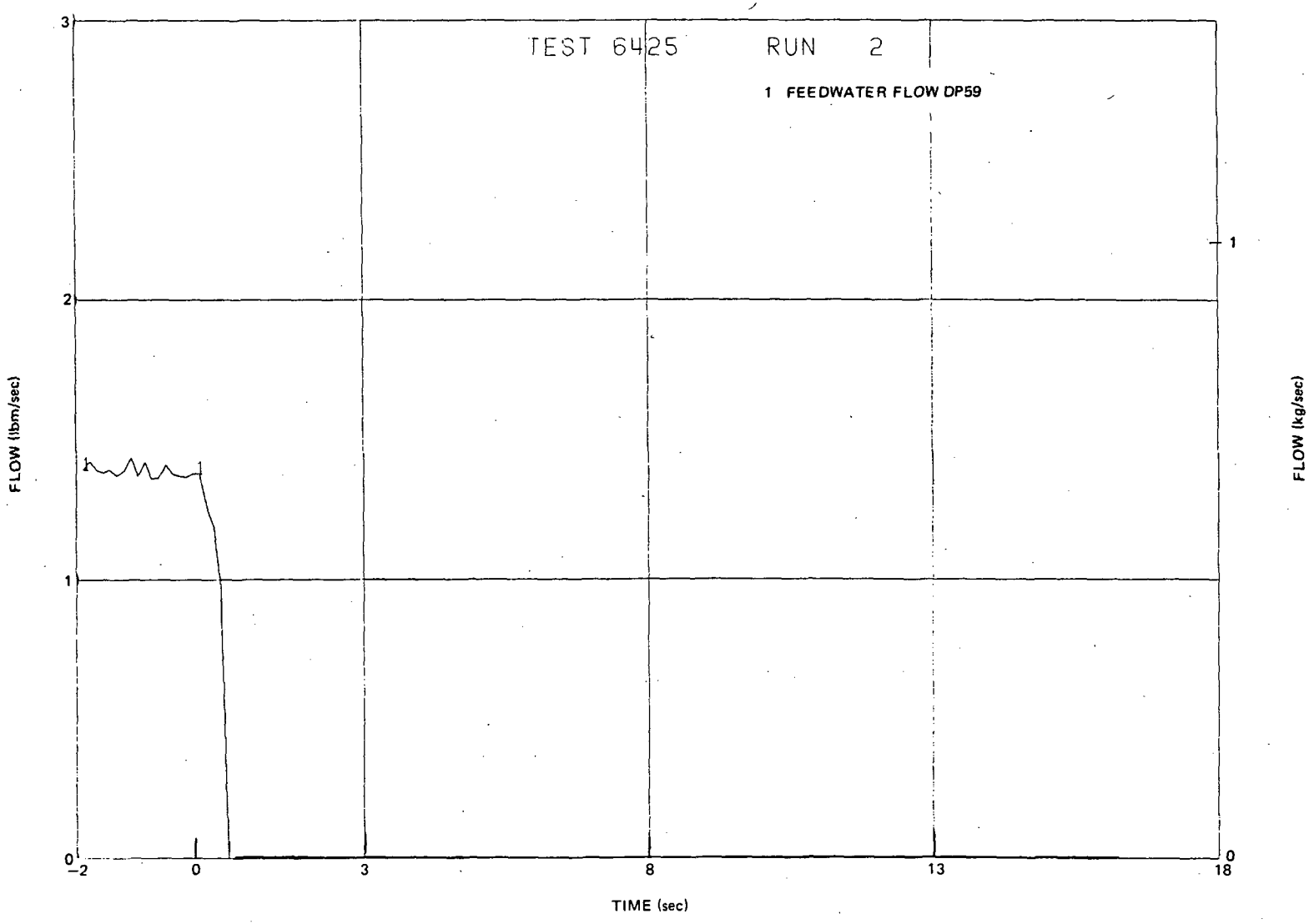

Figure J-73. Feedwater Mass Flow Rate

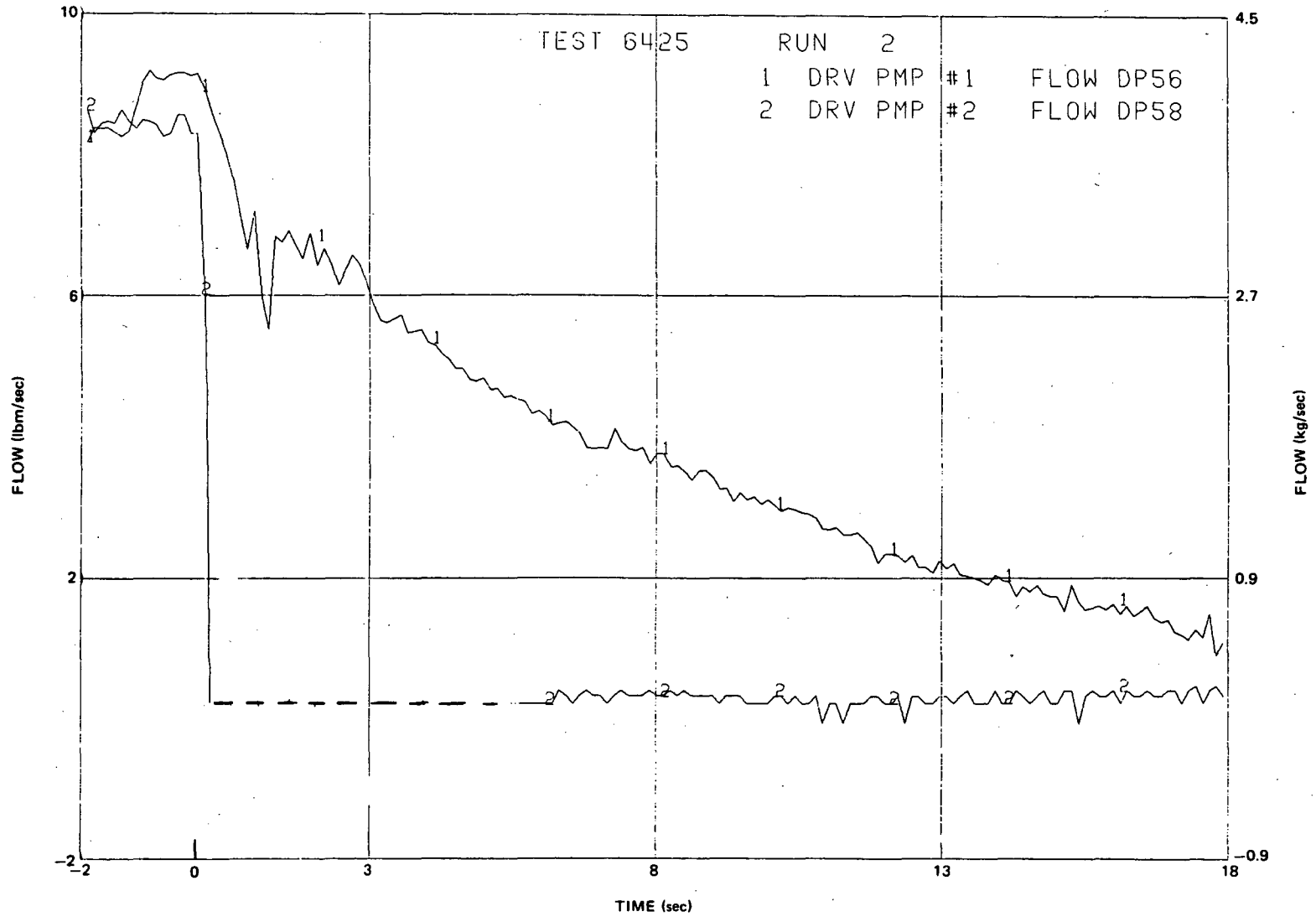

Figure J-74. Recirculation Pump Mass Flow Rates

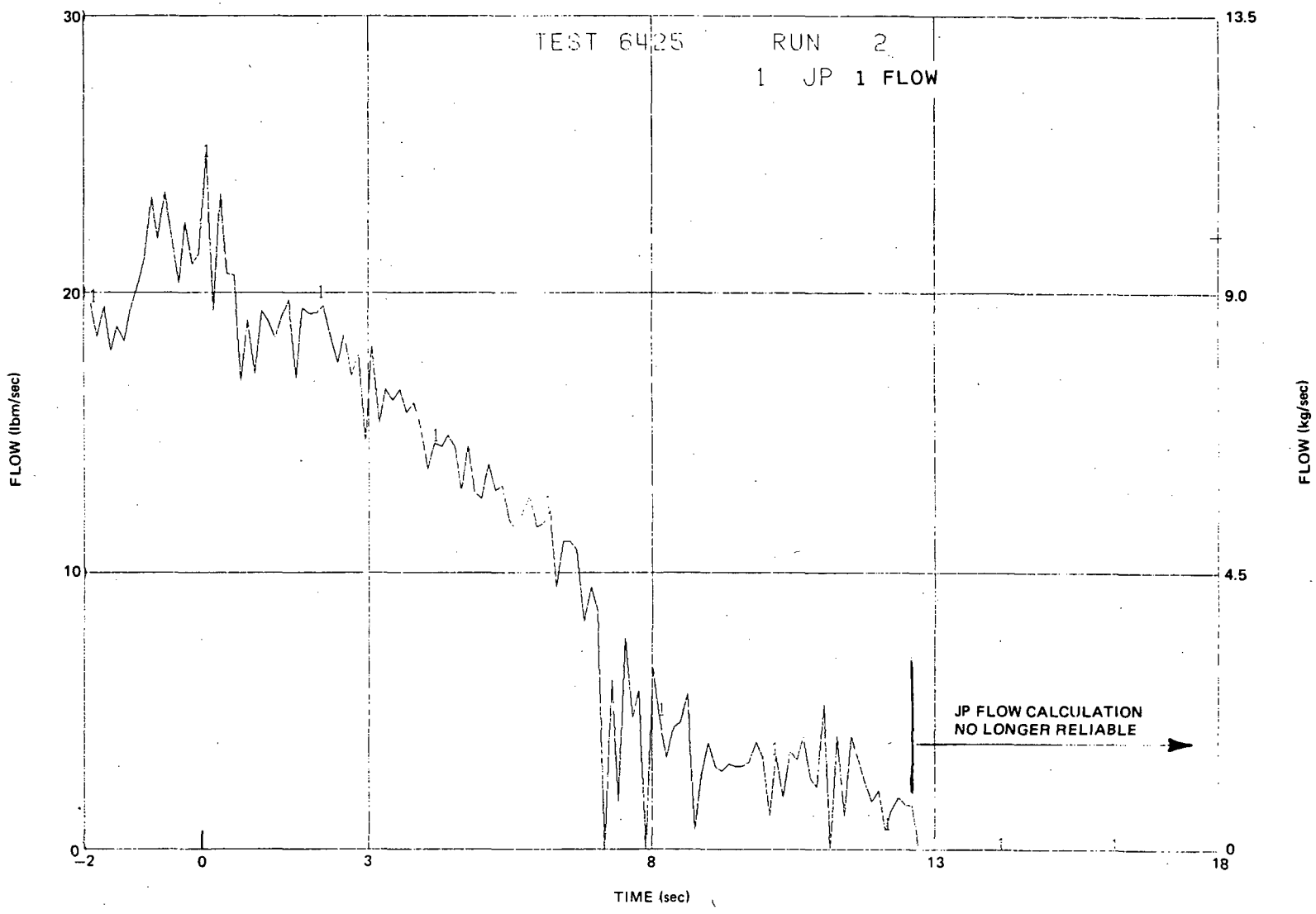

Figure J-75. Intact Loop Jet Pump Mass Flow Rate

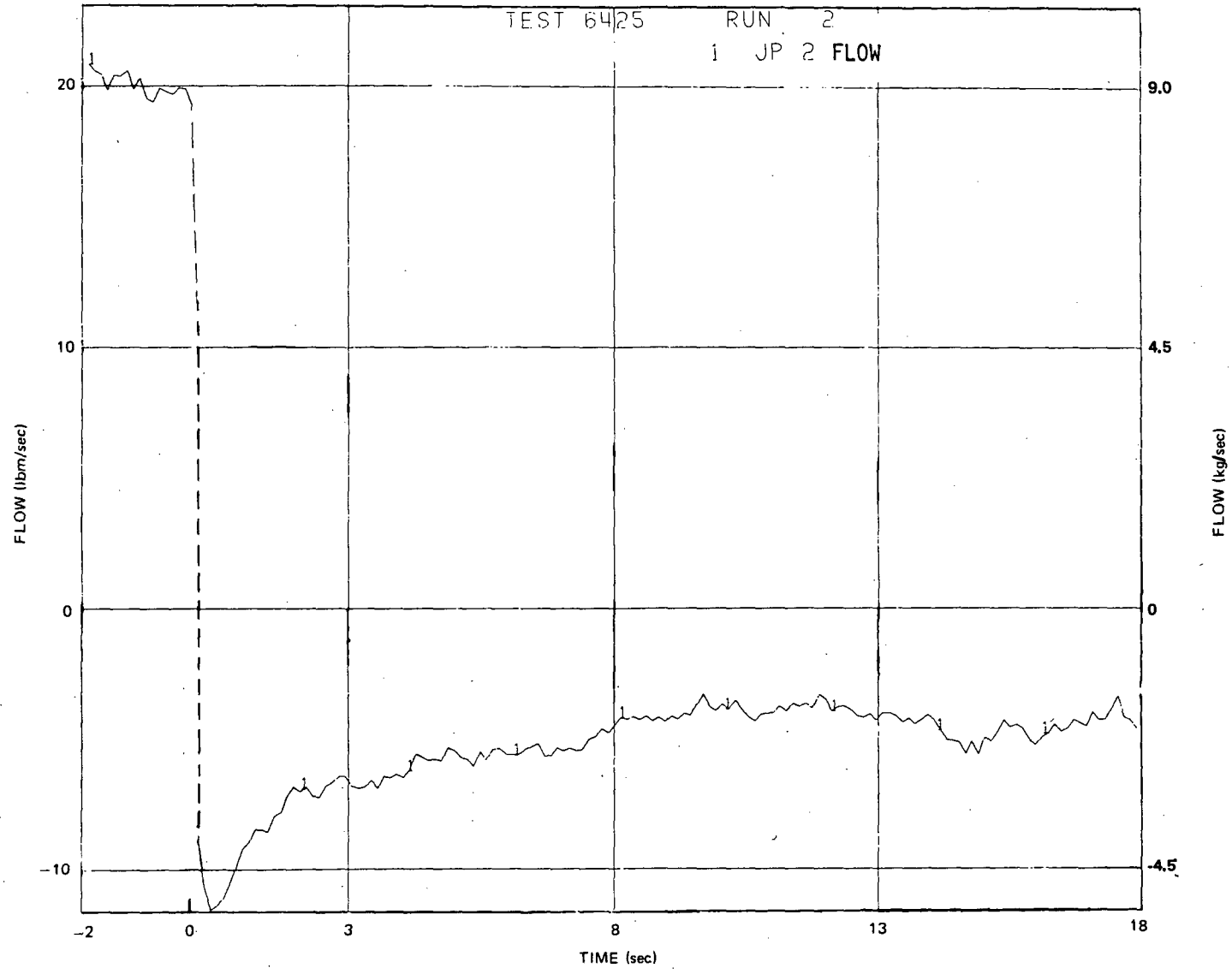

Figure J-76. Broken Loop Jet Pump Mass Flow Rate

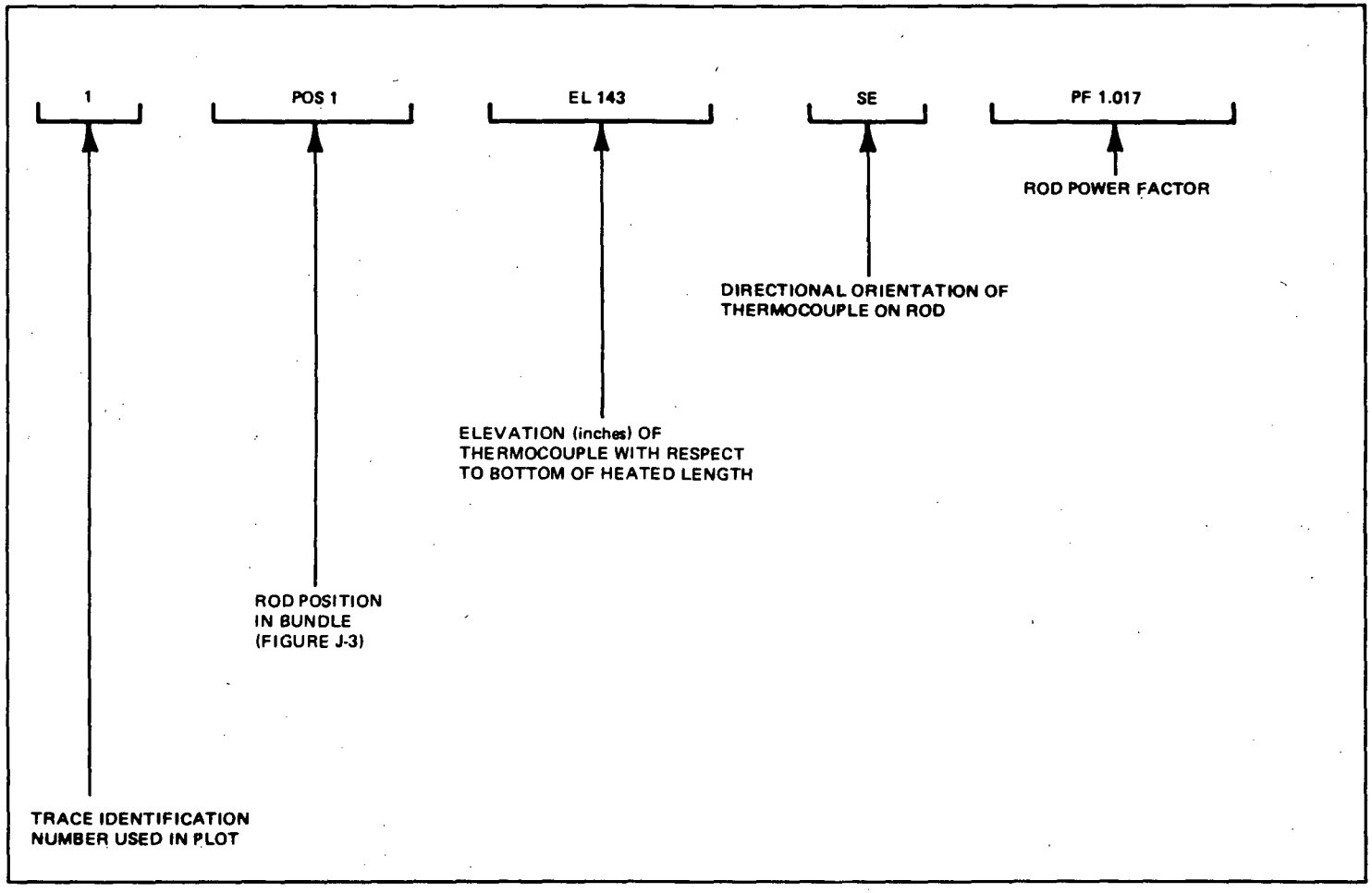

Figure J-77. Guide for Interpreting Legends on Bundle Temperature Plots

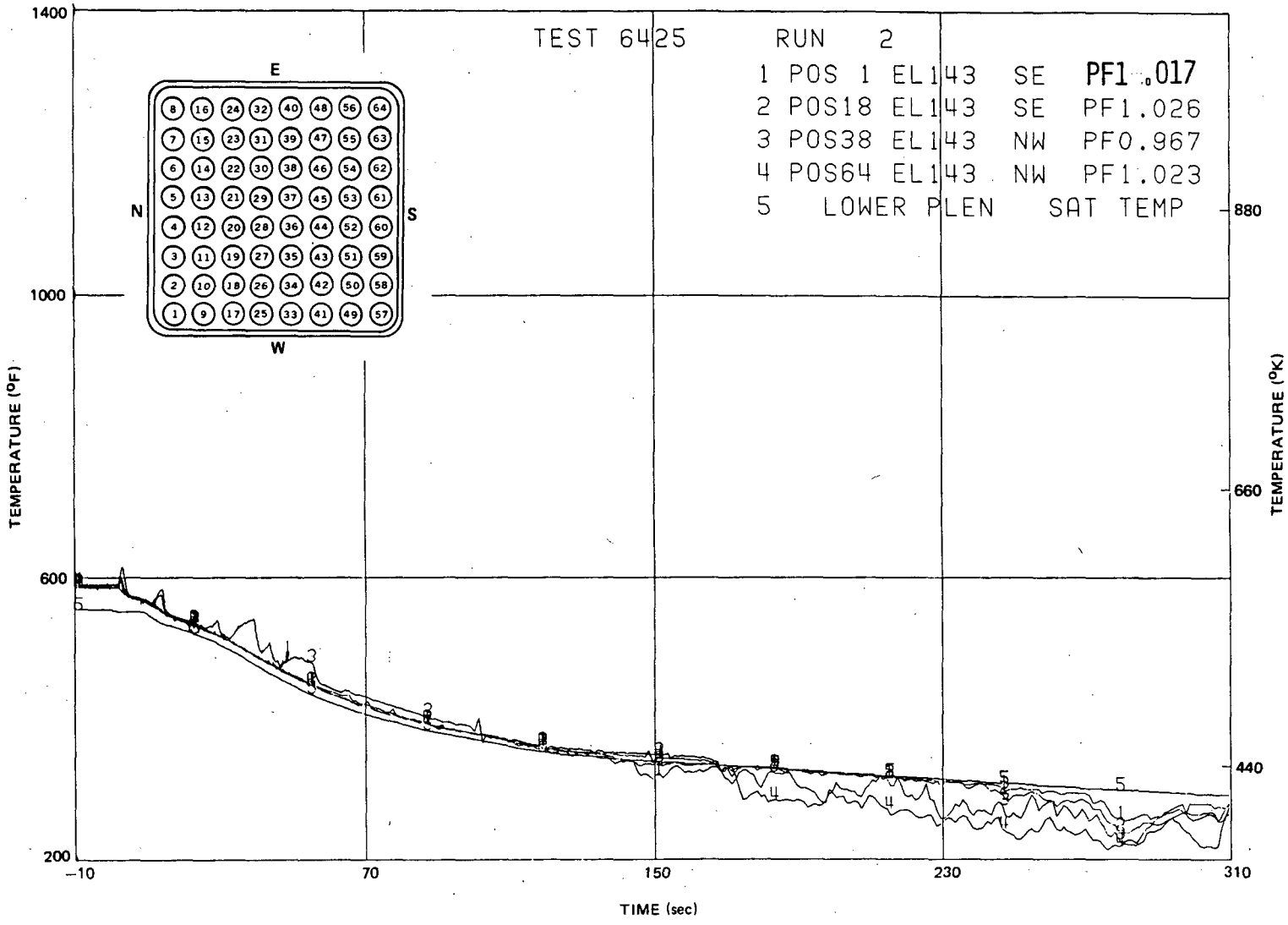

Figure J-78. Inside Clad Temperature-Elevation 143 in.

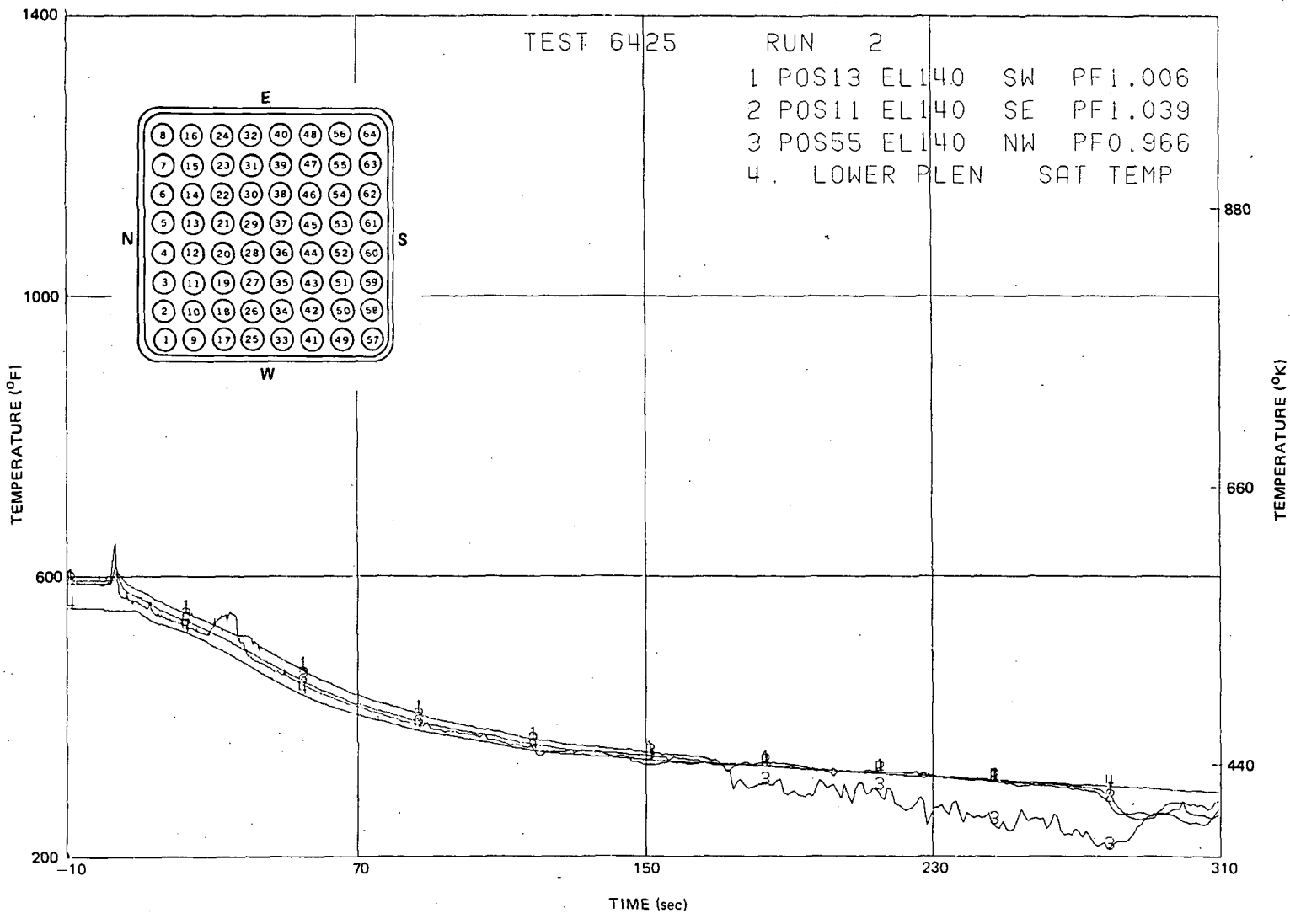

Figure J-79. Inside Clad Temperature-Elevation 140 in.

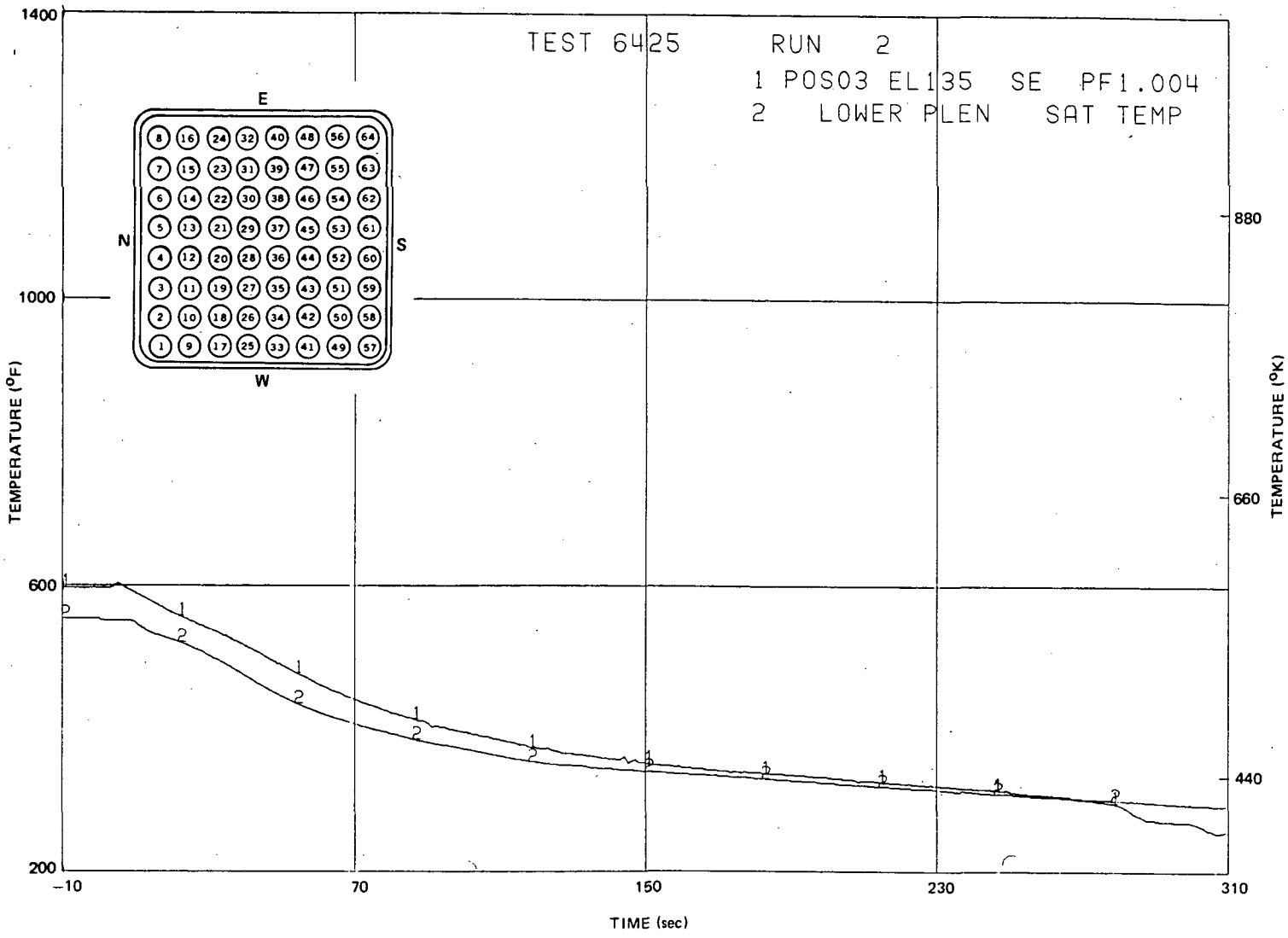

Figure J-80. Inside Clad Temperature-Elevation 135 in.

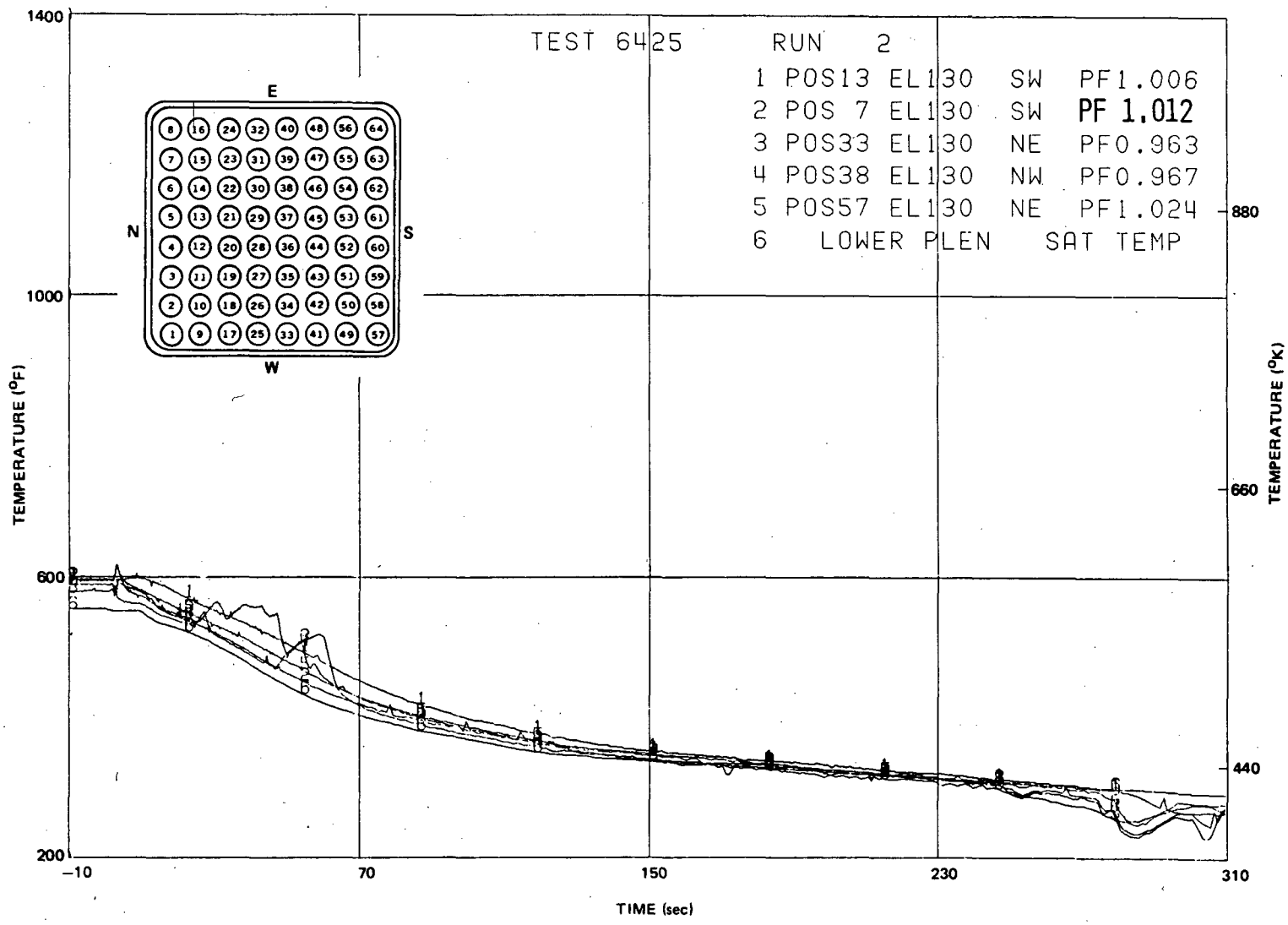

Figure J-81. Inside Clad Temperature-Elevation 130 in.

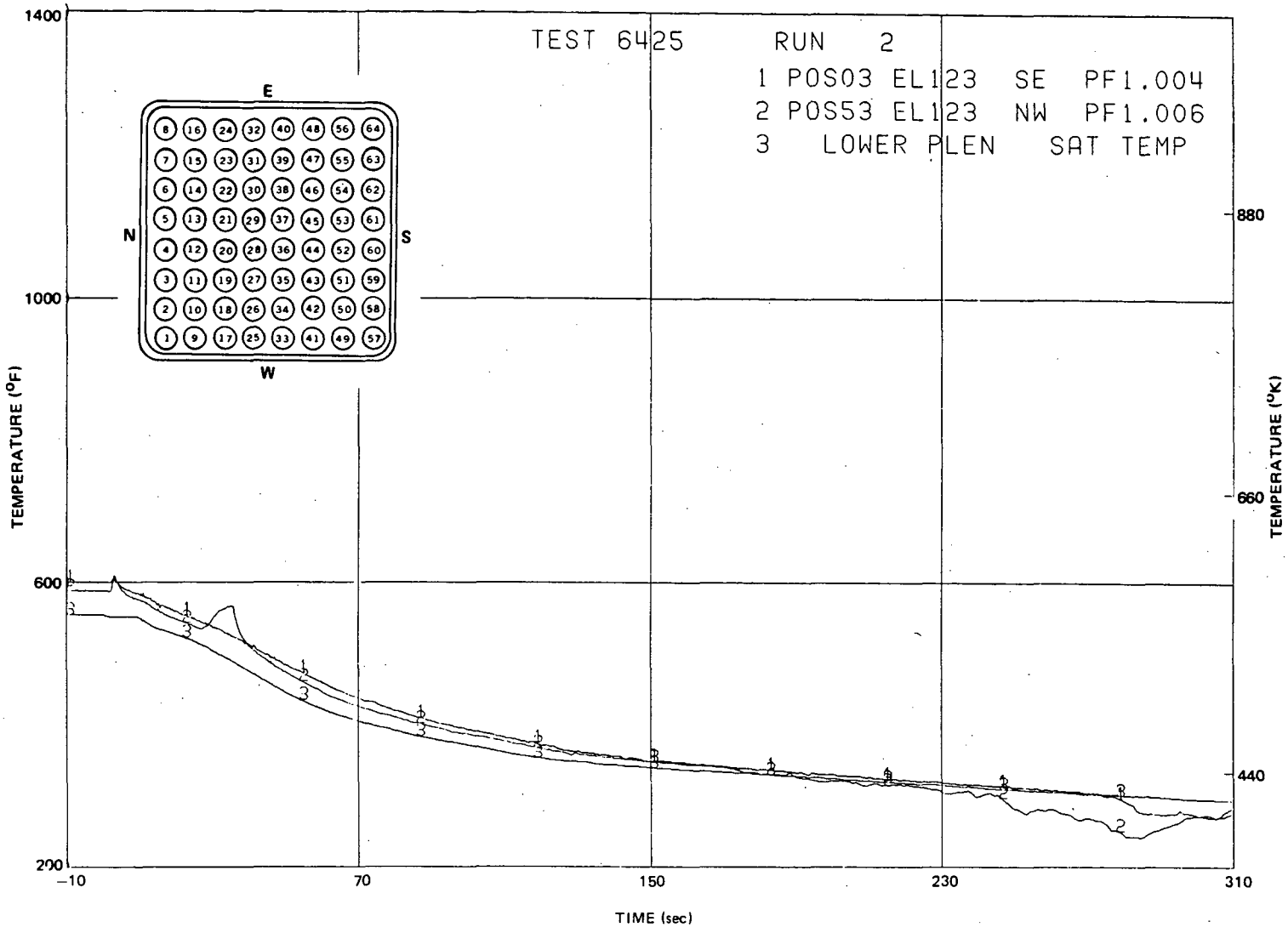

Figure J-82. Inside Clad Temperature-Elevation 123 in.

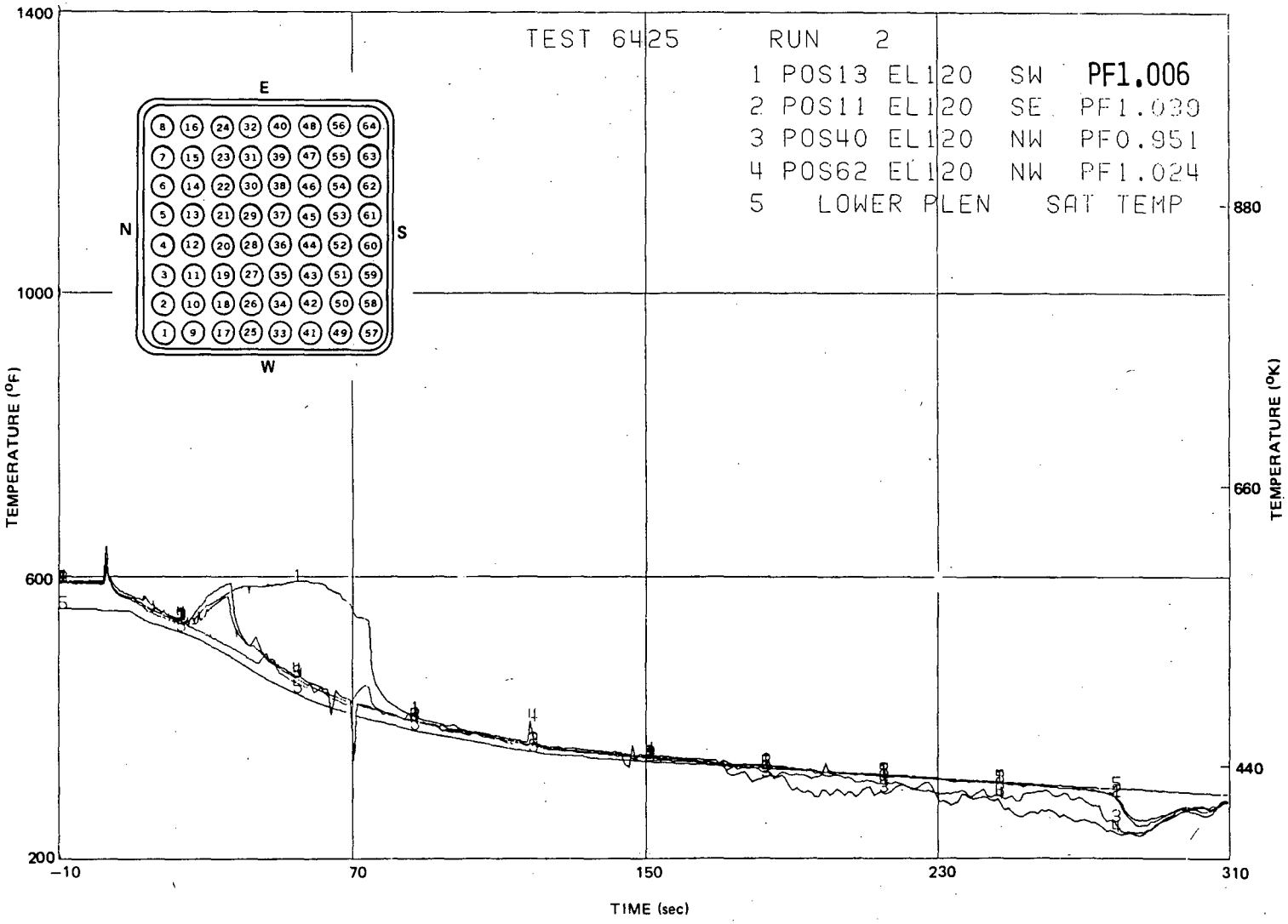

Figure J-83. Inside Clad Temperature-Elevation 120 in.

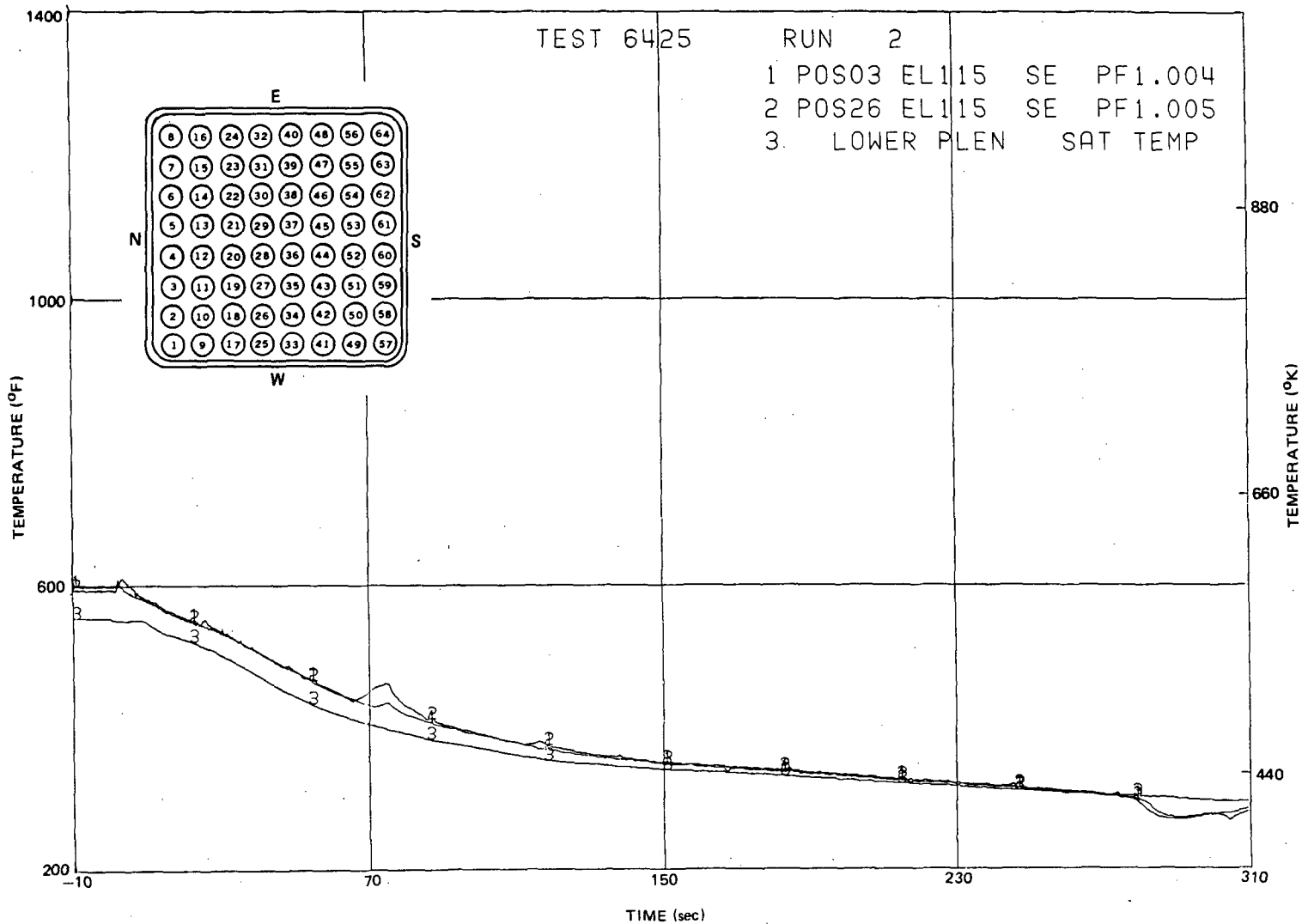

Figure J-84. Inside Clad Temperature-Elevation 115 in.

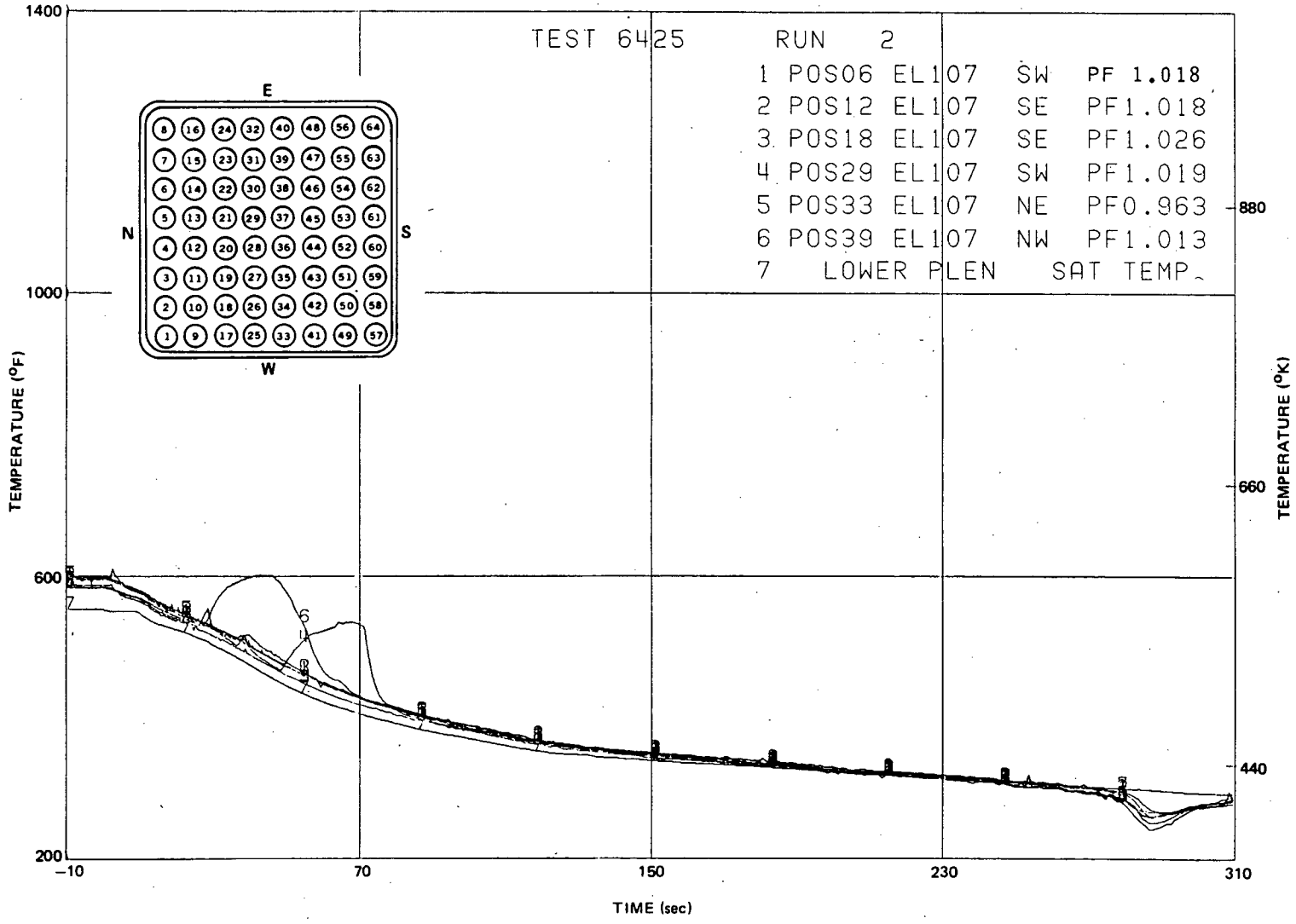

Figure J-85. Inside Clad Temperature-Elevation 107 in.

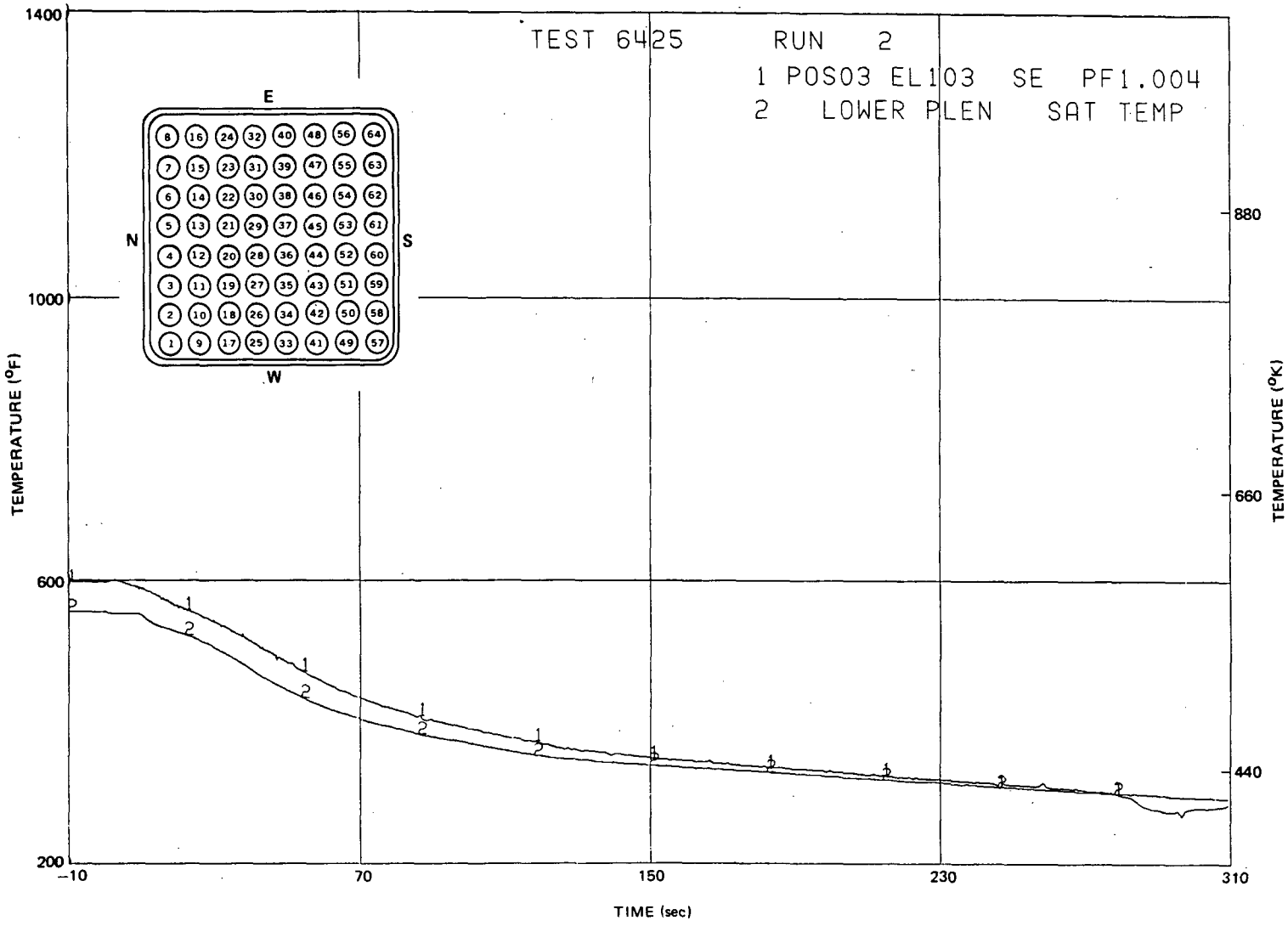

Figure J-86. Inside Clad Temperature-Elevation 103 in.

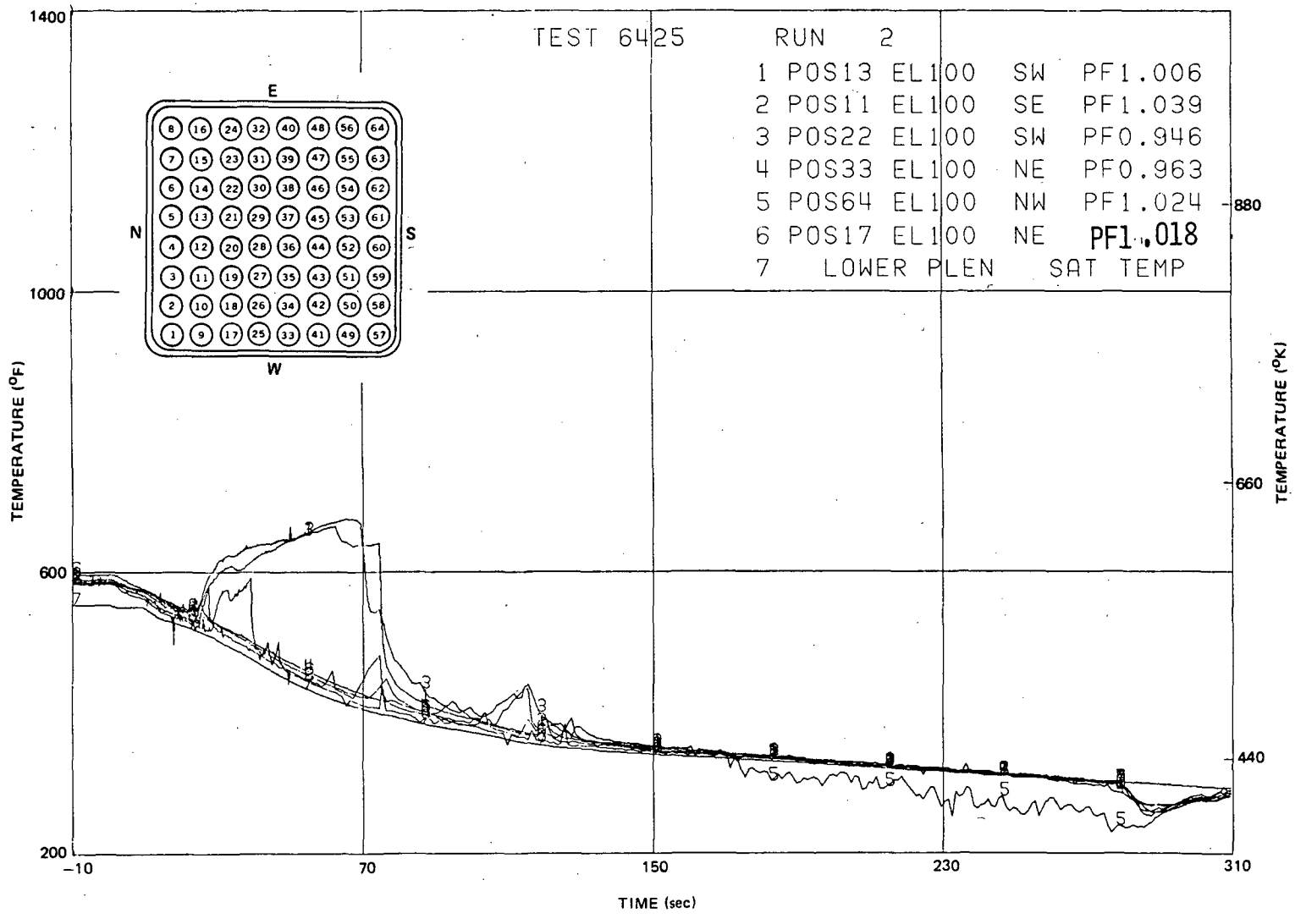

Figure J-87. Inside Clad Temperature-Elevation 100 in.

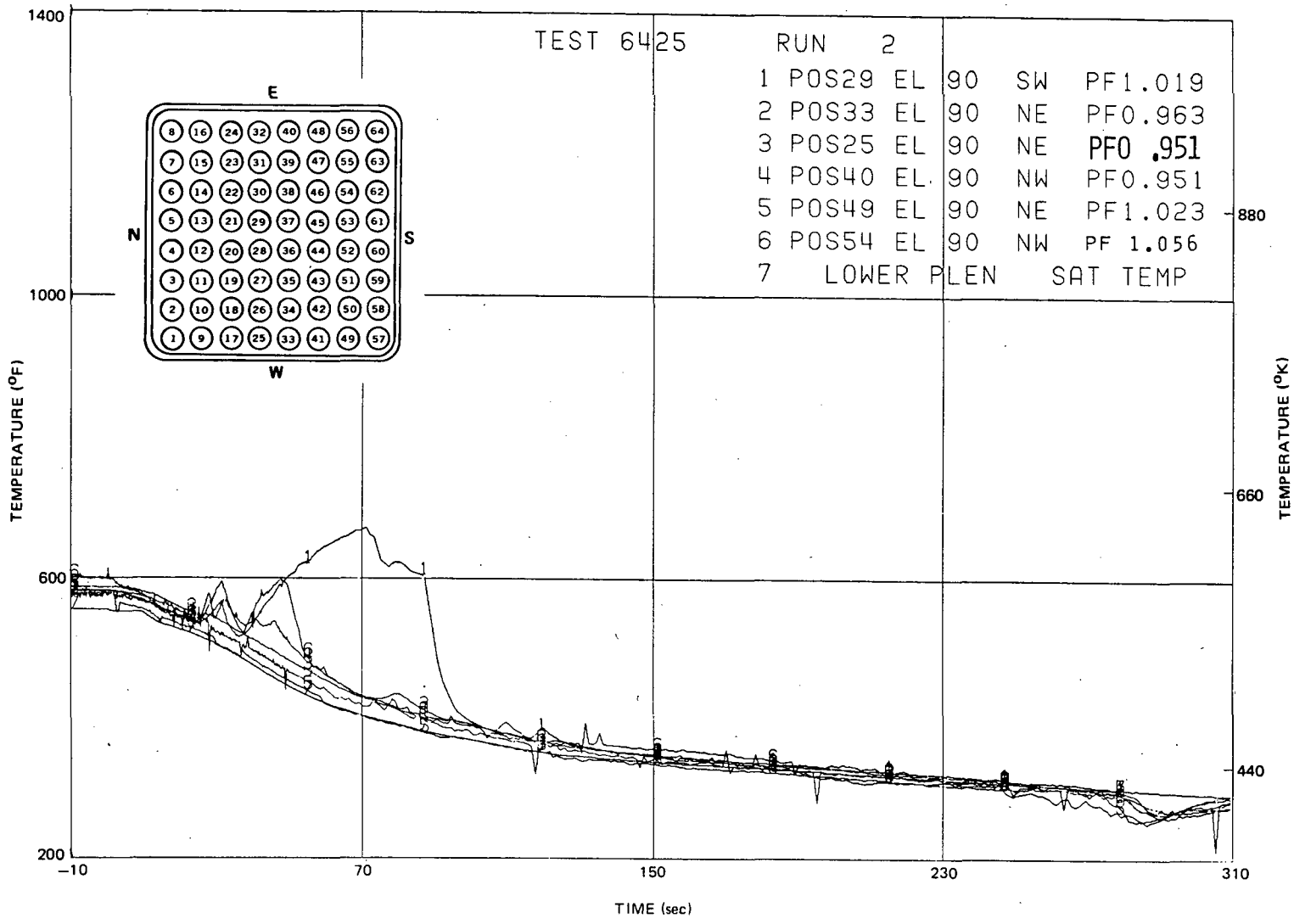

Figure J-88. Inside Clad Temperature-Elevation 90 in.

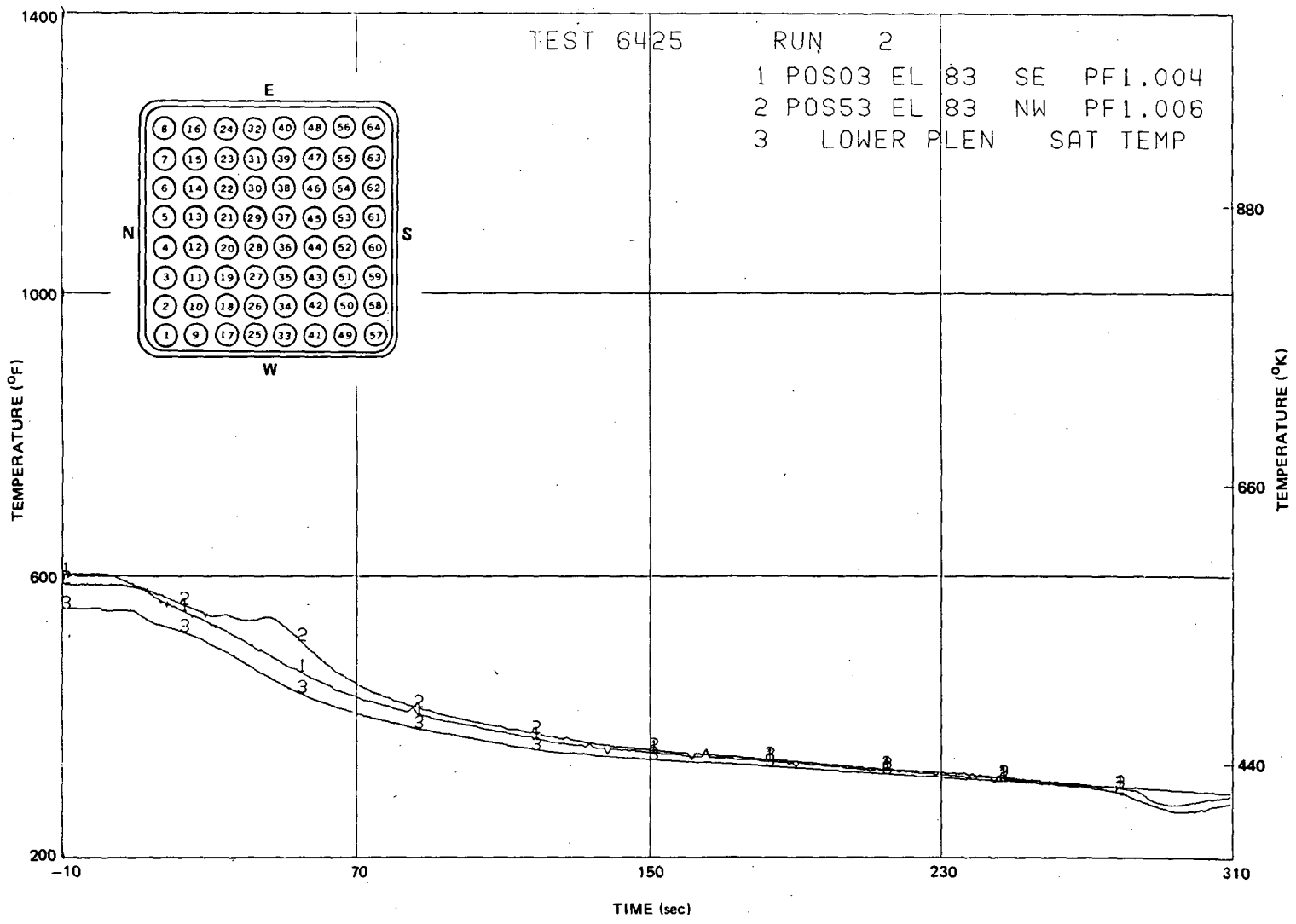

Figure J-89. Inside Clad Temperature-Elevation 83 in.

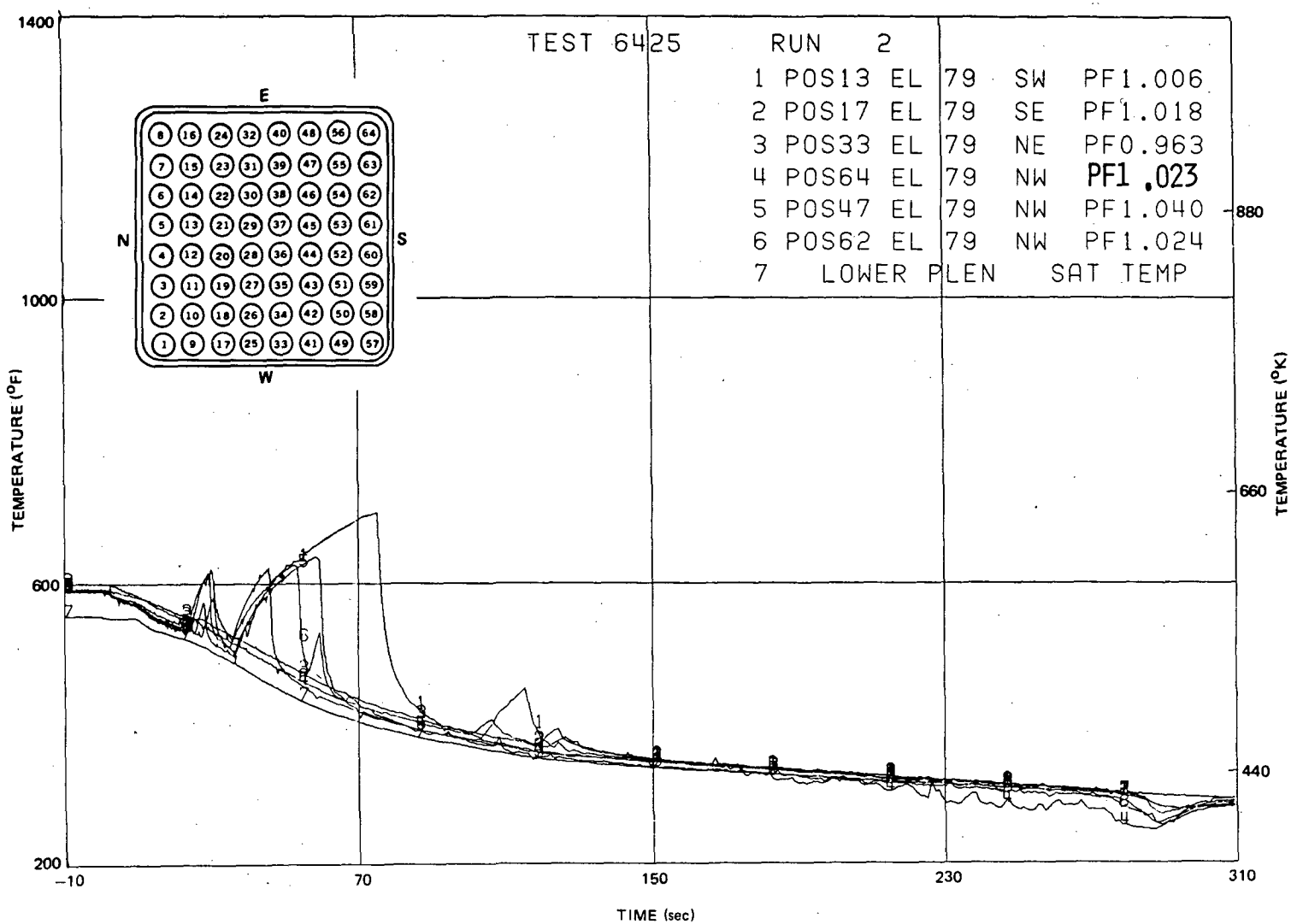

Figure J-90. Inside Clad Temperature-Elevation 79 in.

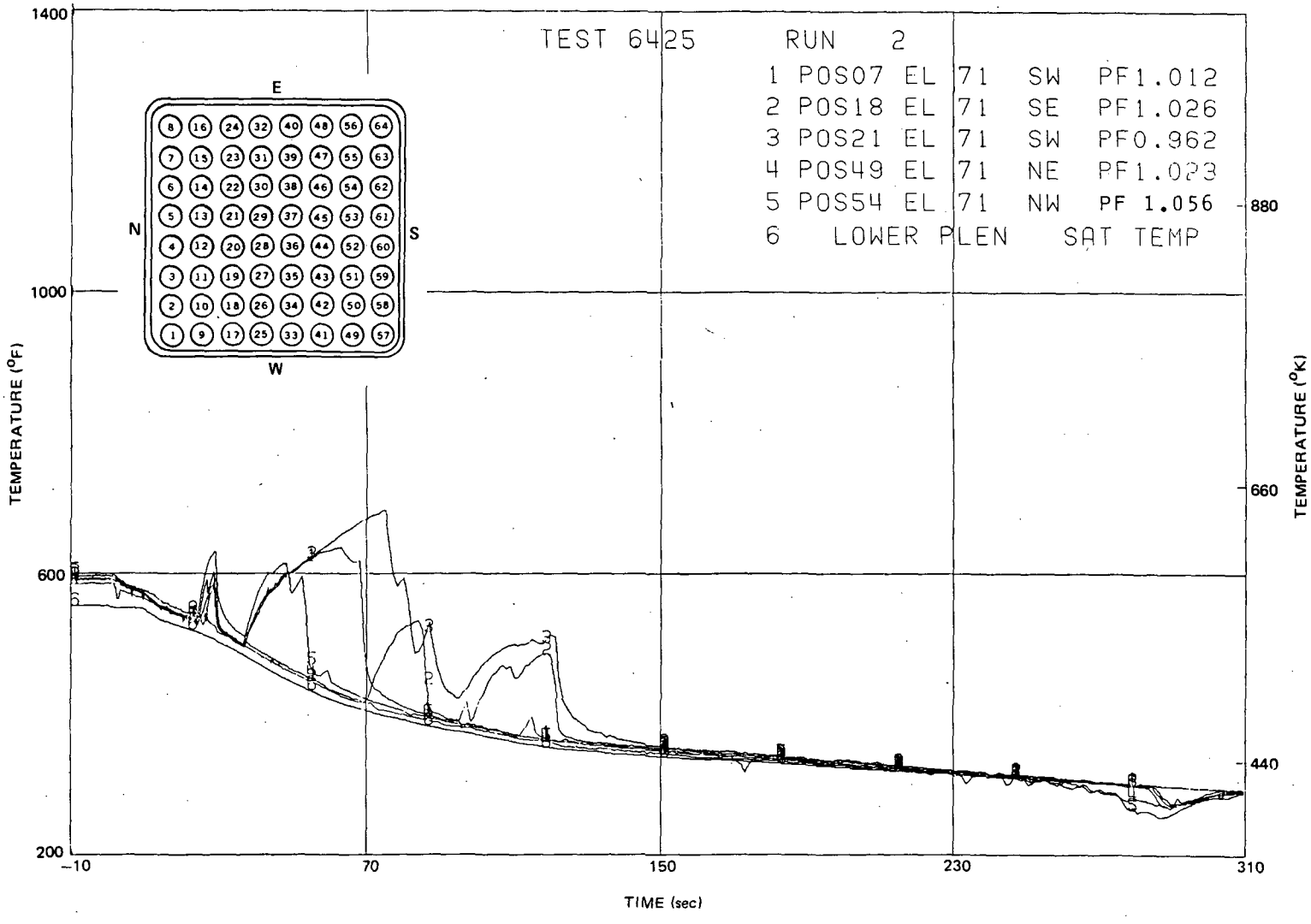

Figure J-91. Inside Clad Temperature-Elevation 71 in.

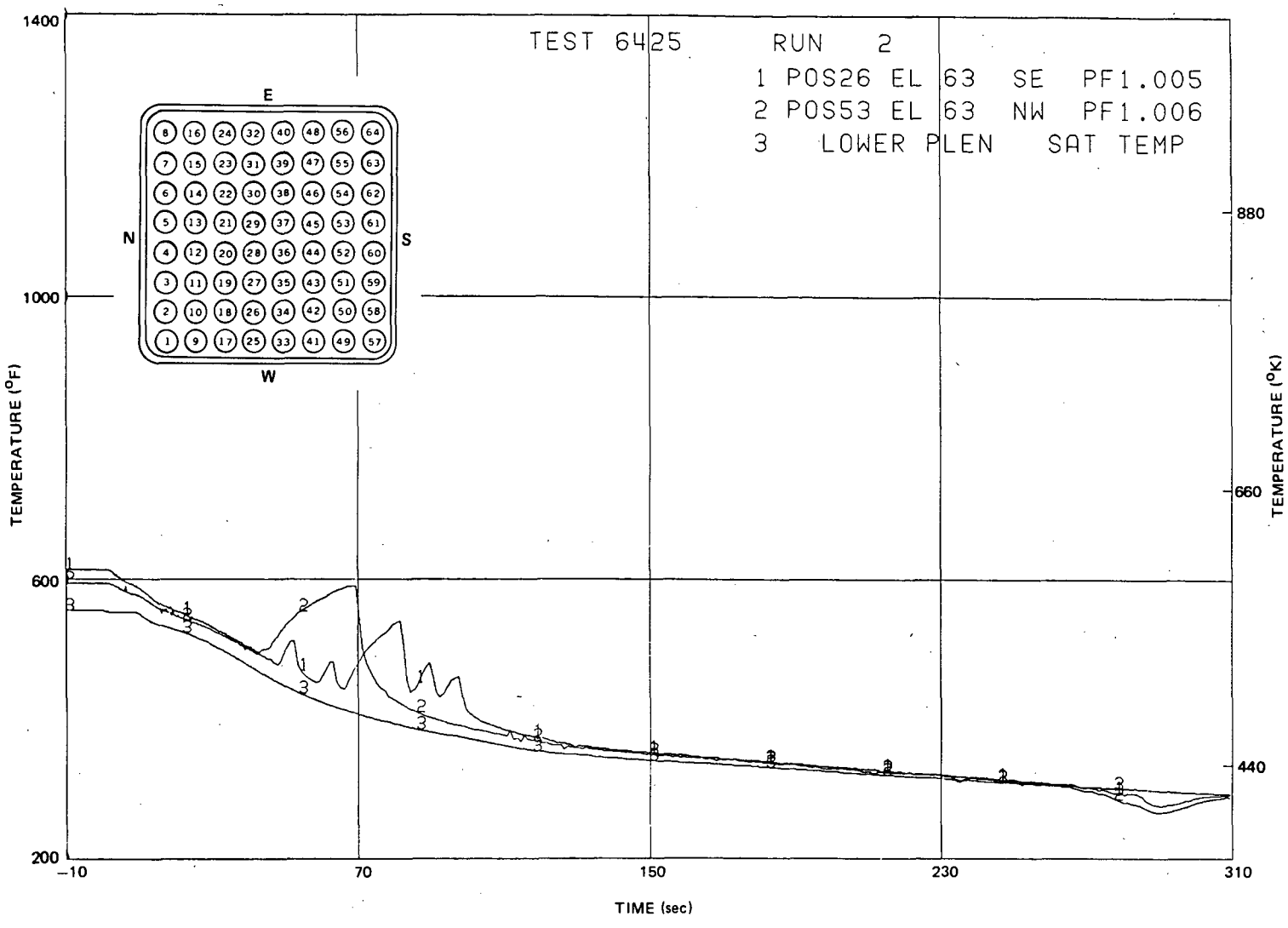

Figure J-92. Inside Clad Temperature-Elevation 63 in.

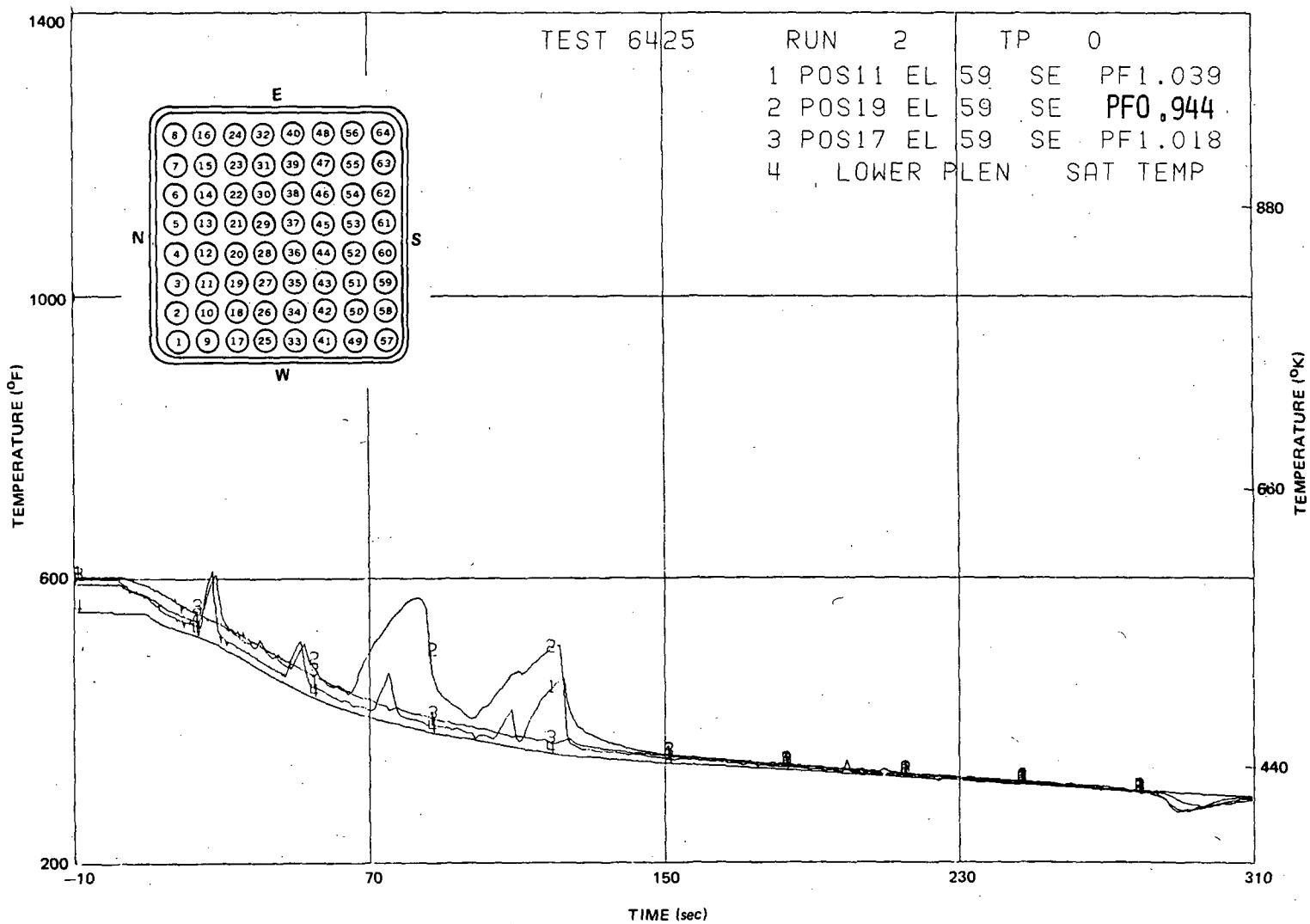

Figure J-93. Inside Clad Temperature-Elevation 59 in.

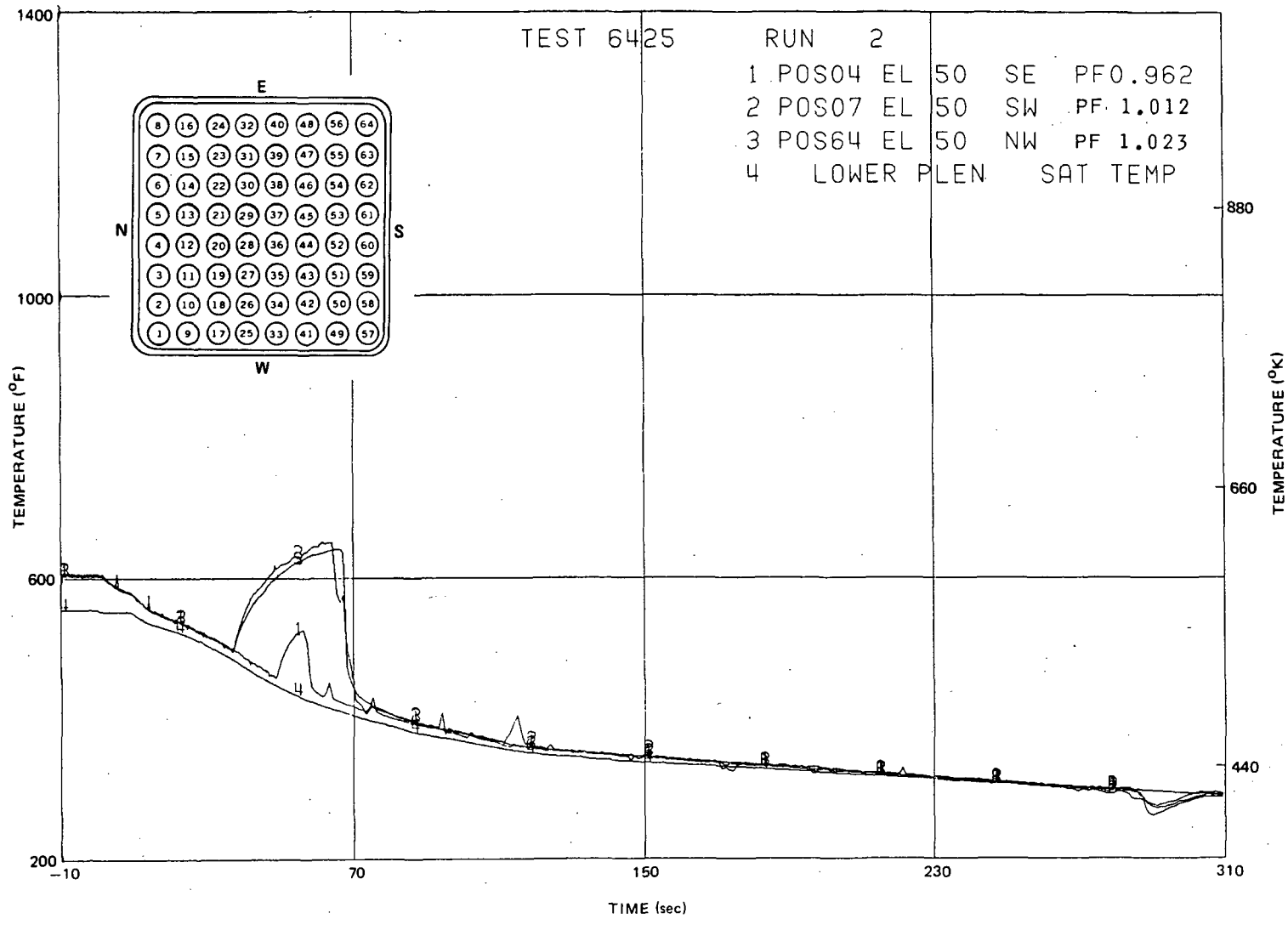

Figure J-94. Inside Clad Temperature-Elevation 50 in.

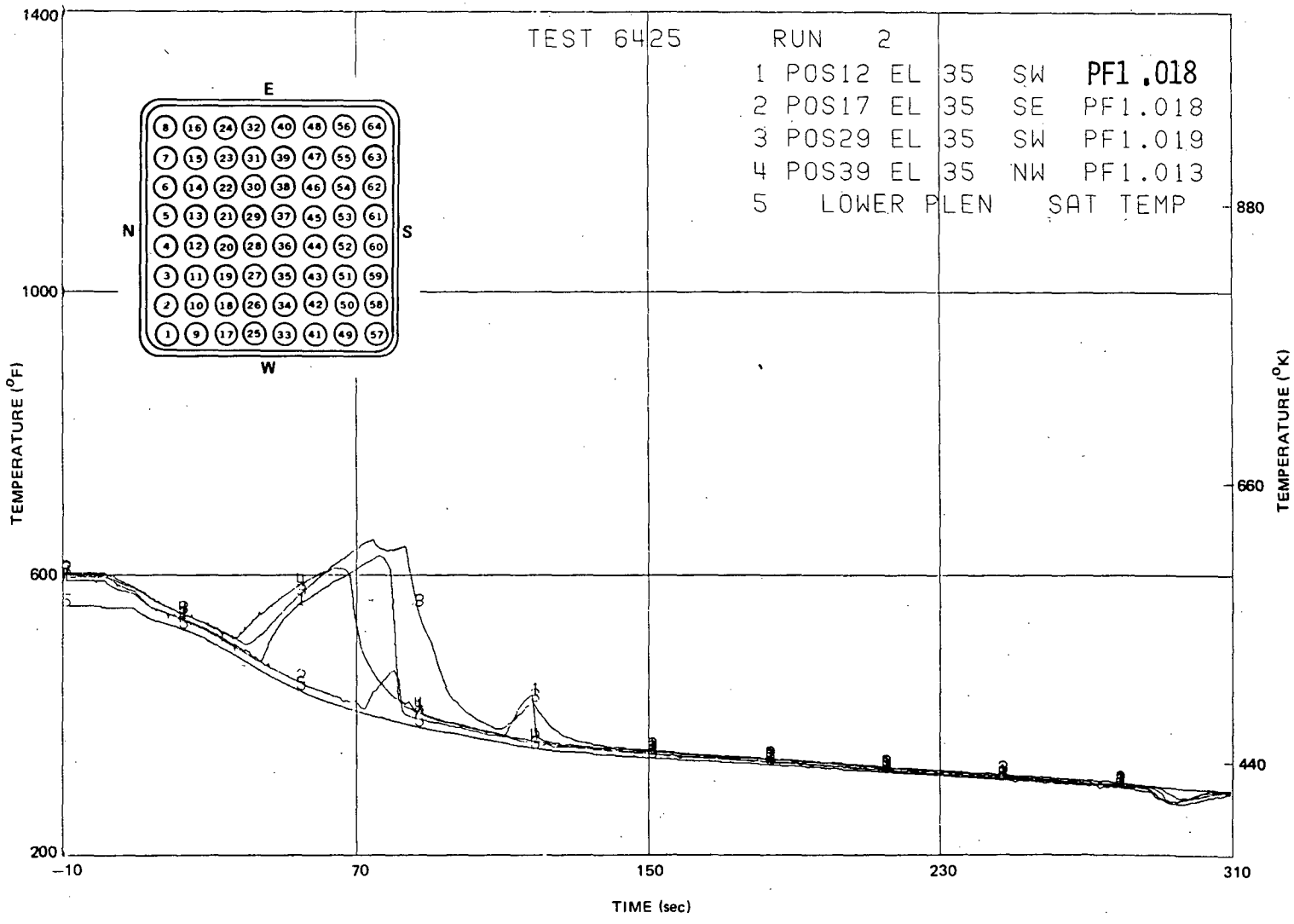

Figure J-95. Inside Clad Temperature-Elevation 35 in.

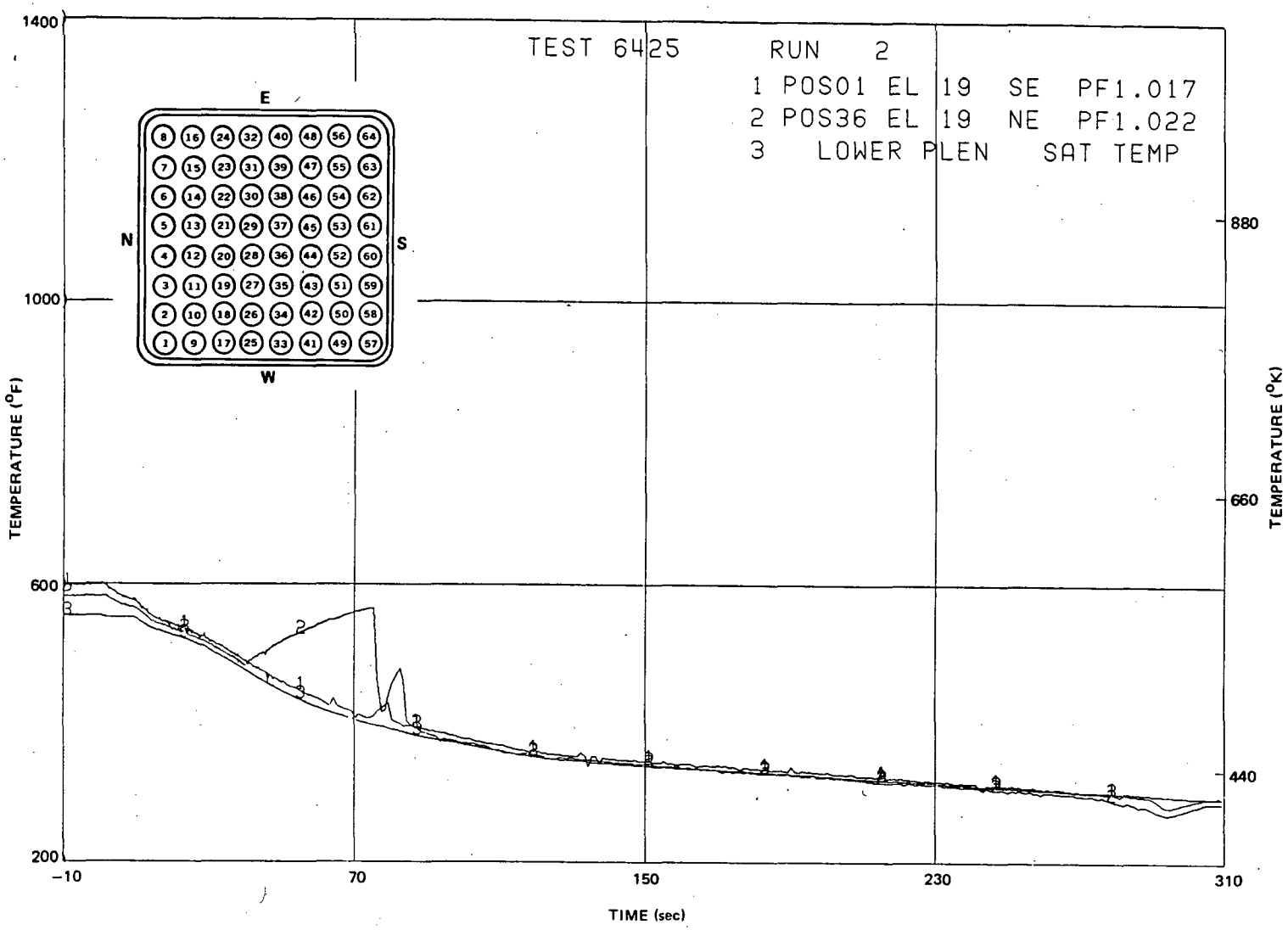

Figure J-96. Inside Clad Temperature-Elevation 19 in.

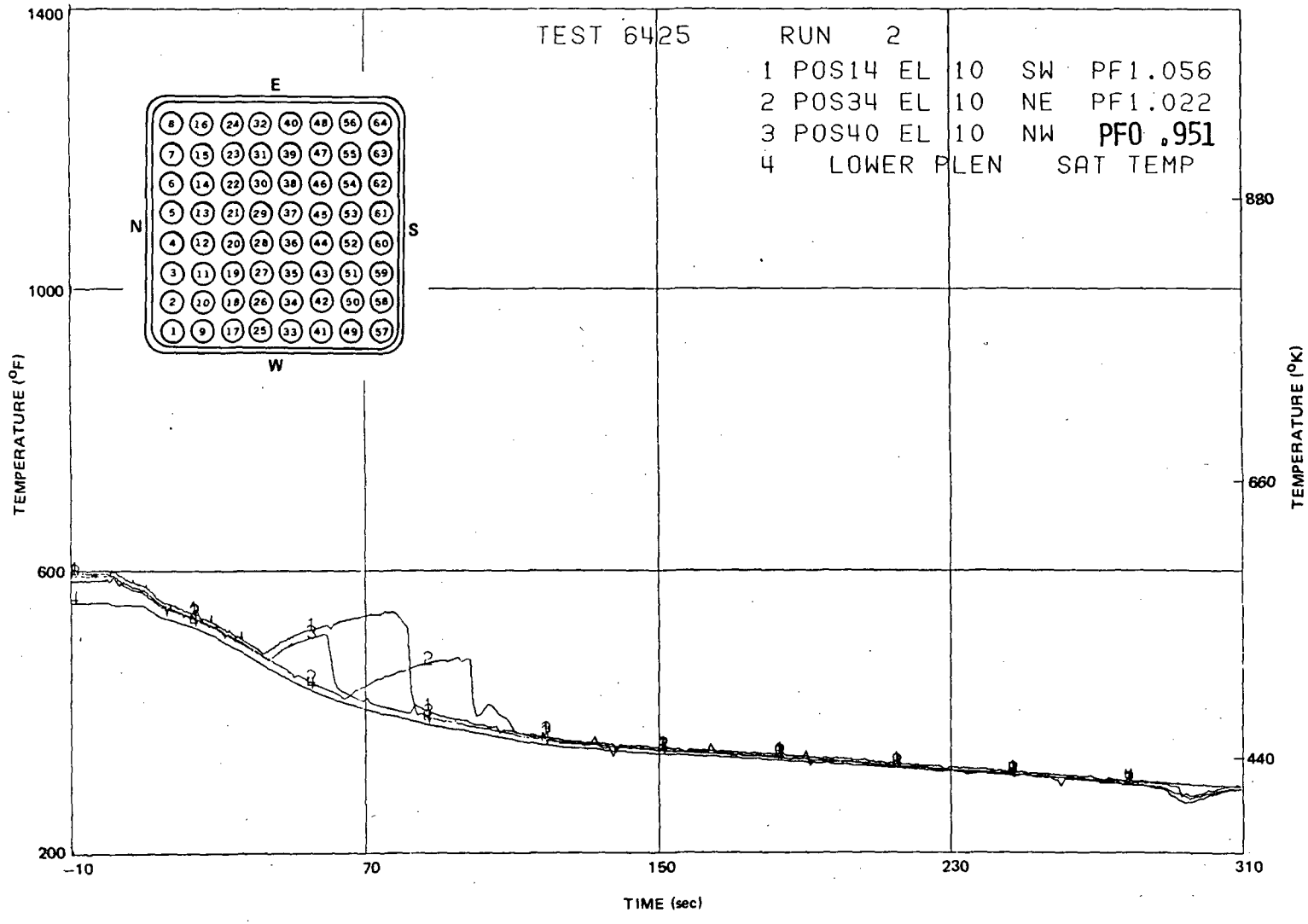

Figure J-97. Inside Clad Temperature-Elevation 10 in.

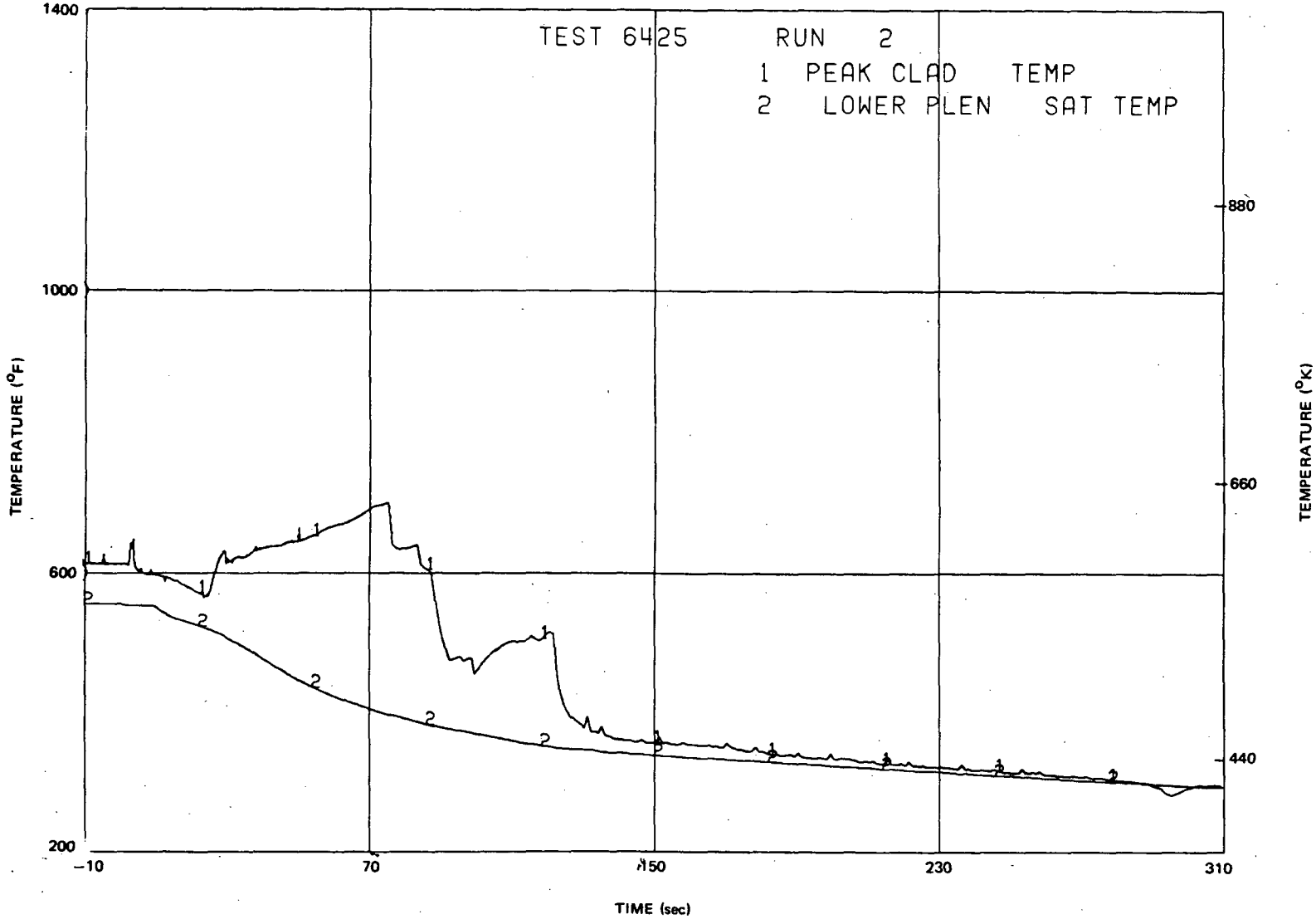

Figure J-98. Peak Clad Temperature

Appendix K

DATA REPORT FOR TEST 6424/RUN 1

Test 6424/1 was a peak power, average ECC flow, nominal ECC temperature test conducted in the TLTA 5A facility. A diagram of the system instrumentation showing measurement nodes is given in Figure K-1. Figure K-2 shows a schematic of the bundle and locations of the pressure transducer taps and thermocouples. The core lattice arrangement and the local peaking factor distribution is shown in Figure K-3.

Tables K-1 and K-2 summarize the initial conditions and sequence of events for Test 6424/1. Primary measurements throughout the transient are given in Figures K-4 to K-38, derived quantities in Figures K-39 to K-66. A guide for interpreting bundle temperature plots is shown in Figure K-67, and the bundle temperature measurements are given in Figures K-68 to K-87. Figure K-88 gives the peak cladding temperature.

Table K-1

PEAK POWER, AVERAGE ECC (6424 RUN 1) INITIAL CONDITIONS

Initial Conditions	
Bundle power	6.49 ± 0.03 MW
Steam dome pressure	1056 ± 5 psia
Lower plenum pressure	1081 ± 5 psia
Lower plenum enthalpy	554 ± 5 Btu/lbm
Initial water level	124 ± 6 in. El
Feedwater enthalpy	45 ± 2 Btu/lbm
Bundle inlet to outlet DP	20 ± 2 psi
Steam flow	8 ± 1 lbm/sec
Feedwater flow	1.1 ± 0.3 lbm/sec
Drive Pump 1 flow	7 ± 1 lbm/sec
Drive Pump 2 flow	8 ± 1 lbm/sec
Jet Pump 1 flow	14 ± 2 lbm/sec
Jet Pump 2 flow	18 ± 2 lbm/sec
Bundle inlet flow	29 ± 5 lbm/sec
ECC fluid temperature	120 ± 15°F

All uncertainty bands are judged from the maximum of data fluctuation and/or absolute uncertainties of the measurements.

Table K-2

SEQUENCE OF EVENTS FOR 6424 RUN 1
(PEAK POWER, AVG. ECC)

Events	Time (sec)
Blowdown valves open	0.0
Bundle power decay initiated	0.5
Feedwater flow stops	0.5
Bypass flow reverses	1.2
Steamline valve completely closed	8.0
Lower plenum bulk flashing	14
Loop 1 isolated	20
HPCS injection begins	27
Lower plenum mixture level reaches jet pump exit plane	34
LPCS, LPCI activated	37
LPCS flow begins	63
LPCI flow begins	71
Bundle quenched	150
End of test	400

NOTES:

1. P - PRESSURE
   DP - DIFFERENTIAL PRESSURE
   T - TEMPERATURE (RTD - RESISTANCE THERM)
   SP - VALVE STEM POSITION
   RO - RESTRICTING ORIFICE
   FE - FLOW ELEMENT
   S - PUMP SPEED
   LP - LEVEL PROBE
   DD - DRAG DISK
   TM - TURBINE METER

2. N305 - 54.88 MEANS NOZZLE NO. 305 IS AT AN ELEVATION OF 54.88 INCHES. IT DOES NOT REFER TO ACTUAL LOCATION OF THE NODAL POINT.

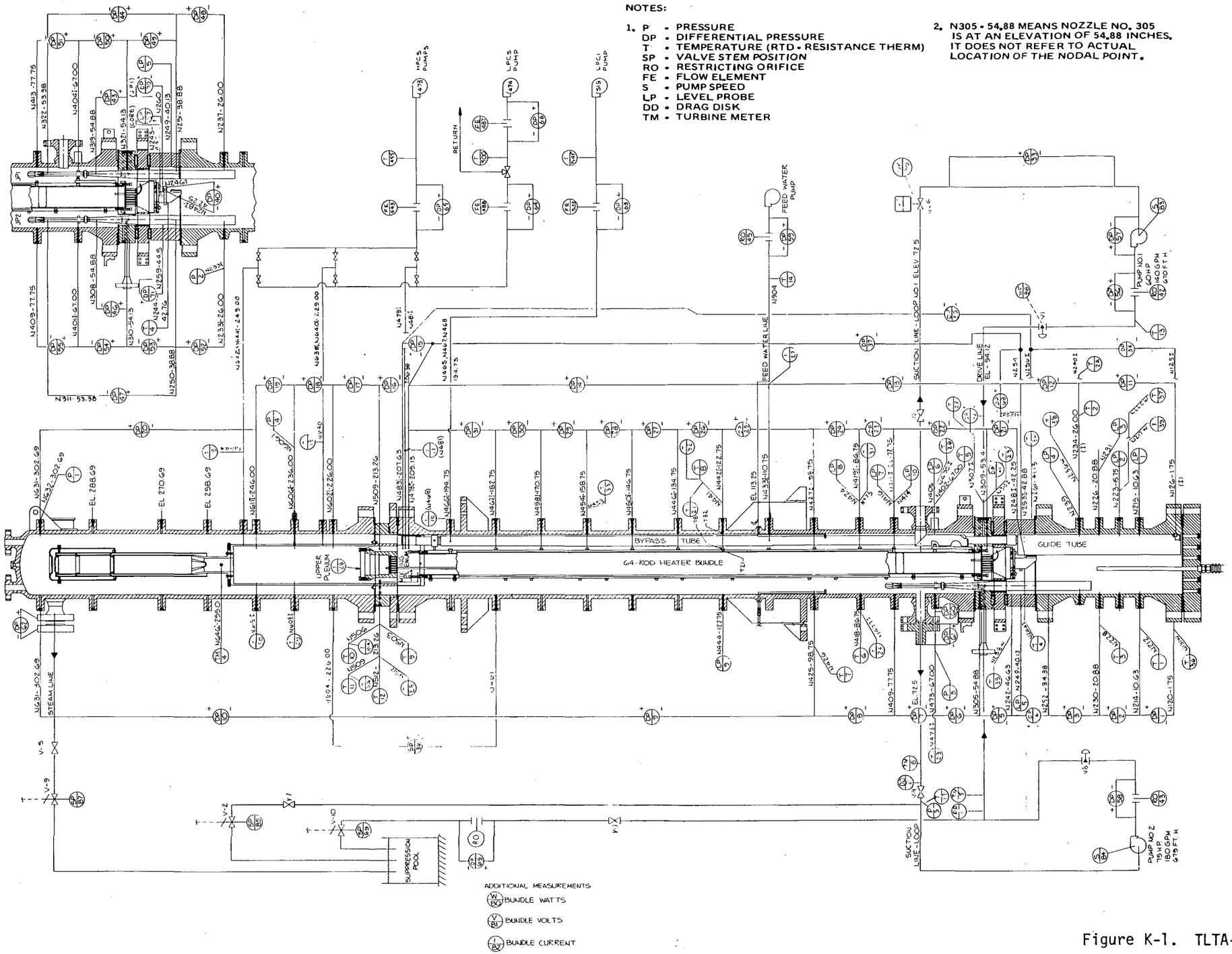

Figure K-1. TLTA-5A Instrumentation

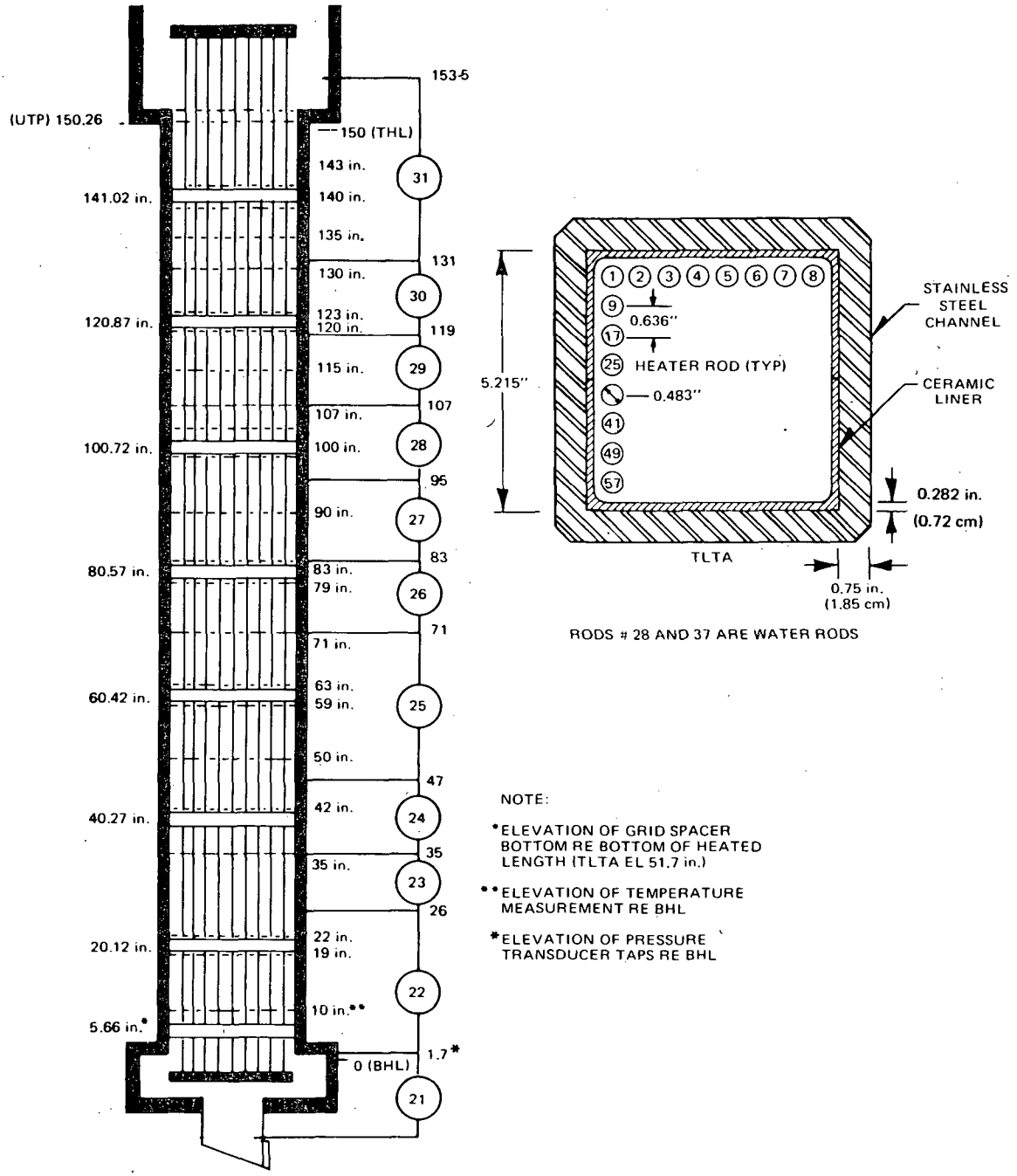

Figure K-2. TLTA-5A Bundle Instrumentation and Dimensions

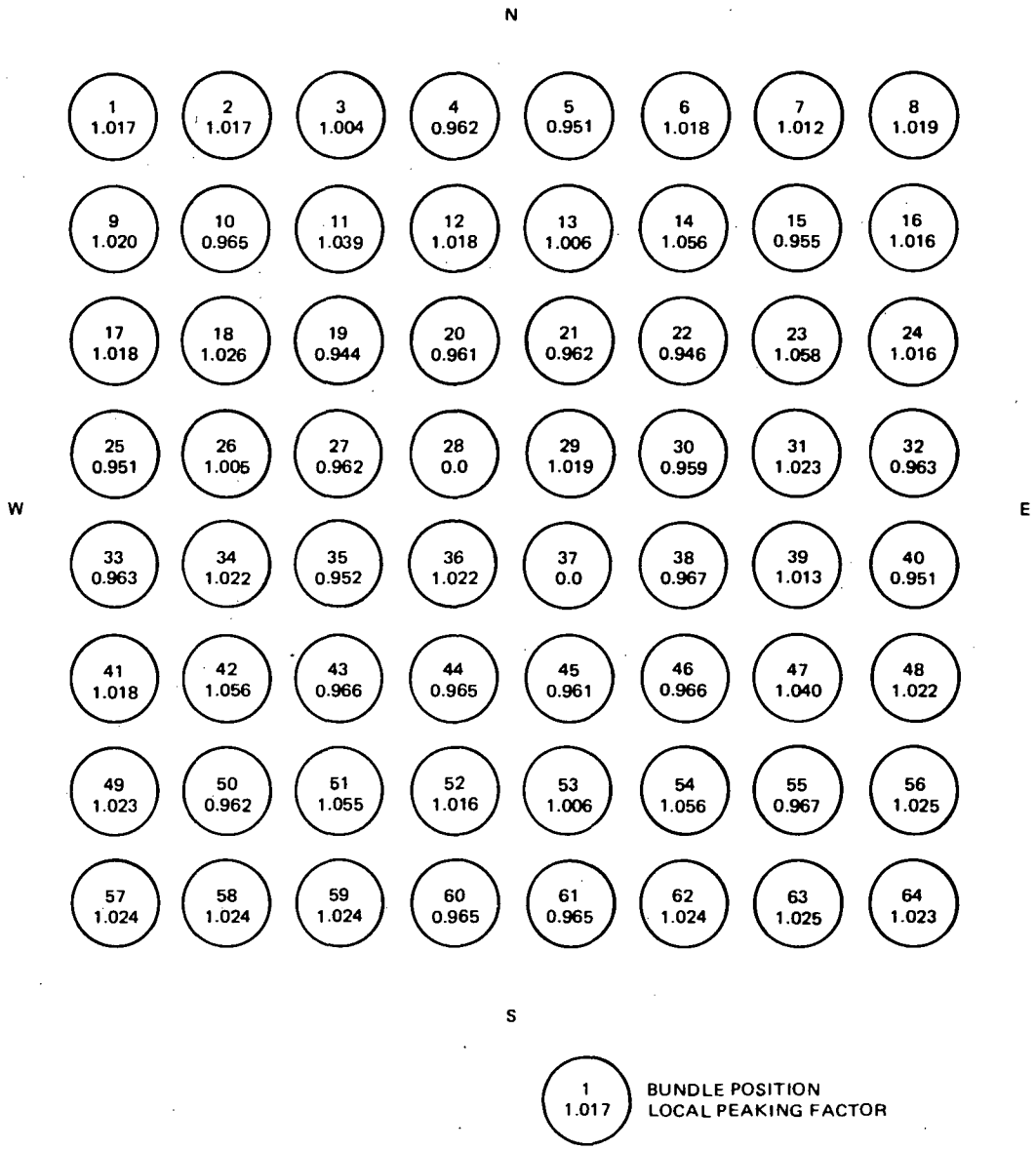

Figure K-3. Local Peaking Factor Distribution

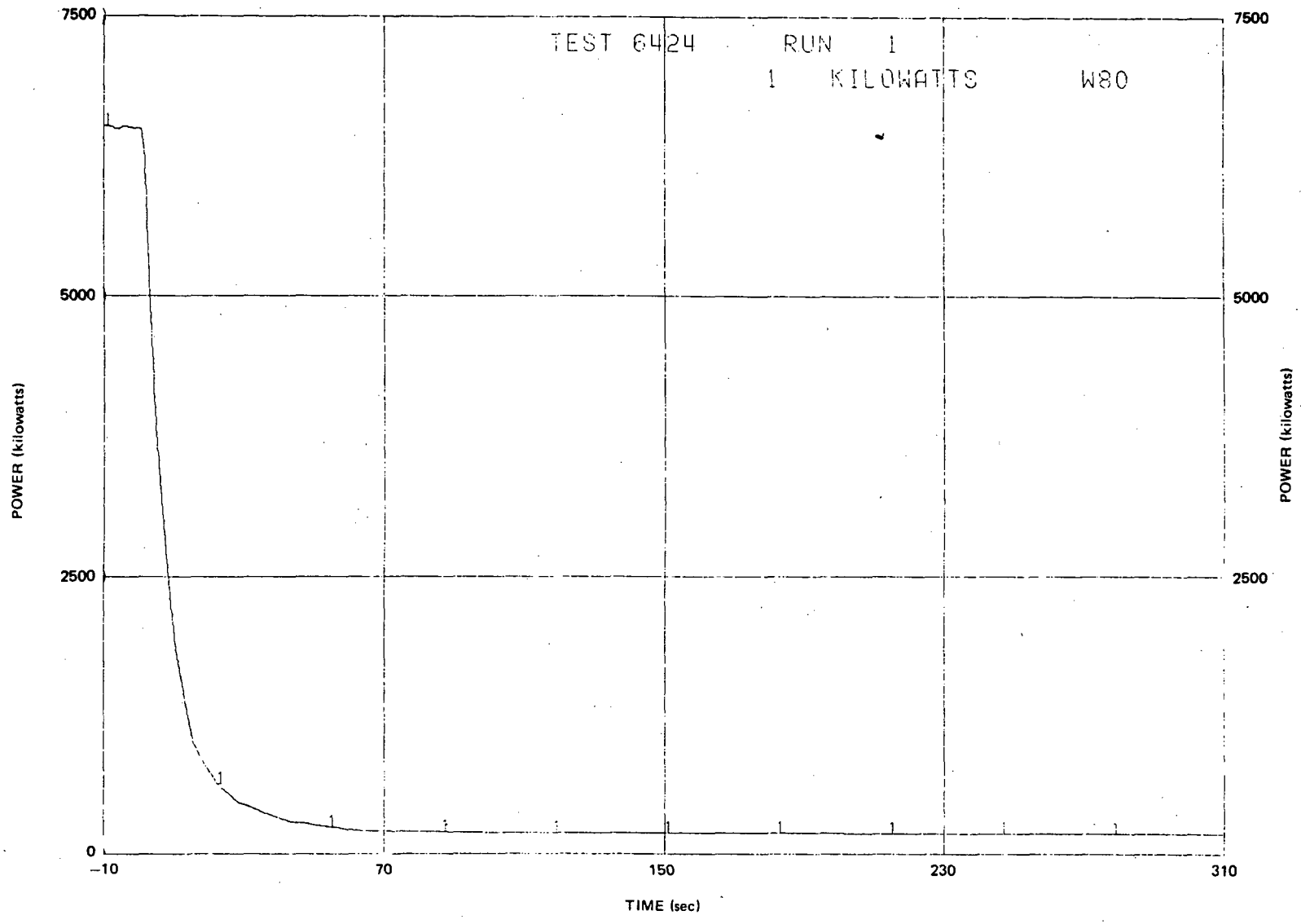

Figure K-4. Bundle Power Decay

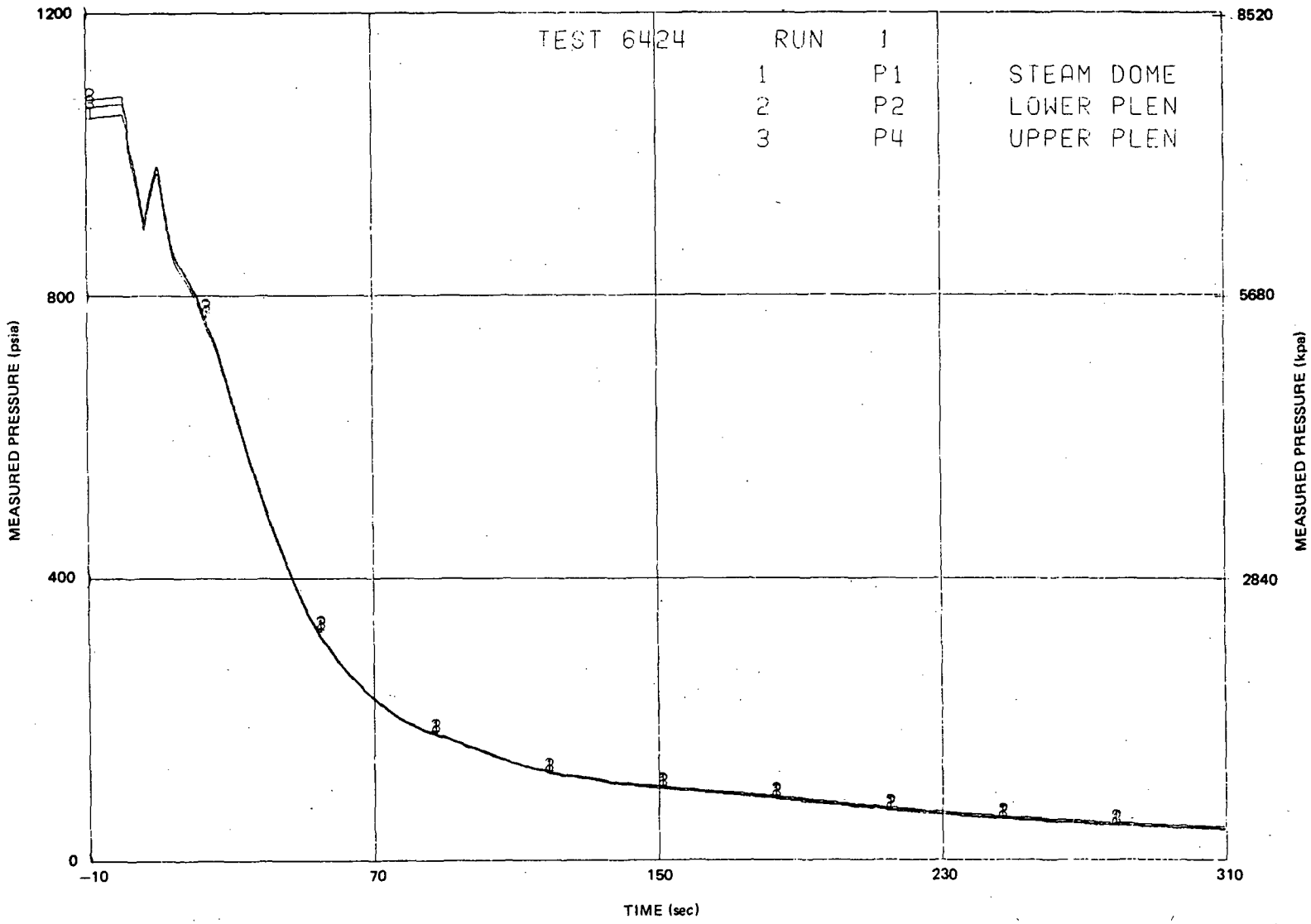

Figure K-5. System Pressures

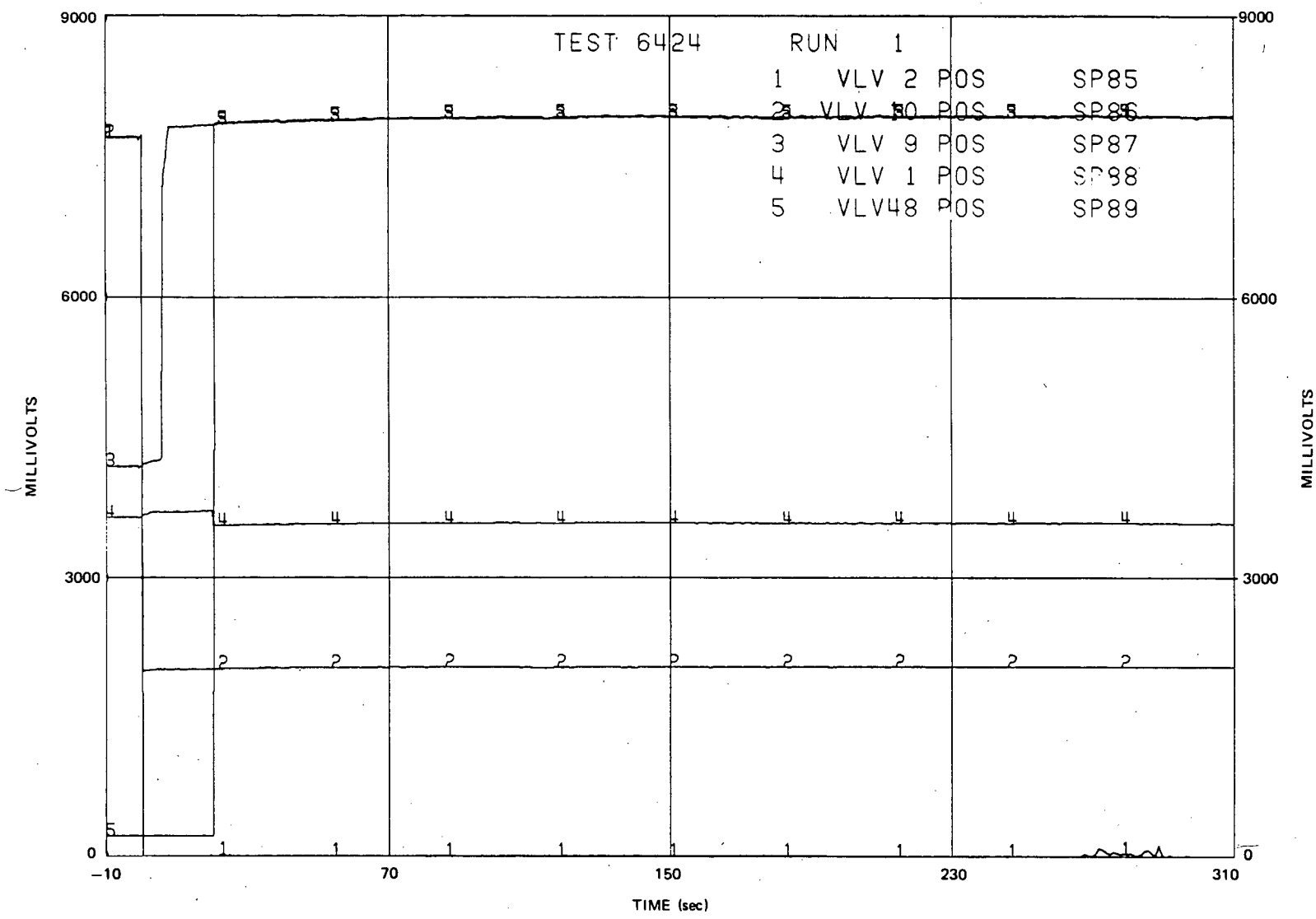

Figure K-6. Valve Positions

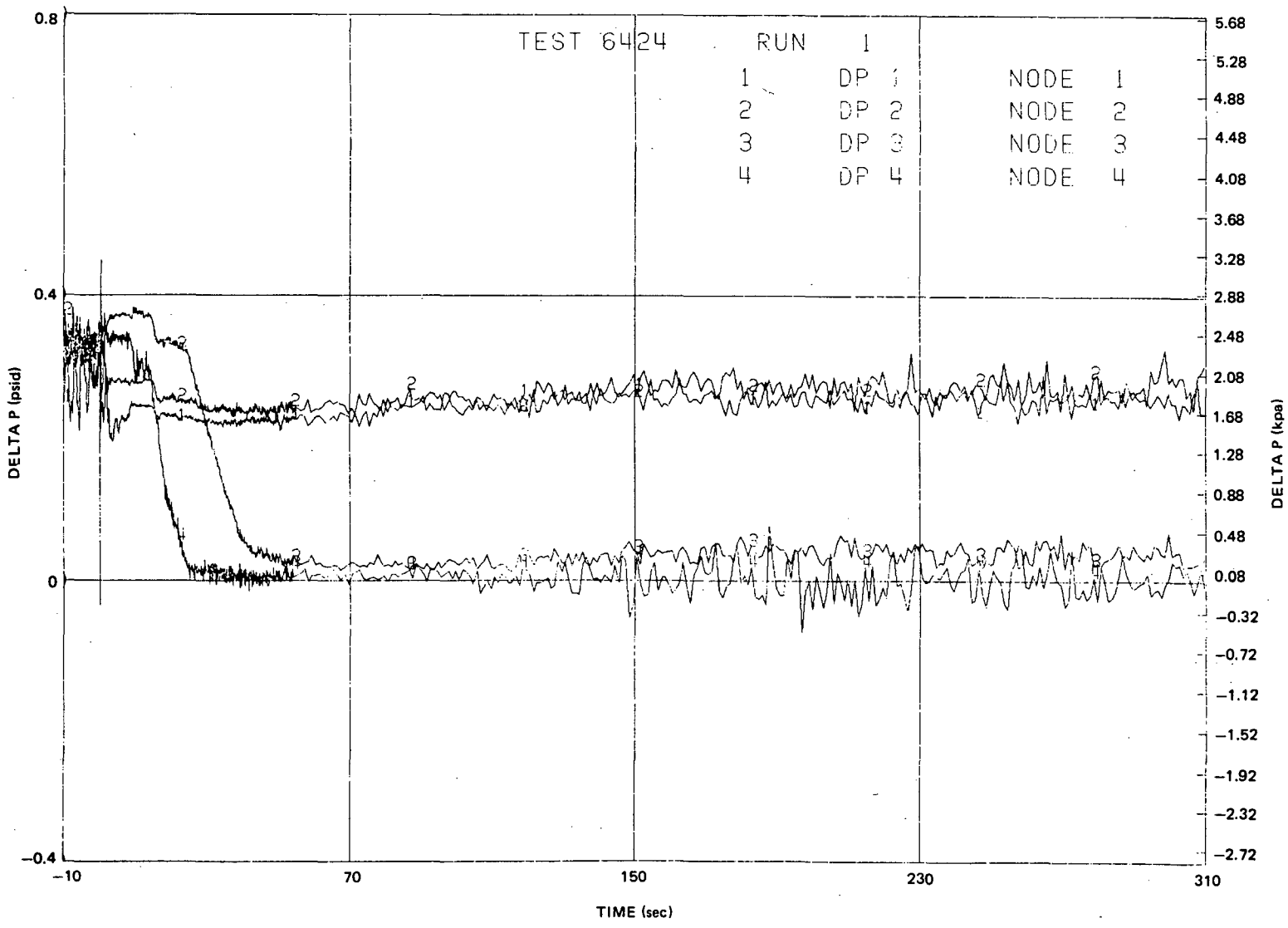

Figure K-7. Lower Plenum Differential Pressures

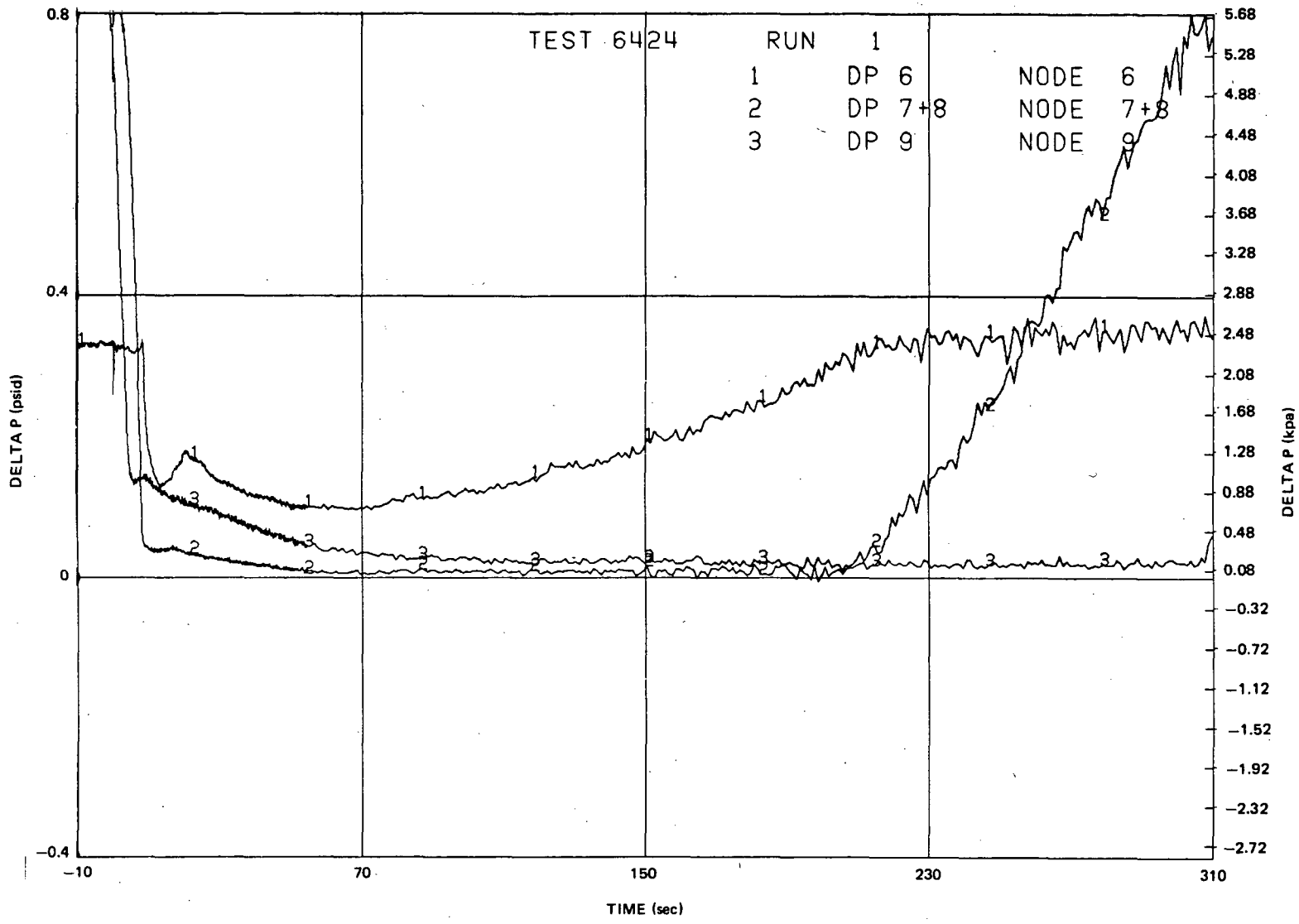

Figure K-8. Annulus Differential Pressures

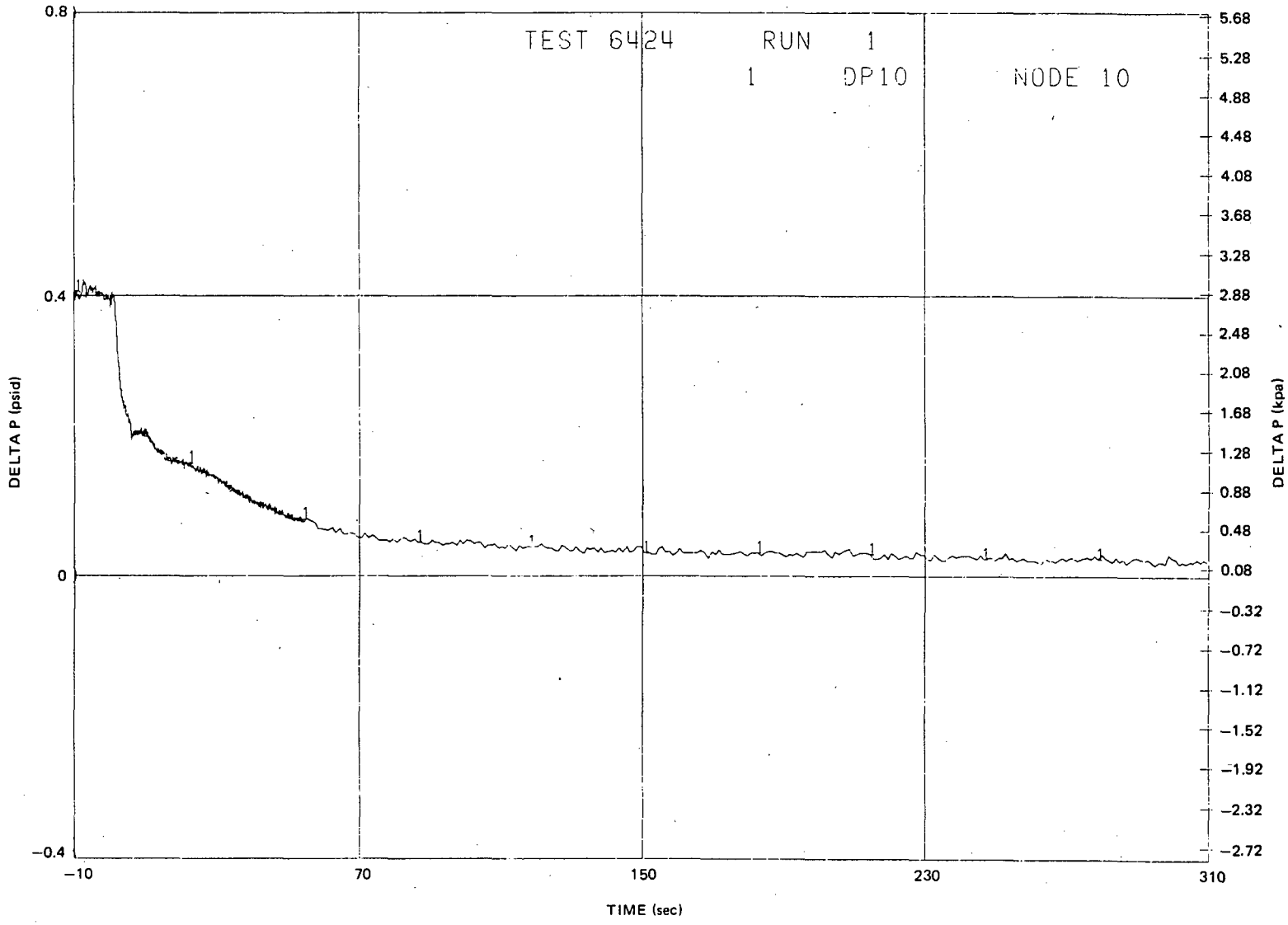

Figure K-9. Upper Annulus Differential Pressure

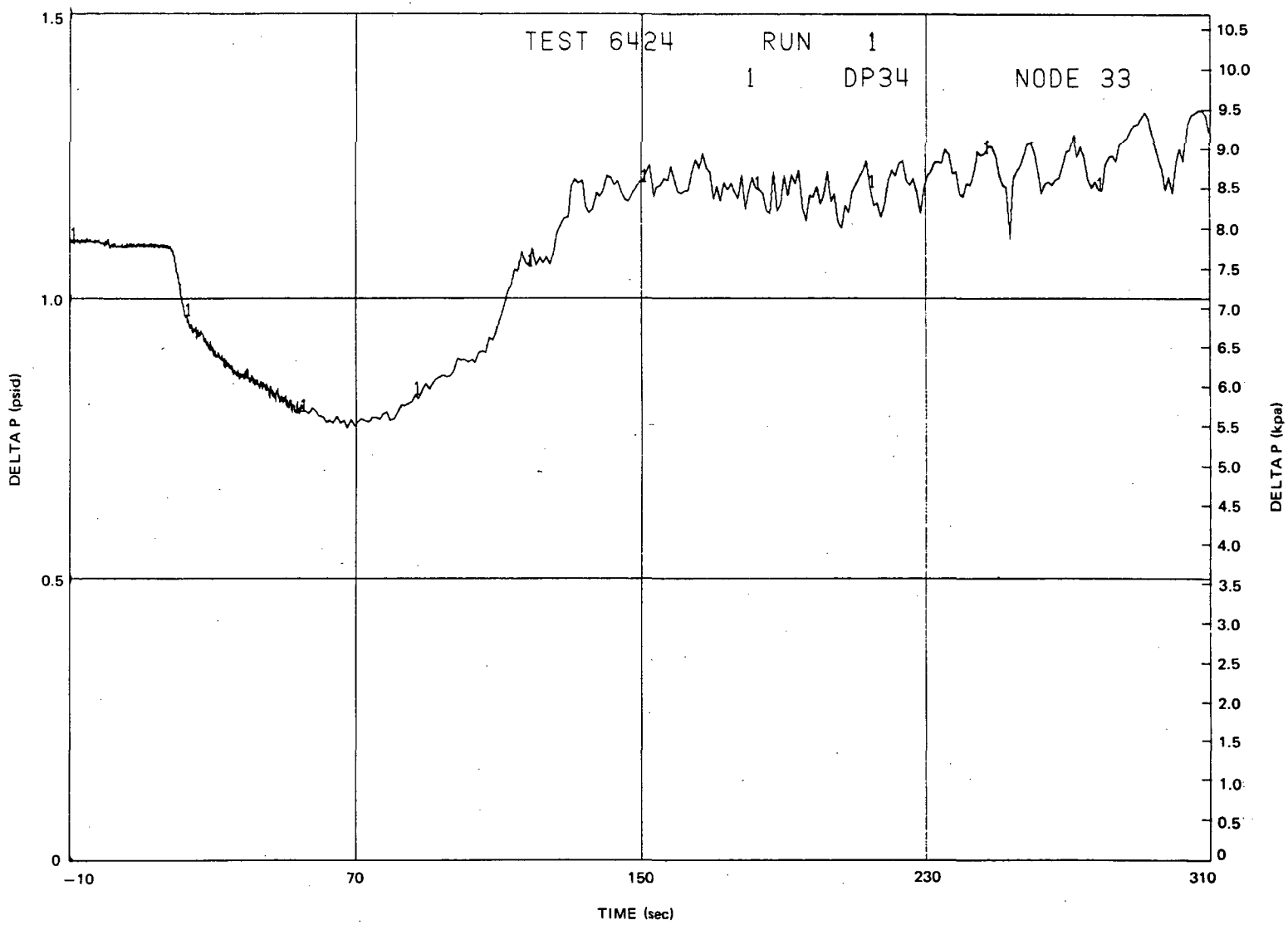

Figure K-10. Guide Tube Differential Pressure

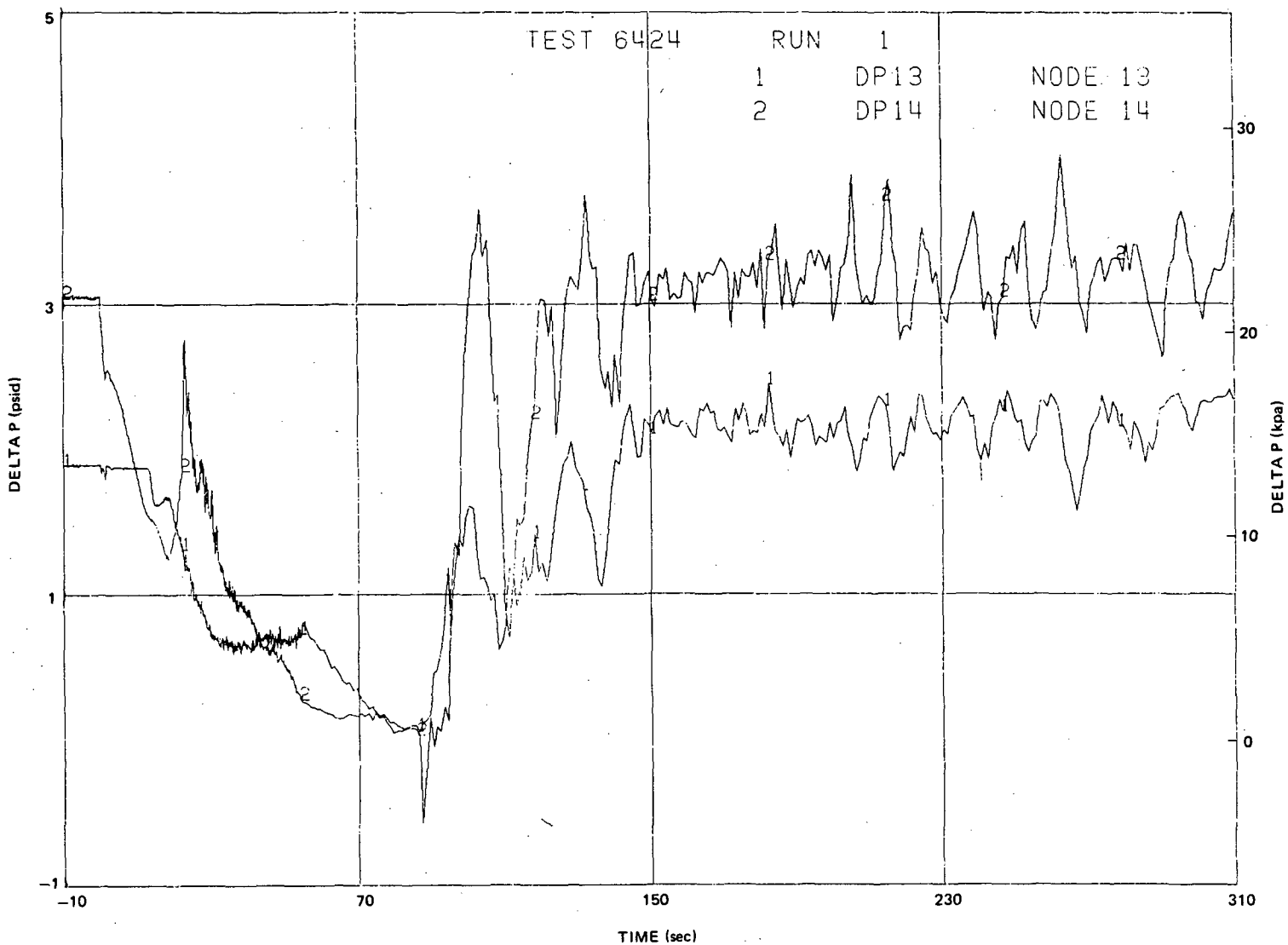

Figure K-11. Bypass Differential Pressures

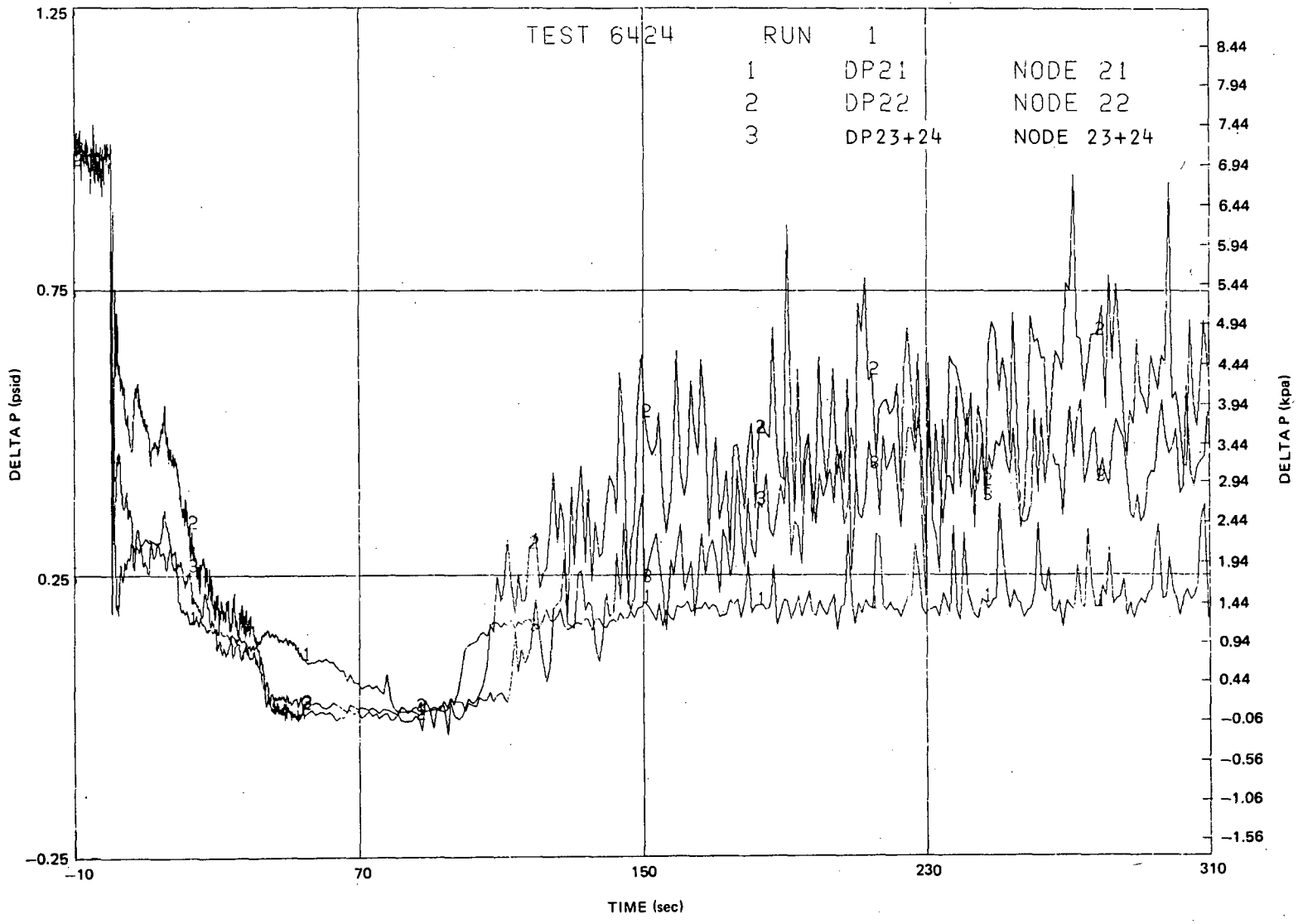

Figure K-12. Lower Bundle Differential Pressures

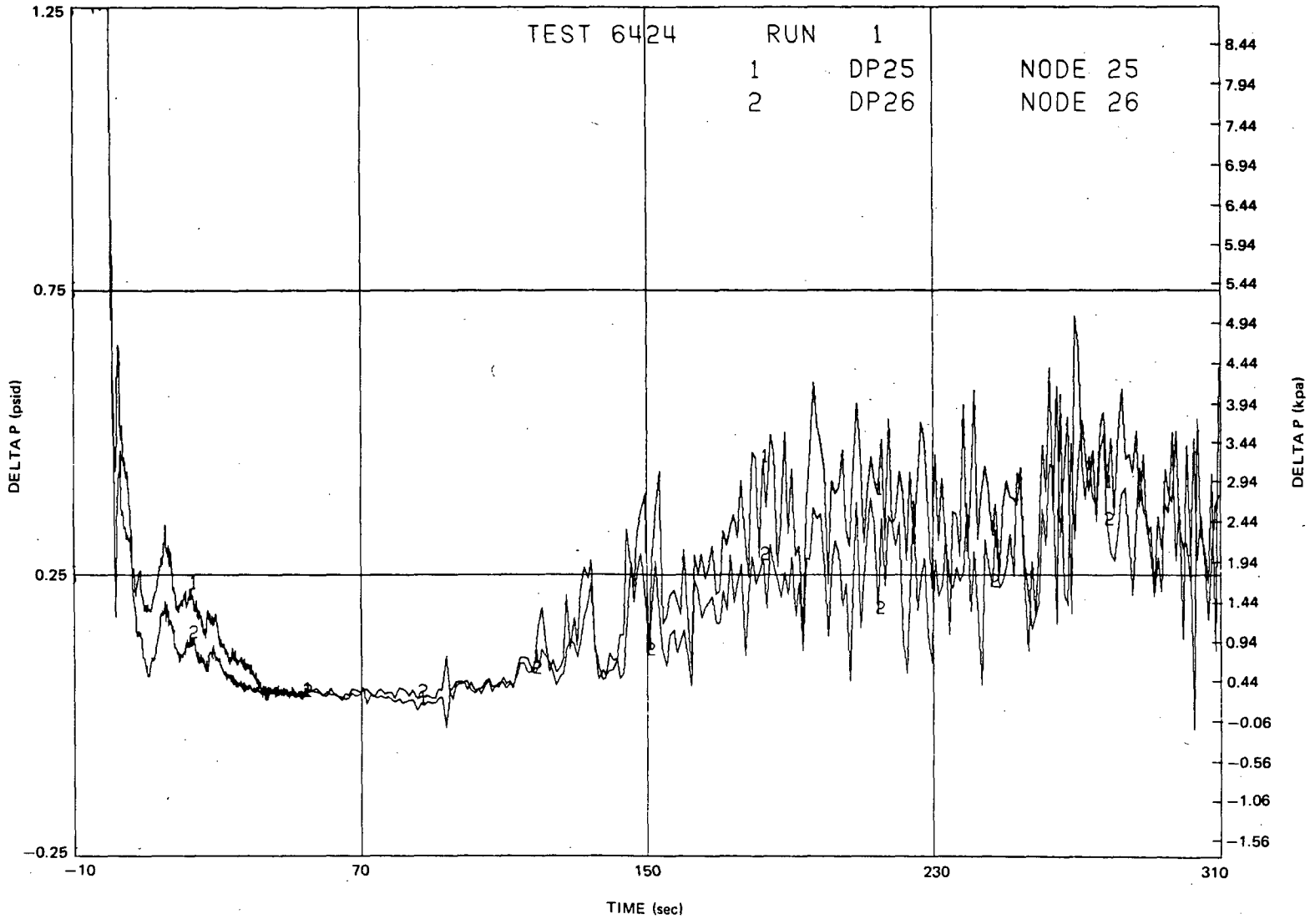

Figure K-13. Middle Bundle Differential Pressures

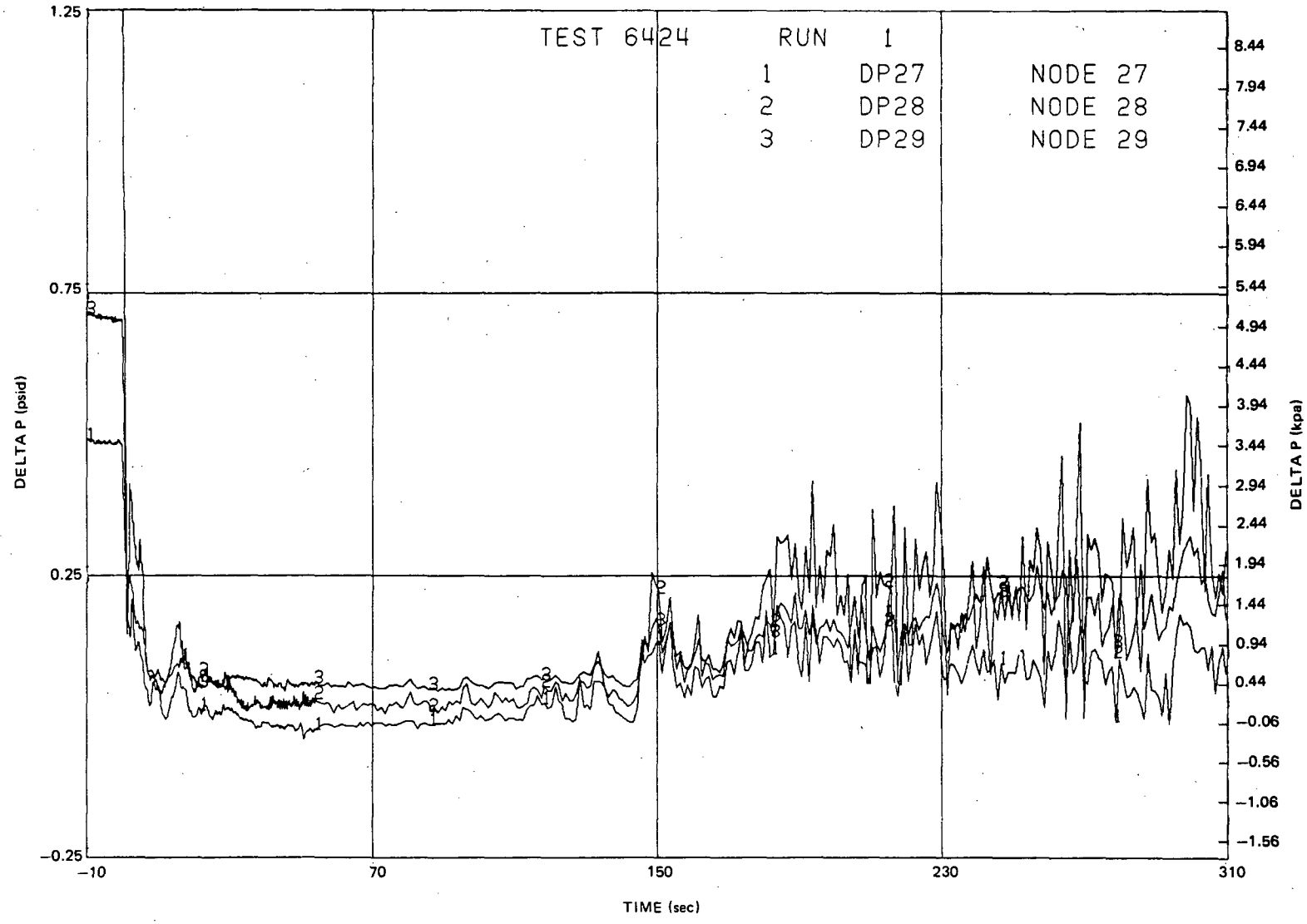

Figure K-14. Upper Bundle Differential Pressures

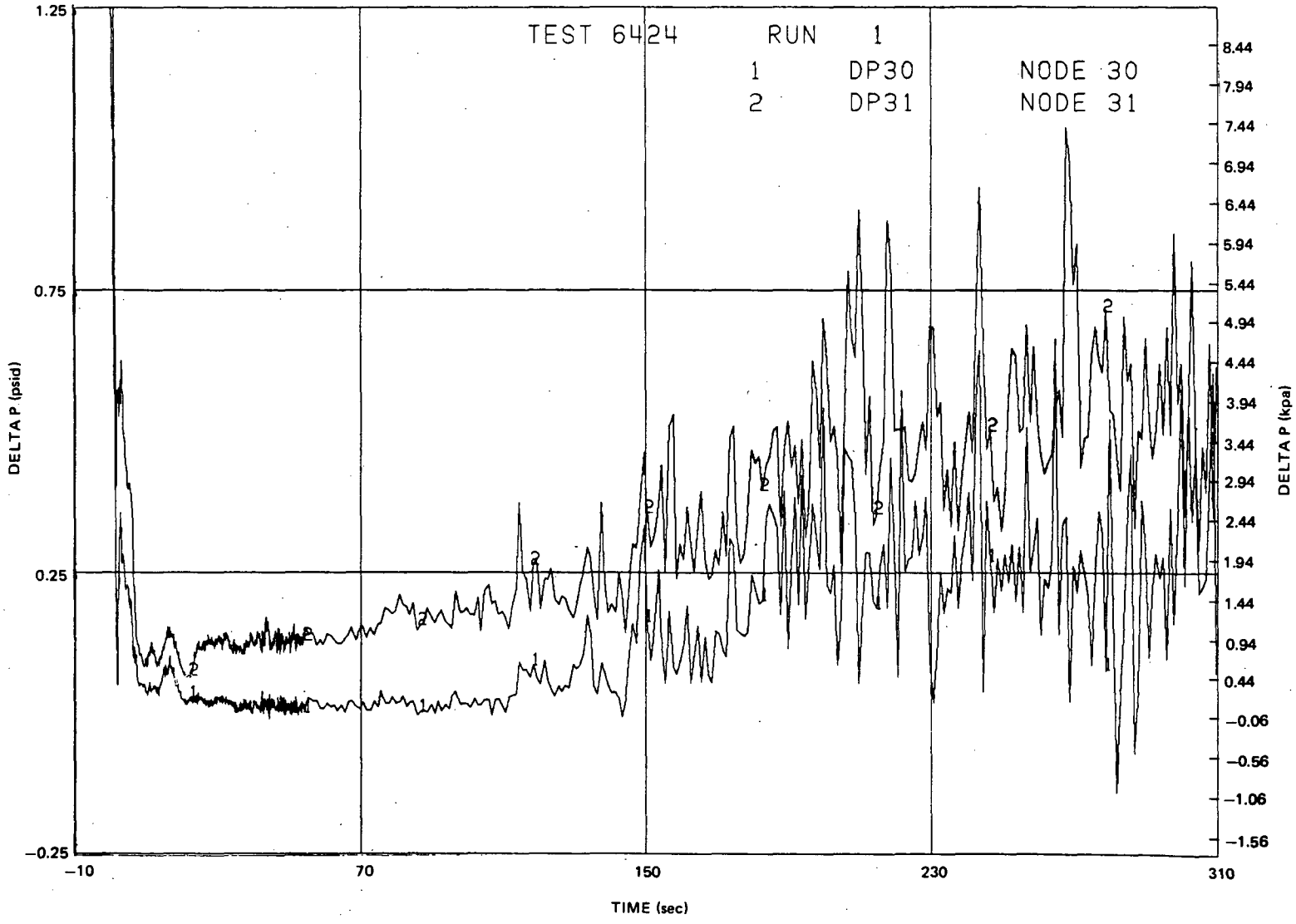

Figure K-15. Top Bundle Differential Pressures

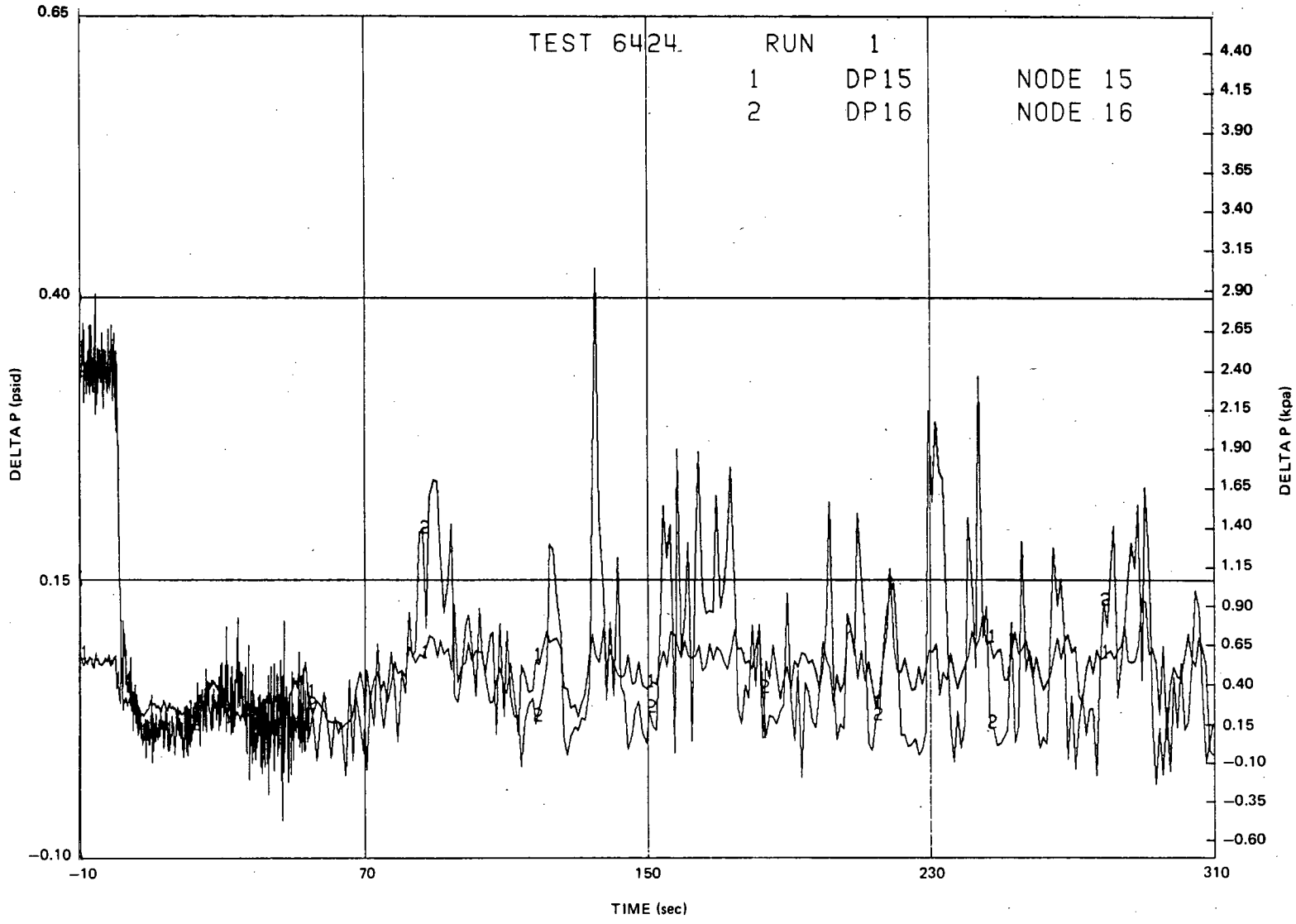

Figure K-16. Mixing Plenum Differential Pressures

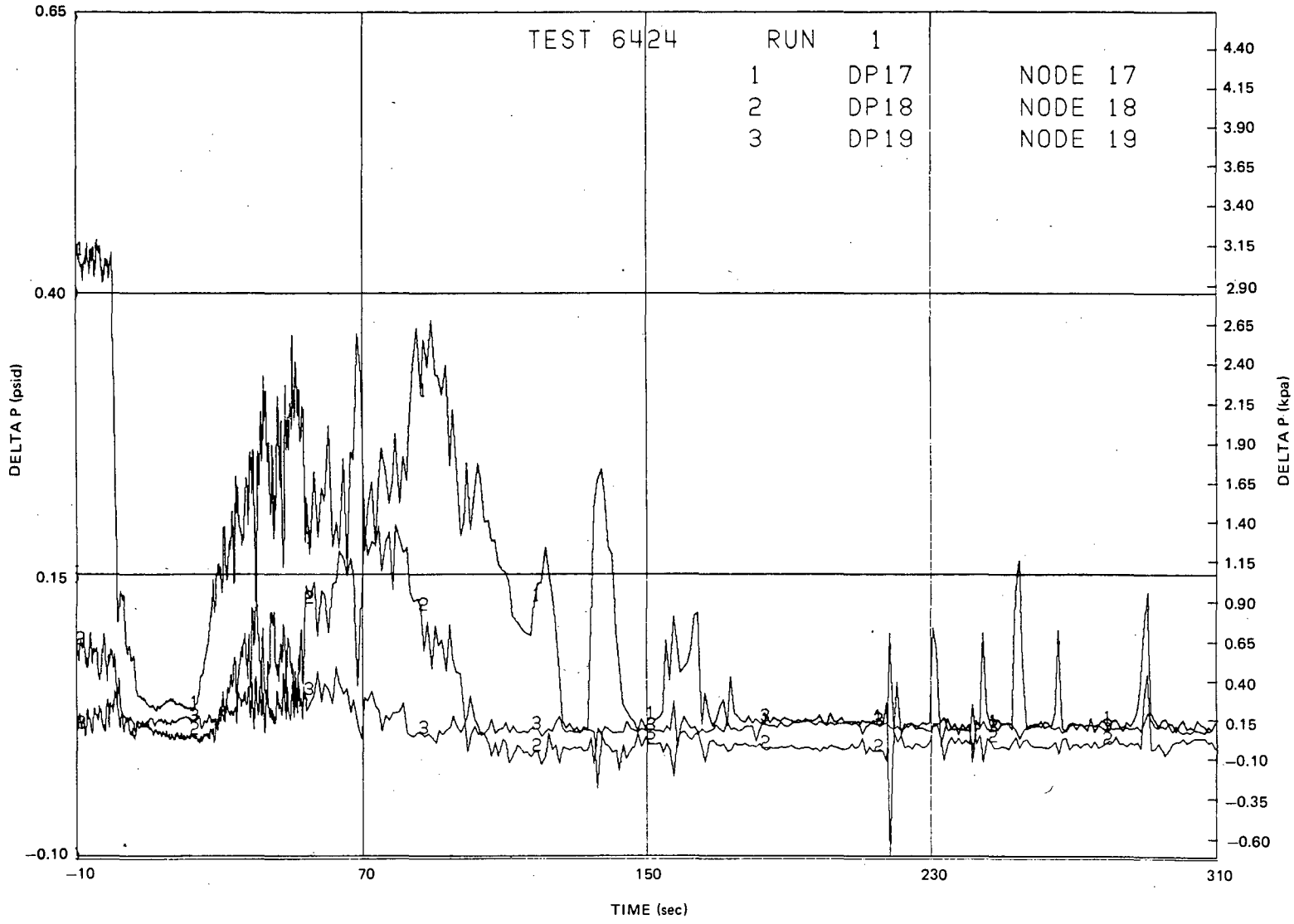

Figure K-17. Upper Plenum Differential Pressures

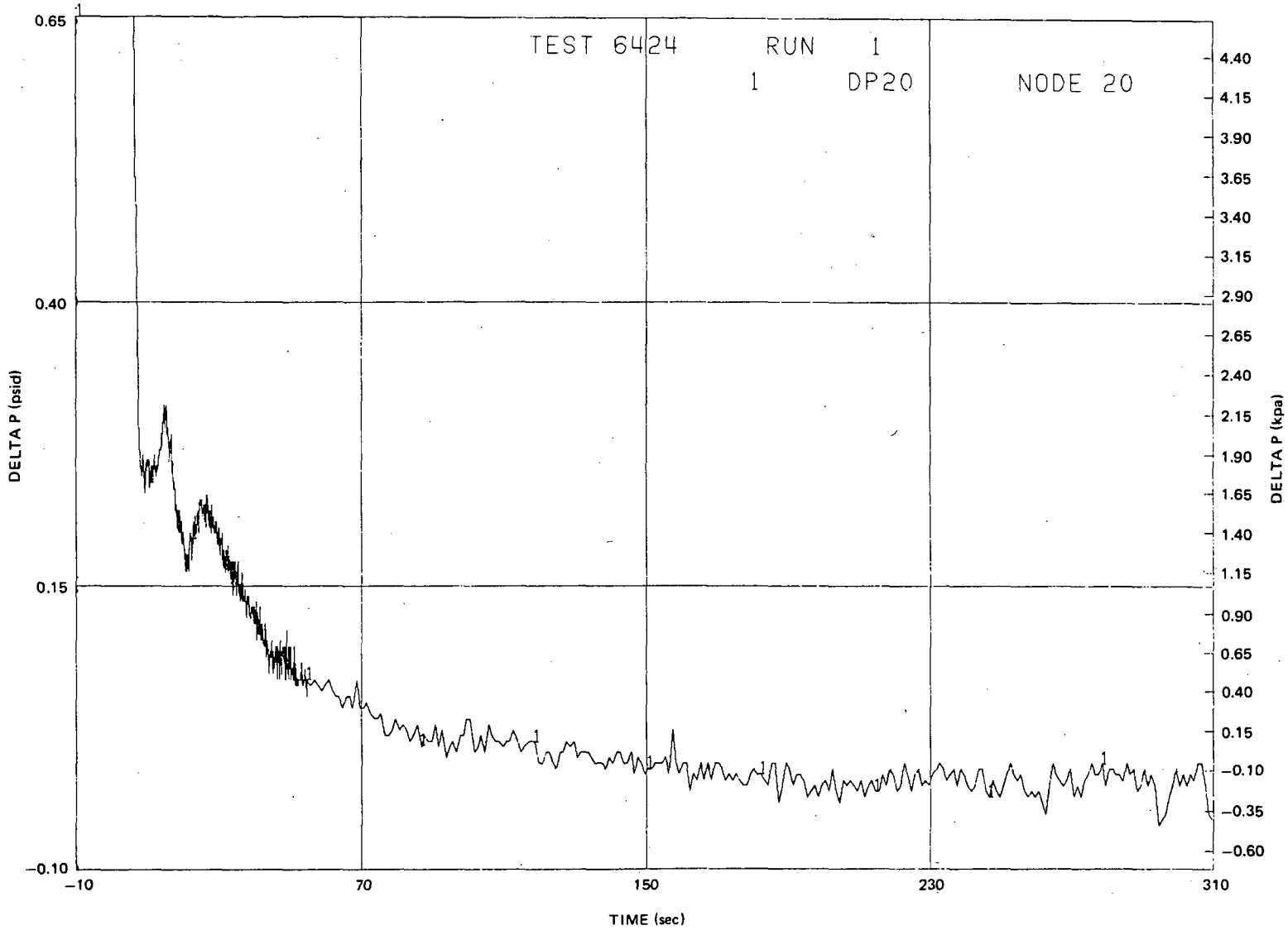

Figure K-18. Steam Separator Differential Pressure

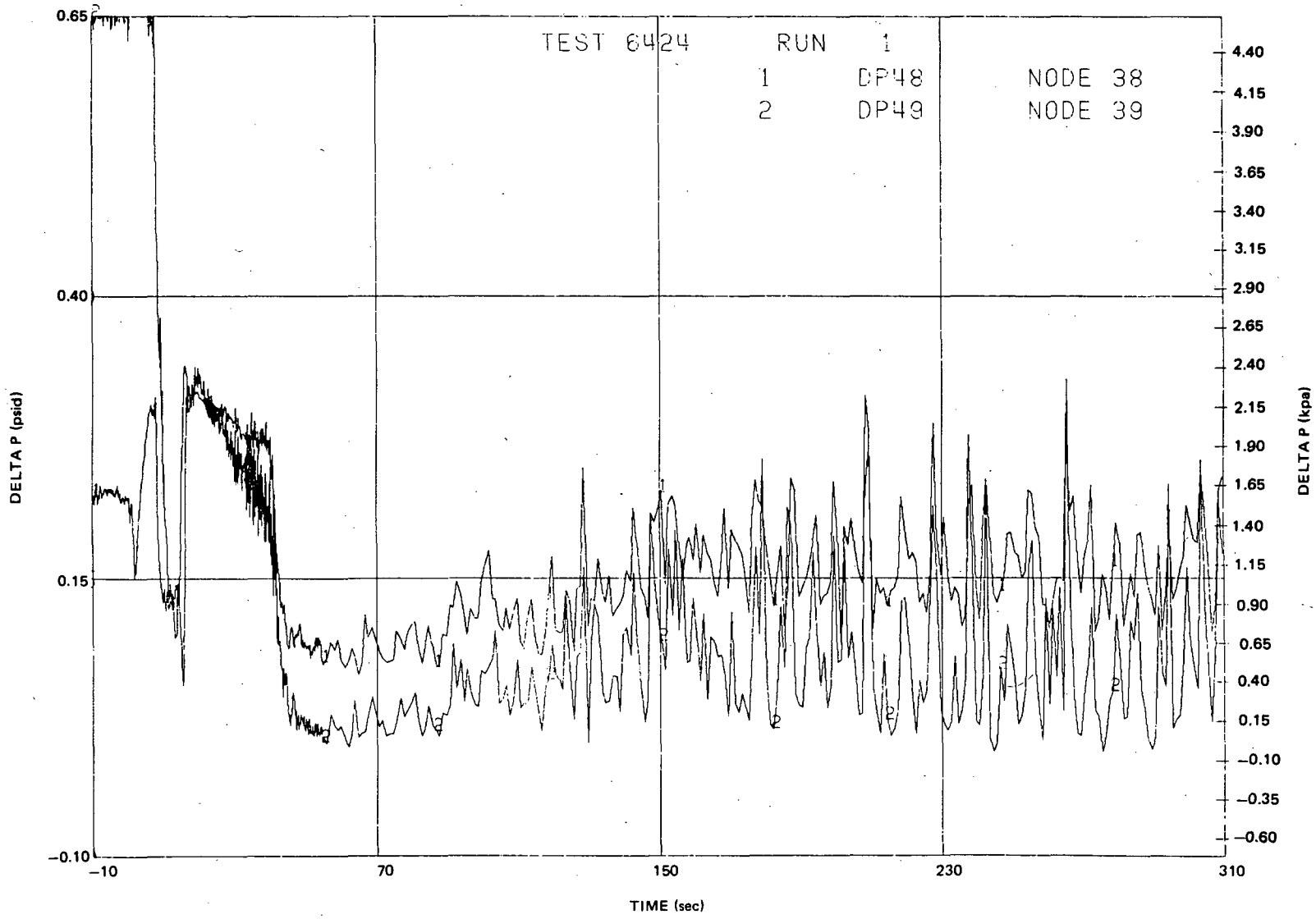

Figure K-19. Intact Loop Jet Pump Differential Pressures

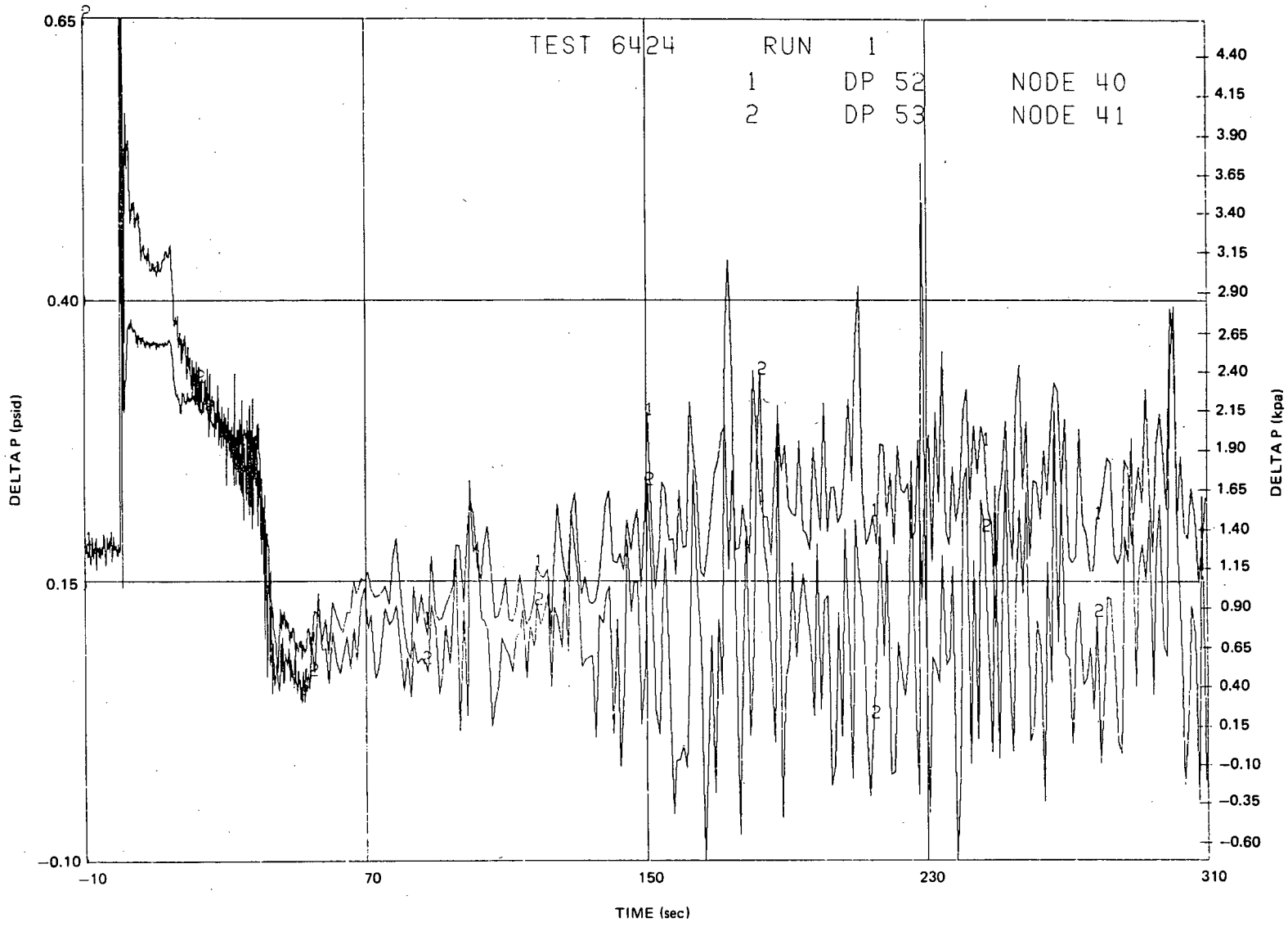

Figure K-20. Broken Loop Jet Pump Differential Pressures

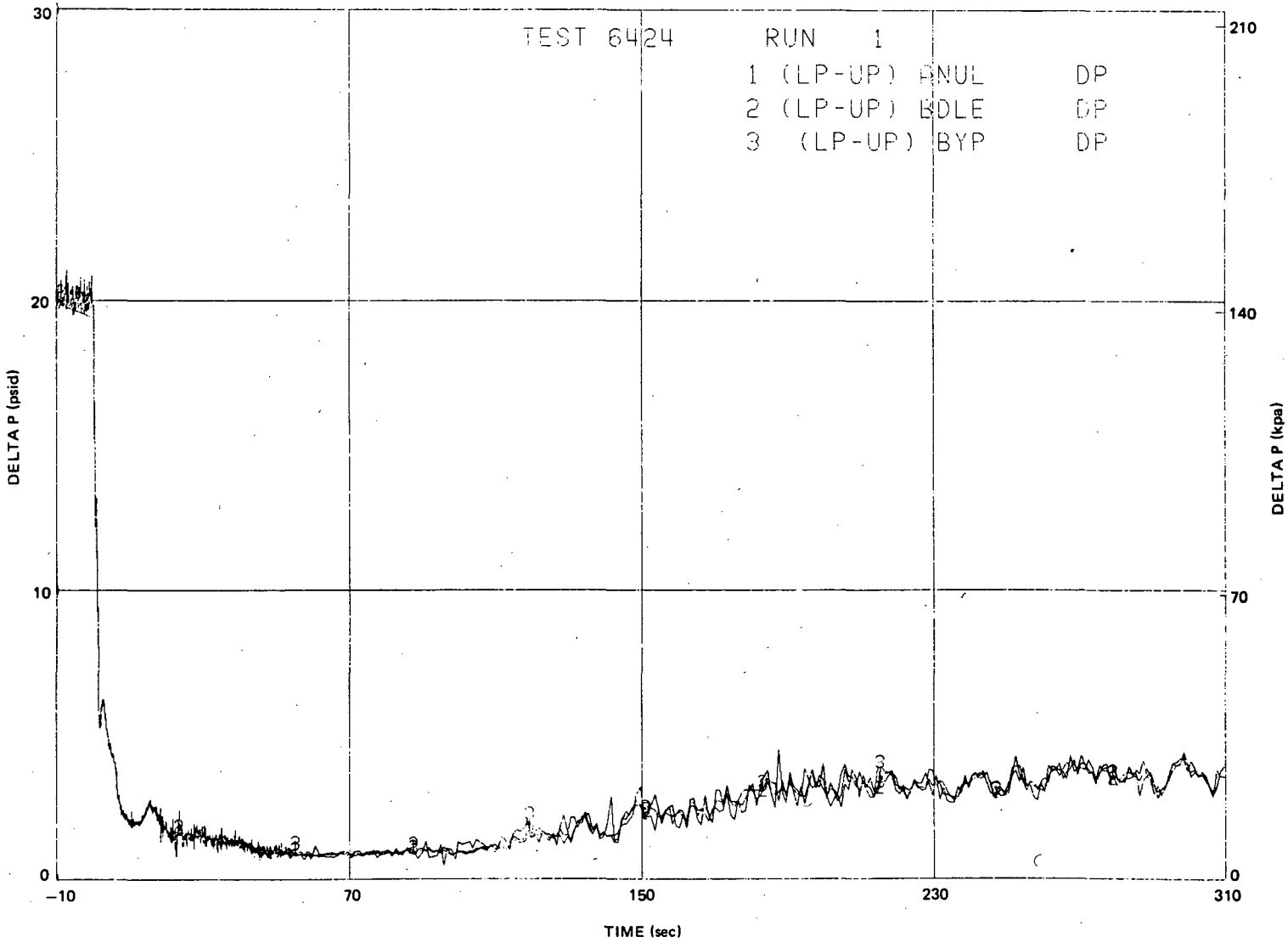

Figure K-21. Lower Plenum to Upper Plenum Differential Pressures for Annulus, Bundle, and Bypass

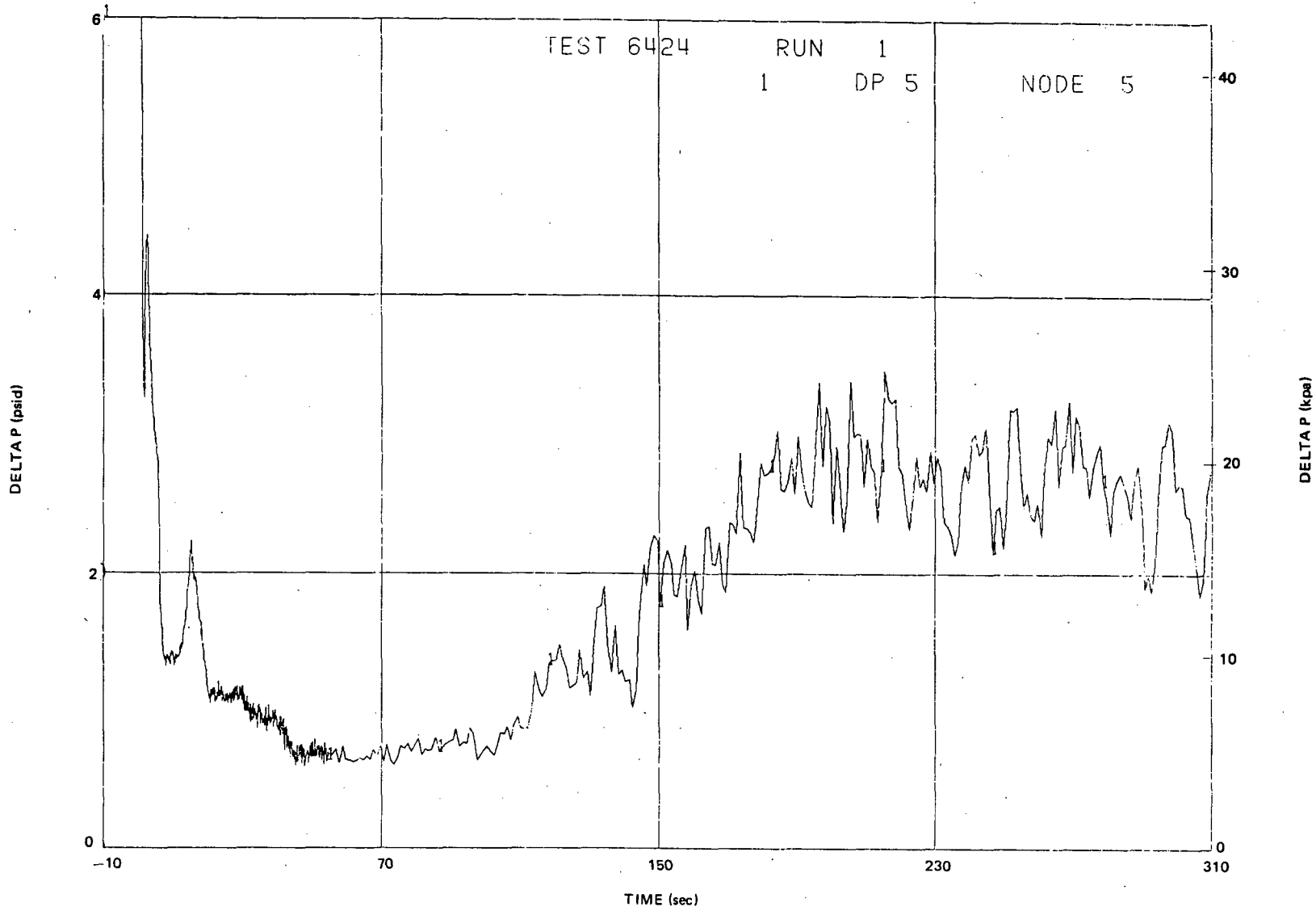

Figure K-22. Lower Plenum to Annulus Differential Pressure

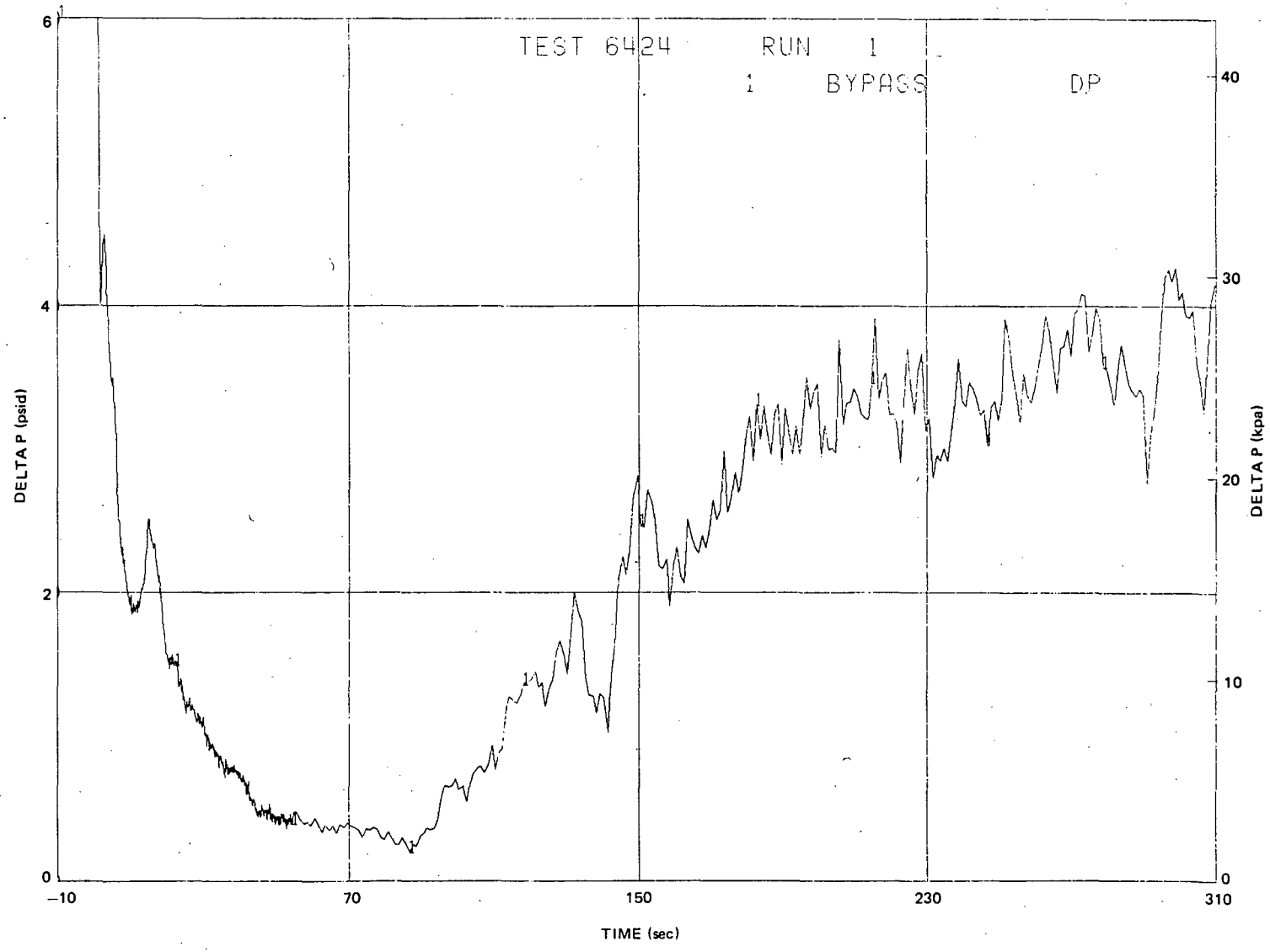

Figure K-23. Bypass Differential Pressure

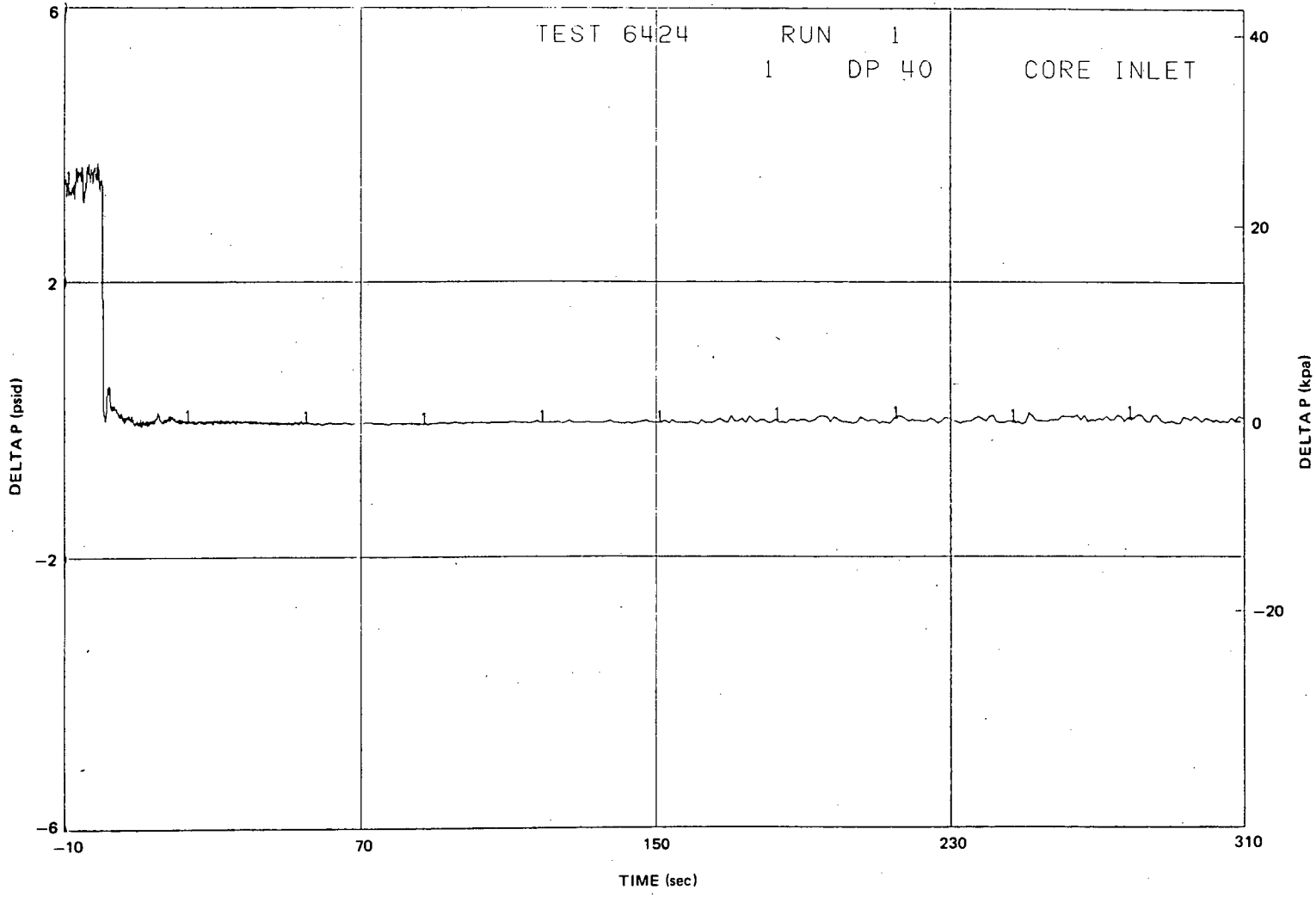

Figure K-24. Bundle Inlet Side Entry Orifice Differential Pressure

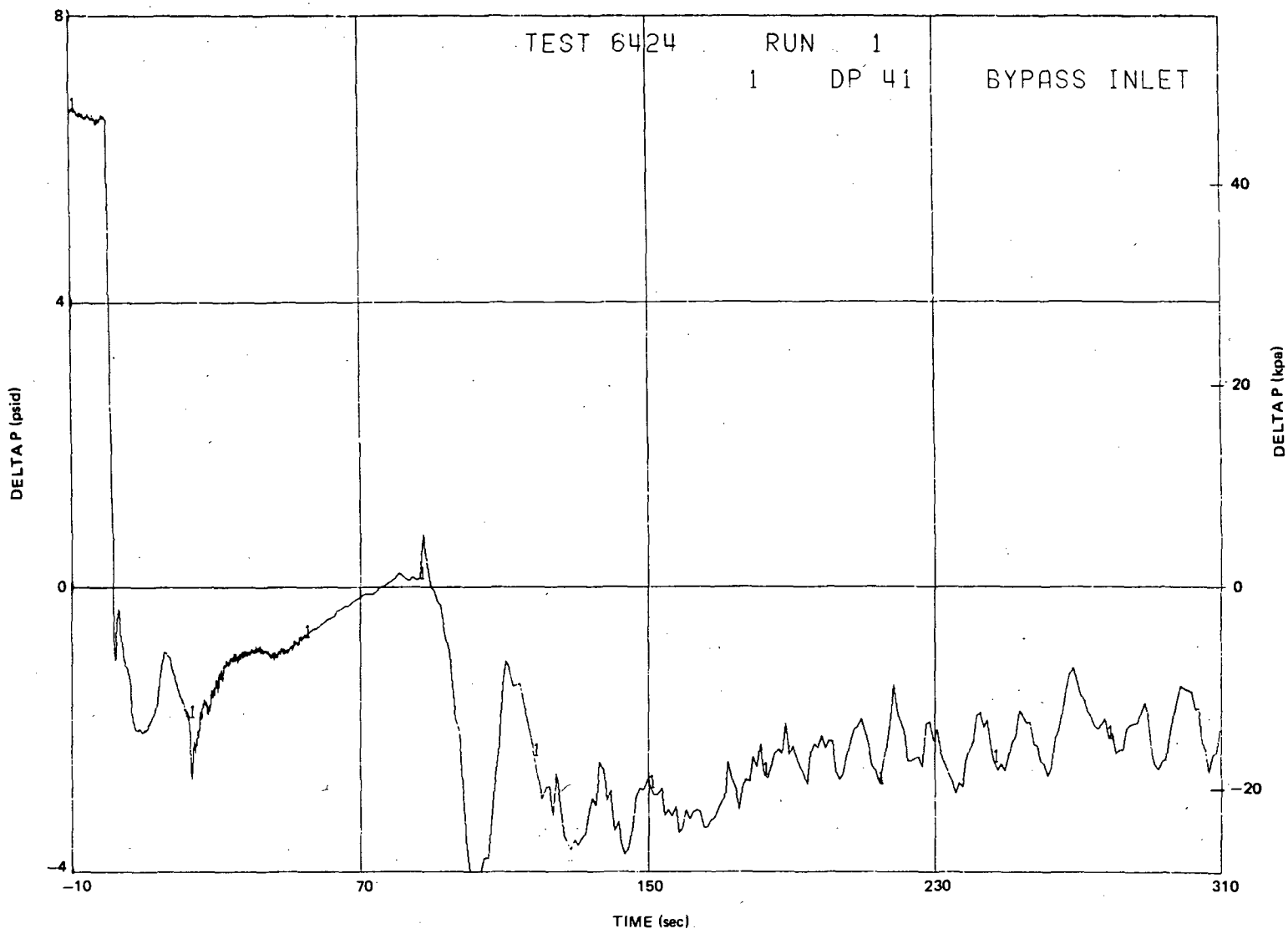

Figure K-25. Bypass Leakage Path Differential Pressure

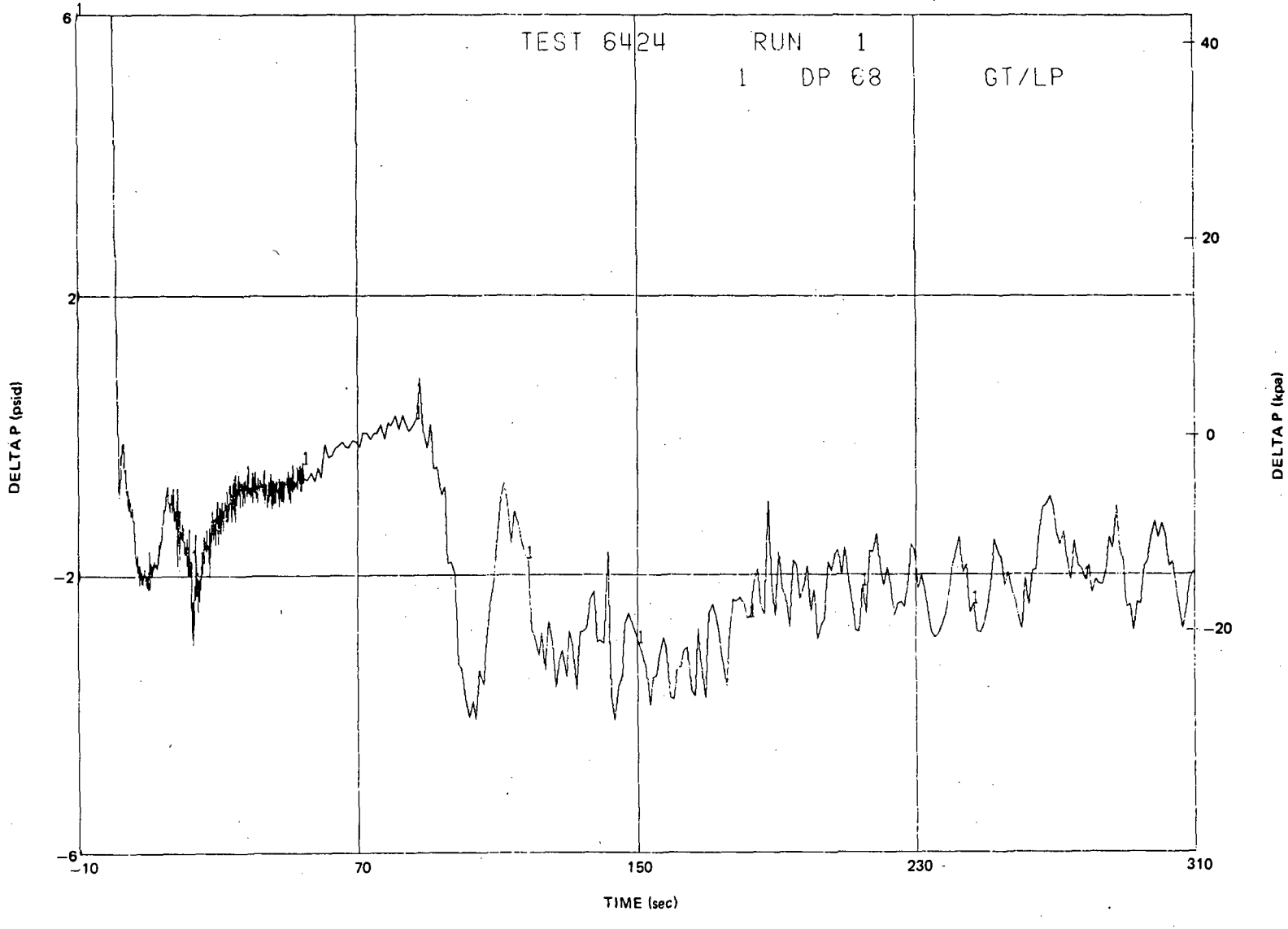

Figure K-26. Lower Plenum to Guide Tube Differential Pressure

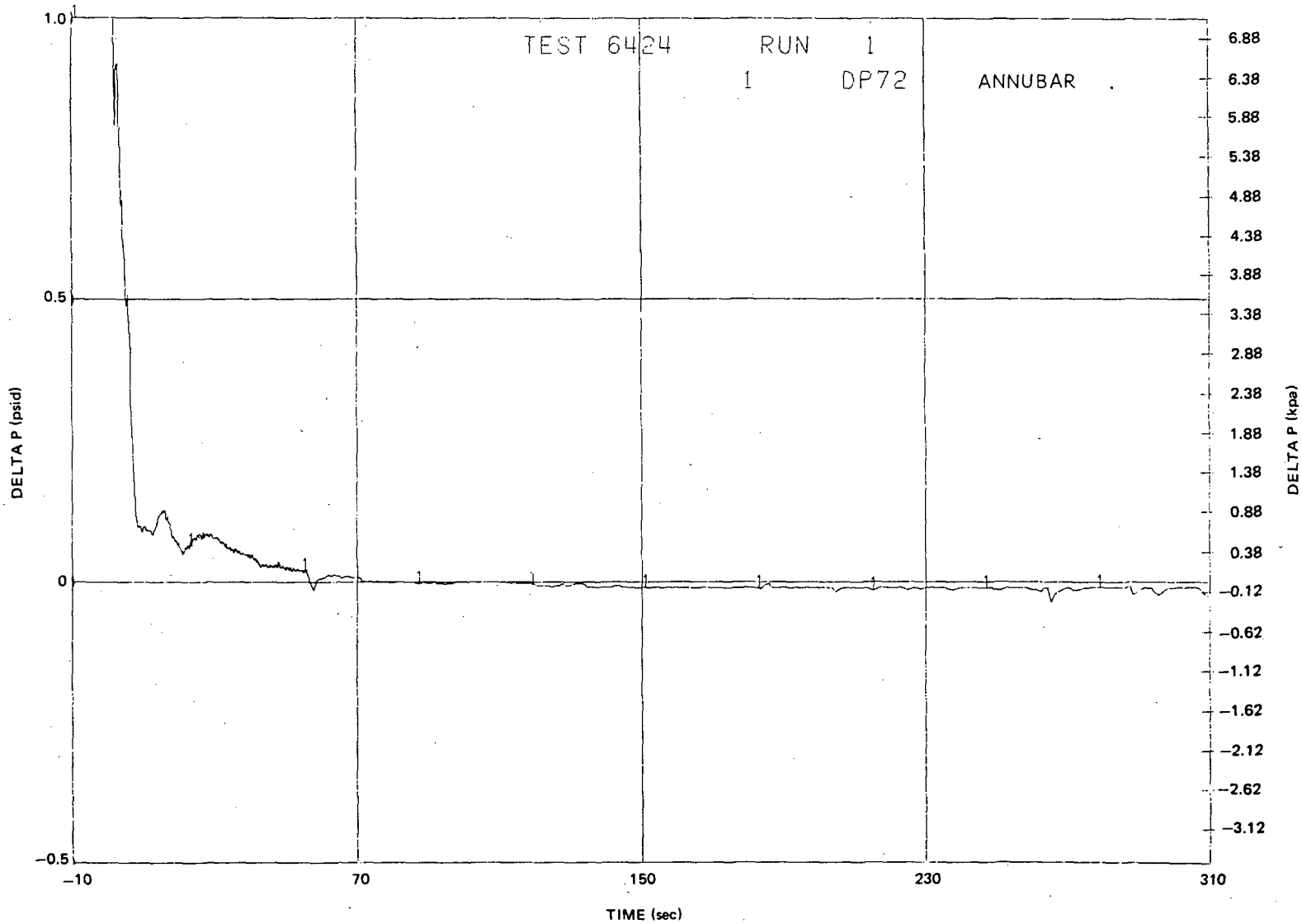

Figure K-27. Upper Plenum Exit Differential Pressure

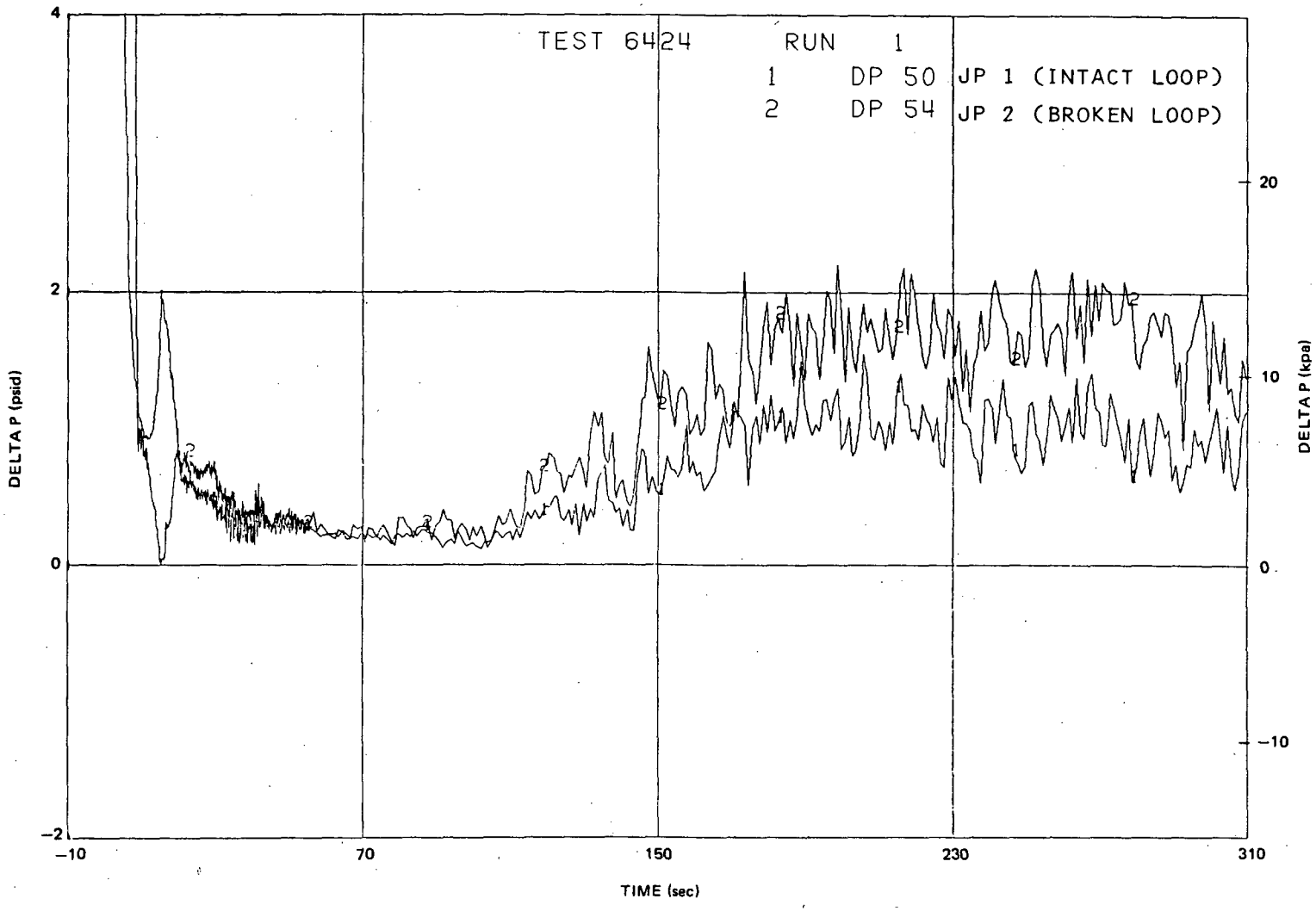

Figure K-28. Intact Loop and Broken Loop Jet Pump Diffuser to Throat Differential Pressures

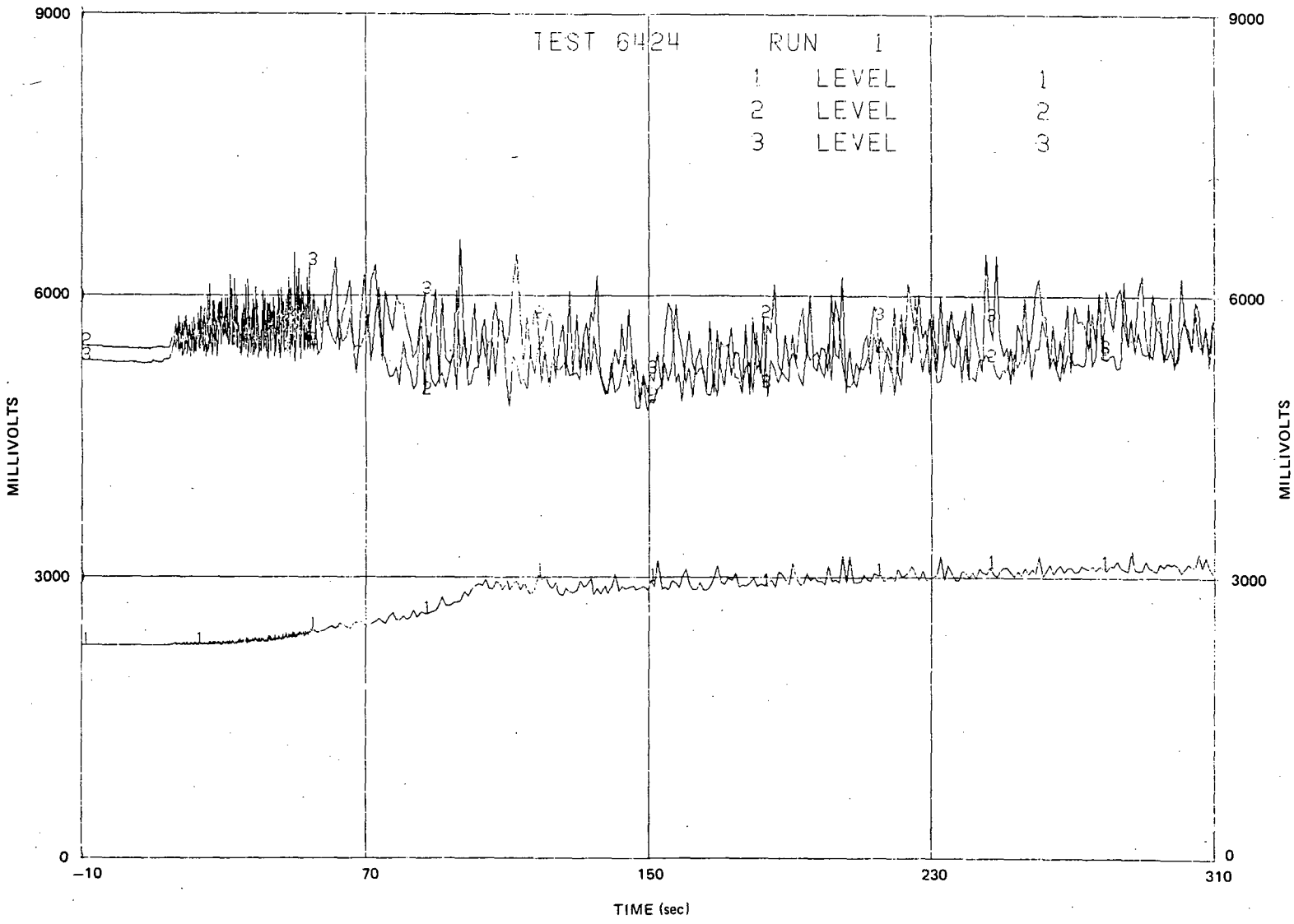

Figure K-29. Bottom Lower Plenum Conductivity Probe Measurements

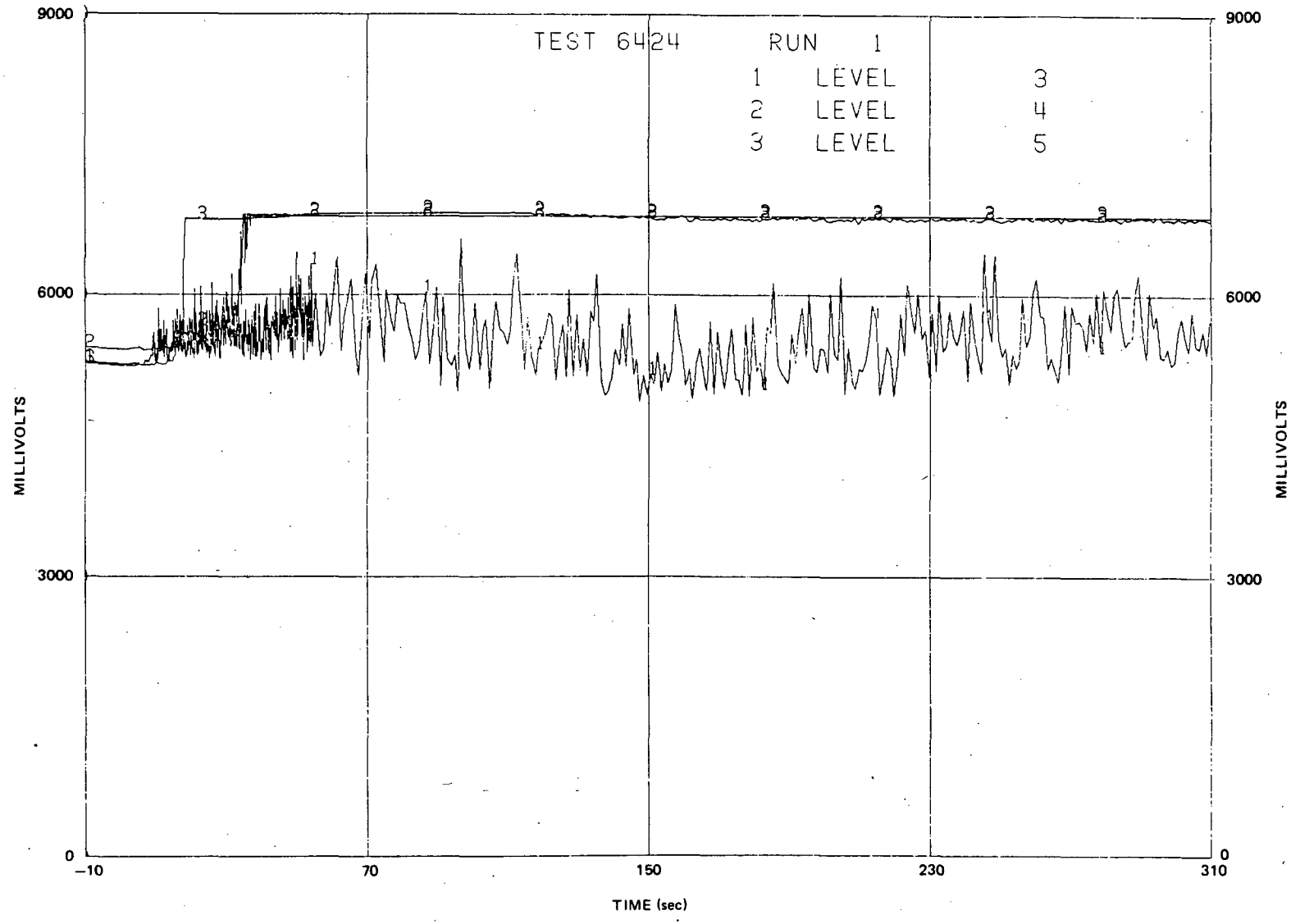

Figure K-30. Upper Lower Plenum Conductivity Probe Measurements

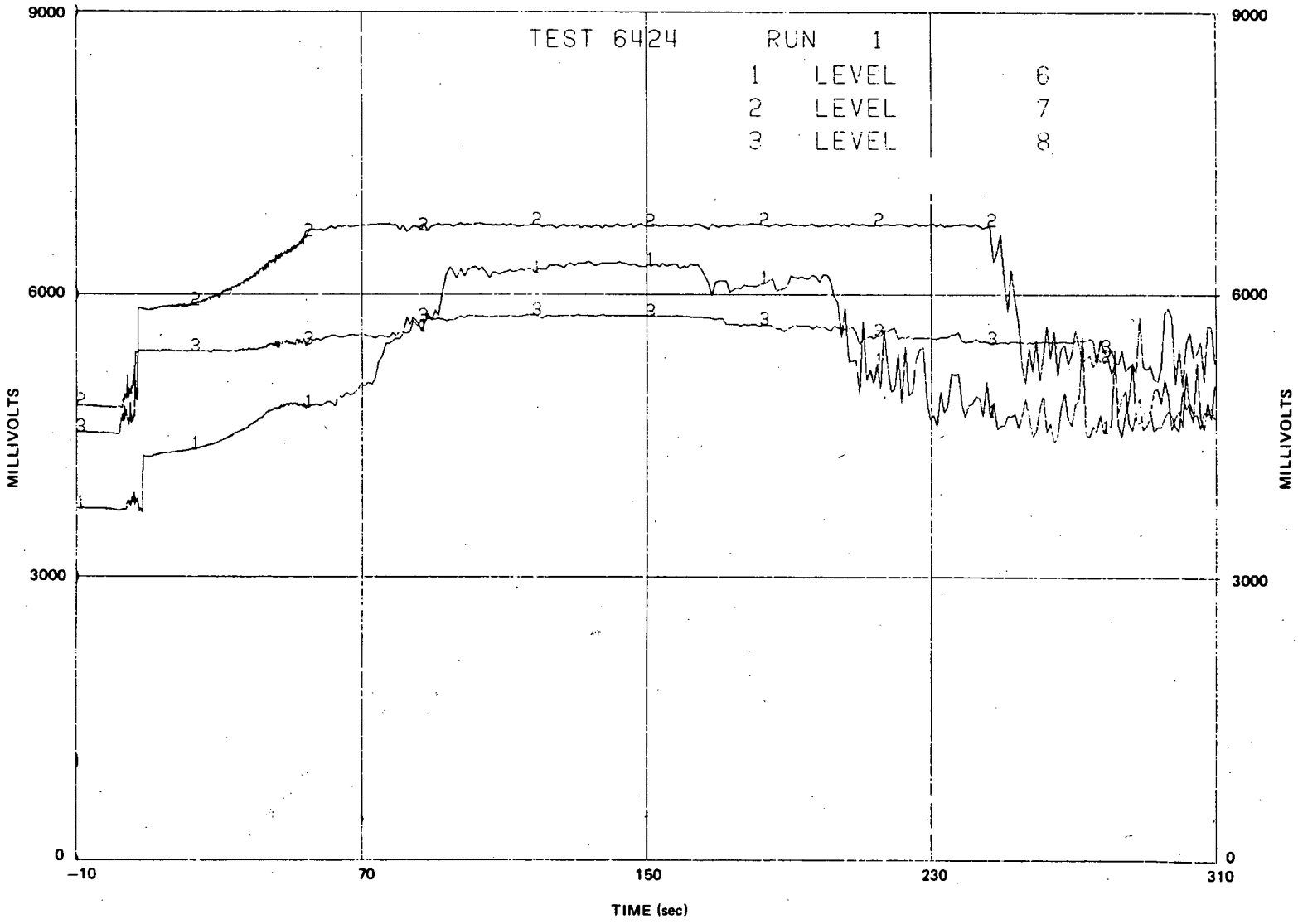

Figure K-31. Lower Annulus Conductivity Probe Measurements

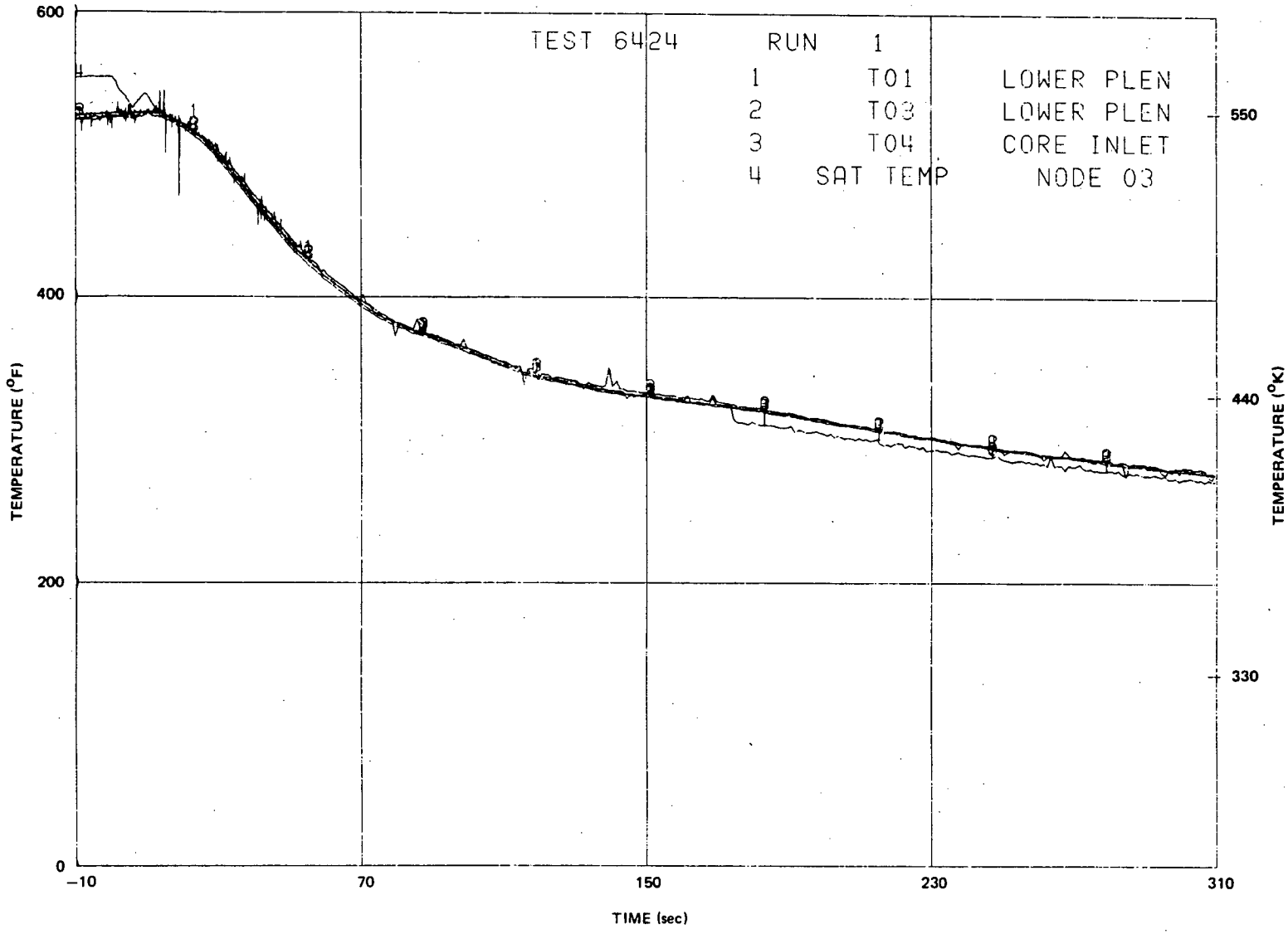

Figure K-32. Lower Plenum Fluid Temperatures

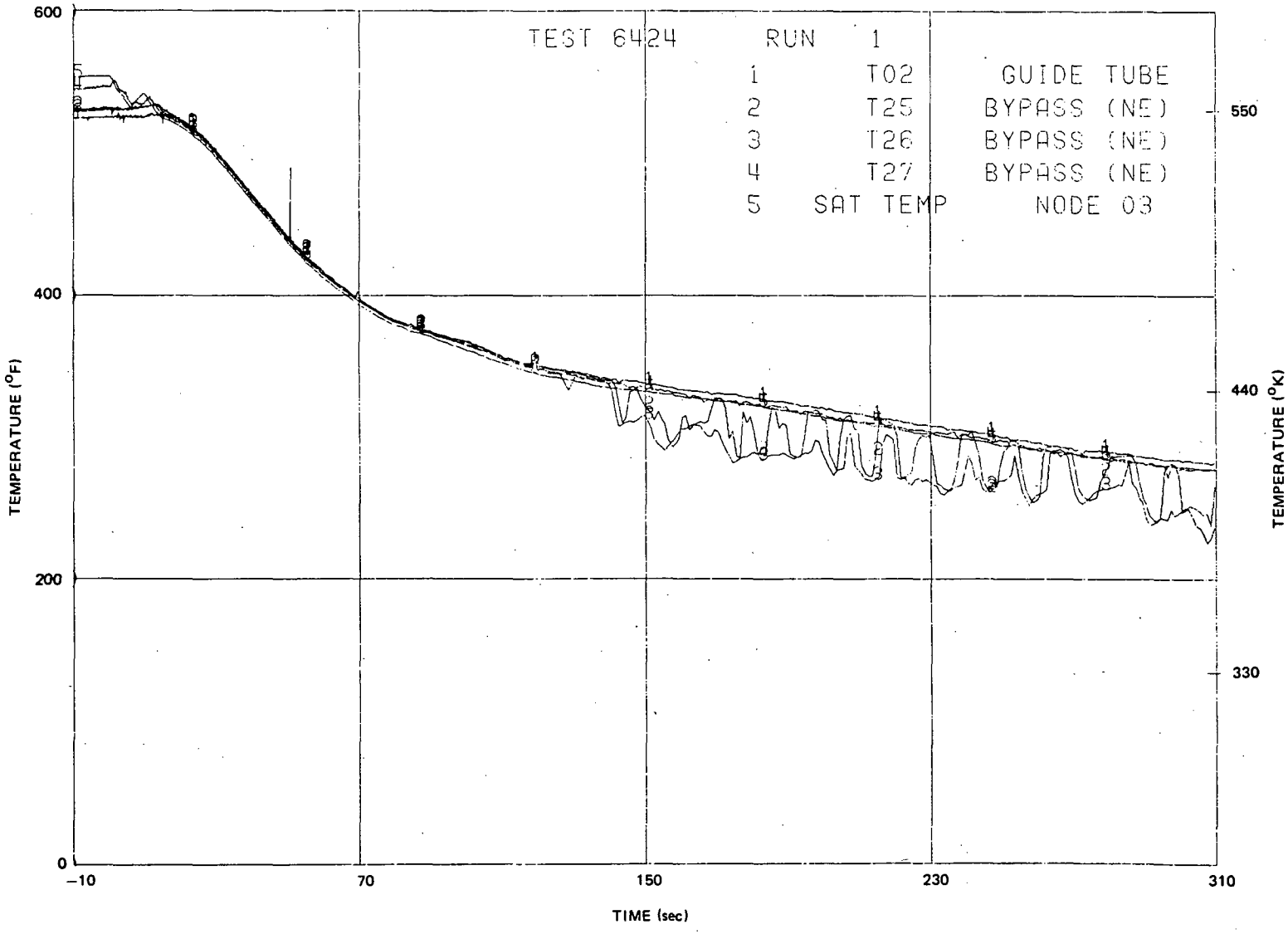

Figure K-33. Guide Tube and Bypass Fluid Temperatures

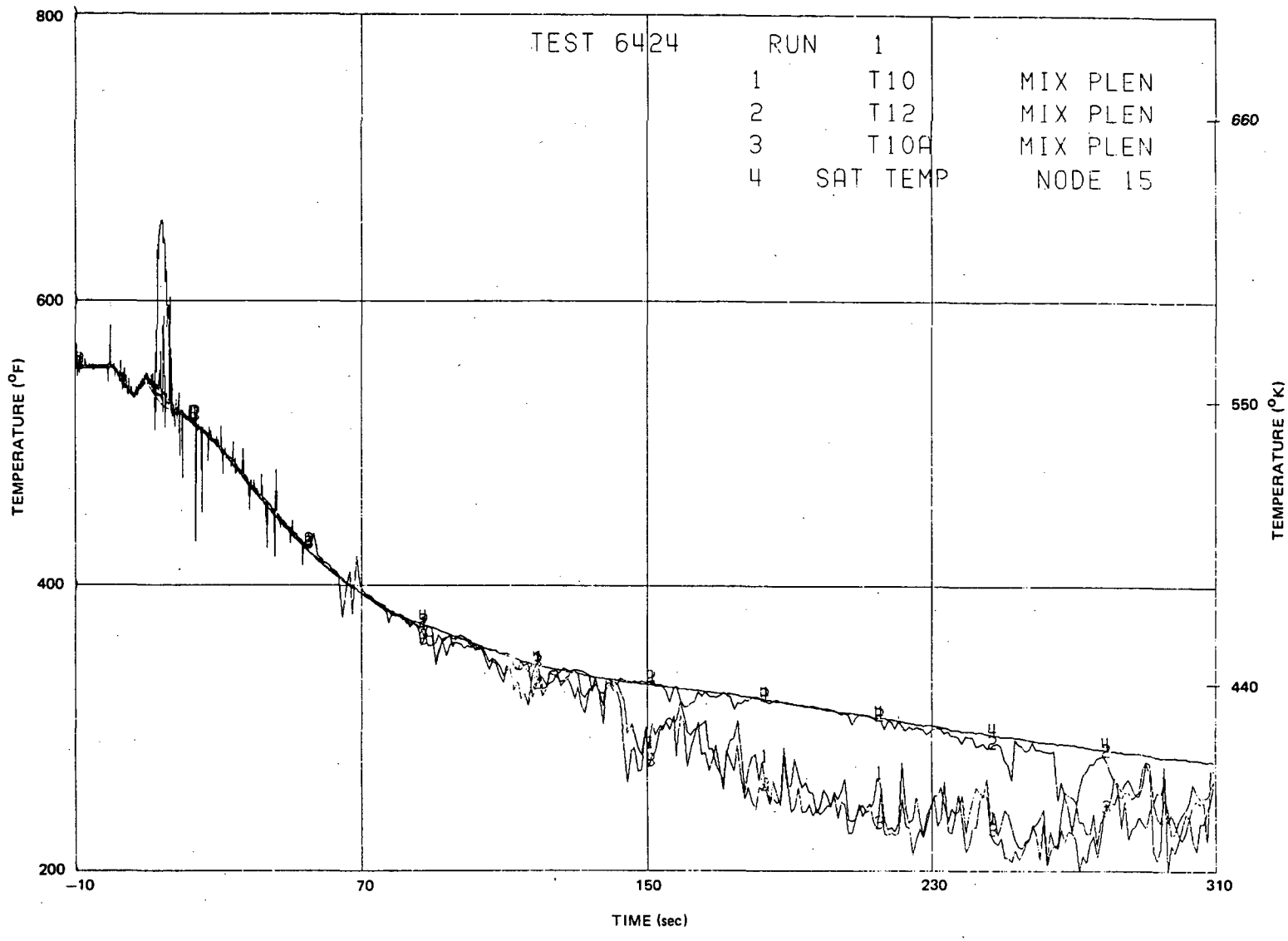

Figure K-34. Mixing Plenum Fluid Temperatures

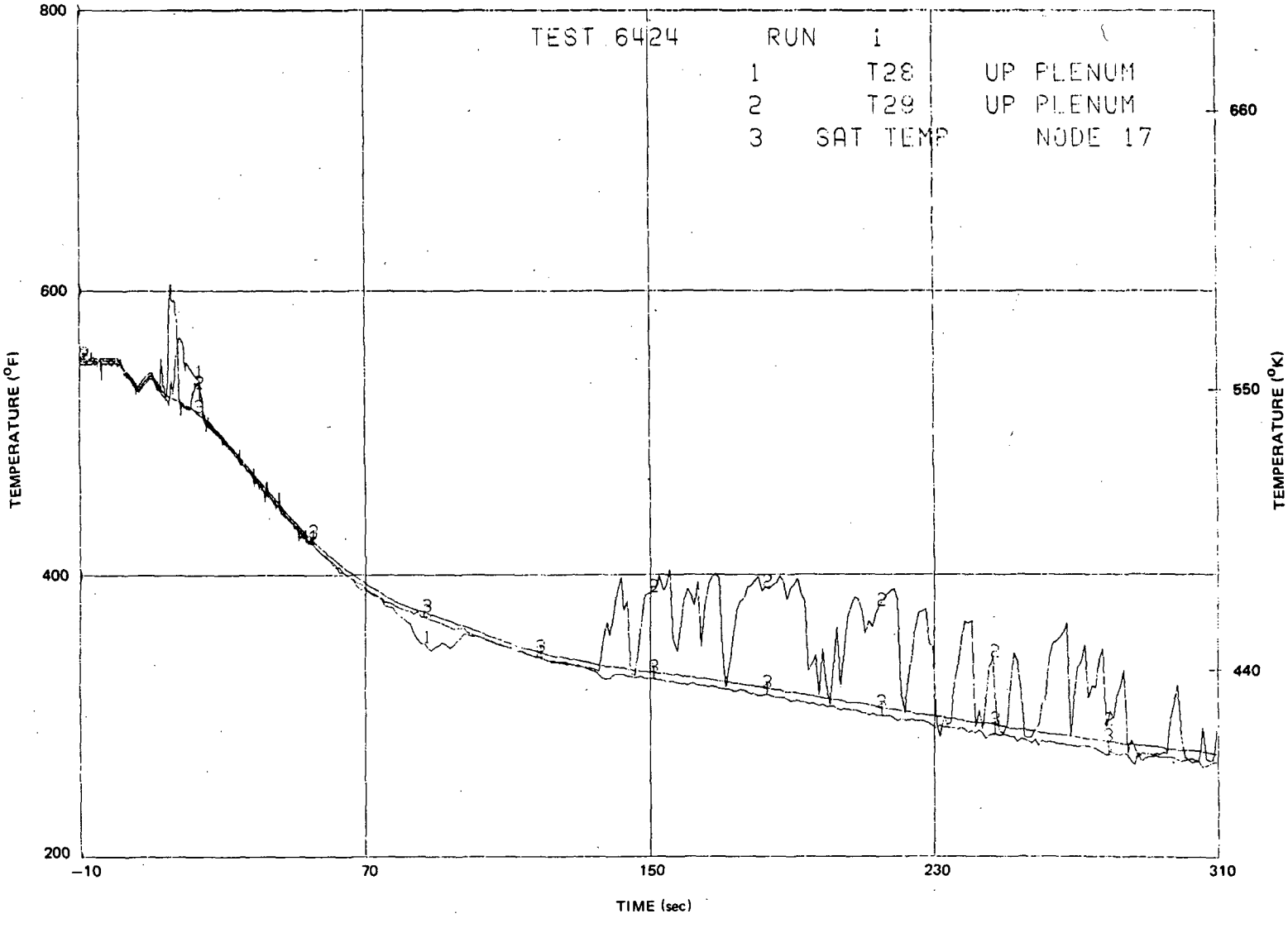

Figure K-35. Upper Plenum Fluid Temperatures

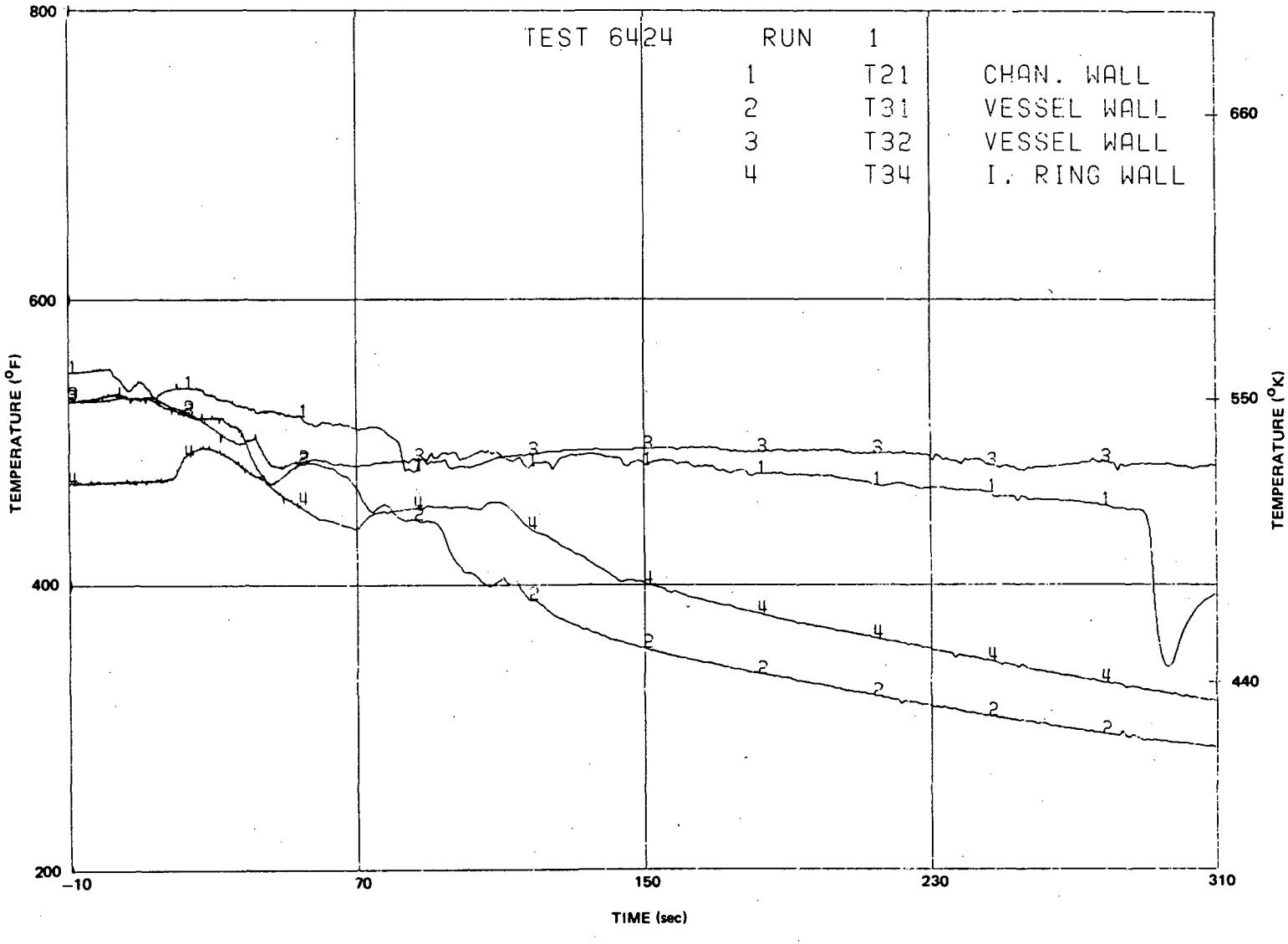

Figure K-36. Wall Temperatures

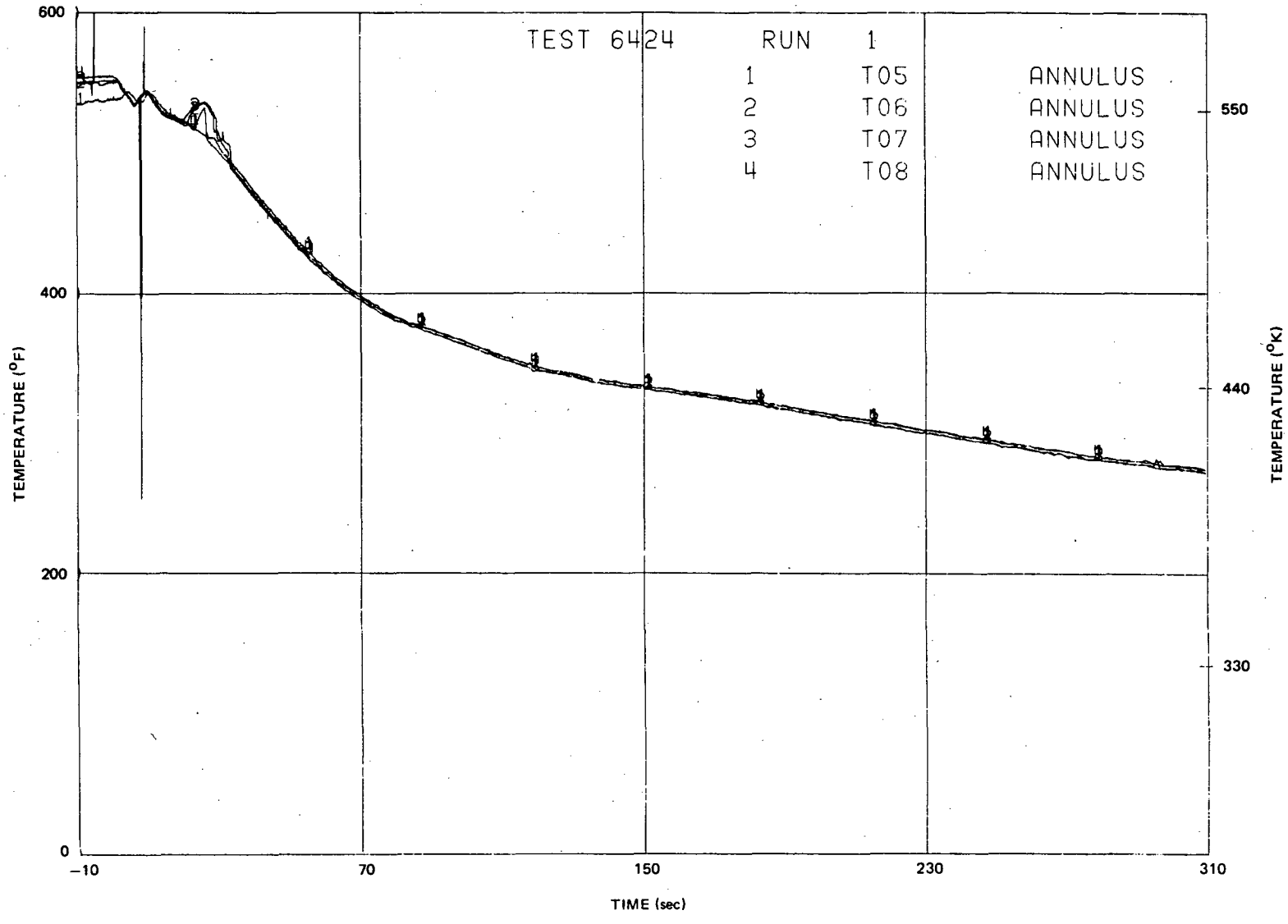

Figure K-37. Annulus Fluid Temperatures

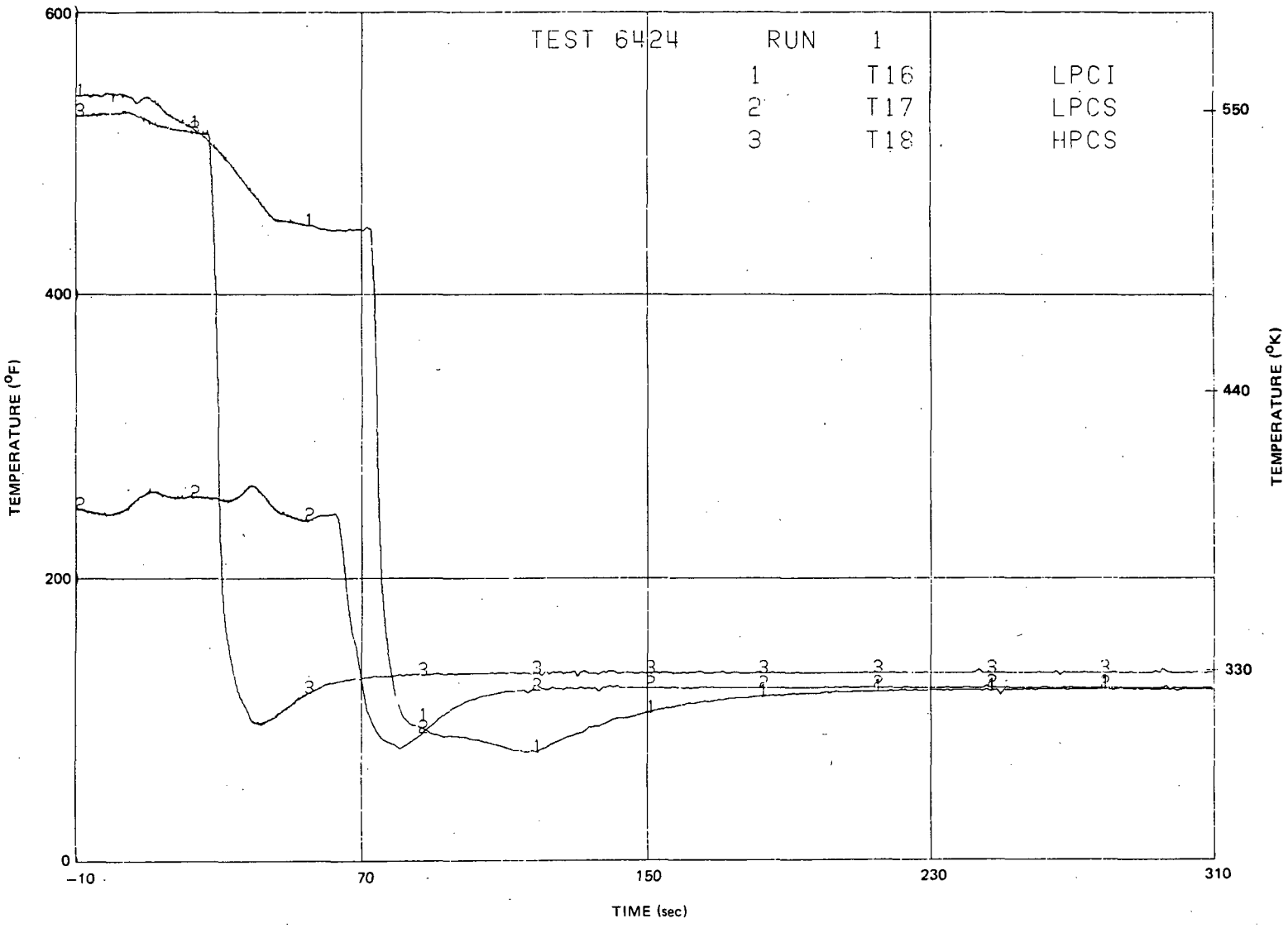

Figure K-38. Emergency Core Cooling Fluid Temperatures

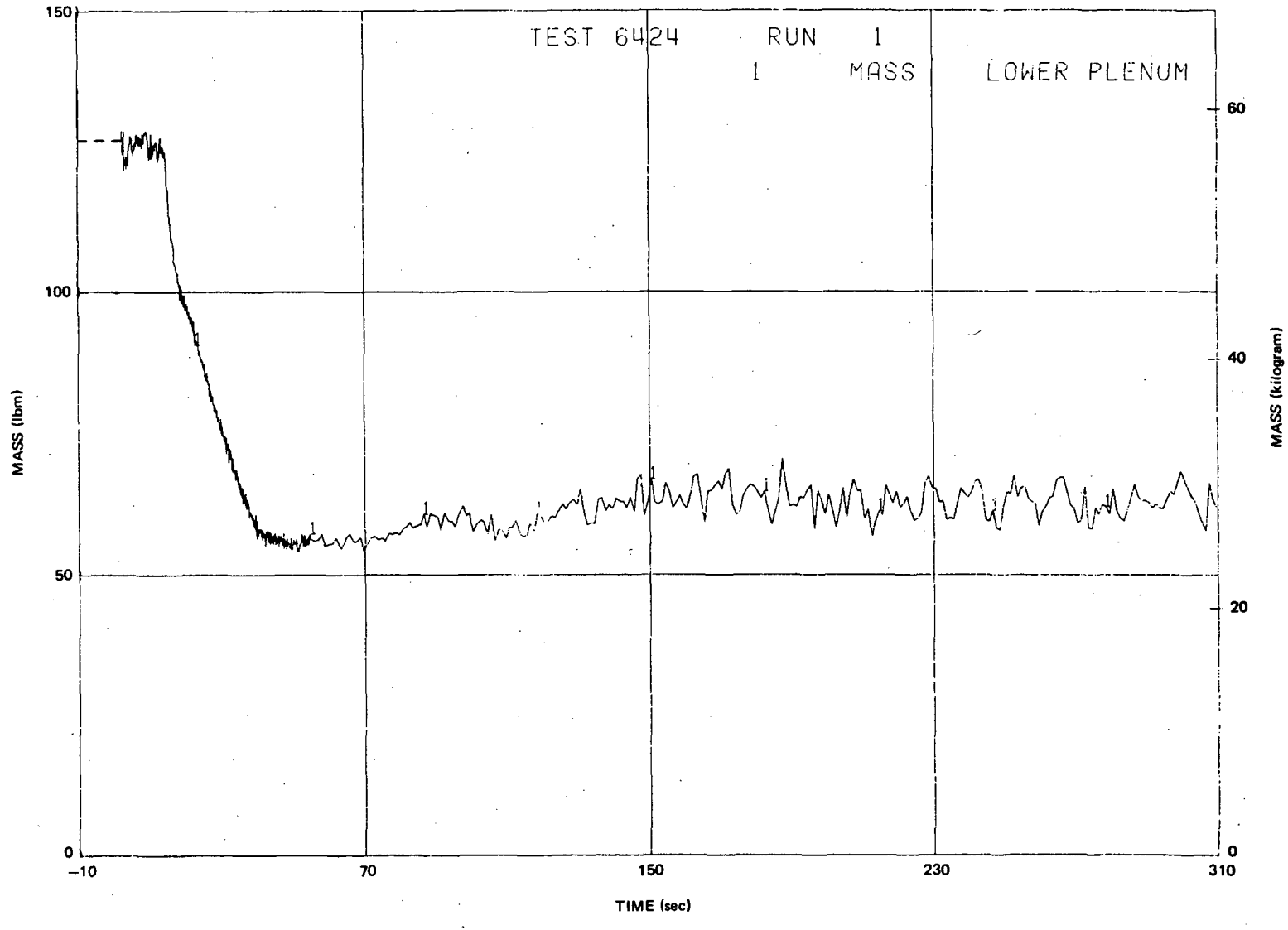

Figure K-39. Lower Plenum Fluid Mass

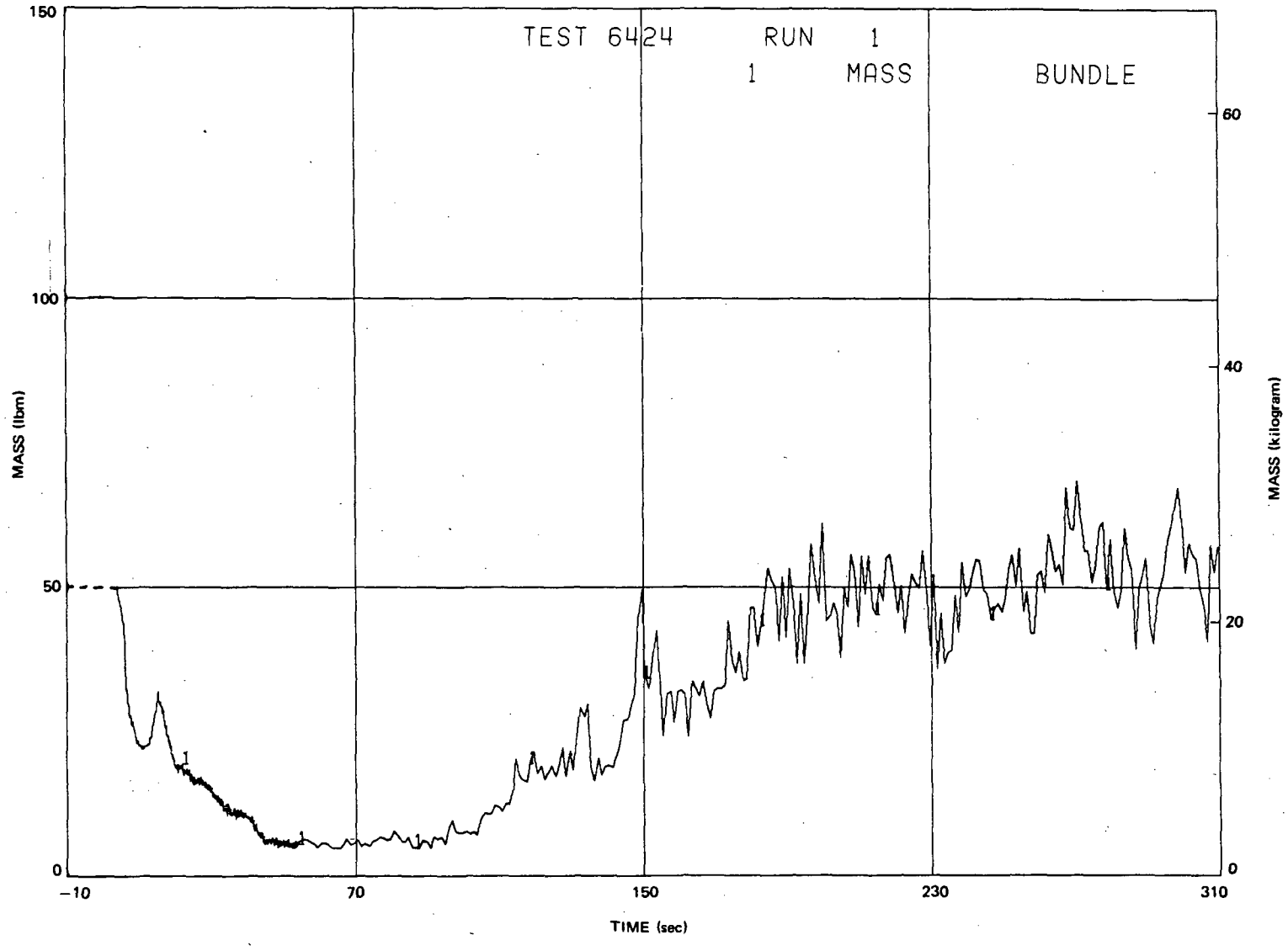

Figure K-40. Bundle Fluid Mass

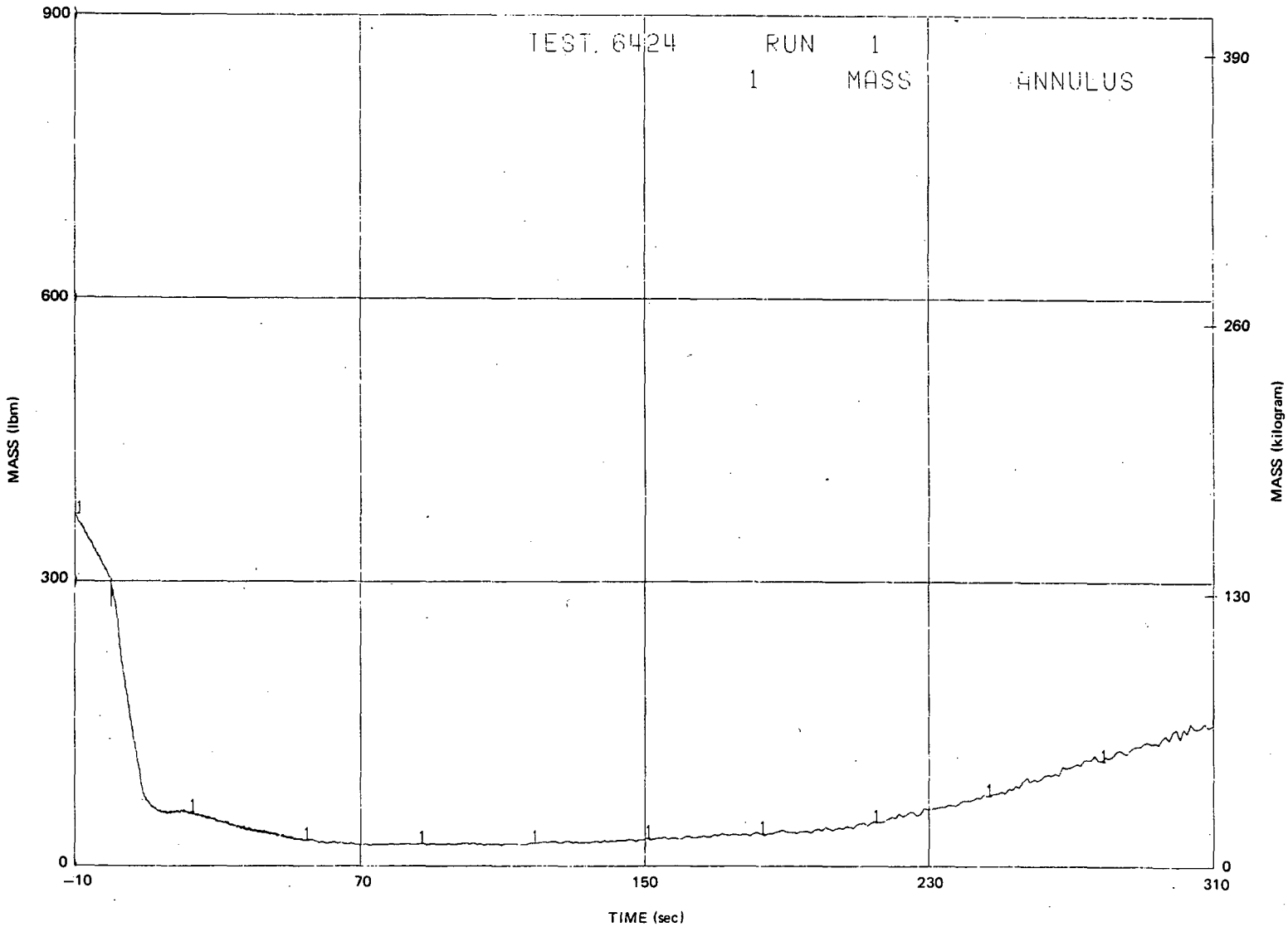

Figure K-41. Annulus Fluid Mass

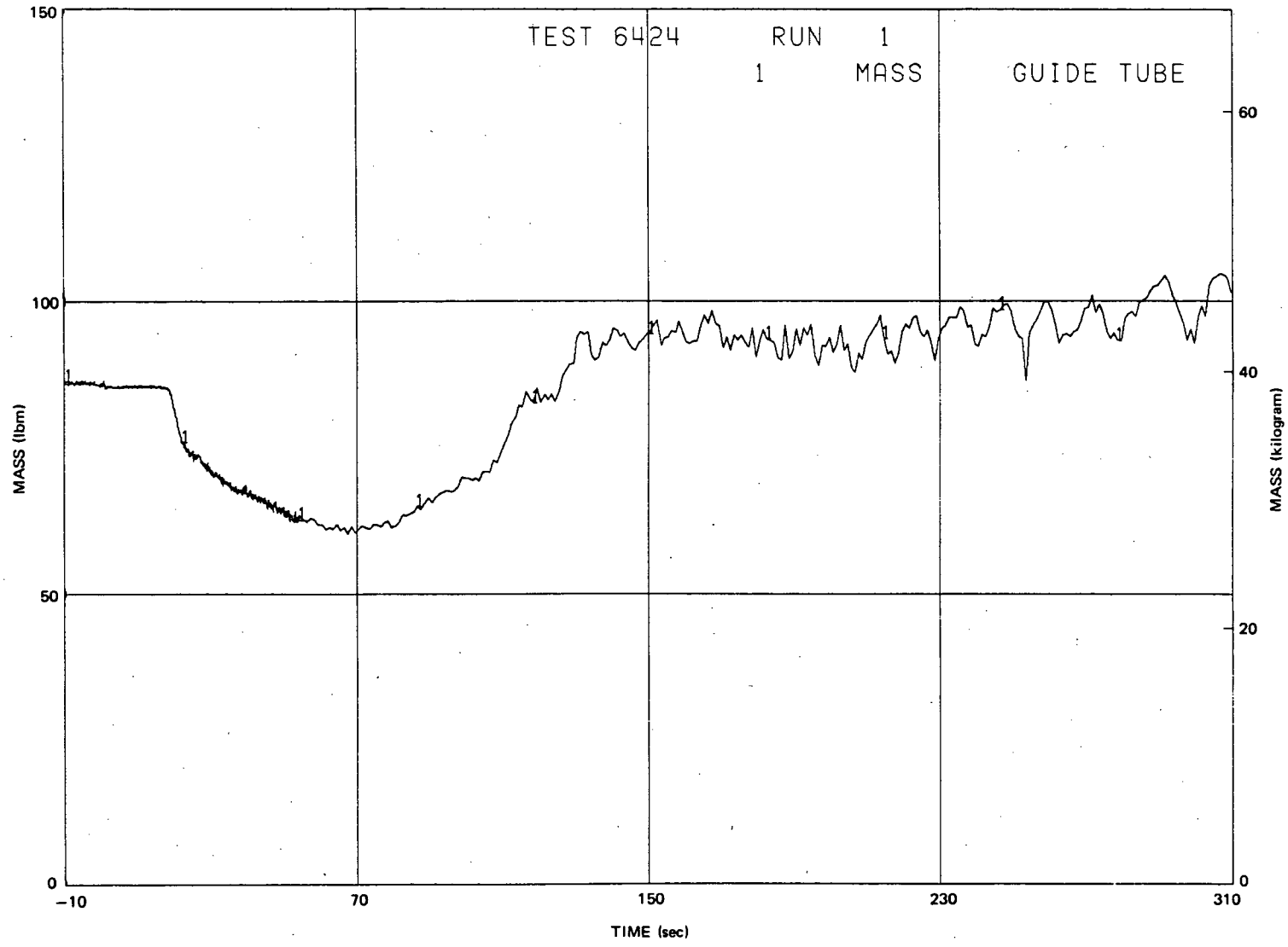

Figure K-42. Guide Tube Fluid Mass

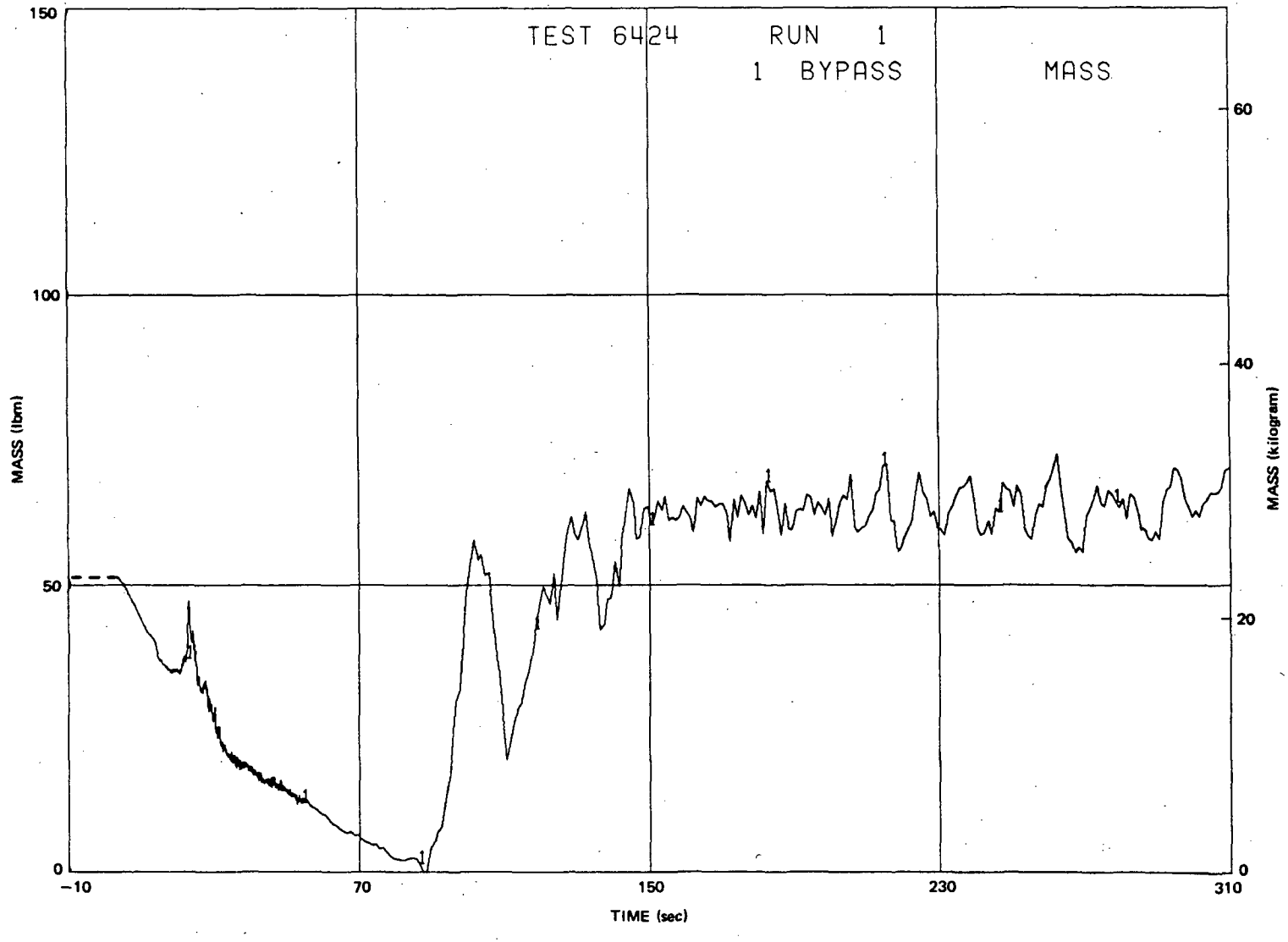

Figure K-43. Bypass Fluid Mass

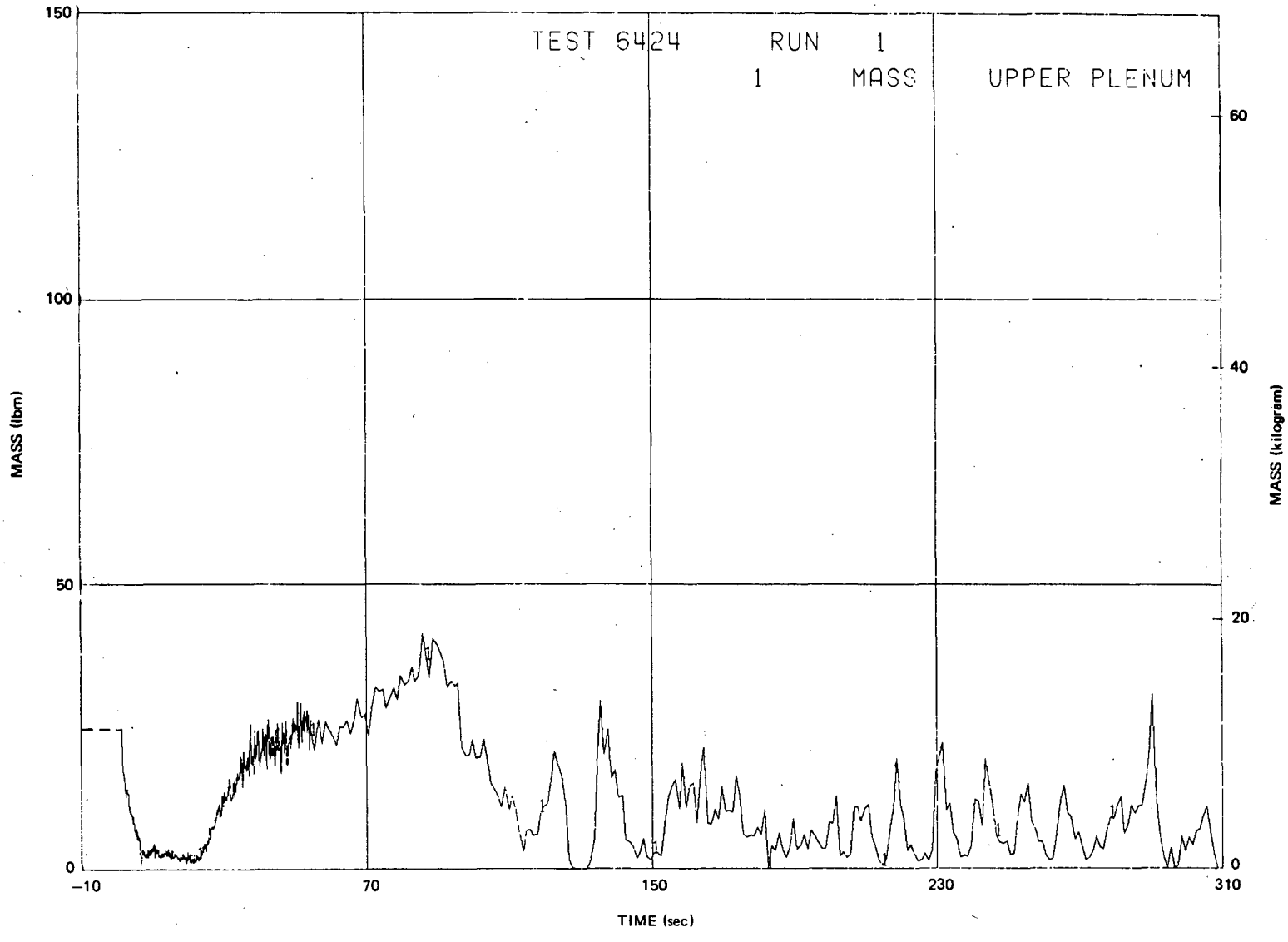

Figure K-44. Upper Plenum Fluid Mass

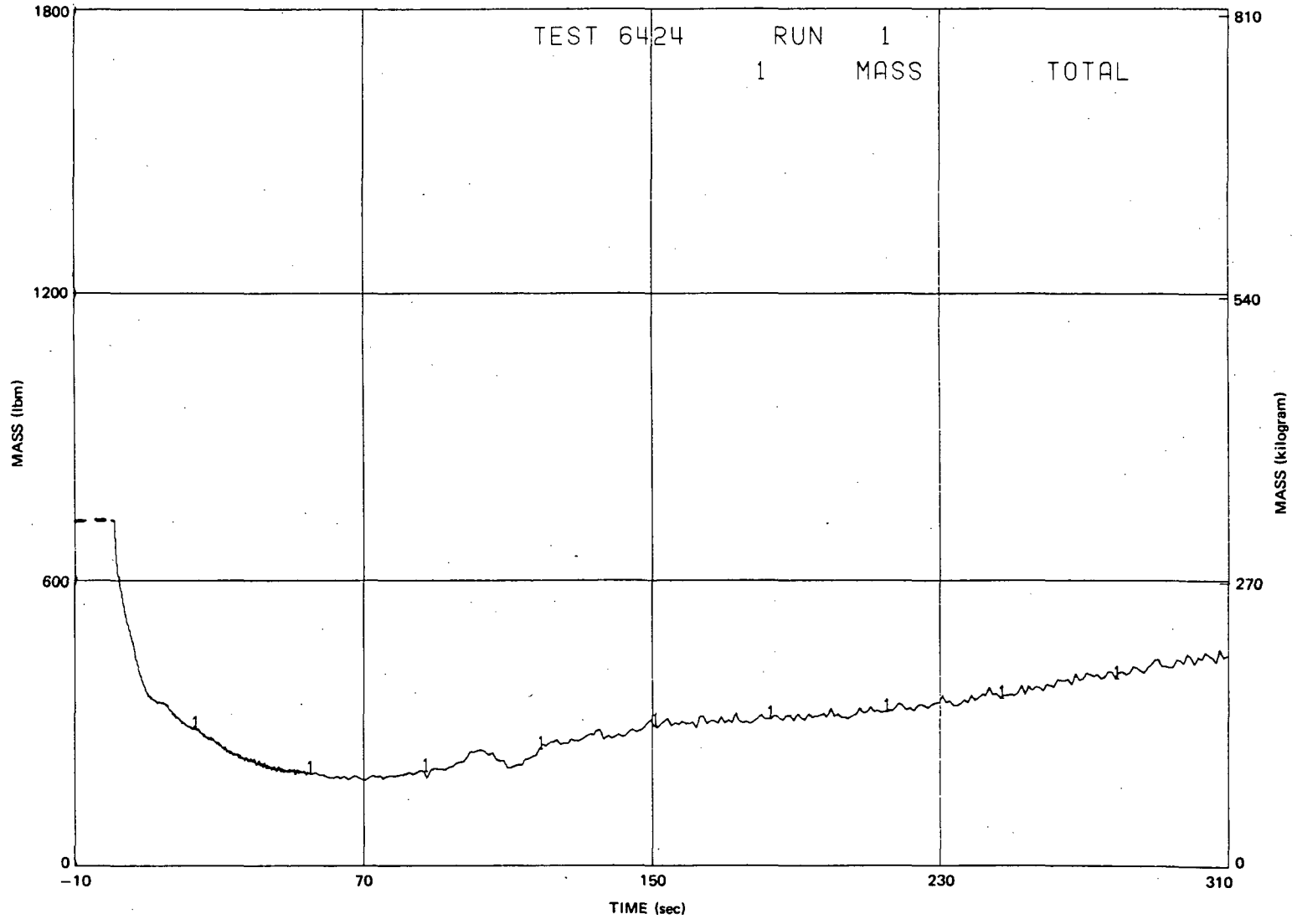

Figure K-45. Total Vessel Fluid Mass

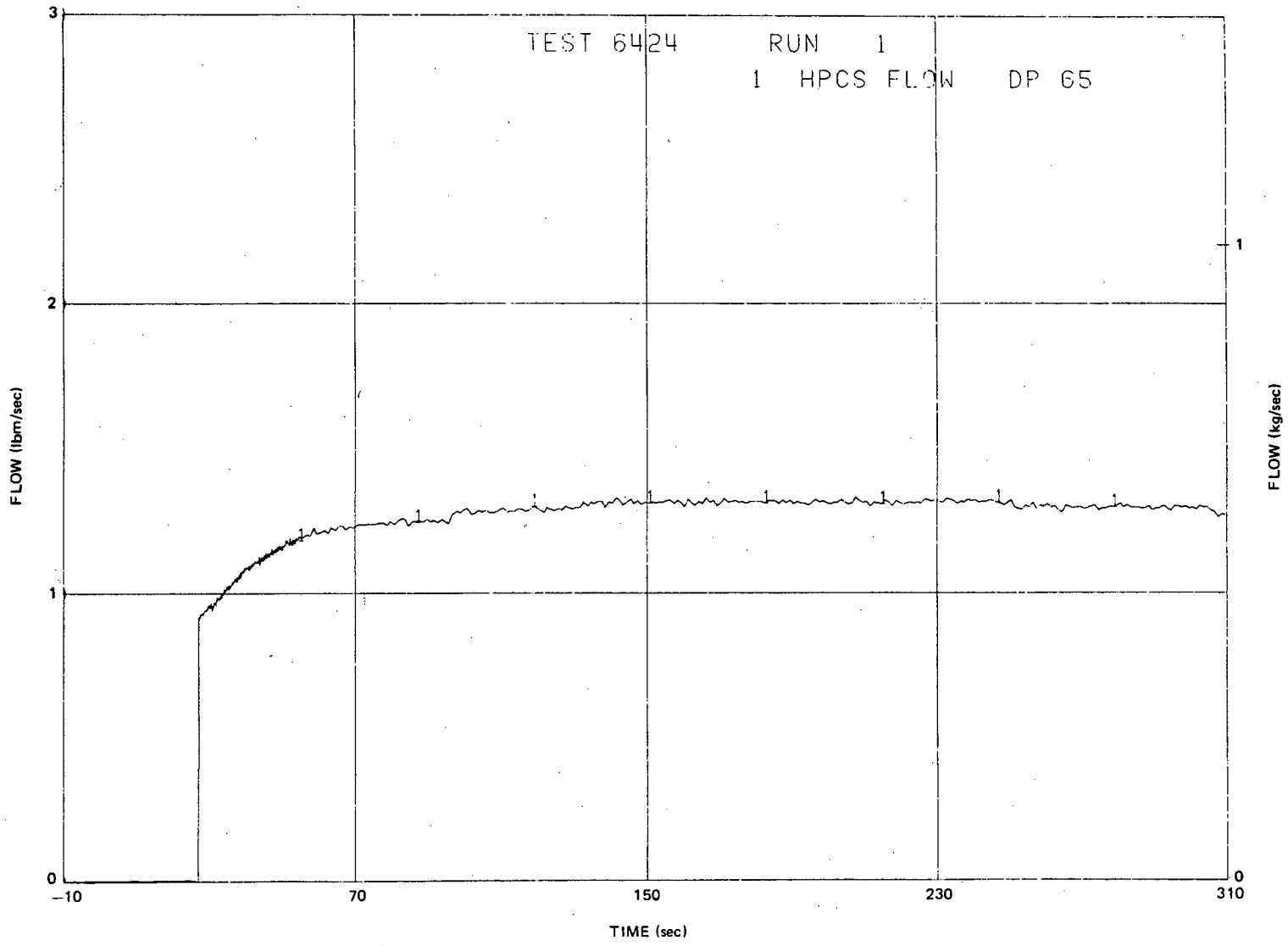

Figure K-46. HPCS Mass Flow Rate

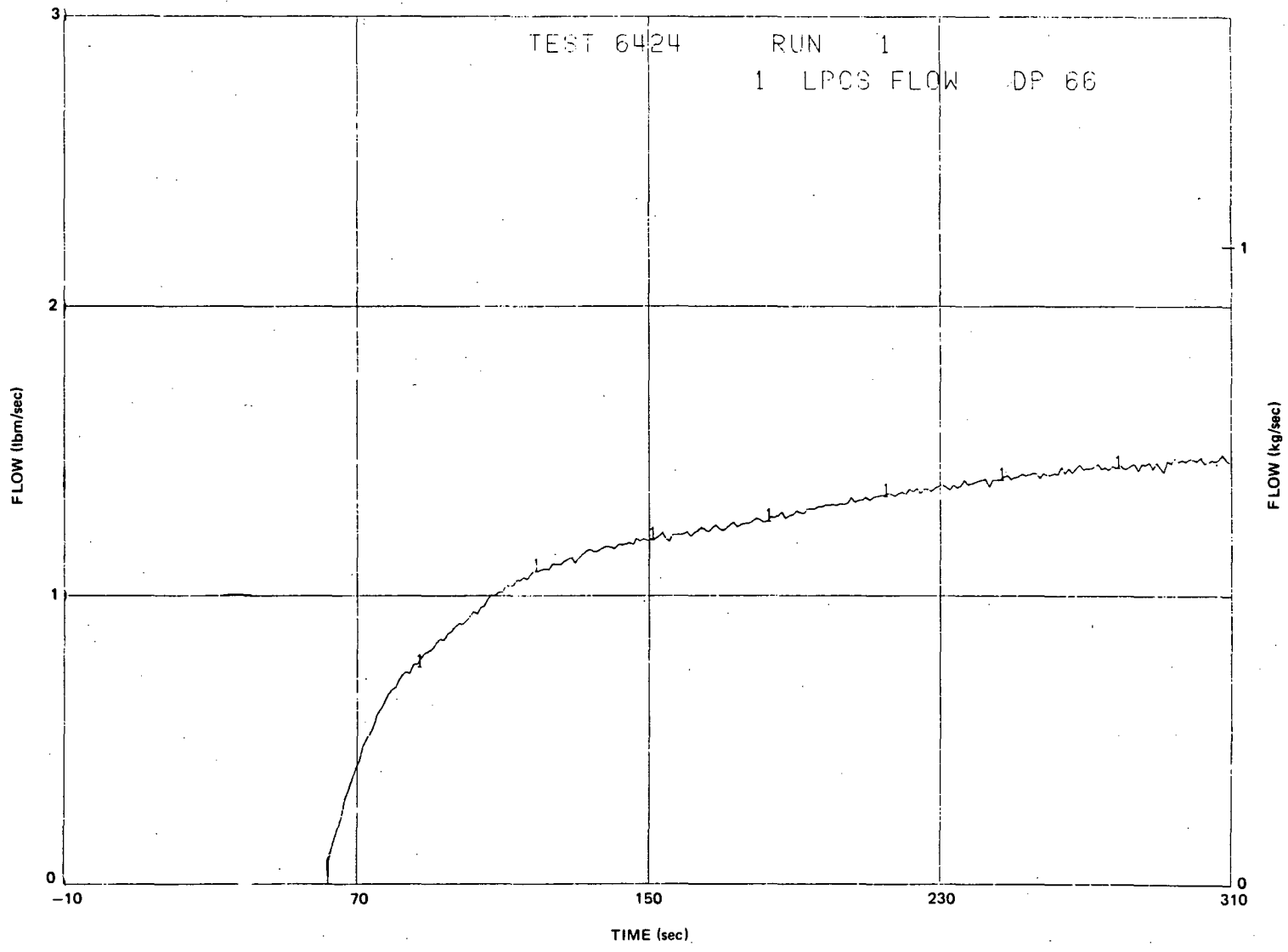

Figure K-47. LPCS Mass Flow Rate

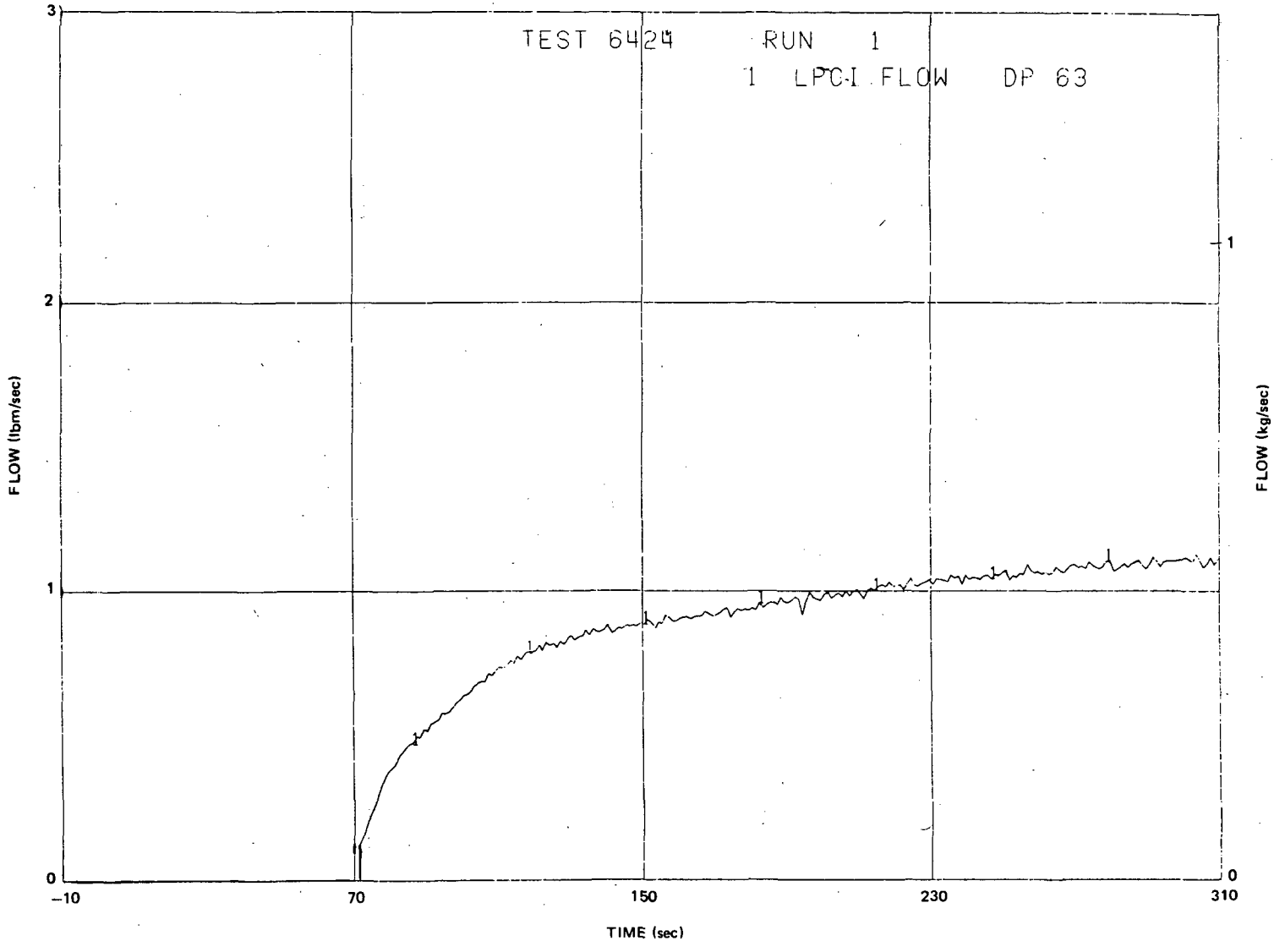

Figure K-48. LPCI Mass Flow Rate

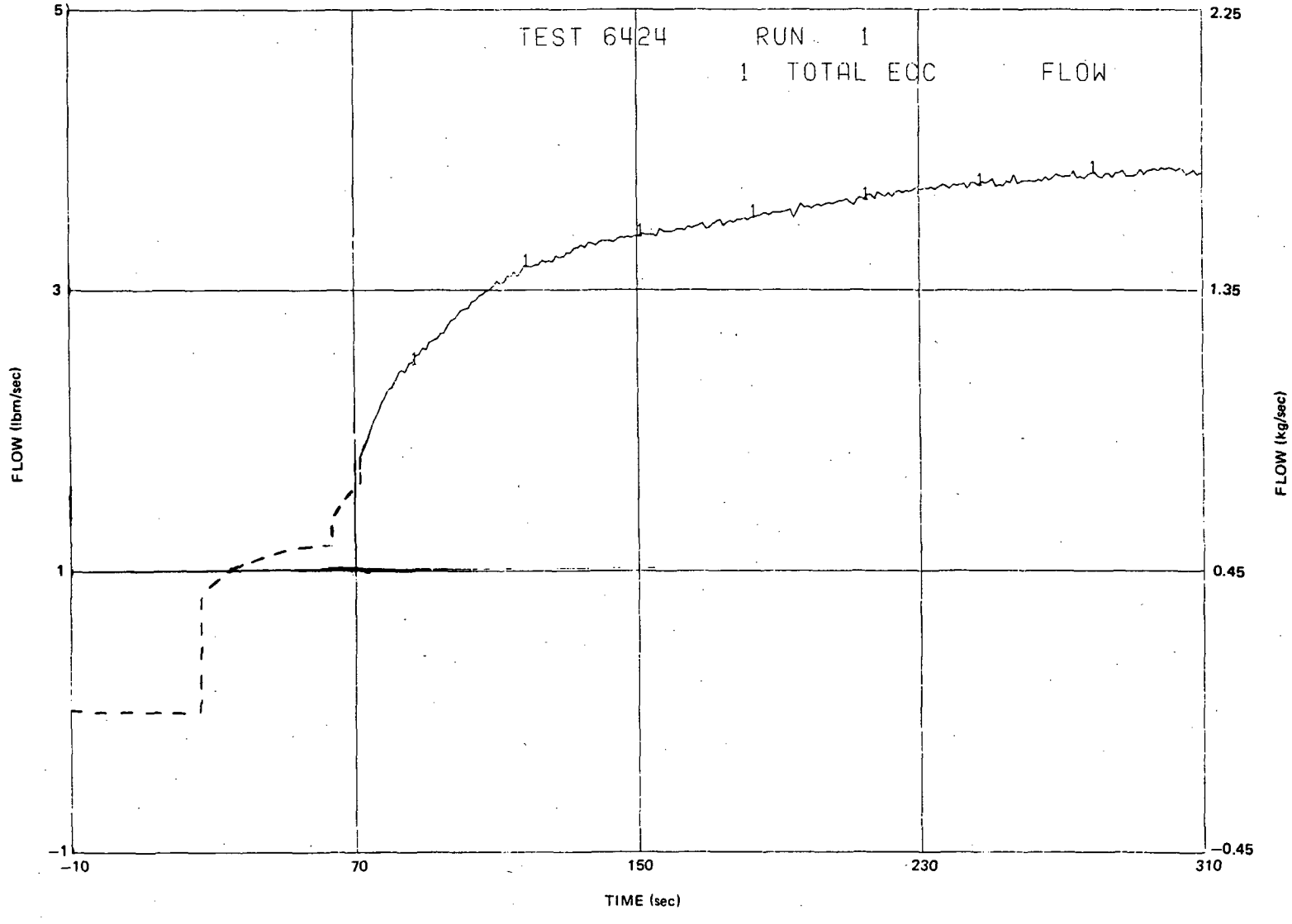

Figure K-49. Total ECC Mass Flow Rate

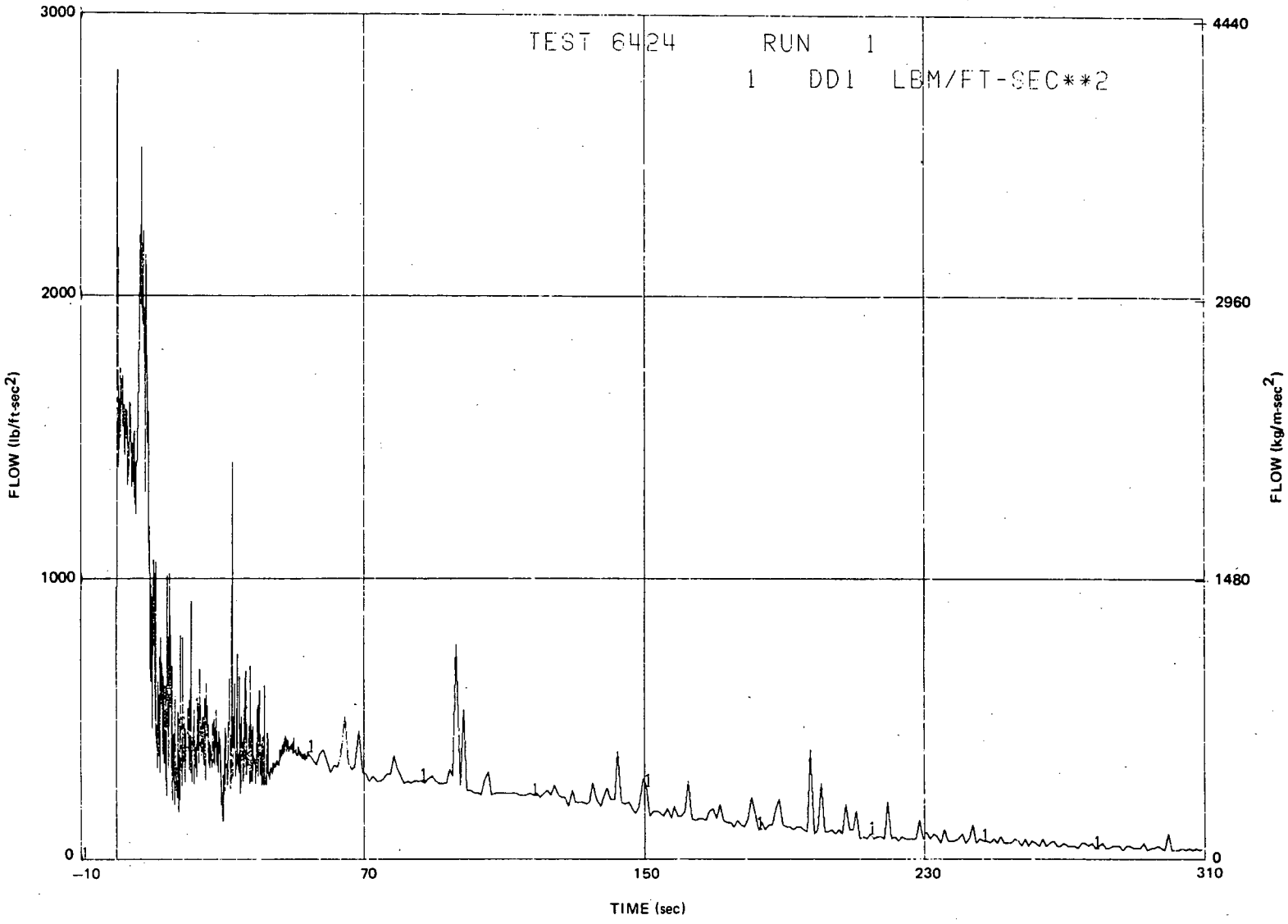

Figure K-50. Drag Disc Measurement on Drive Line Side of Broken Loop

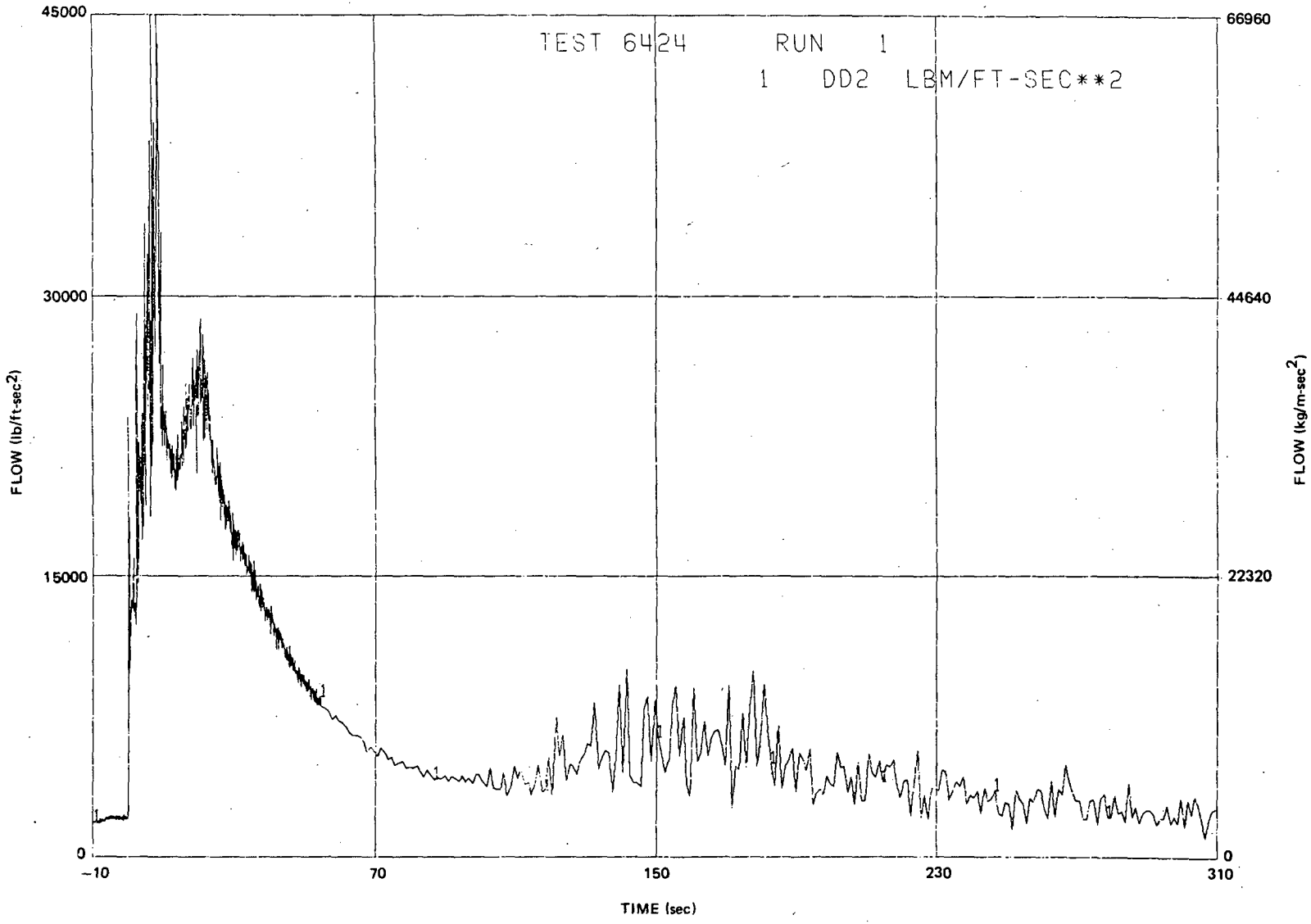

Figure K-51. Drag Disc Measurement on Suction Line Side of Broken Loop

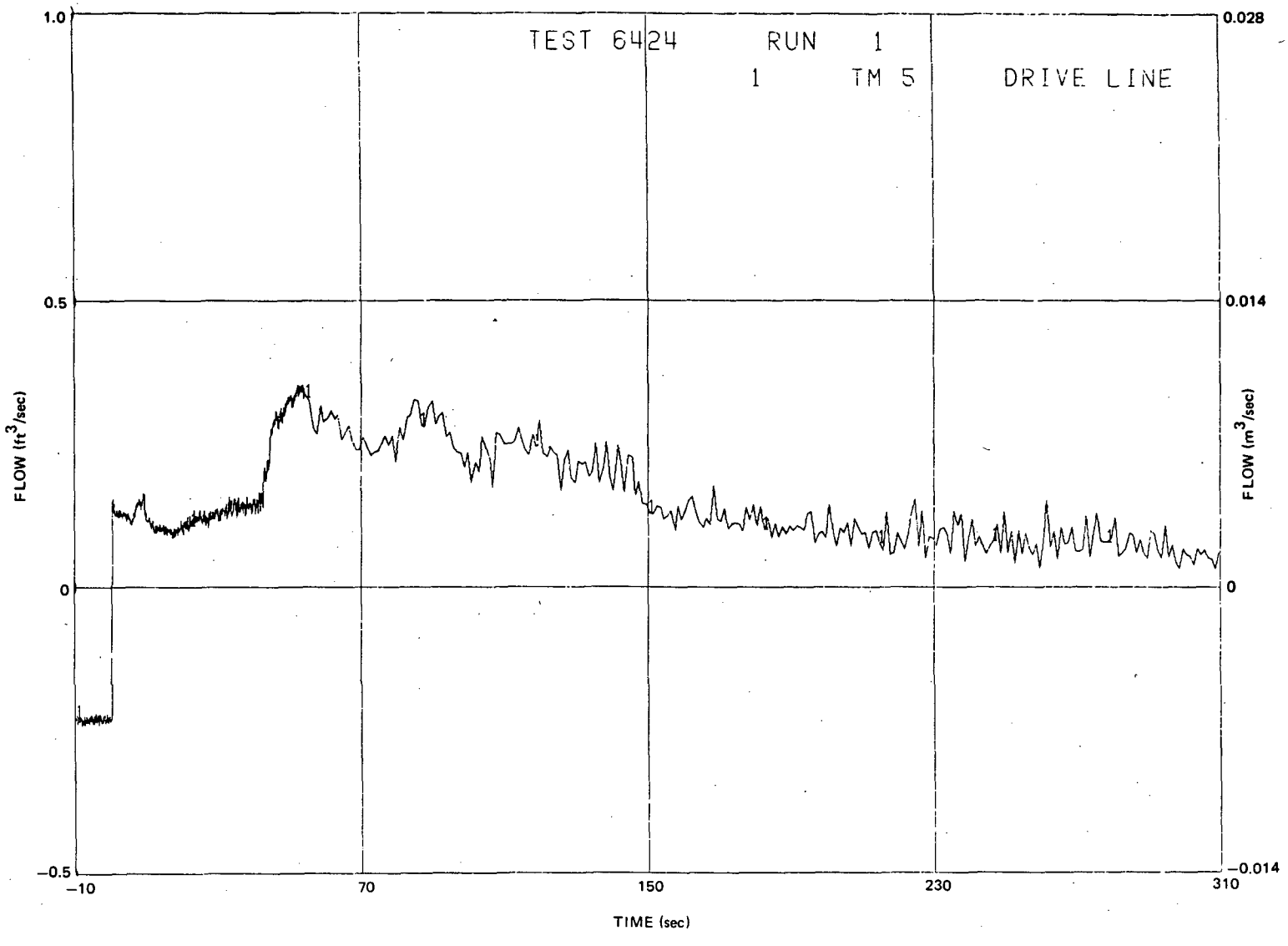

Figure K-52. Turbinemeter Measurement on Drive Line Side of Broken Loop

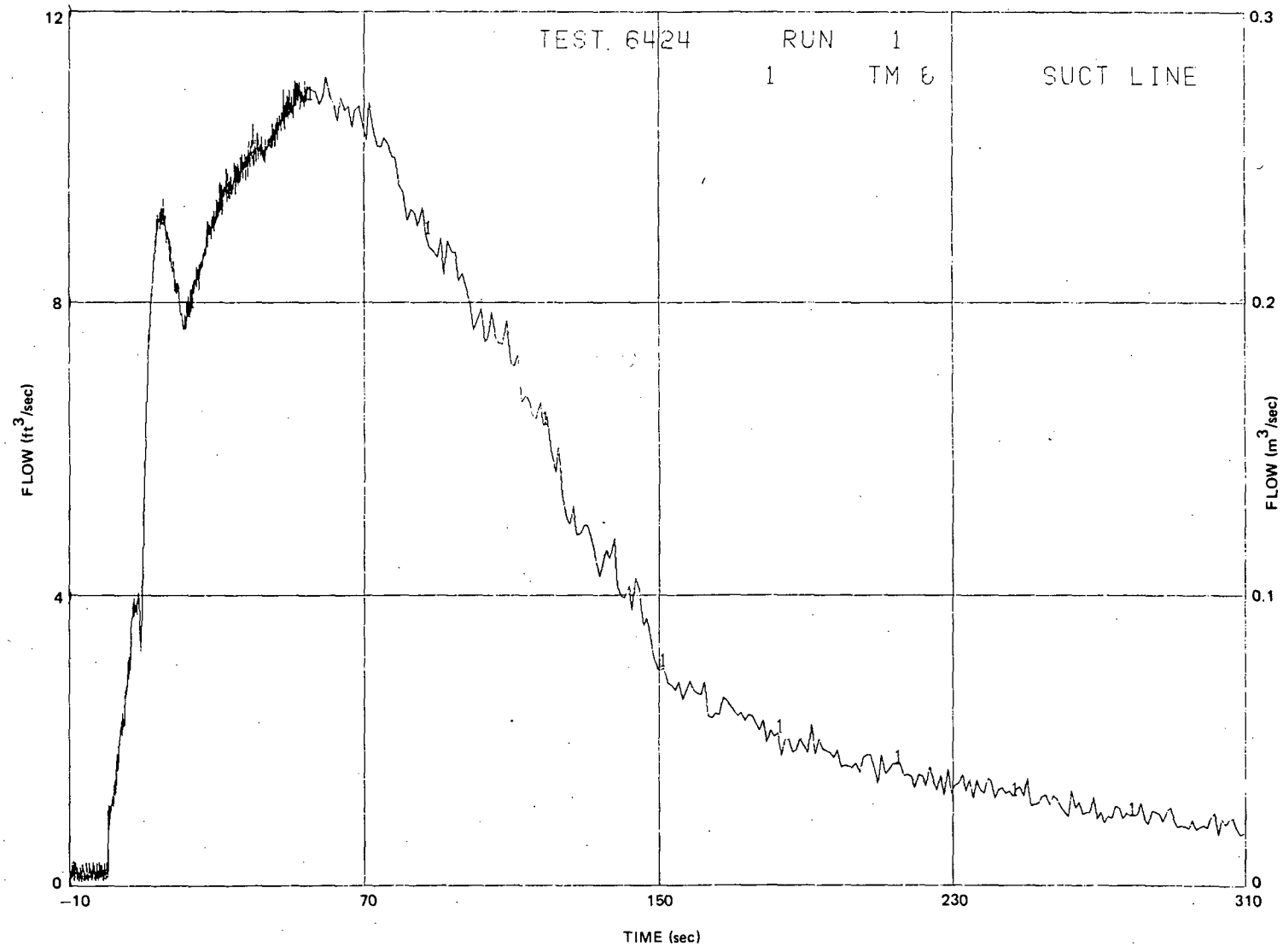

Figure K-53. Turbinemeter Measurement on Suction Line Side of Broken Loop

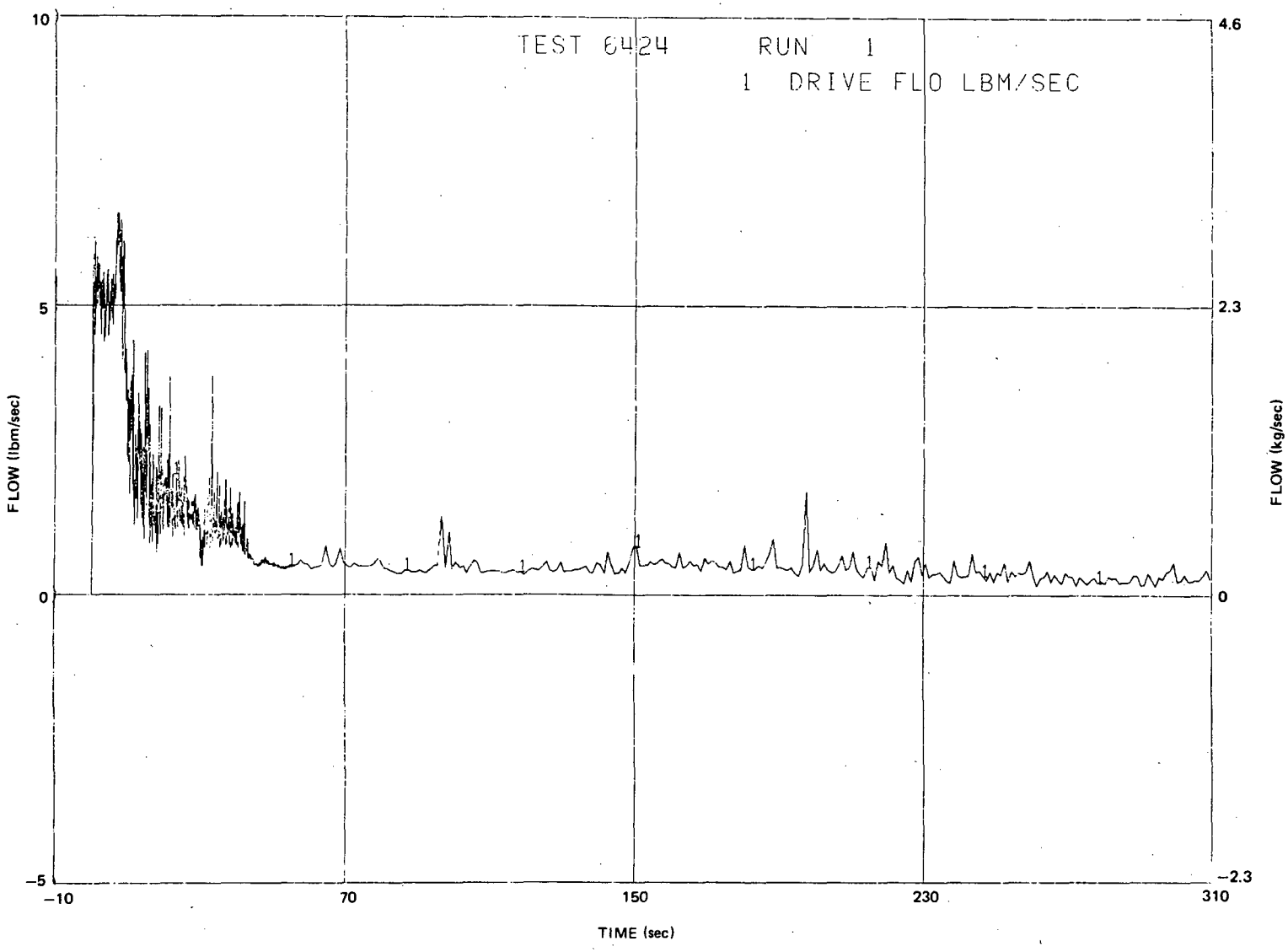

Figure K-54. Drive Line Break Mass Flow Rate

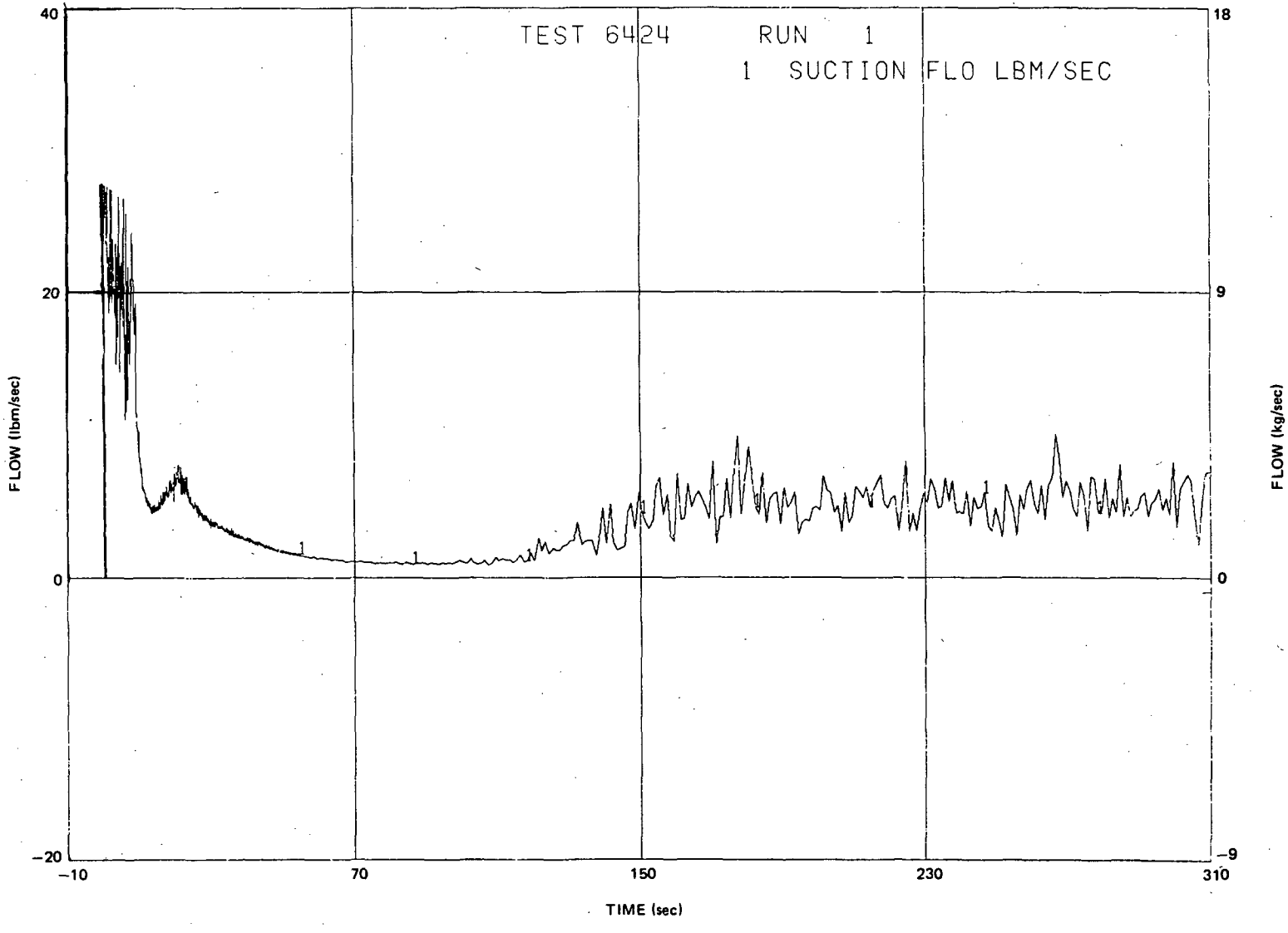

Figure K-55. Suction Line Break Mass Flow Rate

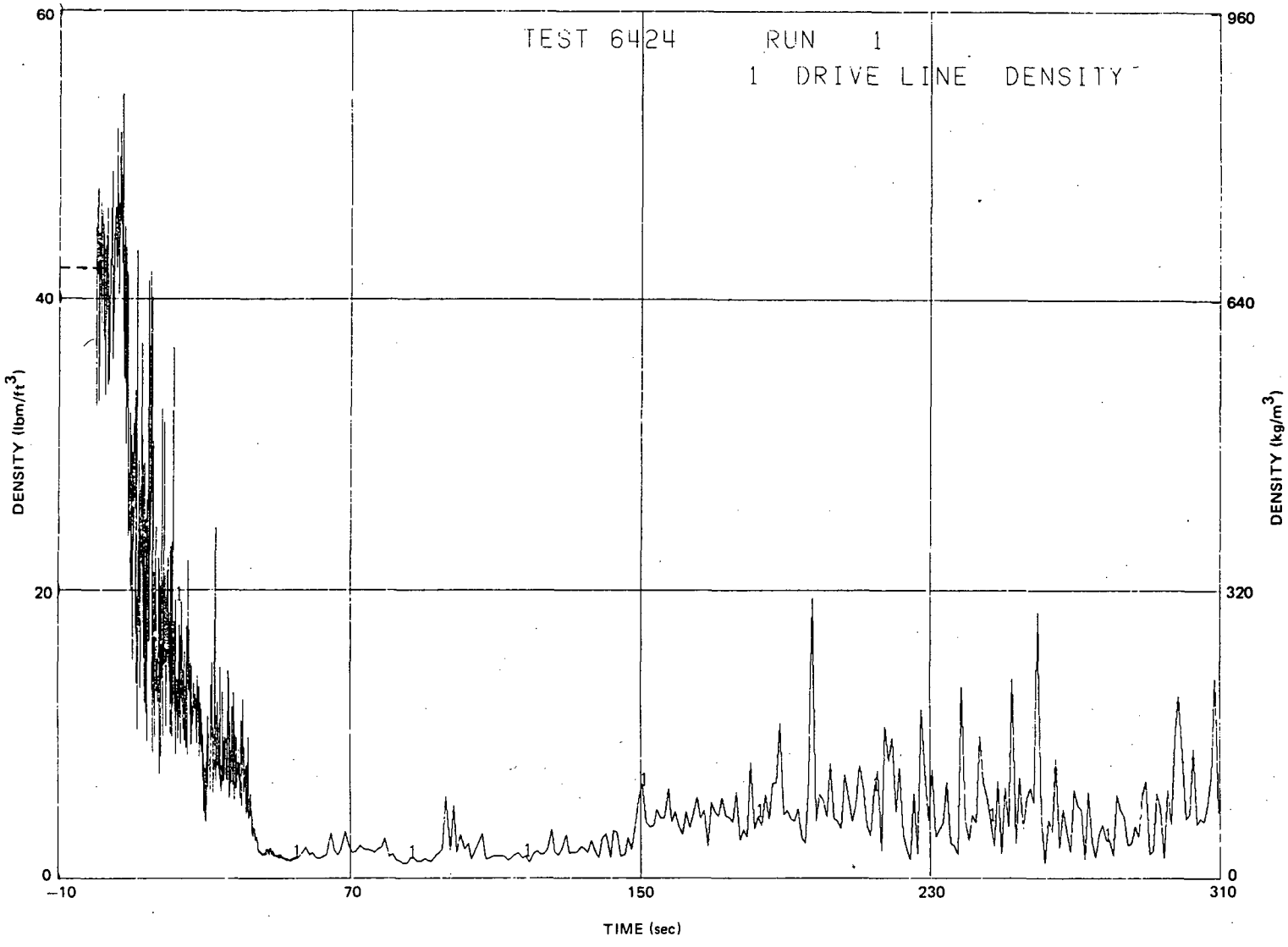

Figure K-56. Drive Line Break Density

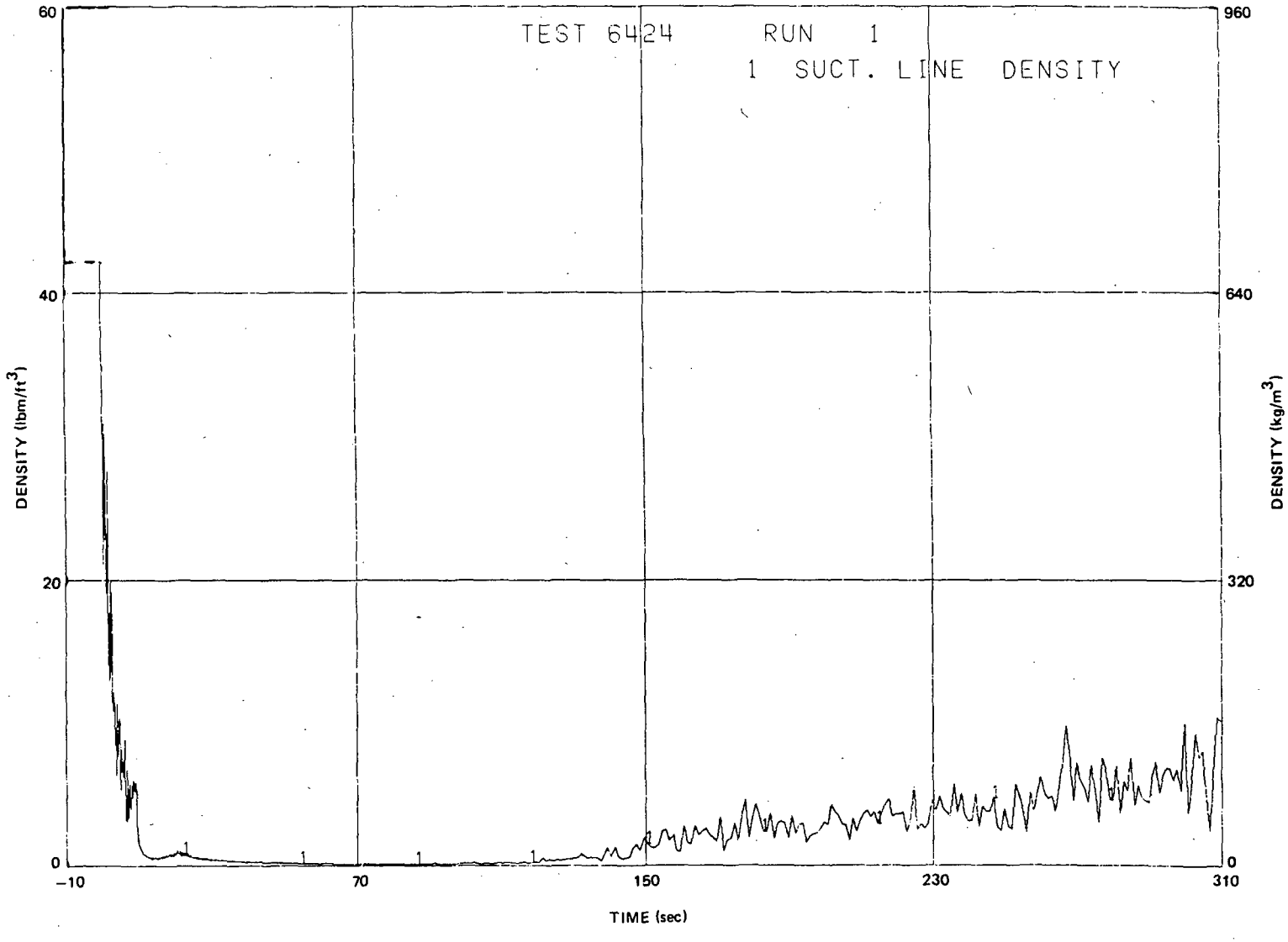

Figure K-57. Suction Line Break Density

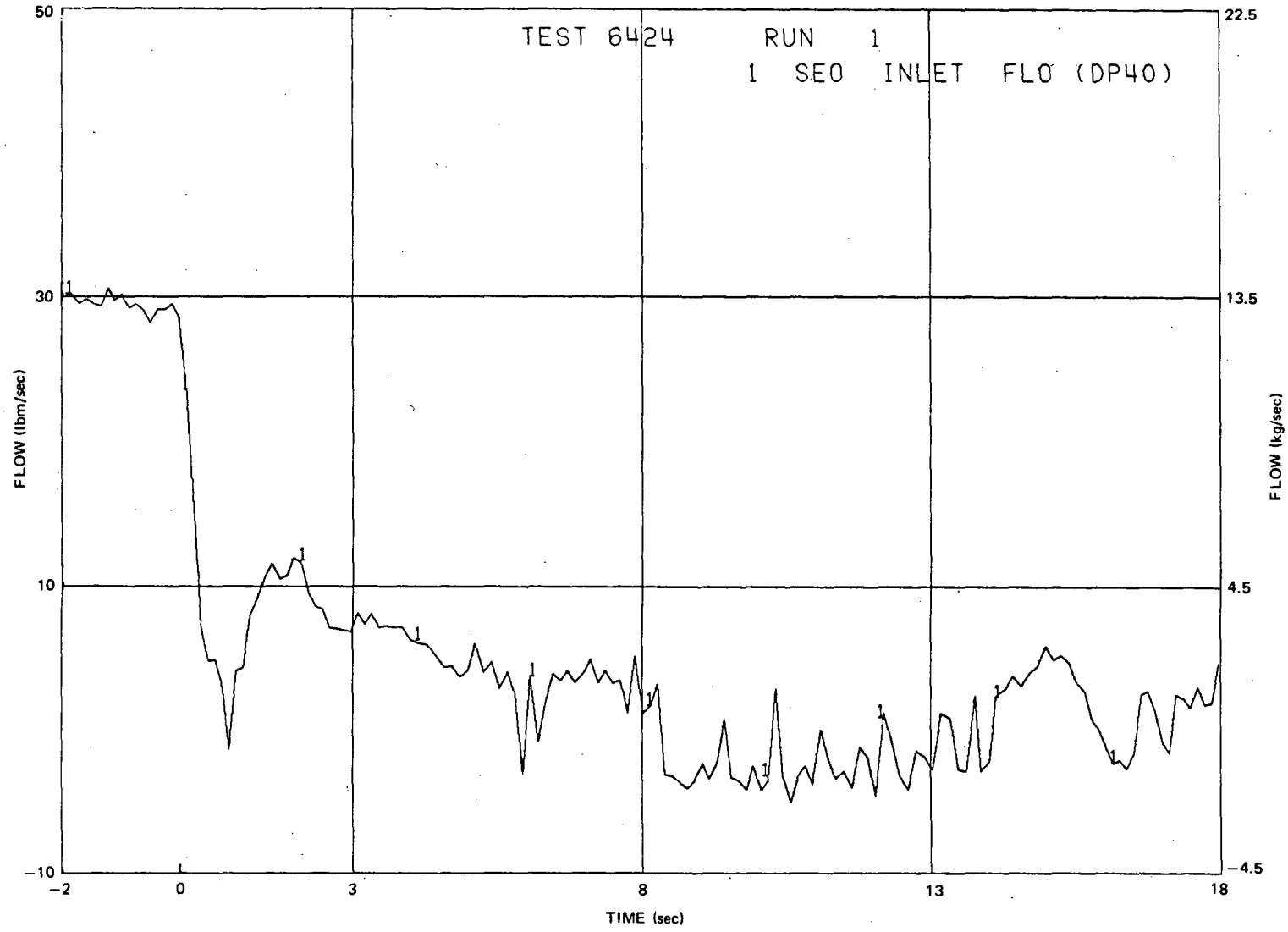

Figure K-58. Bundle Inlet Side Entry Orifice Mass Flow Rate

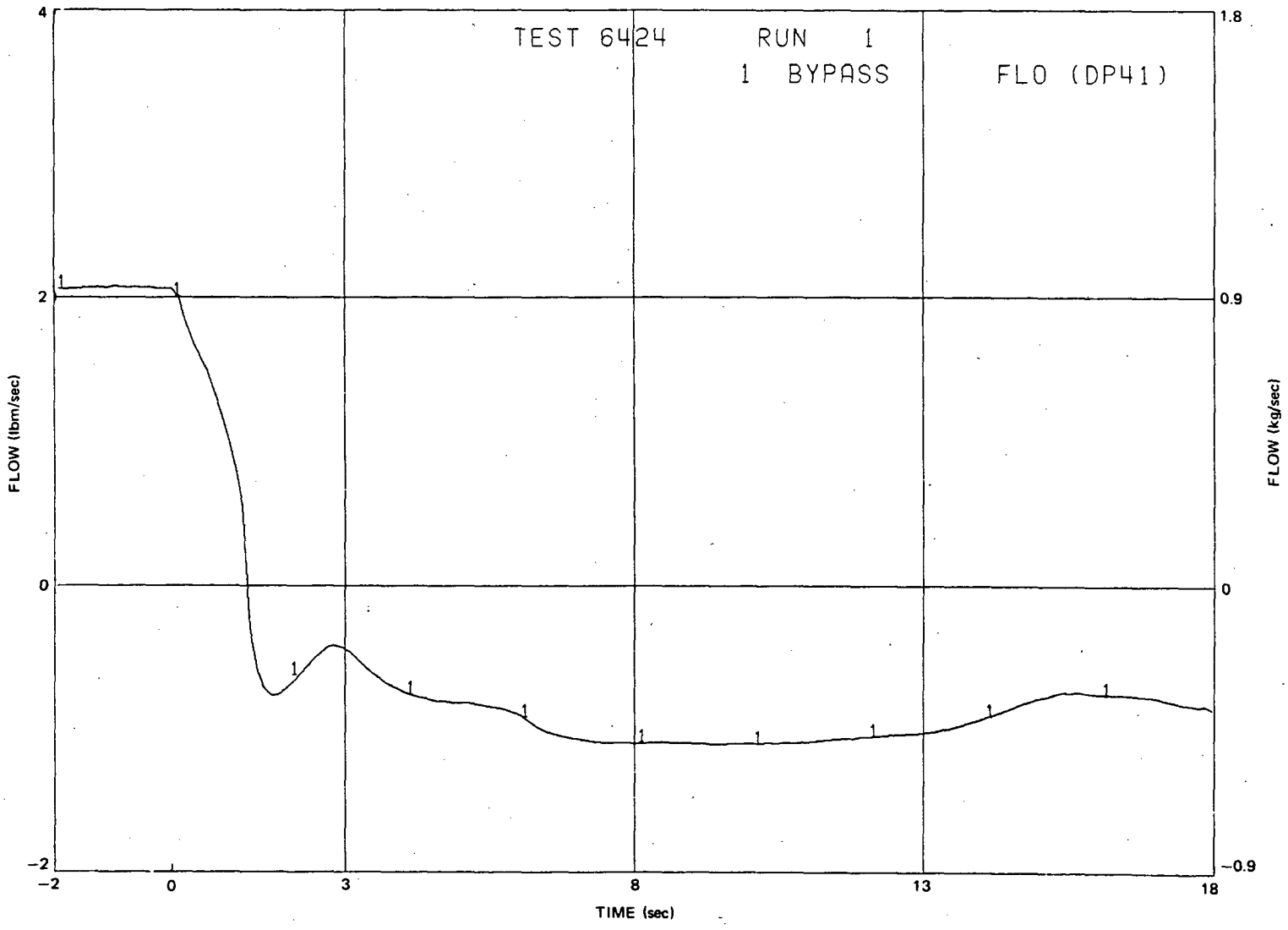

Figure K-59. Bypass Leakage Path Mass Flow Rate

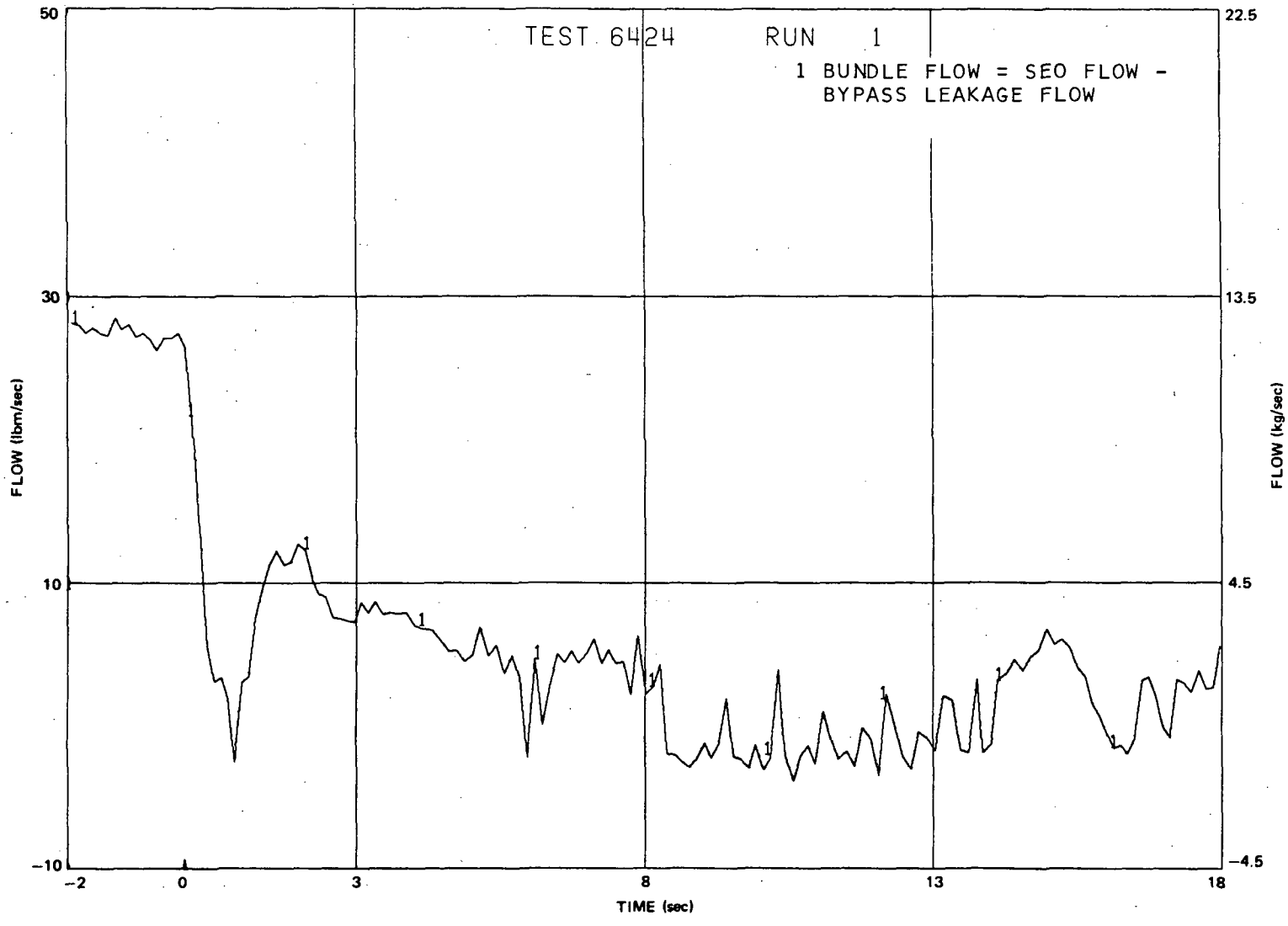

Figure K-60. Bundle Mass Flow Rate

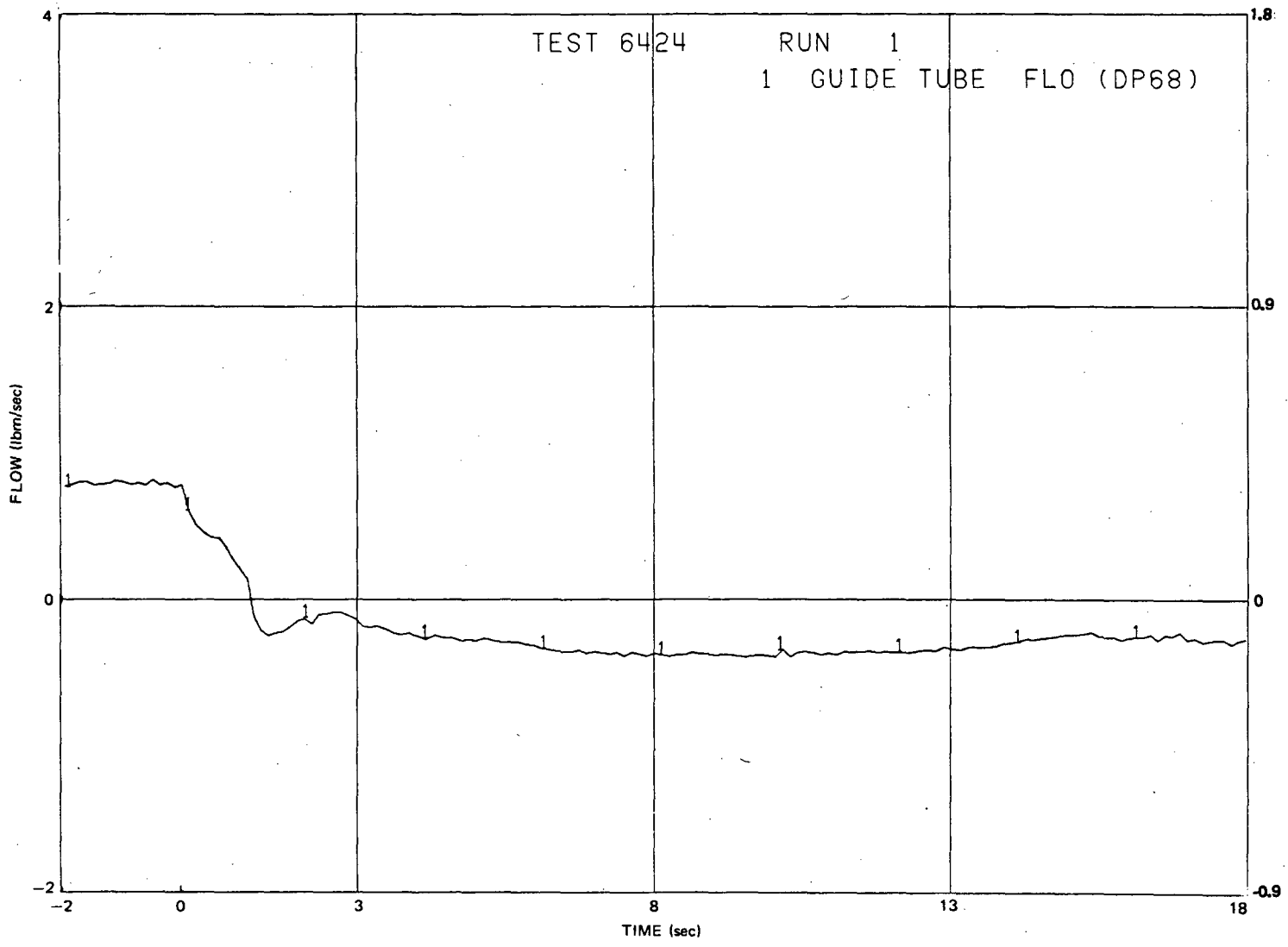

Figure K-61. Lower Plenum to Guide Tube Mass Flow Rate

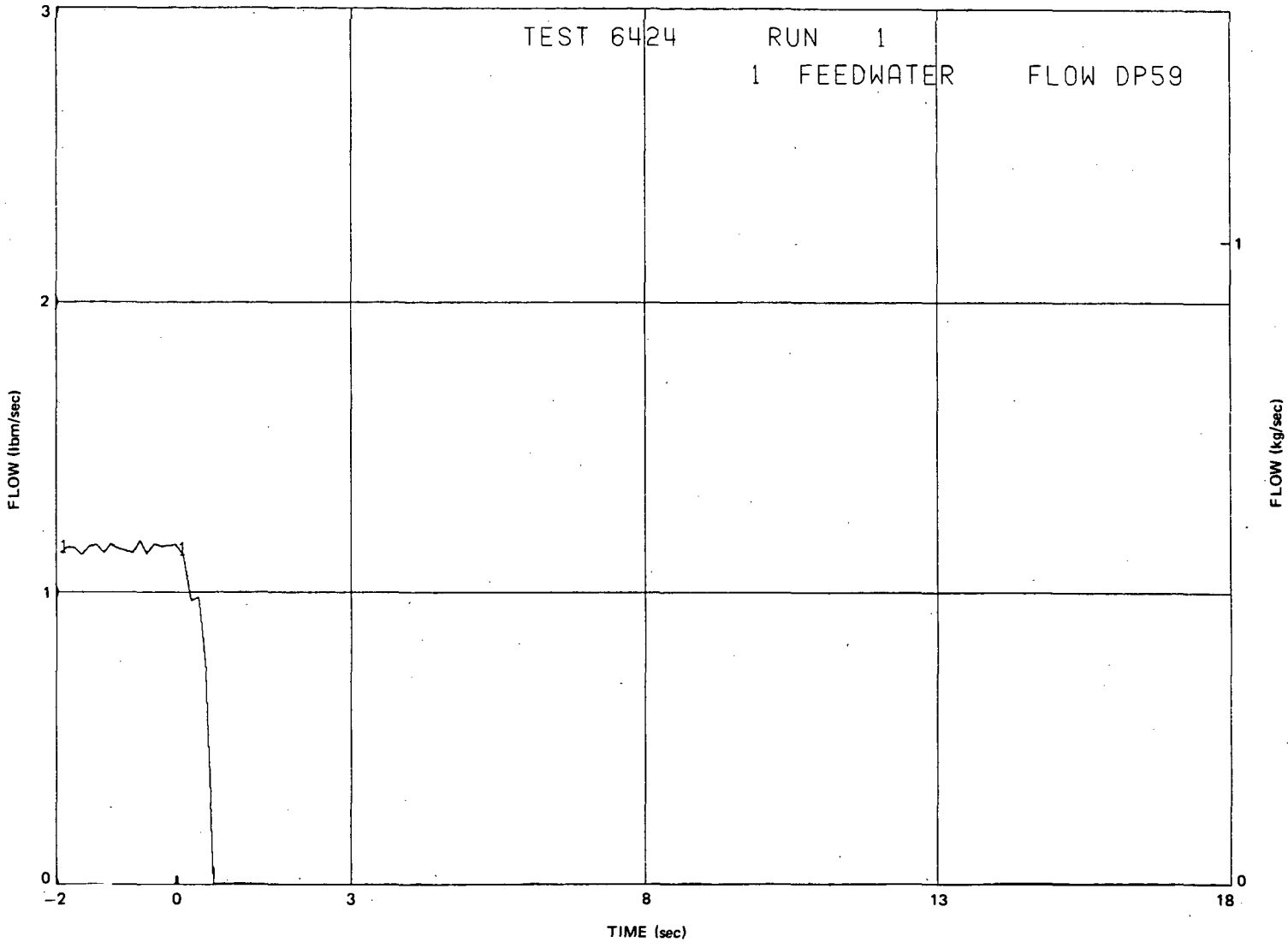

Figure K-62. Feedwater Mass Flow Rate

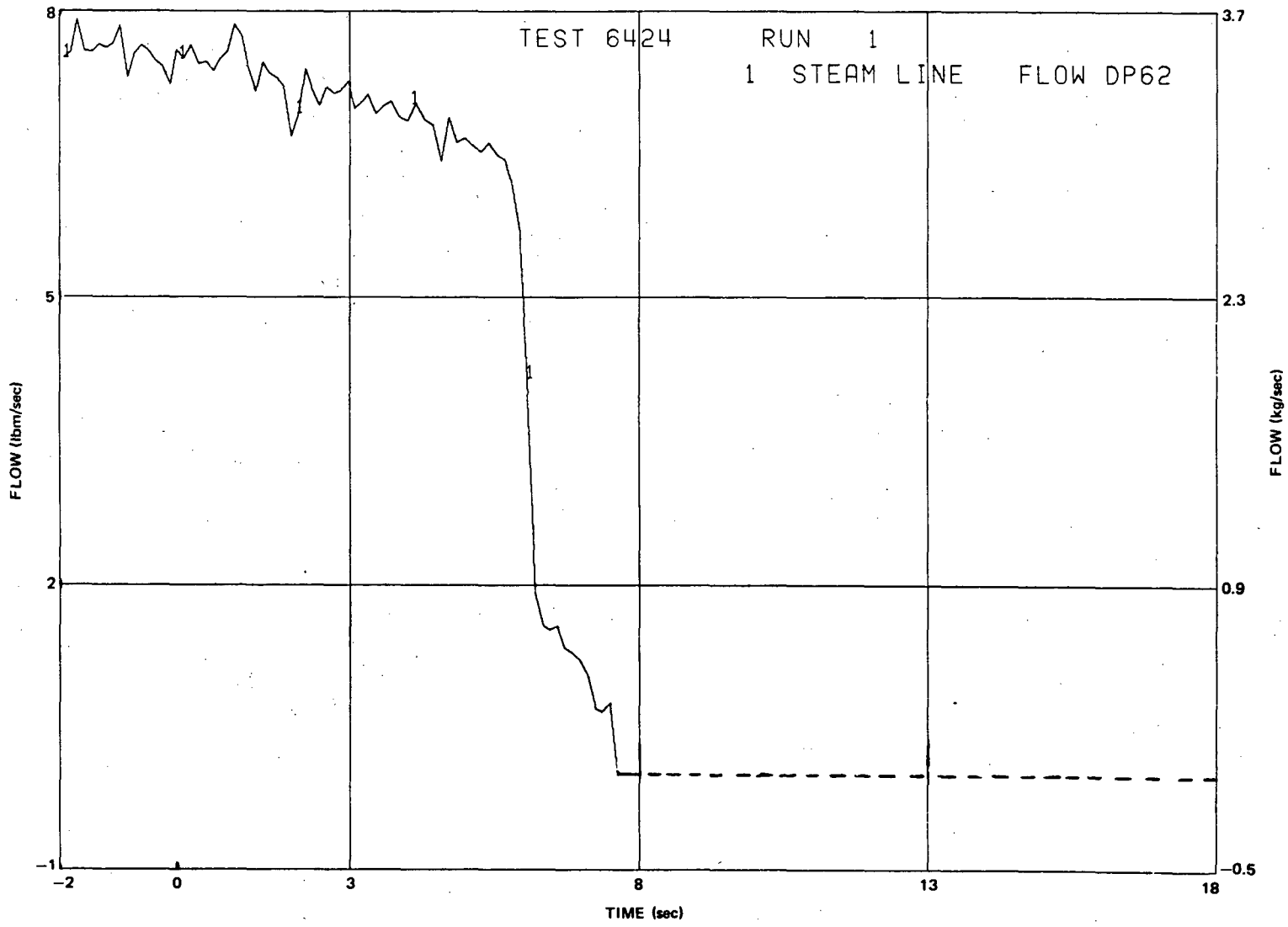

Figure K-63. Steamline Mass Flow Rate

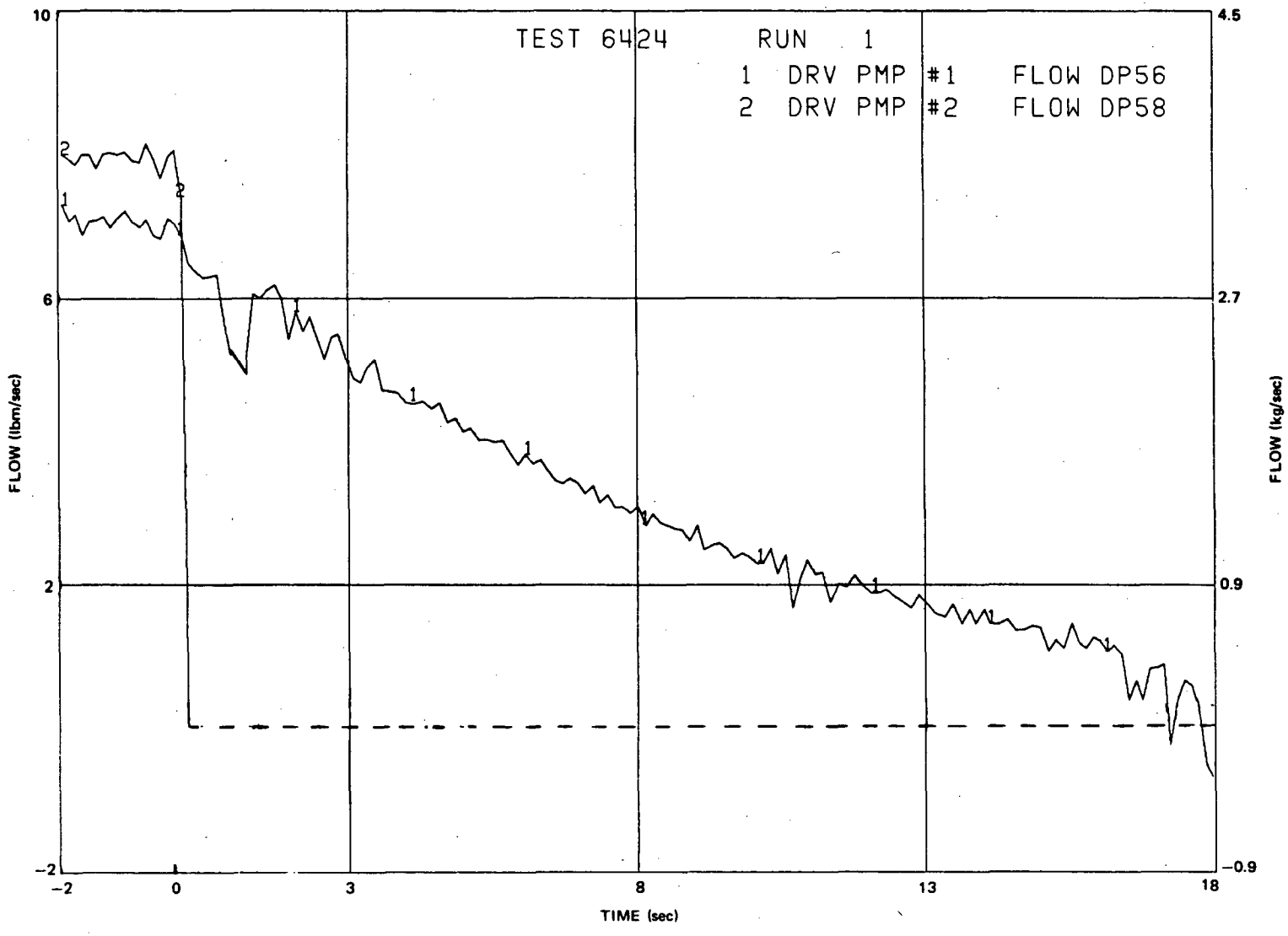

Figure K-64. Recirculation Pump Mass Flow Rates

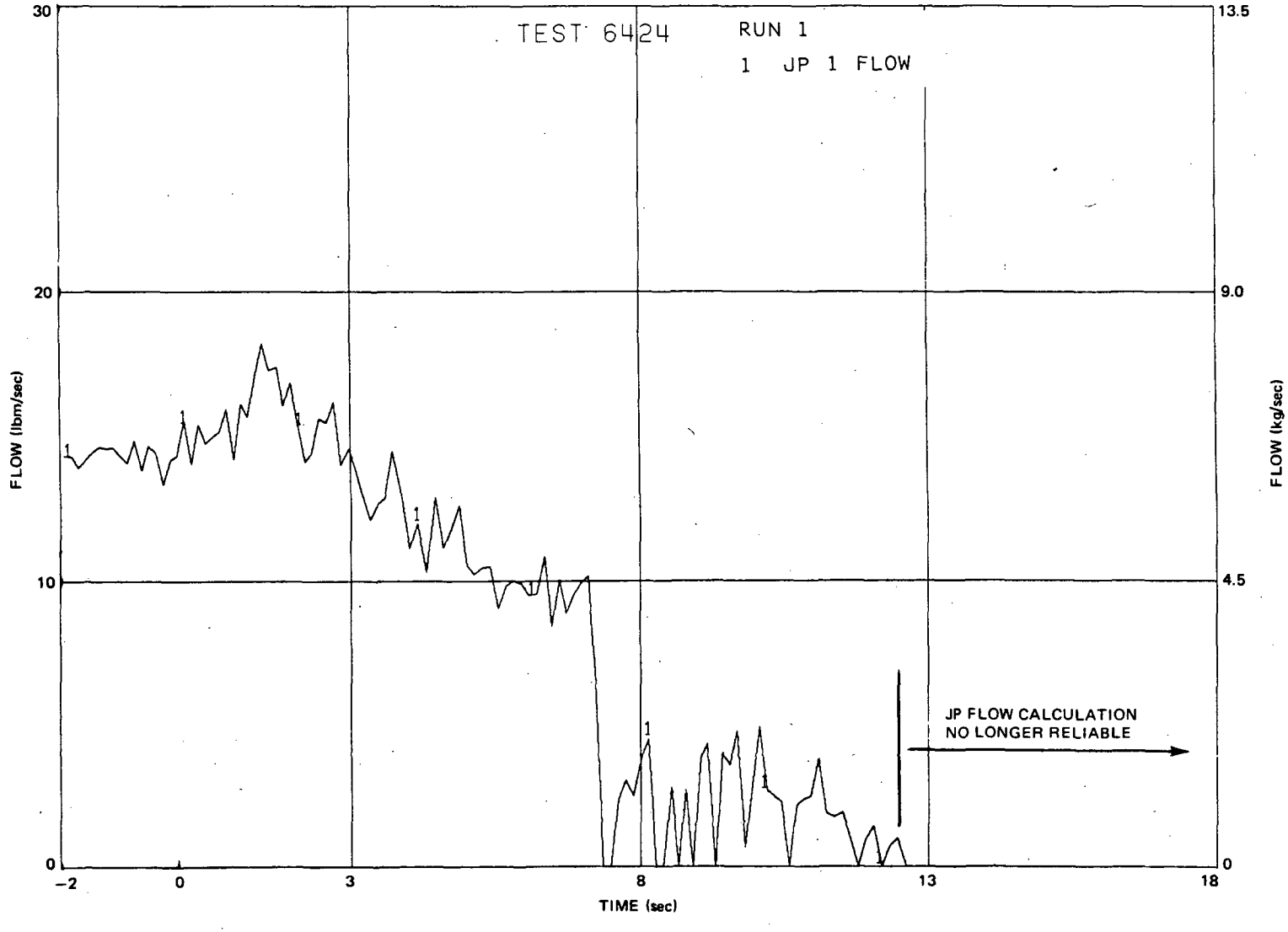

Figure K-65. Intact Loop Jet Pump Mass Flow Rate

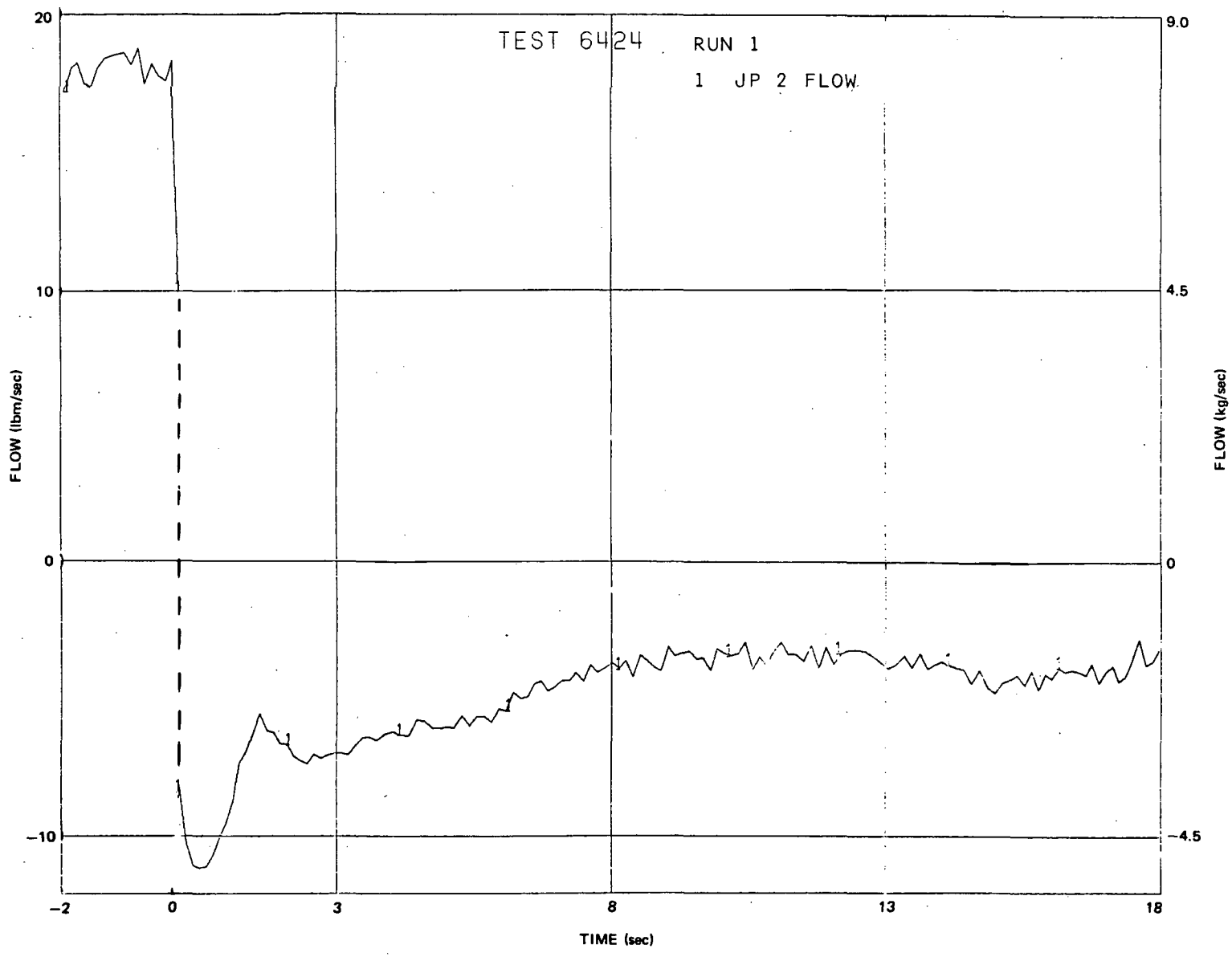

Figure K-66. Broken Loop Jet Pump Mass Flow Rate

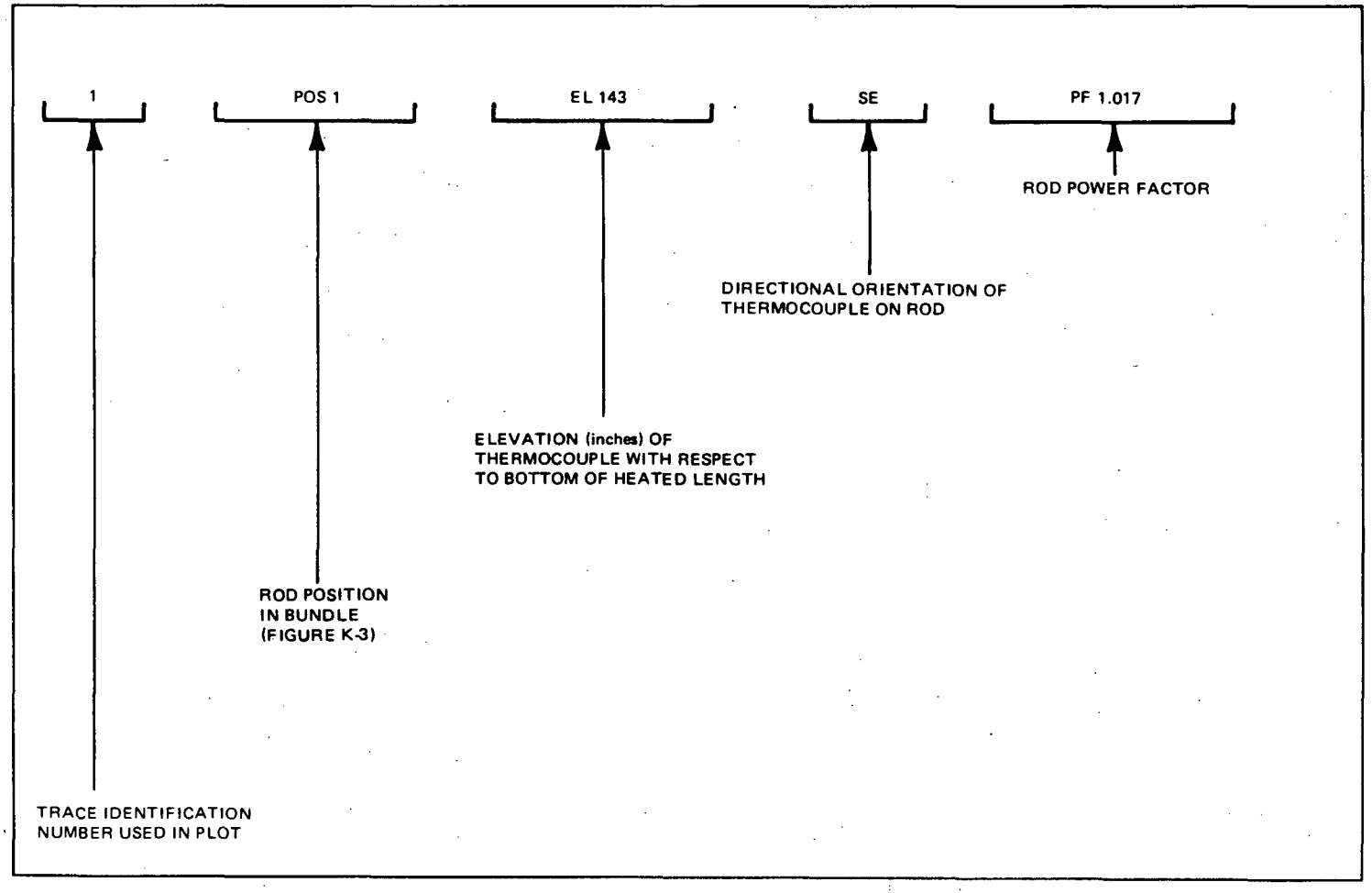

Figure K-67. Guide for Interpreting Legends on Bundle Temperature Plots

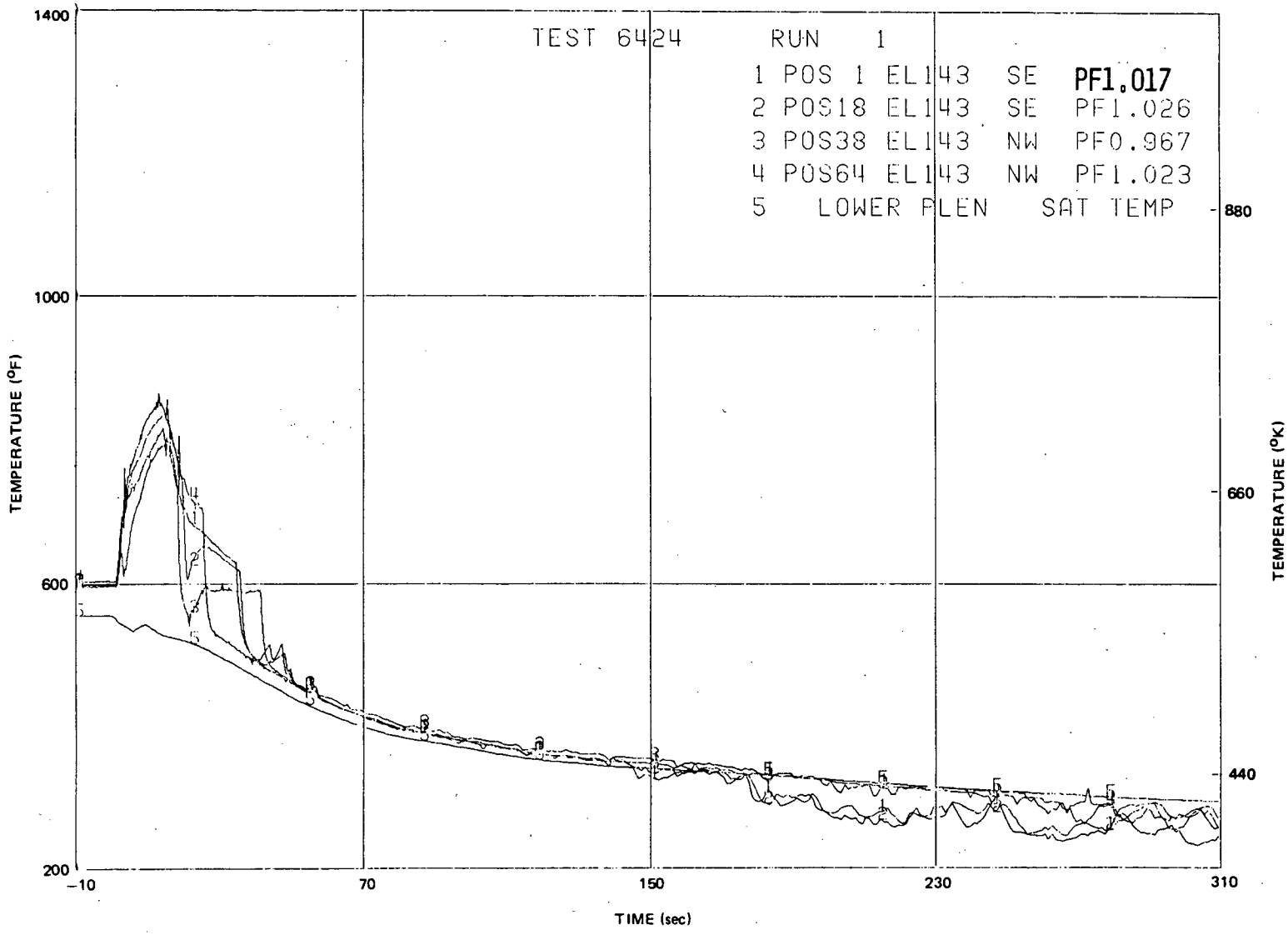

Figure K-68. Inside Clad Temperature-Elevation 143 in.

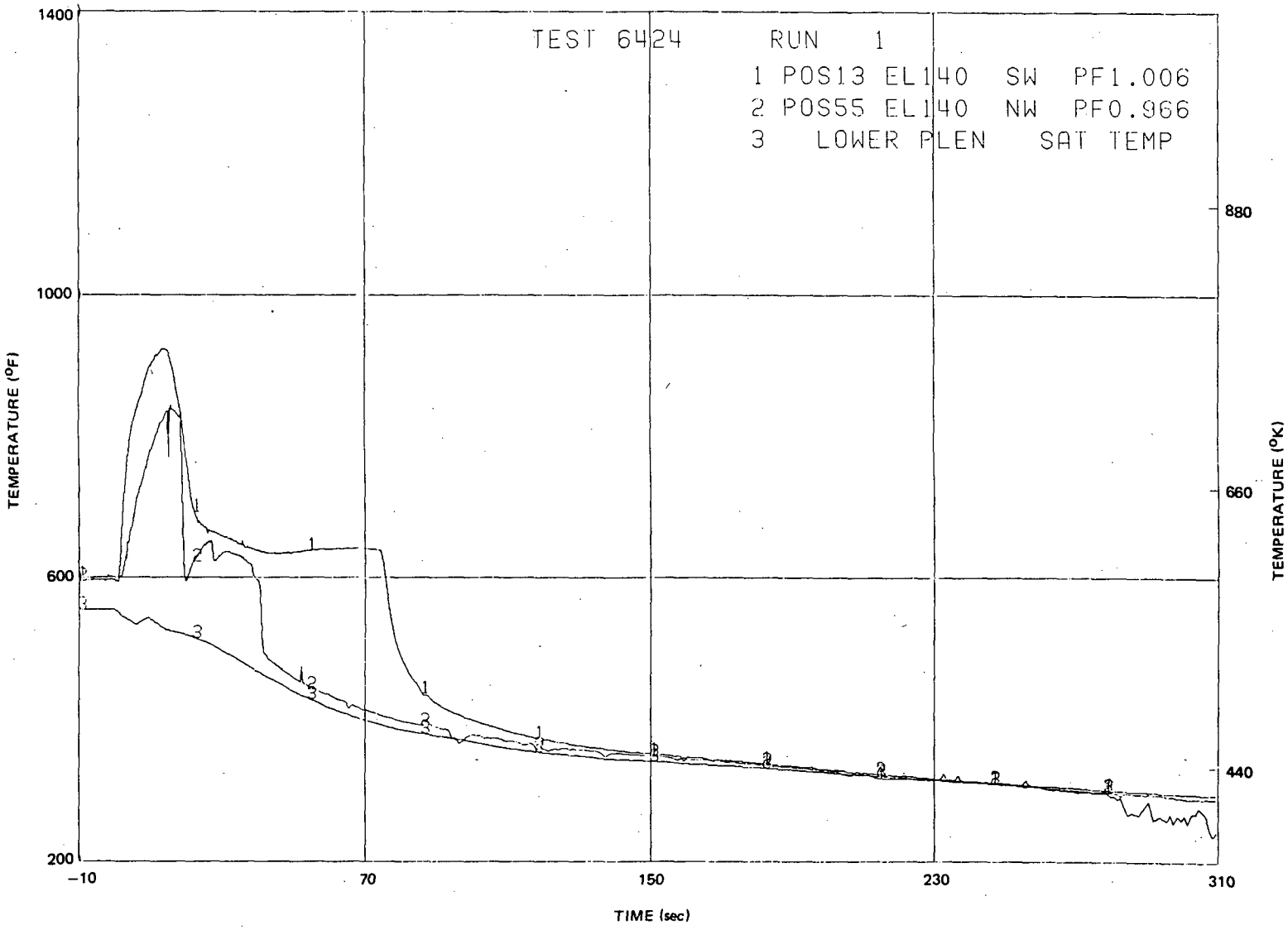

Figure K-69. Inside Clad Temperature-Elevation 140 in.

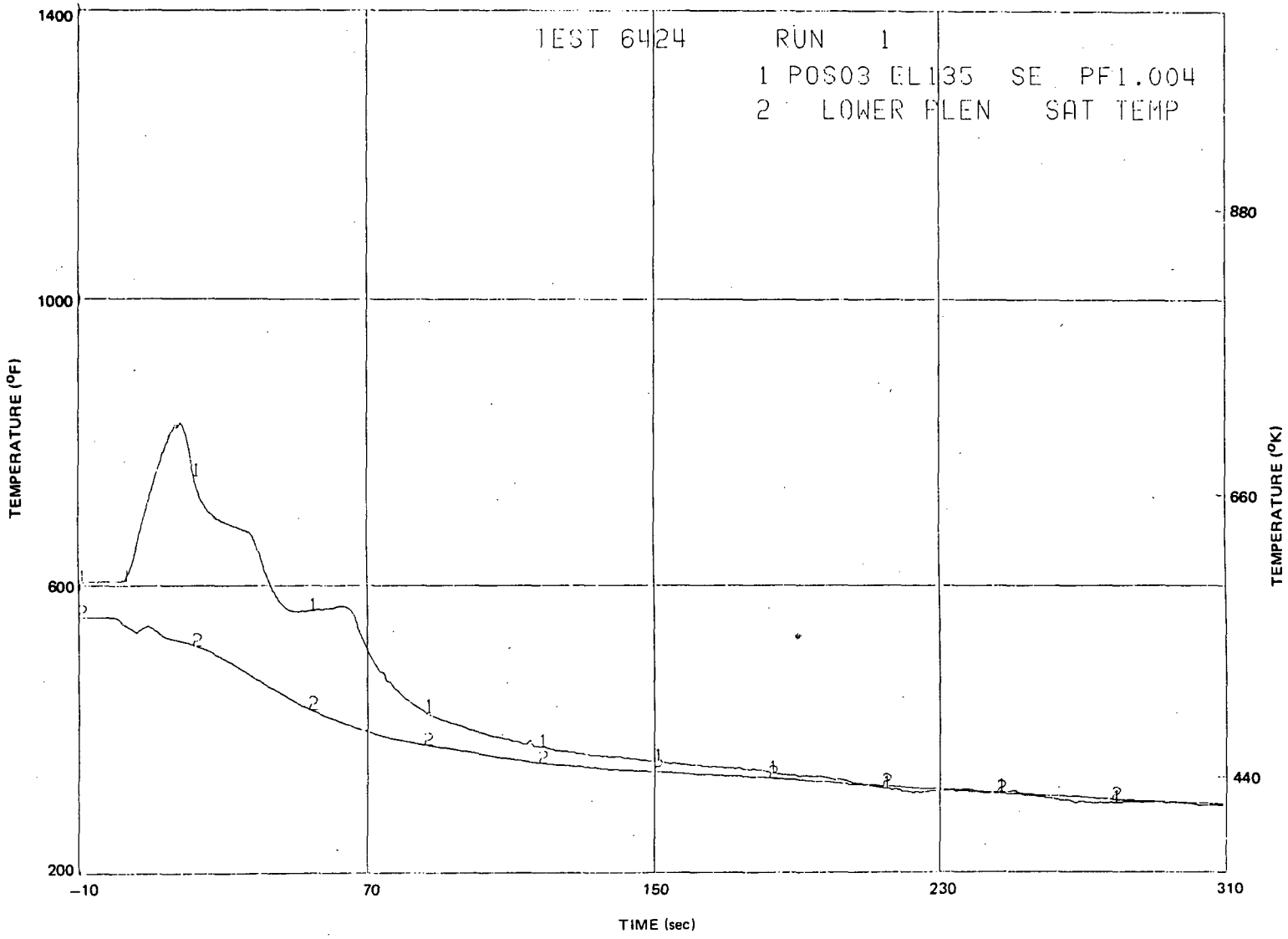

Figure K-70. Inside Clad Temperature-Elevation 135 in.

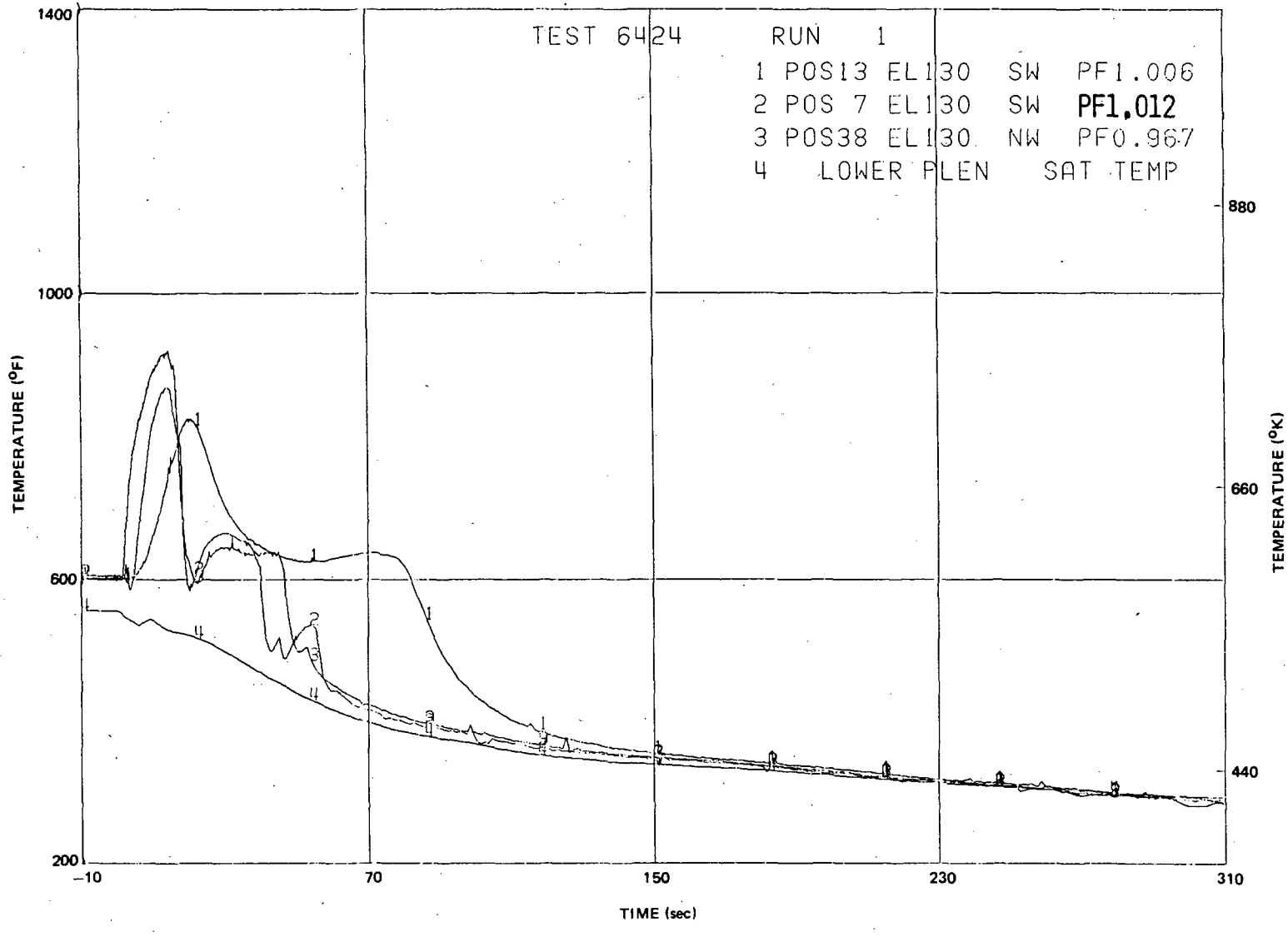

Figure K-71. Inside Clad Temperature-Elevation 130 in.

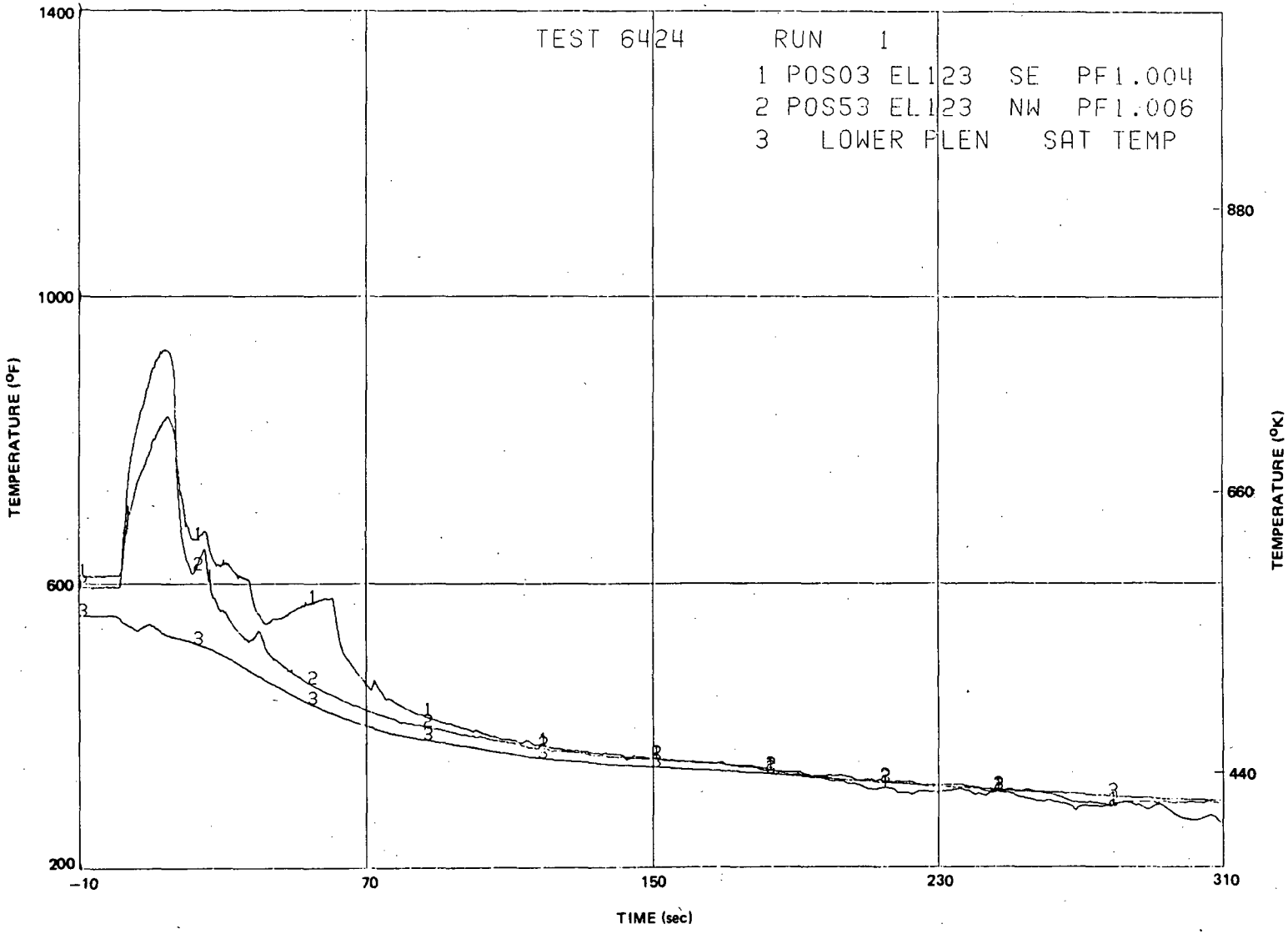

Figure K-72. Inside Clad Temperature-Elevation 123 in.

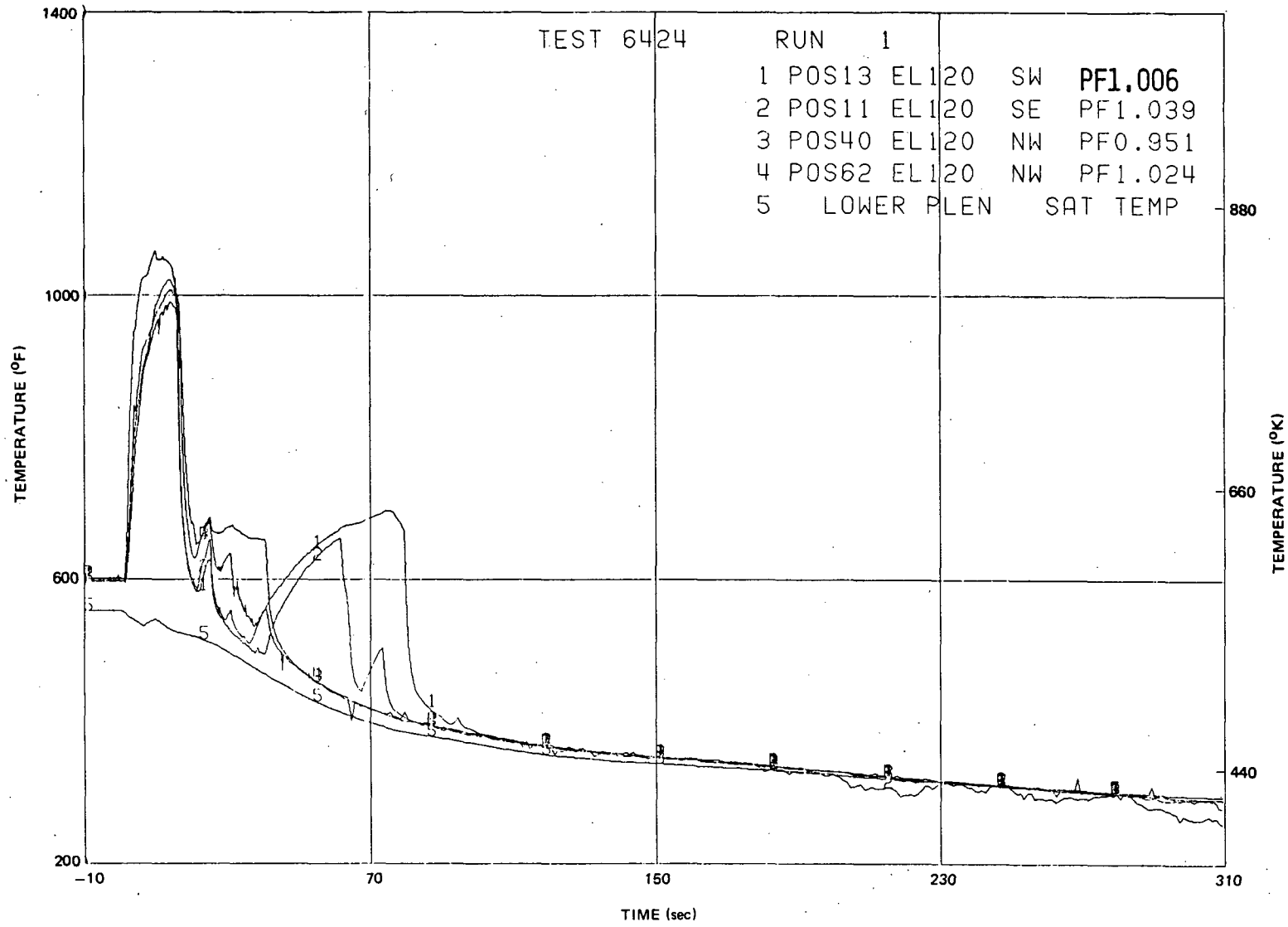

Figure K-73. Inside Clad Temperature-Elevation 120 in.

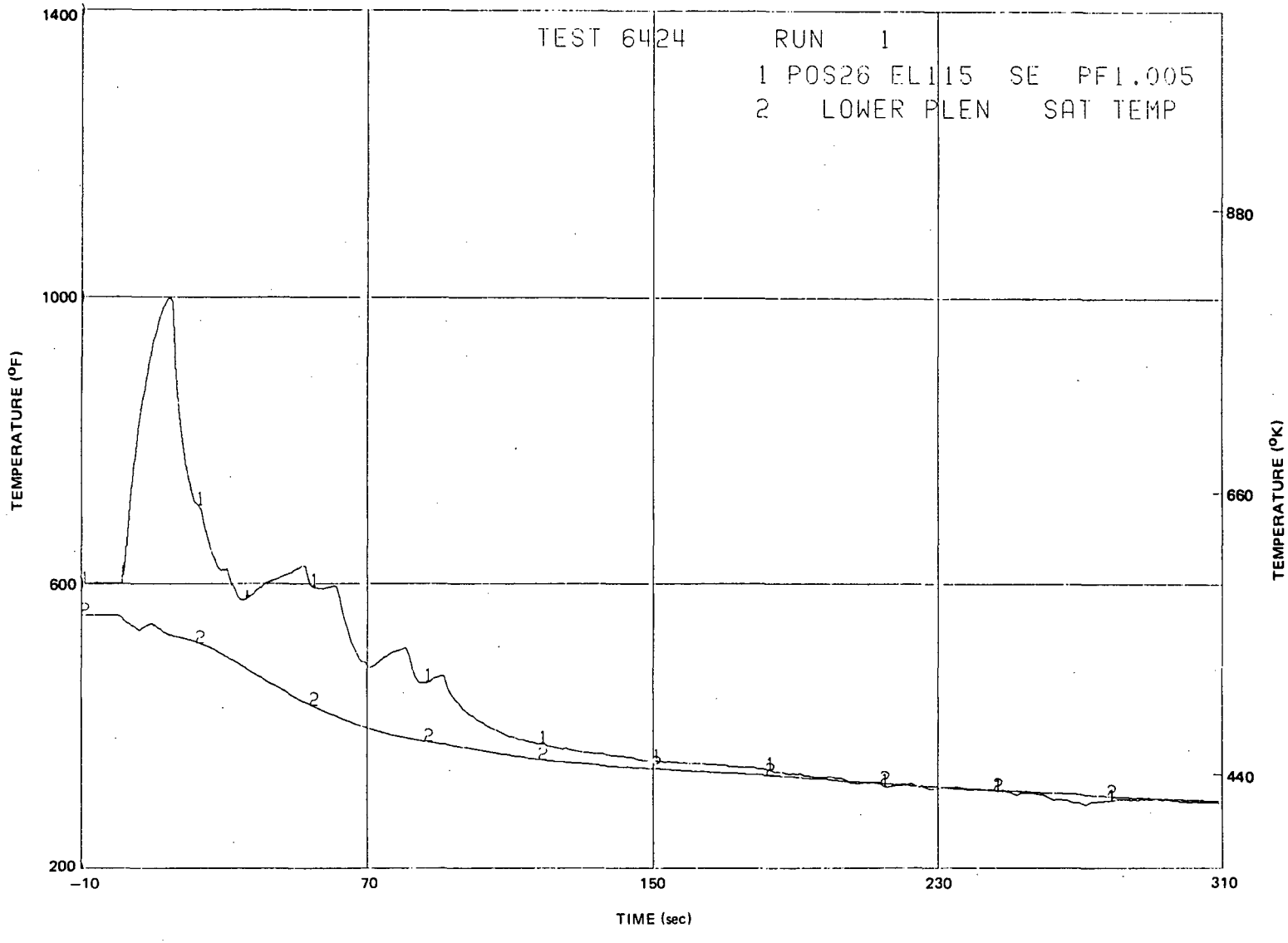

Figure K-74. Inside Clad Temperature-Elevation 115 in.

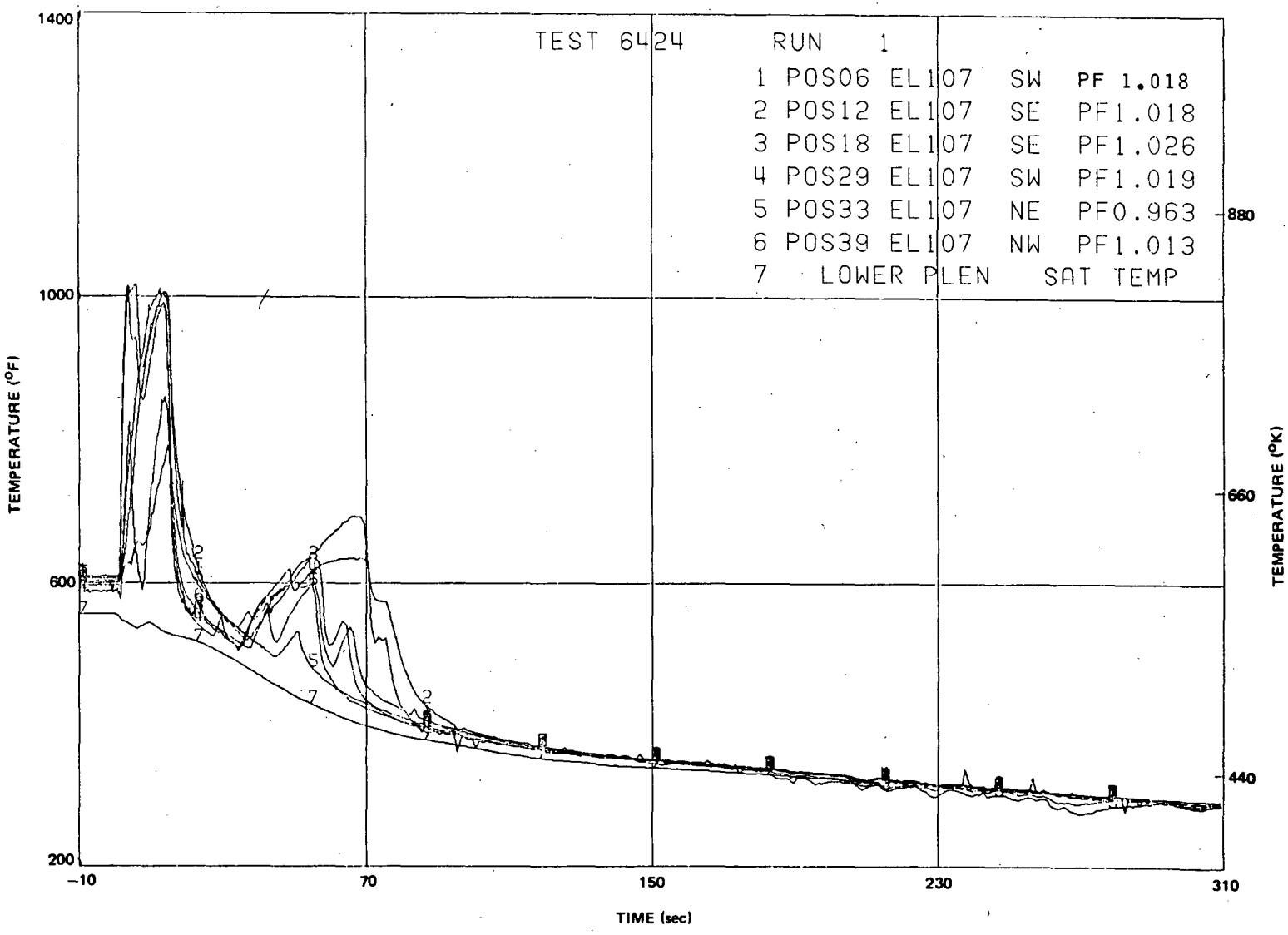

Figure K-75. Inside Clad Temperature-Elevation 107 in.

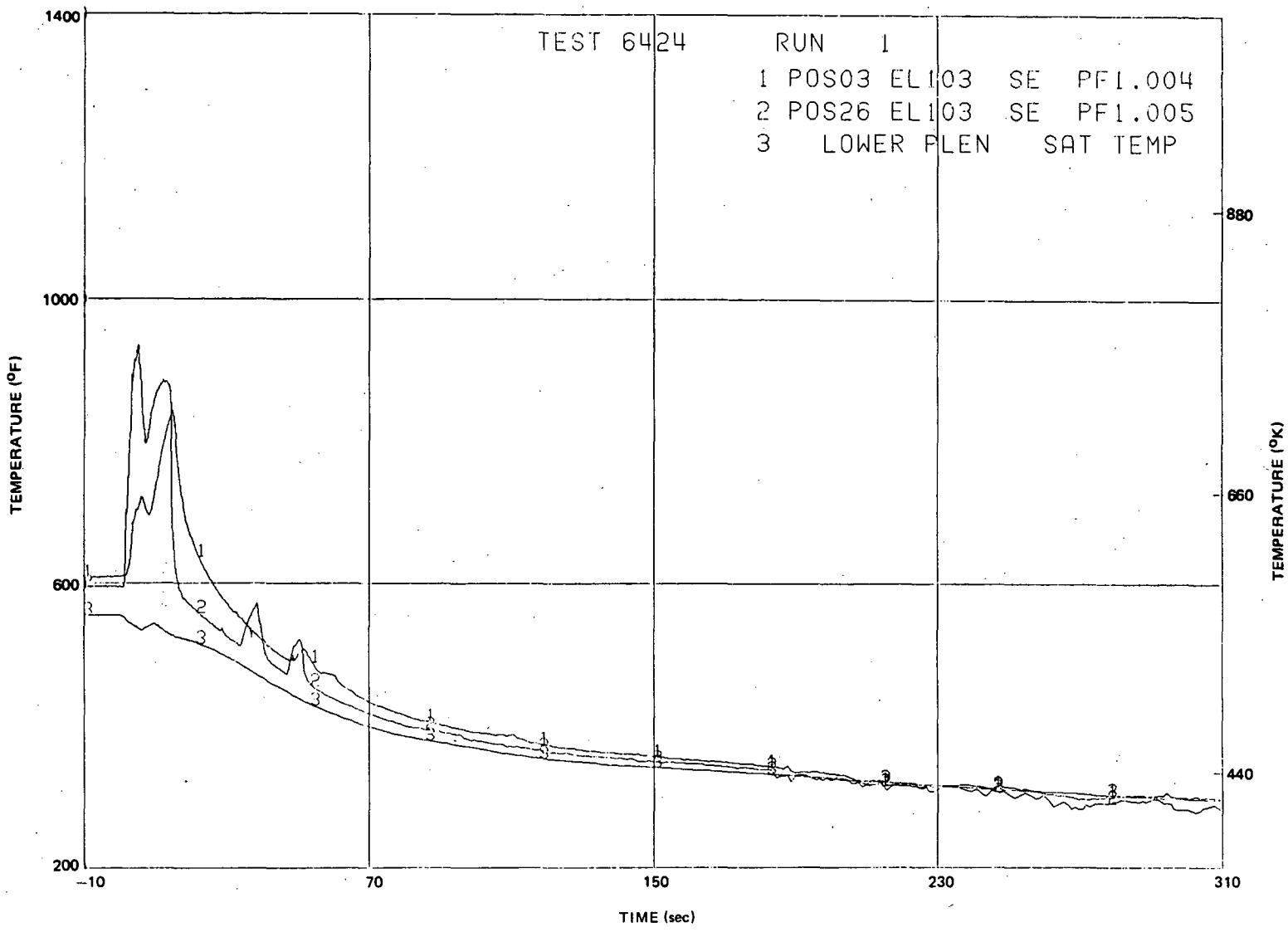

Figure K-76. Inside Clad Temperature-Elevation 103 in.

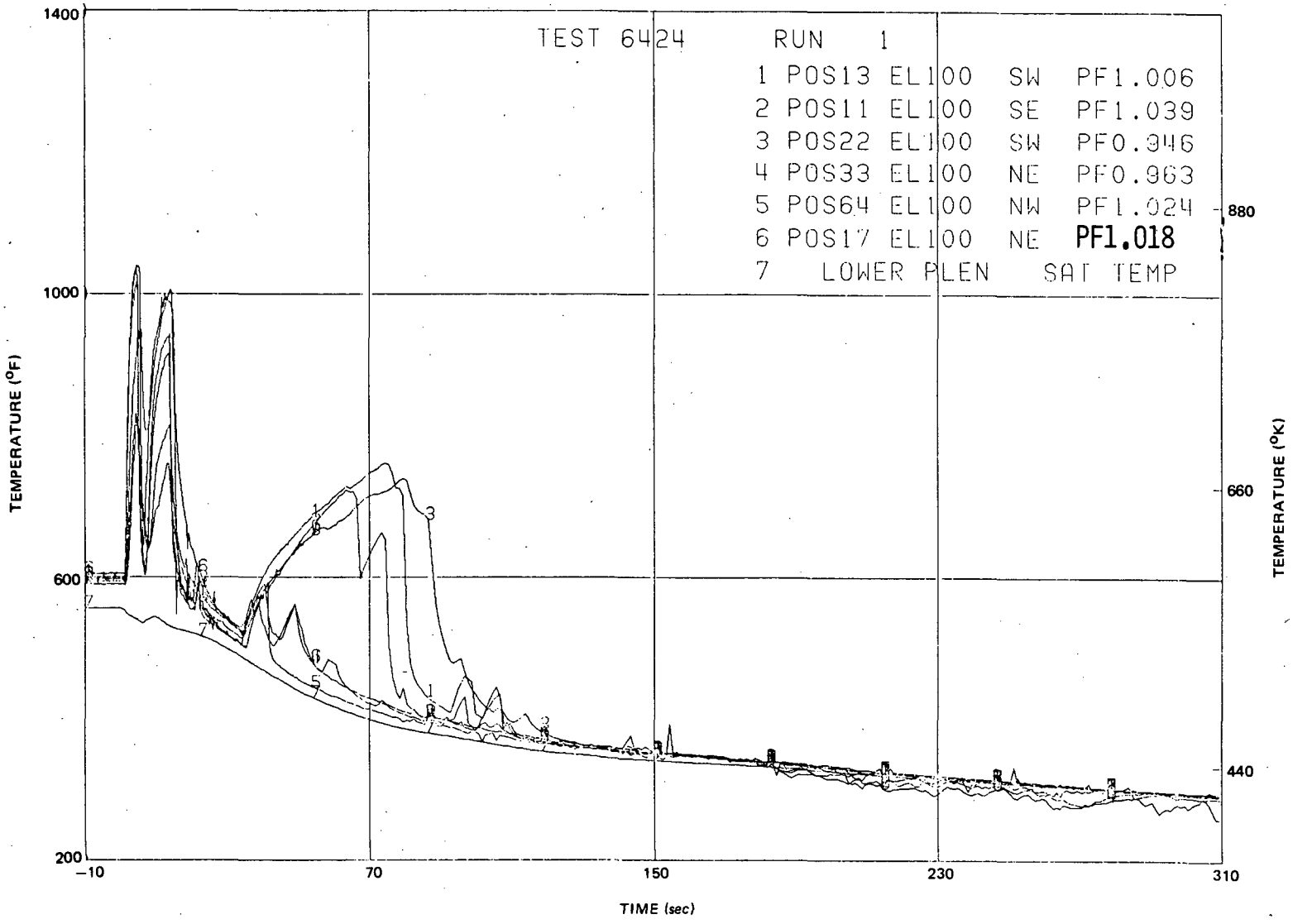

Figure K-77. Inside Clad Temperature-Elevation 100 in.

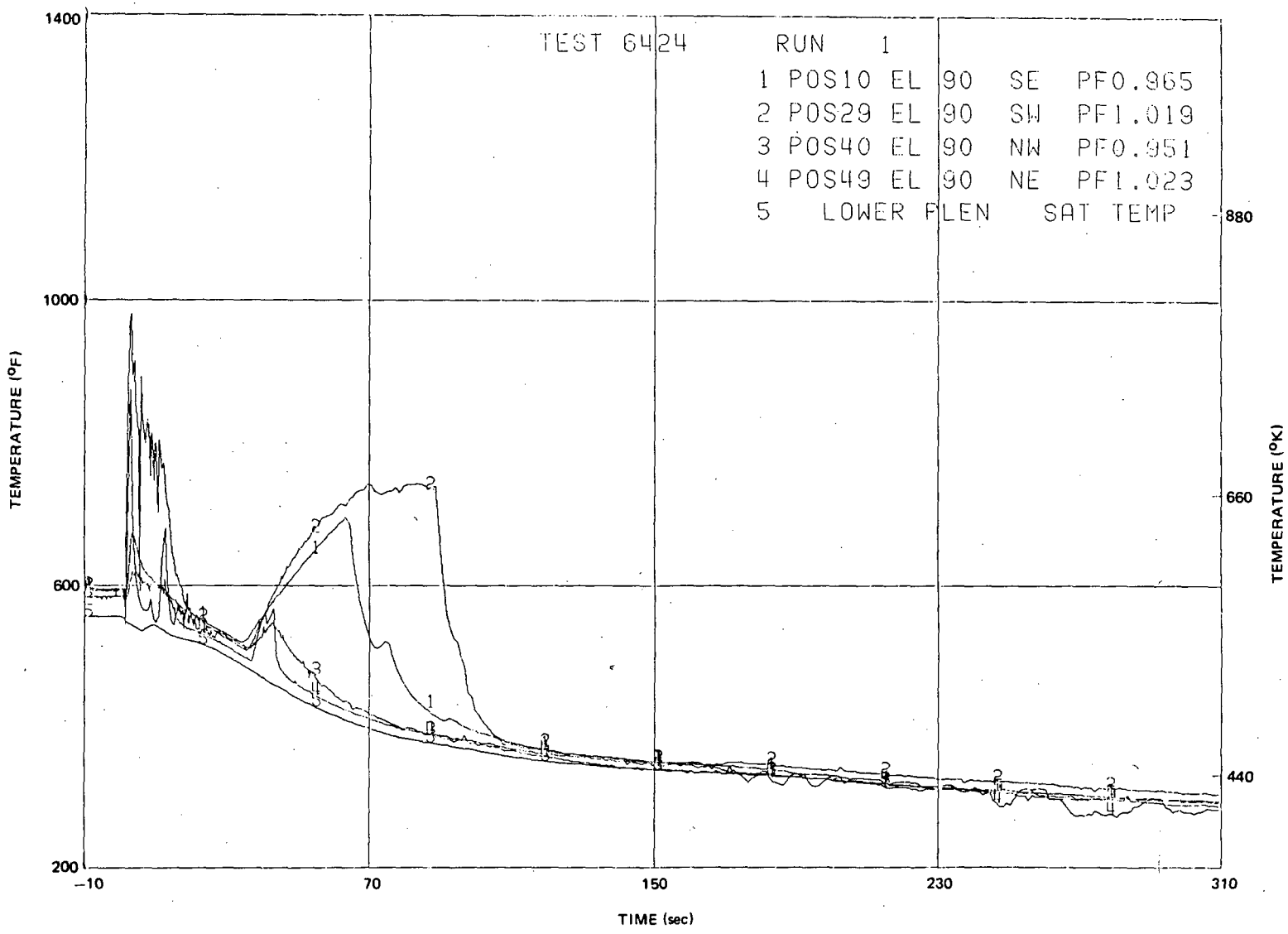

Figure K-78. Inside Clad Temperature-Elevation 90 in.

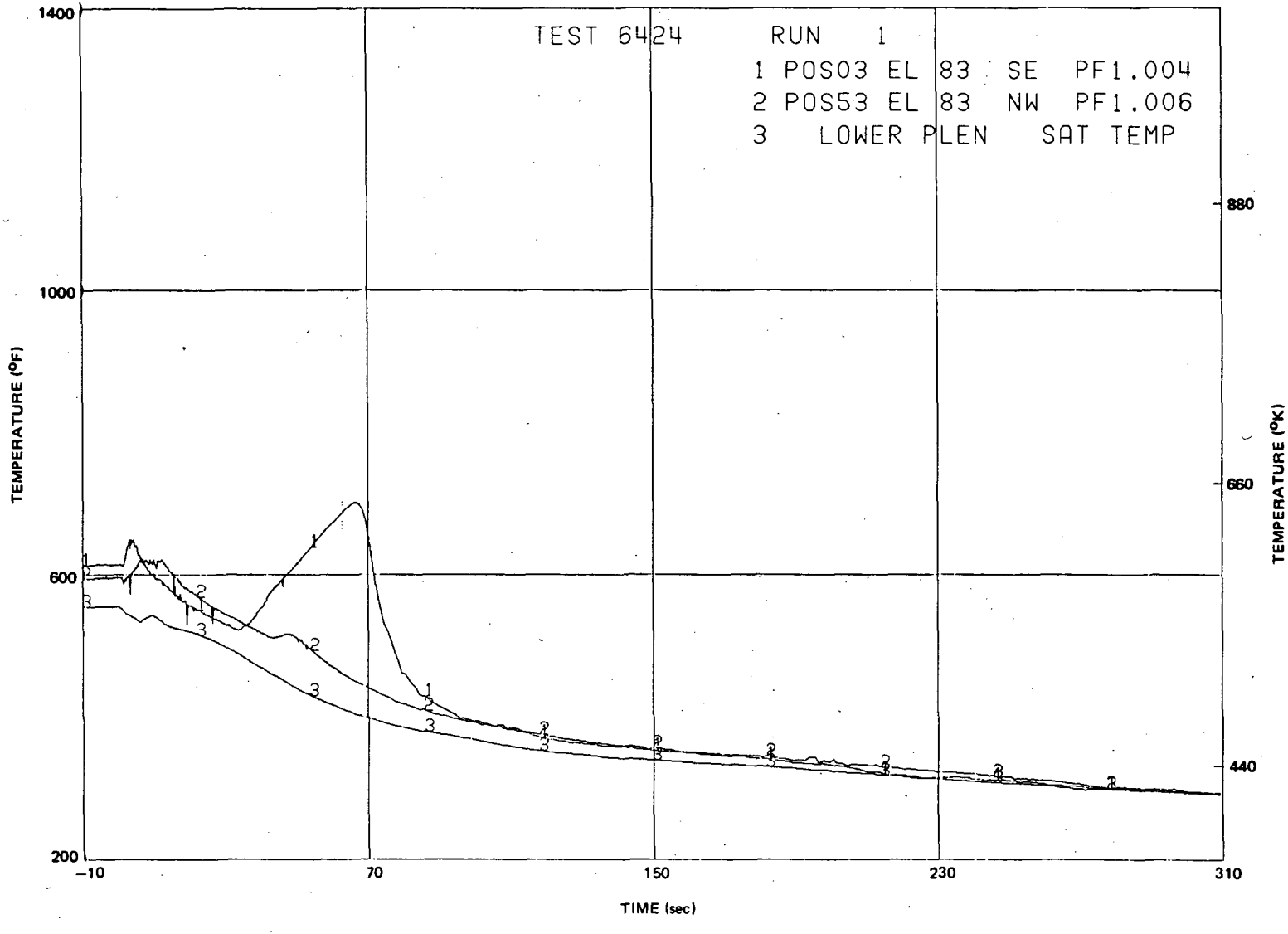

Figure K-79. Inside Clad Temperature-Elevation 83 in.

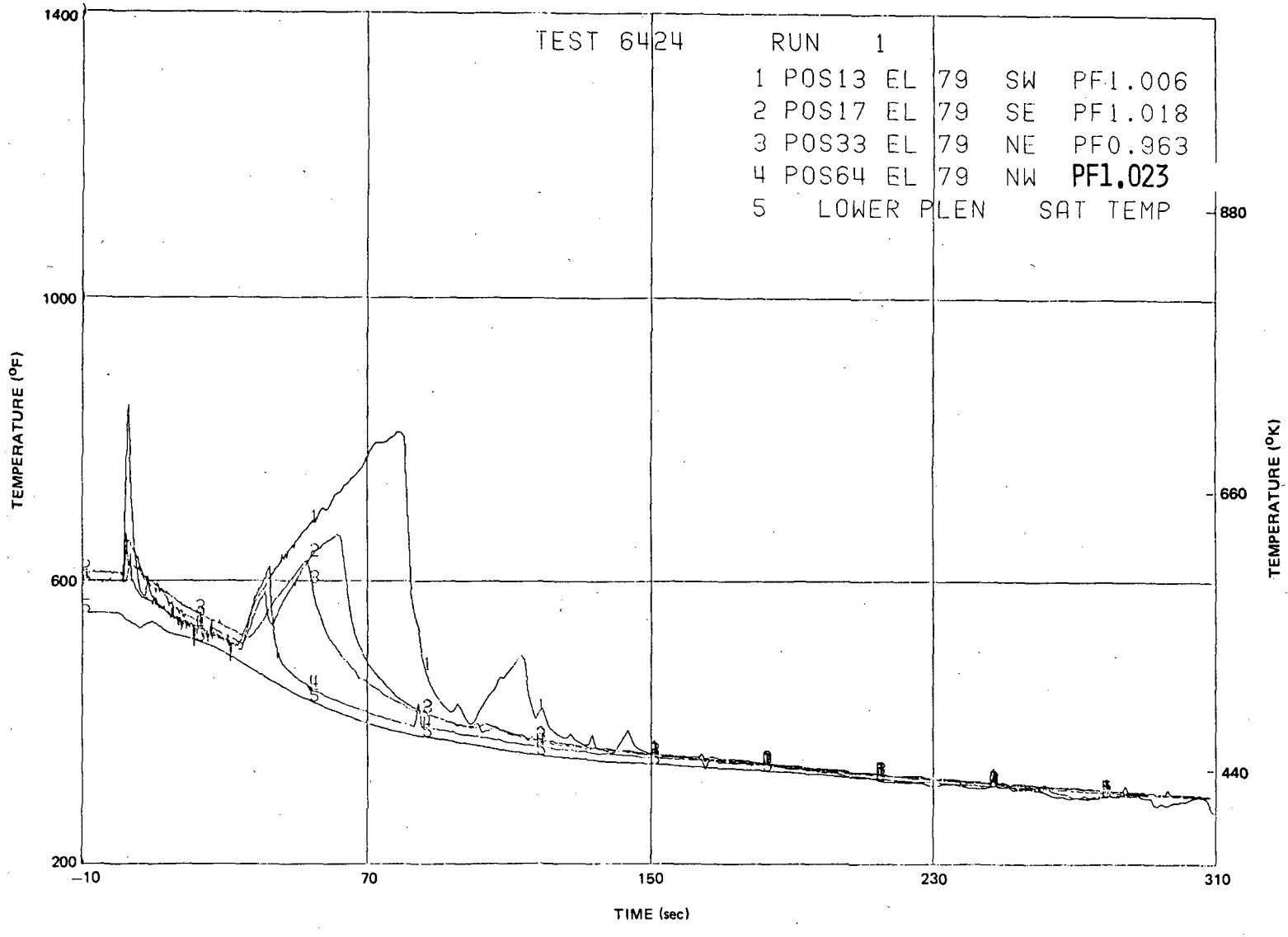

Figure K-80. Inside Clad Temperature-Elevation 79 in.

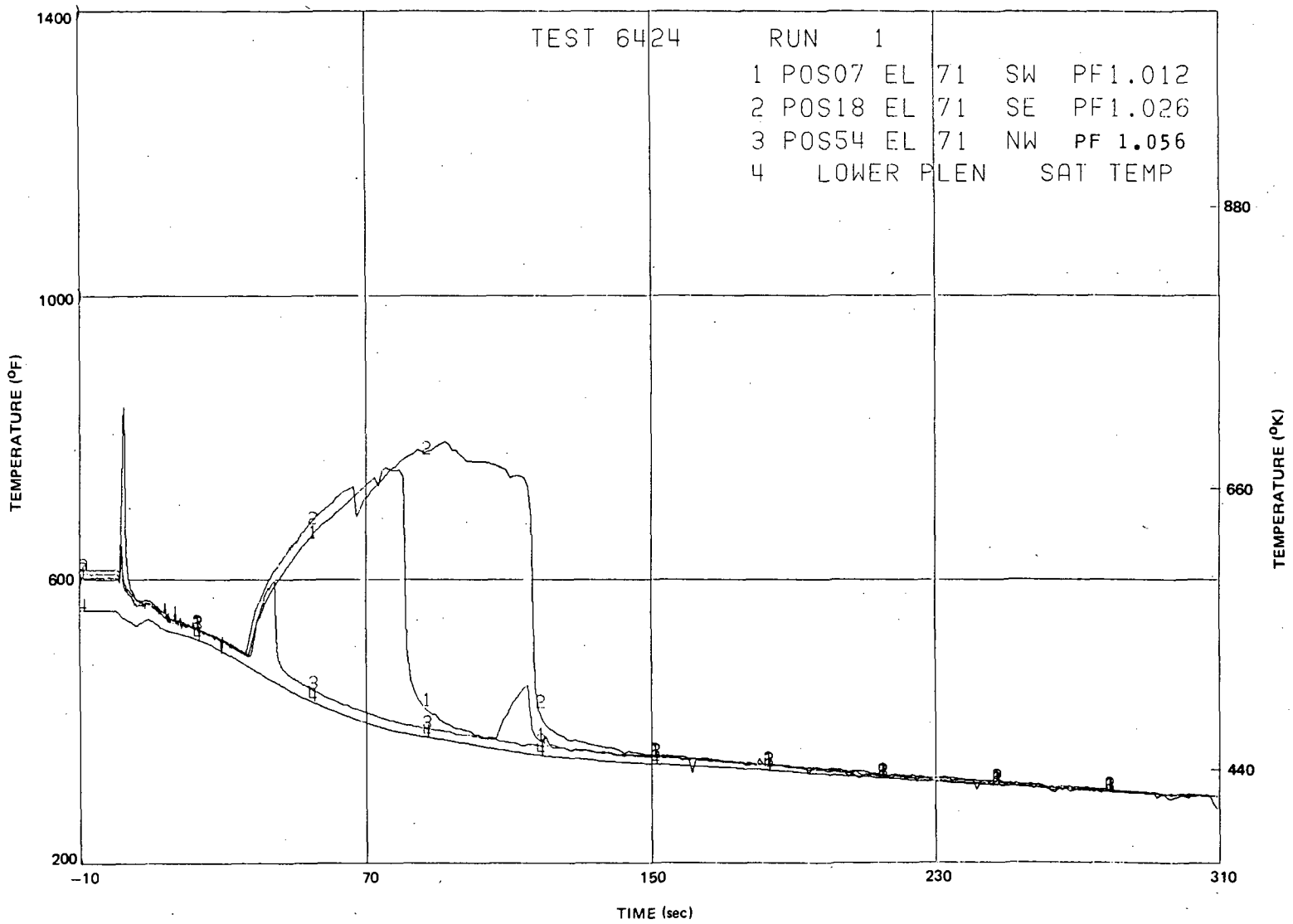

Figure K-81. Inside Clad Temperature-Elevation 71 in.

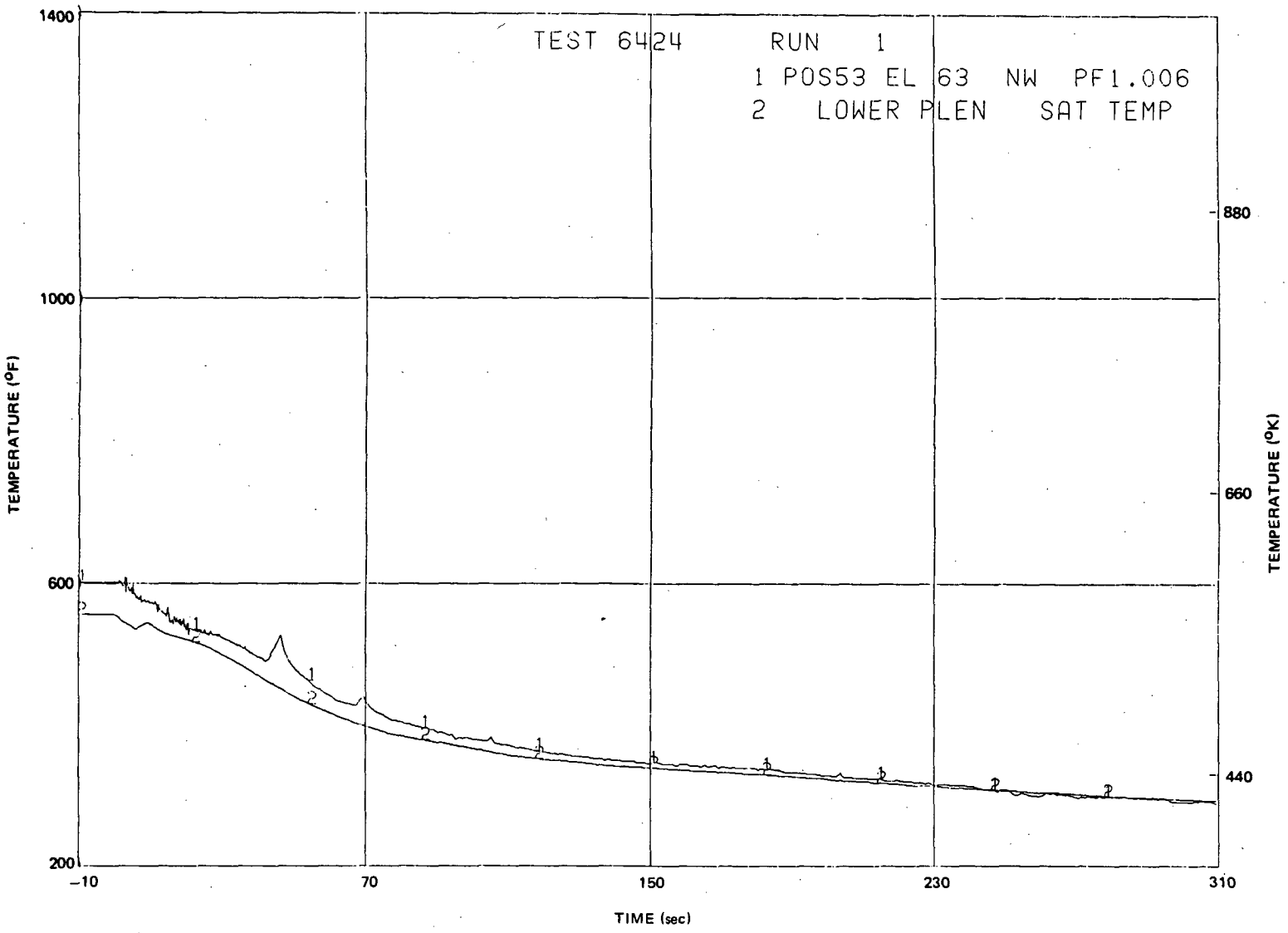

Figure K-82. Inside Clad Temperature-Elevation 63 in.

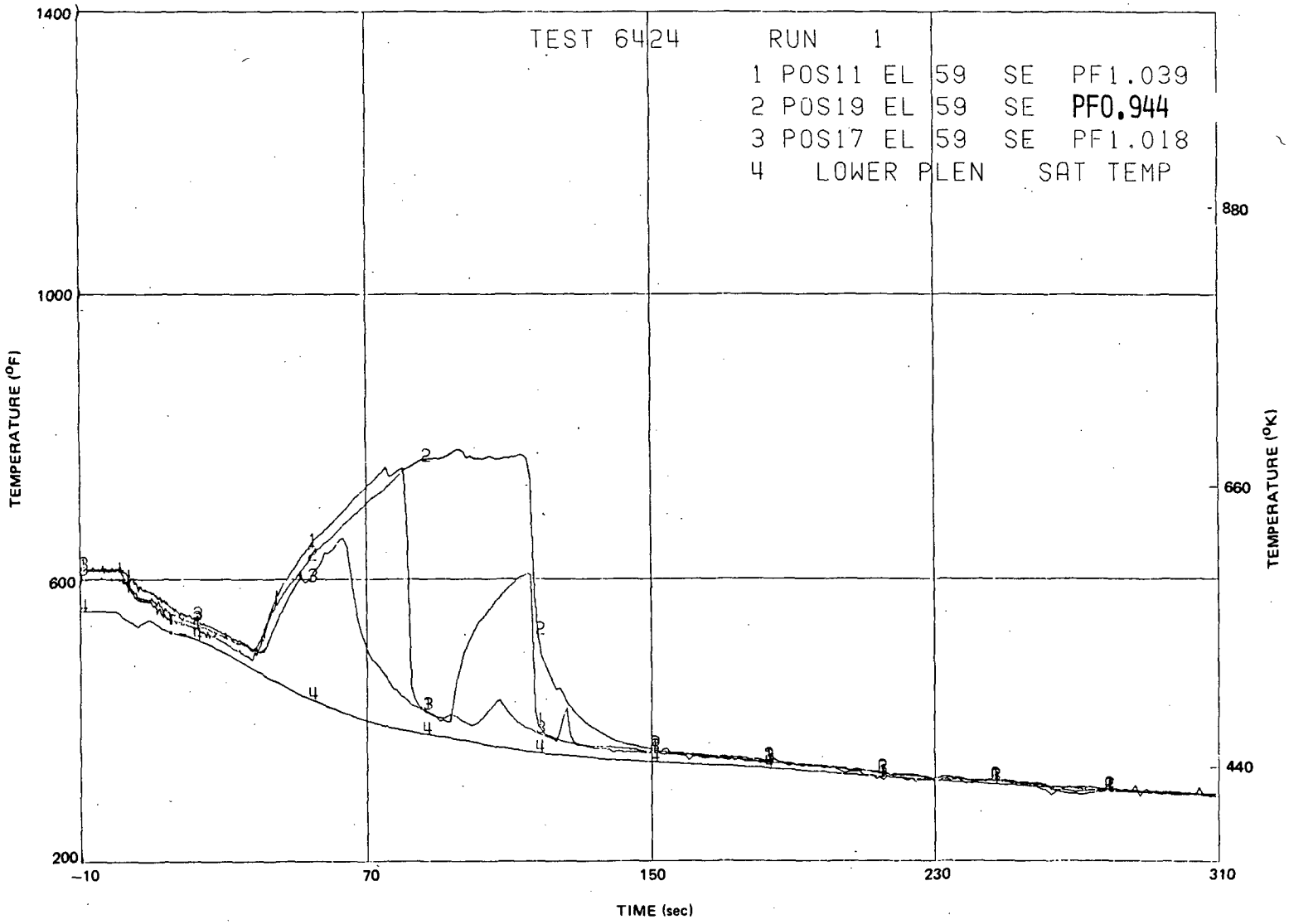

Figure K-83. Inside Clad Temperature-Elevation 59 in.

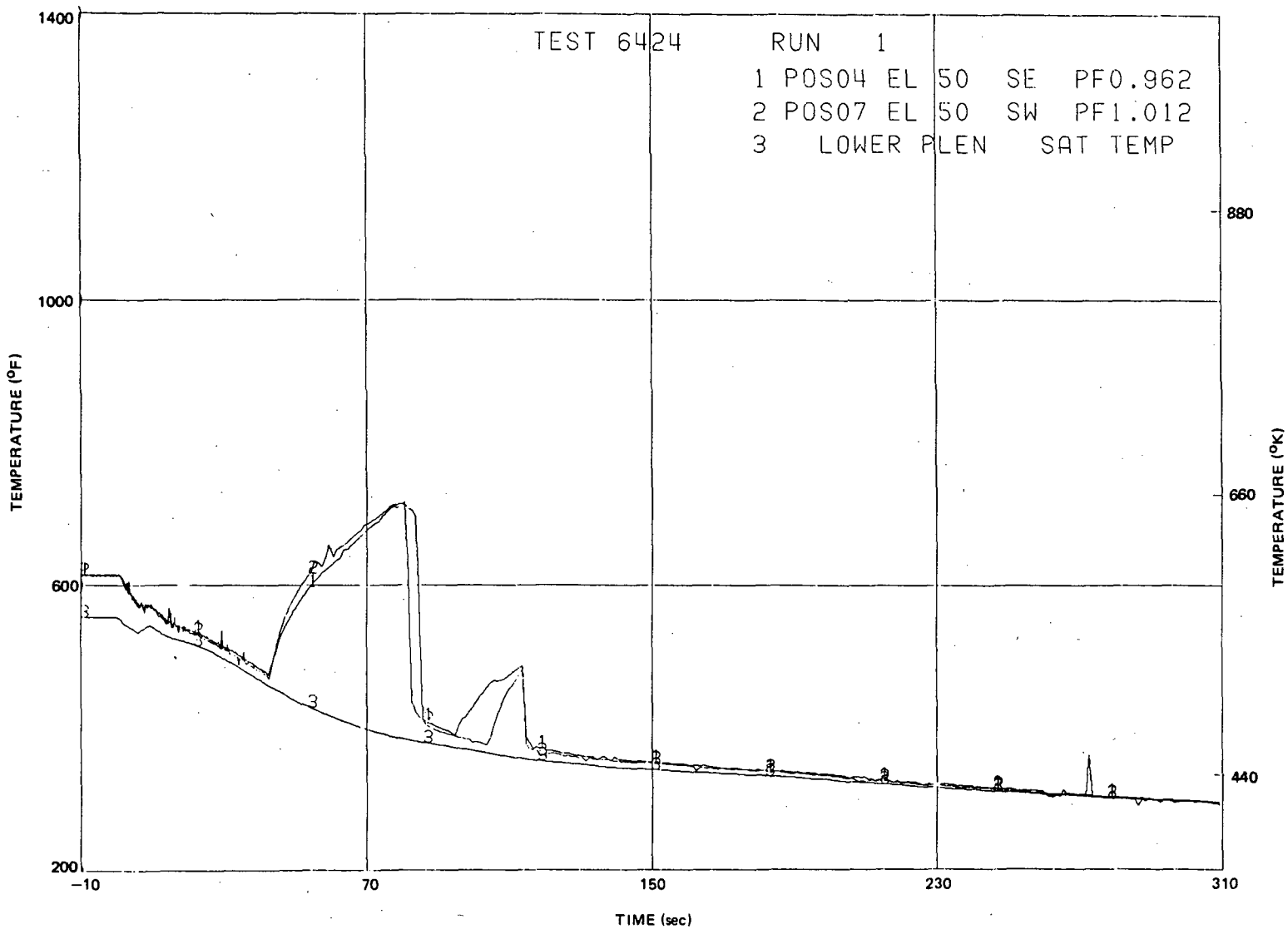

Figure K-84. Inside Clad Temperature-Elevation 50 in.

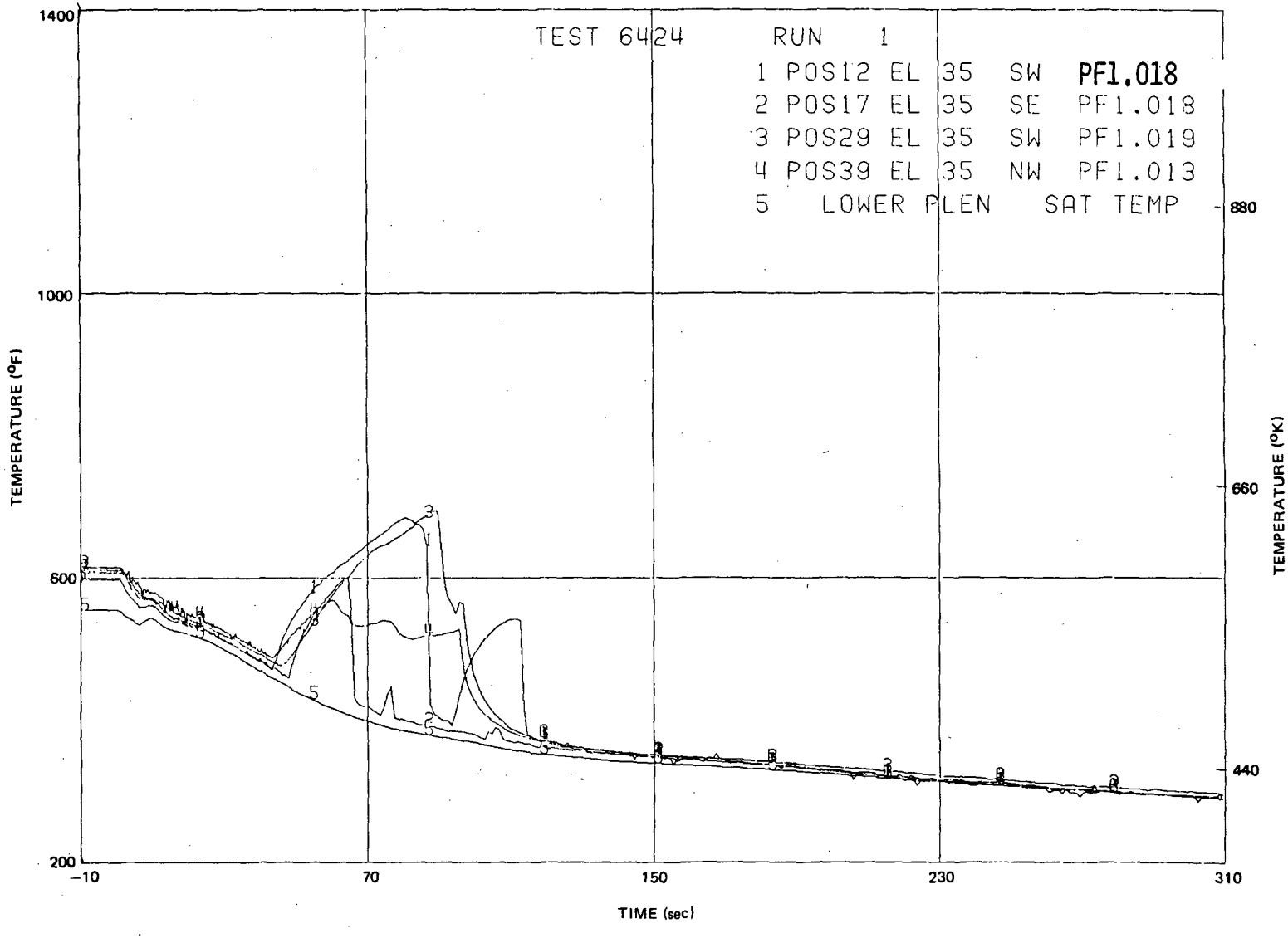

Figure K-85. Inside Clad Temperature-Elevation 35 in.

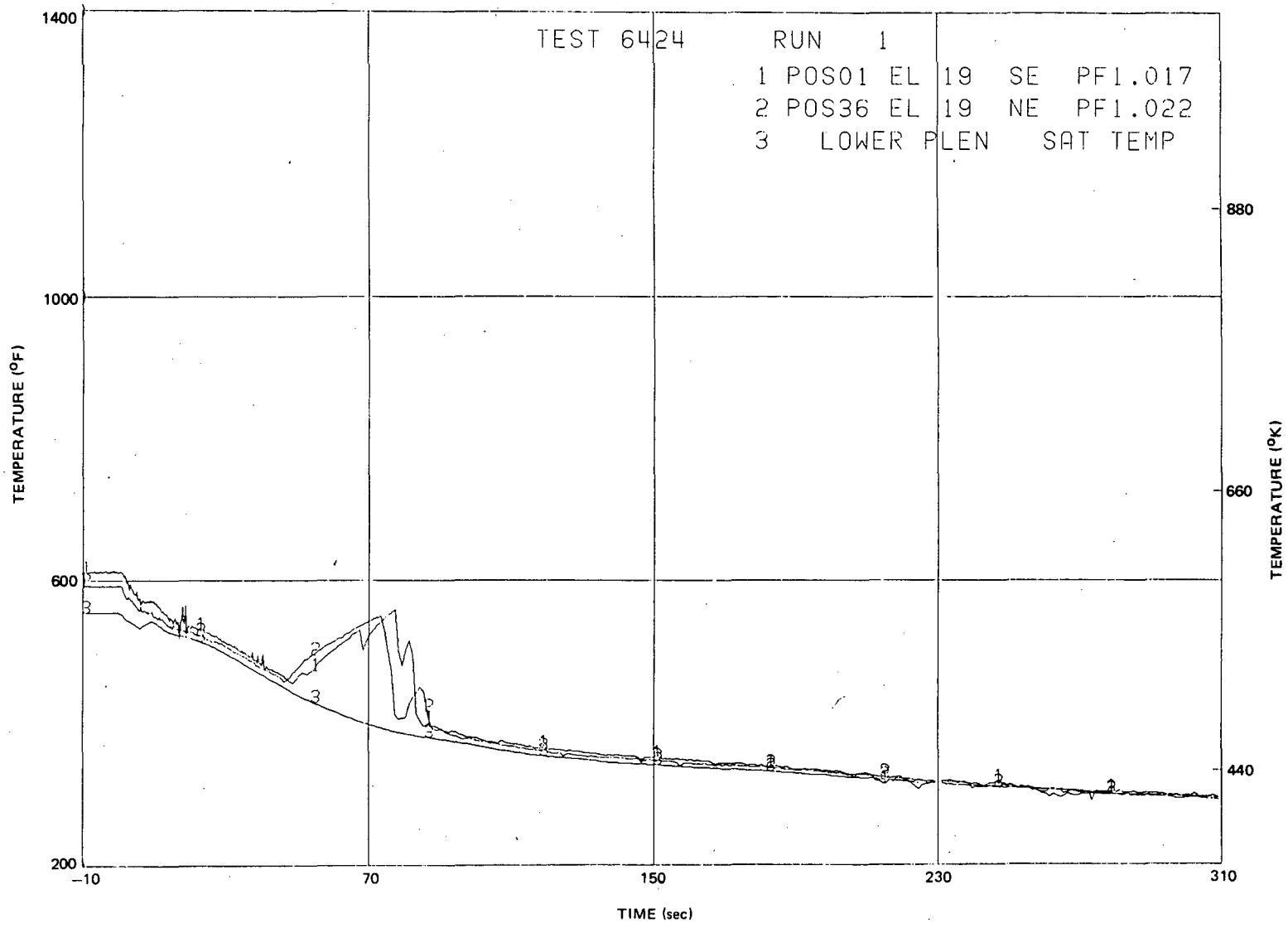

Figure K-86. Inside Clad Temperature-Elevation 19 in.

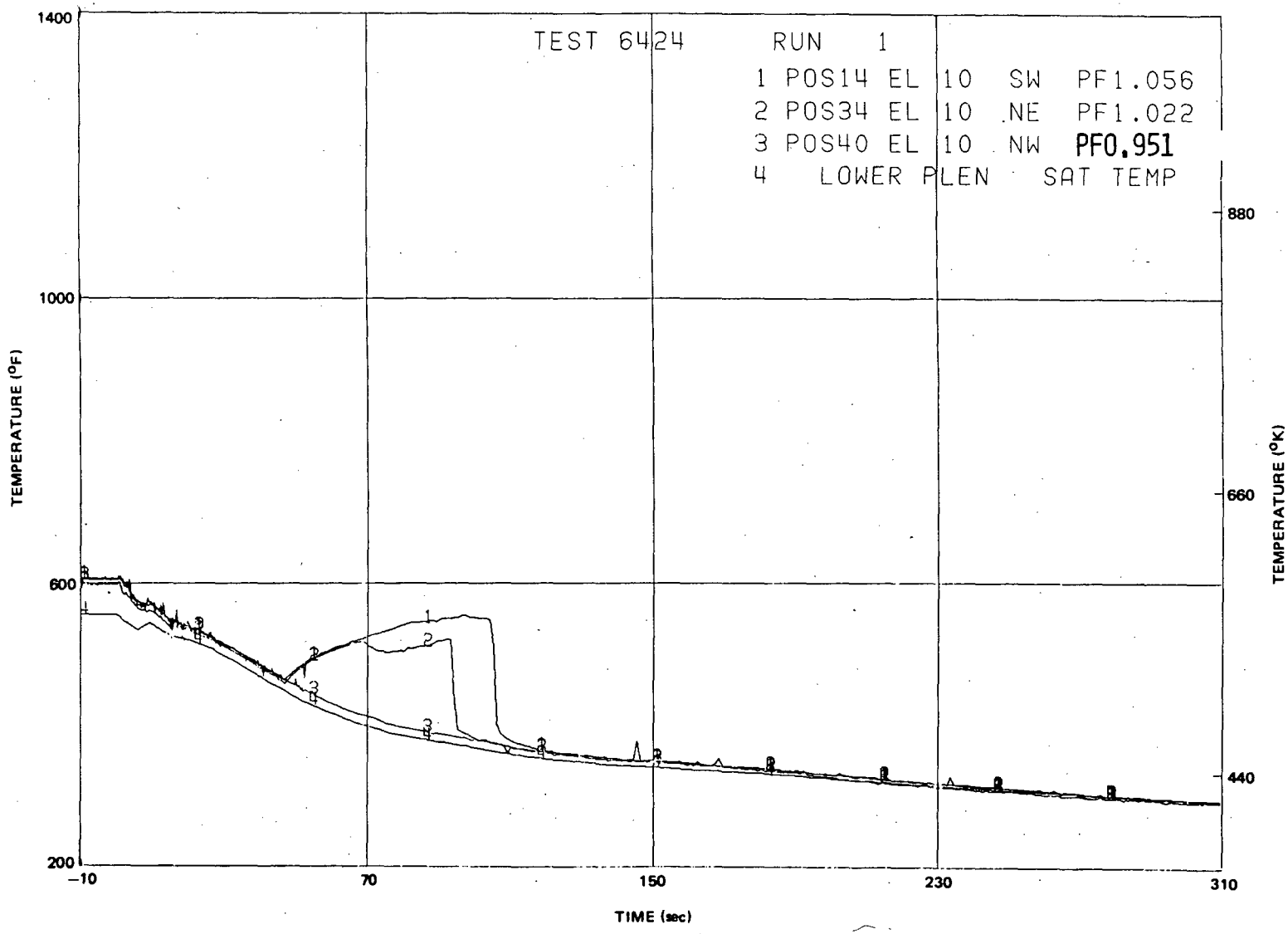

Figure K-87. Inside Clad Temperature-Elevation 10 in.

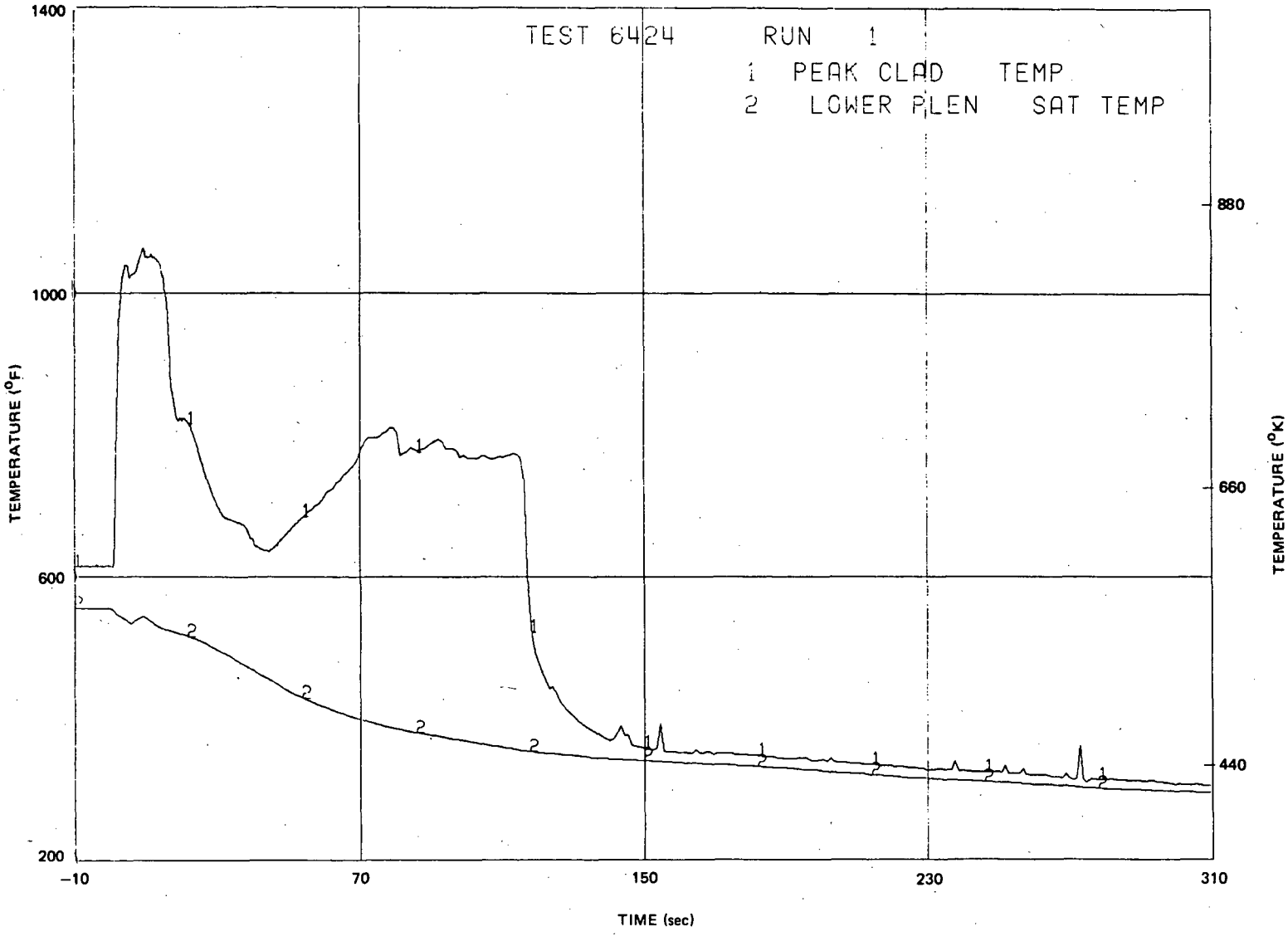

Figure K-88. Peak Clad Temperature

Appendix L

DATA REPORT FOR TEST 6426/RUN 1 AND TEST 6421/RUN 2

Tests 6426/1 and 6421/2 were average power, no ECC injection tests conducted in the TLTA 5A facility. A diagram of the system instrumentation showing measurement nodes is given in Figure L-1. Figure L-2 shows a schematic of the bundle and locations of the pressure transducer taps and thermocouples. The core lattice arrangement and the local peaking factor distribution are shown in Figure L-3.

L-1. MEASUREMENTS FOR TEST 6426/1

Tables L-1 and L-2 summarize the initial conditions and sequence of events for Test 6426/1. Primary measurements throughout the transient are given in Figures L-4 to L-37, derived quantities in Figures L-38 through L-61. A guide for interpreting bundle temperature plots is shown in Figure L-62, and the bundle temperature measurements are given in Figures L-63 to L-77. Figure L-78 gives the peak cladding temperature.

L-2. MEASUREMENTS FOR TEST 6421/2

Primary measurements throughout Test 6421/2 are given in Figures L-79 to L-109, derived quantities in Figures L-110 through L-121. A guide for interpreting bundle temperature plots is shown in Figure L-122, and the bundle temperature measurements are given in Figures L-123 to L-142. Figure L-143 gives the peak cladding temperature.

L-3. DIFFERENCES IN BUNDLE POWER HISTORIES

As discussed in Subsection 3.2.2.2 of the main text, the thermocouple heat-up rate of Test 6426/1 is higher than that of Test 6421/2, even though the two tests are comparable. The heat-up rate difference is attributable to the difference in the bundle power histories. Figure L-144 shows that the bundle power in Test 6421/2 was lower than the power in Test 6426/1. For direct power comparison among all the TLTA 5A tests, Table L-3 is available and gives the digitized power measurements at various times throughout the tests.

Table L-1

BD/ECC 1A TEST 6426 RUN 1 INITIAL CONDITIONS

Initial Conditions	
Bundle power	5.05 ± 0.03 MW
Steam dome pressure	1044 ± 5 psia
Lower plenum pressure	1068 ± 5 psia
Lower plenum enthalpy	526 ± 5 Btu/lbm
Initial water level	123 ± 6 in. El
Feedwater enthalpy	66 ± 2 Btu/lbm
Bundle inlet to outlet DP	15 ± 2 psi
Steam flow	6 ± 1 lbm/sec
Feedwater flow	1.3 ± 0.3 lbm/sec
Drive Pump 1 flow	8.2 ± 1.0 lbm/sec
Drive Pump 2 flow	8.4 ± 1.0 lbm/sec
Jet Pump 1 flow	16 ± 2 lbm/sec
Jet Pump 2 flow	20 ± 2 lbm/sec
Bundle inlet flow	33 ± 5 lbm/sec

All uncertainty bands are judged from the maximum of data fluctuation and/or absolute uncertainties of the measurements.

Table L-2

SEQUENCE OF EVENTS FOR 6426 RUN 1 (AVG. POWER, NO ECC)

Event	Time (sec)
Blowdown valves open	0.0
Bundle power decay initiated	0.5
Blowdown loop jet pump flow reverses	0.1
Feedwater flow stops	0.5
Bypass flow reverses	1.5
Jet pump suction uncovers	6.5
Steamline valve completely closed	7.9
Recirc. suction line begins to uncover	9.2
Lower plenum bulk flashing	13.3
Guide tube flashing	13.8
Core inlet uncovers (SEO center line)	20
Lower plenum mixture level reaches jet pump exit plane	33
End of test	294

Table L-3

POWER MEASUREMENTS FOR ALL TLTA 5A TESTS

Time (Sec)	Power (kW) Test 6421/2	Test 6426/1	Test 6425/2	Test 6424/1	Test 6423/3	Test 6422/3
1	3861.0	5020.0	4988.0	6357.0	6235.0	4785.0
5	2170.0	3008.0	2874.0	3637.0	3413.0	2630.0
10	1072.0	1616.0	1532.0	1922.0	1800.0	1392.0
15	594.1	876.5	847.4	1063.0	1045.0	812.5
20	425.2	591.2	582.4	745.5	681.4	538.7
30	279.6	361.1	364.0	448.5	416.4	332.0
40	209.7	265.0	262.1	329.1	302.9	241.7
50	168.9	209.7	212.6	265.0	238.8	192.2
60	145.6	177.6	177.6	221.3	203.8	163.1
70	136.9	166.0	168.9	209.7	198.0	157.3
80	134.0	163.1	166.0	203.8	186.4	151.4
90	131.0	160.2	157.3	198.0	183.5	154.3
100	131.0	154.3	154.3	192.2	180.6	154.3
120	131.0	154.3	154.3	192.2	180.6	154.3
140	128.1	154.3	154.3	189.3	186.4	154.3
160	131.0	154.3	151.4	186.4	183.5	145.6

NOTES:

1. P - PRESSURE
   DP - DIFFERENTIAL PRESSURE
   T - TEMPERATURE (RTD - RESISTANCE THERM)
   SP - VALVE STEM POSITION
   RO - RESTRICTING ORIFICE
   FE - FLOW ELEMENT
   S - PUMP SPEED
   LP - LEVEL PROBE
   DD - DRAG DISK
   TM - TURBINE METER

2. N305 - 54.88 MEANS NOZZLE NO. 305 IS AT AN ELEVATION OF 54.88 INCHES. IT DOES NOT REFER TO ACTUAL LOCATION OF THE NODAL POINT.

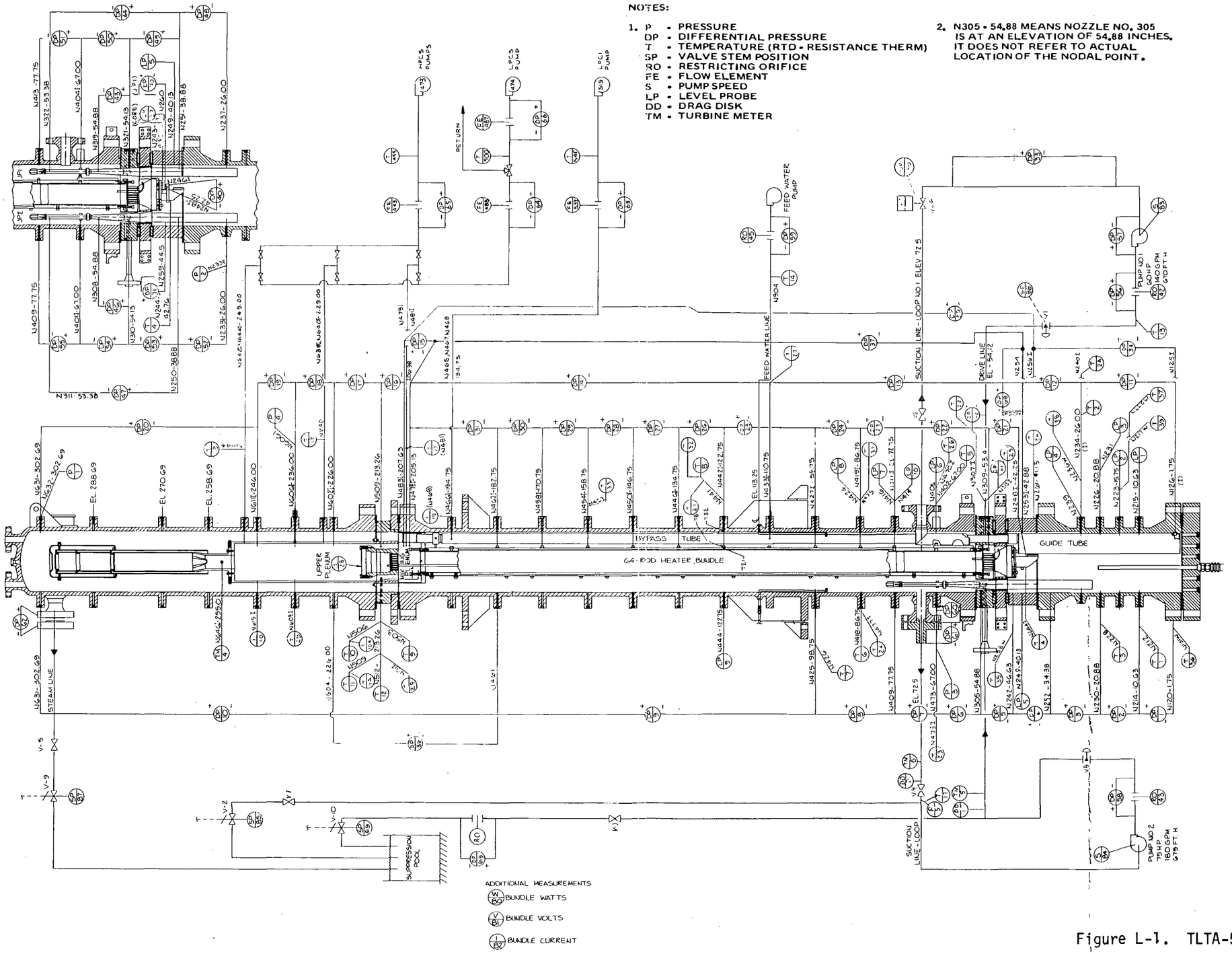

Figure L-1. TLTA-5A Instrumentation

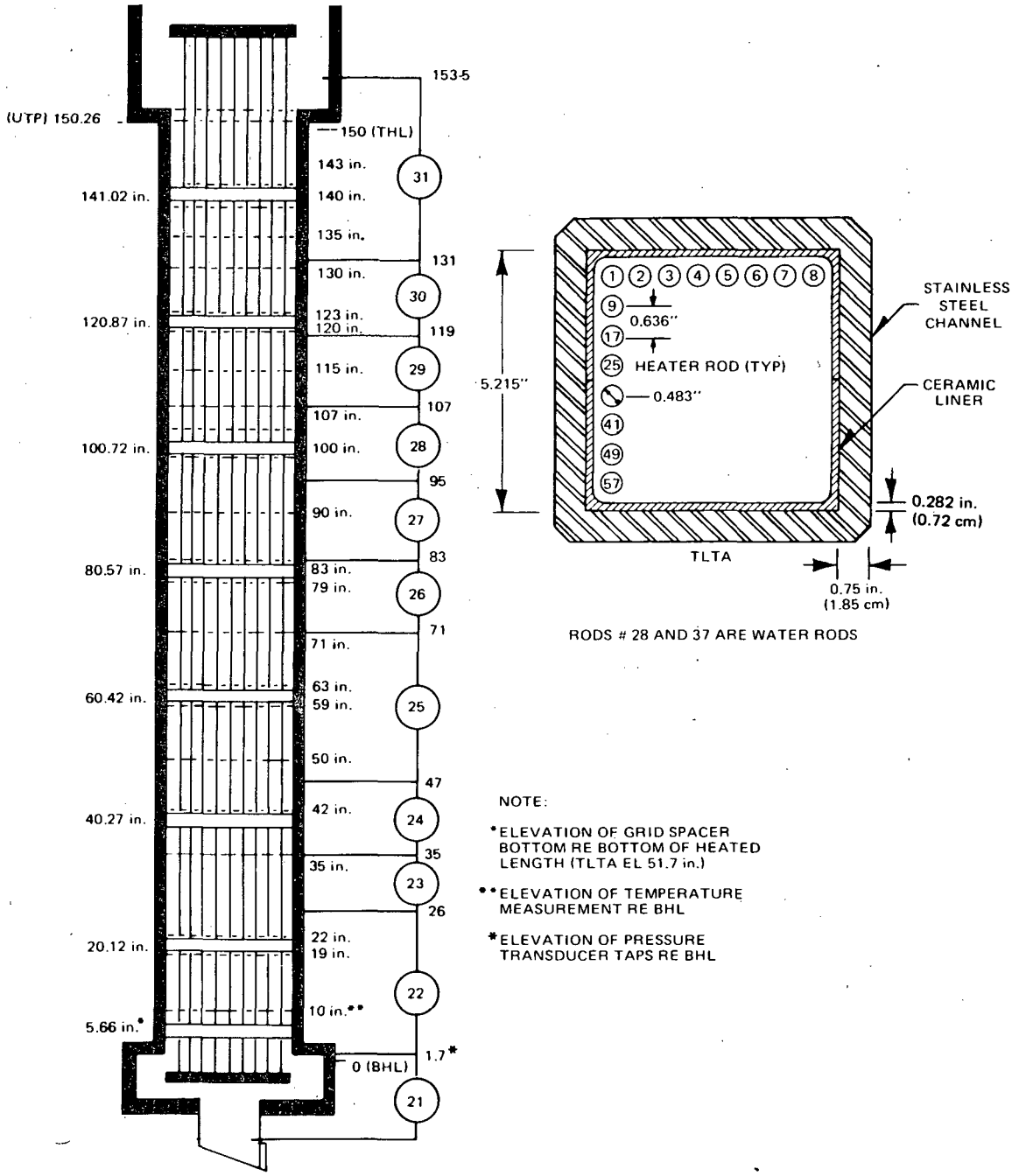

Figure L-2. TLTA-5A Bundle Instrumentation and Dimensions

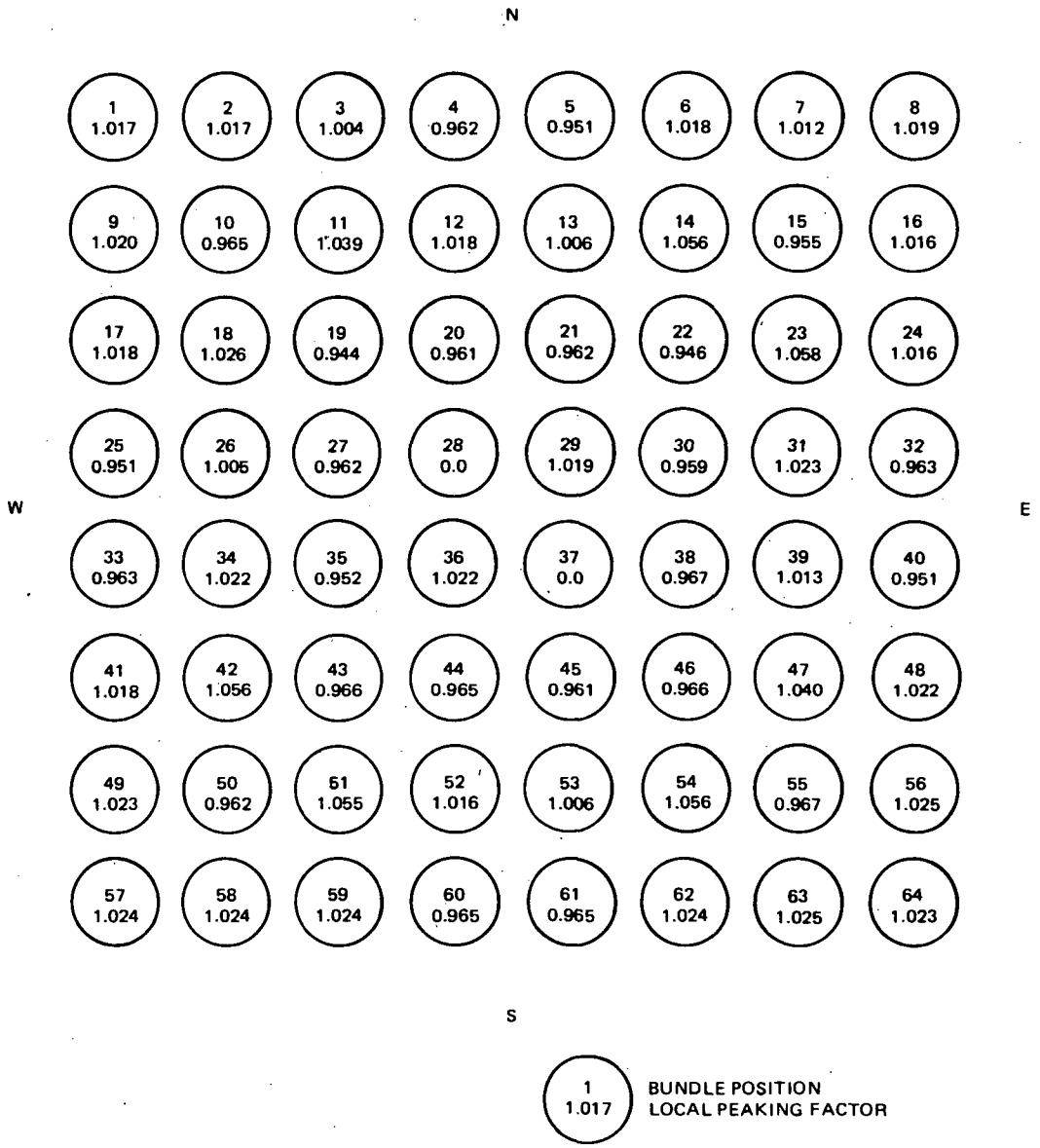

Figure L-3. Local Peaking Factor Distribution

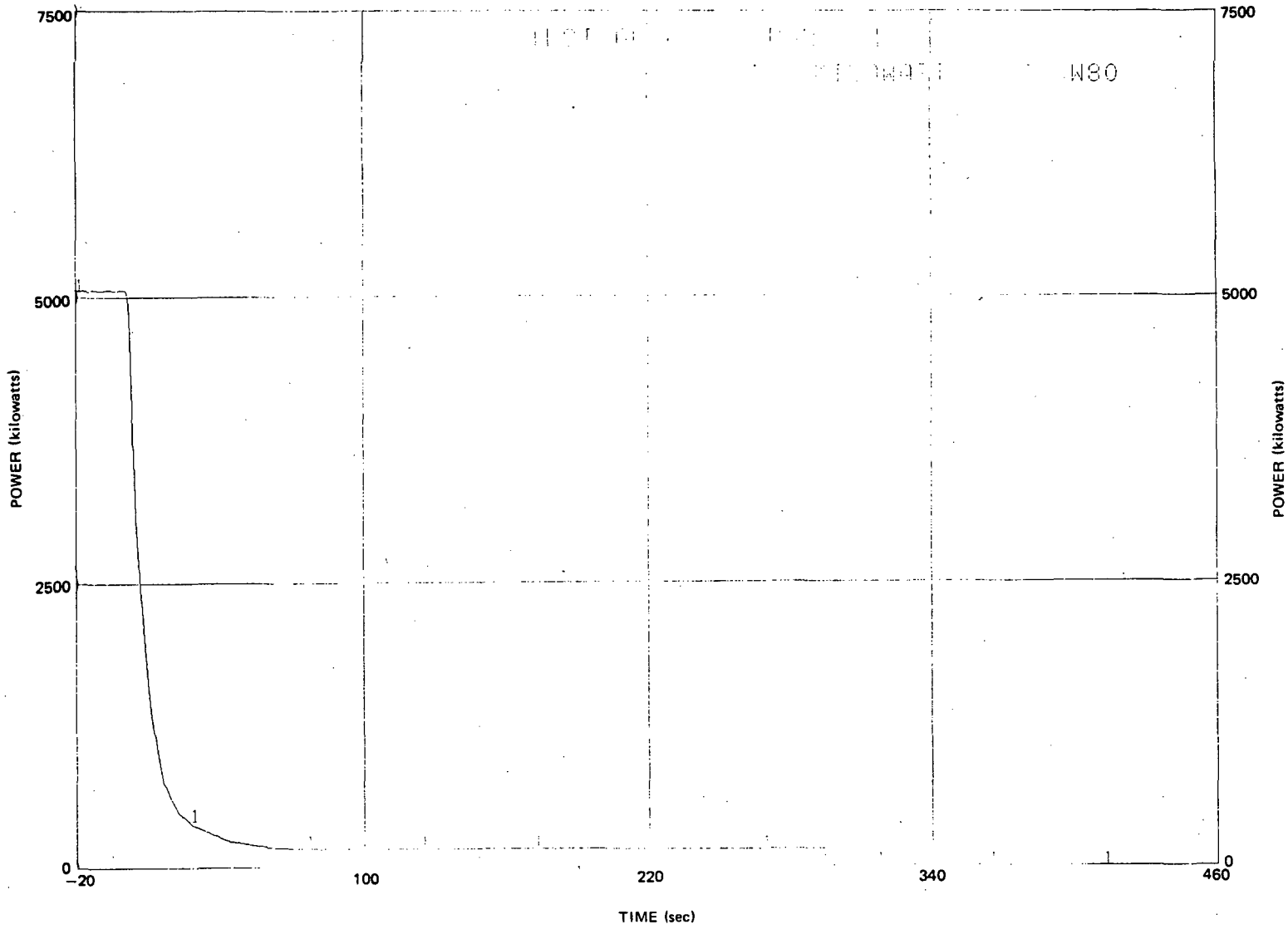

Figure L-4. Bundle Power Decay

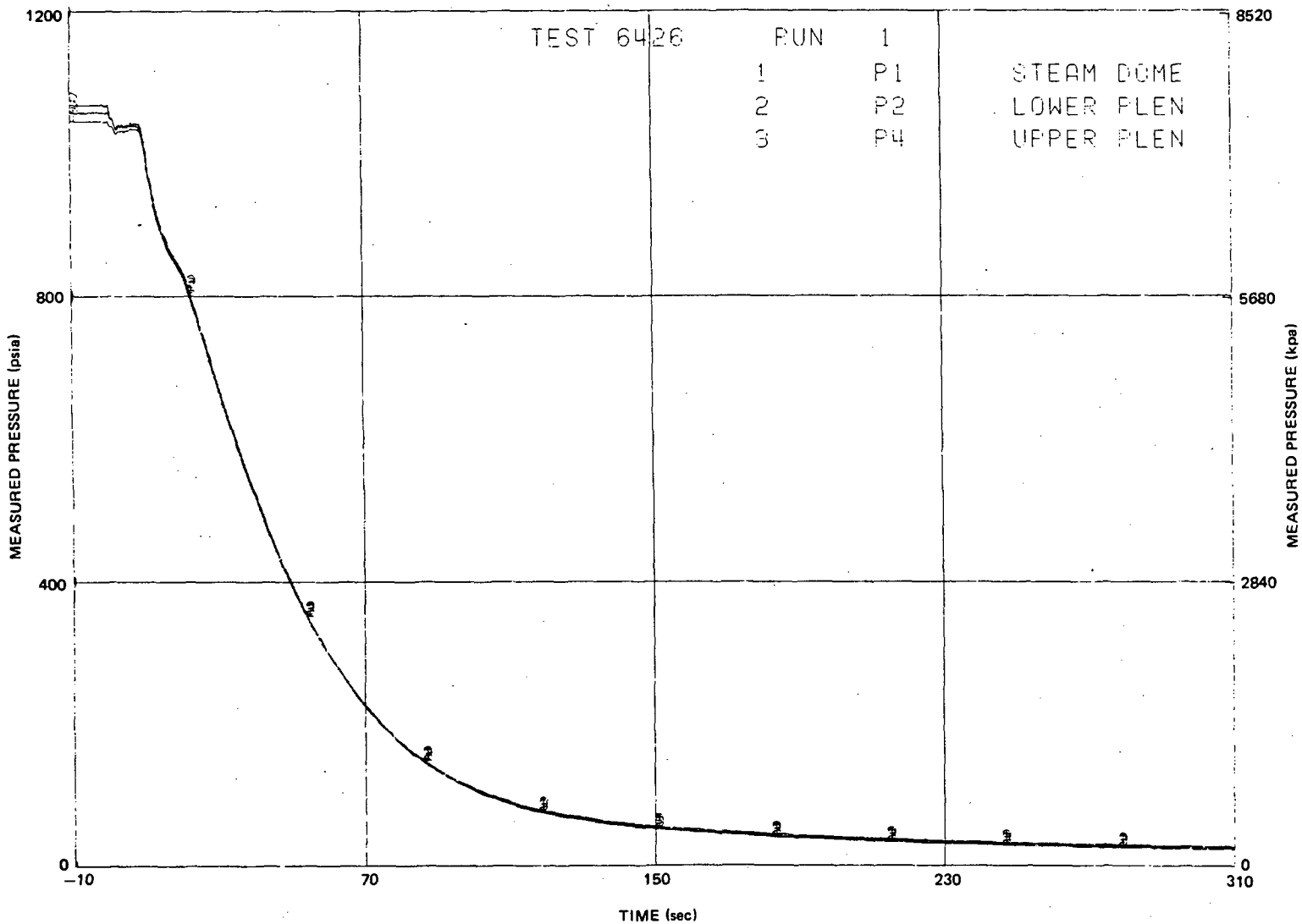

Figure L-5. System Pressures

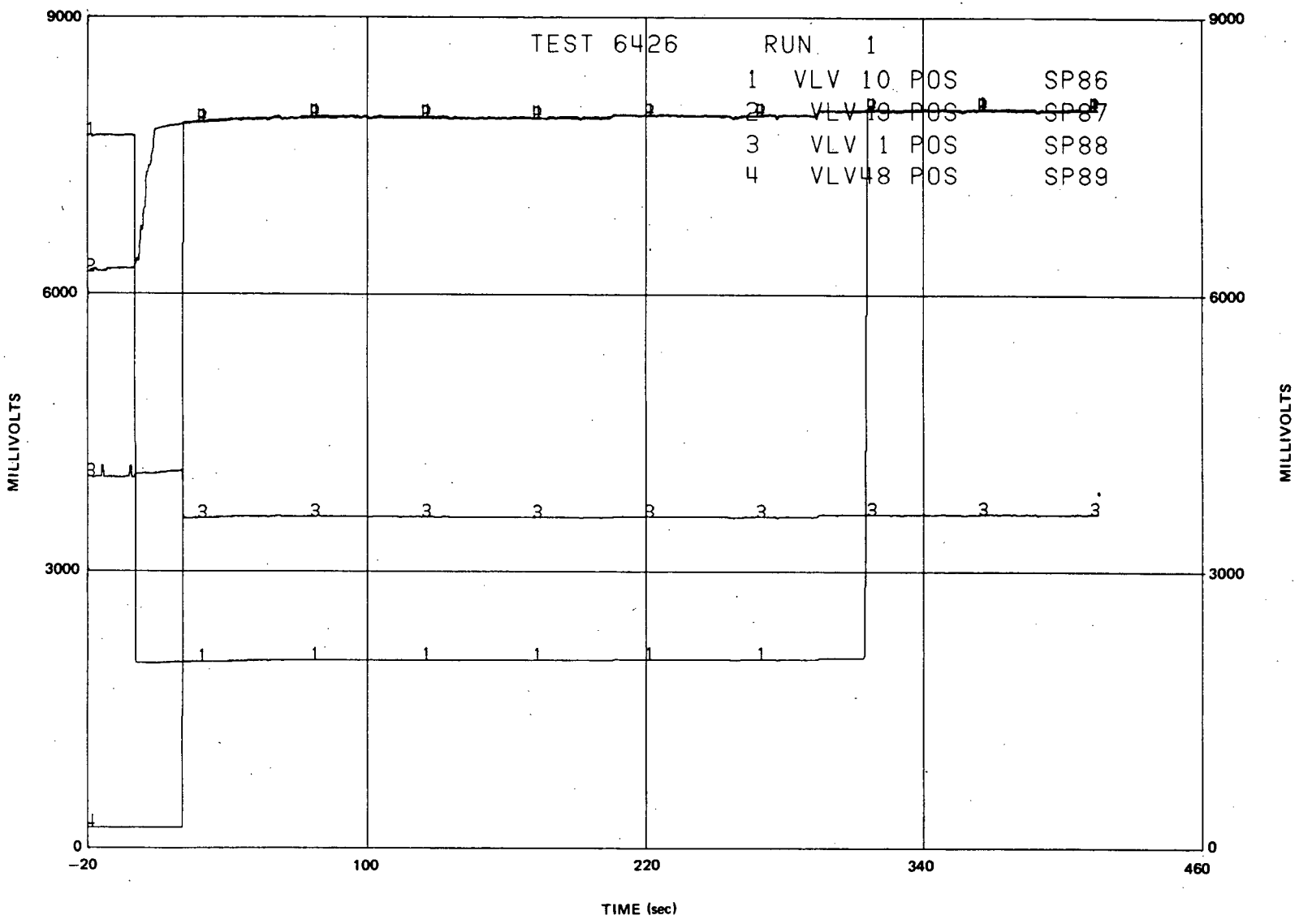

Figure L-6. Valve Positions

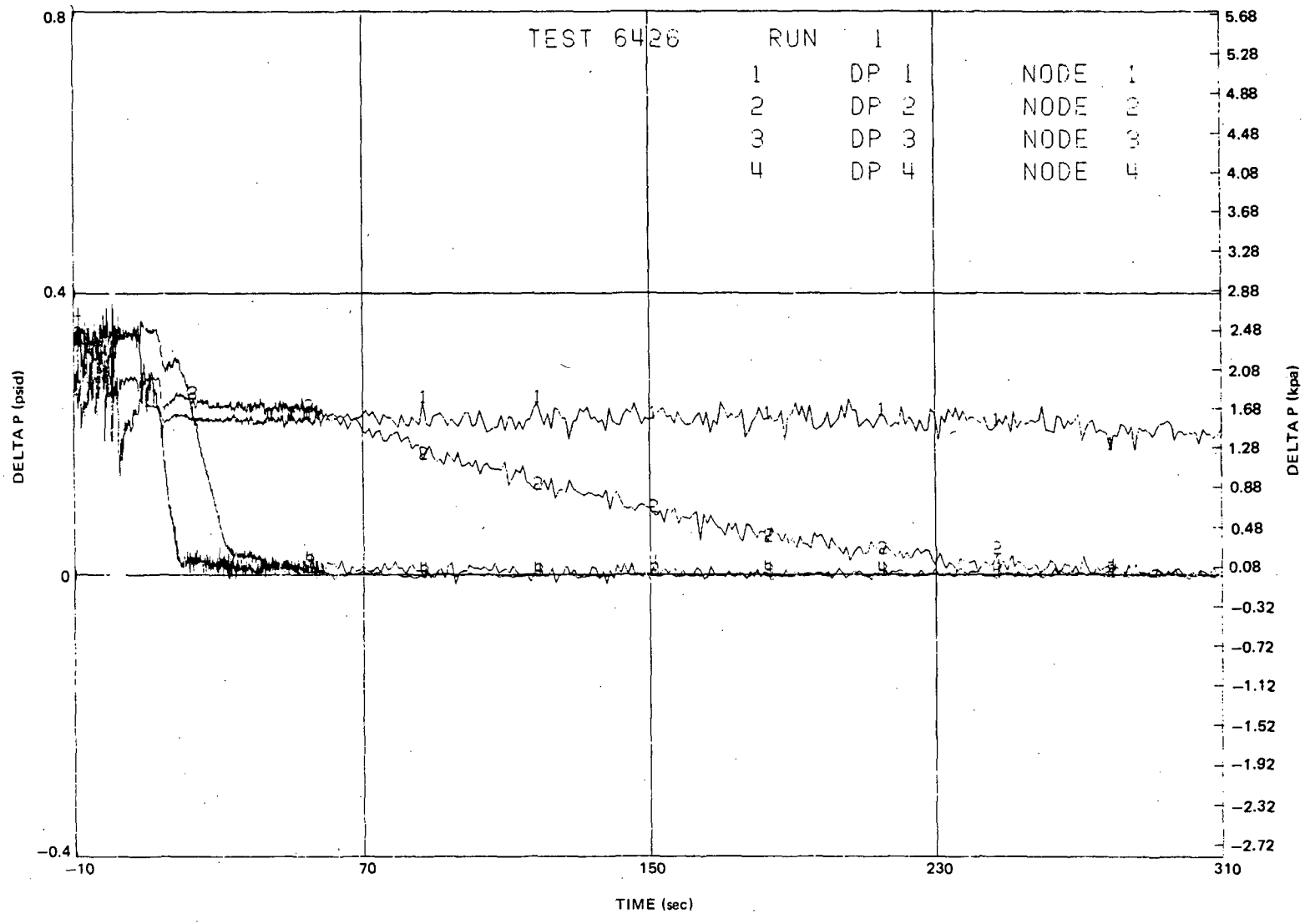

Figure L-7. Lower Plenum Differential Pressures

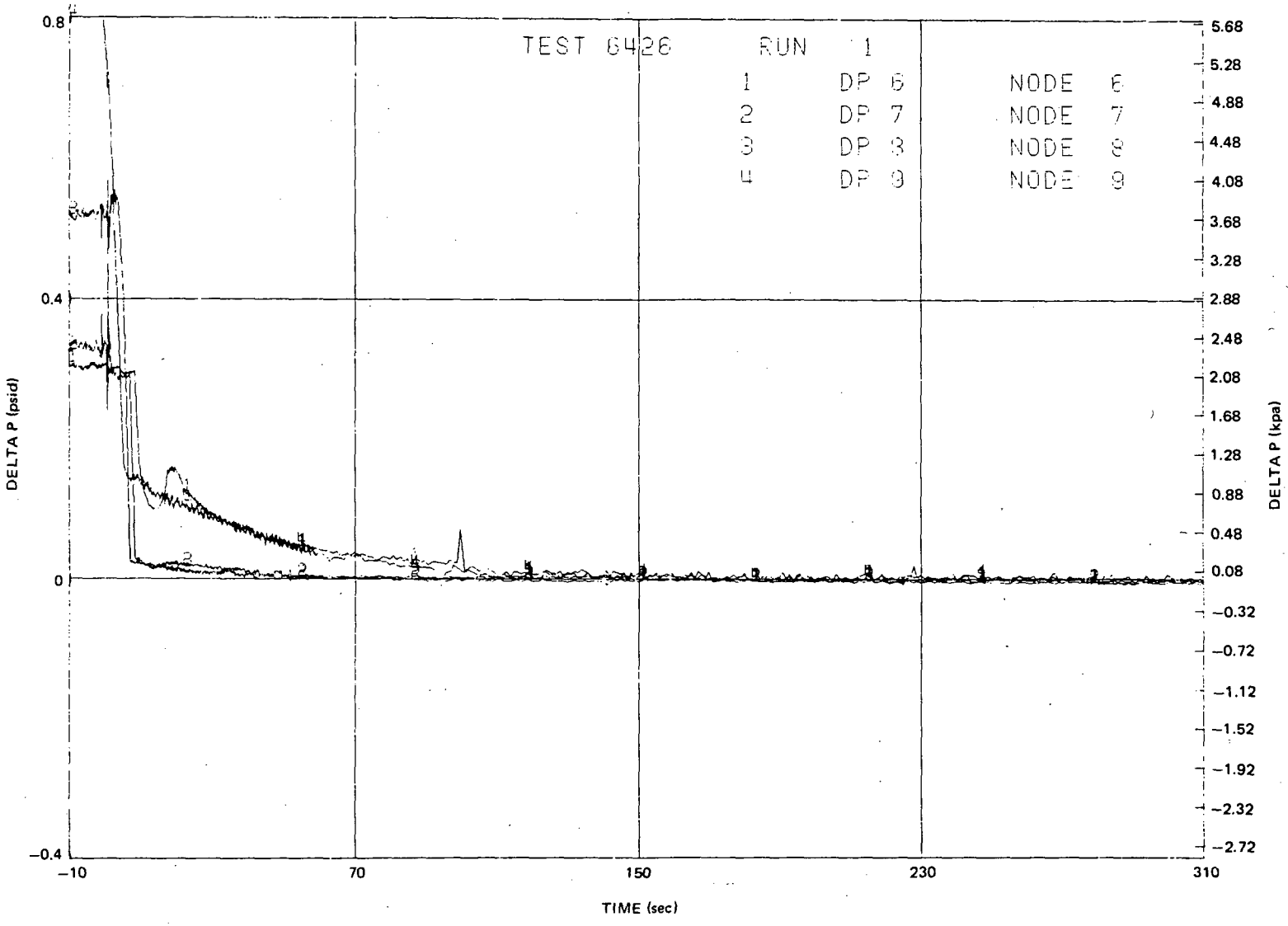

Figure L-8. Annulus Differential Pressures

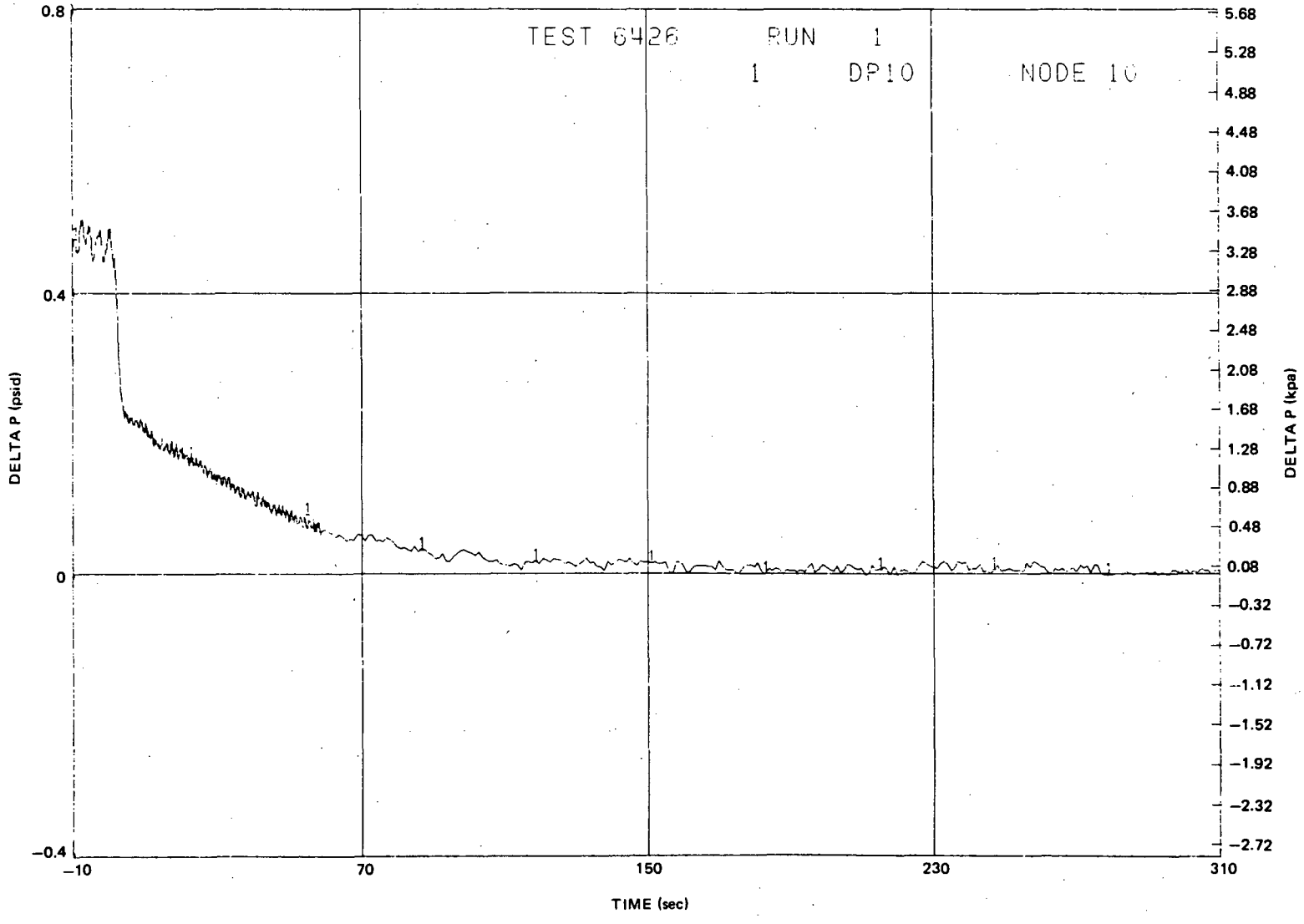

Figure L-9. Upper Annulus Differential Pressure

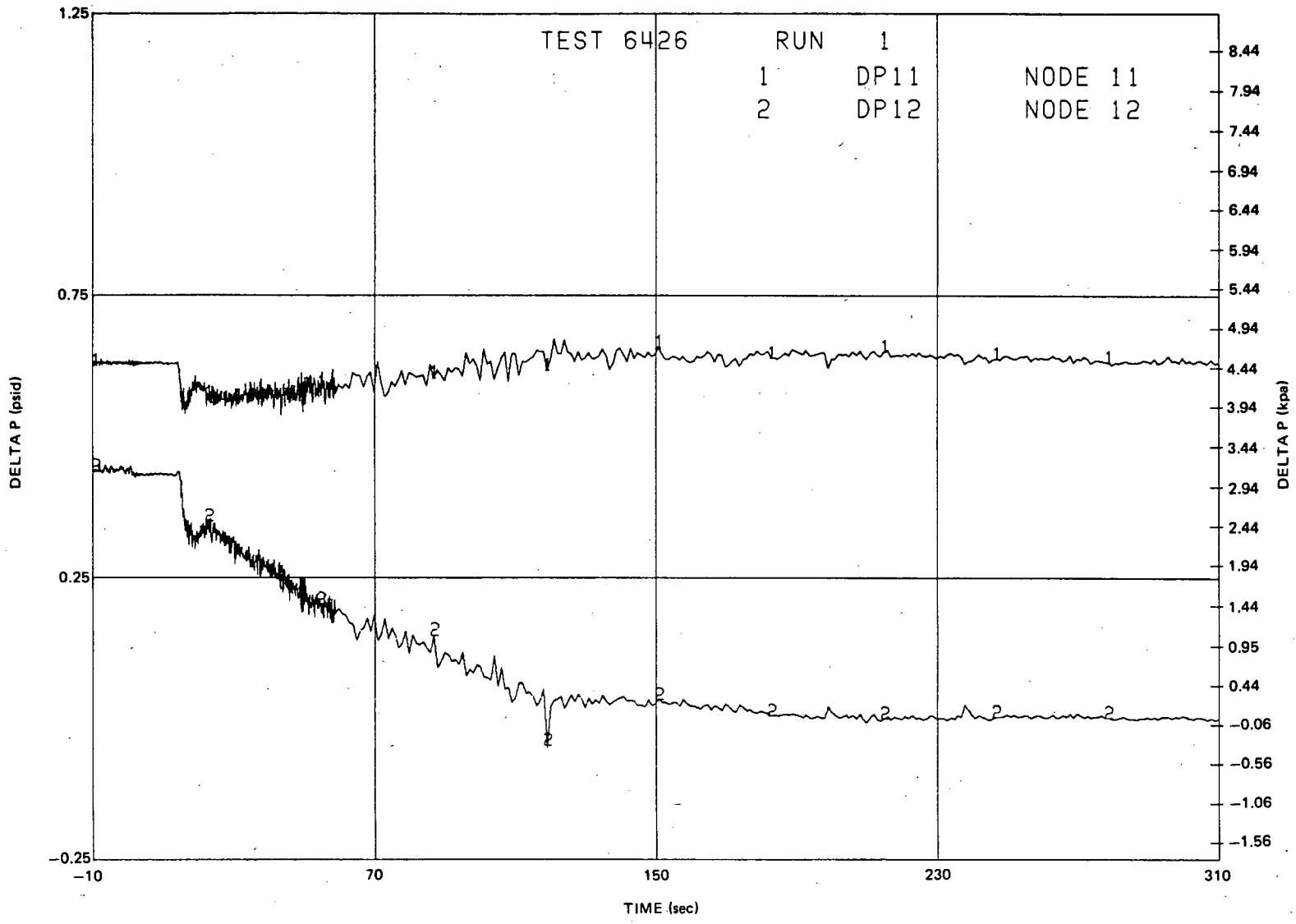

Figure L-10. Guide Tube Differential Pressures

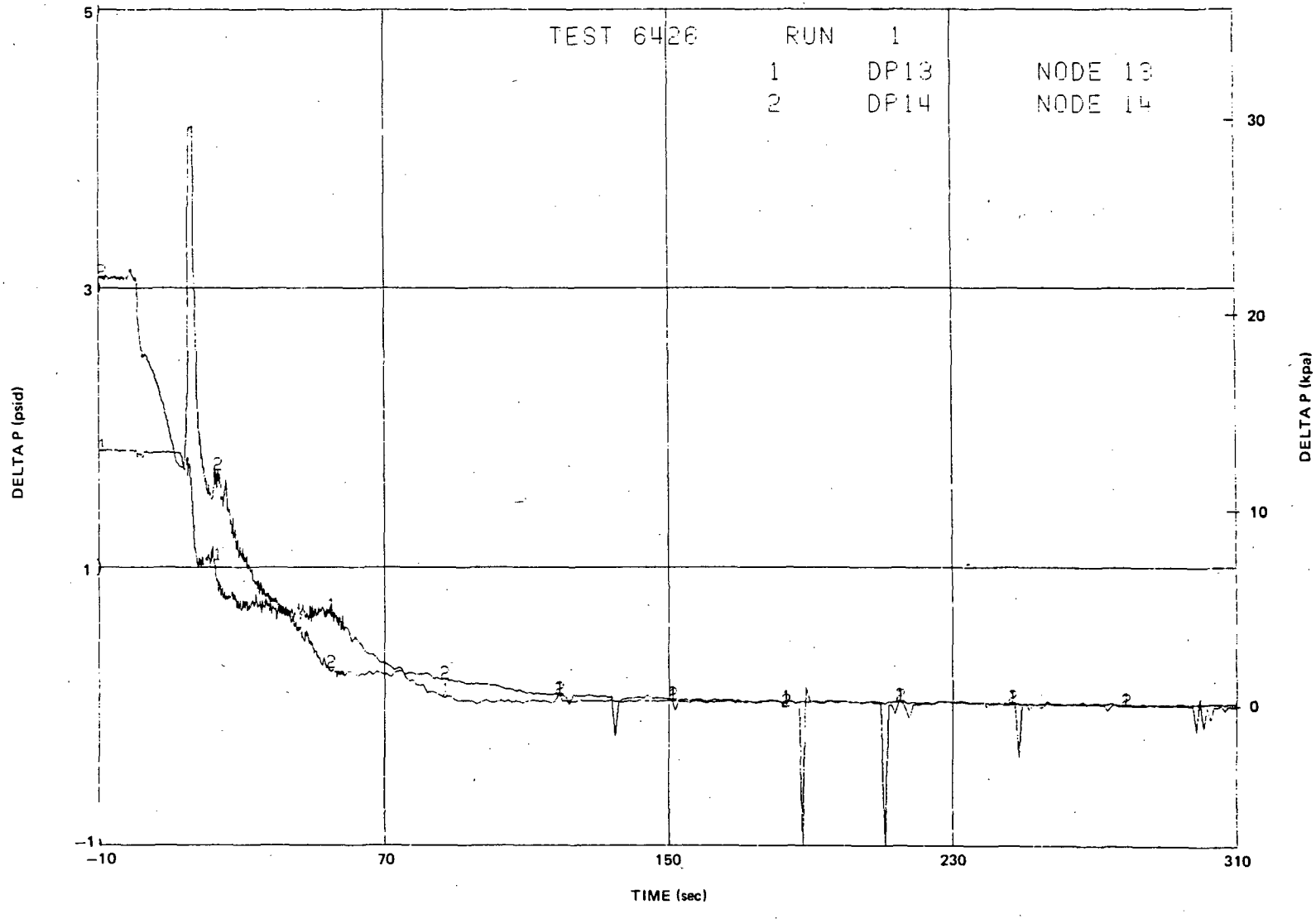

Figure L-11. Bypass Differential Pressures

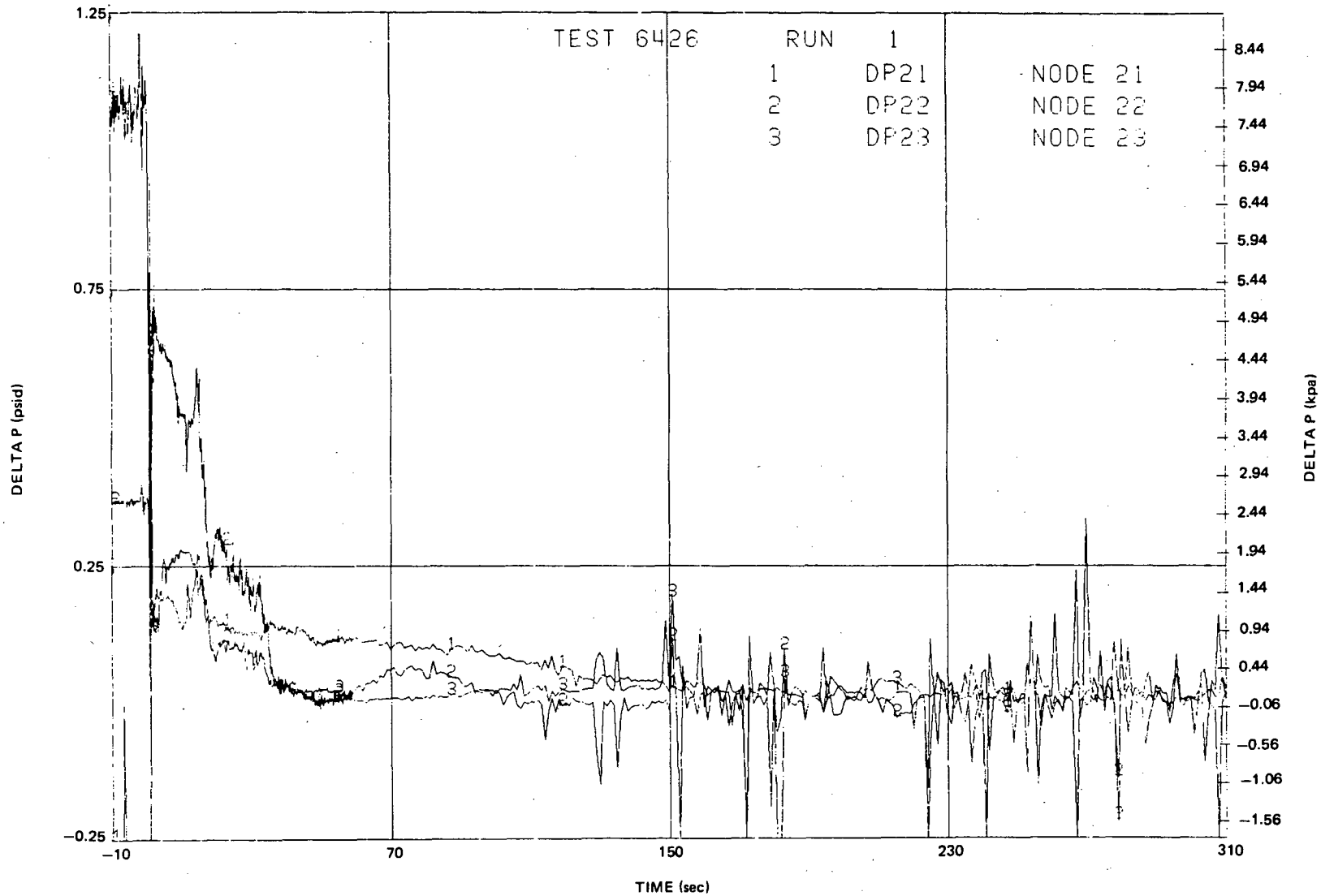

Figure L-12. Lower Bundle Differential Pressures

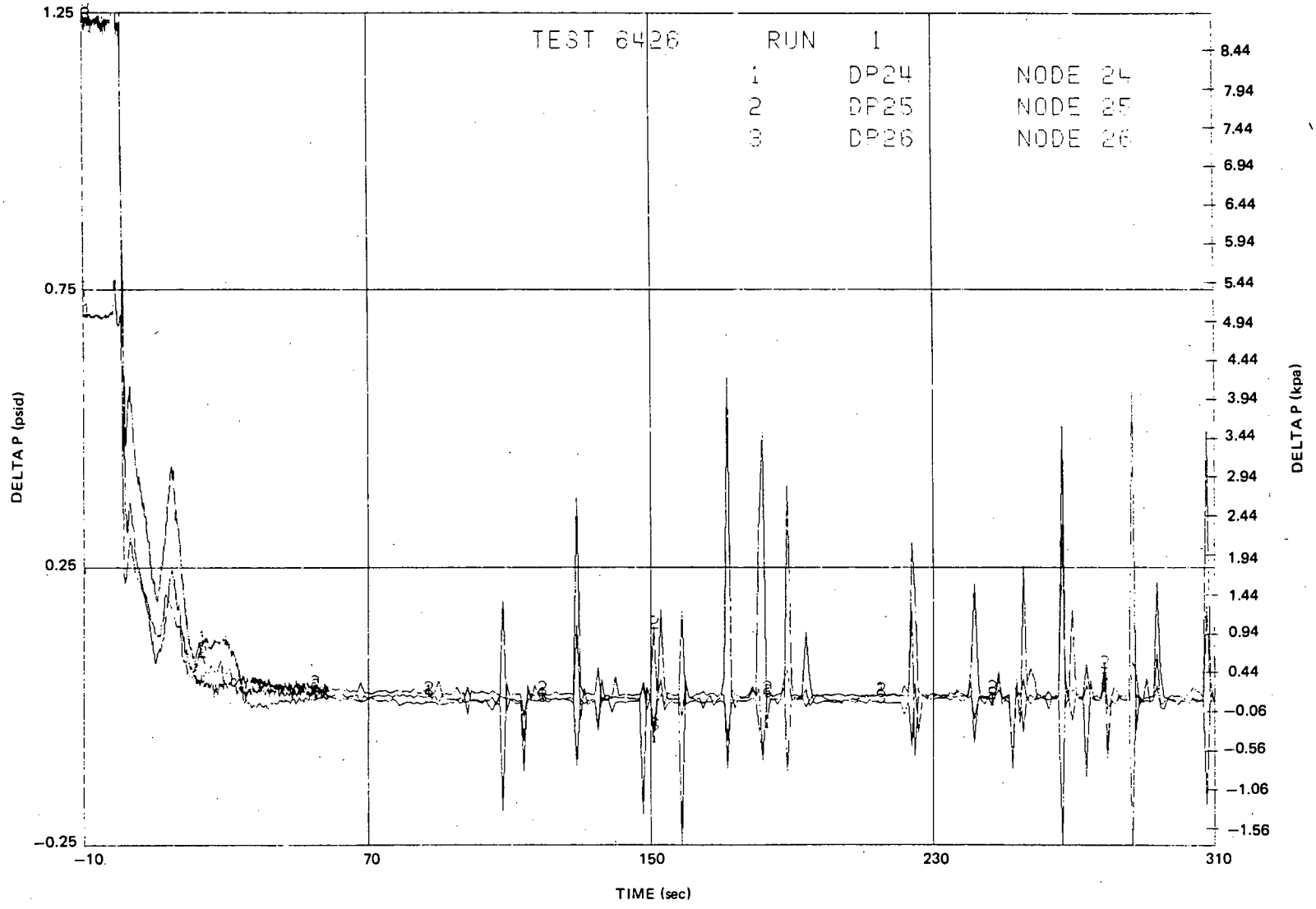

Figure L-13. Middle Bundle Differential Pressures

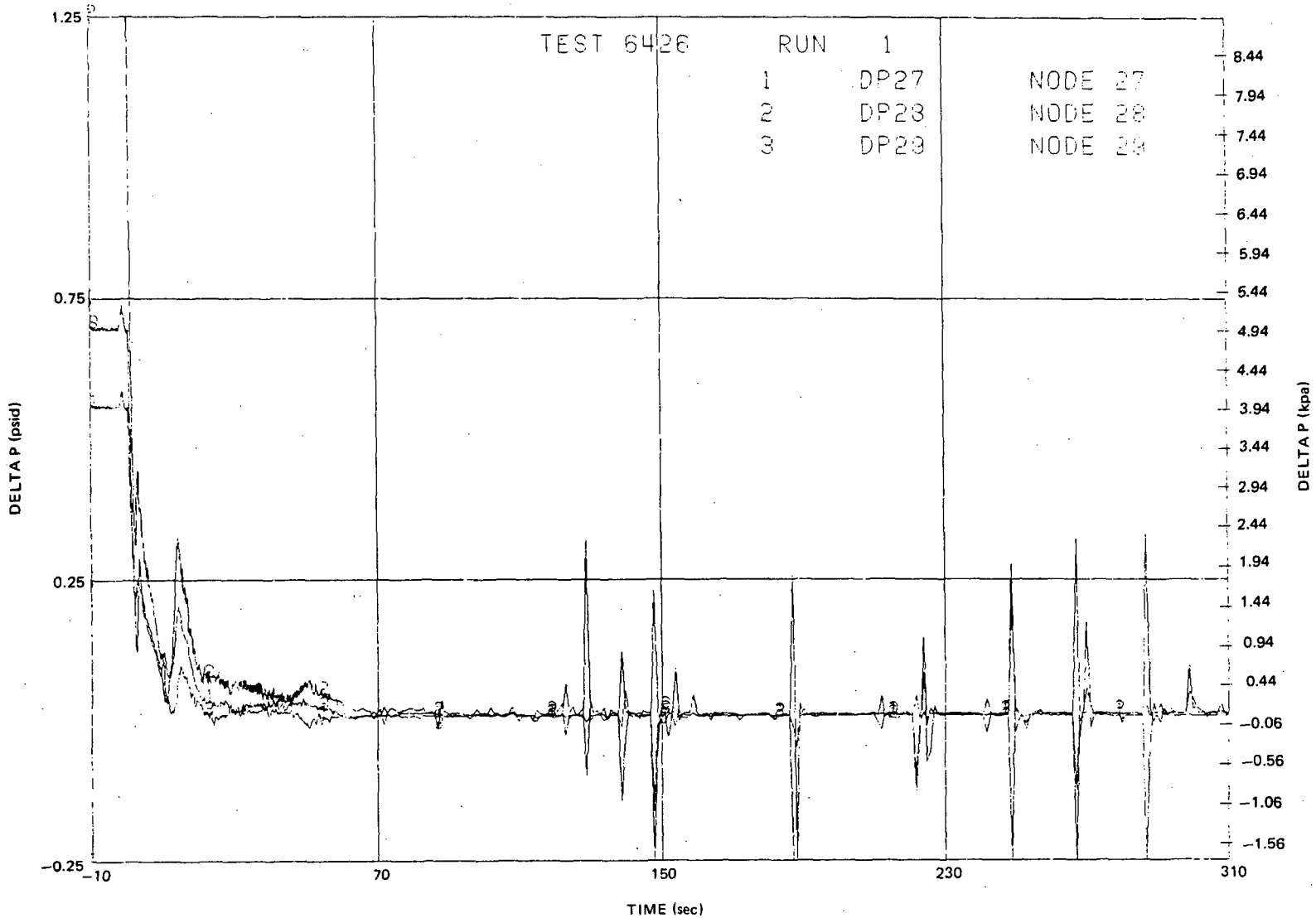

Figure L-14. Upper Bundle Differential Pressures

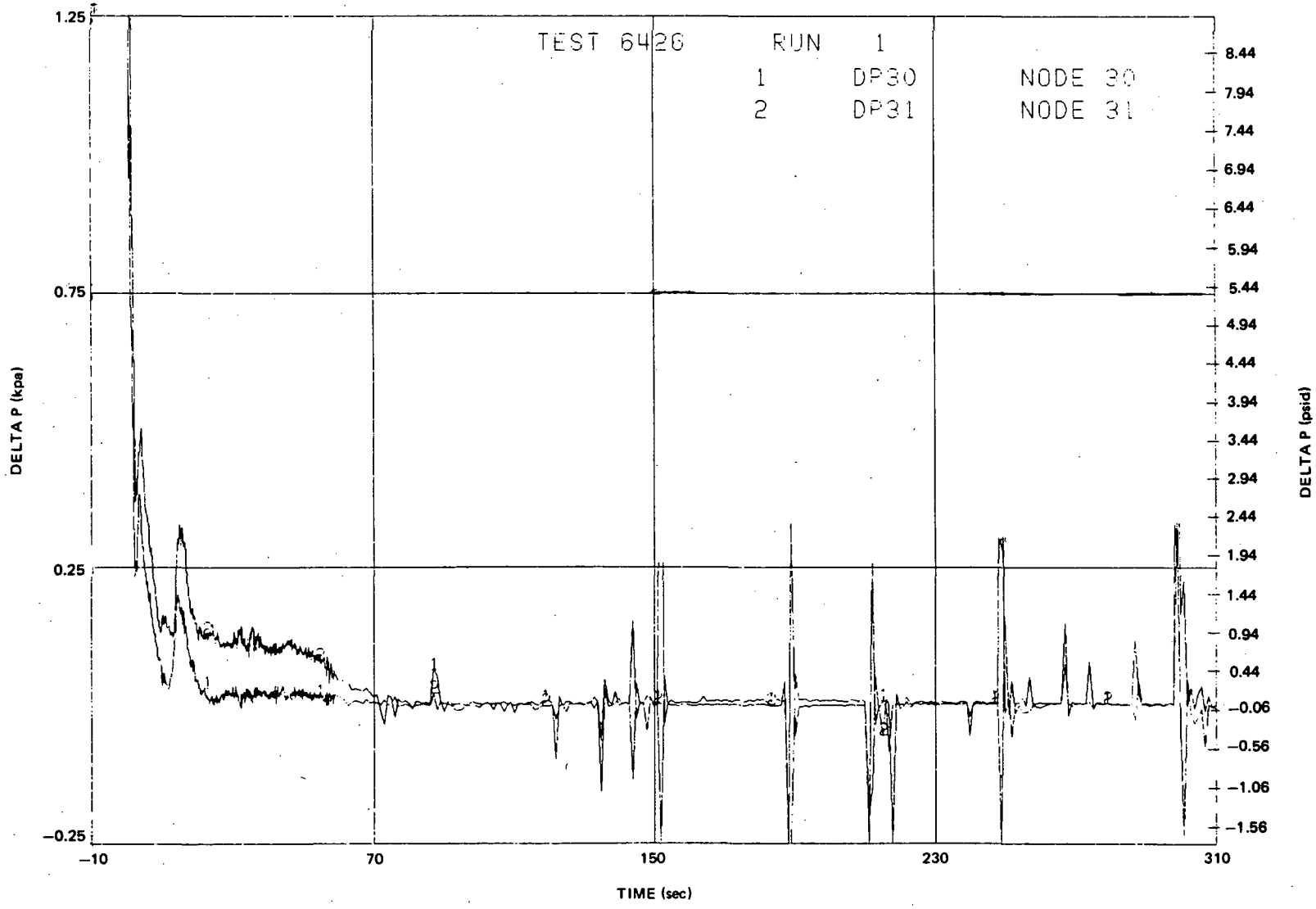

Figure L-15. Top Bundle Differential Pressures

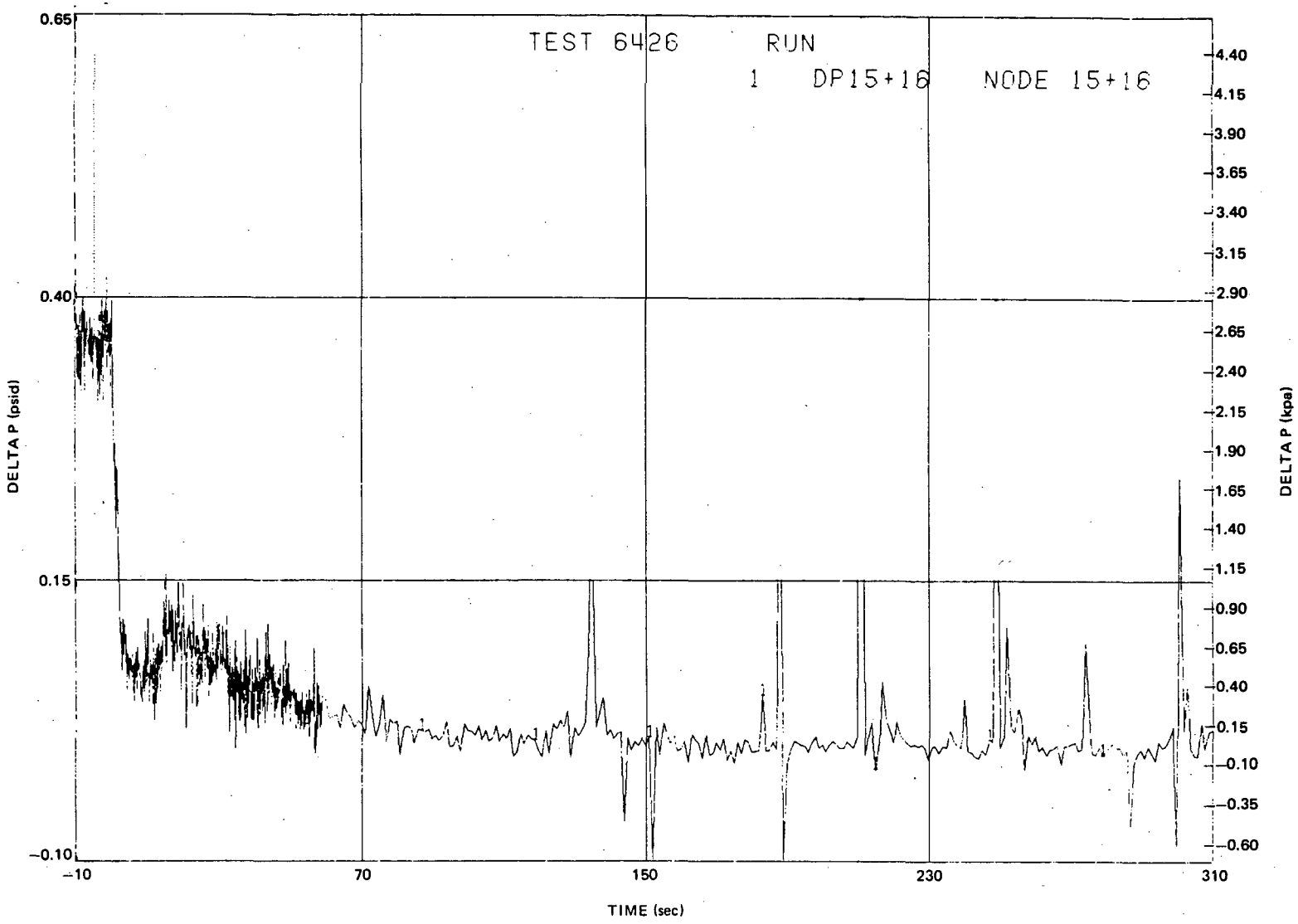

Figure L-16. Mixing Plenum Differential Pressures

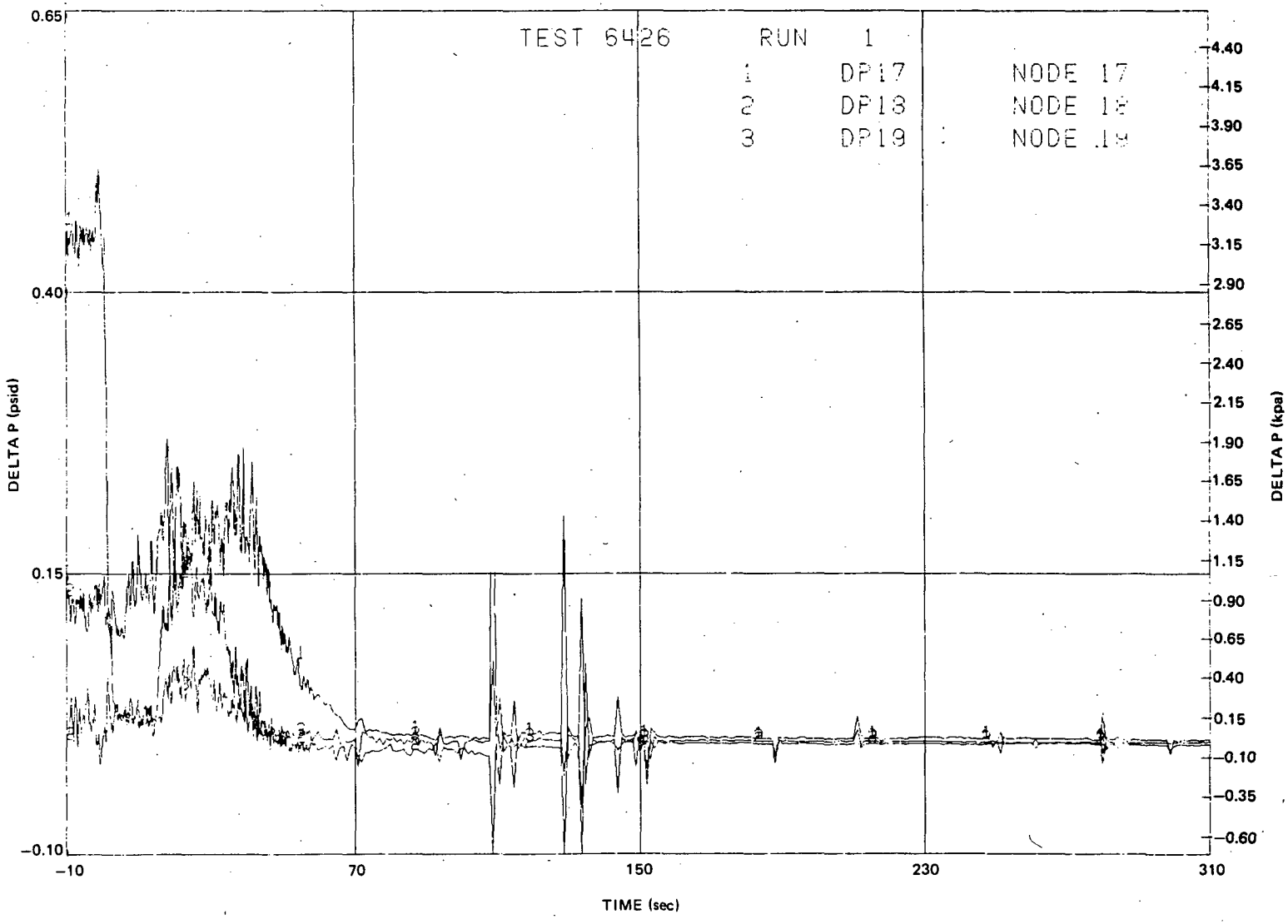

Figure L-17. Upper Plenum Differential Pressures

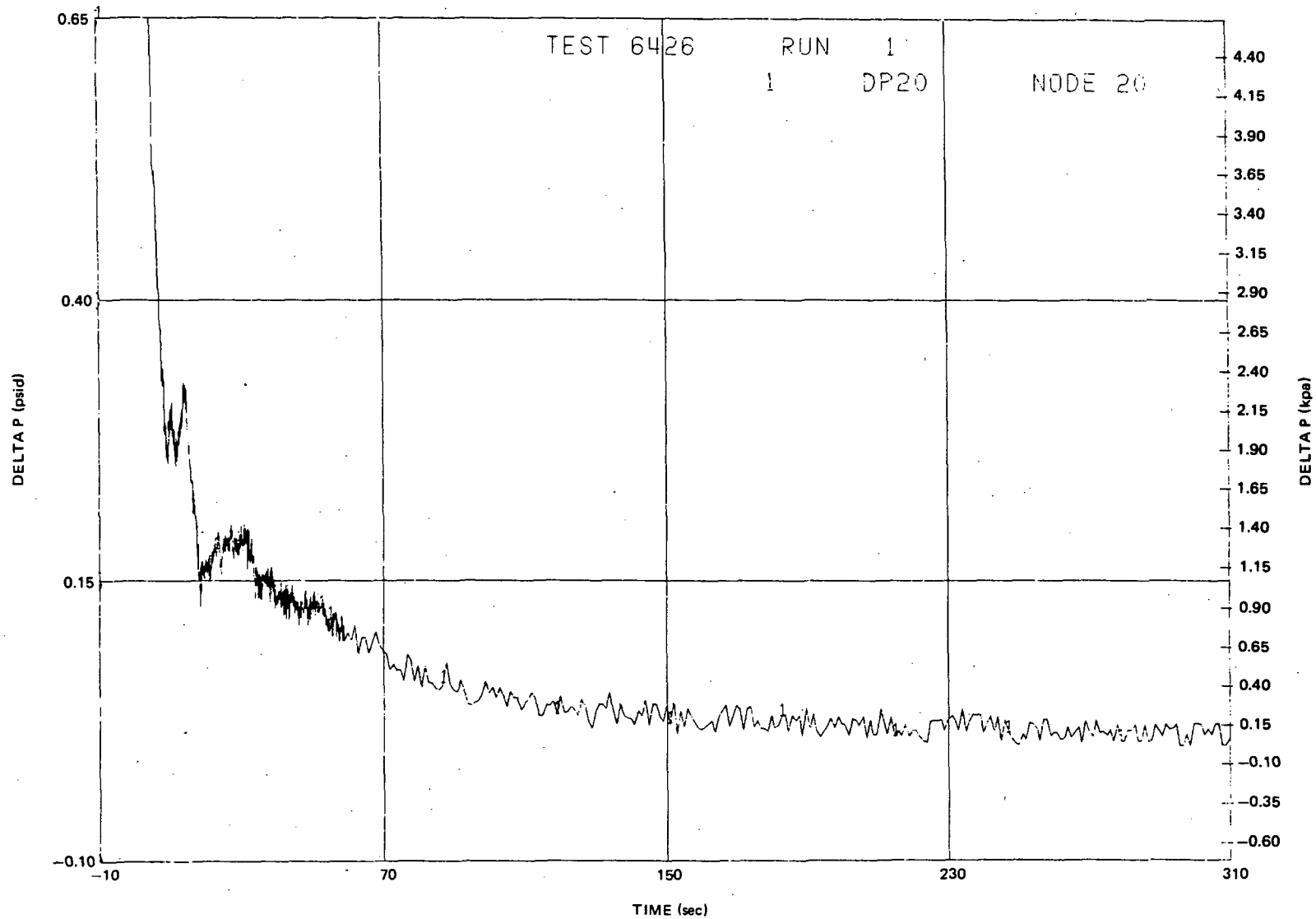

Figure L-18. Steam Separator Differential Pressure

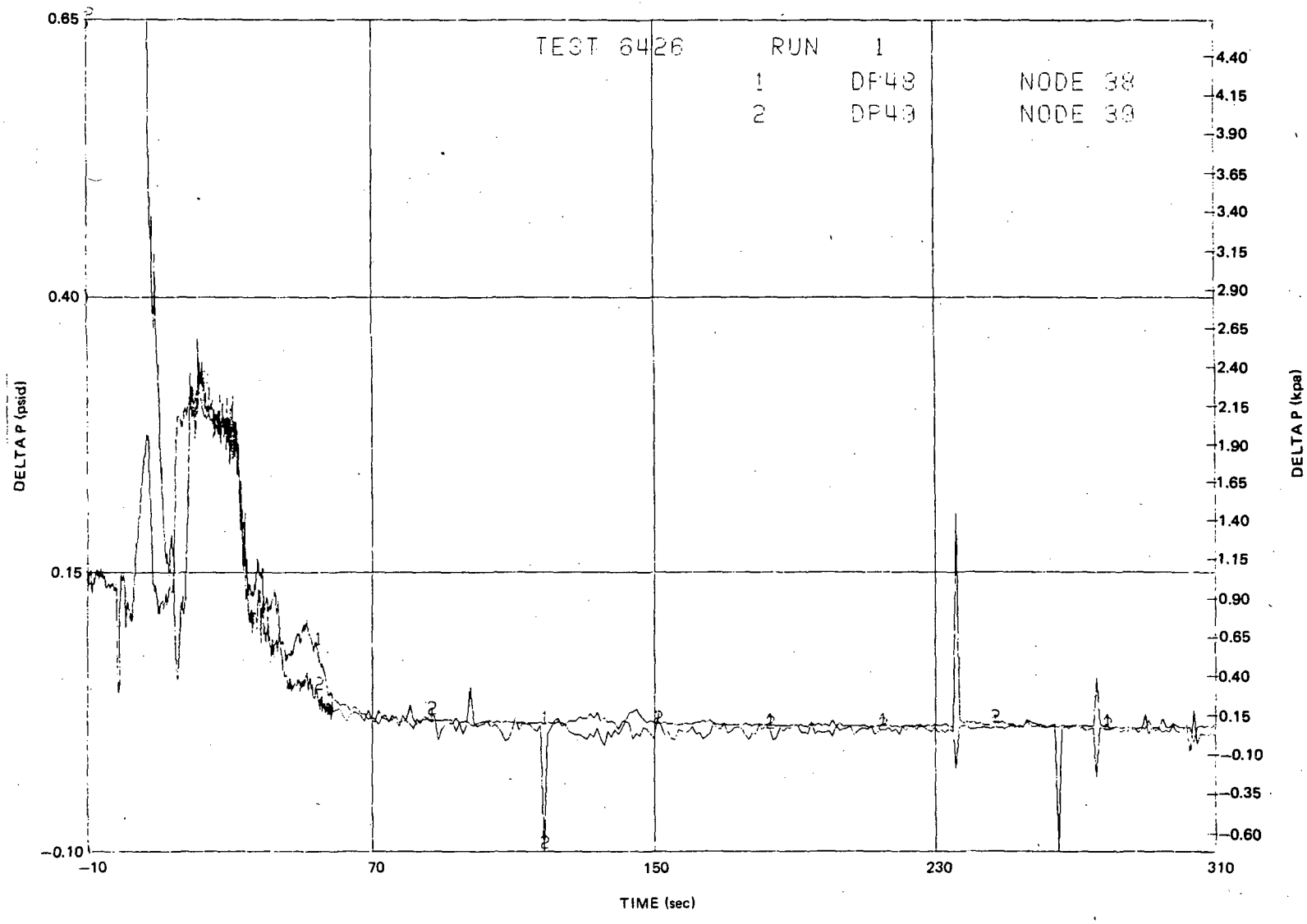

Figure L-19. Intact Loop Jet Pump Differential Pressures

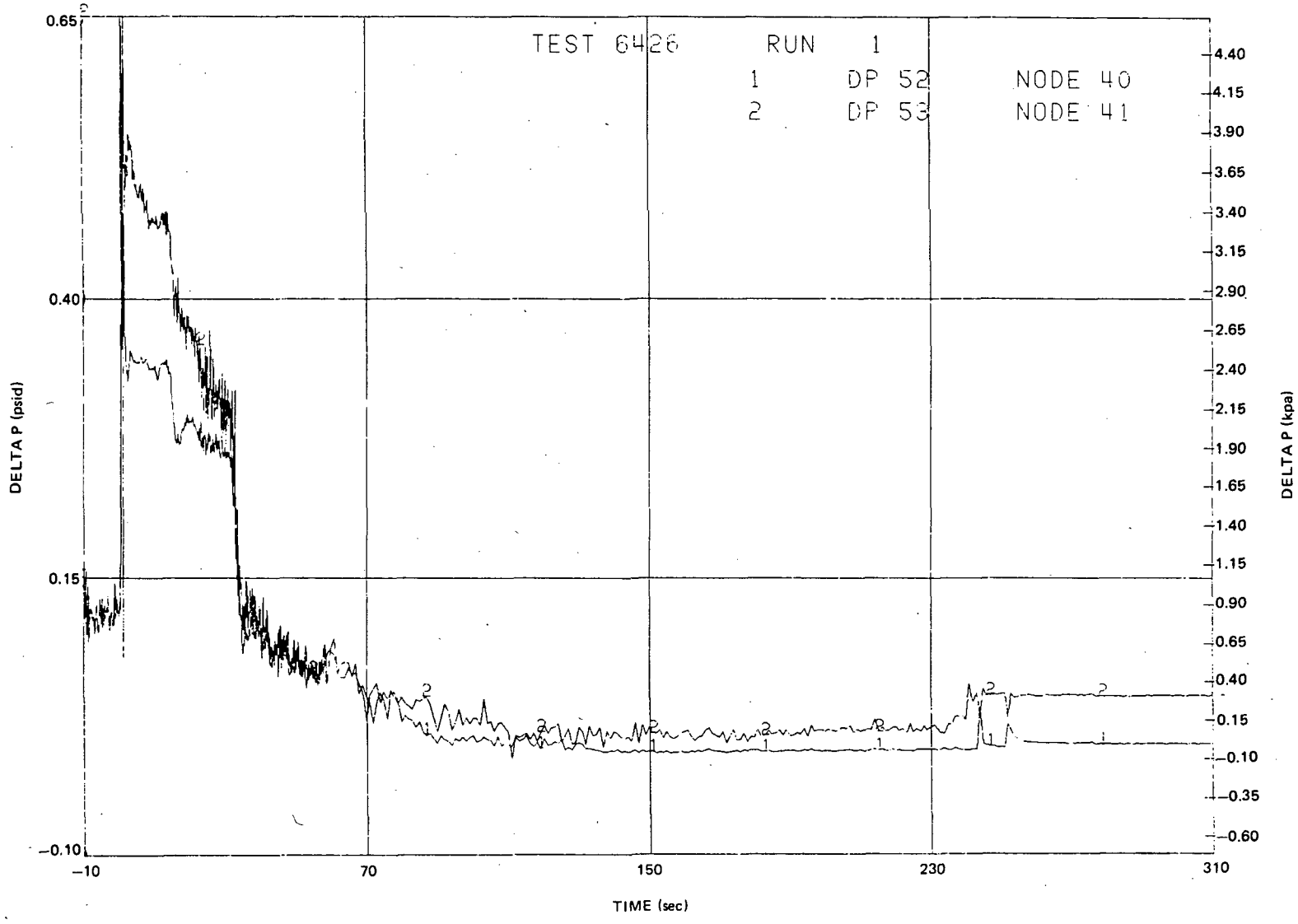

Figure L-20. Broken Loop Jet Pump Differential Pressures

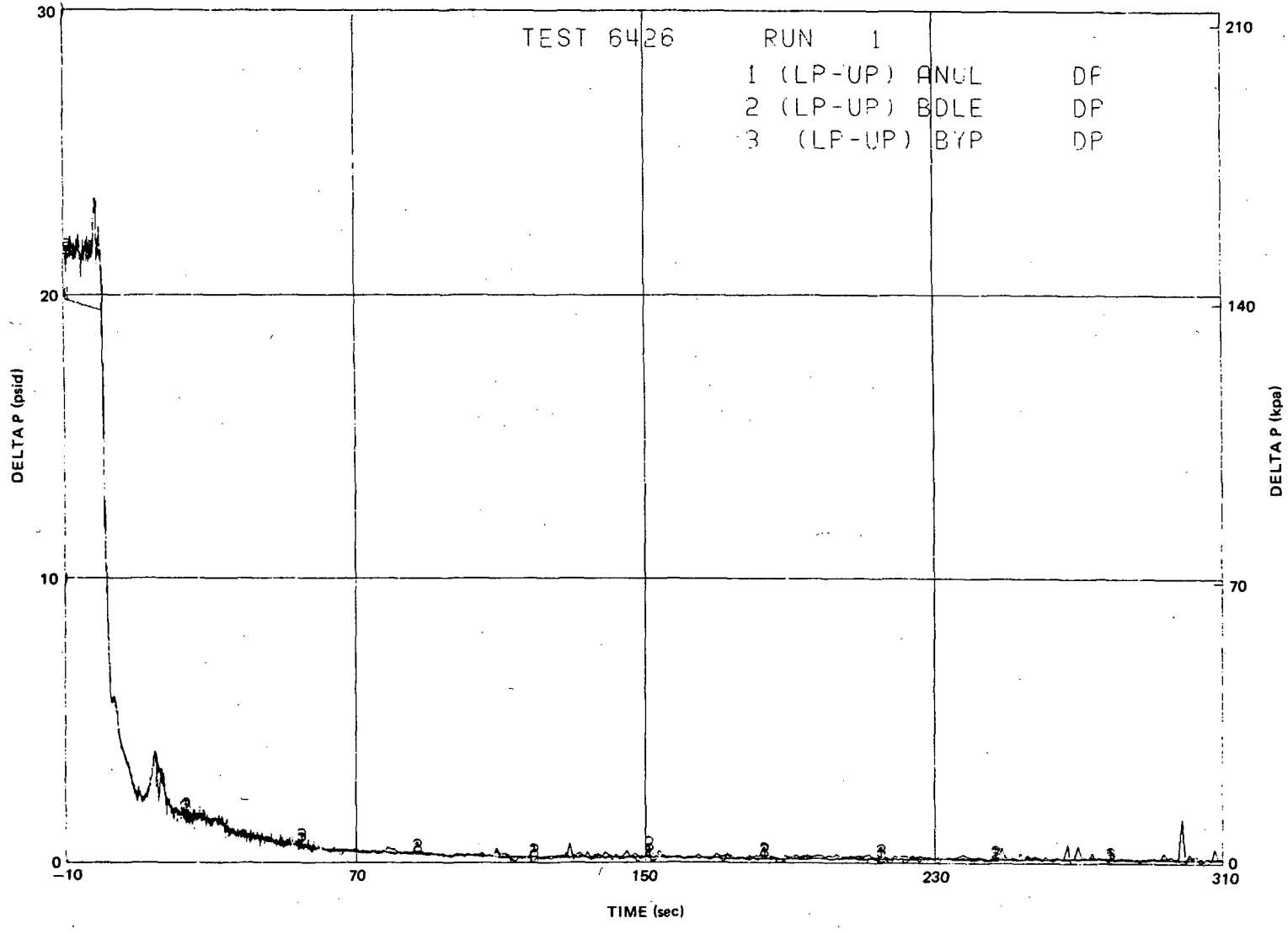

Figure L-21. Lower Plenum to Upper Plenum Differential Pressures for the Annulus, Bundle, and Bypass

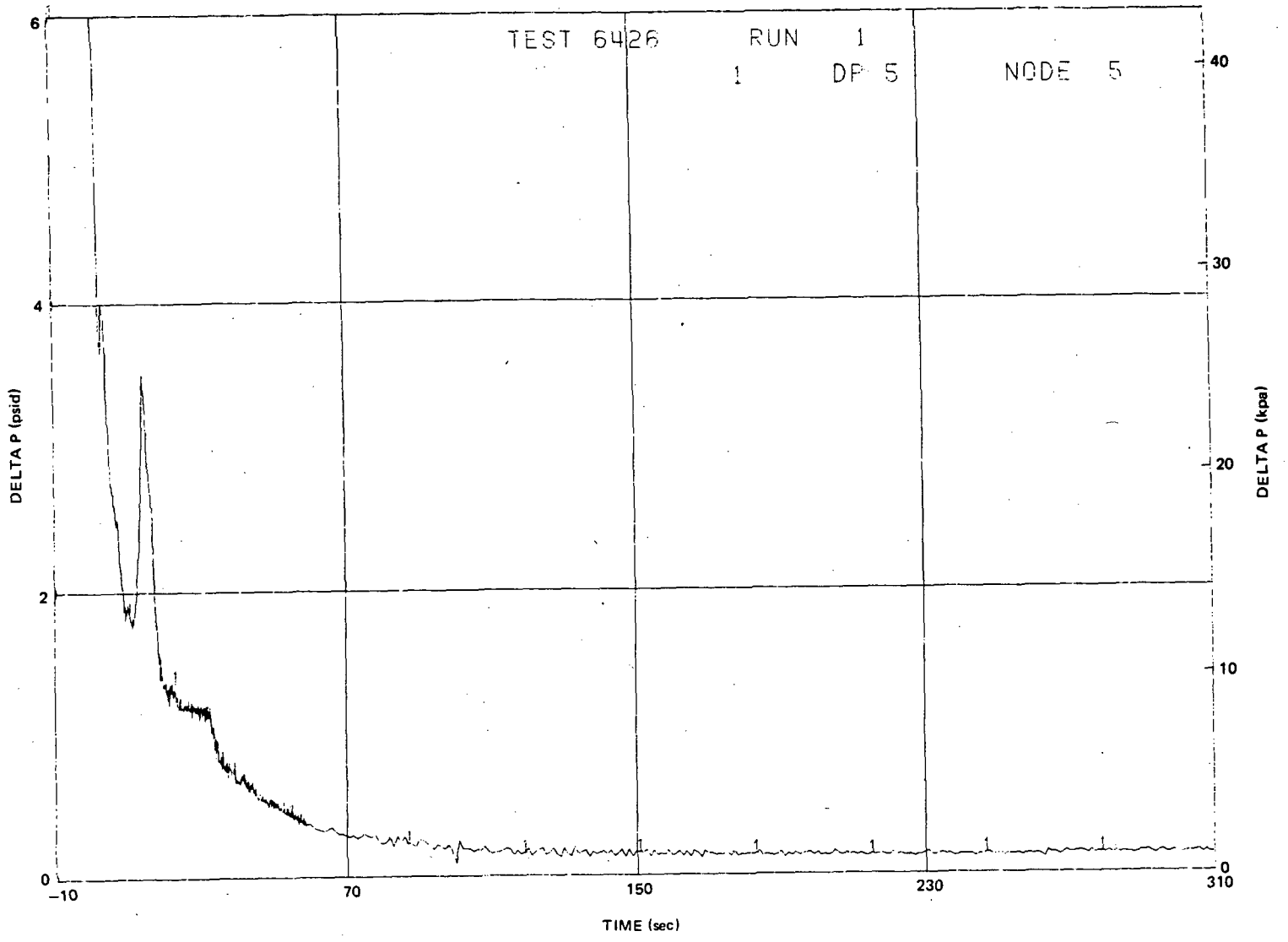

Figure L-22. Lower Plenum to Annulus Differential Pressure

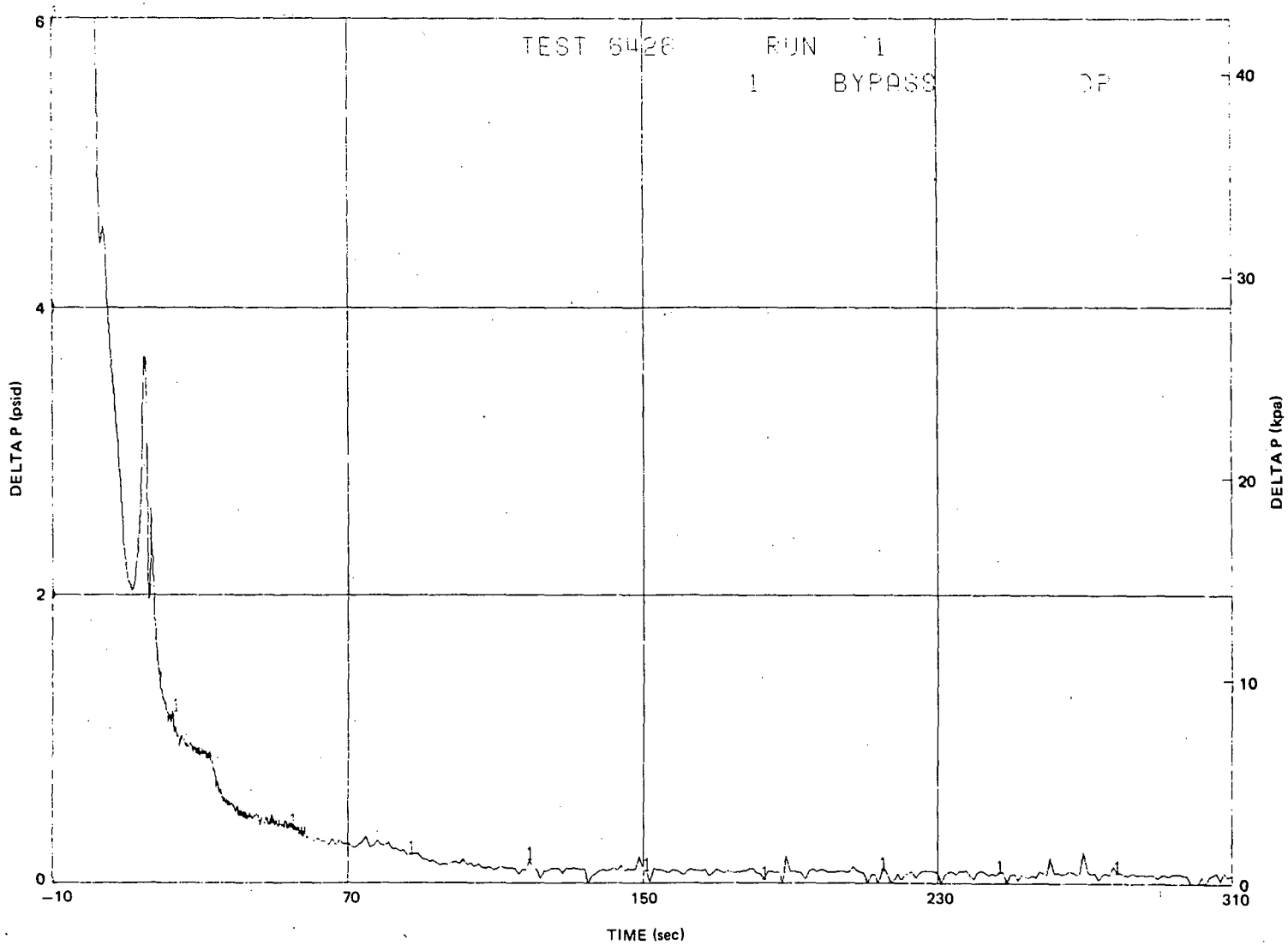

Figure L-23. Bypass Differential Pressure

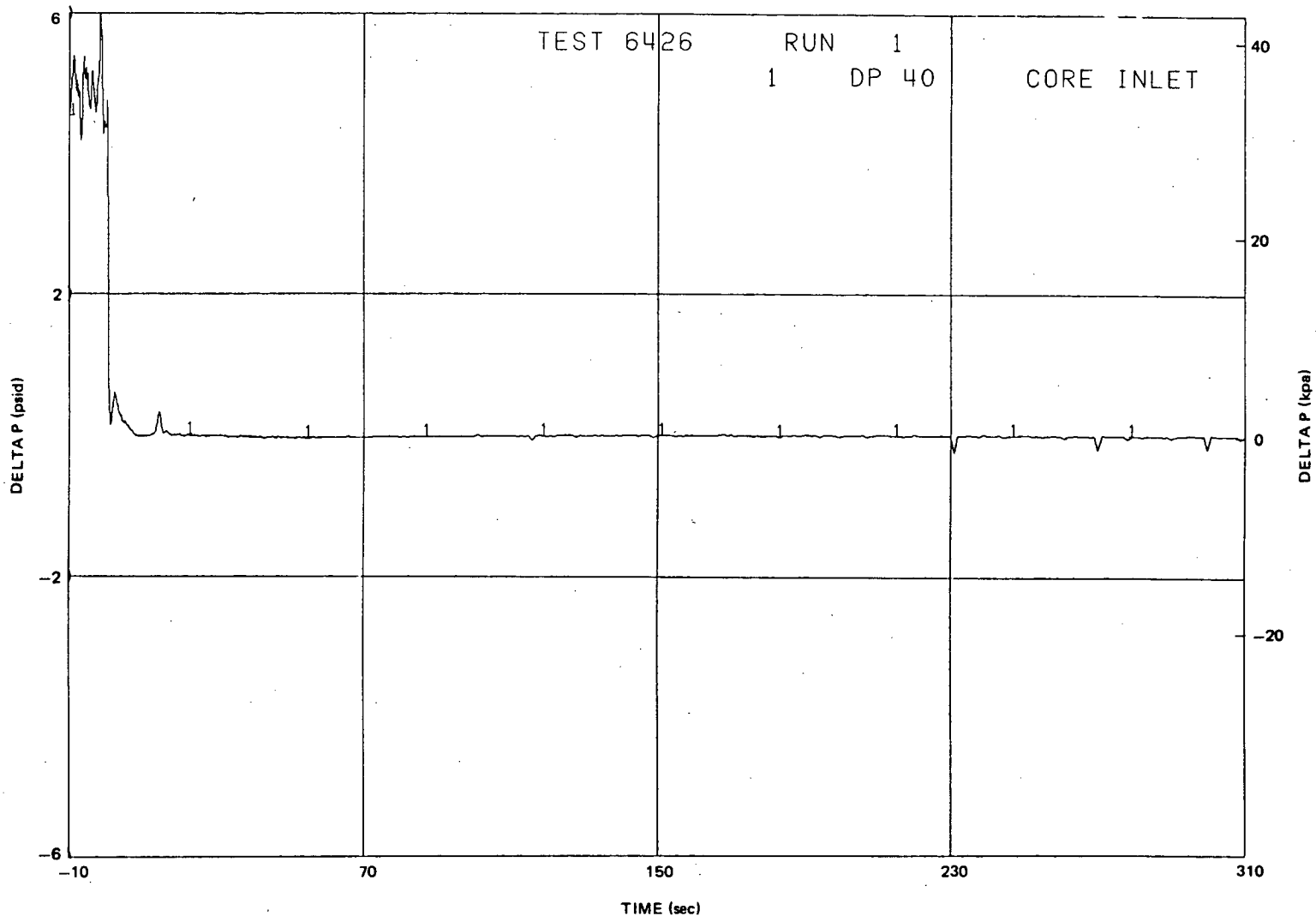

Figure L-24. Bundle Inlet Side Entry Orifice Differential Pressure

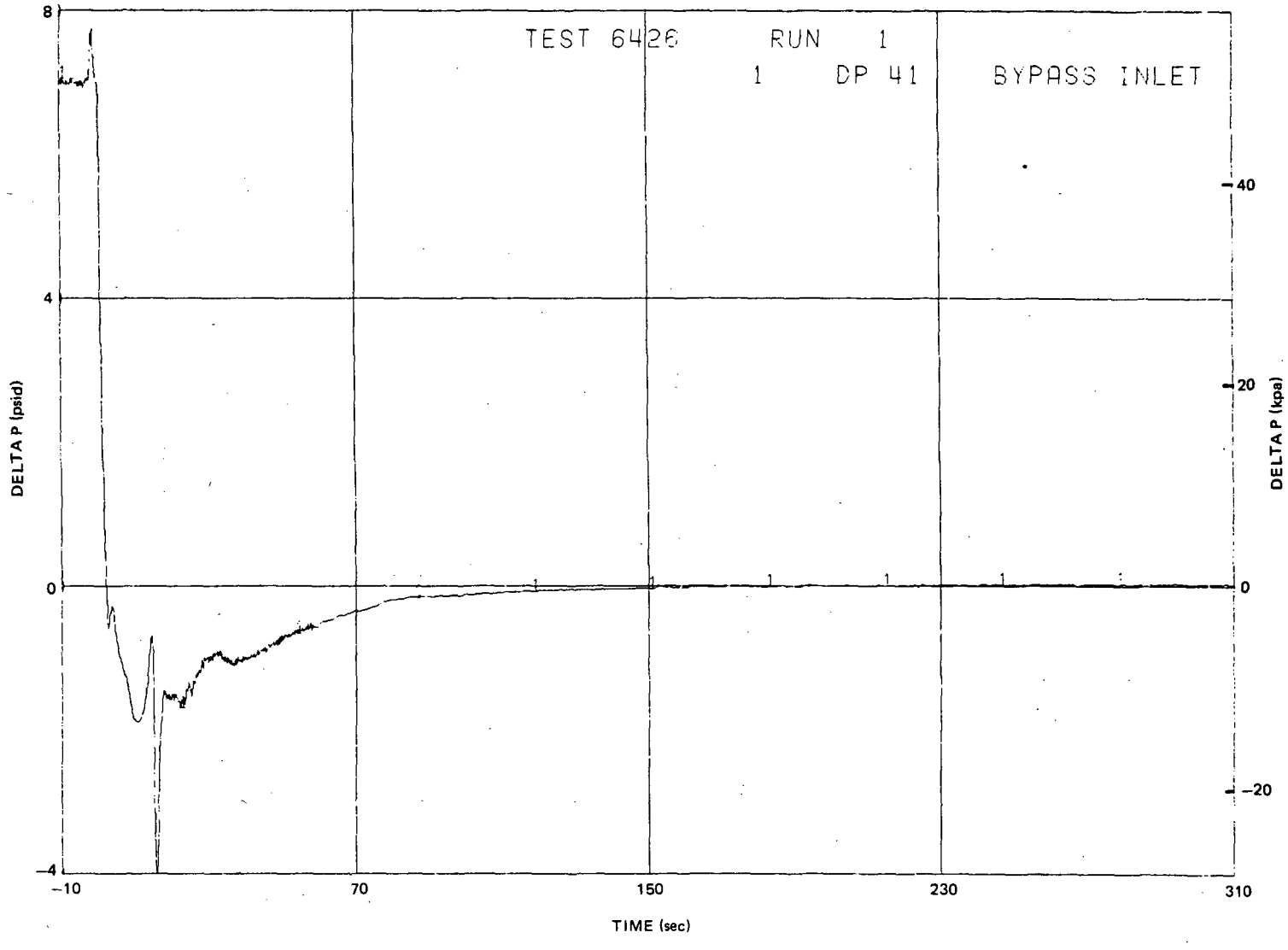

Figure L-25. Bypass Leakage Path Differential Pressure

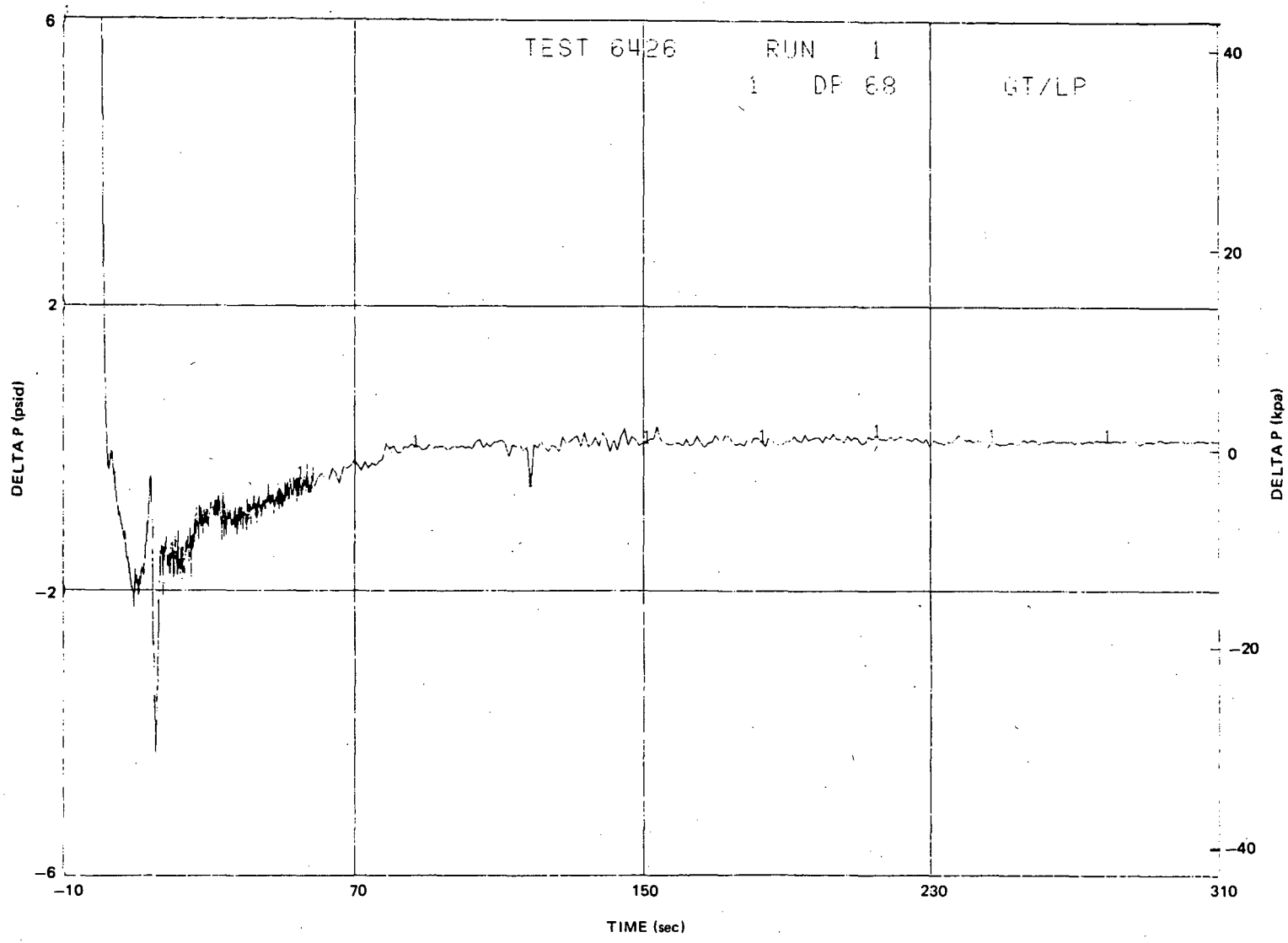

Figure L-26. Lower Plenum to Guide Tube Differential Pressure

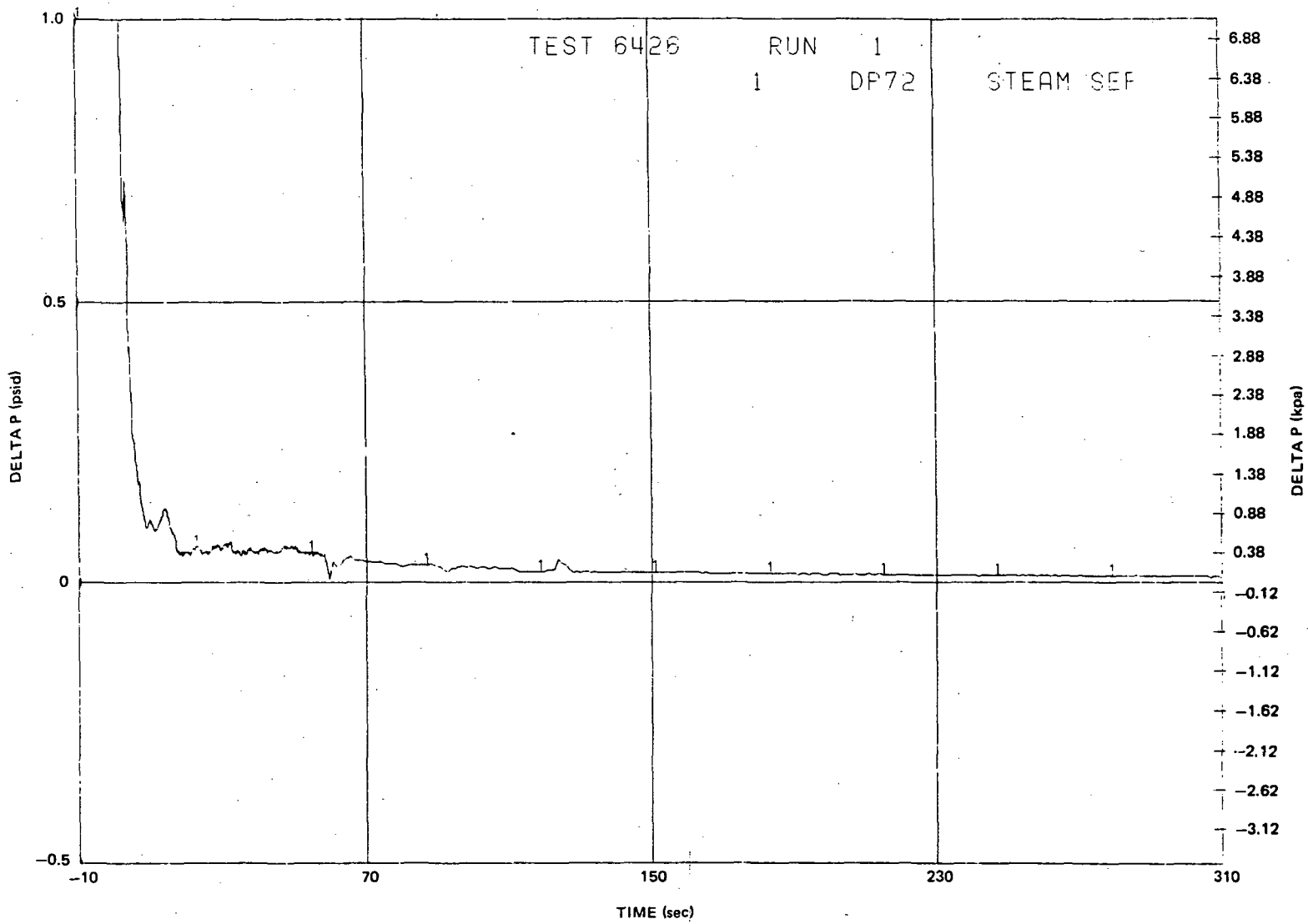

Figure L-27. Upper Plenum Exit Differential Pressure

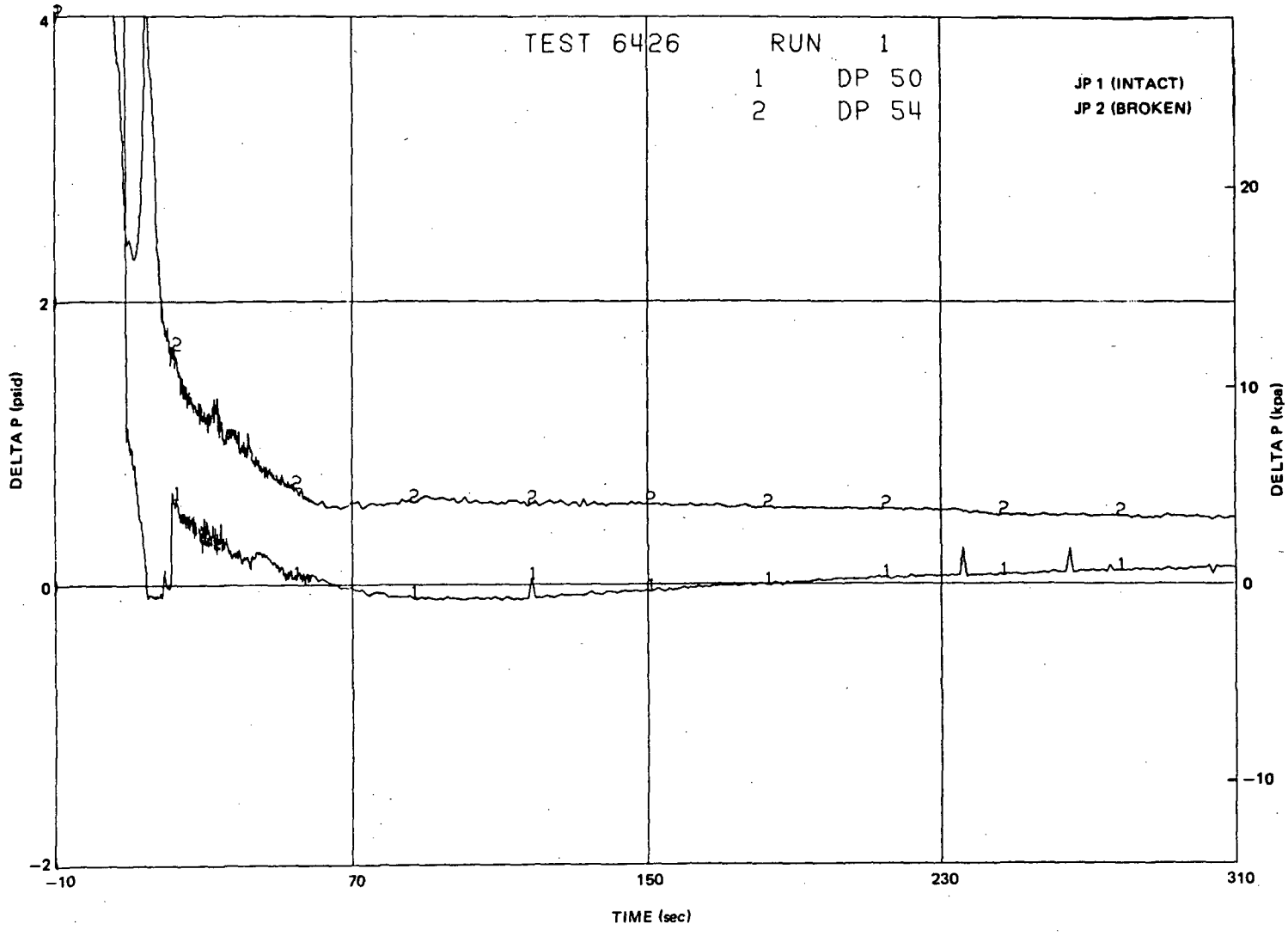

Figure L-28. Intact Loop and Broken Loop Jet Pump Diffuser to Throat Differential Pressure

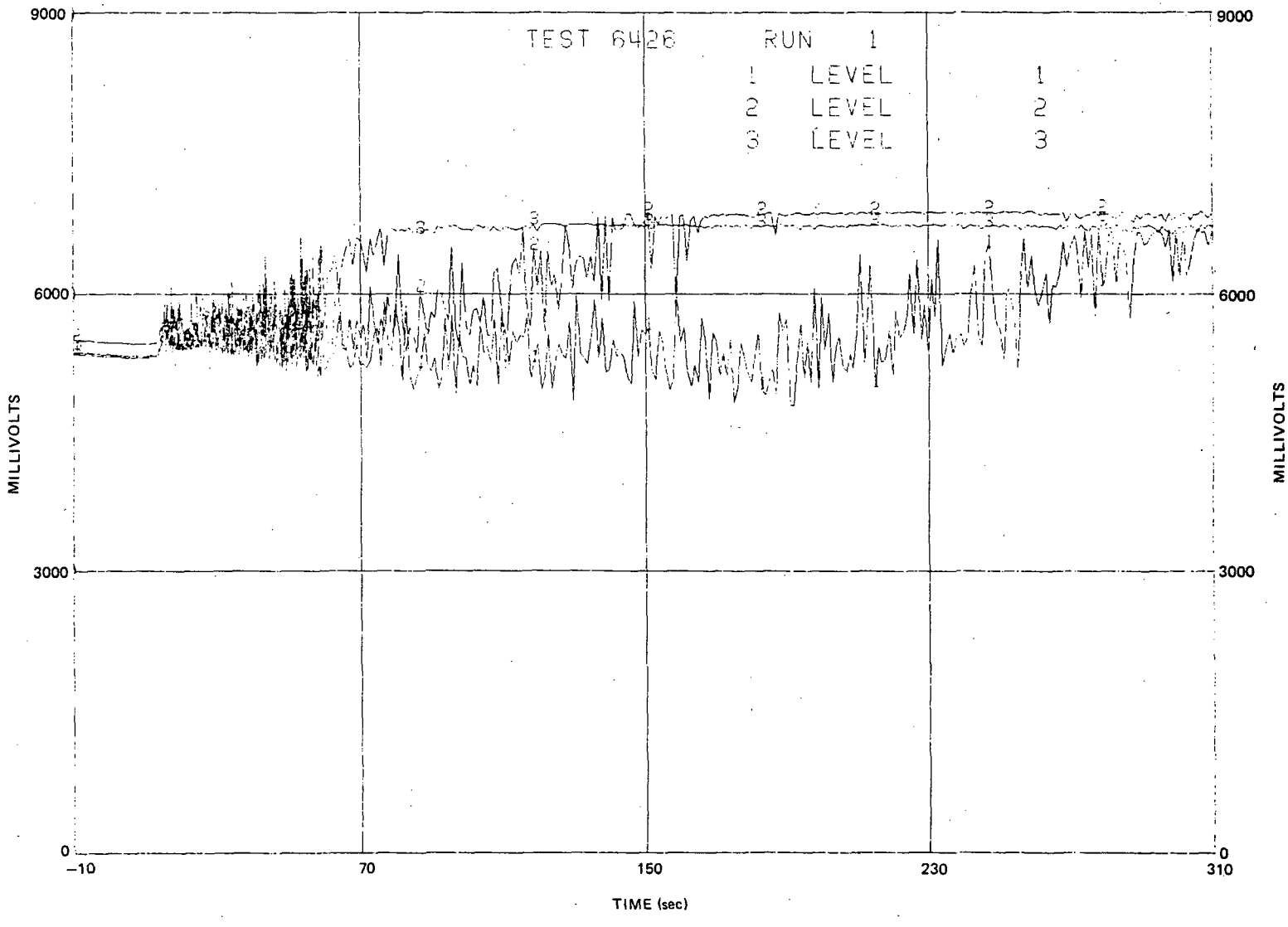

Figure L-29. Bottom Lower Plenum Conductivity Probe Measurements

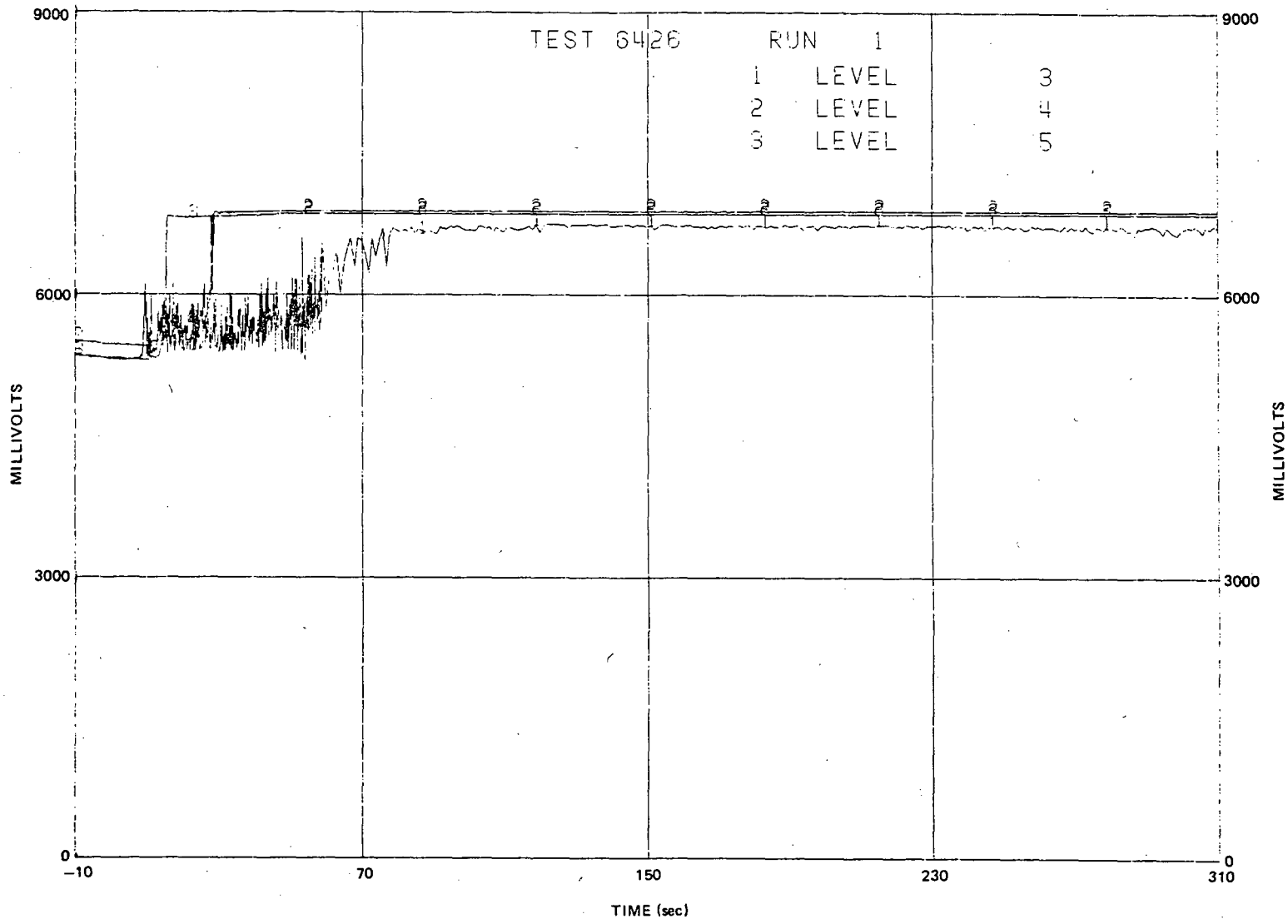

Figure L-30. Upper Lower Plenum Conductivity Probe Measurements

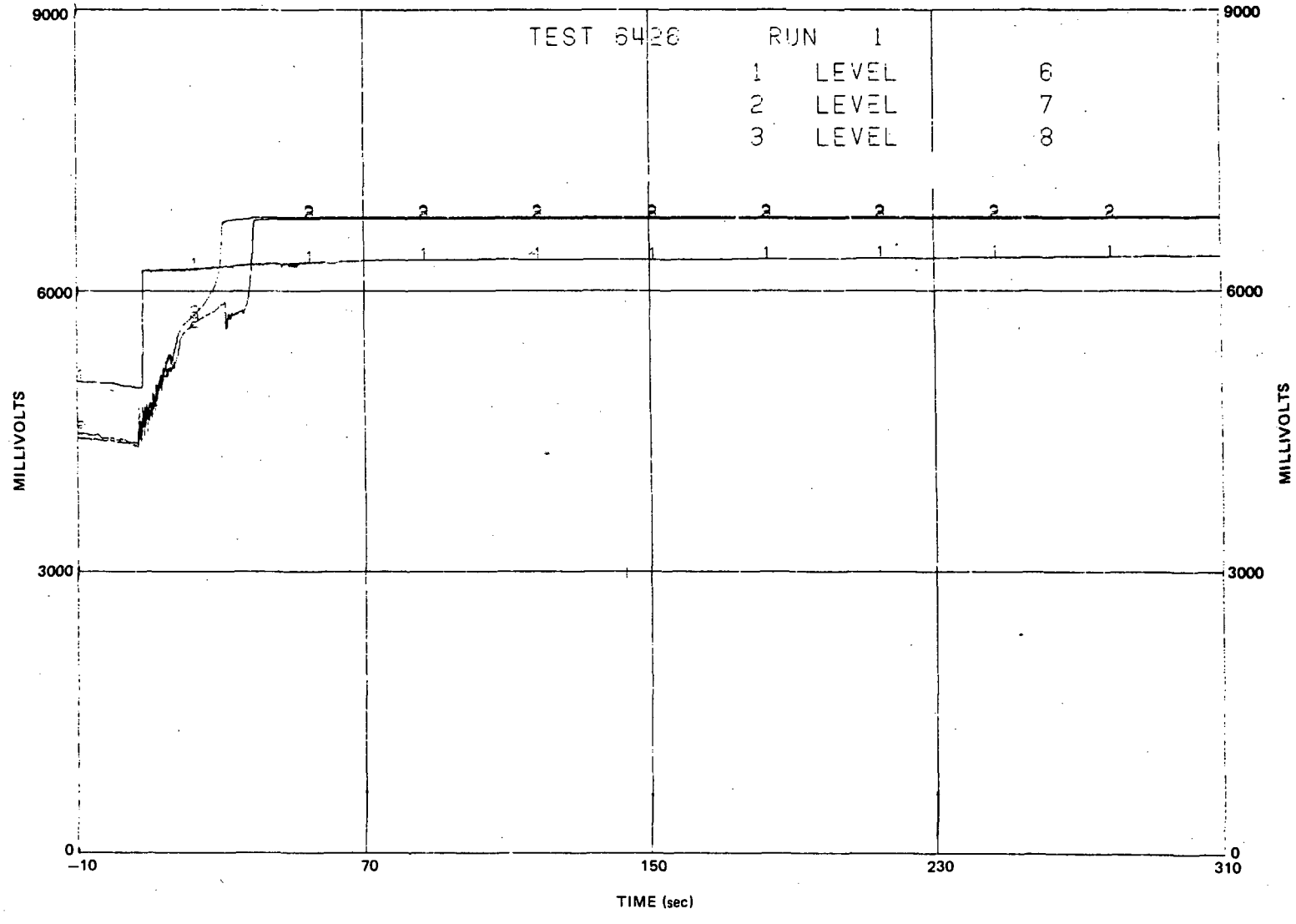

Figure L-31. Lower Annulus Conductivity Probe Measurements

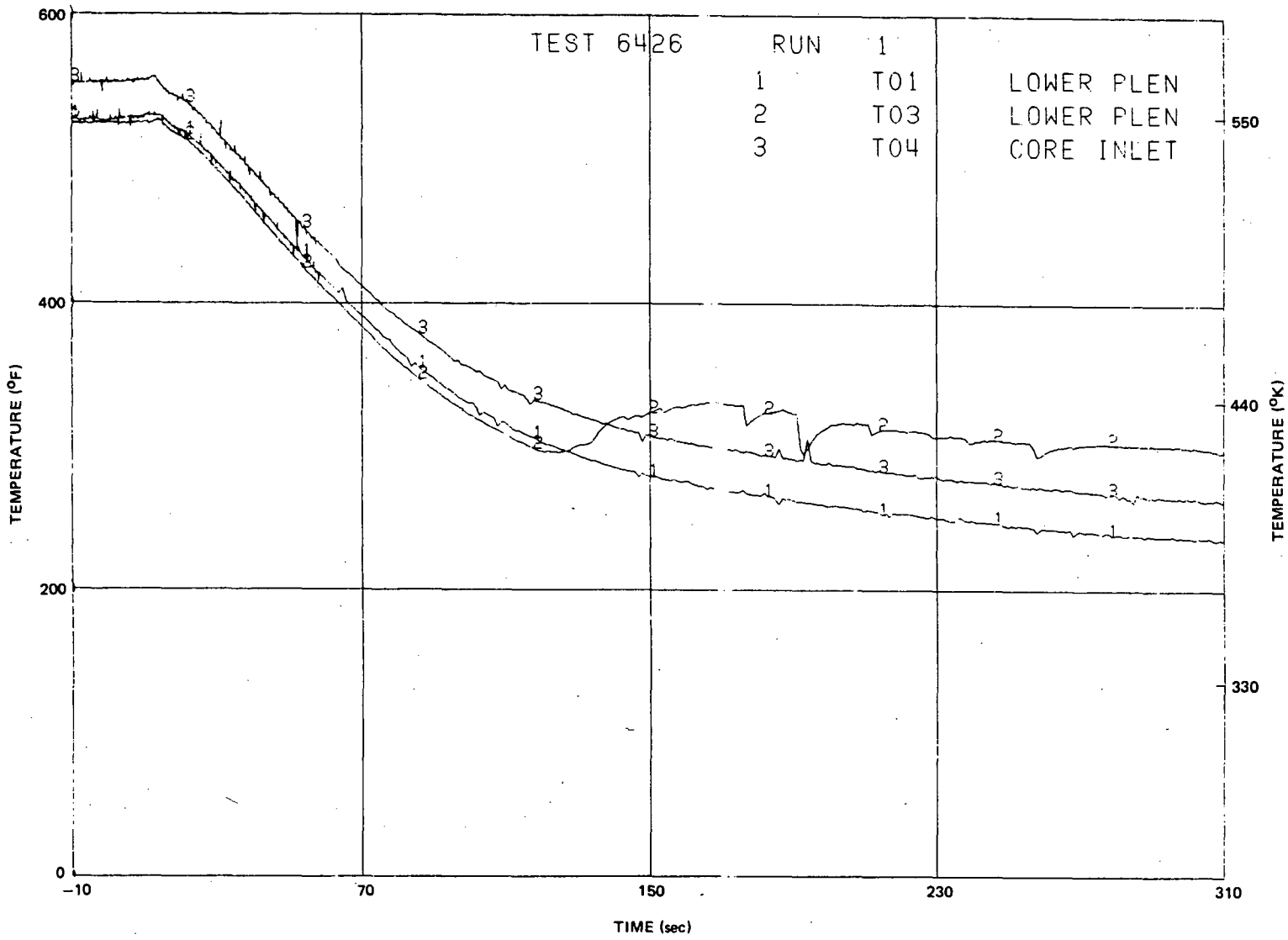

Figure L-32. Lower Plenum Fluid Temperatures

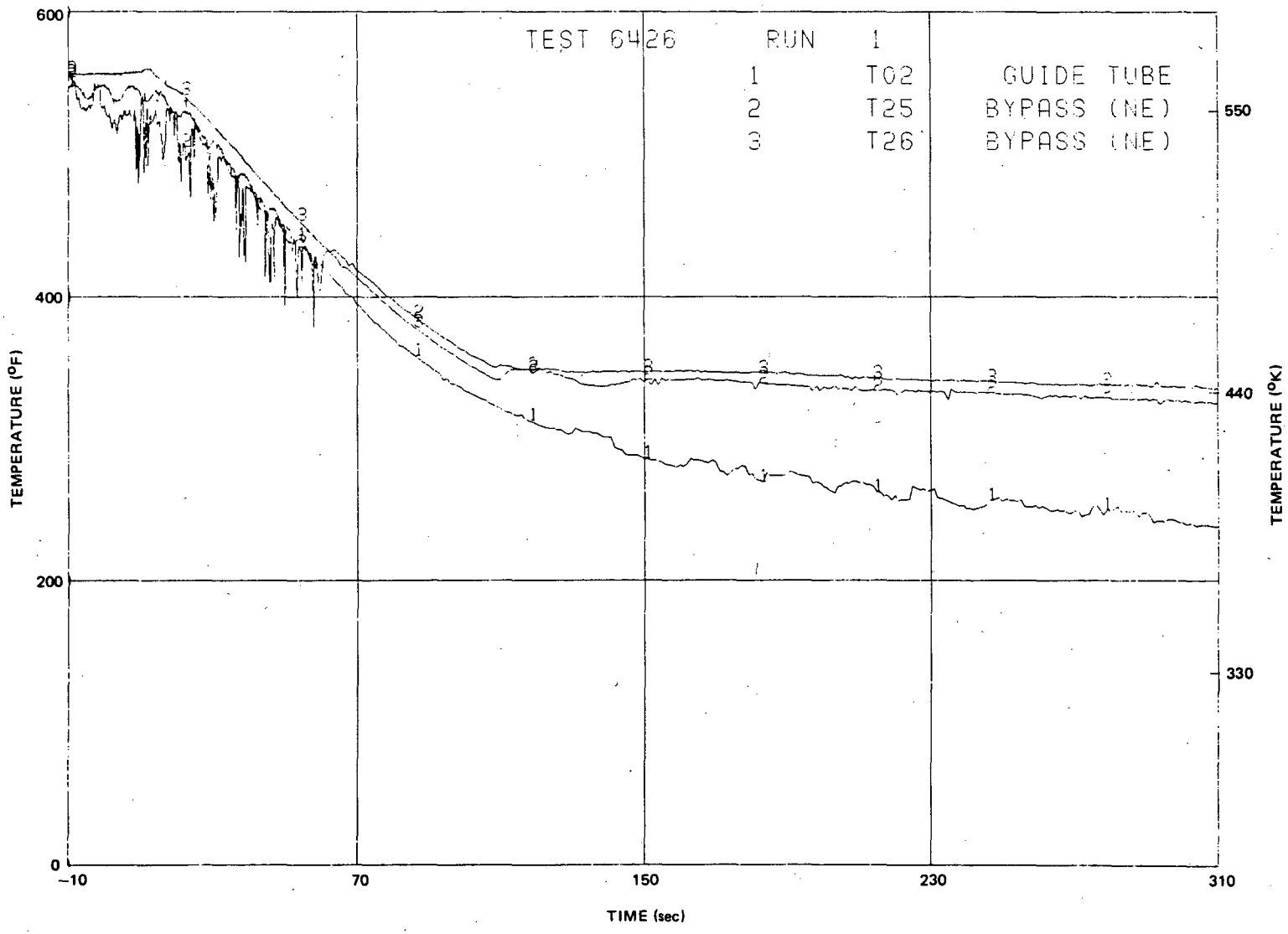

Figure L-33. Guide Tube and Bypass Fluid Temperatures

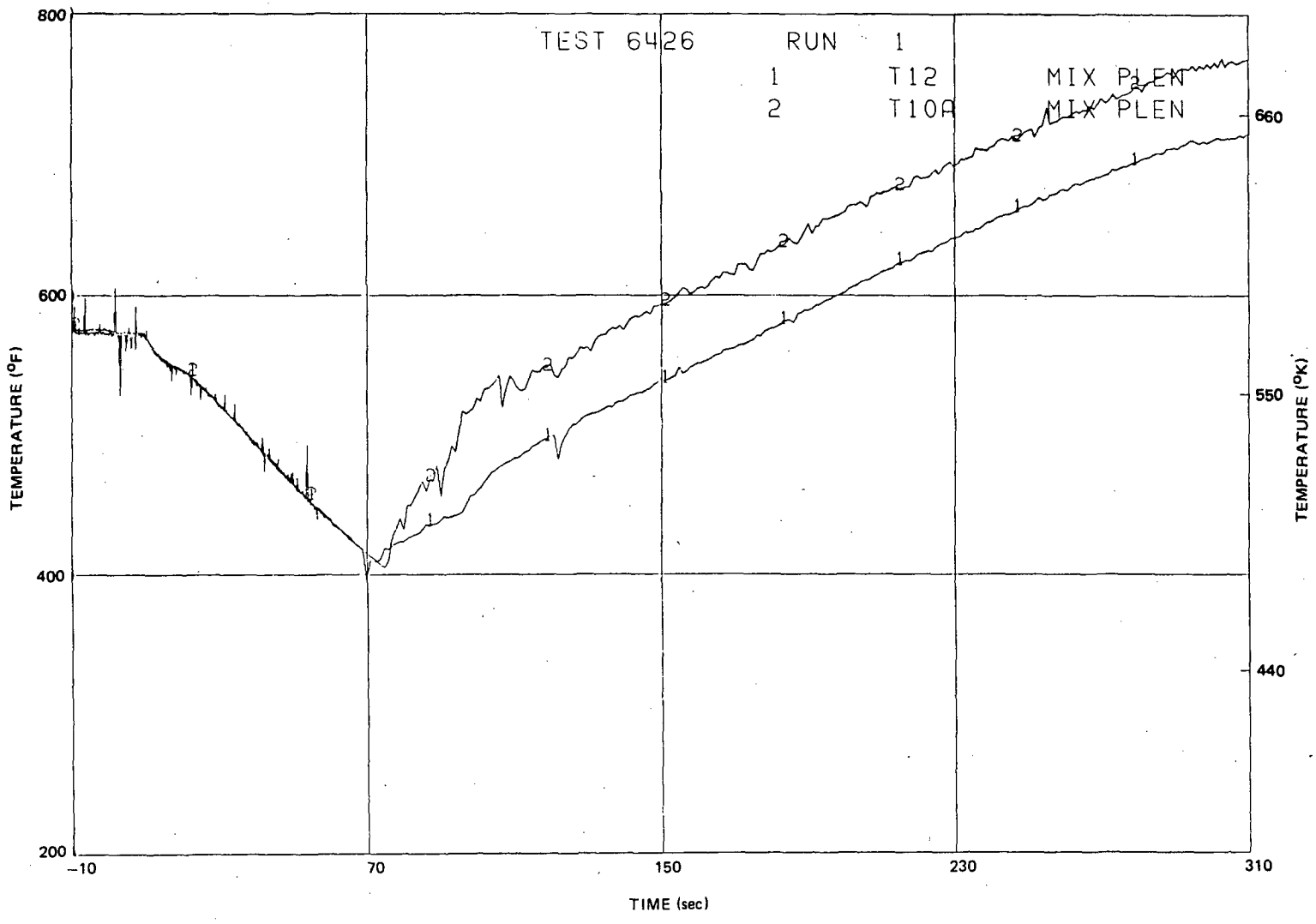

Figure L-34. Mixing Plenum Fluid Temperatures

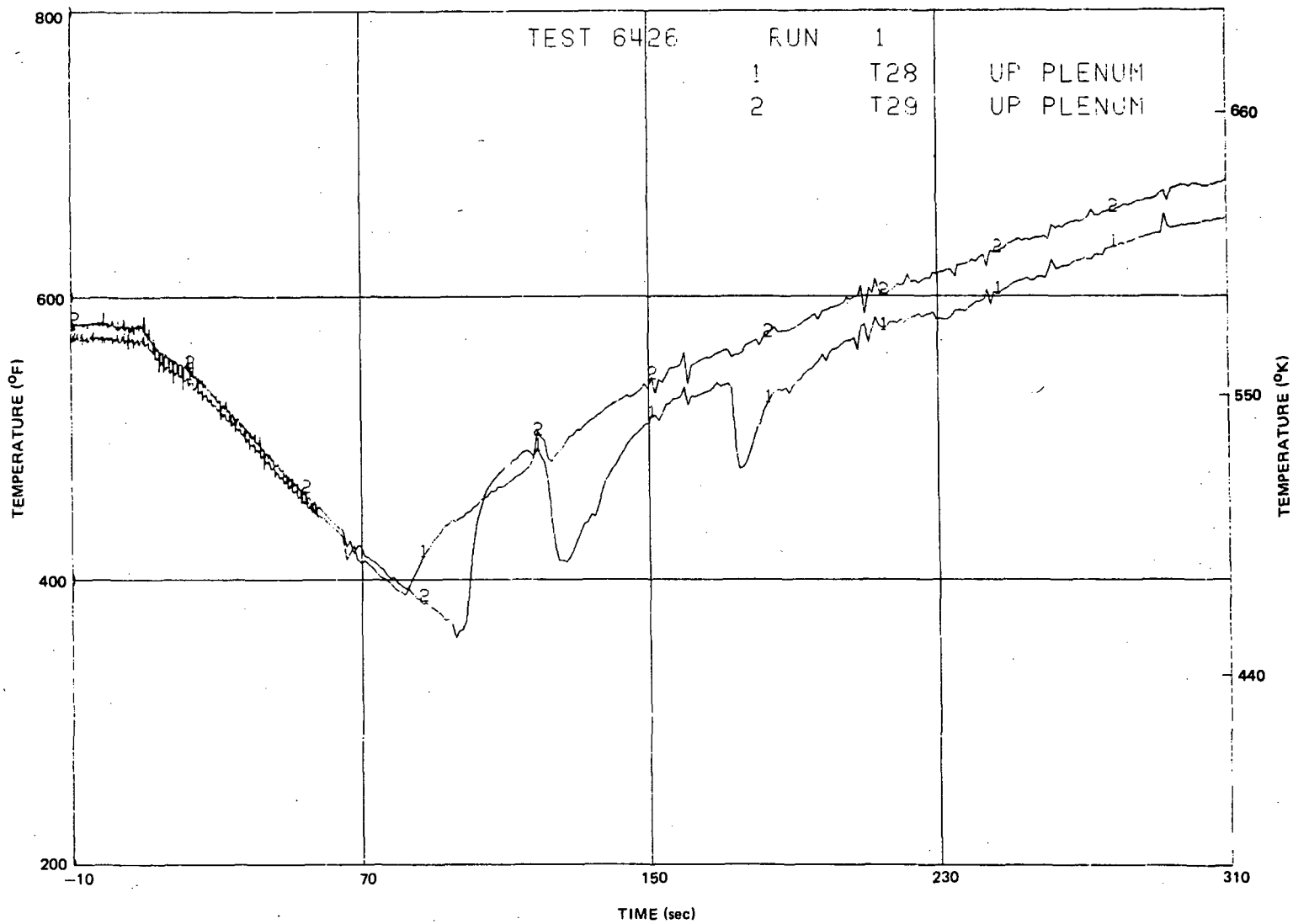

Figure L-35. Upper Plenum Fluid Temperatures

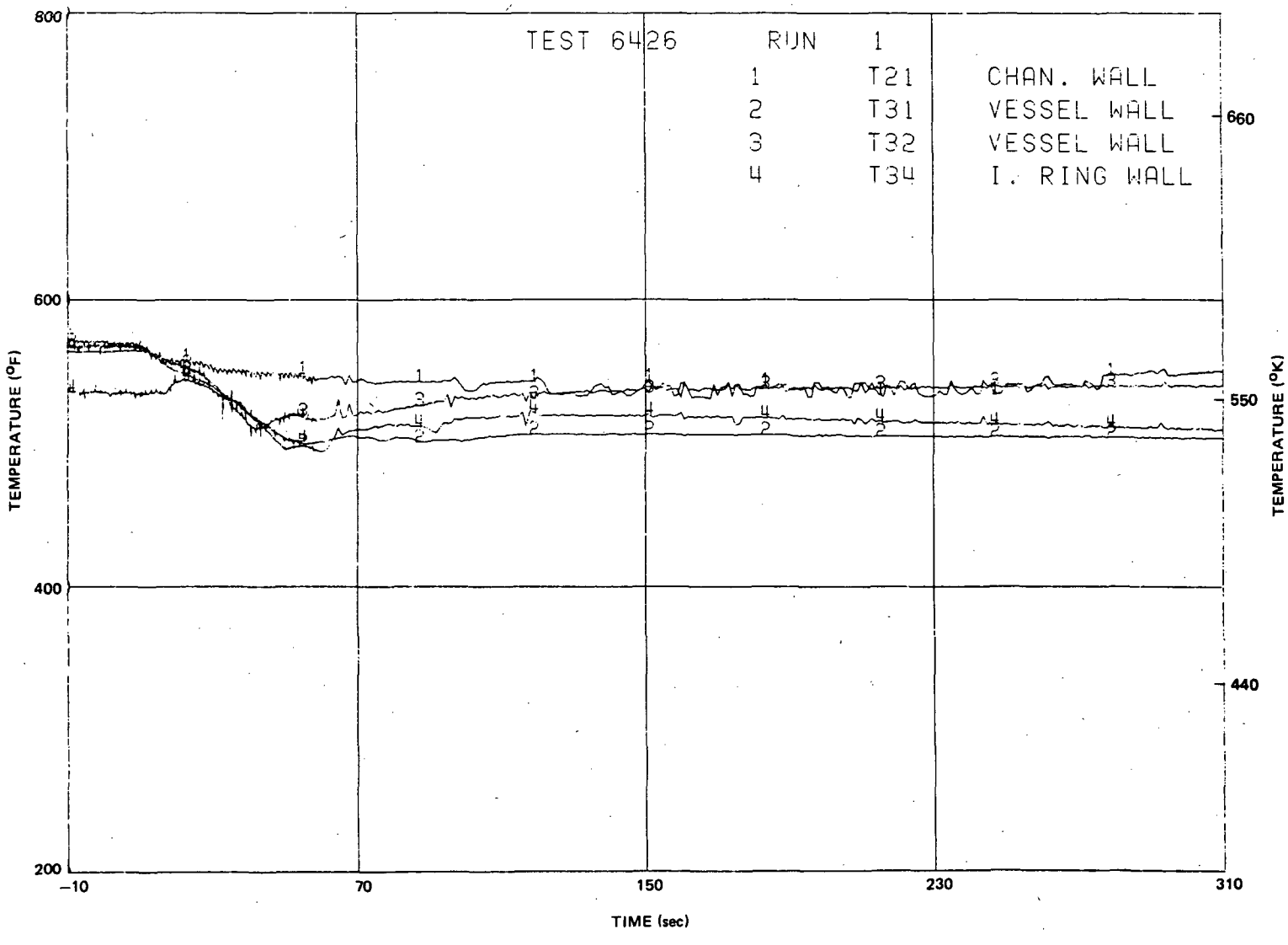

Figure L-36. Wall Temperatures

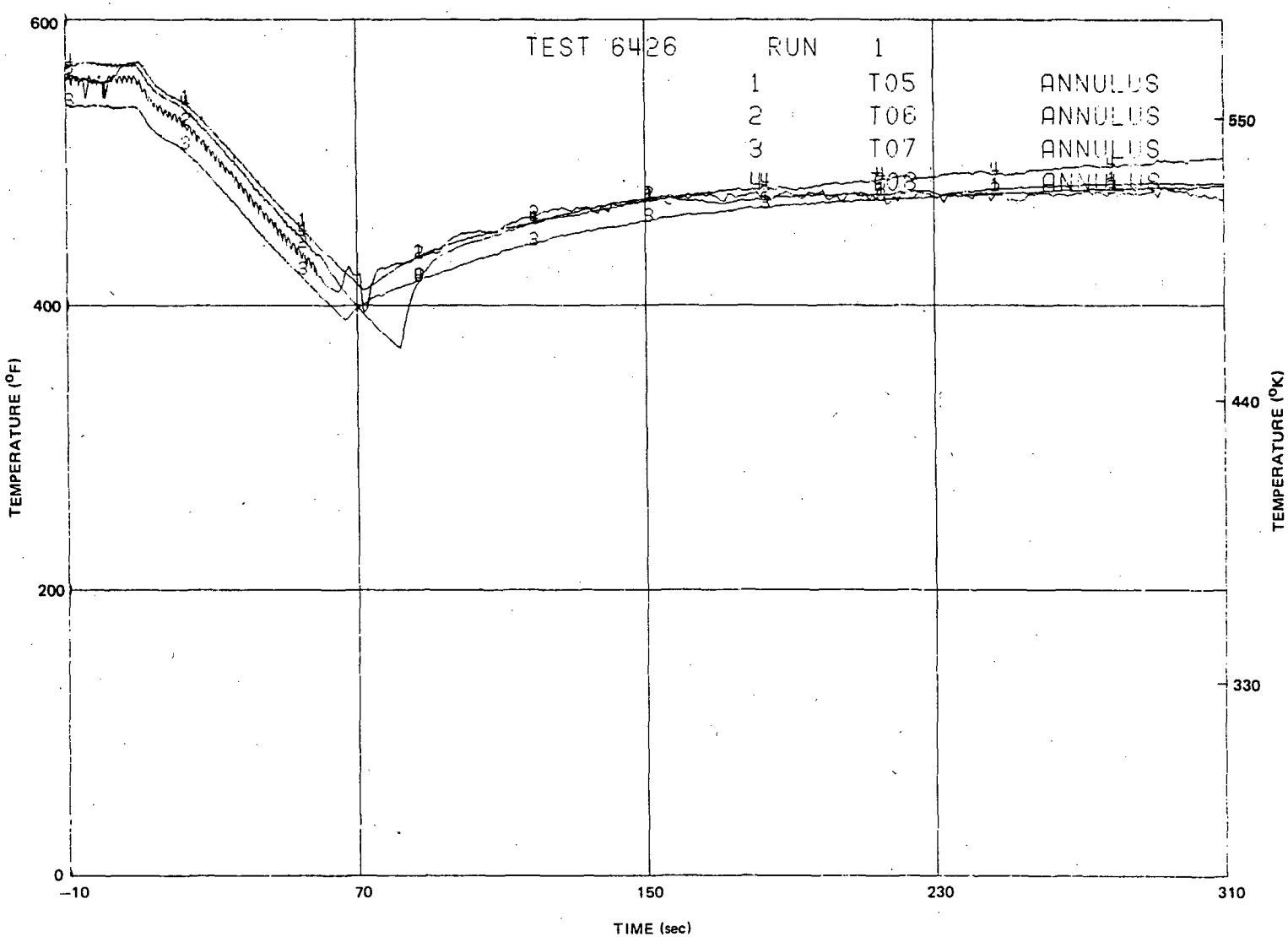

Figure L-37. Annulus Fluid Temperatures

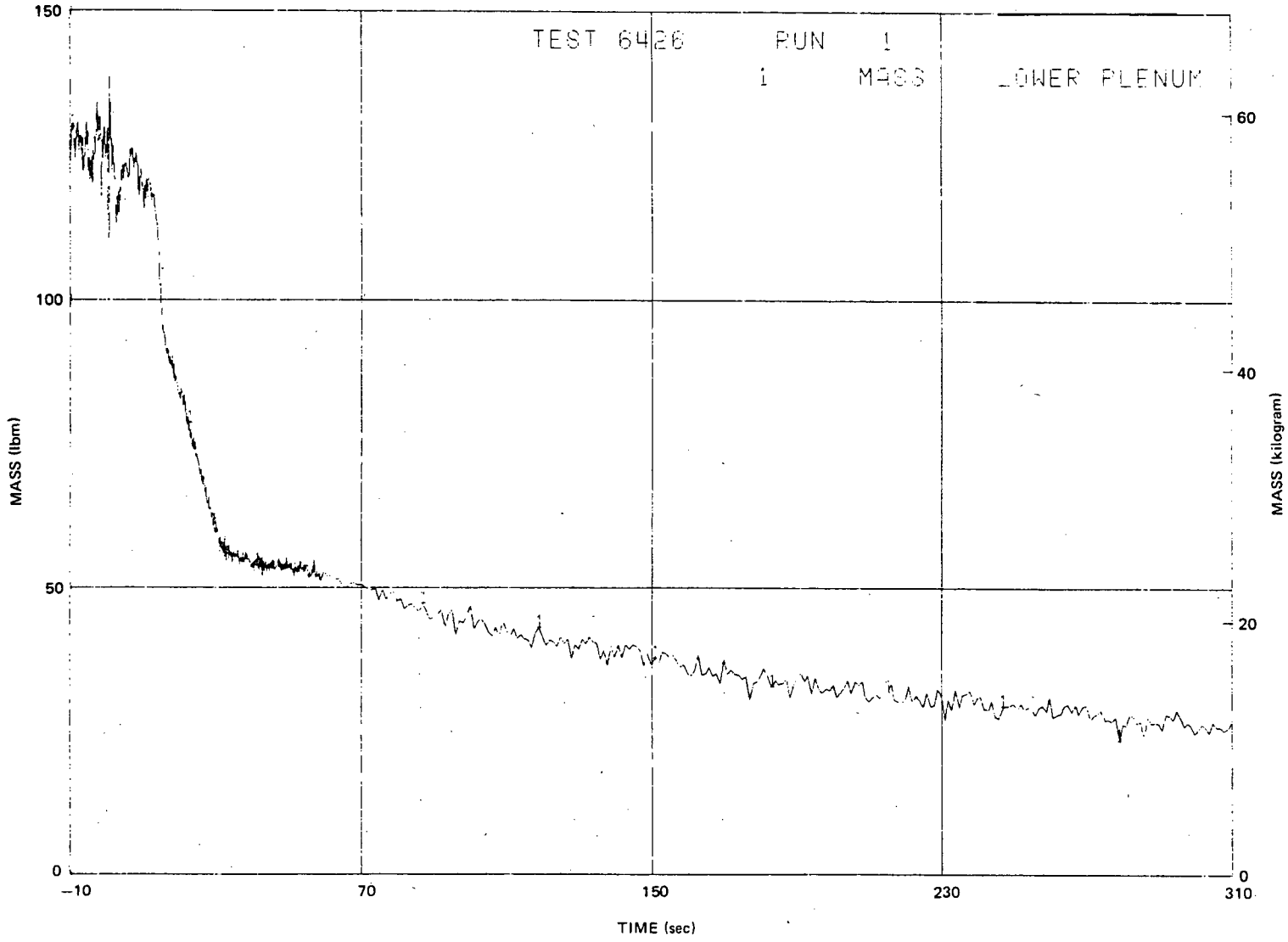

Figure L-38. Lower Plenum Fluid Mass

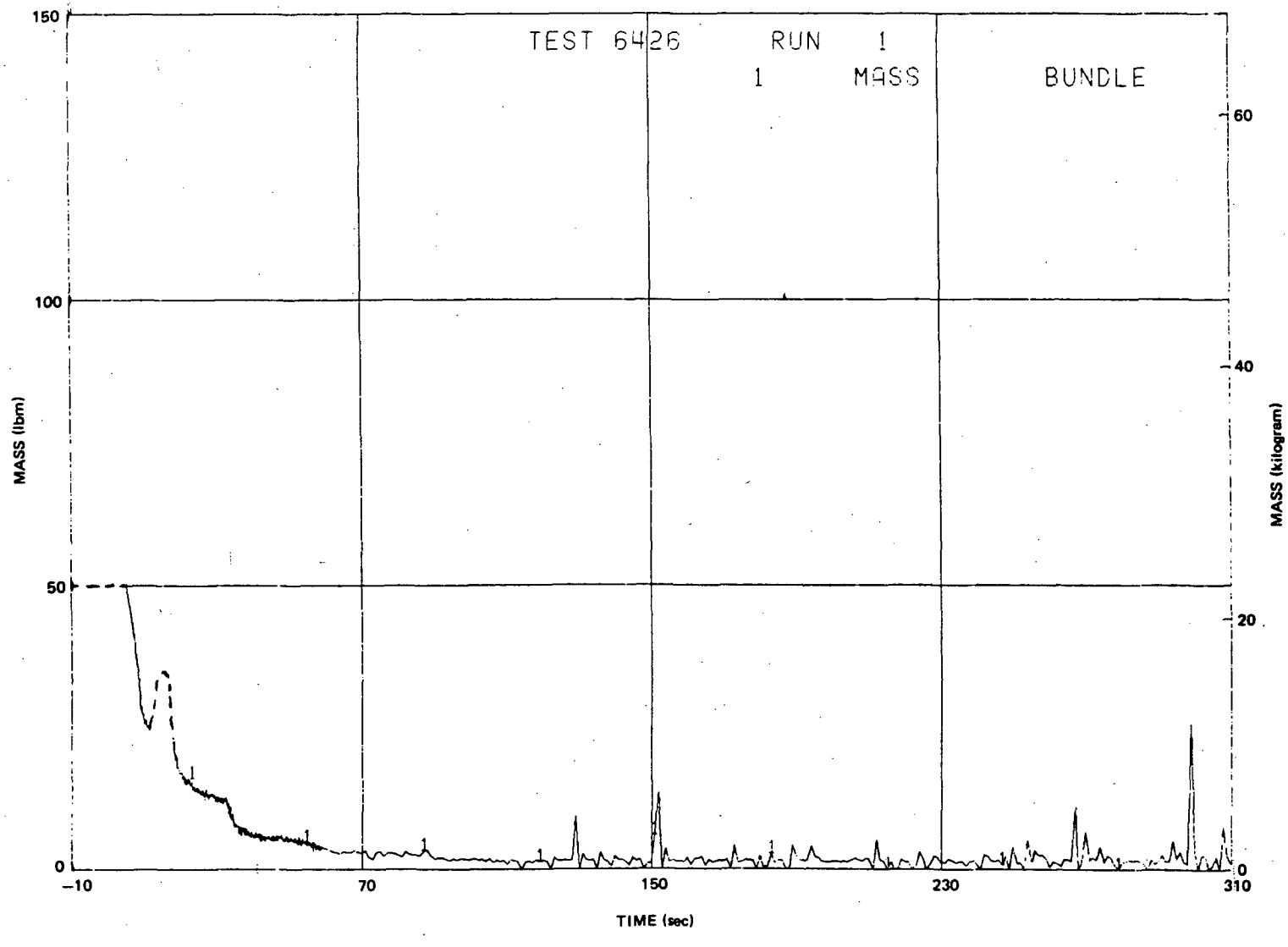
TEST 6426 RUN 1
1 MASS BUNDLE
150
100
50
0
MASS (lbm)
60
40
20
0
MASS (kilogram)
-10
70
150
230
310
TIME (sec)

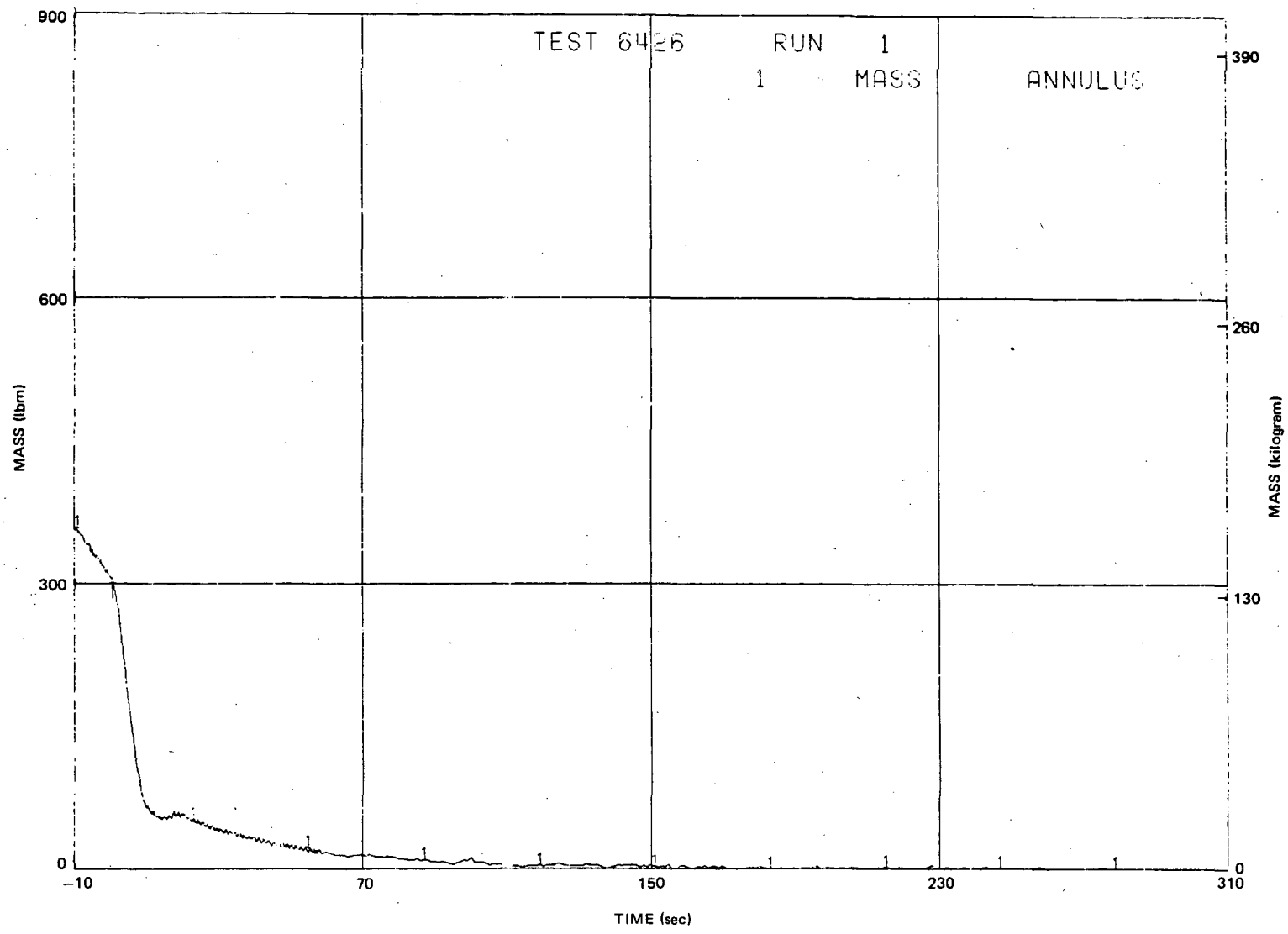

Figure L-40. Annulus Fluid Mass

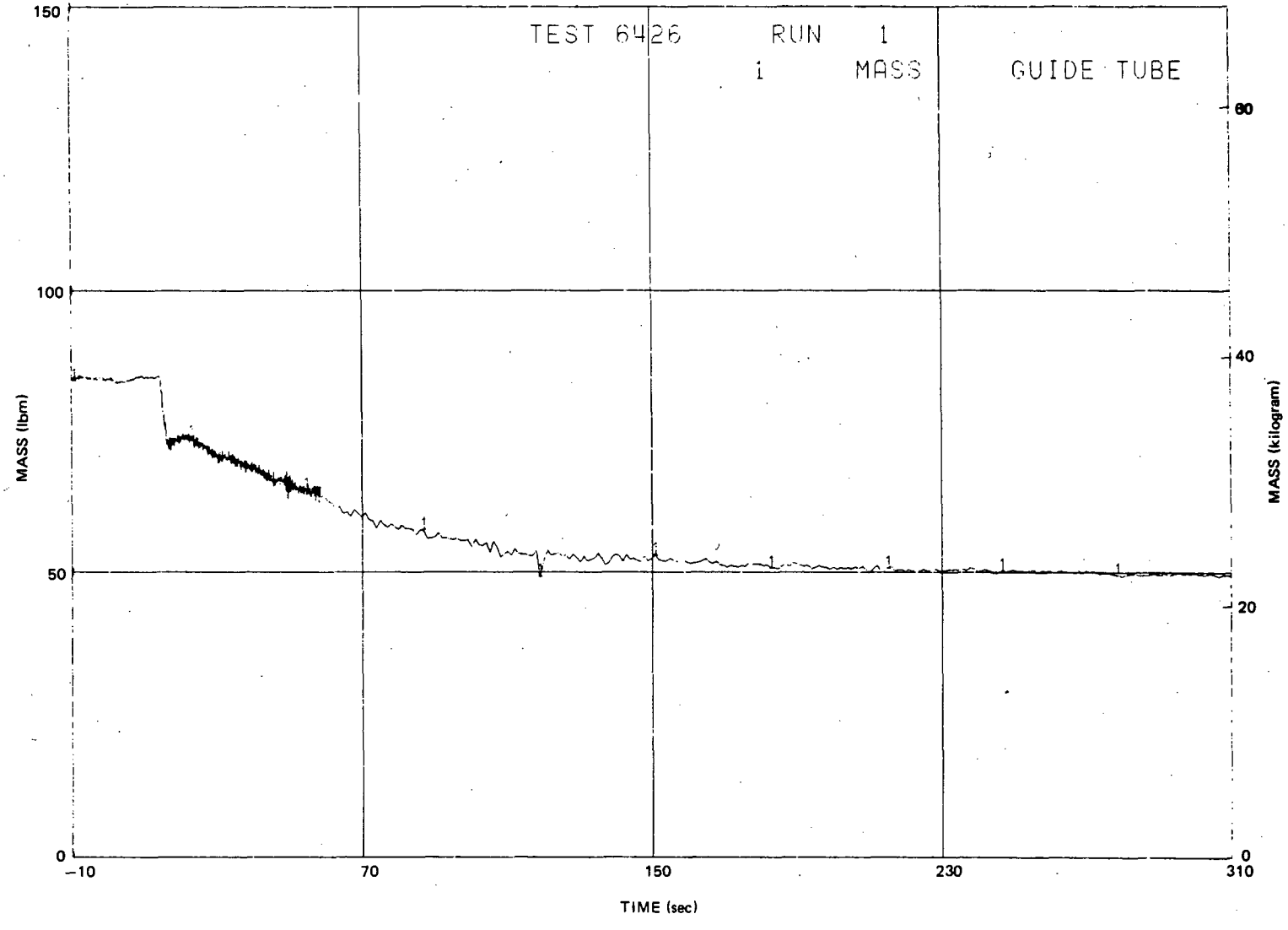

Figure L-41. Guide Tube Fluid Mass

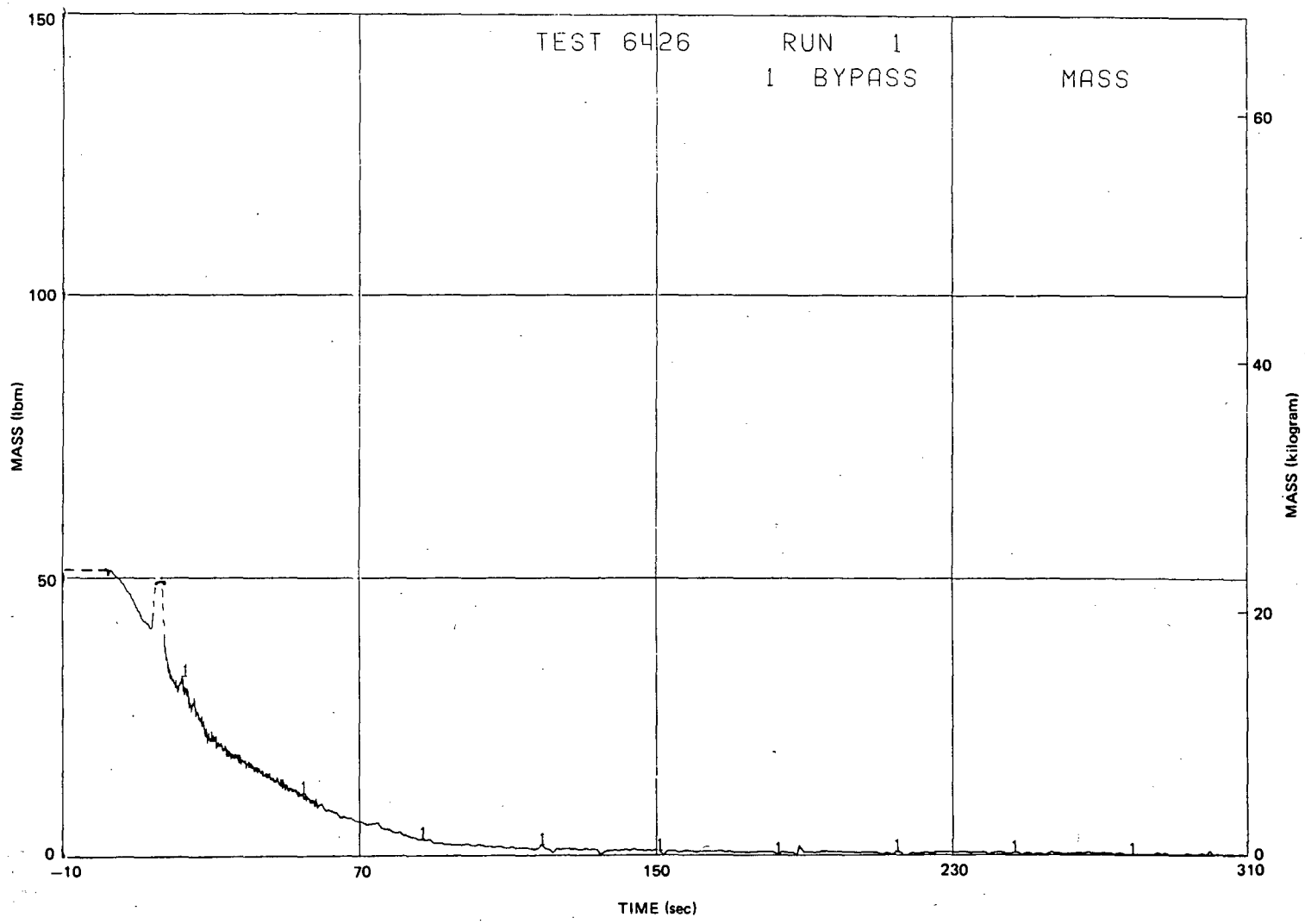
TEST 6426 RUN 1
1 BYPASS
MASS
MASS (lbm)
MASS (kilogram)
TIME (sec)
150
100
50
0
60
40
20
0
−10
70
150
230
310

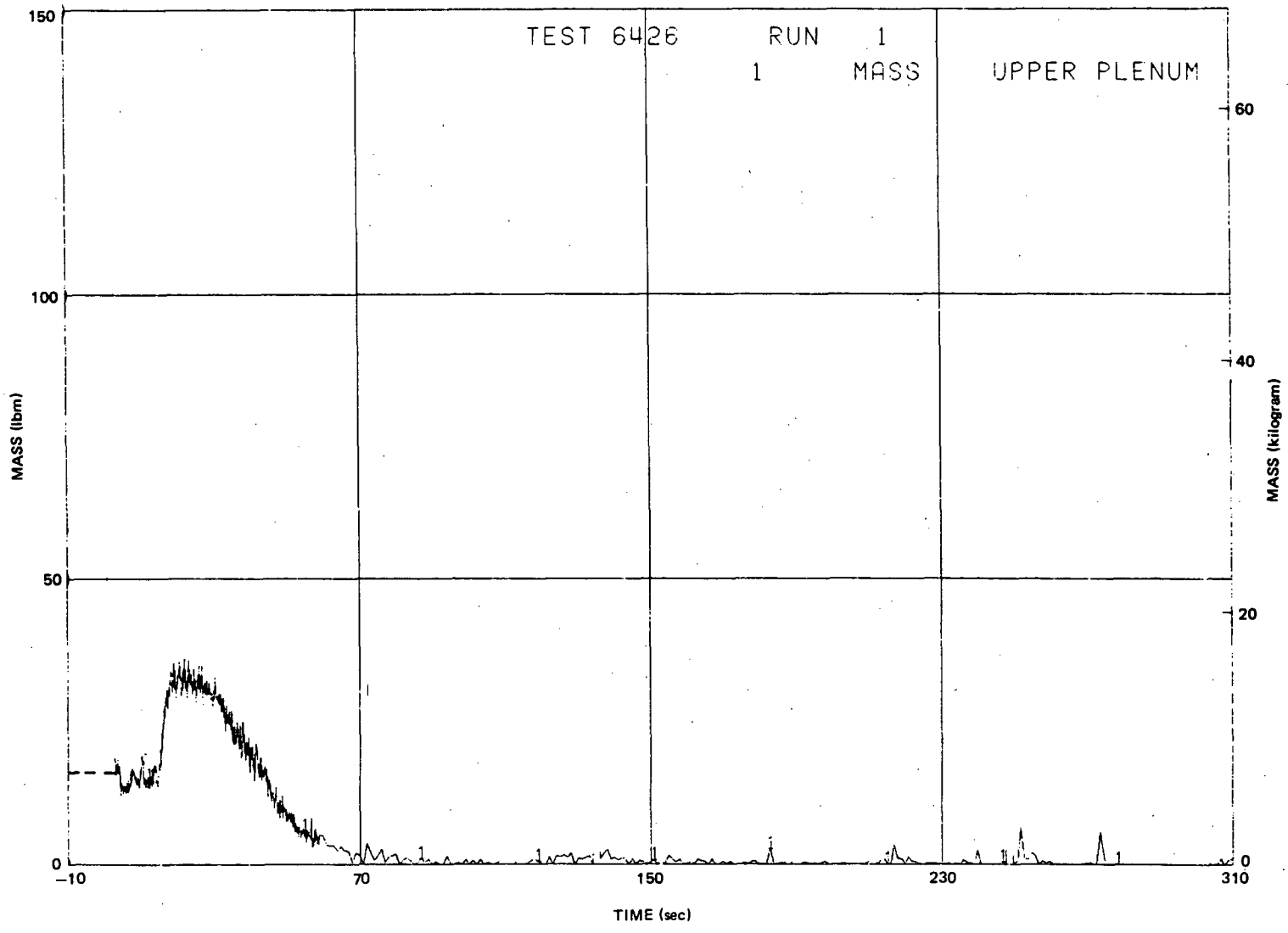

Figure L-43. Upper Plenum Fluid Mass

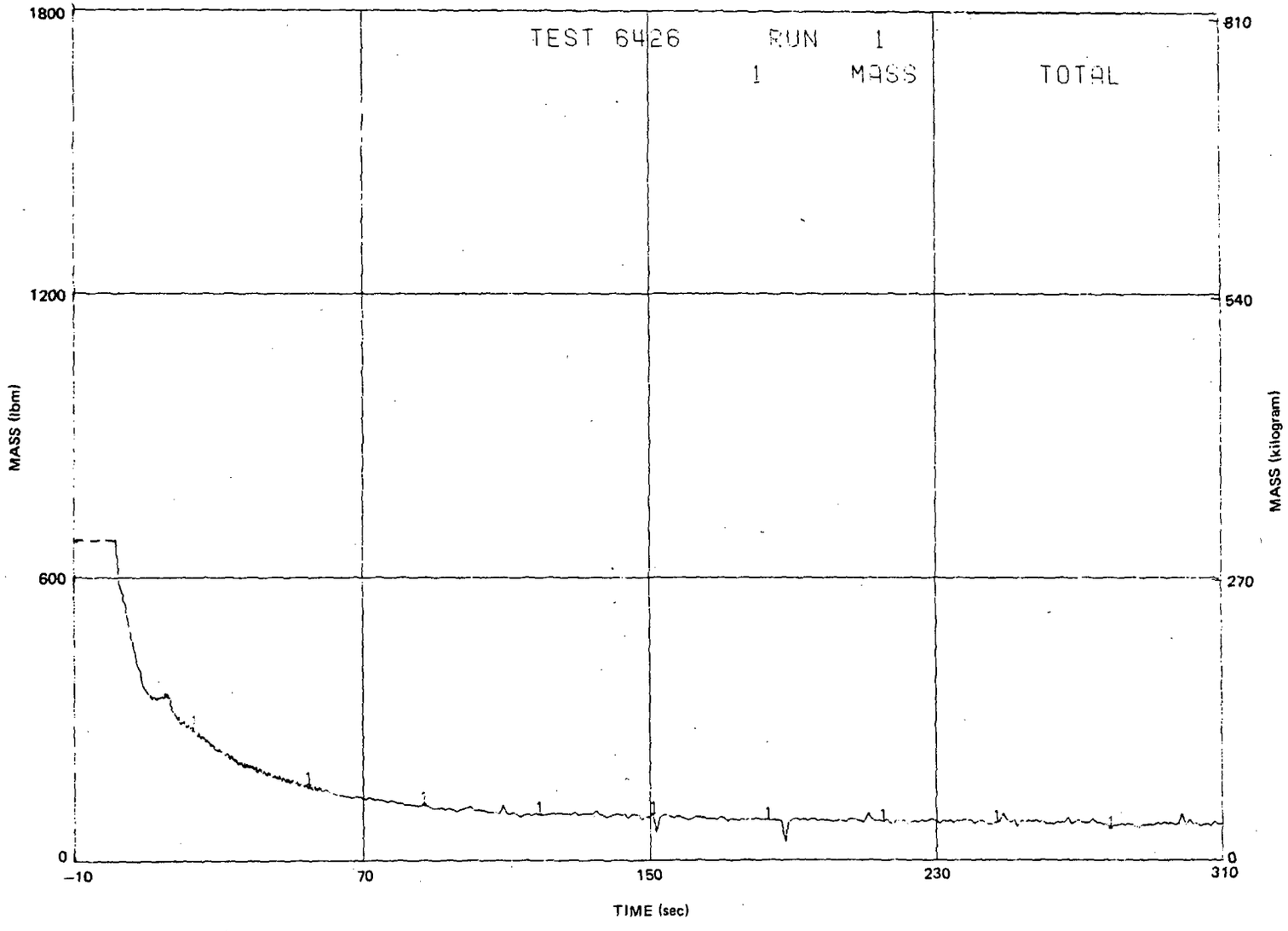

Figure L-44. Total Vessel Fluid Mass

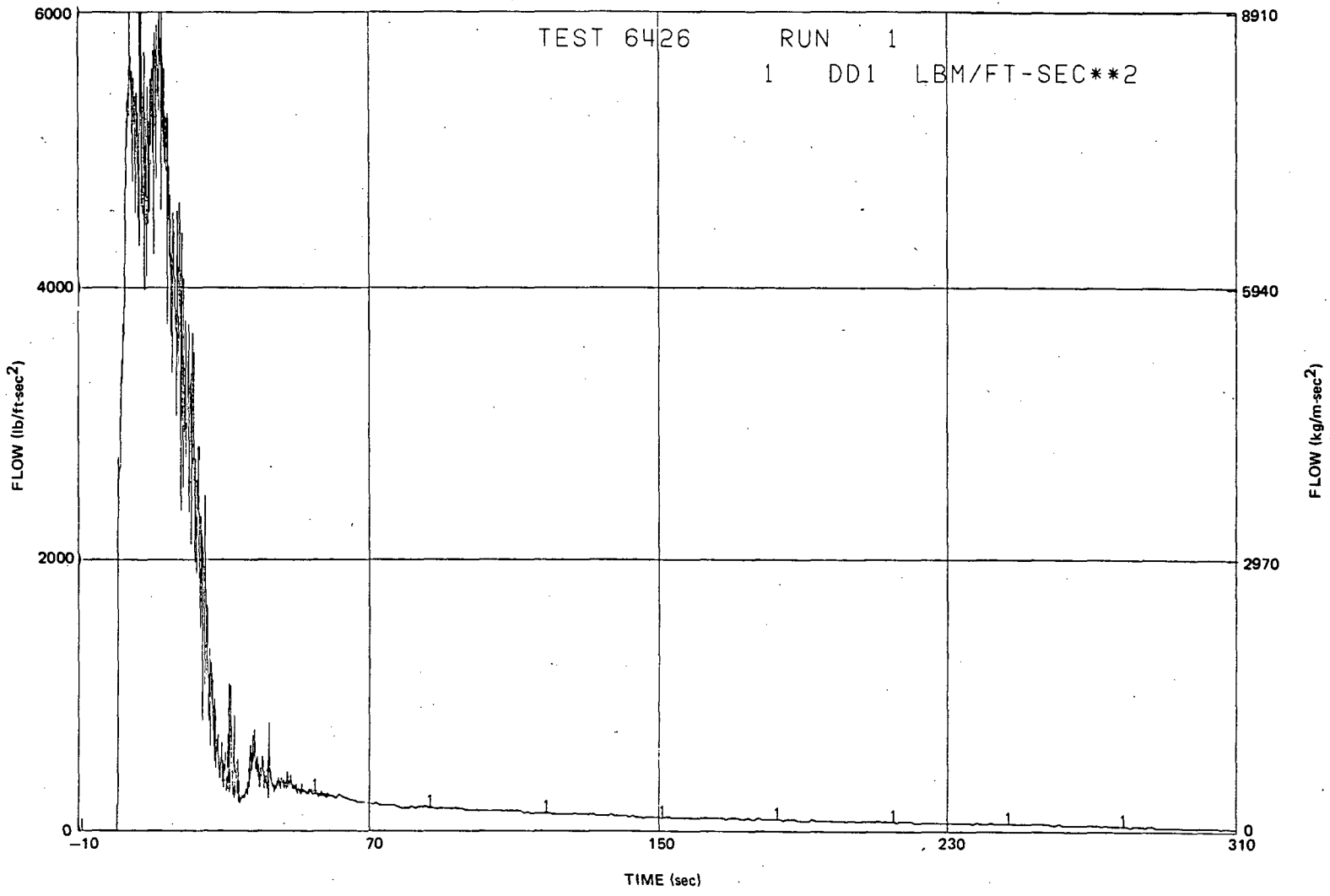

Figure L-45. Drag Disc Measurement on Drive Line Side of Broken Loop

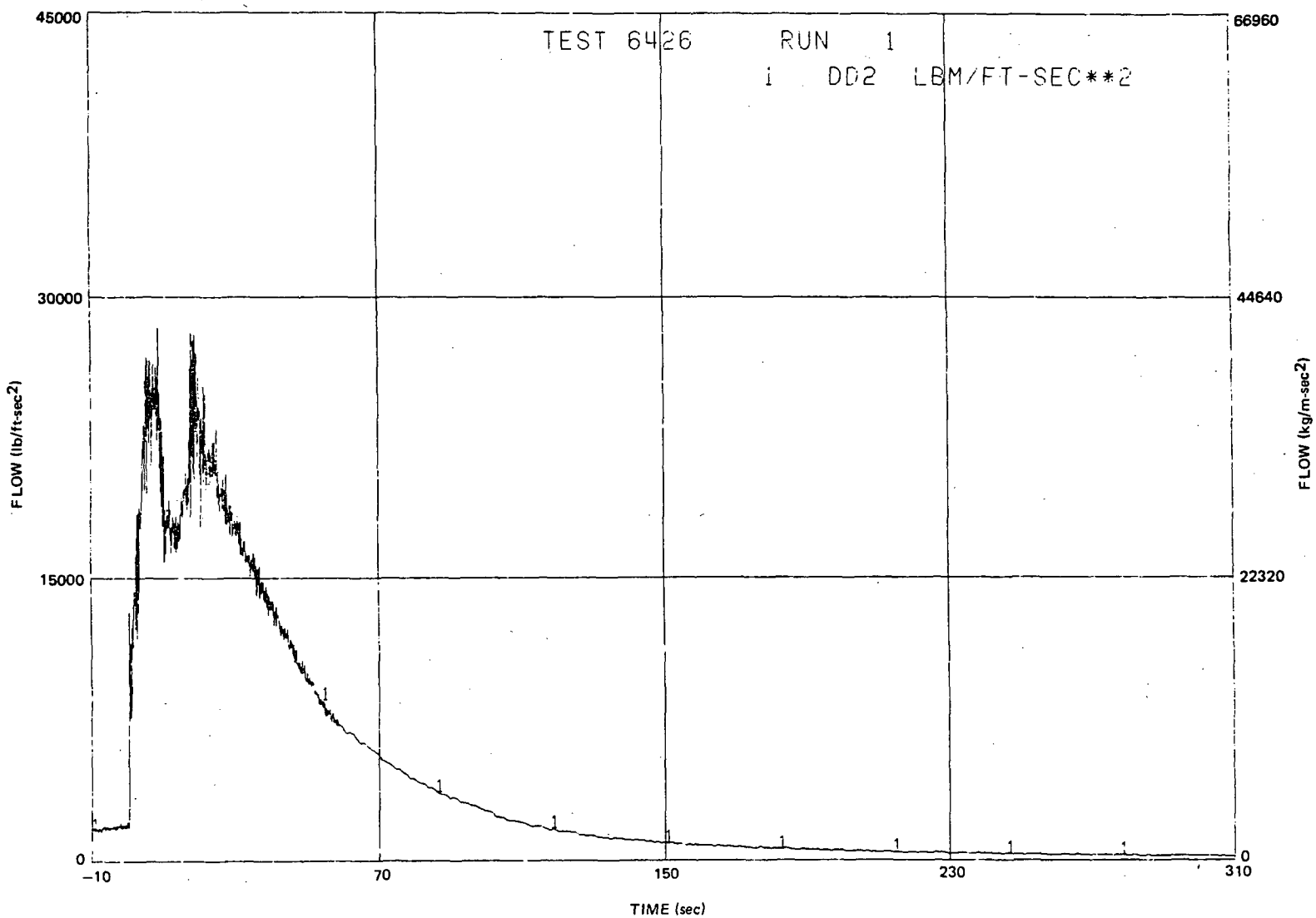

Figure L-46. Drag Disc Measurement on Suction Side of Broken Loop

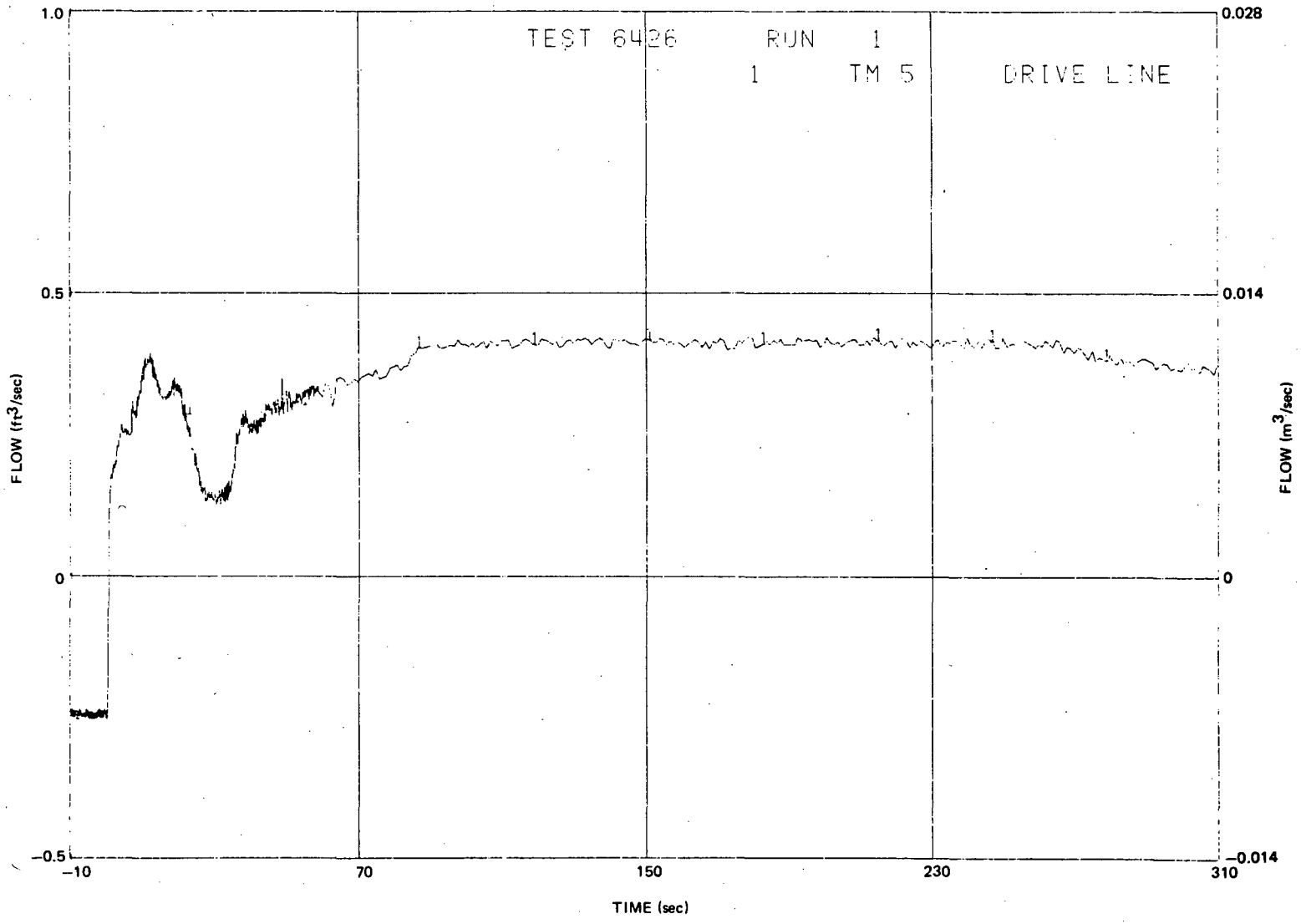

Figure L-47. Turbinemeter Measurement on Drive Line Side of Broken Loop

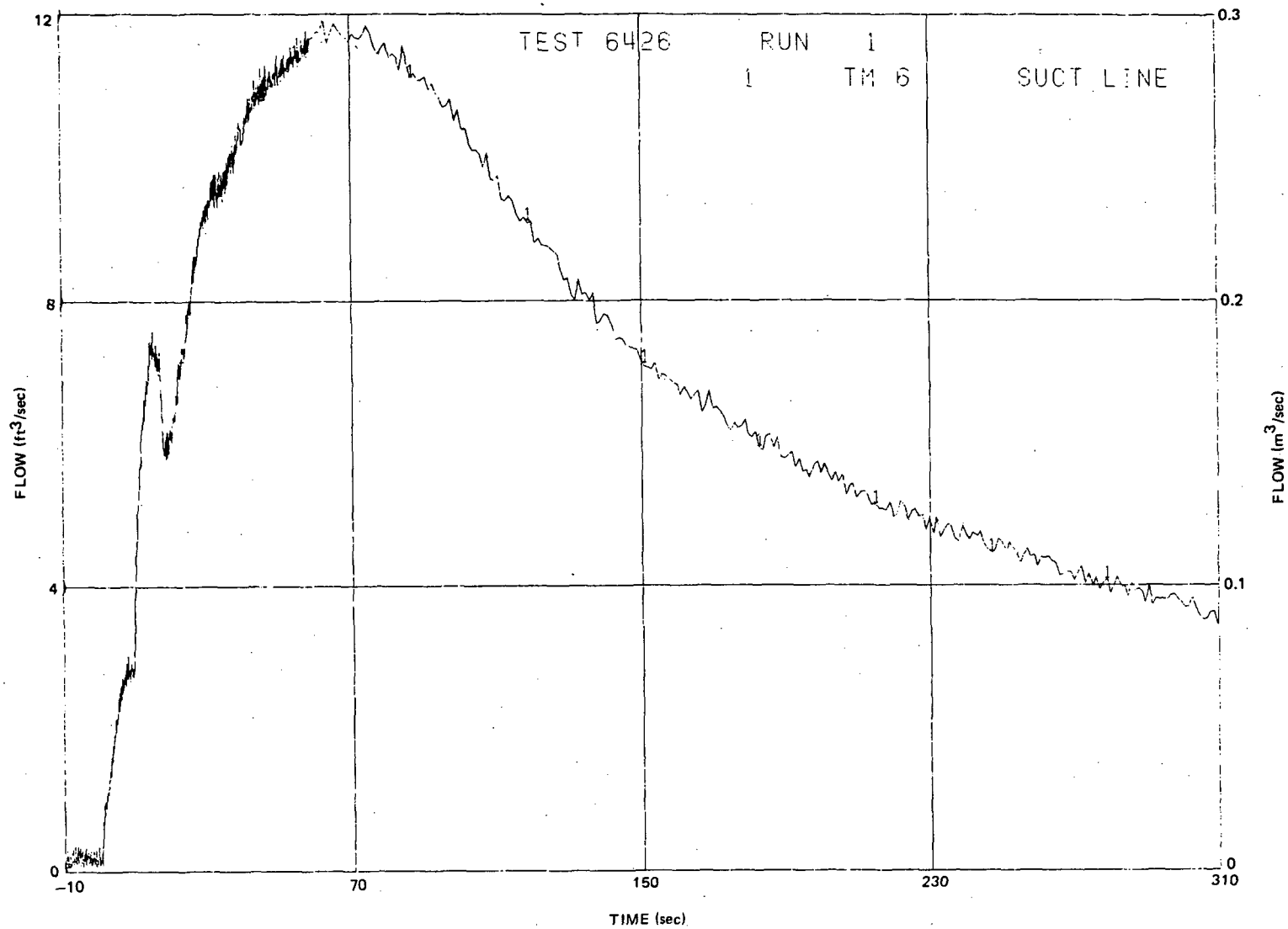

Figure L-48. Turbinemeter Measurement on Suction Line Side of Broken Loop

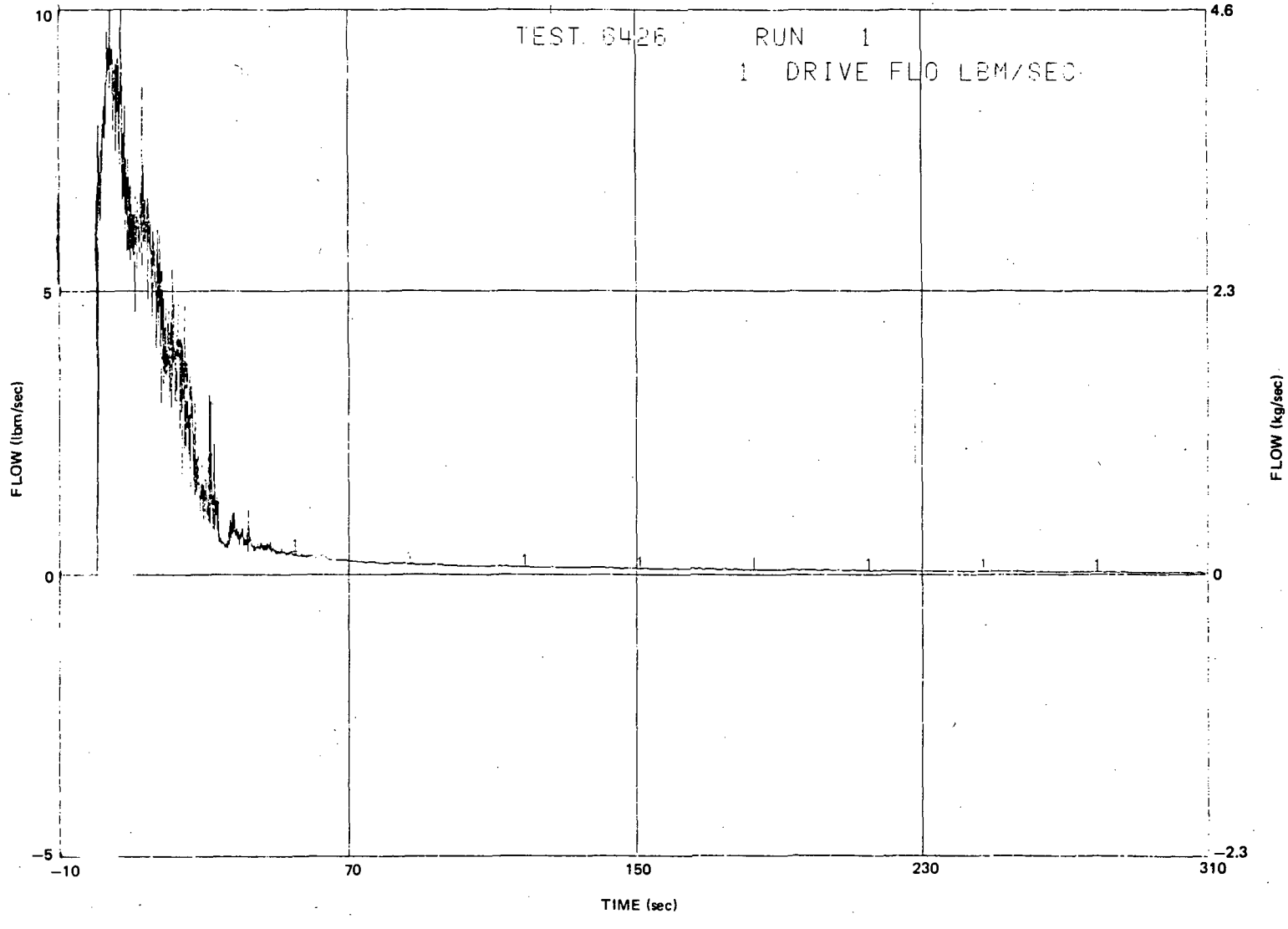

Figure L-49. Drive Line Break Mass Flow Rate

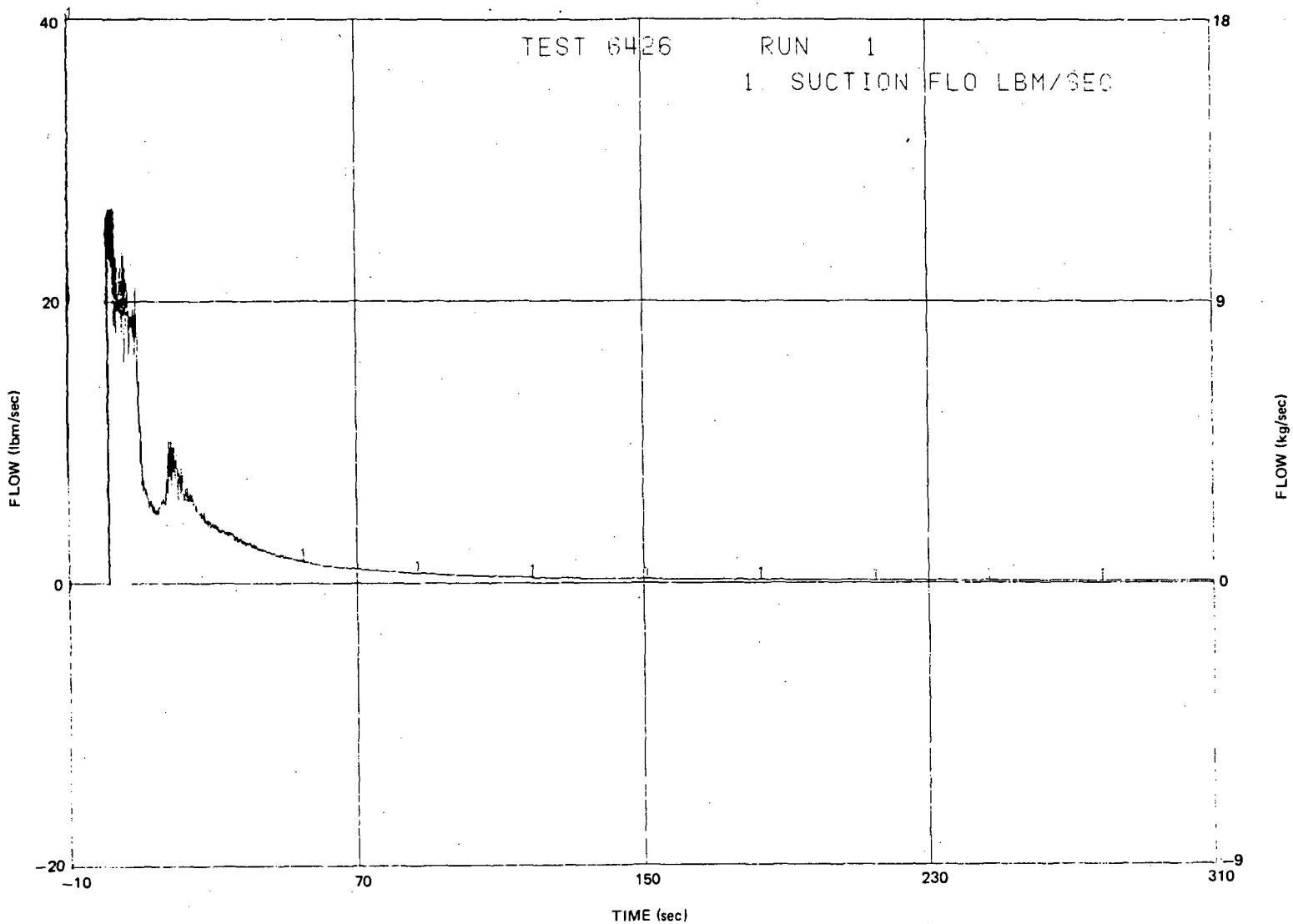

Figure L-50. Suction Line Break Mass Flow Rate

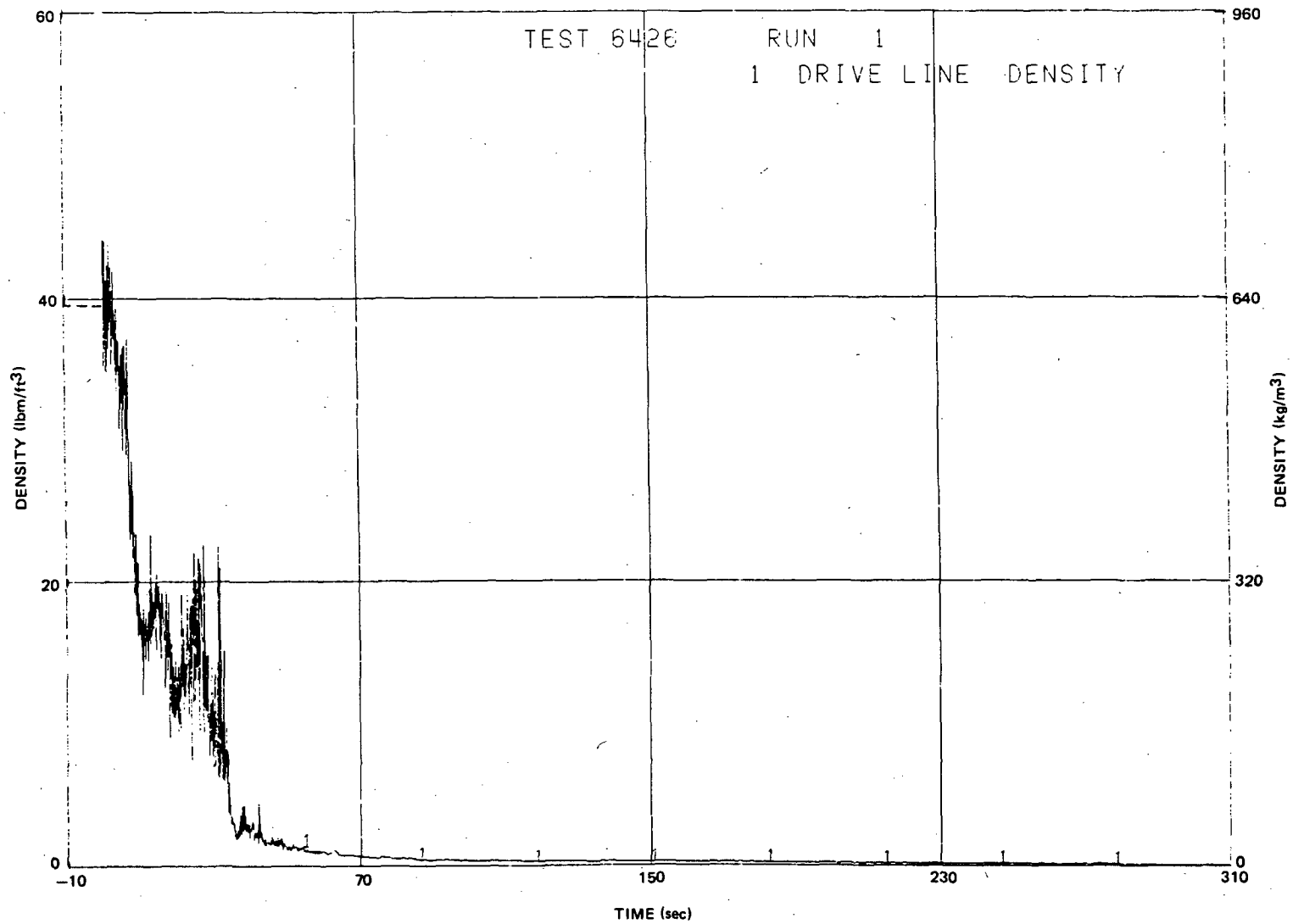

Figure L-51. Drive Line Break Density

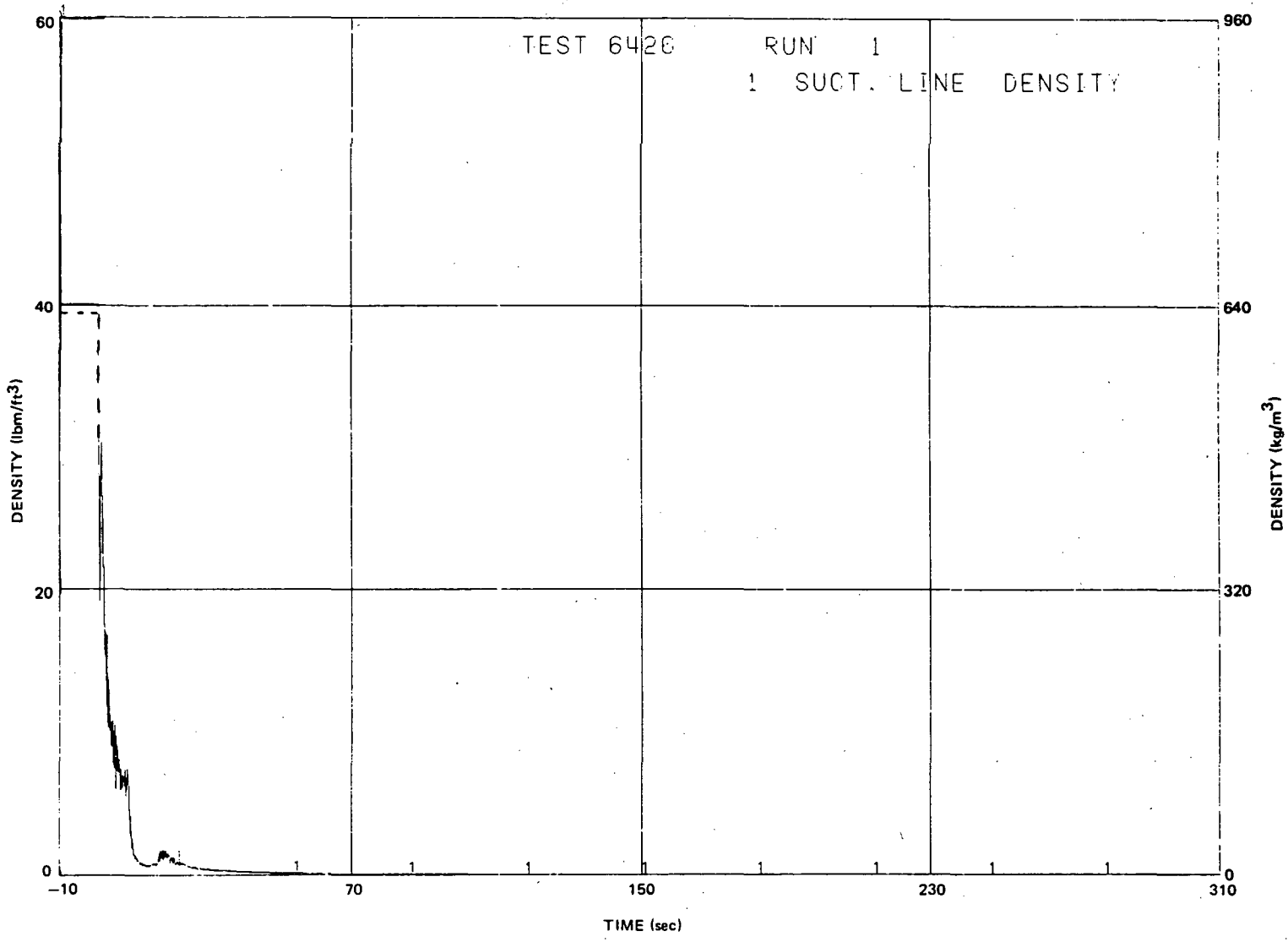

Figure L-52. Suction Line Break Density

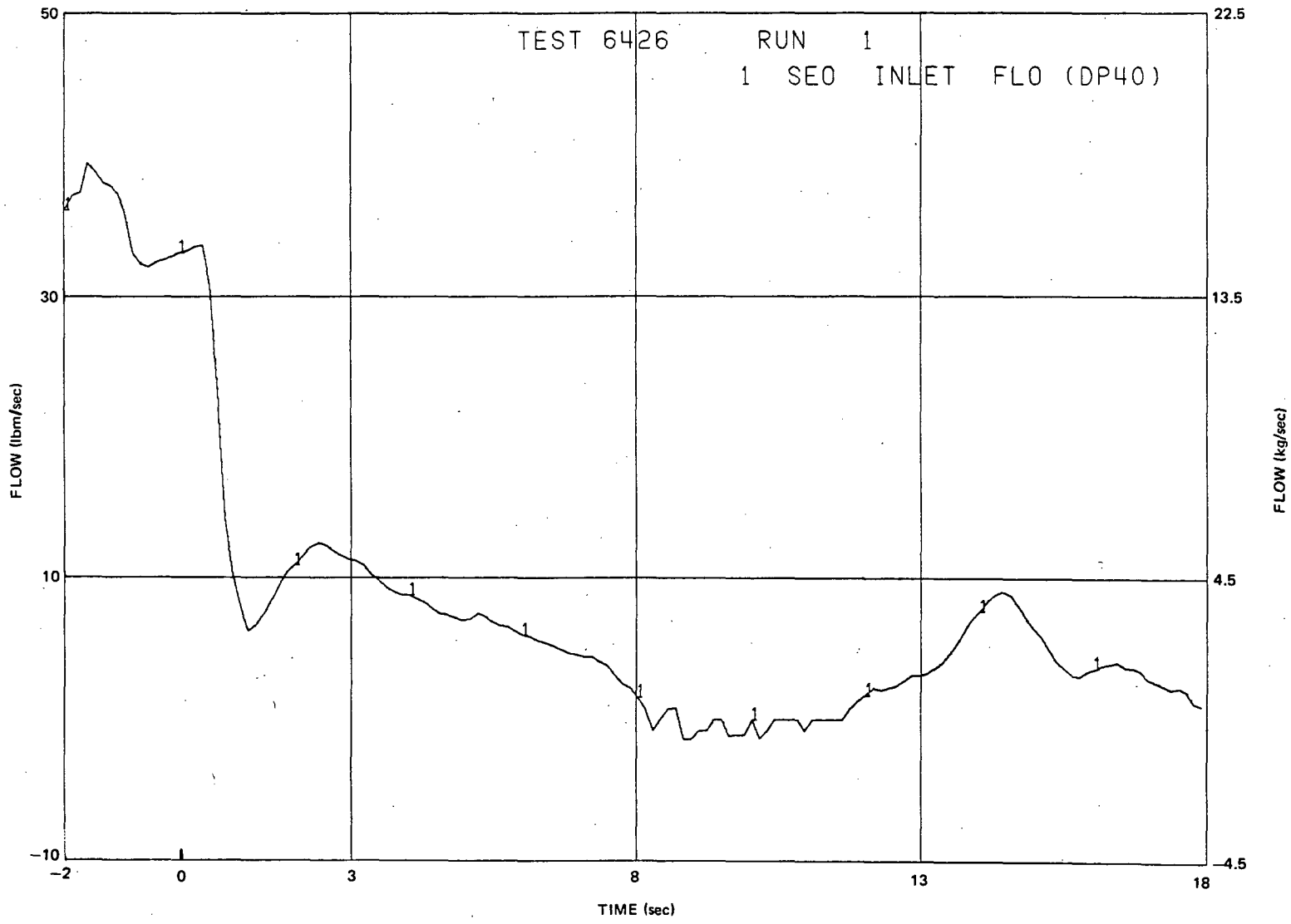

Figure L-53. Bundle Inlet Side Entry Orifice Mass Flow Rate

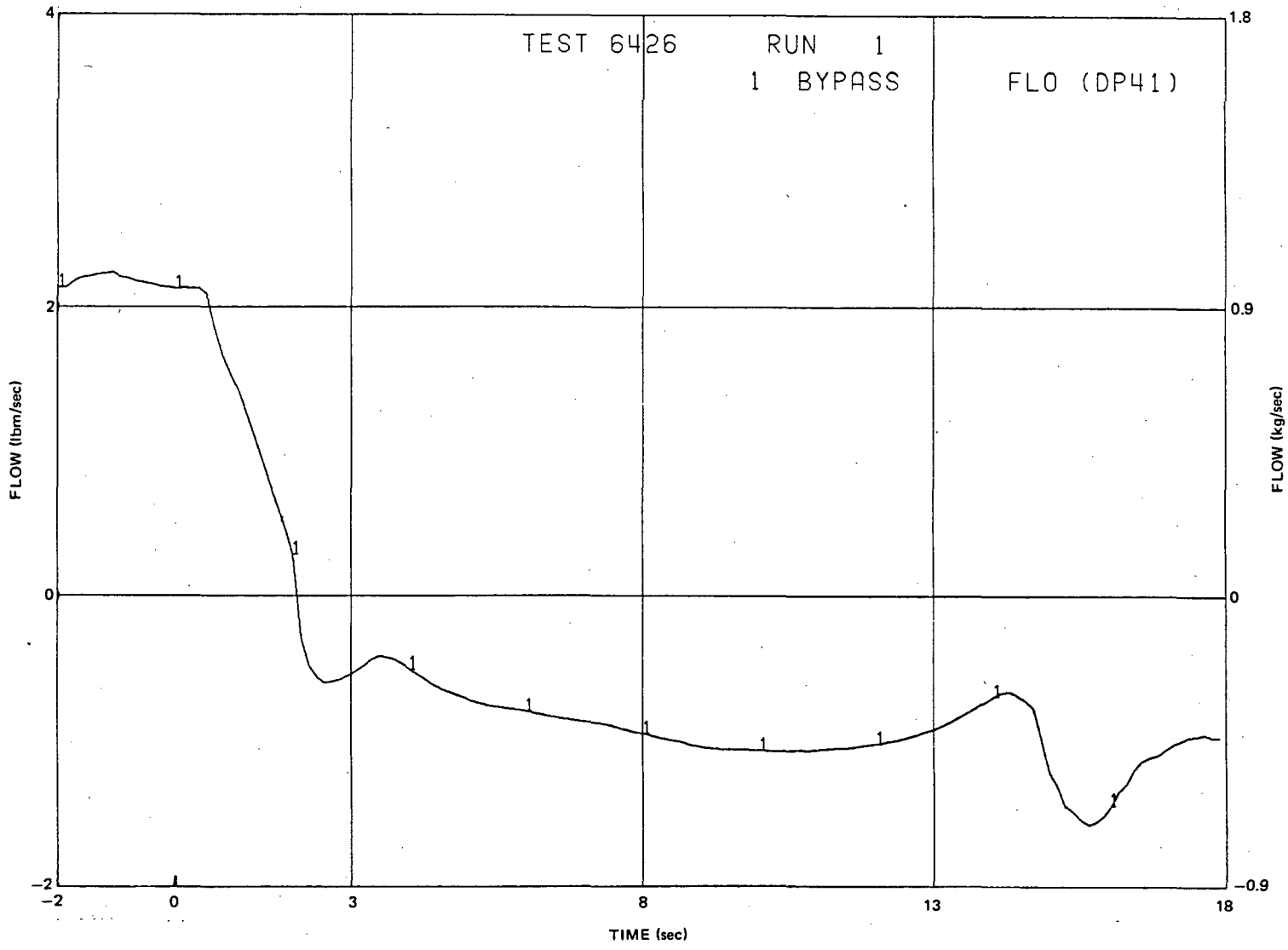

Figure L-54. Bypass Leakage Path Mass Flow Rate

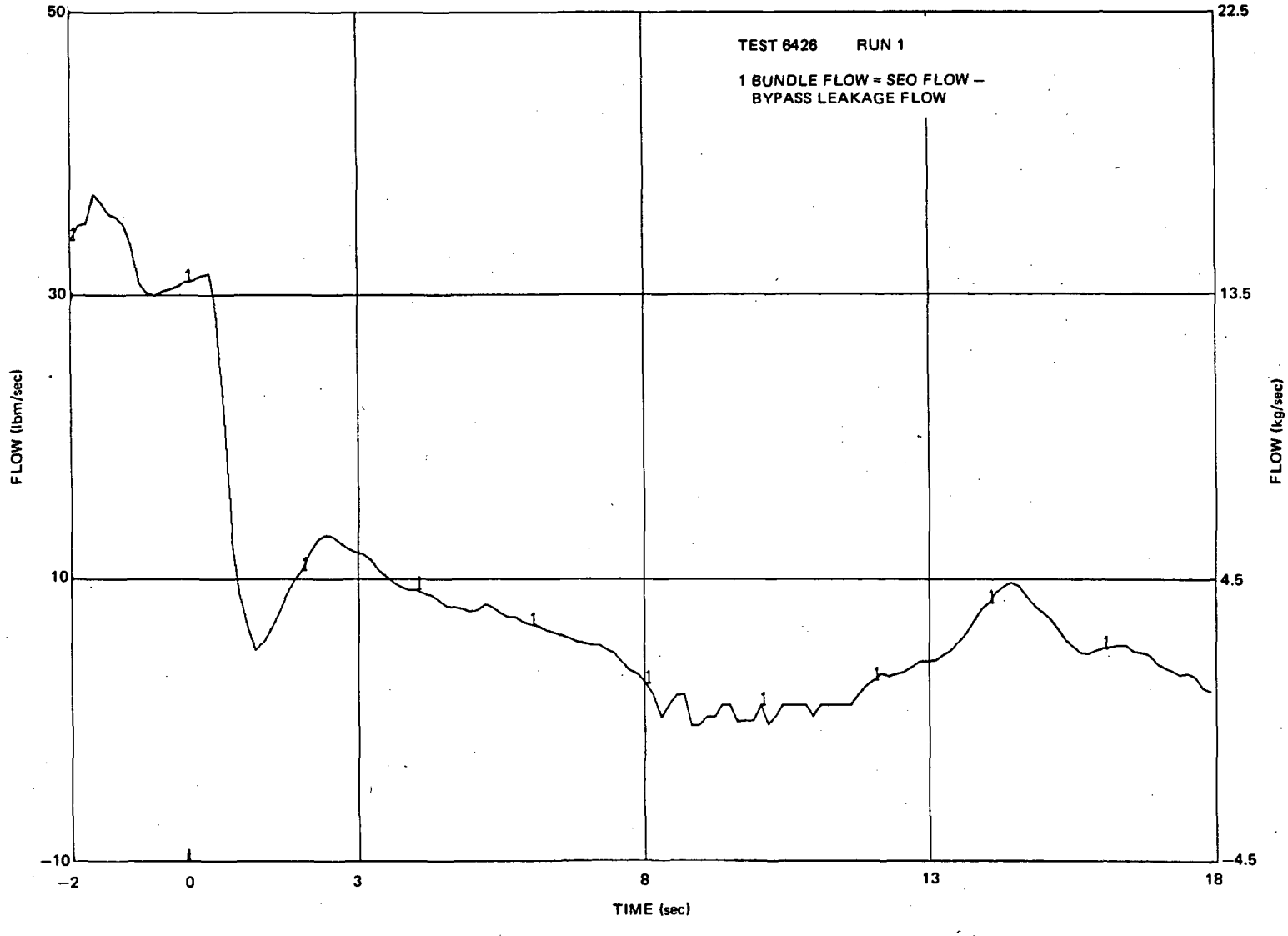

Figure L-55. Bundle Mass Flow Rate

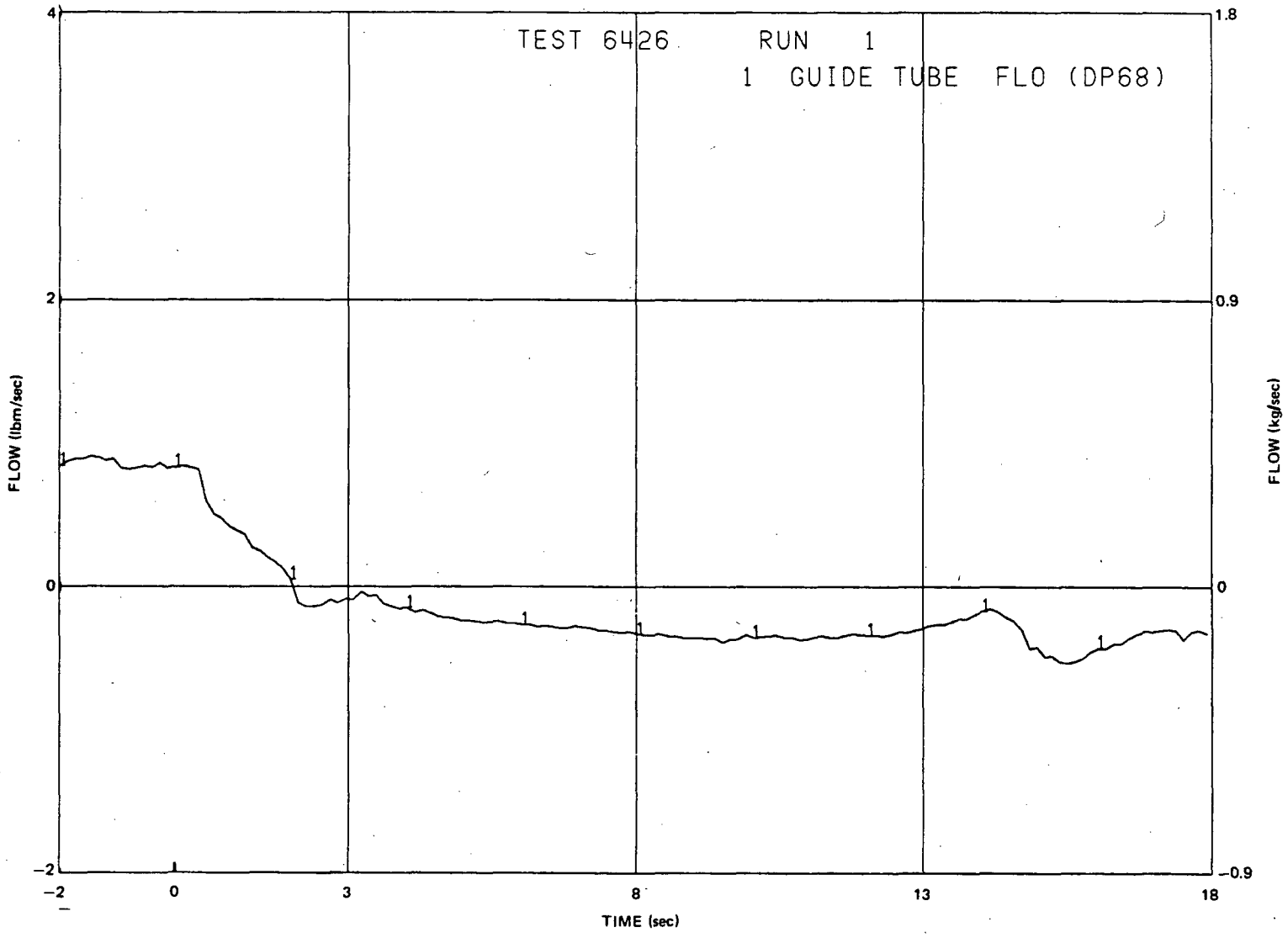

Figure L-56. Lower Plenum to Guide Tube Mass Flow Rate

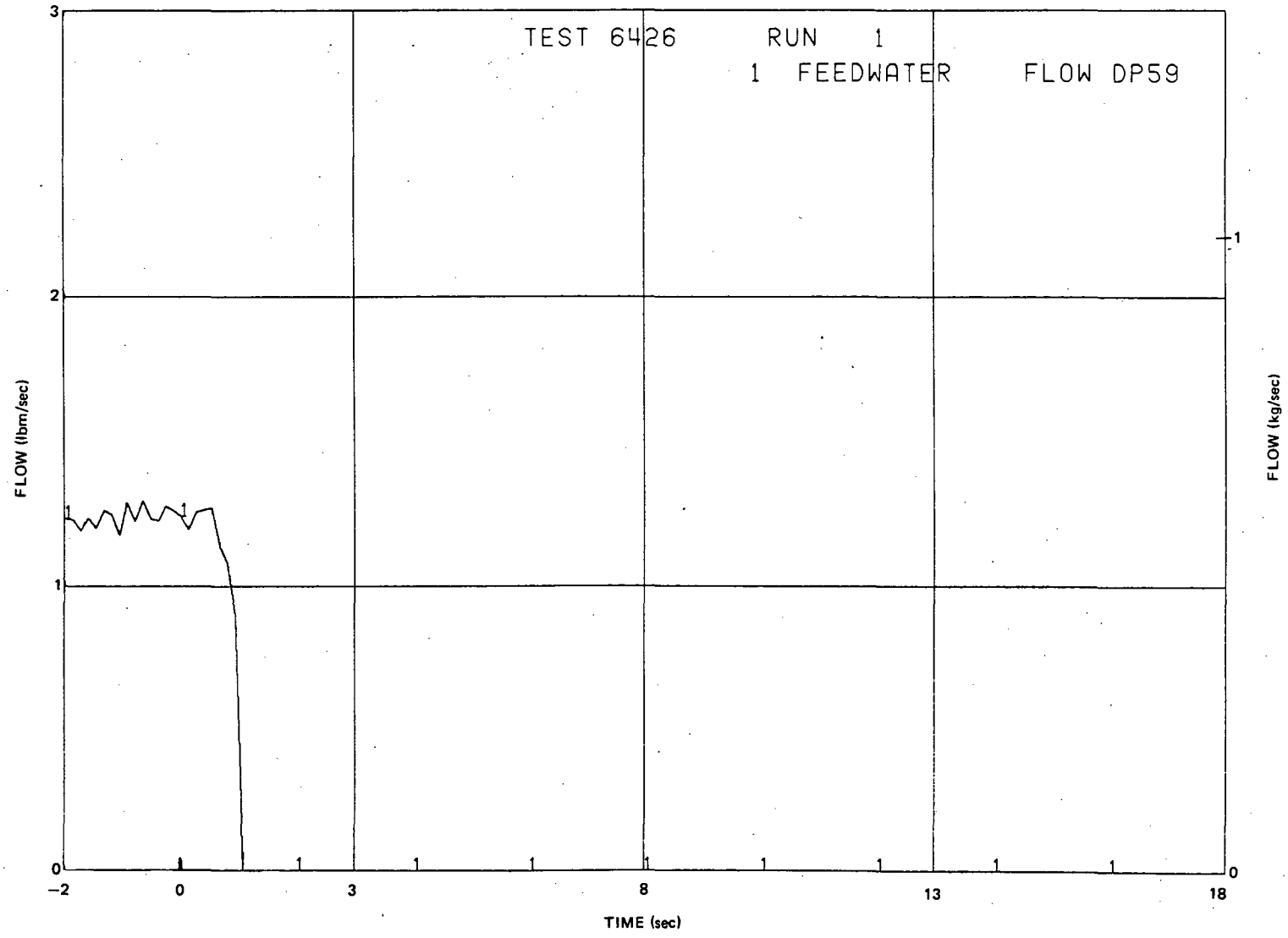

Figure L-57. Feedwater Mass Flow Rate

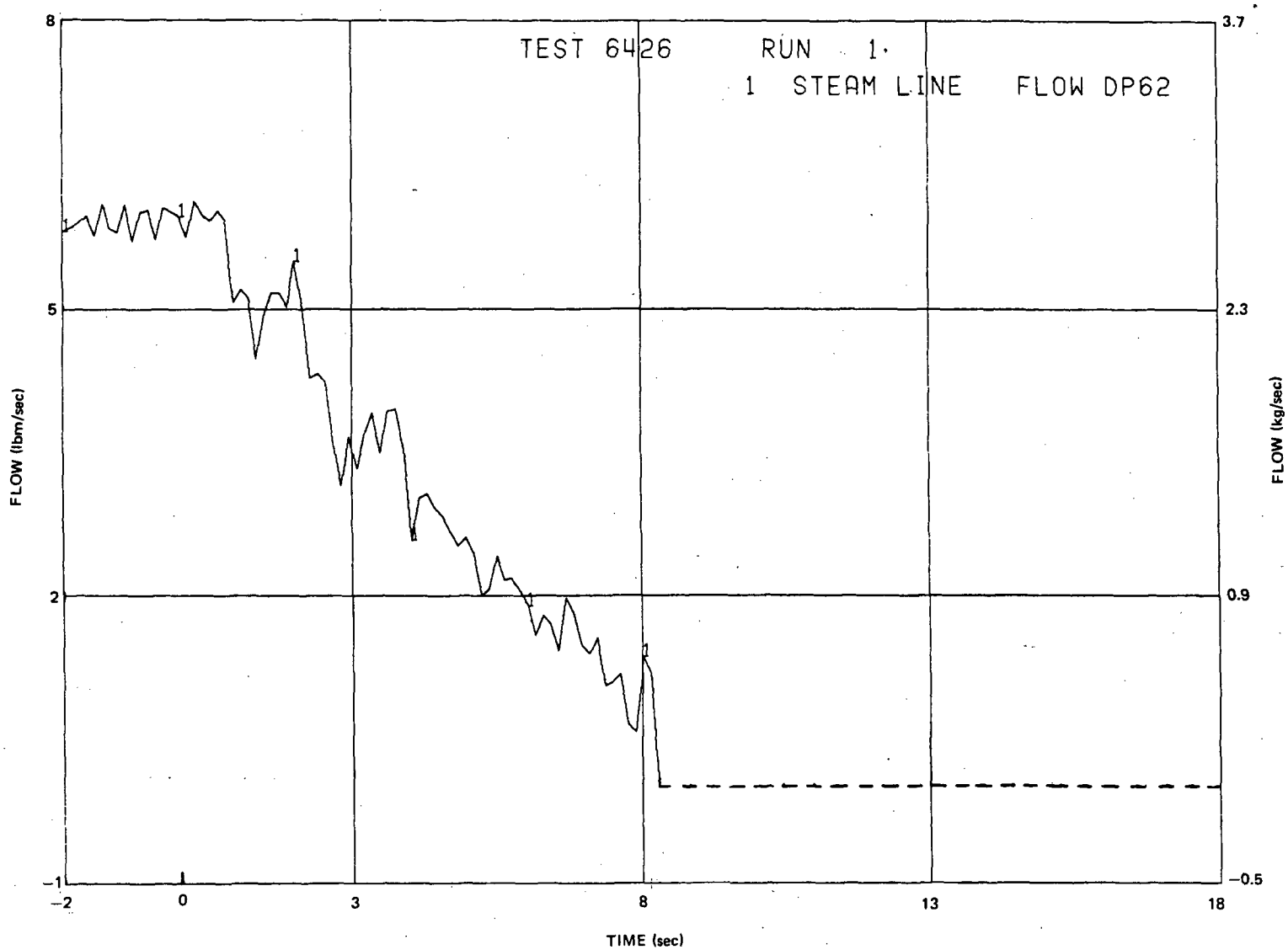

Figure L-58. **Steamline Mass Flow Rate**

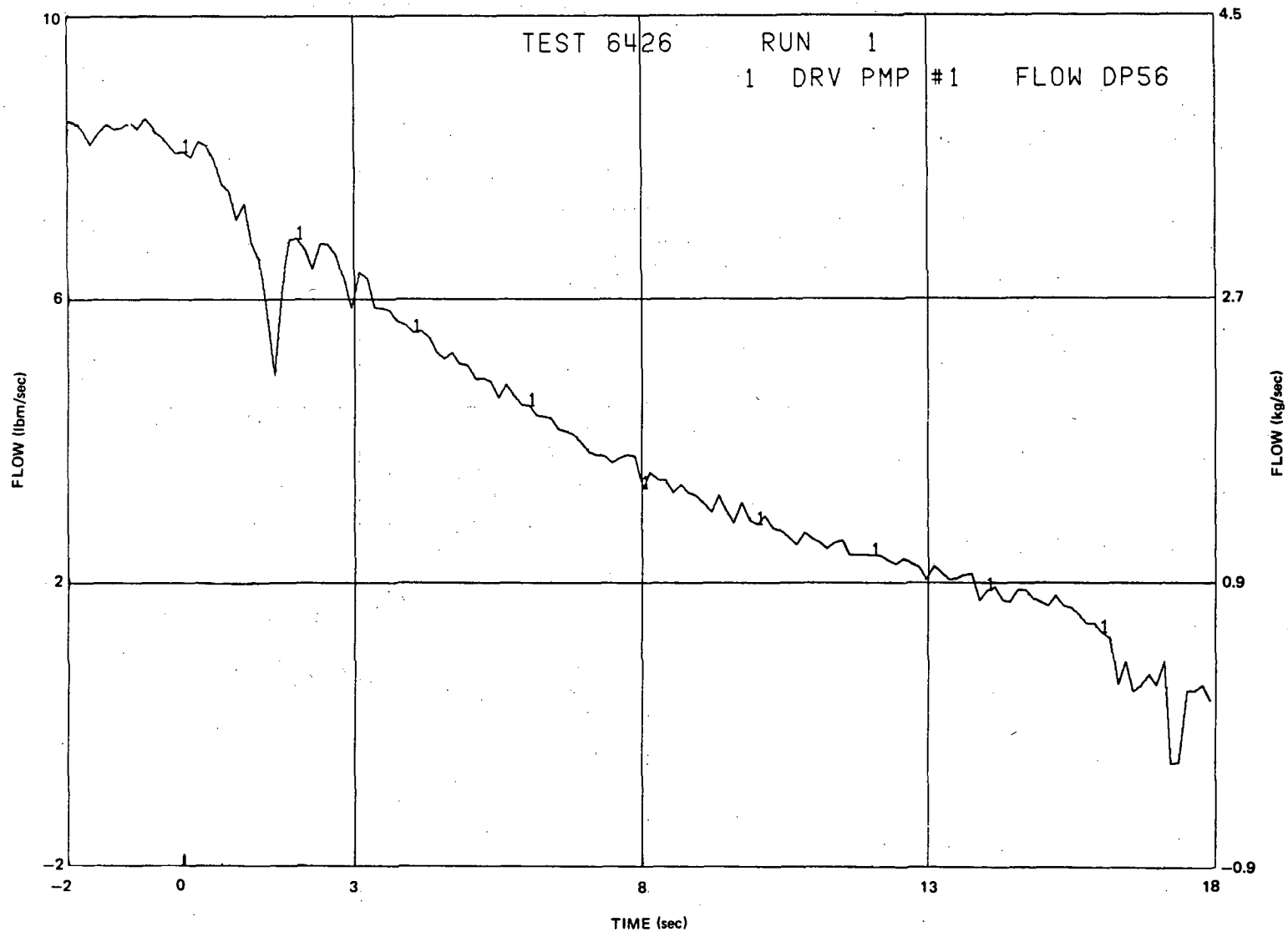

Figure L-59. Intact Loop Recirculation Pump Mass Flow Rate

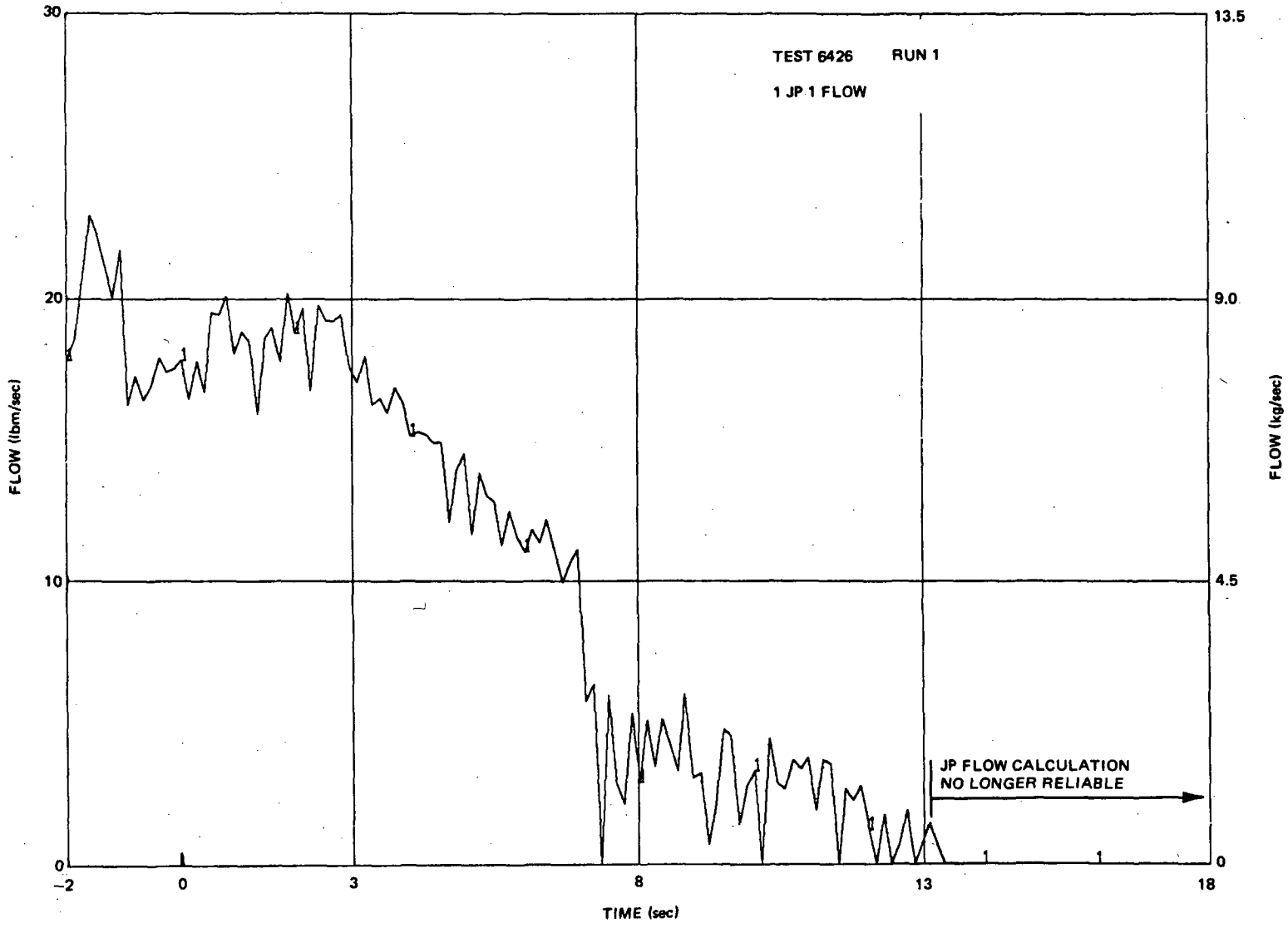

Figure L-60. Intact Loop Jet Pump Mass Flow Rate

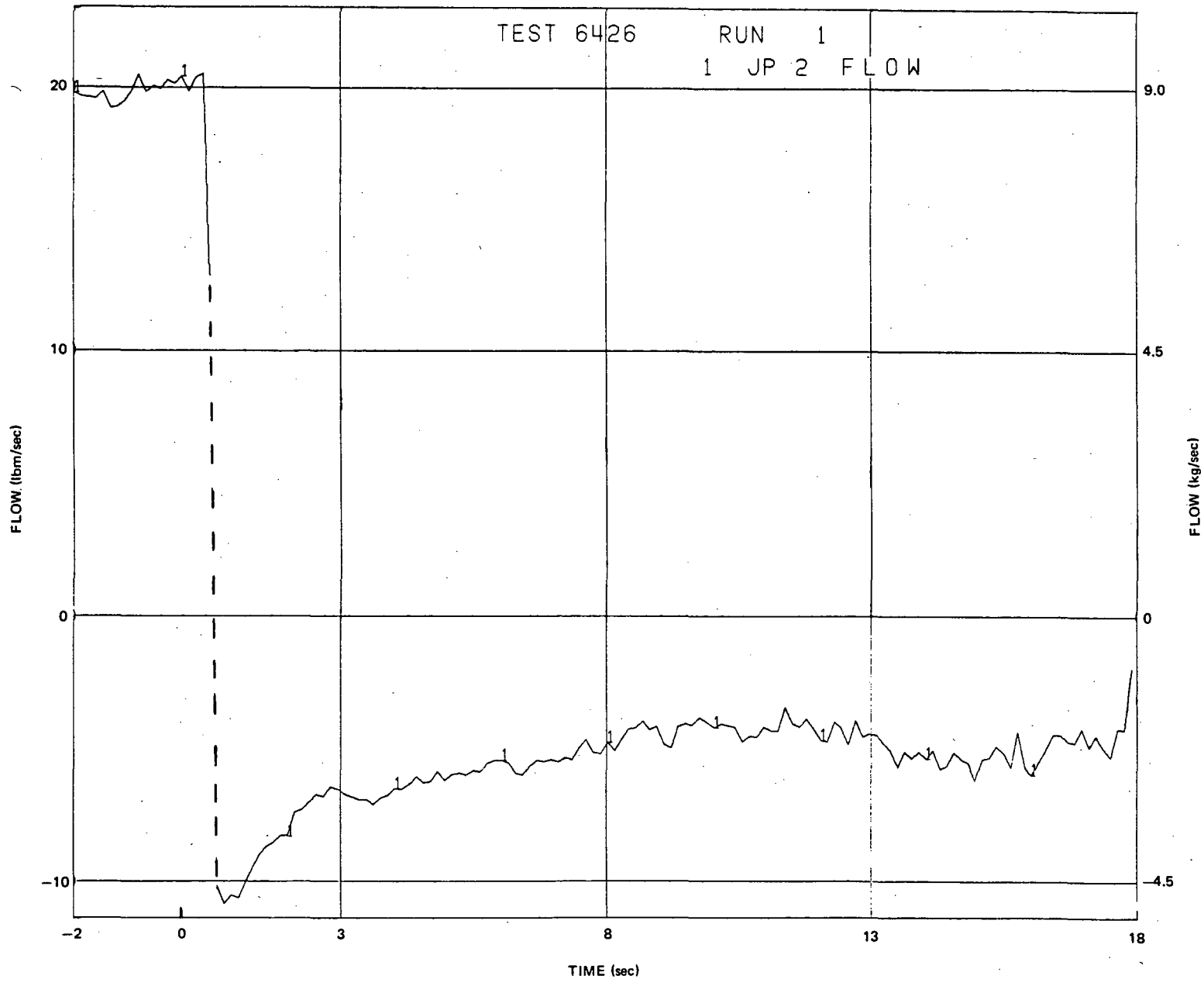

Figure L-61. Broken Loop Jet Pump Mass Flow Rate

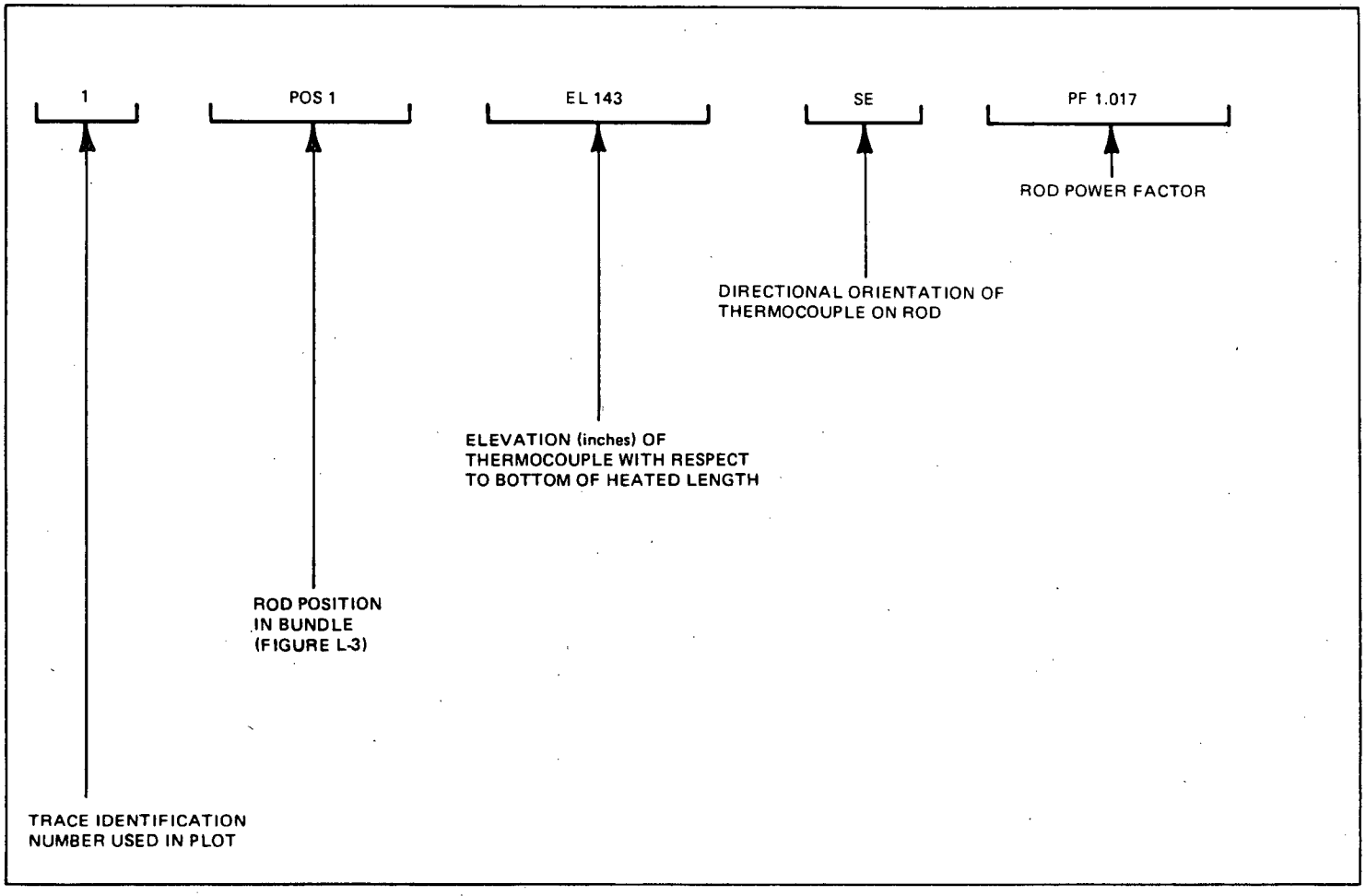

Figure L-62. Guide for Interpreting Legends on Bundle Temperature Plots

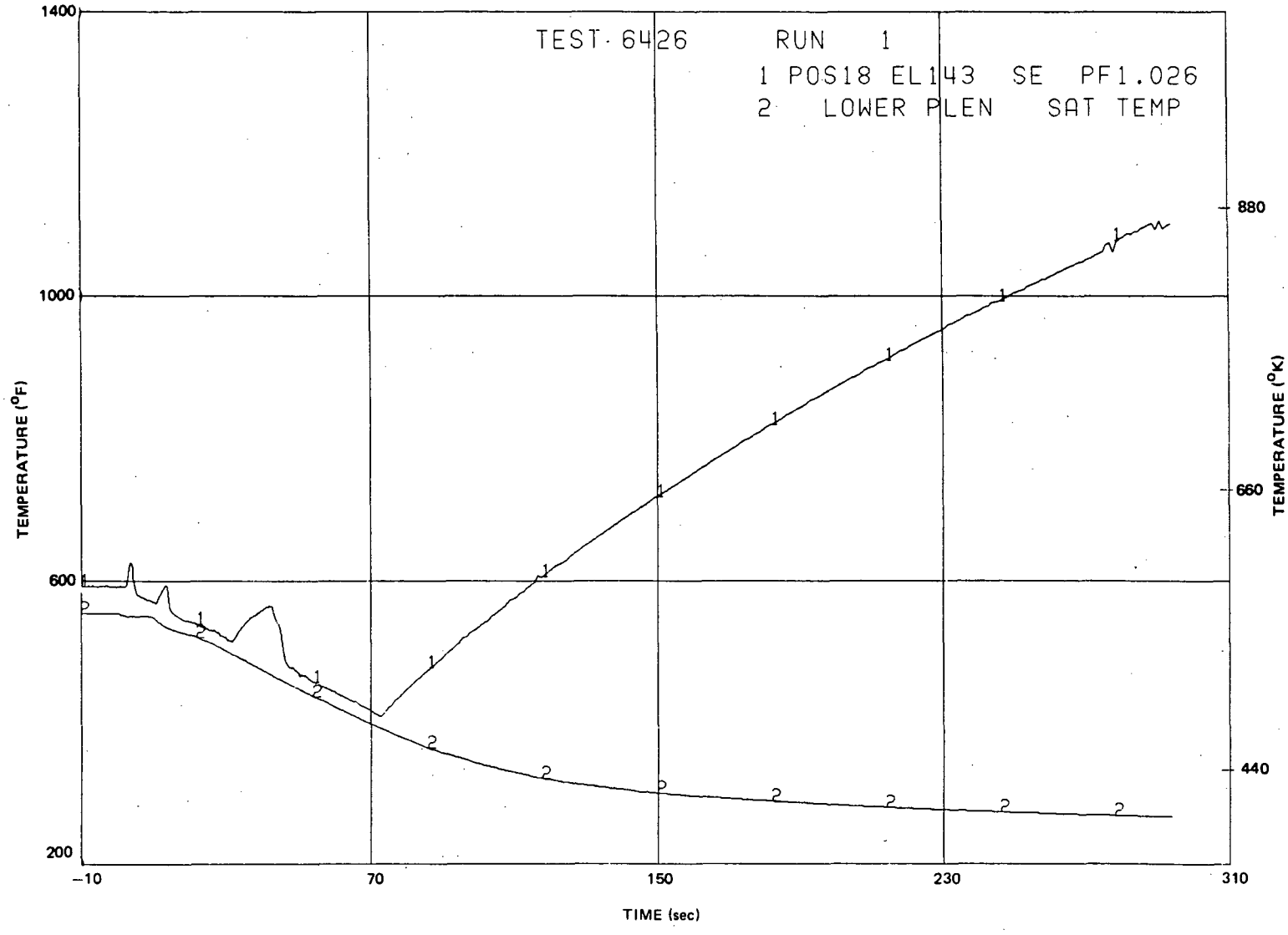

Figure L-63. Inside Clad Temperature - Elevation 143 in.

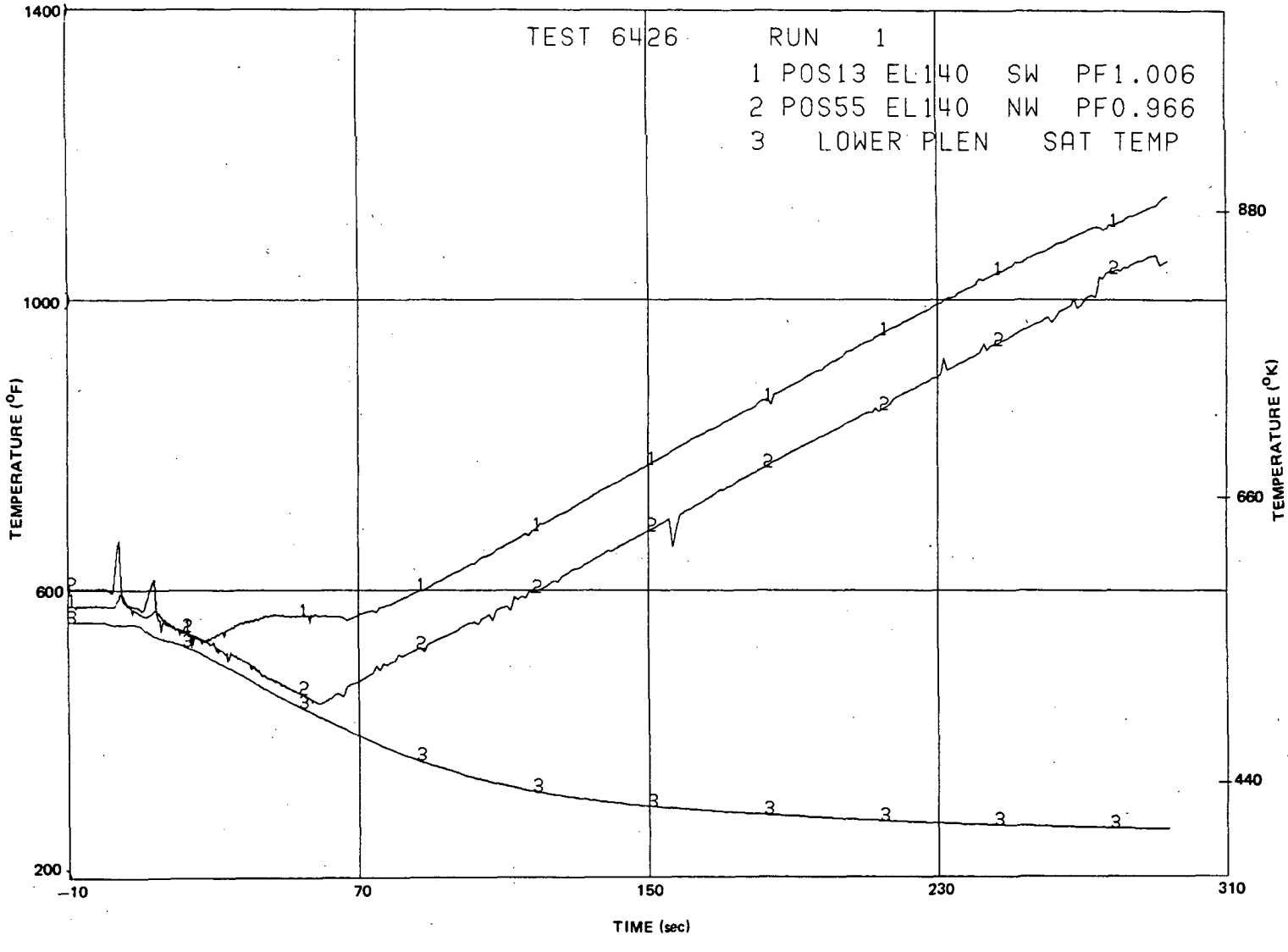

Figure L-64. Inside Clad Temperature - Elevation 140 in.

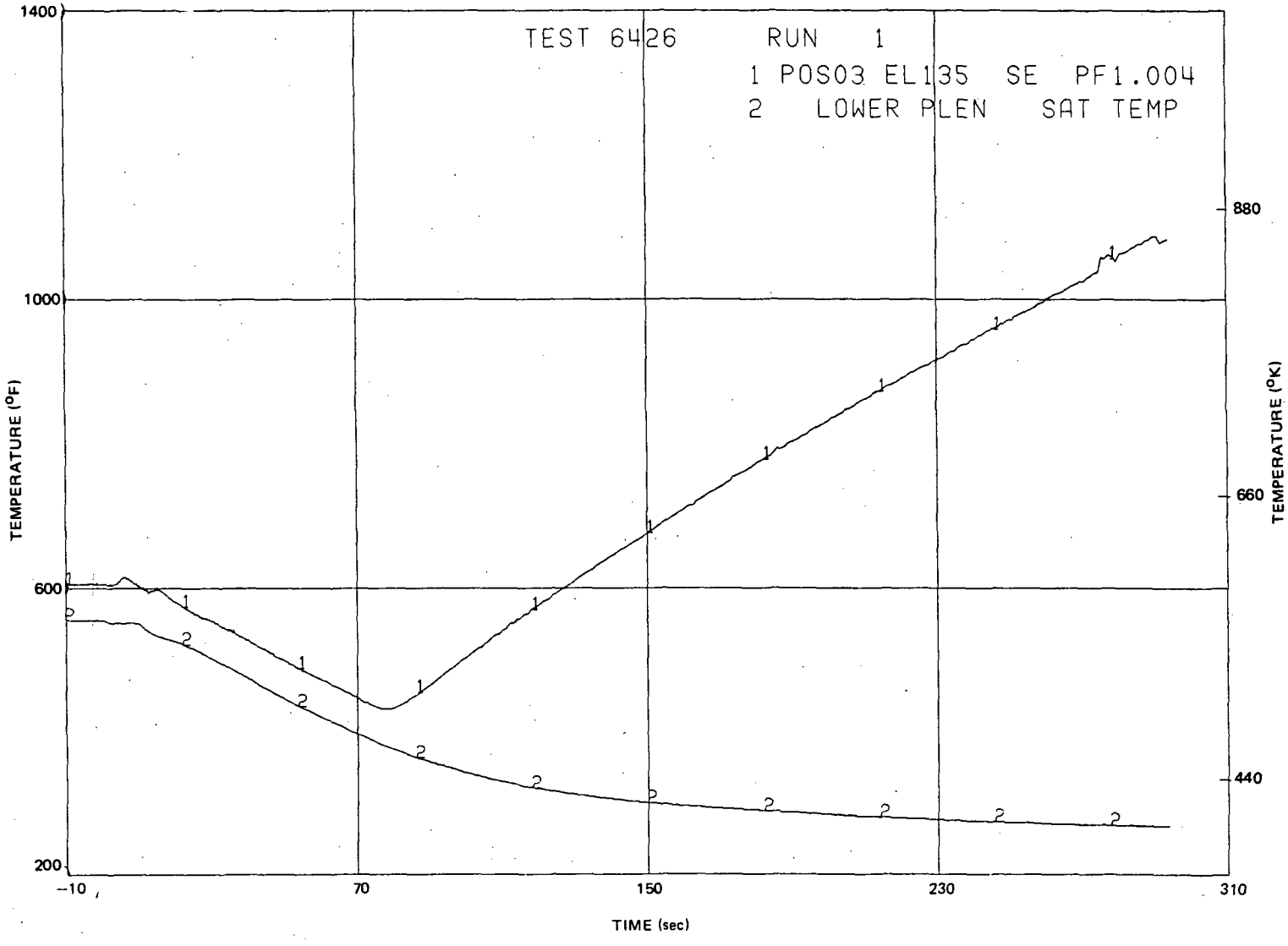

Figure L-65. Inside Clad Temperature - Elevation 135 in.

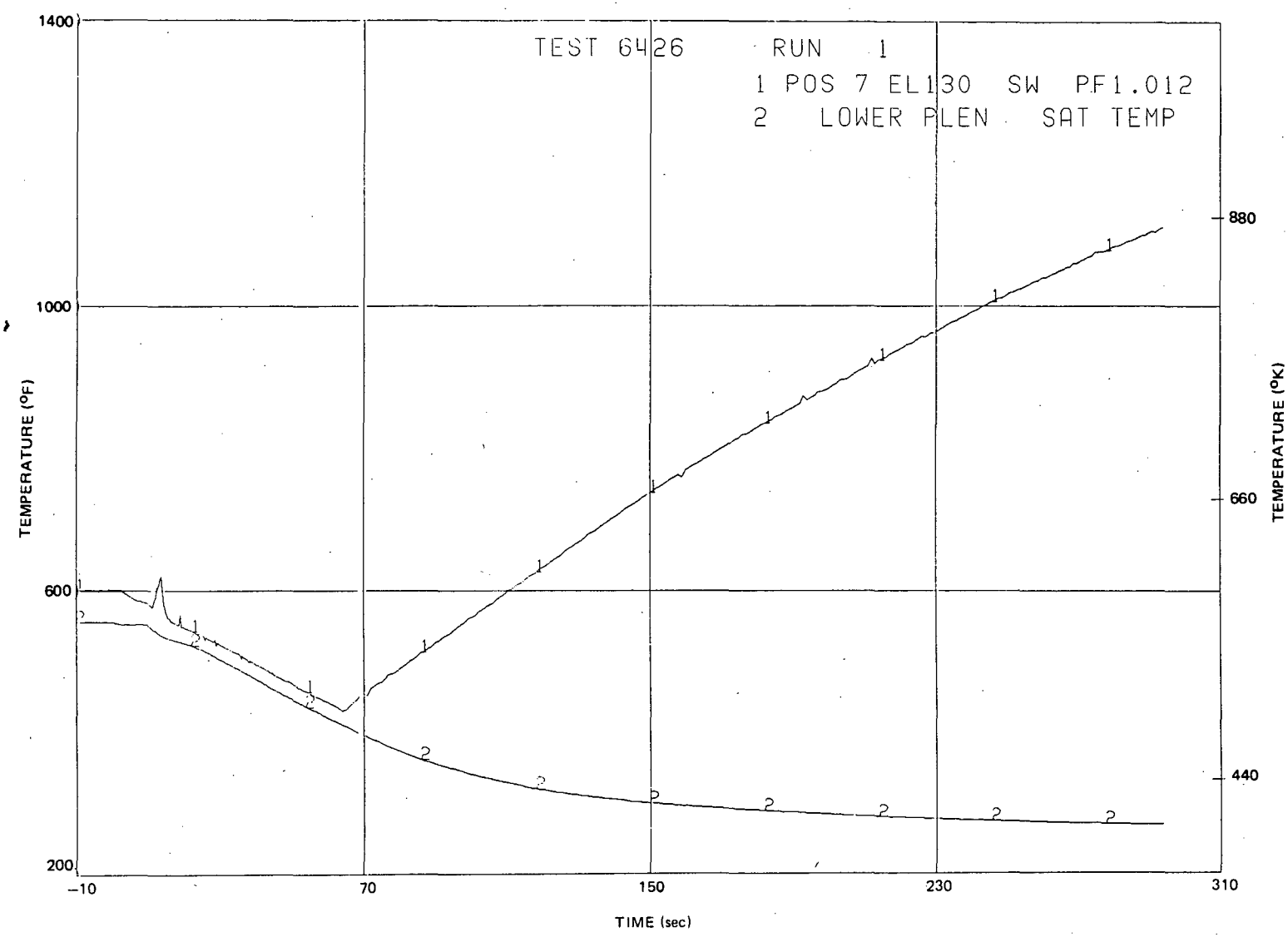

Figure L-66. Inside Clad Temperature - Elevation 130 in.

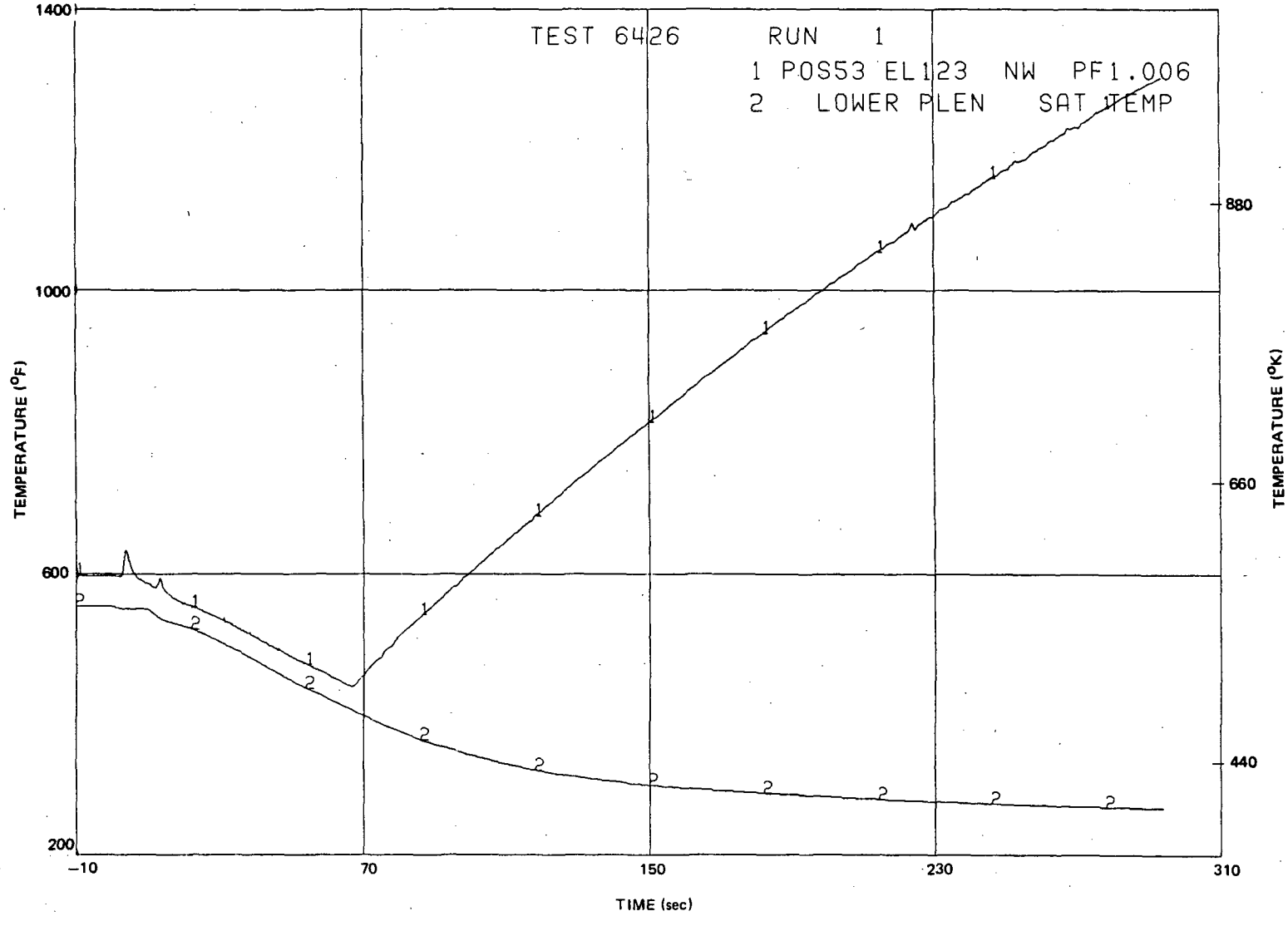

Figure L-67. Inside Clad Temperature - Elevation 123 in.

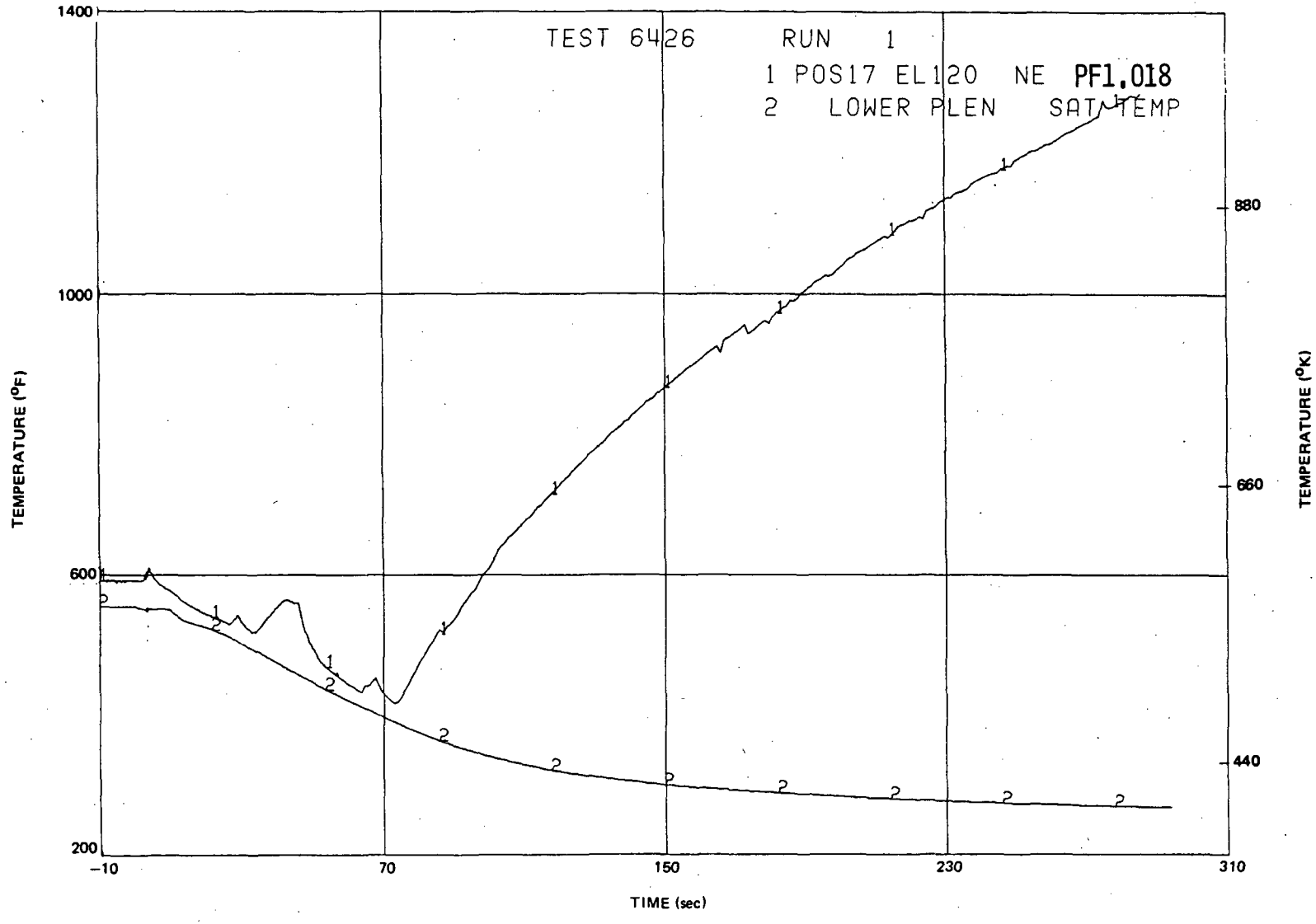

Figure L-68. Inside Clad Temperature - Elevation 120 in.

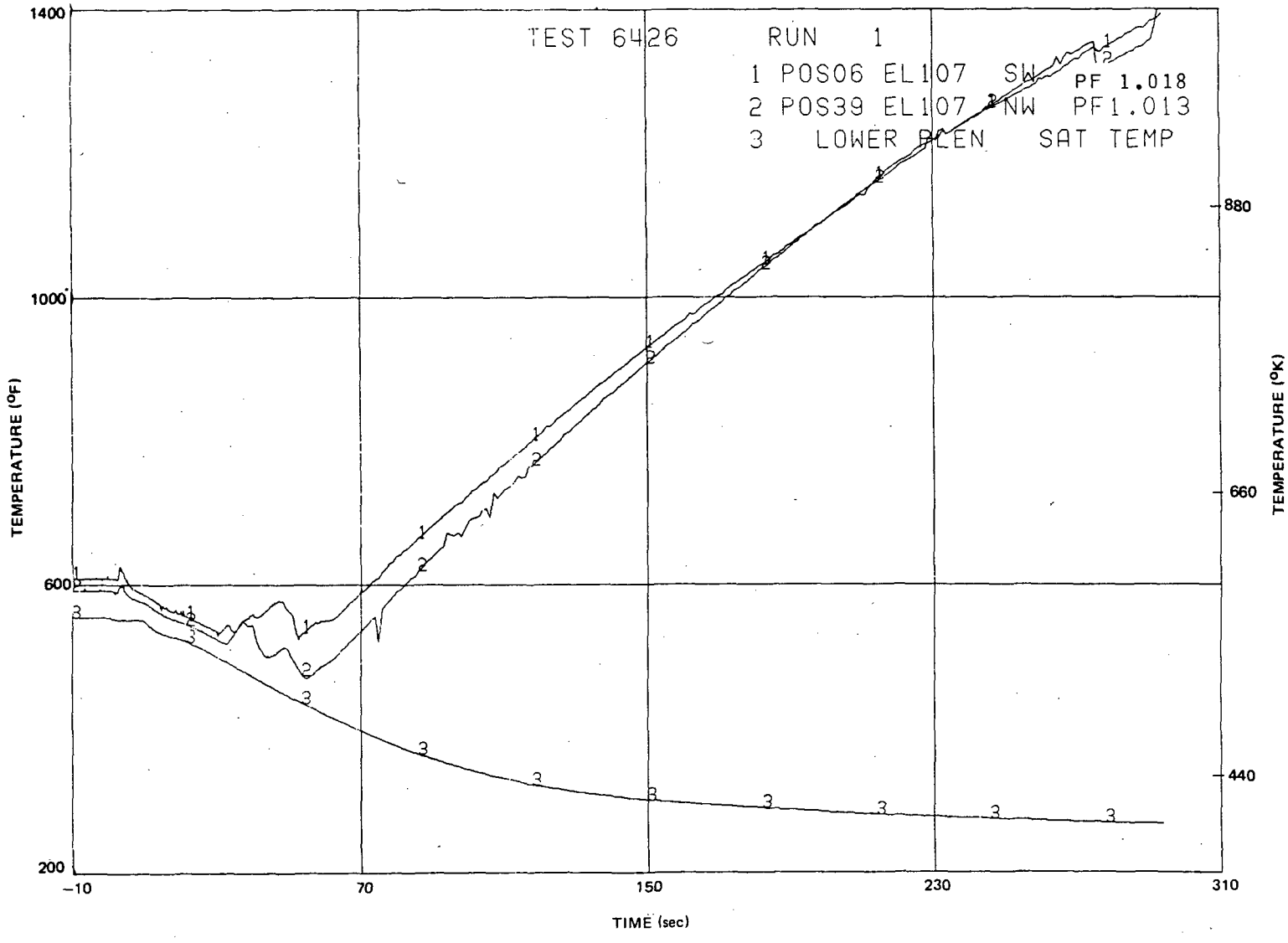

Figure L-69. Inside Clad Temperature - Elevation 107 in.

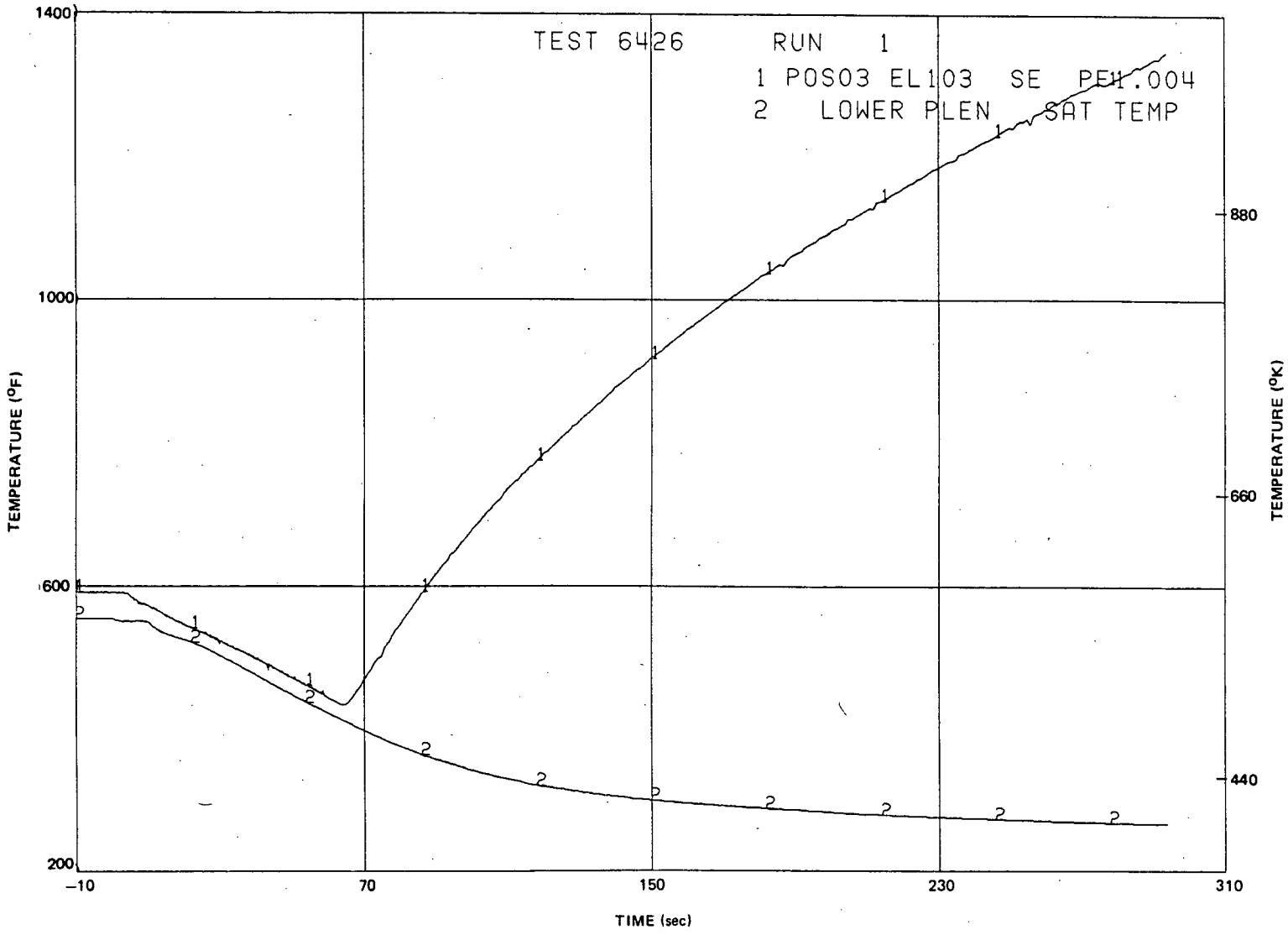

Figure L-70. Inside Clad Temperature - Elevation 103 in.

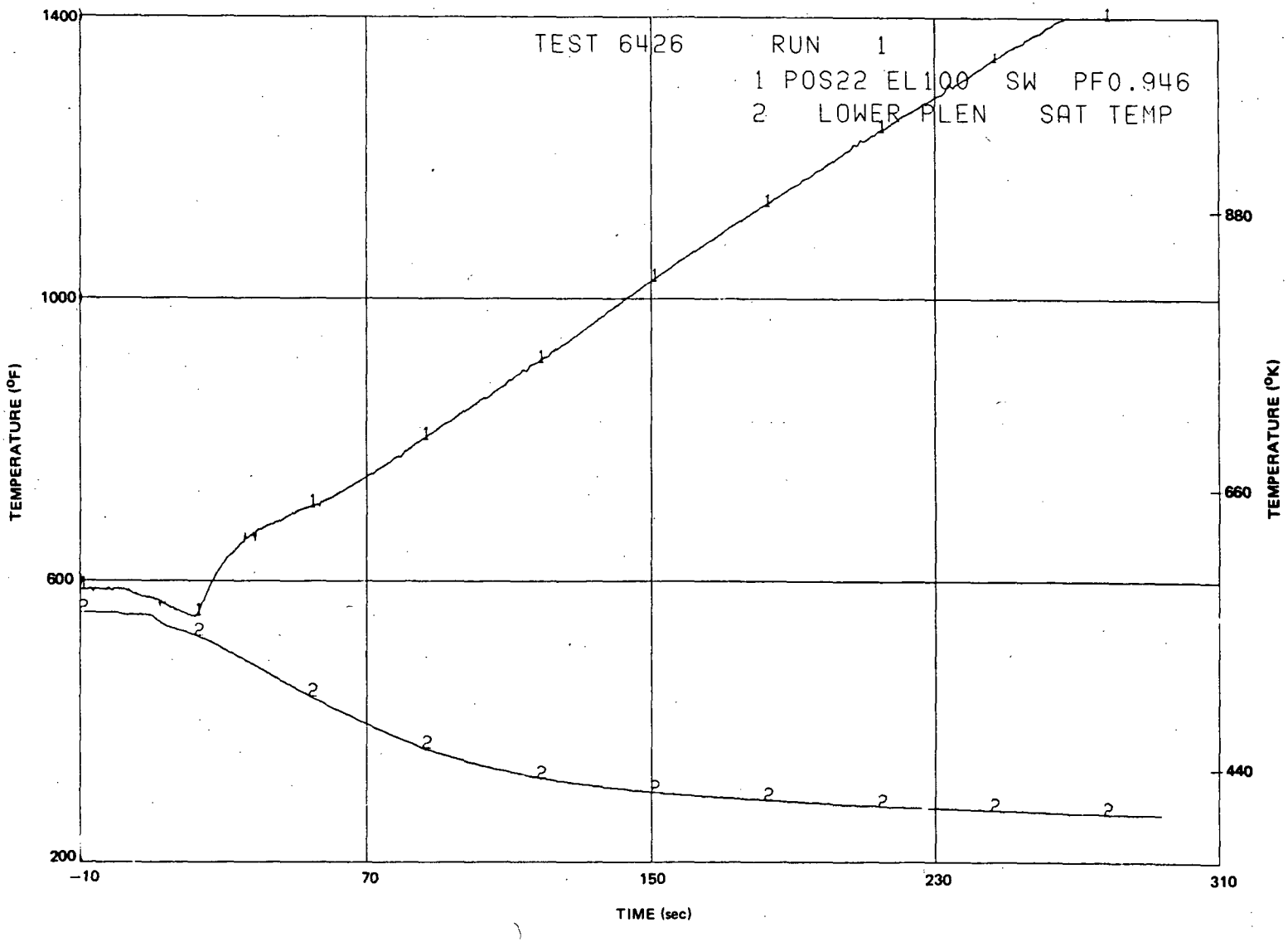

Figure L-71. Inside Clad Temperature - Elevation 100 in.

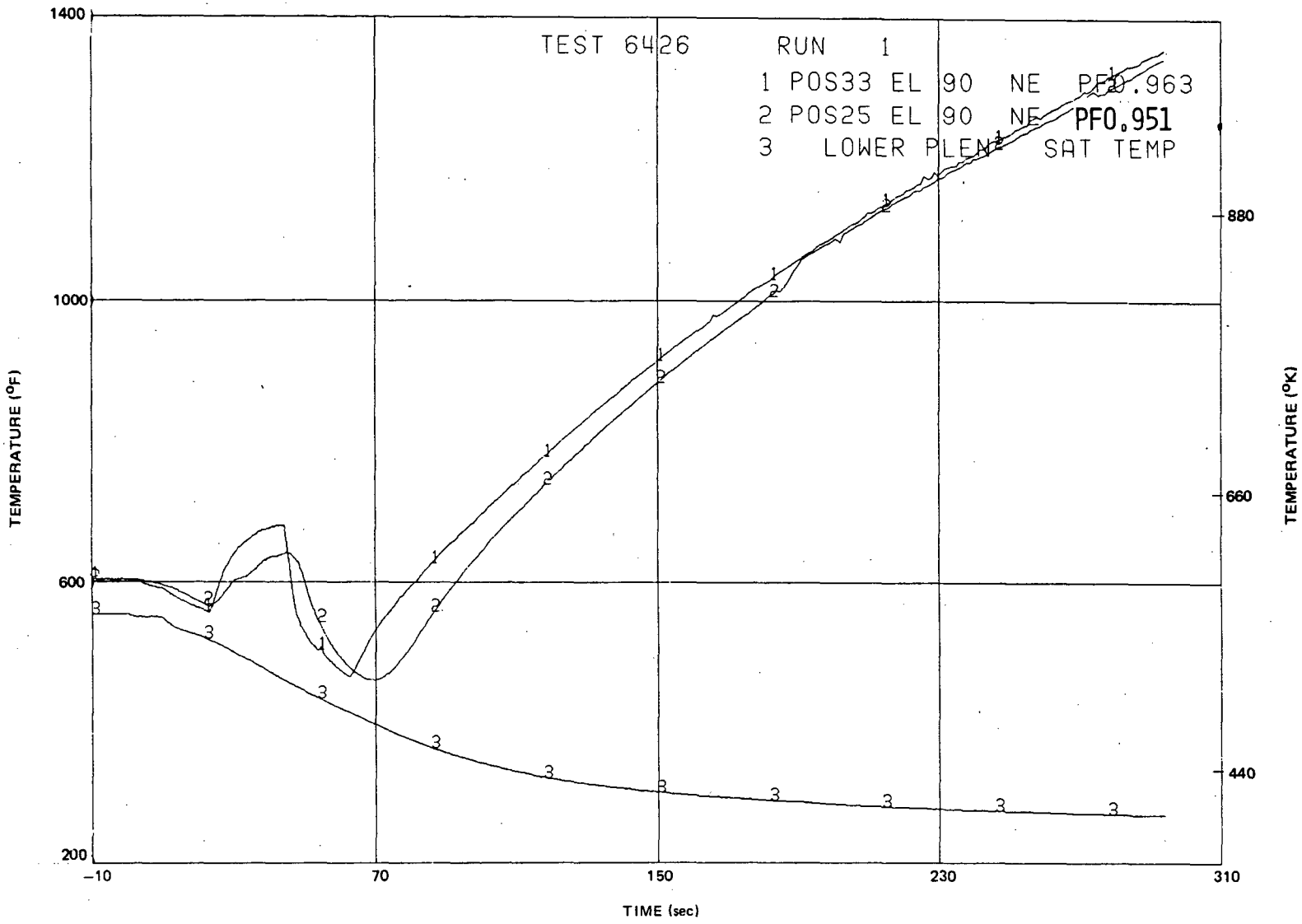

Figure L-72. Inside Clad Temperature - Elevation 90 in.

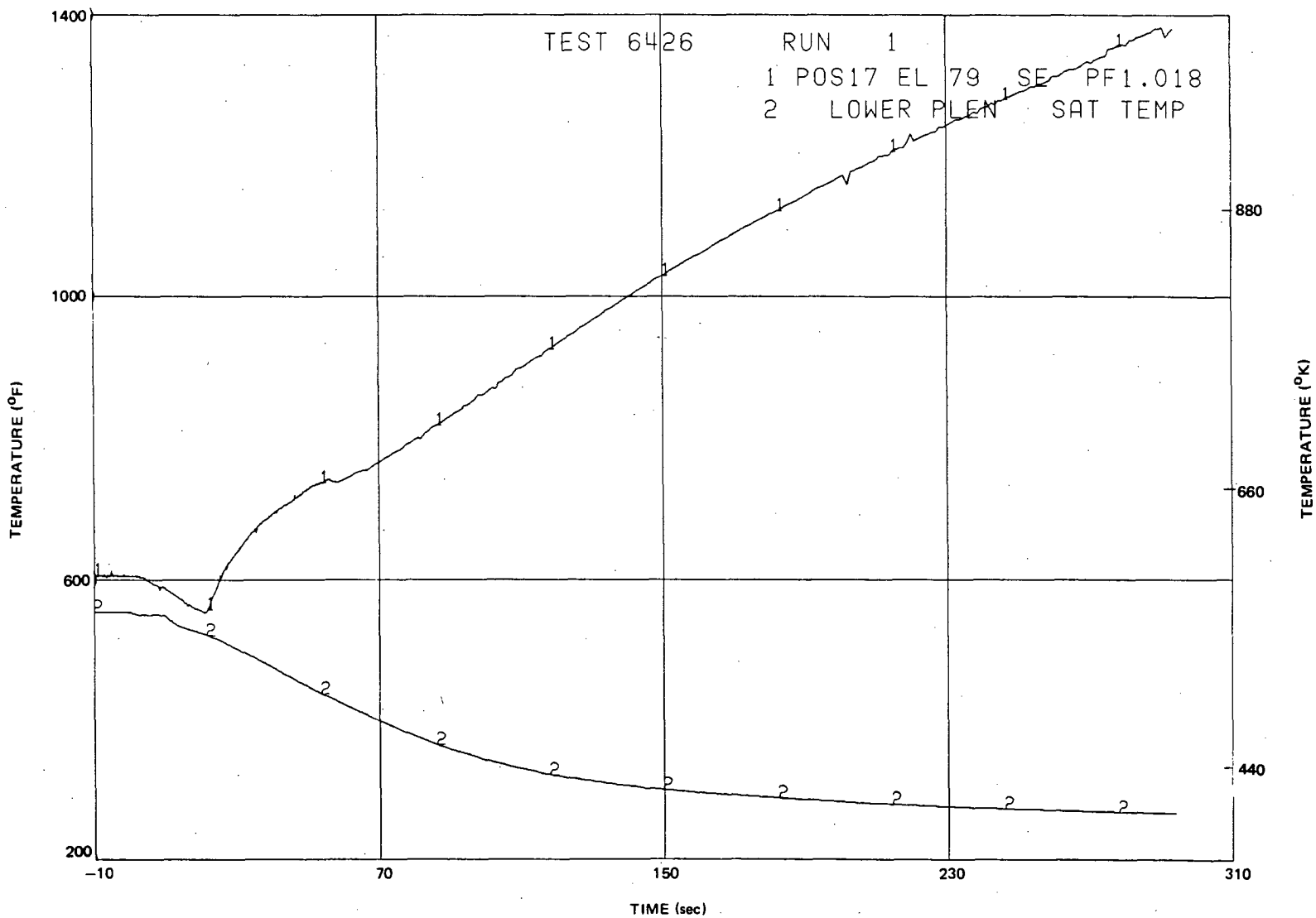

Figure L-73. Inside Clad Temperature - Elevation 79 in.

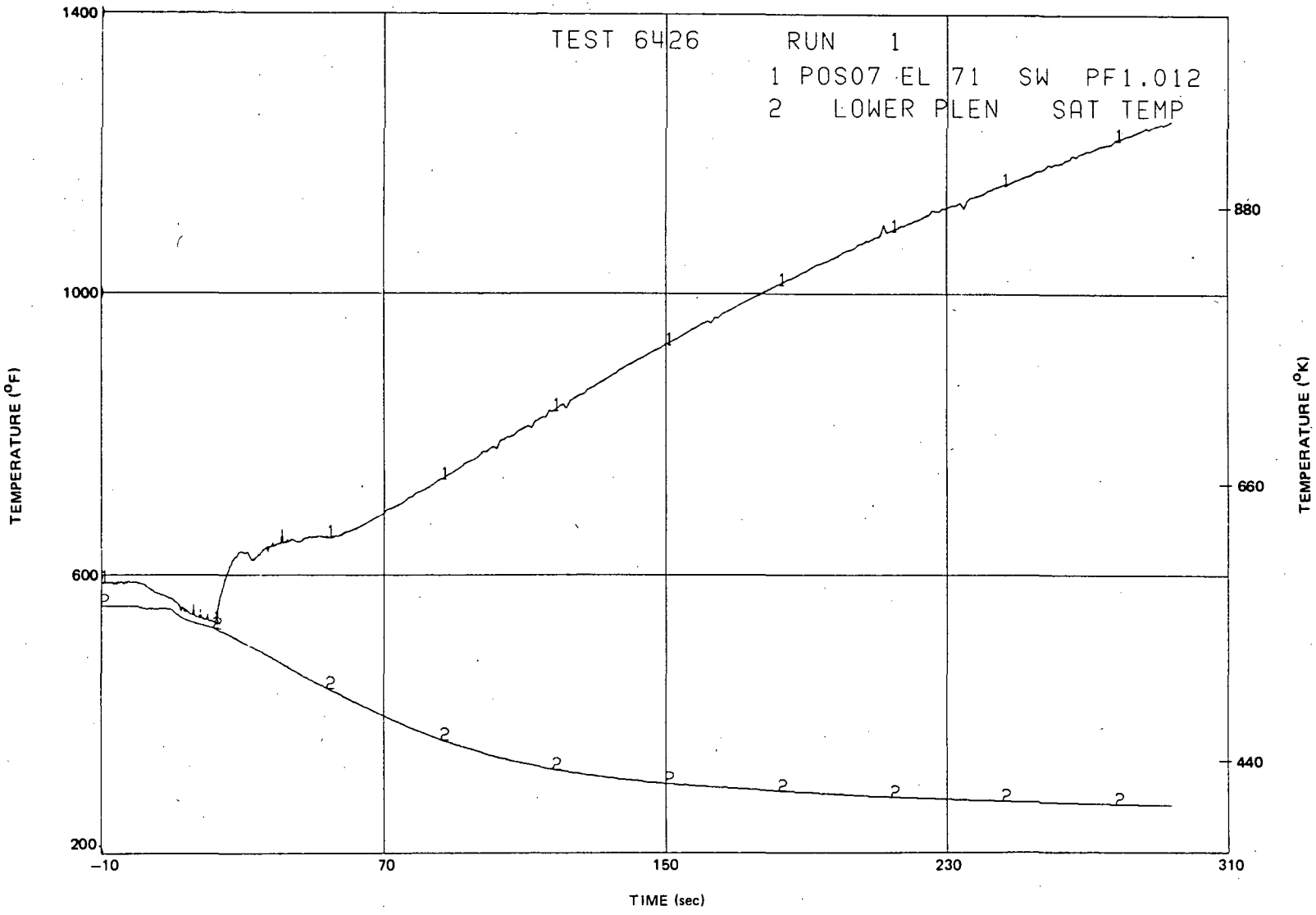

Figure L-74. Inside Clad Temperature - Elevation 71 in.

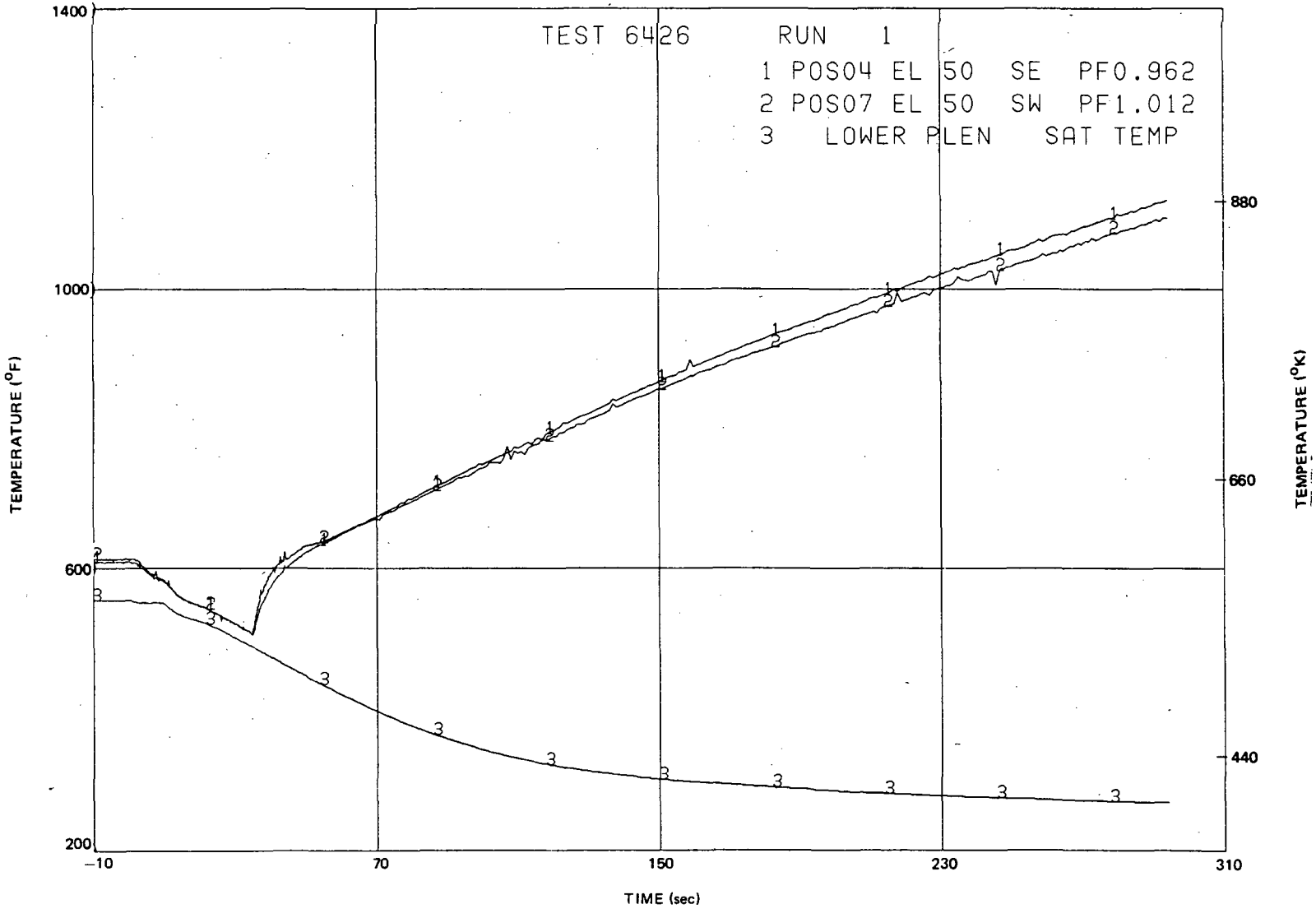

Figure L-75. Inside Clad Temperature - Elevation 50 in.

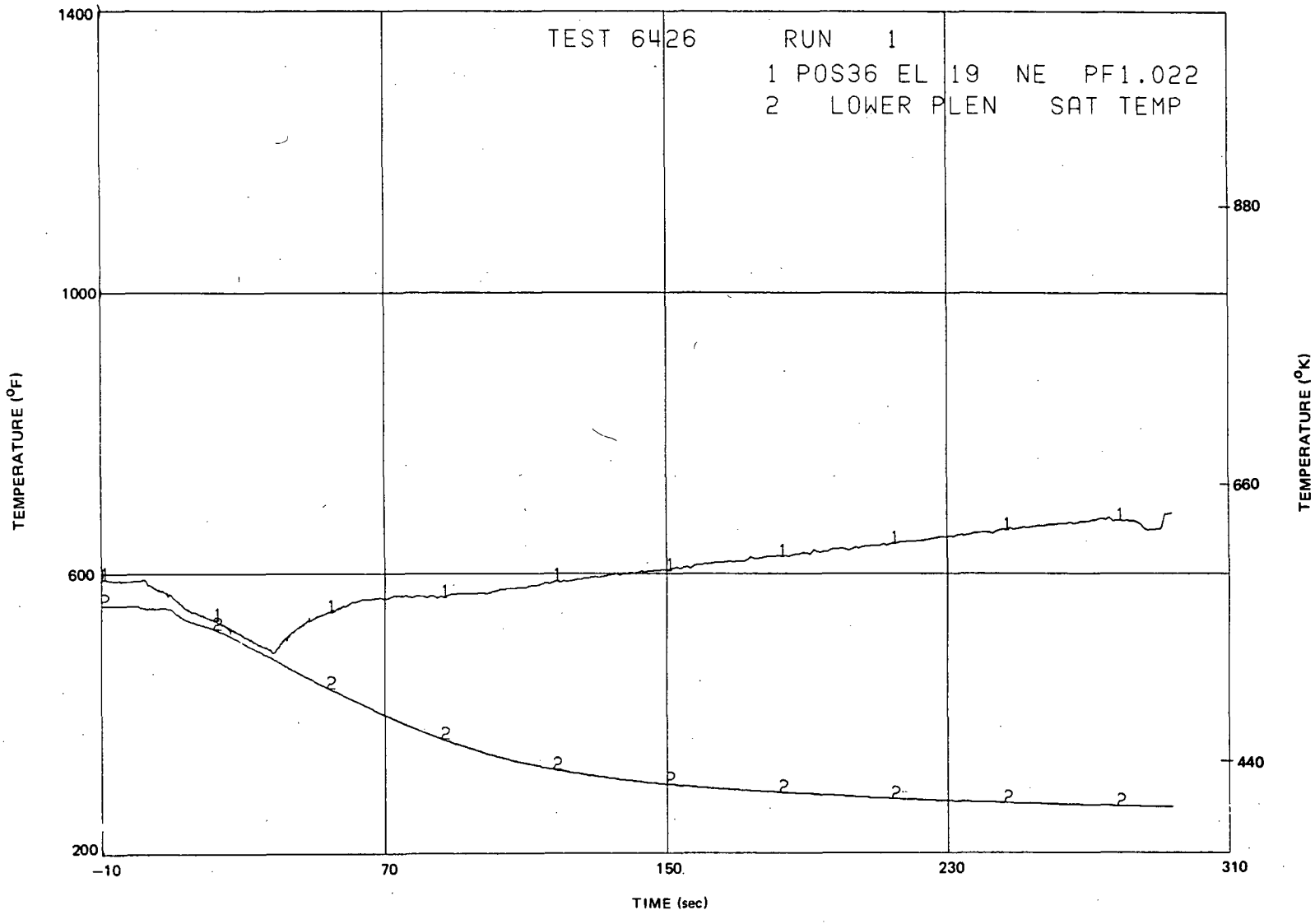

Figure L-76. Inside Clad Temperature - Elevation 19 in.

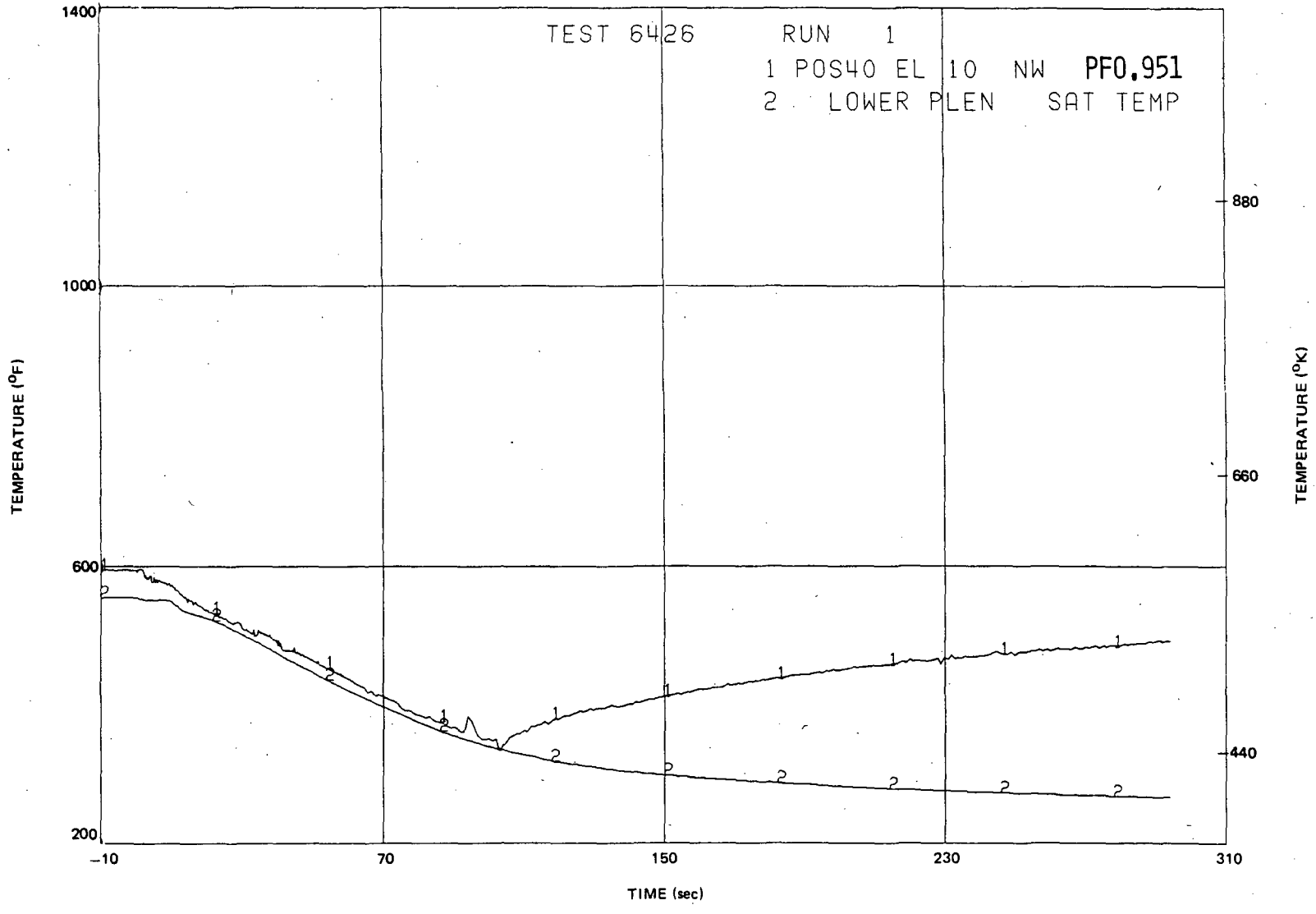

Figure L-77. Inside Clad Temperature - Elevation 10 in.

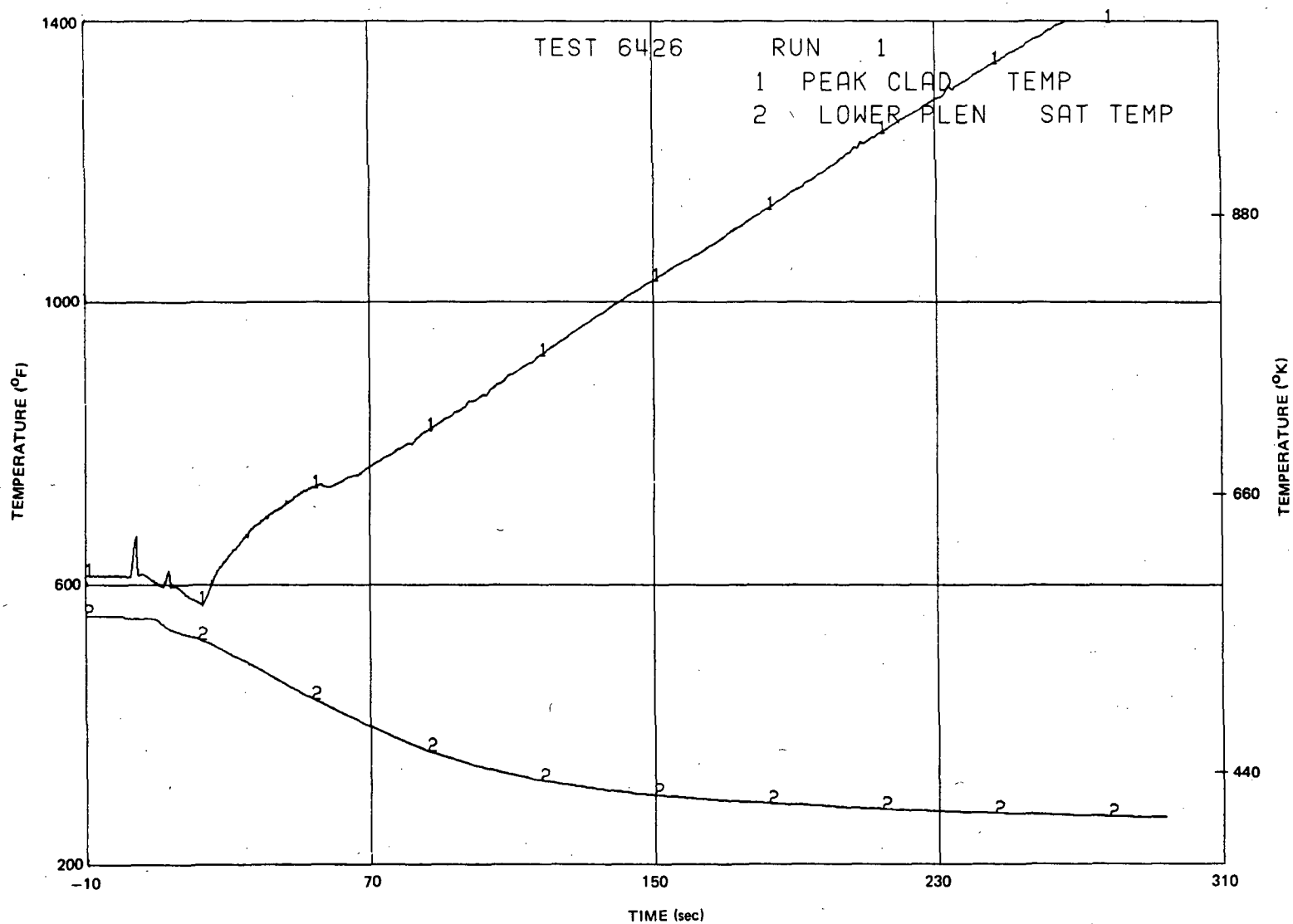

Figure L-78. Peak Clad Temperature

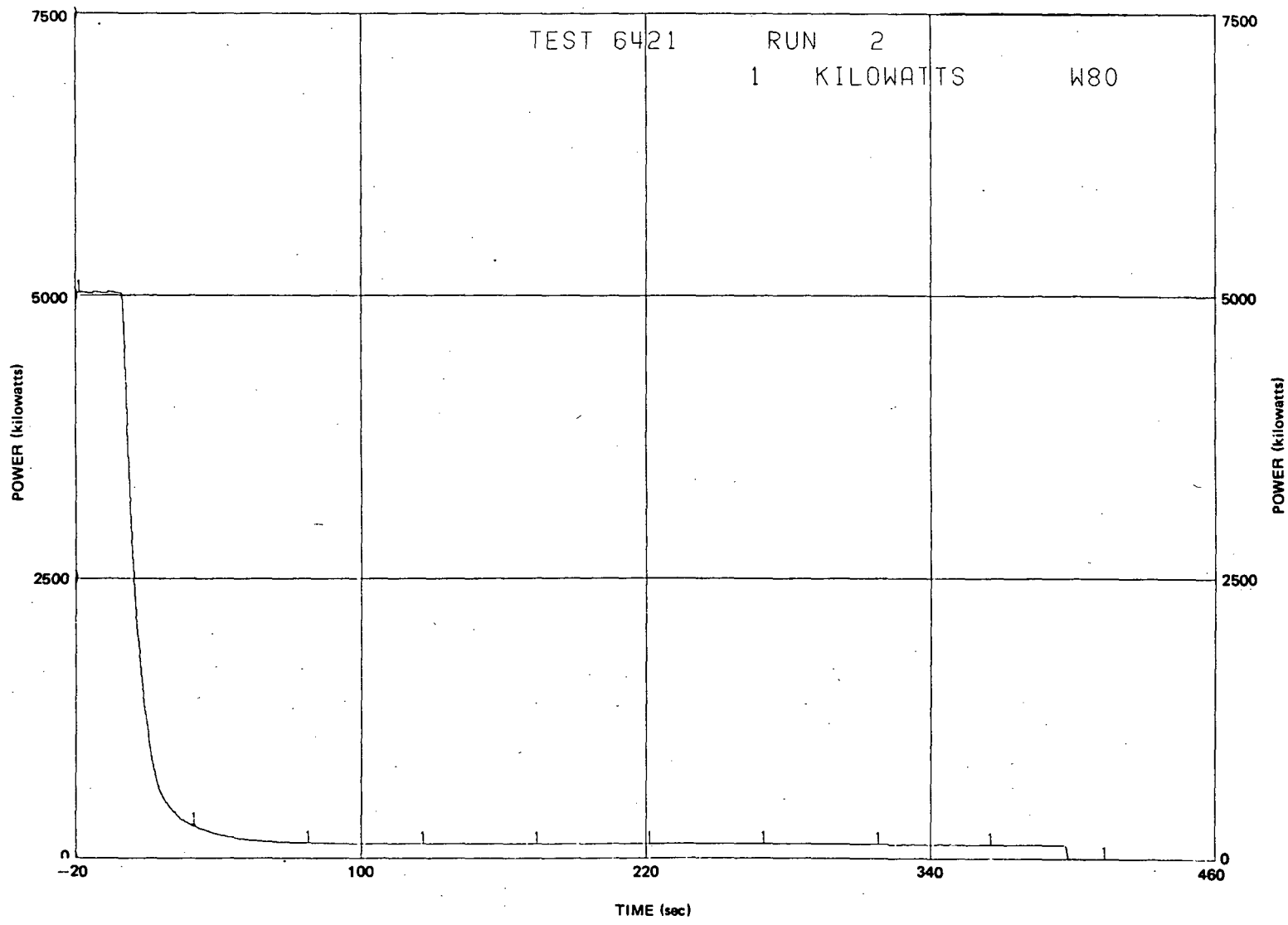

Figure L-79. Bundle Power Decay

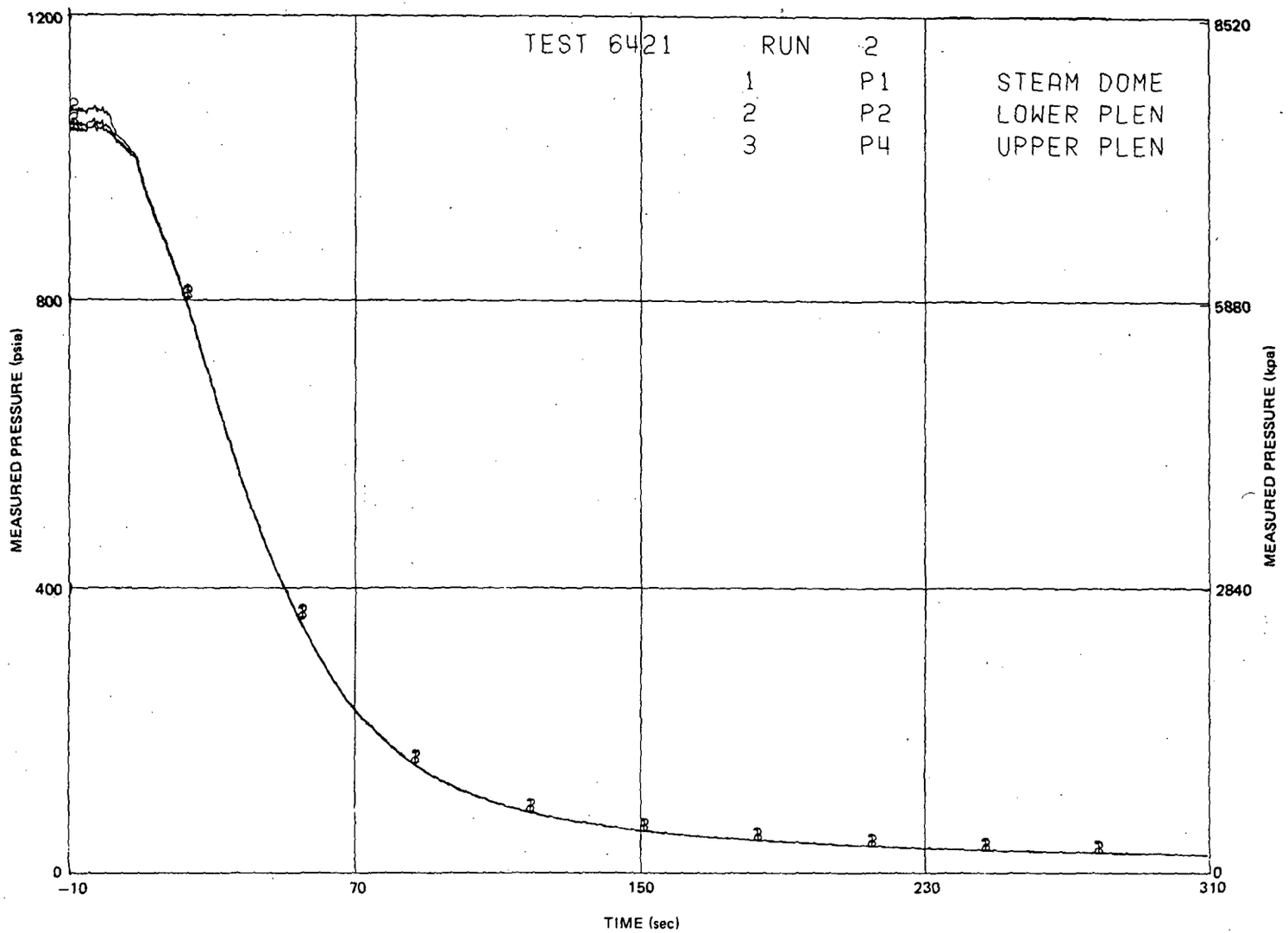

Figure L-80. System Pressures

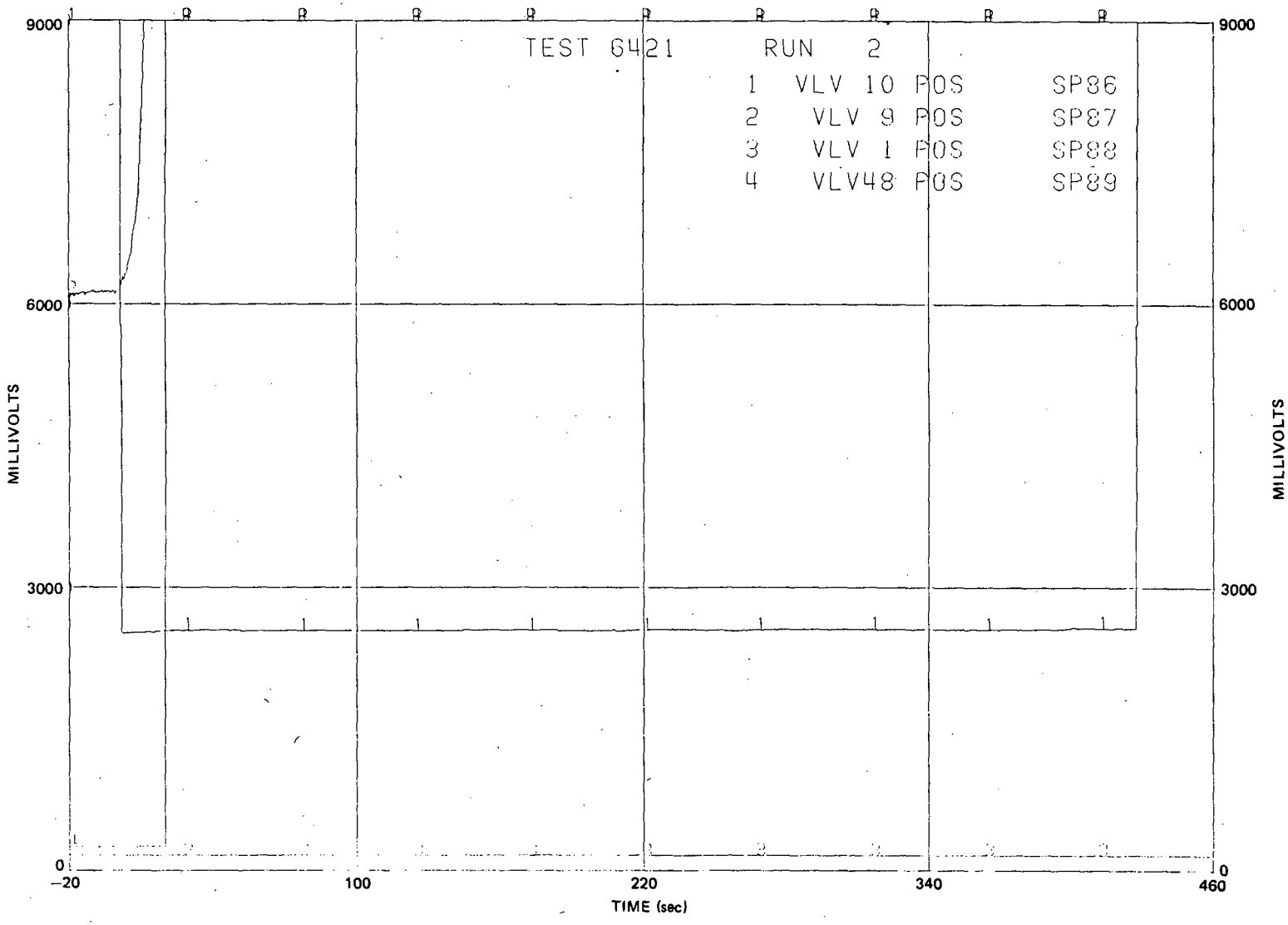

Figure L-81. Valve Positions

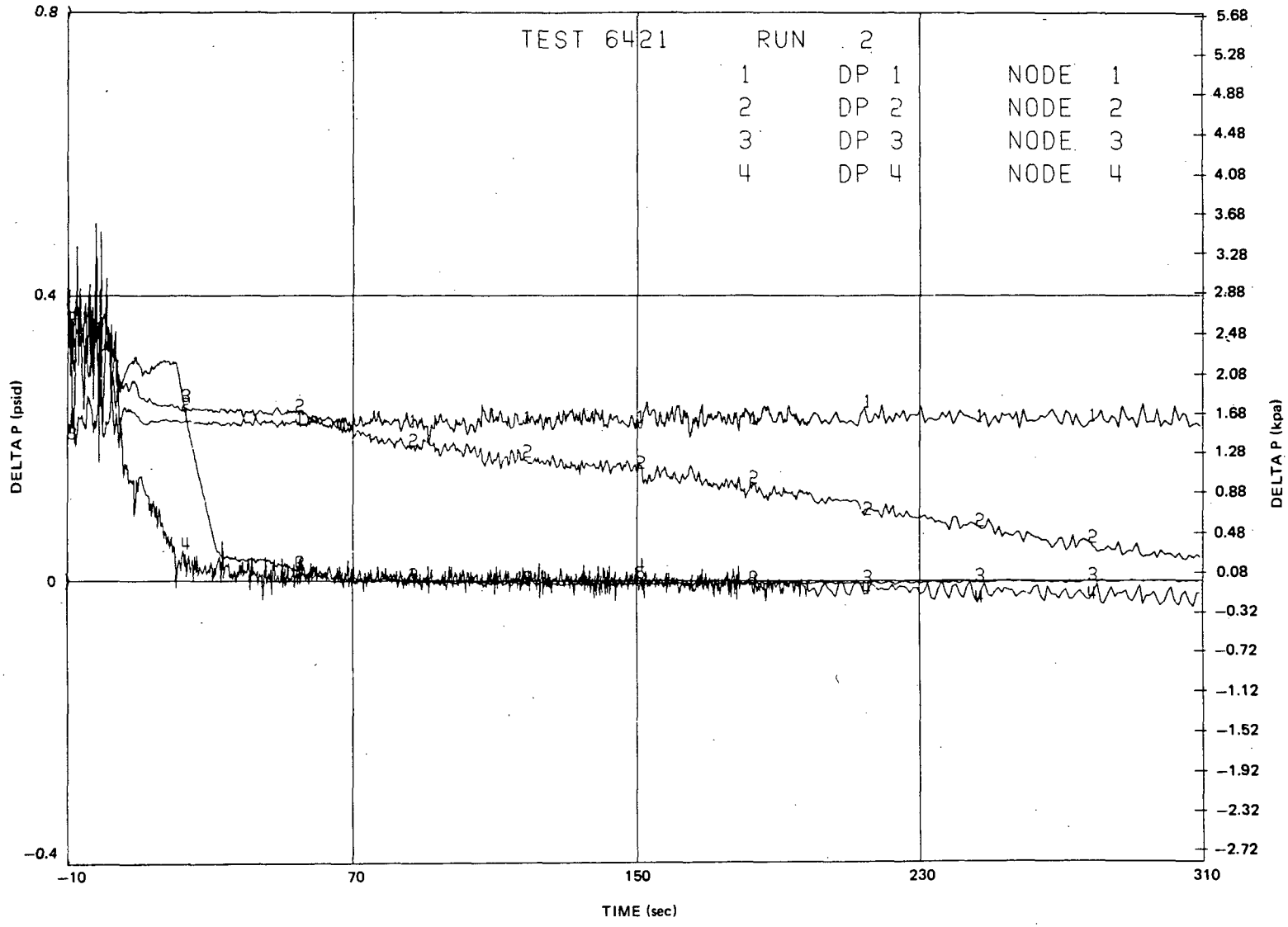

Figure L-82. Lower Plenum Differential Pressures

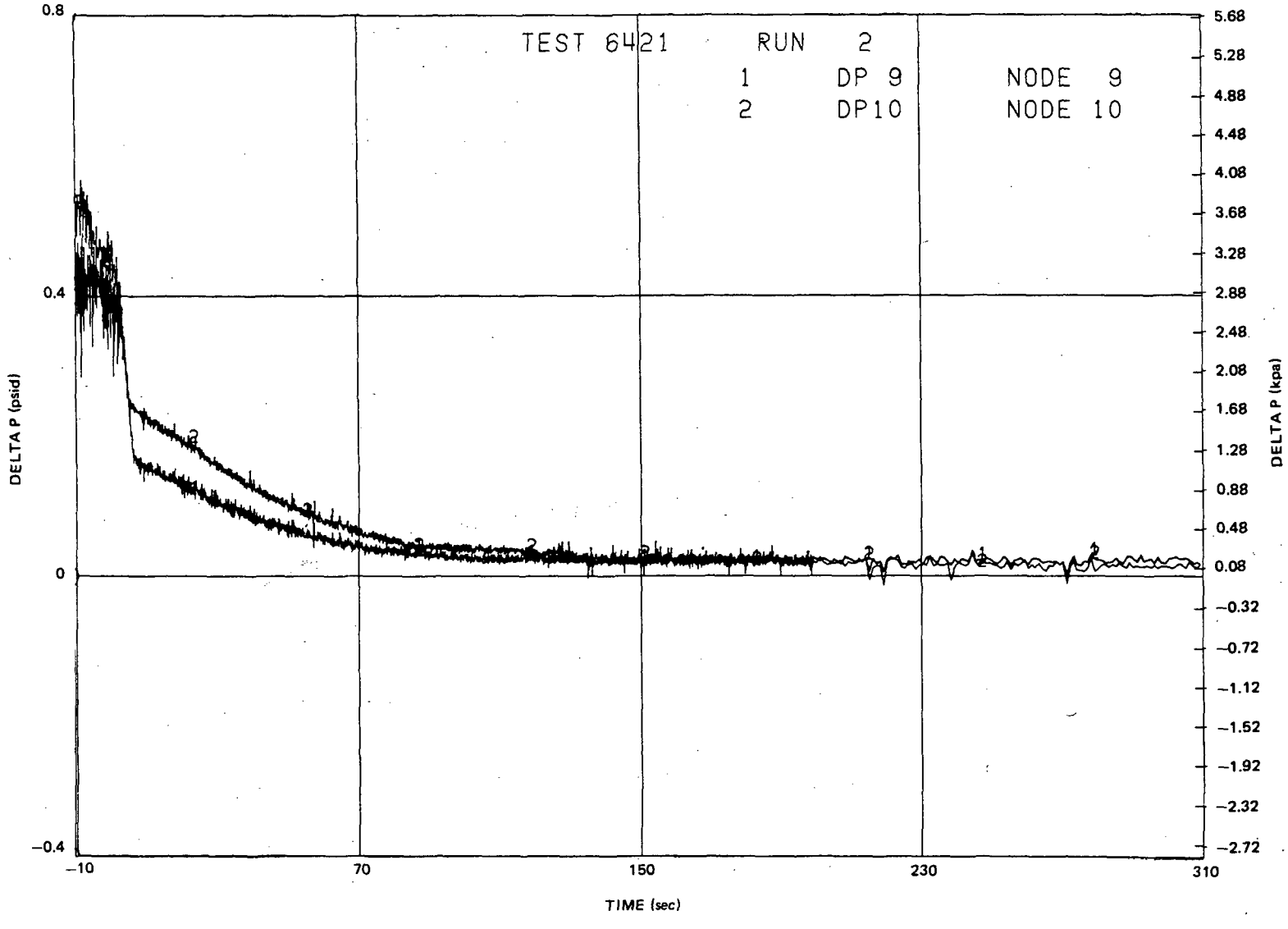

Figure L-83. Upper Annulus Differential Pressures

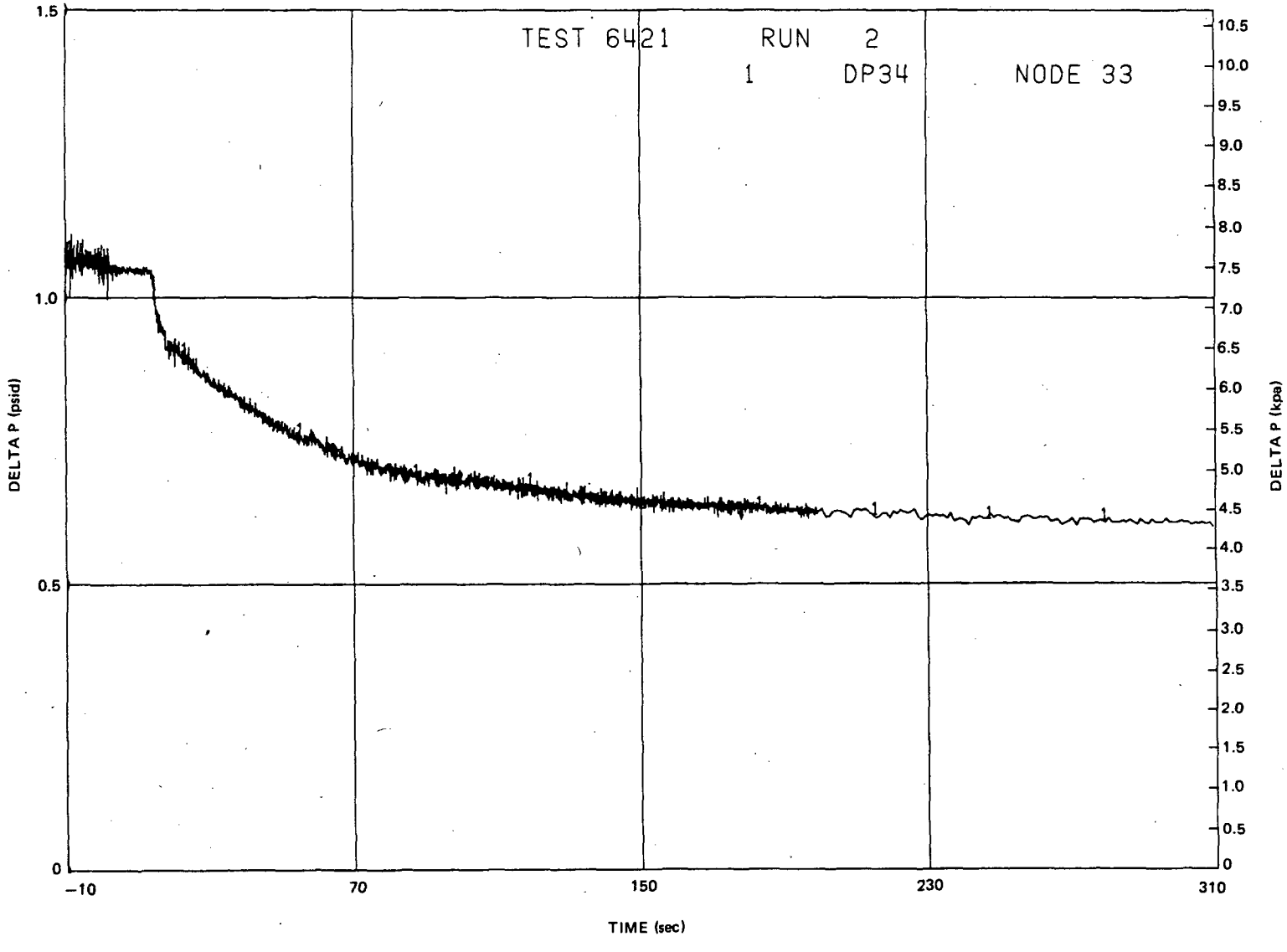

Figure L-84. Guide Tube Differential Pressure

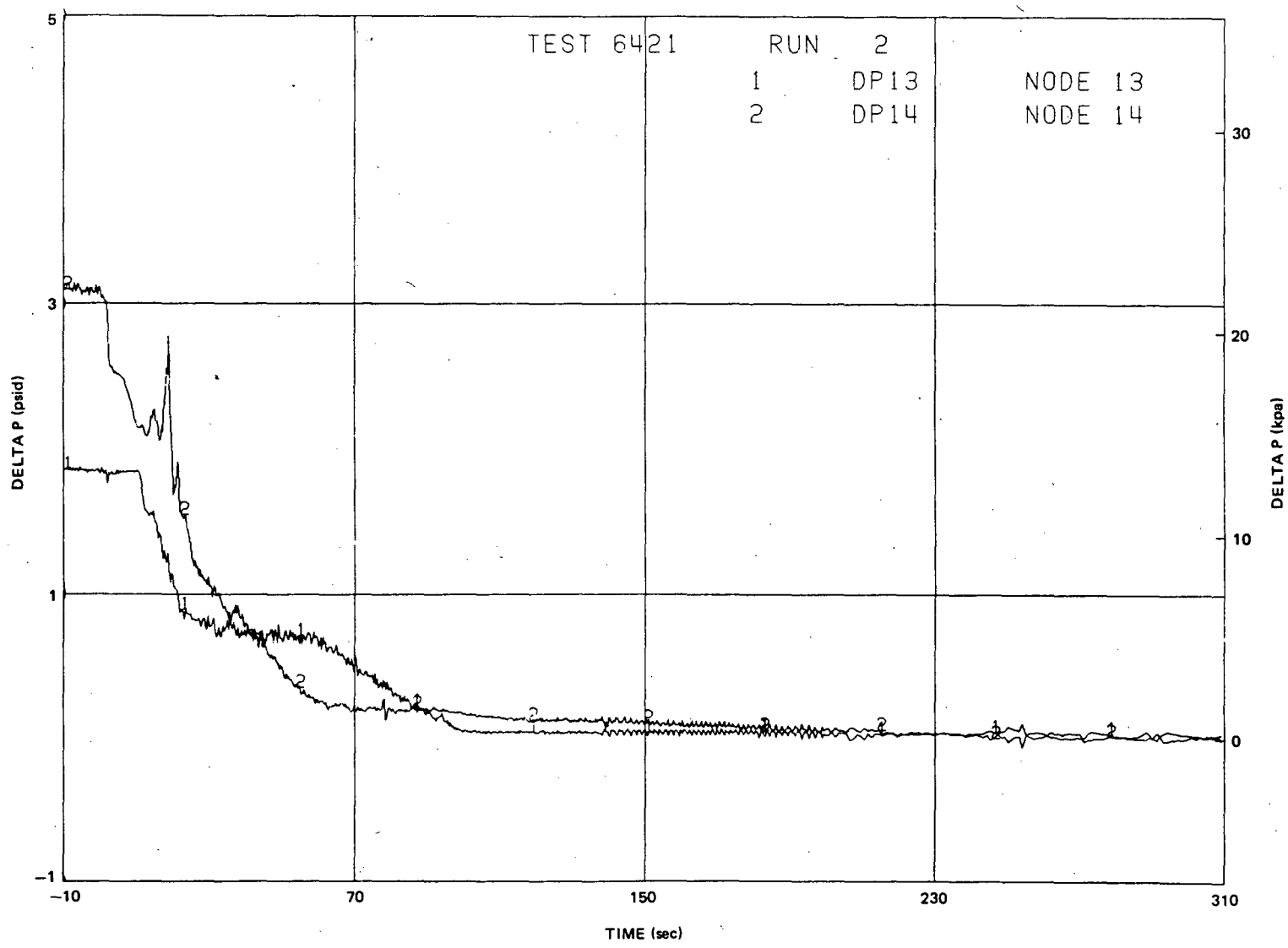

Figure L-85. Bypass Differential Pressures

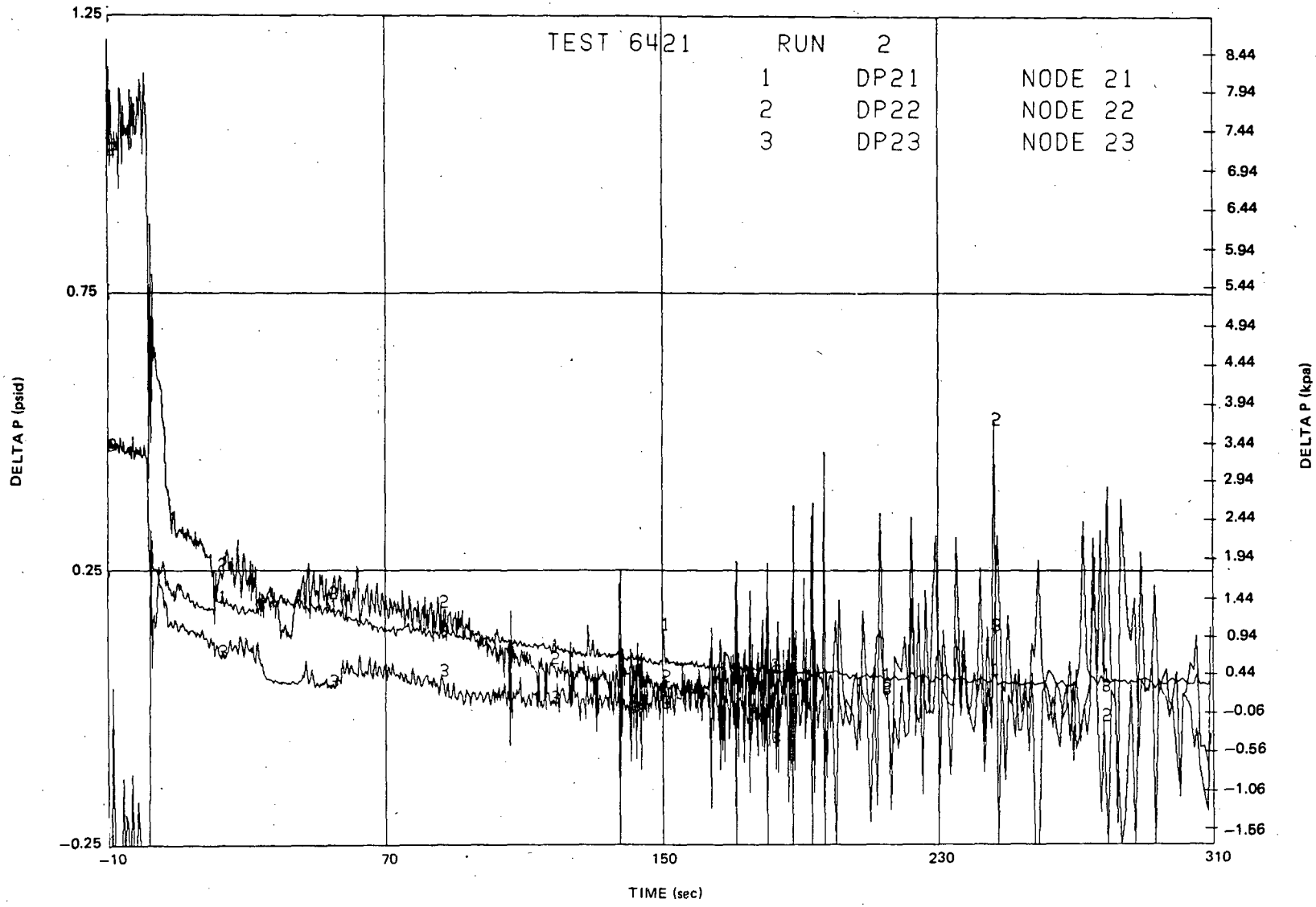

Figure L-86. Lower Bundle Differential Pressures

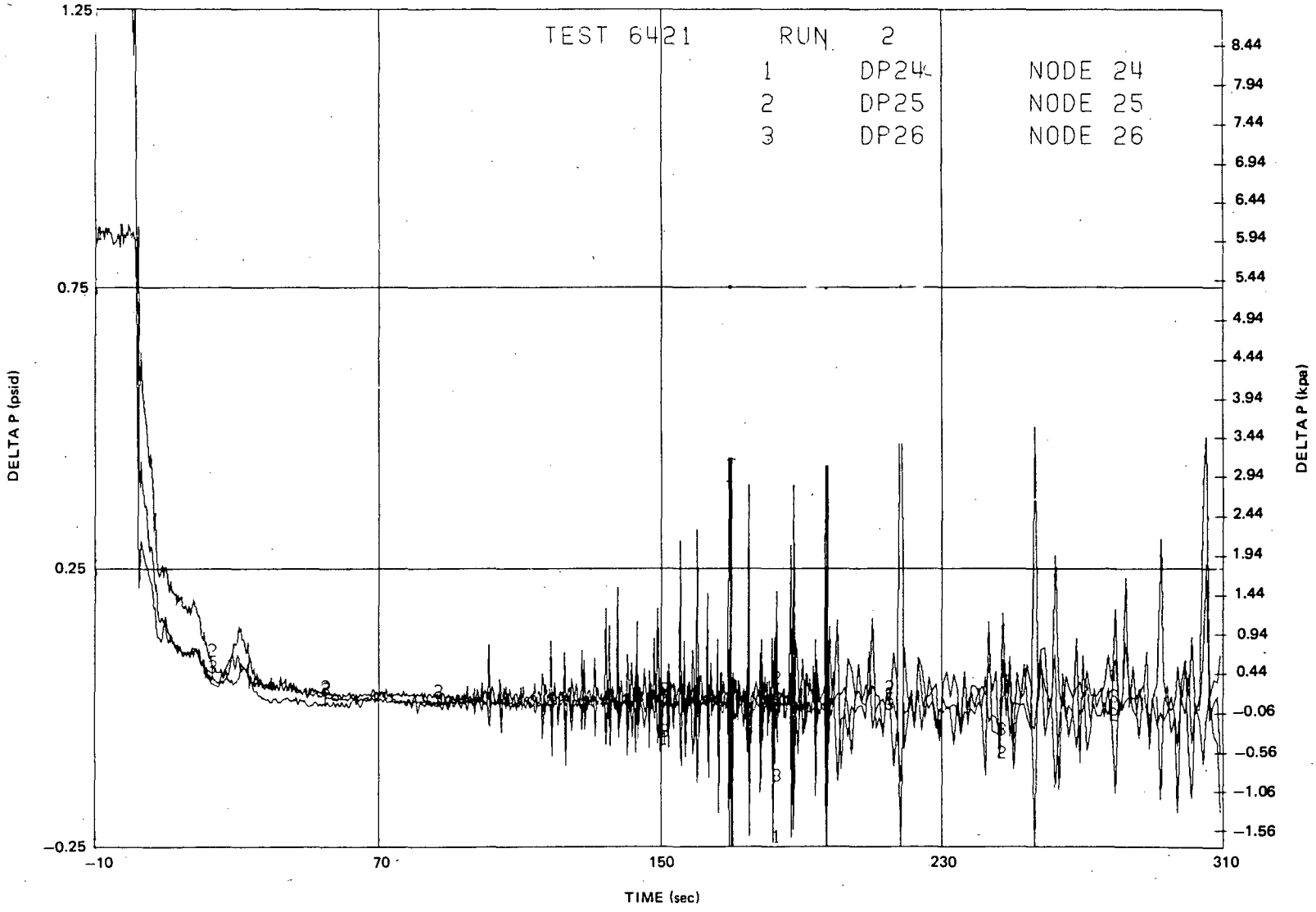

Figure L-87. Middle Bundle Differential Pressures

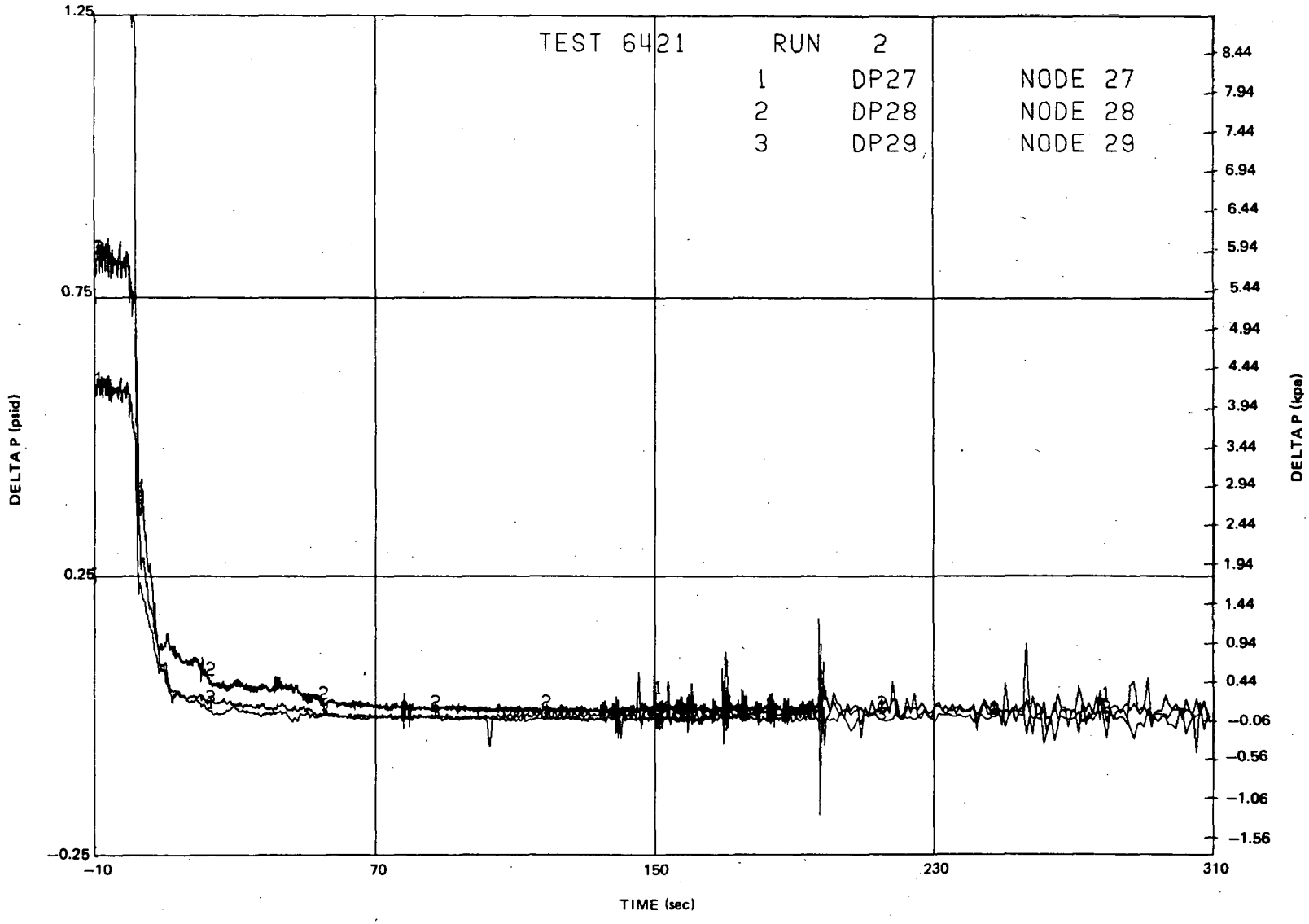

Figure L-88. Upper Bundle Differential Pressures

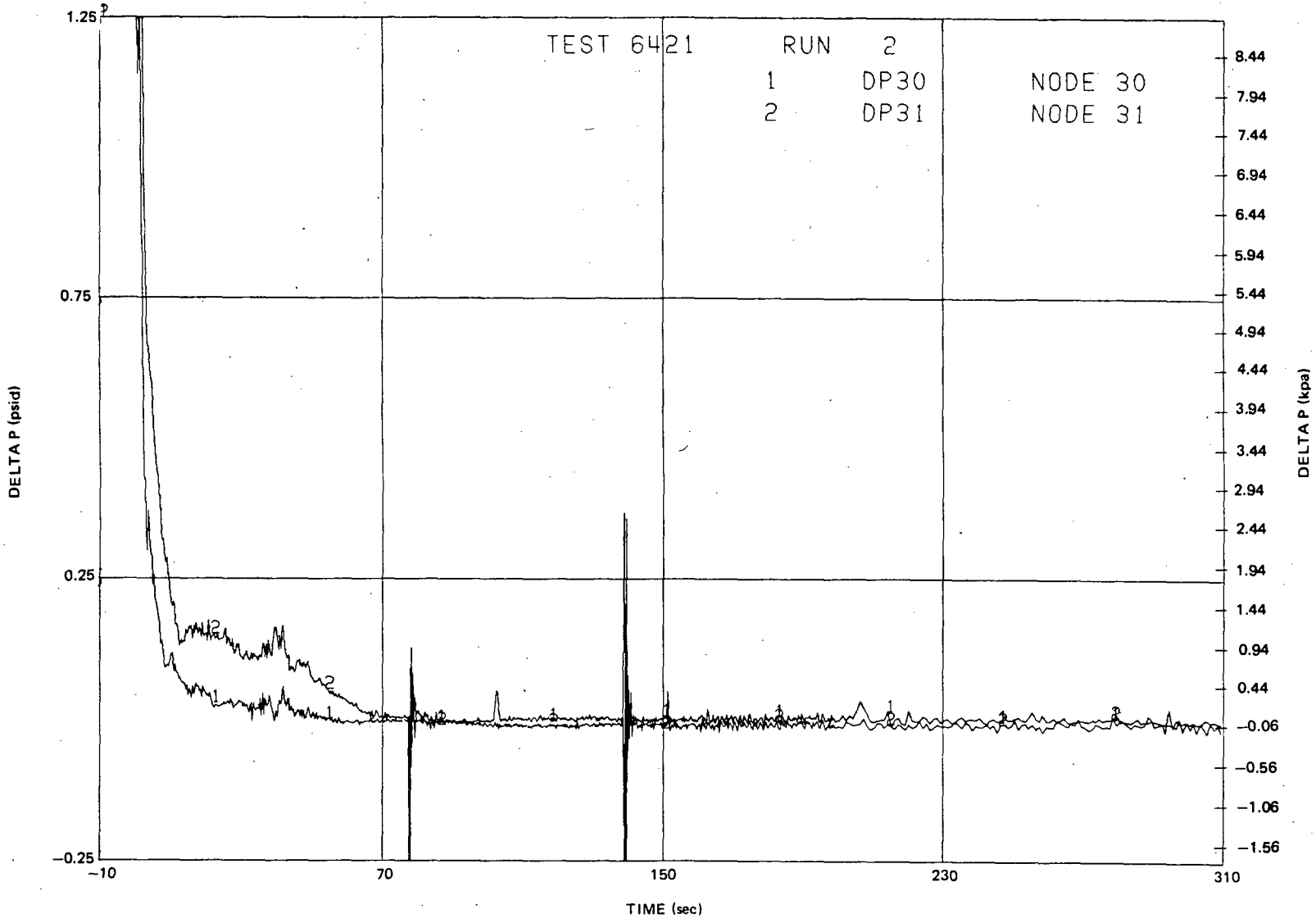

Figure L-89. Top Bundle Differential Pressures

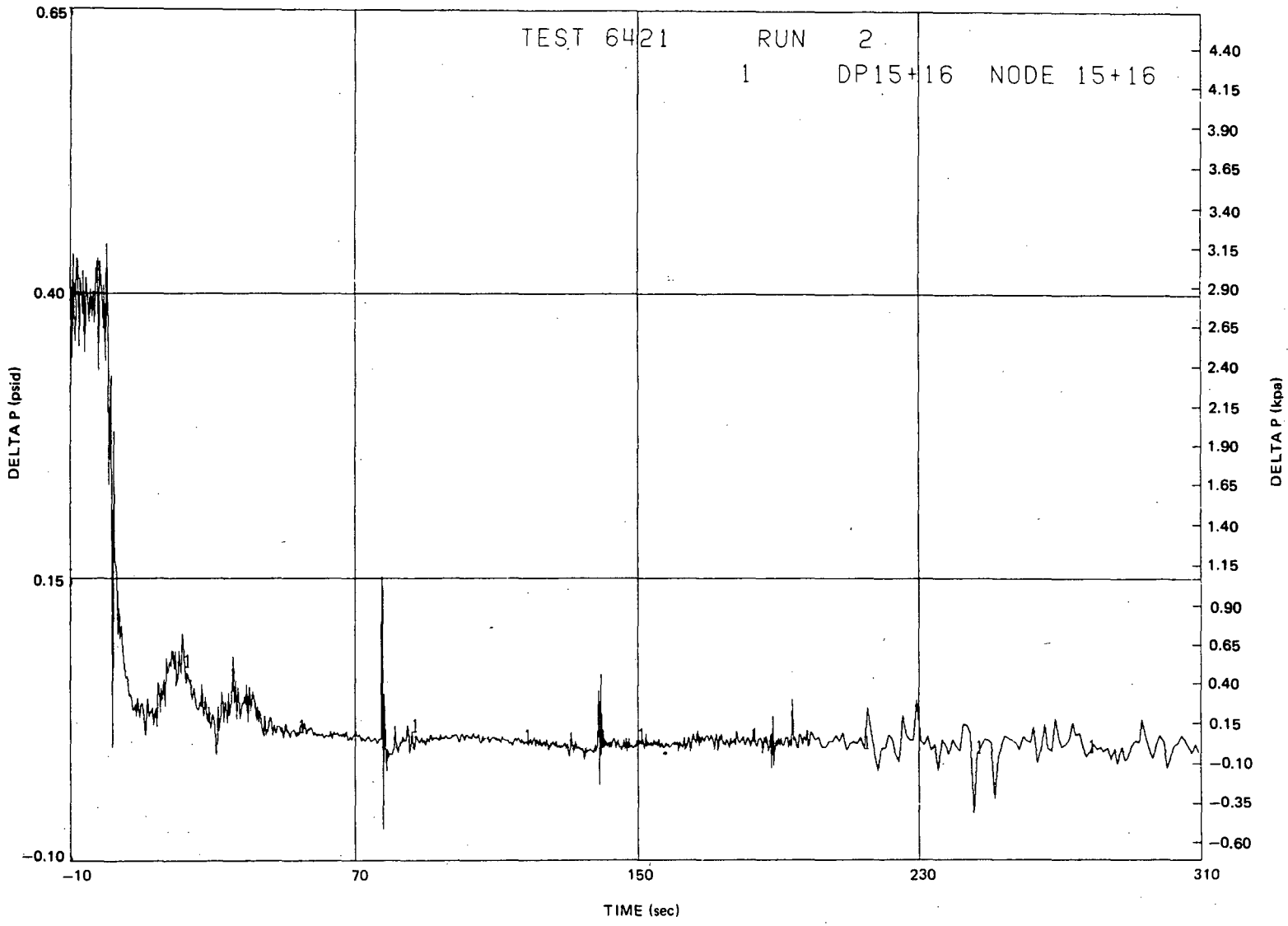

Figure L-90. Mixing Plenum Differential Pressure

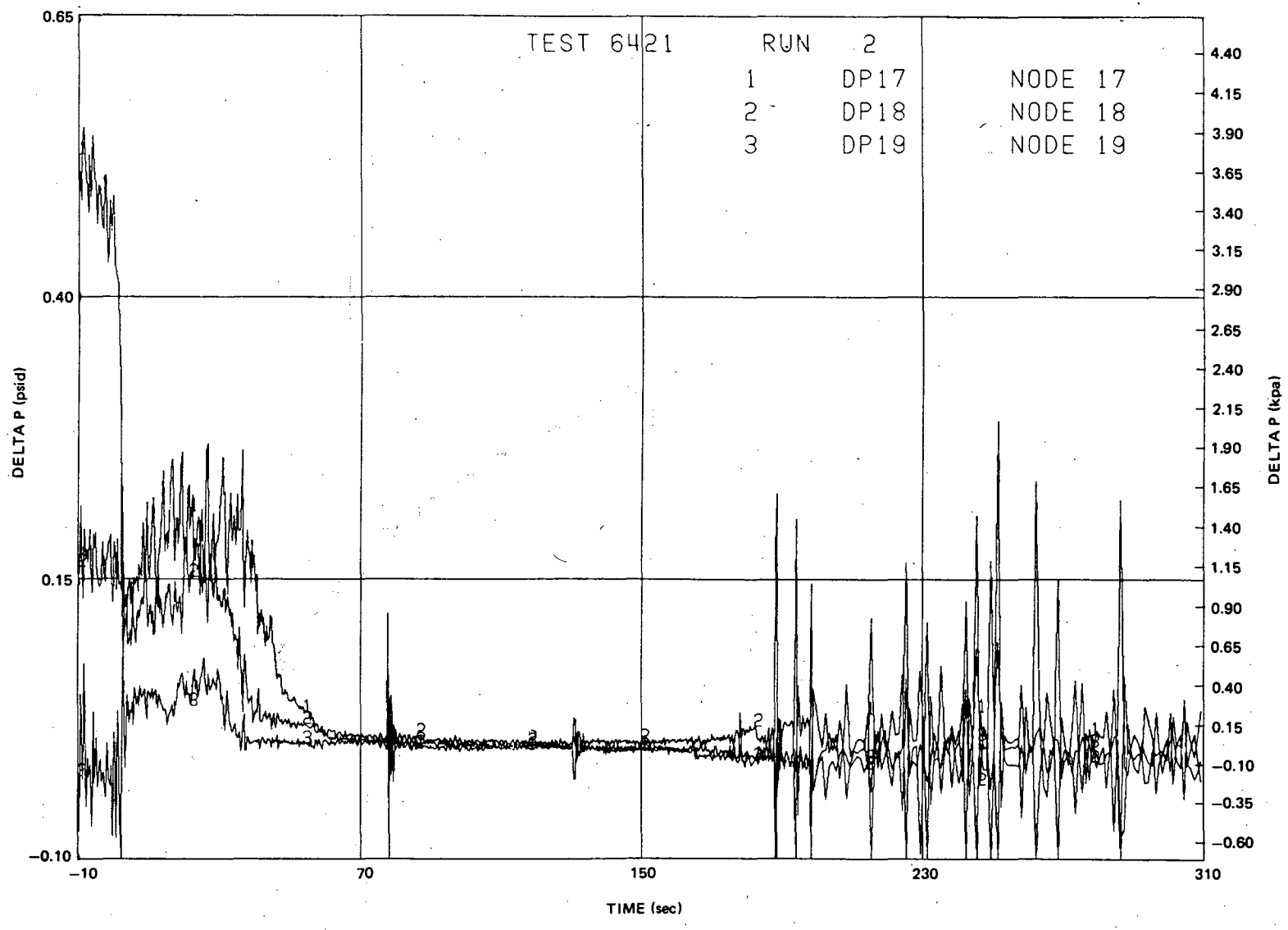

Figure L-91. Upper Plenum Differential Pressures

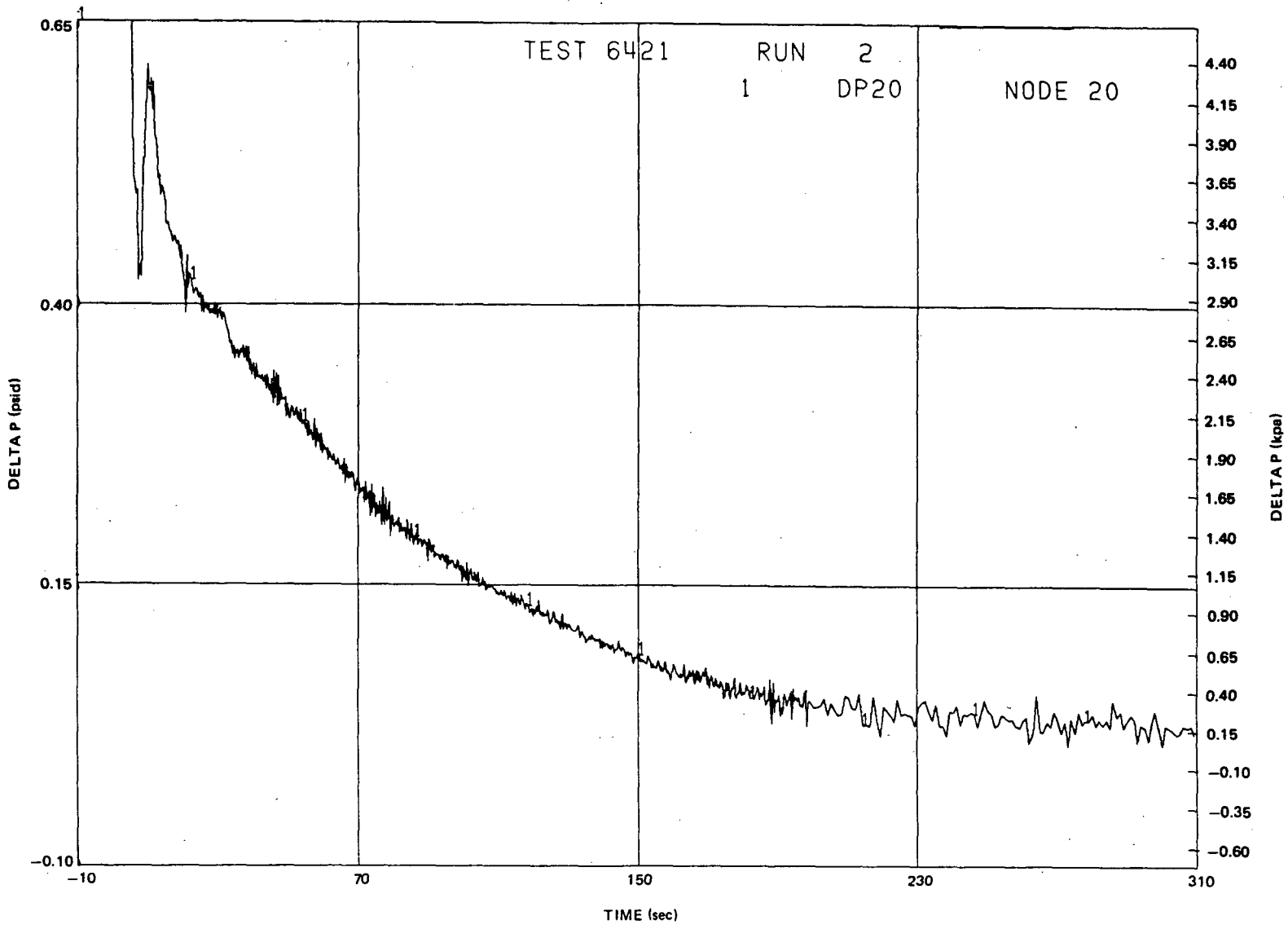

Figure L-92. Steam Separator Differential Pressure

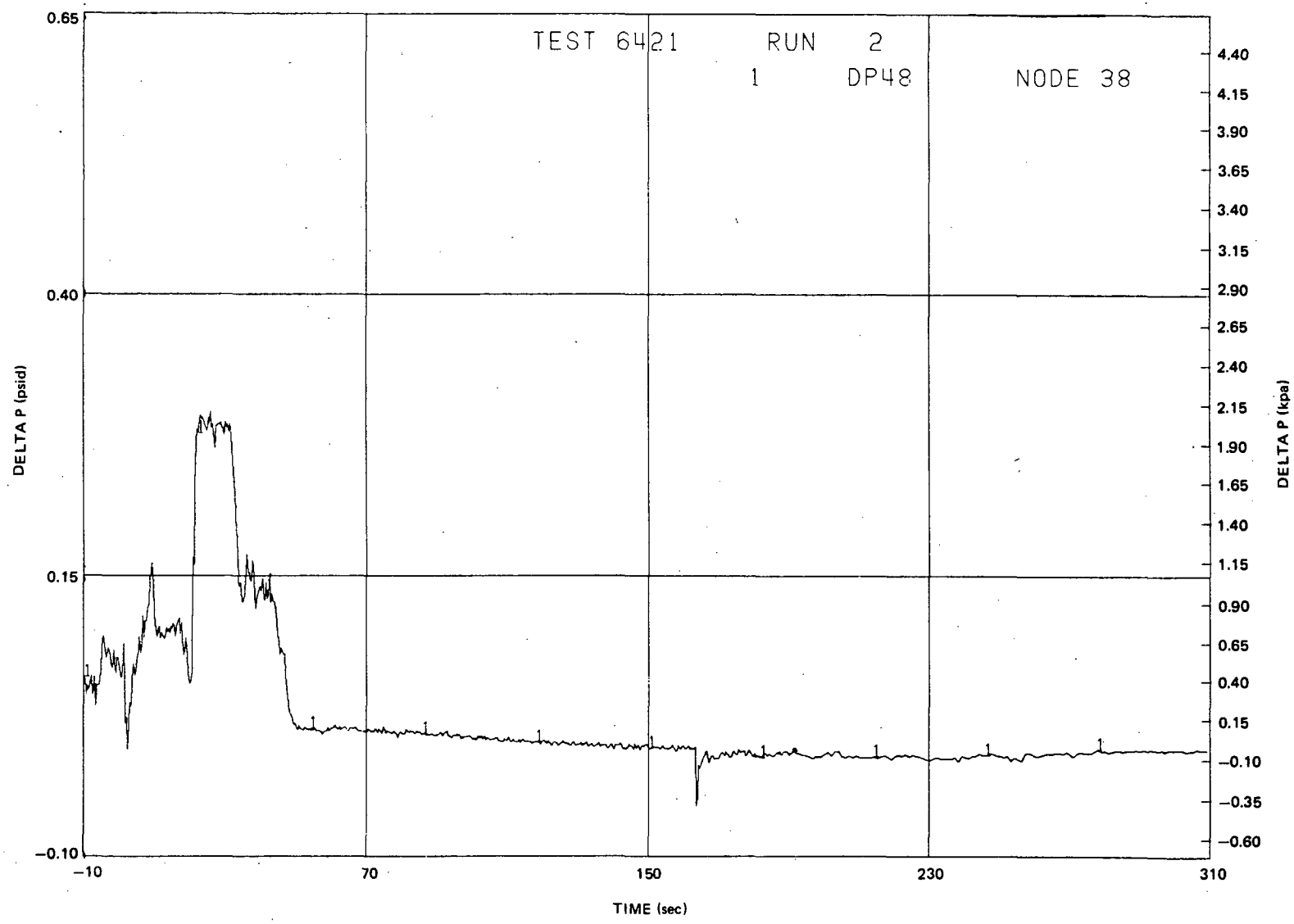

Figure L-93. Intact Loop Jet Pump Differential Pressure

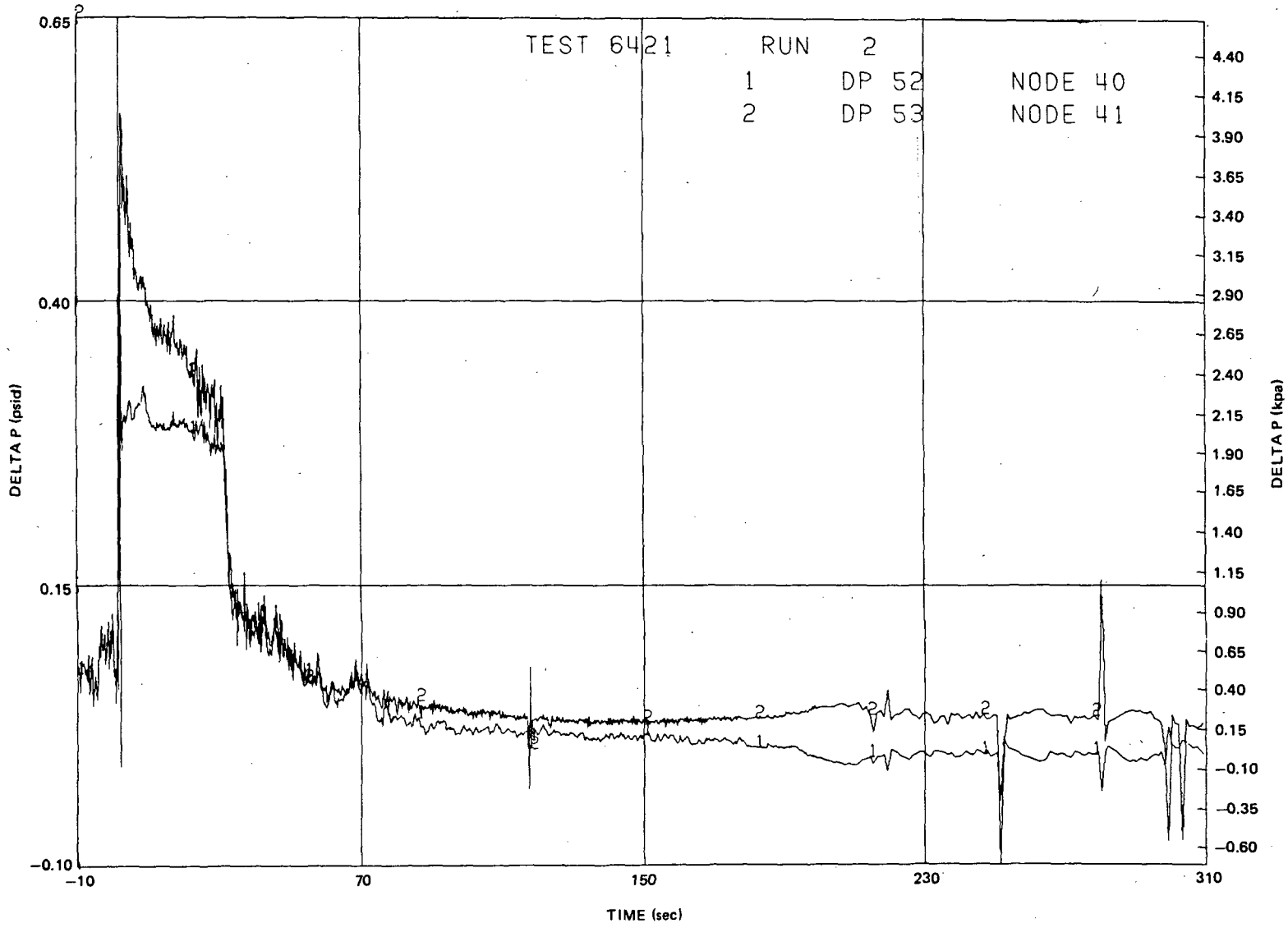

Figure L-94. Broken Loop Jet Pump Differential Pressures

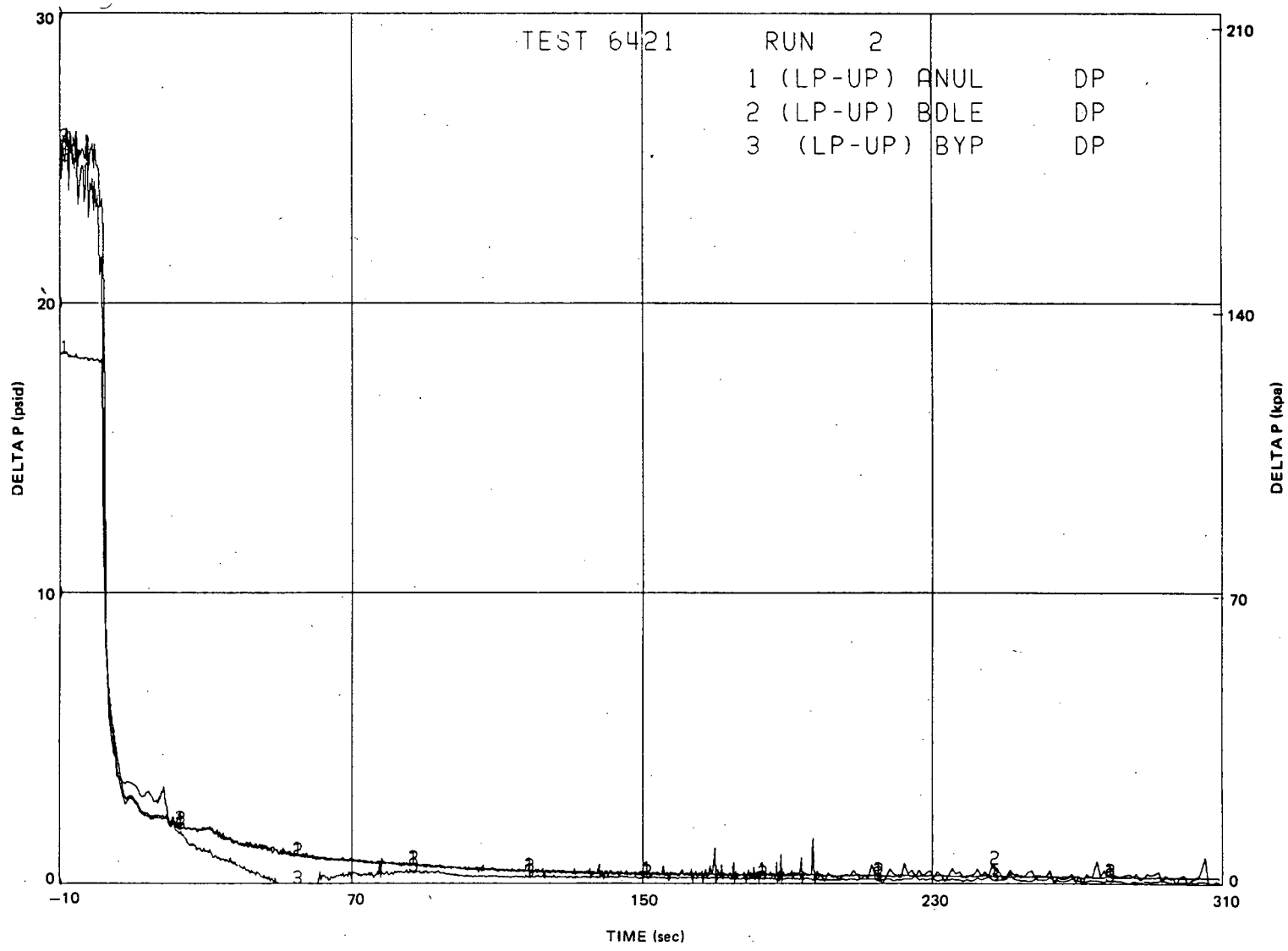

Figure L-95. Lower Plenum to Upper Plenum Differential Pressures for Annulus, Bundle, and Bypass

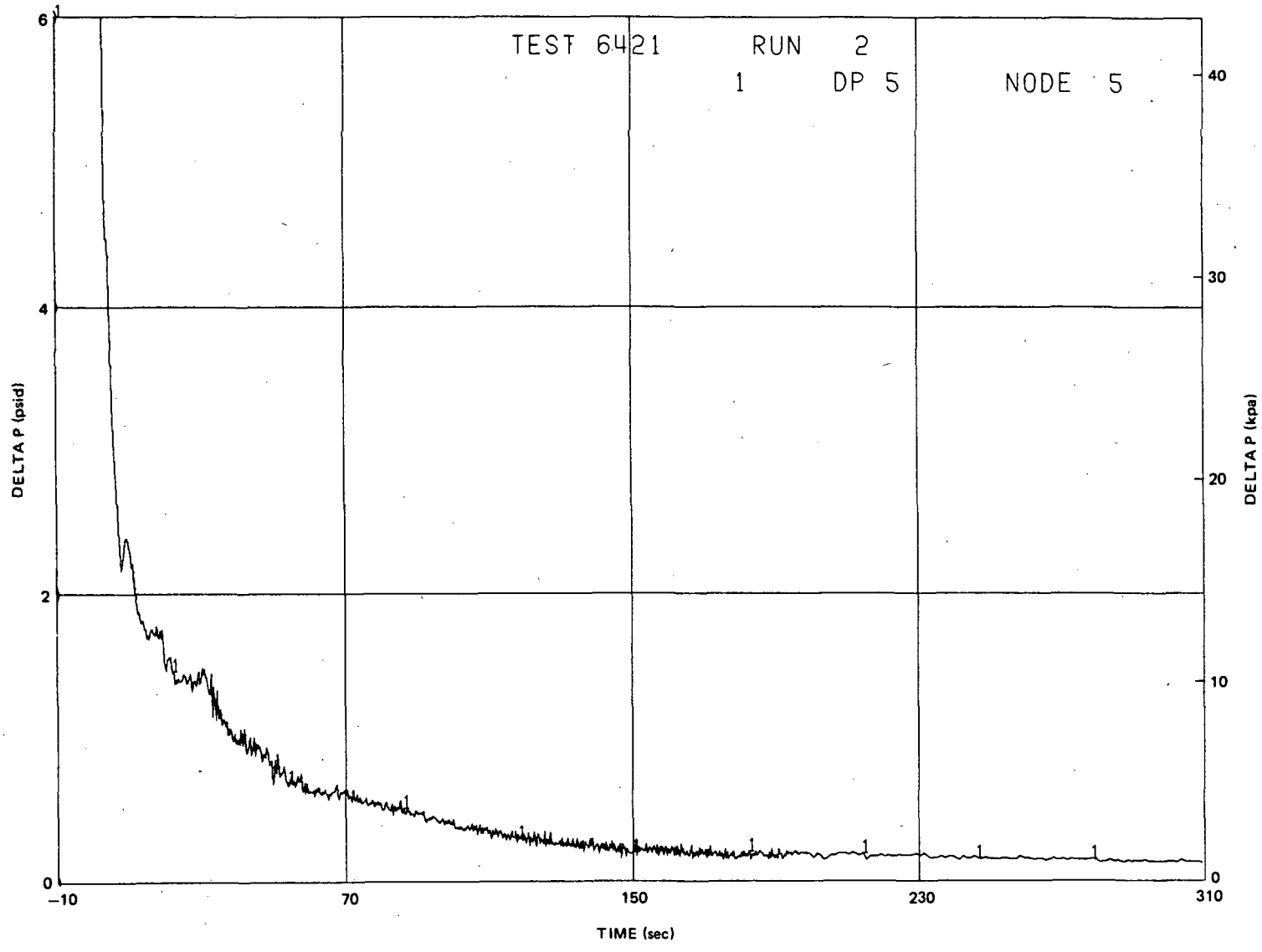

Figure L-96. Lower Plenum to Annulus Differential Pressure

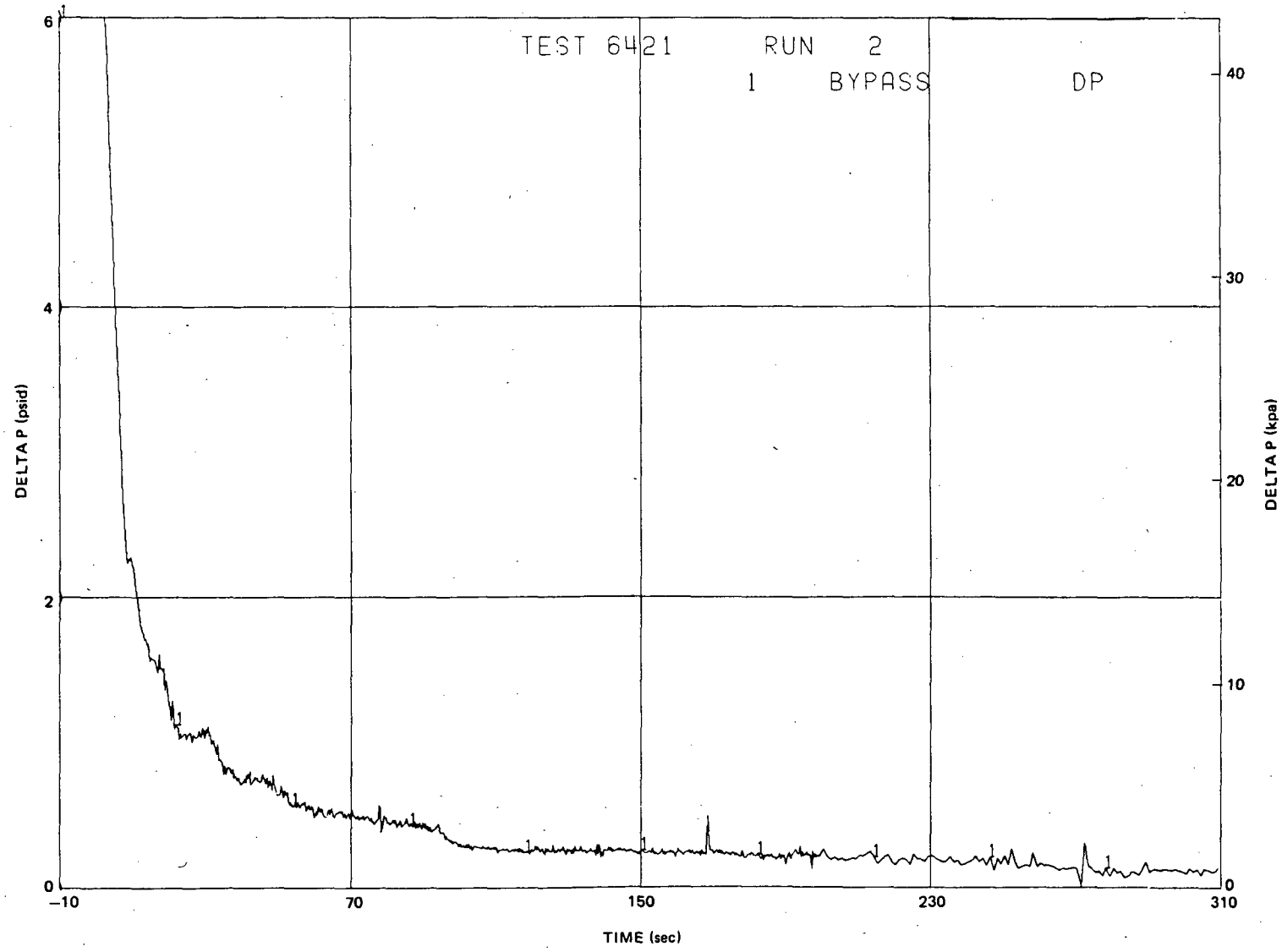

Figure L-97. Bypass Differential Pressure

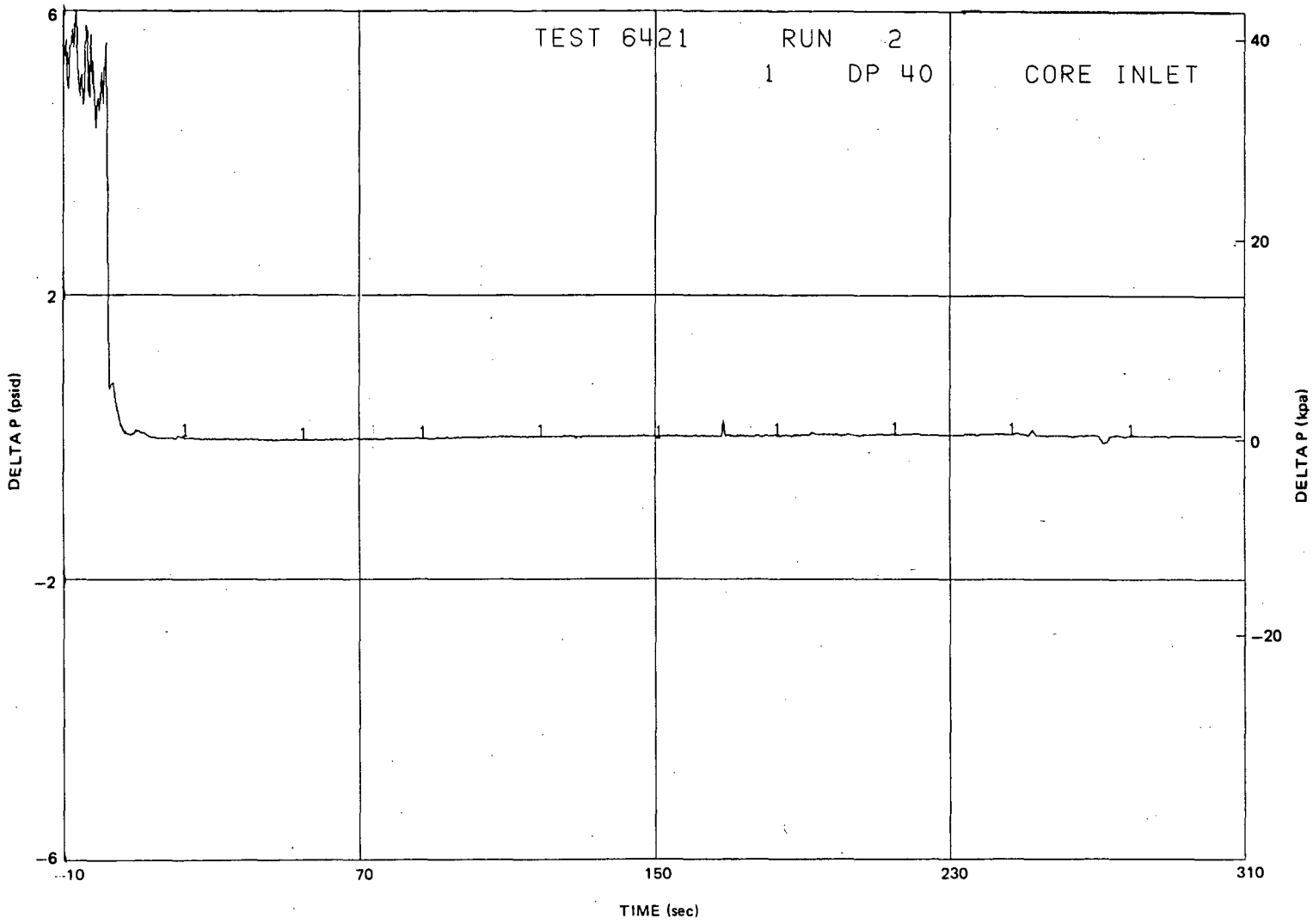

Figure L-98. Bundle Inlet Side Entry Orifice

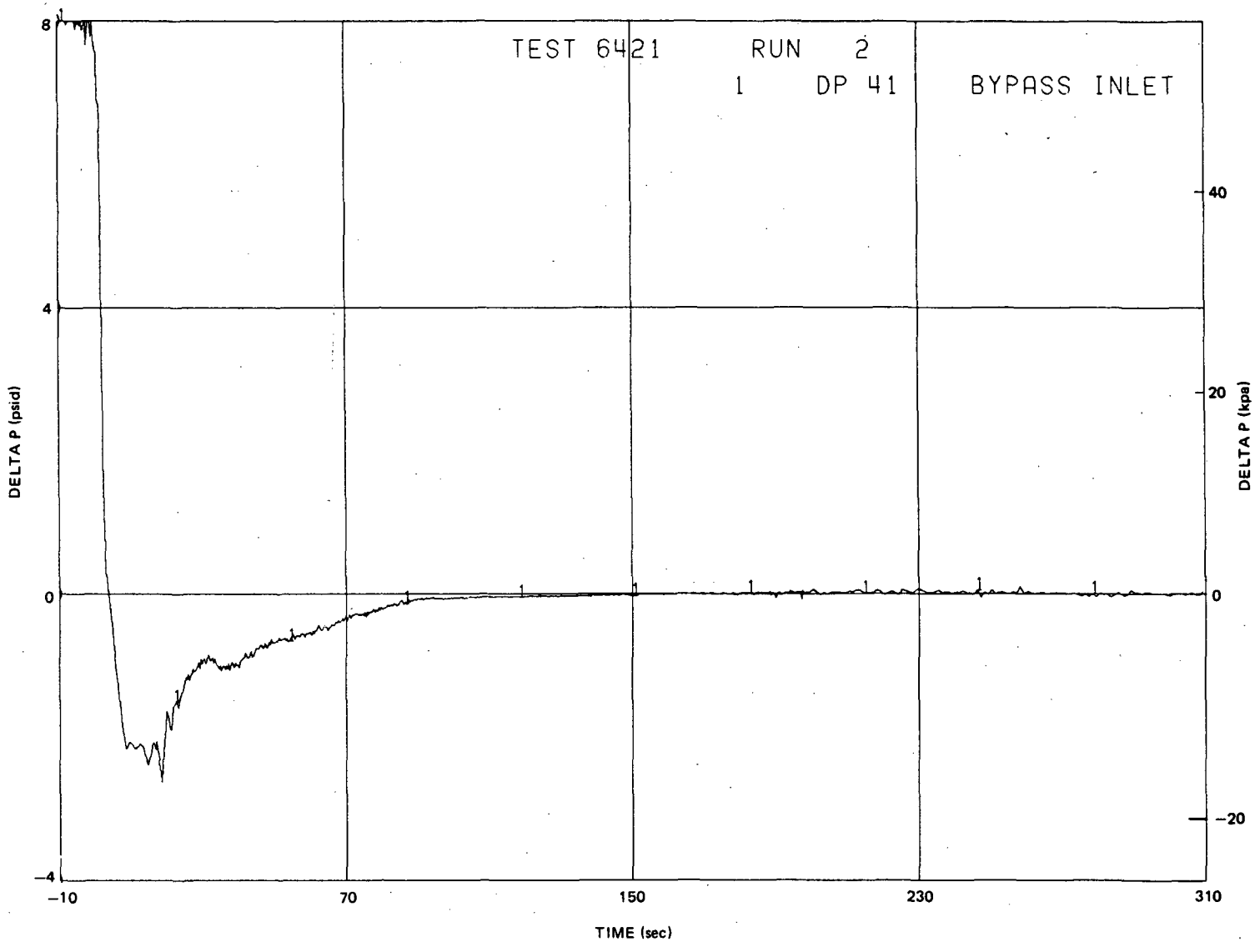

Figure L-99. Bypass Leakage Path Differential Pressure

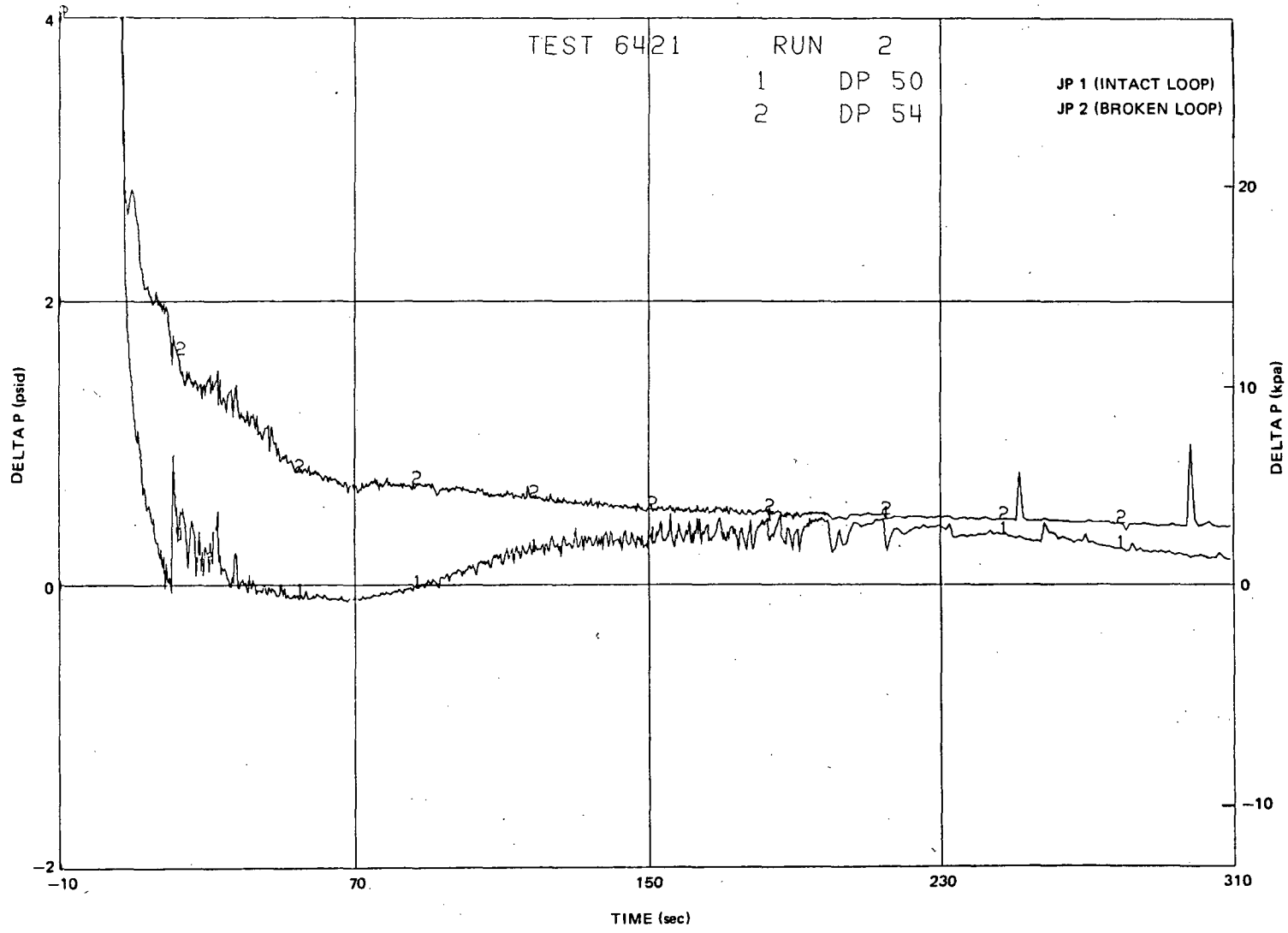

Figure L-100. Intact Loop and Broken Loop Jet Pump Diffuser to Throat Differential Pressures

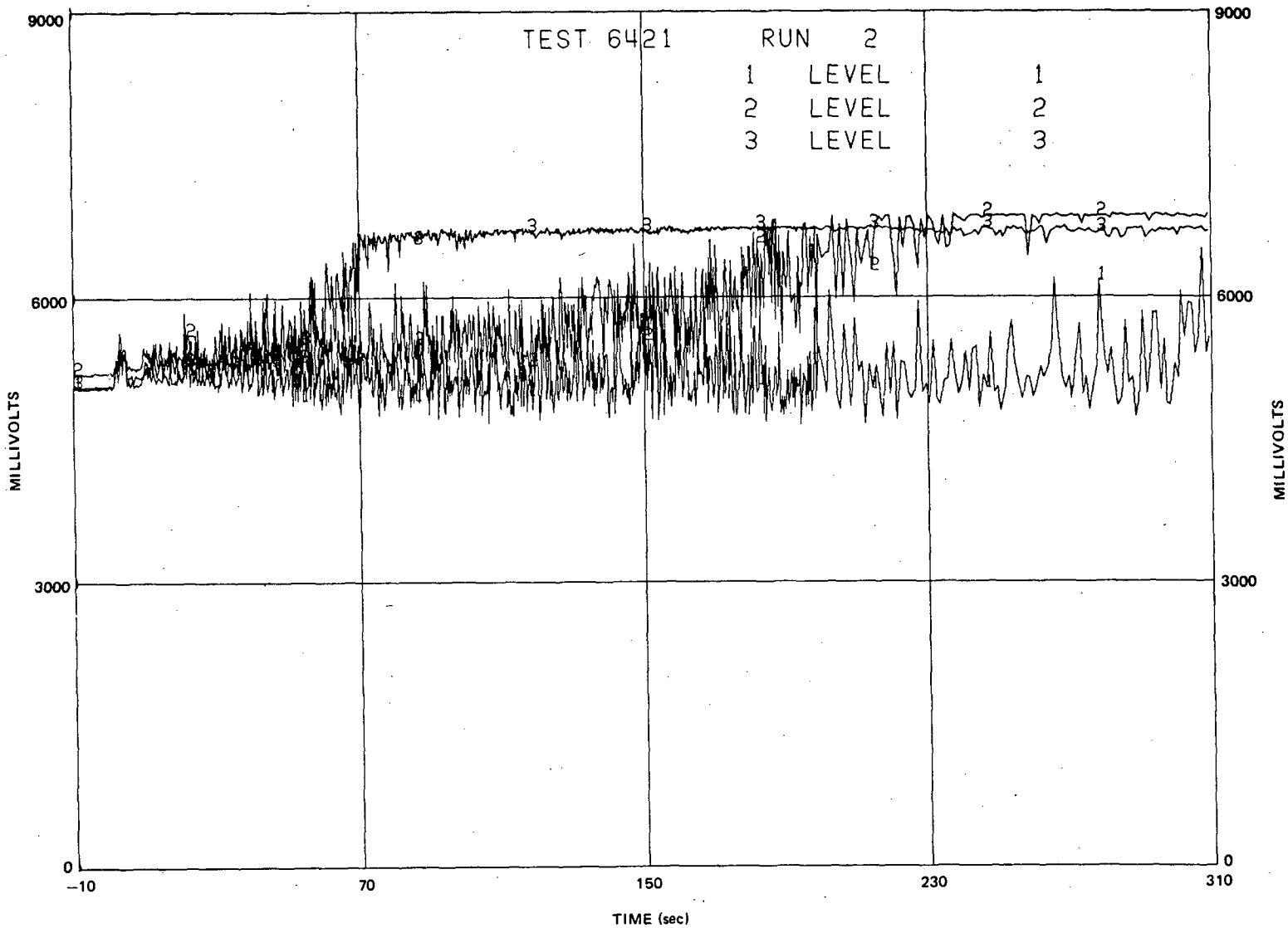

Figure L-101. Bottom Lower Plenum Conductivity Probe Measurements

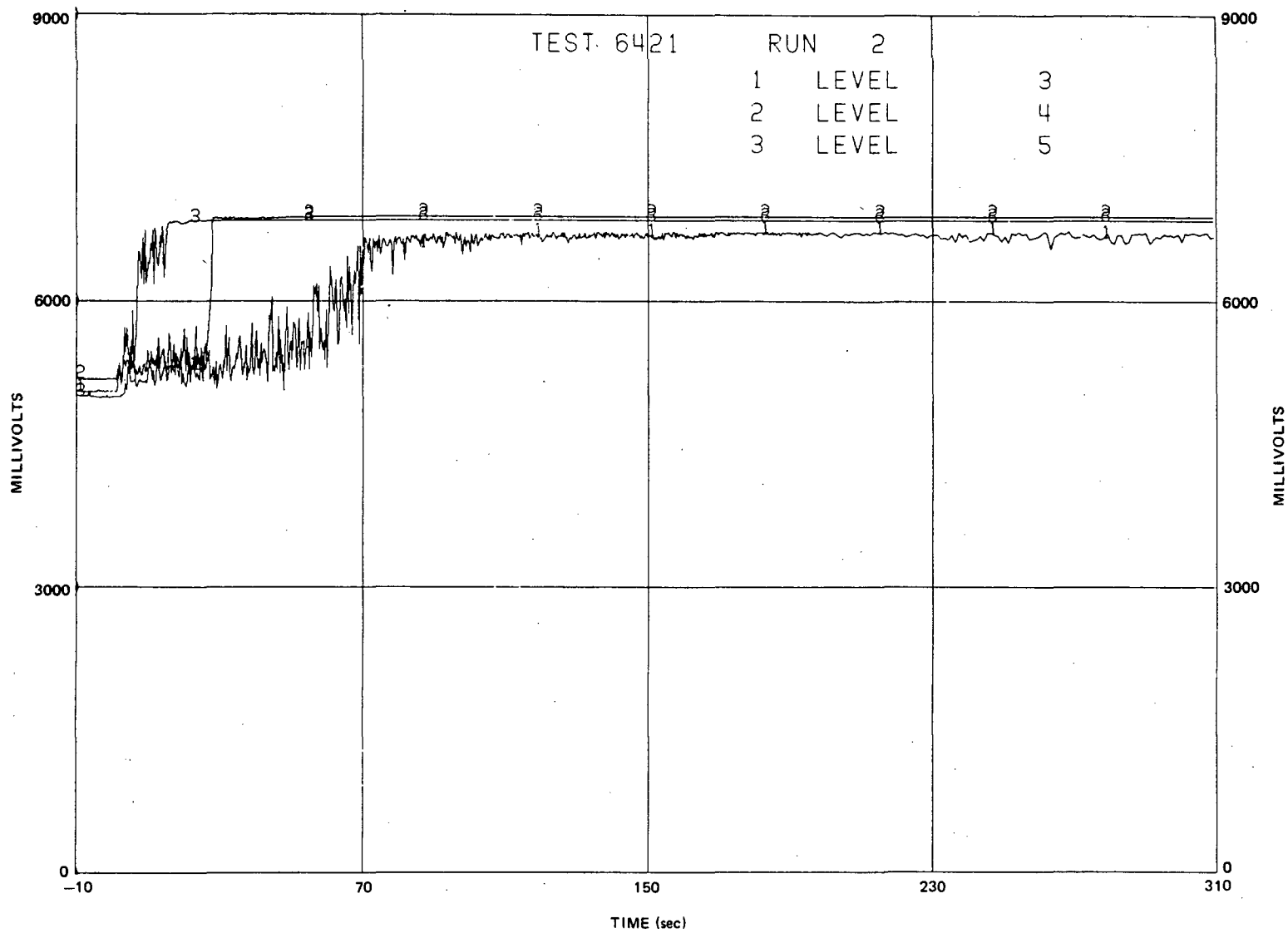

Figure L-102. Upper Lower Plenum Conductivity Probe Measurements

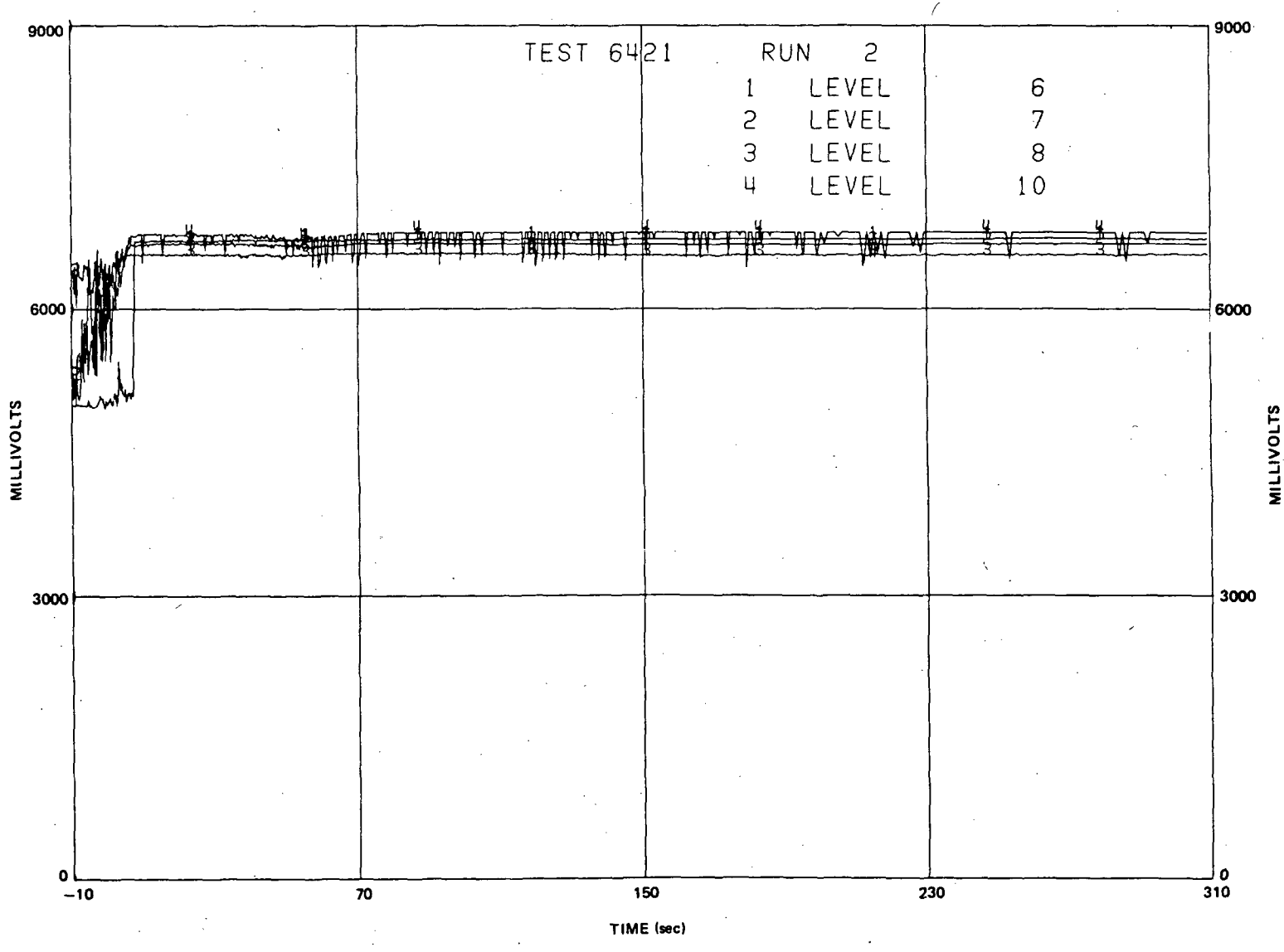

Figure L-103. Lower Annulus Conductivity Probe Measurements

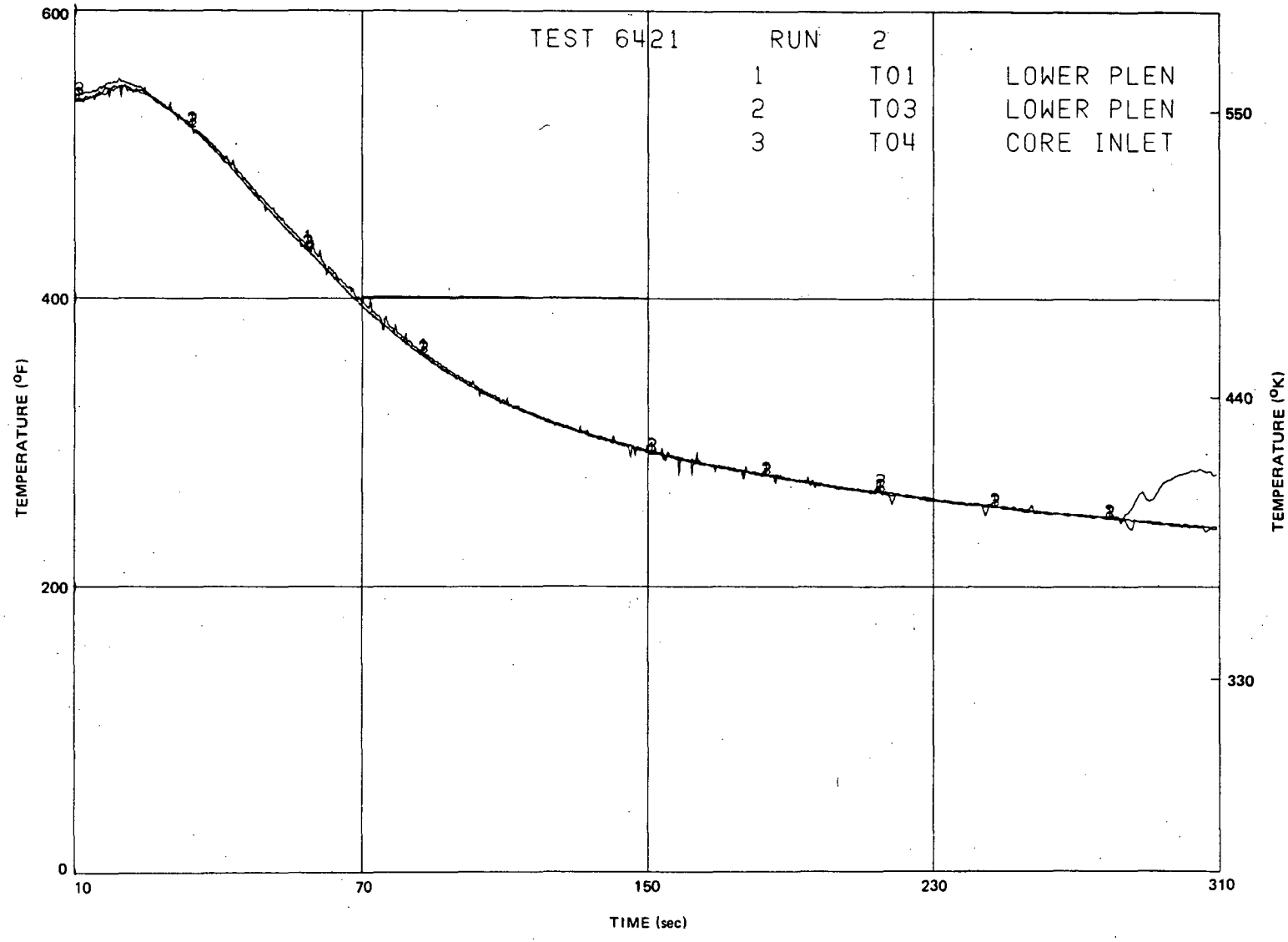

Figure L-104. Lower Plenum Fluid Temperatures

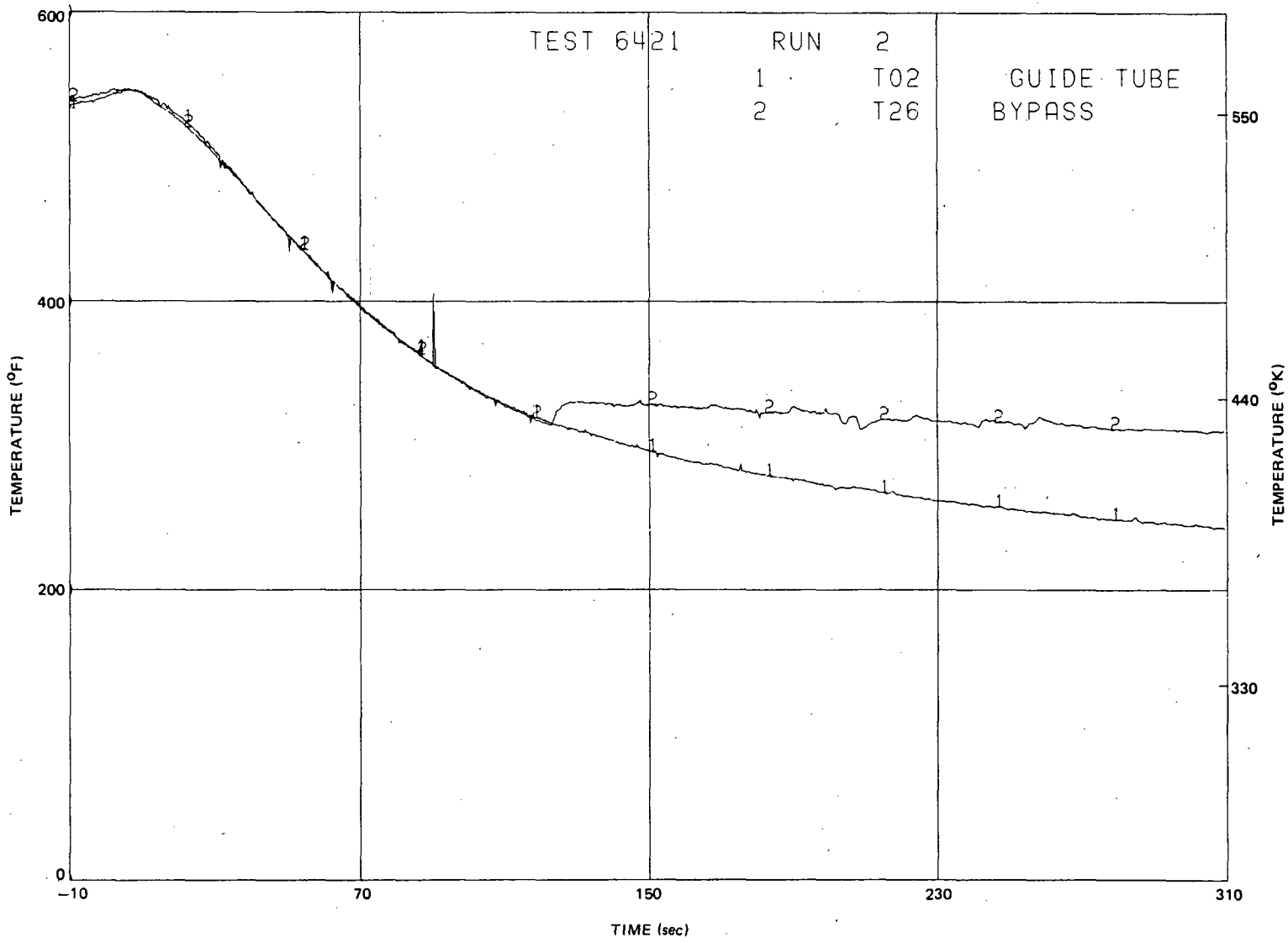

Figure L-105. Guide Tube and Bypass Fluid Temperatures

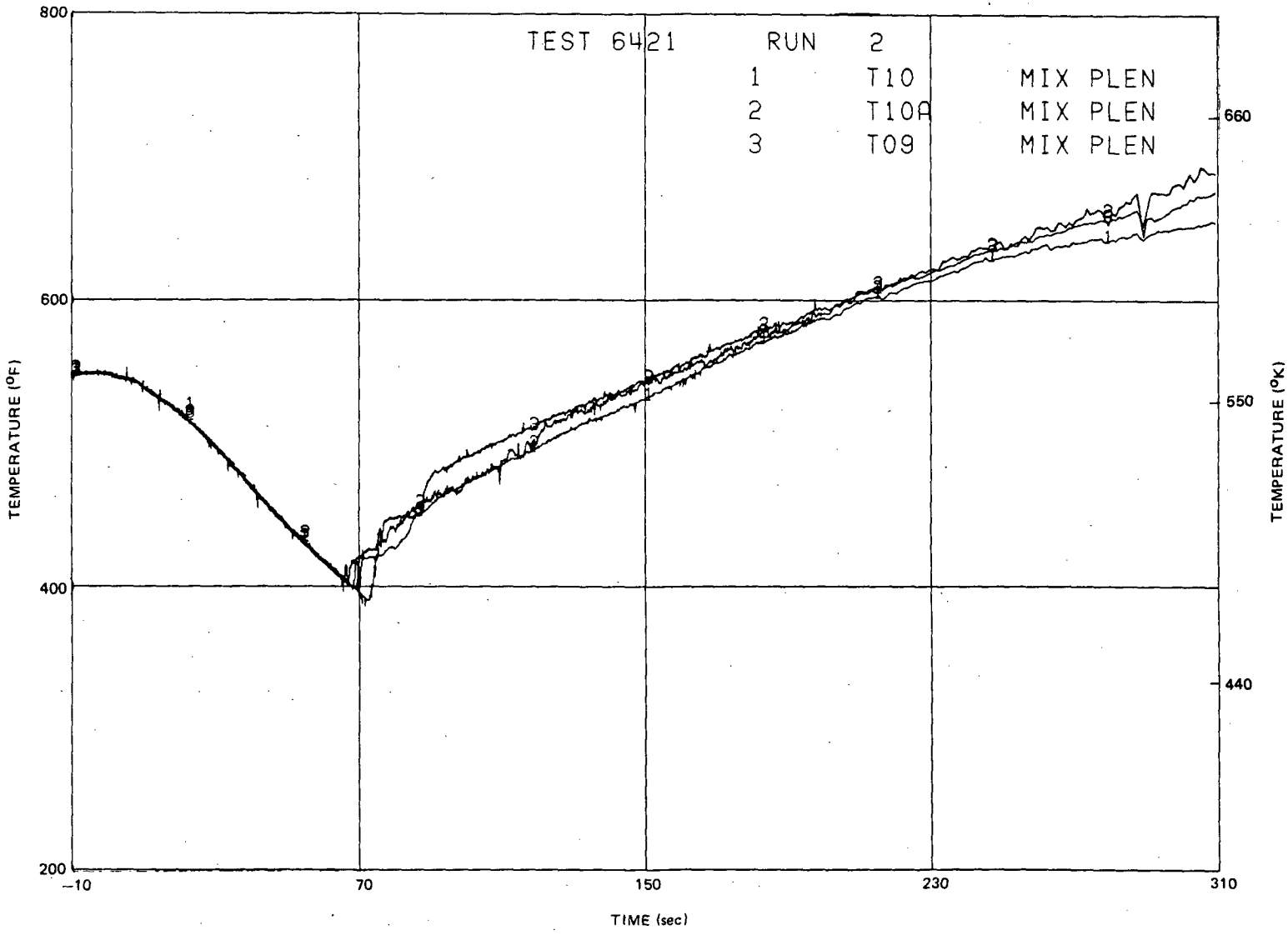

Figure L-106. Mixing Plenum Fluid Temperatures

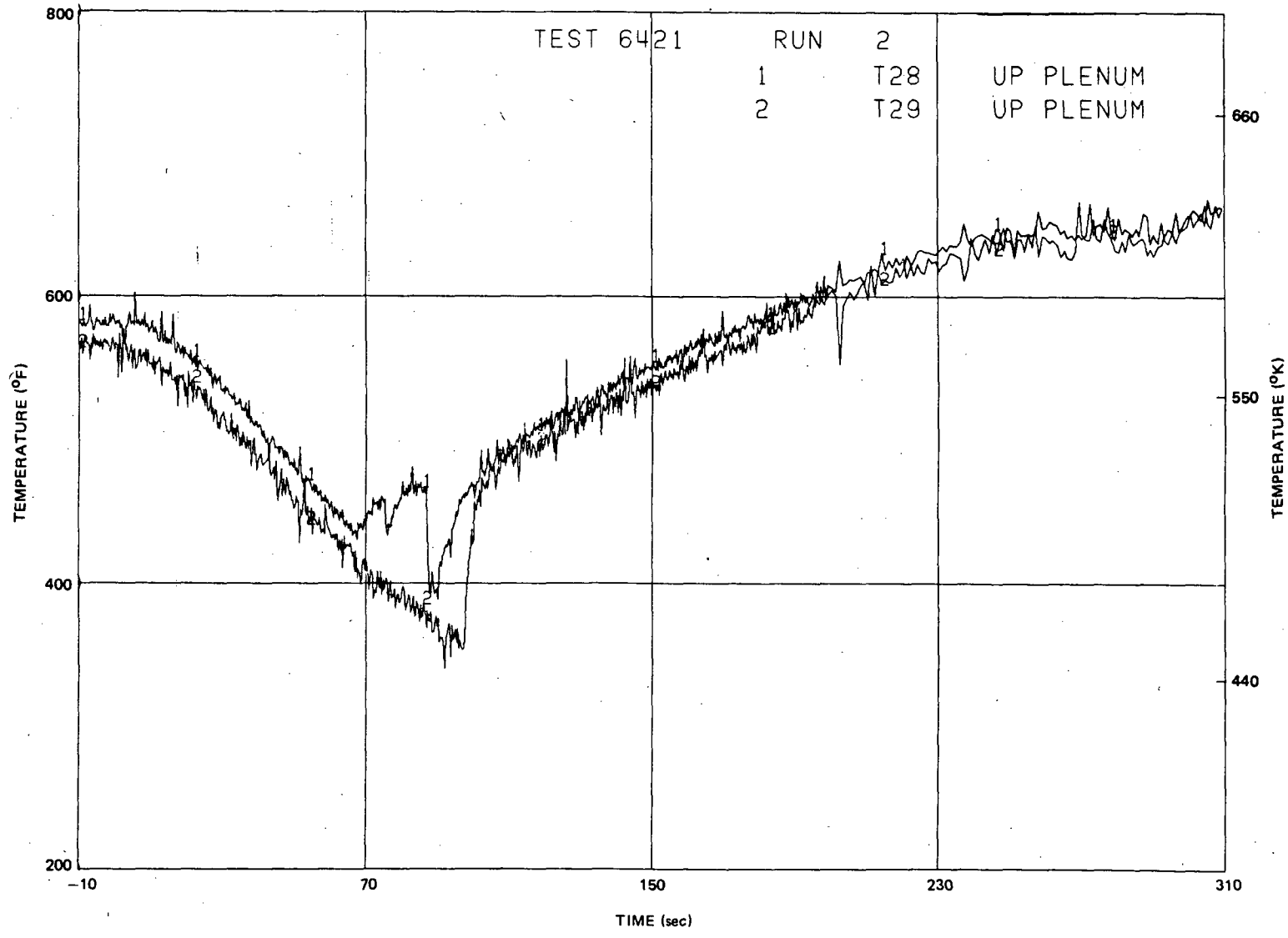

Figure L-107. Upper Plenum Fluid Temperatures

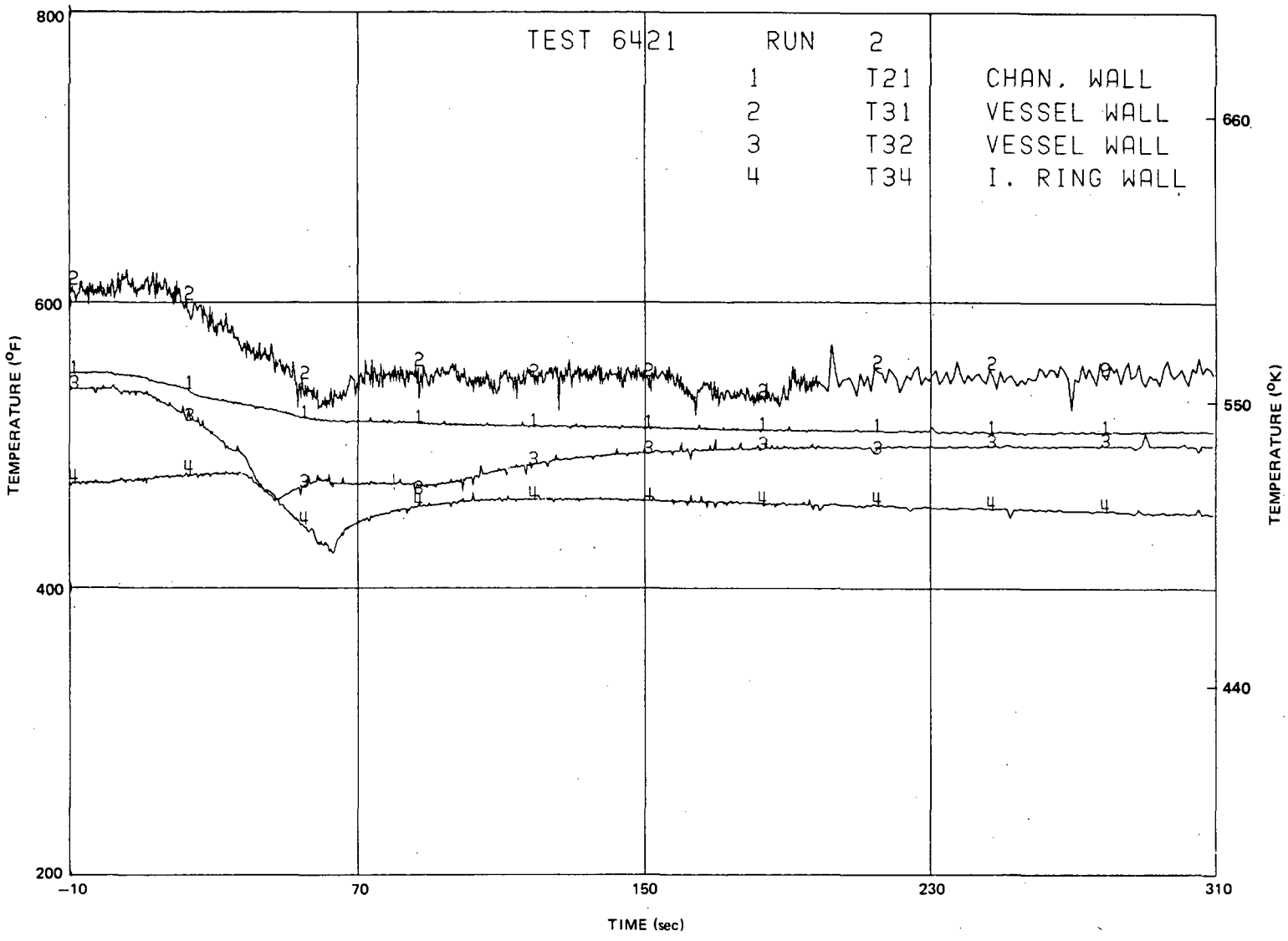

Figure L-108. Wall Temperatures

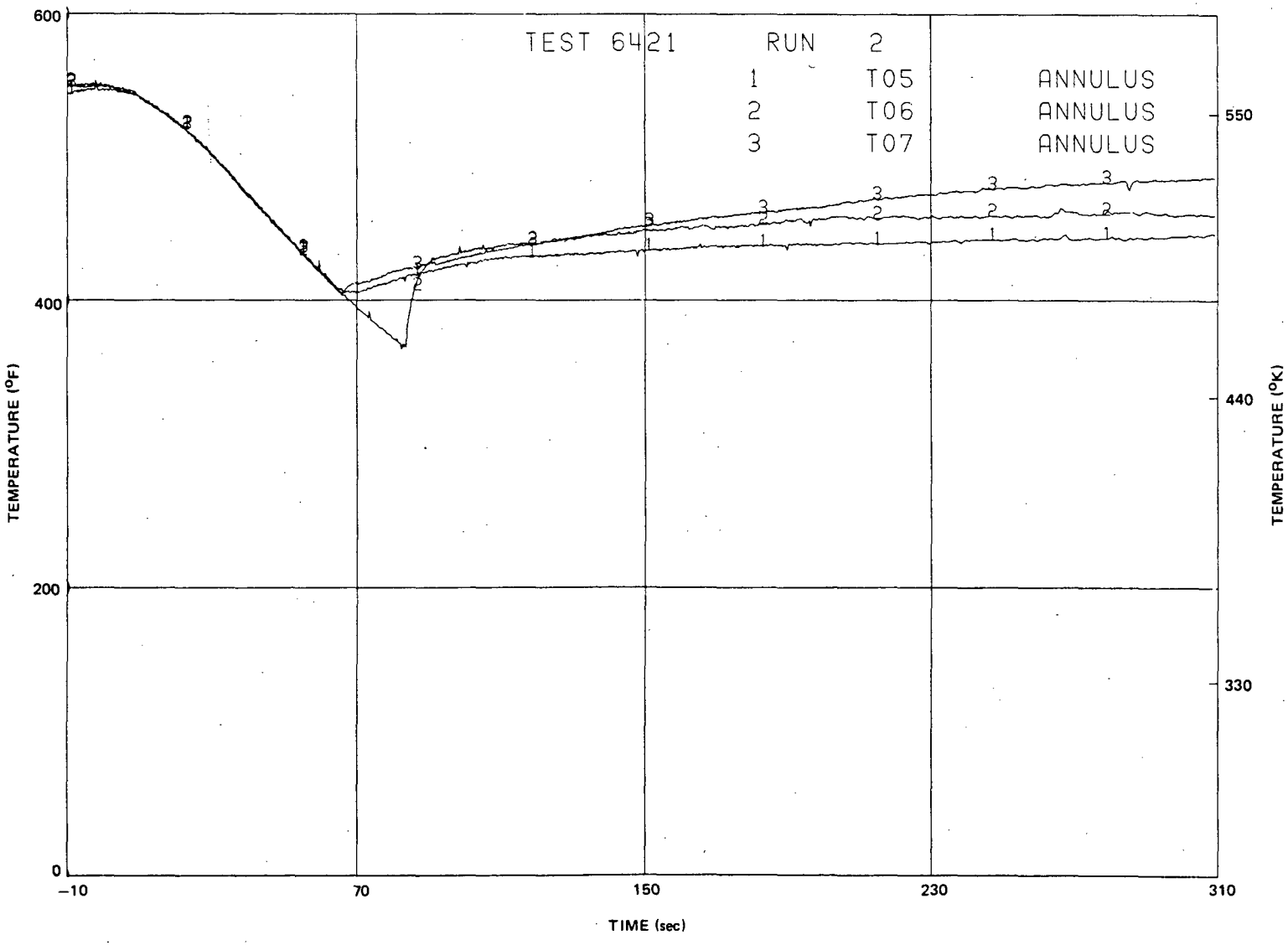

Figure L-109. Annulus Fluid Temperatures

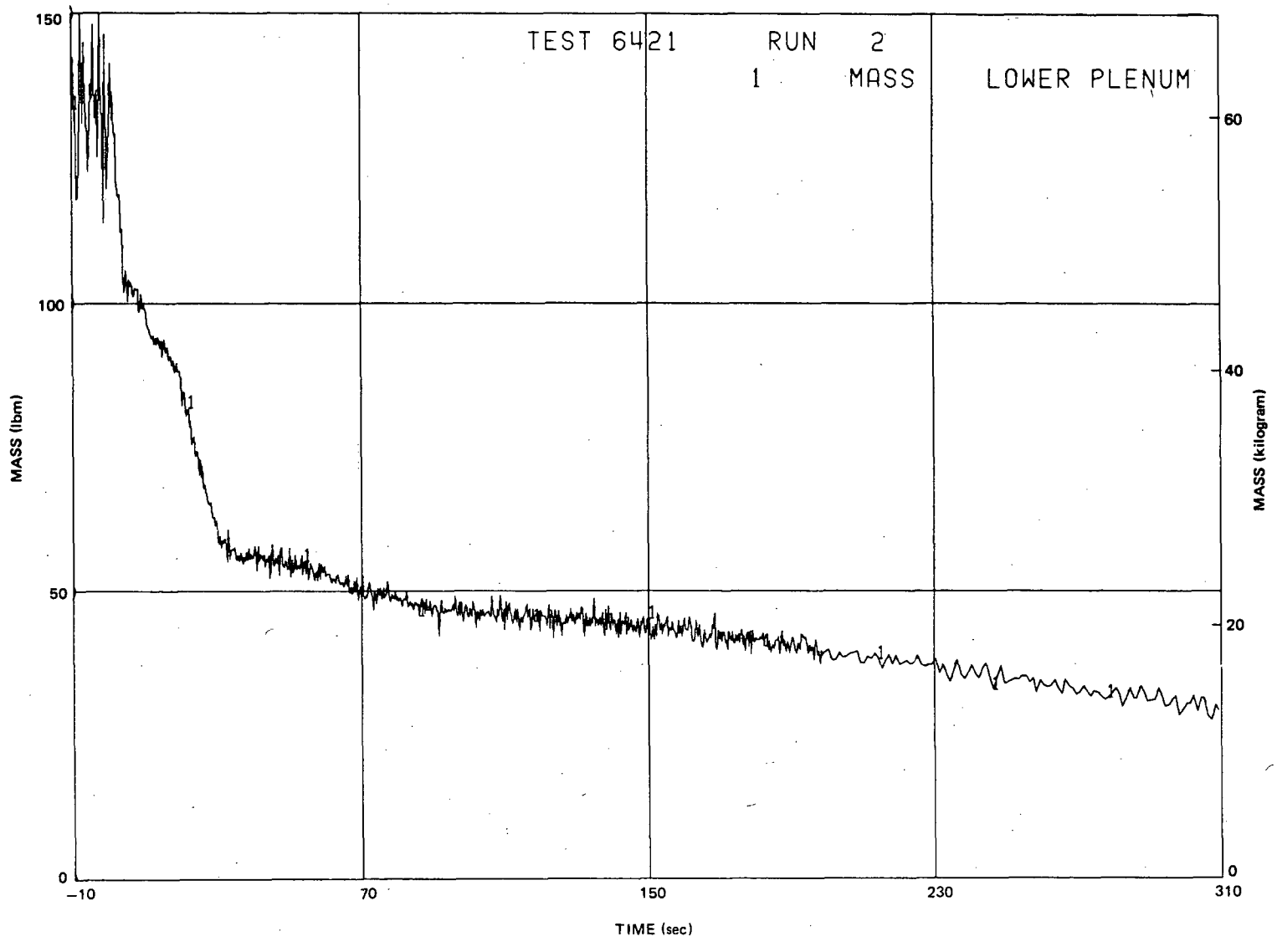

Figure L-110. Lower Plenum Fluid Mass

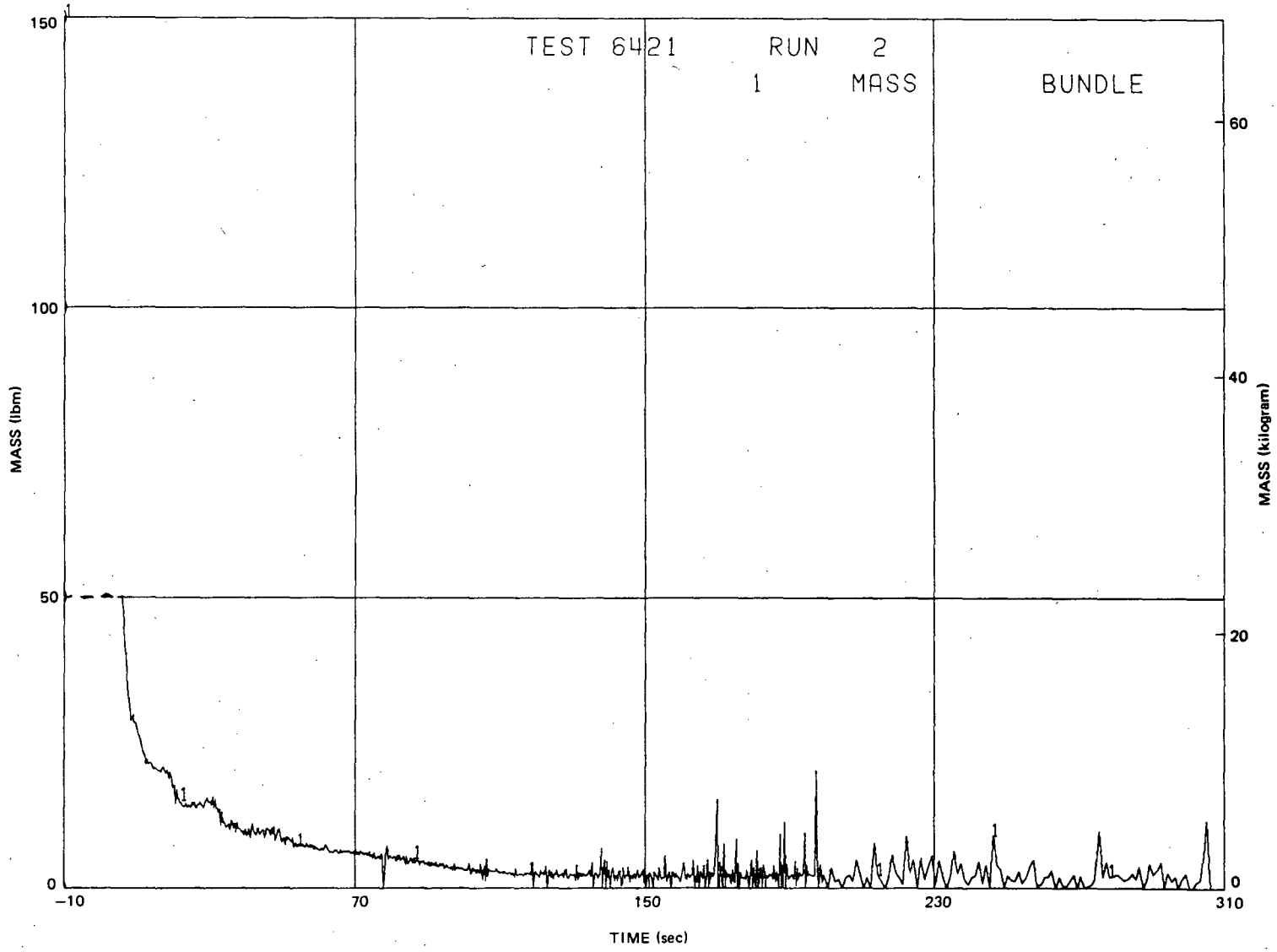

Figure L-111. Bundle Fluid Mass

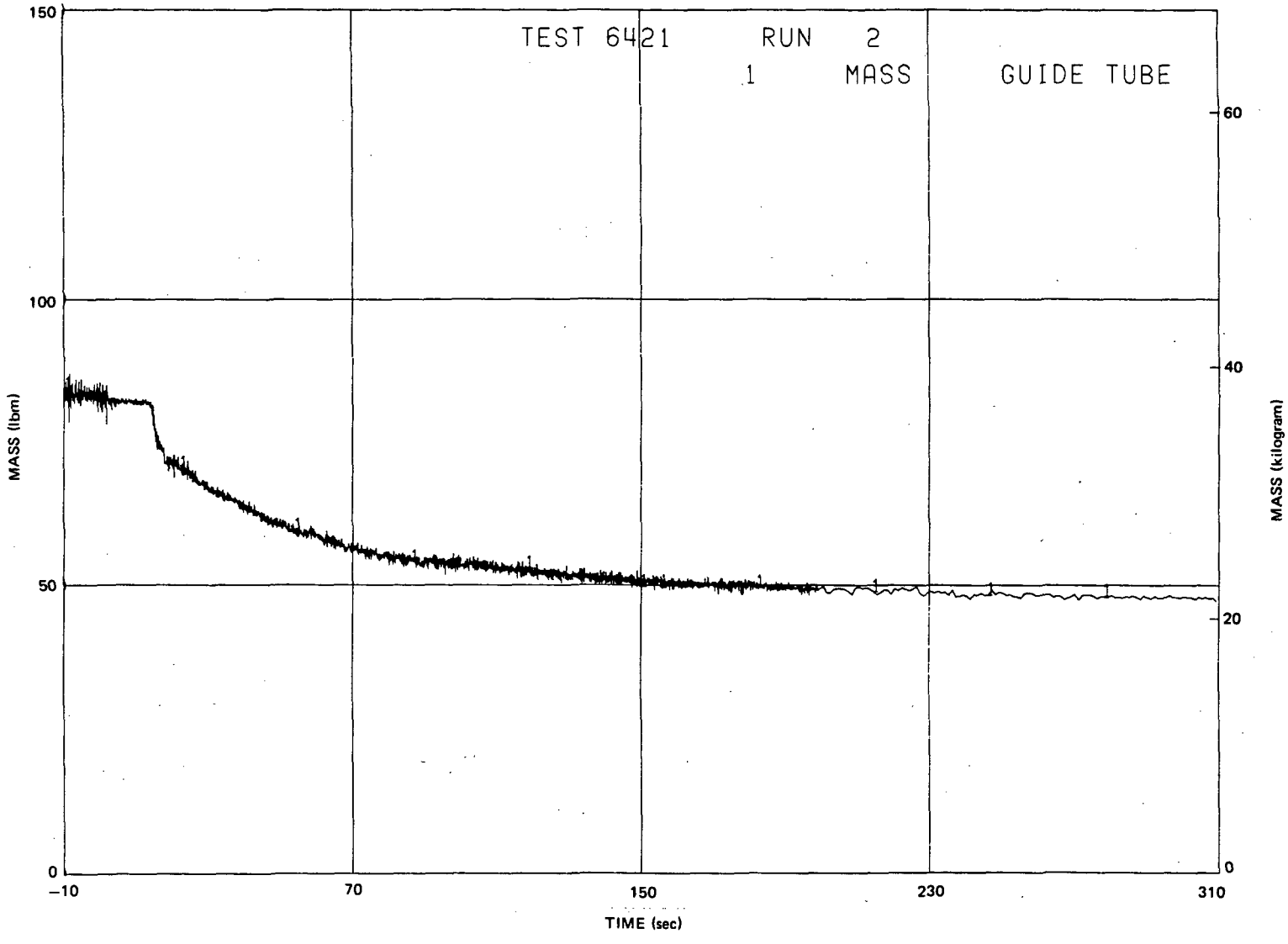

Figure L-112. Guide Tube Fluid Mass

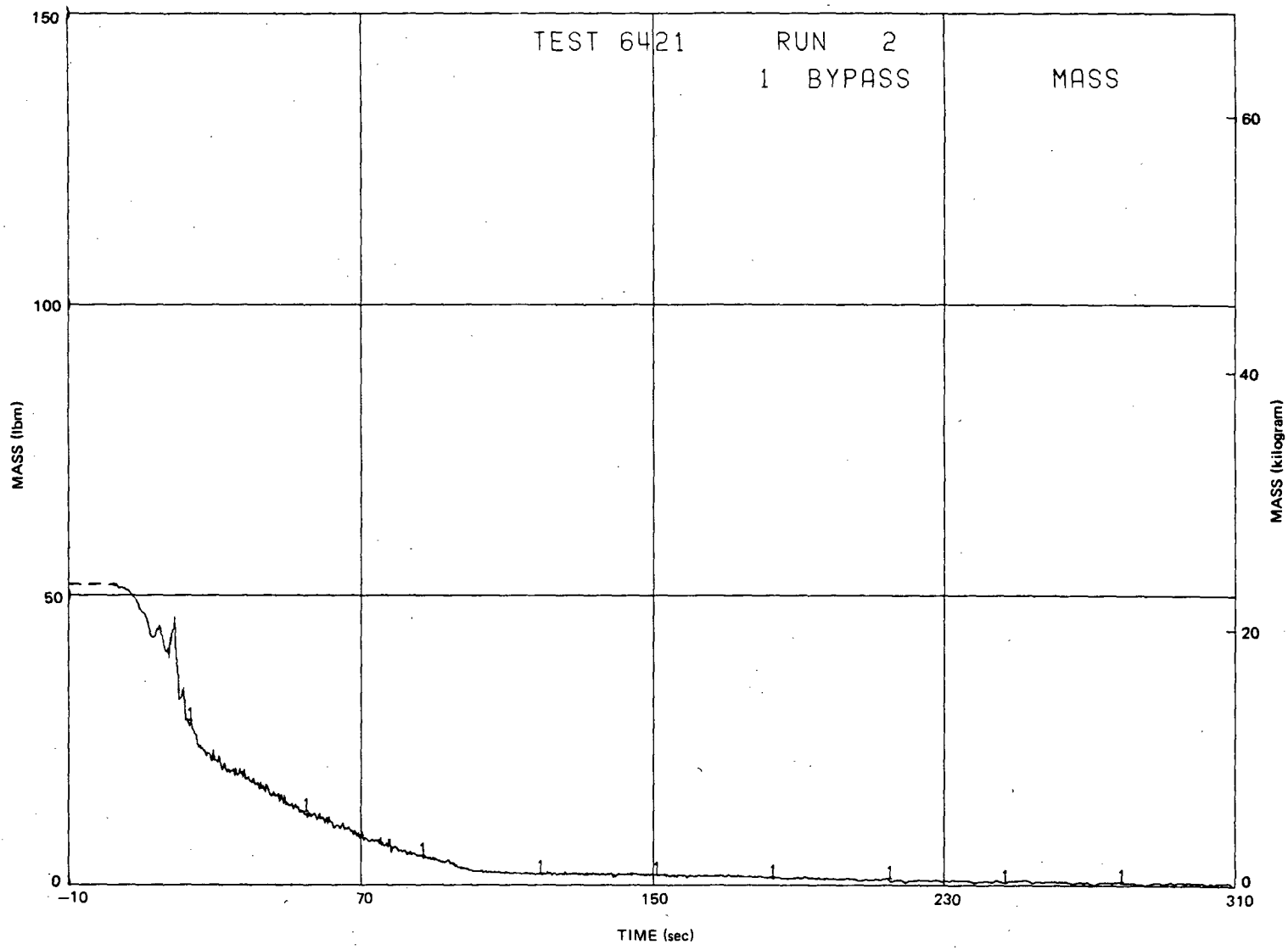

Figure L-113. Bypass Fluid Mass

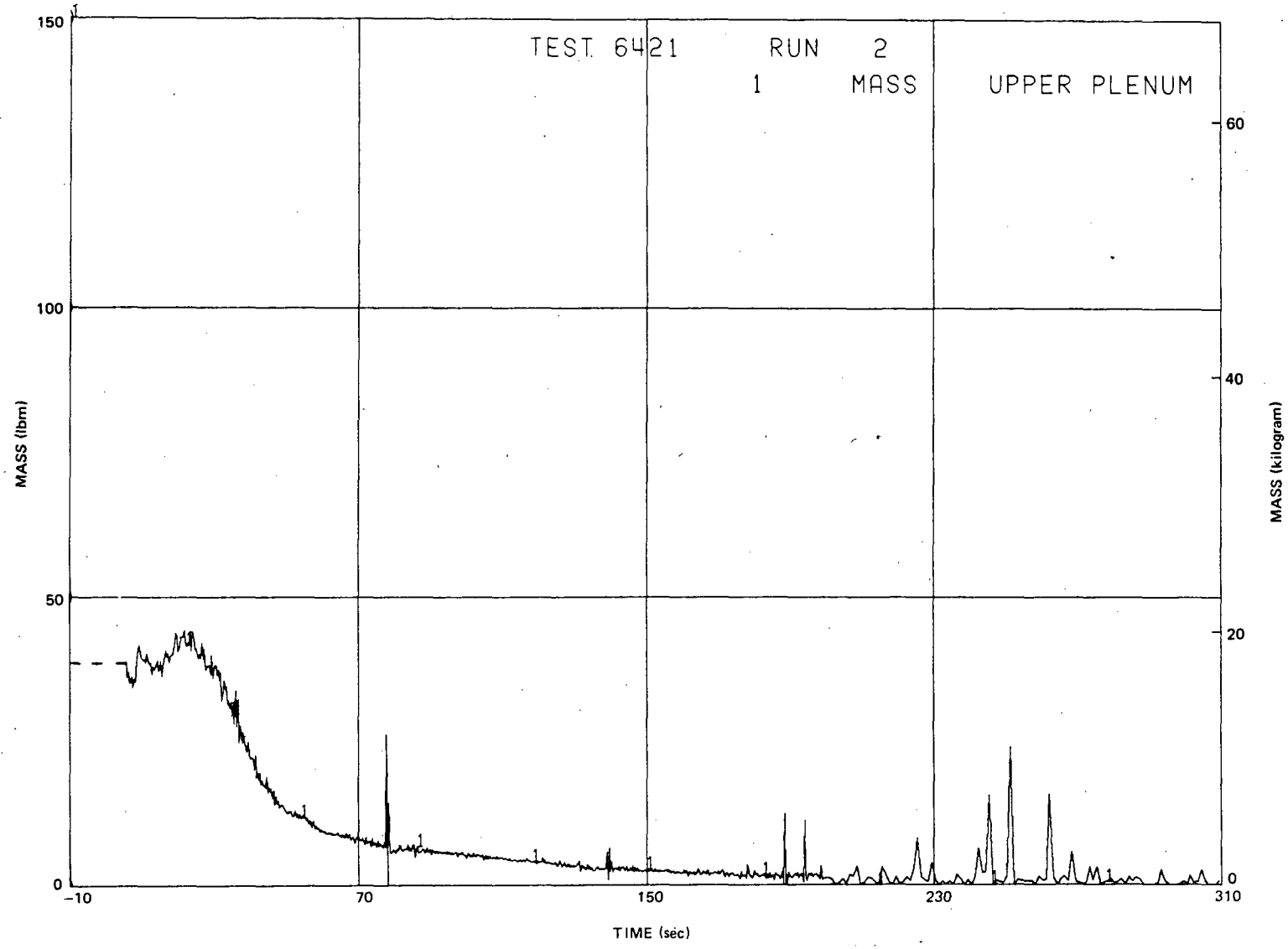

Figure L-114. Upper Plenum Fluid Mass

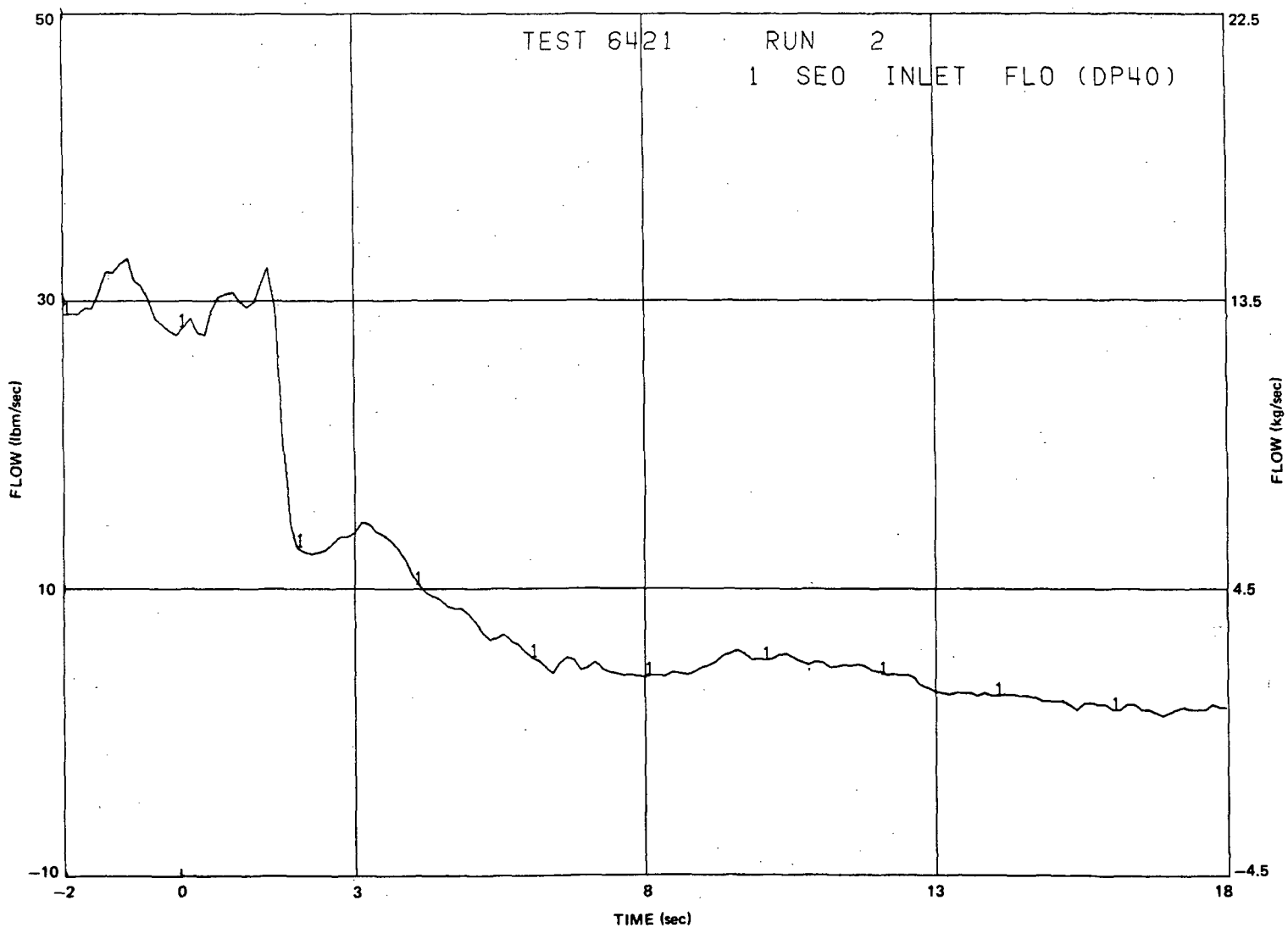

Figure L-115. Bundle Inlet Side Entry Orifice Mass Flow Rate

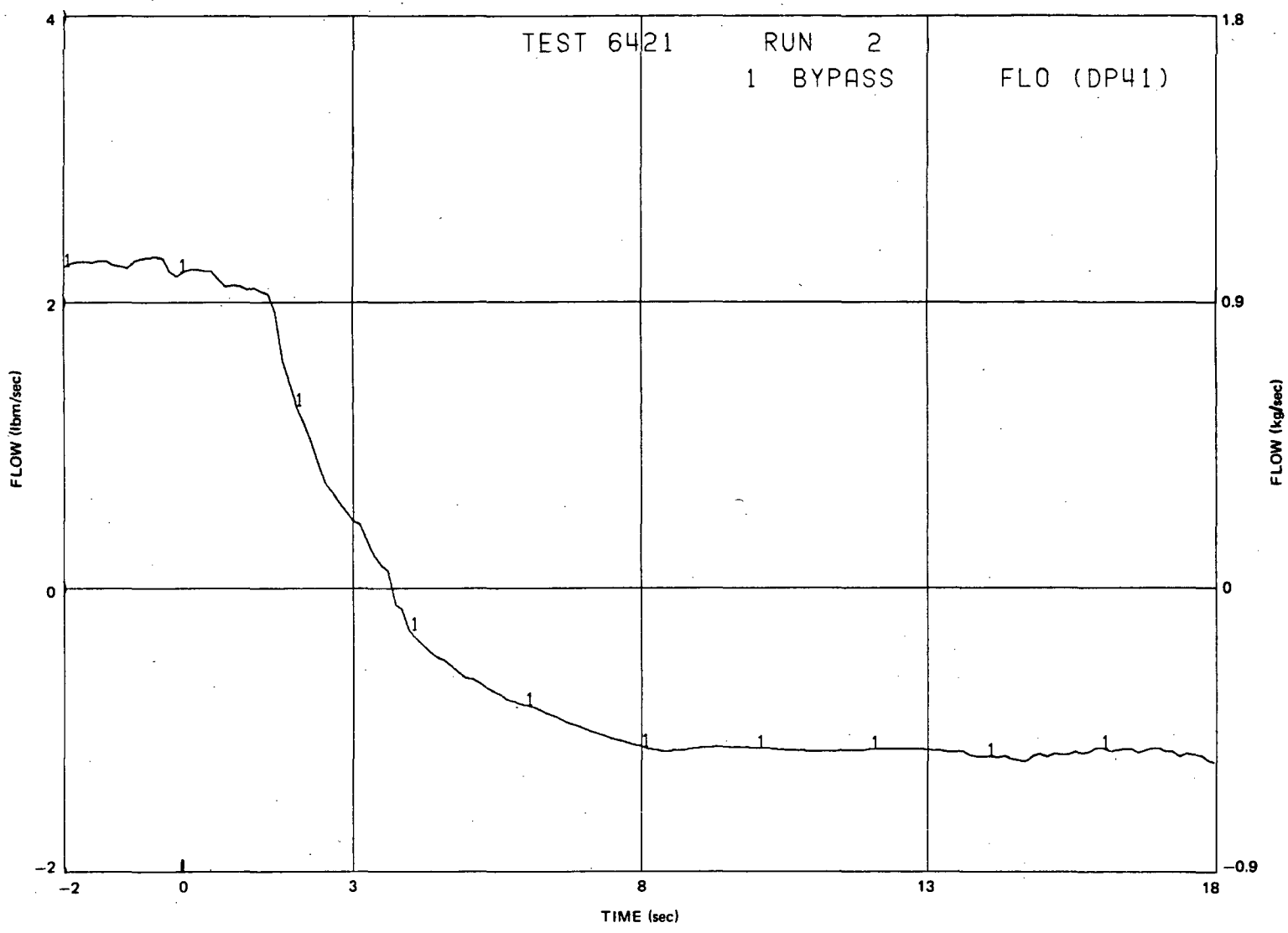

Figure L-116. Bypass Leakage Path Mass Flow Rate

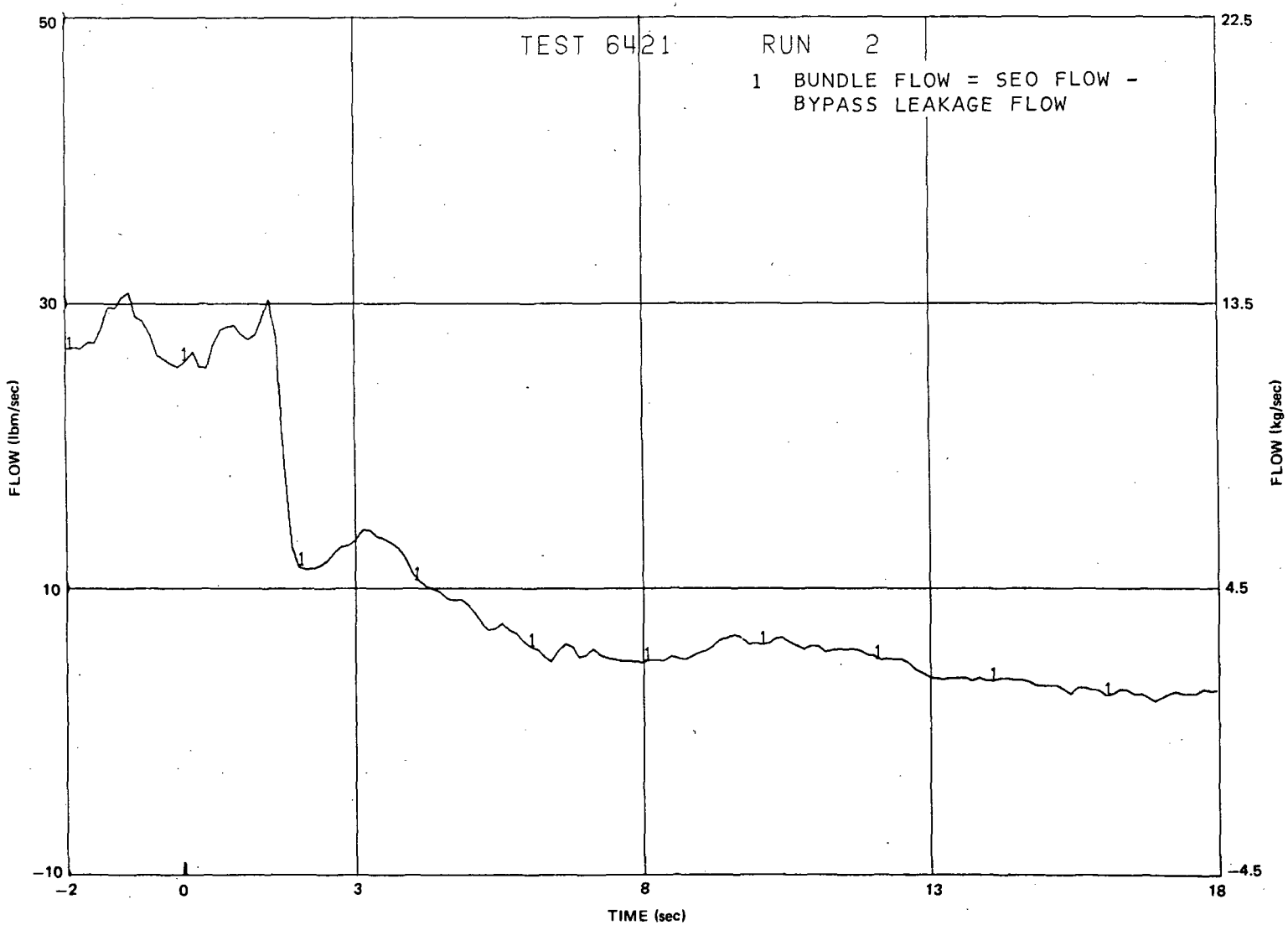

Figure L-117. Bundle Mass Flow Rate

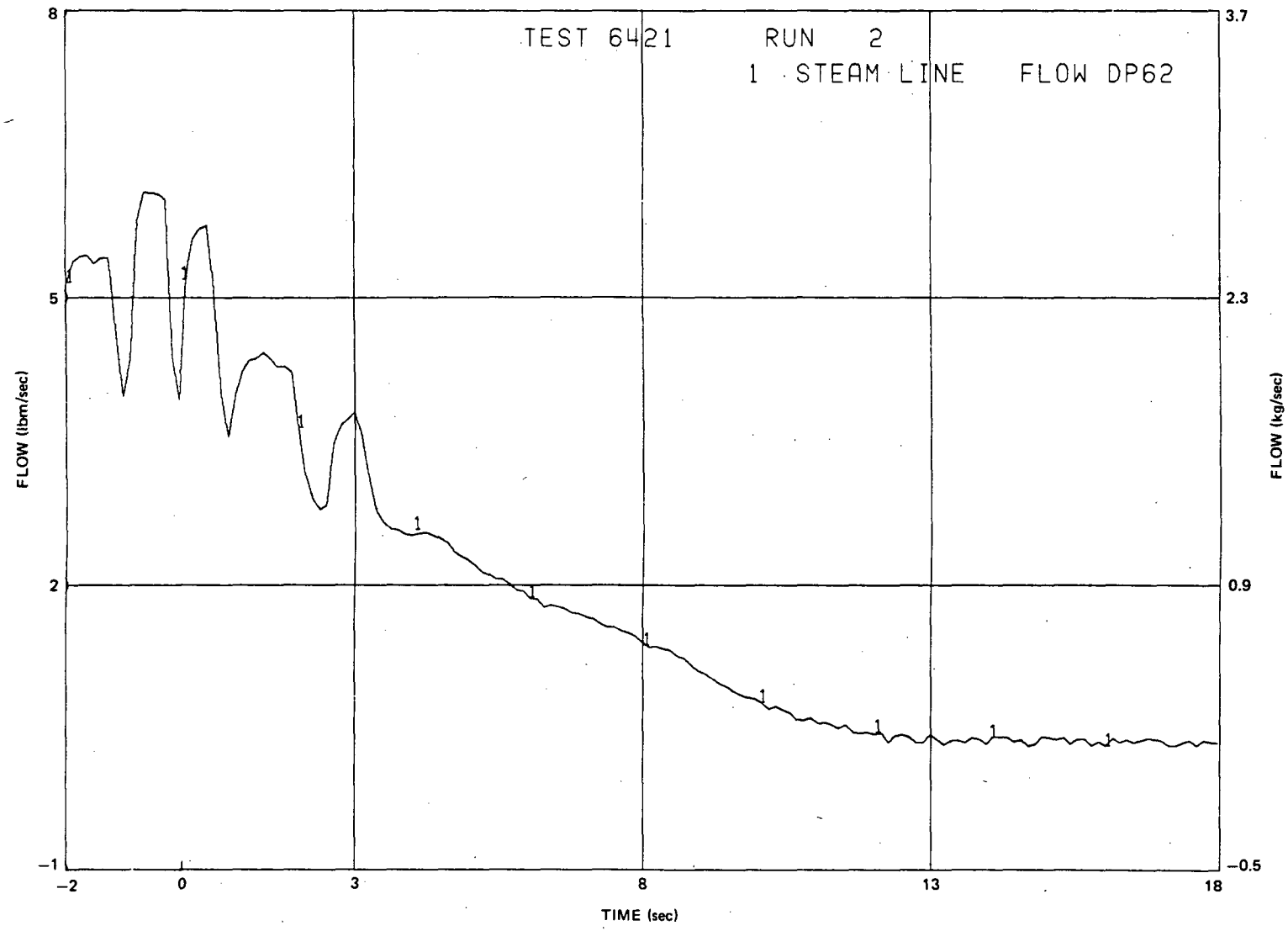

Figure L-118. **Steamline Mass Flow Rate**

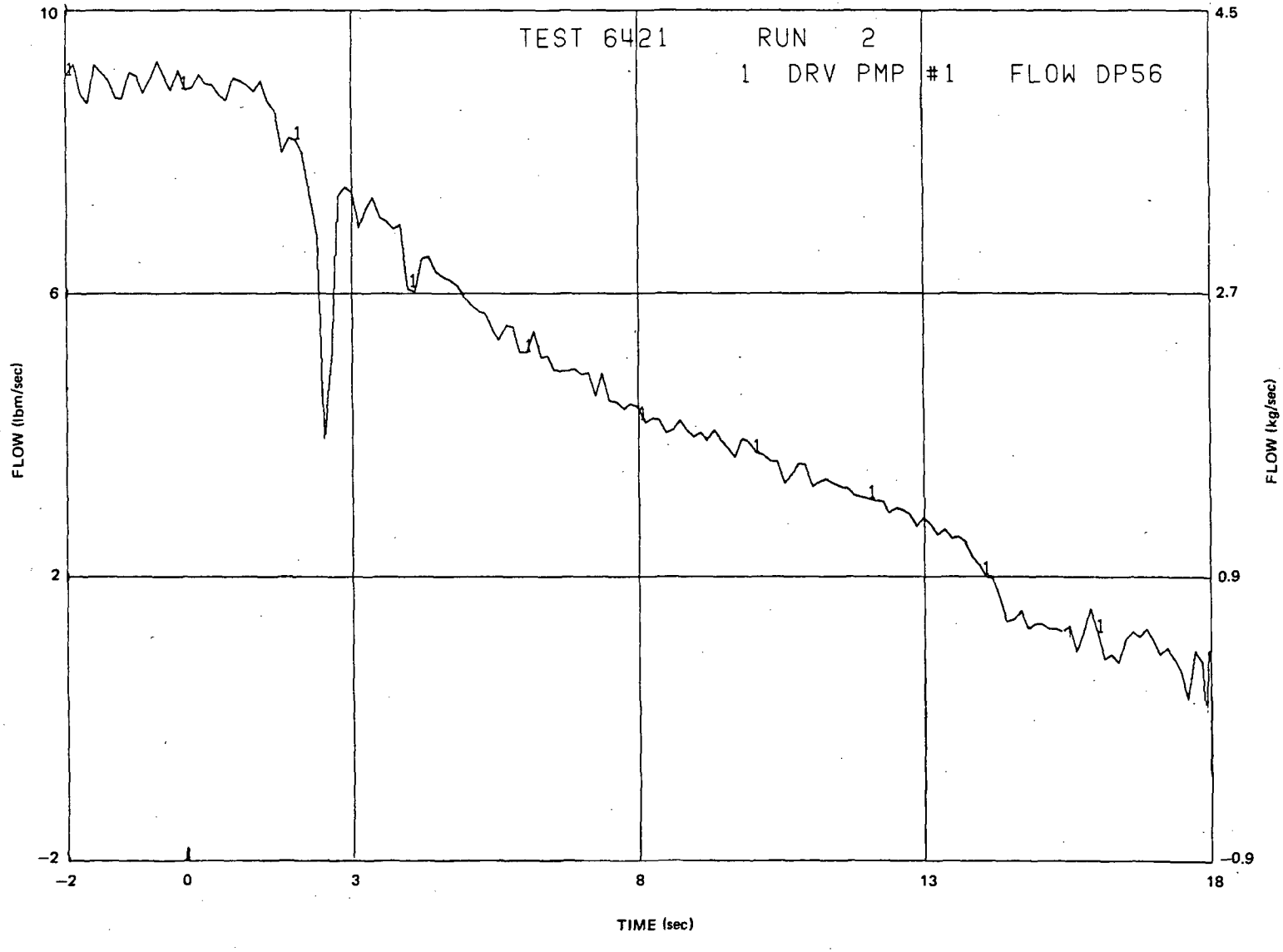

Figure L-119. Intact Loop Recirculation Pump Mass Flow Rate

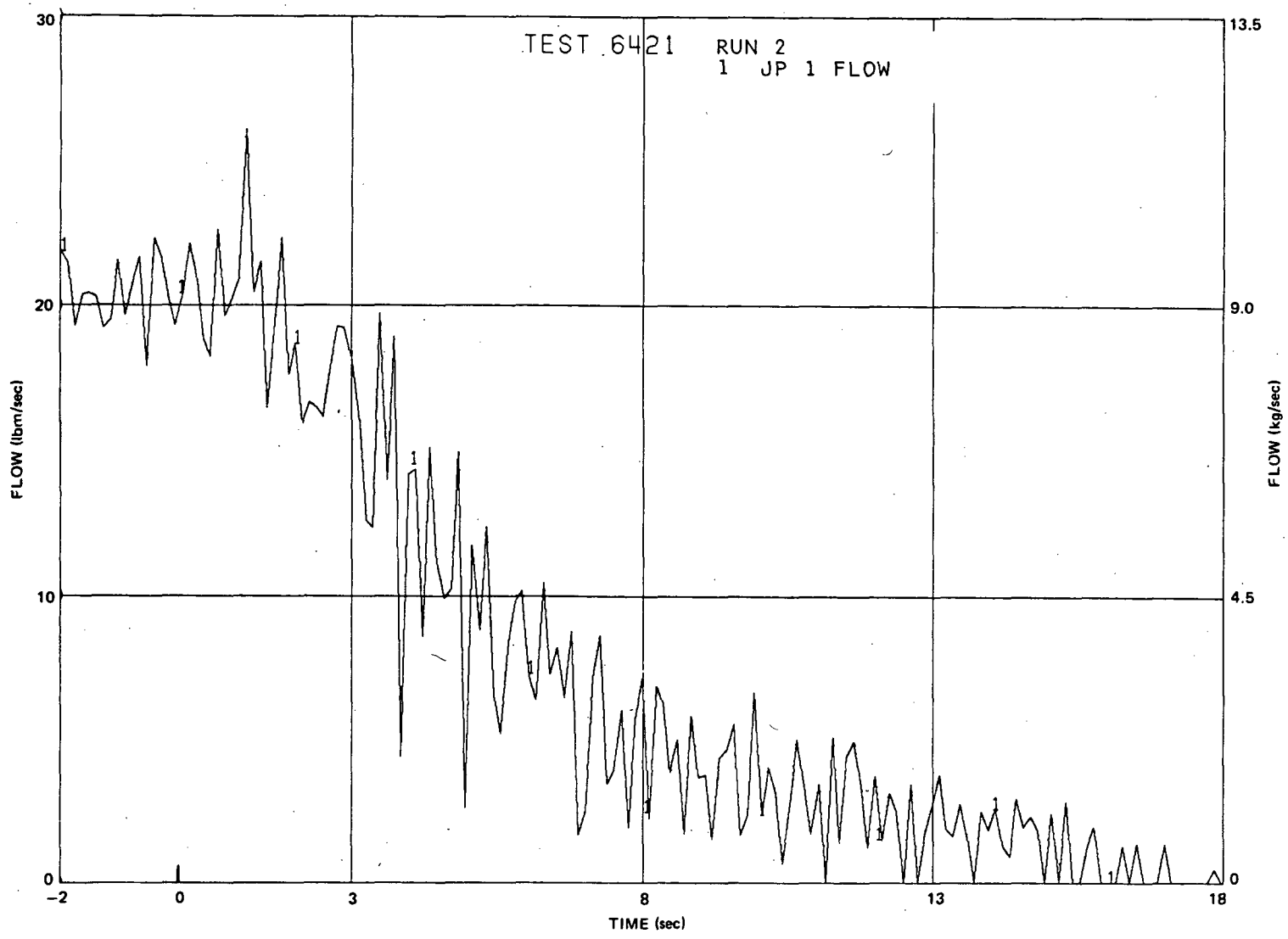

Figure L-120. Intact Loop Jet Pump Mass Flow Rate

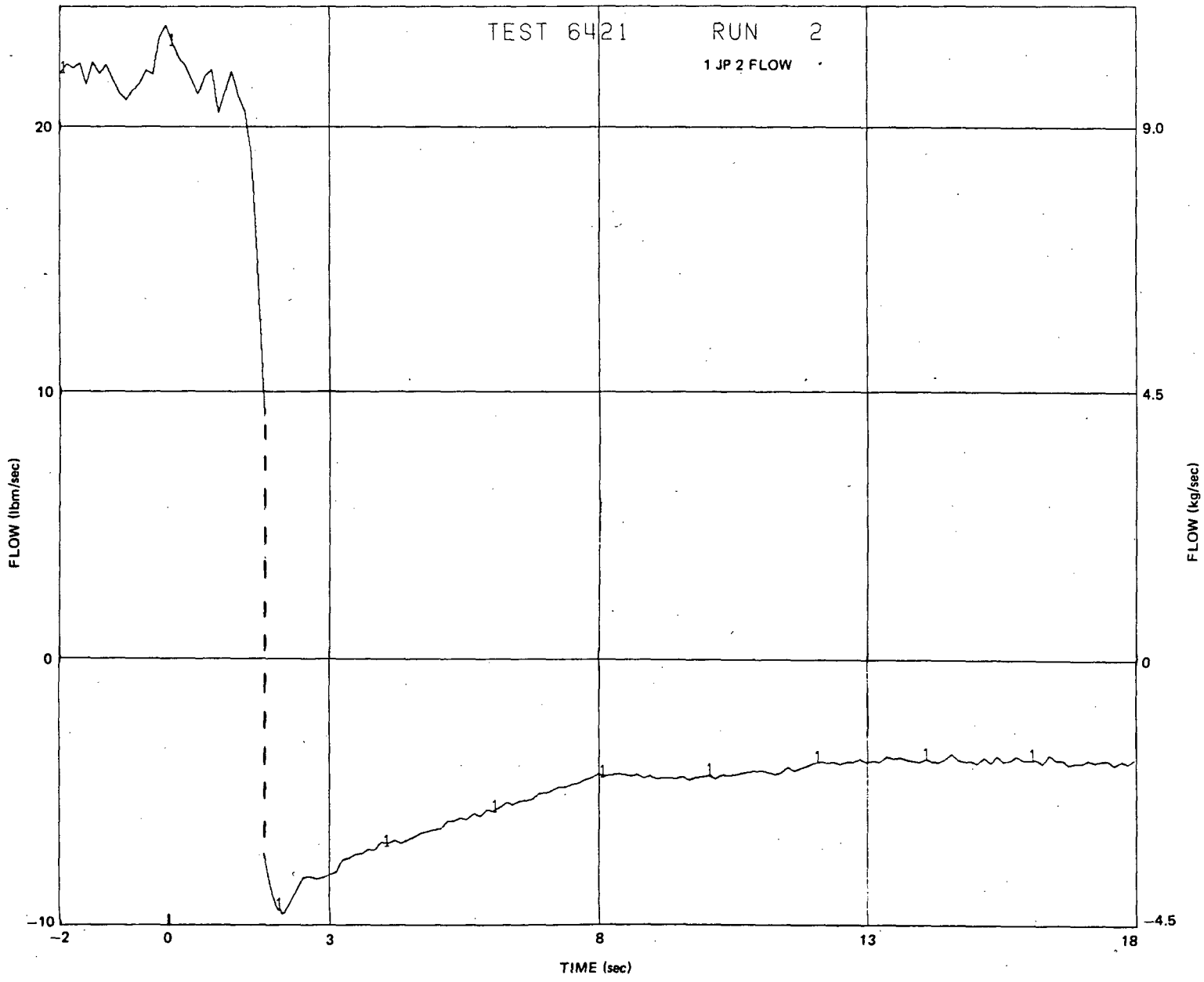

Figure L-121. Broken Loop Jet Pump Mass Flow Rate

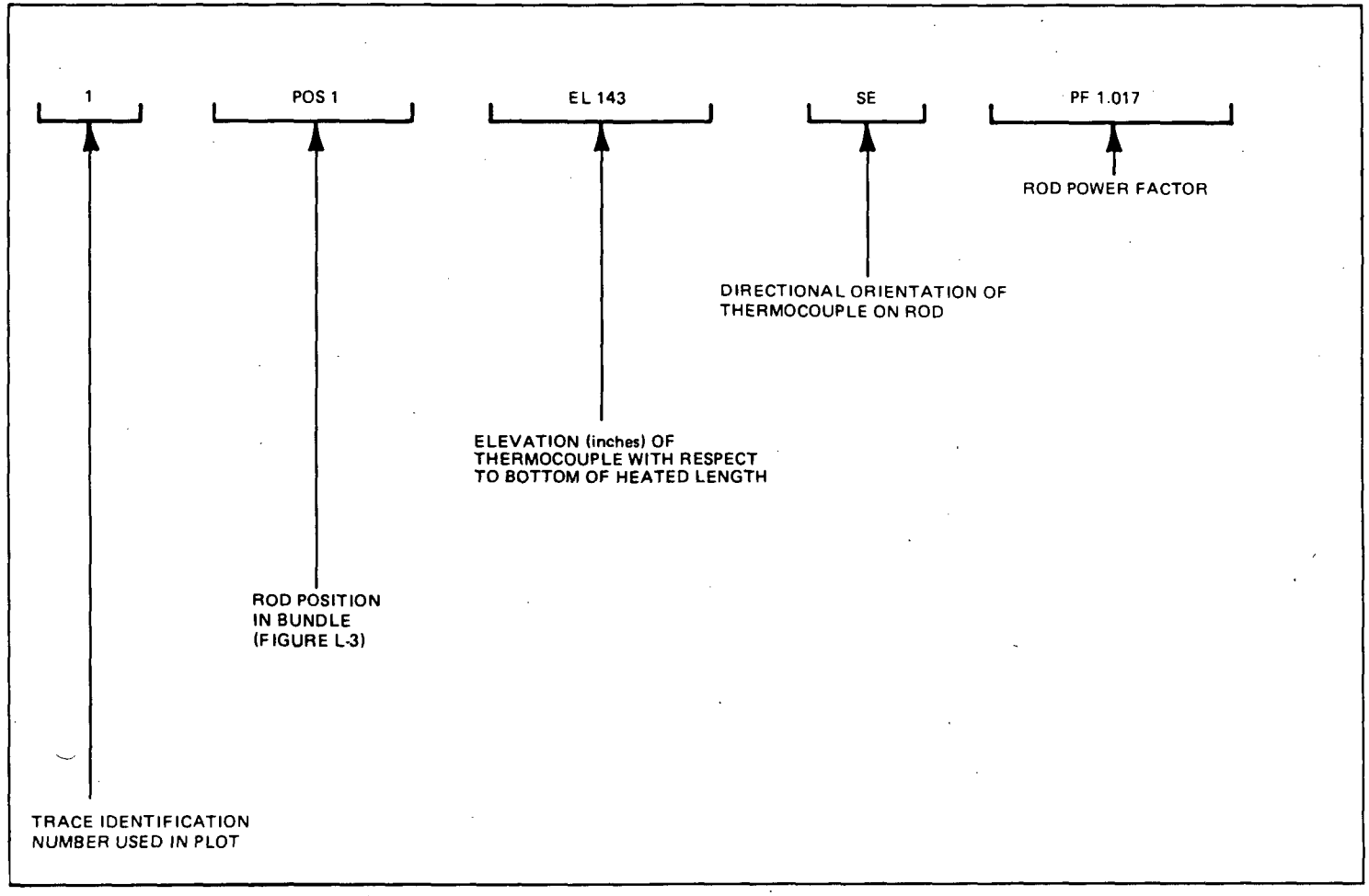

Figure L-122. Guide for Interpreting Legends on Bundle Temperature Plots

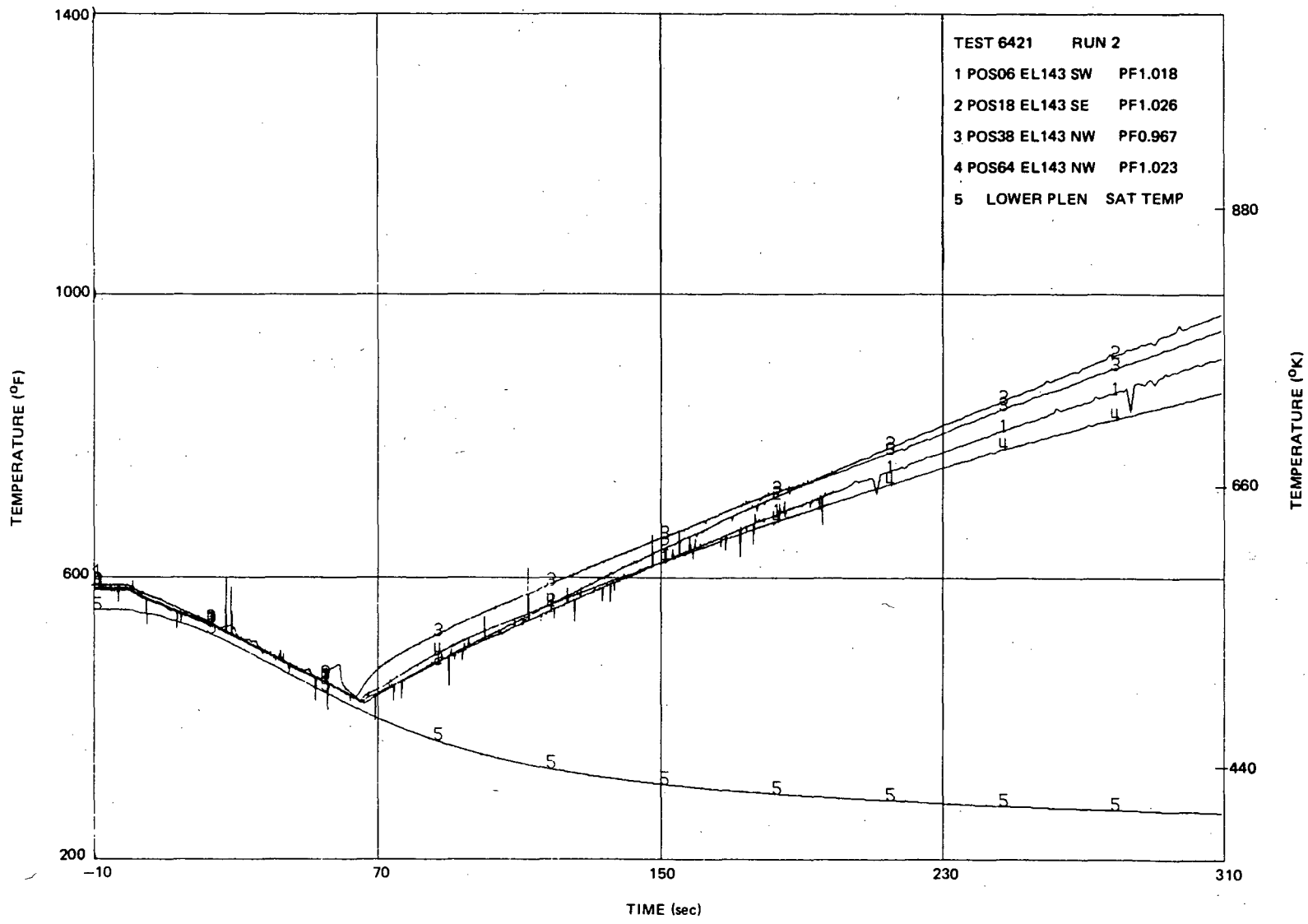

Figure L-123. Inside Clad Temperature - Elevation 143 in.

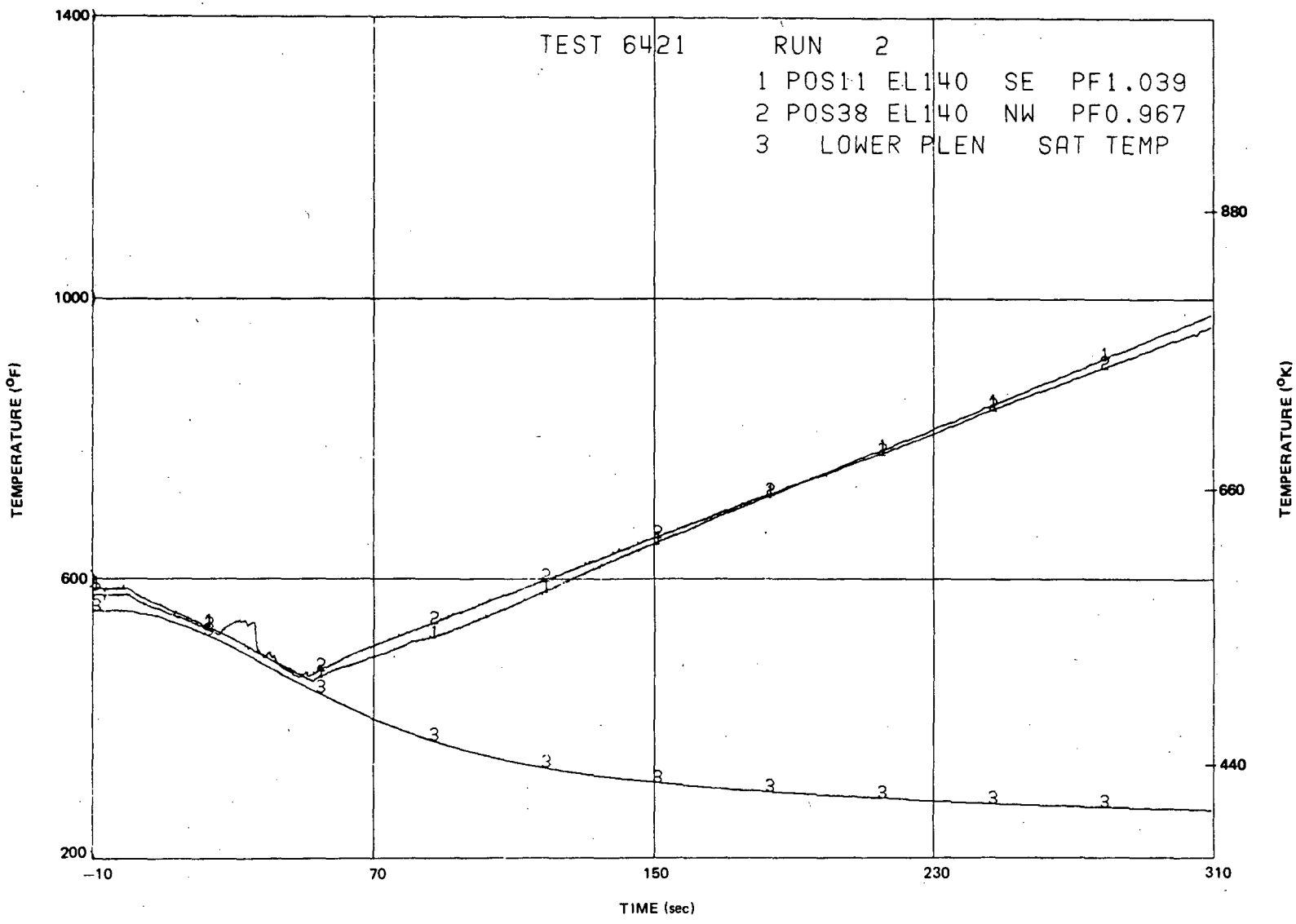

Figure L-124. Inside Clad Temperature - Elevation 140 in.

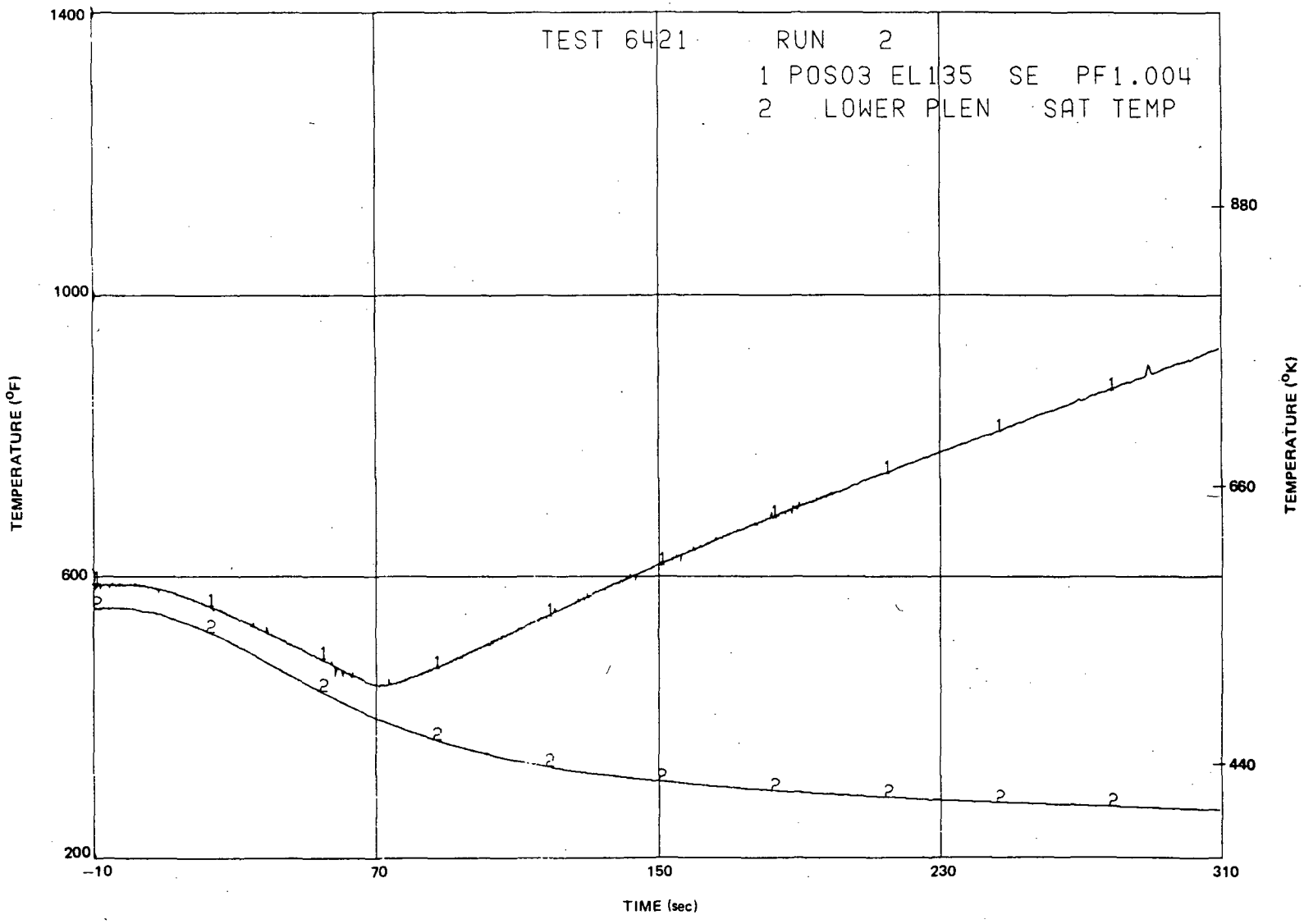

Figure L-125. Inside Clad Temperature - Elevation 135 in.

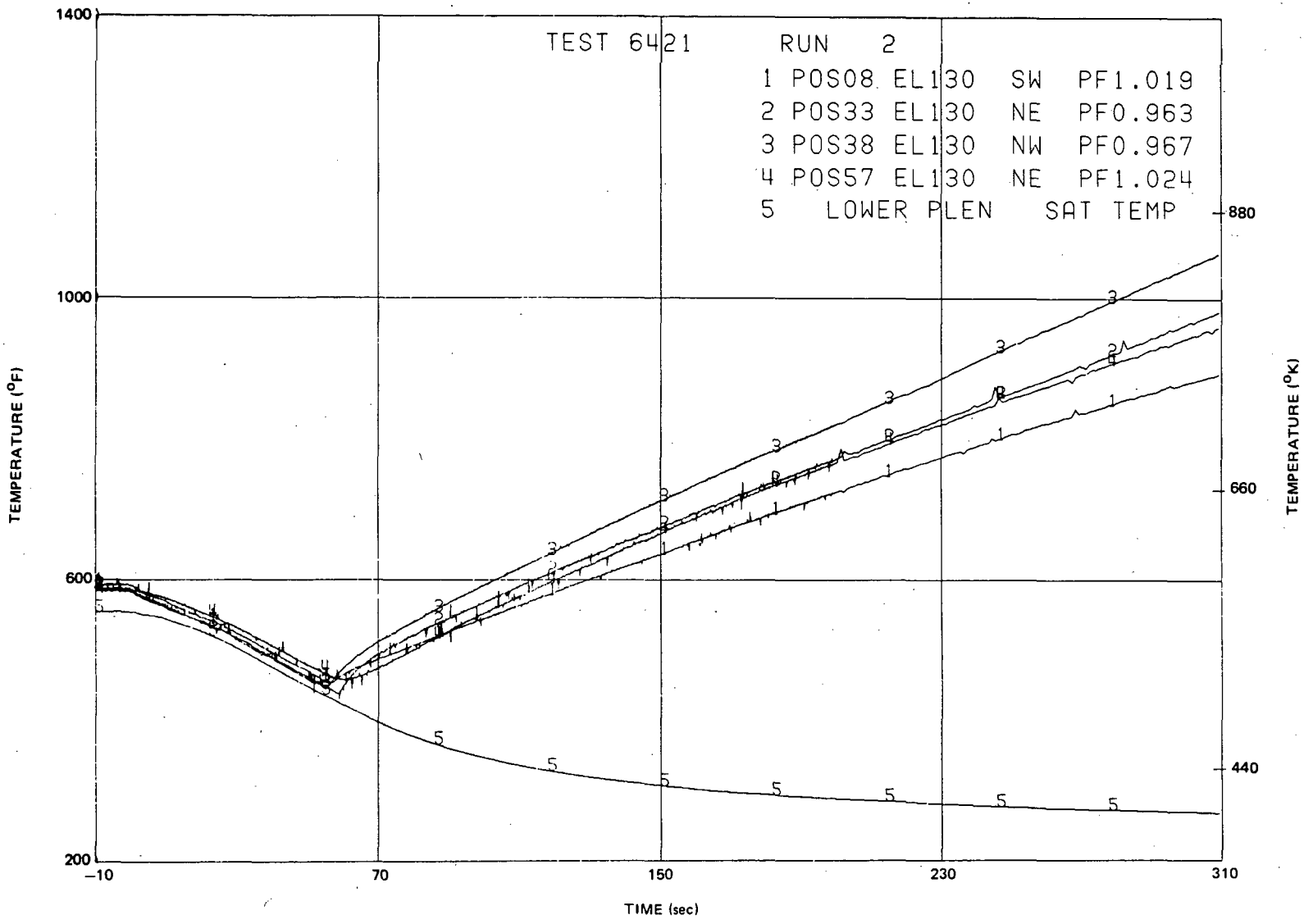

Figure L-126. Inside Clad Temperature - Elevation 130 in.

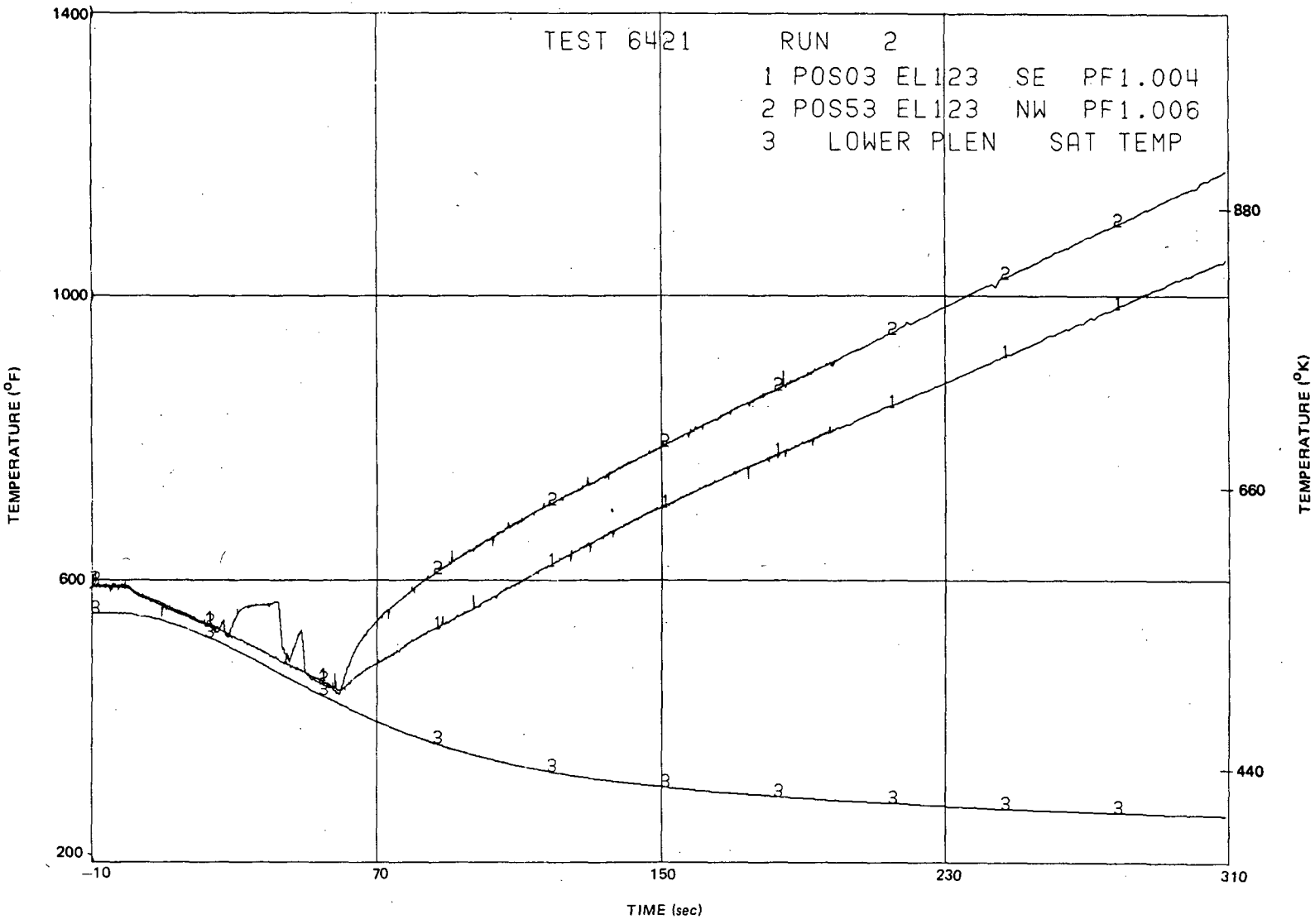

Figure L-127. Inside Clad Temperature - Elevation 123 in.

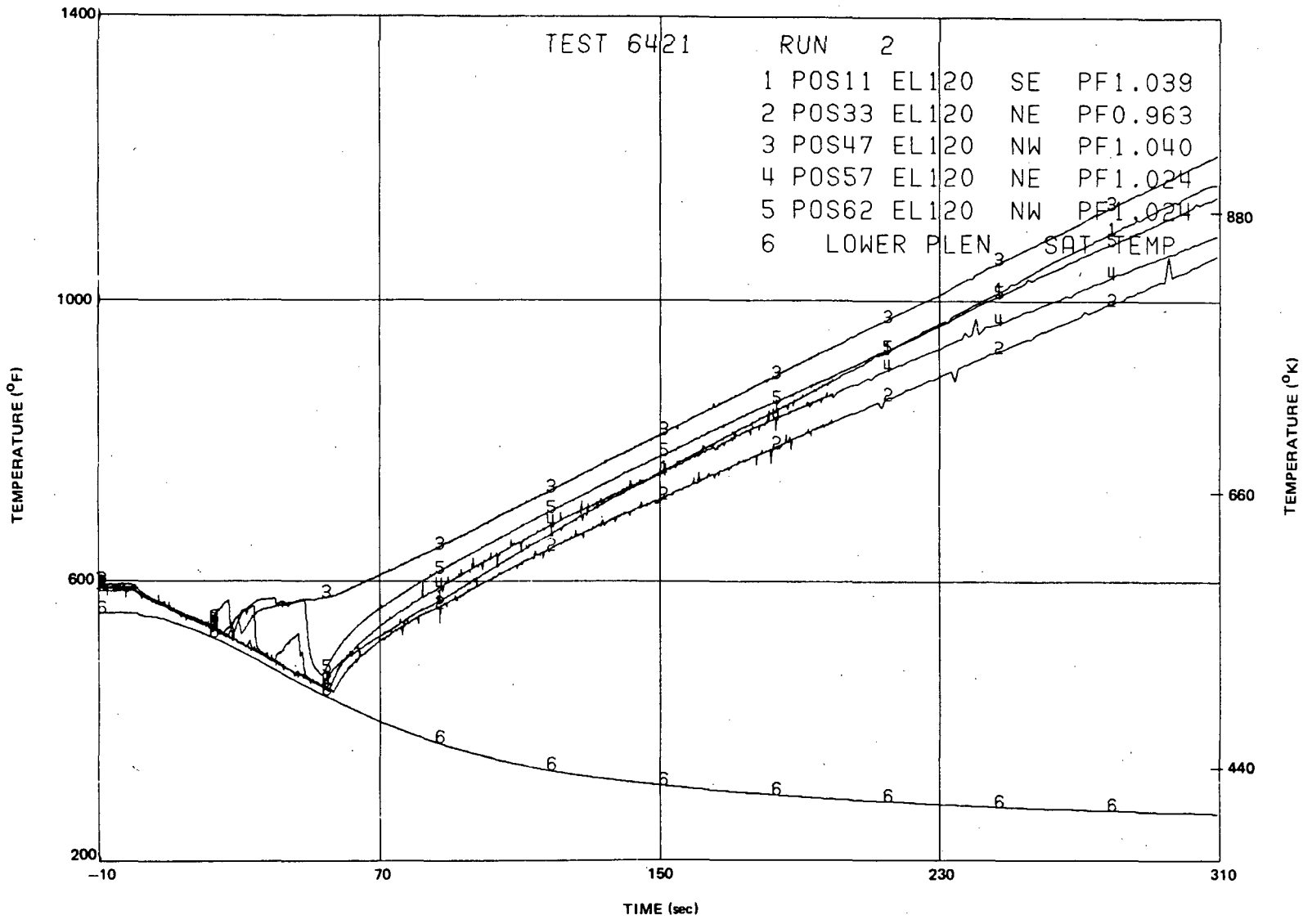

Figure L-128. Inside Clad Temperature - Elevation 120 in.

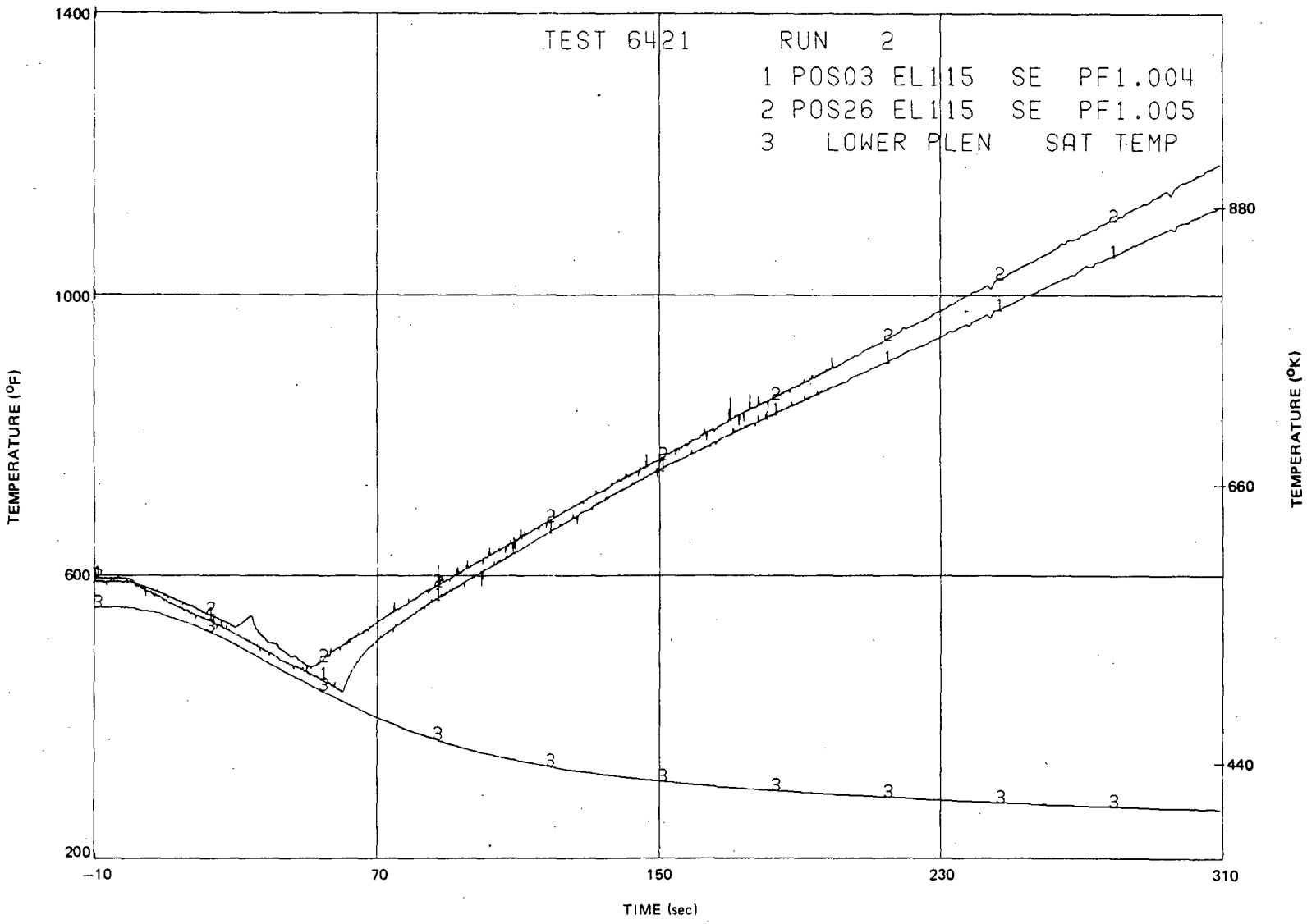

Figure L-129. Inside Clad Temperature - Elevation 115 in.

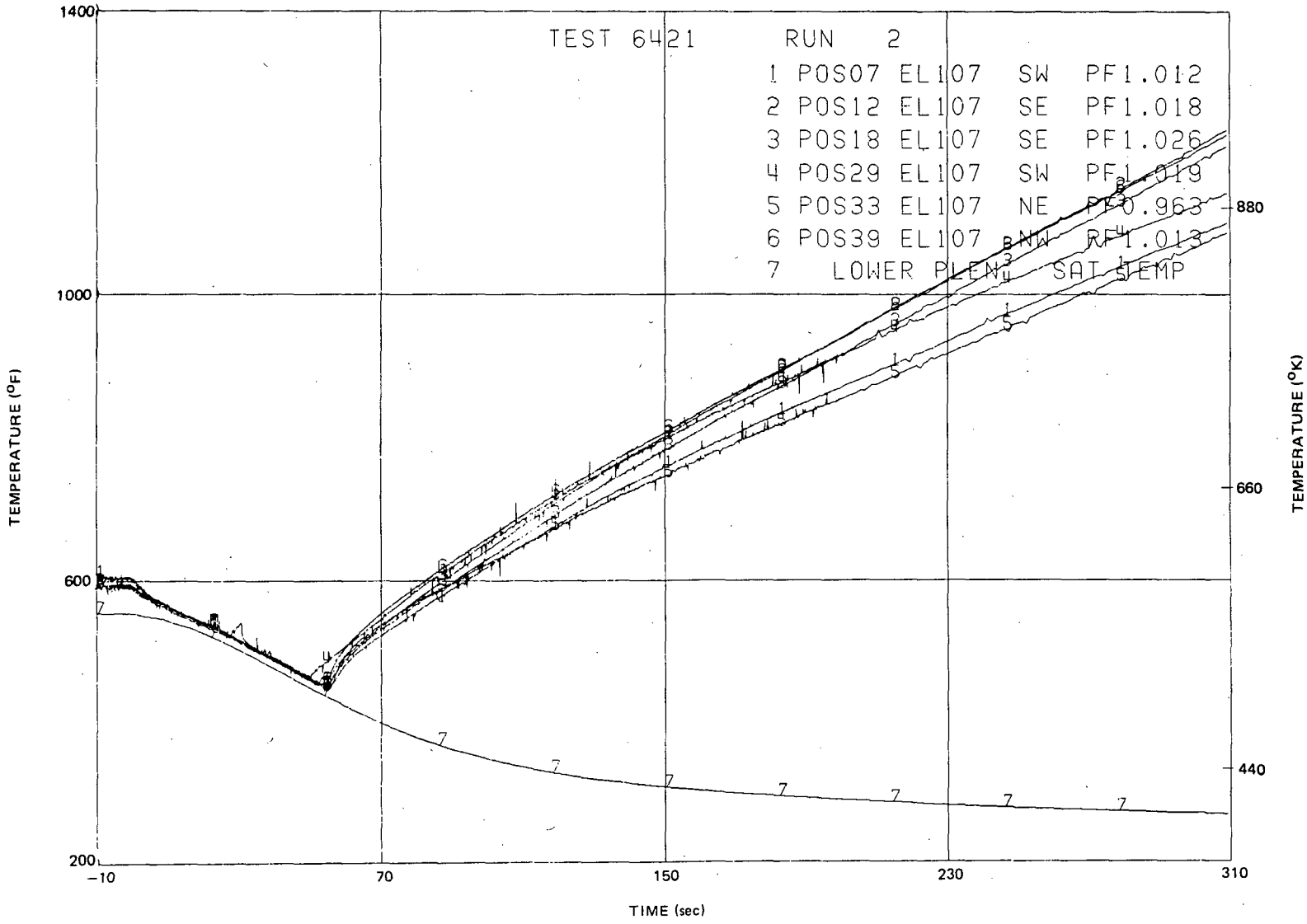

Figure L-130. Inside Clad Temperature - Elevation 107 in.

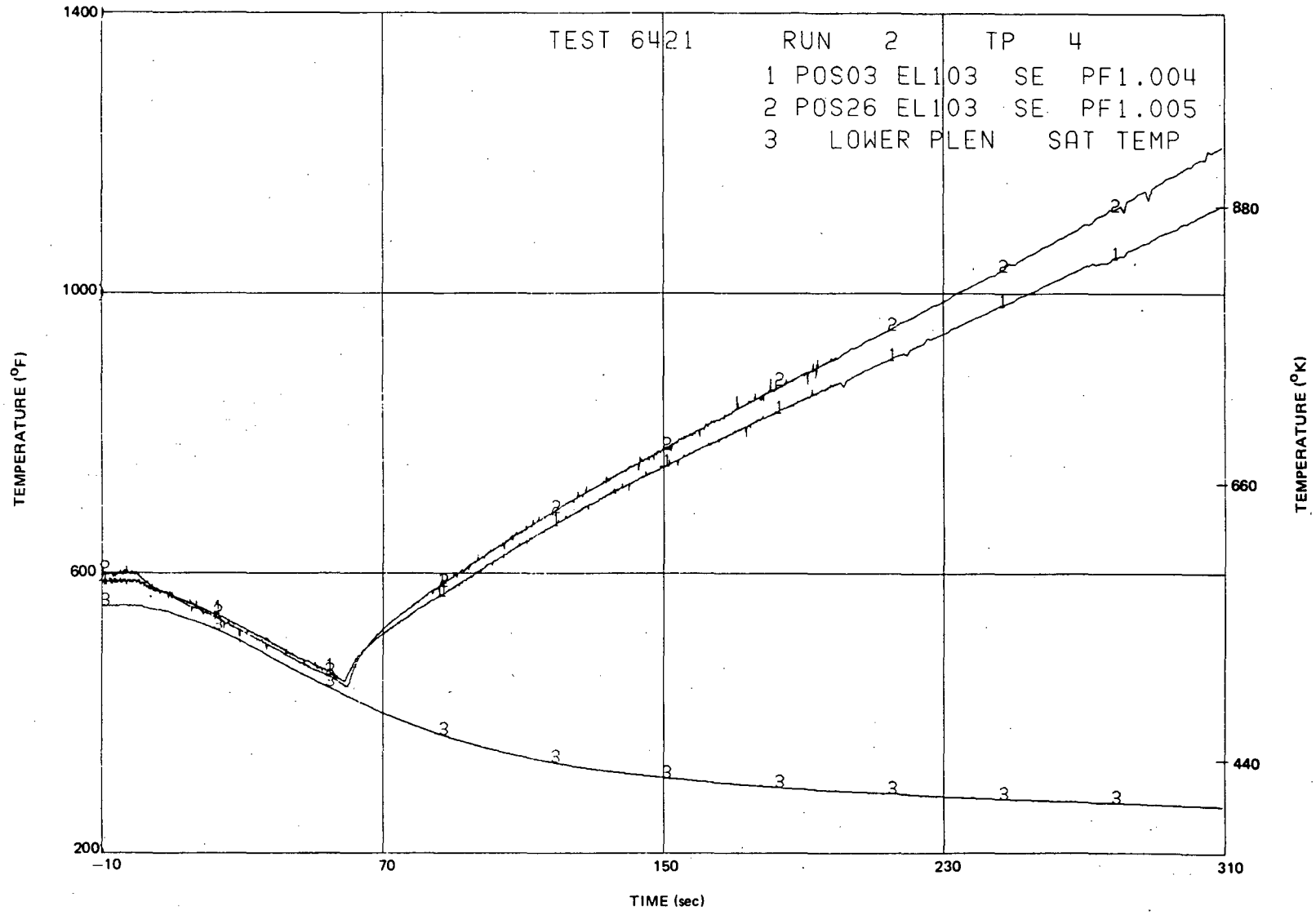

Figure L-131. Inside Clad Temperature - Elevation 103 in.

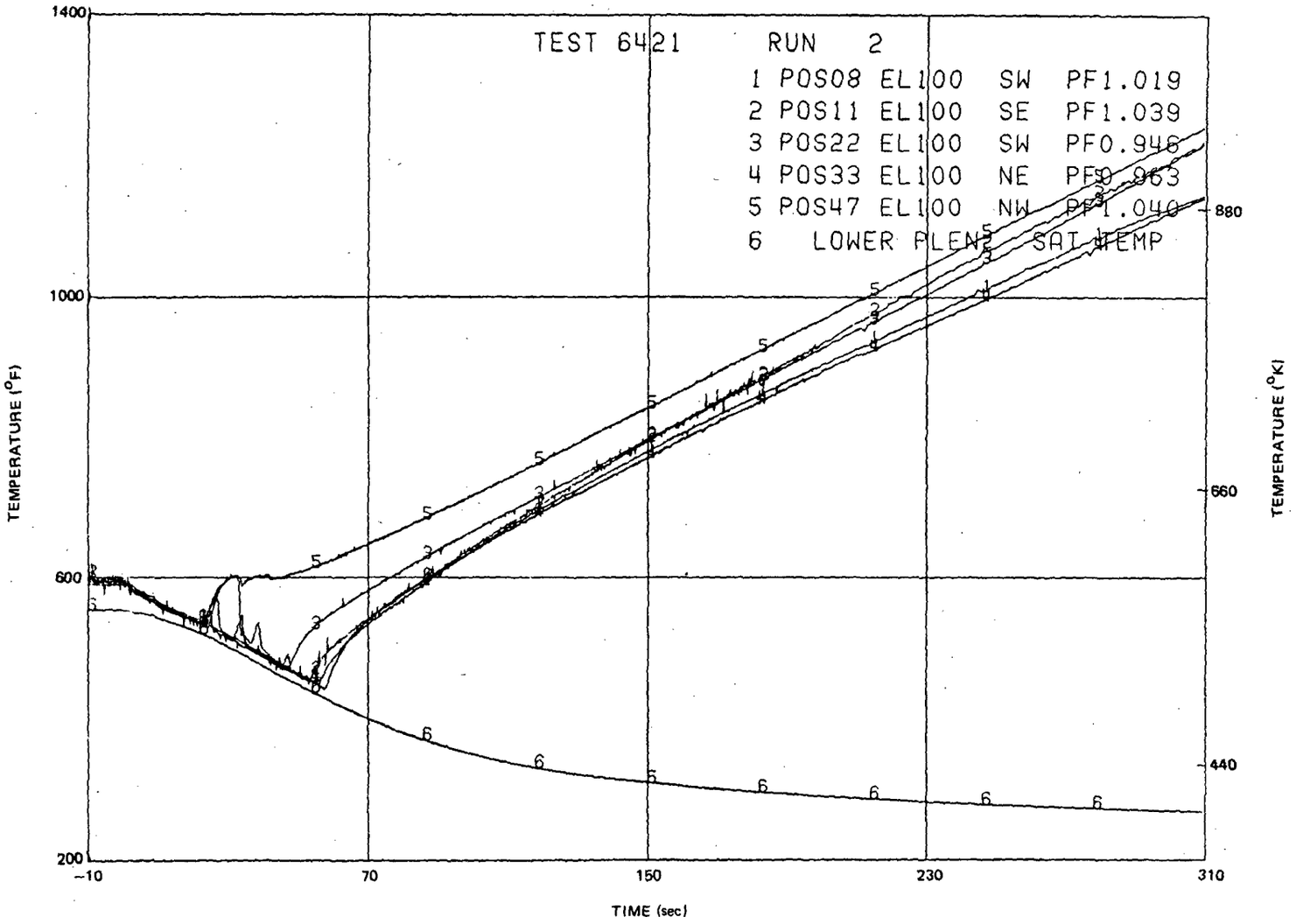

Figure L-132. Inside Clad Temperature - Elevation 100 in.

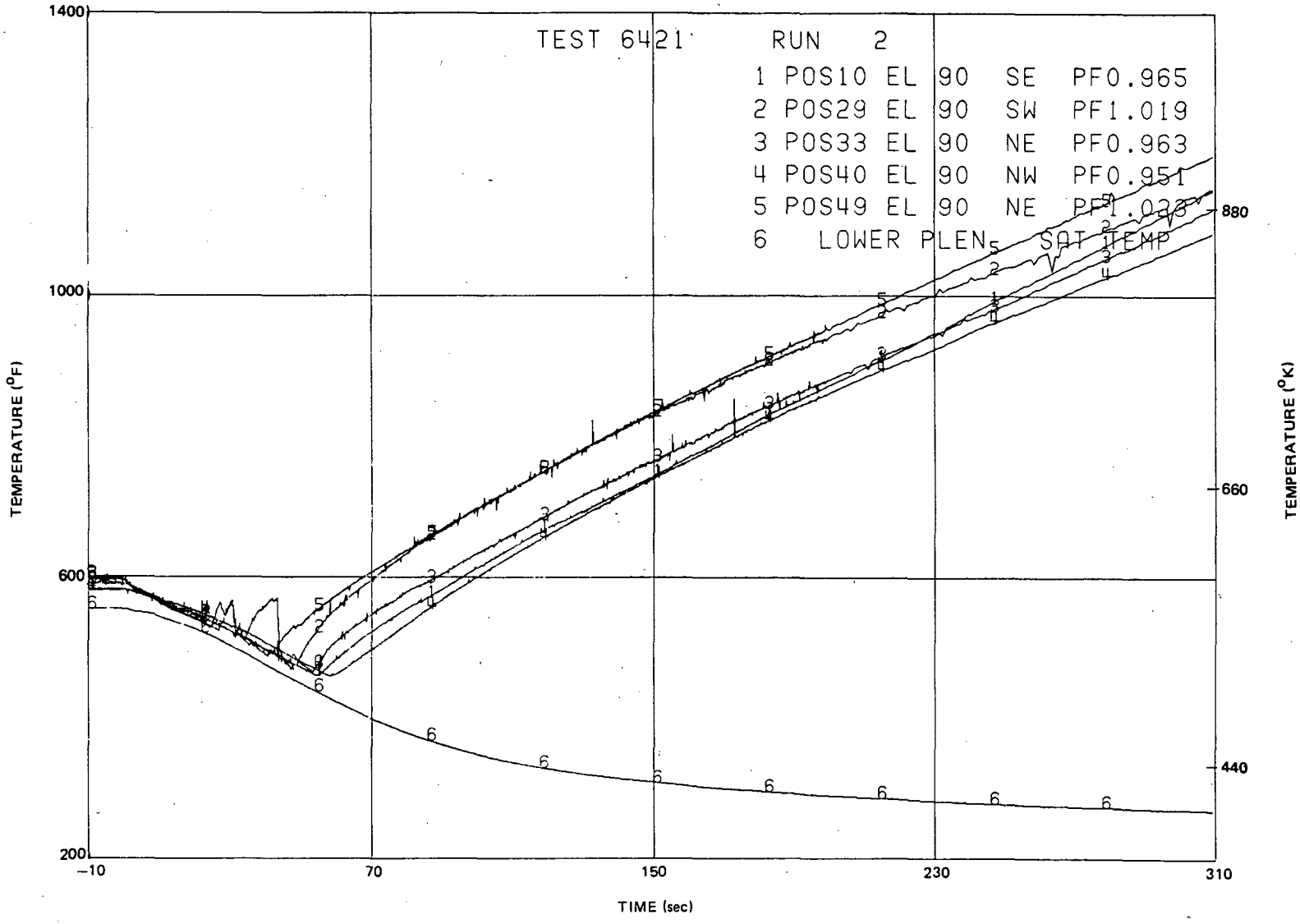

Figure L-133. Inside Clad Temperature - Elevation 90 in.

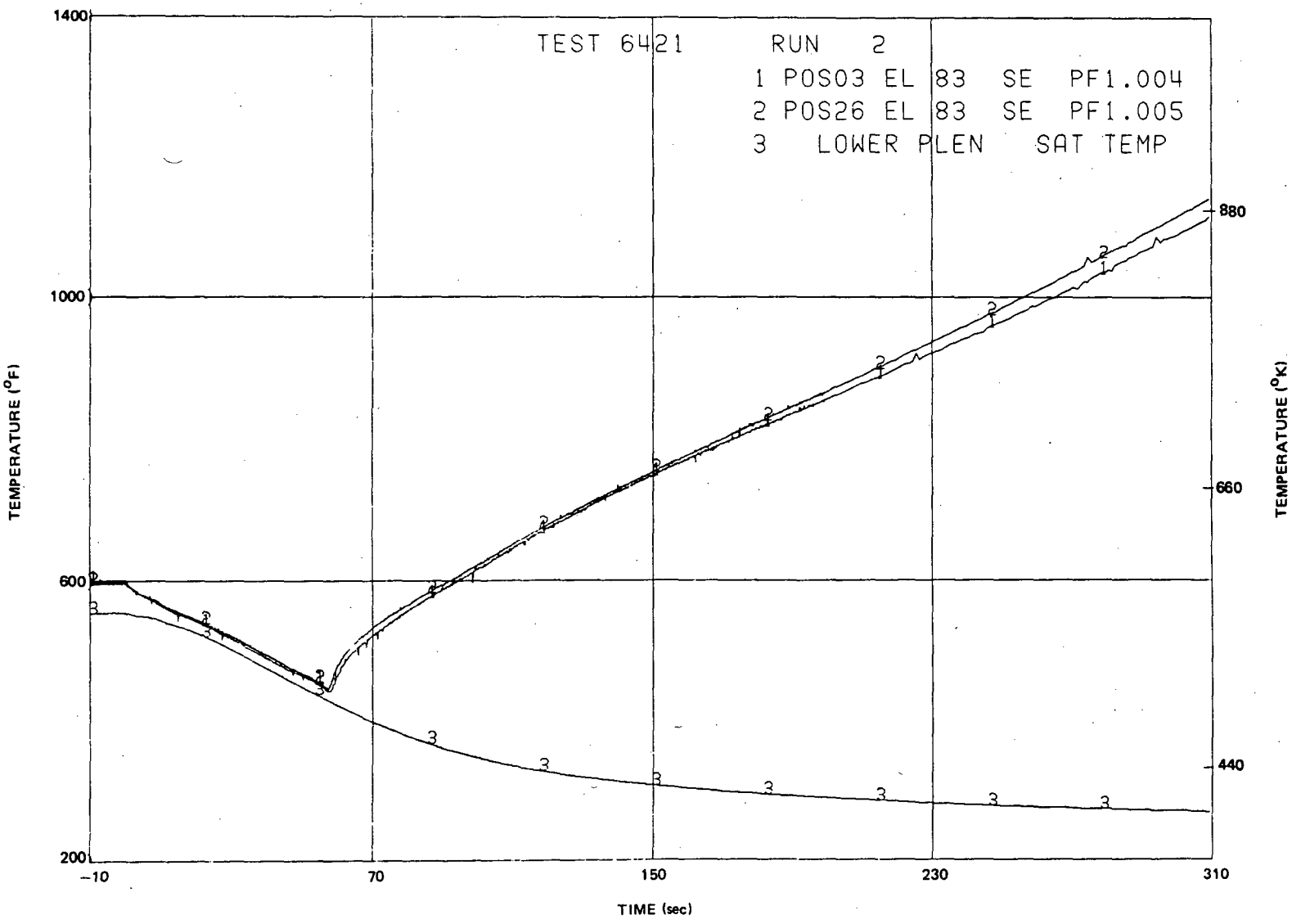

Figure L-134. Inside Clad Temperature - Elevation 83 in.

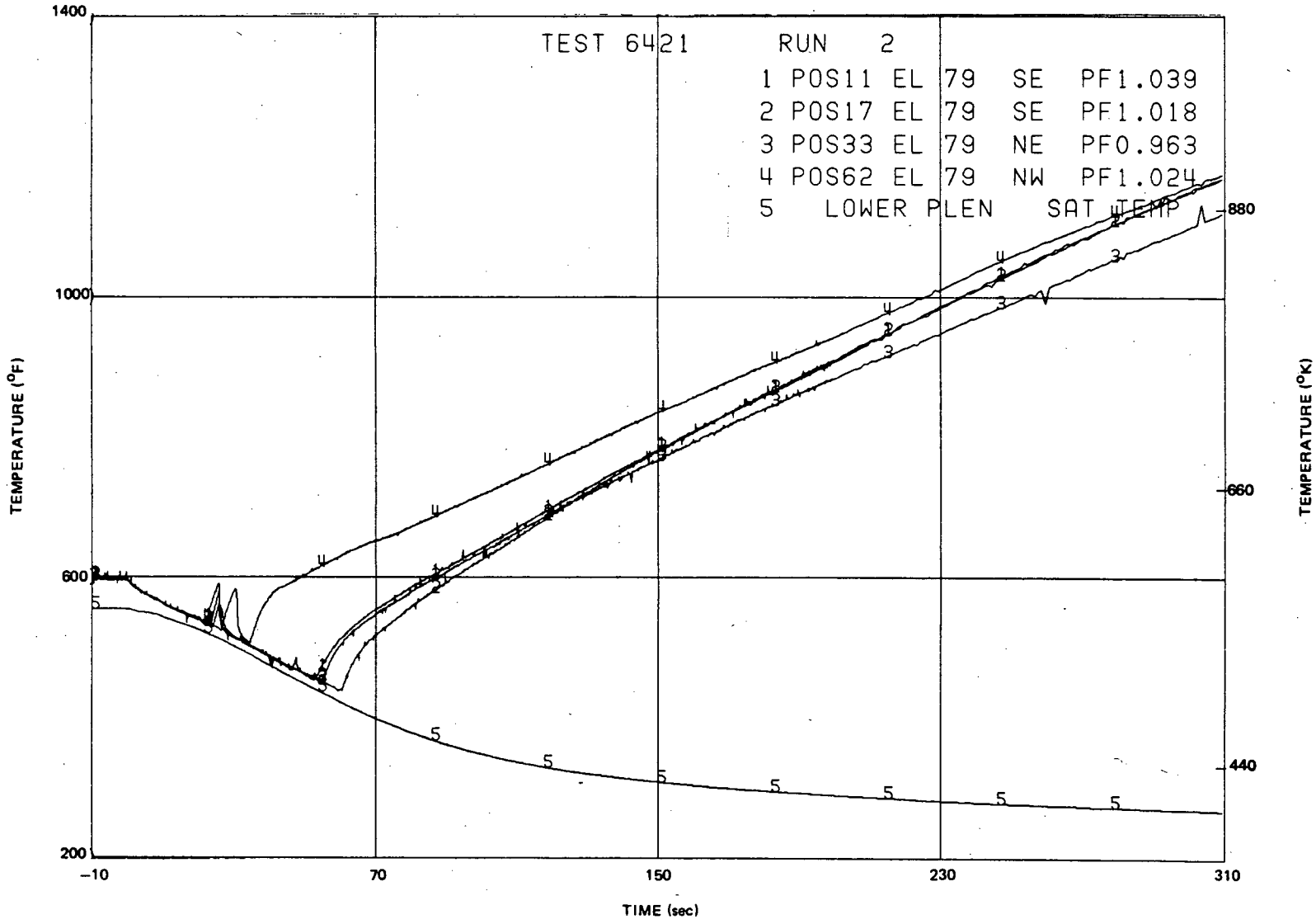

Figure L-135. Inside Clad Temperature - Elevation 79 in.

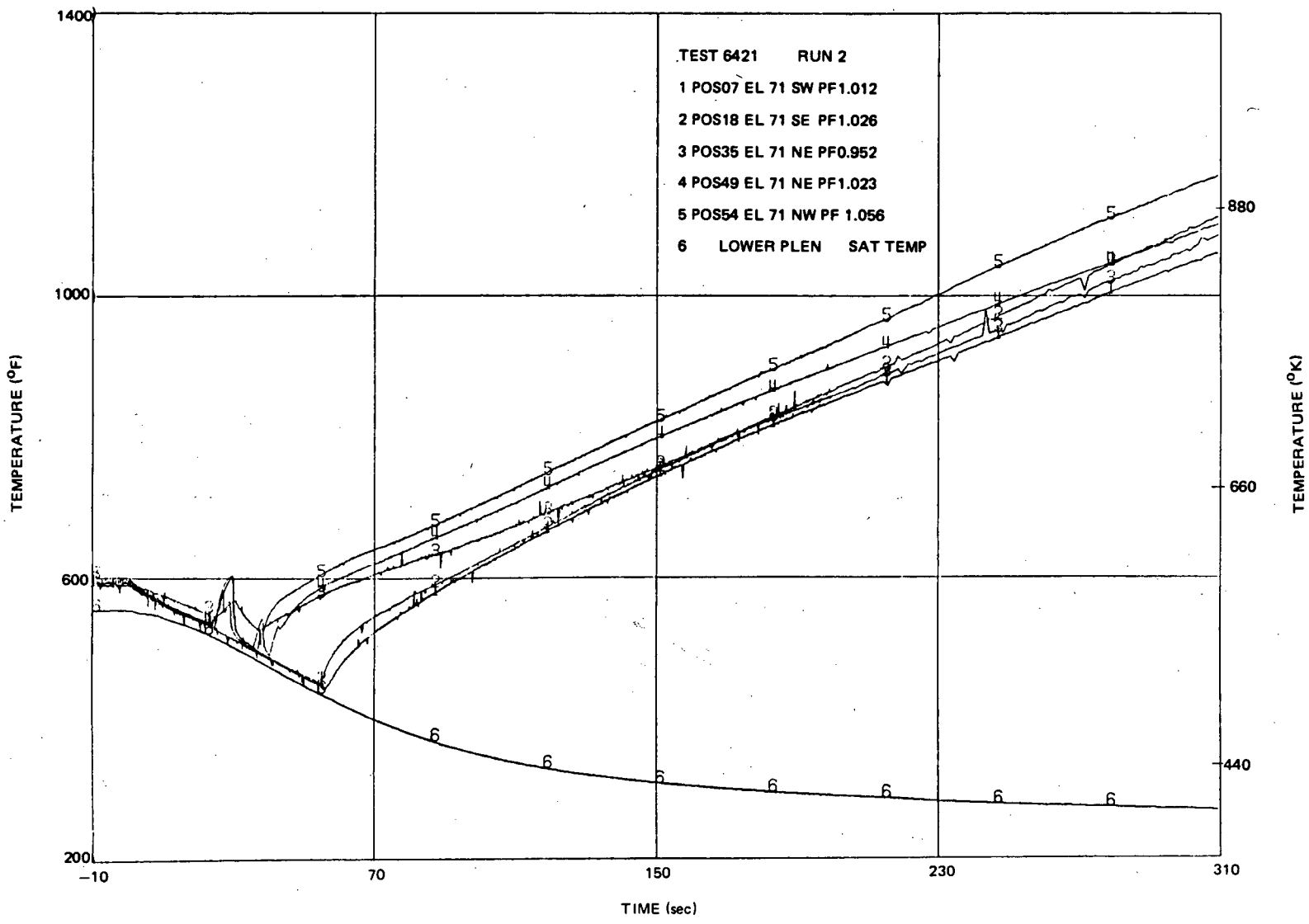

Figure L-136. Inside Clad Temperature - Elevation 71 in.

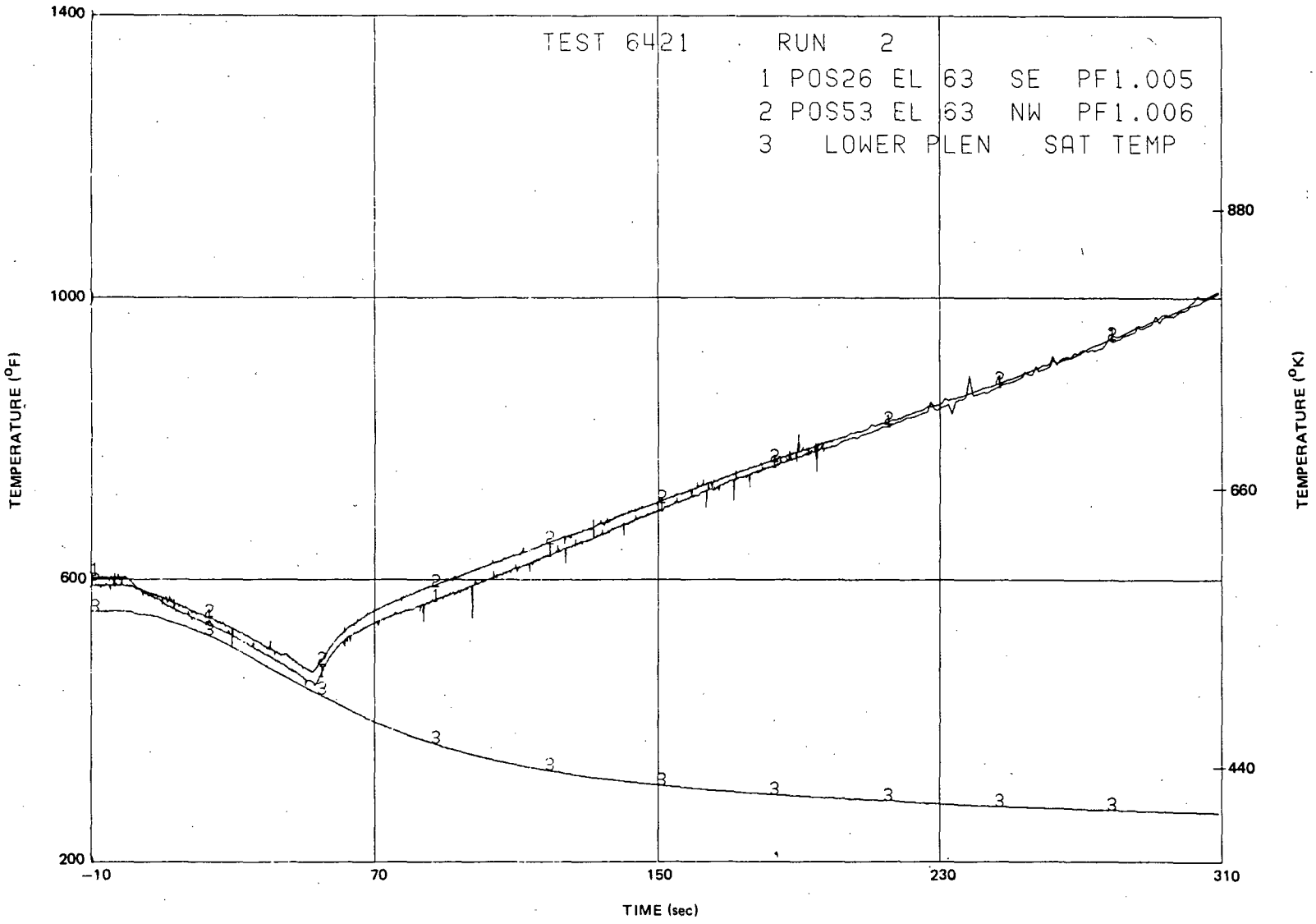

Figure L-137. Inside Clad Temperature - Elevation 63 in.

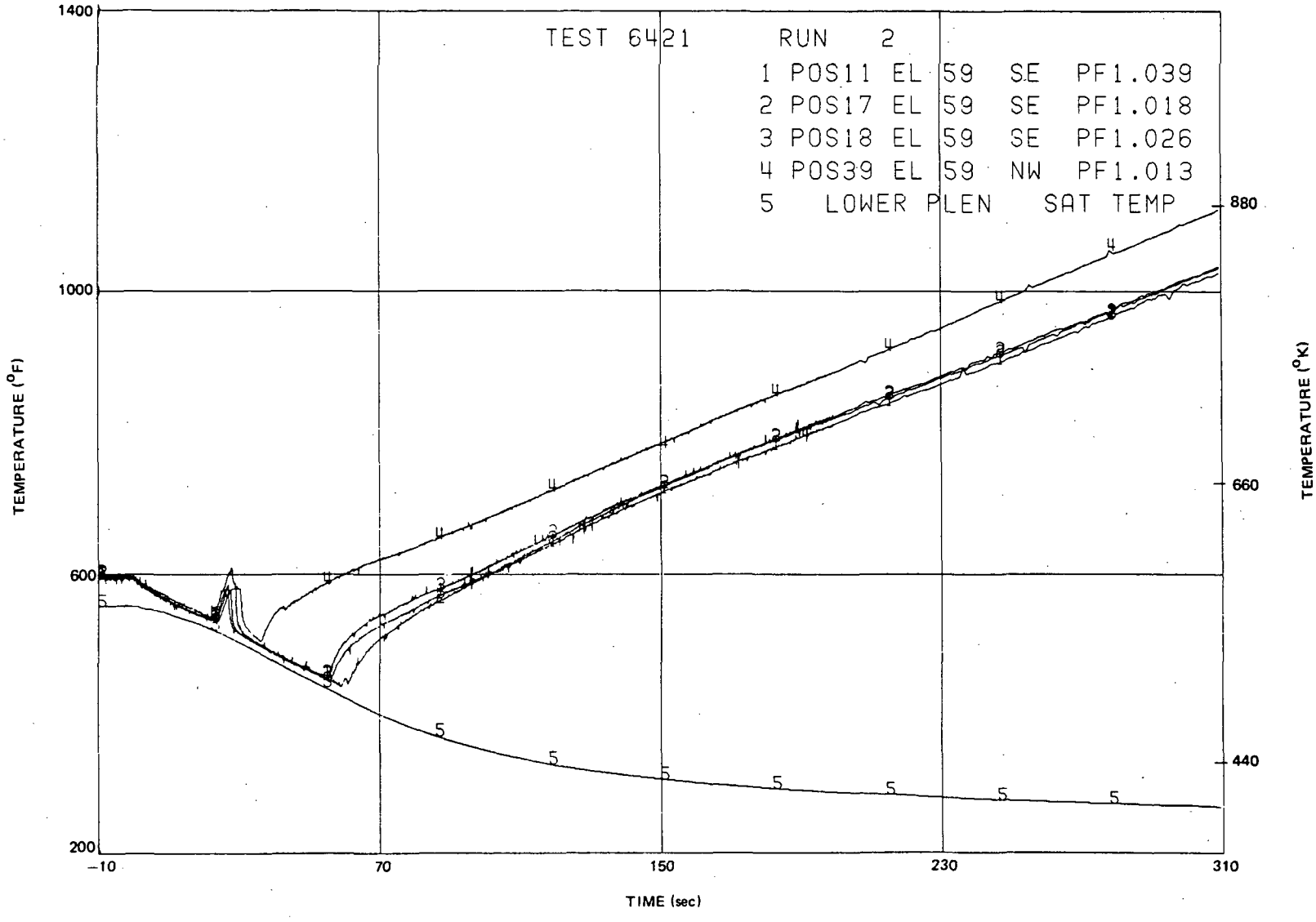

Figure L-138. Inside Clad Temperature - Elevation 59 in.

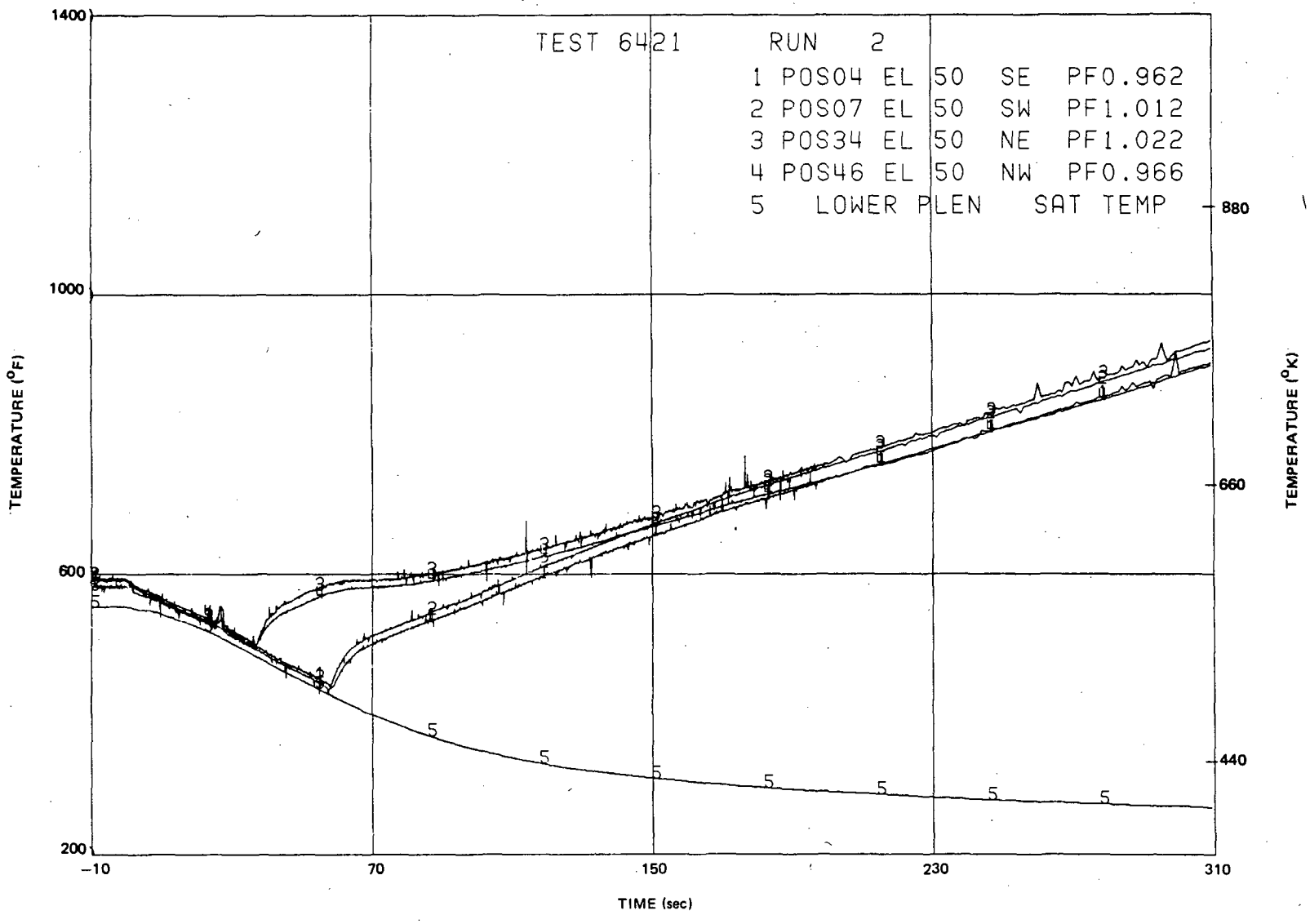

Figure L-139. Inside Clad Temperature - Elevation 50 in.

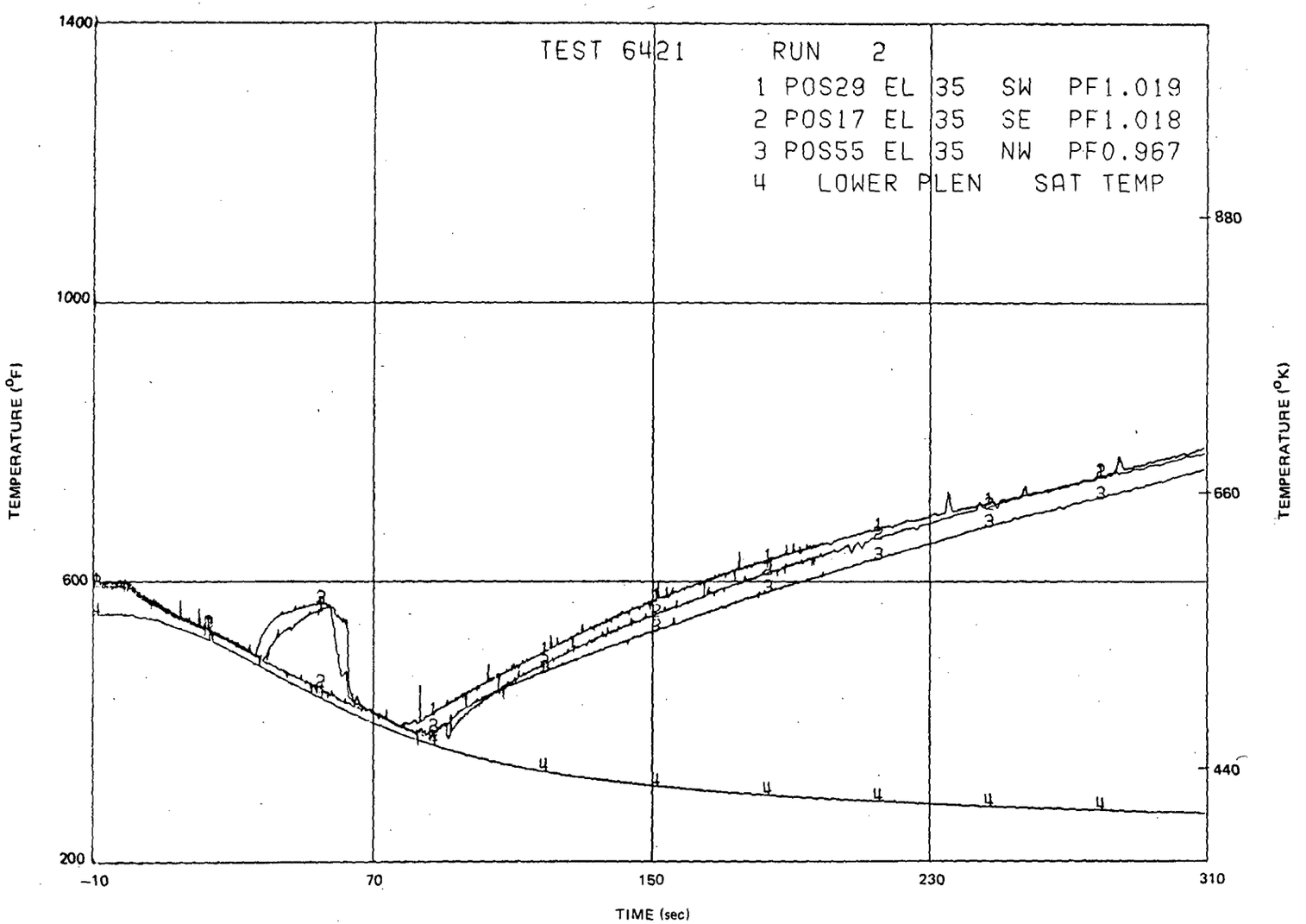

Figure L-140. Inside Clad Temperature - Elevation 35 in.

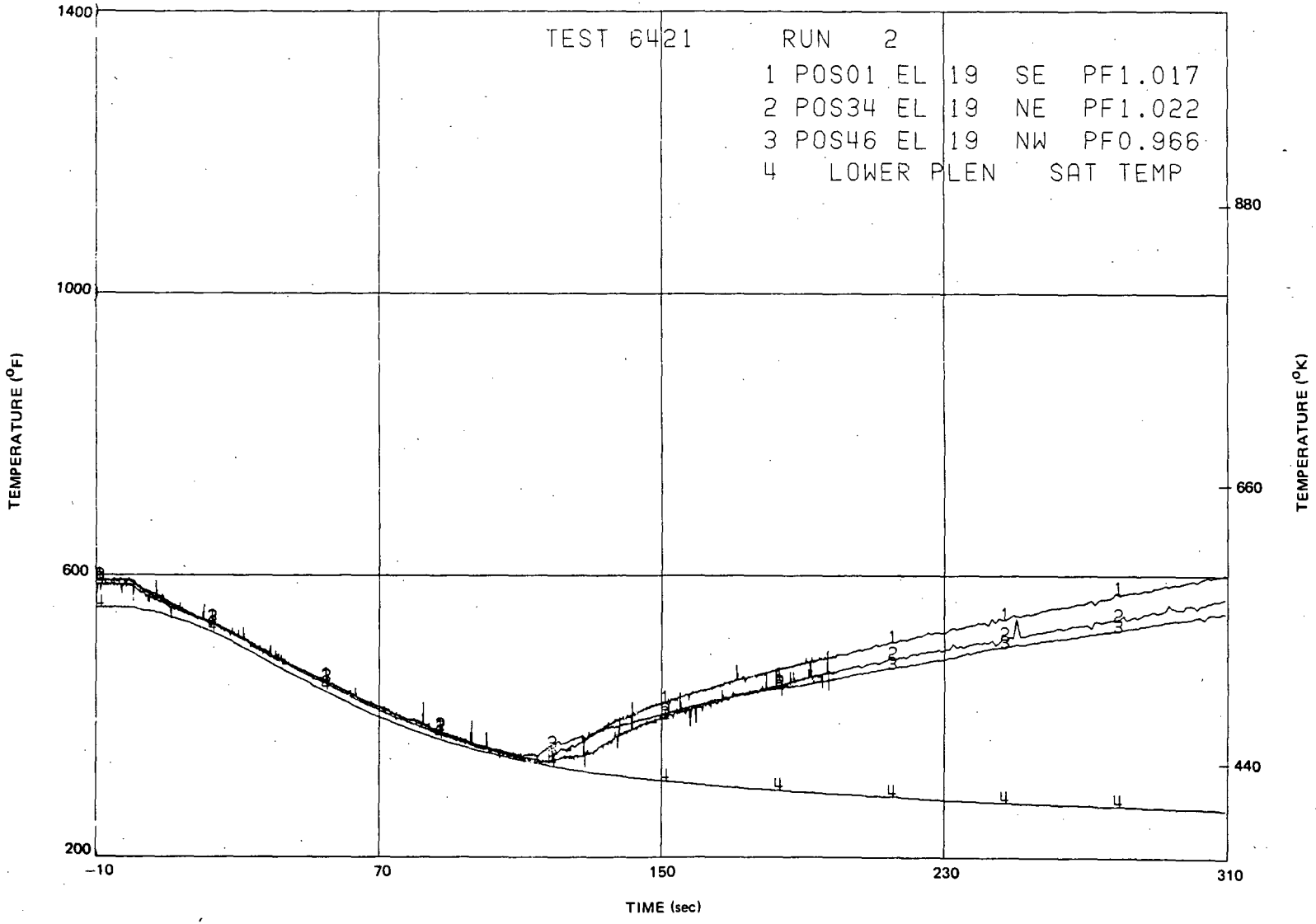

Figure L-141. Inside Clad Temperature - Elevation 19 in.

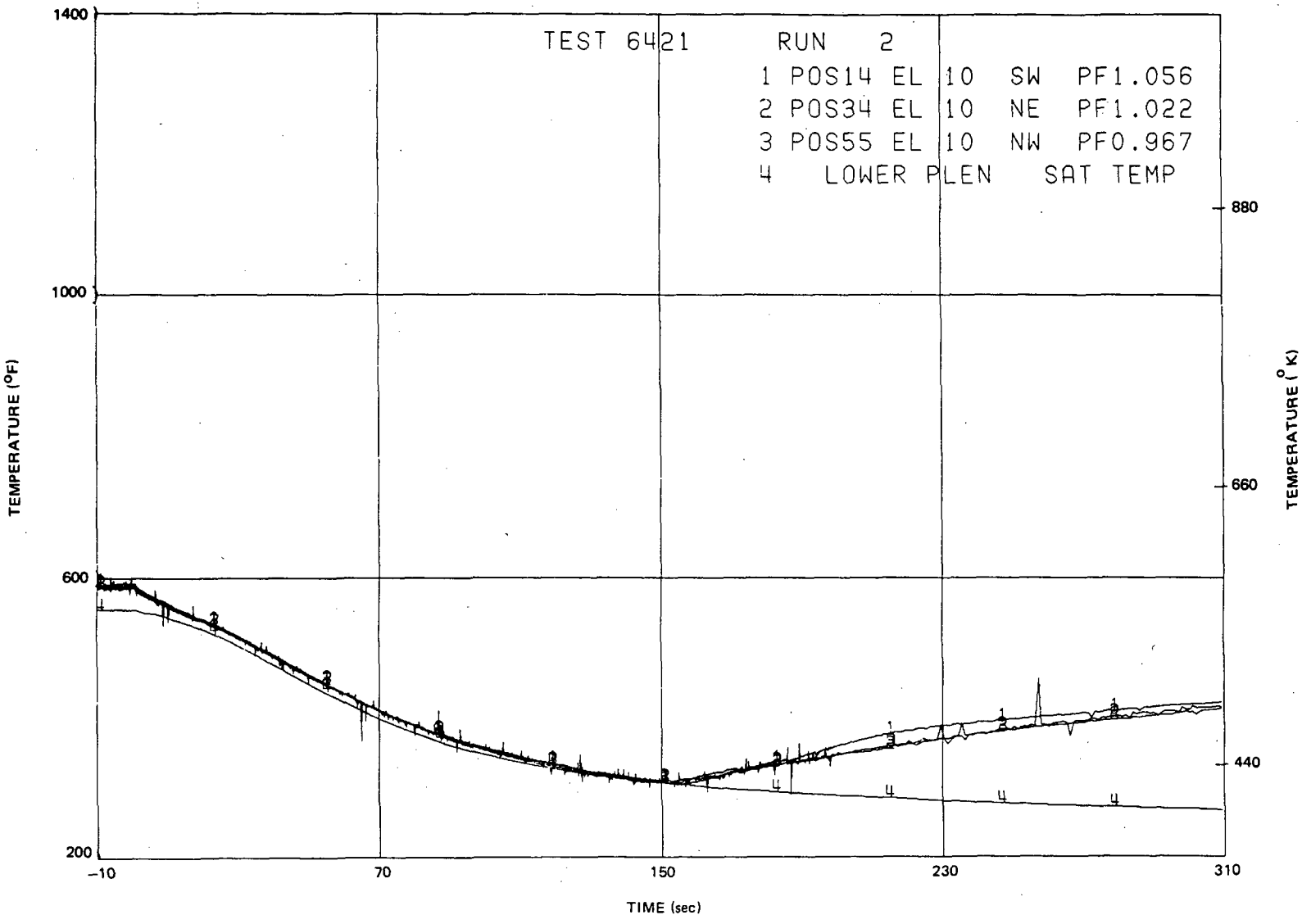

Figure L-142. Inside Clad Temperature - Elevation 10 in.

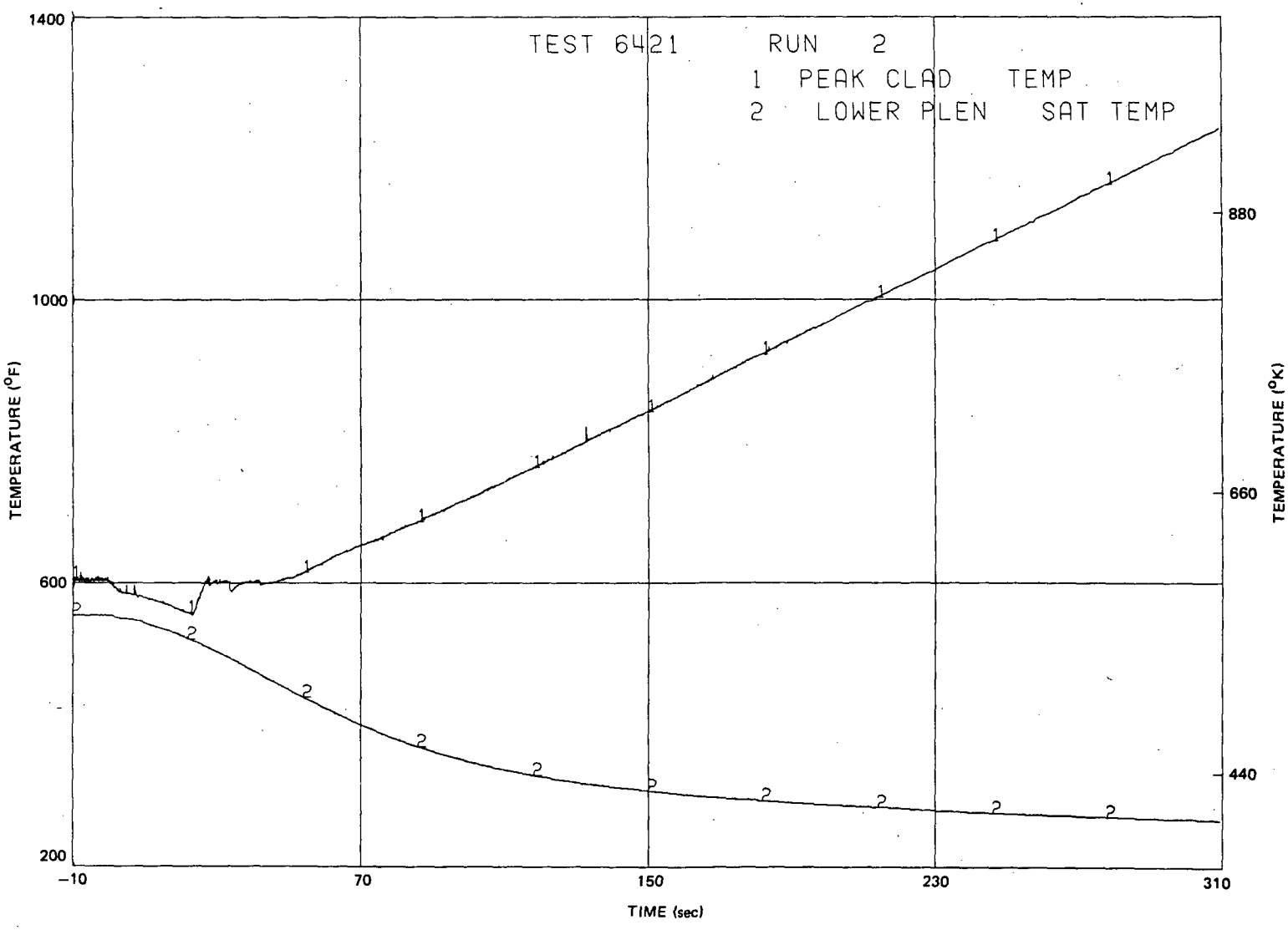

Figure L-143. Peak Clad Temperature

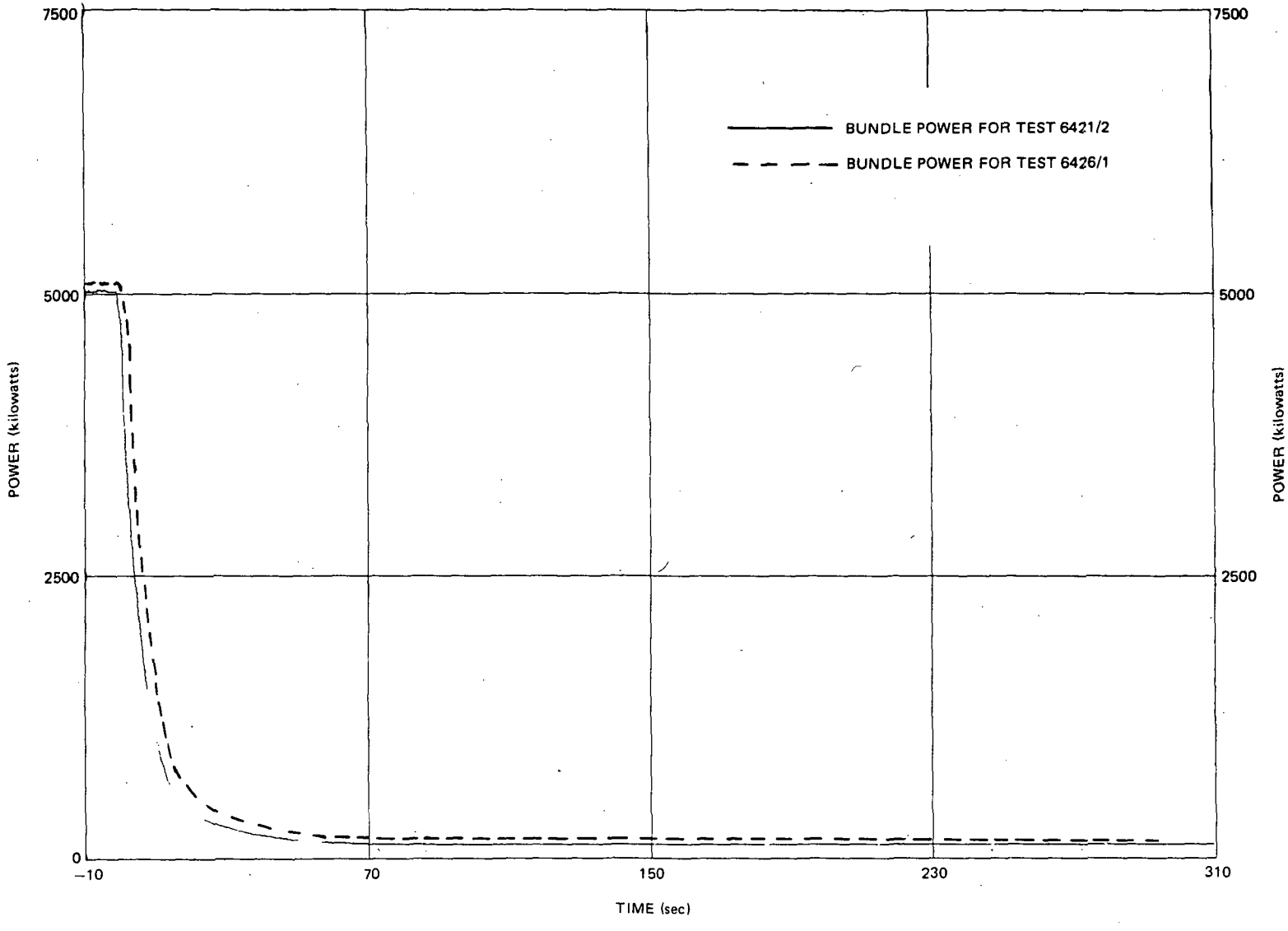

Figure L-144. Comparison of Bundle Power Histories for Tests 6421/2 and 6426/1

Appendix M

DATA REPORT FOR TEST 6422/RUN 3

Test 6422/3 was an average power, average ECC flow, nominal ECC temperature test conducted in the TLTA 5A facility. This test was initially intended to be the reference test. However, owing to improved break flow instrumentation and the addition of a more representative pressure controller to simulate the early system pressure response, Test 6425/2 was chosen as the reference test. Data from Test 6422/3, along with a discussion of the results, are included in this appendix.

A diagram of the system instrumentation showing measurement nodes is given in Figure M-1. Figure M-2 shows a schematic of the bundle and locations of the pressure transducer taps and thermocouples. The core lattice arrangement and the local peaking factor distribution are shown in Figure M-3.

M-1. RESULTS

M-1.1 System Thermal-Hydraulic Response

The test conditions for Test 6422/3 are summarized in Table M-1. The bundle power decay for the test (Figure M-4) was based on ANS-5 for a central-average BWR/6 bundle and included the effect of decay heat and stored heat.

The system pressure response as measured at three locations is presented in Figure M-5. The pressure differences between plena are initially due to the flow and hydrostatic head differences in the system. After the recirculation pumps are tripped and blowdown begins, these pressure differences become small, and the three pressures are seen to be nearly identical. Later in the transient as the system refills, the hydrostatic head difference becomes discernible (Figure M-5).

The ECC injection rates (Figures M-6 through M-9) are governed by the system pressure as the pump characteristics were designed to simulate those of a BWR. Injection commences at 27 sec for HPCS (Figure M-6), 63 sec for LPCS (Figure M-7), and 71 sec for LPCI (Figure M-8). The total amount of ECC injected at any time is included in Figure M-9.

An overview of the system response is presented in Figures M-10 and M-11. The initial system response is similar to the previous scoping test series (Appendix I). Following the onset of lower plenum flashing, the steam generation in the lower plenum holds up inventory in the bundle because of counter current flow limiting (CCFL) at the side entry orifice (SEO) below the bundle. Similarly, CCFL at the upper tieplate and the bypass outlet holds up inventory in the upper plenum. As the blowdown continues, the mixture level in the lower plenum recedes, reaching the jet pump exit plane at ∿34 sec. An alternative path becomes available for the lower plenum vapor to escape, and therefore less vapor vents through the SEO to the bundle. The liquid continuum previously maintained in the bundle by the vapor updraft is now lost, and bulk heat-up within the bundle begins. During this period, the inventory in the upper plenum remains fairly constant (Figures M-10 and M-11), with drainage into the bundle being replenished by continued core spray.

The guide tube/bypass region begins to refill (Figure M-11) shortly after the onset of LPCI injection (∿90 sec). The subcooled LPCI fluid condenses steam in the bypass region and eliminates CCFL at the top of the bypass. The upper plenum is thus partially drained as the bypass is refilled (Figure M-11).

The bundle refloods concomitantly with bypass refill for these reasons: (1) increased hydrostatic head in the bypass region produces increased leakage flow into the bundle, and (2) continuing CCFL at the SEO prevents complete drainage of the bundle inventory into the lower plenum. As the bundle refloods, its hydrostatic head increases, and the leakage flow from the bypass diminishes. The subcooled LPCI fluid that was flowing downward through the bypass region is then forced to flow upward into the upper plenum. This LPCI fluid combines with other subcooled liquid being sprayed into the upper plenum which leads to CCFL breakdown at the top of the bundle. As a result, the bundle reflood is accelerated, and the upper plenum inventory completely drains. The upper plenum remains drained for the balance of the test (Figure M-10).

The filling of the bundle produces a hydrostatic head on the lower plenum fluid and increases the pressure drop across the jet pumps. The pressure drop is sufficient to carry the ECC fluid, which is now draining through the bypass and bundle, out of the lower plenum and into the downcomer region (Figure M-12). The hydrostatic head of the bundle, therefore, prevents the lower plenum from completely refilling. The system achieves pseudo-steady-state for the remainder of the transient except, as discussed below, for two short periods of vapor venting through the bypass region.

Plots of regional mass are included (Figures M-13 through M-19). From these plots the timing and extent of mass transfer from one region to another can be determined. Nodal differential pressures along the bundle are shown in Figures M-20 through M-23. Bundle reflood from the bottom and final reflooding from the top can be observed from these measurements. Nodal differential pressure along the guide tube and bypass are shown in Figures M-24 and M-25.

M-1.2 Bundle Heat-Up Response

The thermal response of the bundle is marked by: (1) low peak cladding temperatures below 700°F, (2) a well cooled bundle (∿Tsat) after 150 sec, and (3) eventual subcooling of the bundle (below Tsat). A guide for interpreting bundle temperature plots is shown in Figure M-26. Peak cladding temperature is presented in Figure M-27, while temperature measurements at different locations are included in Figures M-28 through M-49.

Some dryouts at ∿20 sec are seen at certain locations (Figures M-34, M-36, M-37, M-39, M-40, and M-42) as lower plenum flashing subsides. However, these dryouts are all rewetted at approximately the time of HPCS flow inception. As the elapsed times between the HPCS inception and rod rewetting are rather short, rewet of the dryout rods is attributed to fallback cooling from the inventory in the upper plenum.

Bulk dryout of the bundle occurs at approximately 34 sec when the liquid continuum in the bundle is lost following jet pump exit uncovery in the lower plenum. The bundle heatup is, nevertheless, limited to ∿700°F because of the effectiveness of the HPCS fluid which penetrates the upper region of the bundle and rewets many of the rods. The maximum cladding temperature reaches the peak value before LPCS injection begins (Figure M-27).

The upper half of the bundle becomes further cooled (Figures M-37 through M-49) following LPCS injection, which begins at 63 sec. The remaining dried-out rods in the upper bundle are rewetted, and the upper rod thermocouple measurements indicate saturation temperature.

The lower half of the bundle, by contrast, continues to show local dryout even after the heat-up rate and cladding temperatures have peaked. The region becomes well cooled when the bundle refloods between 110 and 140 sec (Figures M-11 and M-27 through M-36).

With the bundle completely reflooded and with the continuous injection of subcooled ECC, the fluid inventory within the bundle becomes subcooled. This is evident in Figures M-28 to M-49, where it is seen that after about 150 sec the cladding temperatures in the bundle show values below the saturation temperature for the system pressure.

M-1.3 Vapor Venting in Guide Tube/Bypass Region

Vapor venting in the guide tube/bypass region is primarily due to the rapid filling of the bypass region with a two-phase mixture coupled with the inequality of fluid density in the two parallel columns (bundle and bypass).

The guide tube/bypass region refills in 30 sec (from ∿100 to ∿130 sec as shown in Figure M-11). The mass of the guide tube increases from 60 to 90 pounds, the bypass from ∿ 0 to ∿ 65 pounds (Figures M-17 and M-18). Of this increase of ∿ 95 pound mass, the one LPCI system accounts for ∿ 25 pounds; the balance comes from the two-phase fluid in the upper plenum.

When the bypass refills at ∿100 sec, the bundle begins to reflood slowly. The hydrostatic head across the bypass is seen in Figure M-50 to be higher than that across the bundle. The difference in hydrostatic heads, shown in Figure M-51, causes the bypass fluid to flow into the bundle and the guide tube fluid into the lower plenum. The leakage flow from the bypass to the bundle contributes to bundle reflood; that from the guide tube contributes additional vapor to the lower plenum. The combined effects of flashing in the lower plenum and the added vapor flow from the guide tube creates a counter current flow condition at the SEO which prevents liquid drainage from the bundle (Figure M-52a).

The reversed leakage flow from the bypass is accompanied by LPCI downflow. The subcooled LPCI fluid condenses vapor generated in the bypass and the guide tube. The reversed leakage flow as well as the downward LPCI flow diminishes as the bundle refloods and the hydrostatic head difference decreased. On the other hand, the vapor updraft from the guide tube into the bypass increases as the leakage flow into the lower plenum decreases. Because of the decreased, subcooled LPCI downflow and increased guide tube vapor upflow, the vapor must travel higher into the bypass before mixing with the subcooled LPCI fluid. This decreases the bypass fluid density, hence the hydrostatic head, which further reduces the hydrostatic head difference.

The hydrostatic head difference is also diminished by an increase in the bundle fluid density. This comes about when the bundle begins reflooding. As the lower bundle becomes well cooled, less vapor is generated, and, hence, more liquid drains into the bundle from the upper plenum. Finally, as the bypass flow decreases, more subcooled ECC fluid becomes available to flow into the bundle (Figure M-52b). .

The hydrostatic heads become equal to ∿200 sec, and the bypass flow becomes zero (Figure M-51). The LPCI fluid can no longer flow downward and is forced into the upper plenum where it combines with the subcooled sprays and flows into the bundle. This renders the bundle hydrostatic head higher relative to the bypass, and the leakage flow reverts to the forward direction (i.e., fluid flows from bundle to bypass and from lower plenum to guide tube).

The forward leakage flow makes it possible for the vapor to escape from the bypass region. As both the liquid and the vapor flow upward through the bypass, the liquid continuum in the bypass is pushed into the upper plenum (Figure M-25, ∿210 sec), leaving the upper part of the bypass filled with a vapor continuum (Figure M-52c). The vapor continuum is then condensed as it comes into direct contact with either the subcooled LPCI at the top of the bypass or the subcooled spray in the upper plenum. Following this, the vapor flow diminishes, and the LPCI fluid flows downward again to fill the bypass. At the same time, more bundle fluid is allowed to drain into and refill the bypass because the hydrostatic head of the bypass region has been reduced. As the bypass refills, the hydrostatic head difference decreases and with it the forward leakage flow.

The forward leakage flow from the lower plenum to the guide tube allows the lower plenum vapor to escape through the guide tube/bypass region. Consequently, the vapor upflow at the SEO decreases, which allows more liquid downflow from the bundle to the lower plenum. As the bundle drains partially and the hydrostatic head decreases, the jet pump path pressure drop correspondingly decreases. This results in a simultaneous increase of mass influx to and decrease of mass outflux from the lower plenum. Therefore mass inventory in the lower plenum increases (Figure M-53).

The forward leakage flow to the bypass reverses later (Figure M-51) when the partial loss of inventory in the bundle coupled with the refilling of the bypass leads to a reversal of the hydrostatic head difference (Figure M-52d). This allows the restoration of the pseudo-steady-state conditions that precede the vapor venting from the guide tube; for, as the guide tube leakage flow is reversed into the lower

plenum, the combined vapor flow from the guide tube and lower plenum is forced through the SEO. The increase in the vapor flow causes CCFL at the SEO which reduces the liquid drain from the bundle, allowing the bundle to accumulate inventory once again. At the same time, as the hydrostatic head of the bundle increases, the pressure drop across the jet pumps increases correspondingly (Figure M-50). This results in a simultaneous decrease of mass influx to and an increase of mass outflux from the lower plenum. Therefore, mass in the lower plenum decreases until the mixture level returns to that of the jet pump exit plane, and a pseudo-steady-state is momentarily restored (Figures M-10 and M-52d).

The vapor venting process repeats itself later in the transient. However, after this second cycle, a large amount of subcooled liquid enters the guide tube and bypass regions. This, in conjunction with decreased flashing caused by the decreased depressurization rate, diminishes the vapor upflow, and further vapor venting subsides.

This venting process in the bypass region of TLTA is believed to be influenced by the one-dimensional configuration of the TLTA geometry and may not be representative of a BWR. In TLTA, the bypass regional volume is mocked-up by four parallel tubes which communicate from the guide tube to the upper plenum. LPCI fluid is injected equally into each tube. In the BWR, the bypass is a more open, three-dimensional region with LPCI injection at the core shroud wall. Communication between the bypass and guide tube and the bypass and bundle is less influential during the reflood period, as the bypass region has a large plenum effect. Therefore, the venting process observed in TLTA is not expected in a BWR.

Table M-1

TEST CONDITIONS FOR TEST 6422, RUN 3

Initial Conditions

Bundle Power	5.05 ± 0.03 MW
Steam Dome Pressure	1035 ± 5 psia
Lower Plenum Pressure	1062 ± 5 psia
Lower Plenum Enthalpy	524 ± 5 Btu/lbm
Initial Water Level	124 ± 6 in. Elevation
Feedwater Enthalpy	41 ± 2 Btu/lbm
Bundle Inlet to Outlet Pressure Drop	17 $\pm\frac{1}{2}$ psi
Steam Flow	6 + 1 lbm/sec
Feedwater Flow	1.6 ± 0.3 lbm/sec
Drive Pump 1 Flow	8.7 ± 1.0 lbm/sec
Drive Pump 2 Flow	8.5 ± 1.0 lbm/sec
Jet Pump 1 Flow	20 ± 2 lbm/sec
Jet Pump 2 Flow	21 ± 2 lbm/sec
Bundle Inlet Flow	35 ± 5 lbm/sec

Timings

Blowdown Valves Opened	0.00 ± 0.02 sec
Power Decay Initiated	0.40 ± 0.05 sec
HPCS Activated	27 sec
HPCS Flow Begins	27 ± 1 sec
LPCS Activated	37 sec
LPCS Flow Begins	63 ± 2 sec
LPCI Activated	37 sec
LPCI Flow Begins	71 ± 2 sec
Bundle Power Tripped	399 sec
Blowdown Valves Closed	429 sec
ECCS Temperature	120 ± 15°F

All uncertainty bands are judged from the maximum of data fluctuation and/or absolute uncertainties of the measurements.

NOTES:

1. P - PRESSURE
   DP - DIFFERENTIAL PRESSURE
   T - TEMPERATURE (RTD - RESISTANCE THERM)
   SP - VALVE STEM POSITION
   RO - RESTRICTING ORIFICE
   FE - FLOW ELEMENT
   S - PUMP SPEED
   LP - LEVEL PROBE
   DD - DRAG DISK
   TM - TURBINE METER

2. N305 - 54.88 MEANS NOZZLE NO. 305 IS AT AN ELEVATION OF 54.88 INCHES. IT DOES NOT REFER TO ACTUAL LOCATION OF THE NODAL POINT.

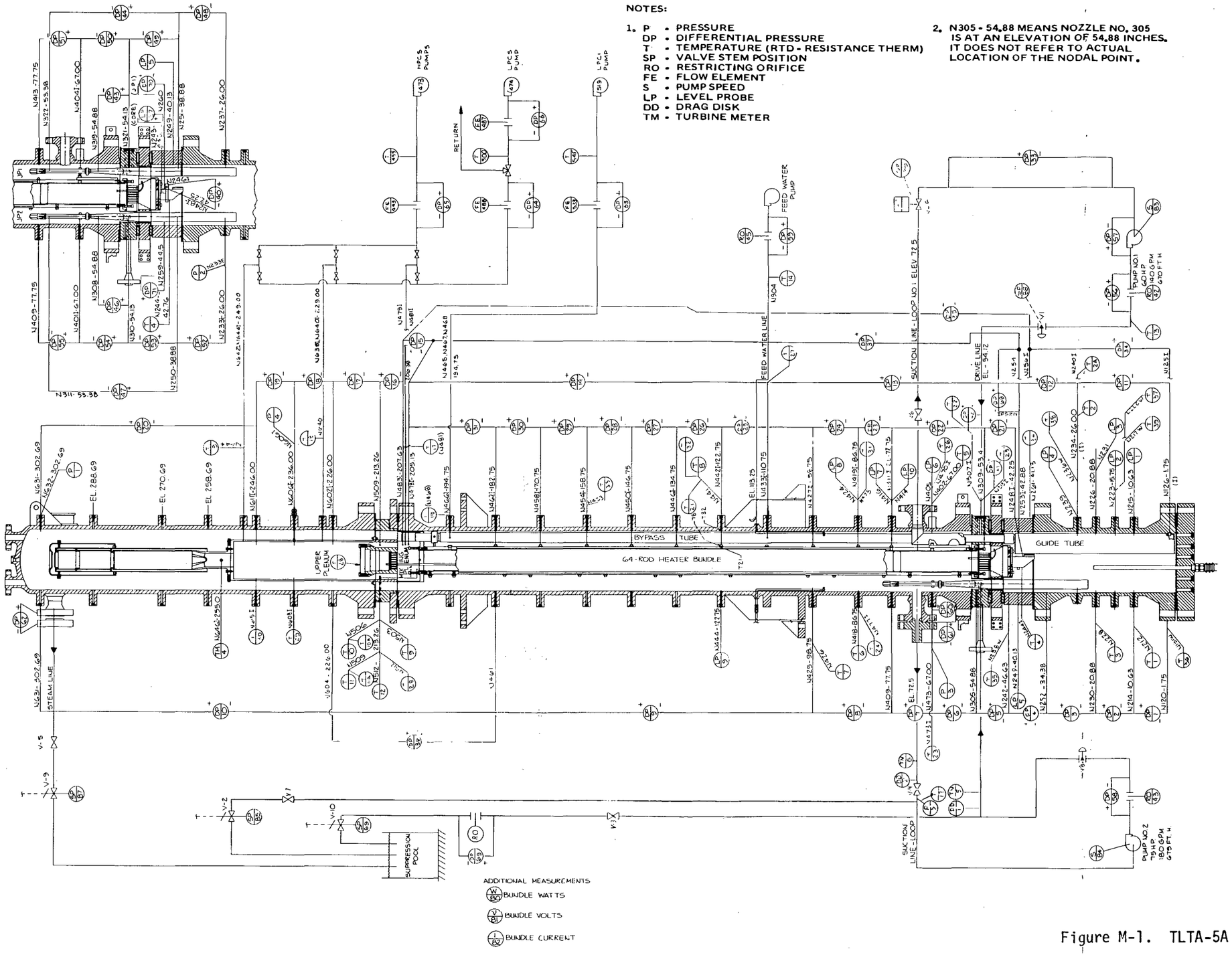

Figure M-1. TLTA-5A Instrumentation

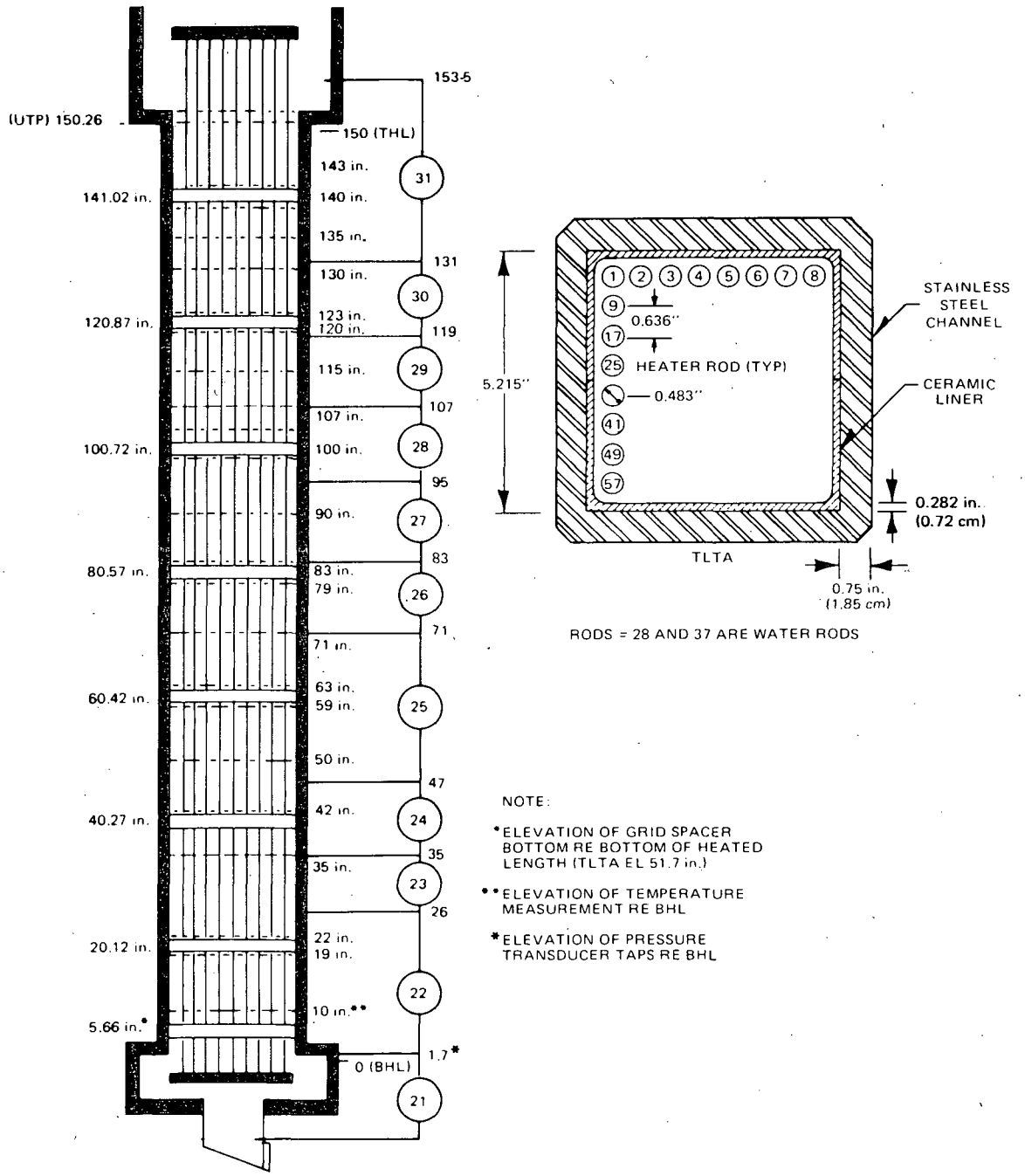

Figure M-2. TLTA-5A Bundle Instrumentation and Dimensions

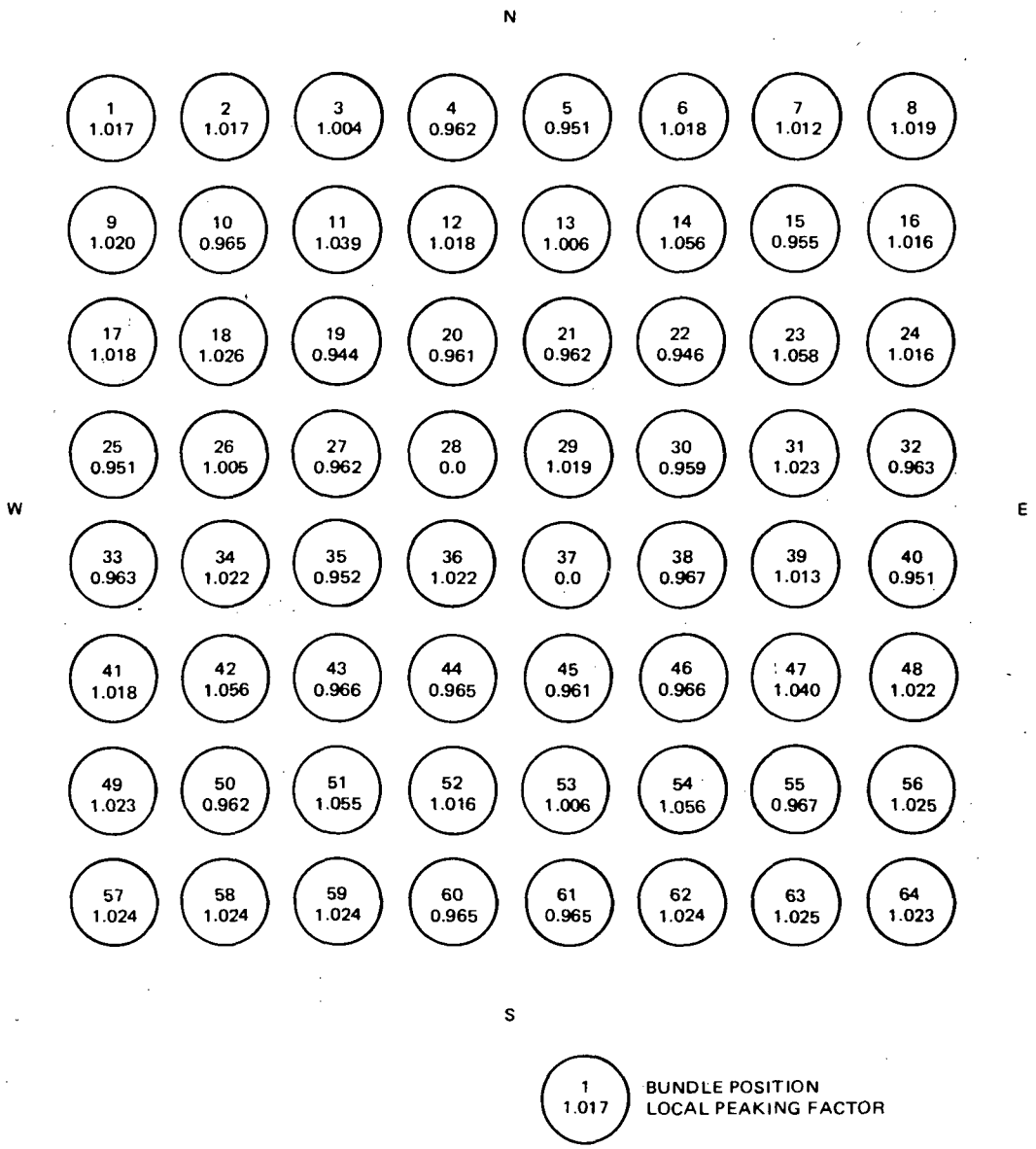

Figure M-3. Local Peaking Factor Distribution

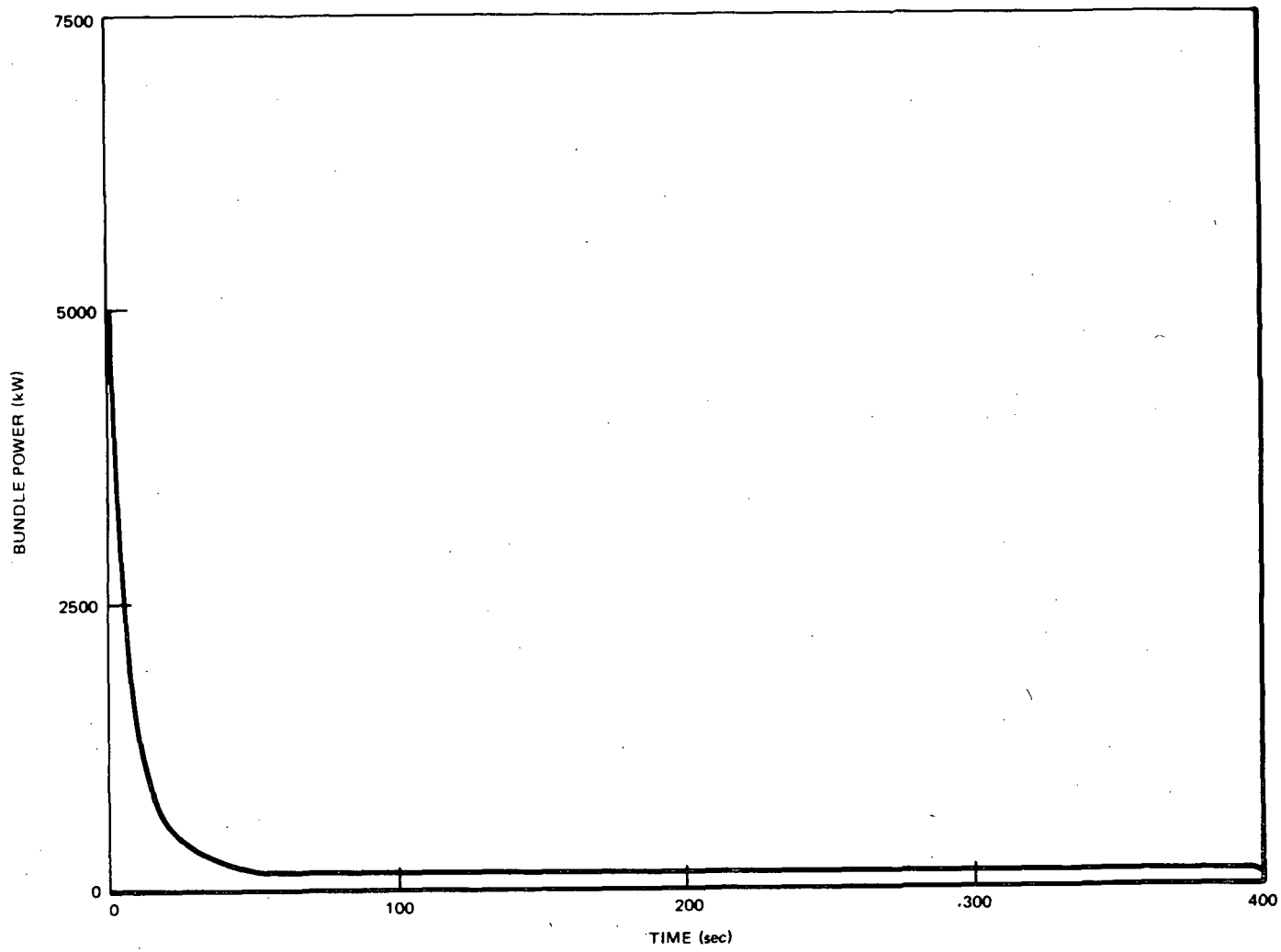

Figure M-4. Bundle Power Decay

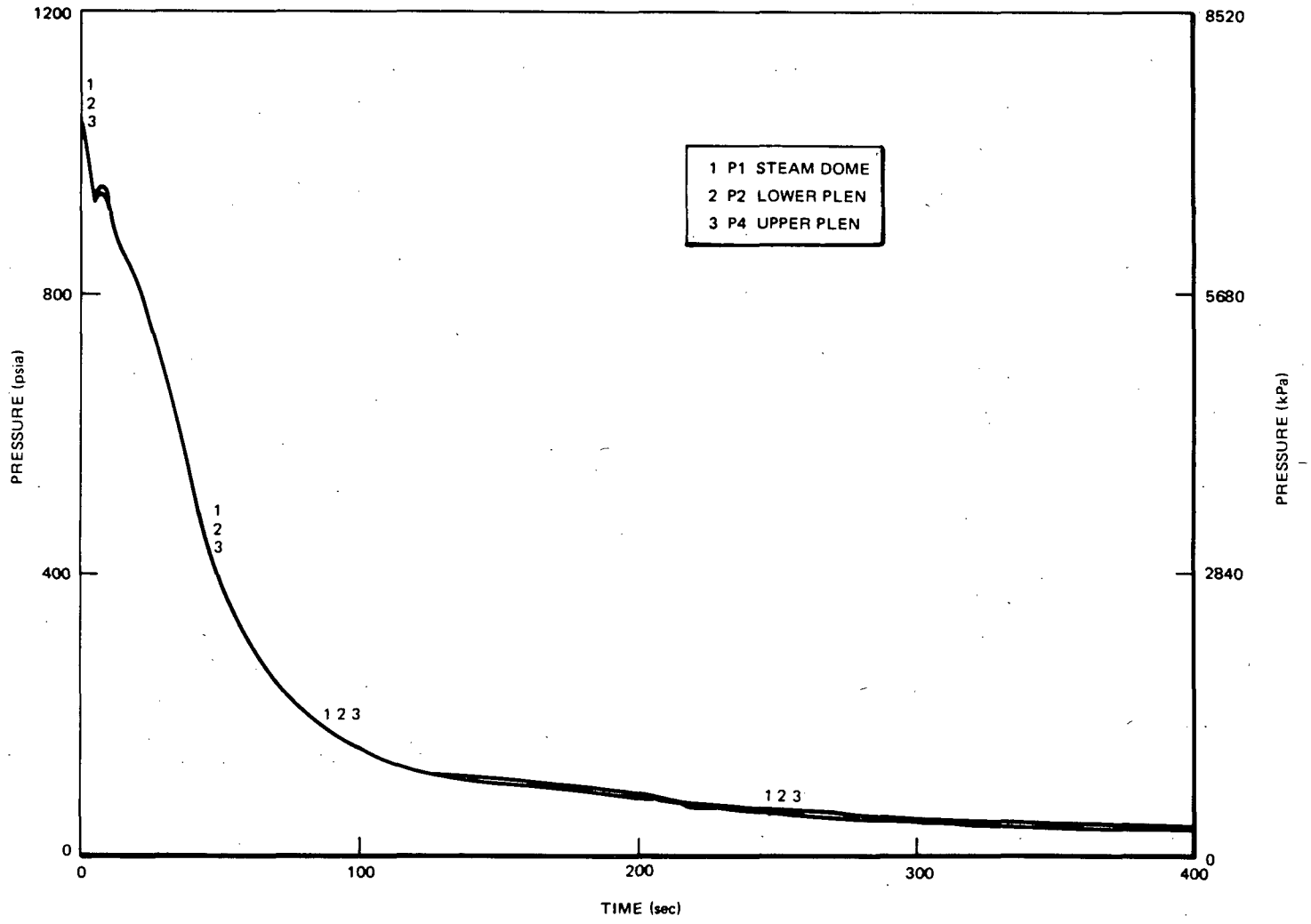

Figure M-5. System Pressures

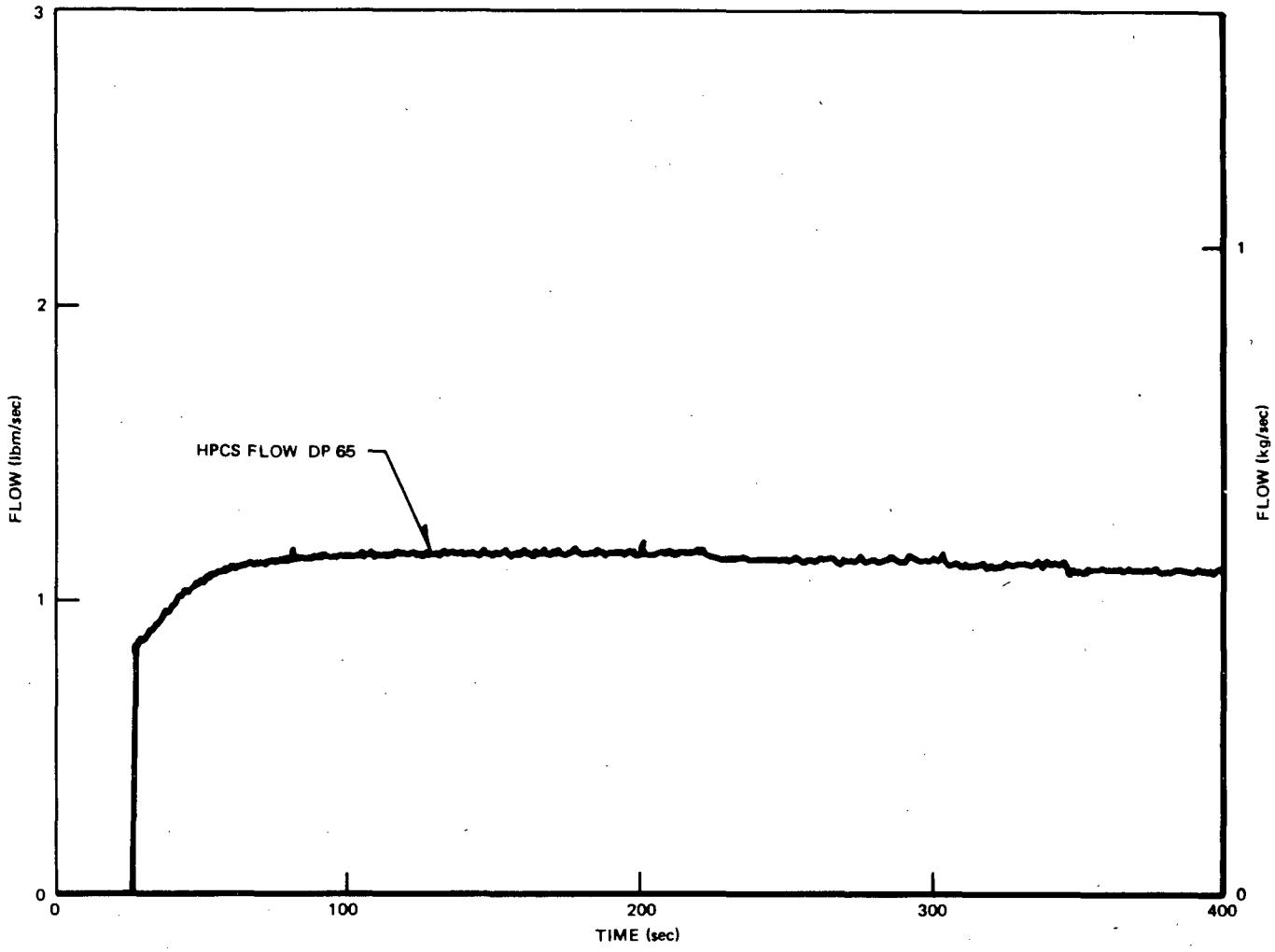

Figure M-6. HPCS Injection Rate

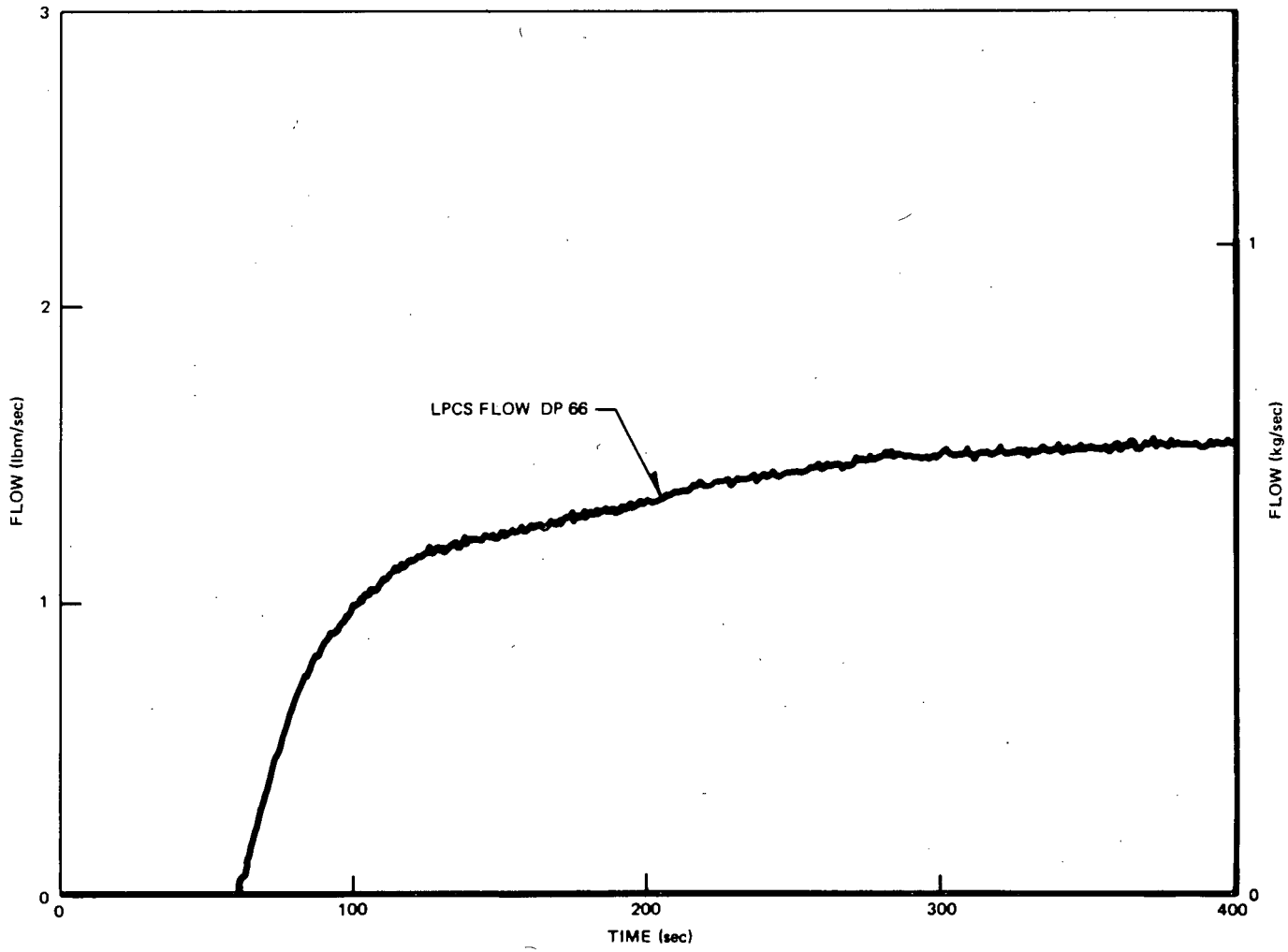

Figure M-7. LPCS Injection Rate

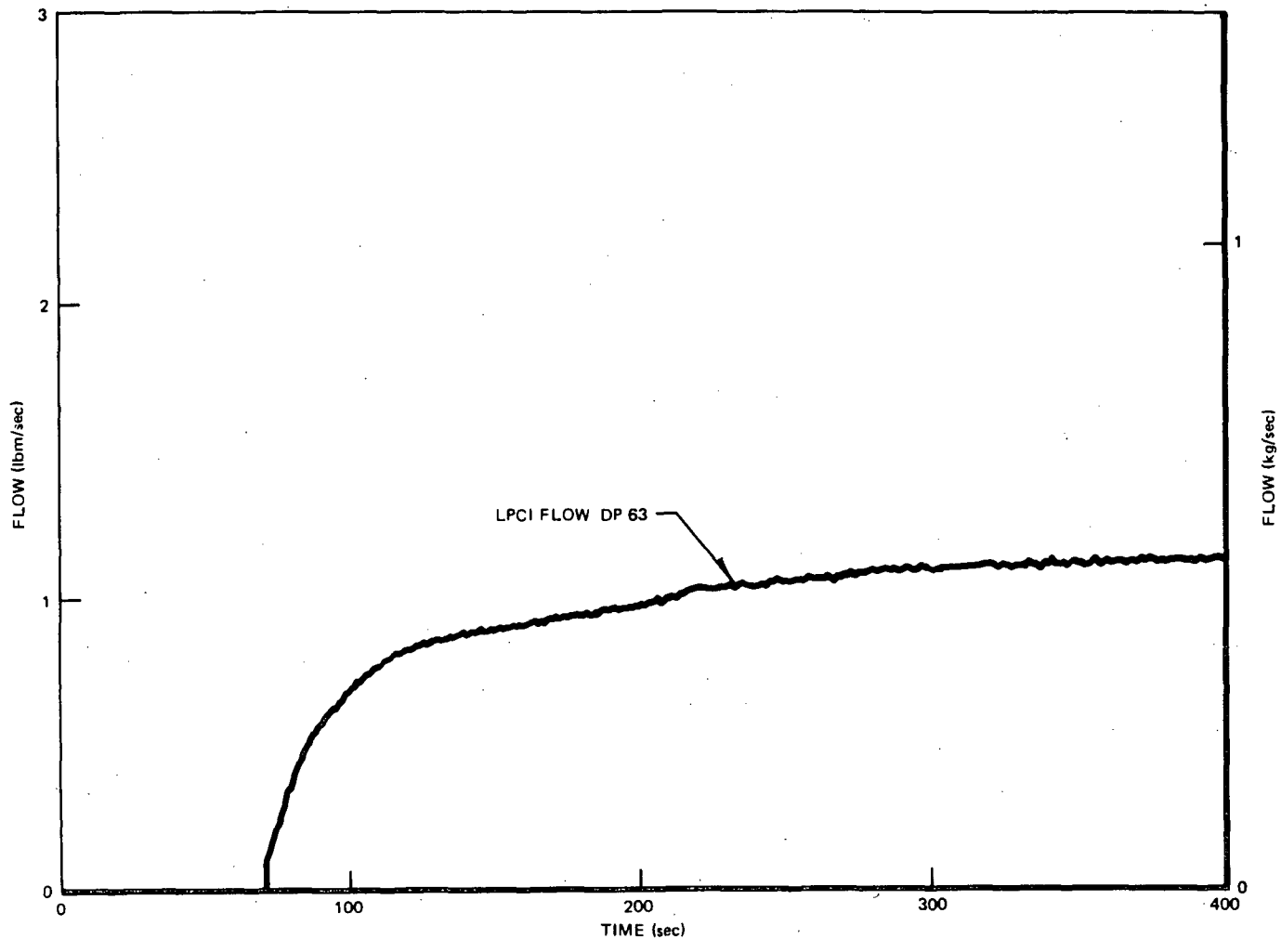

Figure M-8. LPCI Injection Rate

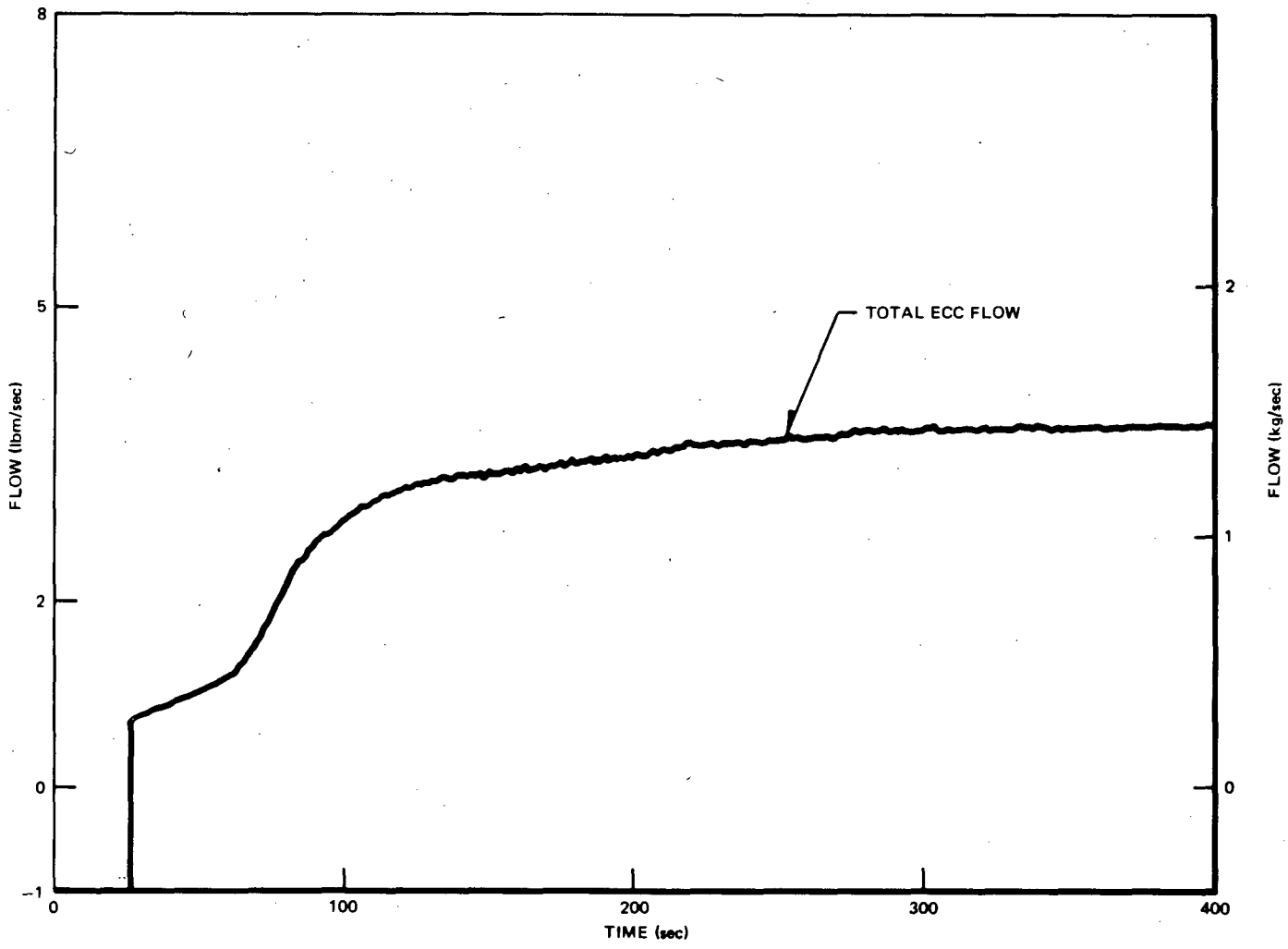

Figure M-9. Total ECC Injection Rate

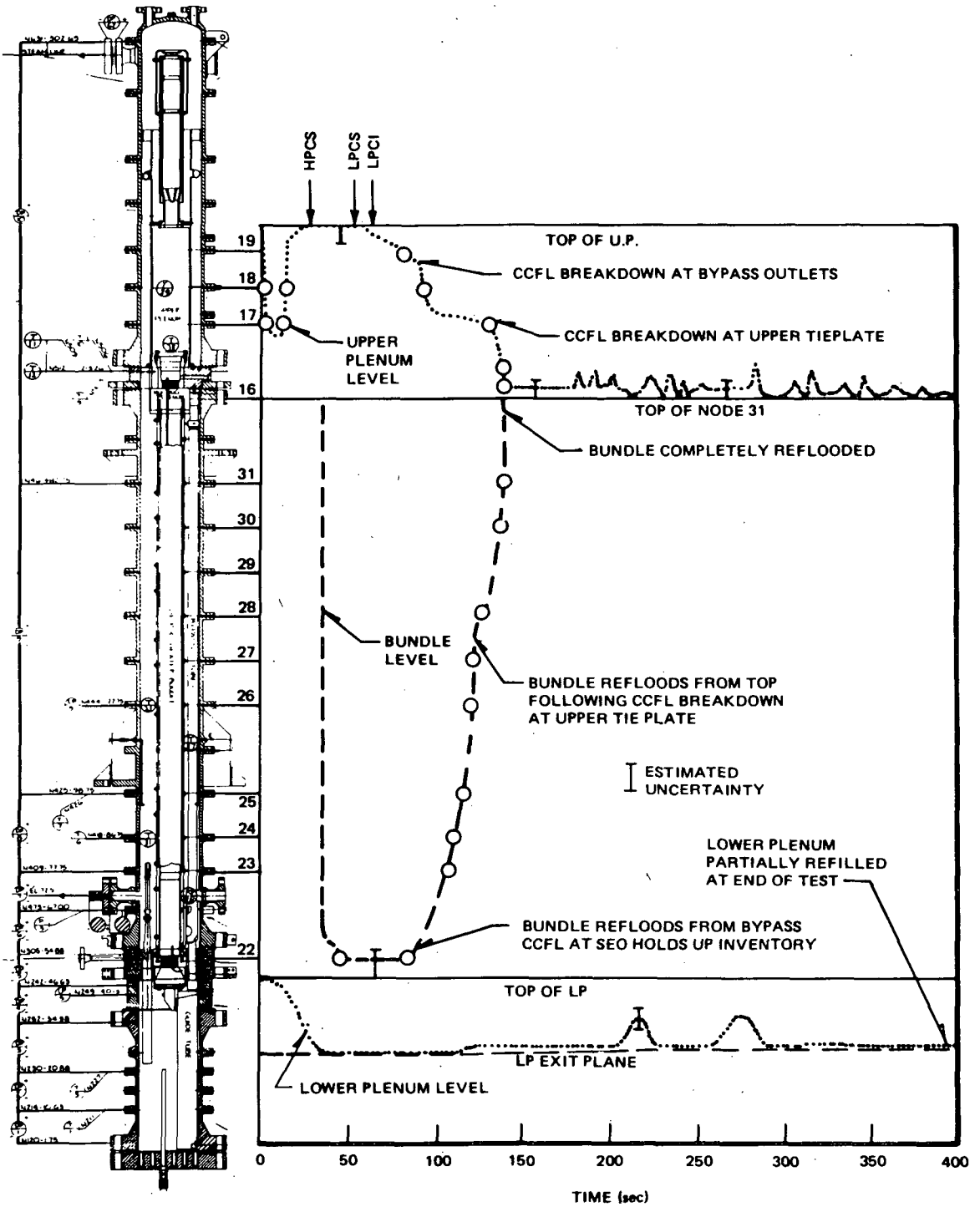

Figure M-10. Mixture Levels along the Bundle Path

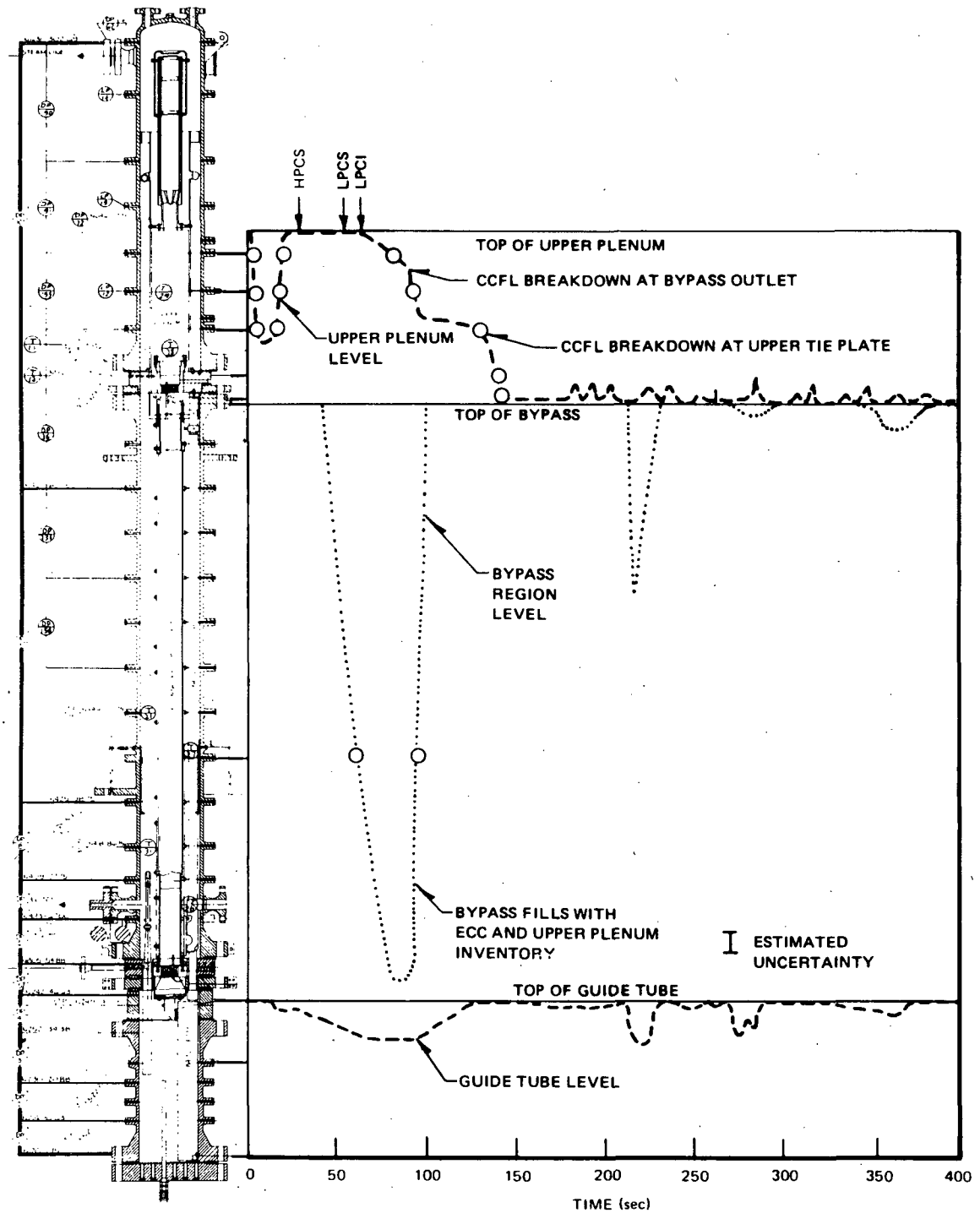

Figure M-11. Mixture Levels along the Bypass Path

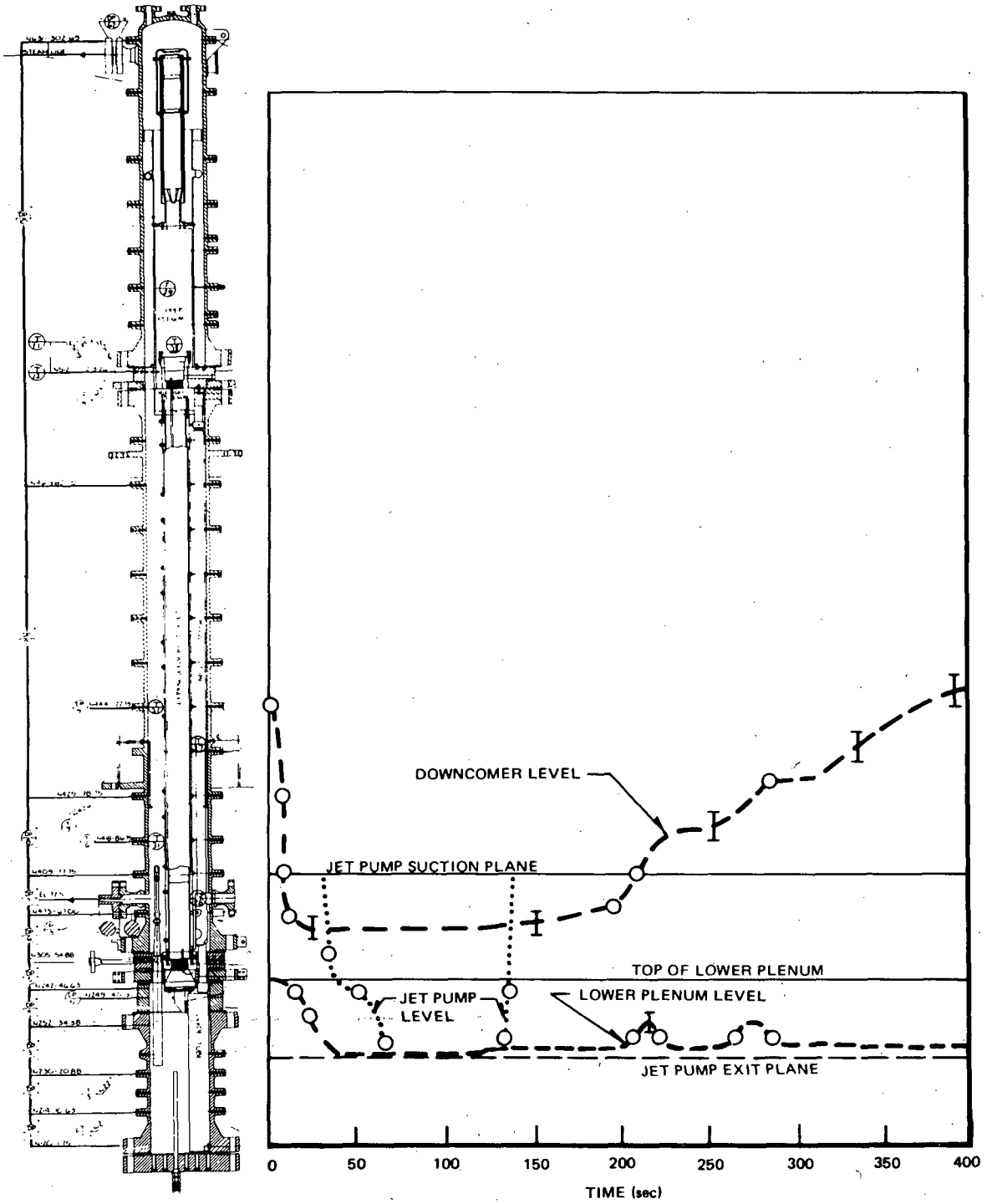

Figure M-12. Mixture Levels along the Jet Pump Path

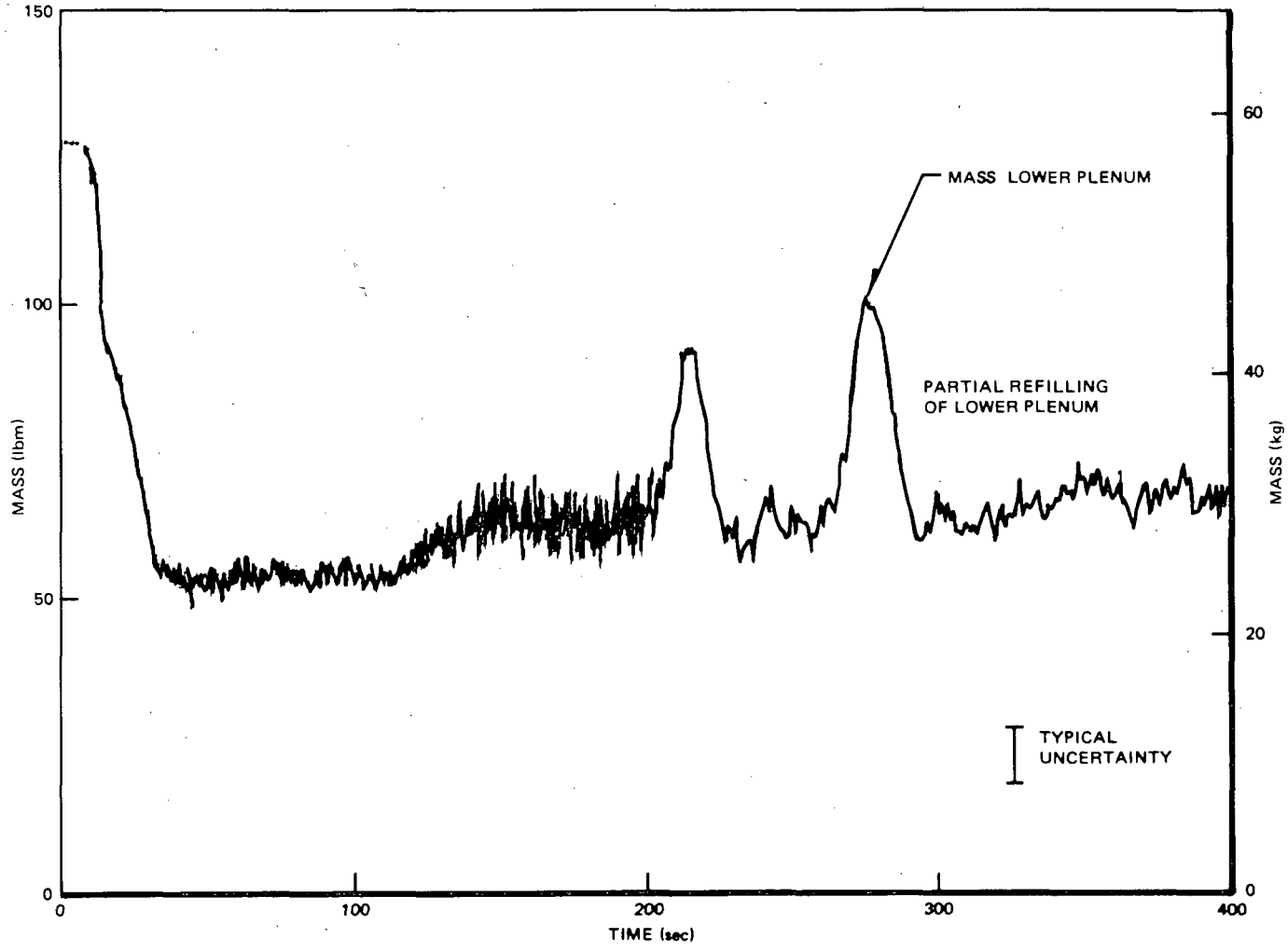

Figure M-13. Lower Plenum Mass

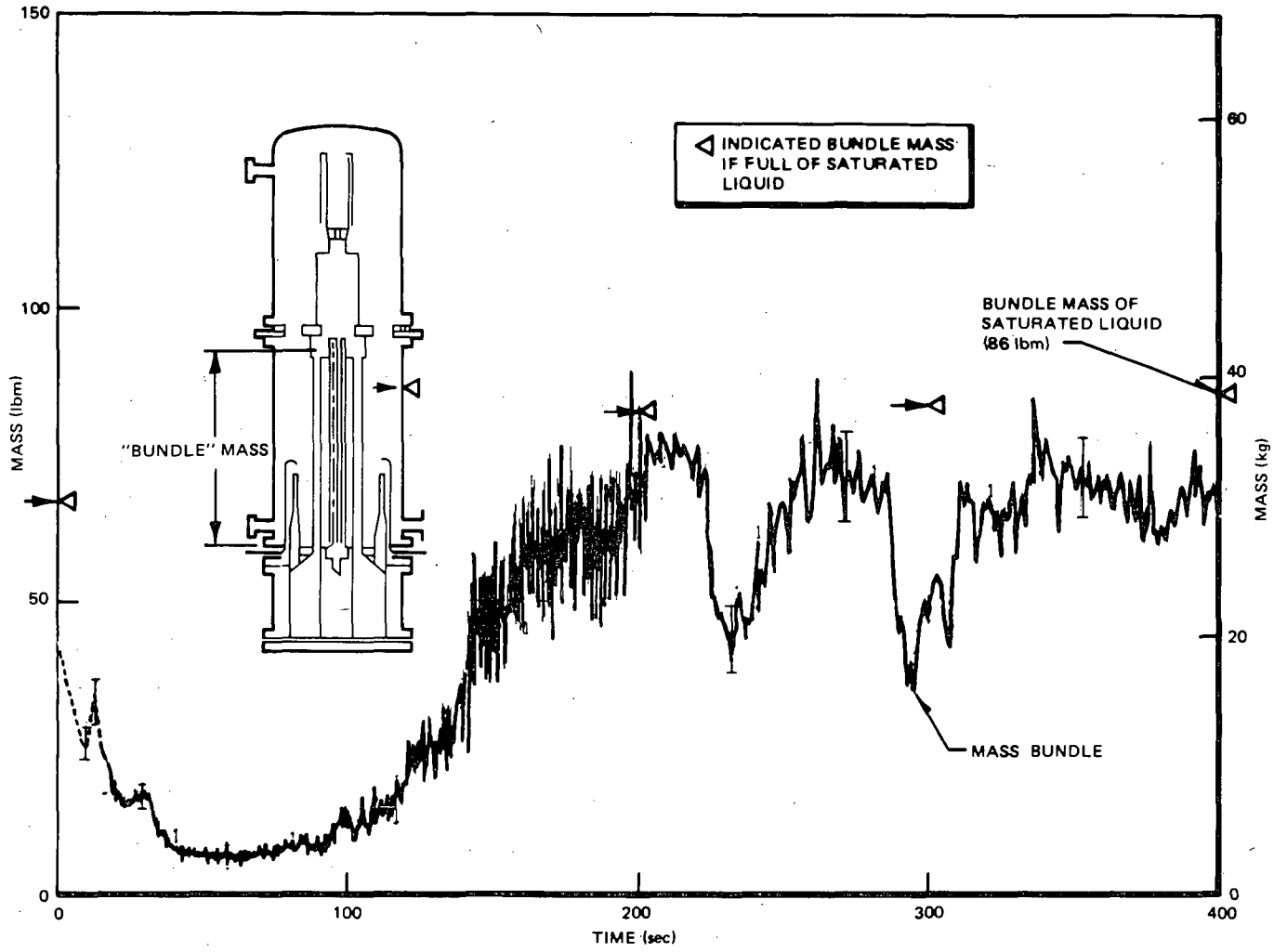

Figure M-14. Bundle Mass

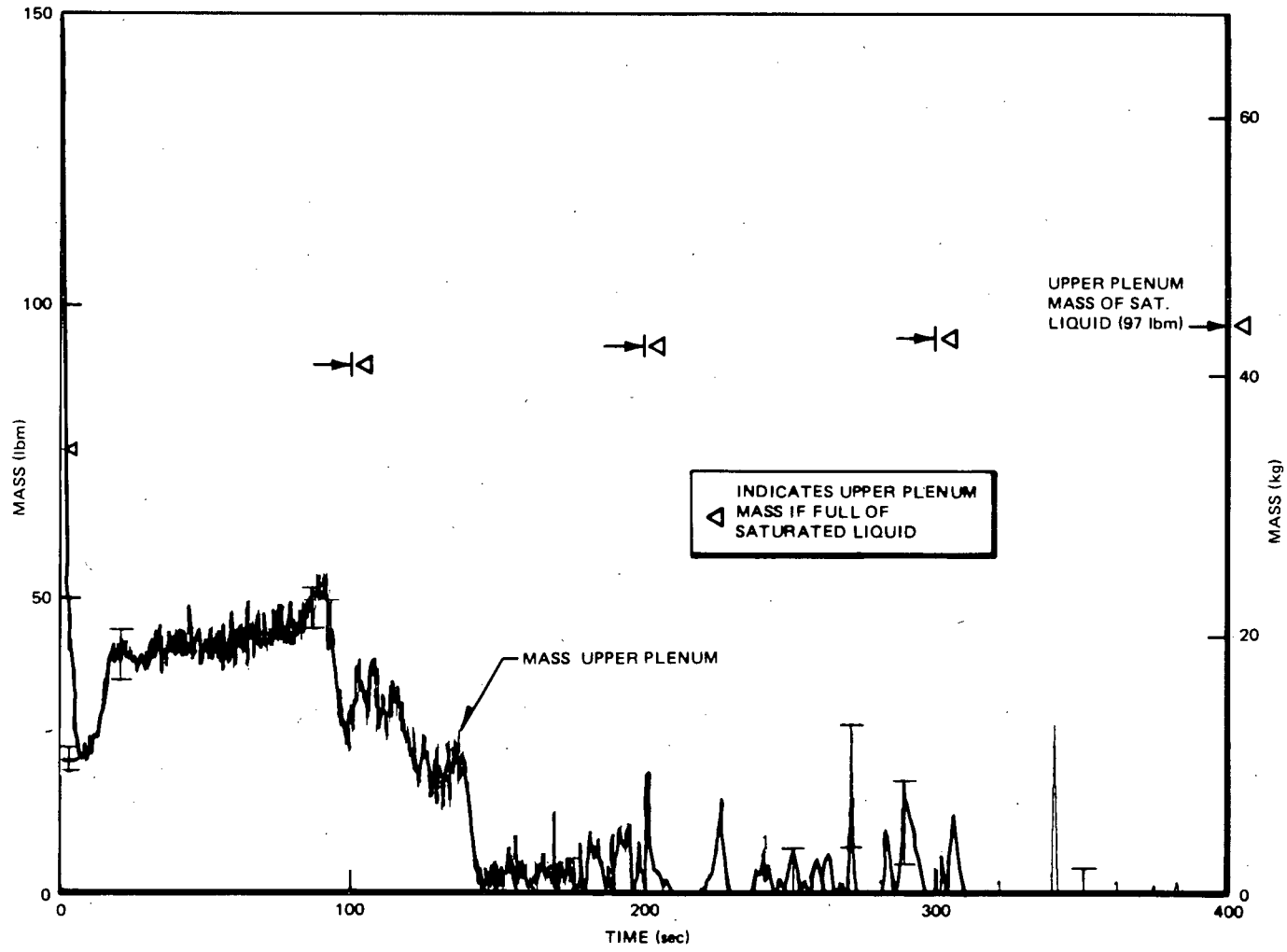

Figure M-15. Upper Plenum Mass

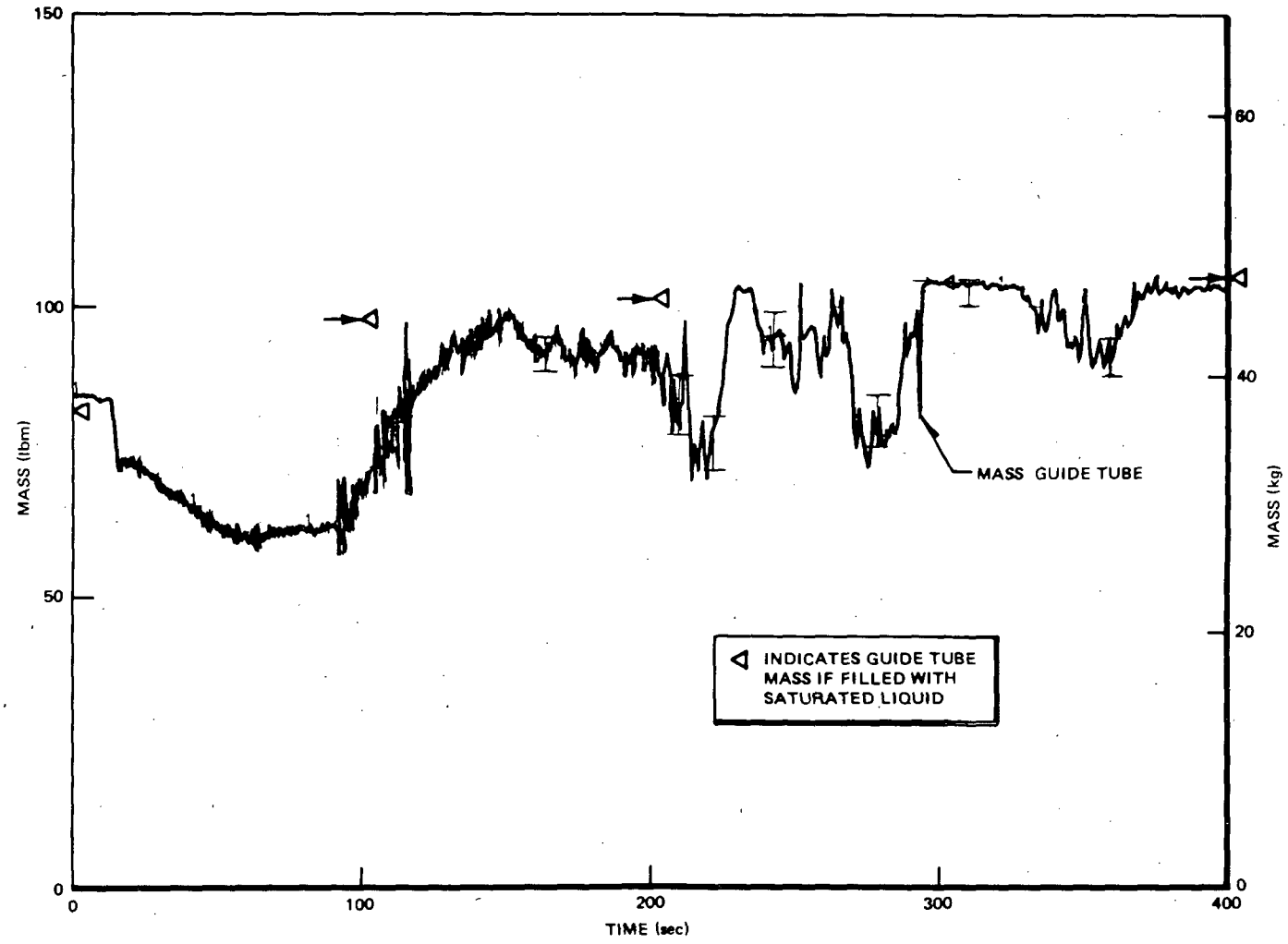

Figure M-16. Guide Tube Mass

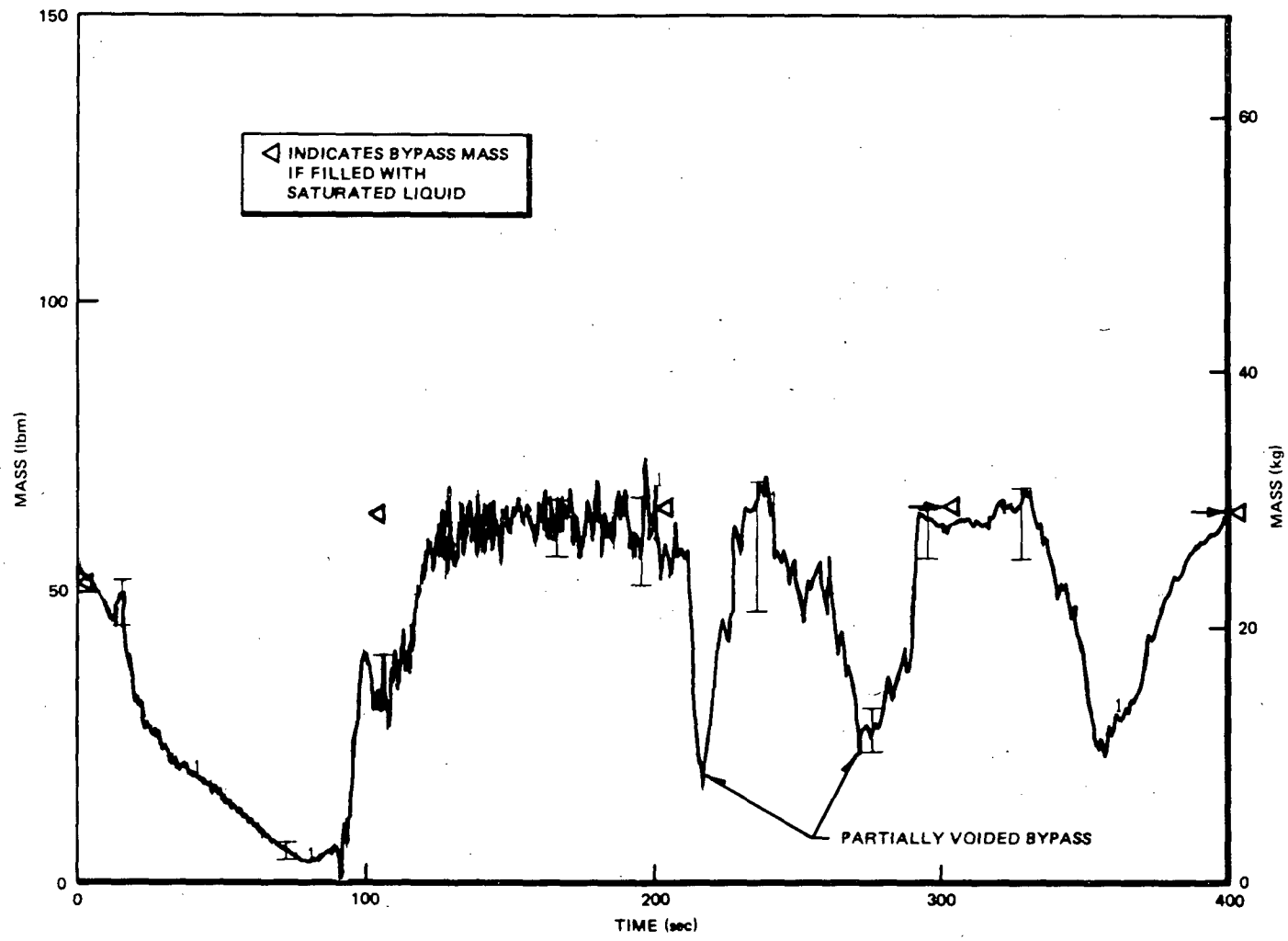

Figure M-17. Bypass Mass

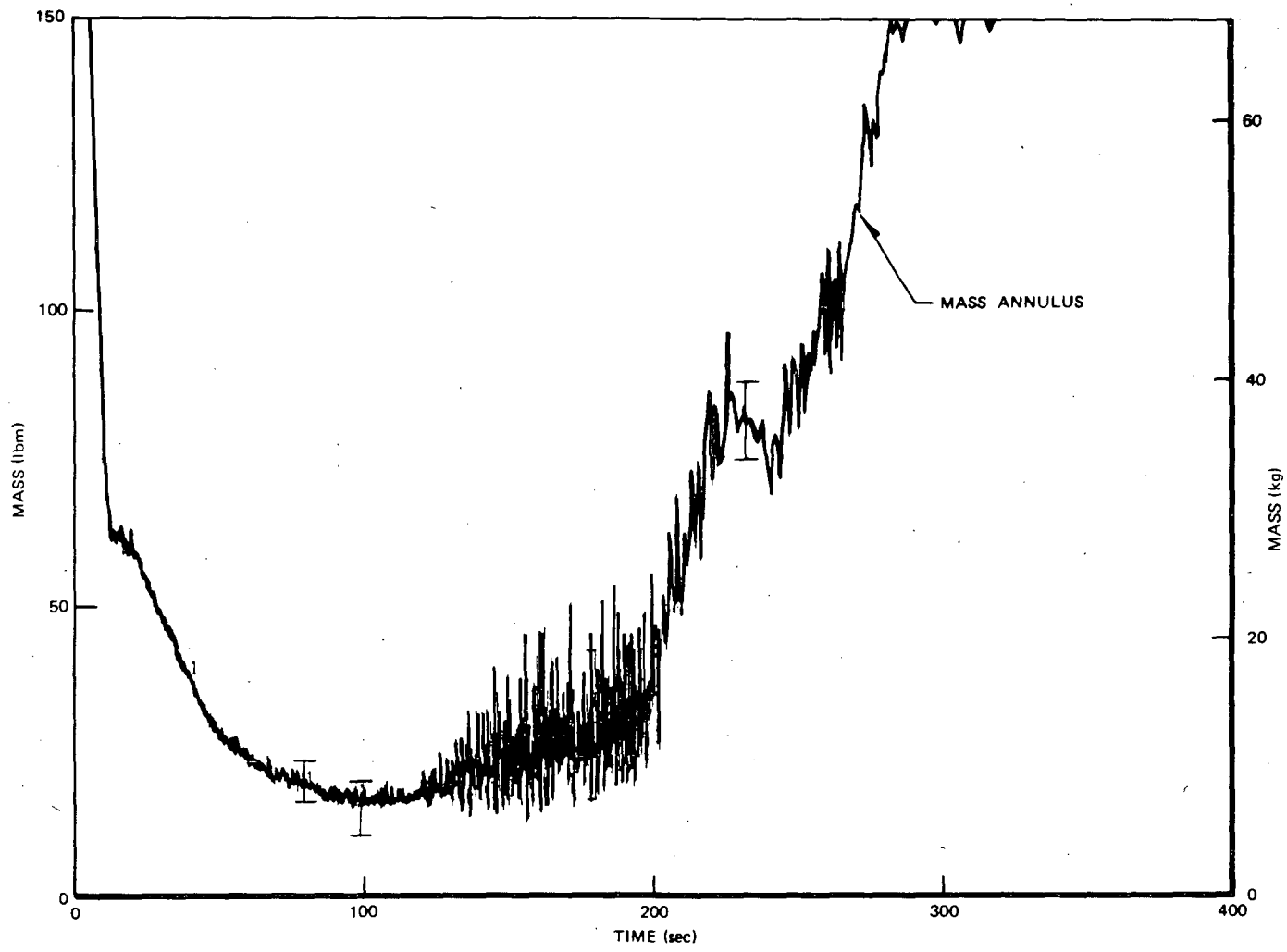

Figure M-18. Annulus Mass

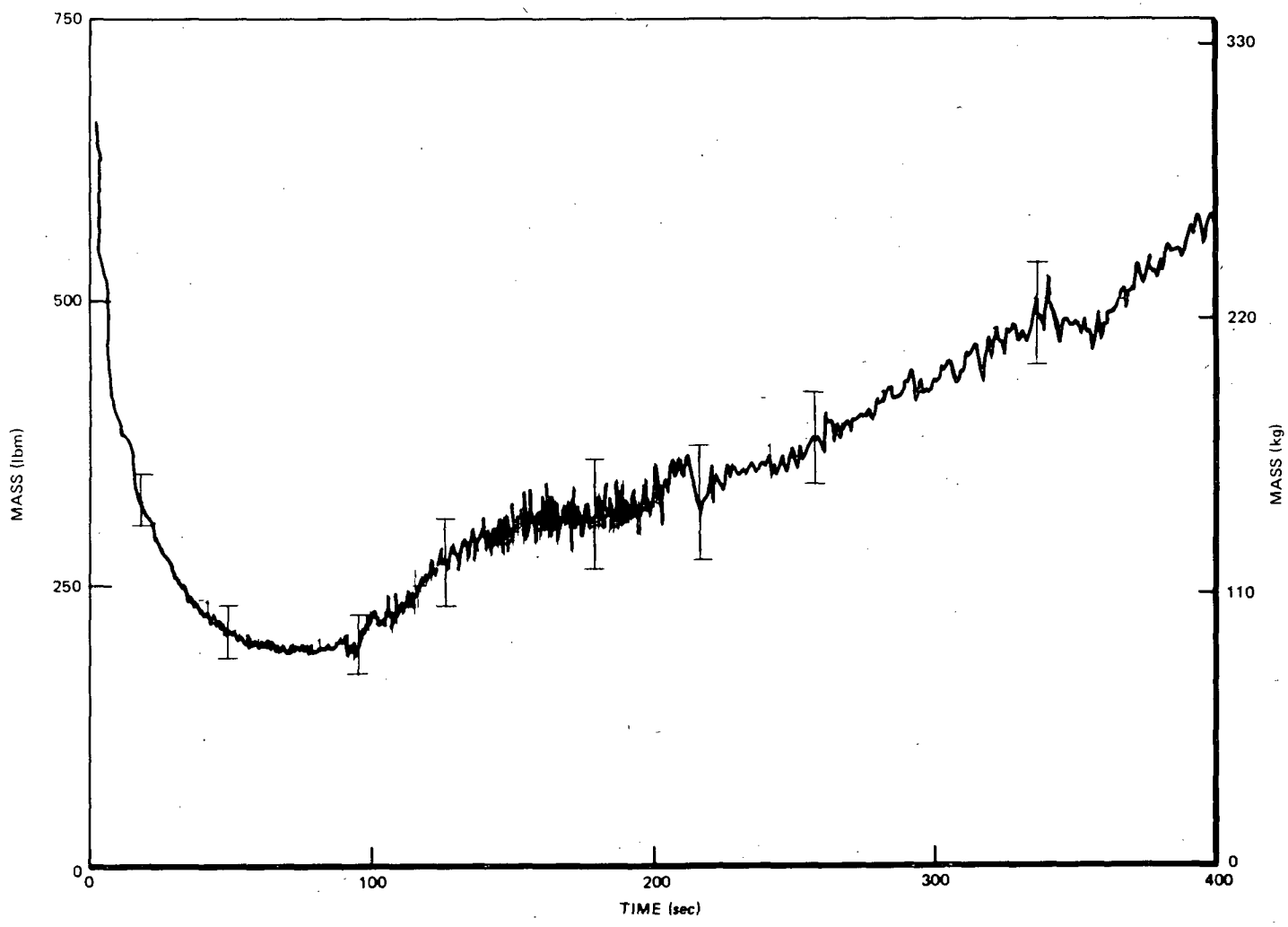

Figure M-19. Total Mass

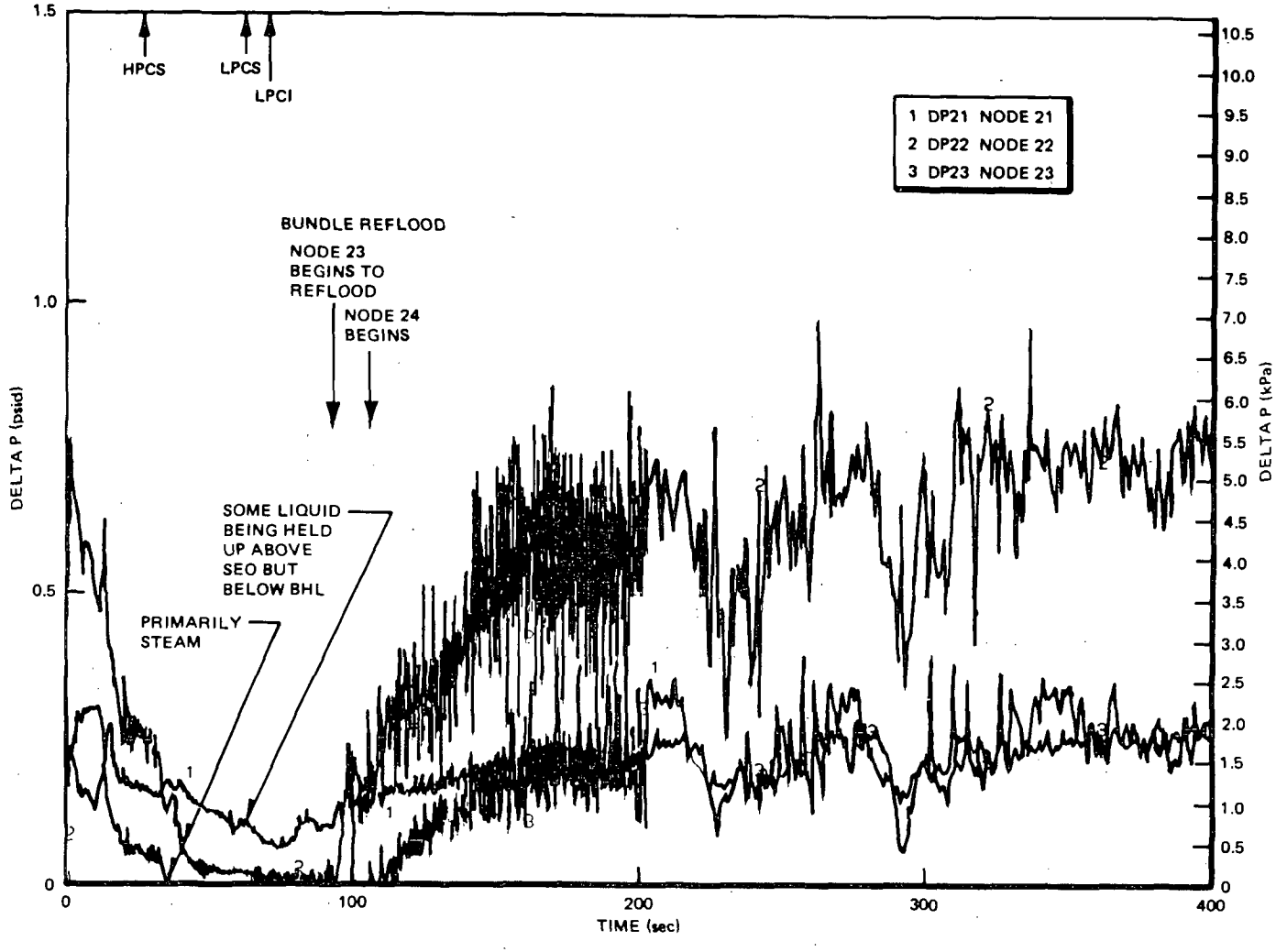

Figure M-20. Lower Bundle Differential Pressures

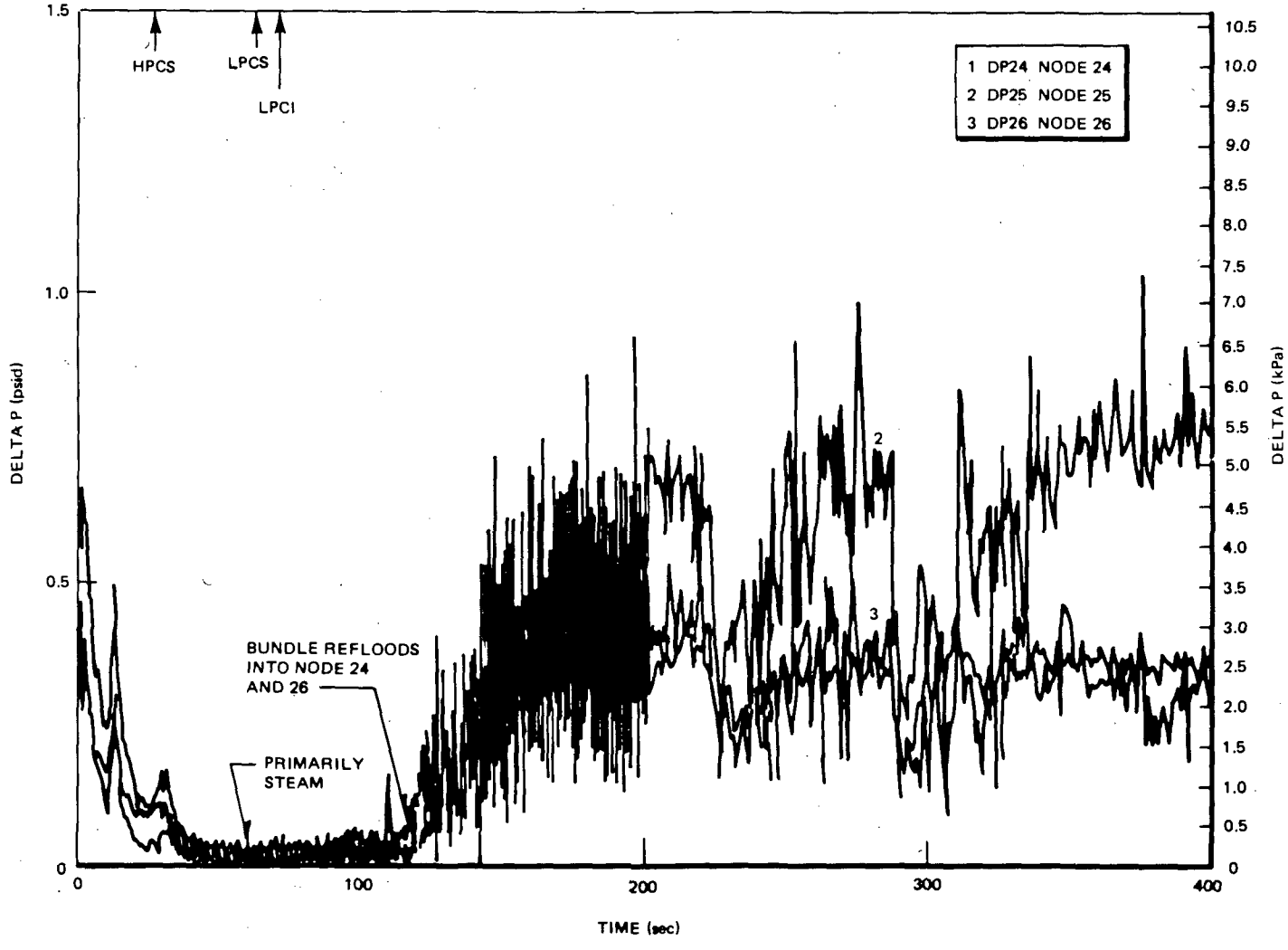

Figure M-21. Lower-Middle Bundle Differential Pressures

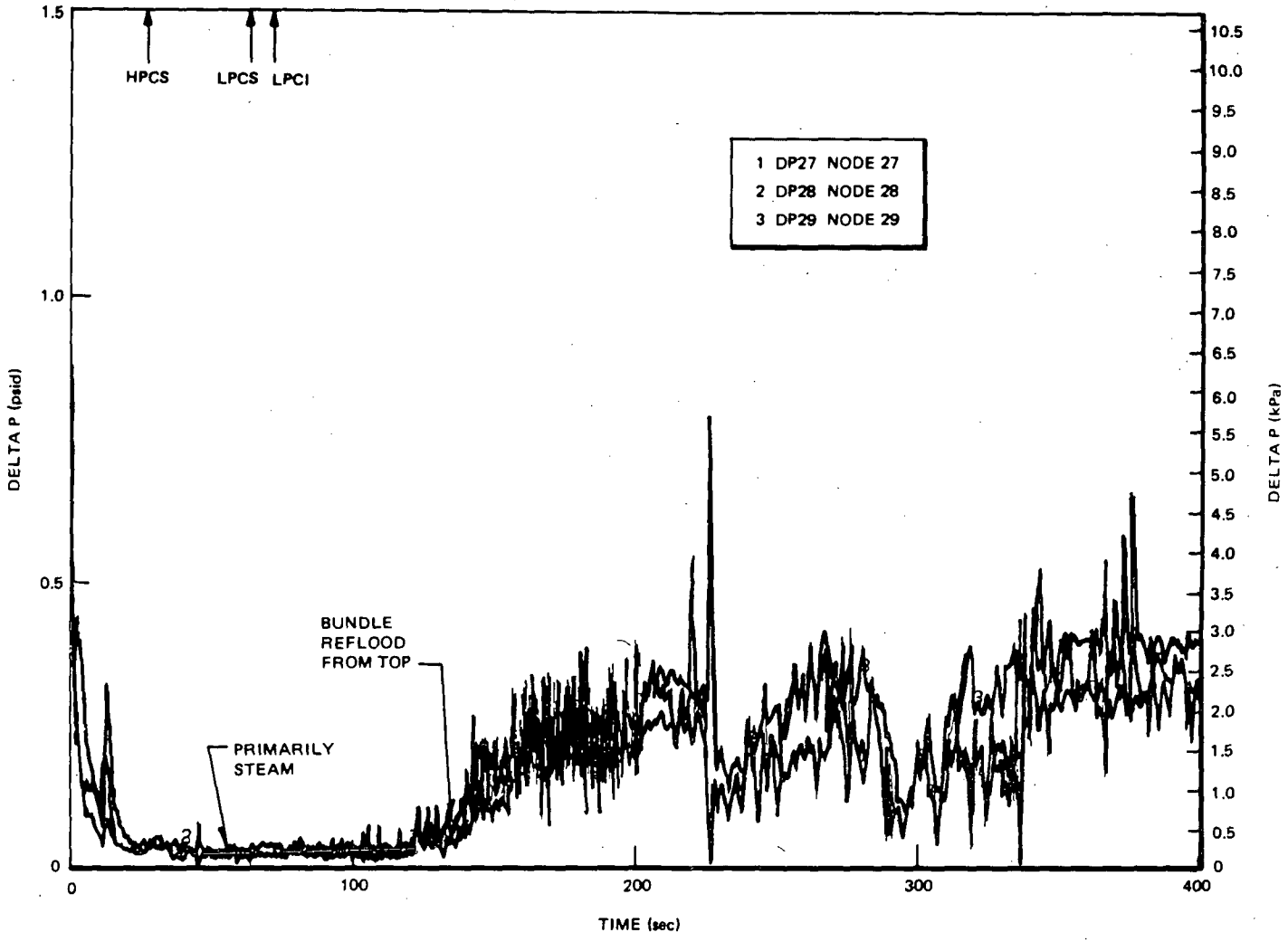

Figure M-22. Upper-Middle Bundle Differential Pressures

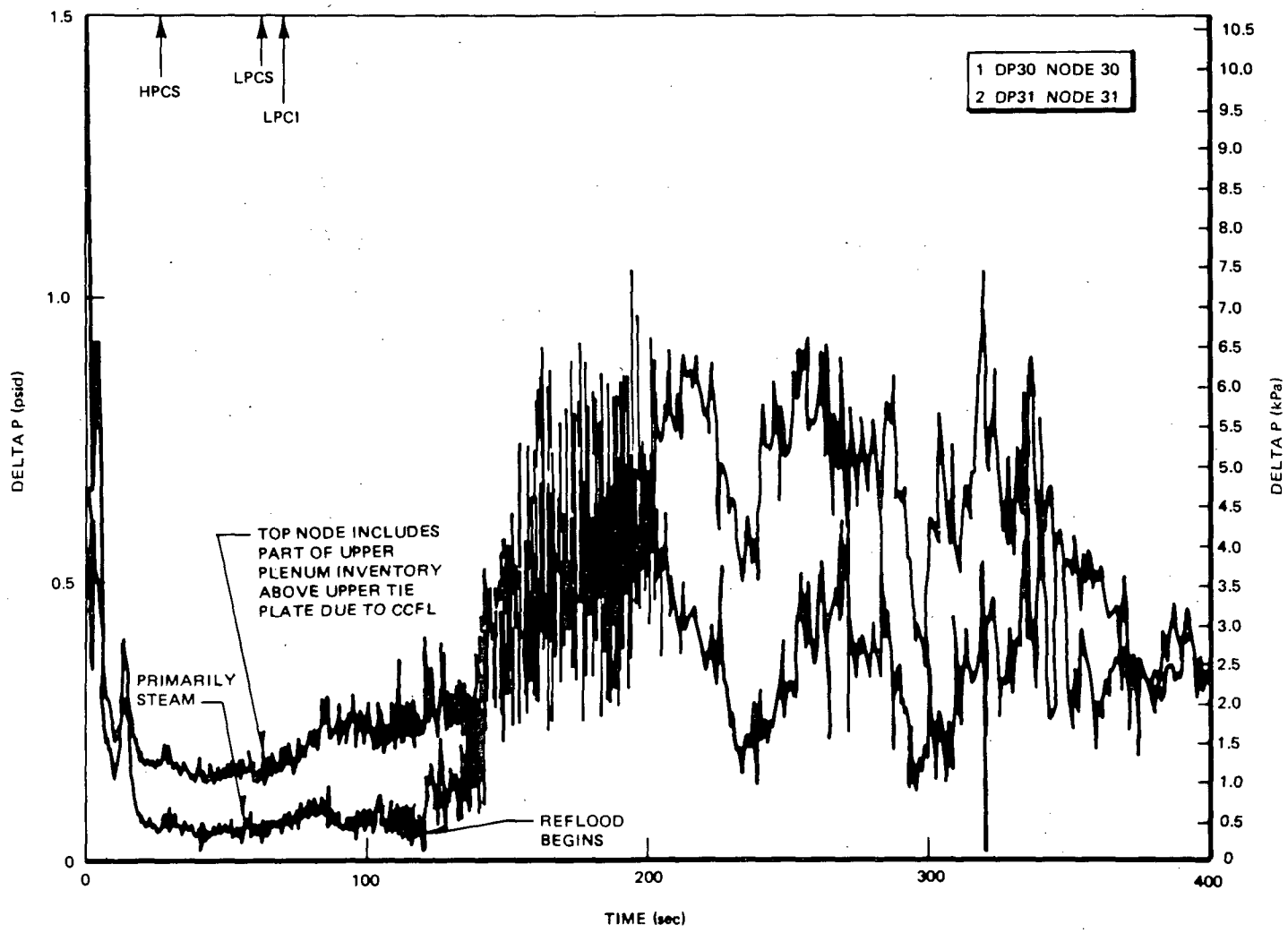

Figure M-23. Upper Bundle Differential Pressures

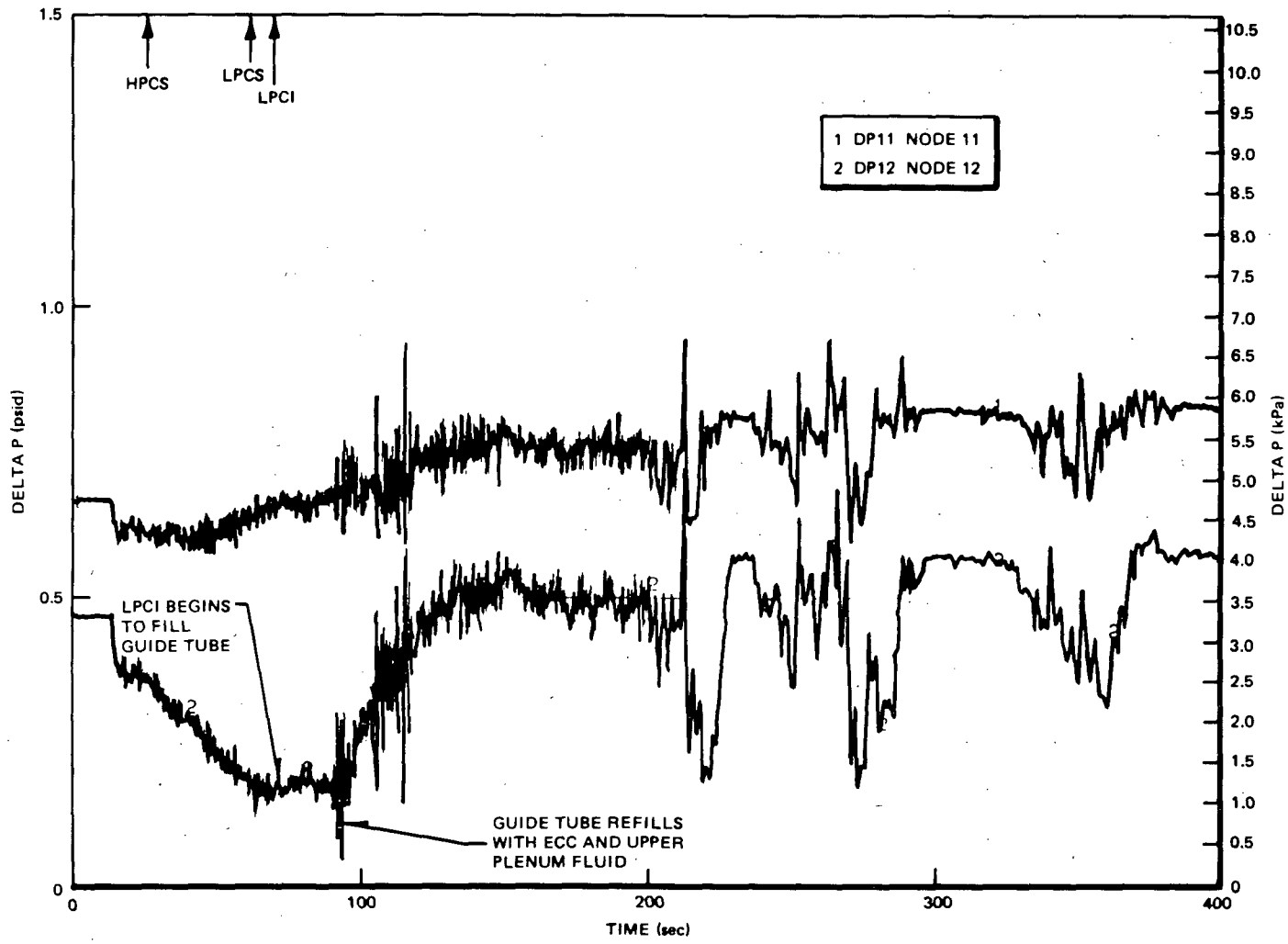

Figure M-24. Guide Tube DPs

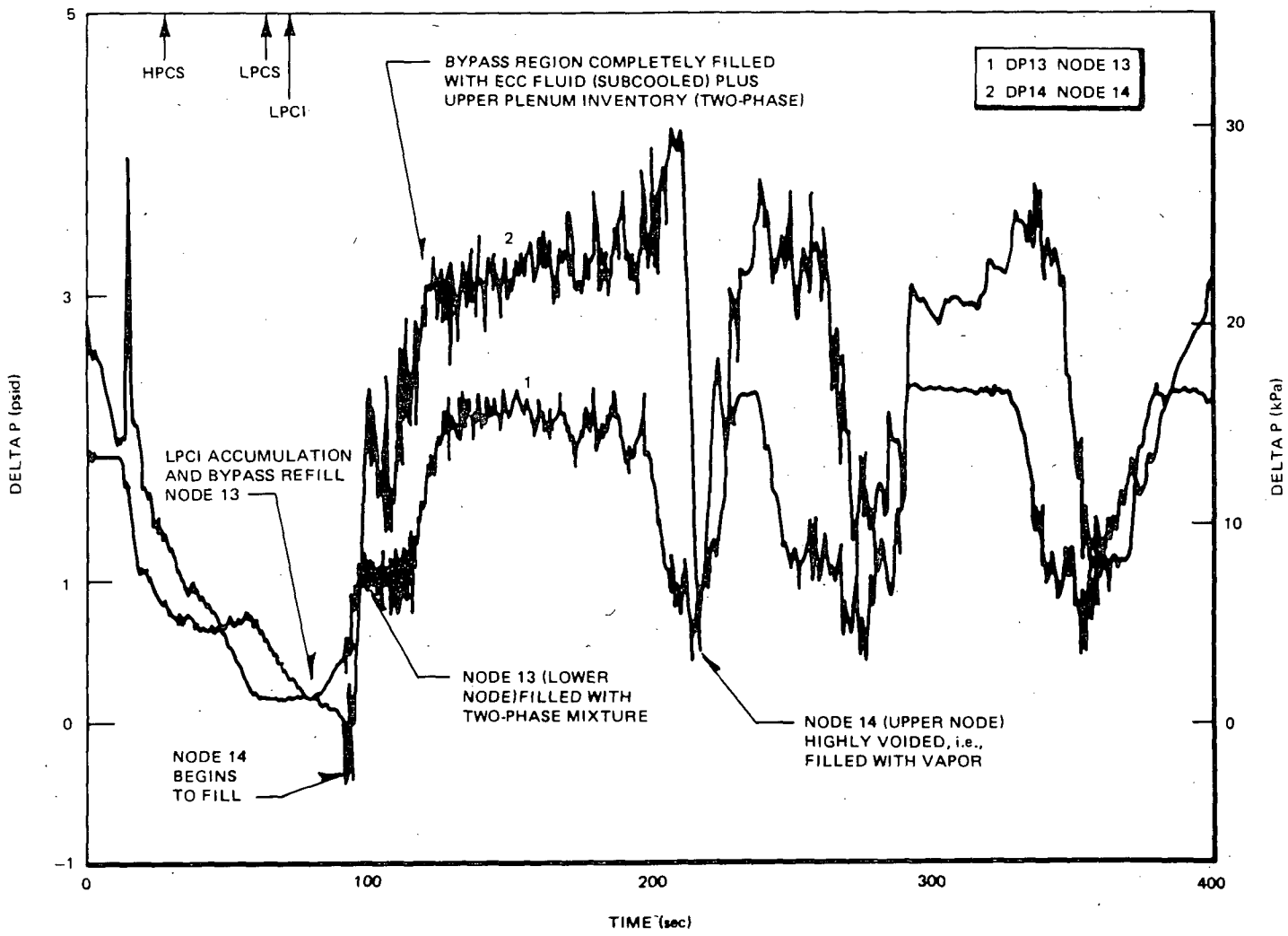

Figure M-25. Bypass Differential Pressures

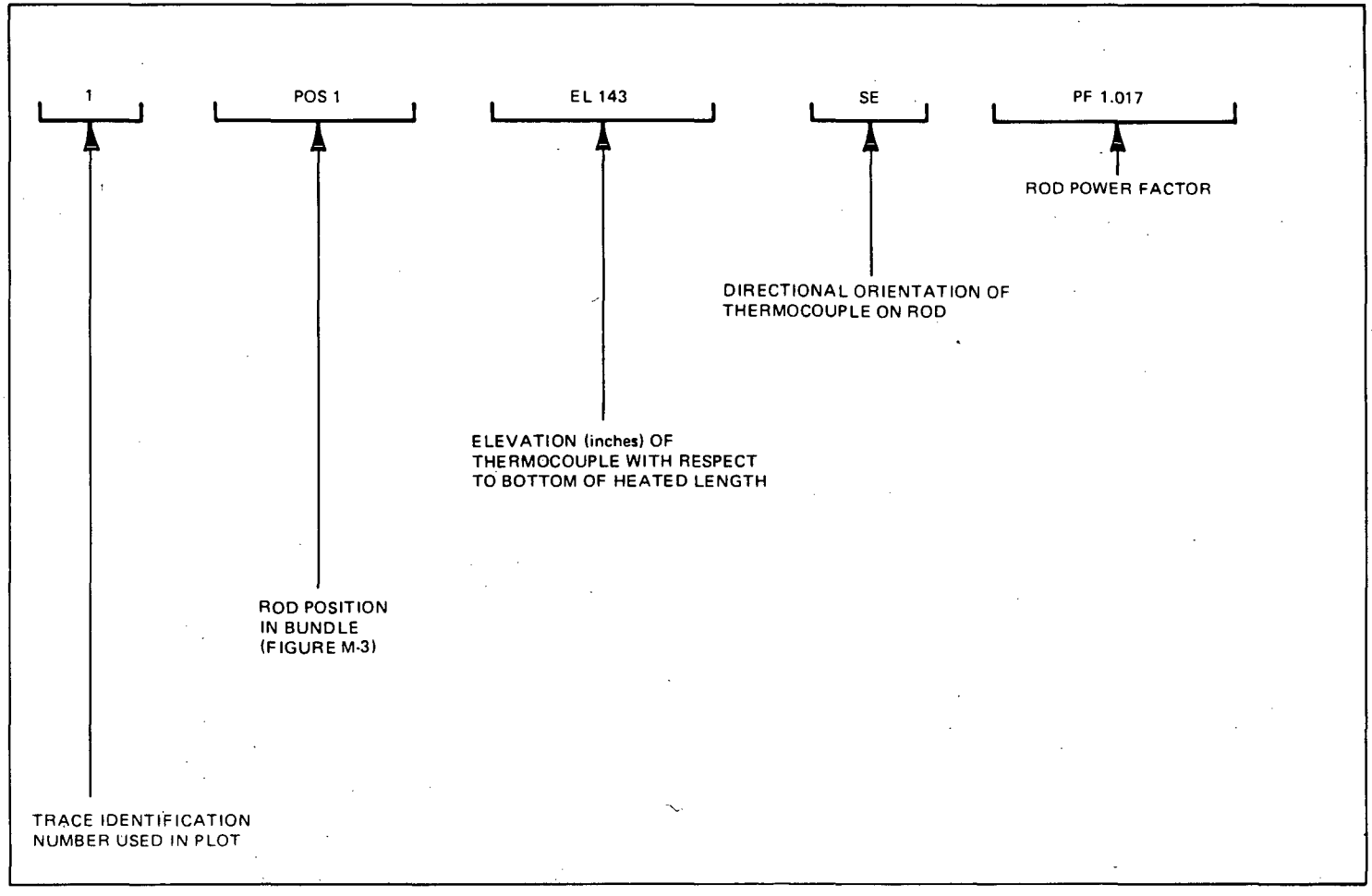

Figure M-26. Guide for Interpreting Legends on Bundle Temperature Plots

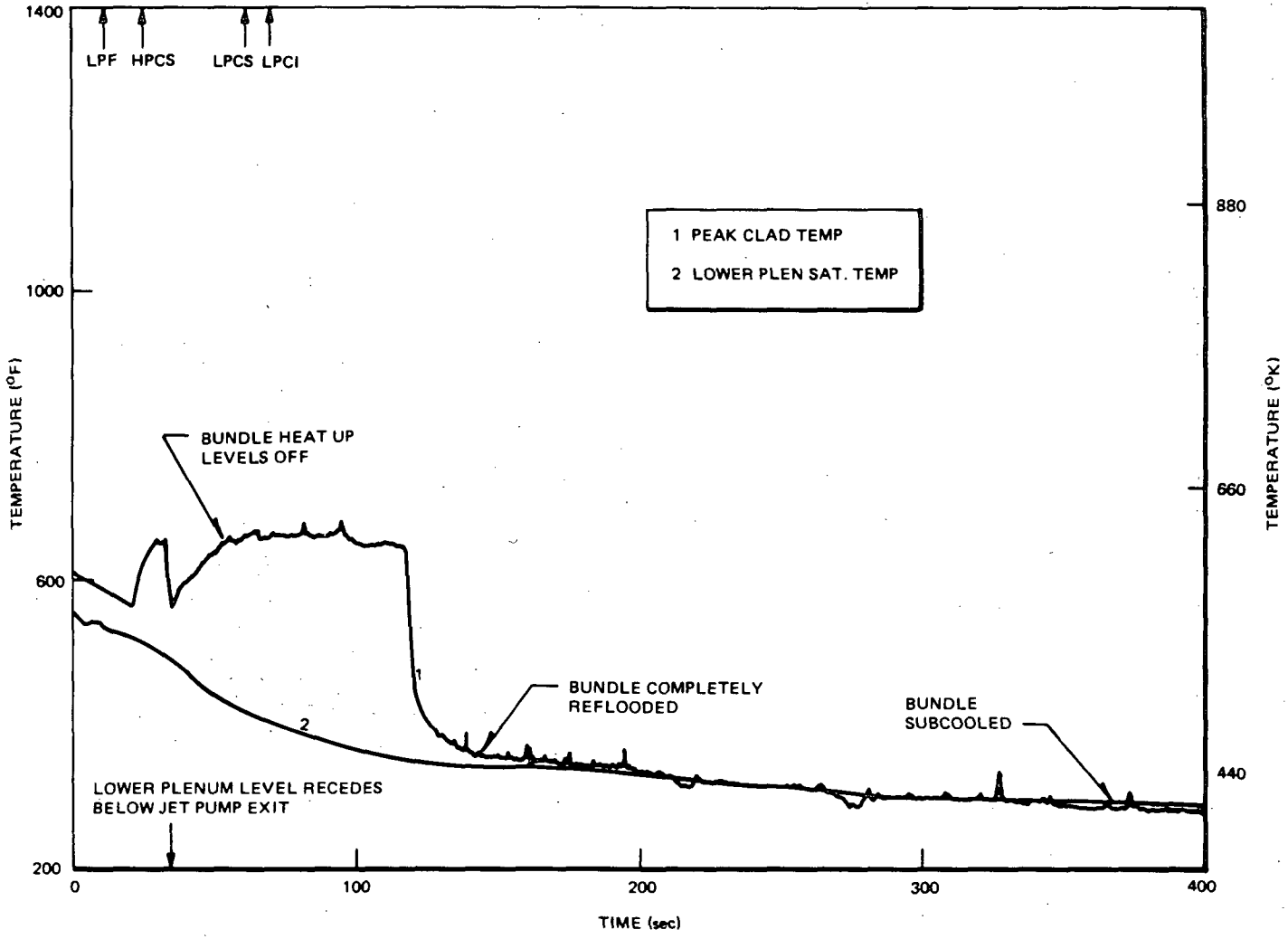

Figure M-27. Peak Cladding Temperature

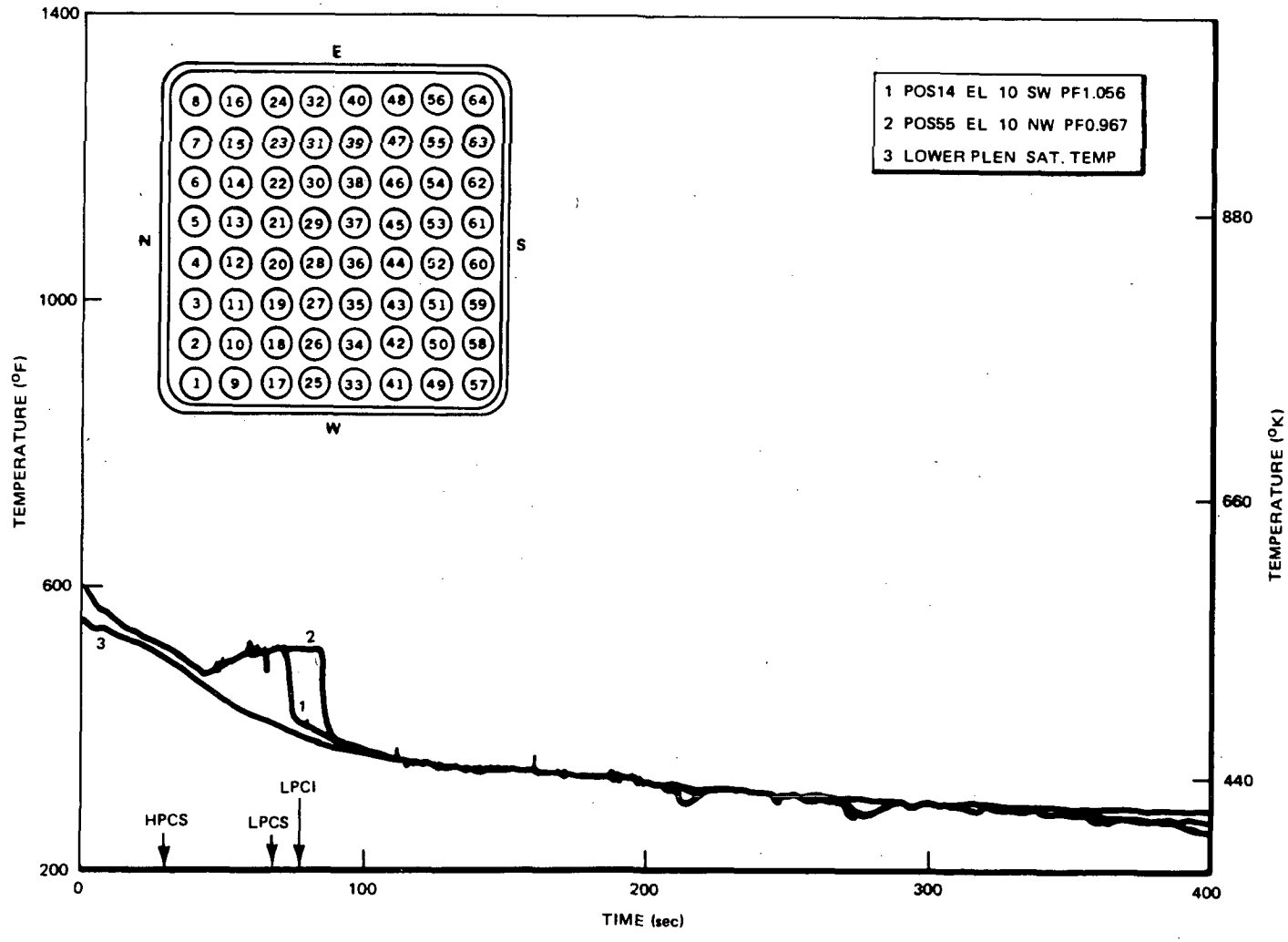

Figure M-28. Rod Cladding Temperature

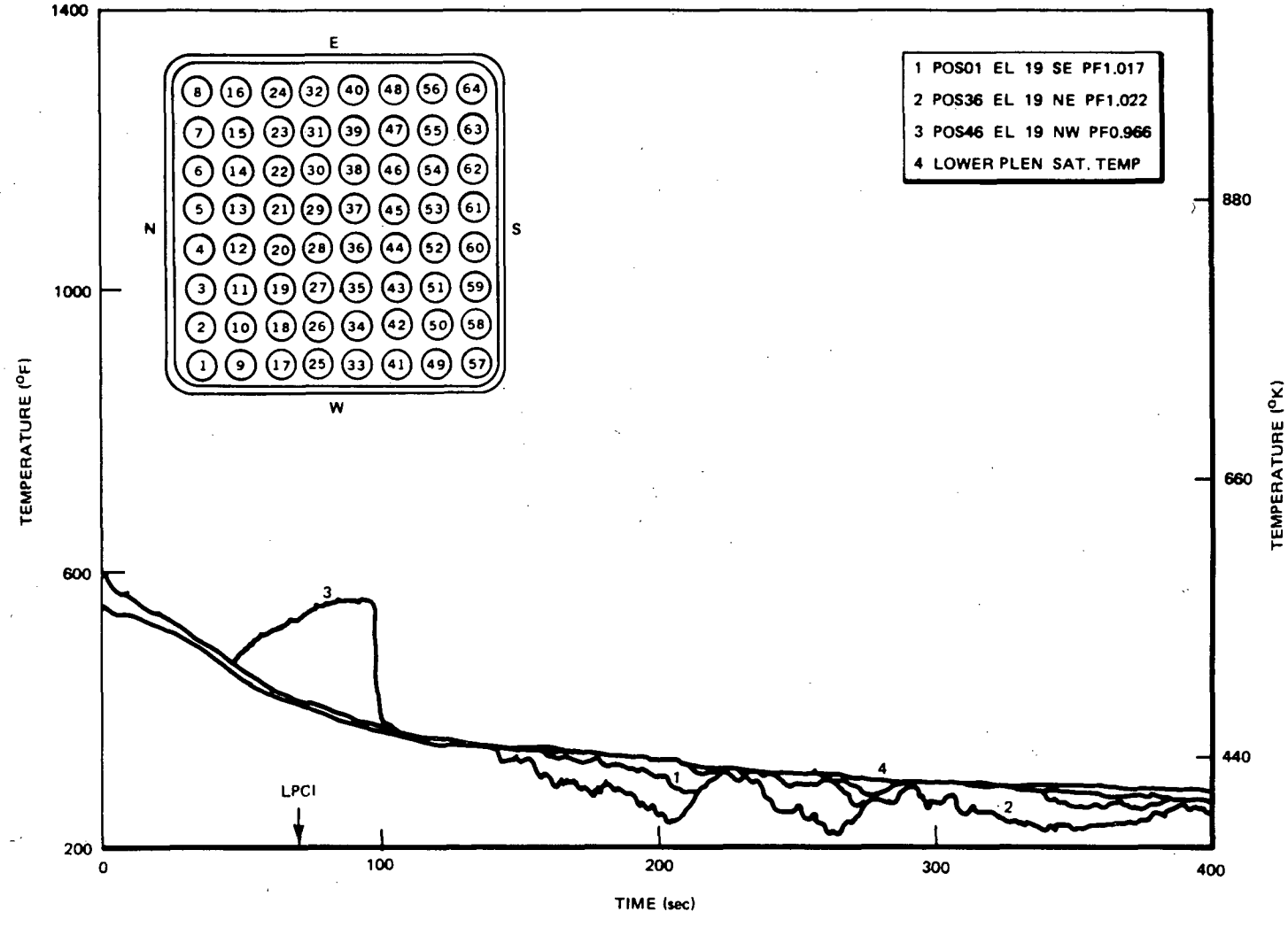

Figure M-29. Rod Cladding Temperature

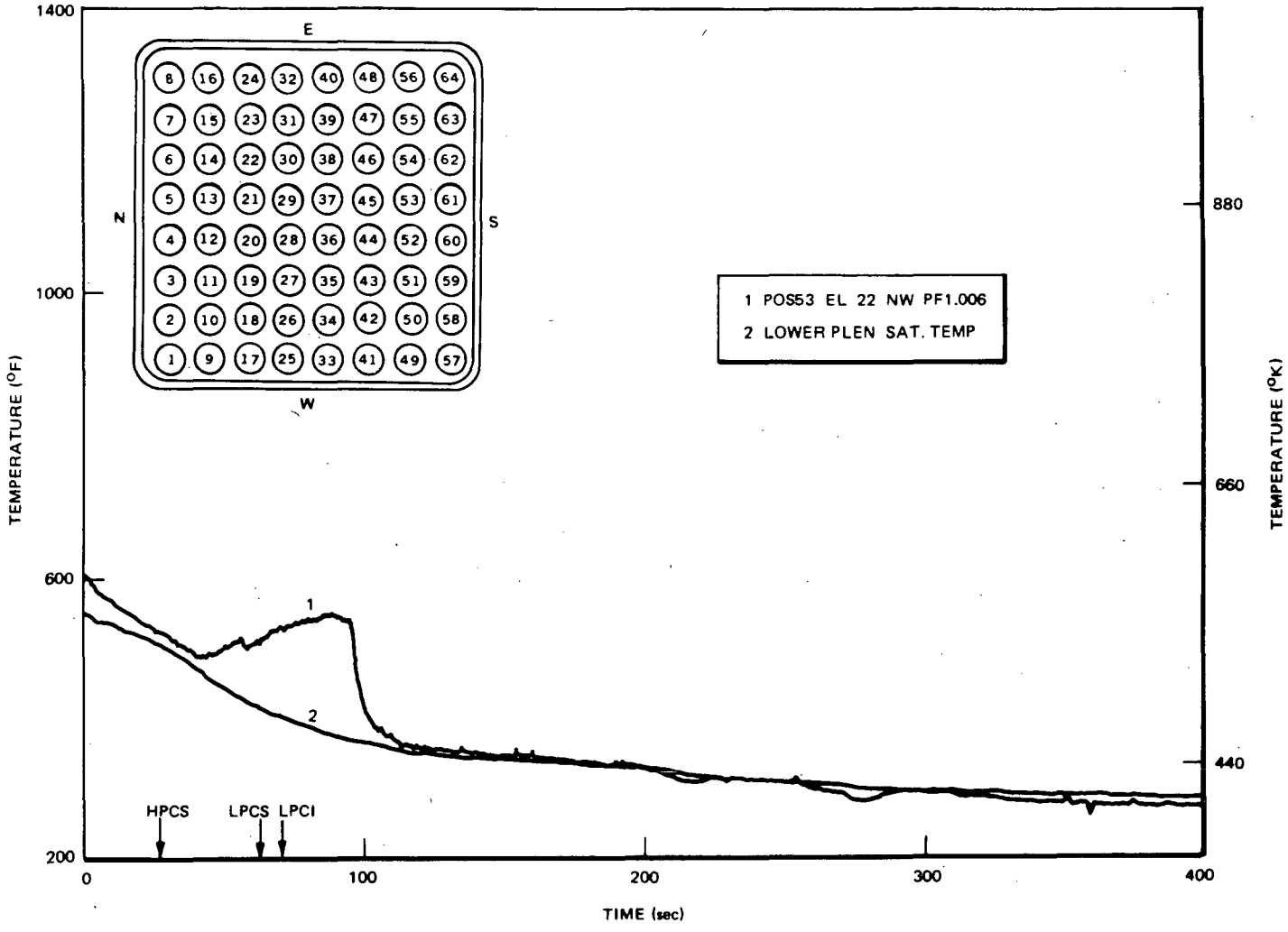

Figure M-30. Rod Cladding Temperature

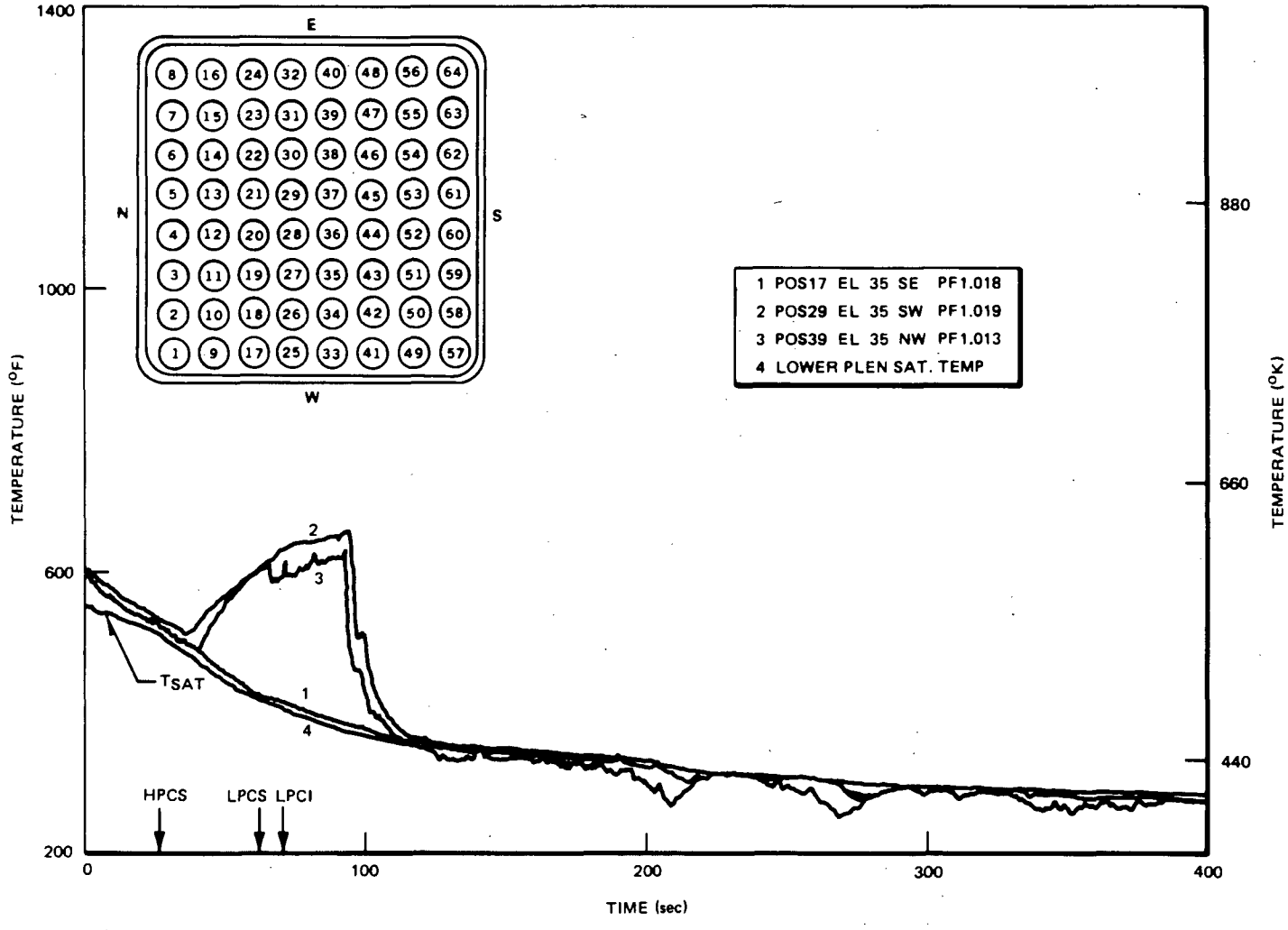

Figure M-31. Rod Cladding Temperature

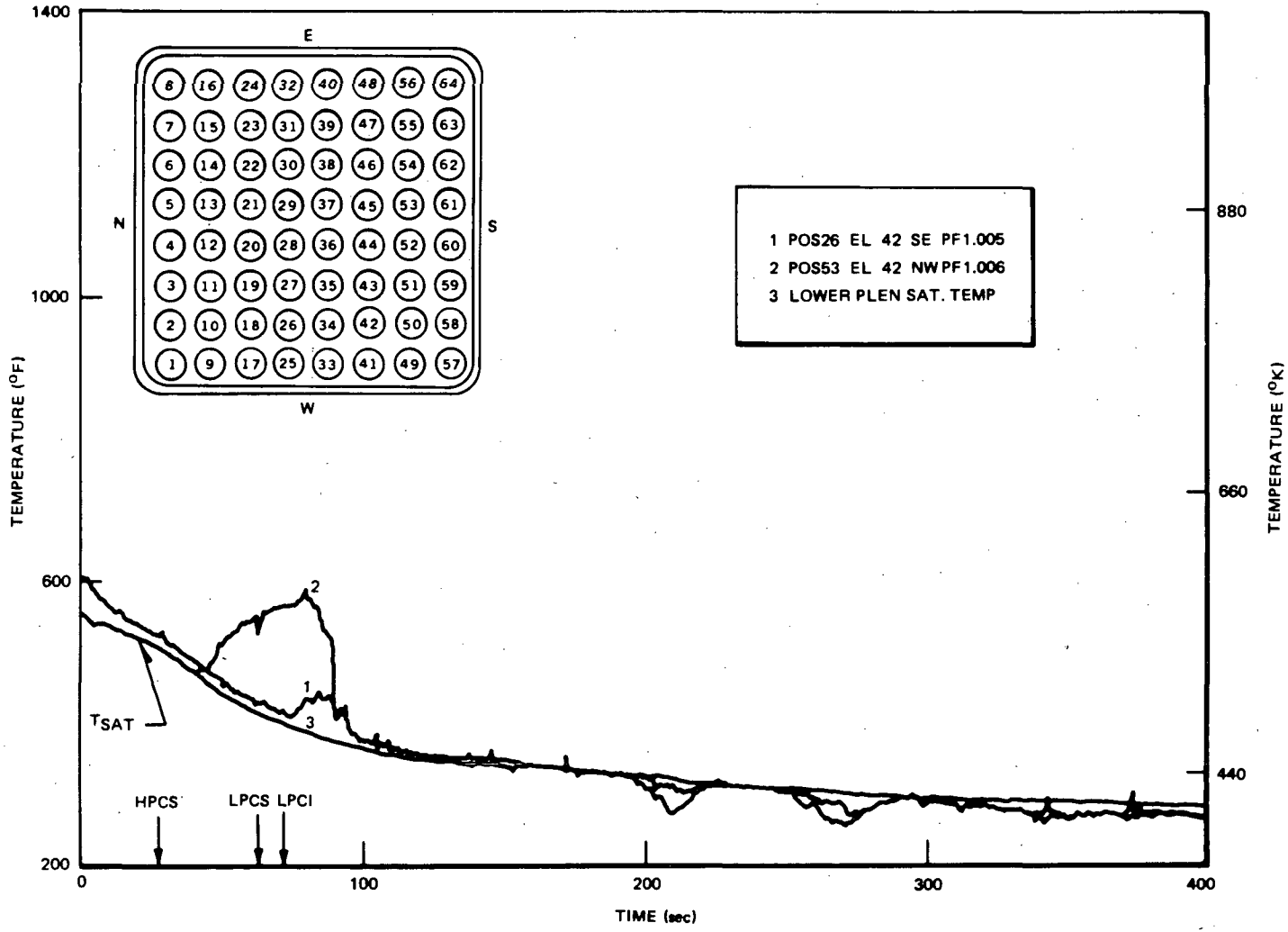

Figure M-32. Rod Cladding Temperature

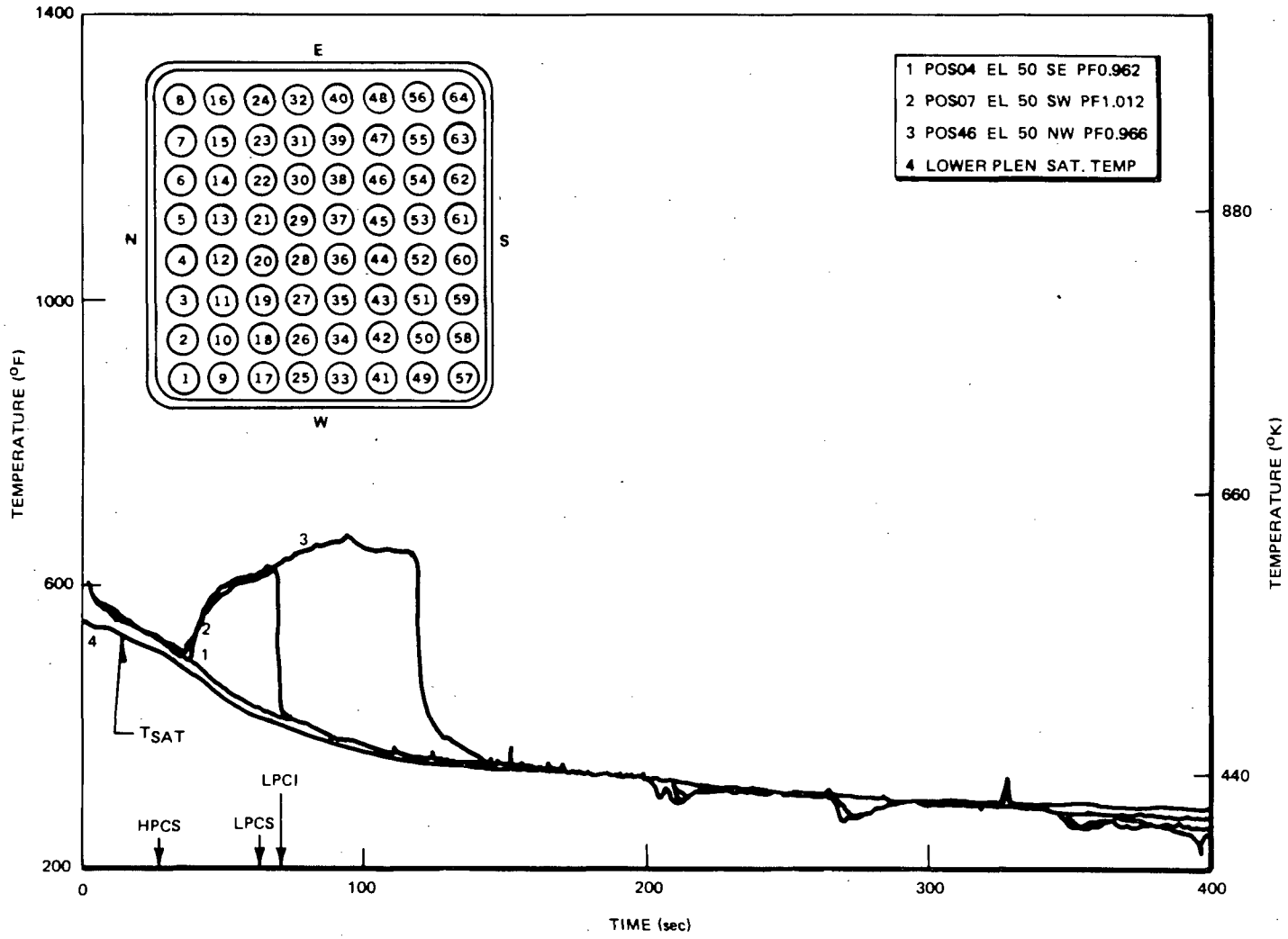

Figure M-33. Rod Cladding Temperature

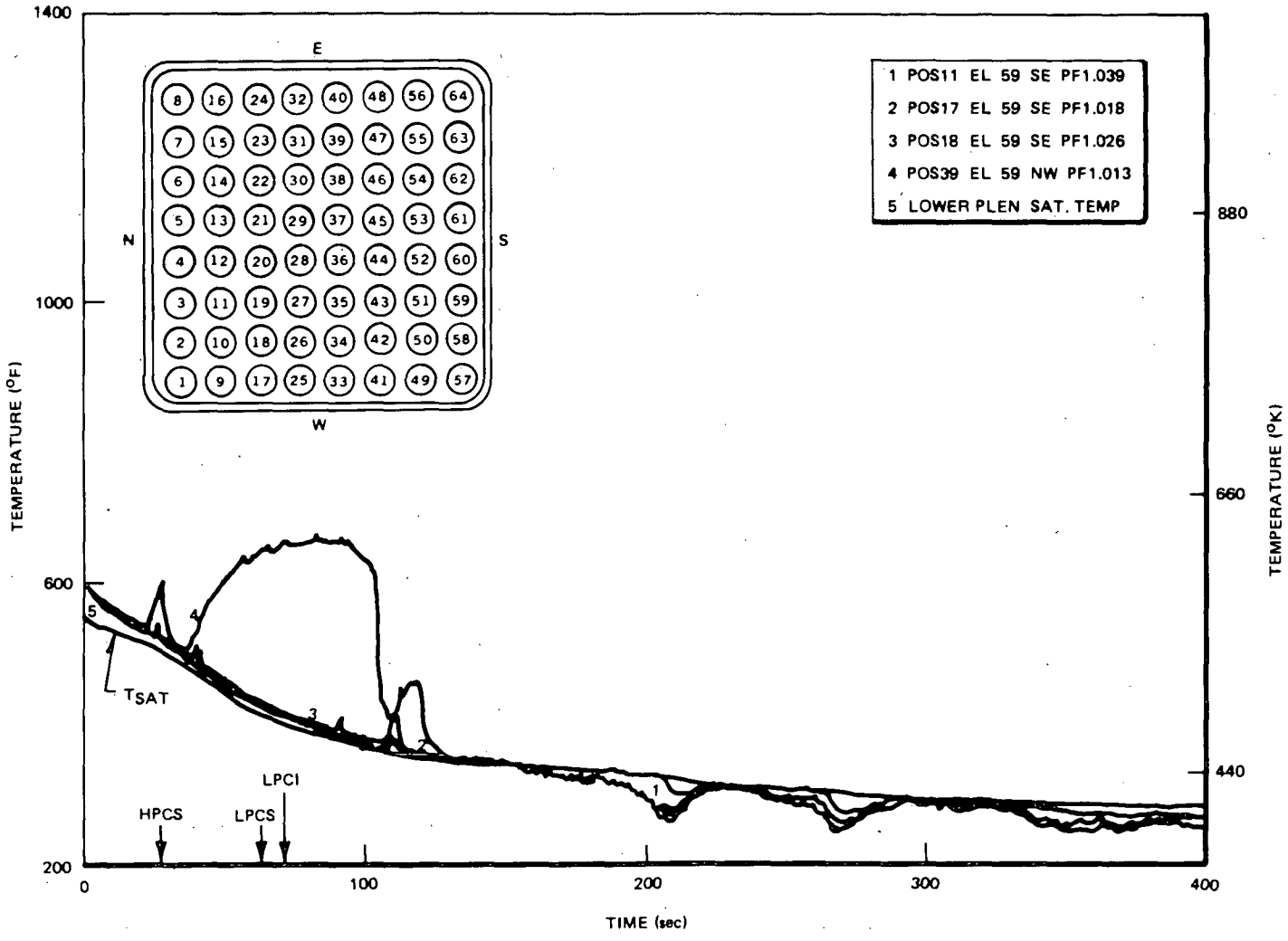

Figure M-34. Rod Cladding Temperature

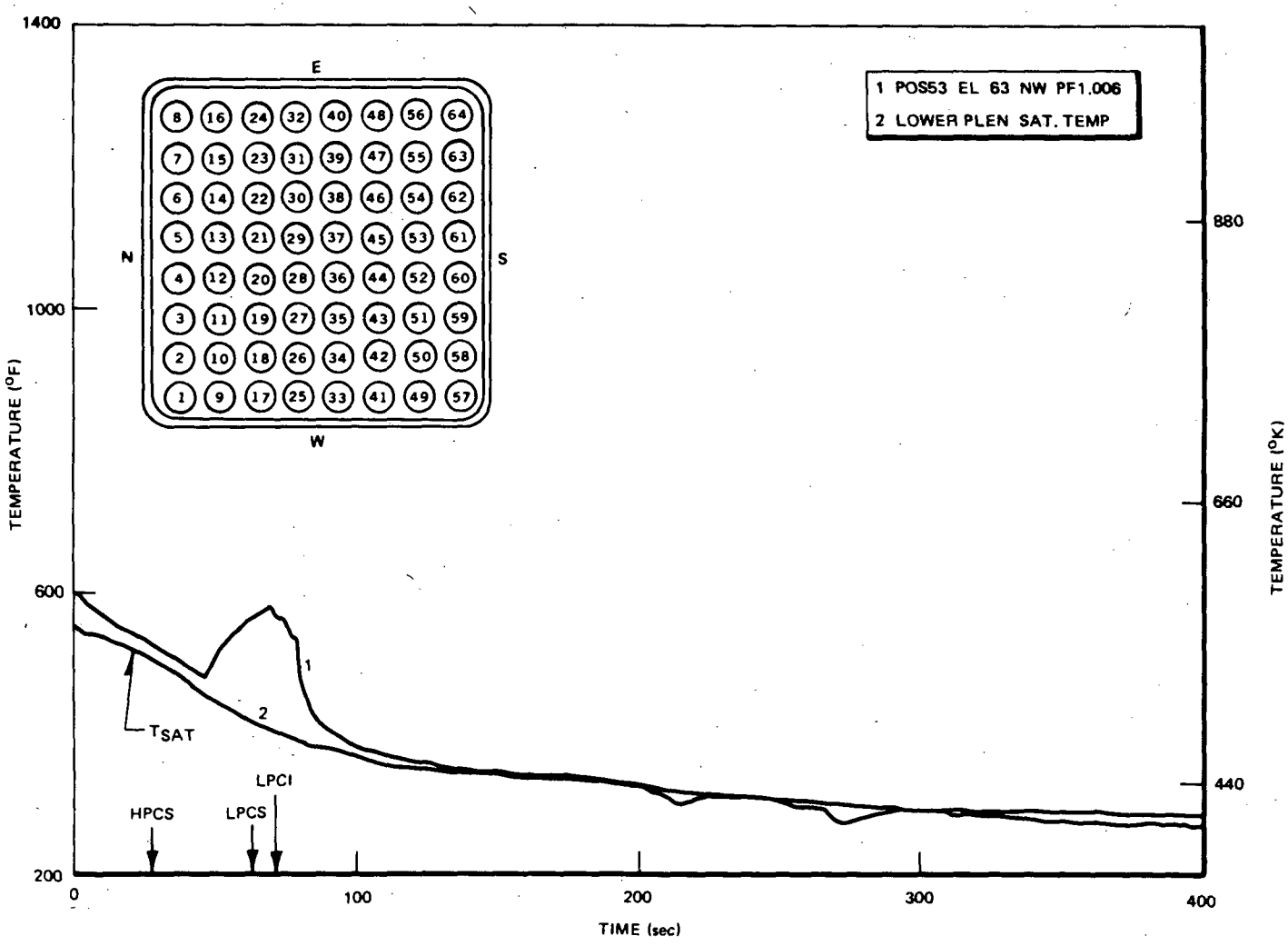

Figure M-35. Rod Cladding Temperature

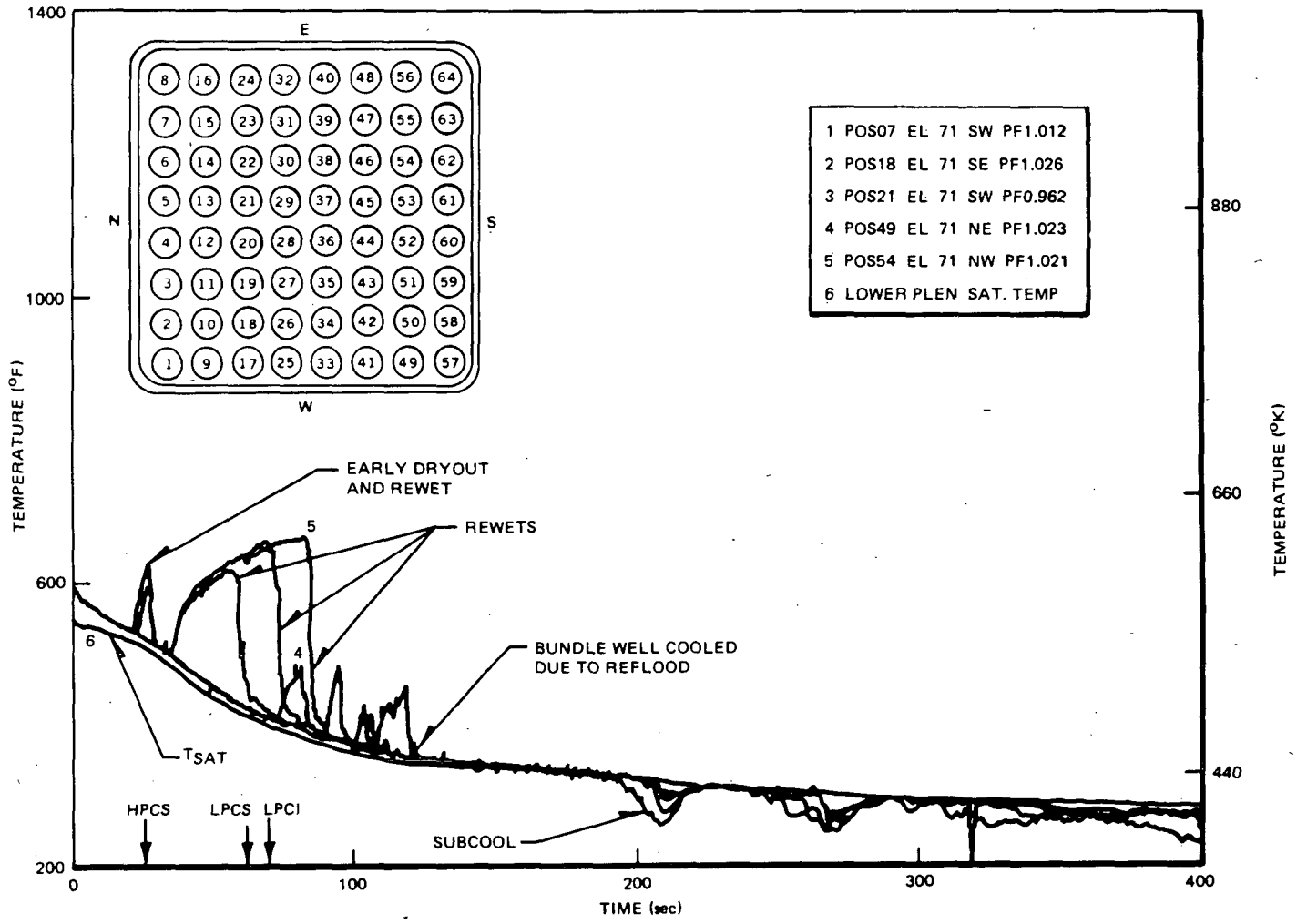

Figure M-36. Rod Cladding Temperature

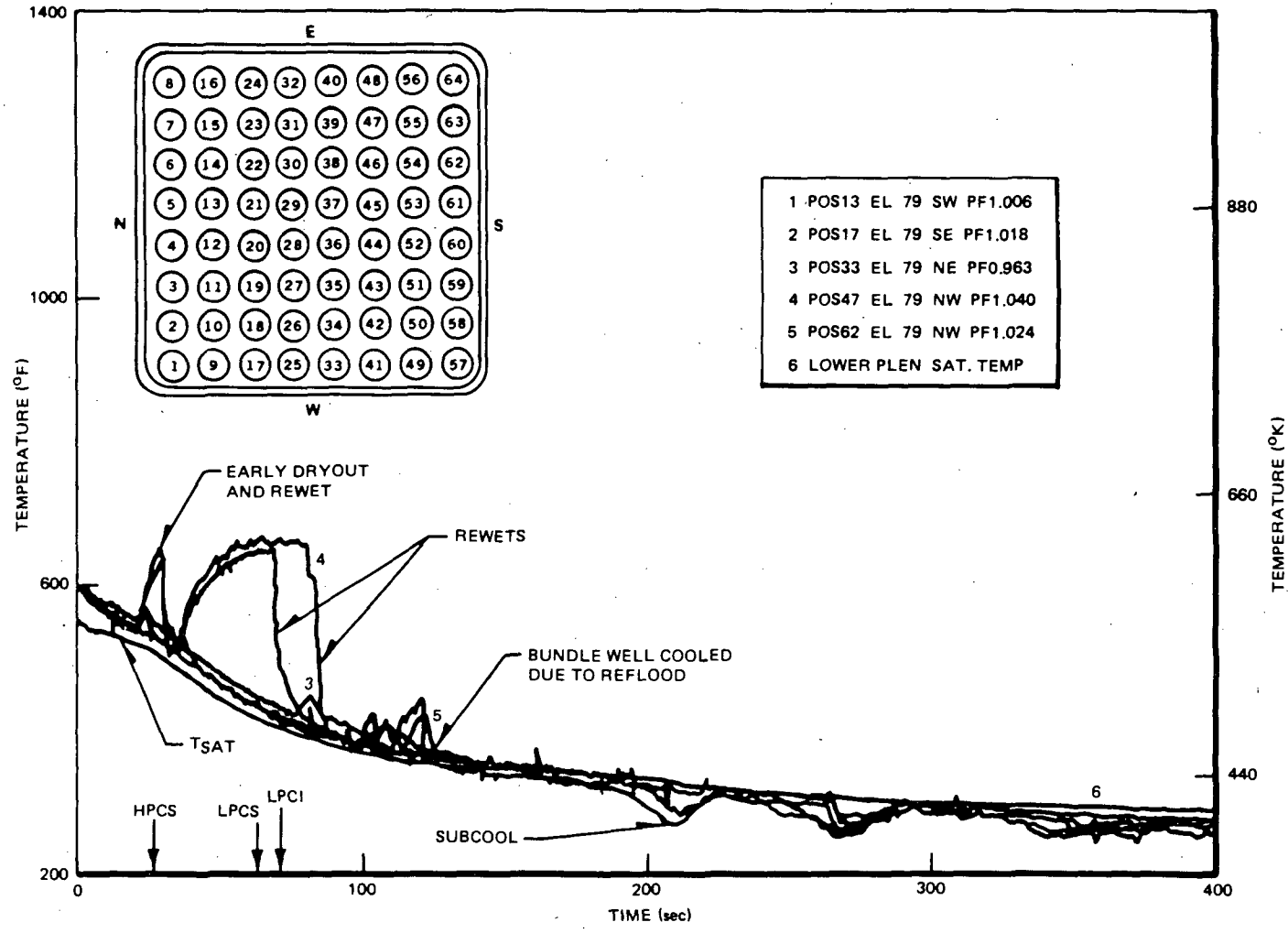

Figure M-37. Rod Cladding Temperature

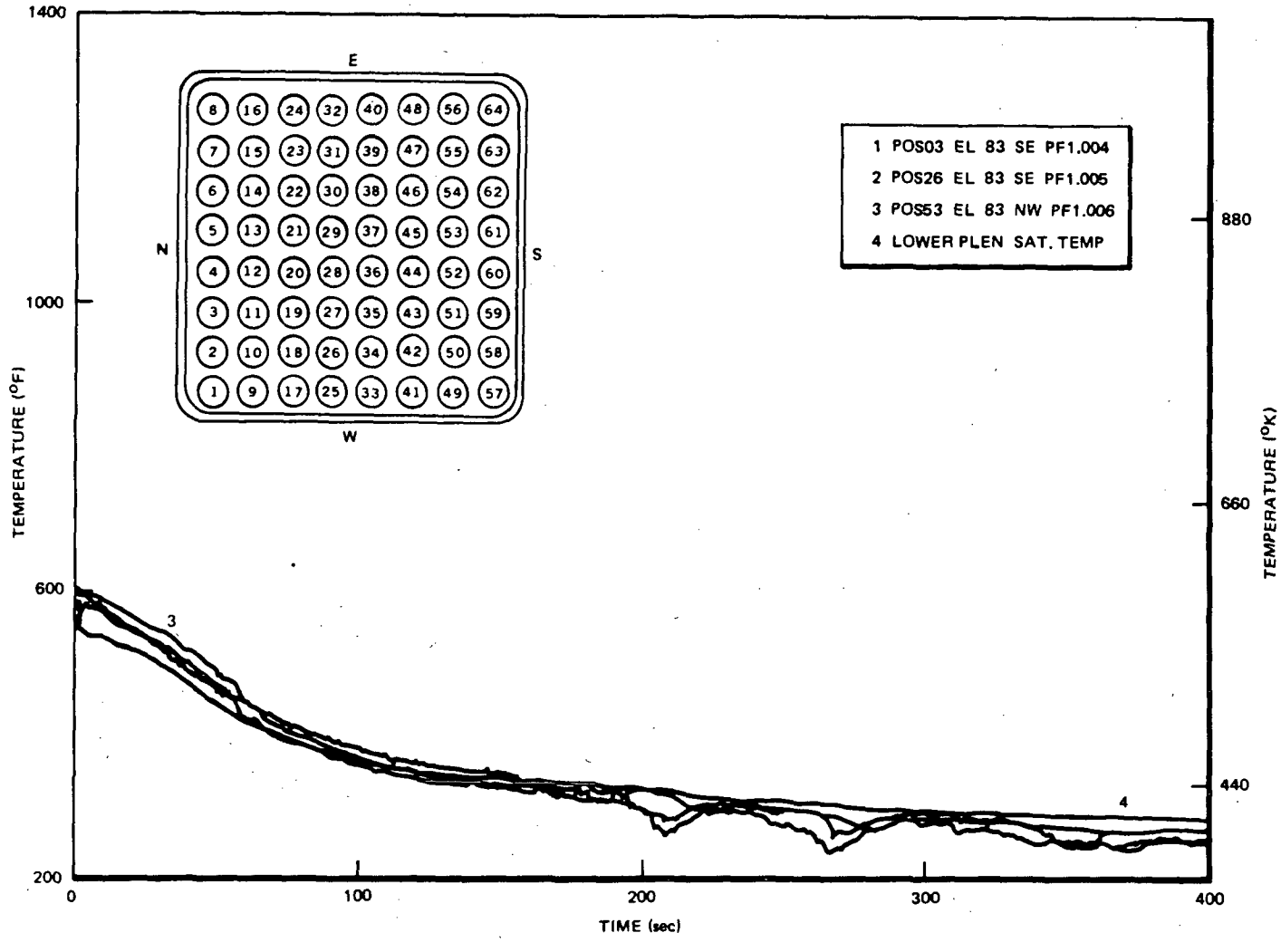

Figure M-38. Rod Cladding Temperature

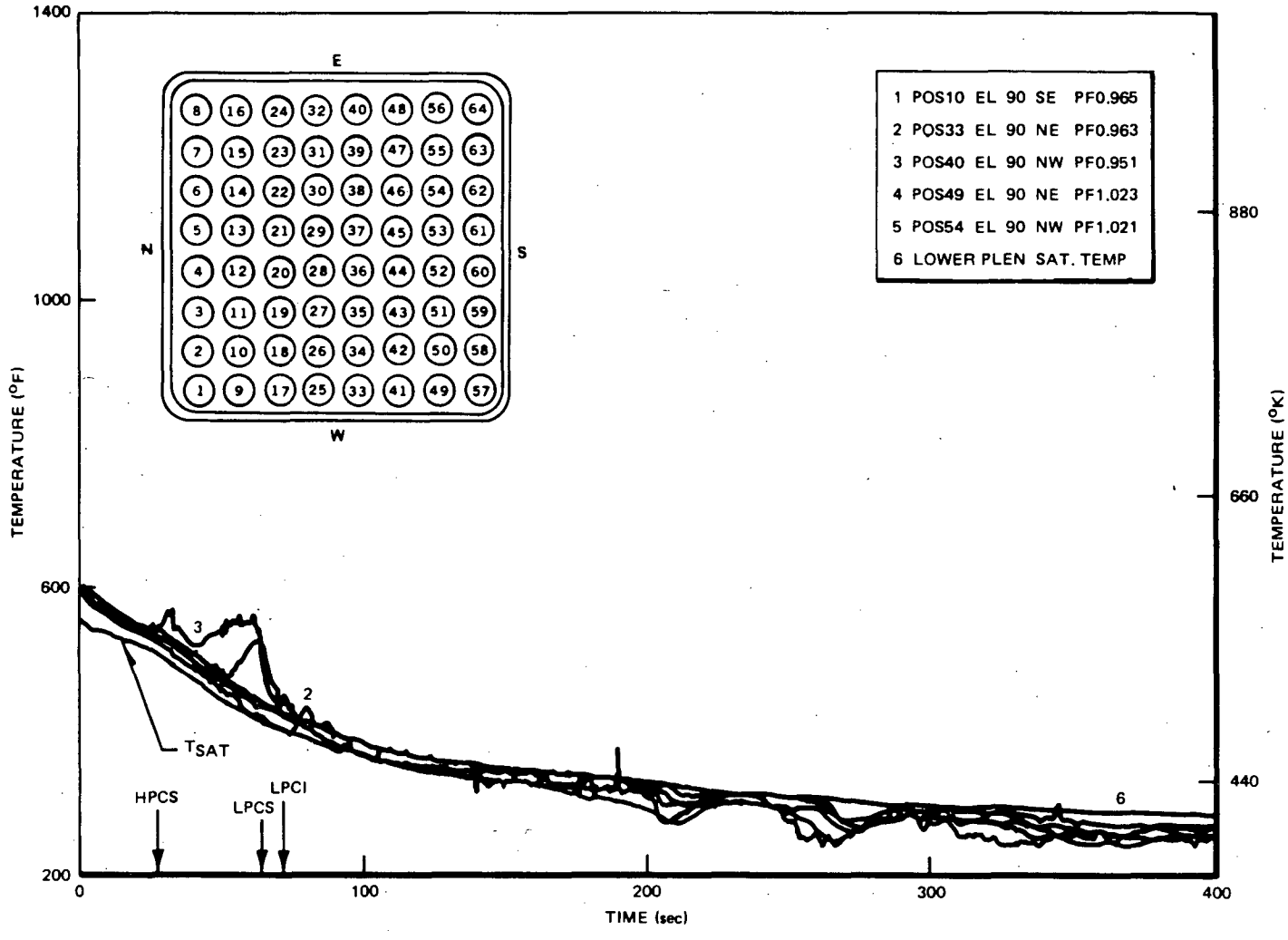

Figure M-39. Rod Cladding Temperature

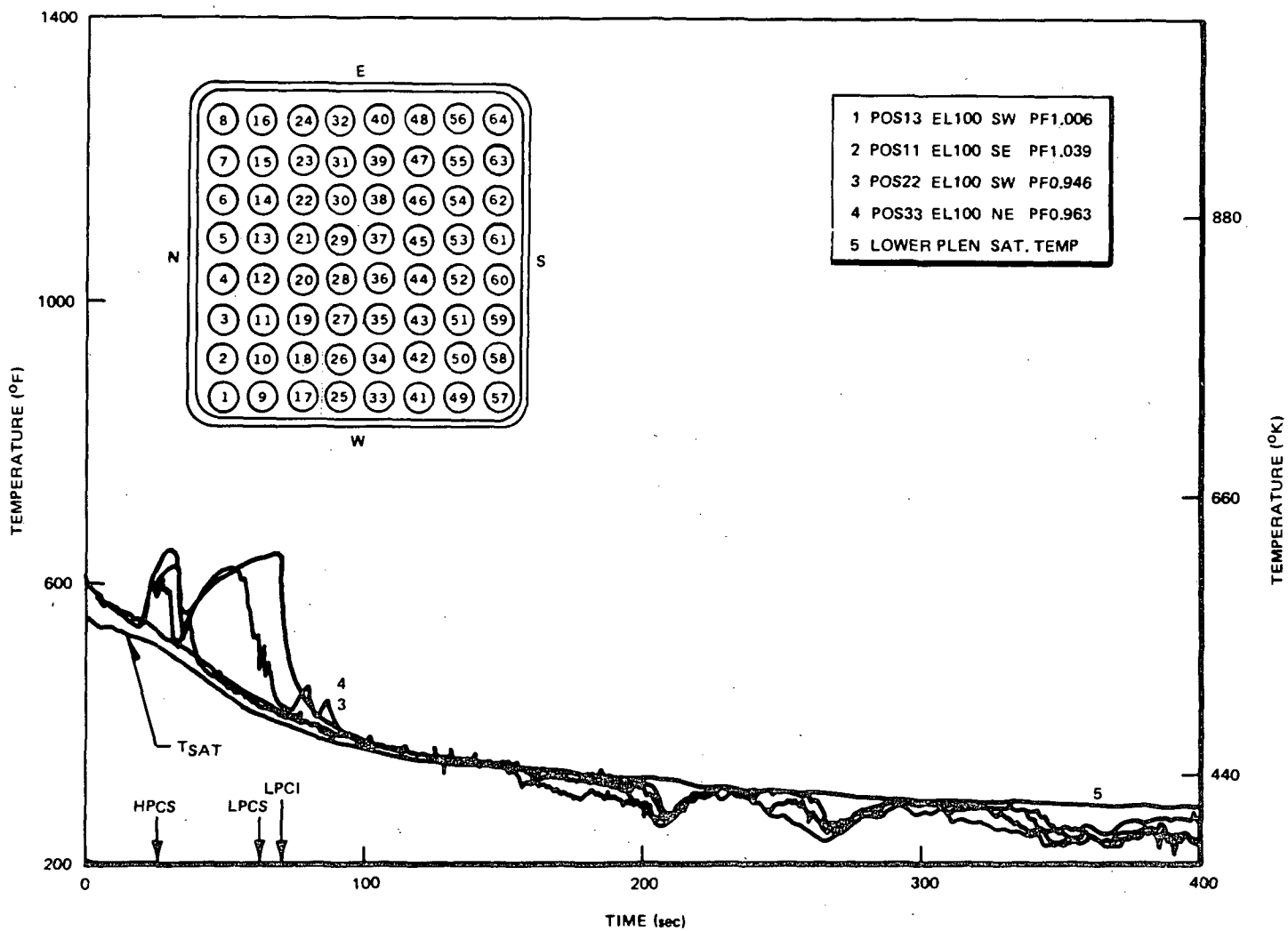

Figure M-40. Rod Cladding Temperature

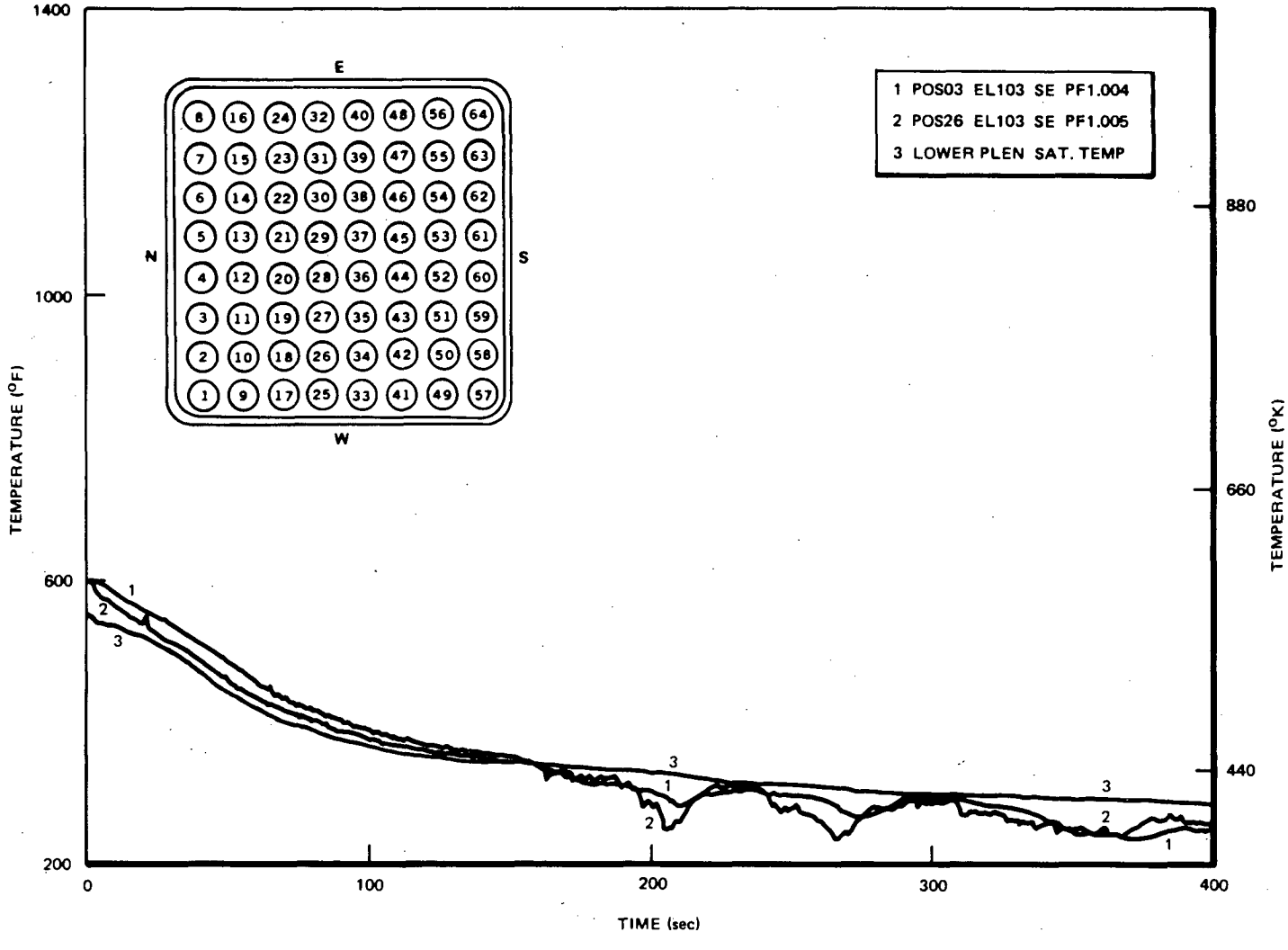

Figure M-41. Rod Cladding Temperature

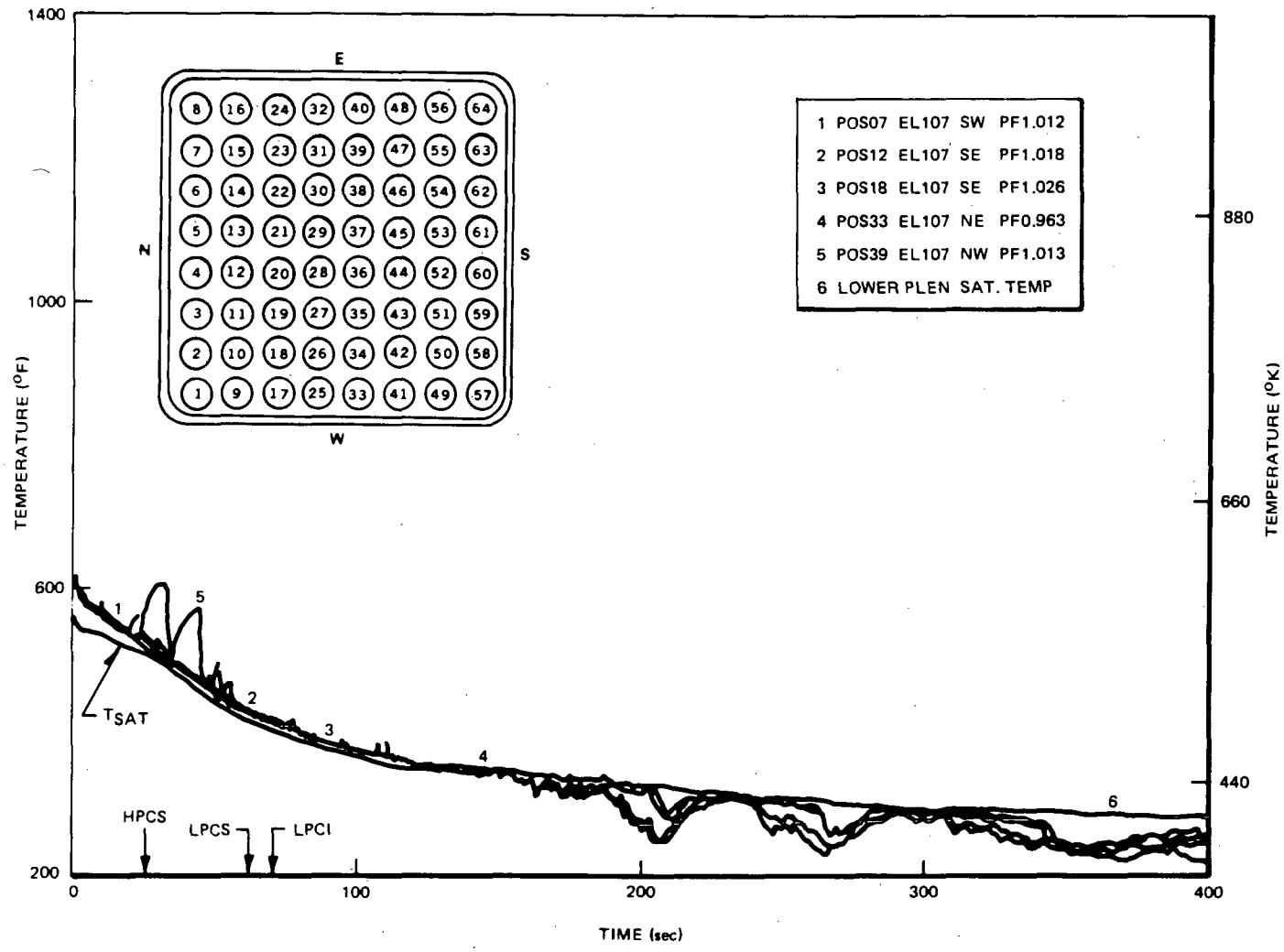

Figure M-42. Rod Cladding Temperature

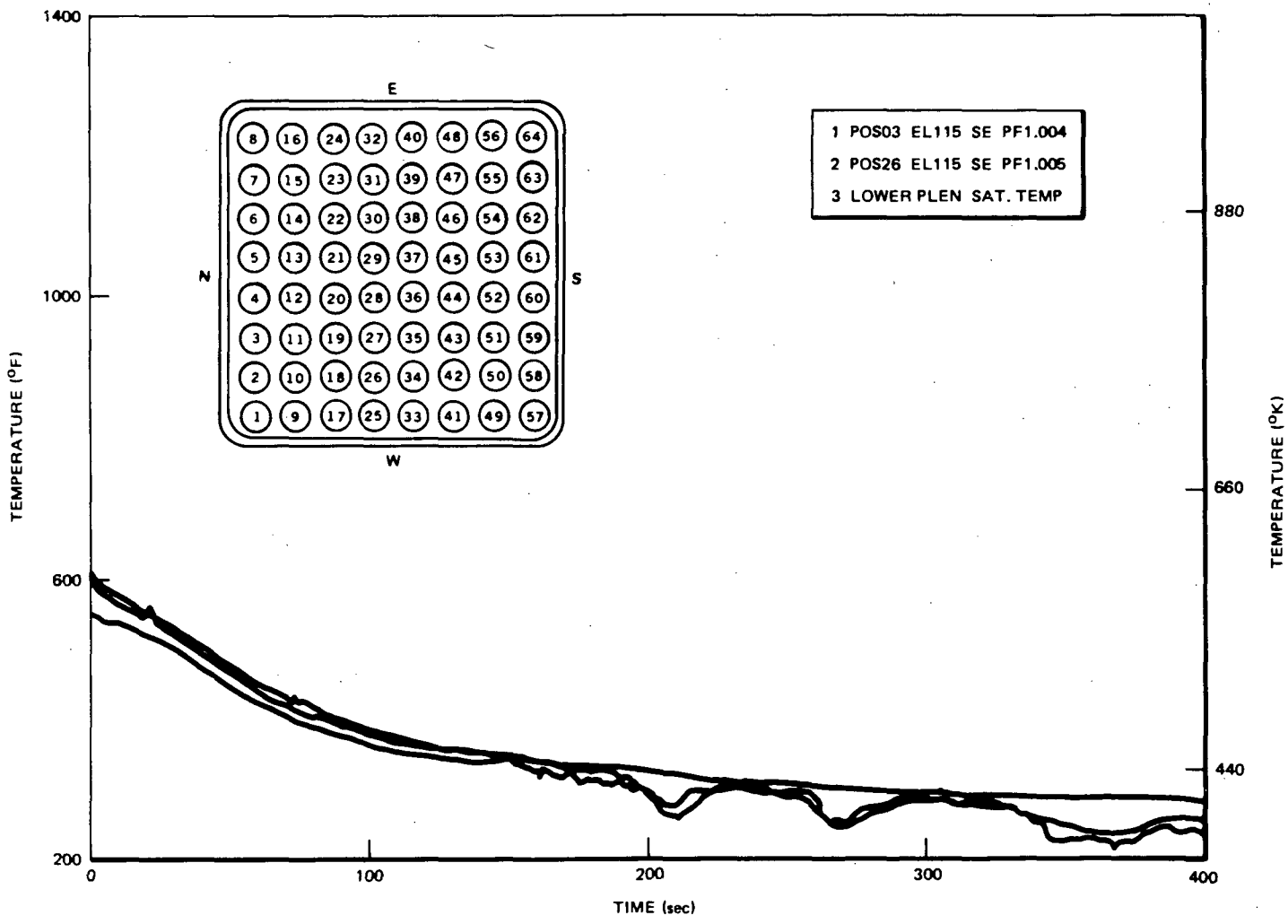

Figure M-43. Rod Cladding Temperature

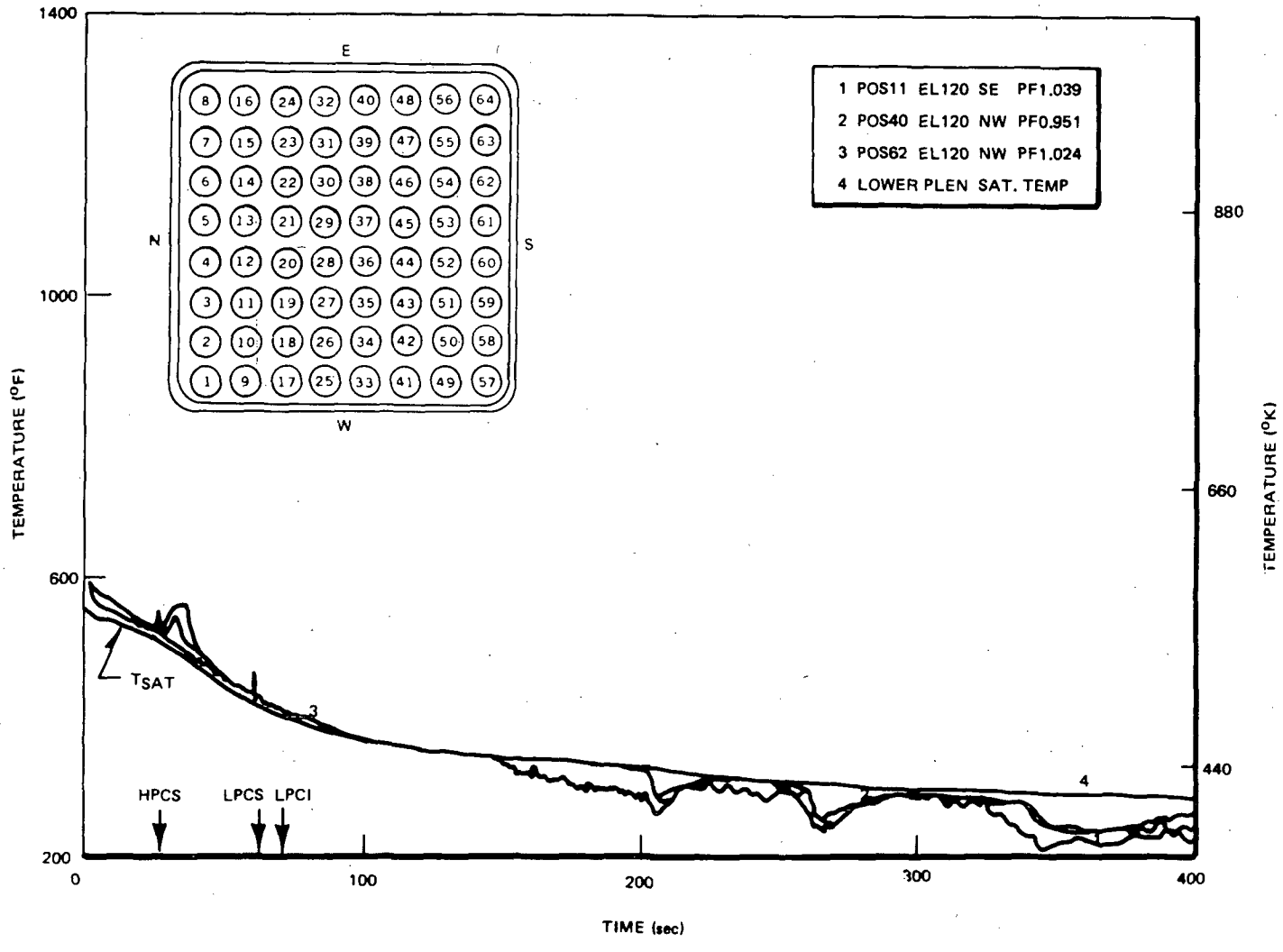

Figure M-44. Rod Cladding Temperature

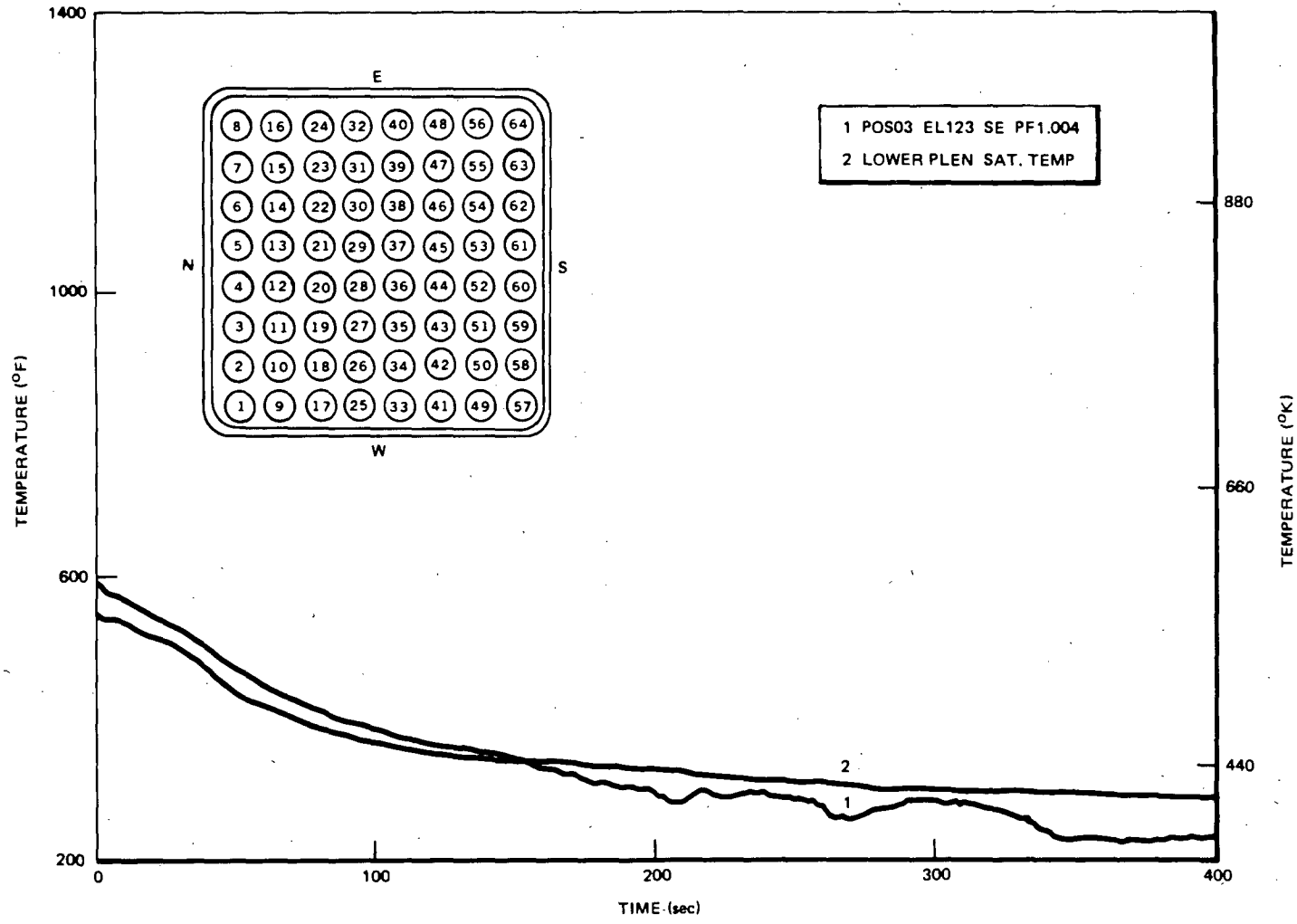

Figure M-45. Rod Cladding Temperature

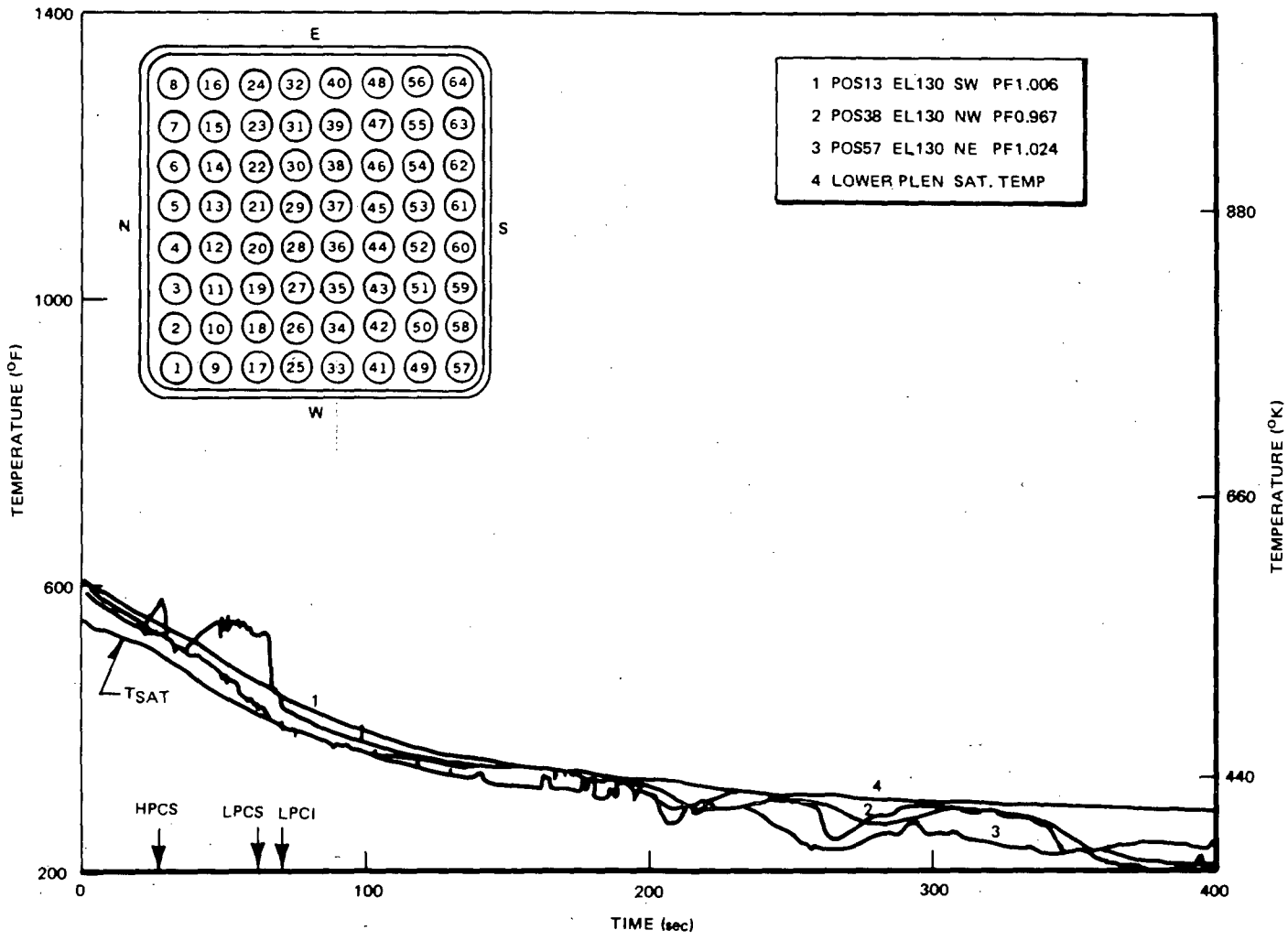

Figure M-46. Rod Cladding Temperature

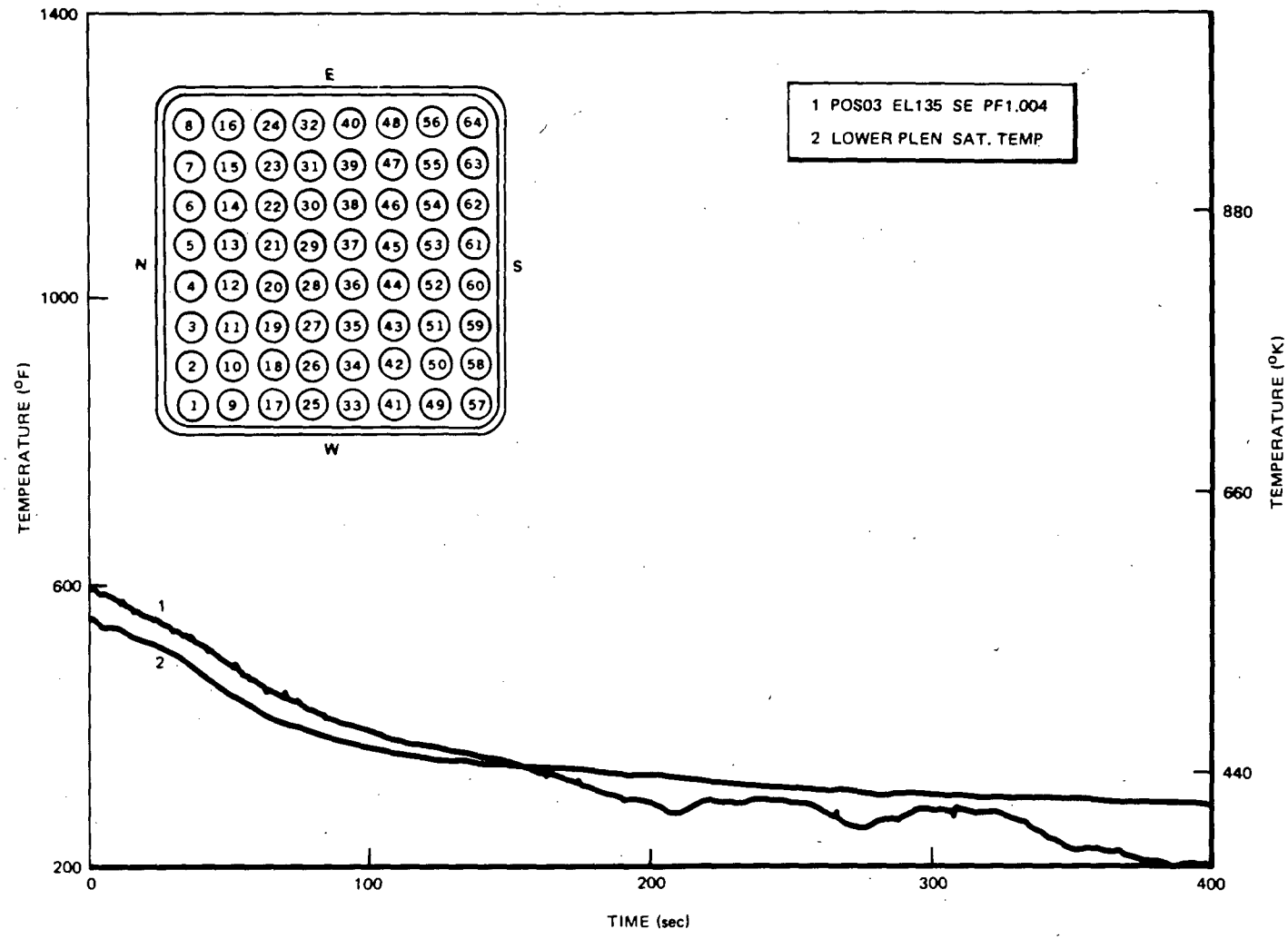

Figure M-47. Rod Cladding Temperature

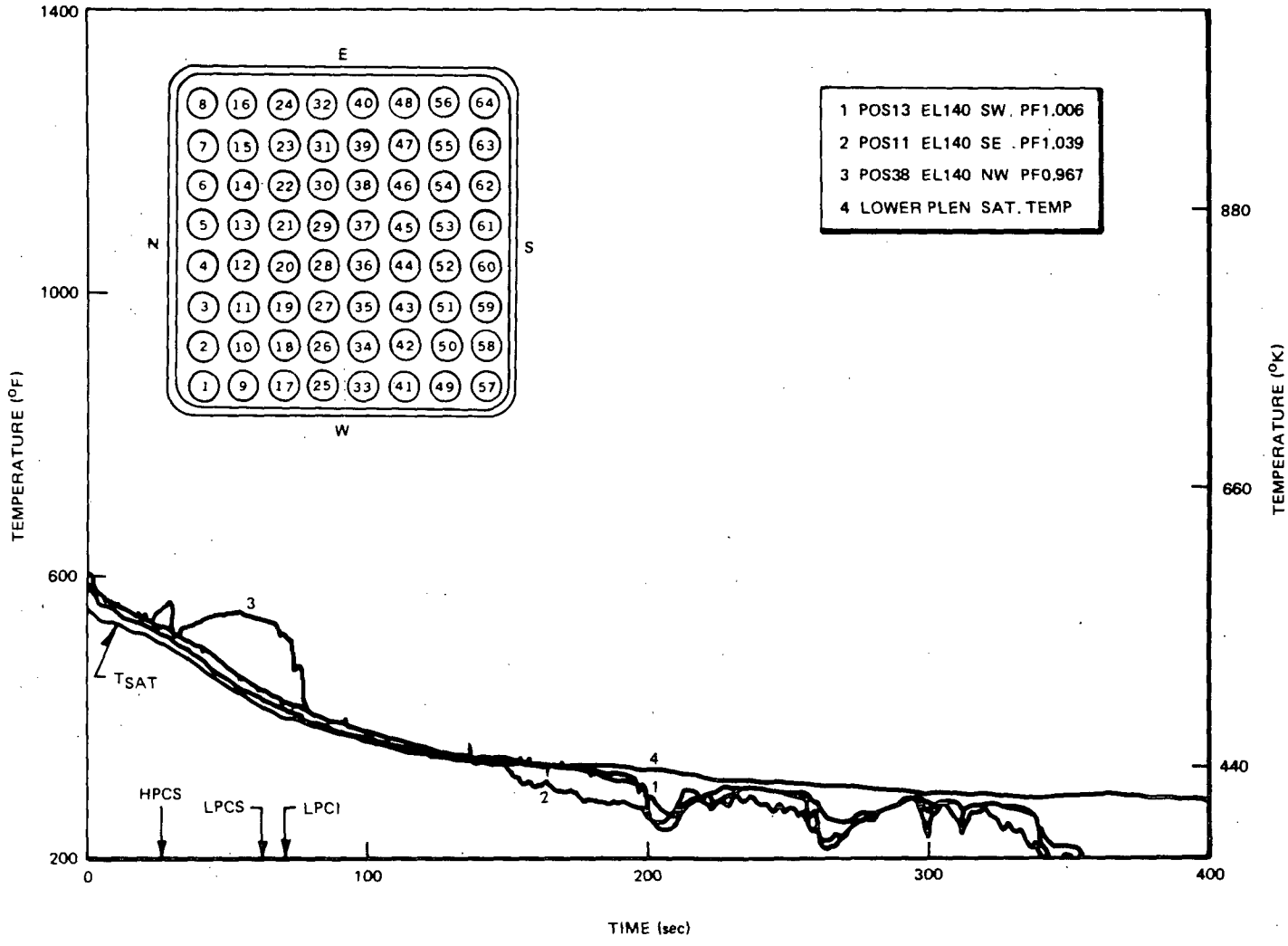

Figure M-48. Rod Cladding Temperature

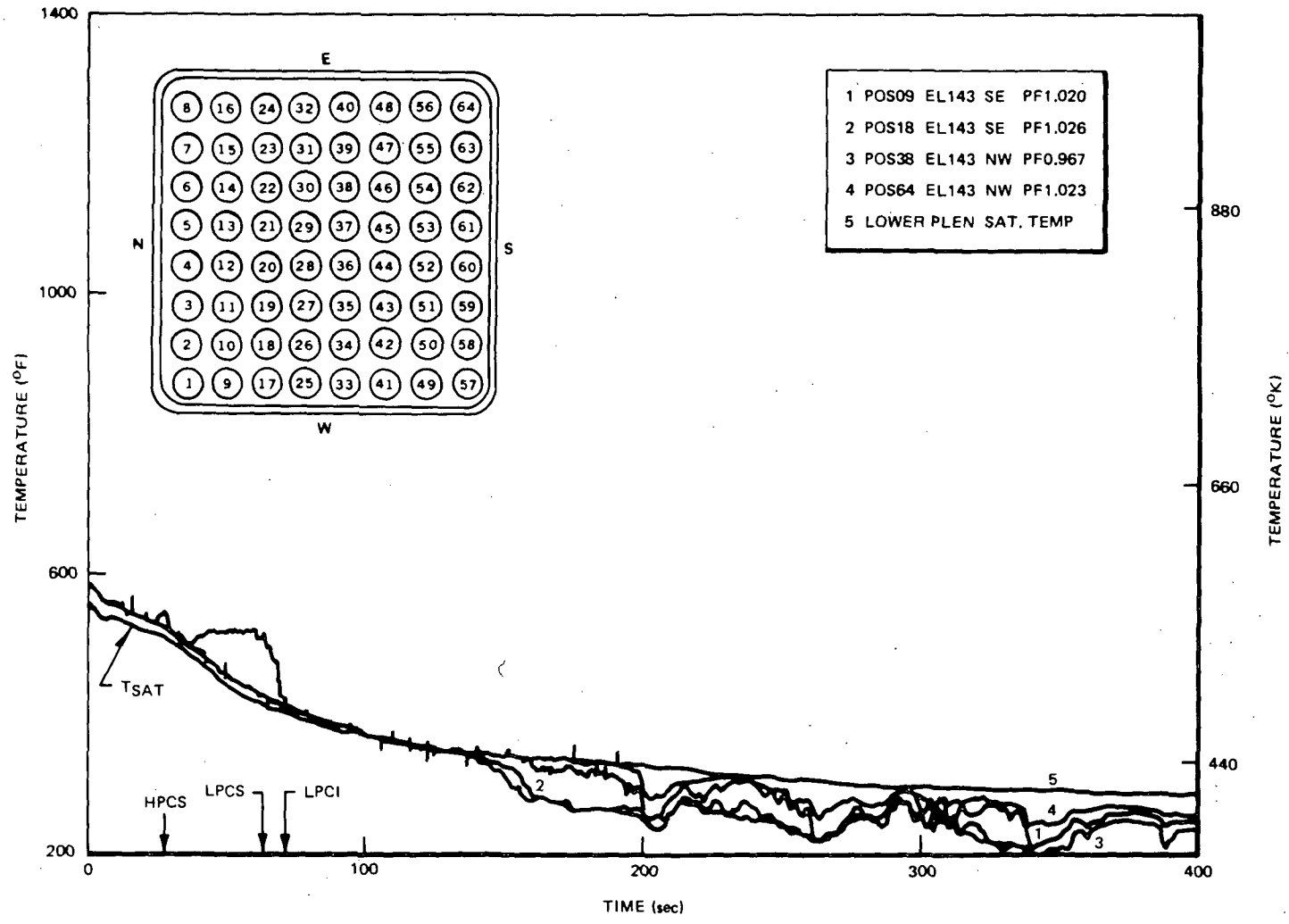

Figure M-49. Rod Cladding Temperature

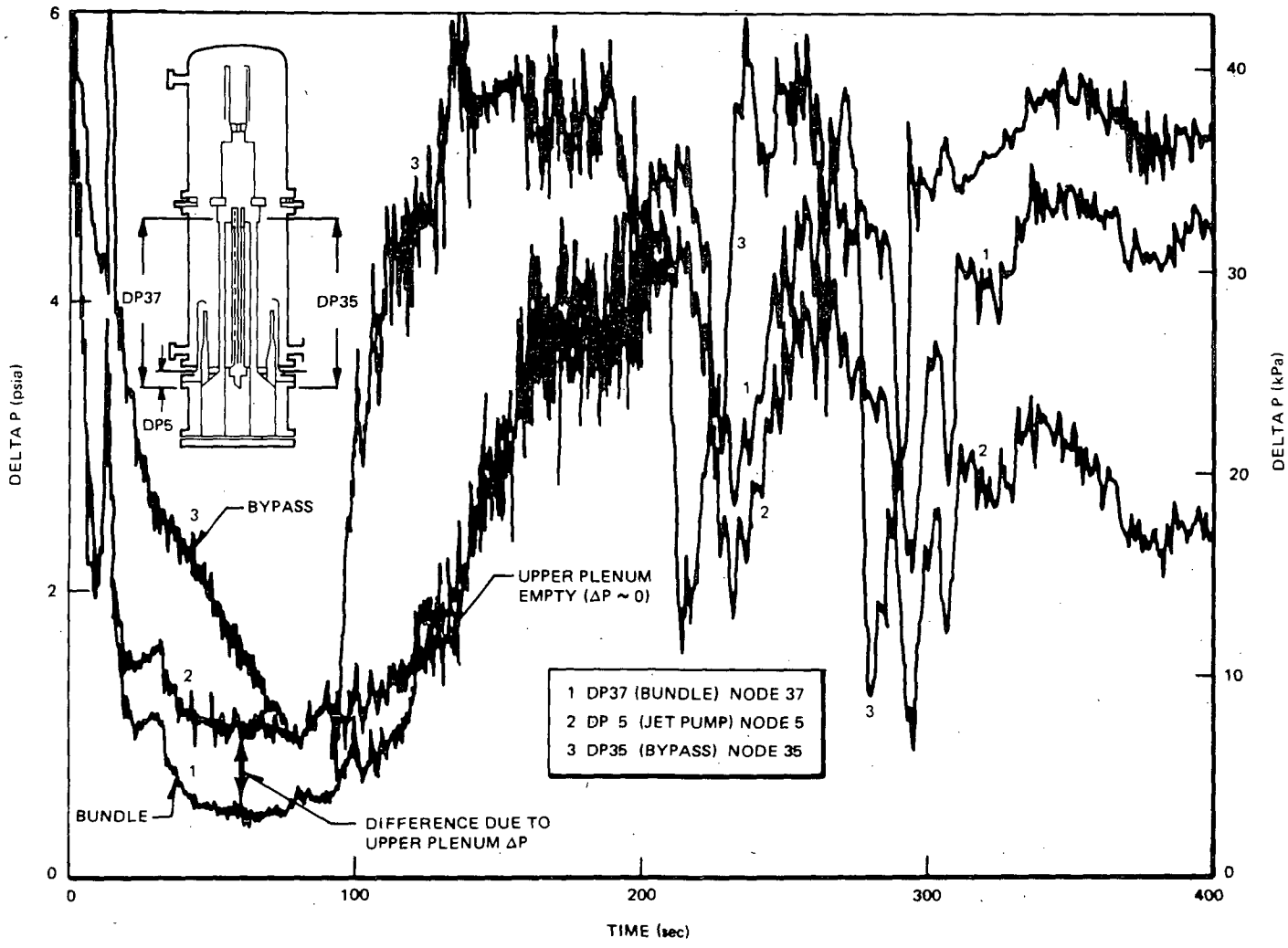

Figure M-50. Parallel Path ΔPs

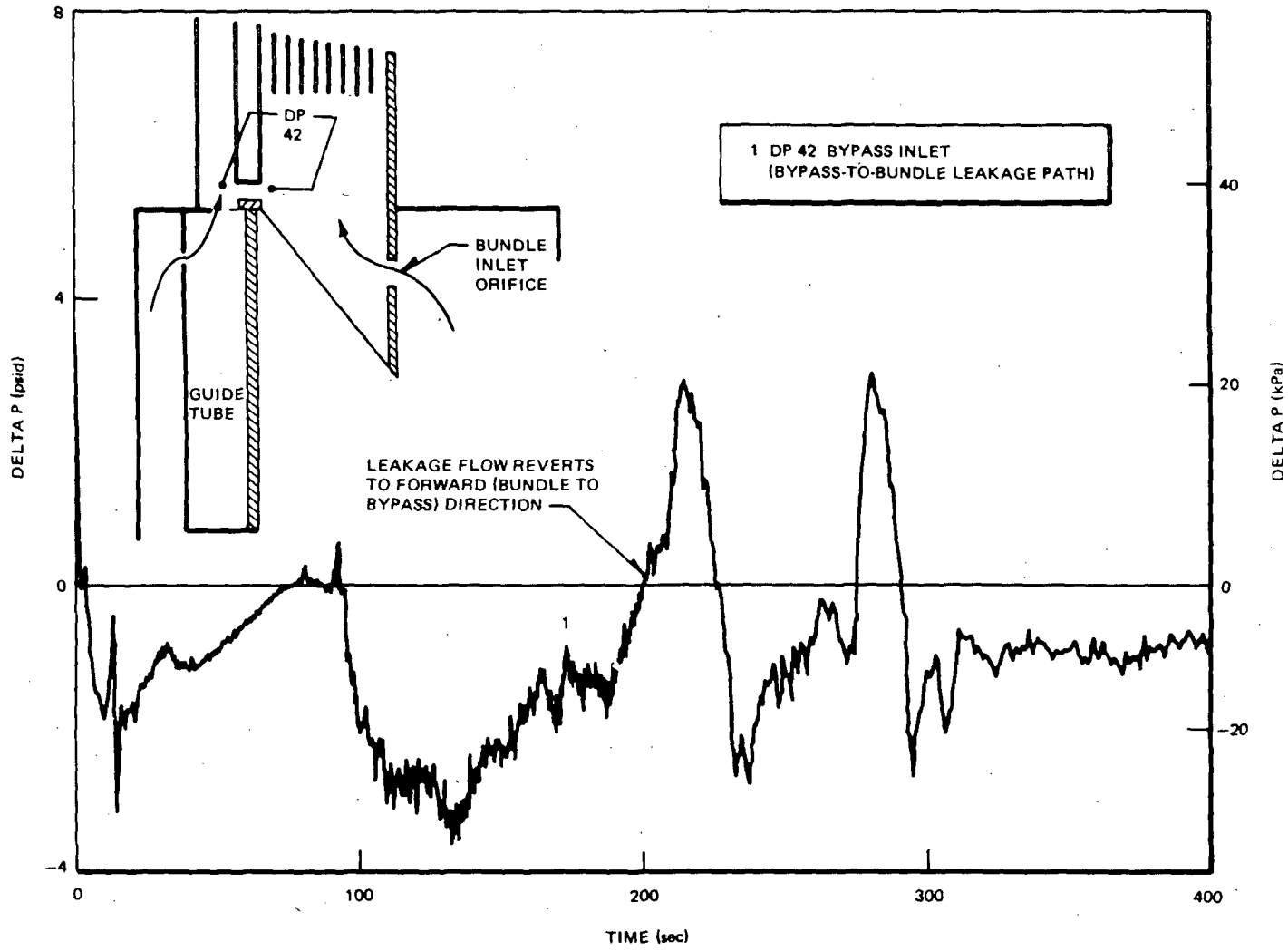

Figure M-51. Leakage Flow ΔPs

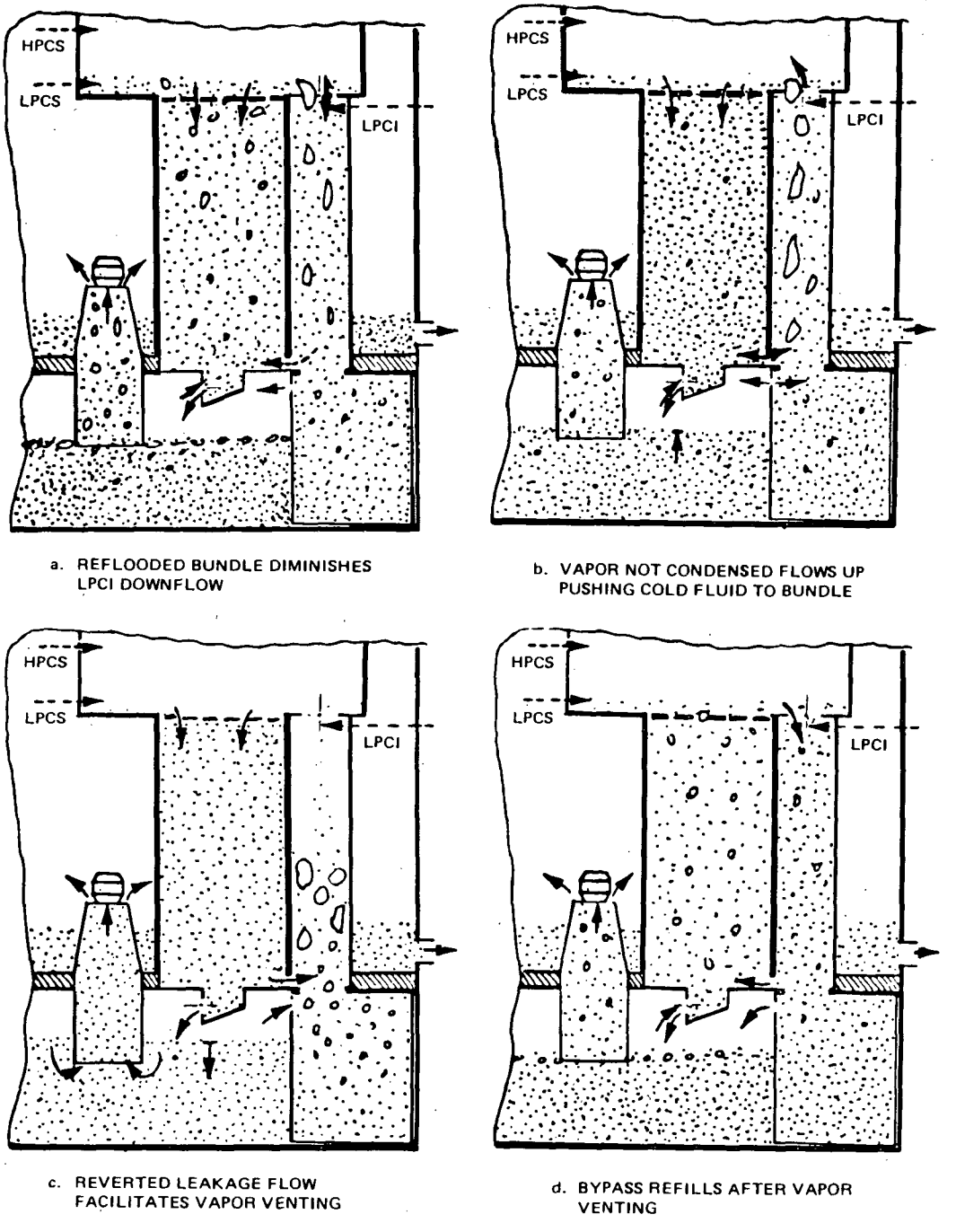

a. REFLOODED BUNDLE DIMINISHES LPCI DOWNFLOW

b. VAPOR NOT CONDENSED FLOWS UP PUSHING COLD FLUID TO BUNDLE

c. REVERTED LEAKAGE FLOW FACILITATES VAPOR VENTING

d. BYPASS REFILLS AFTER VAPOR VENTING

Figure M-52. Vapor Venting Sequence in Bypass for Test 6422, Run 3

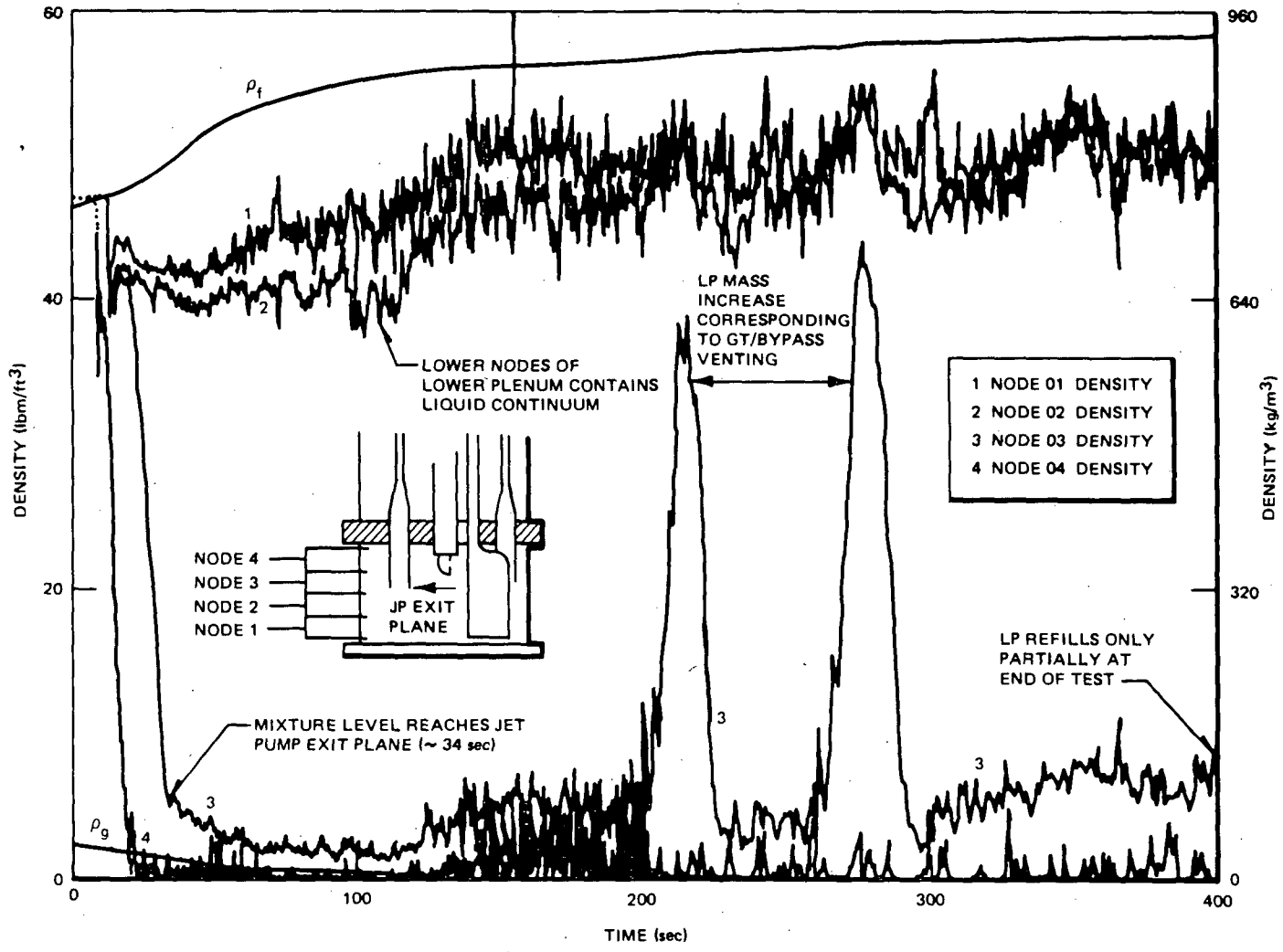

Figure M-53. Lower Plenum Nodal Densities

Appendix N

DATA REPORT FOR TEST 6423/RUN 3

Test 6423/3 was a peak power, low ECC flow, high ECC temperature test conducted in the TLTA 5A facility. A diagram of the system instrumentation showing measurement nodes is given in Figure N-1. Figure N-2 shows a schematic of the bundle and locations of the pressure transducer taps and thermocouples. The core lattice arrangement and the local peaking factor distribution is shown in Figure N-3.

Tables N-1 and N-2 summarize the initial conditions and sequence of events for Test 6423/3. Primary measurements throughout the transient are given in Figures N-4 to N-37, derived quantities in Figures N-38 to N-57. A guide for interpreting bundle temperature plots is shown in Figure N-58, and the bundle temperature measurements are given in Figures N-59 to N-78. Figure N-79 gives the peak cladding temperature.

Table N-1

TEST 6423 RUN 3 INITIAL CONDITIONS

Initial Conditions	
Bundle power	6.46 ± 0.03MW
Steam dome pressure	1037 ± 5 psia
Lower plenum pressure	1065 ± 5 psia
Lower plenum enthalpy	518 ± 5 Btu/lbm
Initial water level	123 ± 6 in. El
Feedwater enthalpy	41 ± 2 Btu/lbm
Bundle inlet to outlet DP	16 ± 2 psi
Steam flow	7 ± 1 lbm/sec
Feed water flow	1.0 ± 0.3 lbm/sec
Drive Pump 1 flow	8.1 ± 1.0 lbm/sec
Drive Pump 2 flow	8.3 ± 1.0 lbm/sec
Jet Pump 1 flow	17 ± 2 lbm/sec
Jet Pump 2 flow	19 ± 2 lbm/sec
Bundle inlet flow	33 ± 5 lbm/sec
ECC fluid temperature	200 ± 15°F

All uncertainty bands are judged from the maximum of data fluctuation and/or absolute uncertainties of the measurements.

Table N-2

SEQUENCE OF EVENTS FOR 6423 RUN 3
(PEAK POWER, LOW ECC)

Event	Time (sec)
Blowdown valves open	0.0
Bundle power decay initiated	0.5
Feedwater flow stops	0.5
Bypass flow reverses	1.5
Steamline valve completely closed	11.5
Lower plenum bulk flashing	15
Loop 1 isolated	20
HPCS injection begins	27
Lower plenum mixture level reaches jet pump exit plane	39
LPCS, LPCI activated	37
LPCS flow begins	65
LPCI flow begins	72
End of test	400

NOTES:

1. P - PRESSURE
   DP - DIFFERENTIAL PRESSURE
   T - TEMPERATURE (RTD - RESISTANCE THERM)
   SP - VALVE STEM POSITION
   RO - RESTRICTING ORIFICE
   FE - FLOW ELEMENT
   S - PUMP SPEED
   LP - LEVEL PROBE
   DD - DRAG DISK
   TM - TURBINE METER

2. N305 - 54.88 MEANS NOZZLE NO. 305 IS AT AN ELEVATION OF 54.88 INCHES. IT DOES NOT REFER TO ACTUAL LOCATION OF THE NODAL POINT.

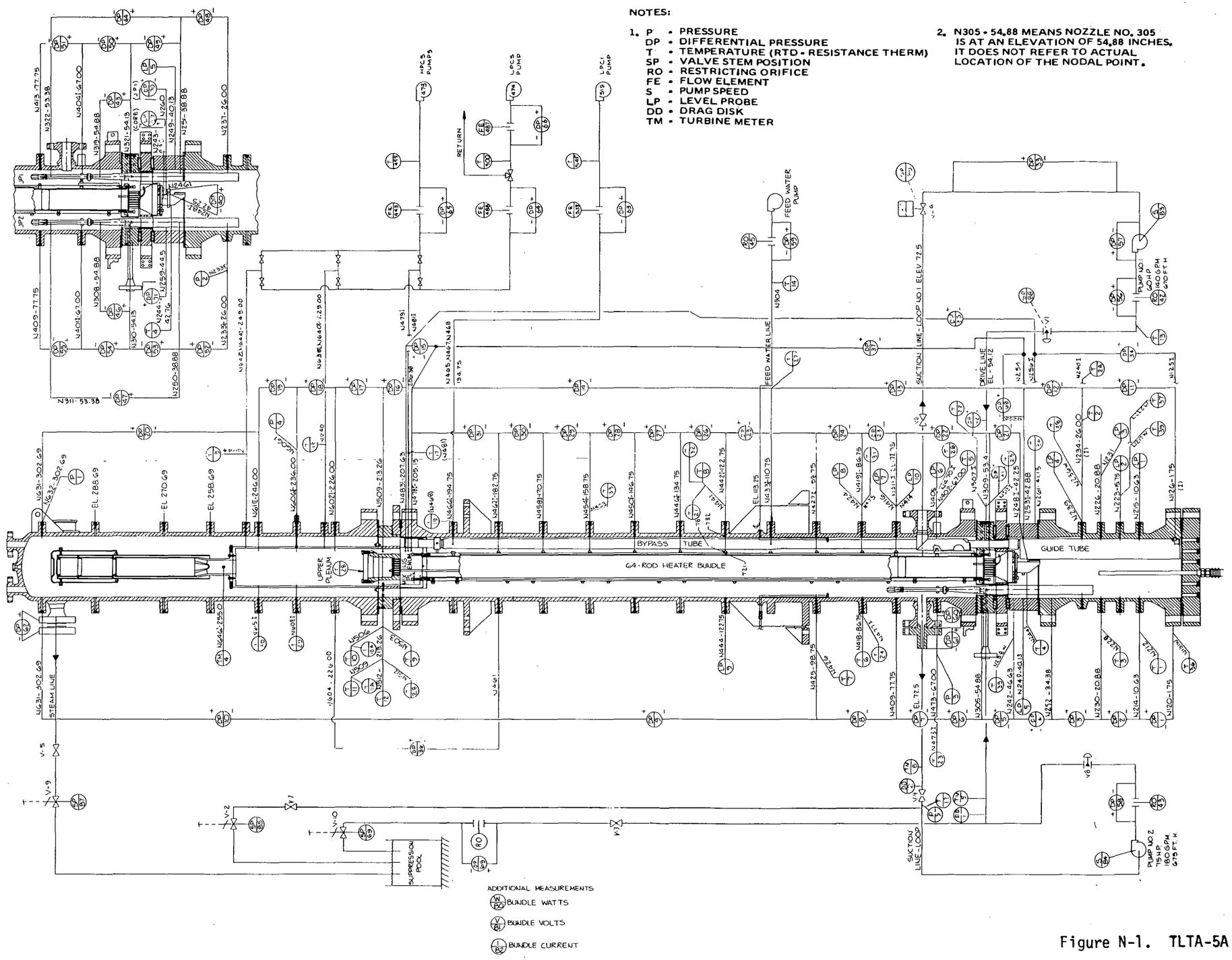

Figure N-1. TLTA-5A Instrumentation

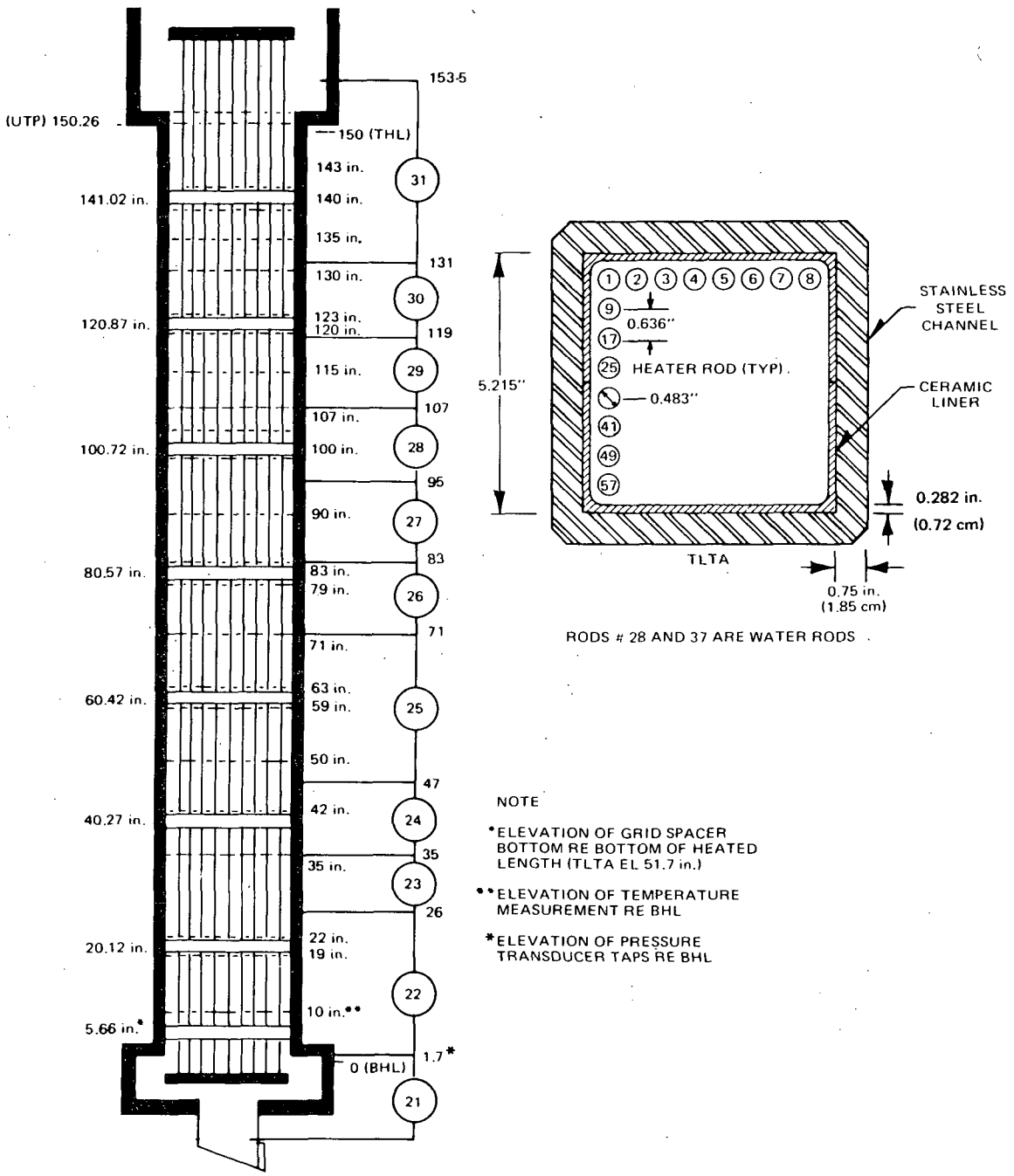

Figure N-2. TLTA-5A Bundle Instrumentation and Dimensions

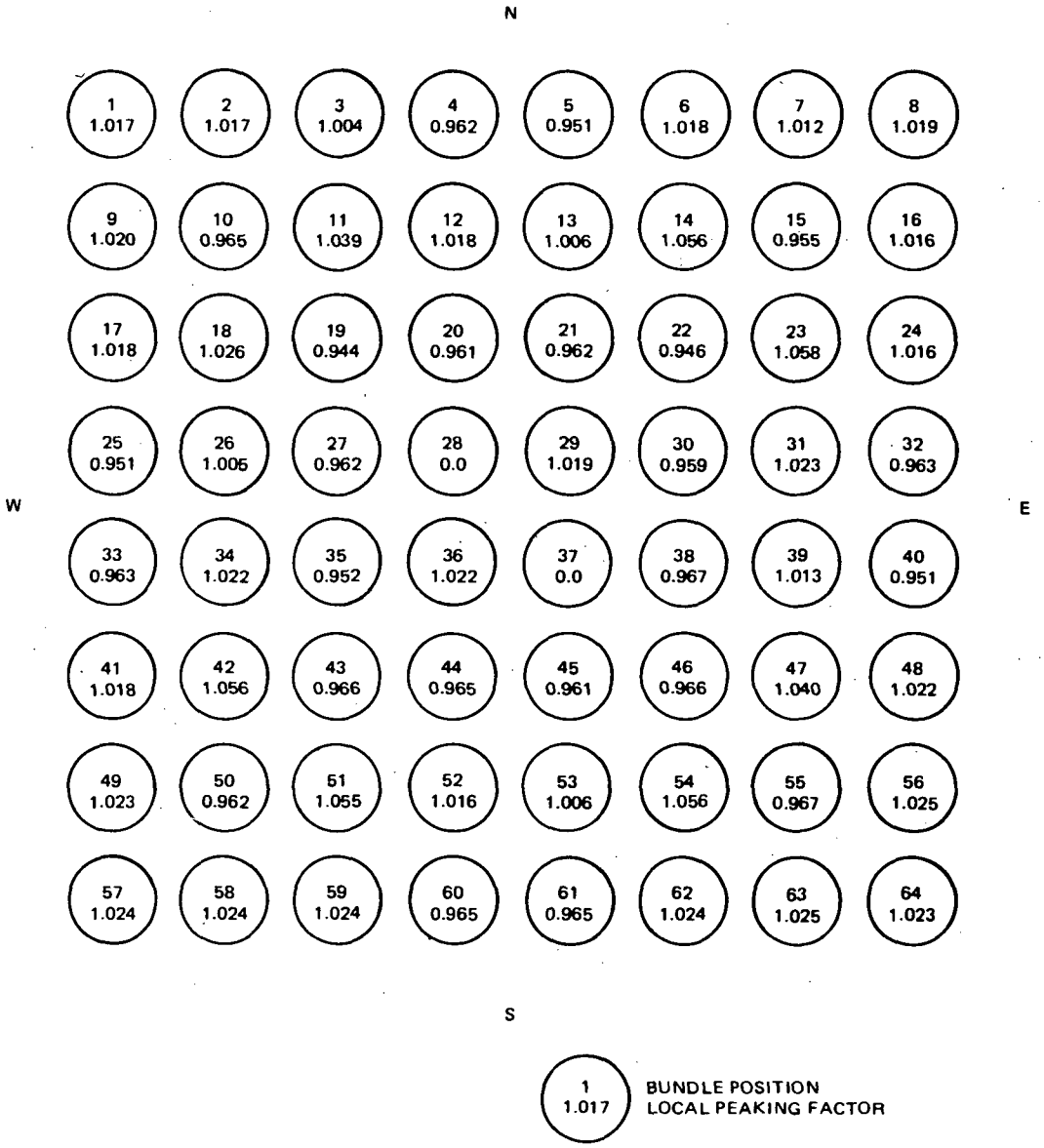

Figure N-3. Local Peaking Factor Distribution

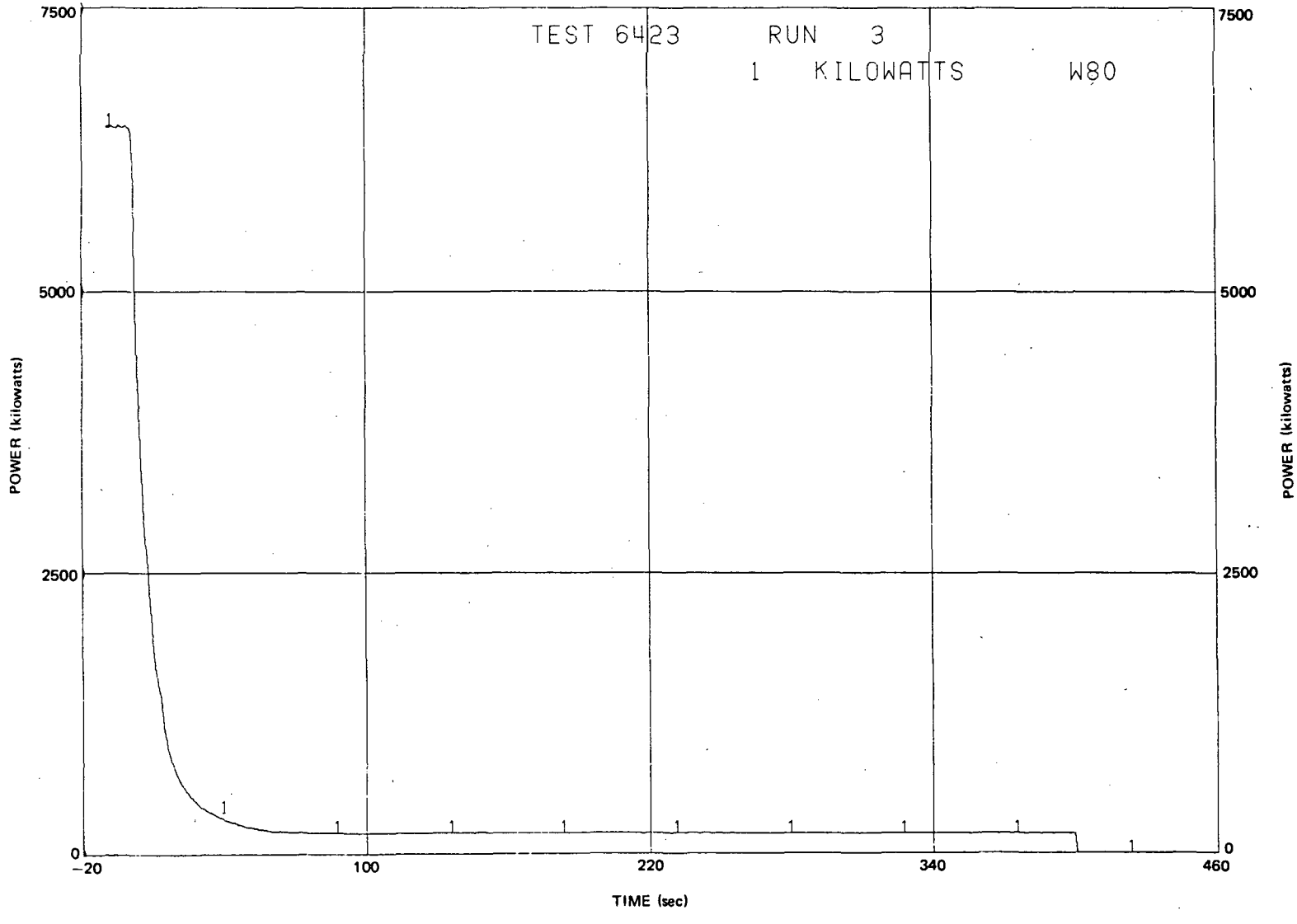

Figure N-4. Bundle Power Decay

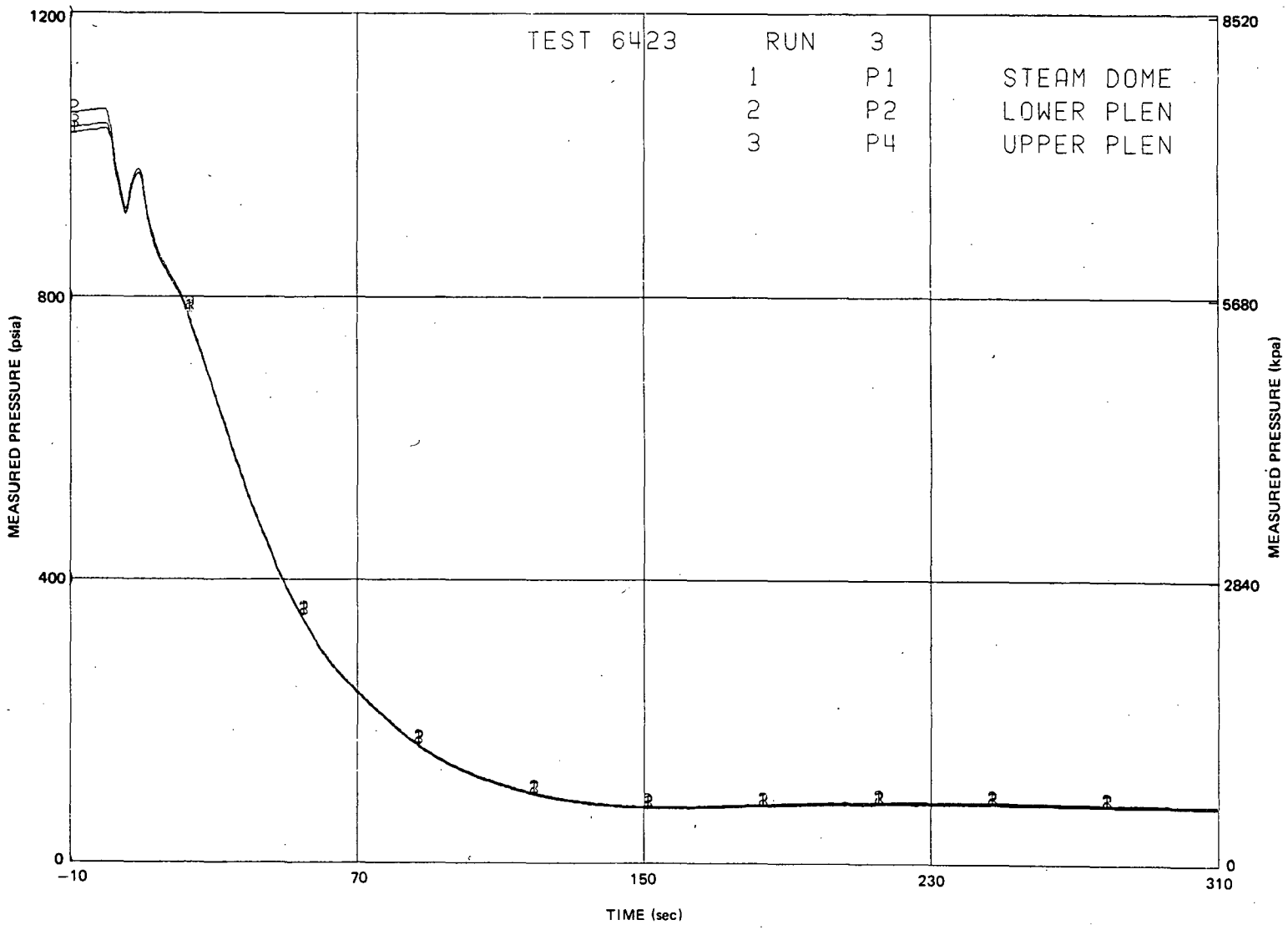

Figure N-5. System Pressures

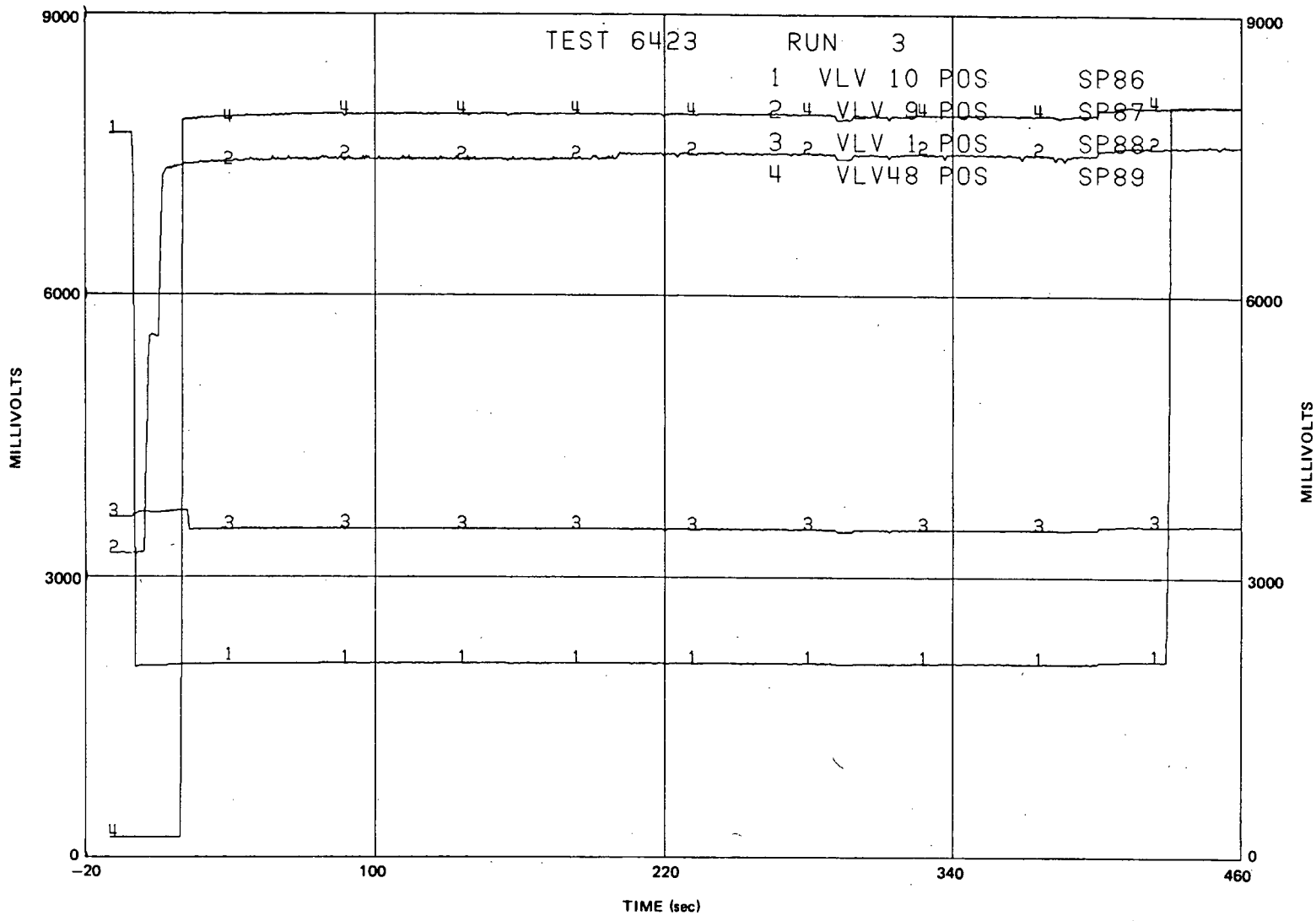

Figure N-6. Valve Positions

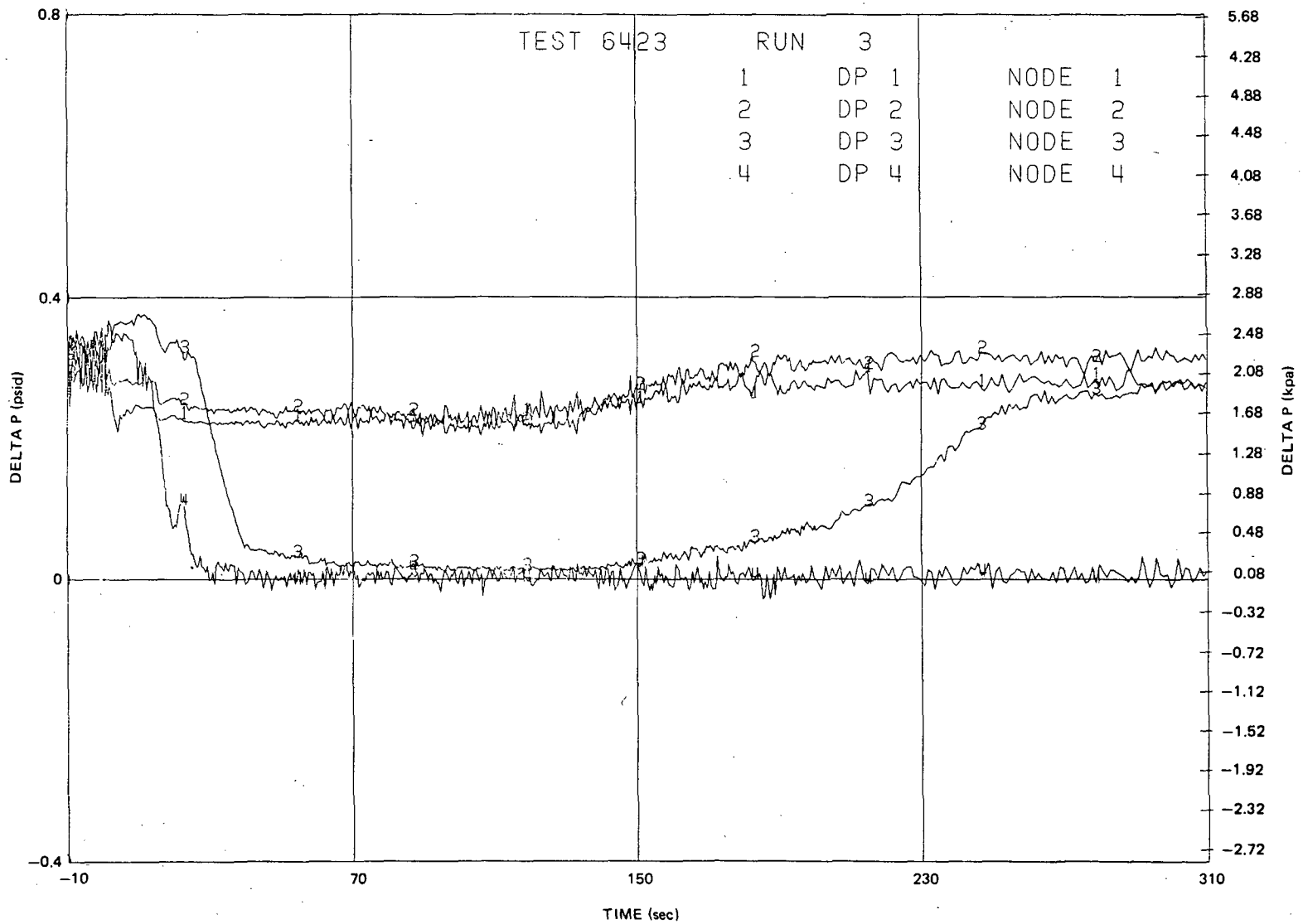

Figure N-7. Lower Plenum Differential Pressures

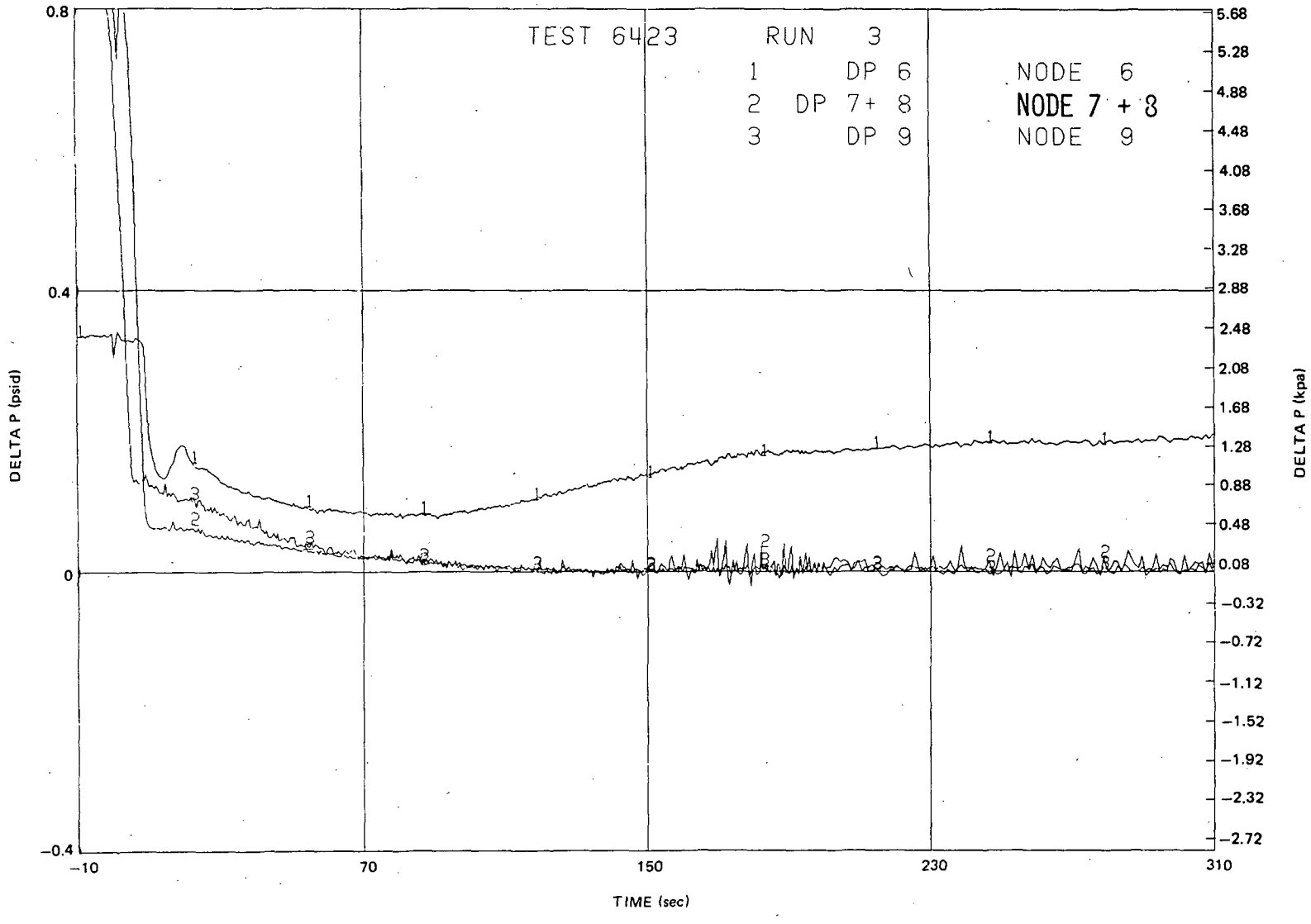

Figure N-8. Annulus Differential Pressures

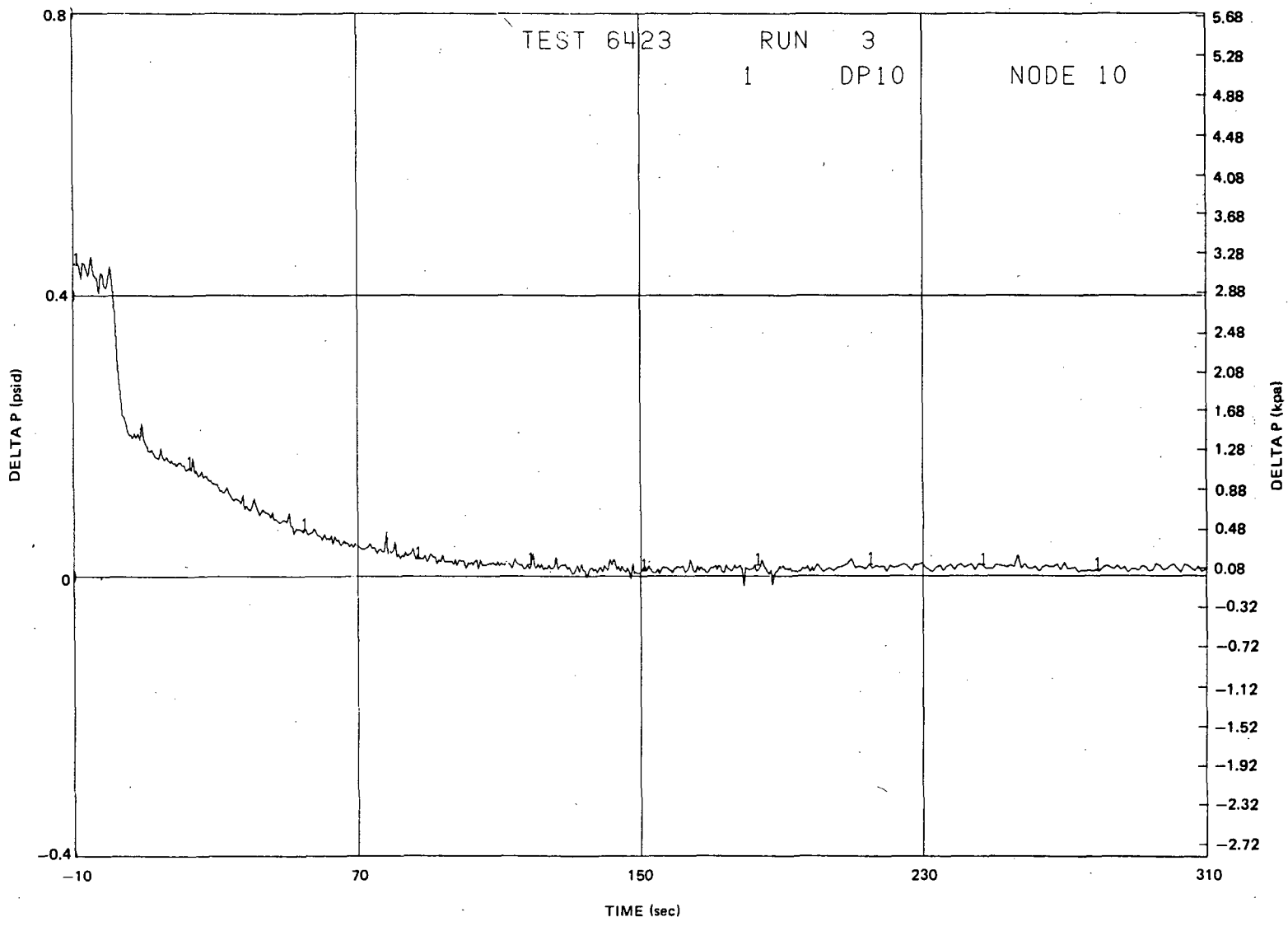

Figure N-9. Upper Annulus Differential Pressure

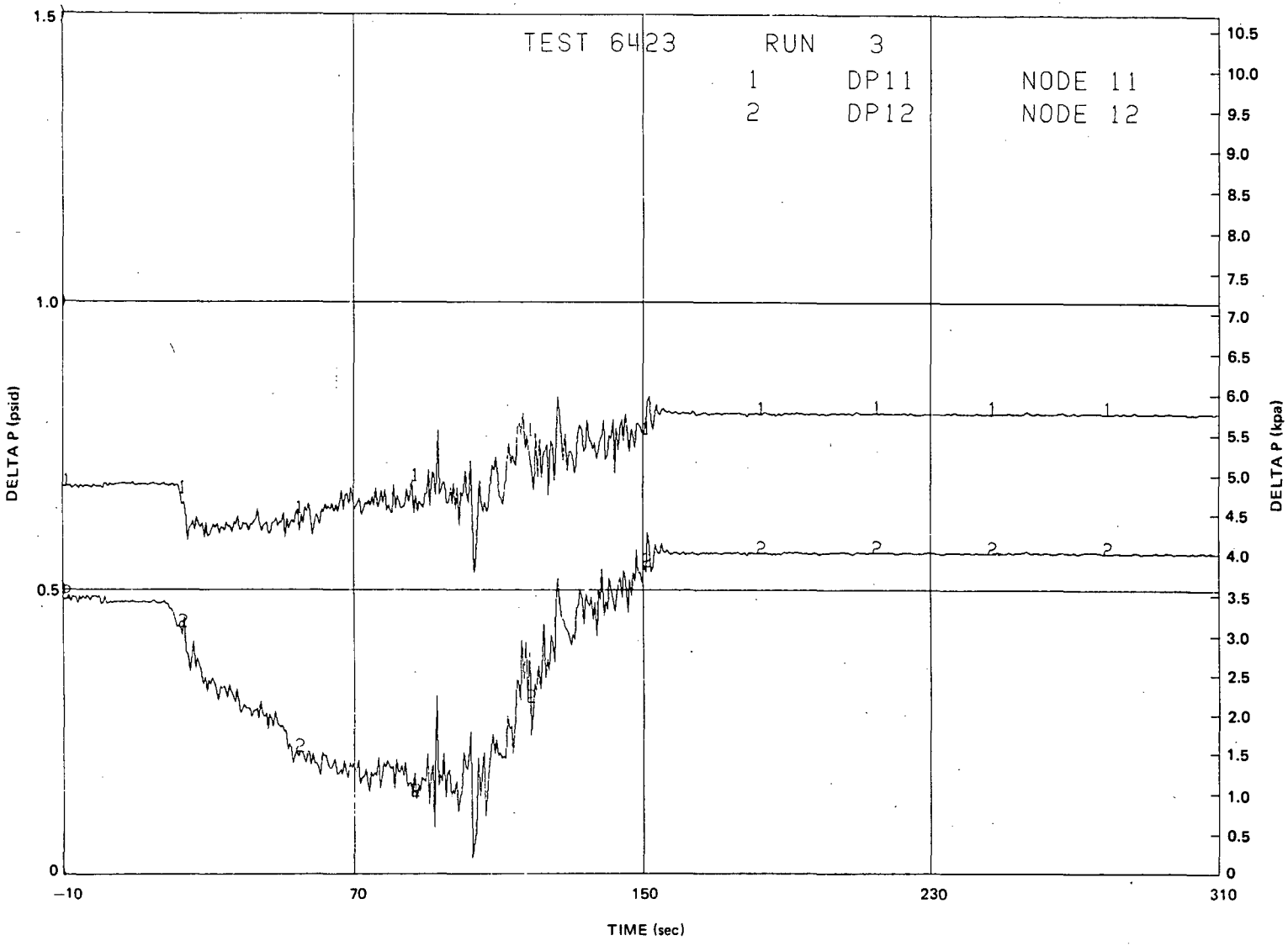

Figure N-10. Guide Tube Differential Pressures

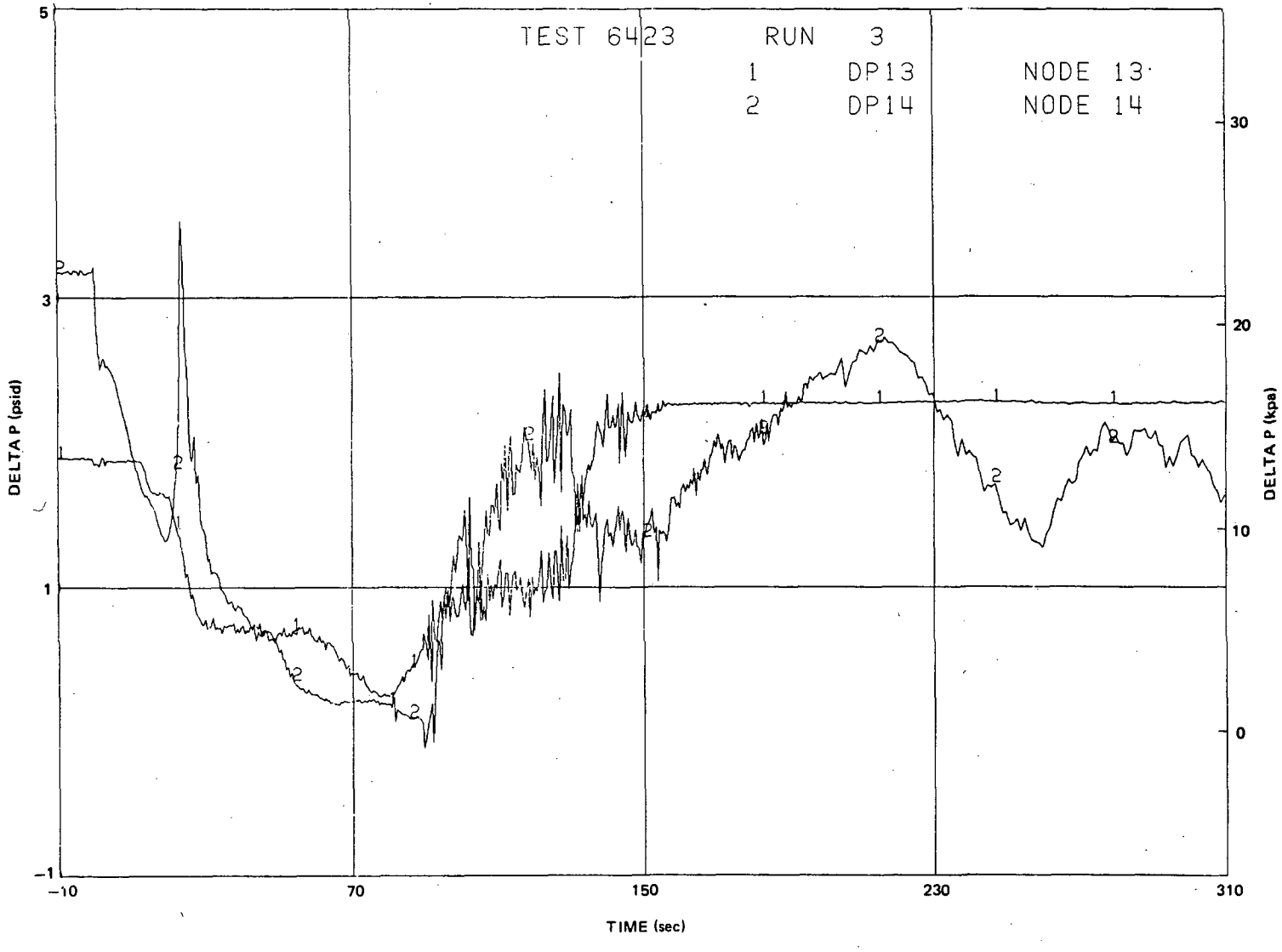

Figure N-11. Bypass Differential Pressures

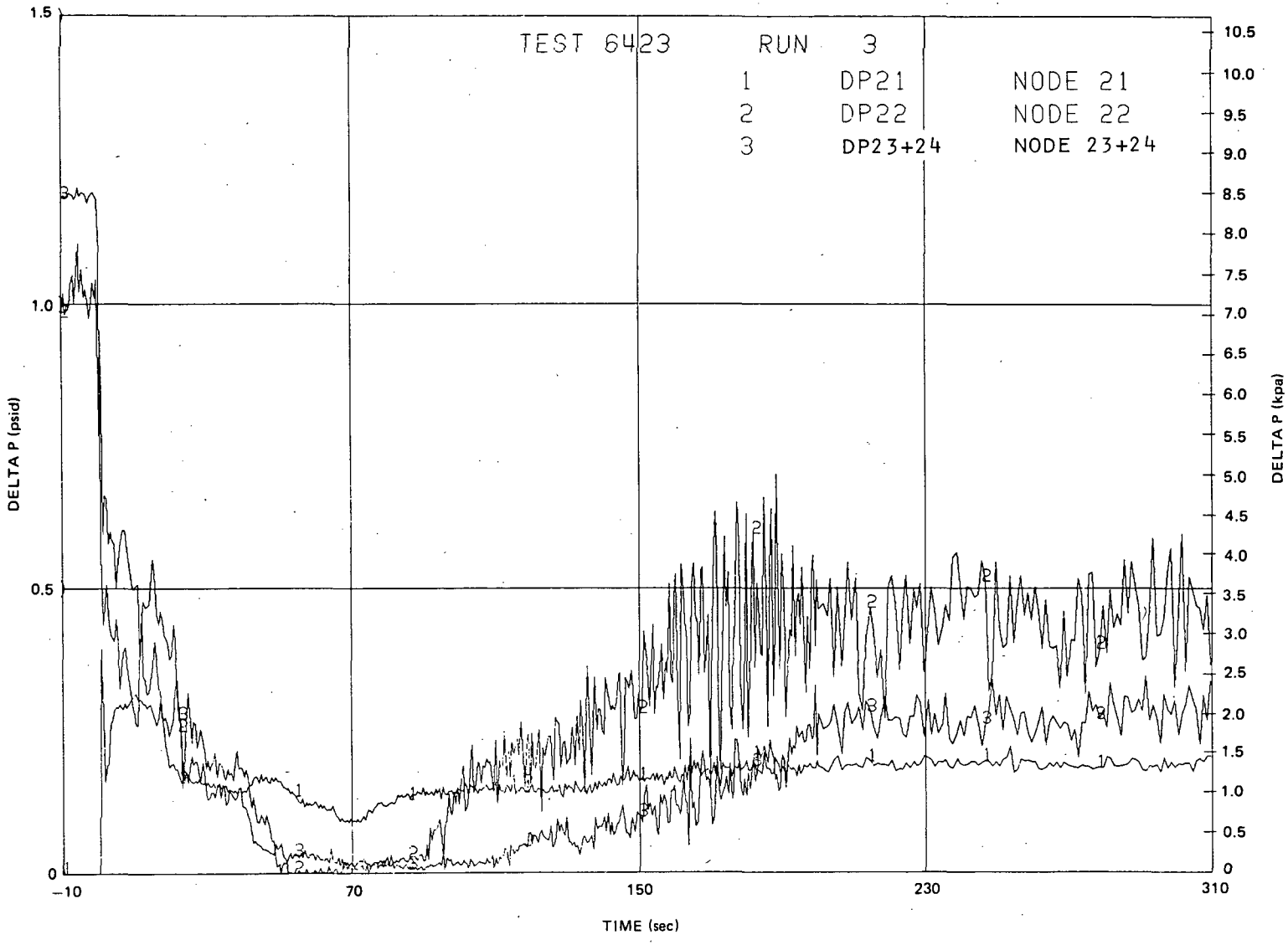

Figure N-12. Lower Bundle Differential Pressures

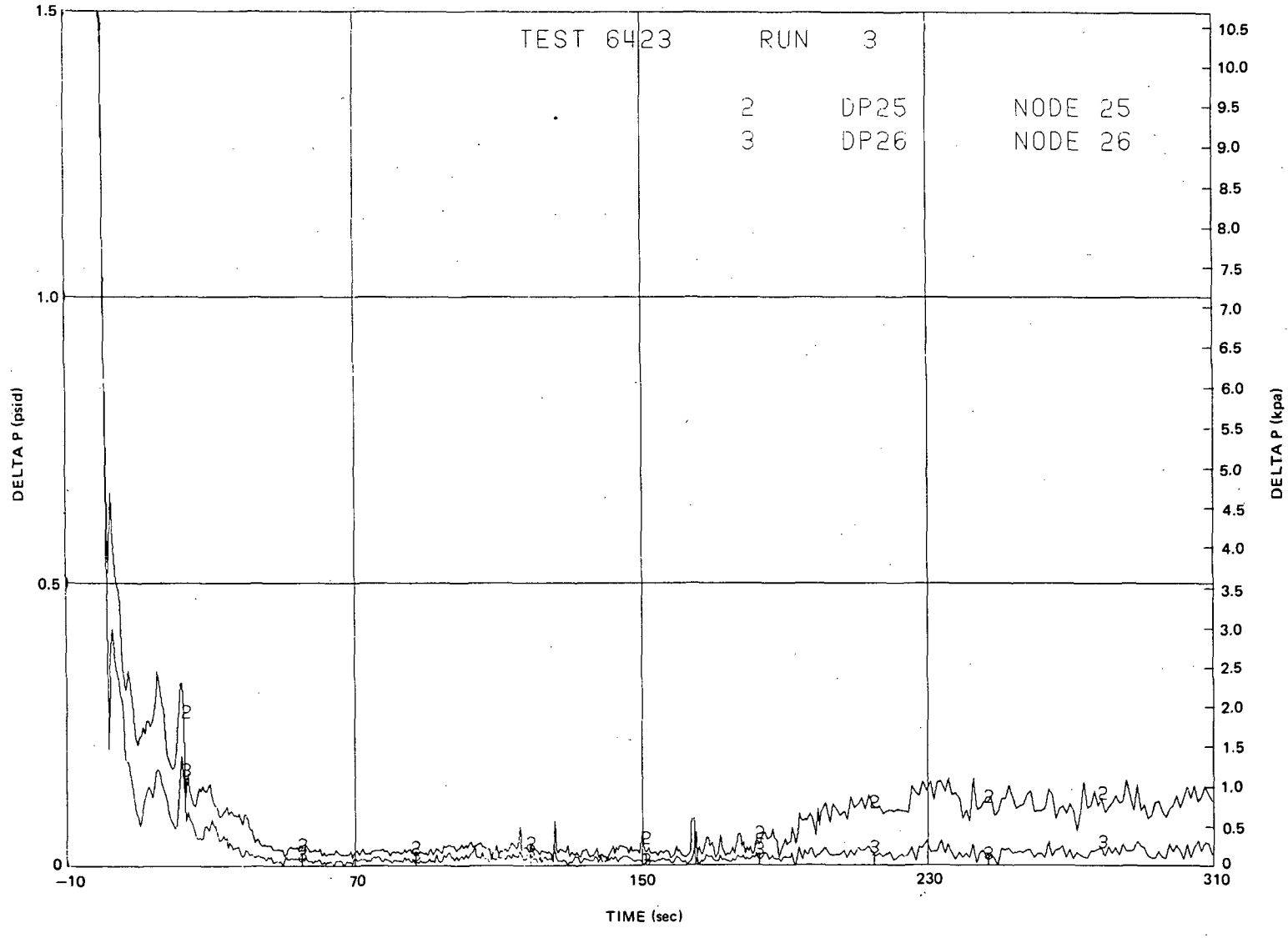

Figure N-13. Middle Bundle Differential Pressures

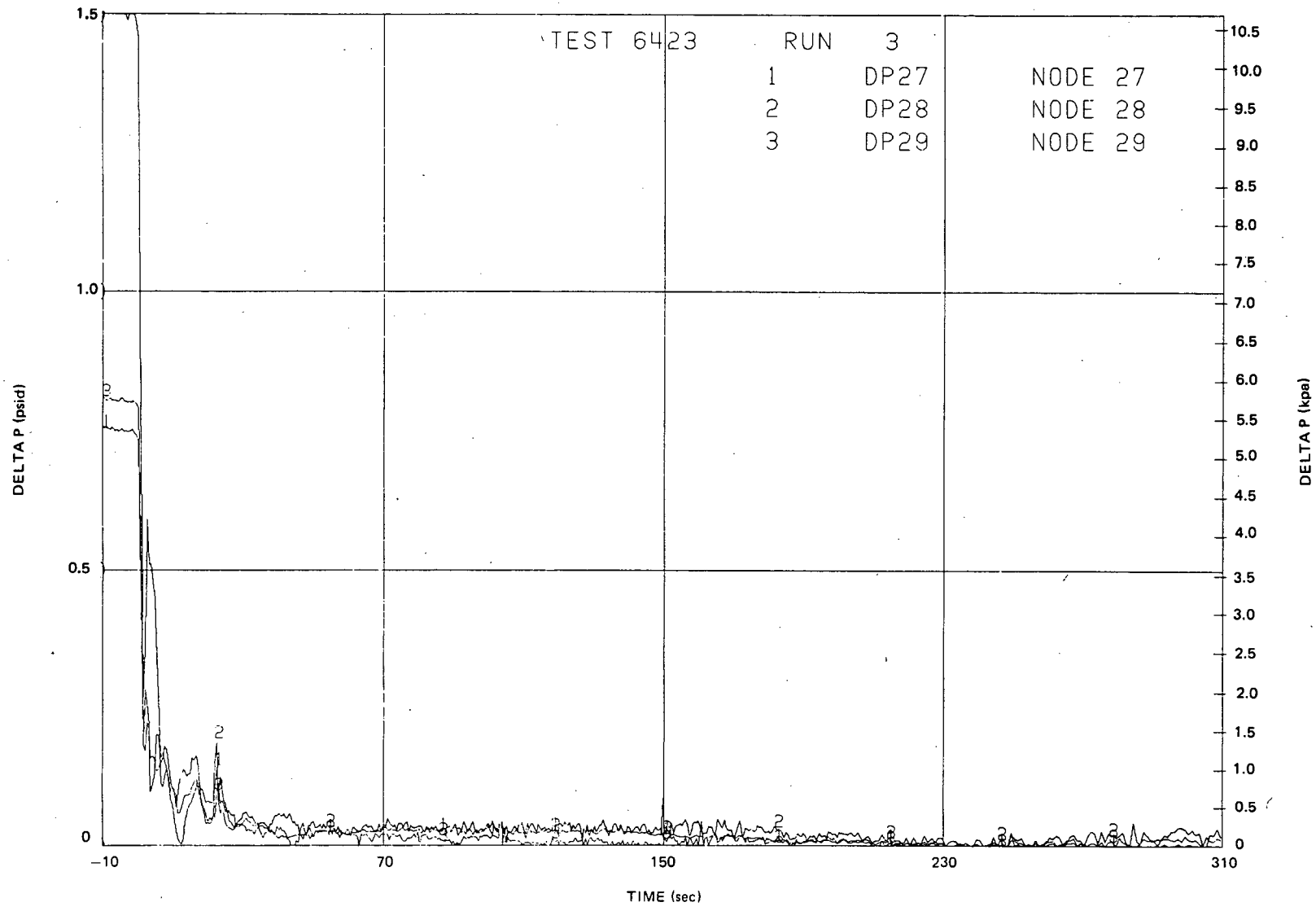

Figure N-14. Upper Bundle Differential Pressures

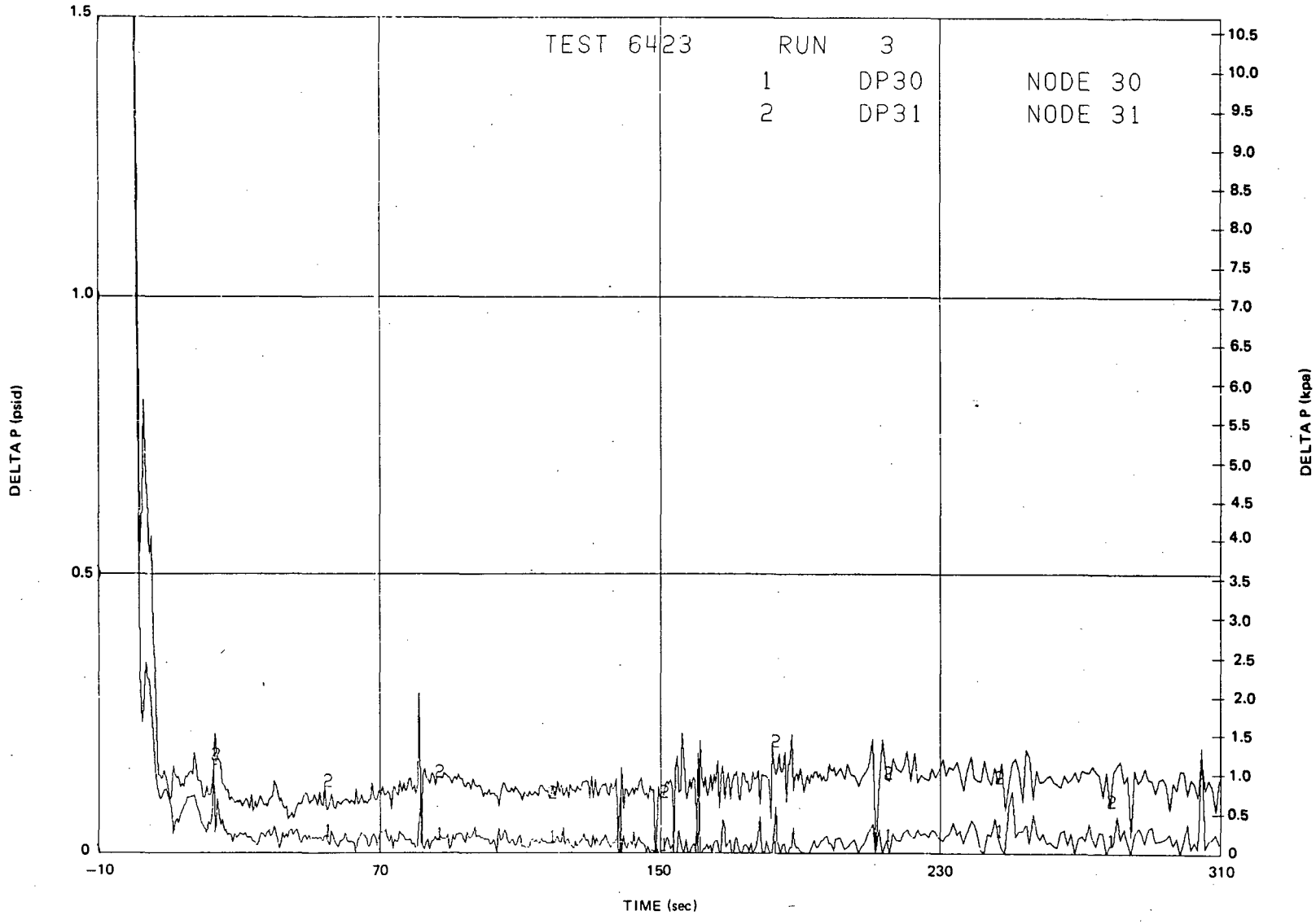

Figure N-15. Top Bundle Differential Pressures

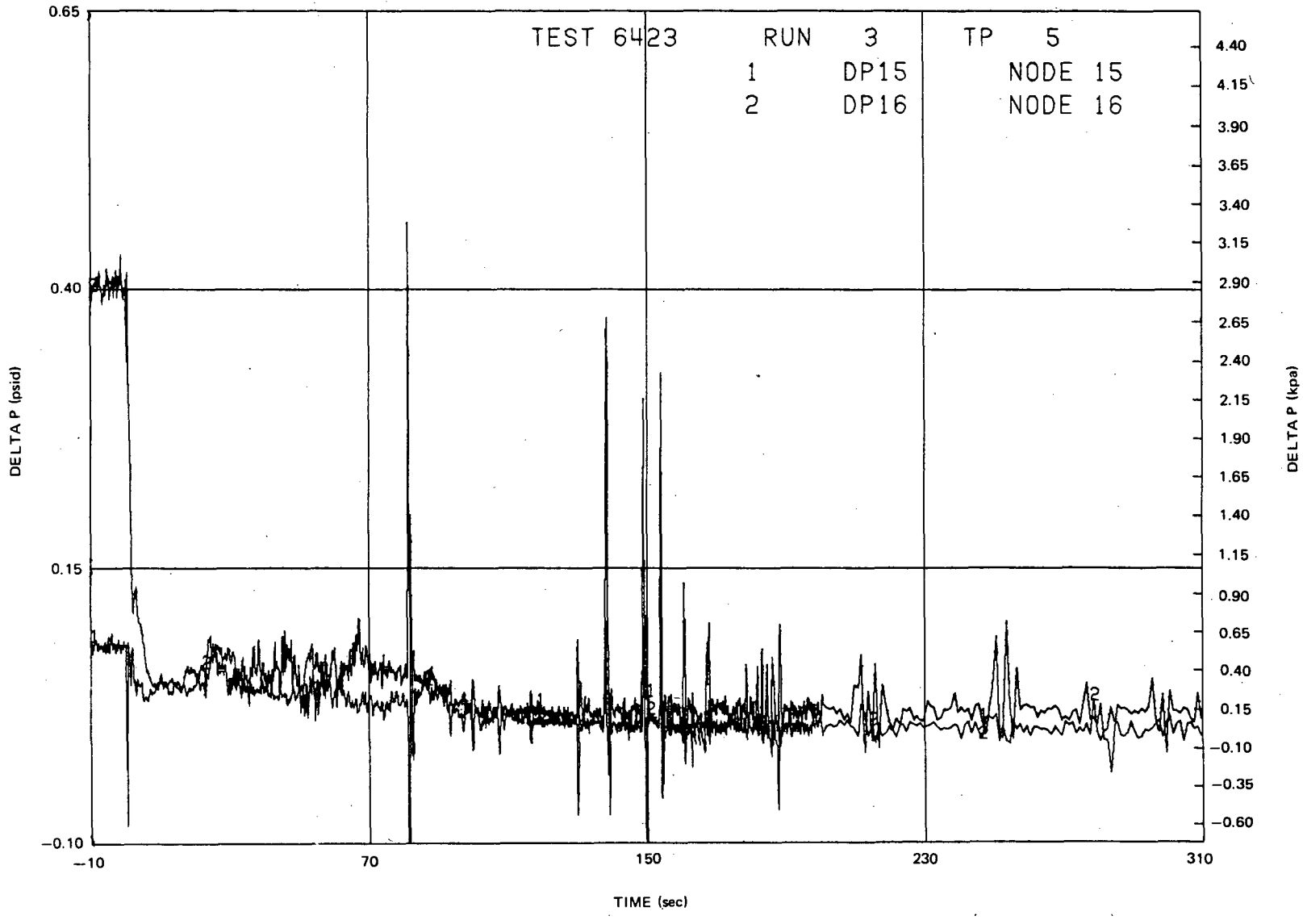

Figure N-16. Mixing Plenum Differential Pressures

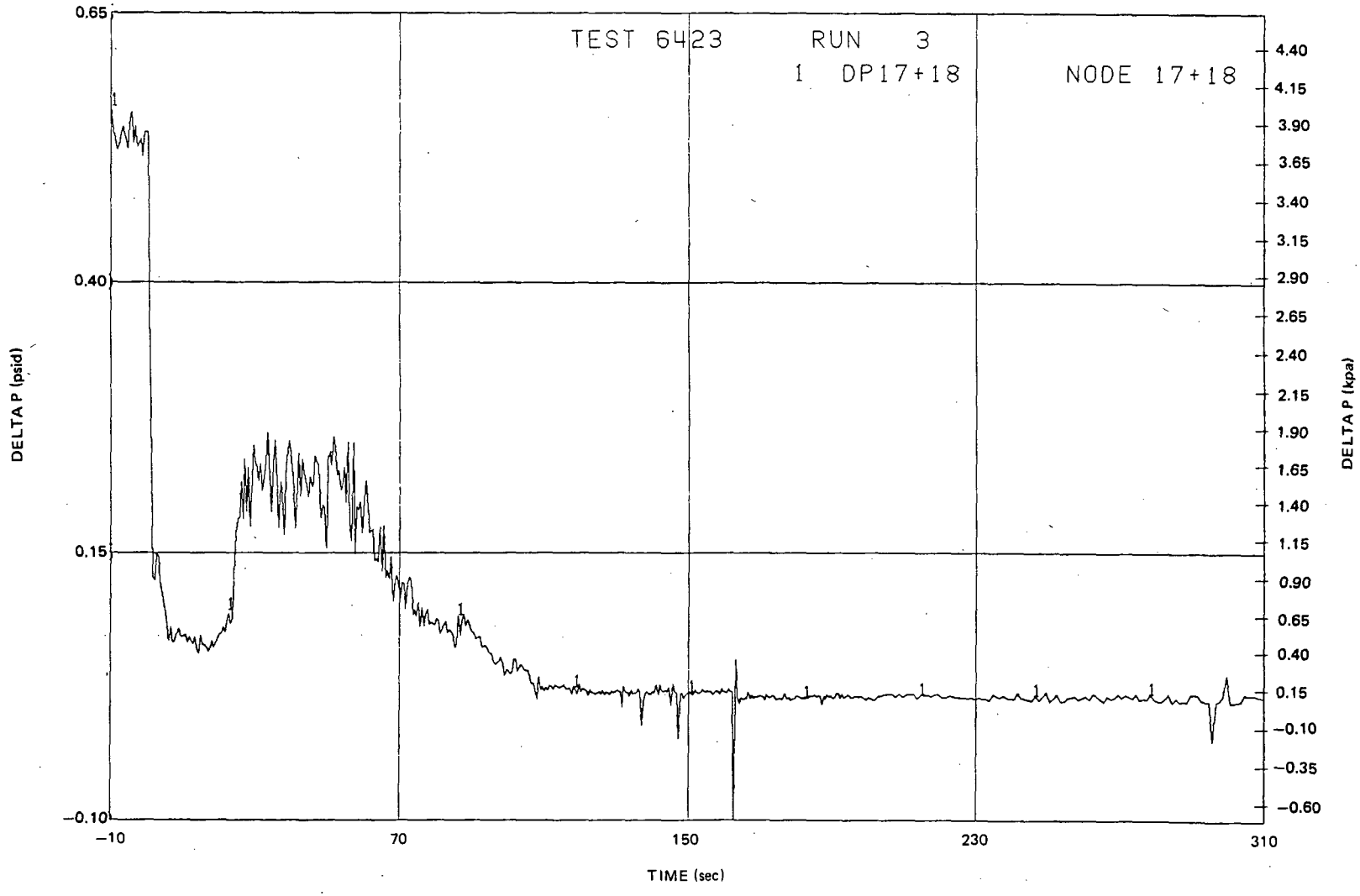

Figure N-17. Upper Plenum Differential Pressures

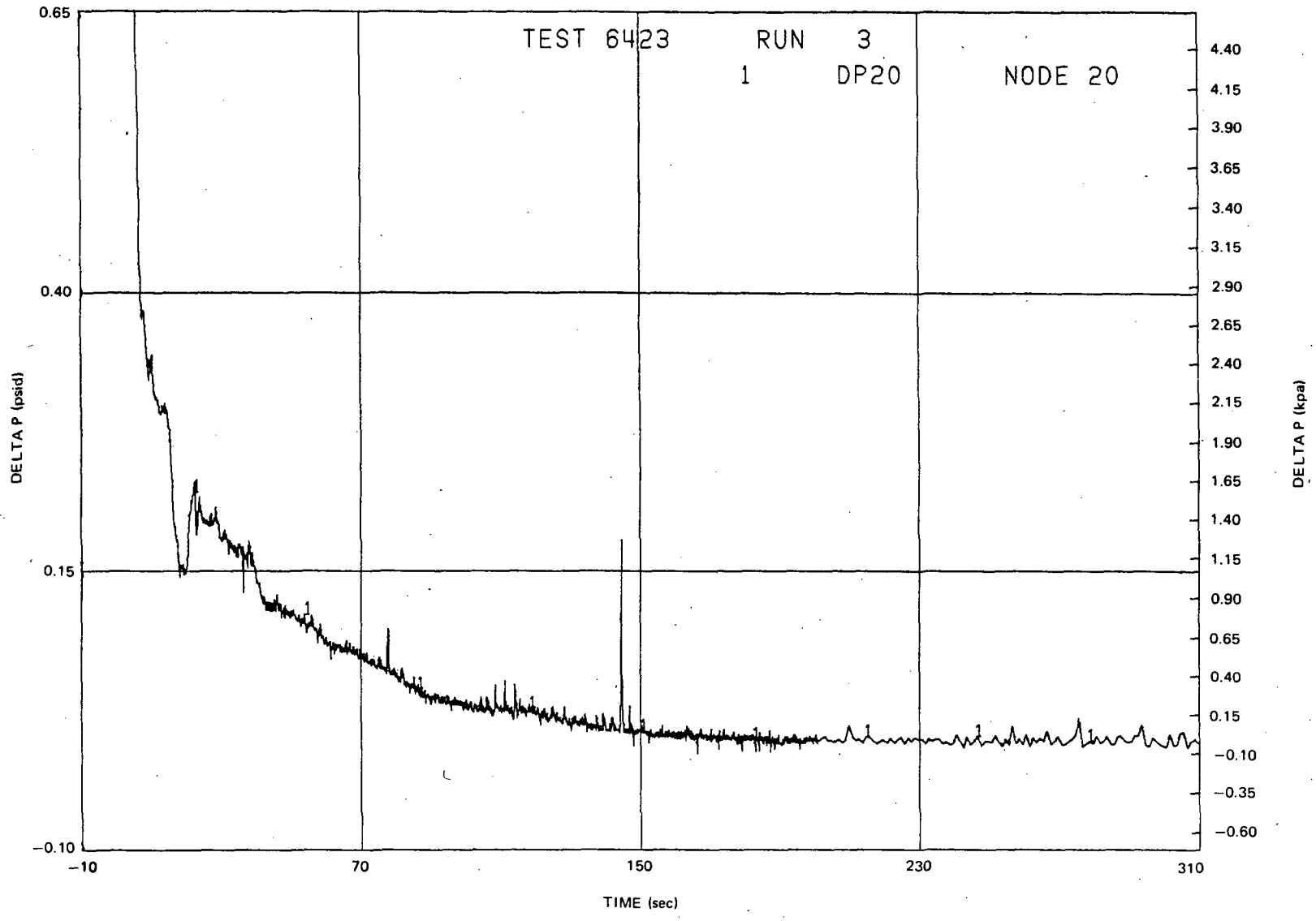

Figure N-18. Steam Separator Differential Pressure

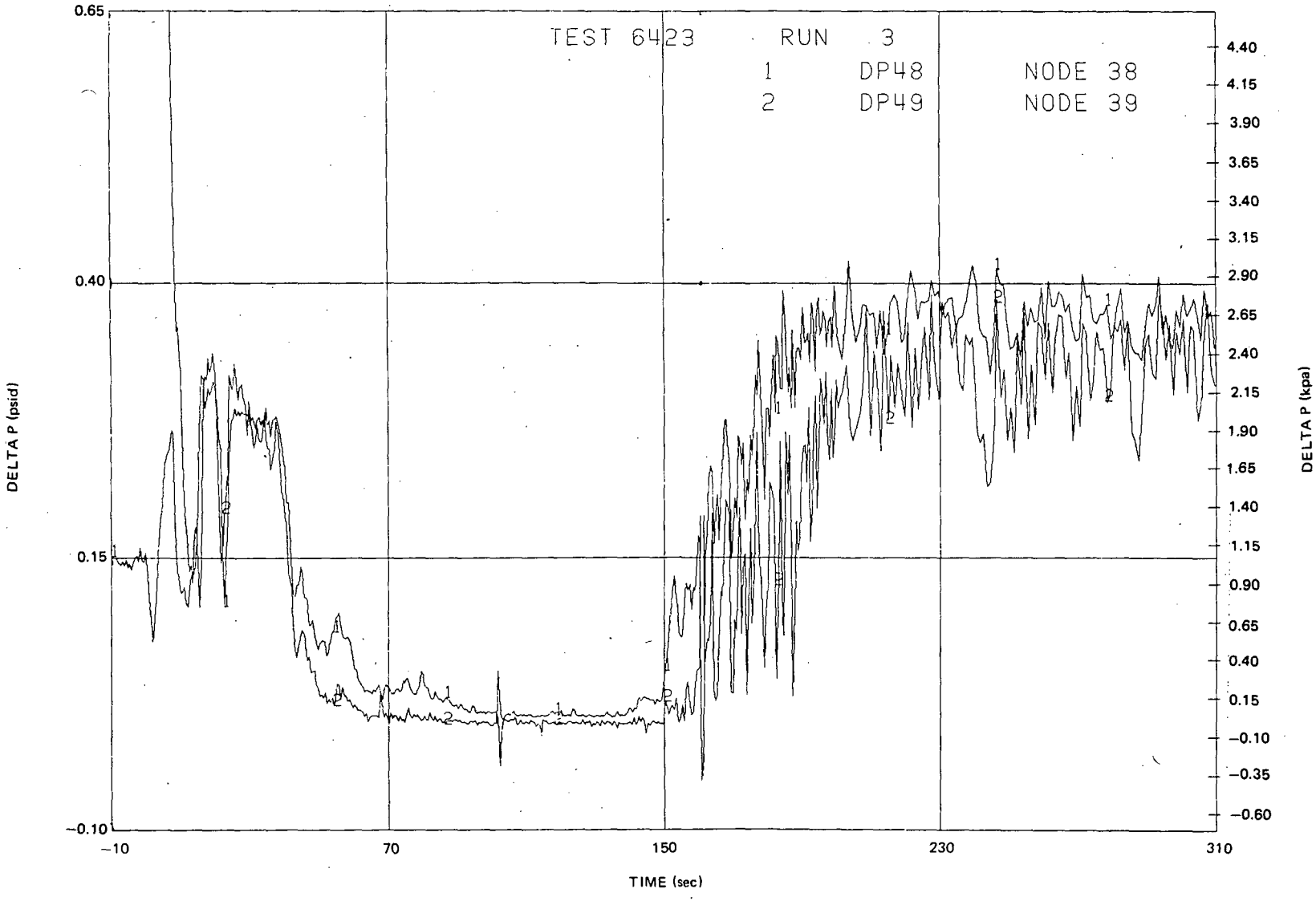

Figure N-19. Intact Loop Jet Pump Differential Pressures

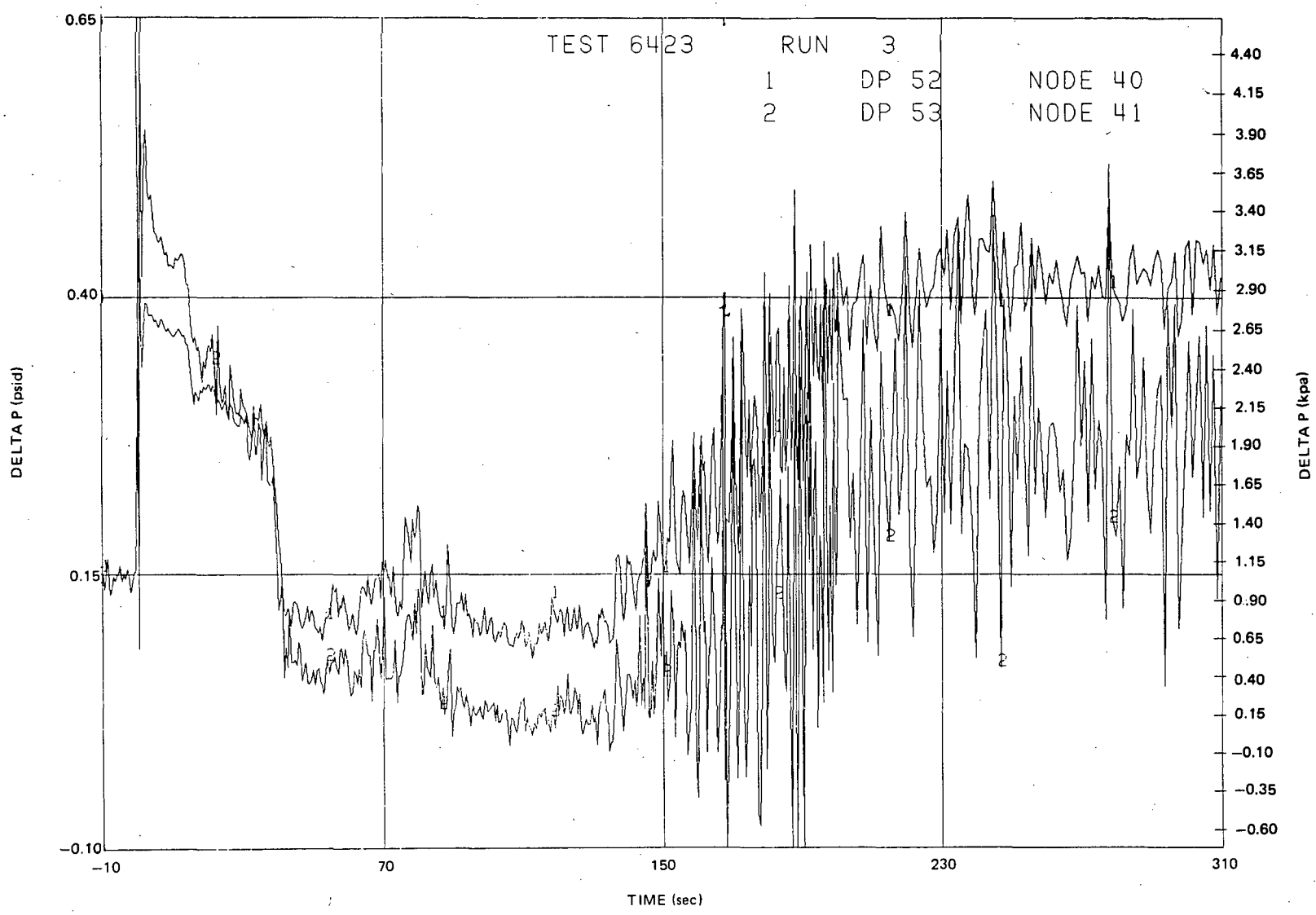

Figure N-20. Broken Loop Jet Pump Differential Pressures

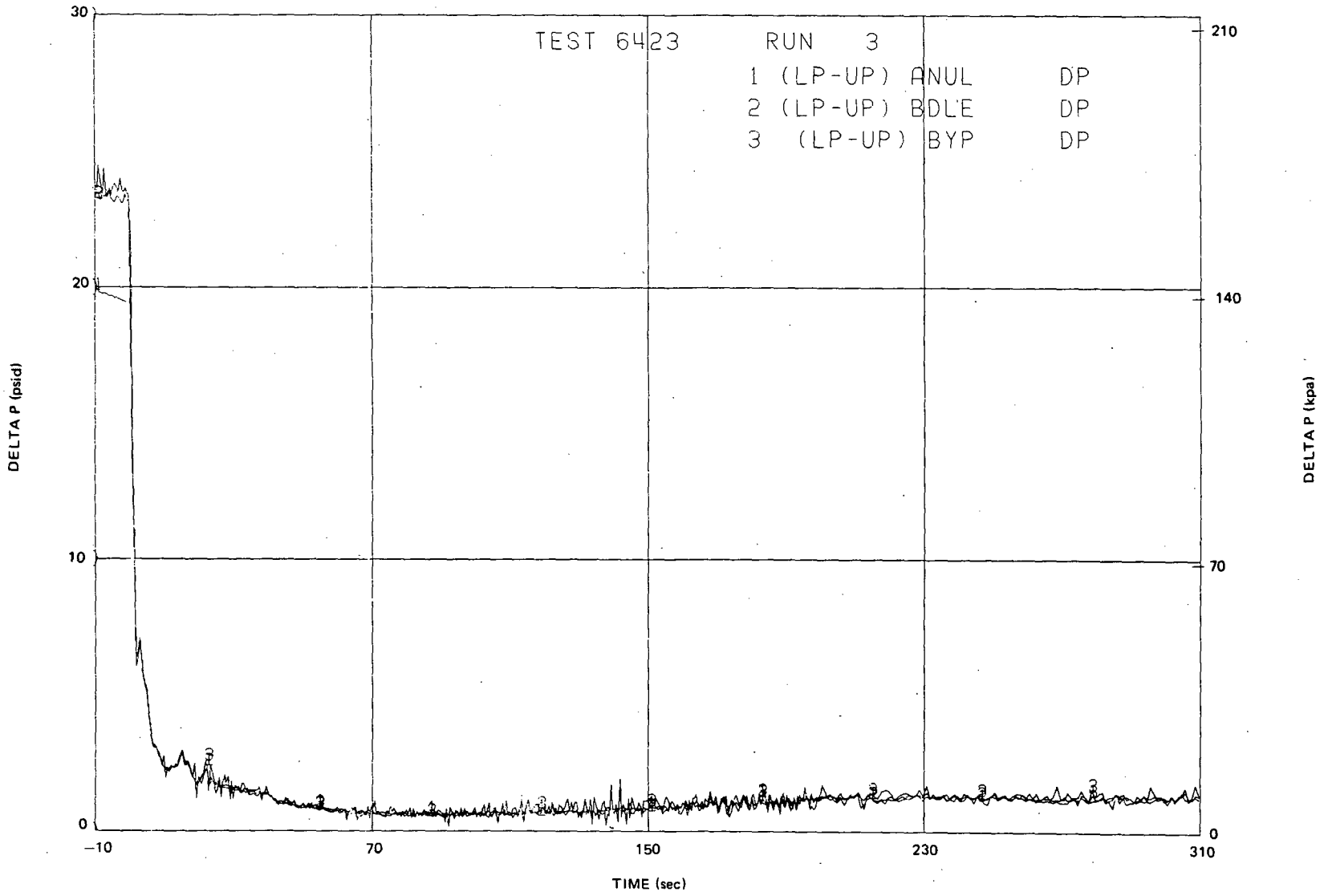

Figure N-21. Lower Plenum to Upper Plenum Differential Pressures for Annulus, Bundle, and Bypass

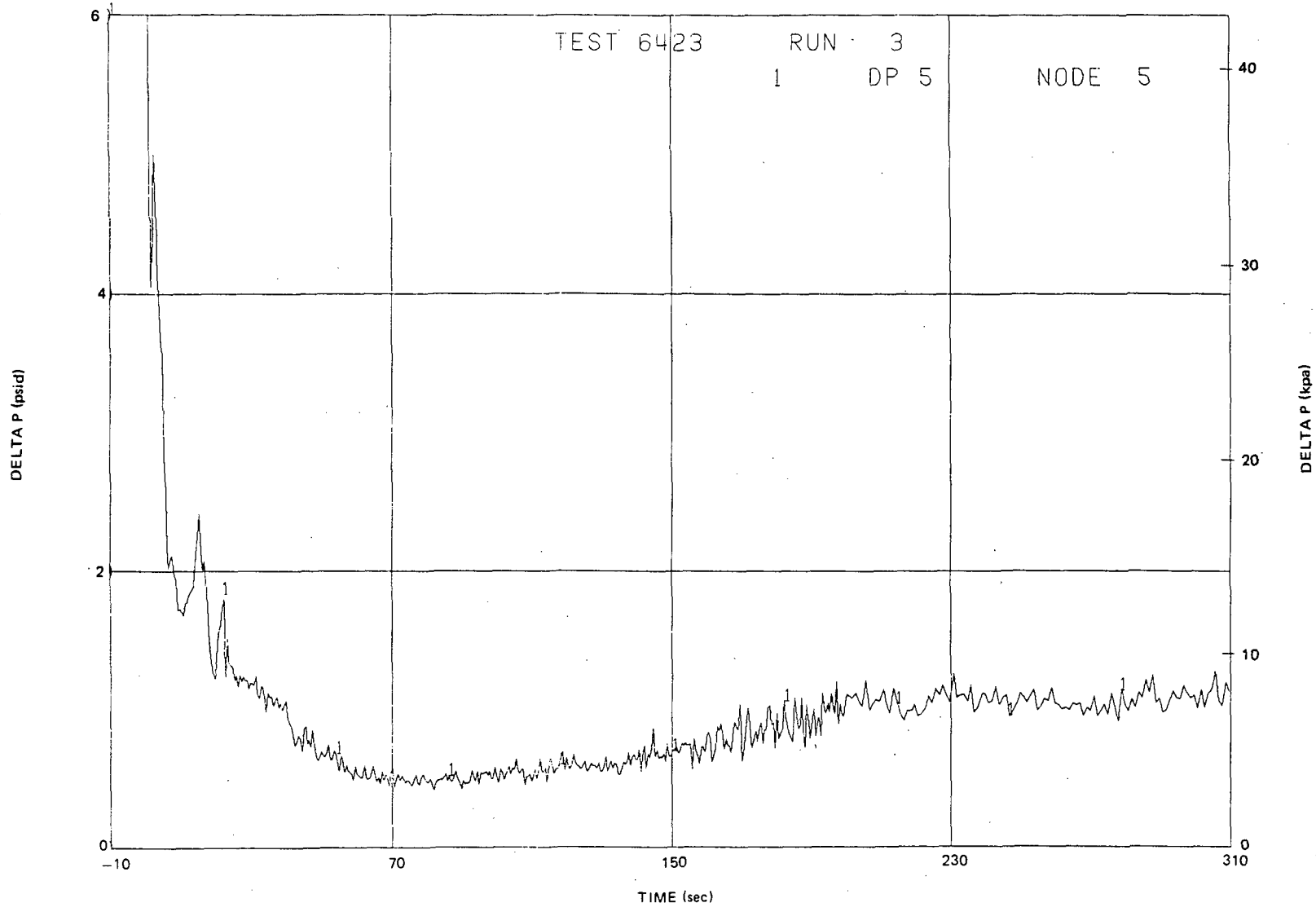

Figure N-22. Lower Plenum to Annulus Differential Pressure

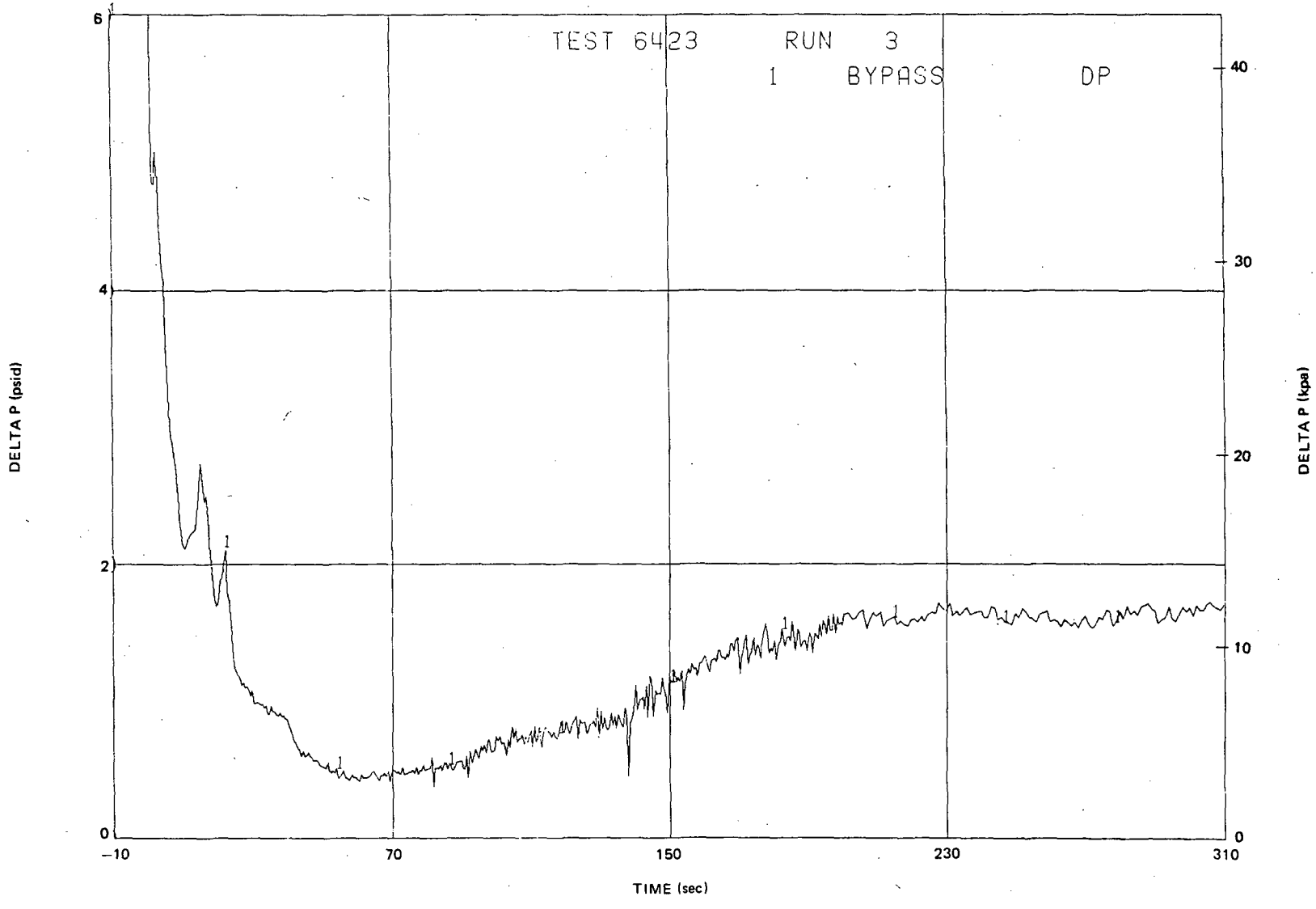

Figure N-23. Bypass Differential Pressure

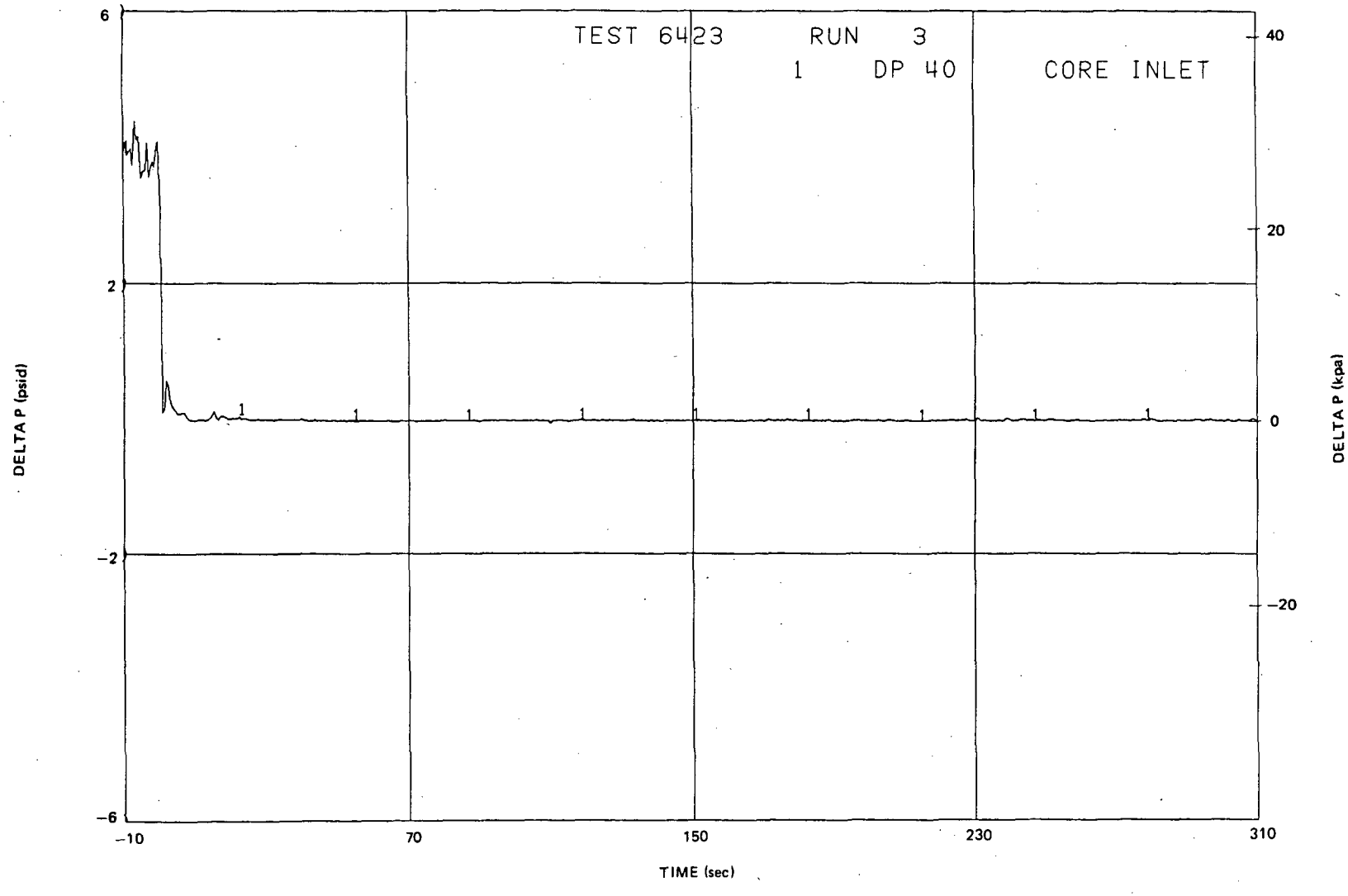

Figure N-24. Bundle Inlet Side Entry Orifice Differential Pressure

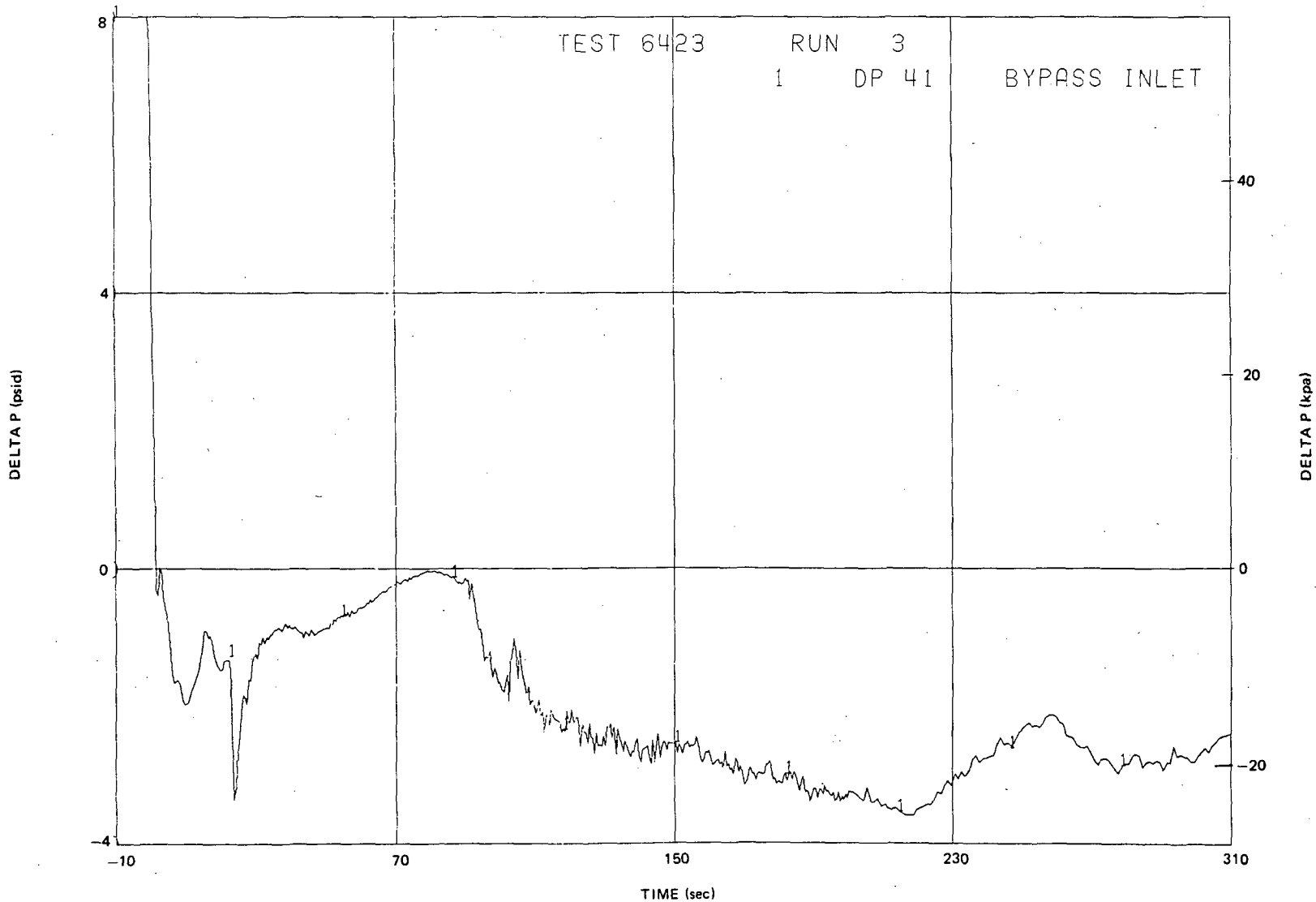

Figure N-25. Bypass Leakage Path Differential Pressure

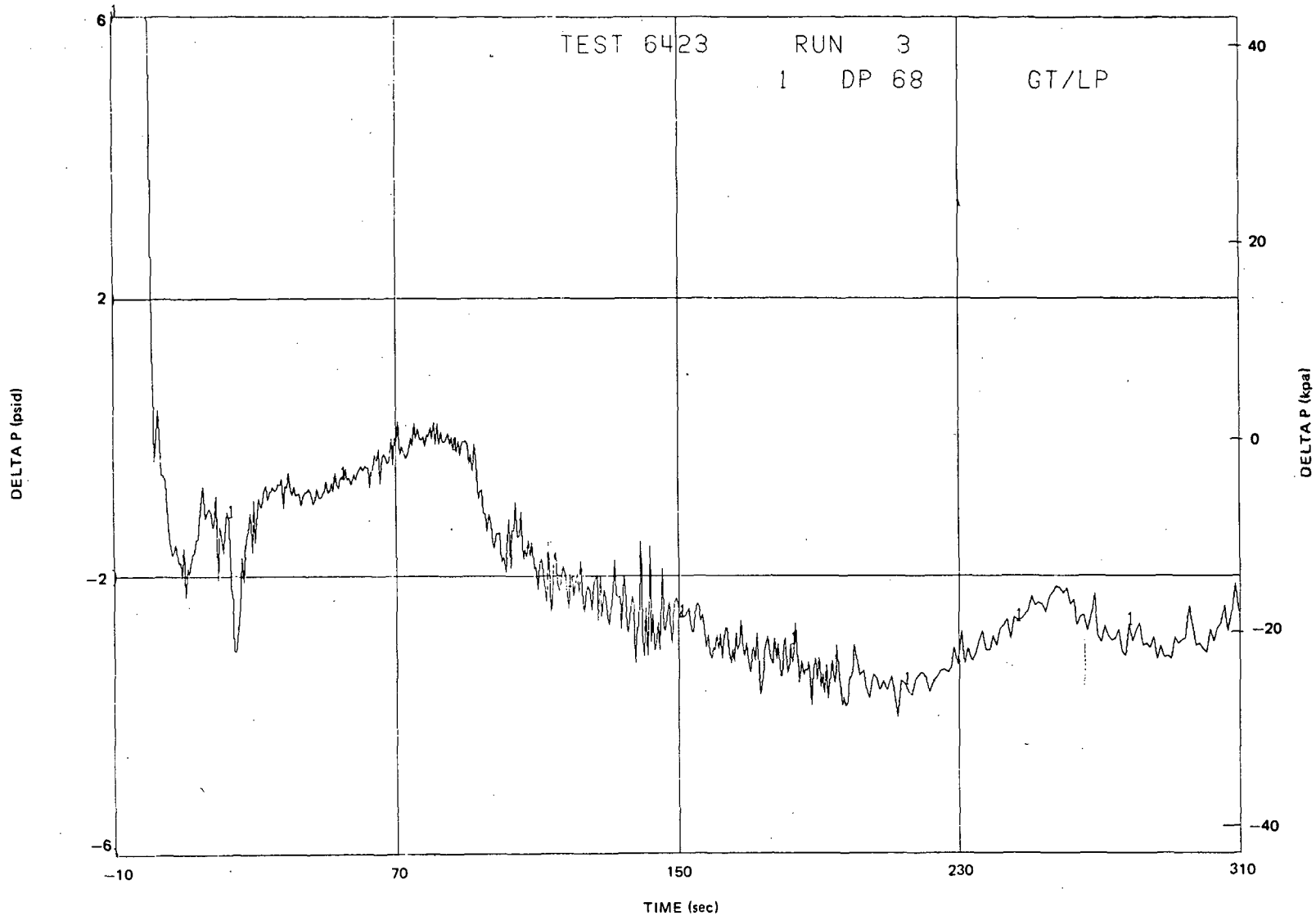

Figure N-26. Lower Plenum to Guide Tube Differential Pressure

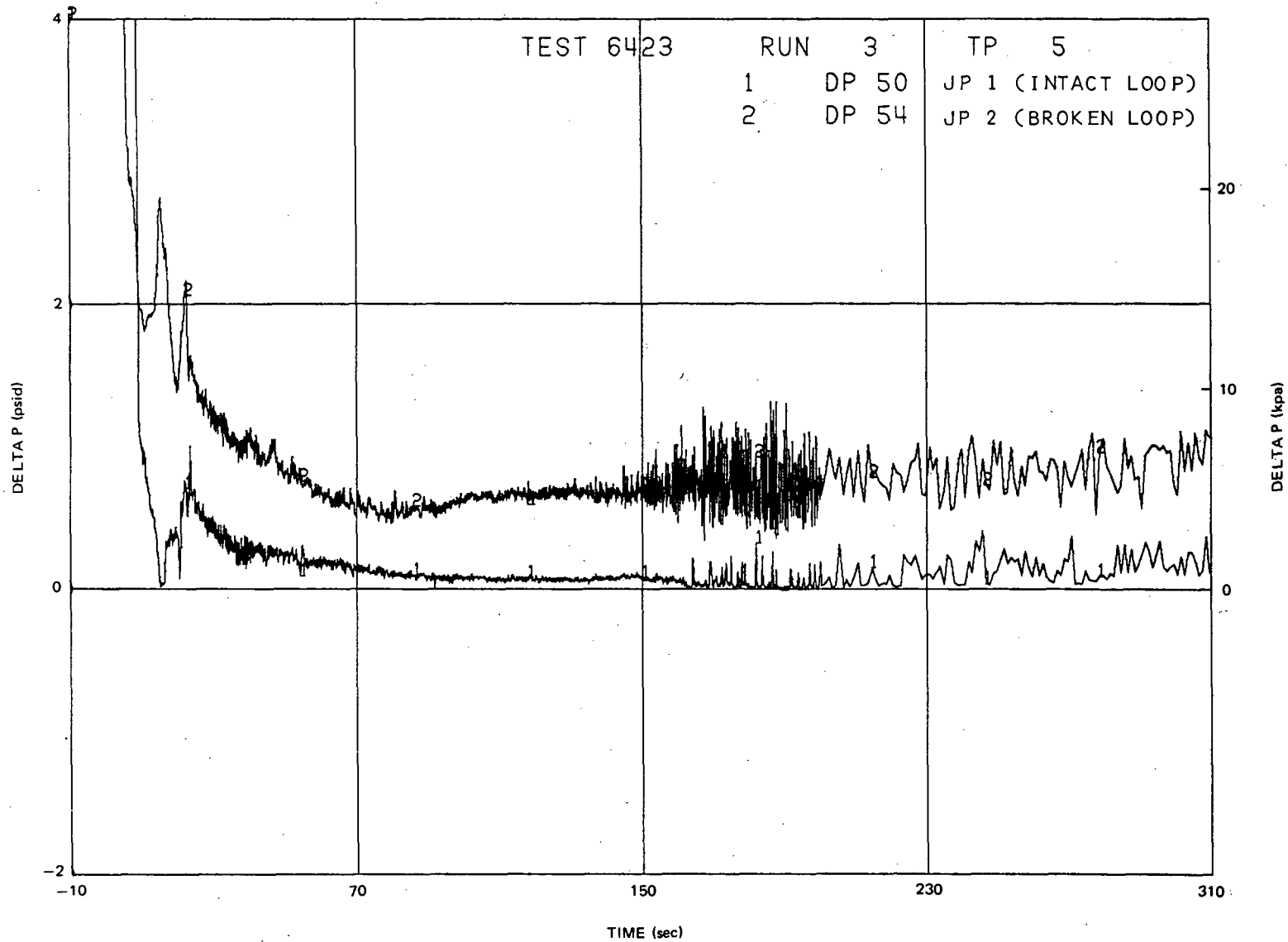

Figure N-27. Intact Loop and Broken Loop Jet Pump Diffuser to Throat Differential Pressures

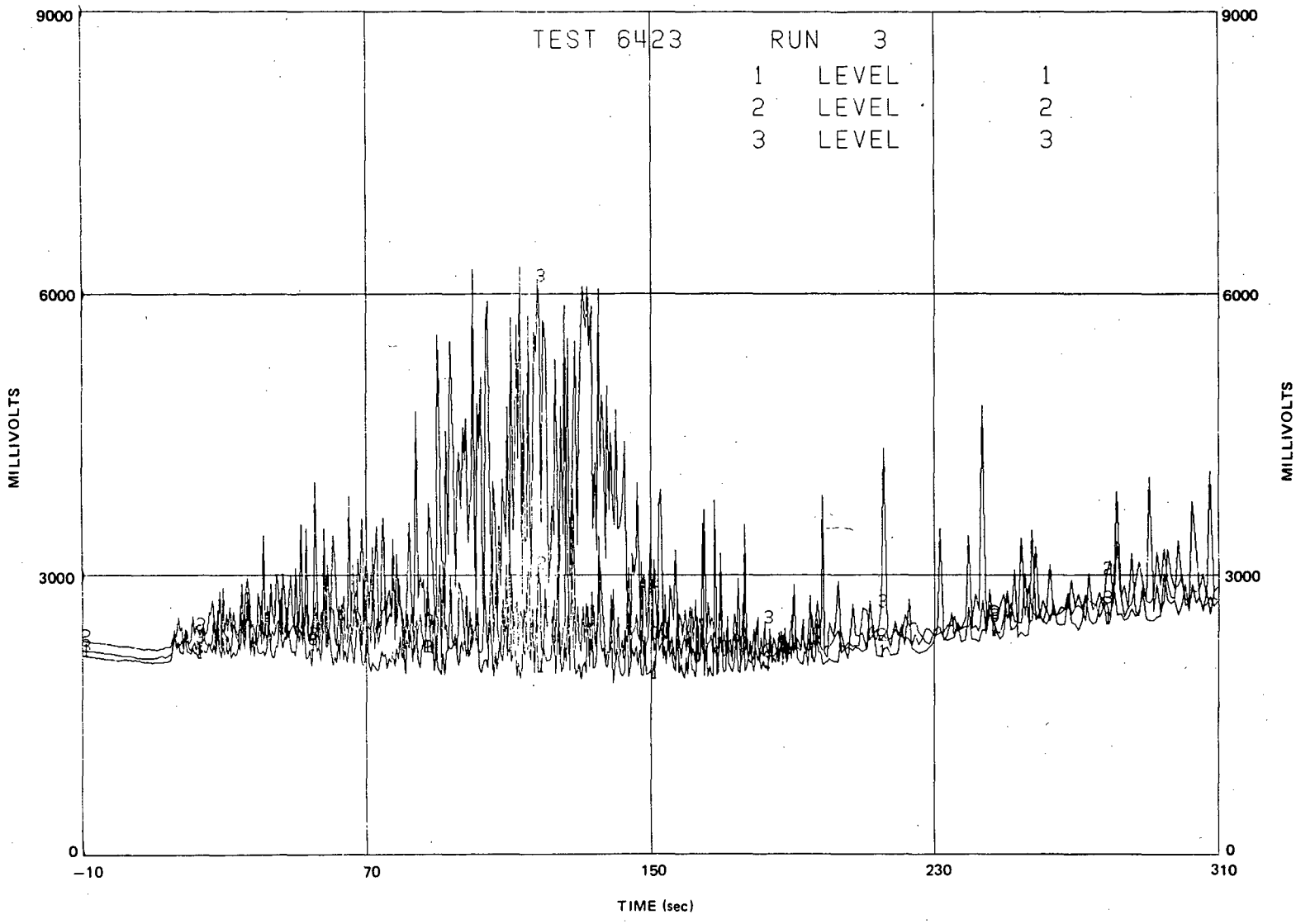

Figure N-28. Bottom Lower Plenum Conductivity Probe Measurements

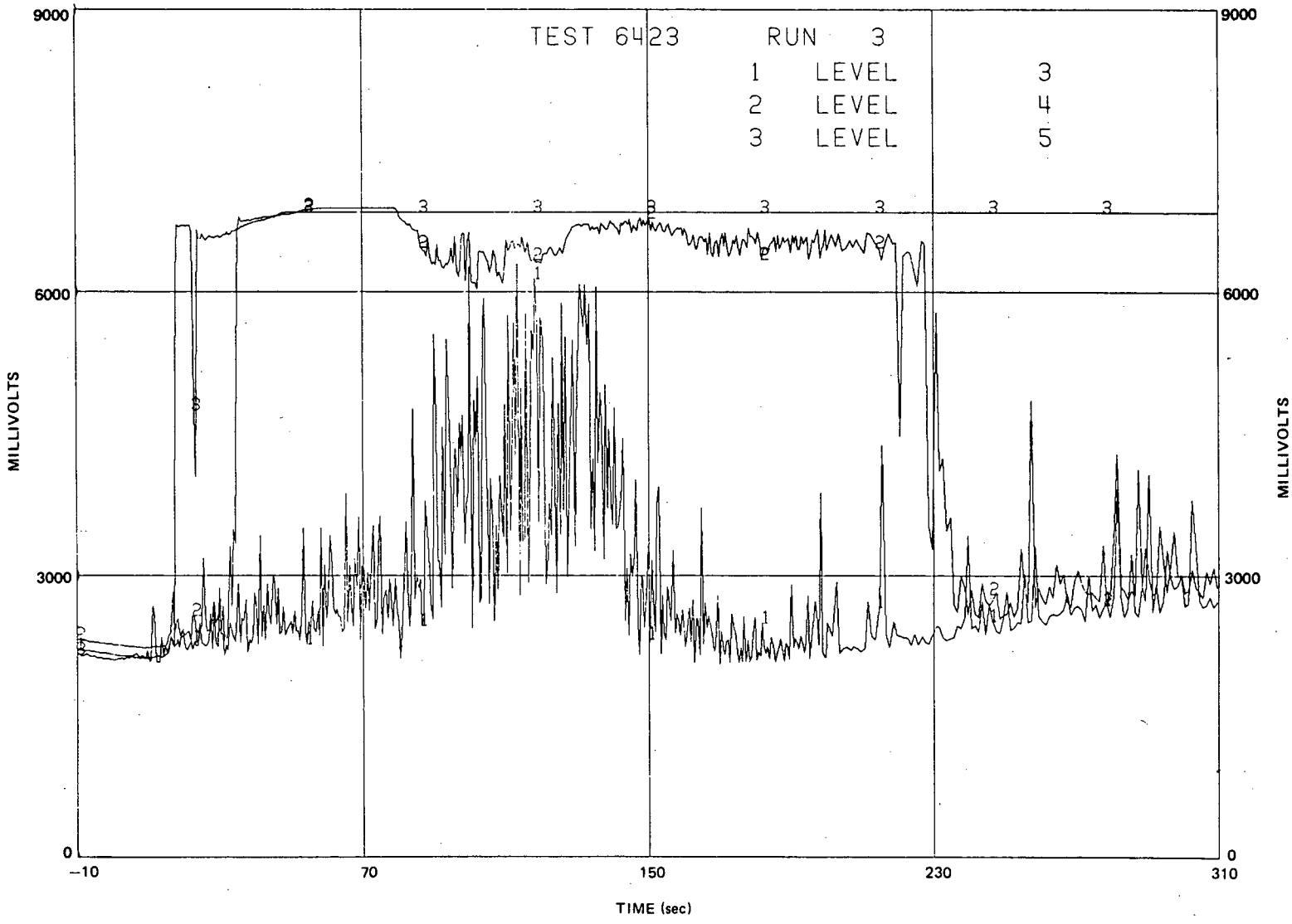

Figure N-29. Upper Lower Plenum Conductivity Probe Measurements

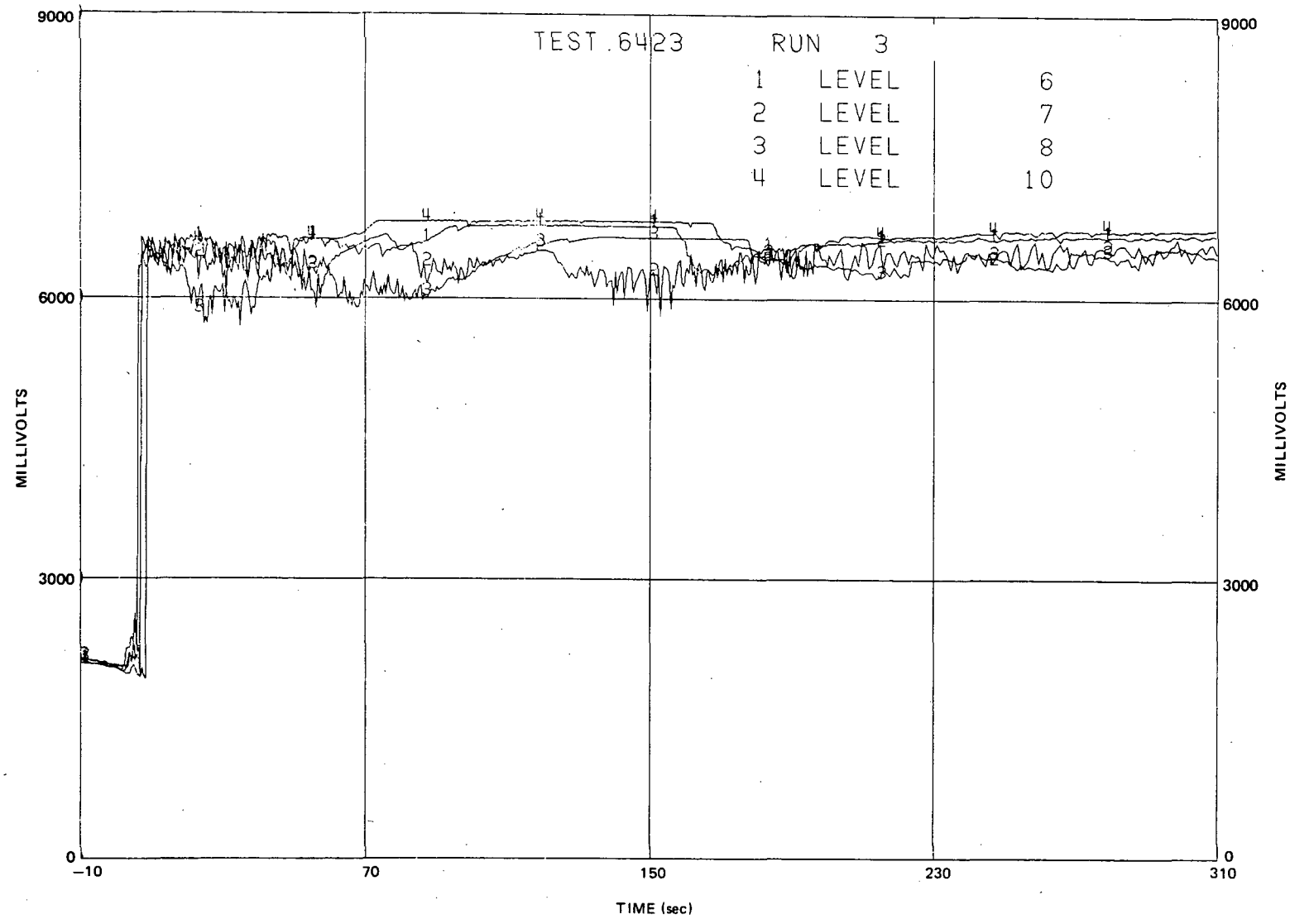

Figure N-30. Lower Annulus Conductivity Probe Measurements

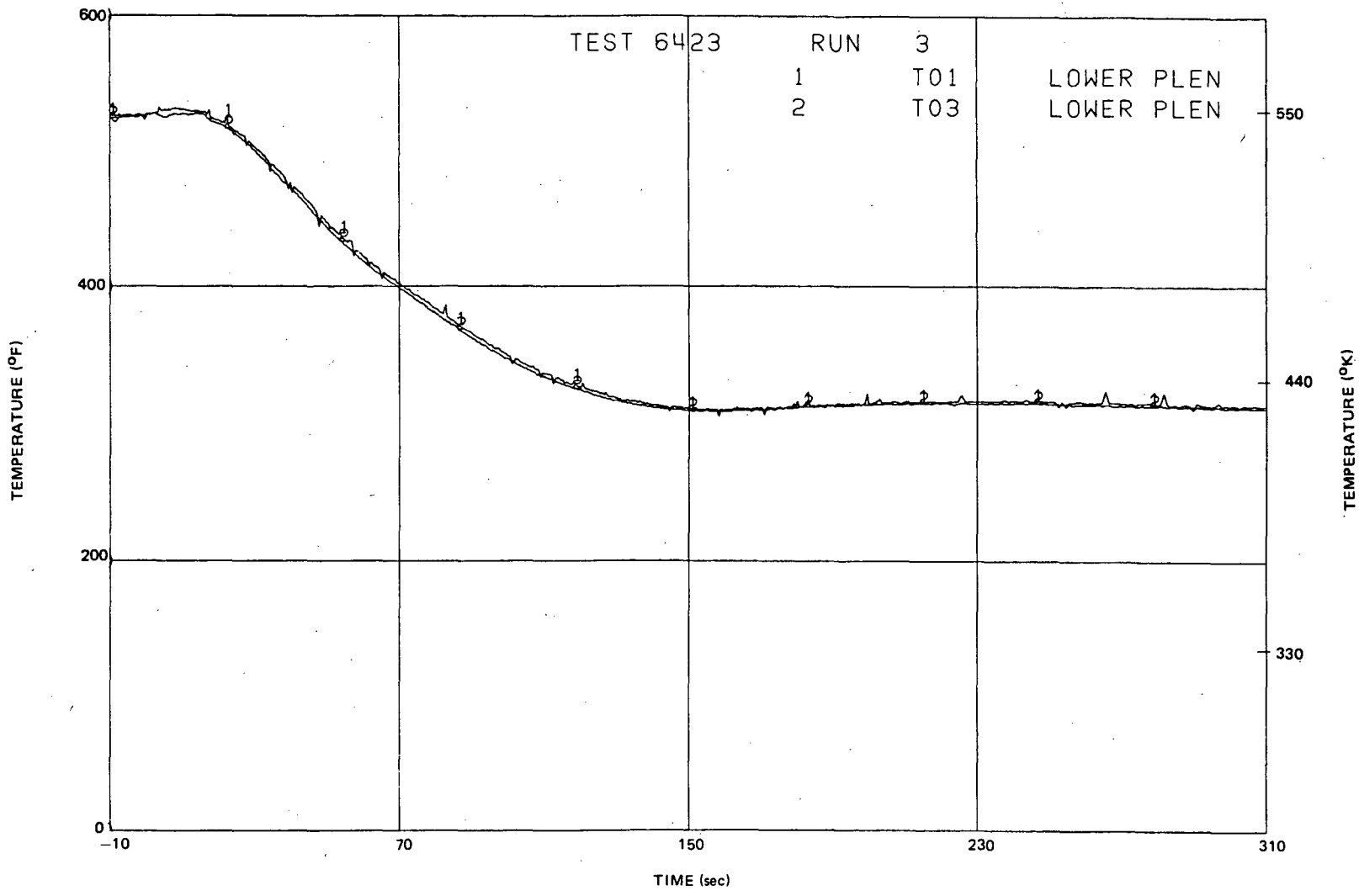

Figure N-31. Lower Plenum Fluid Temperatures

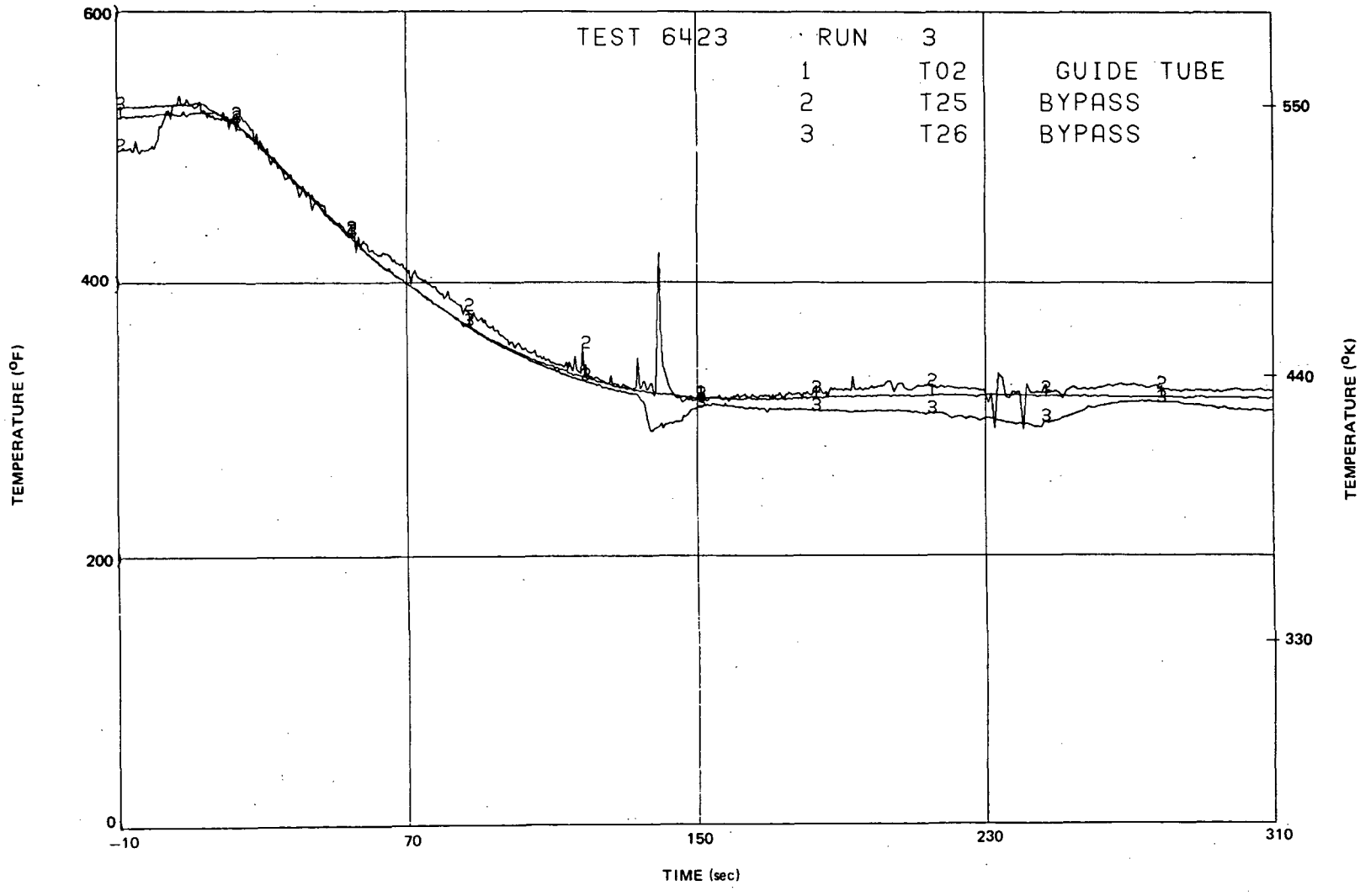

Figure N-32. Guide Tube and Bypass Fluid Temperatures

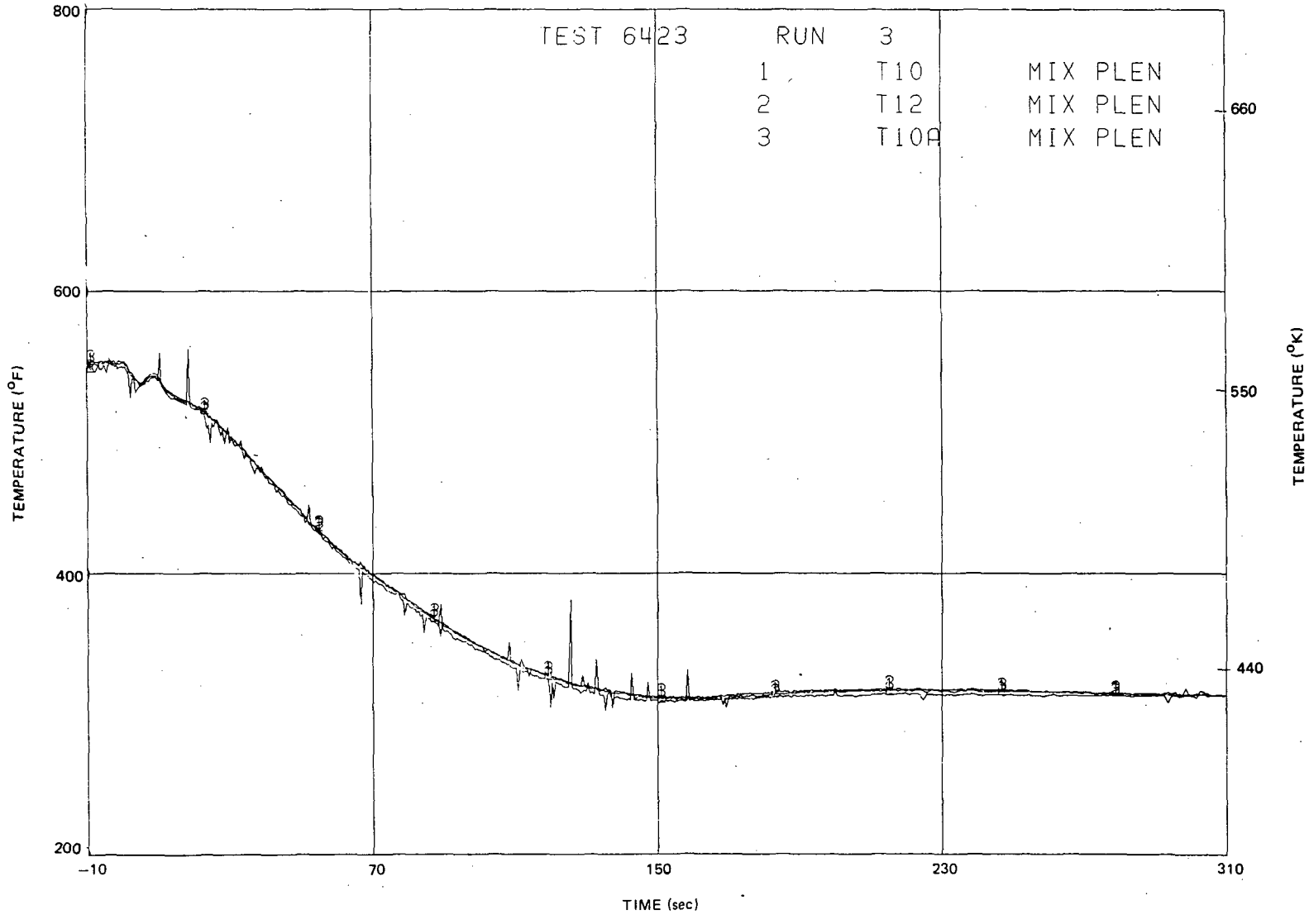

Figure N-33. Mixing Plenum Fluid Temperatures

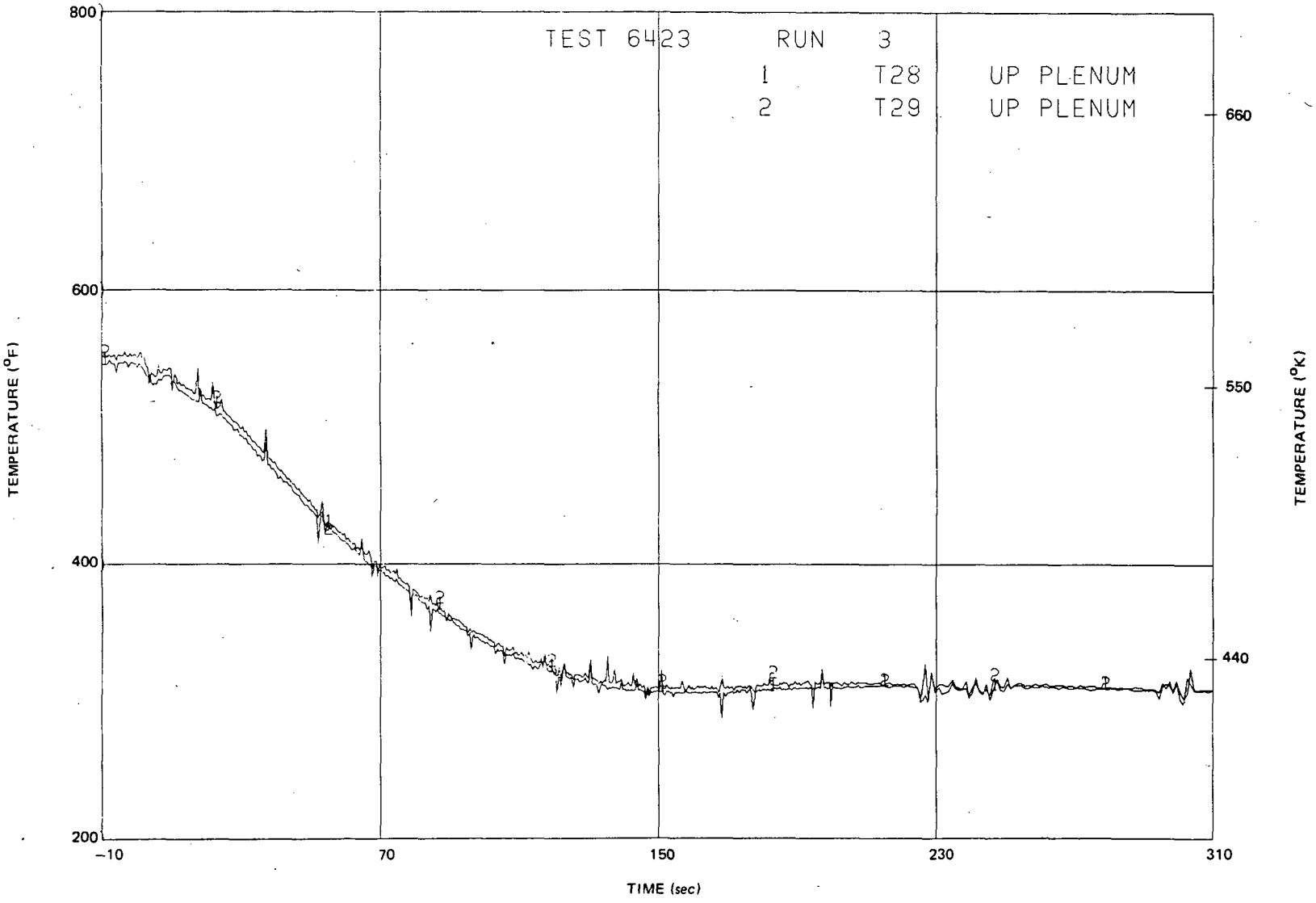

Figure N-34. Upper Plenum Fluid Temperatures

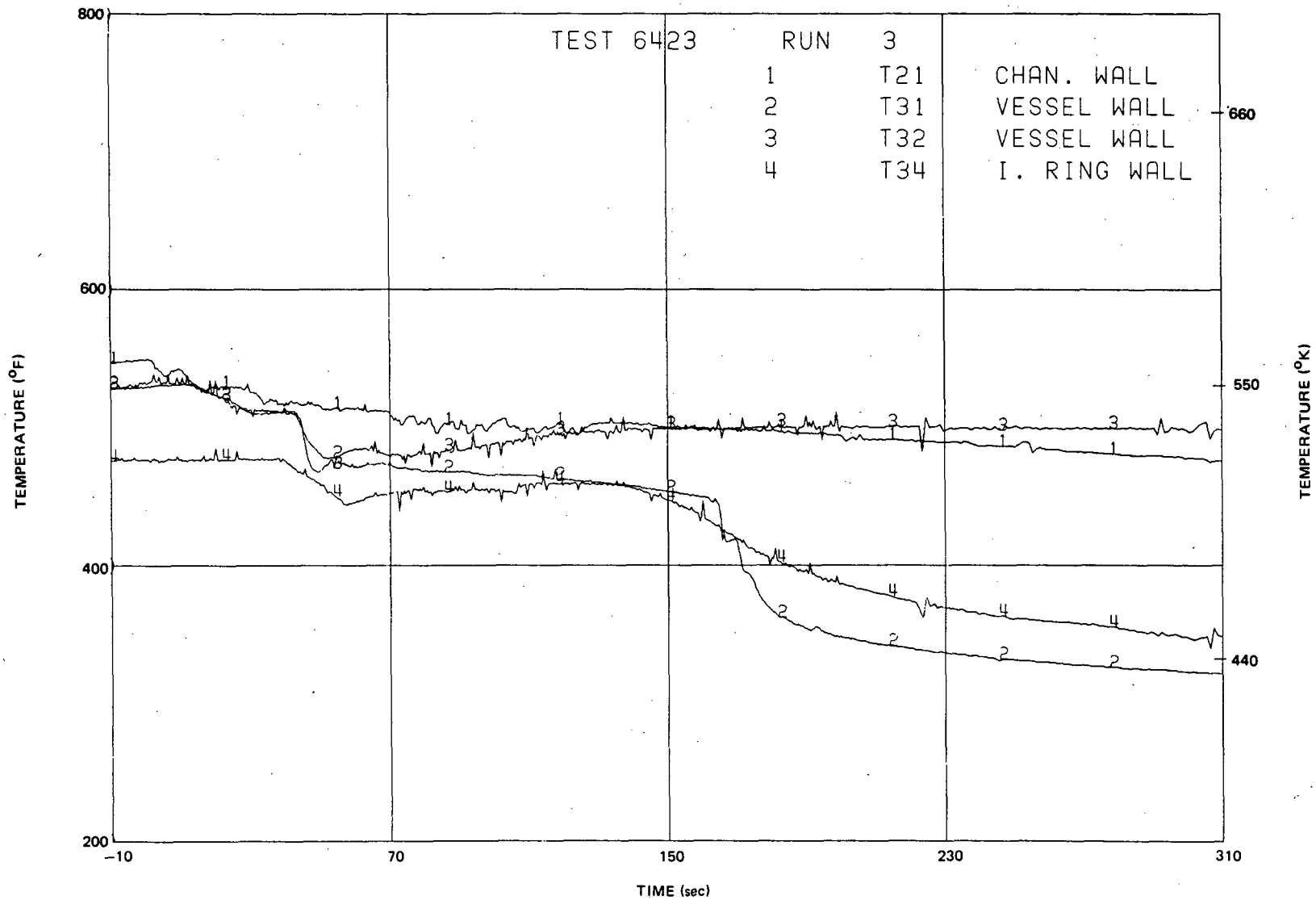

Figure N-35. Wall Temperatures

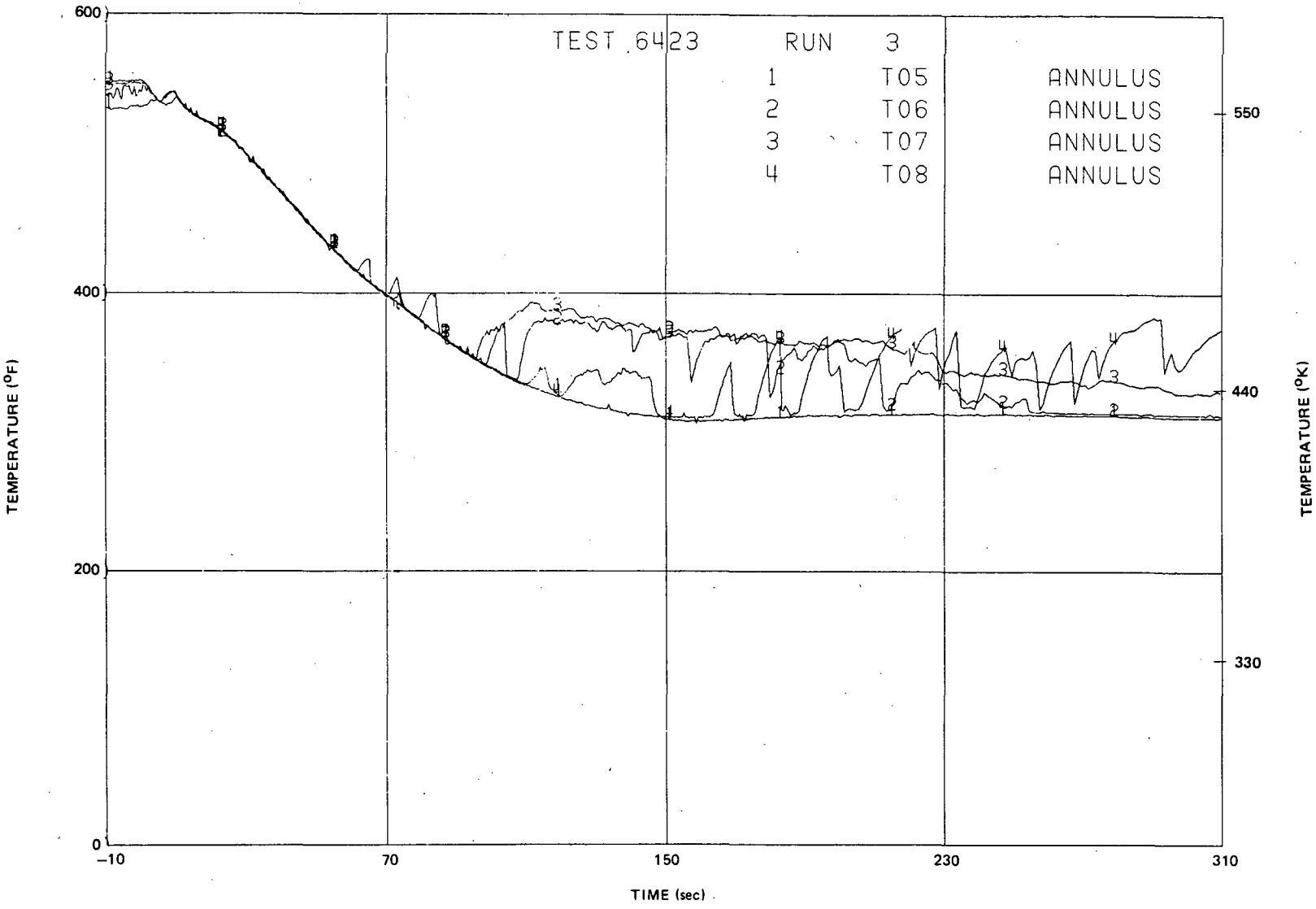

Figure N-36. Annulus Fluid Temperatures

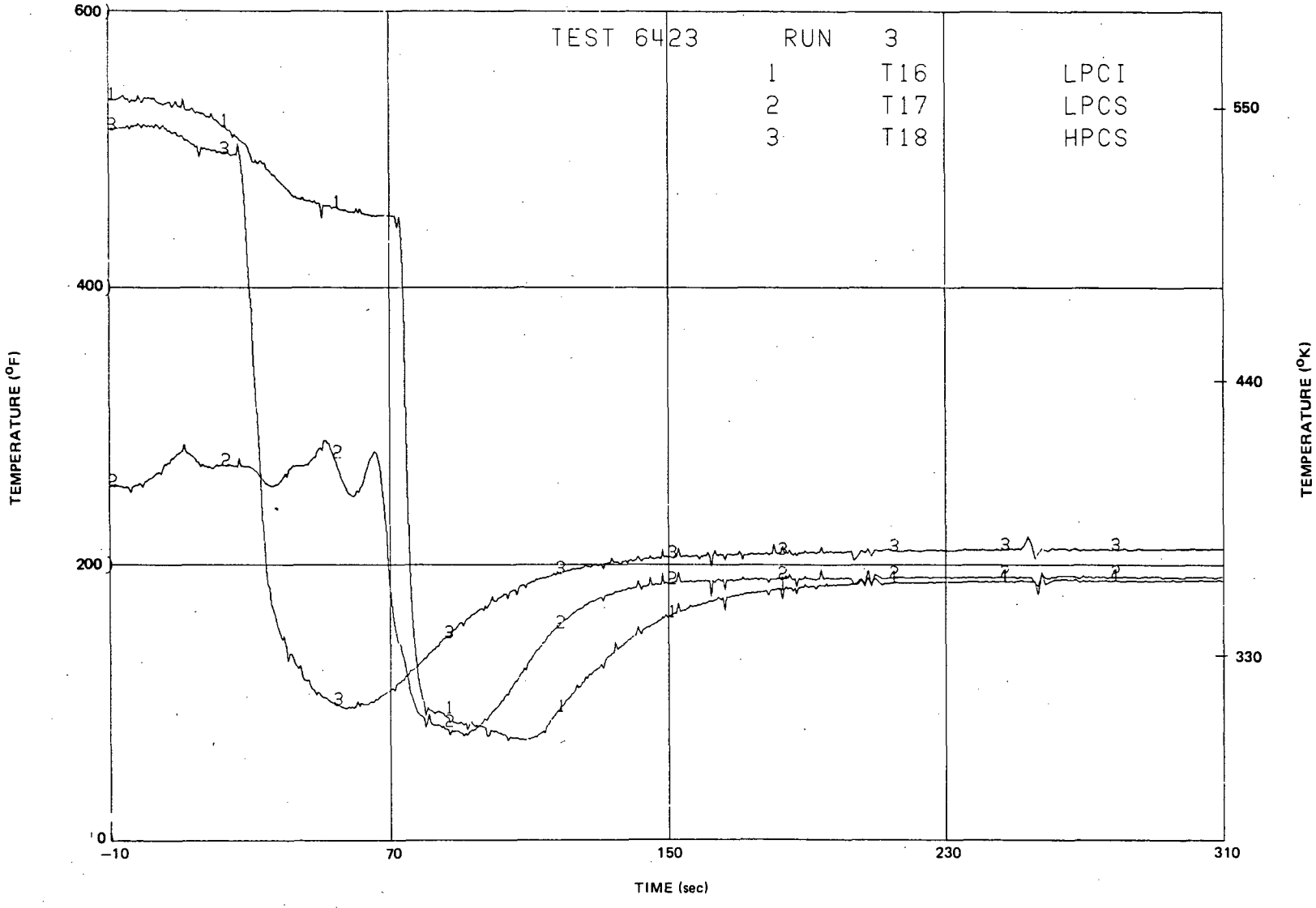

Figure N-37. Emergency Core Cooling Fluid Temperatures

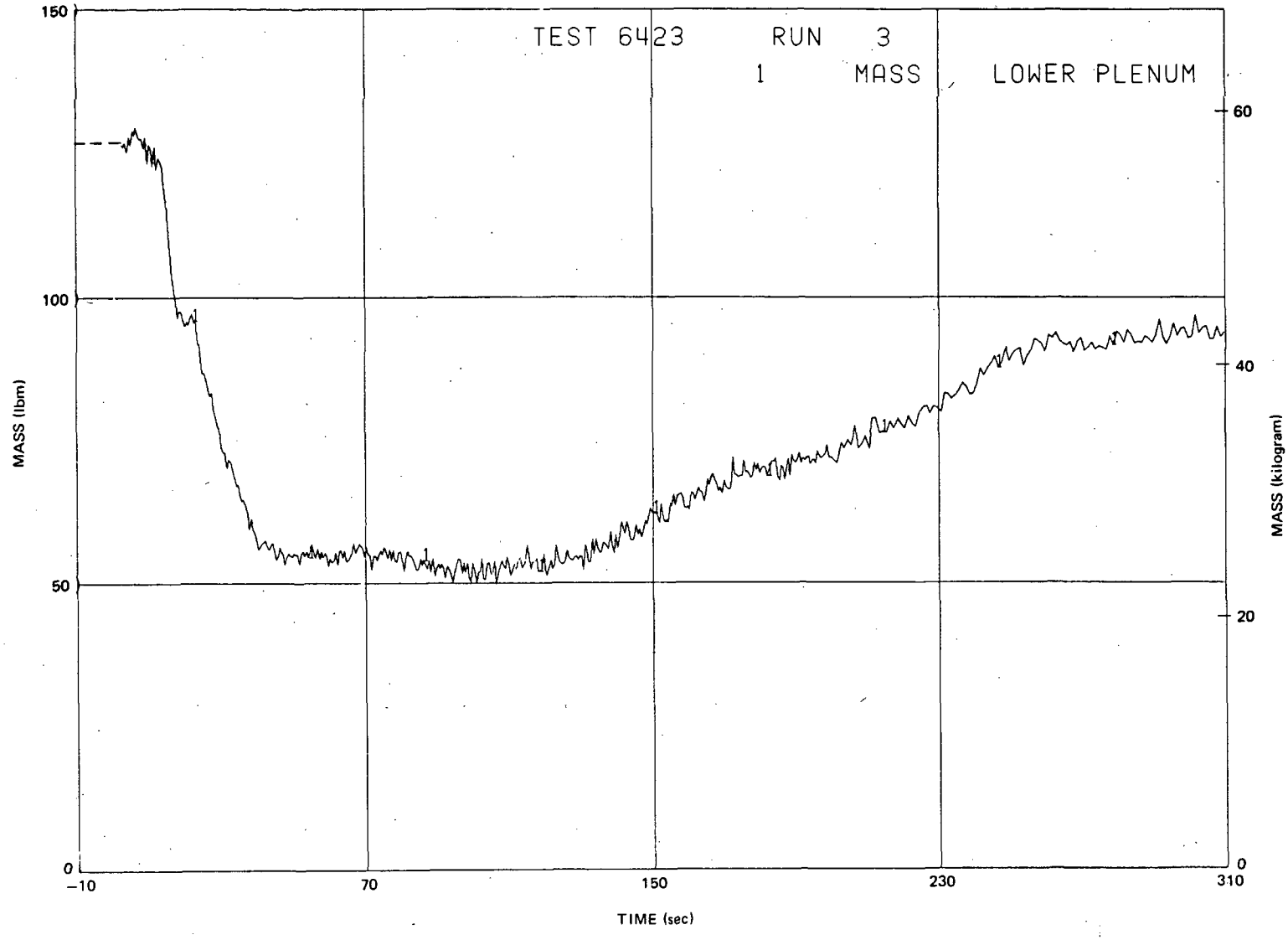

Figure N-38. Lower Plenum Fluid Mass

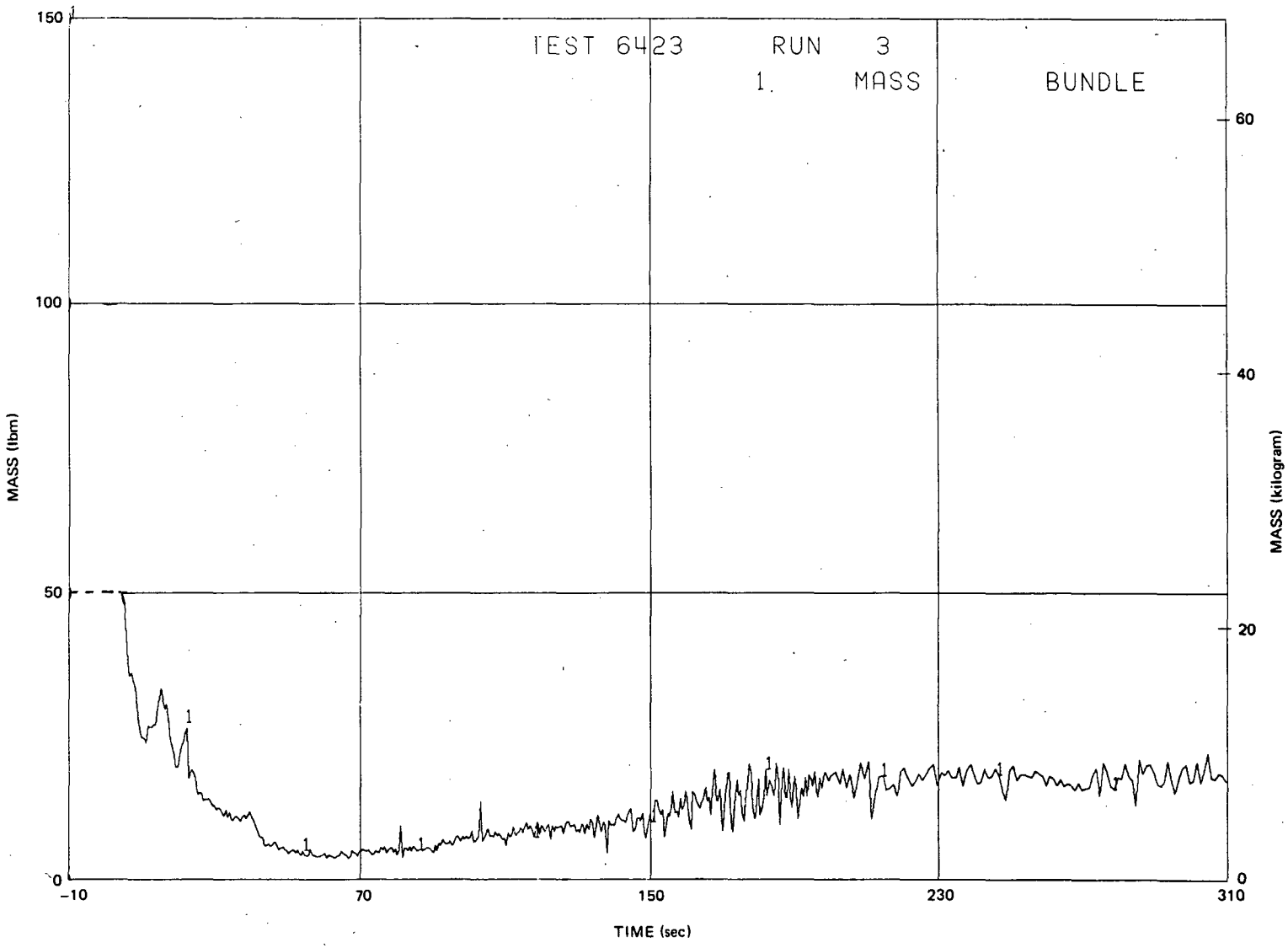

Figure N-39. Bundle Fluid Mass

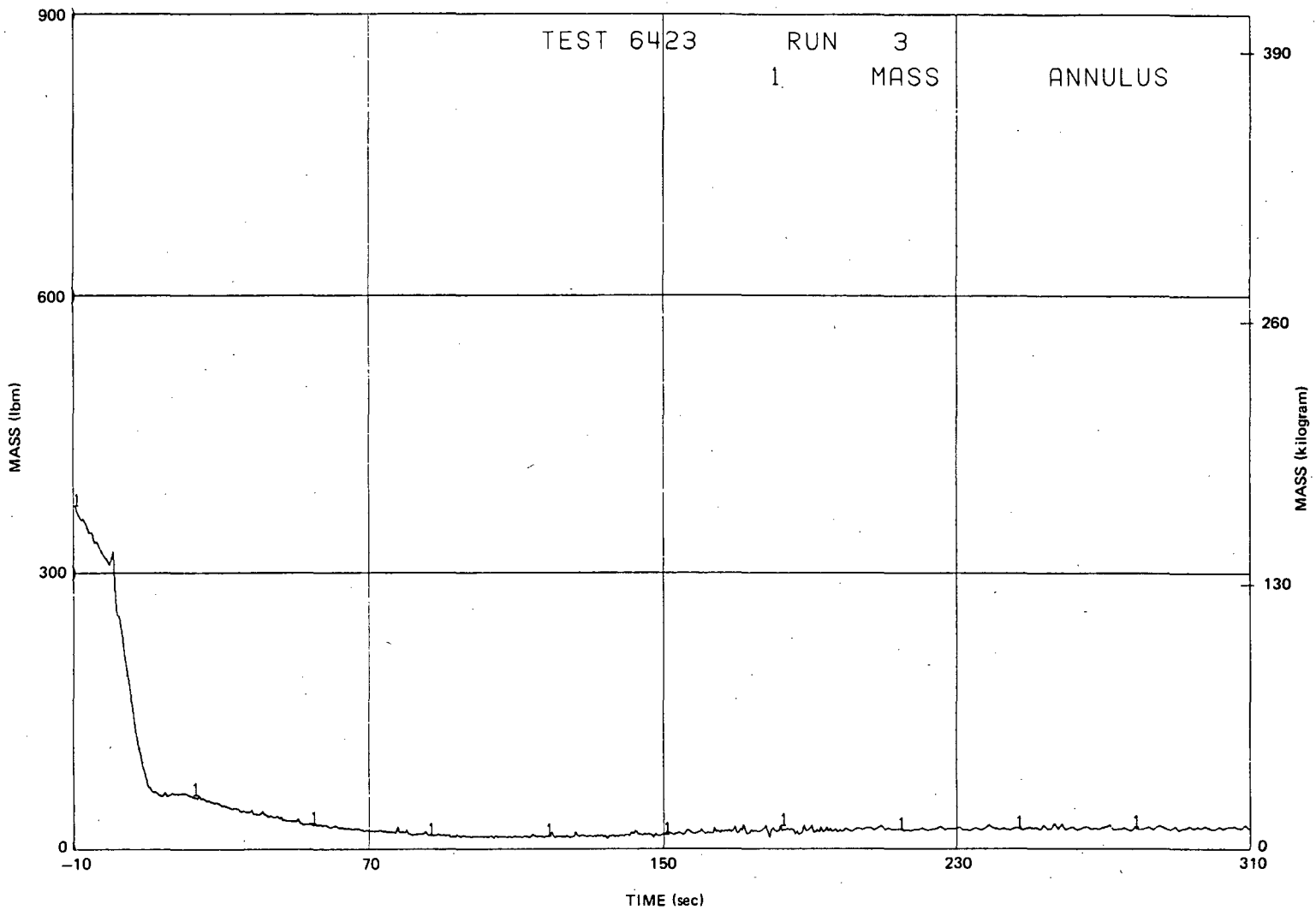

Figure N-40. Annulus Fluid Mass

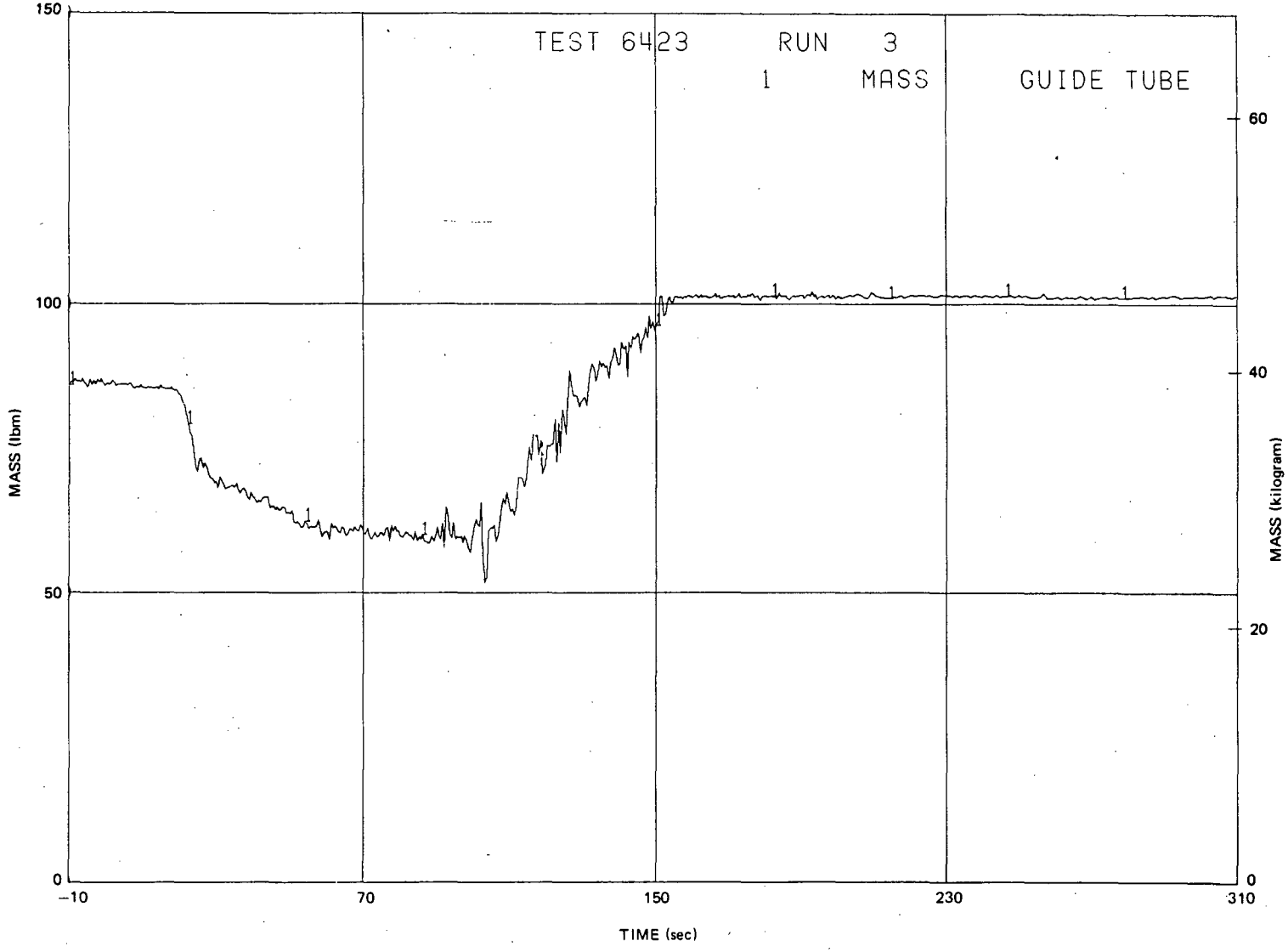

Figure N-41. Guide Tube Fluid Mass

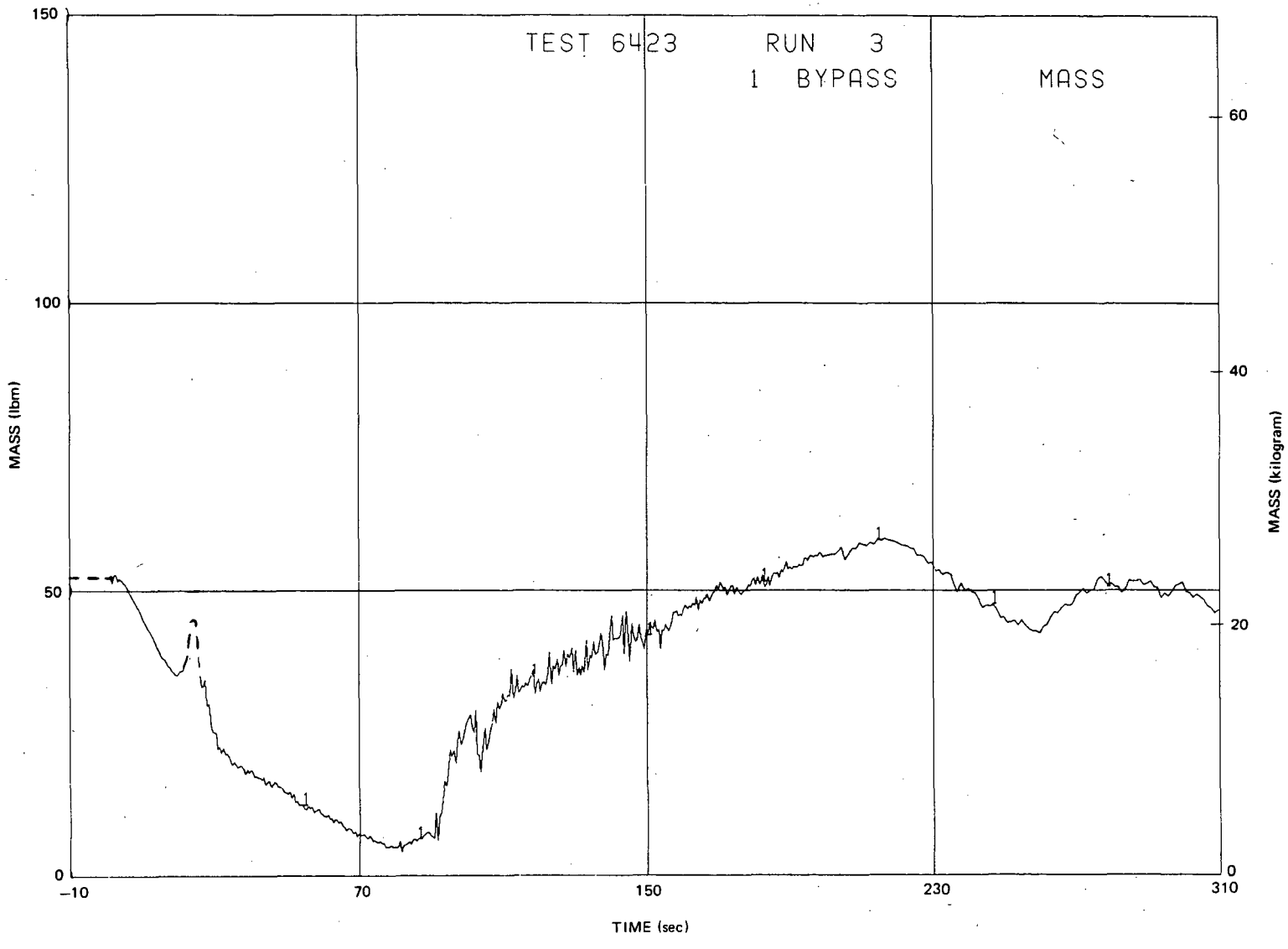

Figure N-42. Bypass Fluid Mass

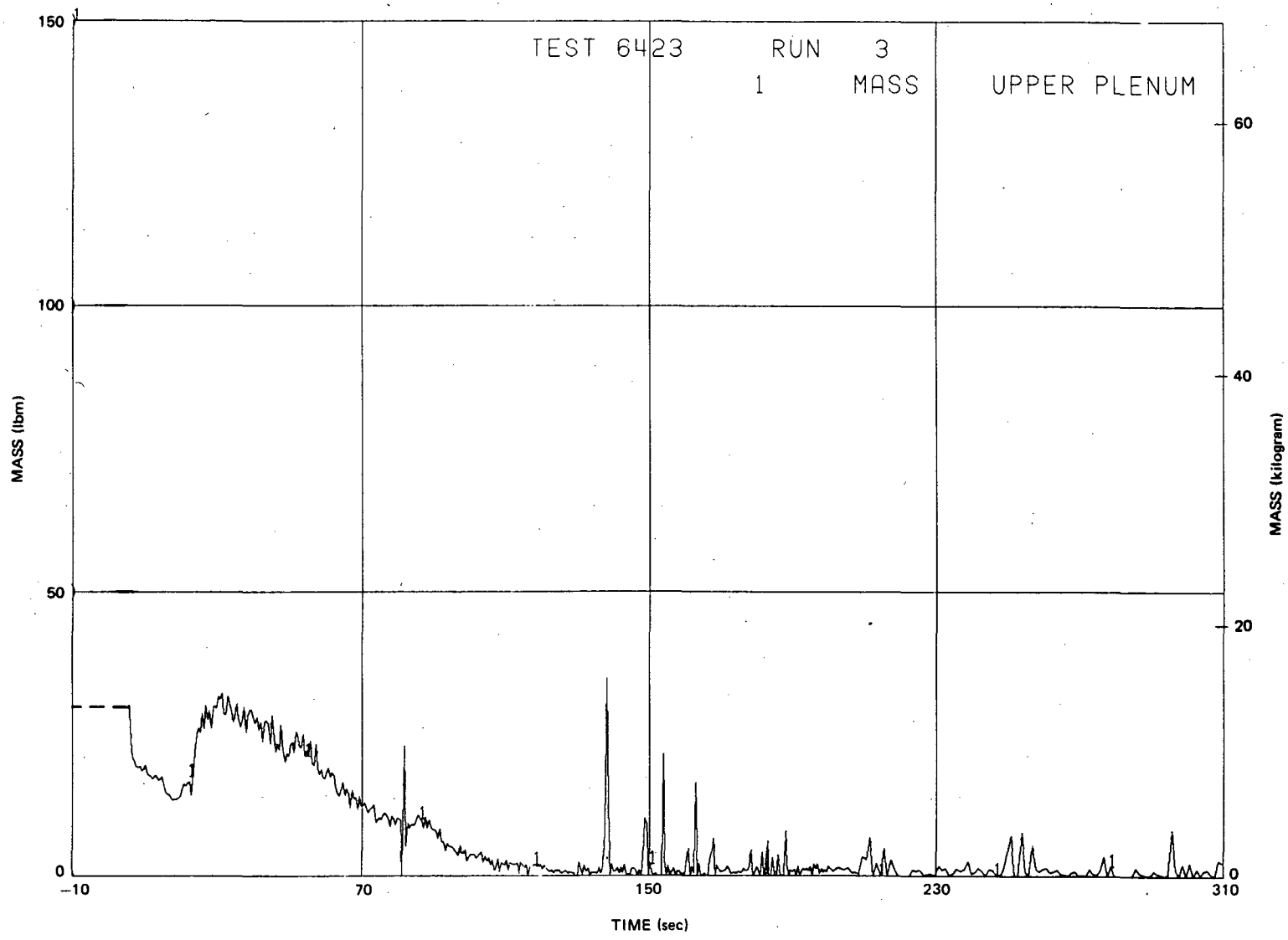

Figure N-43. Upper Plenum Fluid Mass

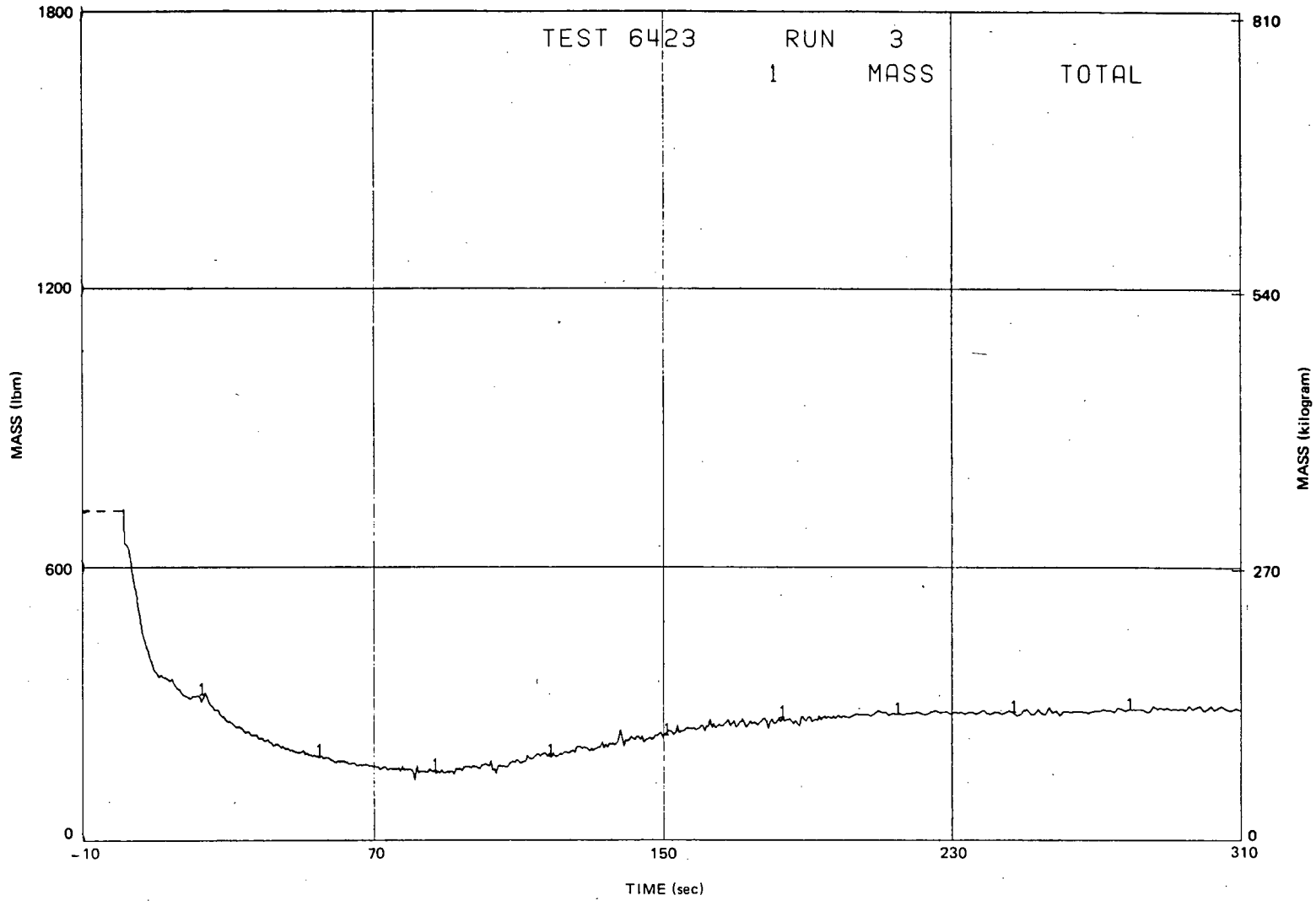

Figure N-44. Total Vessel Fluid Mass

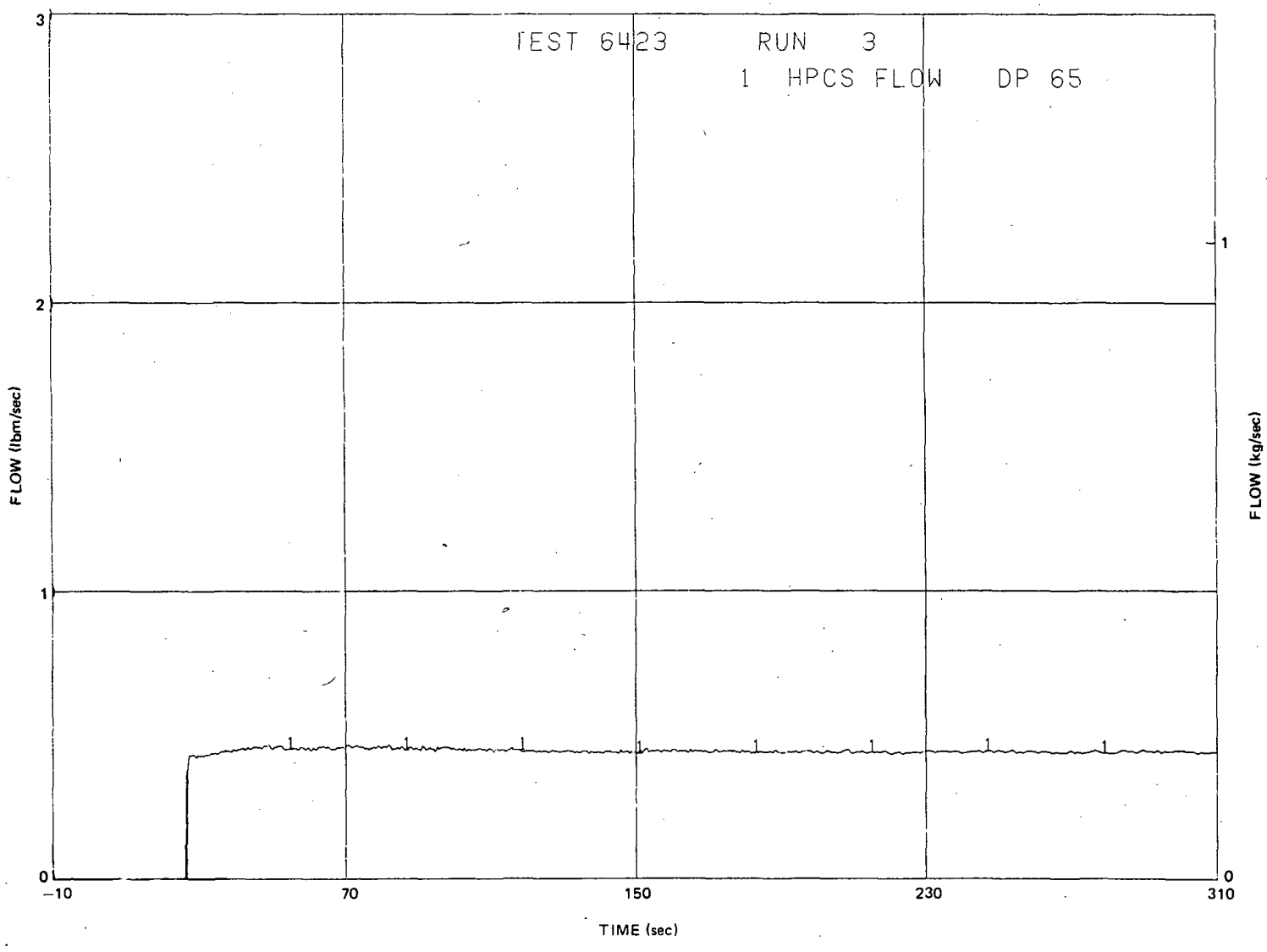

Figure N-45. HPCS Mass Flow Rate

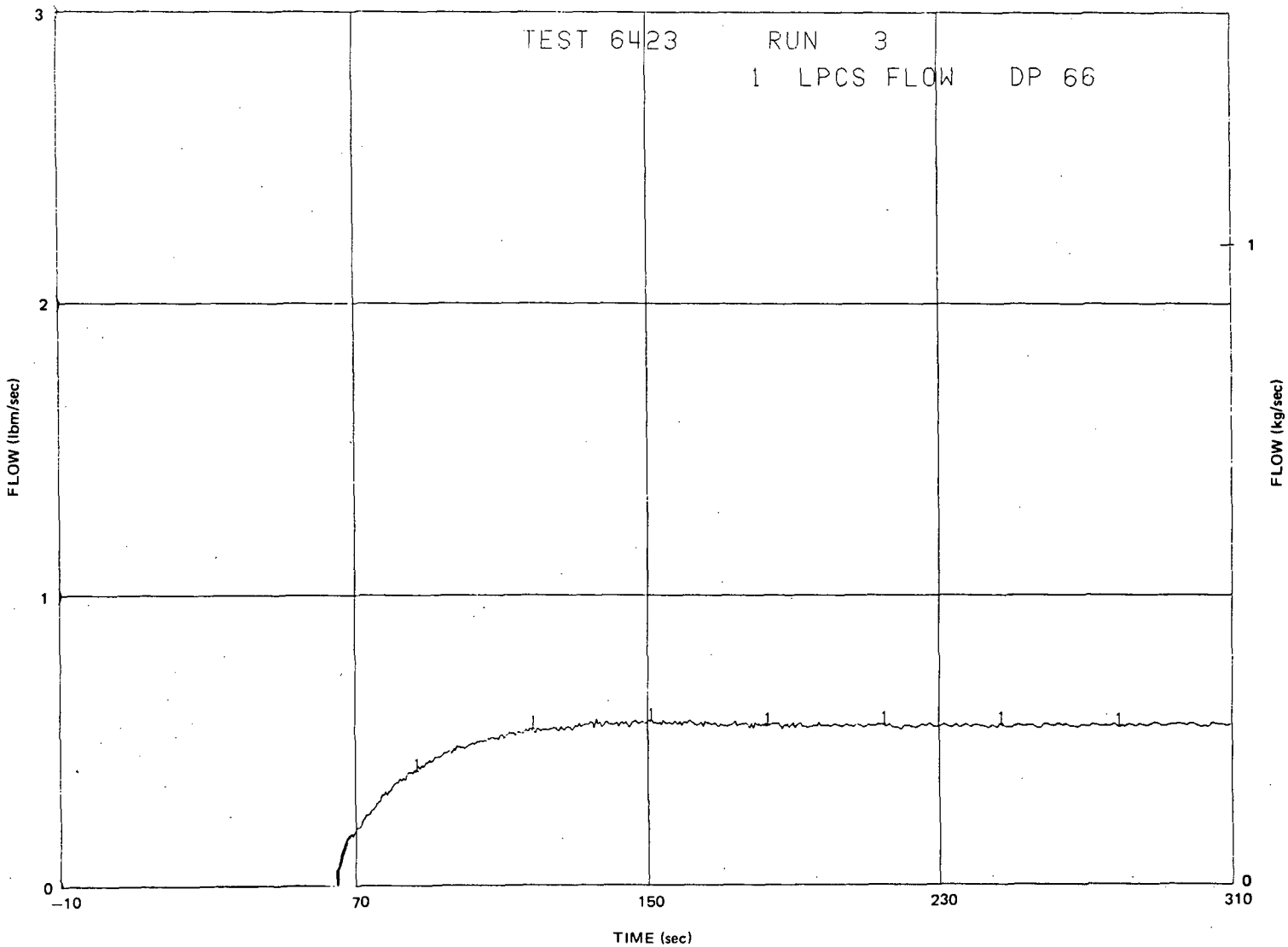

Figure N-46. LPCS Mass Flow Rate

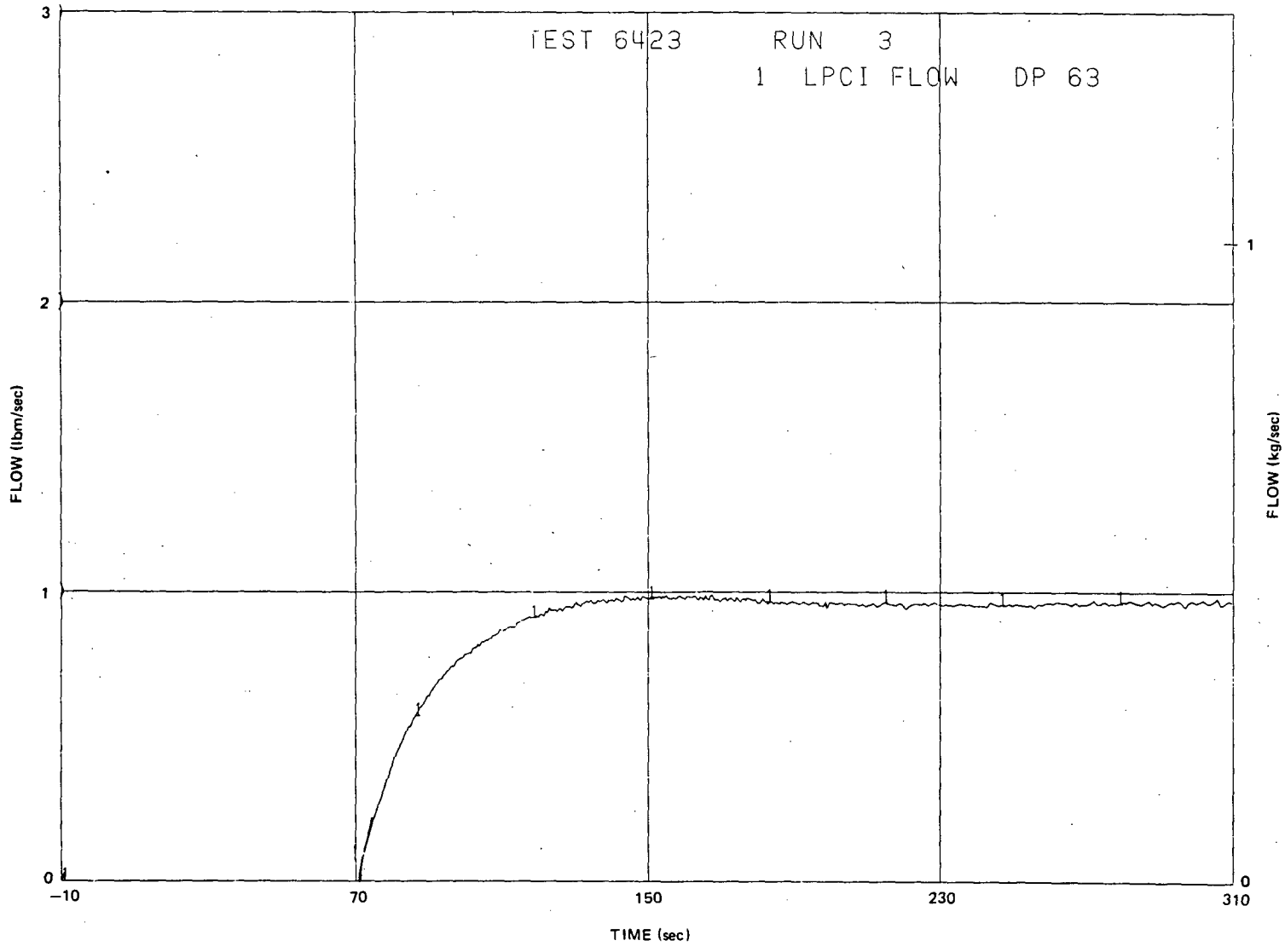

Figure N-47. LPCI Mass Flow Rate

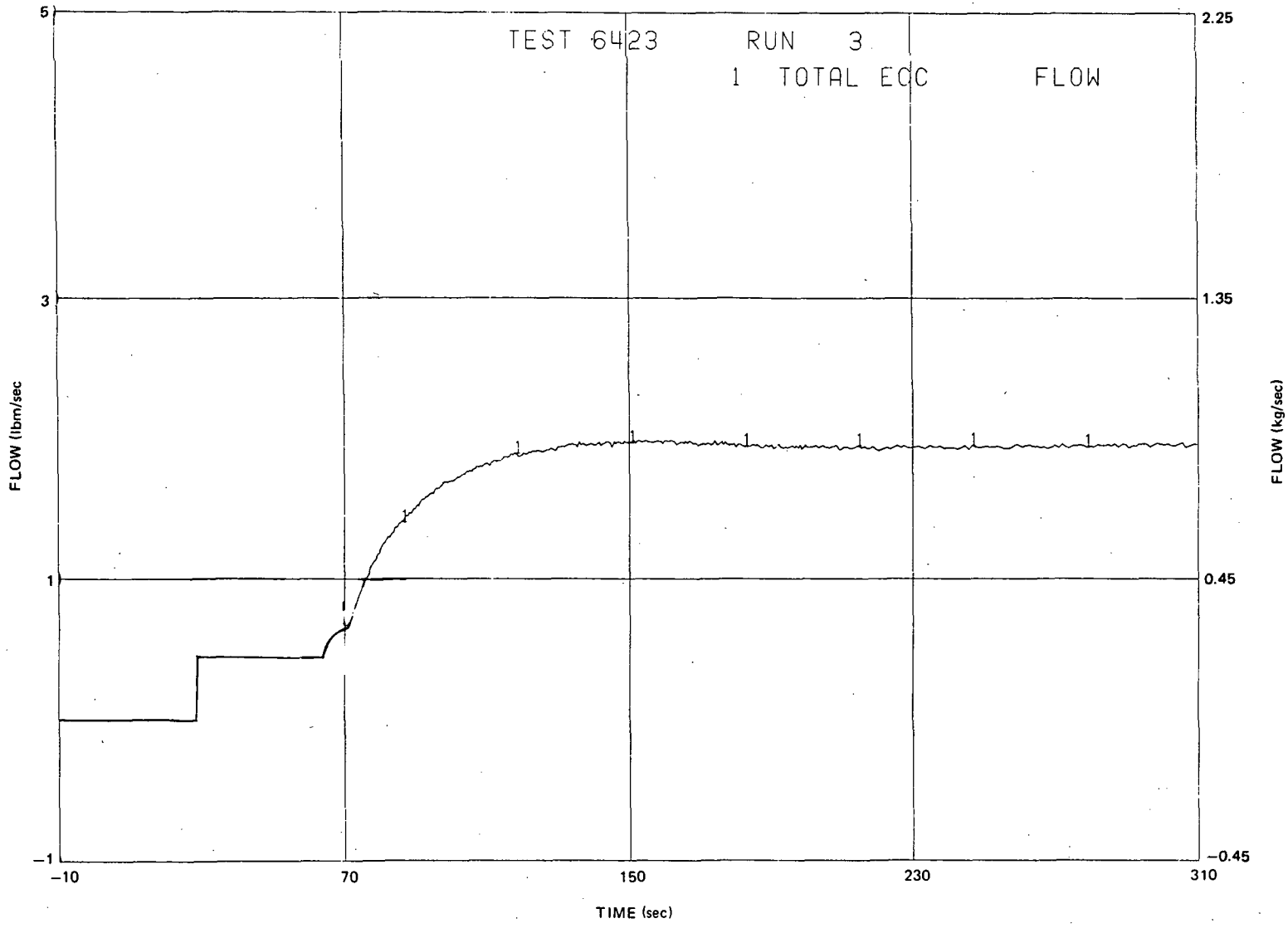

Figure N-48. Total ECC Mass Flow Rate

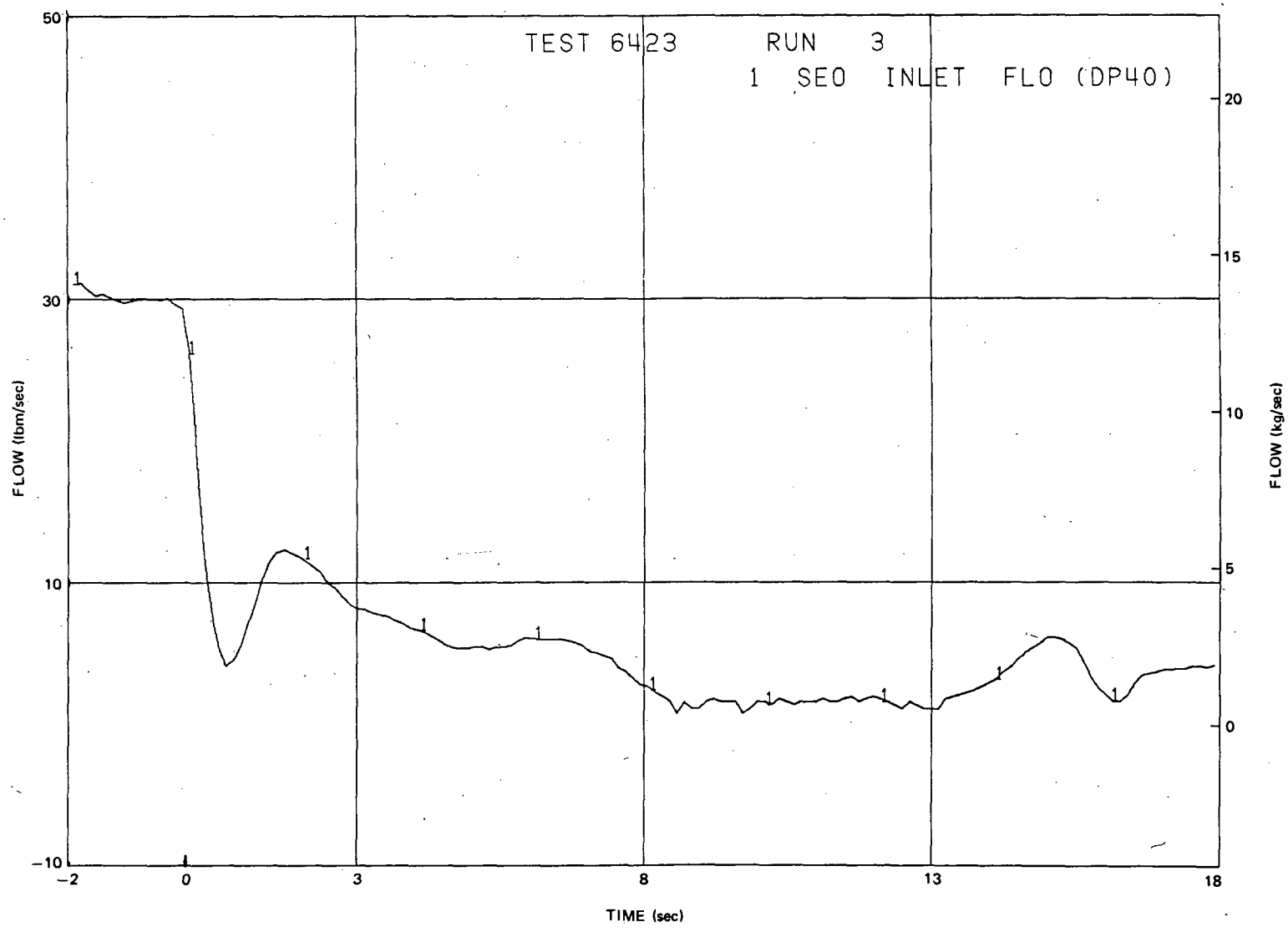

Figure N-49. Bundle Inlet Side Entry Orifice Mass Flow Rate

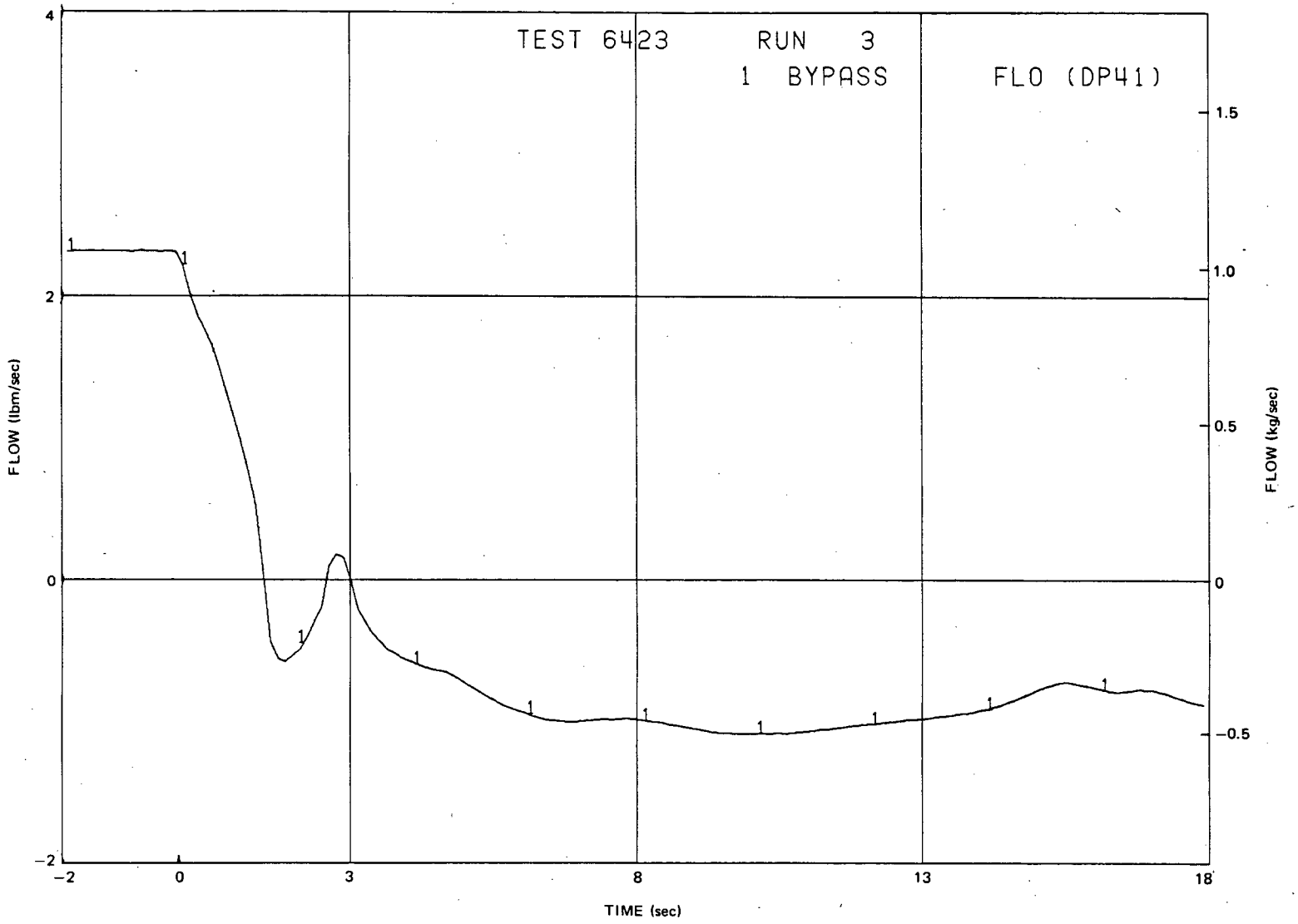

Figure N-50. Bypass Leakage Path Mass Flow Rate

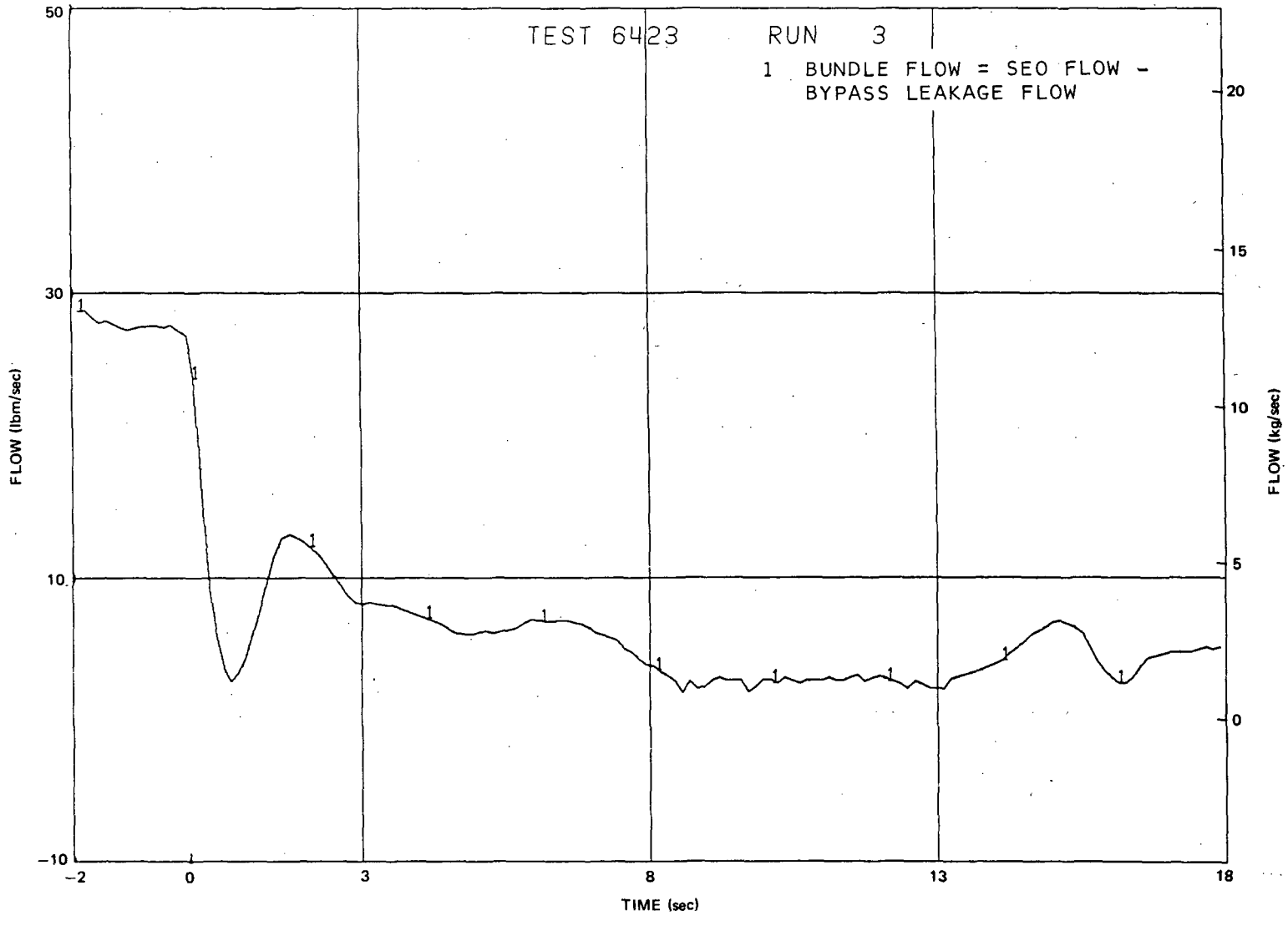

Figure N-51. Bundle Mass Flow Rate

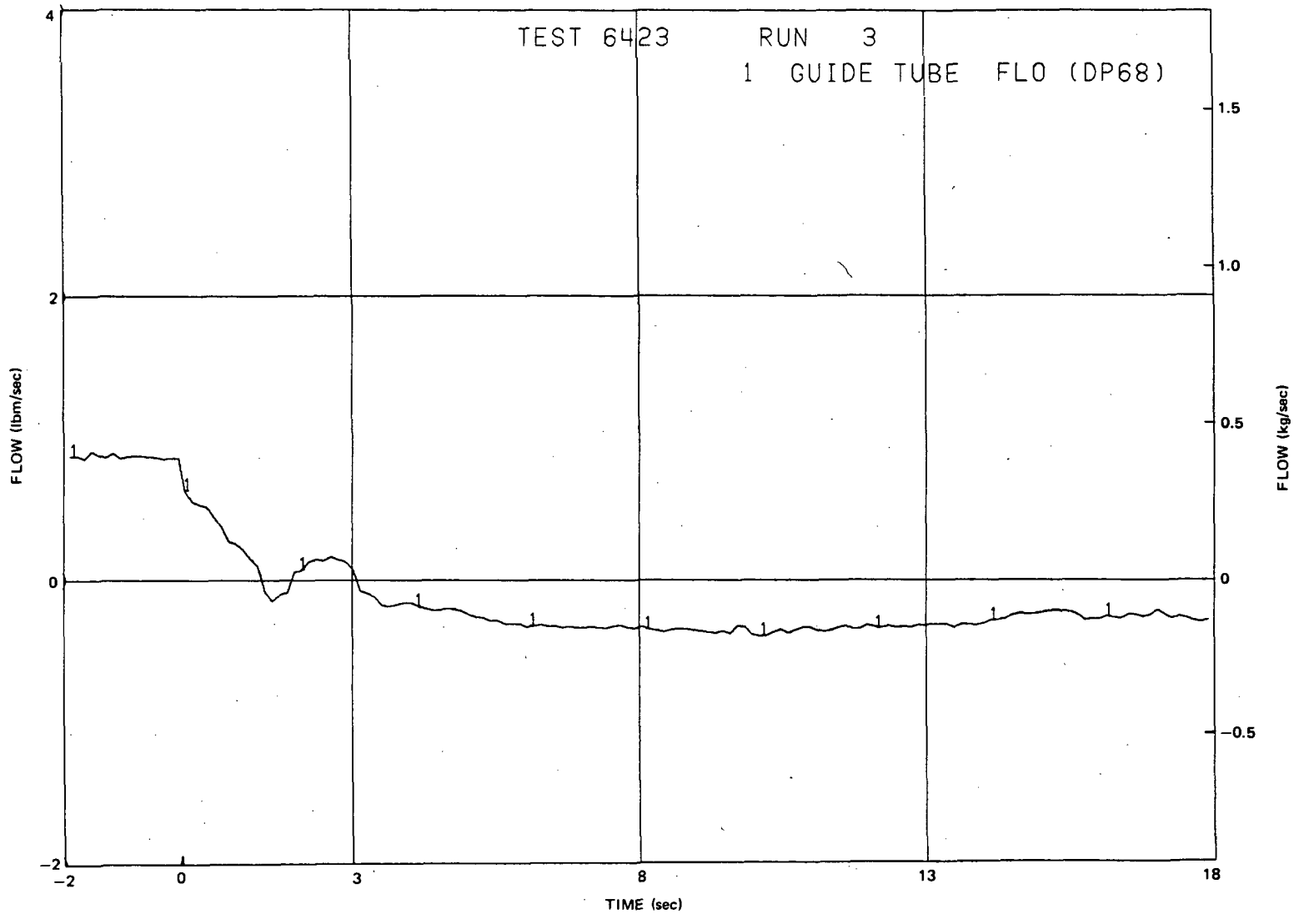

Figure N-52. Lower Plenum to Guide Tube Mass Flow Rate

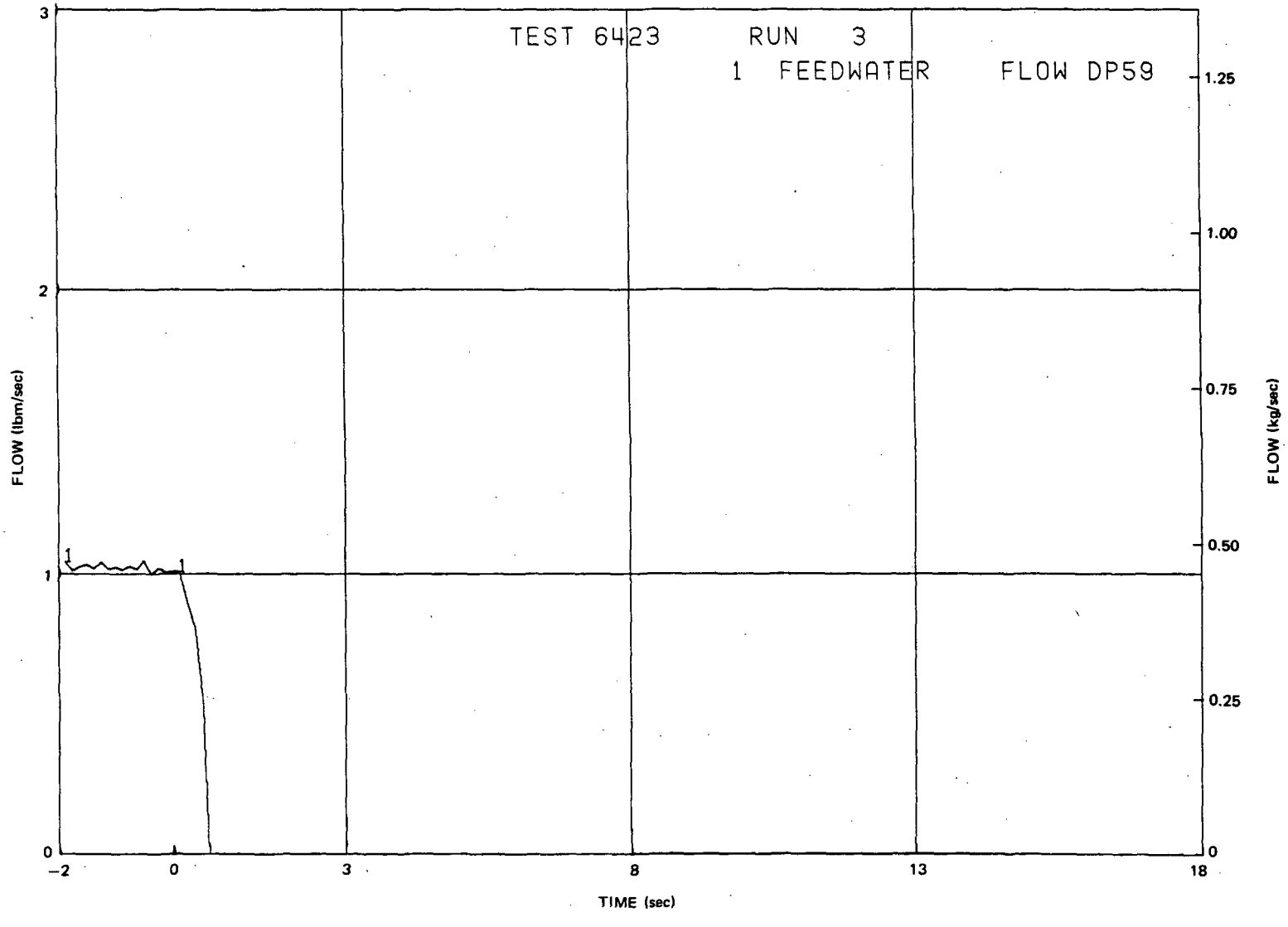

Figure N-53. Feedwater Mass Flow Rate

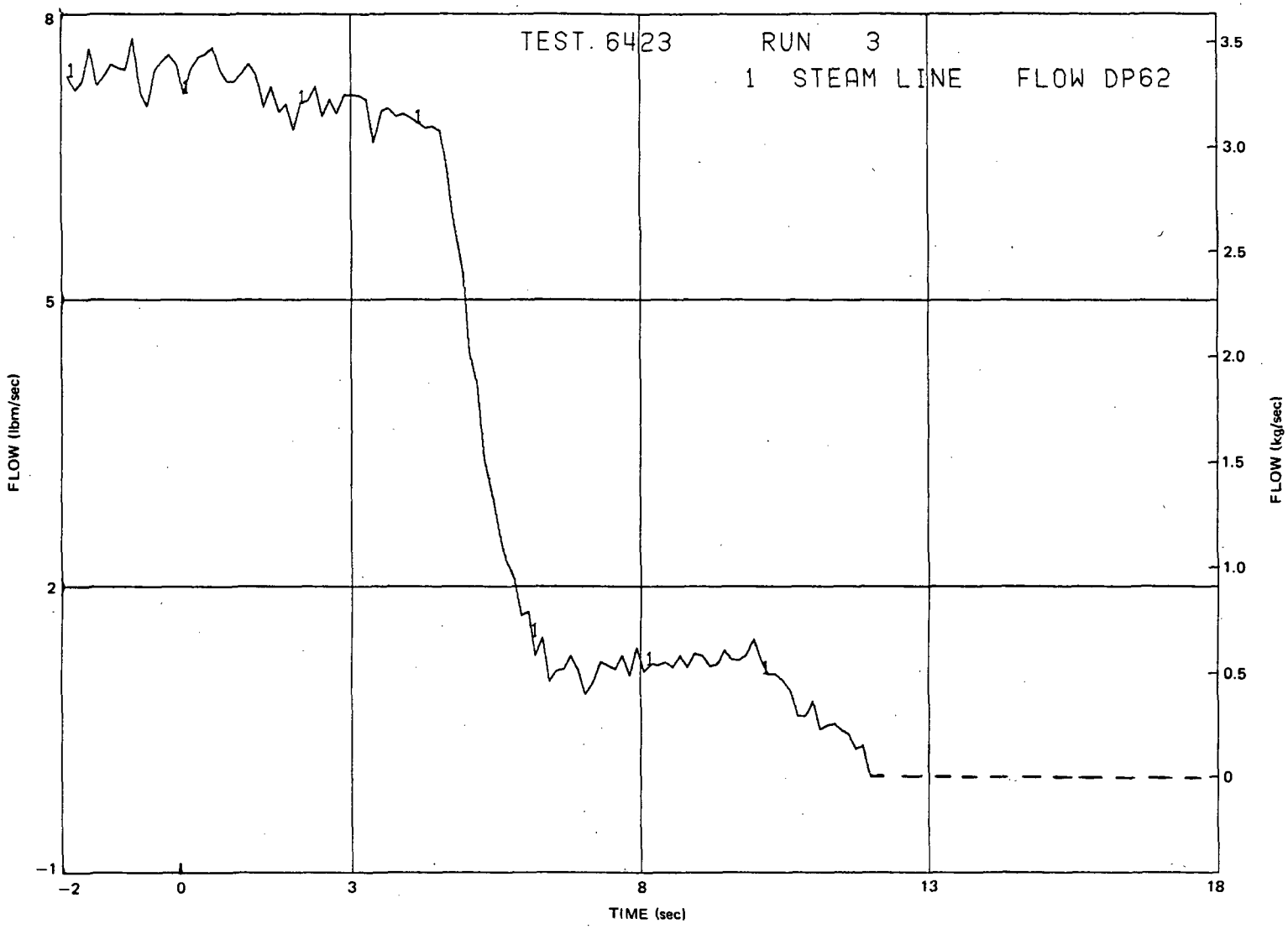

Figure N-54. Steamline Mass Flow Rate

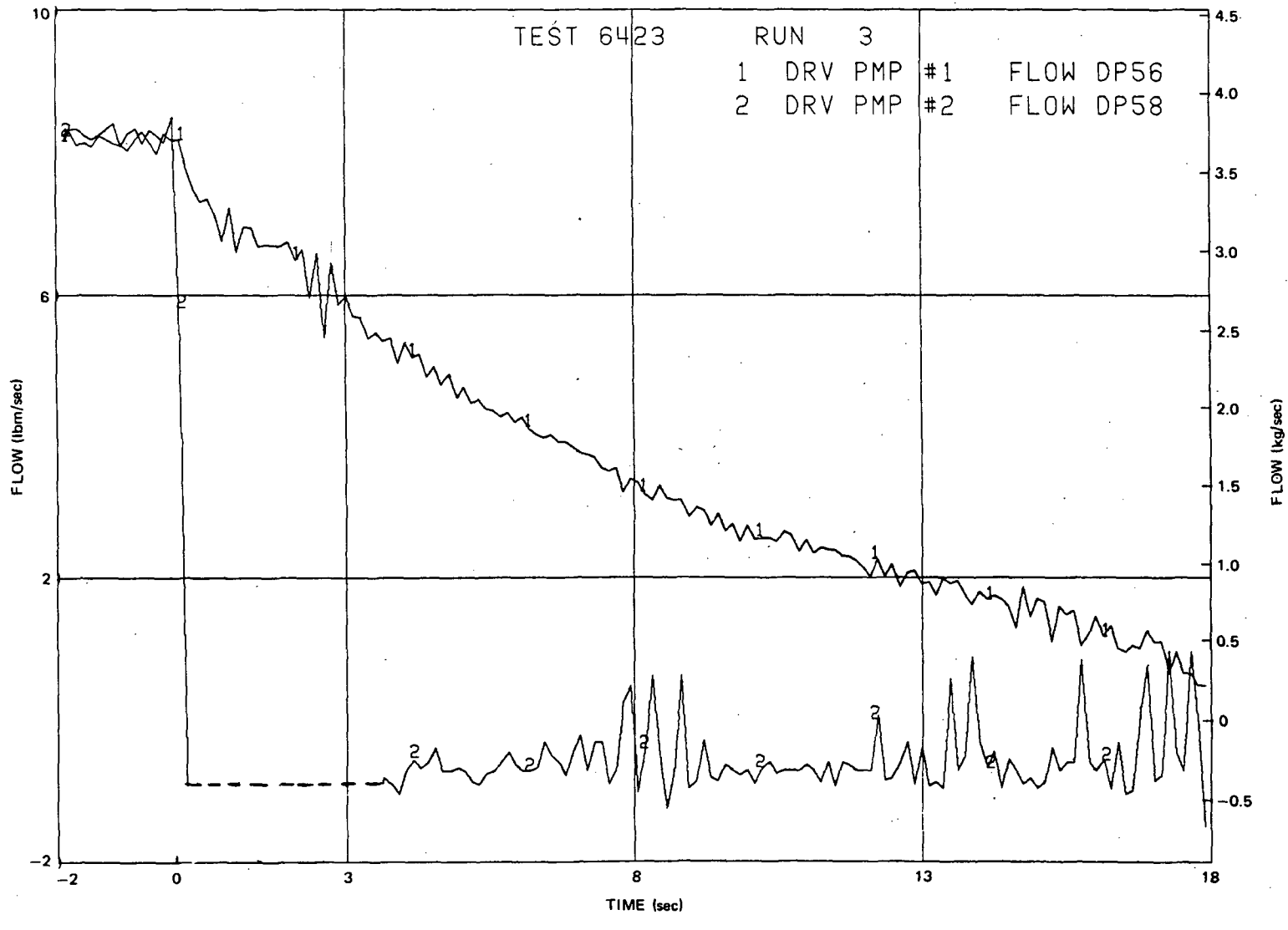

Figure N-55. Recirculation Pump Mass Flow Rates

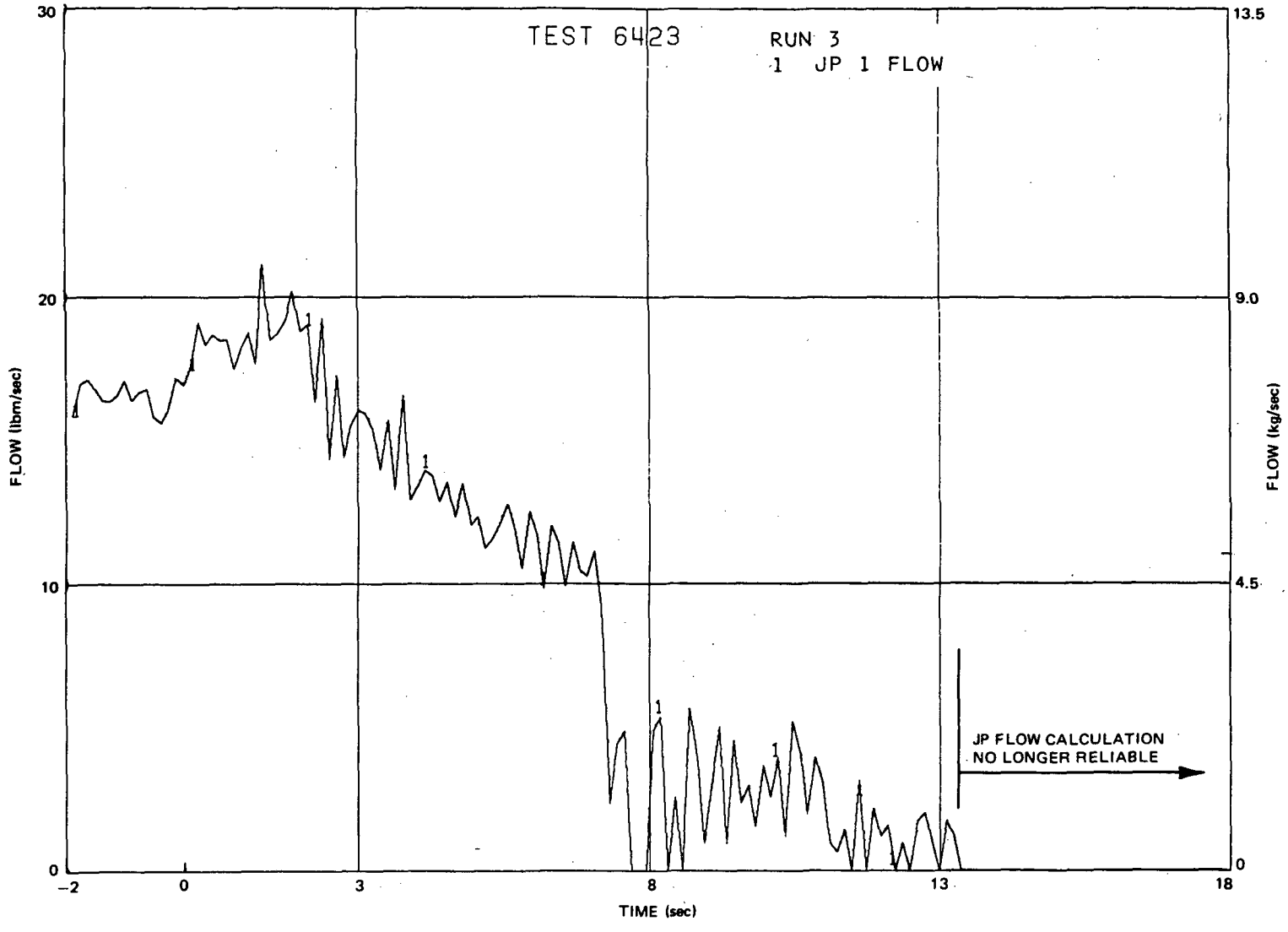

Figure N-56. Intact Loop Jet Pump Mass Flow Rate

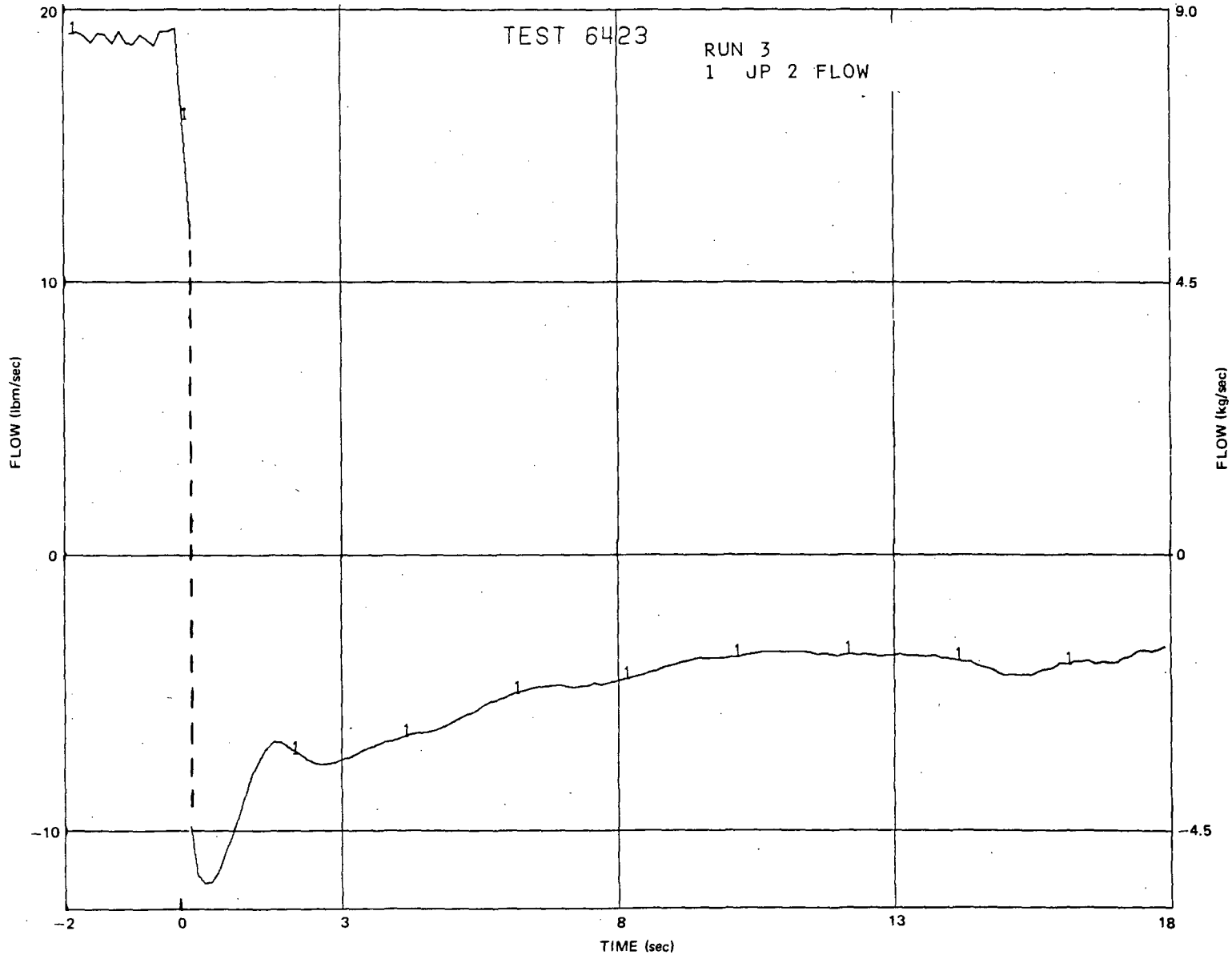

Figure N-57. Broken Loop Jet Pump Mass Flow Rate

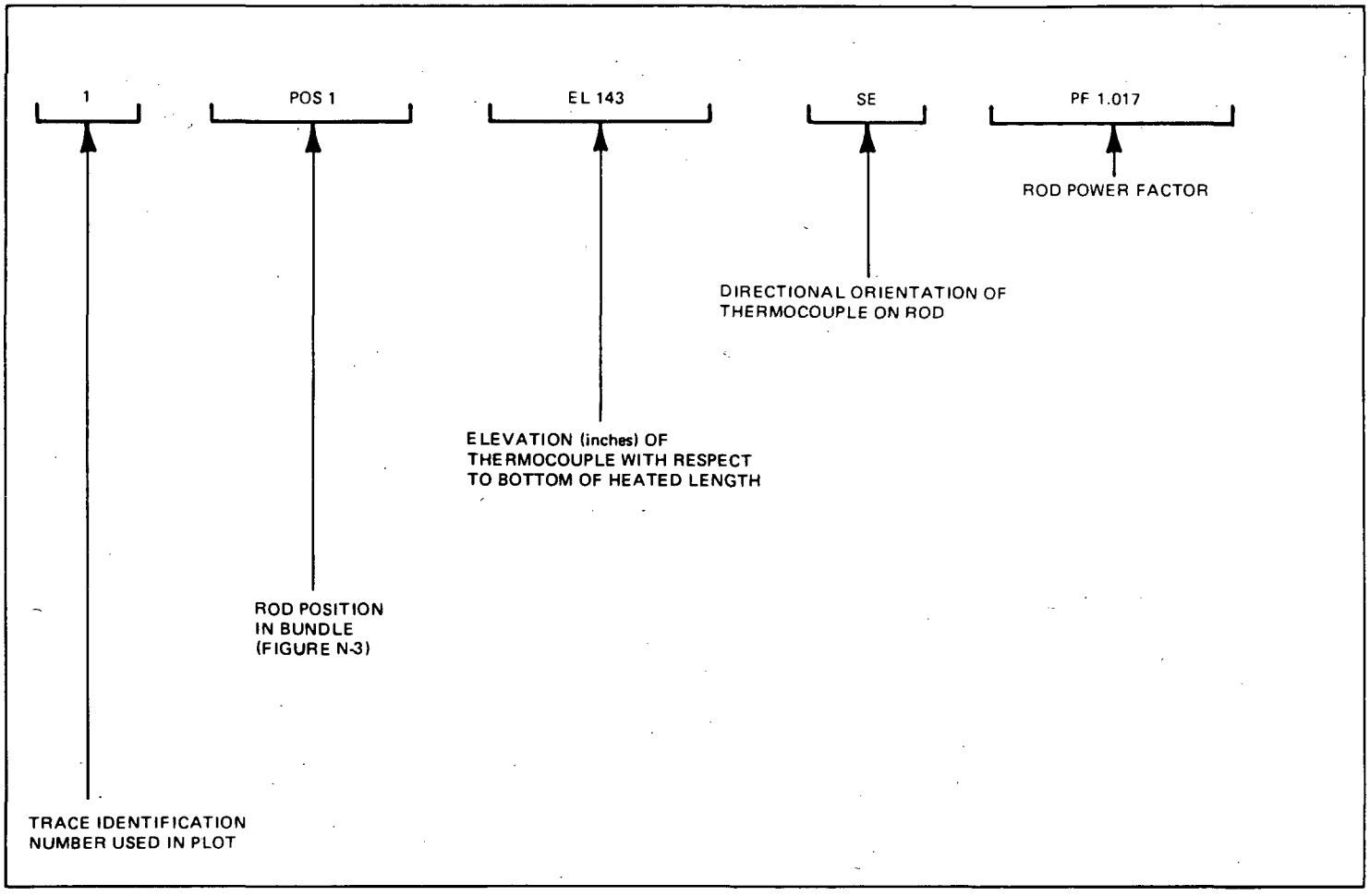

Figure N-58. Guide for Interpreting Legends on Bundle Temperature Plots

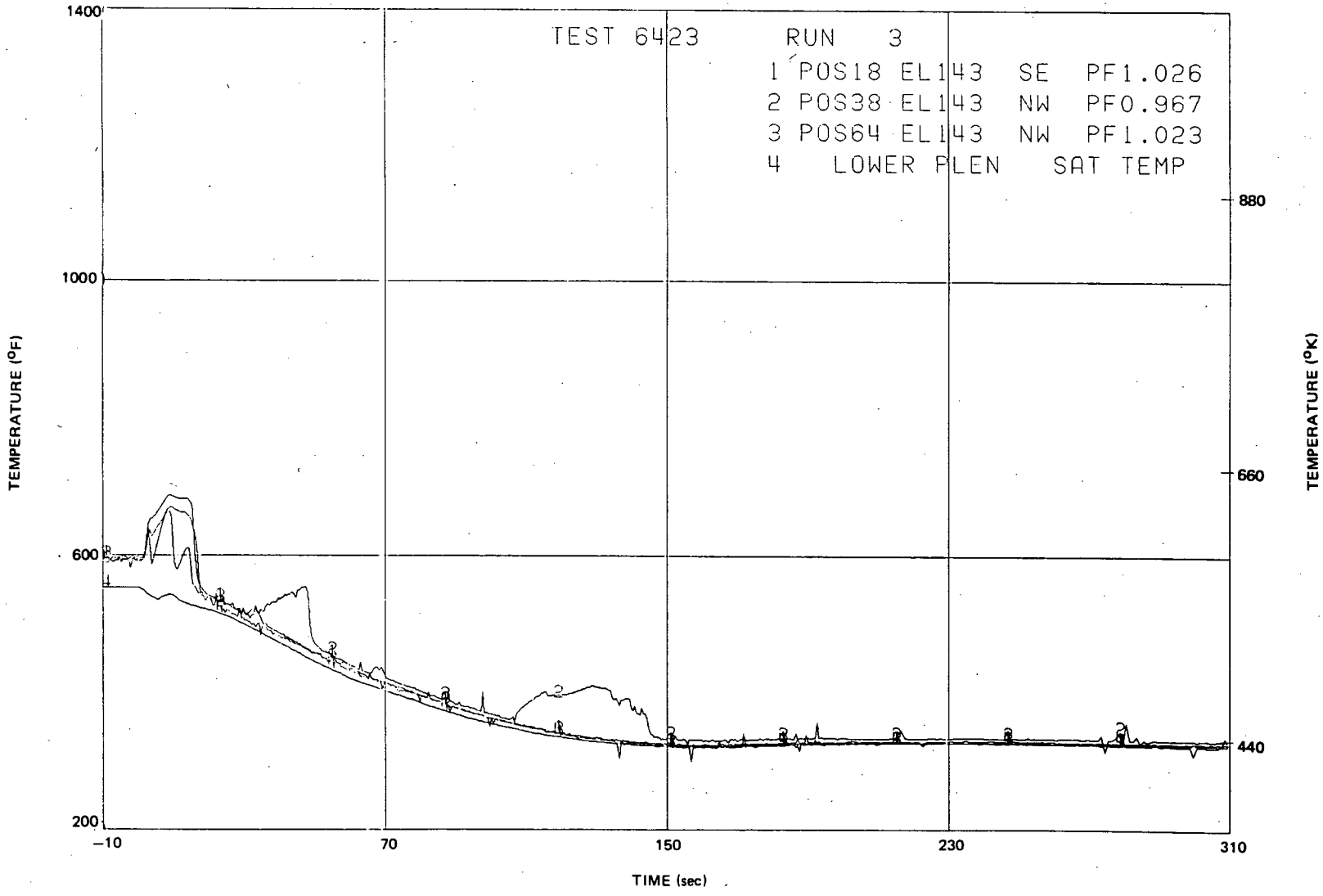

Figure N-59. Inside Clad Temperature - Elevation 143 in.

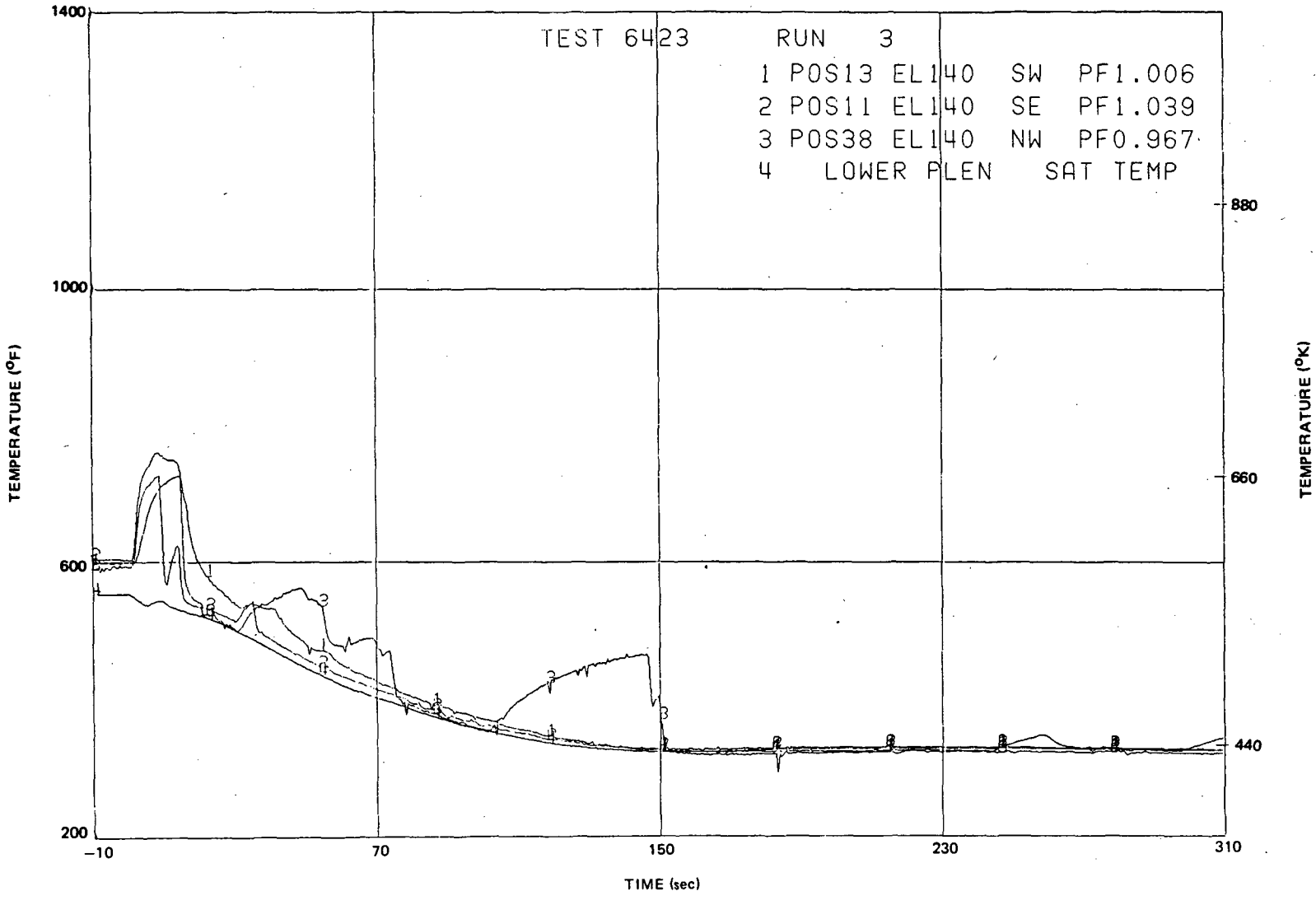

Figure N-60. Inside Clad Temperature - Elevation 140 in.

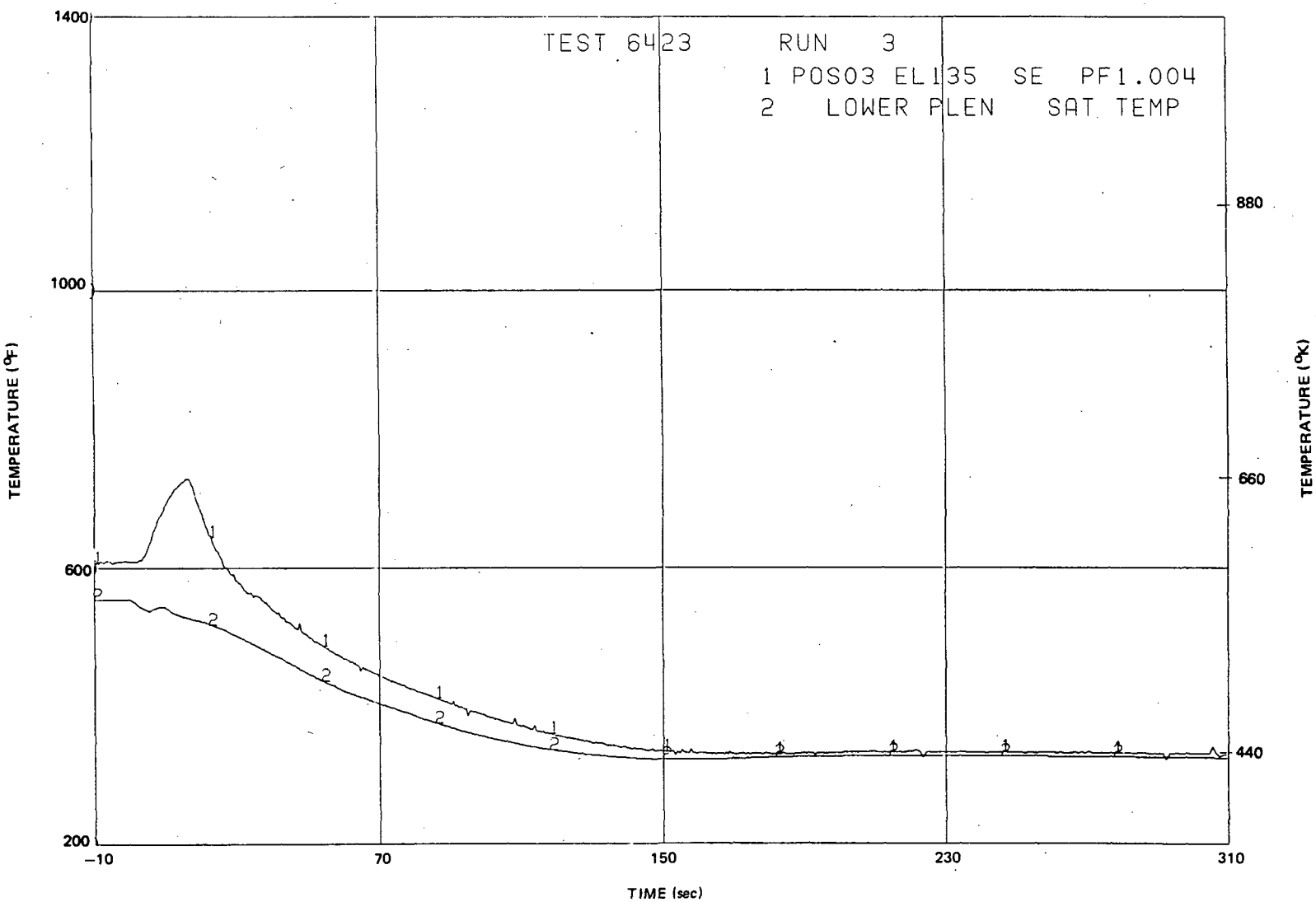

Figure N-61. Inside Clad Temperature - Elevation 135 in.

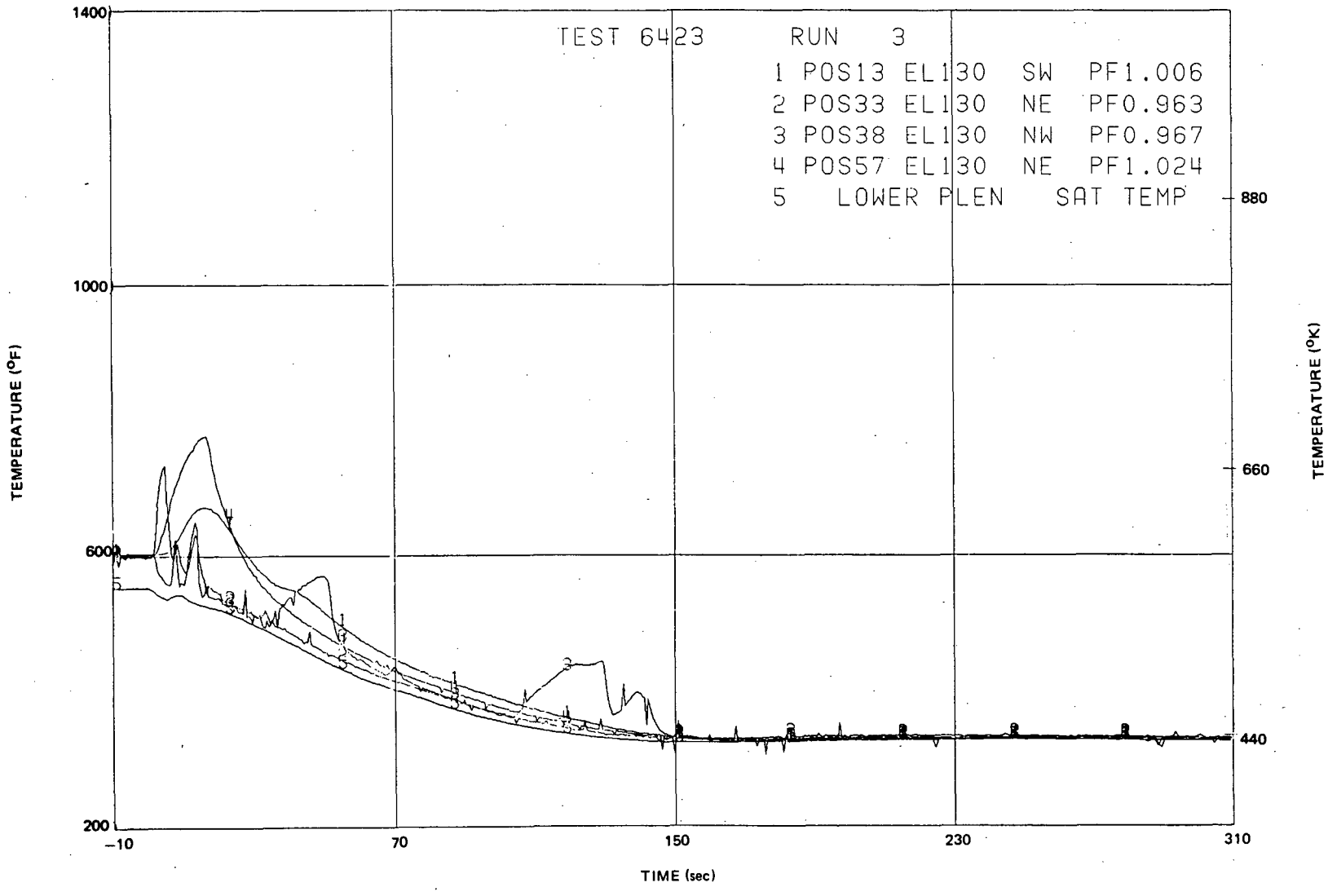

Figure N-62. Inside Clad Temperature - Elevation 130 in.

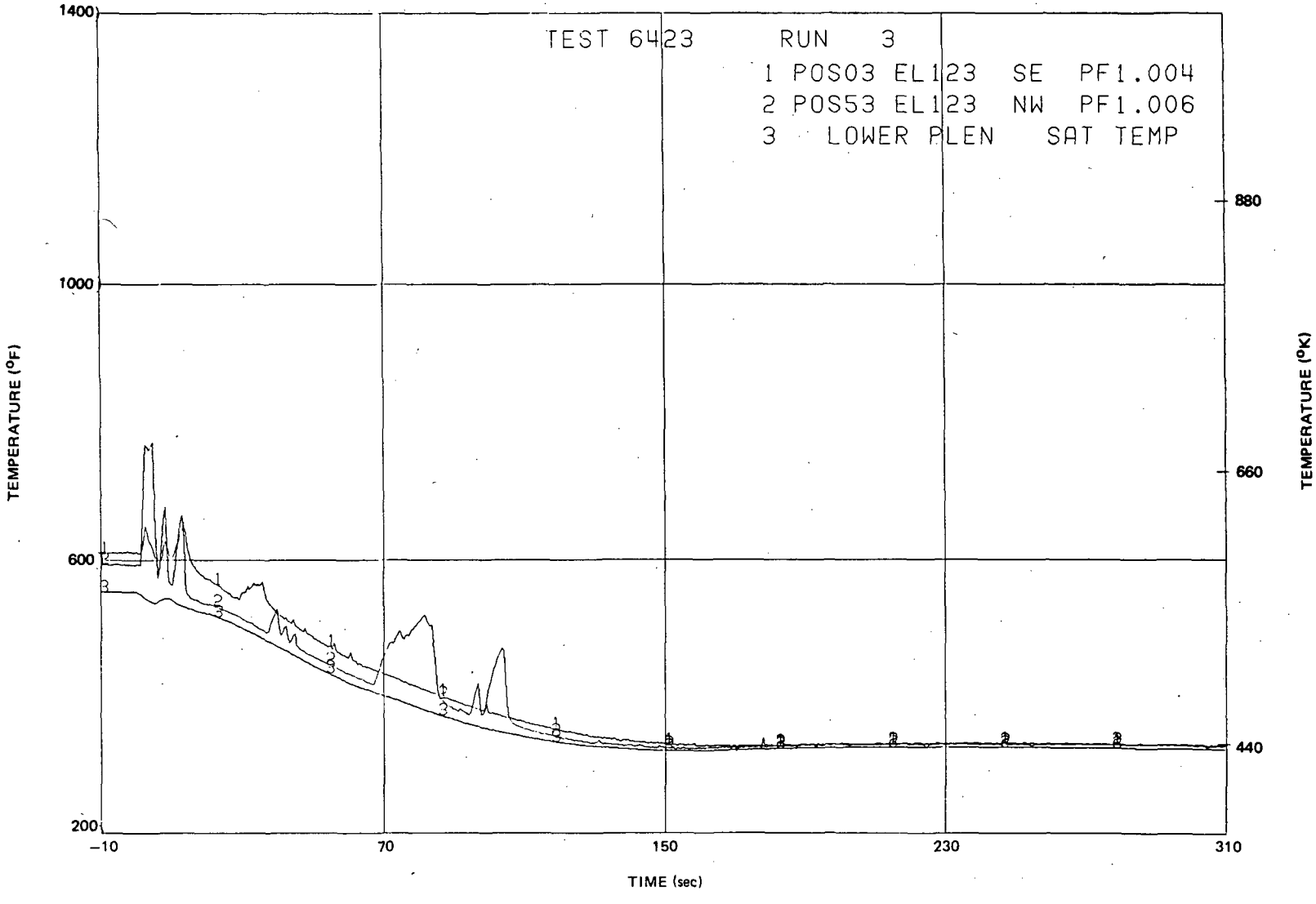

Figure N-63. Inside Clad Temperature - Elevation 123 in.

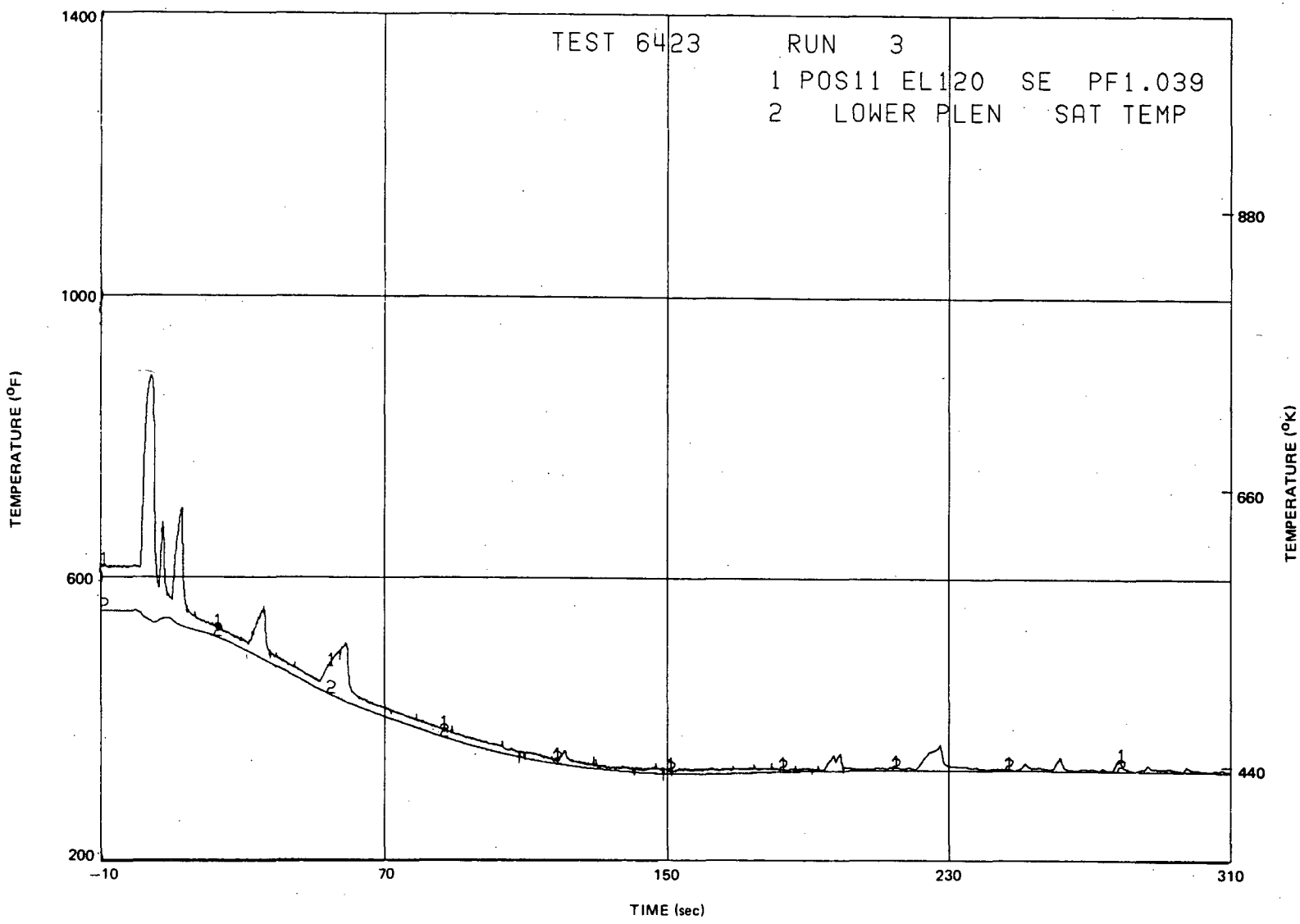

Figure N-64. Inside Clad Temperature - Elevation 120 in.

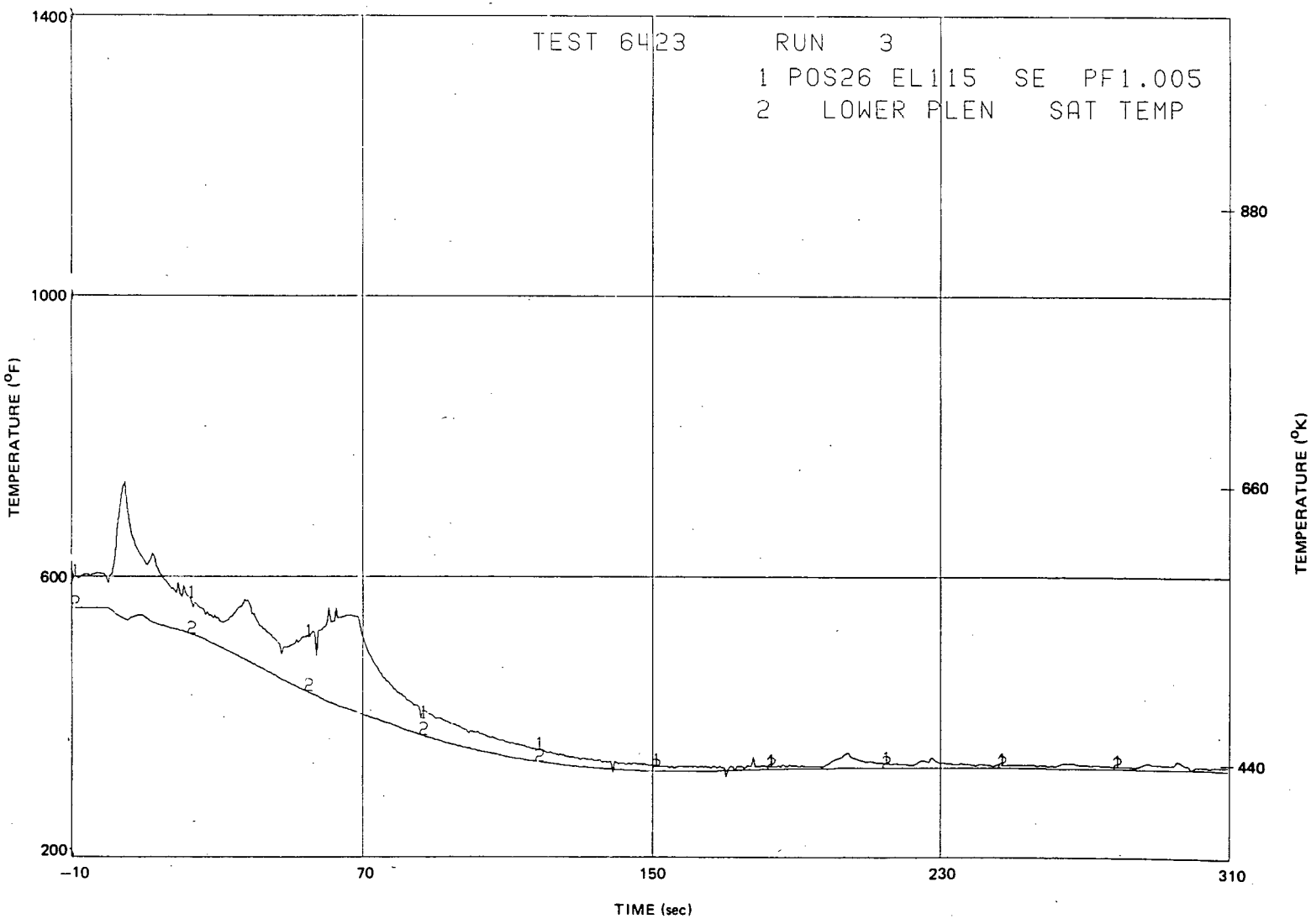

Figure N-65. Inside Clad Temperature - Elevation 115 in.

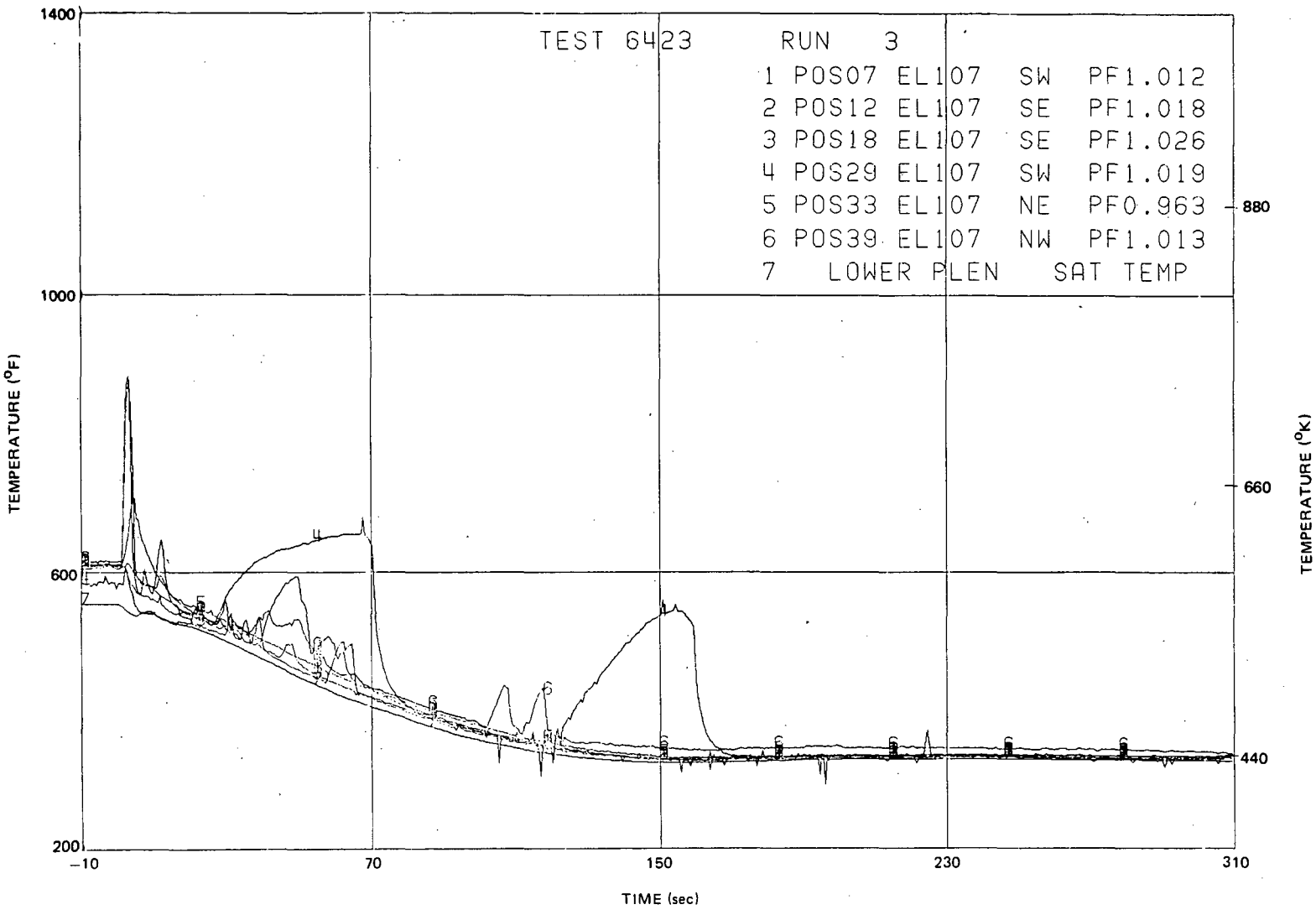

Figure N-66. Inside Clad Temperature - Elevation 107 in.

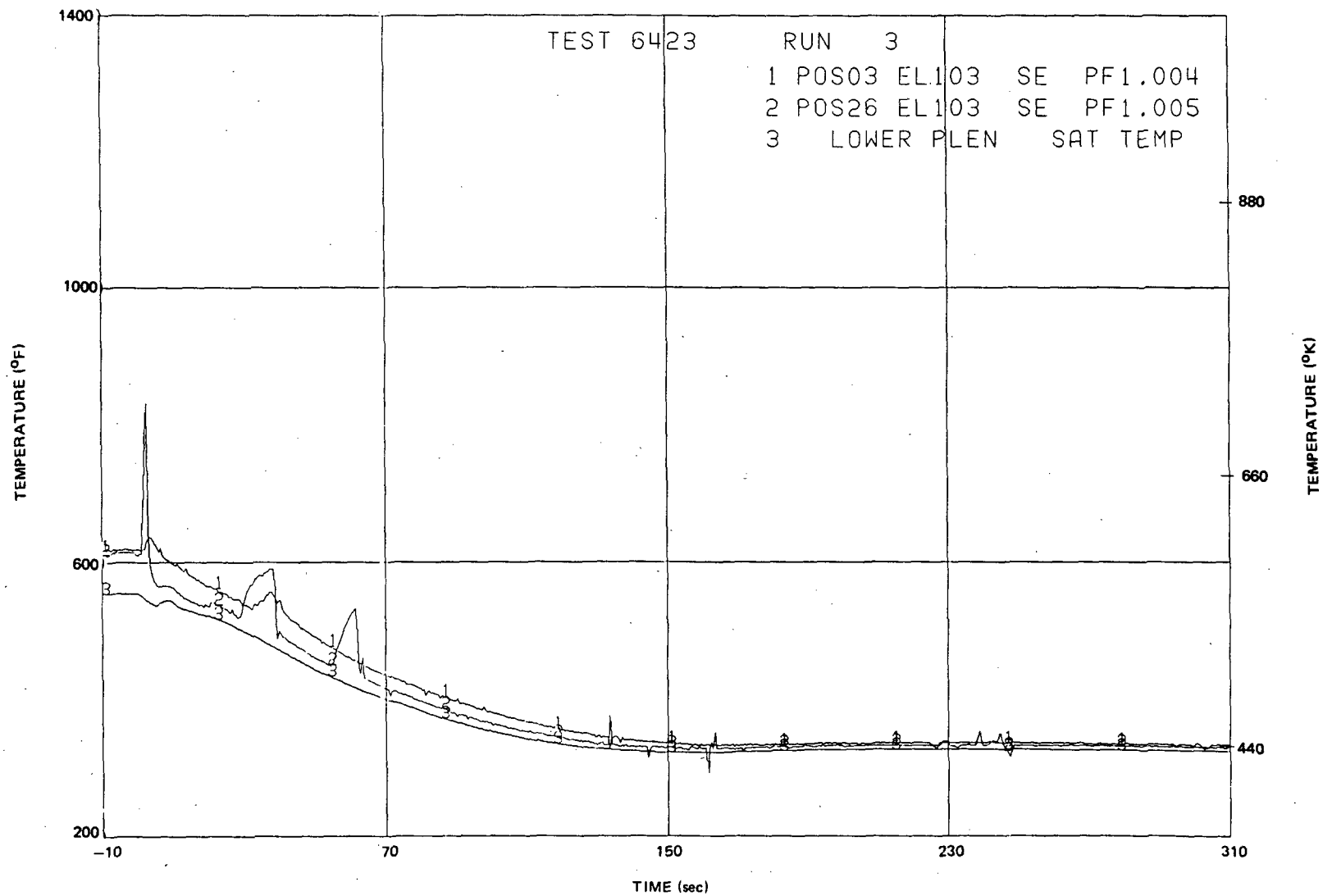

Figure N-67. Inside Clad Temperature - Elevation 103 in.

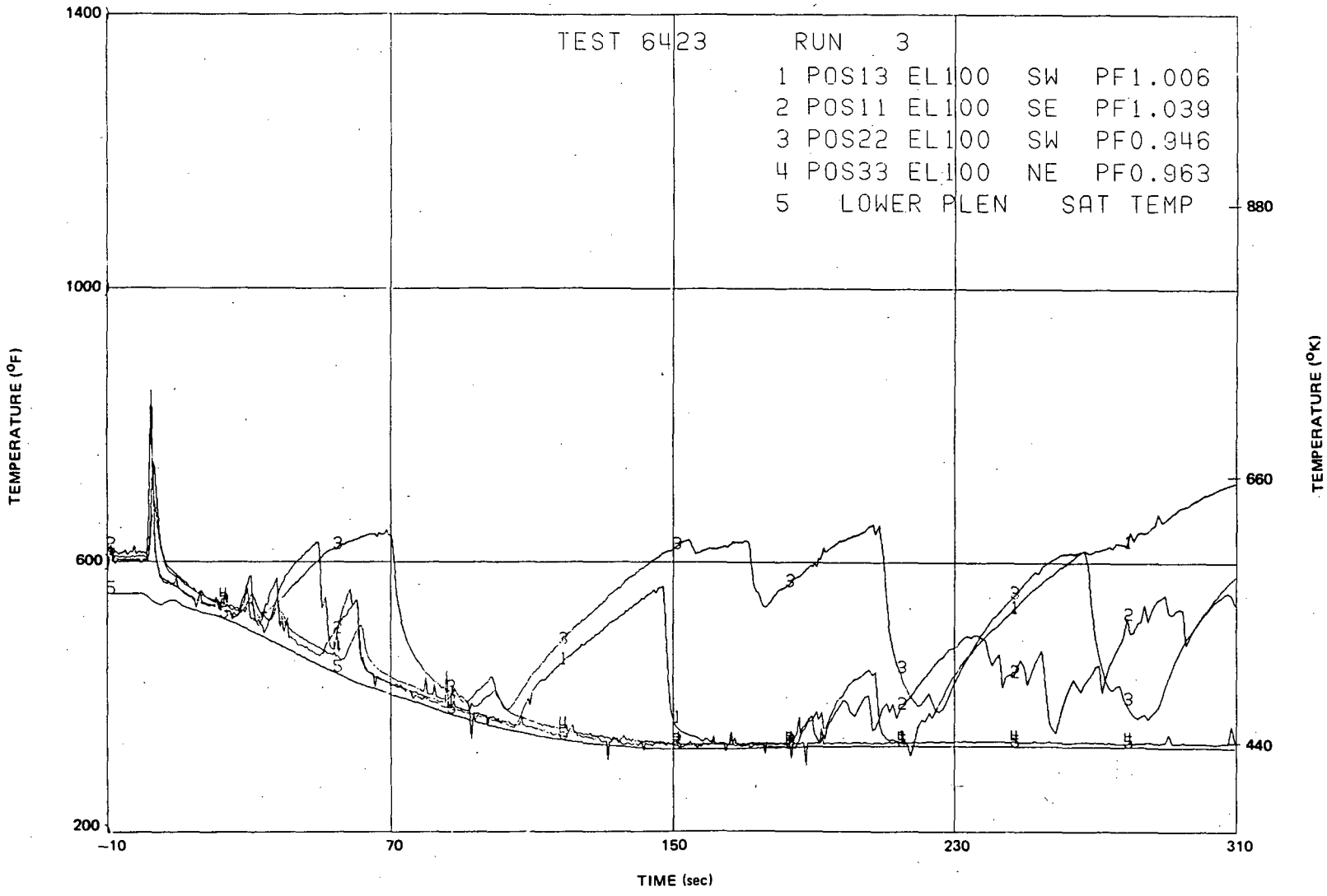

Figure N-68. Inside Clad Temperature - Elevation 100 in.

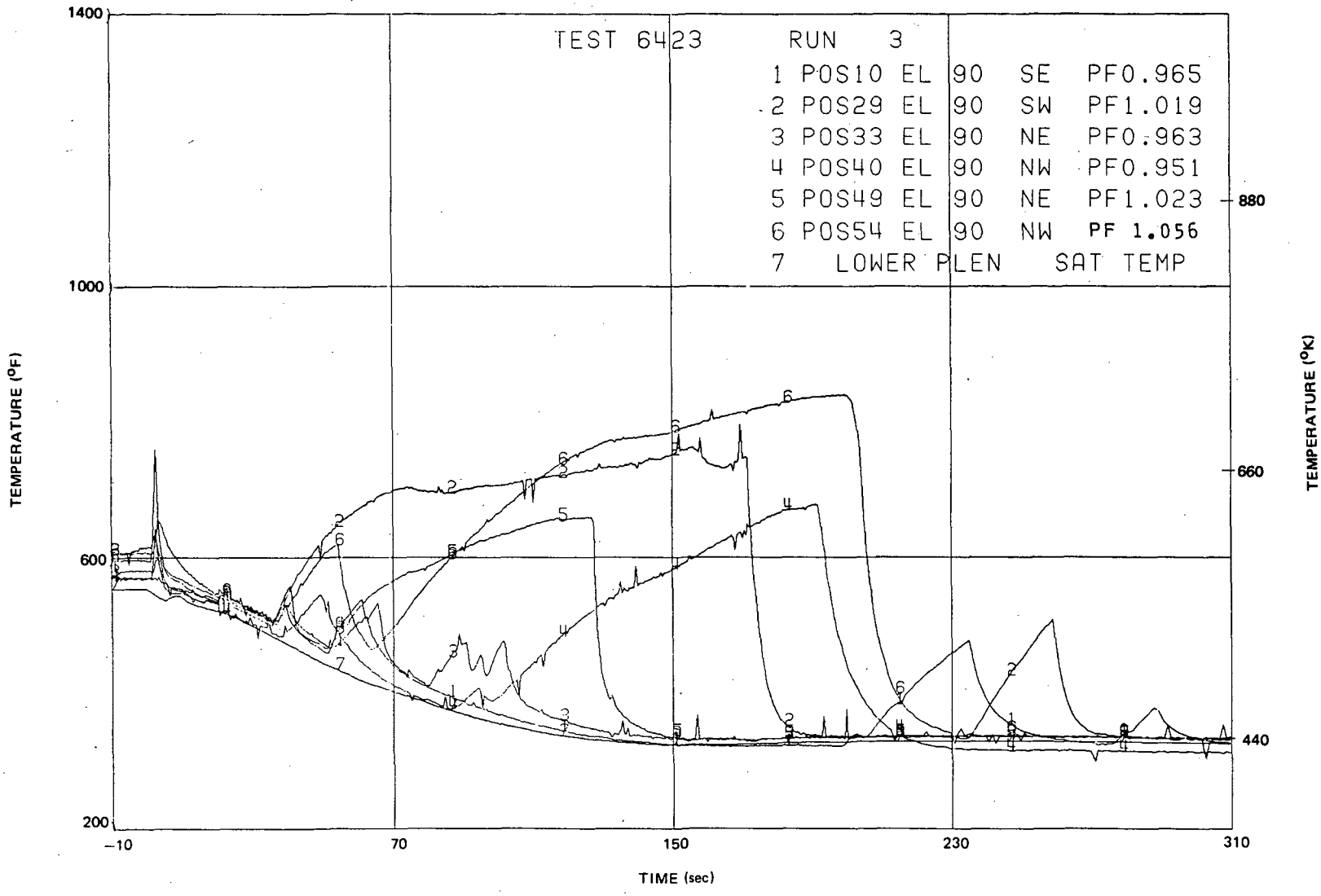

Figure N-69. Inside Clad Temperature - Elevation 90 in.

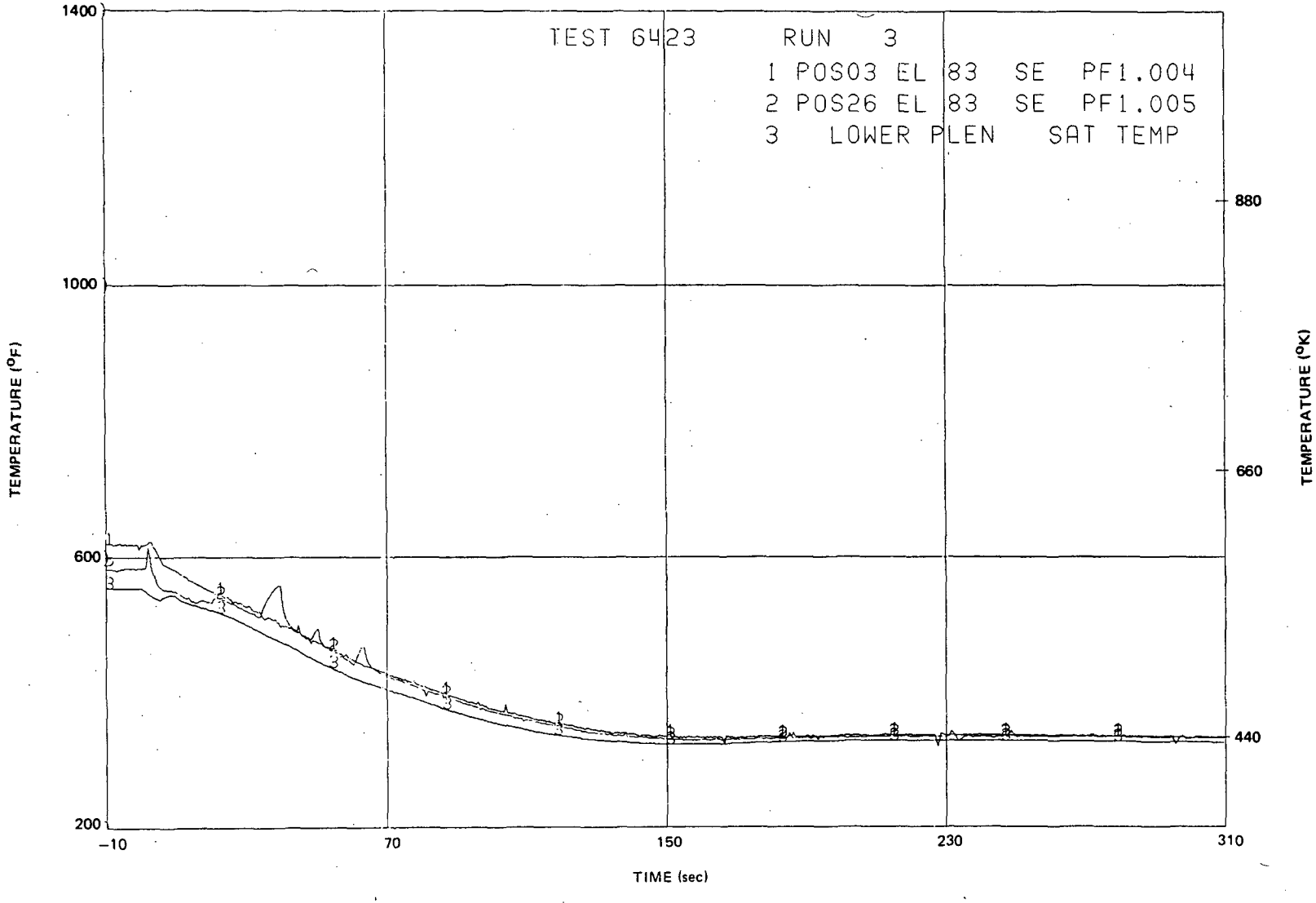

Figure N-70. Inside Clad Temperature - Elevation 83 in.

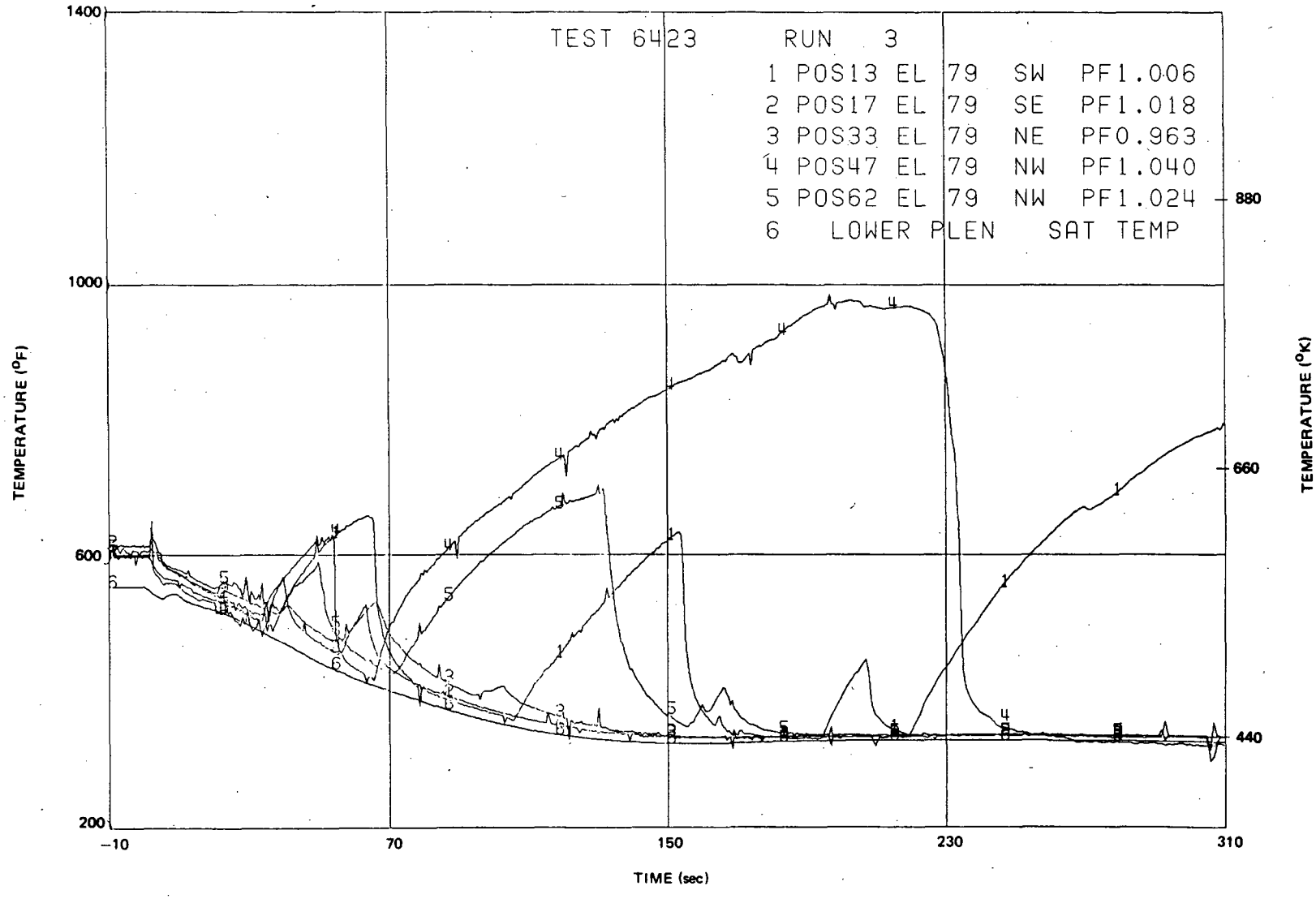

Figure N-71. Inside Clad Temperature - Elevation 79 in.

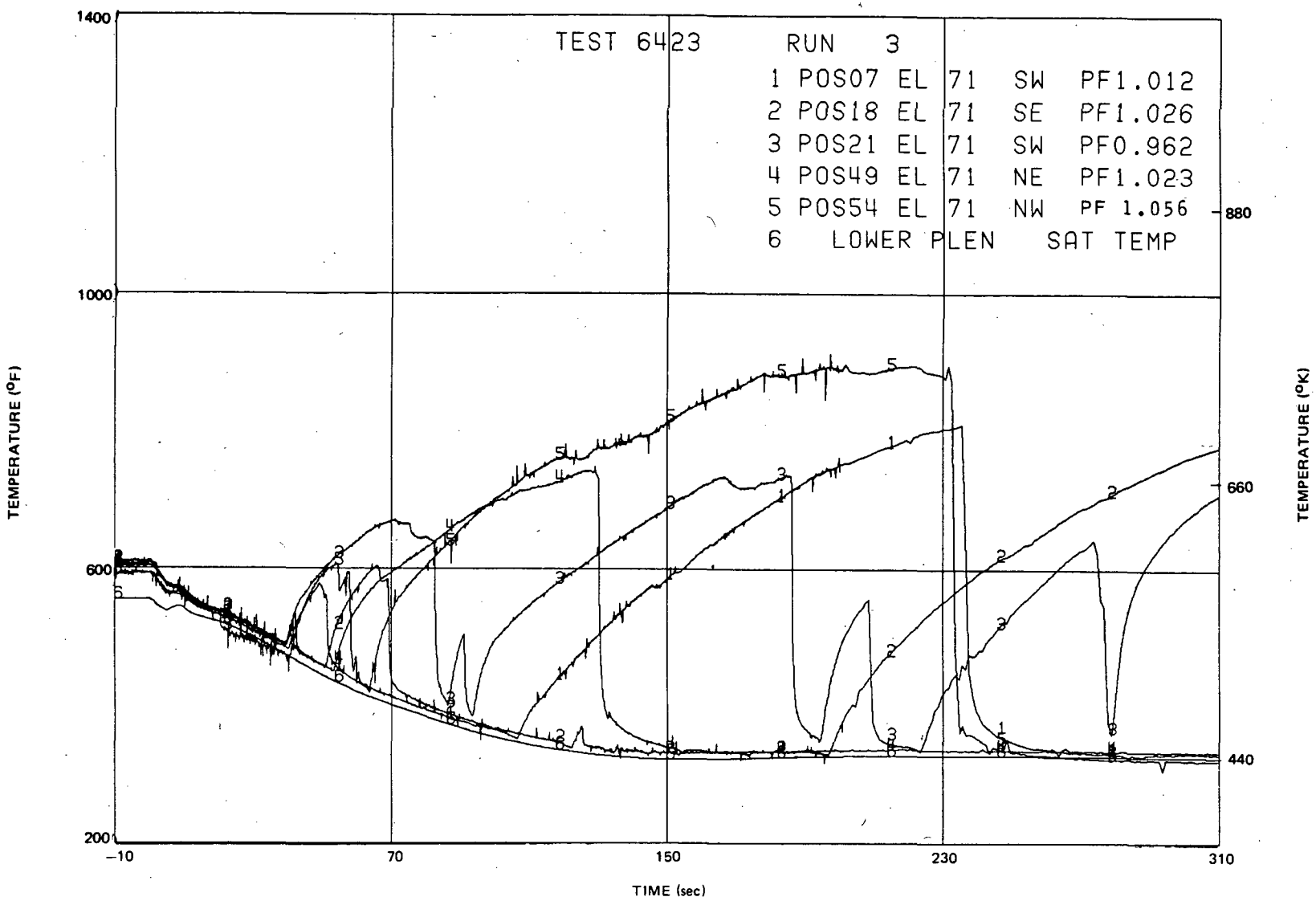

Figure N-72. Inside Clad Temperature - Elevation 71 in.

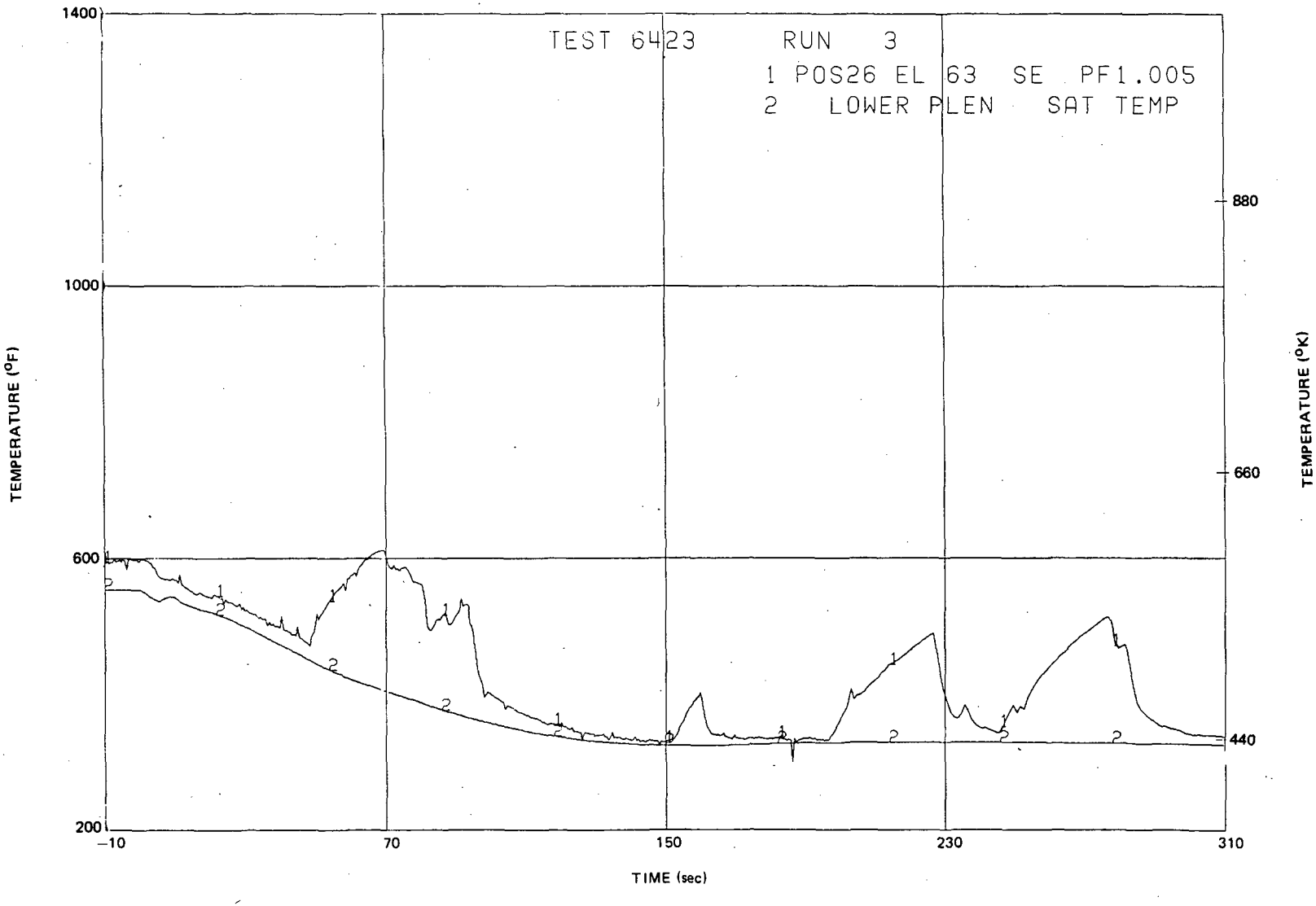

Figure N-73. Inside Clad Temperature - Elevation 63 in.

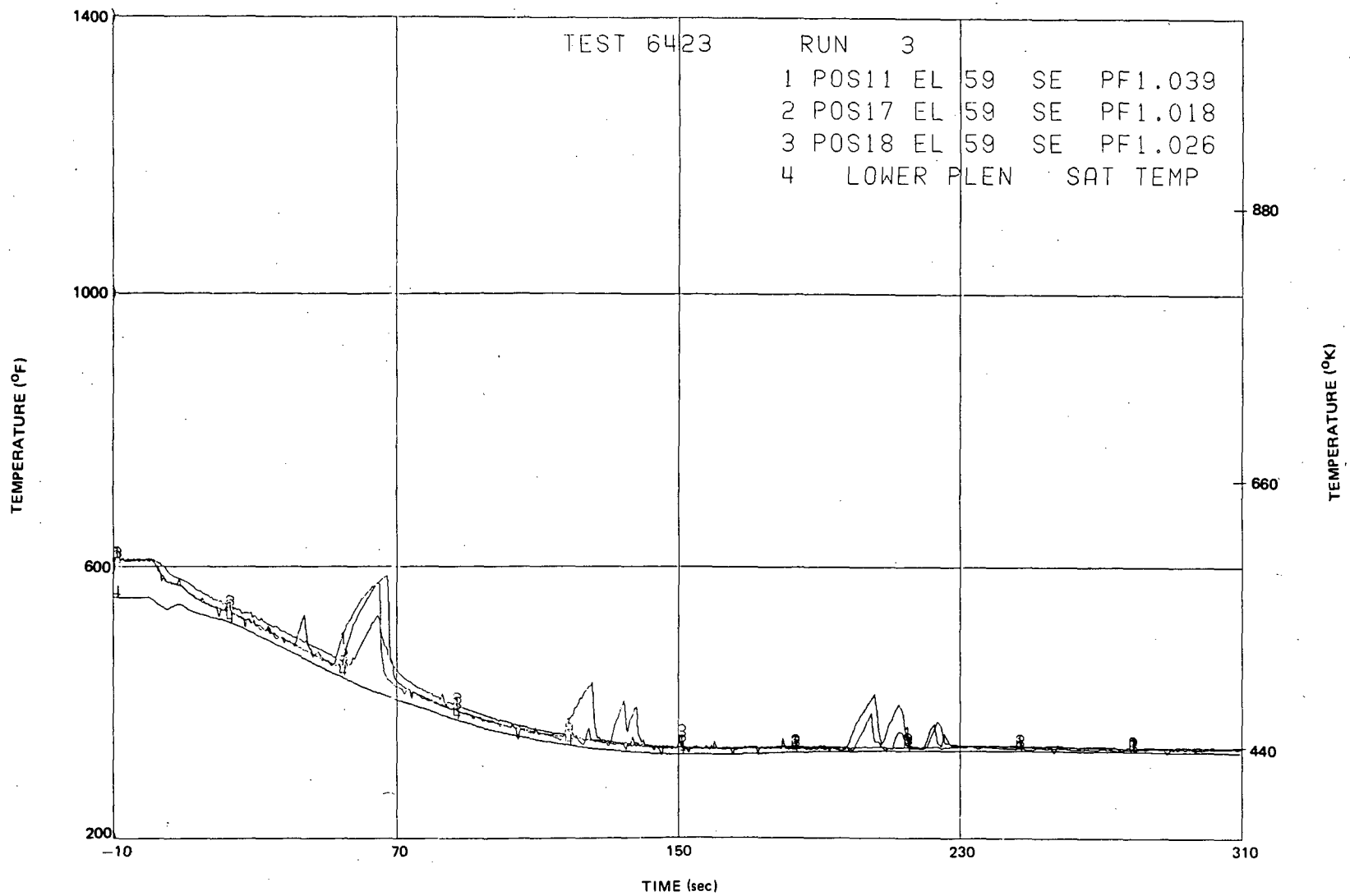

Figure N-74. Inside Clad Temperature - Elevation 59 in.

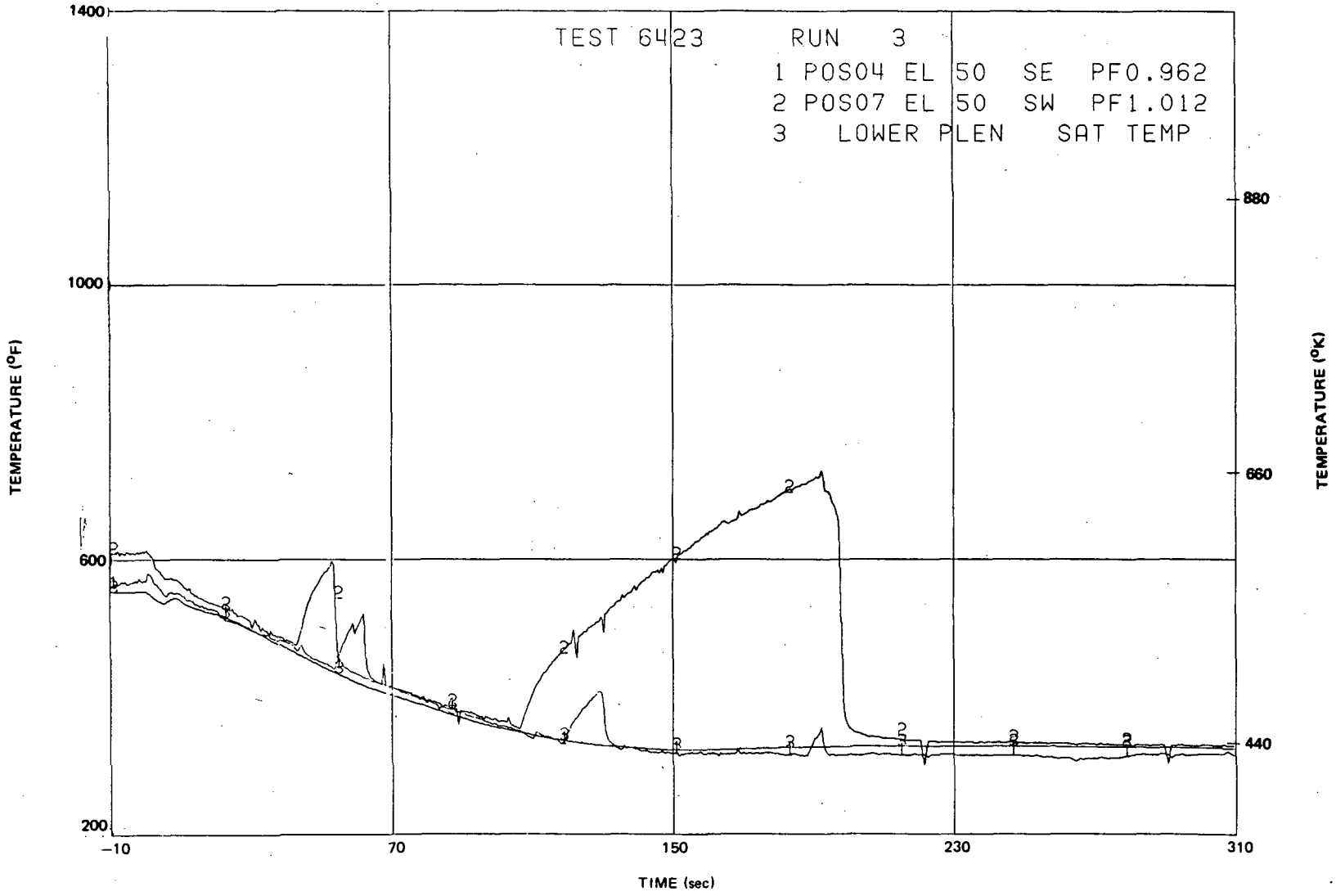

Figure N-75. Inside Clad Temperature - Elevation 50 in.

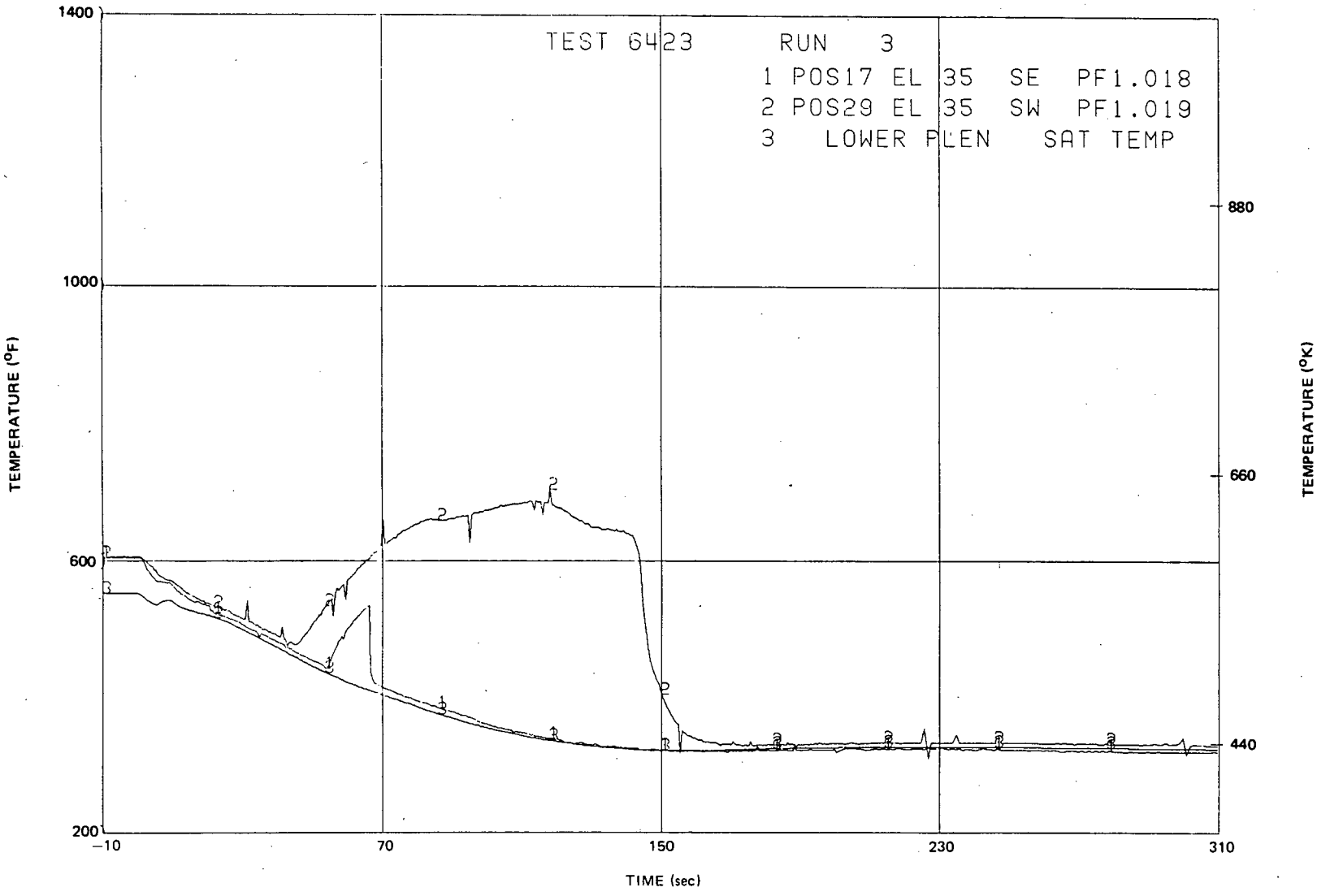

Figure N-76. Inside Clad Temperature - Elevation 35 in.

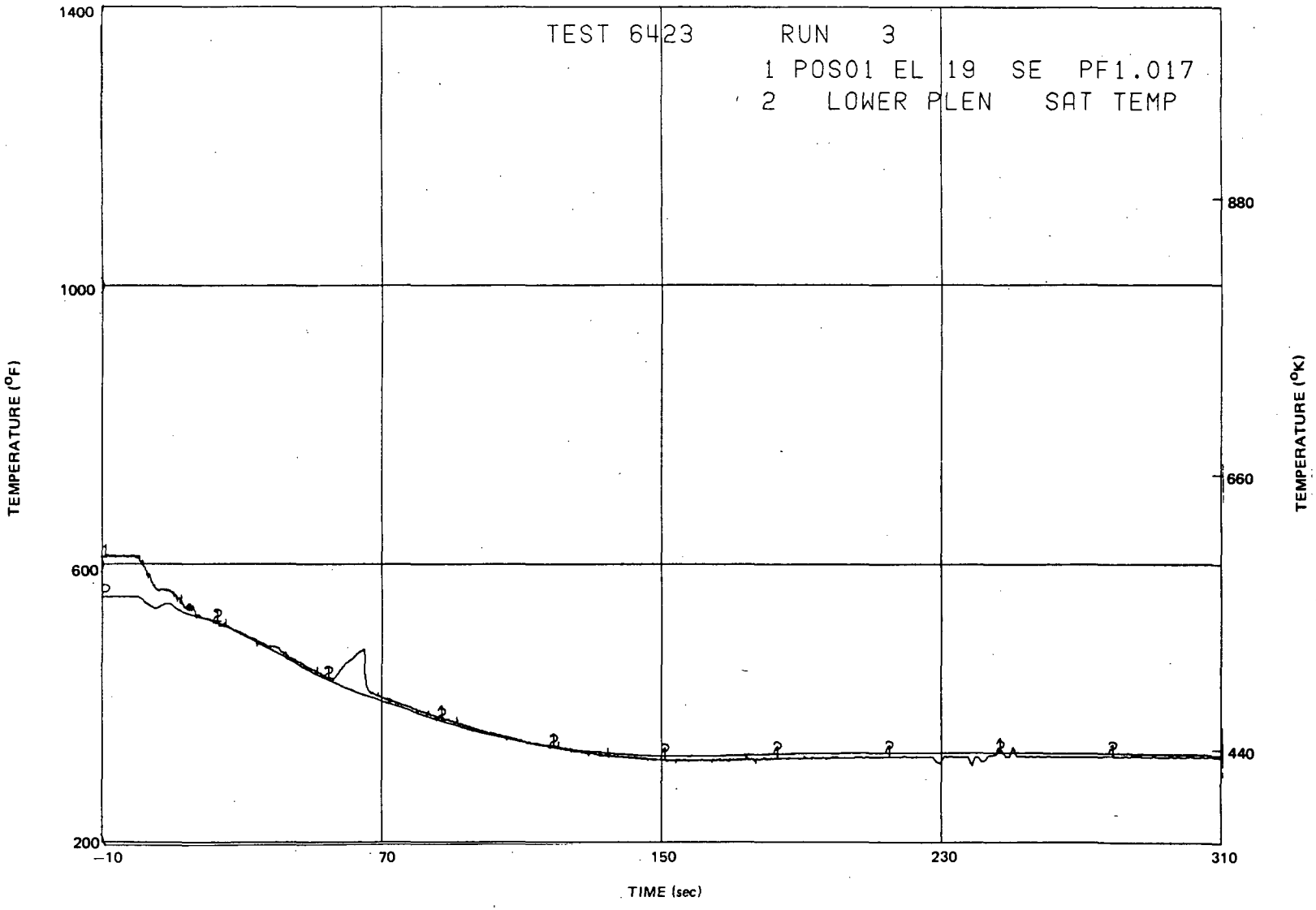

Figure N-77. Inside Clad Temperature - Elevation 19 in.

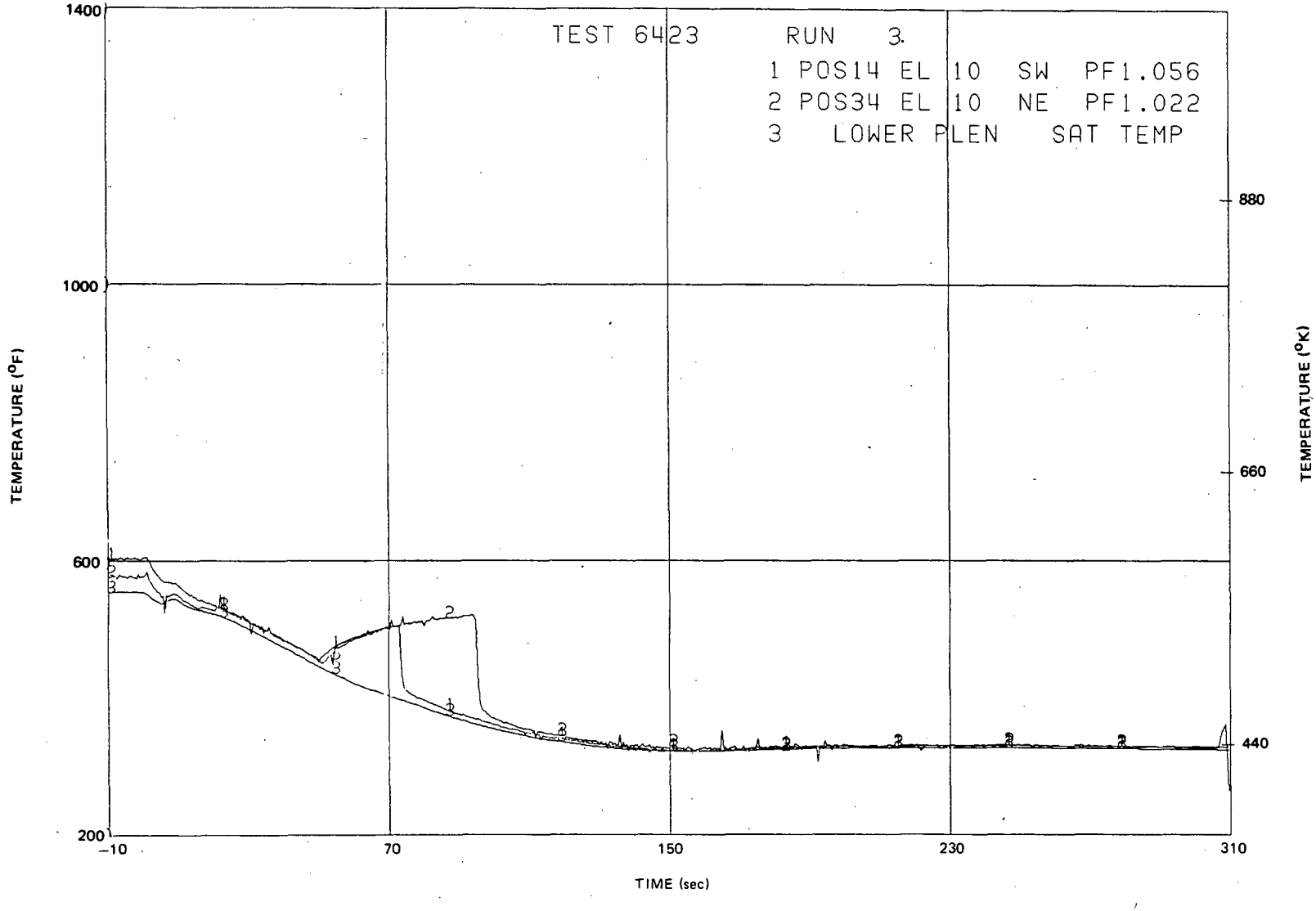

Figure N-78. Inside Clad Temperature - Elevation 10 in.

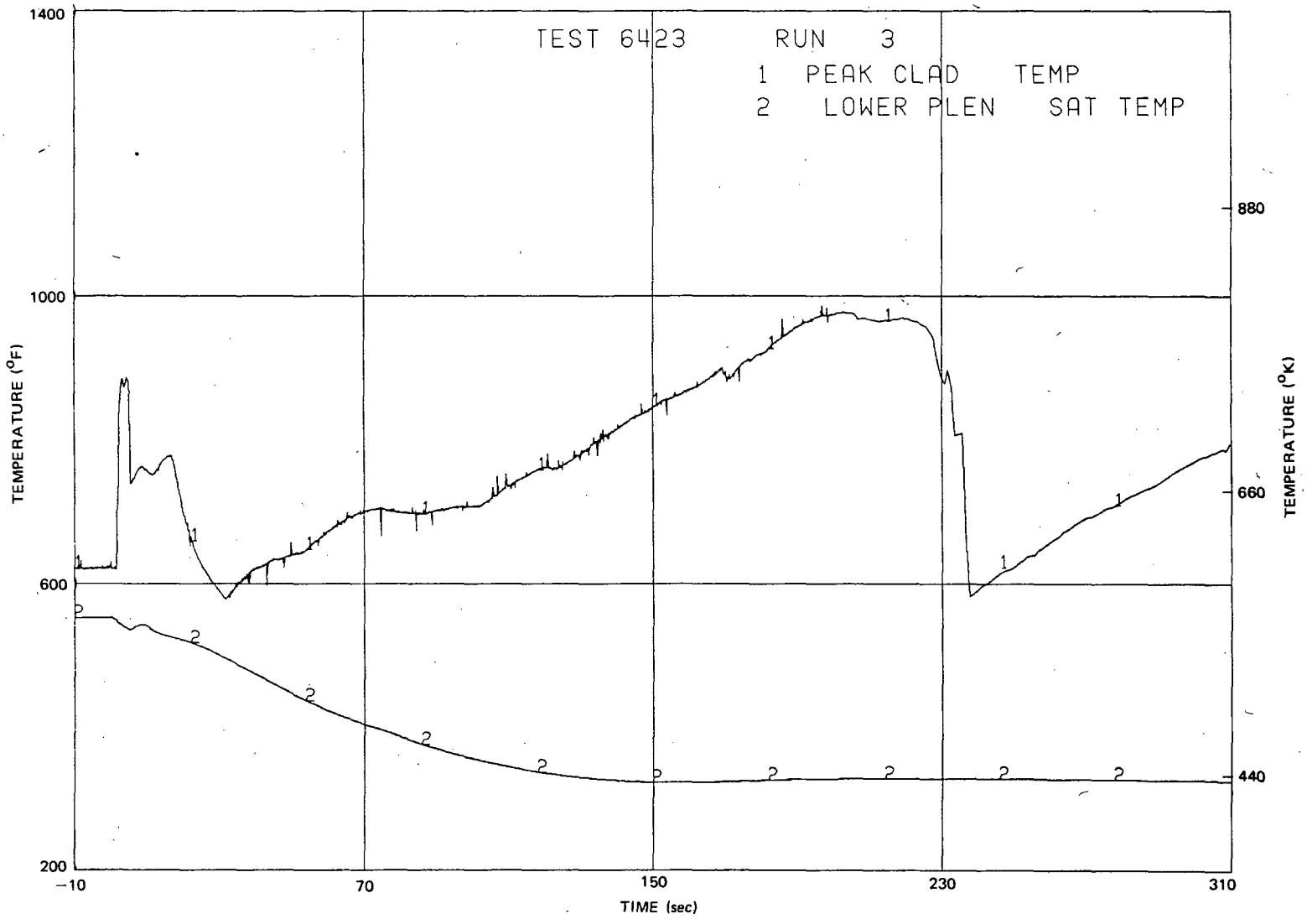

Figure N-79. Peak Clad Temperature

DISTRIBUTION

Division of Reactor Safety Research
U.S. Nuclear Regulatory Commission
Washington, DC 20555
Attn: W. D. Beckner (5)

Division of Reactor Licensing
U.S. Nuclear Regulatory Commission
Washington, DC 20555
Attn: R. K. Frahm

Electric Power Research Institute
4312 Hillview Avenue
Palo Alto, CA 94303
Attn: S. P. Kalra

Argonne National Laboratory
9700 Cass Avenue
Argonne, IL 60439
Attn: P. Lottes, RSR Heat Transfer Coordinator

EG & G
550 Second Street
Idaho Falls, ID 83401
Atn: R. J. Dallman

Safety and Systems Analysis
Nuclear Power Generation Division
Babcock & Wilcox
P. O. Box 1260
Lynchburg, VA 24505
Attn: Dr. B. E. Bingham

Reactor Development Center
Babcock & Wilcox
P. O. Box 1260
Lynchburg, VA 24505
Attn: Mr. D. Montgomery

Safeguards Development
Pressurized Water Reactor Systems Division
P. O. Box 355
Pittsburgh, PA 15230
Attn: Dr. L. E. Hochreiter

C-E Power Systems
Combustion Engineering, Inc.
1000 Prospect Hill Road
Windsor, CT 06095
Attn: Mr. J. D. Crawford

Librarian, General Atomic
P. O. Box 81608
San Diego, CA 92138

Department of Nuclear Engineering
University of California at Berkeley
Berkeley, CA 94720

Department of Nuclear Engineering
Massachusetts Institute of Technology
77 Massachusetts Avenue
Cambridge, MA 02139

Engineering Library
Stanford University Campus
Stanford, CA 94305

Los Alamos Scientific Laboratory
Los Alamos, NM 87544
Attn: C. W. Hirt, Group T-3

Environmental Protection Agency
P. O. Box 15027
Las Vagas, NV 89114

U. S. Nuclear Regulatory Commission
Reactor Analysis Section/Analysis Branch
Washington, DC 20555
Attn: W. Hodges

Mr. Kenneth Randen
ASEA Atom 1
Box 53
S-721 04
Vaesteraas 1, Sweden

Dr. T. Kawai
Hitachi, Limited
Hitachi Works
3-1-1 Saiwai-Cho
Hitachi-Shi, Ibaraki-Ken 317, Japan

Mr. Dieter Ewers
Kraftwerk Union AG
Postfach 700649
D-6000 Frankfurt (Main) 70
Federal Republic of Germany

Dr. H. Hashimoto
Tokyo Shibaura Electric Company
Toshiba Mita Building
13-12, 3-Chome Mita, Minato-Ku
Tokyo, 108, Japan

Mr. E. Annino
AMN Impianti Termici e Nucleari
Casella Postale 190
16151 Genova Sampierdarena
Italy

NRC FORM 335 (7-77)

U.S. NUCLEAR REGULATORY COMMISSION

BIBLIOGRAPHIC DATA SHEET

1. REPORT NUMBER (Assigned by DDC)
NUREG/CR-2229, Vol. 2
EPRI NP-1783
GEAP-24962-2

4. TITLE AND SUBTITLE (Add Volume No., if appropriate)
BWR Large Break Simulation Tests - BWR Blowdown/Emergency Core Cooling Program
Volume 2 - Appendices I-N

2. (Leave blank)

3. RECIPIENT'S ACCESSION NO.

7. AUTHOR(S)
L. S. Lee, G. L. Sozzi, S. A. Allison

5. DATE REPORT COMPLETED
MONTH March | YEAR 1981

9. PERFORMING ORGANIZATION NAME AND MAILING ADDRESS (Include Zip Code)
General Electric Company
175 Curtner Avenue
San Jose, California 95125

DATE REPORT ISSUED
MONTH July | YEAR 1982

6. (Leave blank)

8. (Leave blank)

12. SPONSORING ORGANIZATION NAME AND MAILING ADDRESS (Include Zip Code)
U.S. Nuclear Regulatory Commission
Division of Accident Evaluation
Office of Nuclear Regulatory Research
Washington, D.C. 20555

10. PROJECT/TASK/WORK UNIT NO.

11. CONTRACT NO.
FIN B3014

13. TYPE OF REPORT
Topical Report

PERIOD COVERED (Inclusive dates)
1980-1981

15. SUPPLEMENTARY NOTES

14. (Leave blank)

16. ABSTRACT (200 words or less)

The BD/ECC Program is an experimentally based program jointly sponsored by the Nuclear Regulatory Commission, the Electric Power Research Institute, and the General Electric Company. The BD/ECC 1A Test Phase of this program involves investigating the integral systems effects of emergency core coolant injection during a hypothetical LOCA. Tests were conducted in a BWR system simulator, the Two-Loop Test Apparatus (TLTA) which features a full-size electrically heated bundle. Fluid delivery systems were included to simulate coolant injections.

Tests conducted under this program include large break (design basis accident), small break, and core uncovery under slow loss-of-coolant (boil-off) transients. Three separate topical reports are issued, one for each type of test. This topical covers the large break results. Volume 1 contains the summary, discussion, analysis, and conclusions. Volume 2 contains the data reports.

17. KEY WORDS AND DOCUMENT ANALYSIS

17a. DESCRIPTORS

17b. IDENTIFIERS/OPEN-ENDED TERMS

18. AVAILABILITY STATEMENT
Unlimited

19. SECURITY CLASS (This report)
Unclassified

20. SECURITY CLASS (This page)
Unclassified

21. NO. OF PAGES

22. PRICE
$

NRC FORM 335 (7-77)

*U.S. GOVERNMENT PRINTING OFFICE: 1982-0-361-297/2266

UNITED STATES
NUCLEAR REGULATORY COMMISSION
WASHINGTON, D.C. 20555

OFFICIAL BUSINESS
PENALTY FOR PRIVATE USE, $300

FOURTH CLASS MAIL
POSTAGE & FEES PAID
USNRC
WASH. D. C.
PERMIT No G-67

120555003908 1 ANR2
US NRC
ASLBP
CHAIRMAN
EW439
WASHINGTON DC 20555